frontiers | Research Topics

Translational advances in Alzheimer's, Parkinson's, and other dementia: Molecular mechanisms, biomarkers, diagnosis, and therapies, volume III

Edited by
Chih-Yu Hsu, Woon-Man Kung, Kenneth S. Hettie, Kuangyu Shi and Jiehui Jiang

Published in
Frontiers in Aging Neuroscience
Frontiers in Neuroscience
Frontiers in Pharmacology
Frontiers in Molecular Neuroscience

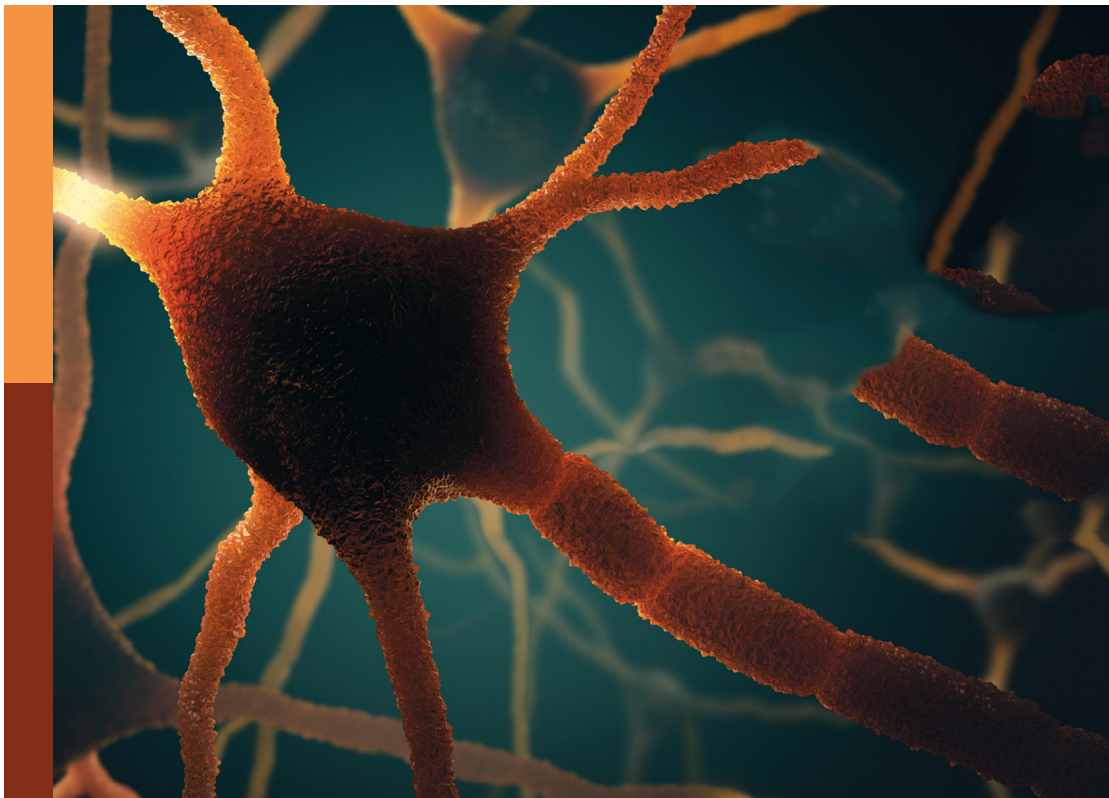

ISSN 1664-8714
ISBN 978-2-8325-4333-7
DOI 10.3389/978-2-8325-4333-7

About Frontiers

Frontiers is more than just an open access publisher of scholarly articles: it is a pioneering approach to the world of academia, radically improving the way scholarly research is managed. The grand vision of Frontiers is a world where all people have an equal opportunity to seek, share and generate knowledge. Frontiers provides immediate and permanent online open access to all its publications, but this alone is not enough to realize our grand goals.

Frontiers journal series

The Frontiers journal series is a multi-tier and interdisciplinary set of open-access, online journals, promising a paradigm shift from the current review, selection and dissemination processes in academic publishing. All Frontiers journals are driven by researchers for researchers; therefore, they constitute a service to the scholarly community. At the same time, the *Frontiers journal series* operates on a revolutionary invention, the tiered publishing system, initially addressing specific communities of scholars, and gradually climbing up to broader public understanding, thus serving the interests of the lay society, too.

Dedication to quality

Each Frontiers article is a landmark of the highest quality, thanks to genuinely collaborative interactions between authors and review editors, who include some of the world's best academicians. Research must be certified by peers before entering a stream of knowledge that may eventually reach the public - and shape society; therefore, Frontiers only applies the most rigorous and unbiased reviews. Frontiers revolutionizes research publishing by freely delivering the most outstanding research, evaluated with no bias from both the academic and social point of view. By applying the most advanced information technologies, Frontiers is catapulting scholarly publishing into a new generation.

What are Frontiers Research Topics?

Frontiers Research Topics are very popular trademarks of the *Frontiers journals series*: they are collections of at least ten articles, all centered on a particular subject. With their unique mix of varied contributions from Original Research to Review Articles, Frontiers Research Topics unify the most influential researchers, the latest key findings and historical advances in a hot research area.

Find out more on how to host your own Frontiers Research Topic or contribute to one as an author by contacting the Frontiers editorial office: frontiersin.org/about/contact

Translational advances in Alzheimer's, Parkinson's, and other dementia: Molecular mechanisms, biomarkers, diagnosis, and therapies, volume III

Topic editors

Chih-Yu Hsu — Fujian University of Technology, China
Woon-Man Kung — Taipei Tzu Chi Hospital, Taiwan
Kenneth S. Hettie — Stanford University, United States
Kuangyu Shi — University of Bern, Switzerland
Jiehui Jiang — Shanghai University, China

Citation

Hsu, C.-Y., Kung, W.-M., Hettie, K. S., Shi, K., Jiang, J., eds. (2024). *Translational advances in Alzheimer's, Parkinson's, and other dementia: Molecular mechanisms, biomarkers, diagnosis, and therapies, volume III*. Lausanne: Frontiers Media SA. doi: 10.3389/978-2-8325-4333-7

Table of contents

08 Editorial: Translational advances in Alzheimer's, Parkinson's, and other dementia: molecular mechanisms, biomarkers, diagnosis, and therapies, volume III
Jiehui Jiang, Kuangyu Shi, Kenneth S. Hettie, Chih-Yu Hsu and Woon-Man Kung

12 Synuclein Motor Dysfunction Composite Scale for the Discrimination of Dementia With Lewy Bodies From Alzheimer's Disease
Ying-Tsung Chen, Satoshi Orimo, Cheng-Yu Wei, Guang-Uei Hung, Shieh-Yueh Yang and Pai-Yi Chiu

20 Cognitive Status and Nutritional Markers in a Sample of Institutionalized Elderly People
María Leirós, Elena Amenedo, Marina Rodríguez, Paula Pazo-Álvarez, Luis Franco, Rosaura Leis, Miguel-Ángel Martínez-Olmos, Constantino Arce and the Rest of NUTRIAGE Study Researchers

37 REPS1 as a Potential Biomarker in Alzheimer's Disease and Vascular Dementia
Jiefeng Luo, Liechun Chen, Xiaohua Huang, Jieqiong Xie, Chun Zou, Mika Pan, Jingjia Mo and Donghua Zou

49 Selective Detection of Misfolded Tau From Postmortem Alzheimer's Disease Brains
Ling Wu, Zerui Wang, Shradha Lad, Nailya Gilyazova, Darren T. Dougharty, Madeleine Marcus, Frances Henderson, W. Keith Ray, Sandra Siedlak, Jianyong Li, Richard F. Helm, Xiongwei Zhu, George S. Bloom, Shih-Hsiu J. Wang, Wen-Quan Zou and Bin Xu

63 Distribution and inter-regional relationship of amyloid-beta plaque deposition in a 5xFAD mouse model of Alzheimer's disease
Ka Chun Tsui, Jaydeep Roy, Sze Chun Chau, Kah Hui Wong, Lei Shi, Chi Him Poon, Yingyi Wang, Tatyana Strekalova, Luca Aquili, Raymond Chuen-Chung Chang, Man-Lung Fung, You-qiang Song and Lee Wei Lim

82 Constructing prediction models for excessive daytime sleepiness by nomogram and machine learning: A large Chinese multicenter cohort study
Penghui Deng, Kun Xu, Xiaoxia Zhou, Yaqin Xiang, Qian Xu, Qiying Sun, Yan Li, Haiqing Yu, Xinyin Wu, Xinxiang Yan, Jifeng Guo, Beisha Tang and Zhenhua Liu

96 Induction of *A Disintegrin and Metalloproteinase with Thrombospondin motifs 1* by a rare variant or cognitive activities reduces hippocampal amyloid-β and consequent Alzheimer's disease risk
Yunjie Qiu, Longze Sha, Xiuneng Zhang, Guanjun Li, Wanwan Zhu and Qi Xu

113 Efficacy of acupuncture in animal models of vascular dementia: A systematic review and network meta-analysis
Guangyao Li, Yuling Shi, Lu Zhang, Chuanghui Yang, Ting Wan, Hang Lv, Wenxuan Jian, Jinghu Li and Min Li

130 Striatal dopaminergic lesions contributed to the disease severity in progressive supranuclear palsy
Ming-Jia Chen, Jia-Ying Lu, Xin-Yi Li, Fang-Yang Jiao, Chuan-Tao Zuo, Jian Wang, Feng-Tao Liu and Yu-Jie Yang for the Progressive Supranuclear Palsy Neuroimage Initiative (PSPNI)

138 White matter hyperintensities in dementia with Lewy bodies are associated with poorer cognitive function and higher dementia stages
Tai-Yi Chen, Po-Chi Chan, Ching-Fang Tsai, Cheng-Yu Wei and Pai-Yi Chiu

148 A diagnosis model of dementia *via* machine learning
Ming Zhao, Jie Li, Liuqing Xiang, Zu-hai Zhang and Sheng-Lung Peng

161 The role of PKC/PKR in aging, Alzheimer's disease, and perioperative neurocognitive disorders
Wenping Lu, Sailan Tang, Ao Li, Qiuyue Huang, Mengyun Dou, Ye Zhang, Xianwen Hu, Raymond Chuen Chung Chang, Gordon Tin Chun Wong and Chunxia Huang

178 Sensing red blood cell nano-mechanics: Toward a novel blood biomarker for Alzheimer's disease
Matteo Nardini, Gabriele Ciasca, Alessandra Lauria, Cristina Rossi, Flavio Di Giacinto, Sabrina Romanò, Riccardo Di Santo, Massimiliano Papi, Valentina Palmieri, Giordano Perini, Umberto Basile, Francesca D. Alcaro, Enrico Di Stasio, Alessandra Bizzarro, Carlo Masullo and Marco De Spirito

192 Mesenchymal stromal cells for the treatment of Alzheimer's disease: Strategies and limitations
Shobha Regmi, Daniel Dan Liu, Michelle Shen, Bhavesh D. Kevadiya, Abantika Ganguly, Rosita Primavera, Shashank Chetty, Reza Yarani and Avnesh S. Thakor

212 Cognitive tasks propagate the neural entrainment in response to a visual 40 Hz stimulation in humans
Elvira Khachatryan, Benjamin Wittevrongel, Mariska Reinartz, Ine Dauwe, Evelien Carrette, Alfred Meurs, Dirk Van Roost, Paul Boon and Marc M. Van Hulle

226 A systematic review and meta-analysis of cognitive and behavioral tests in rodents treated with different doses of D-ribose
Ying Song, Yage Du, Yu An, Jie Zheng and Yanhui Lu

237 Subtyping of early-onset Parkinson's disease using cluster analysis: A large cohort study
Zhou Zhou, Xiaoxia Zhou, Yaqin Xiang, Yuwen Zhao, Hongxu Pan, Juan Wu, Qian Xu, Yase Chen, Qiying Sun, Xinyin Wu, Jianping Zhu, Xuehong Wu, Jianhua Li, Xinxiang Yan, Jifeng Guo, Beisha Tang, Lifang Lei and Zhenhua Liu for Parkinson's Disease, and Movement Disorders Multicenter Database and Collaborative Network in China (PD-MDCNC)

248 Cerebrospinal fluid neurofilament dynamic profiles predict cognitive progression in individuals with *de novo* Parkinson's disease
Ze-Hu Sheng, Ling-Zhi Ma, Jia-Yao Liu, Ya-Nan Ou, Bing Zhao, Ya-Hui Ma and Lan Tan

259 Baduanjin exercise modulates the hippocampal subregion structure in community-dwelling older adults with cognitive frailty
Mingyue Wan, Rui Xia, Huiying Lin, Yu Ye, Pingting Qiu and Guohua Zheng

274 Trilateral association of autophagy, mTOR and Alzheimer's disease: Potential pathway in the development for Alzheimer's disease therapy
Arunkumar Subramanian, T. Tamilanban, Abdulrhman Alsayari, Gobinath Ramachawolran, Ling Shing Wong, Mahendran Sekar, Siew Hua Gan, Vetriselvan Subramaniyan, Suresh V. Chinni, Nur Najihah Izzati Mat Rani, Nagaraja Suryadevara and Shadma Wahab

289 Olfactory functional covariance connectivity in Parkinson's disease: Evidence from a Chinese population
Shouyun Du, Yiqing Wang, Guodong Li, Hongyu Wei, Hongjie Yan, Xiaojing Li, Yijie Wu, Jianbing Zhu, Yi Wang, Zenglin Cai and Nizhuan Wang

301 Serum vitamin levels in multiple system atrophy: A case-control study
Daji Chen, Linlin Wan, Zhao Chen, Xinrong Yuan, Mingjie Liu, Zhichao Tang, You Fu, Sudan Zhu, Xuewei Zhang, Rong Qiu, Beisha Tang and Hong Jiang

312 High clinical diagnostic accuracy of combined salivary gland and myocardial metaiodobenzylguanidine scintigraphy in the diagnosis of Parkinson's disease
Shuangfang Li, Lei Yue, Shuzhen Chen, Zhuang Wu, Jingxing Zhang, Ronghua Hong, Ludi Xie, Kangwen Peng, Chenghong Wang, Ao Lin, Lingjing Jin and Qiang Guan

321 The effect of bright light therapy in migraine patients with sleep disturbance: A prospective, observational cohort study protocol
Tsung-Hsing Lin, Cheng-Chia Yang, Shih-Yu Lee, Ching-Mao Chang, I-Ju Tsai, Cheng-Yu Wei and Chun-Pai Yang

327 Correlation between retinal structure and brain multimodal magnetic resonance imaging in patients with Alzheimer's disease
Xiaoli Hao, Weiwei Zhang, Bin Jiao, Qijie Yang, Xinyue Zhang, Ruiting Chen, Xin Wang, Xuewen Xiao, Yuan Zhu, Weihua Liao, Dongcui Wang and Lu Shen

341 Characteristics of fatigue in Parkinson's disease: A longitudinal cohort study
Xiaoxia Zhou, Yaqin Xiang, Tingwei Song, Yuwen Zhao, Hongxu Pan, Qian Xu, Yase Chen, Qiying Sun, Xinyin Wu, Xinxiang Yan, Jifeng Guo, Beisha Tang, Lifang Lei, Zhenhua Liu and for Parkinson's Disease & Movement Disorders Multicenter Database and Collaborative Network in China (PD-MDCNC)

353 Subjective cognitive decline in patients with Parkinson's disease: an updated review
Juan Huang, Xingxing Yuan, Lin Chen, Binbin Hu, Lijuan Jiang, Ting Shi, Hui Wang and Wei Huang

366 Genetic analysis of dystonia-related genes in Parkinson's disease
Yige Wang, Yuwen Zhao, Hongxu Pan, Qian Zeng, Xiaoxia Zhou, Yaqin Xiang, Zhou Zhou, Qian Xu, Qiying Sun, Jieqiong Tan, Xinxiang Yan, Jinchen Li, Jifeng Guo, Beisha Tang, Qiao Yu and Zhenhua Liu

377 Metabolic changes in the plasma of mild Alzheimer's disease patients treated with Hachimijiogan
Mosaburo Kainuma, Shinobu Kawakatsu, Jun-Dal Kim, Shinji Ouma, Osamu Iritani, Ken-Ichiro Yamashita, Tomoyuki Ohara, Shigeki Hirano, Shiro Suda, Tadanori Hamano, Sotaro Hieda, Masaaki Yasui, Aoi Yoshiiwa, Seiji Shiota, Masaya Hironishi, Kenji Wada-Isoe, Daiki Sasabayashi, Sho Yamasaki, Masayuki Murata, Kouta Funakoshi, Kouji Hayashi, Norimichi Shirafuji, Hirohito Sasaki, Yoshinori Kajimoto, Yukiko Mori, Michio Suzuki, Hidefumi Ito, Kenjiro Ono and Yoshio Tsuboi

388 Identification of diagnostic biomarkers in Alzheimer's disease by integrated bioinformatic analysis and machine learning strategies
Boru Jin, Xiaoqin Cheng, Guoqiang Fei, Shaoming Sang and Chunjiu Zhong

399 Amyloid beta-correlated plasma metabolite dysregulation in Alzheimer's disease: an untargeted metabolism exploration using high-resolution mass spectrometry toward future clinical diagnosis
Jingzhi Yang, Shuo Wu, Jun Yang, Qun Zhang and Xin Dong

414 The differential diagnosis value of radiomics-based machine learning in Parkinson's disease: a systematic review and meta-analysis
Jiaxiang Bian, Xiaoyang Wang, Wei Hao, Guangjian Zhang and Yuting Wang

429 Locus specific endogenous retroviral expression associated with Alzheimer's disease
Tyson Dawson, Uzma Rentia, Jessie Sanford, Carlos Cruchaga, John S. K. Kauwe and Keith A. Crandall

442 Regional homogeneity and functional connectivity of freezing of gait conversion in Parkinson's disease
Yiqing Bao, Yang Ya, Jing Liu, Chenchen Zhang, Erlei Wang and Guohua Fan

452 Alterations of gut microbiota are associated with brain structural changes in the spectrum of Alzheimer's disease: the SILCODE study in Hainan cohort
Beiqi He, Can Sheng, Xianfeng Yu, Liang Zhang, Feng Chen and Ying Han

466 Current and future therapeutic strategies for Alzheimer's disease: an overview of drug development bottlenecks
Yong Peng, Hong Jin, Ya-hui Xue, Quan Chen, Shun-yu Yao, Miao-qiao Du and Shu Liu

482 Identification of disulfidptosis-related genes and subgroups in Alzheimer's disease
Shijia Ma, Dan Wang and Daojun Xie

496 Does serum neurofilament light help predict accelerated cognitive ageing in unimpaired older adults?
Jessica M. Collins, Aidan D. Bindoff, Eddy Roccati, Jane E. Alty, James C. Vickers and Anna E. King

506 Global trends and prospects about synaptic plasticity in Alzheimer's disease: a bibliometric analysis
Yingying Zhang, Junyao Zhang, Yinuo Wang and Junyan Yao

519 The key role of depression and supramarginal gyrus in frailty: a cross-sectional study
Sara Isernia, Valeria Blasi, Gisella Baglio, Monia Cabinio, Pietro Cecconi, Federica Rossetto, Marta Cazzoli, Francesco Blasi, Chiara Bruckmann, Fabrizio Giunco, Sandro Sorbi, Mario Clerici and Francesca Baglio

529 Antidepressant effect of bright light therapy on patients with Alzheimer's disease and their caregivers
Xi Mei, Chenjun Zou, Zizhen Si, Ting Xu, Jun Hu, Xiangping Wu and Chengying Zheng

frontiers | Frontiers in Aging Neuroscience

TYPE Editorial
PUBLISHED 08 January 2024
DOI 10.3389/fnagi.2023.1352988

OPEN ACCESS

EDITED AND REVIEWED BY
Agustin Ibanez,
Latin American Brain Health Institute (BrainLat), Chile

*CORRESPONDENCE
Woon-Man Kung
nskungwm@yahoo.com.tw

RECEIVED 09 December 2023
ACCEPTED 18 December 2023
PUBLISHED 08 January 2024

CITATION
Jiang J, Shi K, Hettie KS, Hsu C-Y and Kung W-M (2024) Editorial: Translational advances in Alzheimer's, Parkinson's, and other dementia: molecular mechanisms, biomarkers, diagnosis, and therapies, volume III. *Front. Aging Neurosci.* 15:1352988. doi: 10.3389/fnagi.2023.1352988

Editorial: Translational advances in Alzheimer's, Parkinson's, and other dementia: molecular mechanisms, biomarkers, diagnosis, and therapies, volume III

Jiehui Jiang [1], Kuangyu Shi [2,3], Kenneth S. Hettie [4,5], Chih-Yu Hsu [6] and Woon-Man Kung [7,8]*

[1]School of Life Science, Institute of Biomedical Engineering, Shanghai University, Shanghai, China, [2]Department of Nuclear Medicine, Inselspital, Bern University Hospital, University of Bern, Bern, Switzerland, [3]Department of Informatics, Technical University of Munich, Munich, Germany, [4]Department of Radiology, Molecular Imaging Program at Stanford (MIPS), Stanford University School of Medicine, Stanford, CA, United States, [5]Department of Otolaryngology - Head and Neck Surgery, Molecular Imaging Program at Stanford (MIPS), Stanford University School of Medicine, Stanford, CA, United States, [6]School of Transportation, Fujian University of Technology, Fuzhou, China, [7]Division of Neurosurgery, Department of Surgery, Taipei Tzu Chi Hospital, Buddhist Tzu Chi Medical Foundation, New Taipei City, Taiwan, [8]Department of Exercise and Health Promotion, College of Kinesiology and Health, Chinese Culture University, Taipei, Taiwan

KEYWORDS

Alzheimer's disease, Parkinson's disease, dementia, neurodegenerative disorders, big data mining, imaging methods, bioinformatic applications

Editorial on the Research Topic
Translational advances in Alzheimer's, Parkinson's, and other dementia: molecular mechanisms, biomarkers, diagnosis, and therapies, volume III

This Research Topic (RT) is a series continuation of two previous prominent RTs, Volume I (Jiang et al., 2022b) and Volume II, (Jiang et al., 2022a) published in 2022. These previous publications reviewed 69 and 57 articles, respectively. Volume III is the latest collection on the topic and comprises 41 globally sourced articles, contributing significant updates from diverse viewpoints on this important theme between 2022 and 2023. In total, 362 authors, including researcher scientists and clinicians, who were actively engaged in the field, contributed to these Research Topics.

The ability to detect neurodegenerative dementia at an early stage continues to receive increased attention. Common etiologies include Alzheimer's disease (AD), Parkinson's disease (PD), and vascular dementia (VD) (Andjelkovic et al., 2023; Andrews et al., 2023; Louis et al., 2023). Study results have shown that changes in the underlying molecular biology of such cognitive impairments are associated with dementia. Recently, research studies have demonstrated that molecular imaging techniques can capture small alternations in patients with dementia. Improvements in biotechnologies, such as primarily positron emission tomography (PET) and magnetic resonance imaging (MRI), continue to demonstrate molecular imaging techniques that capture the small alterations and events in patients with dementia (Borghammer, 2021; Roda et al., 2022). Moreover, artificial

intelligence is emerging as a critical tool in bioinformatics research (Mei et al., 2021; Goyal et al., 2022). However, detection of AD and other dementias in their "early phase" remains a challenge in the current standard of care.

To address current challenges, the articles in this Volume are categorized into sections based on their underlying disciplinary approach, which seeks to identify and/or treat dementia.

Genetics

Luo et al. identified REPS1 as the hub gene for AD and VD based on 3 datasets. Qiu et al. identified a novel rare variant c. - 2067A > C and found that it may reduce Amyloid-β (Aβ) deposition in the hippocampus. Wang et al. implemented whole-exome sequencing (WES) and whole-genome sequencing (WGS) to mine data from 3,959 PD patients and 2,931 healthy controls. The results showed that COL6A3 and TH were associated with PD. Dawson et al. discovered that dysregulated expression of ancient retrovirus insertions in the human genome are present in AD. Ma et al. developed and utilized predictive models to assess the risk of developing the disulfidptosis subtype in patients with AD, finding that disulfidptosis is strongly associated with AD.

Biomarkers: molecular

Leirós et al. reported that higher serum levels of vitamin A, vitamin D, transthyretin (TTR), albumin, selenium (Se), and uric acid (UA) could act as protective factors against cognitive decline based on multiple logistic regression, whereas higher body mass index (BMI) could act as a risk factor. Chen Y.-T. et al. combined plasma α-synuclein level and Motor Dysfunction Questionnaire (MDQ) to discriminate between dementia with Lewy bodies (DLB) and AD. Wu et al. used an engineered tau fragment 4RCF as a substrate to investigate misfolded tau from diseased AD and other tauopathy brains and were able to seed the recombinant 4RCF substrate. Their conclusion from the data were that it may be useful as a biomarker for the diagnosis of AD and related tau lesions. In a study performed by Nardini et al., utilizing the mechanical characteristics of red blood cells, they used a standard linear solid model that was found to demonstrate excellent classifications for determining AD. Lu et al. used different mouse models to find that similar pathogenic features in aging, AD, and perioperative neurocognitive disorder (PND) from dysregulation of protein kinase C (PKC)/protein kinase (PKR) activity may be related to its pathogenesis. Based on the Parkinson's Progression Markers Initiative (PPMI) database, Sheng et al. found that the concentration and changes of Neurofilament light chain protein (NfL) in cerebrospinal fluid (CSF) could be used to identify the cognitive progress in PD patients.

Chen D. et al. surveyed significant changes in the vitamin profile in multiple system atrophy (MSA). The results from receiver operating characteristic (ROC) curves suggested that vitamin A, folate, and vitamin C could discriminate between MSA and normal controls. Yang et al. applied high-resolution mass spectrometry to detect metabolites in AD plasma samples, wherein they found significant fluctuations in the levels of plasma metabolites, PAGln, and L-arginine in the AD group. Using 6 datasets derived from AD frontal cortex samples, Jin et al. employed a combination of bioinformatics analysis and machine learning (ML) to screen out thioredoxin interaction protein (TXNIP), early growth Response 1 (EGR1), and insulin-like growth factor binding protein 5 (IGFBP5), as diagnostic markers for AD. He et al. evaluated the gut microbiota-brain-cognition interaction, wherein their findings suggested that there is an intrinsic association between gut microbiota changes, brain atrophy, and cognitive decline. Collins et al. determined a positive association between plasma NfL levels measured by single molecule array technology and cognitive decline with aging. They suggested that although NfL level was associated with cognitive decline, it did not mediate the relationship between age and cognition.

Biomarkers: imaging

Tsui et al. quantified the comprehensive morphological characteristics of Aβ plaque deposition in the brain using an AD mouse model. In using ^{11}C-CFT coupled with PET imaging, Chen M.-J. et al. determined that there is a significant contribution to the disease severity of progressive supranuclear palsy (PSP) by the striatal dopamine transporter (DAT) bindings (caudate). By utilizing the functional covariance connection strength method, Du et al. indicated that characteristics of olfactory-related brain networks can potentially be used as neuroimaging biomarkers for characterizing PD states.

Li S. et al. performed ^{131}I-metaiodobenzylguanidine (MIBG) scintillation imaging on 37 subjects, wherein they determined that MIBG uptake rate could assist in PD diagnosis. Hao et al. combined retinal imaging and multimodal MRI to show promising results in identifying AD patients. Bao et al. assessed that regional homogeneity (ReHo) and functional connectivity (FC) abnormalities may occur in the basal ganglia, limbic regions, and cognitive control cortex during the early stage of gait freezing. Isernia et al. found that depression fully mediates a relationship between frailty and thickness of the superior limbic and rostral medial frontal gyrus cortex.

Computer-aided diagnosis

Based on the diagnostic data of a questionnaire survey, Zhao et al. discerned the bagging method model to have the best diagnostic effect, whereas principal component analysis (PCA) has the best feature selection effect, both after having compared various models and feature selection algorithms. Deng et al. used nomogram and the XGBoost ML method to establish an effective and relatively accurate prediction model (accuracy of 71.86%) of excessive daytime sleepiness (EDS) in PD.

Therapies

Khachatryan et al. focused on the inclusion of a cognitive task during the Gamma ENtrainment Using Sensory stimulation (GENUS) session. Their results proved that the inclusion had

a positive effect on the strength and extent of the gamma entrainment, followed by an improvement in the therapeutic effect of GENUS (Khachatryan et al.). Zhou Z. et al. performed cluster analysis in a cohort of 1,217 individuals with early-onset PD and identified 3 clinical subtypes (mild, intermediate, and severe). Wan et al. specified that Baduanjin exercise was effective in improving cognition. Kainuma et al. reported that the increase of plasma metabolite levels after 6 months of hachimijiogan (HJG) administration was significantly higher than that of the control group.

Mei et al. investigated the effects of bright light therapy (BLT) on AD patients and caregivers. Their study showed that there was an inhibitory effect of BLT on depression. Lin et al. proposed a prospective, observational cohort study to determine the effects of BLT on migraine patients with sleep disorders.

Reviews

Several reviews are included in this section of the Research Topic. Huang et al. reviewed the work related to PD and subjective cognitive decline (SCD) and they found that PD with SCD occurred with metabolic changes to the brain. Regmi et al. discussed the strategies and limitations of using mesenchymal stem/stromal cells (MSCs) therapy for AD. Subramanian et al. described the different mechanisms and signaling regulations, highlighting the trilateral association of autophagy, the mammalian target of the rapamycin (mTOR) pathway, and AD with a description of inhibiting drugs/molecules of mTOR, a strategic target in AD. Peng et al. investigated bottlenecks in utilizing therapeutic strategies toward AD, wherein they focused on anti-Aβ, anti-tau drugs, and mitochondrial targeted therapy to suggest future directions for AD drug therapies.

Li G. et al. conducted a network meta-analysis that aimed to evaluate the efficacy of acupuncture in animal models of VD, which provided evidence that acupuncture significantly improved cognitive function in rats with VD. Another meta-analysis was conducted by Song et al. to show the effects of D-ribose on cognition in rodents. They summarized the outcomes of eight trials involving 289 rodents and conducted a systematic review. The results of their study identified D-ribose therapy as a cause of cognitive impairment with cognitive ability worsening with increasing dose. Bian et al. conducted a systematic review and meta-analysis to estimate the diagnostic value of image-based ML for PD. The findings from their paper suggested that image-based ML can be used as a potential tool for PD diagnosis. As synaptic plasticity disorders play key roles in AD, Zhang et al. implemented a bibliometric analysis to gain insights into how systematic synaptic plasticity affects the progress of AD.

Miscellaneous

Chen T.-Y. et al. conducted a retrospective analysis and rated white matter hyperintensities (WMHs) visual scores on 449 patients with DLB. This study obtained useful information that WMHs were associated with cognitive impairment (Chen T.-Y. et al.). Zhou X. et al. conducted a longitudinal study that enrolled 2,100 PD subjects and demonstrated that fatigue may be a risk factor for increased disease severity.

Conclusions

A number of articles in this Research Topic collection focus on the application of bioinformatics and computational biology, with some studies discussing disease susceptibility genes. In addition, several researchers used molecular methods, novel imaging techniques, and imaging analysis to explore biomarkers. Even though other novel clinical treatments have not been covered here, the multidisciplinary perspectives of the studies included in the Research Topic facilitate and improve understanding of such disease mechanisms, helping to identify novel potential biomarkers and treatment targets.

Author contributions

JJ: Writing—original draft. KS: Writing—original draft. KH: Writing—review & editing. C-YH: Writing—review & editing. W-MK: Writing—review & editing.

Funding

The author(s) declare that no financial support was received for the research, authorship, and/or publication of this article.

Conflict of interest

The authors declare that the research was conducted in the absence of any commercial or financial relationships that could be construed as a potential conflict of interest.

The author(s) declared that they were an editorial board member of Frontiers, at the time of submission. This had no impact on the peer review process and the final decision.

Publisher's note

References

Andjelkovic, A. V., Situ, M., Citalan-Madrid, A. F., Stamatovic, S. M., Xiang, J., Keep, R., et al. (2023). Blood-brain barrier dysfunction in normal aging and neurodegeneration: mechanisms, impact, and treatments. *Stroke* 54, 661–672. doi: 10.1161/STROKEAHA.122.040578

Andrews, S. J., Renton, A. E., Fulton-Howard, B., Drabiniok, A. P., Marcora, E., and Goate, A. M. l. (2023). The complex genetic architecture of Alzheimer's disease: novel insights and future directions. *Ebiomedicine* 90, 104511. doi: 10.1016/j.ebiom.2023.104511

Borghammer, P. (2021). The α-synuclein origin and connectome model (SOC model) of Parkinson's disease: explaining motor asymmetry, non-motor phenotypes, and cognitive decline. *J. Parkinson Dis.* 11, 455–474. doi: 10.3233/JPD-202481

Goyal, P., Rani, R., and Singh, K. (2022). State-of-the-art machine learning techniques for diagnosis of Alzheimer's disease from mr-images: a systematic review. *Arch. Comput. Method E.* 29, 2737–2780. doi: 10.1007/s11831-021-09674-8

Jiang, J., Shi, K., Huang, Y. H., Hsu, C. Y., Hettie, K., Kung, W., et al. (2022a). Editorial: Translational advances in Alzheimer's, Parkinson's, and other dementia: molecular mechanisms, biomarkers, diagnosis, and therapies, volume II. *Front. Aging Neurosci.* 14, 1045828. doi: 10.3389/fnagi.2022.1045828

Jiang, J., Shi, K., Peng, F., Hsu, C.-., Y., and Kung, W.-, M. (2022b). Editorial: translational advances in Alzheimer's, Parkinson's, and other neurodegenerative dementias. *Front. Aging Neurosci.* 14, 858467. doi: 10.3389/fnagi.2022.858467

Louis, S., Carlson, A. K., Suresh, A., Rim, J., Mays, M., Ontaneda, D., et al. (2023). Impacts of climate change and air pollution on neurologic health, disease, and practice a scoping review. *Neurology* 100, 474–483. doi: 10.1212/WNL.0000000000201630

Mei, J., Desrosiers, C., and Frasnelli, J. (2021). Machine learning for the diagnosis of Parkinson's disease: a review of literature. *Front. Aging Neurosci.* 13, 633752. doi: 10.3389/fnagi.2021.633752

Roda, A. R., Serra-Mir, G., Montoliu-Gaya, L., Tiesseler, L., and Villegas, S. (2022). Amyloid-beta peptide and tau protein crosstalk in Alzheimer's disease. *Neural Regen. Res.* 17, 1666–1674. doi: 10.4103/1673-5374.332127

frontiers | Frontiers in Aging Neuroscience

ORIGINAL RESEARCH
published: 19 May 2022
doi: 10.3389/fnagi.2022.920591

Synuclein Motor Dysfunction Composite Scale for the Discrimination of Dementia With Lewy Bodies From Alzheimer's Disease

*Ying-Tsung Chen[1,2], Satoshi Orimo[3], Cheng-Yu Wei[4], Guang-Uei Hung[5], Shieh-Yueh Yang[6] and Pai-Yi Chiu[7,8]**

[1] Department of Psychiatry, Show Chwan Memorial Hospital, Changhua, Taiwan, [2] Department of Psychiatry, Chang Bing Show Chwan Memorial Hospital, Changhua, Taiwan, [3] Department of Neurology, Kamiyoga Setagaya Street Clinic, Tokyo, Japan, [4] Department of Exercise and Health Promotion, College of Education, Chinese Culture University, Taipei, Taiwan, [5] Department of Nuclear Medicine, Chang Bing Show Chwan Memorial Hospital, Changhua, Taiwan, [6] MagQu Co., Ltd., New Taipei, Taiwan, [7] Department of Neurology, Show Chwan Memorial Hospital, Changhua, Taiwan, [8] Department of Applied Mathematics, Tunghai University, Taichung, Taiwan

OPEN ACCESS

Edited by:
Jiehui Jiang,
Shanghai University, China

Reviewed by:
Wenying Du,
Capital Medical University, China
Andrei Surguchov,
University of Kansas Medical Center, United States
Hsi-Hsien Chou,
Chung Shan Medical University, Taiwan

***Correspondence:**
Pai-Yi Chiu
paiyibox@gmail.com

Specialty section:
This article was submitted to Alzheimer's Disease and Related Dementias, a section of the journal Frontiers in Aging Neuroscience

Received: 14 April 2022
Accepted: 29 April 2022
Published: 19 May 2022

Citation:
Chen Y-T, Orimo S, Wei C-Y, Hung G-U, Yang S-Y and Chiu P-Y (2022) Synuclein Motor Dysfunction Composite Scale for the Discrimination of Dementia With Lewy Bodies From Alzheimer's Disease. Front. Aging Neurosci. 14:920591. doi: 10.3389/fnagi.2022.920591

Background: An abnormal increase of α-synuclein in the brain is the hallmark of dementia with Lewy bodies (DLB). However, the diagnostic power of plasma α-synuclein in DLB is not yet confirmed. Parkinsonism is highly associated with and is one of the core clinical features of DLB. We studied plasma α-synuclein and developed a novel tool that combined plasma α-synuclein level and Motor Dysfunction Questionnaire (MDQ), namely Synuclein Motor Dysfunction Composite Scale (SMDCS), for the clinical discrimination of DLB from Alzheimer's disease (AD).

Methods: This cross-sectional study analyzed participants' demographical data, plasma α-synuclein level, MDQ, structured clinical history questionnaire, neuropsychological and motor function tests, and neuroimaging studies. The power of plasma α-synuclein level, MDQ, and SMDCS for discriminating DLB from non-demented controls (NC) or AD were compared.

Results: Overall, 121 participants diagnosed as 58 DLB, 31 AD, and 31 NC were enrolled. Patients with DLB had significantly higher mean plasma α-synuclein level (0.24 ± 0.32 pg/ml) compared to the NC group (0.08 ± 0.05 pg/ml) and the AD group (0.08 ± 0.05 pg/ml). The DLB group demonstrated higher MDQ (2.95 ± 1.60) compared to the NC (0.42 ± 0.98) or AD (0.44 ± 0.99) groups. The sensitivity/specificity of plasma α-synuclein level, MDQ, and SMDCS for differentiating DLB from non-DLB were 0.80/0.64, 0.83/0.89, and 0.88/0.93, respectively.

Conclusion: Both plasma α-synuclein and MDQ were significantly higher in patients with DLB compared to the NC or AD groups. The novel SMDCS, significantly improved accuracy for the clinical differentiation of DLB from AD or NC.

Keywords: Synuclein Motor Dysfunction Composite Scale, plasma α-synuclein, dementia with Lewy bodies, Alzheimer's disease, Motor Dysfunction Questionnaire

INTRODUCTION

Dementia with Lewy bodies (DLB) is the second most common degenerative dementia (Geser et al., 2005; Zupancic et al., 2011). An abnormal increase in α-synuclein in the brain is the hallmark of Lewy body disease including Parkinson's disease (PD) and DLB (Surguchov, 2022). Evidence of biofluid markers for the diagnosis of PD or DLB is still lacking consensus (Li et al., 2007; Noguchi-Shinohara et al., 2009; Ohrfelt et al., 2009; Spies et al., 2009; Kasuga et al., 2010; Hansson et al., 2014; Lin et al., 2017, 2020). Among these studies, the examination of α-synuclein level in the cerebrospinal fluid (CSF) for the differentiation of DLB from other brain disorders has revealed controversial findings. Some studies have shown no difference (Noguchi-Shinohara et al., 2009; Spies et al., 2009) or decreased levels (Kasuga et al., 2010), while others have demonstrated increased levels (Ohrfelt et al., 2009; Hansson et al., 2014). Recent studies have used serum or plasma α-synuclein for the clinical diagnosis of PD or DLB. However, the practicality and feasibility are still being tested (Li et al., 2007; Laske et al., 2011; Lin et al., 2017, 2020). Discrepancies in plasma or serum studies may be due to the level of α-synuclein stored in red blood cells being high, and hemolysis during sample preparation and processing may confound the quantification of α-synuclein (Barbour et al., 2008; Kasuga et al., 2012). Being a novel biomarker, plasma α-synuclein is seldom studied in patients with DLB. To our knowledge, there is only one published study on this topic (Laske et al., 2011). Unlike Alzheimer's Disease (AD) which uses amyloid and phosphorylated tau in CSF or PET imaging to establish a reliable diagnosis, the determinant imaging or liquid biomarkers in CSF and blood samples for the diagnosis of DLB remains unclear. Hence, more evidence is needed for clinical practice.

Clinical characteristic features including motor and non-motor dysfunctions are still essential for the diagnosis of PD, PD with dementia (PDD), or DLB. In this study, we aimed to test the diagnostic power of plasma α-synuclein for the identification of DLB from AD and non-demented control (NC). In addition, we tested the diagnostic efficacy with our newly developed motor dysfunction questionnaire (MDQ) (**Table A1**) which has been validated with dopamine transporter imaging by comparing motor dysfunctions among DLB, AD, and ND groups (Chiu et al., 2021). Furthermore, we followed the consensus criteria of using both clinical features and biomarkers for the diagnosis of DLB and hypothesized that a simple diagnostic tool, combining both clinical and biomarker information, should improve the detection of DLB. Therefore, we designed a novel, simple, and practical tool which combined a fluid biomarker (plasma α-synuclein level) and a clinical assessment (MDQ), namely, the Synuclein Motor Dysfunction Composite Scale (SMDCS), for the diagnosis of DLB.

MATERIALS AND METHODS

Participants

This was a cross-sectional study. From 2018 to 2020, a consecutive series of NC, AD, and DLB patients were enrolled from two dementia clinics in central Taiwan. For the diagnosis of NC, the individual must have a global Clinical Dementia Rating Scale (CDR) (Morris, 1993) score of 0 OR 0.5 and without significantly impaired activities of daily living (ADL) defined by a total Instrumental ADL score >6 (Lawton and Brody, 1969). Patients with AD were diagnosed according to the criteria for probable AD developed by the National Institute on Aging and the Alzheimer's Association workgroup (NIA-AA) (McKhann et al., 2011). Patients with DLB were diagnosed according to the revised consensus criteria for probable DLB, developed by the fourth report of the DLB consortium (McKeith et al., 2017).

Preparation of Plasma Samples

A 9-ml K3-EDTA tube was used for blood collection. No fasting was required before for blood sampling. The tube was gently inverted several times immediately after blood collection. A swing-out (bucket) rotor was used to centrifuge the blood at room temperature, at 1,500–2,500 × *g*, for 15 min. Aliquots of 0.5-ml plasma were transferred into fresh 2.0-ml tubes. All the aliquoted plasma samples were stored at −80°C within 3 h of blood collection, before the ImmunoMagnetic Reduction (IMR) assays were performed. Plasma samples were collected in 2018–2019 and assayed with IMR (MF-ASC-0060, MagQu) in 2018–2019. The frozen samples are taken directly by MagQu's staff or delivered in dry ice to MagQu Co., Ltd. for IMR measurements. Each reported concentration of a biomarker was the average of duplicated measurements. The IMR analyzer (XacPro-S) was used for assays.

Procedures

All participants were selected from Show Chwan Healthcare Center Dementia Registry database (Chiu et al., 2020; Wang et al., 2020; Zhu et al., 2020). The demographical, clinical, neuropsychological, neuropsychiatric, neuroimaging, and laboratory data were collected. The global severity of dementia was assessed according to the CDR scale and the sum of boxes of CDR (CDR-SB). Cognitive functions were assessed with the Cognitive Abilities Screening Instrument (CASI) (Teng et al., 1994) and the Montreal Cognitive Assessment (MoCA) (Nasreddine et al., 2005). Motor functions were assessed with the motor score of the Unified Parkinson's Disease Rating Scale (UPDRS Part III) (Ballard et al., 1997) and MDQ (Chiu et al., 2021). The novel SMDCS is the sum of the MDQ score and the α-synuclein score. The α-synuclein scores were divided into four according to quartile of the α-synuclein level, from low to high, with a score of 1 representing the lowest quartile and 4 the highest. Neuropsychiatric symptoms were assessed with the 12-domain Neuropsychiatric Inventory (NPI) (Cummings et al., 1994). All patients had results from the following measures: plasma α-synuclein, at least a cerebral CT or MRI, a set of blood screening tests including complete blood count, GOT, GPT, BUN, creatinine, thyroid function, RPR or VDRL, vitamin B12, and folic acid. Furthermore, 96 participants underwent the APOE genetic study, and 82 participants underwent dopamine transporter uptake imaging with ^{99m}Tc-Trodat-1 SPECT. Abnormal dopamine transporter imaging (DaTabN) is one of the indicative biomarkers for the diagnosis of DLB.

TABLE 1 | Demographic and background characteristics of NC (n = 31), AD (n = 31), and DLB (n = 59) patients.

	NC	AD	DLB	F/χ^2	p-Value	*Post hoc*/pair comparison
Age, mean (SD)	68.3 (9.1)	74.1 (8.3)	77.8 (6.6)	15.41	<0.001	NC < AD < DLB
CDR-SB, mean (SD)	0.5 (0.7)	4.9 (3.7)	5.8 (3.8)	24.96	<0.001	NC < AD < DLB
Female, *n* (%)	15 (48.4)	18 (58.1)	28 (47.5)	0.98	NS	NC = AD = DLB
Education, mean (SD)	8.3 (4.0)	6.3 (4.4)	5.7 (5.3)	3.33	0.039	NC > AD = DLB
IADL, mean (SD)	7.8 (0.5)	4.3 (2.9)	3.6 (2.8)	31.18	<0.001	NC > AD > DLB
MoCA, mean (SD)	21.2 (5.9)	11.7 (6.1)	10.6 (6.1)	32.30	<0.001	NC < AD = DLB
CASI, mean (SD)	84.7 (10.7)	59.5 (21.7)	57.5 (18.7)	25.29	<0.001	NC > AD = DLB
NPI, mean (SD)	3.5 (4.4)	7.0 (11.2)	14.6 (16.3)	8.36	<0.001	NC < AD < DLB
UPDRS-M, mean (SD)	7.1 (5.4)	8.9 (11.3)	21.8 (13.8)	8.36	< 0.001	NC = AD < DLB
VH, *n* (%)	1 (3.2)	2 (6.5)	29 (49.2)	30.60	<0.001	NC = AD < DLB
Parkinsonism, *n* (%)	2 (6.5)	3 (9.7)	49 (83.1)	68.86	<0.001	NC = AD < DLB
RBD, *n* (%)	3 (9.7)	5 (16.1)	34 (57.6)	26.97	<0.001	NC = AD < DLB
DaTabN, *n* (%)	3 (13.6)	4 (26.7)	32 (71.1)	22.78	<0.001	NC = AD < DLB
SBR, mean (SD)	1.71 (0.37)	1.59 (0.44)	1.28 (0.39)	22.78	<0.001	NC > AD > DLB
APOE4, *n* (%)	8 (25.8)	17 (58.1)	11 (32.4)	7.66	0.022	NC = DLB < AD

n, number of cases; NC, non-demented control; AD, Alzheimer's Disease; DLB, dementia with Lewy bodies; NA, not applicable; NS, non-significance; CDR-SB, sum of boxes of the Clinical Dementia Rating Scale; α-syn, plasma α-synuclein; HAI-MDQ, Motor Dysfunction Questionnaire in the History-based Artificial Intelligent Clinical Dementia Diagnostic System (HAICDDS), SMDCS: Synuclein Motor Dysfunction Composite Scale; IADL, Instrumental Activities of Daily Living; MoCA, Montreal Cognitive Assessment; CASI, Cognitive Abilities Screening Instrument; NPI, Neuropsychiatric Inventory; UPDRS-M, motor subscale of the Unified Parkinson's Disease Rating Scale; VH, visual hallucinations; RBD, REM sleep behavior disorder; DaTabN, abnormal dopamine transporter imaging in 22 ND, 15 AD, and 45 DLB; SBR, striatal background ratio; APOE4, apolipoprotein E4 allele in 31 ND, 31 AD, and 34 DLB.

Data Analysis

The Chinese version of SPSS for Windows, version 22.0 (IBM, SPSS Inc., Chicago, IL, United States) was used for statistical analyses. Comparisons among the three groups (demographic data, plasma α-synuclein, MDQ, SMDCS, neuropsychological tests, neuropsychiatric symptoms, and UPDRS Part III) were performed with one-way ANOVA. Sex, CDR, APOE4 allele, and clinical features were analyzed using the Chi-square test. The receiver operating characteristic (ROC) curves analysis of plasma α-synuclein, MDQ, and SMDCS were compared between DLB versus non-DLB. Plasma α-synuclein level greater than the cut-off score was defined as α-syn+ group. Dopamine transporter imaging, motor, and non-motor features of SMDCS+ group were compared to SMDCS− group, with odds ratios (OR) adjusted for age and dementia severity by CDR. All calculated p-values were two-tailed. Statistical significance was defined as a p-value of <0.05.

Ethical Consideration

The Committee for Medical Research Ethics of Show Chwan Memorial Hospital reviewed the study, and the Data Inspectorate approved it. All participants signed informed consent before participating in the study.

RESULTS

A total of 121 participants were analyzed in this study, including 59 probable DLB, 31 probable AD, and 31 NC. Comparing the demographical data of the three groups showed that both DLB and AD groups had significantly older age, lower education, higher CDR-SB, lower total CASI score, lower total MoCA score than NC (all $p < 0.001$) (**Table 1**). Compared to the NC and AD groups, patients with DLB also had significantly higher UPDRS Part III, SBR, and frequencies of all clinical features, including fluctuation of cognition, parkinsonism, visual hallucinations and REM sleep behavior disorder (RBD), and total NPI score (all p-value < 0.001). APOE4 allele was significantly higher in patients with AD (58.1%) compared to NC (25.8%) or patients with DLB (32.4%), with a p-value of 0.022 (**Table 1**).

Patients with DLB had significantly higher mean plasma α-synuclein level (0.24 ± 0.32 pg/ml) compared to NC (0.08 ± 0.05 pg/ml) or patients with AD (0.08 ± 0.05 pg/ml). The DLB group also demonstrated higher MDQ score (3.25 ± 1.77) compared to the NC (0.52 ± 1.15) and AD (0.48 ± 1.06) groups. The SMDCS scores were divided according to the cut-off score of 0.085 pg/ml. Therefore, level 0–0.0424, 0.0425–0.0849, 0.0850–0.1274, and >0.1275 pg/ml were scored 0, 1, 2, and 3, respectively.

TABLE 2 | Comparison of plasma α-synuclein, HAI-MDQ, and SMDCS among NC (n = 31), AD (n = 31), and DLB (n = 59) patients.

	NC	AD	DLB	F/χ^2	p-Value	*Post hoc*
α-Syn, mean (SD)	0.08 (0.05)	0.08 (0.05)	0.24 (0.32)	7.12	0.001	NC = AD < DLB
HAI-MDQ, mean (SD)	0.52 (1.15)	0.48 (1.06)	3.25 (1.77)	53.13	<0.001	NC = AD < DLB
SMDCS, mean (SD)	0.97 (1.17)	0.90 (1.16)	4.73 (1.84)	91.89	<0.001	NC = AD < DLB

n, number of cases; NC, non-demented control; AD, Alzheimer's Disease; DLB, dementia with Lewy bodies; α-syn, plasma α-synuclein; HAI-MDQ, Motor Dysfunction Questionnaire in the History-based Artificial Intelligent Clinical Dementia Diagnostic System (HAICDDS); SMDCS, Synuclein Motor Dysfunction Composite Scale.

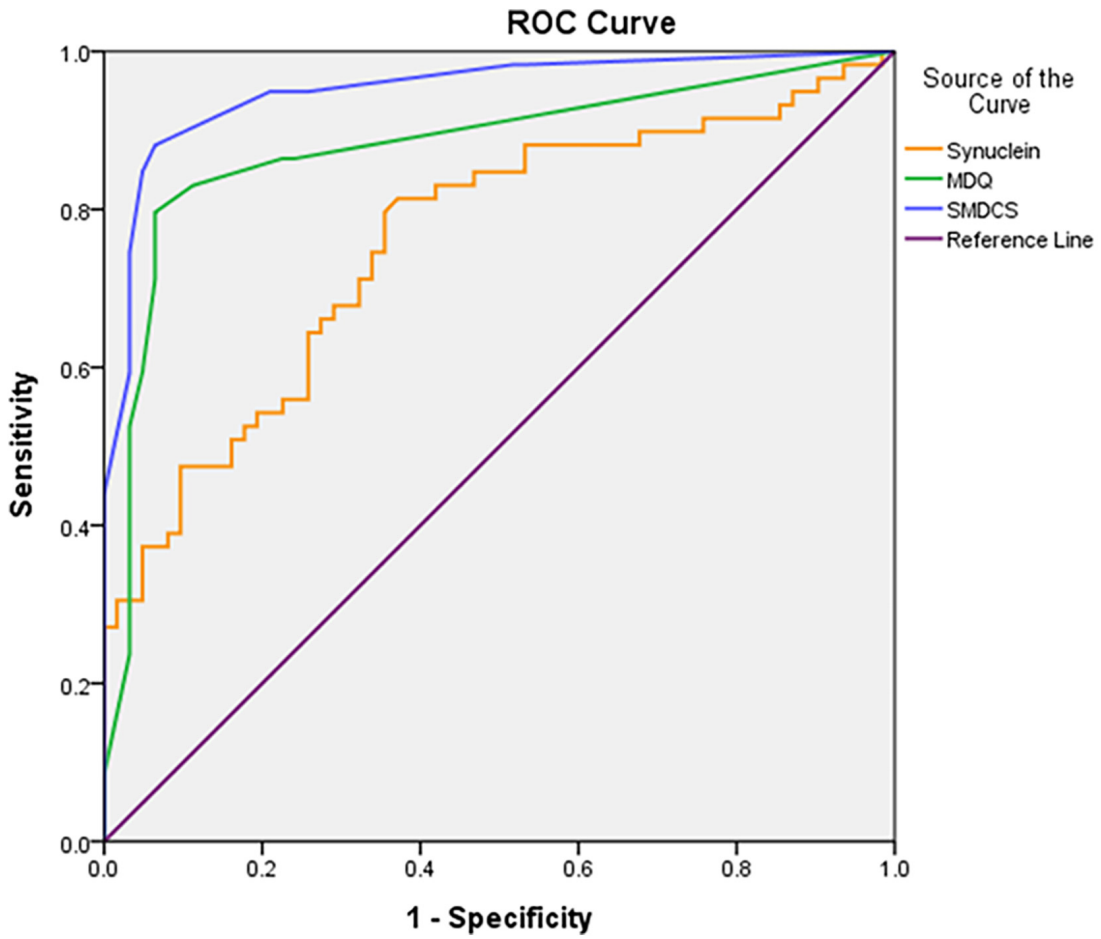

FIGURE 1 | The ROC curves analysis of plasma α-synuclein, MDQ, and SMDCS between DLB versus non-DLB.

The SMDCS revealed a higher total score in patients with DLB (4.73 ± 1.84) compared to that of the NC (0.97 ± 1.17) and AD (0.90 ± 1.06) groups (**Table 2**).

Figure 1 demonstrated the ROC curves analysis of plasma α-synuclein, MDQ, and SMDCS between DLB versus non-DLB. The plasma α-synuclein level differentiated patients with DLB from the non-DLB group, with a cut-off score of >0.085, a sensitivity 0.80, a specificity 0.64, and AUC with 95% CI 0.76 (0.67–0.85). The MDQ differentiated patients with DLB from those in the non-DLB group, with a cut-off score of >1, a sensitivity 0.83, a specificity 0.89, and AUC with 95% CI 0.88 (0.81–0.95). The SMDCS significantly differentiated patients with DLB from the non-DLB group, with a cut-off score of >2, a sensitivity 0.88, a specificity 0.93, and AUC with 95% CI 0.95 (0.91–0.99).

Table 3 shows the background characteristics and clinical DLB features of the SMDCS+ (SMDCS > 2) group compared to the SMDCS− (SMDCS ≤ 2) group among all patients, and the OR adjusted for age and dementia severity by CDR-SB. The comparison of demographical data after adjustment showed that the SMDCS+ group had significantly higher plasma α-synuclein level (OR = 20674.16; $p < 0.001$), higher MDQ (OR = 5.56; $p < 0.001$), higher NPI composite score (OR = 1.05; $p = 0.045$), higher DaTabN (OR = 6.84; $p < 0.001$) with lower SBR (OR = 0.22; $p = 0.028$), higher UPDRS Part III (OR = 1.08; $p = 0.002$), and lower education (OR = 0.99; $p = 0.004$). Moreover, all motor and non-motor DLB features were significantly higher in the SMDCS+ group (**Table 3**).

DISCUSSION

For the clinical diagnosis of DLB, this study prospectively investigated the plasma α-synuclein level (a fluid biomarker) along with a newly designed MDQ (a clinical assessment). Both tools demonstrated higher scores in patients with DLB compared with the non-DLB group. The combination of both diagnostic tools successfully provided a better discrimination power of the diagnosis of DLB, from AD or NC. In this study, plasma samples were collected and assayed with the IMR standardized procedure. The finding of higher plasma α-synuclein levels in patients with DLB compared to the non-DLB group was not consistent with a 2011 study by Laske et al. (2011). However, the elevated plasma

TABLE 3 | Dopamine transporter imaging, motor, and non-motor features of SMDCS + group (n = 56) compared to SMDCS – group (n = 65), odds ratio (OR) adjusted for age and dementia severity by CDR.

	SMDCS+, *n* (%)	SMDCS–, *n* (%)	OR	*p*
α-Syn, mean (SD)	0.24 (0.33)	0.09 (0.05)	20,674.16	<0.001
MDQ, mean (SD)	3.31 (1.33)	0.23 (0.49)	12.01	<0.001
DaTabN, *n* (%)	31 (70.5)	8 (21.1)	7.65	<0.001
SBR, mean (SD)	1.28 (0.41)	1.64 (0.38)	0.11	0.005
UPDRS-M, mean (SD)	22.8 (14.9)	8.2 (7.1)	1.12	<0.001
Motor features of DLB				
Resting tremor, *n* (%)	24 (42.9)	4 (6.2)	13.43	<0.001
Kinetic tremor, *n* (%)	31 (55.4)	4 (6.2)	28.43	<0.001
Bradykinesia, *n* (%)	47 (83.9)	6 (9.2)	40.48	<0.001
Rigidity, *n* (%)	42 (75.0)	1 (0.0)	170.58	<0.001
Postural instability	42 (75.0)	3 (4.6)	42.95	<0.001
Parkinsonism*, *n* (%)	50 (89.3)	1 (1.5)	496.02	<0.001
Non-motor features of DLB				
Fluctuation, *n* (%)	34 (60.7)	10 (15.4)	4.26	0.003
VHs, *n* (%)	24 (42.9)	8 (12.3)	2.92	0.001
RBD, *n* (%)	32 (57.1)	10 (15.4)	8.07	<0.001

n, number of cases; CDR, Clinical Dementia Rating Scale; OR, odds ratio; α-syn, plasma α-synuclein; MDQ, Motor Dysfunction Questionnaire in the History-based Artificial Intelligent Clinical Dementia Diagnostic System (HAICDDS); DaTabN, abnormal dopamine transporter imaging among 22 ND, 15 AD, and 45 DLB; SBR, striatal background ratio in dopamine transporter imaging among 22 ND, 15 AD, and 45 DLB; Parkinsonism, bradykinesia plus at least one other parkinsonian motor symptom/sign; UPDRS-M, motor subscale of the Unified Parkinson's Disease Rating Scale (UPDRS); Fluctuation, fluctuation of cognition; VHs, visual hallucinations; RBD, REM sleep behavior disorder; NS, non-significance.*

α-synuclein levels concurred with similar studies that used IMR to differentiate PD from non-PD (Lin et al., 2017, 2020). In Laske's study, they measured α-synuclein serum concentrations using a commercial ELISA kit. Thus, the discrepancy between our study and Laske's study is probably due to the different preparation methods used for the detection of very low concentrations of α-synuclein in the serum or plasma.

Other important findings in this study also deserved attention. First, demographical data revealed that the participants with DLB in this study had significantly greater motor dysfunctions, including more Parkinsonism and higher UPDRS Part III scores. Besides, patients with DLB also presented higher non-motor features including fluctuation of cognition, VH, and RBD. These findings were compatible with previous studies and the clinical criteria for the diagnosis of DLB (McKeith et al., 2017). In the demographic section of the study, we included other biomarkers which showed higher DaTabN and lower APOE4 allele in patients with DLB compared to those with AD. These findings are also consistent with previous studies.

Second, although a fluid biomarker for the diagnosis of DLB is too novel to become the only indicative or supportive biomarker, findings in our analysis showing that significantly increased levels of plasma α-synuclein in patients with DLB compared to non-DLB patients were evident. This supports the use of a fluid biomarker for the clinical diagnosis of DLB. Findings of significantly higher UPDRS Part III scores in the α-syn + group than in the α-syn – group (18.9 ± 15.7 versus 12.7 ± 14.3; p = 0.028) indicated a good correlation between motor dysfunctions and UPDRS and the plasma α-synuclein level. Significantly lower SBR in the α-syn + group than that in the α-syn – group (1.35 ± 0.42 versus 1.55 ± 0.41; p = 0.047), and a high negative correlation coefficient of plasma α-synuclein level with SBR (−0.36; p = 0.002) indicated a good correlation of the plasma α-synuclein level with reduced dopamine transporter uptake in the striatal areas, which is currently the hallmark of brain imaging study for the diagnosis of DLB. Further studies on fluid biomarkers are warranted for clinical applications.

We assumed that the high rates with different manifestations of Parkinsonian symptoms in the patients with DLB would be noticed by their caregivers. Hence, we used a simple informant-based Parkinsonism questionnaire (MDQ) in this study. We demonstrated that higher MDQ scores (2.95 ± 1.60) among patients with DLB, and much lower scores in the NC (0.42 ± 0.98) and AD (0.44 ± 0.99) groups. These findings revealed that using the MDQ much higher characteristic motor symptoms are observed in patients with DLB compared to non-DLB patients. This finding is compatible with the results of one of our recently published articles (Chiu et al., 2021). Findings of significant higher MDQ in the α-syn + group than in the α-syn – group (2.2 ± 2.0 versus 1.3 ± 1.9; p = 0.023) indicated a good correlation between motor dysfunctions as assessed by MDQ and plasma α-synuclein.

Using either the plasma α-synuclein level (sensitivity: 0.80, specificity: 0.64, and AUC: 0.76) or the HAI-MDQ (sensitivity: 0.83, specificity: 0.89, and AUC: 0.88) to discriminate DLB from non-DLB yielded satisfactory results. However, a combination of both of these tools (SMDCS) further increased the power of discrimination (sensitivity of 0.88, specificity of 0.93, and AUC of 0.95). Therefore, we are looking forward to collecting more data and performing analyses on combined complex clinical data, fluid biomarkers, and neuroimaging markers, supplemented with artificial intelligence and machine learning procedures. So that we can provide a more accurate and efficient diagnostic tool for the clinical detection of DLB.

Third, the associated factors of positive SMDCS in all participants in this study had provided the clinical evidence supporting the value of measuring plasma α-synuclein level combined with a clinical questionnaire for the clinical discrimination of DLB from non-DLB. Findings of much higher SMDCS total scores in the SMDCS + group (4.7 ± 1.8) than that in the SMDCS – group (0.9 ± 1.2) and higher UPDRS Part III scores in the SMDCS + group (22.8 ± 14.9) than in the SMDCS – group (8.2 ± 7.1) indicated a good positive correlation of motor dysfunctions between both tools for the assessment of characteristic Parkinsonism associated with DLB. The correlation coefficient of SMDCS with UPDRS Part III was 0.63 in the later analysis. In other words, the DLB motor features are well detected by using a combined scale of both clinical and biofluid markers. Significantly lower SBR in the SMDCS + group (1.28 ± 0.41) than that in the SMDCS – group (1.64 ± 0.38), and a high negative correlation coefficient of SMDCS with SBR (−0.45) indicated a good correlation of the novel tool with reducing dopamine transporter uptake in the striatal areas, which is currently the hallmark of brain imaging study for the

diagnosis of DLB. Higher rates of the Parkinsonian symptoms including resting tremor, kinetic tremor, bradykinesia, rigidity, and instability as well as non-motor DLB features including DaTabN, RBD, VH, and cognitive fluctuation were found in the SMDCS+ group revealed that the composite questionnaire for the clinical detection of DLB was simple, practical, and reliable.

CONCLUSION

In conclusion, our study showed that both the plasma α-synuclein level and the MDQ score were significantly higher in patients with DLB compared to the NC and AD groups, with a fair diagnostic power. The novel SMDCS which combined both measures is simple and practical. Moreover, the SMDCS demonstrated satisfactory sensitivity and specificity for the clinical differentiation of DLB from AD or NC. The diagnostic value of the novel tool was further confirmed by good correlations with the DAT study and motor subscores of the UPDRS. This simple screening tool can be applied at the bedside, as well as in the clinics, for the screening of motor dysfunctions related to DLB. This could help non-specialists detect DLB more easily in healthcare settings without access to neurologists.

The study has some limitations. First, the sample size in this study was relatively small and included only two hospitals in central Taiwan. Further research studies with larger sample populations for further validation of the findings are needed. Second, the diagnosis of NC, AD, or DLB was based only on the clinical criteria. However, detailed clinical information and DAT imaging may help differentiate DLB from NC or AD. In this study, APOE4 allele was significantly higher in the AD group compared to the DLB and NC groups. Third, the comparison of the plasma α-synuclein level among DLB, AD, and ND was cross-sectional. Therefore, the possible contribution of plasma α-synuclein to the progression of diseases was not able to be speculated in this study. The follow-up of a larger cohort with further observations of the incidence or the progression of dementia should be considered.

DATA AVAILABILITY STATEMENT

The original contributions presented in the study are included in the article/supplementary material, further inquiries can be directed to the corresponding author.

ETHICS STATEMENT

The studies involving human participants were reviewed and approved by the Show Chwan Memorial Hospital. The ethics committee waived the requirement of written informed consent for participation.

AUTHOR CONTRIBUTIONS

Y-TC undertook the literature search and data analysis, edited the author contributions, contributed to revisions of the manuscript, and the final draft of the manuscript. P-YC undertook the literature search and data analysis, contributed to revisions of the manuscript, and the final draft of the manuscript. SO, G-UH, and S-YY contributed to revisions and drafts of the manuscript. All authors contributed to the article and approved the submitted version.

ACKNOWLEDGMENTS

We would like to thank Ming-Tsung Lee at the Research Assistant Center of Show Chwan Memorial Hospital for his feedback and suggestions during the experimental design and statistical analysis stages.

REFERENCES

Ballard, C., McKeith, I., Burn, D., Harrison, R., O'Brien, J., Lowery, K., et al. (1997). The UPDRS scale as a means of identifying extrapyramidal signs in patients suffering from dementia with lewy bodies. *Acta. Neurol. Scand.* 96, 366–371. doi: 10.1111/j.1600-0404.1997.tb00299.x

Barbour, R., Kling, K., Anderson, J. P., Banducci, K., Cole, T., Diep, L., et al. (2008). Red blood cells are the major source of alpha-synuclein in blood. *Neurodegener. Dis.* 5, 55–59. doi: 10.1159/000112832

Chiu, P. Y., Hung, G. U., Wei, C. Y., Tzeng, R. C., and Pai, M. C. (2020). Freezing of speech single questionnaire as a screening tool for cognitive dysfunction in patients with dementia with lewy bodies. *Front. Aging Neurosci.* 12:65. doi: 10.3389/fnagi.2020.00065

Chiu, P. Y., Wei, C. Y., Hung, G. U., and Wu, S. L. (2021). Motor dysfunction questionnaire and dopamine transporter imaging composite scale improve differentiating dementia with lewy bodies from alzheimer's Disease with motor dysfunction. *Front. Aging. Neurosci.* 13:709215. doi: 10.3389/fnagi.2021.709215

Cummings, J. L., Mega, M., Gray, K., Rosenberg-Thompson, S., Carusi, D. A., and Gornbein, J. (1994). The Neuropsychiatric inventory: comprehensive assessment of psychopathology in dementia. *Neurology* 44, 2308–2314. doi: 10.1212/wnl.44.12.2308

Geser, F., Wenning, G. K., Poewe, W., and McKeith, I. (2005). How to diagnose dementia with Lewy bodies: state of the art. *Mov. Dis.* 20(Suppl. 12), S11–S20. doi: 10.1002/mds.20535

Hansson, O., Hall, S., Ohrfelt, A., Zetterberg, H., Blennow, K., Minthon, L., et al. (2014). Levels of cerebrospinal fluid alpha-synuclein oligomers are increased in parkinson's disease with dementia and dementia with lewy bodies compared to alzheimer:s Disease. *Alzheimers Res. Ther.* 6:25. doi: 10.1186/alzrt255

Kasuga, K., Nishizawa, M., and Ikeuchi, T. (2012). alpha-Synuclein as CSF and Blood biomarker of dementia with lewy bodies. *Int. J. Alzheimers Dis.* 2012:437025. doi: 10.1155/2012/437025

Kasuga, K., Tokutake, T., Ishikawa, A., Uchiyama, T., Tokuda, T., Onodera, O., et al. (2010). Differential levels of alpha-synuclein, beta-amyloid42 and tau in CSF between patients with dementia with Lewy bodies and alzheimer's Disease. *J. Neurol. Neurosurg Psychiatry* 81, 608–610. doi: 10.1136/jnnp.2009.197483

Laske, C., Fallgatter, A. J., Stransky, E., Hagen, K., Berg, D., and Maetzler, W. (2011). Decreased alpha-synuclein serum levels in patients with lewy body dementia compared to alzheimer's Disease patients and control subjects. *Dement Geriatr. Cogn. Dis.* 31, 413–416. doi: 10.1159/000329763

Lawton, M. P., and Brody, E. M. (1969). Assessment of older people: self-maintaining and instrumental activities of daily living. *Gerontologist* 9, 179–186. doi: 10.1093/geront/9.3_part_1.179

Li, Q. X., Mok, S. S., Laughton, K. M., McLean, C. A., Cappai, R., Masters, C. L., et al. (2007). Plasma alpha-synuclein is decreased in subjects with Parkinson's disease. *Exp. Neurol.* 204, 583–588. doi: 10.1016/j.expneurol.2006.12.006

Lin, C. H., Yang, S. Y., Horng, H. E., Yang, C. C., Chieh, J. J., Chen, H. H., et al. (2017). Plasma alpha-synuclein predicts cognitive decline in Parkinson's disease. *J. Neurol. Neurosurg Psychiatry* 88, 818–824. doi: 10.1136/jnnp-2016-314857

Lin, W. C., Lu, C. H., Chiu, P. Y., and Yang, S. Y. (2020). Plasma total alpha-synuclein and neurofilament light chain: clinical validation for discriminating Parkinson's Disease from normal control. *Dement Geriatr. Cogn. Dis.* 49, 401–409. doi: 10.1159/000510325

McKeith, I. G., Boeve, B. F., Dickson, D. W., Halliday, G., Taylor, J. P., Weintraub, D., et al. (2017). Diagnosis and management of dementia with lewy bodies: fourth consensus report of the DLB Consortium. *Neurology* 89, 88–100. doi: 10.1212/WNL.0000000000004058

McKhann, G. M., Knopman, D. S., Chertkow, H., Hyman, B. T., Jack, C. R. Jr., Kawas, C. H., et al. (2011). The diagnosis of dementia due to alzheimer's Disease: recommendations from the national institute on aging-alzheimer's association workgroups on diagnostic guidelines for alzheimer's Disease. *Alzheimers Dement* 7, 263–269. doi: 10.1016/j.jalz.2011.03.005

Morris, J. C. (1993). The clinical dementia rating (CDR): current version and scoring rules. *Neurology* 43, 2412–2414. doi: 10.1212/wnl.43.11.2412-a

Nasreddine, Z. S., Phillips, N. A., Bedirian, V., Charbonneau, S., Whitehead, V., Collin, I., et al. (2005). The montreal cognitive assessment, MoCA: a brief screening tool for mild cognitive impairment. *J. Am. Geriatr. Soc.* 53, 695–699. doi: 10.1111/j.1532-5415.2005.53221.x

Noguchi-Shinohara, M., Tokuda, T., Yoshita, M., Kasai, T., Ono, K., Nakagawa, M., et al. (2009). CSF alpha-synuclein levels in dementia with lewy bodies and alzheimer's Disease. *Brain Res.* 1251, 1–6. doi: 10.1016/j.brainres.2008.11.055

Ohrfelt, A., Grognet, P., Andreasen, N., Wallin, A., Vanmechelen, E., Blennow, K., et al. (2009). Cerebrospinal fluid alpha-synuclein in neurodegenerative disorders-a marker of synapse loss? *Neurosci. Lett.* 450, 332–335. doi: 10.1016/j.neulet.2008.11.015

Spies, P. E., Melis, R. J., Sjogren, M. J., Rikkert, M. G., and Verbeek, M. M. (2009). Cerebrospinal fluid alpha-synuclein does not discriminate between dementia disorders. *J. Alzheimers Dis.* 16, 363–369. doi: 10.3233/JAD-2009-0955

Surguchov, A. (2022). "Biomarkers in Parkinson's Disease," in *Neurodegenerative Diseases Biomarkers. Neuromethods*, eds P. V. Peplow, B. Martinez, and T. A. Gennarelli (New York, NY: Humana), 155–180. doi: 10.1016/j.nicl.2017.09.009

Teng, E. L., Hasegawa, K., Homma, A., Imai, Y., Larson, E., Graves, A., et al. (1994). The cognitive abilities screening instrument (CASI): a practical test for cross-cultural epidemiological studies of dementia. *Int. Psychogeriatr.* 6, 45–58. doi: 10.1017/s1041610294001602

Wang, C. T., Hung, G. U., Wei, C. Y., Tzeng, R. C., and Chiu, P. Y. (2020). An informant-based simple questionnaire for visuospatial dysfunction assessment in dementia. *Front. Neurosci.* 14:44. doi: 10.3389/fnins.2020.00044

Zhu, F., Li, X., McGonigle, D., Tang, H., He, Z., Zhang, C., et al. (2020). Analyze informant-based questionnaire for the early diagnosis of senile dementia using deep learning. *IEEE J. Transl. Eng. Health Med.* 8:2200106. doi: 10.1109/JTEHM.2019.2959331

Zupancic, M., Mahajan, A., and Handa, K. (2011). Dementia with lewy bodies: diagnosis and management for primary care providers. *Prim. Care Com. CNS Dis.* 13:CC.11r01190. doi: 10.4088/PCC.11r01190

Conflict of Interest: S-YY was employed by the MagQu Co., Ltd.

The remaining authors declare that the research was conducted in the absence of any commercial or financial relationships that could be construed as a potential conflict of interest.

Publisher's Note: All claims expressed in this article are solely those of the authors and do not necessarily represent those of their affiliated organizations, or those of the publisher, the editors and the reviewers. Any product that may be evaluated in this article, or claim that may be made by its manufacturer, is not guaranteed or endorsed by the publisher.

APPENDIX

TABLE A1 | Composition of the HAICDDS-Motor Dysfunction Questionnaire (HAI-MDQ).
患者是否有下列症狀? (不清楚或是不確定請選否)
Does the patient have the following symptoms? (If uncertain, please answer No.)

Item			
MD1	坐著或靜止不動的時候，肢體或臉部會明顯地顫抖嗎?	□ 不會	□ 會
	Does tremor, or shaking, often in hands, arms, or legs, occur when he/she is sitting or standing still?	□ No	□ Yes
MD2	拿東西, 做動作或是說話的時候, 肢體或臉部會明顯地顫抖嗎?	□ 不會	□ 會
	Does tremor, or shaking, often in hands, arms, or legs, occur when he/she is reaching something, holding position, or talking?	□ No	□ Yes
MD3	動作變得緩慢, 尤其是起步特別困難, 面部表情也明顯減少嗎?	□ 不會	□ 會
	Does movement become slower when he/she try to move from a resting position, and also decreases facial expression?	□ No	□ Yes
MD4	動作變得僵硬, 手腳彎曲的角度受到限制, 走路步伐變小身體會前傾嗎?	□ 不會	□ 會
	Does limited angle or stiff movement occur during moving, the steps become smaller and the posture become stooped?	□ No	□ Yes
MD5	動作變得不穩, 走路不平衡, 有時候好像要跌倒或真的跌倒嗎?	□ 不會	□ 會
	Does balance or posture problems occur during walking and cause frequent falls?	□ No	□ Yes
MD6	若有上述這些動作障礙, 剛開始的時候就常常跌倒?	□ 不會	□ 會
	Did he/she fall often at the beginning if he/she has these motor dysfunctions mentioned above?	□ No	□ Yes
MD7	說話音調變得平淡, 比較沒有抑揚頓挫, 會越講越小聲嗎?	□ 不會	□ 會
	Does the speech reduce pitch range (monotone) and volume (hypophonia)?	□ No	□ Yes

frontiers | Frontiers in Aging Neuroscience

ORIGINAL RESEARCH
published: 24 May 2022
doi: 10.3389/fnagi.2022.880405

Cognitive Status and Nutritional Markers in a Sample of Institutionalized Elderly People

María Leirós[1], Elena Amenedo[1], Marina Rodríguez[1], Paula Pazo-Álvarez[1], Luis Franco[2], Rosaura Leis[3,4,5], Miguel-Ángel Martínez-Olmos[5,6], Constantino Arce[7] and the Rest of NUTRIAGE Study Researchers*

[1] Research Group in Cognitive and Affective Neuroscience (NECEA), Department of Clinical Psychology and Psychobiology, University of Santiago de Compostela, A Coruña, Spain, [2] Economic Analysis and Modeling Group, Instituto de Estudios y Desarrollo de Galicia (IDEGA), Santiago de Compostela, Spain, [3] Pediatric Gastroenterology, Hepatology and Nutrition Unit, Hospital Clínico Universitario de Santiago, Instituto de Investigación Sanitaria de Santiago de Compostela (IDIS), Santiago de Compostela, Spain, [4] Unit of Investigation in Nutrition, Growth and Human Development of Galicia, Department of Forensic Sciences, Pathological Anatomy, Gynecology and Obstetrics, and Pediatrics, University of Santiago de Compostela, Santiago de Compostela, Spain, [5] CIBEROBN (Physiopathology of Obesity and Nutrition), Institute of Health Carlos III (ISCIII), Madrid, Spain, [6] Section of Endocrinology-Nutrition Area, Hospital Clínico Universitario de Santiago de Compostela, Santiago de Compostela, Spain, [7] Department of Social, Basic and Methodology Psychology, University of Santiago de Compostela, Santiago de Compostela, Spain

OPEN ACCESS

Edited by:
Parnetti Lucilla,
University of Perugia, Italy

Reviewed by:
Hudson Sousa Buck,
University of São Paulo, Brazil
Heather M. Wilkins,
University of Kansas Medical Center Research Institute, United States

***Correspondence:**
María Leirós
maria.leiros.lorenzo@usc.es

Specialty section:
This article was submitted to Neurocognitive Aging and Behavior, a section of the journal Frontiers in Aging Neuroscience

Received: *21 February 2022*
Accepted: *19 April 2022*
Published: *24 May 2022*

Citation:
Leirós M, Amenedo E, Rodríguez M, Pazo-Álvare P, Franco L, Leis R, Martínez-Olmos M-Á, Arce C and the Rest of NUTRIAGE Study Researchers (2022) Cognitive Status and Nutritional Markers in a Sample of Institutionalized Elderly People. Front. Aging Neurosci. 14:880405. doi: 10.3389/fnagi.2022.880405

Background: Since many of the risk factors for cognitive decline can be modified by diet, the study of nutrition and its relationships with cognitive status in aging has increased considerably in recent years. However, there are hardly any studies that have assessed cognitive status using a comprehensive set of neuropsychological tests along with measures of functional capacity and mood and that have related it to nutritional status measured from several nutritional parameters that have shown its relationships with cognitive function.

Objective: To test the differences in depressive symptomatology and in several measures of nutritional status between three groups classified according to their cognitive status (CS hereafter).

Method: One hundred thirteen participants from nursing homes in Galicia, Spain, underwent a comprehensive neuropsychological examination, including a general screening test (MMSE) and tests for different cognitive domains along with measures of activities of daily living (ADL) and assessment of depressive symptomatology (GDS-SF). According to established clinical criteria, participants were divided into three CS groups, Cognitively Intact (CI), Mild Cognitive Impairment (MCI), and All-Cause Dementia (ACD). Nutritional status was also examined using blood-derived measures, body mass index (BMI) and a nutritional screening test (MNA-SF). Differences between CS groups in all nutritional variables were studied by one-way ANOVAs with *post-hoc* Bonferroni correction or Kruskal-Wallis with Games-Howell *post-hoc* correction when appropriate. Multinomial logistic regression was also applied to test the association between nutritional variables and CS.

Results: Differences between CS groups were statistically significant for depressive symptomatology, vitamin A and D, albumin, selenium (Se), uric acid (UA), and BMI. The results of multinomial logistic regression found positive associations between groups with better CS and higher concentrations of vitamins A and D, transthyretin (TTR), albumin, Se, and UA, while negative associations were found for BMI.

Conclusion: Higher serum levels of vitamin A, vitamin D, TTR, albumin, Se, and UA could act as protective factors against cognitive decline, whereas higher BMI could act as a risk factor.

Keywords: cognitive status, mild cognitive impairment (MCI), dementia, nutritional status, nutritional markers, blood biomarkers, nursing homes, aging

INTRODUCTION

Demographic trends indicate that population is aging (Klímová and Vališ, 2018). In this context, there is an increase in health problems or conditions whose main risk factor is advanced age, including cognitive impairment (Power et al., 2019). The lack of effective treatments for cognitive impairment makes preventive strategies a public priority to preserve health and quality of life in advanced stages of life (Dye et al., 2017; Ma et al., 2017) and reduce the economic cost in public health resources (Miquel et al., 2018).

The aging process involves changes in cognitive functions associated with advancing age and genetic factors, as well as lifestyle-related variables. Therefore, assessment of the relationships between modifiable lifestyle factors, such as diet, and nutritional status and cognitive status (CS hereafter), is important to characterize nutritional patterns that may have a neuroprotective role, and thus aid in the prevention of cognitive decline.

It has been suggested that individuals at risk for cognitive decline may be identified by combinations of biological markers (Nettiksimmons et al., 2015). Blood-derived measures, compared to other commonly used methods to predict cognitive decline such as magnetic resonance imaging (MRI), fluorodeoxyglucose-Positron emission tomography (PET), cerebrospinal fluid (CSF), or protein levels from lumbar puncture, are less expensive and more familiar to patients and potential research participants (Nettiksimmons et al., 2015).

Taking the previous into account, the aim of this study was to look for nutritional indicators, mostly from blood-derived measures, that differ among groups classified according to their CS. This may help to identify markers that precede cognitive decline or that can identify individuals at risk for cognitive decline and dementia.

The study of nutrition and its relationship to cognitive function and dementia has increased in recent years. Yet, to our knowledge, there is a lack of studies that have assessed cognitive status using a comprehensive set of neuropsychological tests along with measures of activities of daily living (ADL) and assessment of affective state, and that have related it to nutritional status measured from blood-derived measures, anthropometric measures, and a nutritional status screening test combined.

The relationships between blood-derived measures and cognitive function have been widely studied for some biochemical variables and micronutrients, while others remain almost unstudied. The group of vitamins is among the micronutrients that have received most attention and accumulates more evidence on its relationships with cognitive function. For this group, the most studied has been vitamin D because of its neuroprotective, anti-inflammatory, and antioxidant effects (Sultan et al., 2020). Results on vitamin D and cognitive function suggest that its main circulating form, 25-hydroxyvitamin D (25-OH vitamin D), is closely associated to cognitive function and that may play an important role against cognitive decline (Kalueff and Tuohimaa, 2007; Buell and Dawson-Hughes, 2008; Seamans et al., 2010; Schlögl and Holick, 2014; Toffanello et al., 2014; Wilson et al., 2014; Jorde et al., 2015; Kueider et al., 2016; Goodwill et al., 2018; Duchaine et al., 2020; reviews in Dickens et al., 2011; Van der Schaft et al., 2013; Goodwill and Szoeke, 2017; Chai et al., 2019; Sultan et al., 2020). Serum folate and serum vitamin B12 levels have also been related to cognitive decline and dementia, although findings are inconclusive (Elias et al., 2006; Kang et al., 2006; Michelakos et al., 2013; Moore et al., 2014; Rabensteiner et al., 2020; for a review see Rosenberg, 2008; O'Leary et al., 2012). One of the less studied vitamins in this context is vitamin A, and its derived factors such as retinoids. In recent years, there has been an increasing number of studies, mainly in animal models, linking retinoids to the etiology of Alzheimer's Disease (AD) (Goodman and Pardee, 2003; Goodman, 2006; Malaspina and Michael-Titus, 2008; Carratu et al., 2015). Some authors even propose that retinoic acid may have therapeutic properties for the treatment of neurodegenerative diseases such as AD (Lee et al., 2009) given their role in the modulation of neurogenesis, neuronal survival and synaptic plasticity (Olson and Mello, 2010). Nevertheless, to our knowledge studies testing relationships between this vitamin and cognitive function in aging are lacking.

Aging is also associated with increased levels of circulating cytokines and proinflammatory markers (Lim et al., 2013; Michaud et al., 2013) such as interleukins, Tumor Necrosis Factor-α (TNF-α), and C-Reactive Protein (CRP). This group of biochemical parameters is receiving increasing attention as inflammation may affect the central nervous system modulating cognitive function and mediating in cognitive impairment

(Ray et al., 2007; McAfoose and Baune, 2009; Gorelick, 2010; Ownby, 2010; O'Bryant et al., 2010; Valls-Pedret et al., 2012; Koyama et al., 2013; Lim et al., 2013; Michaud et al., 2013; Petersen et al., 2020).

There is also evidence for relationships between cognitive changes in aging and other blood-derived measures, although supported by fewer studies. Thus, serum visceral proteins, such as prealbumin or transthyretin (TTR) and albumin, have been both considered markers of nutritional status (Smith, 2017; Keller, 2019) and cognitive function (Onem et al., 2010; Velayudhan et al., 2012; Nettiksimmons et al., 2015; Araghi et al., 2021). Although selenium (Se) is known to play an antioxidant role as it is the main constituent of antioxidant enzymes that are expressed in different tissues, including the brain (Cardoso et al., 2014), there are few studies on the relationship between Se concentrations and CS or cognitive impairment (Cardoso et al., 2010, 2014; Berr et al., 2012; for a review see Smorgon et al., 2004). Another natural antioxidant compound with beneficial properties is uric acid (UA) (Tuven et al., 2017; for a review see Tana et al., 2018). However, UA may also act as a pro-inflammatory compound and there still exists discussion on its oxidant-antioxidant properties (Sautin and Johnson, 2008). UA levels have been associated with cognitive performance (Annanmaki et al., 2008), MCI (Rinaldi et al., 2003; Pellecchia et al., 2016), different types of dementia (Rinaldi et al., 2003; Kim et al., 2006; Schlesinger and Schlesinger, 2008; Ruggiero et al., 2009; Al-Khateeb et al., 2015; Wen et al., 2017; Xu et al., 2017; Latourte et al., 2018; Serdarevic et al., 2020; Boccardi et al., 2021) and risk of dementia (González-Aramburu et al., 2014; for a review see Schlesinger and Schlesinger, 2008; for a meta-analysis see Khan et al., 2016; Zhou et al., 2021). Other micronutrients or blood biochemistry variables that have been related to CS although studies are more scarce, are serum iron, ferritin, and transferrin (Umur et al., 2011; Yavuz et al., 2012), total cholesterol (TC), High Density Lipoprotein Cholesterol (HDL-C), Low Density Lipoprotein Cholesterol (LDL-C) (Van Exel et al., 2002; Van Vliet, 2012; Crichton et al., 2014; Lv et al., 2016; Ma et al., 2017), zinc (Cuajungco and Fagét, 2003; Lam et al., 2008; Nuttall and Oteiza, 2014), Mean Corpuscular Volume (MCV) (Gamaldo et al., 2013), calcium (Schram et al., 2007), insulin (Stolk et al., 1997), gamma-glutamyl transferase (GGT) (Lee et al., 2020; Tang et al., 2021), alanine aminotransferase (ALT) (Nho et al., 2019), and glucose (Korol and Gold, 1998; Seetharaman et al., 2015).

The study of the relationships between cognitive and nutritional status should also consider anthropometric indexes of obesity, such as Body Mass Index (BMI). Although the relationships between obesity and cognitive function have been widely studied the findings from previous studies are inconclusive (for a meta-analysis see Danat et al., 2019). Obesity has also been linked to depression (Noh et al., 2015). The evidence from epidemiological and clinical trials suggest a bidirectional connection between overweight and psychological health (for a review see Luppino et al., 2010). Given that obesity is a prevalent condition at older ages, and that the study of the relationships between BMI and CS has led to discrepant results, BMI measurement was also included in the present study.

Relationships between cognitive impairment or dementia and depressive symptoms have also been the subject of previous research studies. Depressive symptoms have been related to lower cognitive performance (Ganguli et al., 2006; Godin et al., 2007) and some authors even suggest that depression may be a risk factor for the development of cognitive impairment (Van Den Kommer et al., 2013). However, a meta-analysis by Huang et al. (2011) suggests that dementia may be also a risk factor for depression. Taking the above into account, depressive symptomatology was also assessed in the present study.

In summary, although the relationships between cognitive function and nutritional status are increasingly studied, few studies have included a set of neuropsychological tests to assess the main cognitive domains, measures of functional capacity and affective symptomatology. Moreover, to our knowledge, there are hardly any studies that have examined these relationships by establishing a clinical diagnosis of CS in different groups classified according to the severity of their cognitive impairment and limitations in ADLs, based on recognized criteria and that have combined it with blood biochemical variables and anthropometric and nutritional measures. Therefore, in the present study the main objective was to examine the differences between three groups classified according to their CS in the presence of depressive symptomatology, and in several measures of nutritional status: blood markers, BMI, and the Mini Nutritional Assessment-Short Form (MNA-SF).

MATERIALS AND METHODS

Participants

One hundred ninety-six participants were recruited from 11 public nursery homes from Galicia, Spain. From the original sample, 113 participants from 63 to 97 years were finally included in this study (mean age 83.1 ± 6.2, 62.8% women). The 113 enrolled participants had a complete dataset at the time of data analysis including sociodemographic characteristics, neuropsychological testing, functional capacity, depressive symptoms assessment, blood biomarkers, anthropometric measures, and nutritional assessment. The interval between cognitive and nutritional assessments was less than 6 months for all participants. Exclusion criteria included previous dementia diagnosis, acquired brain damage, current chemotherapy or radiation therapy, and/or an inability to complete the neuropsychological tests due to significant sensory difficulties such as visual and/or hearing impairments not adequately corrected. All the procedures were approved by the Central Ethics and Research Committee of Galicia Autonomous Community (2017/542), and the study was performed in accordance with the ethical standards established in the Declaration of Helsinki. Written consent was obtained from each participant.

Cognitive Status Assessment

Neuropsychological testing was carried out along with ADL assessment and depressive symptomatology examination by the same clinical neuropsychologist. The tests applied were selected to minimize the effects of education and socioeconomic level.

Neuropsychological Examination

A neuropsychological battery composed by tests designed to measure global cognitive function, and specific cognitive domains (attention, learning, memory, visuoconstructive ability, processing speed, and executive function) was applied as follows. The Mini-Mental State Examination (MMSE, Folstein et al., 1975) was used to evaluate global cognitive function. Attention was assessed using Digits subtest (digits forward) of the Wechsler Adult Intelligence Scale (WAIS-IV) (Wechsler, 2008), and Color Trail Test (CTT) (D'Elia et al., 1996) first form. To assess learning and verbal memory processes the administered test was the Rey Auditory Verbal Learning Test (RAVLT, Rey, 1964), and to measure visual immediate memory, the Rey-Osterrieth Complex Figure (ROCF, Rey, 1941) was administered. Working memory was evaluated using digits backward and sequencing of the Digits Subtest (WAIS-IV, Wechsler, 2008). Visuoperceptive and visuoconstructive skills were evaluated with the copy assay of ROCF. Processing speed was evaluated using the Symbol Search and Coding subtest, along with the processing speed index of the WAIS-IV (Wechsler, 2008). Executive function was measured with a phonetic fluency measure using the PMR (Artiola et al., 1999) which was chosen instead of FAS (Borkowski et al., 1967) because these letters are more appropriate for Spanish vocabulary (Artiola et al., 1999), the Five Digits Test (Sedó, 2007) and CTT second form (D'Elia et al., 1996).

Basic and Instrumental Activities of Daily Living

Barthel Index was used to determine participants capacity in basic activities of daily living (BADL, Mahoney and Barthel, 1965). Instrumental activities of daily living (IADL) were assessed using an adaptation of the Lawton and Brody index (Lawton and Brody, 1969), including items for institutionalized participants (i.e., ability to use telephone, shopping, ability to handle finances, public transportation, and nursing home and health services use).

Based on the results obtained from the neuropsychological examination and the performance in ADL, participants were divided in three different CS groups, Cognitively Intact (CI), Mild Cognitive Impairment (MCI), and All Cause Dementia (ACD). This classification was performed by a qualified neuropsychologist following established criteria (see **Table 1**) drawn from the Spanish Neurology Society (SEN; Robles et al., 2002), the Working Group from the National Institute on Aging and Alzheimer's Association (NIA-AA; McKhann et al., 2011; Croisile et al., 2012), the Diagnostic and Statistical Manual of Mental Disorders-Fifth Edition (DSM-V; American Psychiatric Association, 2013) and the International Working Group on Mild Cognitive Impairment (Winblad et al., 2004).

Depressive Symptomatology Evaluation

To evaluate the existence of depressive symptoms the short form of the Geriatric Depression Scale (GDS-SF, Sheikh and Yesavage, 1986) was administered to each participant (see **Table 2**).

Nutritional Screening

Blood Collection and Analyses

Blood samples were drawn from the antecubital vein between 08:00 and 09:30 h after an overnight fast and rest. Blood samples were taken from all study participants in the following types of tubes: EDTA K2 for hemogram and blood bank, separator Gel for clinical chemistry determinations, and Silica, for determination of trace elements. The samples were protected from sunlight and refrigerated. The serum and plasma were separated and cryopreserved at −80°C until the analysis was conducted. Routine blood tests were analyzed at the Central Laboratories of the University Clinical Hospital of Santiago de Compostela. Biochemical, hematological basic and advanced determinations of inflammatory parameters, oxidative stress and bone health analytical procedures were performed with instrumentation and reagents from Siemens Healthineers, and selenium was determined by Inductively Coupled Plasma-Mass Spectrometry from Agilent Technologies, according to the manufacturer's recommendations. Serum 25(OH)D concentrations were quantified using a direct competitive chemiluminescence immunoassay by the LIAISON method. Insulin resistance (IR) was calculated by Homeostatic Model Assessment of IR (HOMA-IR). The normal ranges for the biochemistry variables used are those established by the Galician Public Health Service, reviewed in this case by specialist physicians (see **Table 3**).

Anthropometric Measures

Body weight and height were measured using properly calibrated scales and a height rod or tape measure, correspondingly. Wheelchair weighing scales were used for measuring the weight for participants unable to stand, as measurement of forearm length or from measurement between knee and heel following the criteria from The "Must" Explanatory Booklet (Malnutrition Advisory Group [MAG], 2003). BMI was calculated for every participant, following the World Health Organization (WHO) criteria (WHO, 2021).

Nutritional Assessment

The Mini Nutritional Assessment-Short Form (MNA-SF; Rubenstein et al., 2001) is a screening tool to help identifying elderly participants who are malnourished or at risk of malnutrition. This instrument has been validated by Kaiser et al. (2009) and was administered to all participants.

Statistical Analyses

To test for possible sex differences between the CS groups (CI, MCI, and ACD) a Chi-Square test was run. Differences in age, years of education, depressive symptoms, and nutritional variables were tested by one-way ANOVAs with Bonferroni *post-hoc* correction for pairwise multiple comparisons. For ANOVA analyses, the assumption of homogeneity of variances was tested by Levenne's statistic and normality by the Kolmogorov-Smirnov test for all variables. For variables that did not meet one or both assumptions, the corresponding non-parametric Kruskal-Wallis test was applied to explore differences between groups and the Games-Howell test for pairwise comparisons.

Multinomial logistic regression was used to predict the probability of belonging to the CS group as the dependent variable, on the different variables of nutritional status considered as continuous. The reference group was ACD, and the results are

TABLE 1 | Diagnostic criteria (differential: column 1; common: columns 2–5) to classify participants according to their cognitive status.

Diagnostic criteria for MCI	Cognitive deficits do not interfere with BADL and IADL	Cognitive deficits are not attributable to delusions, psychiatric disorders and/or active medication	Cognitive impairment is detected and diagnosed by a combination of the participant's medical history and neuropsychological assessment	There is impairment in at least two of the following cognitive domains assessed: attention, learning and memory, information processing speed, executive functions, and visuoperceptive and visuoconstructive abilities	A cognitive domain is considered impaired when the scores obtained in at least one of the tests used to assess a cognitive domain are below 2SD of the mean of a population of similar age and education
Diagnostic criteria for ACD	Cognitive deficits do interfere with the ADL				

MCI, Mild Cognitive Impairment; ACD, All Cause Dementia; BADL, Basic Activities of Daily Living; IADL, Instrumental Activities of Daily Living; ADL, Activities of Daily Living; SD, standard deviation.

TABLE 2 | Sample demographic characteristics.

Variables and measurement units	Total sample *N* = 113	CI *n* = 32	MCI *n* = 49	ACD *n* = 32
Age, years (*M* ±*SD*)	83.09 ±6.21	82.15 ±5.04	83.95 ±6.58	82.71 ±6.67
Sex				
Female (*n*)	71	18	32	21
Male (*n*)	42	14	17	11
Education, years (*M* ±*SD*)	6.79 ±3.45	8.84 ±3.90	6.32 ±2.99	5.46 ±2.74
GDS-SF				
No symptoms (*n*)	50	18	23	9
Light (*n*)	50	13	20	17
Moderate (*n*)	10	1	6	4
Severe (*n*)	3			2

SD, Standard Deviation; CI, Cognitively Intact; MCI, Mild Cognitive Impairment; ACD, All Cause Dementia; GDS-SF, Geriatric Depression Scale-Short Form.

expressed as Odds Ratios (OR) (see **Table 4**). For these statistical analyses, blood biochemical variables that have been shown to be associated with cognitive functions in previous literature were selected. These included blood count parameters, lipid profile, glycemic profile, protein profile, liver profile, vitamins, minerals, and inflammatory factors (see **Table 3**). *P*-values < 0.05 were considered significant. Statistical analyses were performed with SPSS software (version 25, SPSS, Inc., Chicago, IL, United States).

RESULTS

Demographic characteristics, and descriptive statistics for depressive symptoms and nutritional variables are summarized in **Tables 2**, **3** using means and standard deviations for continuous variables or frequencies for categorical variables. According to the diagnostic criteria (**Table 1**), 28.3% participants were classified as CI, 43.4% as MCI and 28.3% as ACD. There were no significant differences in age [$F_{(2,\ 112)} = 0.89$, $p = 0.41$] or sex (χ^2, $p = 0.66$) between groups. However, differences in education years were significant [$F_{(2,\ 112)} = 9.74$, $p < 0.001$], with participants in CI group having more years of schooling compared to MCI ($p < 0.002$) and ACD ($p < 0.001$). Differences in depressive symptoms were also statistically significant [$F_{(2,\ 112)} = 6.04$, $p < 0.005$], with greater presence of symptomatology in the ACD group compared to CI group ($p < 0.005$) (see **Figure 1**). According to the data obtained from the MNA-SF, 81.2% of the total sample was classified as having normal nutritional status (see **Table 3**). ANOVAs and multinomial logistic regression results (see **Table 4**) that have reached statistical significance are presented in the following sections.

Vitamins

Analysis of variance showed significant differences between the groups in serum vitamin A concentrations [$F_{(2,\ 112)} = 6.65$, $p < 0.005$] and *post hoc* pairwise comparisons confirmed those differences between CI and ACD groups ($p < 0.001$). The assumption of homogeneity of variances was met, although the variable vitamin A was not normally distributed according to the results of the Kolmogorov-Smirnov test [$F_{(2,\ 112)} = 0.11$, $p < 0.005$]. Kruskal-Wallis test was administered as the corresponding non-parametric technique [$H_{(2,\ 112)} = 11.94$, $p < 0.005$] confirming the results found by the ANOVA analysis. Regression results (**Table 4**) showed that higher levels of serum vitamin A were positively associated with greater odds of belonging to CI or MCI groups with respect to the reference group (ACD). The serum 25-OH vitamin D concentrations also differed significantly across groups [$F_{(2,\ 112)} = 3.12$, $p < 0.05$]. *Post hoc* pairwise comparisons supported those differences between the MCI and ACD groups ($p < 0.05$) and indicated that MCI participants had higher levels of this vitamin than ACD participants, with no differences between CI

TABLE 3 | Descriptive statistics (*M* ±*SD*) for blood biomarkers, BMI, and MNA-SF scores.

Nutritional variables	Normal values and measurement units	Total sample *N* = 113	CI *n* = 32	MCI *n* = 49	ACD *n* = 32
Vitamin A-Retinol	30–80, μg/dL	55.97 ±19.86	63.56 ±18.94	57.18 ±20.96	46.53 ±15.25
25-OH Vitamin D	30–150, ng/mL	14.04 ±9.76	14.21 ±9.17	16.12 ±11.22	10.68 ±?6.80
TTR	15–36, mg/dL	24.77 ±5.84	26.12 ±6.94	25.22 ±5.30	22.75 ±5.03
Albumin	4–5.2, g/dL	4.22 ± 0.26	4.20 ± 0.24	4.29 ± 0.19	4.15 ± 0.34
Se	<151, mcg/L	89.62 ±18.90	86.25 ±14.16	96.75 ±19.77	82.09 ±18.29
UA	2.4–7, mg/dL	5.97 ±1.69	6.28 ±1.46	6.18 ±1.77	5.33±1.67
Vitamin B12-Cobalamin	180–1,900, pg/mL	446.98 ±237.37	425.25 ±147.41	471.91 ±244.93	430.53 ±295.28
Folate	2.7–17, ng/mL	8.45 ±9.89	7.30 ±5.54	7.62 ±3.49	10.85 ±17.20
TNF	0–8.1, pg/mL	21.66 ±19.91	16.77 ±10.43	24.76 ±25.42	21.79 ±16.84
hs-CRP	0.1–0.3, mg/dL	0.71 ±1.39	0.99 ±2.21	0.64 ± 0.99	0.53 ± 0.66
IL-1	<5, pg/mL	6.74 ±6.10	6.23 ±4.21	7.33 ±7.54	6.35 ±5.23
IL-6	0–5, pg/mL	10.50 ±8.65	11.56 ±10.84	10.51 ±9.13	9.40 ±4.62
Magnesium	1.7–2.2 mg/dL	2.05 ±0.25	2.04 ±0.30	2.07 ± 0.23	2.01 ± 0.21
Zinc	65–140, μg/dL	97.12 ±18.45	97.62 ±12.93	97.93 ±20.19	95.37 ±20.66
Iron	60–170, μg/dL	73.14 ±26.49	74.06 ±29.56	74.34 ±24.80	70.37 ±26.41
Ferritin	Total sample Men 12–300, ng/mL Women 12–150, ng/mL	100.72 ±20.68 136.69 ±160.55 79.45 ±83.49	124.31 ±133.58 163.43 ±56.34 93.89 ±188.34	82.67 ±91.71 97.76 ±77.18 74.66 ±98.78	104.78 ±143.69 162.81 ±213.81 74.38 ±79.51
Creatinine	0.4–1.3, mg/dL	1.01 ± 0.45	1.11 ± 0.53	0.99 ± 0.31	0.93 ± 0.51
Urea	13–50, mg/dL	59.19 ±30.63	62.18 ±34.08	61.91 ±29.28	52.03 ±28.76
AST/GOT	10–40, UI/L	22.01 ±6.12	21.74 ±5.79	21.95 ±6.90	22.34 ±5.27
ALT/GPT	3–41, UI/L	19.83 ±8.60	19.43 ±6.87	21.28 ±10.34	18.00 ±6.90
GGT	8–73, UI/L	37.00 ±43.93	40.00 ±52.10	32.95 ±36.27	40.18 ±46.64
Hemoglobin	13.5–17.5, g/dL	13.09 ±1.57	12.97 ±1.75	13.39 ±1.50	12.75 ±1.44
MCV	83–102, fl	91.10 ±5.73	91.14 ±7.25	91.67 ±4.76	90.19 ±5.46
MCH	27–31, pg	30.30 ±2.14	30.45 ±2.56	30.41 ±1.84	29.99 ±2.15
TC	120–255, mg/dL	172.01 ±39.32	171.81 ±40.53	175.20 ±38.23	167.31Q ±40.49
LDL-C	55–125, mg/dL	102.39 ±33.49	103.40 ±35.75	104.26 ±31.51	98.50 ±34.83
HDL-C	34–91, mg/dL	46.63 ±12.65	45.21 ±12.93	46.30 ±12.67	48.53 ±12.51
TG	27–150, mg/dL	115.04 ±48.99	116.31 ±51.75	123.24 ±51.45	101.21 ±39.88
TP	6.4–8.5, g/dL	6.85 ± 0.46	6.78 ± 0.46	6.92 ± 0.47	6.83 ± 0.44
Glucose	74–105, mg/dL	95.70 ±23.82	92.19 ±20.13	100.51 ±28.86	91.84 ±17.03
Insulin	2–15, mUI/L	11.39 ±9.63	10.07 ±7.42	10.48 ±7.48	14.09 ±13.50
Platelets	135–369, ×103/μL	216.42 ±78.42	215.28 ±73.46	208.91 ±62.91	229.06 ±102.16
Inorganic phosphate	2.5–4.5, mg/dL	3.37 ± 0.48	3.39 ± 0.53	3.37 ± 0.41	3.35 ± 0.52
BMI	Kg/m^2	29.70 ±5.10	29.32 ±5.43	28.58 ±4.51	31.78 ±5.15
BMI, group (n)					
Underweight	<18.5, Kg/m^2	1	6	11	1
Normal weight Pre-obesity	18.5–24.9, Kg/m^2 25.29.9, Kg/m^2	19 40	13 13	20 18	2 7
Obesity	>30, Kg/m^2	53			22
MNA-SF, total score	0–14 points	12.71 ±1.89	12.81 ±2.00	12.91±1.77	12.31±1.95
MNA-SF, group (*n*)					
Normal nutritional status	12–14 points	91	28	40	23
At risk of malnutrition	8–11points	17	2	7	8
Possible malnutrition	0–7 points	4	2	1	1

25-OH vitamin D, 25-hydroxyvitamin D; TTR, transthyretin; Se, selenium; UA, Uric Acid; TNF, Tumor Necrosis Factor; hs-CRP, high sensitivity C-Reactive protein; IL-1, Interleukin 1beta; IL-6, Interleukin 6; AST/GOT, Aspartate Aminotransferase; ALT/GPT, Alanine aminotransferase; GGT, Gamma-glutamyl transferase; MCV; Mean Corpuscular Volume; MCH, Mean Corpuscular Hemoglobin; TC, Total cholesterol; LDL-C, Low-Density Lipoprotein Cholesterol; HDL-C, High-Density Lipoprotein Cholesterol; TG, Triglycerides; TP, Total Proteins; BMI, Body Mass Index; MNA-SF, Mini Nutritional Assessment Short Form.

and MCI groups. The assumption of homogeneity of variances was met, although the variable vitamin D was also not normally distributed according to the results of the Kolmogorov-Smirnov test [$F_{(2,\ 112)} = 0.21$, $p < 0.001$]. The Kruskal-Wallis test [$H_{(2,\ 112)} = 9.52$, $p < 0.05$] confirmed the results found by the ANOVA analysis. Higher blood vitamin D levels were positively related to higher odds of belonging to MCI compared to ACD, according to regression results. The results for the CI group were not statistically significant.

Proteins

There were no significant variations in serum TTR concentrations across groups, according to ANOVA. The hypothesis of homogeneity of variances and the assumption of normality were satisfied. No significant differences were detected in pairwise comparisons either. According to the regression results (**Table 4**), higher levels of serum TTR were positively associated with a higher likelihood of belonging to the CI group with respect to ACD. The results for the MCI group did not

TABLE 4 | Multinomial logistic regression results.

	Cognitively intact (CI)			Mild cognitive impairment (MCI)		
	OR (95%CI)	**Wald test**	***P*-value**	**OR (95%CI)**	**Wald test**	***P*-value**
Vitamin A	1.05 (1.02, 1.09)	10.84	0.001	1.04 (1.01, 1.07)	6.32	0.01
Vitamin D	1.06 (0.99, 1.15)	2.95	0.09	1.08 (1.01, 1.16)	5.34	0.05
TTR	1.11 (1.01, 1.22)	5.17	0.05	1.08 (0.99, 1.18)	3.52	0.06
Albumin	2.01 (0.32, 12.72)	0.55	0.46	9.75 (1.55, 61.43)	5.88	0.01
Se	1.02 (0.98, 1.05)	1.13	0.29	1.06 (1.02, 1.09)	11.27	0.001
SUA	1.46 (1.05, 2.02)	5.08	0.05	1.41 (1.04, 1.90)	5.08	0.05
BMI	0.90 (0.82, 1.00)	3.72	0.05	0.88 (0.80, 0.96)	7.17	0.01

OR, odds ratio; d.f. = 1. Reference category, All Cause Dementia (ACD).

reach statistical significance (**Table 4**). ANOVA analyses revealed significant differences in serum albumin concentrations across CS groups [$F_{(2,\ 112)} = 3.43$, $p < 0.05$], and *post hoc* pairwise comparisons between MCI and ACD groups corroborated those differences ($p < 0.05$). The assumption of homogeneity of variances was not met, so Games-Howell as robust technique of equality of means was also applied to confirm the results, although no significant differences were found between the groups. The variable albumin was not either normally distributed according to the results of the Kolmogorov-Smirnov test [$F_{(2,\ 112)} = 0.13$, $p < 0.001$]. Kruskal-Wallis test was administered as the corresponding non-parametric technique [$H_{(2,\ 112)} = 7.39$, $p < 0.05$] confirming the results found by the ANOVA analysis. Higher serum albumin concentrations were positively associated with greater odds of belonging to the MCI group with respect to ACD group, according to regression results. Statistical significance was not reached in the results for the CI group.

Antioxidants

Significant differences between the groups in serum Se concentrations were found [$F_{(2,\ 112)} = 7.23$, $p < 0.001$] and *post hoc* pairwise comparisons confirmed those differences between CI and MCI groups ($p < 0.05$) and between MCI and ACD groups ($p < 0.001$). The hypothesis of homogeneity of variances and the assumption of normality were satisfied. Regression results showed that higher serum Se concentrations were positively associated with increased odds of belonging to MCI group with respect to ACD group (**Table 4**). Additionally, ANOVA showed significant differences between CS groups in serum UA concentrations [$F_{(2,\ 112)} = 3.33$, $p < 0.05$]. *Post hoc* pairwise comparisons did not reach statistical significance. The assumption of homogeneity of variances was met, although UA was not normally distributed according to the results of the Kolmogorov-Smirnov test [$F_{(2,\ 112)} = 0.09$, $p < 0.05$]. Kruskal-Wallis test was administered [$H_{(2,\ 112)} = 6.09$, $p < 0.05$] confirming the results found by the ANOVA analysis. Also, higher levels of serum UA were positively associated with greater odds of belonging to the CI and MCI groups with respect to the ACD group according to regression results.

Body Mass Index

Significant differences in BMI between CS groups were found in ANOVA analyses [$F_{(2,\ 112)} = 4.12$, $p < 0.05$] and *post hoc* pairwise comparisons confirmed those differences between MCI and ACD groups ($p < 0.05$). The hypothesis of homogeneity of variances and the assumption of normality were satisfied. Regression results showed that higher levels of BMI were negatively associated with greater odds of belonging to MCI group with respect to the reference group (see **Table 4**). The results for the CI group did not reach statistical significance. However, it is worth highlighting that the mean BMI for the groups with better CS (CI and MCI) was in the overweight range, while the mean BMI for the most cognitively impaired group (ACD) was in the obese range (see **Table 3**).

DISCUSSION

Because nutritional status could be considered as a potential marker for cognitive decline and a target in the search for preventive strategies to delay the onset or progression of cognitive impairment, in the current study, we examined the differences in nutritional status, assessed by blood markers, BMI and the MNA-SF nutritional screening test, across three groups of institutionalized older participants classified according to their CS. Additionally, the possible differences in depressive symptomatology between CS groups were also examined.

Significant differences between CS groups were found for concentrations of vitamin A, vitamin D, albumin, Se, UA, and BMI. Moreover, better CS was associated with higher concentrations of vitamins A and D, TTR, albumin, Se and UA, while worse CS was associated with higher BMI. Finally, depressive symptomatology was greater in the ACD group compared to CI group.

In the following sections we will discuss our results in the context of previous literature. For a smoother reading the cognitive assessment and/or the diagnostic criteria applied by the studies included in the discussion are indicated in **Table 5**.

Vitamins

In the present study higher levels of vitamin A were associated with better CS and with greater odds of belonging to the CI and MCI groups compared with ACD group. Very little has been found in the previous literature on vitamin A concentrations and cognitive function in aging. Significant reductions in serum vitamin A levels were found in participants with dementia (Raszewski et al., 2016) and in AD patients

TABLE 5 | Cognitive assessment or diagnostic criteria applied by the studies included in the discussion section.

References	Cognitive assessment and/or diagnostic criteria
Al-Khateeb et al. (2015)	Cognitive testing: MMSE. AD diagnosis: NINCDS-ADRDA criteria.
Annanmaki et al. (2008)	Cognitive testing: MMSE, the Information and Similarities subtests of the WAIS-R, the Picture completion and Block design subtests of the WAIS-R, the Digit span and Digit symbol subtests of the WAIS-R, the Logical memory subtest of the WMS-R, the Word list subtest of the WMS-III, the Visual reproduction subtest of the WMS-R, and the Trail making and Rule shift cards tests from the Behavioral Assessment of the Dysexecutive Syndrome. Also, verbal fluency was assessed with asking the subject to list as many animals in a minute as they could and then words that begin with the letter K. Computerized tasks included Simple Reaction Time, two-choice Reaction Time and 10-choice Reaction Time.
Annweiler et al. (2010a)	Cognitive testing: SPMSQ. Cognitive impairment was defined as a score less than 8 in the SPMSQ.
Annweiler et al. (2012)	MCI diagnosis: the International Working Group on Mild Cognitive Impairment criteria.
Araghi et al. (2021)	Cognitive testing: 20-word list for recall, the Alice Heim 4-I test, and verbal fluency assessed via the "S" words and semantic fluency via "animal" words tests. Dementia ascertainment: National hospital episode statistics and the data extracted from hospital medical records and coded using the ICD-10.
Boccardi et al. (2021)	Cognitive testing: MMSE, the Babcock Story Recall test and the immediate and delayed recall of the Rey's Auditory Verbal Learning Test, Token test, the Category Fluency test, Visual Search test and the Letter Fluency test, the copy drawing test and the CDR. MCI diagnosis: Petersen (2004) criteria. AD diagnosis: NINCDS-ADRDA criteria.
Bourdel-Marchasson et al. (2001)	Cognitive testing: MMSE AD diagnosis: DSM-III and NINCDS/ADRDA criteria
Duchaine et al. (2020)	Cognitive testing: 3MS. Cognitive impairment-no dementia diagnosis: DSM-III-R and the ICD-10 criteria. All cause dementia diagnosis: DSM-III-R or the DSM-IV criteria. AD diagnosis: NINCDS-ADRDA criteria.
Feart et al. (2017)	Cognitive testing: MMSE, the Isaacs Set Test, the Benton Visual Retention Test, TMT A and B and the Free and Cued Selective Reminding Test. Dementia diagnosis: DSM-IV. AD diagnosis: NINCDS-ADRDA criteria.
González-Aramburu et al. (2014)	Cognitive testing: MMSE. Dementia diagnosis: made in accordance with the recommendations of the Movement Disorders Society Task Force: PD developed prior to the onset of dementia, PD was associated with a decreased global cognitive efficiency (MMSE < 26), cognitive deficiency was severe enough to impair daily life, and there was impairment in more than one cognitive domain.
Granic et al. (2015)	Cognitive testing: MMSE and the attention subsets of the Cognitive Drug Research computerized assessment system Normal cognitive status was set for MMSE scores of 26 or more. Incident cognitive impairment was defined as crossing the 25-point threshold of the MMSE.
Han et al. (2011)	AD diagnosis: NINCDS- ADRDA criteria
Jorde et al. (2015)	Cognitive testing: MMSE, the word recall testing immediate verbal and visual memory, the digit–symbol coding test, and the finger tapping test.
Kim et al. (2006)	Cognitive testing: MMSE AD diagnosis: DSM-IV and NINCD-ADRDA criteria.
Koch et al. (2021)	Cognitive testing: California Verbal Learning Test, Rey Osterrieth figure, WAIS-R block design, Boston Naming Test, Animal fluency, WAIS-R digit span forward, TMT A and B, Stroop color/word test, number of colors named, National Adult Reading Test, Raven's Colored Progressive Matrice, the 3MS, the CDR and the Alzheimer's Disease Assessment Scale. VD diagnosis: the State of California Alzheimer's disease diagnostic and treatment centers criteria. Mixed dementia diagnosis: DSM-IV criteria. AD diagnosis: NINCDS-ADRD criteria.
Latourte et al. (2018)	Cognitive testing: MMSE and the Isaacs Set Test. Participants were further examined by a physician who performed additional neuropsychological testing and assessed the degree of impairment. Dementia diagnosis: DSM-IV criteria. AD diagnosis: NINCDS-ADRDA criteria VD diagnosis: the National Institute of Neurological Disorders and the Stroke-Association Internationale pour la Recherche et l'Enseignement en Neurosciences criteria.
Licher et al. (2017)	Cognitive testing: MMSE and the Geriatric Mental Schedule organic level. Participants with a MMSE score under 26 or Geriatric Mental Schedule score over 0 underwent further investigation including the Cambridge Examination for Mental Disorders of the Elderly. Dementia diagnosis: DSM-III-R criteria. AD diagnosis: NINCDS–ADRDA criteria.

(Continued)

TABLE 5 | (Continued)

References	Cognitive assessment and/or diagnostic criteria
Ma et al. (2020)	Dementia diagnosis: Doctors diagnosed dementia or Alzheimer's disease reported by the participants who were capable of participating personally in the study. The adapted short-form Informant Questionnaire on Cognitive Decline in the Elderly was completed by an informant to compare the present functional and cognitive performance with the prior performance during the past 2 years. A threshold of 3.38 or more on the Informant Questionnaire on Cognitive Decline in the Elderly was used to define dementia. Third, records from the Hospital Episode Statistics were used to identify dementia patients.
Ng et al. (2008)	Cognitive testing: MMSE Poor cognitive performance: a total score of 23 or less on the MMSE.
Pellecchia et al. (2016)	Cognitive testing: Verbal Span, Trail Making Test and interference task of Stroop Color-Word Test, Rey's auditory verbal learning test, clock drawing test, Rey–Osterrieth complex figure test, phonological fluency task, frontal assessment battery, Benton judgment of line orientation test, and Constructional apraxia test and nouns and verbs denomination tasks. Parkinsonism was diagnosed by movement disorder specialists experienced in parkinsonian disorders. MCI diagnosis: Litvan et al. (2012) criteria.
Przybelski and Binkley (2007)	Cognitive testing: MMSE
Raszewski et al. (2016)	Cognitive testing: MMSE Dementia diagnosis: DSM-IV criteria AD diagnosis: NINCDS-ADRDA criteria
Rinaldi et al. (2003)	Cognitive testing: MMSE, Clock Drawing test, Babckock story recall, Auditory Verbal Learning test, Corsi Block Tapping test, Token test, Category Naming test, the Controlled Oral Word Association test, the Visual Search test, the Digit forward and backward test, the Raven's colored progressive matrices and the CDR scale. MCI diagnosis: Subjective complaint of defective memory, normal ADL, normal general cognitive functioning, abnormal memory for age as demonstrated by a performance of at least 1.5 SD below the age norm, absence of dementia and a CDR scale of 0.5. AD diagnosis: NINCDS-ADRDA criteria
Ruggiero et al. (2009)	Cognitive testing: MMSE. Those with a score over 26 points were considered as non-demented, while those with a score under 21 were considered as possibly demented and directly scheduled for the second-stage screening procedure. Participants with an MMSE score between 22 and 26 received additional neuropsychological testing using Word-Pairing Test (WAIS-R), Digit Test—Number Memory (WAIS-R) and the Caltagirone drawings. Dementia diagnosis: DSM-IV criteria.
Schmeidler et al. (2019)	Cognitive testing: Shipley Vocabulary, Similarities, TMT A and B, Letter Fluency, Boston Naming, Target Cancelation: Shapes and Letters and Word List: Delayed Recall, Immediate Recall, and Recognition.
Tien et al. (2019)	Cognitive testing: CDR scale, the 12-item memory test, modified 15-item Boston naming test, category verbal fluency test, forward and backward digit span test, and trail making A test. MCI diagnosis: established criteria by International Working Group on Mild Cognitive Impairment and Petersen (2004). AD diagnosis: National Institute on Aging-Alzheimer's Association criteria.
Toffanello et al. (2014)	Cognitive testing: MMSE Cognitive impairment was defined as scores under 24 in the MMSE. Cognitive decline was defined as a decline of 3 or more points at the follow up.
Velayudhan et al. (2012)	Cognitive testing: MMSE. Cognitive decline: Rapid cognitive decline was defined as a drop of 2 or more points over a period of 1 year on the MMSE scores. AD diagnosis: NINCDS- ADRDA criteria.
Wang et al. (2018)	Cognitive testing: MMSE. MCI diagnosis: Memory deterioration or other type of cognitive impairment confirmed by the MMSE, when basic cognitive functions were preserved, and subjects were not affected by any type of dementia.
Wilson et al. (2014)	Cognitive testing: 3MS and The Digit Symbol Substitution Test
Xue et al. (2017)	Cognitive testing: A list consisting of 10 Chinese words for immediate and delayed recall, orientation by recalling today's date, the day of the week and current season, numerical ability by a serial subtraction of 7 starting from 100 and drawing by reproducing a picture of two pentagons overlapped.
Zhang et al. (2018)	Cognitive testing: MMSE

NINCDS/ADRDA, National Institute of Neurological and Communicative Disorders and Stroke and the Alzheimer's disease and Related Disorders Association; WAIS-R, Wechsler Adult Intelligence Scale–Revised; WMS-R, Wechsler Memory Scale-Revised; WMS-III, Wechsler Memory Scale-Third Edition; SPMSQ, Pfeiffer Short Portable Mental State Questionnaire; ICD-10, International Classification of Diseases, 10th revision; CDR, Clinical Dementia Rating Scale; DSM-III, Diagnostic and Statistical Manual of Mental Disorders 3th edition; 3MS, the Modified Mini-Mental State; DSM-III-R, Diagnostic and Statistical Manual of Mental Disorders 3th edition revised; DSM-IV, Diagnostic and Statistical Manual of Mental Disorders 4th edition; TMT, Trail Making Test.

(Bourdel-Marchasson et al., 2001; Rinaldi et al., 2003). Rinaldi et al. (2003) also examined the associations with MCI, and found peripheral levels of antioxidants, such as UA, vitamin C, vitamin E, and vitamin A, were similarly lower in patients with MCI and AD compared to controls. The above presented findings from this study go a step further, given that the CI group presented the highest vitamin A levels, followed by the MCI group and finally the ACD group, so it appears that

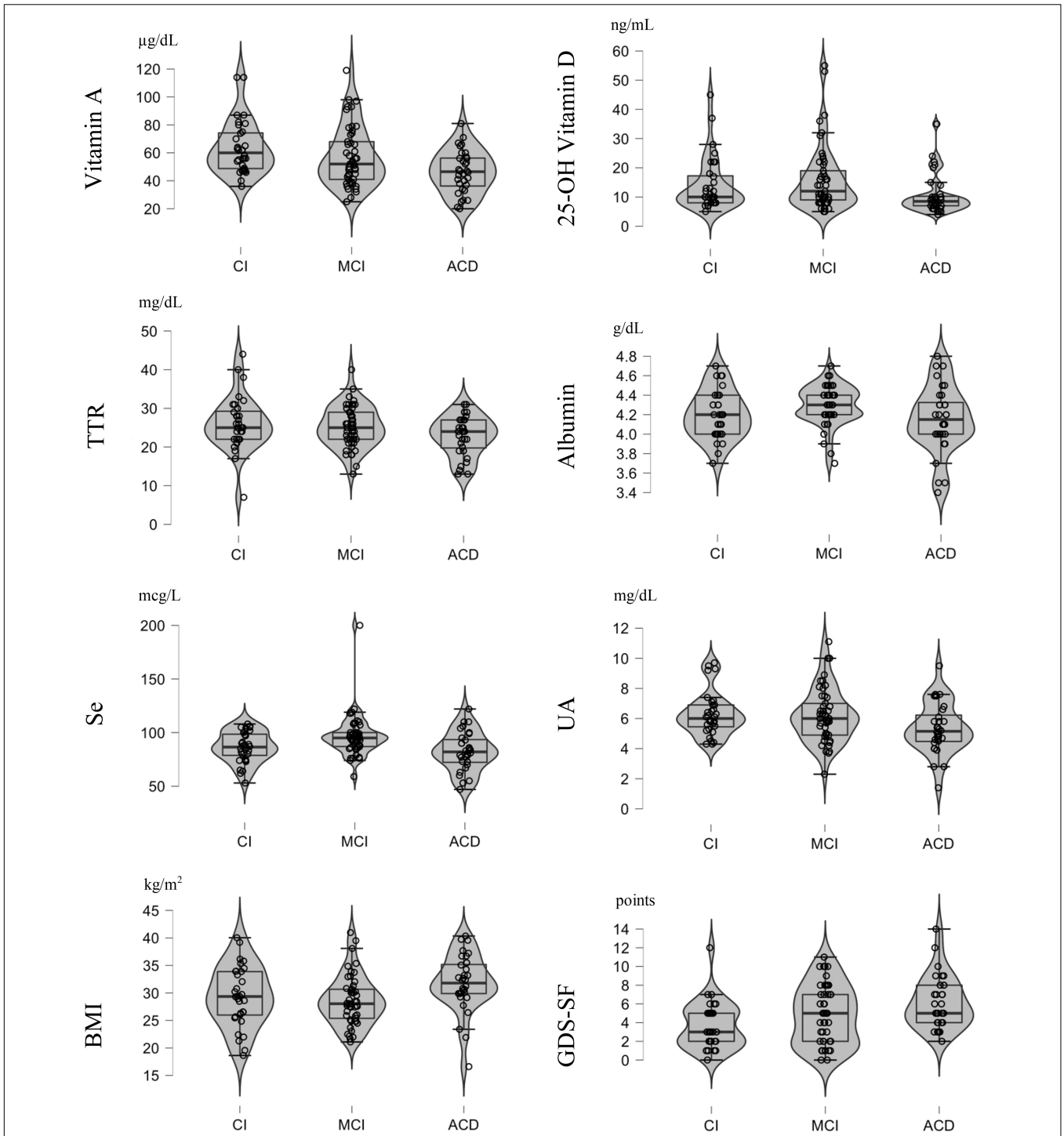

FIGURE 1 | Distribution graphs of the variables which achieved statistically significant differences across cognitive status groups (CI, Cognitively Intact; MCI, Middle Cognitive Impairment; ACD, All Cause Dementia).

CS decreases as vitamin A concentrations does (see **Table 3**). Bourdel-Marchasson et al. (2001) suggested that lower plasma retinol in well-nourished elderly AD patients compared to control subjects may mean that this antioxidant vitamin has been consumed by excessive free radical production and Rinaldi et al. (2003) propose that given that MCI may represent a prodromal stage for AD, and oxidative damage is one of the earliest pathophysiological events in AD, increasing antioxidant intake in patients with MCI could be beneficial to reduce the risk of progression to dementia.

Due to its anticholinesterase, antioxidant and anti-inflammatory potential, vitamin A has been shown to have a memory-restoring function in mice (Sodhi and Singh, 2013) and to inhibit the formation and extension of beta-amyloid fibrins (Ono and Yamada, 2012). Likewise, it has been reported that brain fluid or plasma concentrations of vitamin A and beta-carotene are lower in AD and that an increase in their concentrations has been shown to slow the progression of dementia, due to their antioxidant, cell-protective, and antiaggregatory effects in *in vitro* and *in vivo* models (Ono and Yamada, 2012). Conversely, in a recent study Koch et al. (2021) found no relationship between plasma concentrations of retinol, tocopherol and carotenoids among other antioxidants and the risk of mixed dementia, vascular dementia (VD) or AD. Further studies are needed to understand the relationships between vitamin A and cognition, especially in aging.

In the present study, higher serum 25-OH vitamin D concentrations were found in the groups with better CS and were associated with higher odds of belonging to the MCI group compared to the ACD group. This vitamin has received the most attention in the study of the association between its serum levels and cognitive functioning both in the elderly without impairment and in those with cognitive impairment or dementia, although a significant number of studies have only used measures of global cognitive screening or in combination with some test of attention or memory functions. Moreover, the results obtained are not free of divergences. Specifically, in non-impaired participants associations between higher 25-OH vitamin D levels and better cognitive function examined through global screening tests have been previously reported (Przybelski and Binkley, 2007; Annweiler et al., 2010a; Wilson et al., 2014) whereas studies having included global cognitive performance screening measures along with tests for specific cognitive domains have reported divergent results (**Table 5**). Thus, Jorde et al. (2015) found that performance in the MMSE and specific measures of memory, psychomotor speed, attention, and logical reasoning test improved with increasing serum 25-OH vitamin D, while Granic et al. (2015) found low and high season-specific 25-OH vitamin D quartiles to be associated with poorer performance compared with those participants in the middle quartiles in attention tasks. Concerning the association between 25-OH vitamin D and cognitive decline, MCI, or dementia the results indicate that lower levels are related to higher risk of cognitive decline (Toffanello et al., 2014; Wilson et al., 2014; Feart et al., 2017) and dementia (Licher et al., 2017), that MCI patients present lower mean serum 25OHD concentrations (Annweiler et al., 2012), and that older participants with vitamin D deficiency and insufficiency compared to those with vitamin D sufficiency, had double risk of all cause dementia (Feart et al., 2017). Conversely, Duchaine et al. (2020) did not find significant associations between 25-OH vitamin D and cognitive decline or dementia. Even found that higher 25-OH vitamin D levels were associated to increased risk of dementia and AD for women. Overall, the evidence collected through multiple systematic reviews and meta-analyses confirms the relationships between higher vitamin D levels and better cognitive performance or lower risk of cognitive impairment or dementia (Annweiler et al., 2009; Dickens et al., 2011; Van der Schaft et al., 2013; Goodwill and Szoeke, 2017; Sommer et al., 2017; Chai et al., 2019; Sultan et al., 2020). Vitamin D has been associated with many neurological functions, and its deficiency with neurological dysfunction (for a review see Annweiler et al., 2010b). Although there are a growing number of studies examining the relationships between vitamin D concentrations and different types of dementia, there are hardly any studies examining the differences between different cognitive statuses that have been classified according to the severity of cognitive impairment and the impact it causes in the activities of daily living, following established criteria after a comprehensive neuropsychological examination. The present results add further support to the well-established knowledge of the neuroprotective attributes of vitamin D (Kalueff and Tuohimaa, 2007; for a review see Buell and Dawson-Hughes, 2008).

Proteins

In our sample, higher levels of TTR were positively associated with better CS and with a higher likelihood of belonging to the CI group with respect to ACD. In agreement with the present results, previous studies have found that higher TTR levels were associated with better cognitive function. Araghi et al. (2021) found in participants at mean age 55 that higher global and specific-domain cognitive scores in memory, reasoning, and verbal fluency were linked with higher serum TTR. Also, in AD participants, lower plasma TTR levels were found when compared to non-demented controls (Han et al., 2011; Velayudhan et al., 2012). More specifically, Velayudhan et al. (2012) found that TTR levels were significantly lower in AD cases with rapid cognitive decline and with severe cognitive impairment and that TTR levels may additionally be predictive of subsequent cognitive decline. However, Araghi et al. (2021) failed to found such predictive properties. Conversely, a more recent study by Tien et al. (2019) found higher plasma TTR levels in MCI patients when compared to healthy participants, and even that higher plasma TTR was associated with the conversion from MCI to AD dementia.

Regarding albumin, higher concentrations were found in the groups with better CS (CI and MCI) and its levels were positively associated with a greater likelihood of belonging to the MCI group with respect to ACD. These findings are in the line of previous studies like Wang et al. (2018) who found that low serum albumin levels were associated with an increased risk of MCI. Ng et al. (2008) also found that poor cognitive performance increased with decreasing quintiles of albumin, and multivariate analyses showed that the lowest quintile of albumin was associated with a twofold increased risk of poorer cognitive performance, independent of other nutritional or risk factors. In the existent research on albumin concentrations and dementia, Kim et al. (2006) found significant reductions in albumin concentrations in AD patients compared to controls.

Finally, it should be emphasized that the majority of participants in the present study were within normal ranges for serum prealbumin and serum albumin levels. Since both proteins are considered markers of nutritional status (Smith, 2017; Keller, 2019), this is congruent with the results of the MNA-SF, which

also indicated that most participants had normal nutritional status (see **Table 3**).

Antioxidants

In this study, higher Se levels were found for the groups with better CS and were also associated with increased odds of belonging to MCI group with respect to ACD group. Although there are few studies on the relationship between Se concentrations and CS or cognitive impairment, these results are consistent with previous literature which indicates that serum Se levels are significantly lower in patients with dementia and in patients with cognitive impairment without dementia (Smorgon et al., 2004; Cardoso et al., 2014). In fact, it has been proposed that deficiency in Se may act as a risk factor for cognitive decline (Berr et al., 2012; Cardoso et al., 2014). Moreover, a systematic review conducted by Loef et al. (2011) found that there is still insufficient evidence for a role of Se in the treatment for AD, but that it may have a potential preventive relevance. The findings on this mineral may be explained by the antioxidant role that it plays for the central nervous system and other body tissues (Rahman, 2007; Mehdi et al., 2013; Cardoso et al., 2014).

Higher serum UA concentrations were found for the group with better CS and with greater odds of belonging to the CI and MCI groups with respect to the ACD group. These findings are in agreement with previous studies that have found lower serum UA levels in patients with MCI (Rinaldi et al., 2003; Xue et al., 2017), and that low UA concentrations can even act as a risk factor for MCI (Xue et al., 2017). Moreover, lower serum UA levels have been also related to VD (Xu et al., 2017) and AD (Rinaldi et al., 2003; Kim et al., 2006; Al-Khateeb et al., 2015; Boccardi et al., 2021). Low UA concentrations have been also found in patients with Parkinson's Disease (PD) (Wen et al., 2017; for a review see Schlesinger and Schlesinger, 2008) and are associated to worse cognitive performance (Annanmaki et al., 2008) and later occurrence of MCI in early PD stages (Pellecchia et al., 2016). However, other authors did not find serum UA levels to have a significant impact on the risk of dementia in PD (González-Aramburu et al., 2014). Some of these findings have been reported in a systematic review and meta-analysis by Khan et al. (2016) who concluded that serum UA was lower in patients with dementia, specifically, the associations were stronger with AD and Parkinson's Disease Dementia (PDD) than with VD. There is also evidence on the relationship between low serum concentrations of UA and increased risk of dementia. A recent systematic review and meta-analysis by Zhou et al. (2021) found low concentrations of UA to act as a potential risk factor for AD and PDD but not for VD. However, it has also been found evidence in the opposite direction and higher concentrations of UA have been associated with an increased likelihood of dementia. Latourte et al. (2018) found increased risk of dementia with higher serum UA levels, analyses by dementia subtypes showed stronger associations with mixed or VD than with AD dementia. Ruggiero et al. (2009) also found higher UA concentrations in persons affected by dementia. The present results would give support to the proposed antioxidant role of UA, which has been implied in reducing plasma oxidative stress, eliminating free radicals, and playing a preventive role against neurodegenerative processes (Tuven et al., 2017; for a review see Tana et al., 2018).

Body Mass Index

In our sample, the two groups with better CS (CI and MCI) had lower BMI compared with ACD group, whose mean values were within obesity range. Additionally, a lower BMI was also associated to increased odds of belonging to MCI group with respect to ACD group. These findings are in agreement with the results of a systematic review conducted by Gorospe and Dave (2007) where increased BMI was associated with an increased risk of dementia. Furthermore, a recent study conducted by Ma et al. (2020) found that having a higher body weight or abdominal obesity are associated with a higher incidence of dementia. There is also evidence related to specific cognitive functions. Poorer language and executive functions performance was associated with higher BMI in a sample of moderately old men, while relatively better performance was associated with higher BMI in the oldest-old (Schmeidler et al., 2019). Zhang et al. (2018) found that participants in the highest BMI quartile had highest mean MMSE scores, and the lowest mean MMSE scores were found in those classified in the lowest BMI quartile. Nevertheless, the findings on BMI have been generally inconsistent, as on a meta-analysis conducted by Danat et al. (2019) thirteen studies found an inverse association between dementia and BMI, while three studies showed a positive association.

The inconsistency of these findings could be due to comorbidity with other chronic conditions such as diabetes, differences between the populations studied (e.g., European, or Asian population), differences in sex and age, as well as body fat distribution. Several mechanisms have been proposed to explain the associations between obesity and impaired cognitive function, including inflammation, elevated leptin, insulin resistance, neuronal degradation, and impaired brain metabolism or blood flow (Nguyen et al., 2014; Anjum et al., 2018).

Inflammatory markers, such as high levels of CRP have been found in the obese, where increased brain atrophy, increased white matter hyperintensities, and decreased total gray matter brain volume have also been observed (Prickett et al., 2015). In the present study, inflammatory markers such as IL, TNF, and CRP were analyzed in all participants and no significant differences were found among CS groups. Other suggested mechanisms underlying the relation between CS and obesity are related to comorbidities, which are common among obese adults, such as insulin resistance and type 2 diabetes, hypertension, impaired glucose tolerance, and dyslipidemia (Miquel et al., 2018). Again, the present results did not show significant differences among CS groups in glucose, insulin, or parameters of lipid profile. Thereafter, the above referred possible relationship between obesity and inflammation or other comorbidities cannot be established in this study.

LIMITATIONS

The present study has some limitations. First, no significant differences were found between the CS groups in biochemical

variables that have been related to cognitive function in previous literature, such as vitamin B12, folate, glucose, cholesterol, or inflammatory markers. Second, associations between CS and nutritional status were examined in a cross-sectional design, which does not allow us to analyze the progression in CS of the participants. Third, given the cross-sectional design of the study, the main conclusion should be taken with caution. Finally, having included only institutionalized participants may make the present results less generalizable to the general population, but the study design emphasized the need to have more control of access to the population to obtain both CS and nutritional data in a more homogeneous setting.

CONCLUSION

To our knowledge, this is the first study to examine the relationships between cognitive and nutritional status by establishing the CS of the participants and classifying them into three groups based on the results obtained from a comprehensive neuropsychological examination comprising the main cognitive domains and assessment of ADLs following established clinical criteria, assessment of depressive symptomatology and including, to explore nutritional status, a wide variety of blood biomarkers, anthropometric measures, and a nutritional screening test.

From the present results it can be concluded that increased serum concentrations of vitamin A, vitamin D, TTR, albumin, Se and UA could act as a protective factor against cognitive impairment, whereas higher BMI could act as a risk factor. Ideally, future work should include large samples of institutionalized and independently living elderly, comprehensive neurocognitive screening and adequate assessment of nutritional status including multiple measures, as well as intervention and longitudinal designs to test the effects on cognitive function resulting from nutritional interventions and change over time.

DATA AVAILABILITY STATEMENT

The raw data supporting the conclusions of this article will be made available by the authors, without undue reservation.

ETHICS STATEMENT

The studies involving human participants were reviewed and approved by the Central Ethics and Research Committee of Galicia Autonomous Community (2017/542). The patients/participants provided their written informed consent to participate in this study.

REST OF THE MEMBERS OF NUTRIAGE STUDY RESEARCHERS

Melchor Fernández, Carlos Dieguez, Lucía Gayoso, Lourdes Vázquez Oderiz, Ángeles Romero, and Nicolás Piedrafita.

AUTHOR CONTRIBUTIONS

ML performed the cognitive status assessment in all participants. ML and EA analyzed, interpreted the data, and wrote the manuscript. ML, MR, EA, and PP-Á designed the study, and collected and interpreted the data. LF, CA, ML, EA, and PP-Á designed the data analyses. RL and M-ÁM-O supervised the collection and analysis of nutritional data, and critically reviewed the manuscript. Melchor Fernández, Carlos Dieguez, Lucía Gayoso, Lourdes Vázquez Oderiz, Ángeles Romero, and Nicolás Piedrafita involved in the design, data collection and funding management of the NUTRIAGE study. All authors contributed to the article and approved the submitted version.

FUNDING

NUTRIAGE (0359_NUTRIAGE_1_E) was a research project 75% co-financed by the Interreg V-A Spain-Portugal Program (POCTEP) 2014–2020 through the European Regional Development Fund (ERDF) of the European Union.

ACKNOWLEDGMENTS

We thank the participants for their collaboration, as well as the management of the nursing homes and their workers who facilitated the organization of the participants and the collection of data.

REFERENCES

Al-Khateeb, E., Althaher, A., Al-Khateeb, M., Al-Musawi, H., Azzouqah, O., Al-Shweiki, S., et al. (2015). Relation between uric acid and Alzheimer's disease in elderly Jordanians. *J. Alzheimers Dis.* 44, 859–865. doi: 10.3233/JAD-142037

American Psychiatric Association (2013). *Diagnostic and Statistical Manual of Mental Disorders*, 5th Edn. Washington, DC: American Psychiatric Association.

Anjum, I., Fayyaz, M., Wajid, A., Sohail, W., and Ali, A. (2018). Does obesity increase the risk of dementia: a literature review. *Cureus* 10:e2660. doi: 10.7759/cureus.2660

Annanmaki, T., Pessala-Driver, A., Hokkanen, L., and Murros, K. (2008). Uric acid associates with cognition in Parkinson's disease. *Parkinsonism Relat. Disord.* 14, 576–578. doi: 10.1016/j.parkreldis.2007.11.001

Annweiler, C., Allali, G., Allain, P., Bridenbaugh, S., Schott, A. M., Kressig, R. W., et al. (2009). Vitamin D and cognitive performance in adults: a systematic review. *Eur. J. Neurol.* 16, 1083–1089. doi: 10.1111/j.1468-1331.2009.02755.x

Annweiler, C., Fantino, B., Schott, A. M., Krolak-Salmon, P., Allali, G., and Beauchet, O. (2012). Vitamin D insufficiency and mild cognitive impairment: cross-sectional association. *Eur. J. Neurol.* 19, 1023–1029. doi: 10.1111/j.1468-1331.2012.03675.x

Annweiler, C., Schott, A. M., Allali, G., Bridenbaugh, S. A., Kressig, R. W., Allain, P., et al. (2010a). Association of vitamin D deficiency with cognitive impairment in older women: cross-sectional study. *Neurology* 74, 27–32. doi: 10.1212/WNL.0b013e3181beecd3

Annweiler, C., Schott, A. M., Berrut, G., Chauviré, V., Le, Gall D, Inzitari, M., et al. (2010b). Vitamin D and ageing: neurological issues. *Neuropsychobiology* 62, 139–150. doi: 10.1159/000318570

Araghi, M., Shipley, M. J., Anand, A., Mills, N. L., Kivimaki, M., Singh-Manoux, A., et al. (2021). Serum transthyretin and risk of cognitive decline and dementia: 22-year longitudinal study. *Neurol. Sci.* 42, 5093–5100. doi: 10.1007/s10072-021-05191-5

Artiola, L., Hermosillo, D., Heaton, R., and Pardee, R. E. (1999). *Manual de Normas y Procedimientos Para la Batería Neuropsicológica en Español*. Tucson, AZ: m Press.

Berr, C., Arnaud, J., and Akbaraly, T. N. (2012). Selenium and cognitive impairment: a brief-review based on results from the EVA study. *BioFactors* 38, 139–144. doi: 10.1002/biof.1003

Boccardi, V., Carino, S., Marinelli, E., Lapenna, M., Caironi, G., Bianco, A. R., et al. (2021). Uric acid and late-onset Alzheimer's disease: results from the ReGAl 2.0 project. *Aging Clin. Exp. Res.* 33, 361–366. doi: 10.1007/s40520-020-01541-z

Borkowski, J. G., Benton, A. L., and Spreen, O. (1967). Word fluency and brain damage. *Neuropsychologia* 5, 135–140. doi: 10.1016/0028-3932(67)90015-2

Bourdel-Marchasson, I., Delmas-Beauviex, M. C., Peuchant, E., Richard-Harston, S., Decamps, A., Reigneir, B., et al. (2001). Antioxidant defences and oxidative stress markers in erythrocytes and plasma from normally nourished elderly Alzheimer patients. *Age Ageing* 30, 235–241. doi: 10.1093/ageing/30.3.235

Buell, J. S., and Dawson-Hughes, B. (2008). Vitamin D and neurocognitive dysfunction: preventing "D"ecline? *Mol. Aspects Med.* 29, 415–422. doi: 10.1016/j.mam.2008.05.001

Cardoso, B., Silva Bandeira, V., Jacob-Filho, W., and Franciscato Cozzolino, S. M. (2014). Selenium status in elderly: relation to cognitive decline. *J. Trace Elements Med. Biol.* 28, 422–426. doi: 10.1016/j.jtemb.2014.08.009

Cardoso, B. R., Ong, T. P., Jacob-Filho, W., Jaluul, O., Freitas, M. I. D. Á, and Cozzolino, S. M. F. (2010). Nutritional status of selenium in Alzheimer's disease patients. *Br. J. Nutr.* 103, 803–806. doi: 10.1017/S0007114509992832

Carratu, M., Marasco, C., Signorile, A., Scuderi, C., and Steardo, L. (2015). Are retinoids a promise for Alzheimer's disease management? *Curr. Med. Chem.* 19, 6119–6125. doi: 10.2174/0929867311209066119

Chai, B., Gao, F., Wu, R., Dong, T., Gu, C., Lin, Q., et al. (2019). Vitamin D deficiency as a risk factor for dementia and Alzheimer's disease: an updated meta-analysis. *BMC Neurol.* 19:284. doi: 10.1186/s12883-019-1500-6

Crichton, G. E., Elias, M. F., Davey, A., Sullivan, K. J., and Robbins, M. A. (2014). Higher HDL cholesterol is associated with better cognitive function: the maine-syracuse study. *J. Int. Neuropsychol. Soc.* 29, 961–970. doi: 10.1017/S1355617714000885

Croisile, B., Auriacombe, S., Etcharry-Bouyx, F., and Vercelletto, M. (2012). The new 2011 recommendations of the National Institute on Aging and the Alzheimer's Association on diagnostic guidelines for Alzheimer's disease: preclinal stages, mild cognitive impairment, and dementia. *Rev. Neurol.* 168, 471–482. doi: 10.1016/j.neurol.2011.11.007

Cuajungco, M. P., and Fagét, K. Y. (2003). Zinc takes the center stage: its paradoxical role in Alzheimer's disease. *Brain Res. Rev.* 41, 44–56. doi: 10.1016/S0165-0173(02)00219-9

Danat, I. M., Clifford, A., Partridge, M., Zhou, W., Bakre, A. T., Chen, A., et al. (2019). Impacts of overweight and obesity in older age on the risk of dementia: a systematic literature review and a meta-analysis. *J. Alzheimers Dis.* 70, 87–99. doi: 10.3233/JAD-180763

D'Elia, L., Satz, P., Uchiyama, C. L., and White, T. (1996). *PAR | CTT | Color Trails Test. Color Trails Test*. Available online at: https://www.parinc.com/Products/Pkey/77 (accessed 2022).

Dickens, A. P., Lang, I. A., Langa, K. M., Kos, K., and Llewellyn, D. J. (2011). Vitamin D, cognitive dysfunction and dementia in older adults. *CNS Drugs* 25, 629–639. doi: 10.2165/11593080-000000000-00000

Duchaine, C. S., Talbot, D., Nafti, M., Giguère, Y., Dodin, S., Tourigny, A., et al. (2020). Vitamin D status, cognitive decline and incident dementia: the Canadian Study of Health and Aging. *Can. J. Public Health* 111, 312–321. doi: 10.17269/s41997-019-00290-5

Dye, L., Boyle, N. B., Champ, C., and Lawton, C. (2017). The relationship between obesity and cognitive health and decline. *Proc. Nutr. Soc.* 76, 443–454. doi: 10.1017/S0029665117002014

Elias, M. F., Robbins, M. A., Budge, M. M., Elias, P. K., Brennan, S. L., Johnston, C., et al. (2006). Homocysteine, folate, and vitamins B6 and B12 blood levels in relation to cognitive performance: the Maine-Syracuse study. *Psychosom. Med.* 68, 547–554. doi: 10.1097/01.psy.0000221380.92521.51

Feart, C., Helmer, C., Merle, B., Herrmann, F. R., Annweiler, C., Dartigues, J. F., et al. (2017). Associations of lower vitamin D concentrations with cognitive decline and long-term risk of dementia and Alzheimer's disease in older adults. *Alzheimers Dement.* 13, 1207–1216. doi: 10.1016/j.jalz.2017.03.003

Folstein, M. F., Folstein, S. E., and McHugh, P. R. (1975). Mini-mental state. A practical method for grading the cognitive state of patients for the clinician. *J. Psychiatr. Res.* 12, 189–198. doi: 10.1016/0022-3956(75)90026-6

Gamaldo, A. A., Ferrucci, L., Rifkind, J., Longo, D. L., and Zonderman, A. B. (2013). Relationship between mean corpuscular volume and cognitive performance in older adults. *J. Am. Geriatr. Soc.* 61, 84–89. doi: 10.1111/jgs.12066

Ganguli, M., Du, Y., Dodge, H. H., Ratcliff, G. G., and Chang, C. C. H. (2006). Depressive symptoms and cognitive decline in late life: a prospective epidemiological study. *Arch. Gen. Psychiatry* 63, 153–160. doi: 10.1001/archpsyc.63.2.153

Godin, O., Dufouil, C., Ritchie, K., Dartigues, J. F., Tzourio, C., Pérès, K., et al. (2007). Depressive symptoms, major depressive episode and cognition in the elderly: the three-city study. *Neuroepidemiology* 28, 101–108. doi: 10.1159/000101508

González-Aramburu, I., Sánchez-Juan, P., Sierra, M., Fernández-Juan, E., Sánchez-Quintana, C., Berciano, J., et al. (2014). Serum uric acid and risk of dementia in Parkinson's disease. *Parkinsonism Relat. Disord.* 20, 637–639. doi: 10.1016/j.parkreldis.2014.02.023

Goodman, A. B. (2006). Retinoid receptors, transporters, and metabolizers as therapeutic targets in late onset Alzheimer disease. *J. Cell. Physiol.* 209, 598–603. doi: 10.1002/jcp.20784

Goodman, A. B., and Pardee, A. B. (2003). Evidence for defective retinoid transport and function in late onset Alzheimer's disease. *Proc. Natl. Acad. Sci. U.S.A.* 100, 2901–2905. doi: 10.1073/pnas.0437937100

Goodwill, A. M., Campbell, S., Simpson, S., Bisignano, M., Chiang, C., Dennerstein, L., et al. (2018). Vitamin D status is associated with executive function a decade later: data from the Women's Healthy Ageing Project. *Maturitas* 107, 56–62. doi: 10.1016/j.maturitas.2017.10.005

Goodwill, A. M., and Szoeke, C. (2017). A Systematic review and meta-analysis of the effect of low Vitamin D on cognition. *J. Am. Geriatr. Soc.* 65, 2161–2168. doi: 10.1111/jgs.15012

Gorelick, P. B. (2010). Role of inflammation in cognitive impairment: results of observational epidemiological studies and clinical trials. *Ann. N. Y. Acad. Sci.* 1207, 155–162. doi: 10.1111/j.1749-6632.2010.05726.x

Gorospe, E. C., and Dave, J. K. (2007). The risk of dementia with increased body mass index. *Age Ageing* 36, 23–29. doi: 10.1093/ageing/afl123

Granic, A., Hill, T. R., Kirkwood, T. B. L., Davies, K., Collerton, J., Martin-Ruiz, C., et al. (2015). Serum 25-hydroxyvitamin D and cognitive decline in the very old: the Newcastle 85+ study. *Eur. J. Neurol.* 22, 106–115. doi: 10.1111/ene.12539

Han, S. H., Jung, E. S., Sohn, J. H., Hong, H. J., Hong, H. S., Kim, J. W., et al. (2011). Human serum transthyretin levels correlate inversely with Alzheimer's disease. *J. Alzheimers Dis.* 25, 77–84. doi: 10.3233/JAD-2011-102145

Huang, C. Q., Wang, Z. R., Li, Y. H., Xie, Y. Z., and Liu, Q. X. (2011). Cognitive function and risk for depression in old age: a meta-analysis of published literature. *Int. Psychogeriatr.* 23, 516–525. doi: 10.1017/S1041610210000049

Jorde, R., Mathiesen, E. B., Rogne, S., Wilsgaard, T., Kjærgaard, M., Grimnes, G., et al. (2015). Vitamin D and cognitive function: the tromsø study. *J. Neurol. Sci.* 355, 155–161. doi: 10.1016/j.jns.2015.06.009

Kaiser, M. J., Bauer, J. M., Ramsch, C., Uter, W., Guigoz, Y., Cederholm, T., et al. (2009). Validation of the Mini Nutritional Assessment short-form (MNA§-SF): a practical tool for identification of nutritional status. *J. Nutr. Health Aging* 13, 782–788. doi: 10.1007/s12603-009-0214-7

Kalueff, A. V., and Tuohimaa, P. (2007). Neurosteroid hormone Vitamin D and its utility in clinical nutrition. *Curr. Opin. Clin. Nutr. Metab. Care* 10, 12–19. doi: 10.1097/MCO.0b013e328010ca18

Kang, J. H., Irizarry, M. C., and Grodstein, F. (2006). Prospective study of plasma folate, Vitamin B12, and cognitive function and decline. *Epidemiology* 17, 650–657. doi: 10.1097/01.ede.0000239727.59575.da

Keller, U. (2019). Nutritional laboratory markers in malnutrition. *J. Clin. Med.* 8:775. doi: 10.3390/jcm8060775

Khan, A. A., Quinn, T. J., Hewitt, J., Fan, Y., and Dawson, J. (2016). Serum uric acid level and association with cognitive impairment and dementia: systematic review and meta-analysis. *Age* 38:16. doi: 10.1007/s11357-016-9871-8

Kim, T. S., Pae, C. U., Yoon, S. J., Jang, W. Y., Lee, N. J., Kim, J. J., et al. (2006). Decreased plasma antioxidants in patients with Alzheimer's disease. *Int. J. Geriatr. Psychiatry* 21, 344–348. doi: 10.1002/gps.1469

Klímová, B., and Vališ, M. (2018). Nutritional interventions as beneficial strategies to delay cognitive decline in healthy older individuals. *Nutrients* 10:905. doi: 10.3390/nu10070905

Koch, M., Furtado, J. D., Cronjé, H. T., DeKosky, S. T., Fitzpatrick, A. L., Lopez, O. L., et al. (2021). Plasma antioxidants and risk of dementia in older adults. *Alzheimers Dement.* 7:e12208. doi: 10.1002/trc2.12208

Korol, D. L., and Gold, P. E. (1998). Glucose, memory, and aging. *Am. J. Clin. Nutr.* 67, 764S–771S. doi: 10.1093/ajcn/67.4.764S

Koyama, A., O'Brien, J., Weuve, J., Blacker, D., Metti, A. L., and Yaffe, K. (2013). The role of peripheral inflammatory markers in dementia and Alzheimer's disease: a meta-analysis. *J. Gerontol. Ser. A Biol. Sci. Med. Sci.* 68, 433–440. doi: 10.1093/gerona/gls187

Kueider, A. M., Tanaka, T., An, Y., Kitner-Triolo, M. H., Palchamy, E., Ferrucci, L., et al. (2016). State and trait-dependent associations of Vitamin-D with brain function during aging. *Neurobiol. Aging* 39, 38–45. doi: 10.1016/j.neurobiolaging.2015.11.002.State

Lam, P. K., Kritz-Silverstein, D., Barrett-Connor, E., Milne, D., Nielsen, F., Gamst, A., et al. (2008). Plasma trace elements and cognitive function in older men and women: the Rancho Bernardo study. *J. Nutr. Health Aging* 12, 22–27. doi: 10.1007/BF02982160

Latourte, A., Soumaré, A., Bardin, T., Perez-Ruiz, F., Debette, S., and Richette, P. (2018). Uric acid and incident dementia over 12 years of follow-up: a population-based cohort study. *Ann. Rheum. Dis.* 77, 328–335. doi: 10.1136/annrheumdis-2016-210767

Lawton, M. P., and Brody, E. M. (1969). Assessment of older people: self-maintaining and instrumental activities of daily living. *Gerontologist* 9, 179–186. doi: 10.1093/geront/9.3_part_1.179

Lee, H. P., Casadesus, G., Zhu, X., Lee, H. G., Perry, G., Smith, M. A., et al. (2009). All-trans retinoic acid as a novel therapeutic strategy for Alzheimer's disease. *Expert Rev. Neurotherap.* 9, 1615–1621. doi: 10.1586/ern.09.86

Lee, Y. B., Han, K., Park, S., Kim, S. M., Kim, N. H., Choi, K. M., et al. (2020). Gamma-glutamyl transferase variability and risk of dementia: a nationwide study. *Int. J. Geriatr. Psychiatry* 35, 1105–1114. doi: 10.1002/gps.5332

Licher, S., De Bruijn, R. F. A. G., Wolters, F. J., Zillikens, M. C., Ikram, M. A., and Ikram, M. K. (2017). Vitamin D and the risk of dementia: the rotterdam study. *J. Alzheimers Dis.* 60, 989–997. doi: 10.3233/JAD-170407

Lim, A., Krajina, K., and Marsland, A. L. (2013). Peripheral inflammation and cognitive aging. *Inflamm. Psychiatry* 28, 175–187. doi: 10.1159/000346362

Litvan, I., Goldman, J. G., Tröster, A. I., Schmand, B. A., Weintraub, D., Petersen, R. C., et al. (2012). Diagnostic criteria for mild cognitive impairment in Parkinson's disease: movement disorder society task force guidelines. *Mov. Disord.* 27, 349–356. doi: 10.1002/mds.24893

Loef, M., Schrauzer, G. N., and Walach, H. (2011). Selenium and Alzheimer's disease: a systematic review. *J. Alzheimers Dis.* 26, 81–104. doi: 10.3233/JAD-2011-110414

Luppino, F. S., De Wit, L. M., Bouvy, P. F., Stijnen, T., Cuijpers, P., Penninx, B. W. J. H., et al. (2010). Overweight, obesity, and depression: a systematic review and meta-analysis of longitudinal studies. *Arch. Gen. Psychiatry* 67, 220–229. doi: 10.1001/archgenpsychiatry.2010.2

Lv, Y. B., Yin, Z. X., Chei, C. L., Brasher, M. S., Zhang, J., Kraus, V. B., et al. (2016). Serum cholesterol levels within the high normal range are associated with better cognitive performance among Chinese elderly. *J. Nutr. Health Aging* 20, 280–287. doi: 10.1007/s12603-016-0701-6

Ma, C., Yin, Z., Zhu, P., Luo, J., Shi, X., and Gao, X. (2017). Blood cholesterol in late-life and cognitive decline: a longitudinal study of the Chinese elderly. *Mol. Neurodegener.* 12:24. doi: 10.1186/s13024-017-0167-y

Ma, Y., Ajnakina, O., Steptoe, A., and Cadar, D. (2020). Higher risk of dementia in English older individuals who are overweight or obese. *Int. J. Epidemiol.* 49, 1353–1365. doi: 10.1093/ije/dyaa099

Mahoney, F. I., and Barthel, D. (1965). Functional evaluation: the Barthel Index. *Maryland State Med. J.* 14, 56–61.

Malaspina, A., and Michael-Titus, A. T. (2008). Is the modulation of retinoid and retinoid-associated signaling a future therapeutic strategy in neurological trauma and neurodegeneration? *J. Neurochem.* 104, 584–595. doi: 10.1111/j.1471-4159.2007.05071.x

Malnutrition Advisory Group [MAG] (2003). *The "MUST" Explanatory Booklet*. Manchester: MAG.

McAfoose, J., and Baune, B. T. (2009). Evidence for a cytokine model of cognitive function. *Neurosci. Biobehav. Rev.* 33, 355–366. doi: 10.1016/j.neubiorev.2008.10.005

McKhann, G. M., Knopman, D. S., Chertkow, H., Hyman, B. T., Jack, C. R., Kawas, C. H., et al. (2011). The diagnosis of dementia due to Alzheimer's disease: recommendations from the National Institute on Aging-Alzheimer's Association workgroups on diagnostic guidelines for Alzheimer's disease. *Alzheimers Dement.* 7, 263–269. doi: 10.1016/j.jalz.2011.03.005

Mehdi, Y., Hornick, J. L., Istasse, L., and Dufrasne, I. (2013). Selenium in the environment, metabolism and involvement in body functions. *Molecules* 18, 3292–3311. doi: 10.3390/molecules18033292

Michaud, M., Balardy, L., Moulis, G., Gaudin, C., Peyrot, C., Vellas, B., et al. (2013). Proinflammatory cytokines, aging, and age-related diseases. *J. Am. Med. Direct. Assoc.* 14, 877–882. doi: 10.1016/j.jamda.2013.05.009

Michelakos, T., Kousoulis, A. A., Katsiardanis, K., Dessypris, N., Anastasiou, A., Katsiardani, K. P., et al. (2013). Serum folate and B12 levels in association with cognitive impairment among seniors: results from the VELESTINO study in greece and meta-analysis. *J. Aging Health* 25, 589–616. doi: 10.1177/0898264313482488

Miquel, S., Champ, C., Day, J., Aarts, E., Bahr, B. A., Bakker, M., et al. (2018). Poor cognitive ageing: vulnerabilities, mechanisms and the impact of nutritional interventions. *Ageing Res. Rev.* 42, 40–55. doi: 10.1016/j.arr.2017.12.004

Moore, E. M., Ames, D., Mander, A. G., Carne, R. P., Brodaty, H., Woodward, M. C., et al. (2014). Among vitamin B12 deficient older people, high folate levels are associated with worse cognitive function: combined data from three cohorts. *J. Alzheimers Dis.* 39, 661–668. doi: 10.3233/JAD-131265

Nettiksimmons, J., Ayonayon, H., Harris, T., Phillips, C., Rosano, C., Satterfield, S., et al. (2015). Development and validation of risk index for cognitive decline using blood-derived markers. *Neurology* 84, 696–702. doi: 10.1212/WNL.0000000000001263

Ng, T. P., Feng, L., Niti, M., and Yap, K. B. (2008). Albumin, haemoglobin, BMI and cognitive performance in older adults. *Age Ageing* 37, 423–429. doi: 10.1093/ageing/afn102

Nguyen, J. C. D., Killcross, A. S., and Jenkins, T. A. (2014). Obesity and cognitive decline: role of inflammation and vascular changes. *Front. Neurosci.* 8:375. doi: 10.3389/fnins.2014.00375

Nho, K., Kueider-Paisley, A., Ahmad, S., Mahmoudiandehkordi, S., Arnold, M., Risacher, S. L., et al. (2019). Association of altered liver enzymes with Alzheimer disease diagnosis, cognition, neuroimaging measures, and cerebrospinal fluid biomarkers. *JAMA Netw. Open* 2, 1–20. doi: 10.1001/jamanetworkopen.2019.7978

Noh, J. W., Kwon, Y. D., Park, J., and Kim, J. (2015). Body mass index and depressive symptoms in middle aged and older adults. *BMC Public Health* 15:310. doi: 10.1186/s12889-015-1663-z

Nuttall, J. R., and Oteiza, P. I. (2014). Zinc and the aging brain. *Genes Nutr.* 9:379. doi: 10.1007/s12263-013-0379-x

O'Bryant, S. E., Xiao, G., Barber, R., Reisch, J., Doody, R., Fairchild, T., et al. (2010). A serum protein-based algorithm for the detection of Alzheimer disease. *Arch. Neurol.* 67, 1077–1081. doi: 10.1001/archneurol.2010.215

O'Leary, F., Allman-Farinelli, M., and Samman, S. (2012). Vitamin B12 status, cognitive decline and dementia: a systematic review of prospective cohort studies. *Br. J. Nutr.* 108, 1948–1961. doi: 10.1017/S0007114512004175

Olson, C. R., and Mello, C. V. (2010). Significance of Vitamin A to brain function, behavior and learning. *Mol. Nutr. Food Res.* 54, 489–495. doi: 10.1002/mnfr.200900246

Onem, Y., Terekeci, H., Kucukardali, Y., Sahan, B., Solmazgül, E., Şenol, M. G., et al. (2010). Albumin, hemoglobin, body mass index, cognitive and functional performance in elderly persons living in nursing homes. *Arch. Gerontol. Geriatr.* 50, 56–59. doi: 10.1016/j.archger.2009.01.010

Ono, K., and Yamada, M. (2012). Vitamin A and Alzheimer's disease. *Geriatr. Gerontol. Int.* 12, 180–188. doi: 10.1111/j.1447-0594.2011.00786.x

Ownby, R. L. (2010). Neuroinflammation and cognitive aging. *Curr. Psychiatry Rep.* 12, 39–45. doi: 10.1007/s11920-009-0082-1

Pellecchia, M. T., Savastano, R., Moccia, M., Picillo, M., Siano, P., Erro, R., et al. (2016). Lower serum uric acid is associated with mild cognitive impairment

in early Parkinson's disease: a 4-year follow-up study. *J. Neural Trans.* 123, 1399–1402. doi: 10.1007/s00702-016-1622-6

Petersen, M., Hall, J., Parsons, T., Johnson, L., and O'Bryant, S. (2020). Combining select blood-based biomarkers with neuropsychological assessment to detect mild cognitive impairment among Mexican Americans. *J. Alzheimers Dis.* 75, 739–750. doi: 10.3233/JAD-191264

Petersen, R. C. (2004). Mild cognitive impairment as a diagnostic entity. *J. Intern. Med.* 256, 183–194. doi: 10.1111/j.1365-2796.2004.01388.x

Power, R., Prado-Cabrero, A., Mulcahy, R., Howard, A., and Nolan, J. M. (2019). The role of nutrition for the aging population: implications for cognition and Alzheimer's disease. *Annu. Rev. Food Sci. Technol.* 10, 619–639. doi: 10.1146/annurev-food-030216-030125

Prickett, C., Brennan, L., and Stolwyk, R. (2015). Examining the relationship between obesity and cognitive function: a systematic literature review. *Obes. Res. Clin. Pract.* 9, 93–113. doi: 10.1016/j.orcp.2014.05.001

Przybelski, R. J., and Binkley, N. C. (2007). Is vitamin D important for preserving cognition? A positive correlation of serum 25-hydroxyvitamin D concentration with cognitive function. *Arch. Biochem. Biophys.* 460, 202–205. doi: 10.1016/j.abb.2006.12.018

Rabensteiner, J., Hofer, E., Fauler, G., Fritz-Petrin, E., Benke, T., Dal-Bianco, P., et al. (2020). The impact of folate and vitamin B12 status on cognitive function and brain atrophy in healthy elderly and demented Austrians, a retrospective cohort study. *Aging* 12, 15478–15491. doi: 10.18632/aging.103714

Rahman, K. (2007). Studies on free radicals, antioxidants, and co-factors. *Clin. Interv. Aging* 2, 219–236.

Raszewski, G., Chwedorowicz, R., Chwedorowicz, A., and Rothenberg, K. G. (2016). Homocysteine, antioxidant vitamins and lipids as biomarkers of neurodegeneration in Alzheimer's disease versus non-Alzheimer's dementia. *Ann. Agric. Environ. Med.* 23, 193–196. doi: 10.5604/12321966.1196878

Ray, S., Britschgi, M., Herbert, C., Takeda-Uchimura, Y., Boxer, A., Blennow, K., et al. (2007). Classification and prediction of clinical Alzheimer's diagnosis based on plasma signaling proteins. *Nat. Med.* 13, 1359–1362. doi: 10.1038/nm1653

Rey, A. (1941). L'examen psychologique dans les cas d'encéphalopathie traumatique. *Arch. Psychol.* 28, 286–340.

Rey, A. (1964). *L'examen Clinique en Psychologie*. Paris: Presse Universitaires de France.

Rinaldi, P., Polidori, M. C., Metastasio, A., Mariani, E., Mattioli, P., Cherubini, A., et al. (2003). Plasma antioxidants are similarly depleted in mild cognitive impairment and in Alzheimer's disease. *Neurobiol. Aging* 24, 915–919. doi: 10.1016/S0197-4580(03)00031-9

Robles, A., Del Ser, T., Alom, J., Peña-Casanova, J., Barquero, M. S., Bermejo, F., et al. (2002). Propuesta de criterios para el diagnóstico clínico del deterioro cognitivo ligero, la demencia y la enfermedad de Alzheimer. *Neurologia* 17, 17–32.

Rosenberg, I. H. (2008). Effects of folate and vitamin B12 on cognitive function in adults and the elderly. *Food Nutr. Bull.* 29(2 Suppl), S132–S142. doi: 10.1177/15648265080292s118

Rubenstein, L. Z., Harker, J. O., Salvà, A., Guigoz, Y., and Vellas, B. (2001). Screening for undernutrition in geriatric practice: developing the Short-Form Mini-Nutritional Assessment (MNA-SF). *J. Gerontol. Ser. A Biol. Sci. Med. Sci.* 56, 366–372. doi: 10.1093/gerona/56.6.M366

Ruggiero, C., Cherubini, A., Lauretani, F., Bandinelli, S., Maggio, M., Di Iorio, A., et al. (2009). Uric acid and dementia in community-dwelling older persons. *Dement. Geriatr. Cogn. Disord.* 27, 382–389. doi: 10.1159/000210040

Sautin, Y. Y., and Johnson, R. J. (2008). Uric acid: the oxidant-antioxidant paradox. *Nucl. Nucl. Nucleic Acids* 27, 608–619. doi: 10.1080/15257770802138558

Schlesinger, I., and Schlesinger, N. (2008). Uric acid in Parkinson's disease. *Mov. Disord.* 23, 1653–1657. doi: 10.1002/mds.22139

Schlögl, M., and Holick, M. F. (2014). Vitamin D and neurocognitive function. *Clin. Interv. Aging* 9, 559–568. doi: 10.2147/CIA.S51785

Schmeidler, J., Mastrogiacomo, C. N., Beeri, M. S., Rosendorff, C., and Silverman, J. M. (2019). Distinct age-related associations for body mass index and cognition in cognitively healthy very old veterans. *Int. Psychogeriatr.* 31, 895–899. doi: 10.1017/S1041610218001412

Schram, M. T., Trompet, S., Kamper, A. M., De Craen, A. J. M., Hofman, A., Euser, S. M., et al. (2007). Serum calcium and cognitive function in old age. *J. Am. Geriatr. Soc.* 55, 1786–1792. doi: 10.1111/j.1532-5415.2007.01418.x

Seamans, K. M., Hill, T. R., Scully, L., Meunier, N., Andrillo-Sanchez, M., Polito, A., et al. (2010). Vitamin D status and measures of cognitive function in healthy older European adults. *Eur. J. Clin. Nutr.* 64, 1172–1178. doi: 10.1038/ejcn.2010.117

Sedó, M. (2007). *Test de los Cinco Dígitos*. Available online at: http://web.teaediciones.com (accessed 2022).

Seetharaman, S., Andel, R., McEvoy, C., Aslan, A. K. D., Finkel, D., and Pedersen, N. L. (2015). Blood glucose, diet-based glycemic load and cognitive aging among dementia-free older adults. *J. Gerontol. Ser. A Biol. Sci. Med. Sci.* 70, 471–479. doi: 10.1093/gerona/glu135

Serdarevic, N., Stanciu, A. E., Begic, L., and Uncanin, S. (2020). Serum Uric Acid Concentration in Patients with Cerebrovascular Disease (Ischemic Stroke and Vascular Dementia). *Med. Arch. (Sarajevo, Bosnia and Herzegovina)* 74, 95–99. doi: 10.5455/medarh.2020.74.95-99

Sheikh, J. I., and Yesavage, J. A. (1986). Geriatric Depression Scale (GDS): recent evidence and development of a shorter version. *Clin. Gerontol.* 5, 165–173. doi: 10.1300/J018v05n01_09

Smith, S. H. (2017). Using albumin and prealbumin to assess nutritional status. *Nursing* 47, 65–66. doi: 10.1097/01.NURSE.0000511805.83334.df

Smorgon, C., Mari, E., Atti, A. R., Dalla Nora, E., Zamboni, P. F., Calzoni, F., et al. (2004). Trace elements and cognitive impairment: an elderly cohort study. *Arch. Gerontol. Geriatr.* 38, 393–402. doi: 10.1016/j.archger.2004.04.050

Sodhi, R. K., and Singh, N. (2013). All-trans retinoic acid rescues memory deficits and neuropathological changes in mouse model of streptozotocin-induced dementia of Alzheimer's type. *Prog. NeuroPsychopharmacol. Biol. Psychiatry* 40, 38–46. doi: 10.1016/j.pnpbp.2012.09.012

Sommer, I., Griebler, U., Kien, C., Auer, S., Klerings, I., Hammer, R., et al. (2017). Vitamin D deficiency as a risk factor for dementia: a systematic review and meta-analysis. *BMC Geriatr.* 17:16. doi: 10.1186/s12877-016-0405-0

Stolk, R. P., Breteler, M., Ott, A., Pols, H., Lamberts, S., Grobbee, D. E., et al. (1997). Insulin and cognitive function elderly population. *Diabetes Care* 20, 792–795. doi: 10.2337/diacare.20.5.792

Sultan, S., Taimuri, U., Basnan, S. A., Ai-Orabi, W. K., Awadallah, A., Almowald, F., et al. (2020). Low Vitamin D and its association with cognitive impairment and dementia. *J. Aging Res.* 2020, 6097820. doi: 10.1155/2020/6097820

Tana, C., Ticinesi, A., Prati, B., Nouvenne, A., and Meschi, T. (2018). Uric acid and cognitive function in older individuals. *Nutrients* 10:975. doi: 10.3390/nu10080975

Tang, Z., Chen, X., Zhang, W., Sun, X., Hou, Q., Li, Y., et al. (2021). Association Between gamma-glutamyl transferase and mild cognitive impairment in Chinese women. *Front. Aging Neurosci.* 13:630409. doi: 10.3389/fnagi.2021.630409

Tien, Y. T., Lee, W. J., Liao, Y. C., Wang, W. F., Jhang, K. M., Wang, S. J., et al. (2019). Plasma transthyretin as a predictor of amnestic mild cognitive impairment conversion to dementia. *Sci. Rep.* 9:18691. doi: 10.1038/s41598-019-55318-0

Toffanello, E. D., Coin, A., Perissinotto, E., Zambon, S., Sarti, S., Veronese, N., et al. (2014). Vitamin D deficiency predicts cognitive decline in older men and women: the Pro.V.A. Study. *Neurology* 83, 2292–2298. doi: 10.1212/WNL.0000000000001080

Tuven, B., Soysal, P., Unutmaz, G., Kaya, D., and Isik, A. T. (2017). Uric acid may be protective against cognitive impairment in older adults, but only in those without cardiovascular risk factors. *Exp. Gerontol.* 89, 15–19. doi: 10.1016/j.exger.2017.01.002

Umur, E. E., Oktenli, C., Celik, S., Tangi, F., Sayan, O., Sanisoglu, Y. S., et al. (2011). Increased iron and oxidative stress are separately related to cognitive decline in elderly. *Geriatr. Gerontol. Int.* 11, 504–509. doi: 10.1111/j.1447-0594.2011.00694.x

Valls-Pedret, C., Lamuela-Raventós, R. M., Medina-Remón, A., Quintana, M., Corella, D., Pintó, X., et al. (2012). Polyphenol-rich foods in the mediterranean diet are associated with better cognitive function in elderly subjects at high cardiovascular risk. *J. Alzheimers Dis.* 29, 773–782. doi: 10.3233/JAD-2012-111799

Van Den Kommer, T. N., Comijs, H. C., Aartsen, M. J., Huisman, M., Deeg, D. J. H., and Beekman, A. T. F. (2013). Depression and cognition: how do they

interrelate in old age? *Am. J. Geriatr. Psychiatry* 21, 398–410. doi: 10.1016/j.jagp.2012.12.015

Van der Schaft, J., Koek, H. L., Dijkstra, E., Verhaar, H. J. J., van der Schouw, Y. T., and Emmelot-Vonk, M. H. (2013). The association between vitamin D and cognition: a systematic review. *Ageing Res. Rev.* 12, 1013–1023. doi: 10.1016/j.arr.2013.05.004

Van Exel, E., De Craen, A. J. M., Gussekloo, J., Houx, P., Bootsma-Van Der Wiel, A., Macfarlane, P. W., et al. (2002). Association between high-density lipoprotein and cognitive impairment in the oldest old. *Ann. Neurol.* 51, 716–721. doi: 10.1002/ana.10220

Van Vliet, P. (2012). Cholesterol and late-life cognitive decline. *J. Alzheimers Dis.* 30(Suppl 2), S147–S162. doi: 10.3233/JAD-2011-111028

Velayudhan, L., Killick, R., Hye, A., Kinsey, A., Güntert, A., Lynham, S., et al. (2012). Plasma transthyretin as a candidate marker for Alzheimer's disease. *J. Alzheimers Dis.* 28, 369–375. doi: 10.3233/JAD-2011-110611

Wang, L., Wang, F., Liu, J., Zhang, Q., and Lei, P. (2018). Inverse relationship between baseline serum albumin levels and risk of mild cognitive impairment in elderly: a seven-year retrospective cohort study. *Tohoku J. Exp. Med.* 246, 51–57. doi: 10.1620/tjem.246.51

Wechsler, D. (2008). *Wechsler Adult Intelligence Scale*, 4th Edn. Washington, DC: PsycNET.

Wen, M., Zhou, B., Chen, Y.-H., Ma, Z.-L., Gou, Y., Zhang, C.-L., et al. (2017). Serum uric acid levels in patients with Parkinson's disease: a meta-analysis. *PLoS One* 12:e0173731. doi: 10.1371/journal.pone.0173731

WHO (2021). *Body Mass Index-BMI*. Geneva: WHO.

Wilson, V. K., Houston, D. K., Kilpatrick, L., Lovato, J., Yaffe, K., Cauley, J. A., et al. (2014). Relationship between 25-hydroxyvitamin D and cognitive function in older adults: the health, aging and body composition study. *J. Am. Geriatr. Soc.* 62, 636–641. doi: 10.1111/jgs.12765

Winblad, B., Palmer, K., Kivipelto, M., Jelic, V., Fratiglioni, L., Wahlund, L. O., et al. (2004). Mild cognitive impairment - Beyond controversies, towards a consensus: report of the International Working Group on Mild Cognitive Impairment. *J. Intern. Med.* 256, 240–246. doi: 10.1111/j.1365-2796.2004.01380.x

Xu, Y., Wang, Q., Cui, R., Lu, K., Liu, Y., and Zhao, Y. (2017). Uric acid is associated with vascular dementia in Chinese population. *Brain Behav.* 7:e00617. doi: 10.1002/brb3.617

Xue, L. L., Liu, Y. B., Xue, H. P., Xue, J., Sun, K. X., Wu, L. F., et al. (2017). Low uric acid is a risk factor in mild cognitive impairment. *Neuropsychiatr. Dis. Treat.* 13, 2363–2367. doi: 10.2147/NDT.S145812

Yavuz, B. B., Cankurtaran, M., Haznedaroglu, I. C., Halil, M., Ulger, Z., Altun, B., et al. (2012). Iron deficiency can cause cognitive impairment in geriatric patients. *J. Nutr. Health Aging* 16, 220–224. doi: 10.1007/s12603-011-0351-7

Zhang, T., Yan, R., Chen, Q., Ying, X., Zhai, Y., Li, F., et al. (2018). Body mass index, waist-to-hip ratio and cognitive function among Chinese elderly: a cross-sectional study. *BMJ Open* 8:22055. doi: 10.1136/bmjopen-2018-022055

Zhou, Z., Zhong, S., Liang, Y., Zhang, X., Zhang, R., Kang, K., et al. (2021). Serum uric acid and the risk of dementia: a systematic review and meta-analysis. *Front. Aging Neurosci.* 13:625690. doi: 10.3389/fnagi.2021.625690

Conflict of Interest: The authors declare that the research was conducted in the absence of any commercial or financial relationships that could be construed as a potential conflict of interest.

Publisher's Note: All claims expressed in this article are solely those of the authors and do not necessarily represent those of their affiliated organizations, or those of the publisher, the editors and the reviewers. Any product that may be evaluated in this article, or claim that may be made by its manufacturer, is not guaranteed or endorsed by the publisher.

frontiers | Frontiers in Aging Neuroscience

ORIGINAL RESEARCH
published: 22 June 2022
doi: 10.3389/fnagi.2022.894824

REPS1 as a Potential Biomarker in Alzheimer's Disease and Vascular Dementia

Jiefeng Luo[1†], Liechun Chen[1†], Xiaohua Huang[2†], Jieqiong Xie[1], Chun Zou[1], Mika Pan[1], Jingjia Mo[3] and Donghua Zou[1*]*

[1] Department of Neurology, The Second Affiliated Hospital of Guangxi Medical University, Nanning, China, [2] Department of Neurology, The Affiliated Hospital of Youjiang Medical University for Nationalities, Baise, China, [3] Department of General Medicine, The Second Affiliated Hospital of Guangxi Medical University, Nanning, China

OPEN ACCESS

Edited by:
Kuangyu Shi,
University of Bern, Switzerland

Reviewed by:
Heather M. Wilkins,
University of Kansas Medical Center Research Institute, United States
Meiyan Wang,
Salk Institute for Biological Studies, United States
Xuan Ye,
Novartis Institutes for BioMedical Research, United States

***Correspondence:**
Donghua Zou
zoudonghua@gxmu.edu.cn
Jingjia Mo
mojingjia2017@163.com

[†] These authors have contributed equally to this work

Specialty section:
This article was submitted to Alzheimer's Disease and Related Dementias, a section of the journal Frontiers in Aging Neuroscience

Received: 12 March 2022
Accepted: 07 June 2022
Published: 22 June 2022

Citation:
Luo J, Chen L, Huang X, Xie J, Zou C, Pan M, Mo J and Zou D (2022) REPS1 as a Potential Biomarker in Alzheimer's Disease and Vascular Dementia. Front. Aging Neurosci. 14:894824. doi: 10.3389/fnagi.2022.894824

Vascular dementia (VD) and Alzheimer's disease (AD) are common types of dementia for which no curative therapies are known. In this study, we identified hub genes associated with AD and VD in order to explore new potential therapeutic targets. Genes differentially expressed in VD and AD in all three datasets (GSE122063, GSE132903, and GSE5281) were identified and used to construct a protein–protein interaction network. We identified 10 modules containing 427 module genes in AD and VD. Module genes showing an area under the diagnostic curve > 0.60 for AD or VD were used to construct a least absolute shrinkage and selection operator model and were entered into a support vector machine-recursive feature elimination algorithm, which identified REPS1 as a hub gene in AD and VD. Furthermore, REPS1 was associated with activation of pyruvate metabolism and inhibition of Ras signaling pathway. Module genes, together with differentially expressed microRNAs from the dataset GSE46579, were used to construct a regulatory network. REPS1 was predicted to bind to the microRNA hsa_miR_5701. Single-sample gene set enrichment analysis was used to explore immune cell infiltration, which suggested a negative correlation between REPS1 expression and infiltration by plasmacytoid dendritic cells in AD and VD. In conclusion, our results suggest core pathways involved in both AD and VD, and they identify REPS1 as a potential biomarker of both diseases. This protein may aid in early diagnosis, monitoring of treatment response, and even efforts to prevent these debilitating disorders.

Keywords: Alzheimer's disease, vascular dementia, biomarker, REPS1, Ras signaling pathway

INTRODUCTION

Age-related neurodegeneration affects more than 36 million people around the world. The most common cause of dementia is Alzheimer's disease (AD), which shows insidious onset and leads to progressive deterioration of cognitive and physical function as well as mood. By 2050, more than 115 million around the world may be affected by AD (Reisberg et al., 1997). Various factors seem to affect risk of AD-related dementia, such as diabetes, hypertension, and smoking (Luchsinger et al., 2005). The pathogenesis of AD may even involve the individual's own immune system: natural and adaptive immune responses involving monocytes, macrophages, neutrophils, and peripheral blood T cells may contribute to the disease (Polfliet et al., 2001; Ziegler-Heitbrock, 2007;

Baik et al., 2014; Gate et al., 2020). Studies in Tg2576/p75 NTR ± mice suggest that reducing amyloid β accumulation can improve cognitive deficits (Jian et al., 2016), but no treatments are yet available to cure or prevent AD (Tan et al., 2014).

The second most common type of dementia is vascular dementia (VD; O'Brien and Thomas, 2015), which can coexist with AD and other age-related neurological disorders (Gorelick et al., 2011). As populations age, the overall incidence of dementia doubles every 5.1 years, that of AD doubles every 4.5 years, and that of VD doubles every 5.3 years (Jorm and Jolley, 1998). AD and VD appear to be closely related in terms of risk factors and symptoms (Ashraf et al., 2016). Better understanding of the etiology of both diseases, and exploration of the overlap between them, may help clinicians diagnose and treat them.

Such work can take the form of identifying appropriate biomarkers of the two diseases (Biomarkers Definitions Working Group, 2001), particularly molecules that can be assayed in a cost-effective, minimally invasive way, such as in blood. In AD, for example, levels of the microRNA (miRNA) miR-34a may aid in early diagnosis (Jian et al., 2017). The protein RBM8A may regulate many genes related to AD pathophysiology (Zou D. et al., 2019). Furthermore, we identified hub genes associated with molecular subtypes as potential biomarkers for AD, as well as candidate therapeutic targets (Ma et al., 2022). Identifying biomarkers for AD and VD may help individualize treatment for patients as a function of their precise symptoms.

In the present study, our aim was to search for biomarkers of AD and VD using bioinformatics and to explore their potential biological role in the two diseases.

MATERIALS AND METHODS

Data Preprocessing

Gene expression data from the datasets GSE122063, GSE132903, GSE5281, and GSE46579 were downloaded from the Gene Expression Omnibus[1] (Barrett et al., 2013). The data in GSE122063 were obtained using the GPL16699 platform and included 56 AD, 36 VD, and 44 healthy brain tissue samples. The age of patients at death (mean ± SD, year) were 78.6 ± 8.5 for healthy controls, 81.4 ± 10.1 for VD patients and 80.9 ± 7.4 for AD patients. These three groups in the GSE122063 dataset did not differ significantly in age, sex, or time to death. Data in GSE5281 were obtained using the GPL570 platform and included 87 AD and 74 normal brain tissue samples. The age of patients at death ranged from 63 to 102 years. Data in GSE132903 were obtained using the GPL10558 platform and included 97 AD and 98 non-dementia control samples. Age of patients at death range of 195 samples were 70–102 years. Data on miRNA expression in GSE46579 were obtained using the GPL11154 platform and included 48 AD patients and 22 normal blood samples.

Gene expression profiles were normalized using the "normalize Between Arrays" function of the limma package in R (Ritchie et al., 2015). The workflow for this study is shown in **Figure 1**.

[1]https://www.ncbi.nlm.nih.gov/geo/

Analysis of Differential Gene Expression

Differentially expressed mRNAs (DEmRs) between AD and healthy individuals or between VD and healthy individuals were identified in datasets GSE122063, GSE5281, and GSE132903 using the limma package. DEmRs that were upregulated across all three datasets or downregulated across all three datasets, and whose differential expression was associated with an adjusted $P < 0.05$, were considered to be associated with dementia. The Himsc package in R was used to assess similarity of gene expression across different samples based on cumulative distribution curves.

Functional Enrichment of Differentially Expressed Genes

We analyzed enrichment of DEmRs in Gene Ontology terms and Kyoto Encyclopedia of Genes and Genomes (KEGG) pathways using the clusterProfiler package in R (Yu et al., 2012). Enrichment was defined as $P < 0.05$. Interactions between DEmRs and cellular processes were explored using gene set enrichment analysis (GSEA; Mootha et al., 2003; Subramanian et al., 2005).

Protein–Protein Interaction Network

A protein–protein interaction (PPI) network was constructed from intersecting genes whose k_core was greater than 500. The Molecular Complex Detection algorithm was performed to monitor PPI network modules with Cytoscape. From this network we identified module genes related to AD and VD.

Feature Genes

The least absolute shrinkage and selection operator (LASSO) model and support vector machine-recursive feature elimination (SVM-RFE) algorithm were used to screen for feature genes. LASSO was performed within the glmnet package in R (Friedman et al., 2010). LASSO applies a penalty function to shrink the regression coefficient to 0 for variables that influence outcomes less. In this way, the method can converge toward a more accurate prediction model.

Support vector machine is a powerful binary classifier that establishes a classification hyperplane as a decision surface. SVM-RFE is an SVM-based machine learning method that reduces the eigenvectors generated by SVM in order to optimize the variables in a prediction model. The SVM-RFE algorithm was performed within the 1071 package in R (Huang et al., 2014), and potential biomarkers associated with $P < 0.05$ for diagnosing AD or VD were retained.

The ability of module genes to diagnose AD and VD was assessed by calculating the area under receiver operating characteristic curves (AUC) using the "coxph" function in the survival package (Barakat et al., 2019). Only module genes associated with AUC > 0.85 and $P < 0.01$ were retained.

Network of MicroRNAs and Their Target Genes

We used the limma package to identify DEmiRs from the dataset GSE46579. For the three DEmiRs showing the largest | log

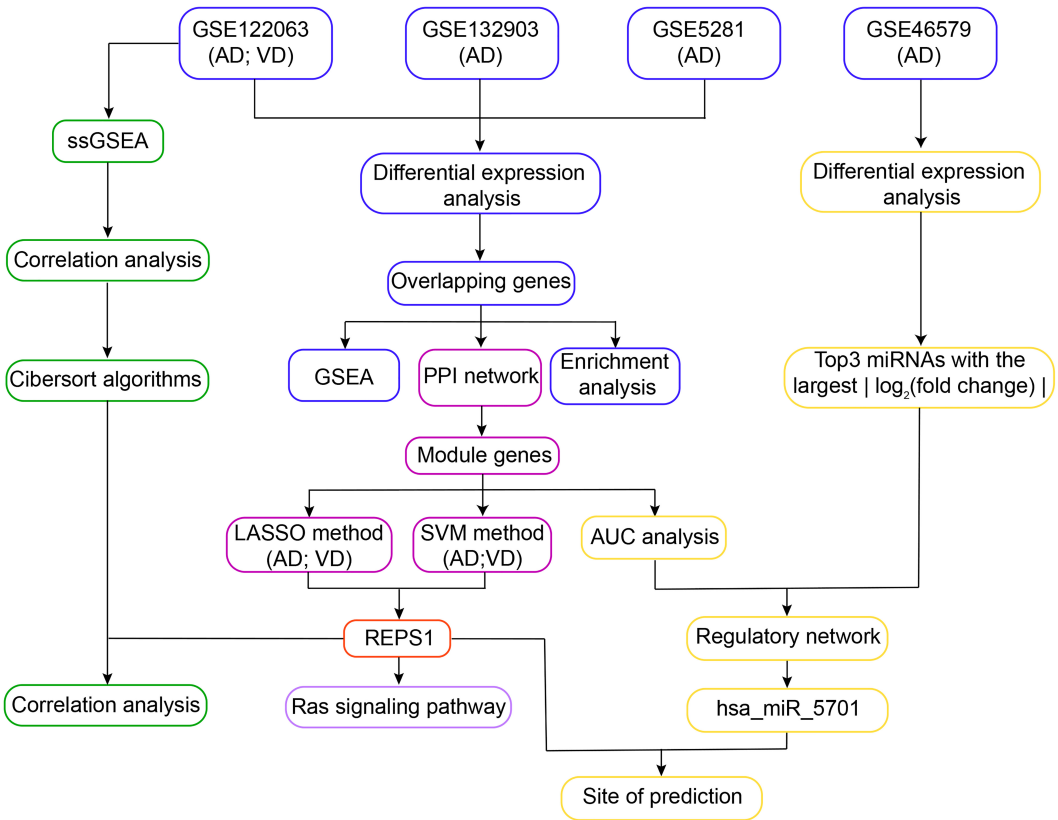

FIGURE 1 | Workflow of the study. In *Step 1,* differentially expressed genes in Alzheimer's disease (AD) and vascular dementia (VD) were identified in three datasets (GSE122063, GSE132903, and GSE5281). The differentially expressed genes overlapping across all three datasets were subjected to functional enrichment analysis and gene set enrichment analysis (GSEA). In *Step 2,* overlapping differentially expressed genes were used to construct a protein–protein interaction (PPI) network, leading to identification of module genes. REPS1 was identified as a hub gene using the least absolute shrinkage and selection operator (LASSO) and the support vector machine-recursive feature elimination (SVM-RFE) algorithm. In *Step 3,* module genes and the three differentially regulated microRNAs (miRNAs) showing the largest | $\log_2$ (fold change)| were used to construct a regulatory network. We found evidence that REPS1 binds hsa_miR_5701. In *Step 4,* single-sample gene set enrichment analysis was performed on the expression profiles of AD and VD in GSE122063. We also explored immune cell infiltration and correlation between REPS1 and biological pathways in AD and VD. AUC, area under the receiver operating characteristic curve.

(fold change)|, we predicted their potential target genes using TargetScan[2]. The resulting regulatory network was visualized using Cytoscape (Shannon et al., 2003), and potential functional aspects were explored using Metascape (Zhou et al., 2019).

Single-Sample Gene Set Enrichment Analysis

Single-sample gene set enrichment analysis (ssGSEA) was used to explore the infiltration and activity of 24 immune cell types using marker gene sets (Bindea et al., 2013). The ssGSEA scores were standardized across immune cell types using the "normalizeBetweenArrays" function in the limma package. Radar plots were used to assess the potential correlations of immune cell infiltration between AD and VD. We used CIBERSORT[3] to assess infiltration levels of immune cells. To identify genes associated with immune cell infiltration patterns, we calculated the immune cell types for the three datasets GSE122063, GSE132903, and GSE5281 using the limma package (Law et al., 2014).

Statistical Analysis

The analyses of the present study were performed using the BioInforCloud platform. DEmRNAs and DEmiRs between AD and healthy individuals or between VD and healthy individuals were analyzed using an unpaired *t* test method within the limma package. Differences were considered significant if associated with $P < 0.05$.

RESULTS

Identification of Differentially Expressed Genes in Vascular Dementia and Alzheimer's Disease

We first identified differentially expressed genes among AD, VD, and control brain tissues (**Figure 2A**). A total of 1,965

[2]www.targetscan.org/vert_72

[3]https://cibersort.stanford.edu/

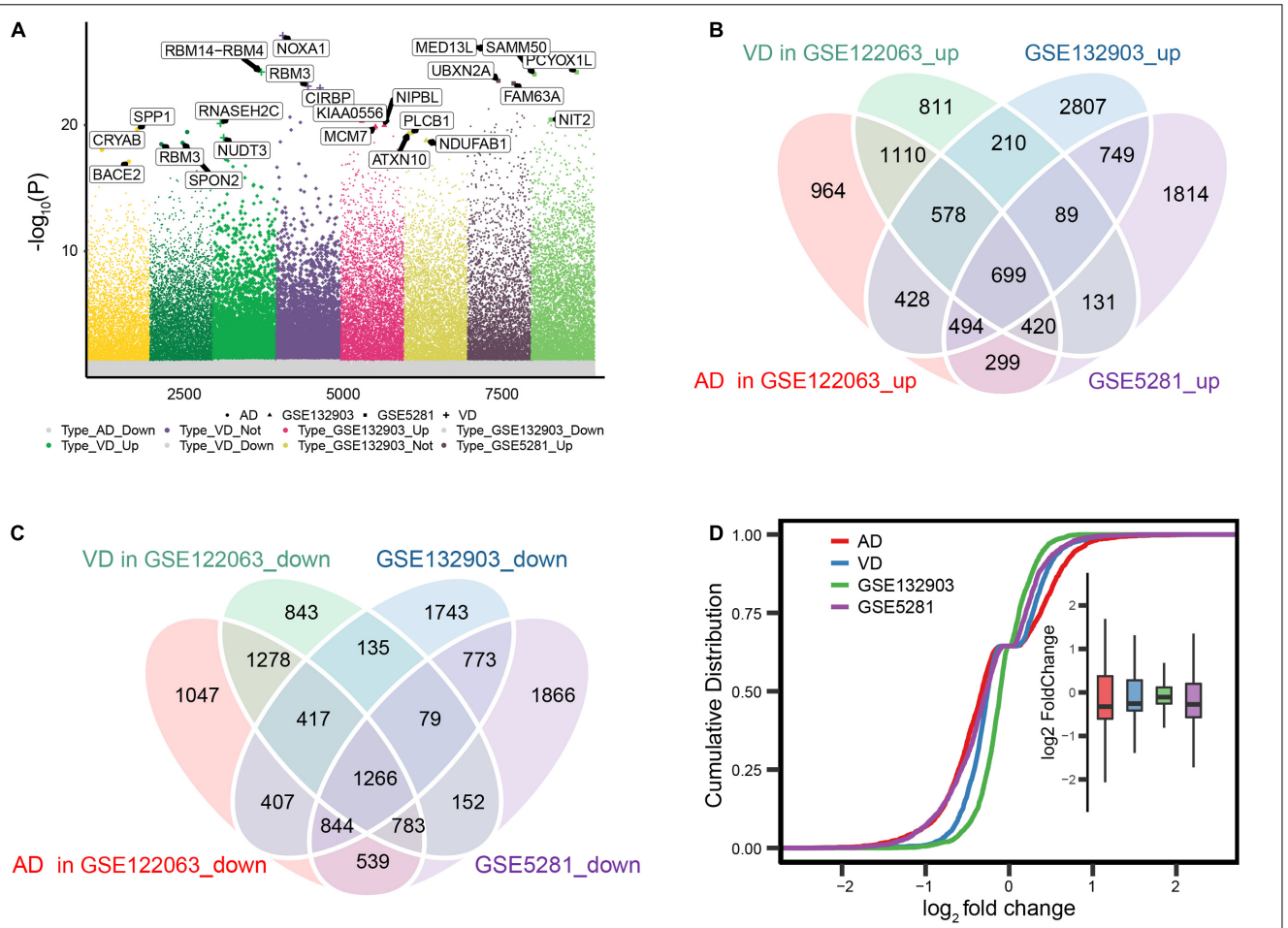

FIGURE 2 | Differential gene expression in Alzheimer's disease (AD) and vascular dementia (VD). **(A)** Differentially expressed genes were identified between controls and patients with AD or VD in the datasets GSE122063, GSE132903, and GSE5281. **(B, C)** Overlap of differentially expressed genes that were up- or downregulated in the two disorders. **(D)** Cumulative distribution plots showing similarity in the expression of differentially expressed genes across datasets.

differentially expressed genes overlapped across the three datasets (**Figures 2B,C**), of which 699 were consistently upregulated and 1,266 consistently downregulated in AD and VD. Expression levels of overlapping differentially expressed genes were most similar between AD and control samples in the datasets GSE122063 and GSE5281 (**Figure 2D**).

Potential Functions of Overlapping Differentially Expressed Genes

Differentially expressed genes overlapping across the datasets GSE122063, GSE5281, and GSE132903 were enriched in biological processes involved in AD, mTOR signaling, and Ras signaling (**Figure 3A**), including purine nucleoside triphosphate metabolism, cellular respiration, and nucleoside triphosphate metabolism (**Figure 3B**).

Gene set enrichment analysis showed that the differentially expressed genes were involved in alanine aspartate and glutamate metabolism, cholinergic synapses and neuroactive ligand-receptor interactions, all of which were activated in AD (**Figure 3C**). Moreover, overlapping genes were predicted to inhibit B cell receptor signaling, interactions between cytokines and their receptors, and NF-kappa B signaling in AD (**Figure 3D**).

Identification of Hub Genes Using Least Absolute Shrinkage and Selection Operator and Support Vector Machine-Recursive Feature Elimination

The PPI network revealed 10 modules containing 427 module genes (**Figure 4A**), of which 14 showed AUC > 0.85 for both AD and VD (**Figure 4B**). From module genes in AD, LASSO identified 13 genes (**Figure 4C**) and SVM-RFE identified 182 genes (**Figure 4D**).

From the overlap between the genes identified by LASSO and SVM-RFE, we identified 13 feature genes: GLRX5, FDX1, TRMT11, GABBR1, SERPINA3, REPS1, IFIT2, ANAPC13, CASP7, DNAJC10, IFT52, TBL1Y, and NDUFV3.

From module genes in VD, LASSO identified 11 genes (**Figure 4E**) and SVM-RFE identified 17 genes (**Figure 4F**). From

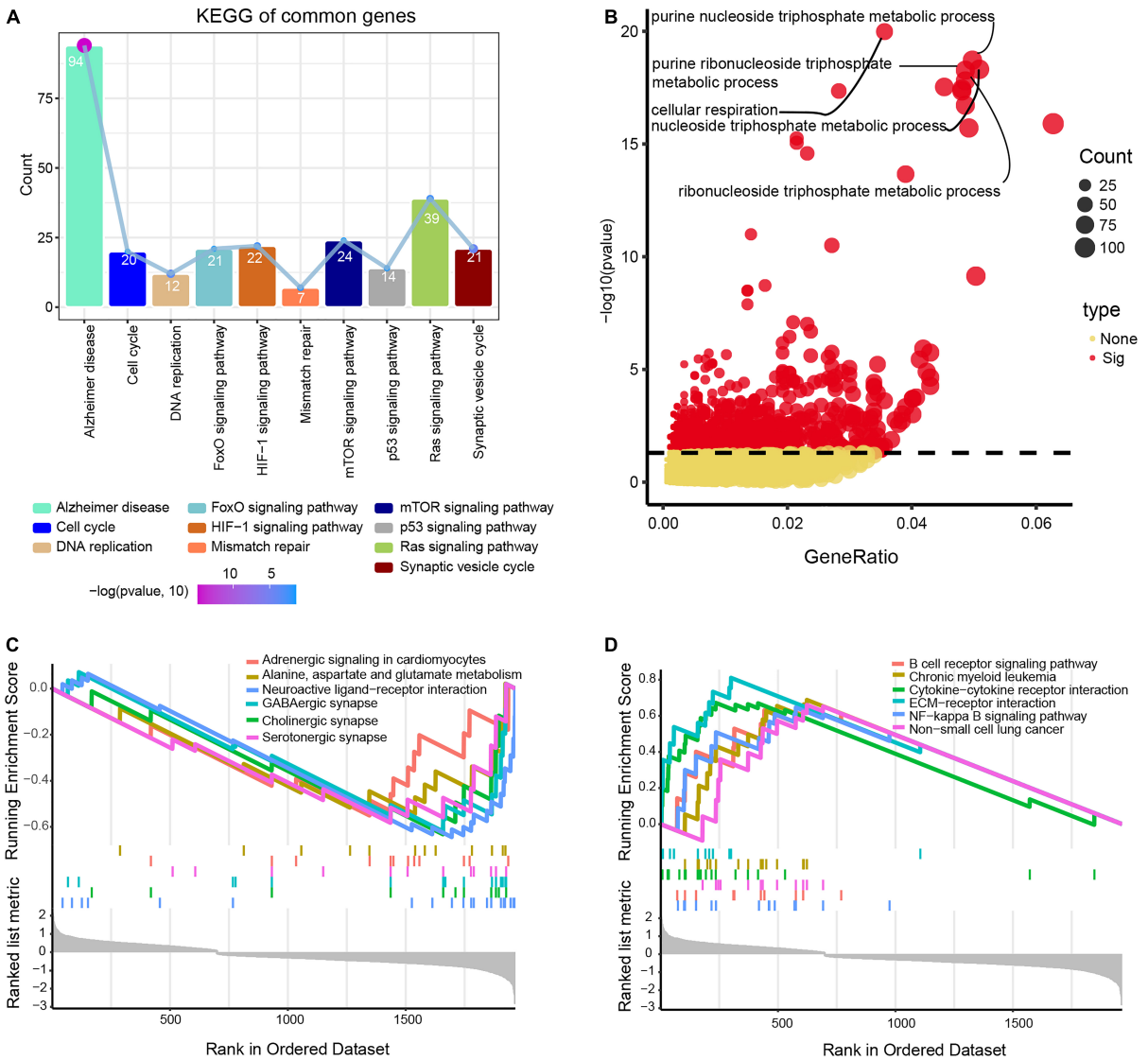

FIGURE 3 | Potential functions of differentially expressed genes in Alzheimer's disease (AD) and vascular dementia (VD). **(A)** Enrichment of genes in Kyoto Encyclopedia of Genes and Genomes (KEGG) pathways. **(B)** Enrichment of genes in Gene Ontology biological processes. **(C, D)** Lists of the top six pathways that the genes were predicted to **(C)** activate or **(D)** inhibit, based on gene set enrichment analysis. Enriched genes were defined as genes strongly expressed in AD/VD tissues that showed high enrichment scores.

the overlap, we identified six feature genes: RAB5A, ALDOC, REPS1, KLHL21, PCF11, and CCT6B.

REPS1 appeared among the overlap genes base on both AD and VD, so we focused on it in subsequent bioinformatic analyses.

Regulatory Network of DEmiRs in Alzheimer's Disease

We identified 161 DEmiRs between AD and controls in the dataset GSE46579, of which 64 were upregulated and 97 were downregulated (**Figure 5A**). These DEmiRs were involved in RNA metabolism, organelle localization, the citric acid cycle and the respiratory electron transport (**Figure 5B**). The three DEmiRs showing the highest $|\log_2$ (fold change)$|$ were involved in p53 signaling, pyruvate metabolism, and endomembrane system organization (**Figure 5C**). The DEmiR hsa-miR-5701 was predicted to bind to REPS1 (**Figure 5D**).

Immune Cell Infiltration in Vascular Dementia and Alzheimer's Disease

Immune cell infiltration was compared between AD or VD patients and controls in the datasets GSE132903, GSE5281, and GSE122063. Patients showed significantly greater infiltration by Effective Memory T Cell (Tem), plasmacytoid dendritic cells (pDCs) and activated dendritic cells (aDCs; **Figure 6A**). REPS1, which was downregulated in patients relative to controls (**Figure 6B**), correlated positively with

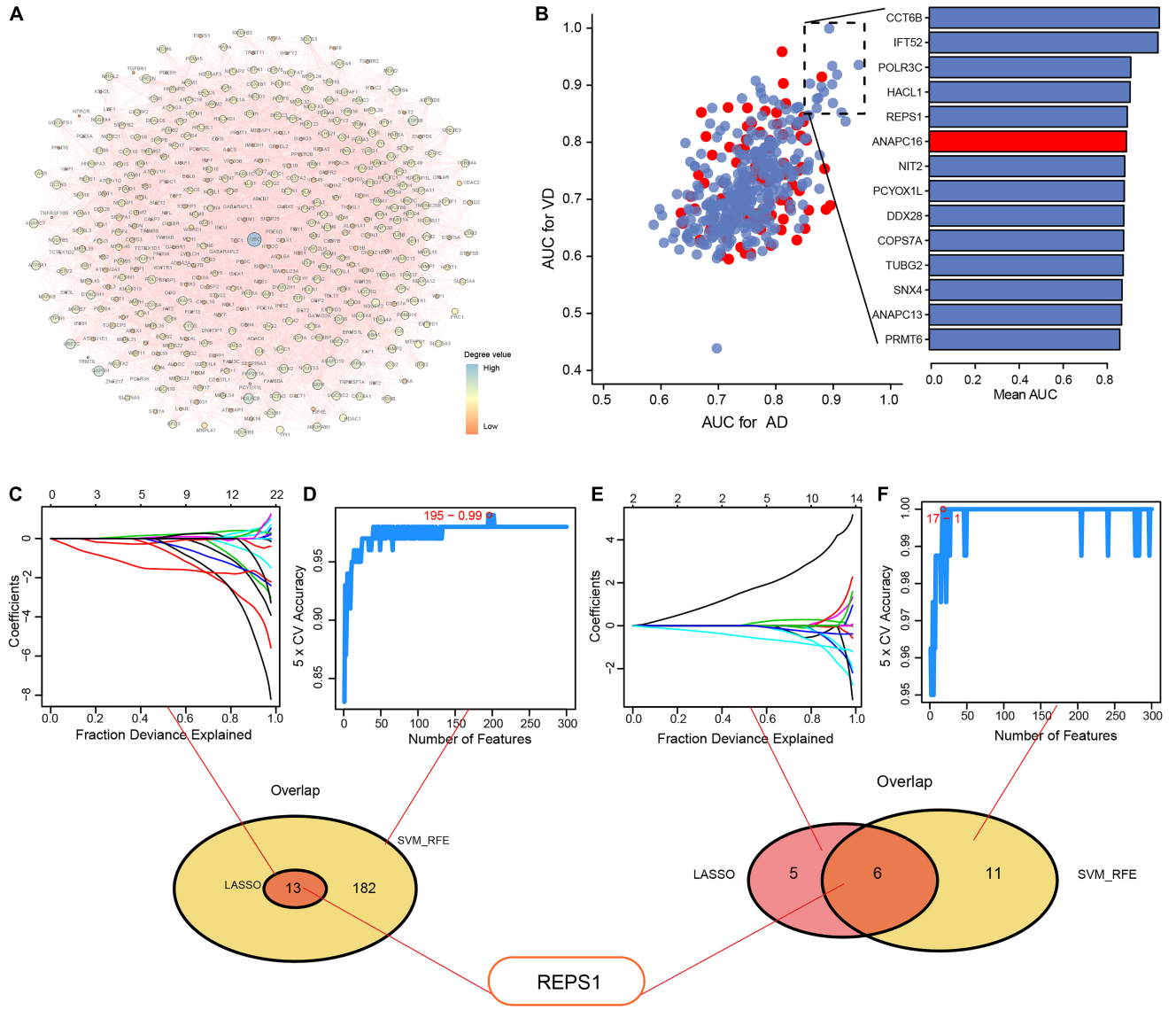

FIGURE 4 | Identification of hub genes using LASSO and SVM-RFE. **(A)** Protein–protein interaction network to reveal module genes. **(B)** Evaluation of the diagnostic value of module genes involved in Alzheimer's disease (AD) and vascular dementia (VD), based on the area under the receiver operating characteristic curve (AUC). Red indicates upregulated genes; blue, downregulated genes. **(C–F)** Module genes were entered into LASSO and SVM-RFE to obtain the overlapping feature genes in **(C, D)** AD or **(E, F)** VD. Feature genes are identified using different colors in **(C)** and **(E)**. LASSO, least absolute shrinkage and selection operator; SVM-RFE, support vector machine-recursive feature elimination.

infiltration by follicular T helper cells and eosinophils in AD (**Figure 6C**), or with T helper 2 cells in VD (**Figure 6D**). Conversely, REPS1 correlated negatively with pDCs in AD (**Figure 6E**) and VD (**Figure 6F**). Plasma cells were the most abundant infiltrating cell type in AD and VD (**Figure 6G** and **Supplementary Table 1**).

Potential Role of REPS1 in Vascular Dementia and Alzheimer's Disease

In AD and VD, REPS1 correlated negatively with cell growth, and it was predicted to activate cellular redox homeostasis (**Figure 7A**). Based on KEGG pathway enrichment, REPS1 was predicted to activate pyruvate metabolism and to inhibit Ras signaling (**Figures 7B,C**).

DISCUSSION

AD and VD are age-related diseases that seriously affect quality of life. Age is a vital risk factor associated with AD (Armstrong, 2019), and as patients age, their disorder becomes more severe. In this study, REPS1 was identified as a potential biomarker of both disorders and Ras signaling as one of the

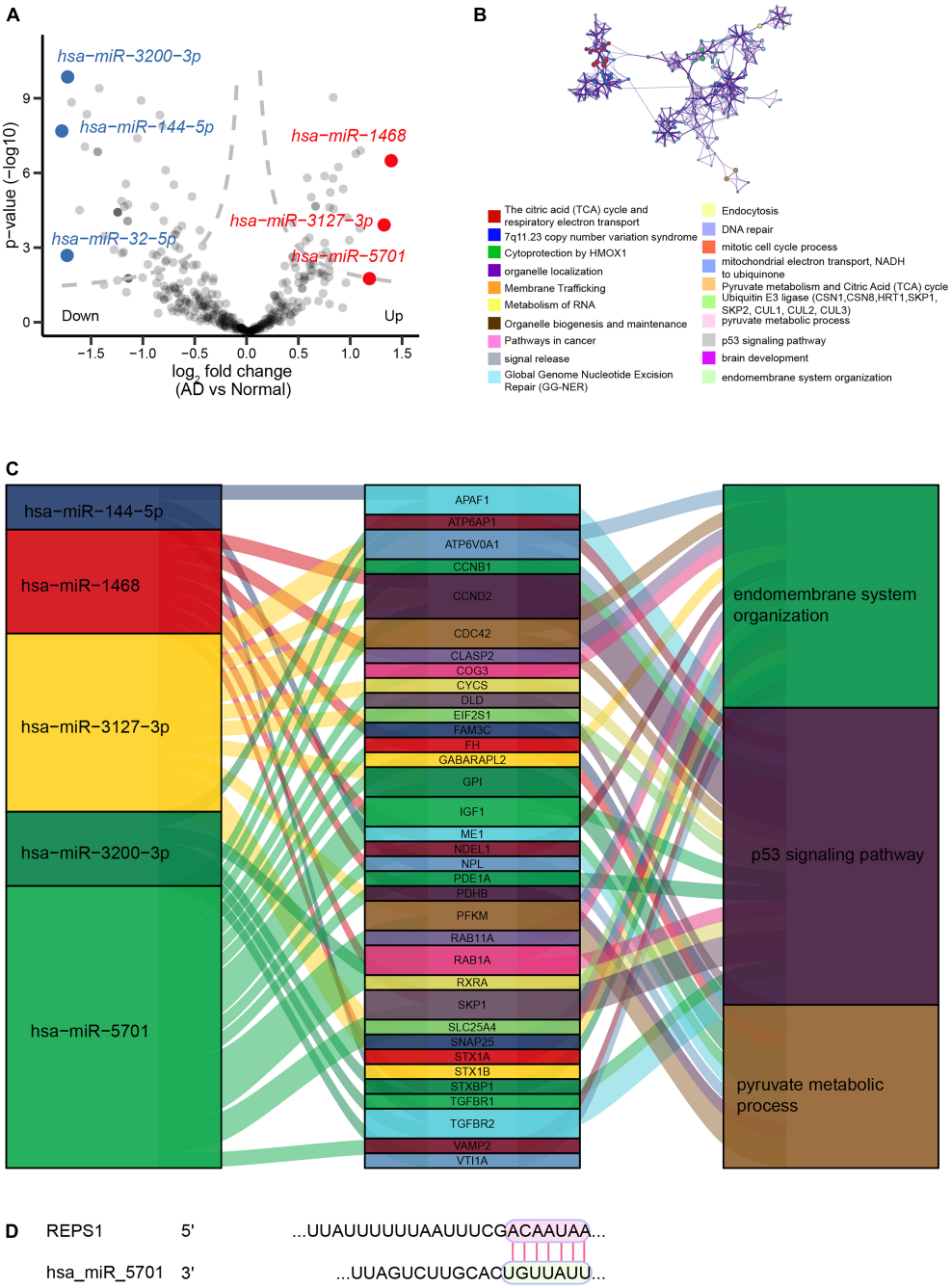

FIGURE 5 | Regulatory network of miRNAs in Alzheimer's disease (AD). **(A)** Volcano plot of differentially expressed miRNAs between AD and controls in the dataset GSE46579. Red indicates the top three upregulated miRNAs, while blue indicates the top three downregulated miRNAs. **(B)** Enrichment analysis of the three differentially expressed miRNAs showing the largest | $\log_2$ (fold change)| . **(C)** Sankey plots showing the biological functions potentially affected by the regulatory relationships between differentially expressed miRNAs and differentially expressed genes. **(D)** Predicted binding between REPS1 and hsa-miR-5701, based on TargetScan.

drivers of pathogenesis. Given that neurodegeneration involves complex networks of interacting genes and pathways (Jian et al., 2021), we adopted a genomic rather than "candidate gene" approach to understanding the landscape of changes that may help explain AD and VD. Our results may aid in the early diagnosis, treatment and even prevention of these debilitating disorders.

Our analyses suggest that genes differentially expressed in AD and VD may be involved in NF-kappa B signaling and Ras signaling. These results are consistent with previous studies

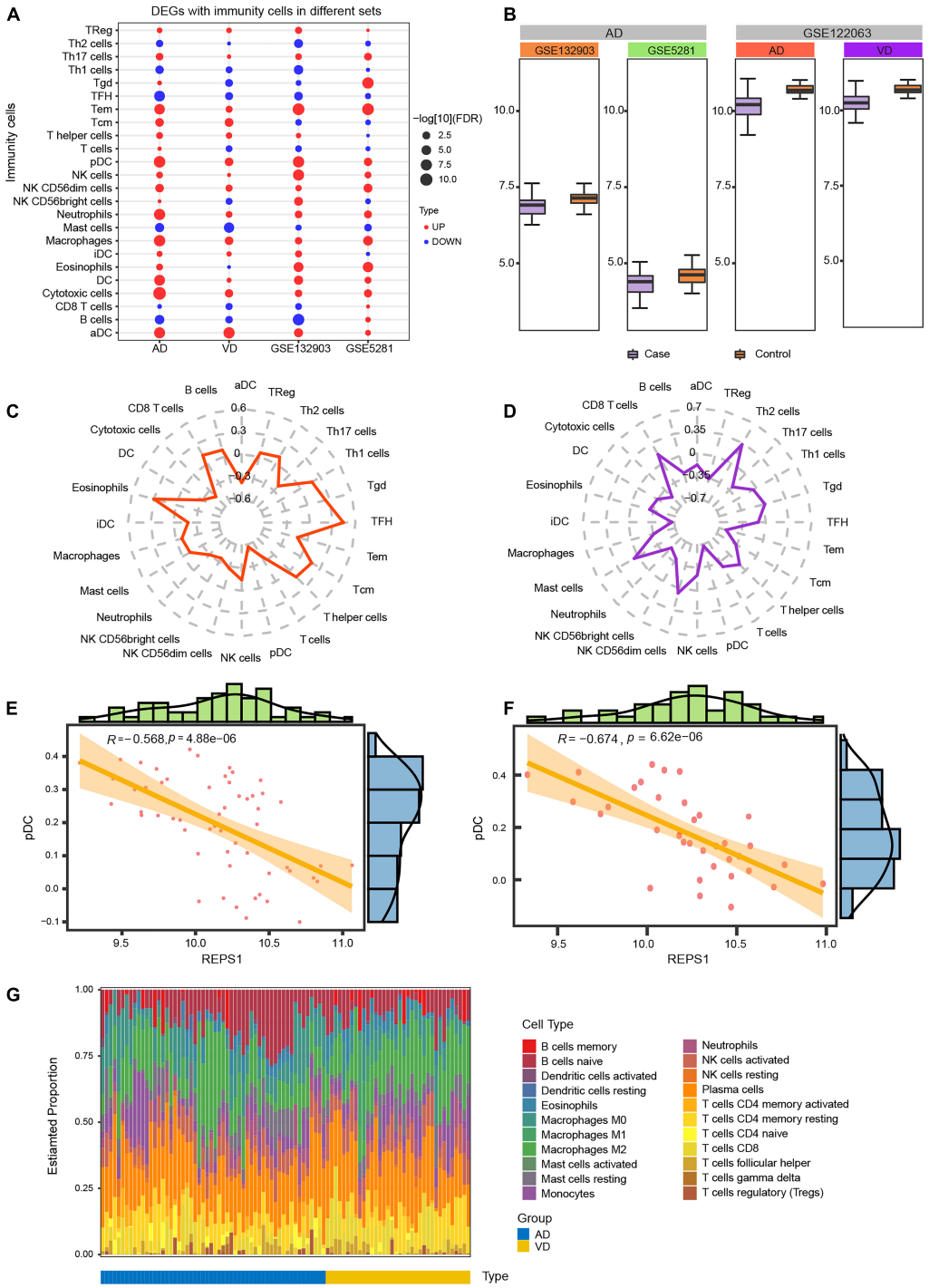

FIGURE 6 | Degree of infiltration by immune cells in Alzheimer's disease (AD) and vascular dementia (VD). **(A)** Differential infiltration by immune cells in the datasets GSE122063 (AD and VD), GSE132903, and GSE5281. **(B)** Expression of REPS1 in the datasets GSE122063 (AD and VD), GSE132903, and GSE5281. **(C, D)** Correlation of REPS1 expression with infiltration by 24 types of immune cells in AD and VD. **(E, F)** REPS1 negatively correlated with plasmacytoid dendritic cells (pDCs) in AD and VD. **(G)** Estimated proportions of 22 immune cell types in AD (blue) or VD (yellow).

(Kirouac et al., 2017; Zou C. et al., 2019; Zhou et al., 2021). Furthermore, among that biological process further study is needed in order to determine which metabolic processes are up- or downregulated in AD or VD. LASSO or SVM-RFE methods identified 13 feature genes in AD samples. Among these, SERPINA3 (Norton et al., 2021), IFIT2 (Puig-Butille et al., 2014),

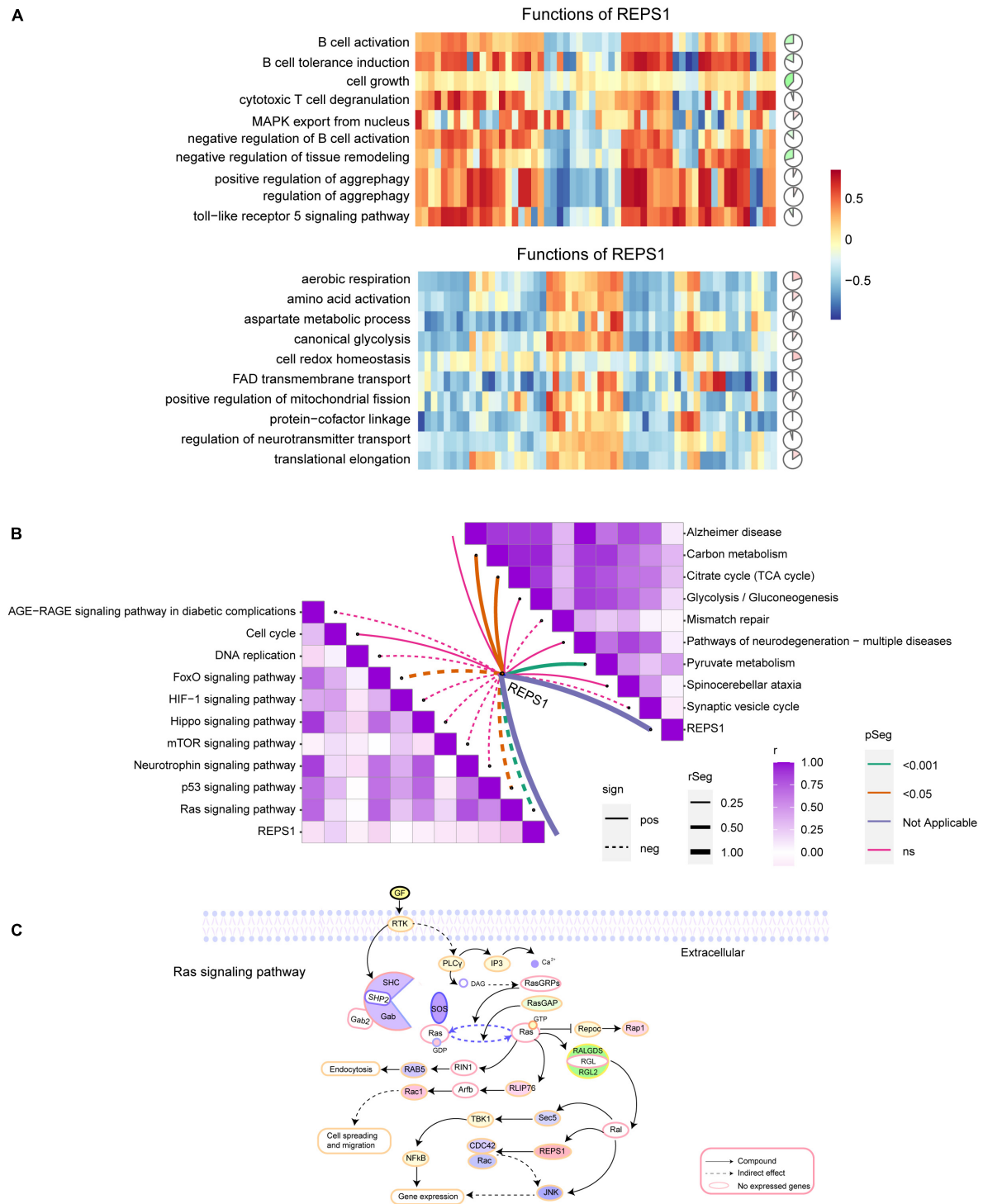

FIGURE 7 | Correlation of REPS1 and pathways. **(A)** Correlations between REPS1 and biological processes. Red indicates activation, and green indicates inhibition. **(B)** Correlation between REPS1 and functional pathways. Solid lines indicate positive correlations, and dotted lines indicate negative correlations. **(C)** Schematic illustrating how REPS1 may trigger downstream Ras signaling.

and CASP7 (Zhang et al., 2019) have previously been proposed to play vital roles in AD. In contrast, we are unaware of previous studies linking AD to the genes REPS1, GLRX5, FDX1, TRMT11, GABBR1, ANAPC13, DNAJC10, IFT52, TBL1Y, or NDUFV3. Six feature genes overlapped between LASSO and SVM-RFE methods as associated with VD, and none of these genes has

previously been linked to VD. These feature genes merit further study for their potential roles in AD or VD. As a key feature gene in AD and VD based on both LASSO and SVM-RFE methods, REPS1 became the focus of the present study. REPS1 is expressed ubiquitously; it is more abundant in heart and testis, and less abundant in brain, kidney, colon, and lung (Xu et al., 2001). Mutations in REPS1 can reduce palmitoylation as well as altered acylation in genetic diseases (Chamberlain and Shipston, 2015). Such alterations have been linked to AD and Huntington's disease (Chavda et al., 2014). Moreover, REPS1 is predicted to be regulated by hsa_miR_5701, which emerged as one of the three DEmiRs showing the largest change in expression in AD and VD. This is the first report linking hsa_miR_5701 to neurological disease. It has already been linked to prognosis of patients with lung squamous cell carcinoma (Gan et al., 2019), and it can inhibit the proliferation of cervical cancer cells (Pulati et al., 2019).

Communication among different cell types in the central nervous system may contribute to AD (Vainchtein and Molofsky, 2020). We found evidence that aDCs and macrophages show substantial infiltration in both AD and VD. Dendritic cell-based therapy may be a more effective treatment for age-related diseases, such as AD (Cheng et al., 2015). The number of microglia, which act as phagocytic immune cells to clear material from the central nervous system, appears to decrease during AD progression (Hoozemans et al., 2011; Heneka, 2017). Furthermore, we observed here a negative correlation between pDCs and AD/VD. These considerations suggest that immune responses weaken over time in AD and VD. Furthermore, CIBERSORT analysis showed extensive infiltration by plasma cells in AD/VD. Age-dependent plasma cell accumulation may contribute to cognitive decline and to behavioral or neurodegenerative disorders in humans (Hepworth et al., 2021).

The function of REPS1 appears to depend on its Eps15 homology domain, which mediates PPIs (Nakashima et al., 1999). REPS1 may interact *via* this domain with downstream effectors, such as the Ras-Ral signaling pathway (Datson et al., 2011). We found REPS1 to correlate positively with pyruvate metabolism and the citrate cycle, both of which have been linked to neuroinflammation and neurodegeneration (Garabadu et al., 2019). We also found REPS1 to correlate positively with the cell cycle. Dysregulation of the cell cycle is a cancer hallmark, and early disruptions in the cell cycle in AD may cause oncogenic signal transduction (Raina et al., 2000). Conversely, we found that REPS1 correlated negatively with Ras signaling. PKC–Ras signaling can be upregulated to compensate for loss of M1 muscarinic acetylcholine receptor activity and thereby mitigate dementia symptoms in elderly (Chen et al., 2020), and our results imply that the same may be true for AD. REPS1 interacts with Ral protein, proteins that activate Cdc42 and Rac GTPases that inhibit JNK, so our results implicate all these proteins in AD and VD.

Our findings should be interpreted with caution because they are based entirely on bioinformatic analyses. Experimental studies should explore whether levels of REPS1 protein change in the brains of individuals with VD or AD.

CONCLUSION

In this study, we identified REPS1 as a potential biomarker of AD and VD and as a candidate therapeutic target. Our results also implicate Ras signaling in the two neurodegenerative disorders.

DATA AVAILABILITY STATEMENT

The original contributions presented in this study are included in the article/**Supplementary Material**; further inquiries can be directed to the corresponding authors.

ETHICS STATEMENT

Ethical review and approval was not required for the study on human participants in accordance with the local legislation and institutional requirements. Written informed consent for participation was not required for this study in accordance with the national legislation and the institutional requirements. Written informed consent was obtained from the individual(s) for the publication of any potentially identifiable images or data included in this article.

AUTHOR CONTRIBUTIONS

DZ and JM conceived and designed the study. JL, LC, and XH performed analyses as well as collected and analyzed the data. All authors prepared the figures and tables, and wrote the manuscript. All authors reviewed the manuscript and approved its submission.

FUNDING

This study was supported by the National Natural Science Foundation of China (82060210), the Nanning Excellent Young Scientist Program and Guangxi Beibu Gulf Economic Zone Major Talent Program (RC20190103).

ACKNOWLEDGMENTS

The authors would like to thank Shaowen Mo and Qiong Song for assisting with bioinformatics analysis on the BioInforCloud platform.

SUPPLEMENTARY MATERIAL

The Supplementary Material for this article can be found online at: https://www.frontiersin.org/articles/10.3389/fnagi.2022.894824/full#supplementary-material

Supplementary Table 1 | Estimated proportions of 22 immune cell types in AD.

REFERENCES

Armstrong, R. A. (2019). Risk factors for Alzheimer's disease. *Folia Neuropathol.* 57, 87–105.

Ashraf, G. M., Chibber, S., Mohammad, Zaidi, S. K., Tabrez, S., Ahmad, A., et al. (2016). Recent updates on the association between Alzheimer's disease and vascular dementia. *Med. Chem.* 12, 226–237. doi: 10.2174/1573406411666151030111820

Baik, S. H., Cha, M. Y., Hyun, Y. M., Cho, H., Hamza, B., Kim, D. K., et al. (2014). Migration of neutrophils targeting amyloid plaques in Alzheimer's disease mouse model. *Neurobiol. Aging* 35, 1286–1292. doi: 10.1016/j.neurobiolaging.2014.01.003

Barakat, A., Mittal, A., Ricketts, D., and Rogers, B. A. (2019). Understanding survival analysis: actuarial life tables and the Kaplan-Meier plot. *Br. J. Hosp. Med.* 80, 642–646. doi: 10.12968/hmed.2019.80.11.642

Barrett, T., Wilhite, S. E., Ledoux, P., Evangelista, C., Kim, I. F., Tomashevsky, M., et al. (2013). NCBI GEO: archive for functional genomics data sets–update. *Nucleic Acids Res.* 41, D991–D995. doi: 10.1093/nar/gks1193

Bindea, G., Mlecnik, B., Tosolini, M., Kirilovsky, A., Waldner, M., Obenauf, A. C., et al. (2013). Spatiotemporal dynamics of intratumoral immune cells reveal the immune landscape in human cancer. *Immunity* 39, 782–795. doi: 10.1016/j.immuni.2013.10.003

Biomarkers Definitions Working Group (2001). Biomarkers and surrogate endpoints: preferred definitions and conceptual framework. *Clin. Pharmacol. Ther.* 69, 89–95. doi: 10.1067/mcp.2001.113989

Chamberlain, L. H., and Shipston, M. J. (2015). The physiology of protein S-acylation. *Physiol. Rev.* 95, 341–376.

Chavda, B., Arnott, J. A., and Planey, S. L. (2014). Targeting protein palmitoylation: selective inhibitors and implications in disease. *Expert Opin. Drug Discov.* 9, 1005–1019. doi: 10.1517/17460441.2014.933802

Chen, M. W., Zhu, H., Xiong, C. H., Li, J. B., Zhao, L. X., Chen, H. Z., et al. (2020). PKC and Ras are involved in M1 muscarinic receptor-mediated modulation of AMPA receptor GluA1 subunit. *Cell. Mol. Neurobiol.* 40, 547–554. doi: 10.1007/s10571-019-00752-x

Cheng, J., Lin, X., Morgan, D., Gordon, M., Chen, X., Wang, Z. H., et al. (2015). Dendritic and Langerhans cells respond to Abeta peptides differently: implication for AD immunotherapy. *Oncotarget* 6, 35443–35457. doi: 10.18632/oncotarget.6123

Datson, N. A., Polman, J. A., de Jonge, R. T., van Boheemen, P. T., van Maanen, E. M., Welten, J., et al. (2011). Specific regulatory motifs predict glucocorticoid responsiveness of hippocampal gene expression. *Endocrinology* 152, 3749–3757. doi: 10.1210/en.2011-0287

Friedman, J., Hastie, T., and Tibshirani, R. (2010). Regularization paths for generalized linear models via coordinate descent. *J. Stat. Softw.* 33, 1–22.

Gan, Z., Zou, Q., Lin, Y., Huang, X., Huang, Z., Chen, Z., et al. (2019). Construction and validation of a seven-microRNA signature as a prognostic tool for lung squamous cell carcinoma. *Cancer Manag. Res.* 11, 5701–5709. doi: 10.2147/CMAR.S191637

Garabadu, D., Agrawal, N., Sharma, A., and Sharma, S. (2019). Mitochondrial metabolism: a common link between neuroinflammation and neurodegeneration. *Behav. Pharmacol.* 30, 642–652. doi: 10.1097/FBP.0000000000000505

Gate, D., Saligrama, N., Leventhal, O., Yang, A. C., Unger, M. S., Middeldorp, J., et al. (2020). Clonally expanded CD8 T cells patrol the cerebrospinal fluid in Alzheimer's disease. *Nature* 577, 399–404. doi: 10.1038/s41586-019-1895-7

Gorelick, P. B., Scuteri, A., Black, S. E., Decarli, C., Greenberg, S. M., Iadecola, C., et al. (2011). Vascular contributions to cognitive impairment and dementia: a statement for healthcare professionals from the American heart association/American stroke association. *Stroke* 42, 2672–2713.

Heneka, M. T. (2017). Inflammasome activation and innate immunity in Alzheimer's disease. *Brain Pathol.* 27, 220–222. doi: 10.1111/bpa.12483

Hepworth, M. R., Greenhalgh, A. D., and Cook, P. C. (2021). B cells on the brain: meningeal IgA and a novel gut-brain firewall. *Immunol. Cell Biol.* 99, 17–20. doi: 10.1111/imcb.12412

Hoozemans, J. J., Rozemuller, A. J., van Haastert, E. S., Eikelenboom, P., and van Gool, W. A. (2011). Neuroinflammation in Alzheimer's disease wanes with age. *J. Neuroinflammation* 8:171. doi: 10.1186/1742-2094-8-171

Huang, M. L., Hung, Y. H., Lee, W. M., Li, R. K., and Jiang, B. R. (2014). SVM-RFE based feature selection and Taguchi parameters optimization for multiclass SVM classifier. *ScientificWorldJournal* 2014:795624. doi: 10.1155/2014/795624

Jian, C., Lu, M., Zhang, Z., Liu, L., Li, X., Huang, F., et al. (2017). miR-34a knockout attenuates cognitive deficits in APP/PS1 mice through inhibition of the amyloidogenic processing of APP. *Life Sci.* 182, 104–111. doi: 10.1016/j.lfs.2017.05.023

Jian, C., Wei, L., Mo, R., Li, R., Liang, L., Chen, L., et al. (2021). Microglia mediate the occurrence and development of Alzheimer's disease through ligand-receptor axis communication. *Front. Aging Neurosci.* 13:731180. doi: 10.3389/fnagi.2021.731180

Jian, C., Zou, D., Luo, C., Liu, X., Meng, L., Huang, J., et al. (2016). Cognitive deficits are ameliorated by reduction in amyloid beta accumulation in Tg2576/p75(NTR+/-) mice. *Life Sci.* 155, 167–173. doi: 10.1016/j.lfs.2016.05.011

Jorm, A. F., and Jolley, D. (1998). The incidence of dementia: a meta-analysis. *Neurology* 51, 728–733.

Kirouac, L., Rajic, A. J., Cribbs, D. H., and Padmanabhan, J. (2017). Activation of Ras-ERK signaling and GSK-3 by amyloid precursor protein and amyloid beta facilitates neurodegeneration in Alzheimer's disease. *eNeuro* 4:ENEURO.0149-16.2017. doi: 10.1523/ENEURO.0149-16.2017

Law, C. W., Chen, Y., Shi, W., and Smyth, G. K. (2014). voom: precision weights unlock linear model analysis tools for RNA-seq read counts. *Genome Biol.* 15:R29. doi: 10.1186/gb-2014-15-2-r29

Luchsinger, J. A., Reitz, C., Honig, L. S., Tang, M. X., Shea, S., and Mayeux, R. (2005). Aggregation of vascular risk factors and risk of incident Alzheimer disease. *Neurology* 65, 545–551. doi: 10.1212/01.wnl.0000172914.08967.dc

Ma, M., Liao, Y., Huang, X., Zou, C., Chen, L., Liang, L., et al. (2022). Identification of Alzheimer's disease molecular subtypes based on parallel large-scale sequencing. *Front. Aging Neurosci.* 14:770136. doi: 10.3389/fnagi.2022.770136

Mootha, V. K., Lindgren, C. M., Eriksson, K. F., Subramanian, A., Sihag, S., Lehar, J., et al. (2003). PGC-1alpha-responsive genes involved in oxidative phosphorylation are coordinately downregulated in human diabetes. *Nat. Genet.* 34, 267–273. doi: 10.1038/ng1180

Nakashima, S., Morinaka, K., Koyama, S., Ikeda, M., Kishida, M., Okawa, K., et al. (1999). Small G protein Ral and its downstream molecules regulate endocytosis of EGF and insulin receptors. *EMBO J.* 18, 3629–3642. doi: 10.1093/emboj/18.13.3629

Norton, E. S., Da Mesquita, S., and Guerrero-Cazares, H. (2021). SERPINA3 in glioblastoma and Alzheimer's disease. *Aging* 13, 21812–21813. doi: 10.18632/aging.203603

O'Brien, J. T., and Thomas, A. (2015). Vascular dementia. *Lancet* 386, 1698–1706.

Polfliet, M. M., Goede, P. H., van Kesteren-Hendrikx, E. M., van Rooijen, N., Dijkstra, C. D., and van den Berg, T. K. (2001). A method for the selective depletion of perivascular and meningeal macrophages in the central nervous system. *J. Neuroimmunol.* 116, 188–195. doi: 10.1016/s0165-5728(01)00282-x

Puig-Butille, J. A., Escamez, M. J., Garcia-Garcia, F., Tell-Marti, G., Fabra, A., Martinez-Santamaria, L., et al. (2014). Capturing the biological impact of CDKN2A and MC1R genes as an early predisposing event in melanoma and non melanoma skin cancer. *Oncotarget* 5, 1439–1451. doi: 10.18632/oncotarget.1444

Pulati, N., Zhang, Z., Gulimilamu, A., Qi, X., and Yang, J. (2019). HPV16(+) -miRNAs in cervical cancer and the anti-tumor role played by miR-5701. *J. Gene Med.* 21:e3126. doi: 10.1002/jgm.3126

Raina, A. K., Zhu, X., Rottkamp, C. A., Monteiro, M., Takeda, A., and Smith, M. A. (2000). Cyclin' toward dementia: cell cycle abnormalities and abortive oncogenesis in Alzheimer disease. *J. Neurosci. Res.* 61, 128–133. doi: 10.1002/1097-4547(20000715)61:2<128::AID-JNR2>3.0.CO;2-H

Reisberg, B., Burns, A., Brodaty, H., Eastwood, R., Rossor, M., Sartorius, N., et al. (1997). Diagnosis of Alzheimer's disease. Report of an international psychogeriatric association special meeting work group under the cosponsorship of Alzheimer's disease international, the European federation of neurological societies, the world health organization, and the world psychiatric association. *Int. Psychogeriatr.* 9(Suppl. 1), 11–38. doi: 10.1017/s1041610297004675

Ritchie, M. E., Phipson, B., Wu, D., Hu, Y., Law, C. W., Shi, W., et al. (2015). limma powers differential expression analyses for RNA-sequencing and microarray studies. *Nucleic Acids Res.* 43:e47. doi: 10.1093/nar/gkv007

Shannon, P., Markiel, A., Ozier, O., Baliga, N. S., Wang, J. T., Ramage, D., et al. (2003). Cytoscape: a software environment for integrated models of biomolecular interaction networks. *Genome Res.* 13, 2498–2504. doi: 10.1101/gr.1239303

Subramanian, A., Tamayo, P., Mootha, V. K., Mukherjee, S., Ebert, B. L., Gillette, M. A., et al. (2005). Gene set enrichment analysis: a knowledge-based approach for interpreting genome-wide expression profiles. *Proc. Natl. Acad. Sci. U.S.A.* 102, 15545–15550. doi: 10.1073/pnas.0506580102

Tan, C. C., Yu, J. T., Wang, H. F., Tan, M. S., Meng, X. F., Wang, C., et al. (2014). Efficacy and safety of donepezil, galantamine, rivastigmine, and memantine for the treatment of Alzheimer's disease: a systematic review and meta-analysis. *J. Alzheimers Dis.* 41, 615–631. doi: 10.3233/JAD-132690

Vainchtein, I. D., and Molofsky, A. V. (2020). Astrocytes and microglia: in sickness and in health. *Trends Neurosci.* 43, 144–154. doi: 10.1016/j.tins.2020.01.003

Xu, J., Zhou, Z., Zeng, L., Huang, Y., Zhao, W., Cheng, C., et al. (2001). Cloning, expression and characterization of a novel human REPS1 gene. *Biochim. Biophys. Acta* 1522, 118–121. doi: 10.1016/s0167-4781(01)00310-4

Yu, G., Wang, L. G., Han, Y., and He, Q. Y. (2012). clusterProfiler: an R package for comparing biological themes among gene clusters. *OMICS* 16, 284–287. doi: 10.1089/omi.2011.0118

Zhang, X., Zhu, C., Beecham, G., Vardarajan, B. N., Ma, Y., Lancour, D., et al. (2019). A rare missense variant of CASP7 is associated with familial late-onset Alzheimer's disease. *Alzheimers Dement.* 15, 441–452. doi: 10.1016/j.jalz.2018.10.005

Zhou, F., Chen, D., Chen, G., Liao, P., Li, R., Nong, Q., et al. (2021). Gene set index based on different modules may help differentiate the mechanisms of Alzheimer's disease and vascular dementia. *Clin. Interv. Aging* 16, 451–463. doi: 10.2147/CIA.S297483

Zhou, Y., Zhou, B., Pache, L., Chang, M., Khodabakhshi, A. H., Tanaseichuk, O., et al. (2019). Metascape provides a biologist-oriented resource for the analysis of systems-level datasets. *Nat. Commun.* 10:1523. doi: 10.1038/s41467-019-09234-6

Ziegler-Heitbrock, L. (2007). The CD14+ CD16+ blood monocytes: their role in infection and inflammation. *J. Leukoc. Biol.* 81, 584–592. doi: 10.1189/jlb.0806510

Zou, C., Wang, J., Huang, X., Jian, C., Zou, D., and Li, X. (2019). Analysis of transcription factor- and ncRNA-mediated potential pathogenic gene modules in Alzheimer's disease. *Aging* 11, 6109–6119. doi: 10.18632/aging.102169

Zou, D., Li, R., Huang, X., Chen, G., Liu, Y., Meng, Y., et al. (2019). Identification of molecular correlations of RBM8A with autophagy in Alzheimer's disease. *Aging* 11, 11673–11685. doi: 10.18632/aging.102571

Conflict of Interest: The authors declare that the research was conducted in the absence of any commercial or financial relationships that could be construed as a potential conflict of interest.

Publisher's Note: All claims expressed in this article are solely those of the authors and do not necessarily represent those of their affiliated organizations, or those of the publisher, the editors and the reviewers. Any product that may be evaluated in this article, or claim that may be made by its manufacturer, is not guaranteed or endorsed by the publisher.

frontiers | Frontiers in Aging Neuroscience

ORIGINAL RESEARCH
published: 20 July 2022
doi: 10.3389/fnagi.2022.945875

Selective Detection of Misfolded Tau From Postmortem Alzheimer's Disease Brains

Ling Wu[1,2†], Zerui Wang[3†], Shradha Lad[2], Nailya Gilyazova[1], Darren T. Dougharty[2], Madeleine Marcus[2], Frances Henderson[2], W. Keith Ray[2], Sandra Siedlak[3], Jianyong Li[2], Richard F. Helm[2], Xiongwei Zhu[3], George S. Bloom[4], Shih-Hsiu J. Wang[5], Wen-Quan Zou[3] and Bin Xu[1,2,6]**

[1] Department of Pharmaceutical Sciences, Biomanufacturing Research Institute and Technology Enterprise (BRITE), North Carolina Central University, Durham, NC, United States, [2] Department of Biochemistry, Virginia Polytechnic Institute and State University, Blacksburg, VA, United States, [3] Department of Pathology, Case Western Reserve University, Cleveland, OH, United States, [4] Departments of Biology, Cell Biology, and Neuroscience, University of Virginia, Charlottesville, VA, United States, [5] Department of Pathology and Neurology, Duke University Medical Center, Durham, NC, United States, [6] School of Neuroscience, Virginia Polytechnic Institute and State University, Blacksburg, VA, United States

Tau aggregates are present in multiple neurodegenerative diseases known as "tauopathies," including Alzheimer's disease, Pick's disease, progressive supranuclear palsy, and corticobasal degeneration. Such misfolded tau aggregates are therefore potential sources for selective detection and biomarker discovery. Six human tau isoforms present in brain tissues and both 3R and 4R isoforms have been observed in the neuronal inclusions. To develop selective markers for AD and related rare tauopathies, we first used an engineered tau protein fragment 4RCF as the substrate for ultrasensitive real-time quaking-induced conversion analyses (RT-QuIC). We showed that misfolded tau from diseased AD and other tauopathy brains were able to seed recombinant 4RCF substrate. We further expanded to use six individual recombinant tau isoforms as substrates to amplify misfolded tau seeds from AD brains. We demonstrated, for the first time to our knowledge, that misfolded tau from the postmortem AD brain tissues was able to specifically seed all six full-length human tau isoforms. Our results demonstrated that RT-QuIC analysis can discriminate AD and other tauopathies from non-AD normal controls. We further uncovered that 3R-tau isoforms displayed significantly faster aggregation kinetics than their 4R-tau counterparts under conditions of both no seeding and seeding with AD brain homogenates. In summary, our work offers potential new avenues of misfolded tau detection as potential biomarkers for diagnosis of AD and related tauopathies and provides new insights into isoform-specific human tau aggregation.

Keywords: selective detection, RT-QuIC, Alzheimer's disease, protein aggregation, tau isoforms

OPEN ACCESS

Edited by:
Woon-Man Kung,
Chinese Culture University, Taiwan

Reviewed by:
Takehiro Nakagaki,
Nagasaki University, Japan
Myung Chul Choi,
KAIST, South Korea
Samir Abu Rumeileh,
Martin Luther University of Halle-Wittenberg, Germany
Balaji Krishnan,
University of Texas Medical Branch at Galveston, United States

***Correspondence:**
Bin Xu
bxu@nccu.edu
Wen-Quan Zou
wxz6@case.edu

† These authors have contributed equally to this work

Specialty section:
This article was submitted to Alzheimer's Disease and Related Dementias, a section of the journal Frontiers in Aging Neuroscience

Received: *17 May 2022*
Accepted: *21 June 2022*
Published: *20 July 2022*

Citation:
Wu L, Wang Z, Lad S, Gilyazova N, Dougharty DT, Marcus M, Henderson F, Ray WK, Siedlak S, Li J, Helm RF, Zhu X, Bloom GS, Wang S-HJ, Zou W-Q and Xu B (2022) Selective Detection of Misfolded Tau From Postmortem Alzheimer's Disease Brains. Front. Aging Neurosci. 14:945875. doi: 10.3389/fnagi.2022.945875

Abbreviations: AD, Alzheimer's disease; CBD, Corticobasal degeneration; CNS, Central nervous system; Cryo-EM, Cryo-electron microscopy; CSF, Cerebrospinal fluid; MT, Microtubule; NFT, Neurofibrillary tangle; PBS, Phosphate-buffered saline; PHF, Paired helical filament; PiD, Pick's disease; PMCA, Protein misfolding cyclic amplification; PSP, Progressive supranuclear palsy; RFU, Relative fluorescence unit; RT-QuIC, Real-time quaking-induced conversion; TEM, Transmission electron microscopy; ThT, Thioflavin T.

INTRODUCTION

Alzheimer's disease (AD) is characterized by the accumulation in the brain of two types of abnormal structures in the brain, extracellular Aβ amyloid plaques and intraneuronal tau neurofibrillary tangles (Braak and Braak, 1991; Selkoe, 2001). Until recently, plaques and tangles were thought not only to represent molecular hallmarks of AD, but also to cause the synaptic dysfunction and neuronal death that lead to the memory and cognitive deficits characteristic of AD patients (Bloom, 2014; Spires-Jones and Hyman, 2014). Several lines of evidence have suggested that pathological changes in tangles correlate better with neuronal dysfunction than Aβ deposits (Wilcock and Esiri, 1982; Nelson et al., 2012). Moreover, a close relationship between tau aggregates and neuronal loss is well established in hippocampus and cerebral cortex tissues (Goedert and Spillantini, 2017). Tau aggregates are present not only in AD brains, but also in multiple neurodegenerative diseases known as "tauopathies" (Arai et al., 2001; Lee et al., 2001), including Pick's disease (PiD), progressive supranuclear palsy (PSP), and corticobasal degeneration (CBD). Six tau isoforms are expressed in adult human brain, produced by alternative mRNA splicing of transcripts from *MAPT* gene. These isoforms contain either three or four microtubule-binding repeats (3R or 4R tau) and 0-2 N-terminal inserts (0N, 1N, or 2N tau) (**Figure 1A**) (Goedert et al., 1989). Significantly, isoform composition and morphology of tau filaments can differ between tauopathies, suggesting the existence of distinct misfolded tau strains, molecular heterogeneity and complexity of these tauopathy diseases (Kaufman et al., 2016; Dujardin et al., 2018; Vaquer-Alicea et al., 2021). In AD, both 3R and 4R isoforms make up the neuronal inclusions, whereas in PiD, 3R isoforms predominate in the neuronal deposits. The assembly of 4R tau into filaments is a characteristic of PSP and CBD. Transmission of the AD pathology and related tauopathies is not fully understood, but is believed to be through "prion-like seeding" mechanisms that ultimately yield intercellular spreading of toxic tau aggregates (Guo and Lee, 2011, Guo et al., 2016; Swanson et al., 2017; Gibbons et al., 2019; Vaquer-Alicea and Diamond, 2019; Goedert, 2020).

Traditionally, definitive diagnosis of AD relies on postmortem neuropathological examination and confirmation of the presence of both neurofibrillary tangles and Aβ plaques. More recently, clinical diagnosis of AD and AD-related dementia (ADRD) is supported by imaging biomarkers such as positron emission tomography which is relatively expensive for patients, or by CSF biomarkers such as Aβ42, Aβ42/40 ratio, phosphorylated tau, and total tau which involves an invasive spinal tap procedure. Identifying biomarkers for the development of non-invasive or minimally invasive and inexpensive testing across AD and ADRD is an urgent and unmet need. Many protein misfolding diseases, such as AD (Chiti and Dobson, 2017), Parkinson's disease (Lee and Trojanowski, 2006), prion disease (Prusiner, 2013), and type 2 diabetes (Westermark et al., 2011; Wu et al., 2021), involve analogous pathological accumulation of disease-specific amyloidogenic protein in the form of self-seeding filaments or sub-filamentous deposits. An ultrasensitive detection method of misfolded proteins, named real-time quaking-induced conversion (RT-QuIC), originated from prion disease detection (Moda et al., 2014; Orru et al., 2017; Wang et al., 2019), gained significant application for *in vitro* amplification in a number of neurodegenerative diseases, such as Aβ oligomers in AD (Salvadores et al., 2014) and α-synuclein in Parkinson's disease (Fairfoul et al., 2016; Shahnawaz et al., 2017; Groveman et al., 2018; Wang et al., 2020). Using engineered short fragments of tau (K19 or K12) or a mixture of tau fragments (K19 + τ306, K18 + K19) as substrates, specific detection of the prion-like tau seeding activities by RT-QuIC assays had been reported with autopsy brain tissues of AD, Pick's disease, and chronic traumatic encephalopathy (Saijo et al., 2017; Kraus et al., 2019; Metrick et al., 2020). However, whether other tau fragments (such as K18-mimicking 4RCF alone), can serve as effective substrates to amplify the misfolded tau seeds relevant to the pathogenesis of AD and related tauopathies are not well studied. 4RCF tau is an engineered, truncated tau fragment spanning 2N4R amino acid sequence 244-372 (four repeat segments of 2N4R; **Figure 2A**), the essential segments that contribute to 4R tau aggregation. Of particular interest and importance, full-length wild-type human tau isoforms, the *bona fide* forms of tau protein in the brain, have not been studied as effective seeding substrates for AD and related tauopathies. Given the complexity of molecular pathology of AD and related tauopathies, a diverse set of tau substrate constructs will provide a versatile toolbox for selective detection of AD and other tauopathies in diagnosis, differentiation, and disease course prognostication using ultrasensitive detection technologies such as RT-QuIC and protein misfolding cyclic amplification (PMCA) (Saá et al., 2005; Shahnawaz et al., 2020).

In this study, we demonstrated that prion-like seeding activities of misfolded tau from post-mortem AD brains with not only a novel engineered tau fragment 4RCF, but also all six full-length 3R-tau and 4R-tau isoforms as effective substrates. The results suggested that selective use of various recombinant human tau isoforms or fragments may be critical in developing RT-QuIC-based diagnosing, characterizing, and predicting consequences of AD and non-AD tauopathies. Our kinetic measurements also revealed isoform-specific aggregation properties that 3R tau isoforms aggregated significantly faster than their 4R counterparts, which may have physiological or pathological significance as we gain better understanding of poorly understood functions of six tau isoforms in human brains.

MATERIALS AND METHODS

Plasmid Constructs

Expression vectors for his-tagged versions of all six wild-type human tau isoforms were kindly provided by the late Dr. Lester "Skip" Binder and Dr. Nicolas Kanaan of Michigan State University. 4RCF construct (four microtubule-binding repeats and cysteine-free construct containing C291S and C322S mutations) was first PCR-amplified of 4R repeats sequence from 2N4R tau plasmid and cloned into the same expression vector using *Nde*I and *Xho*I restriction sites, followed by site-directed mutagenesis at Cys291 and Cys322 sites using QuikChange Site-directed mutagenesis kit (Agilent, Santa Clara, CA). All

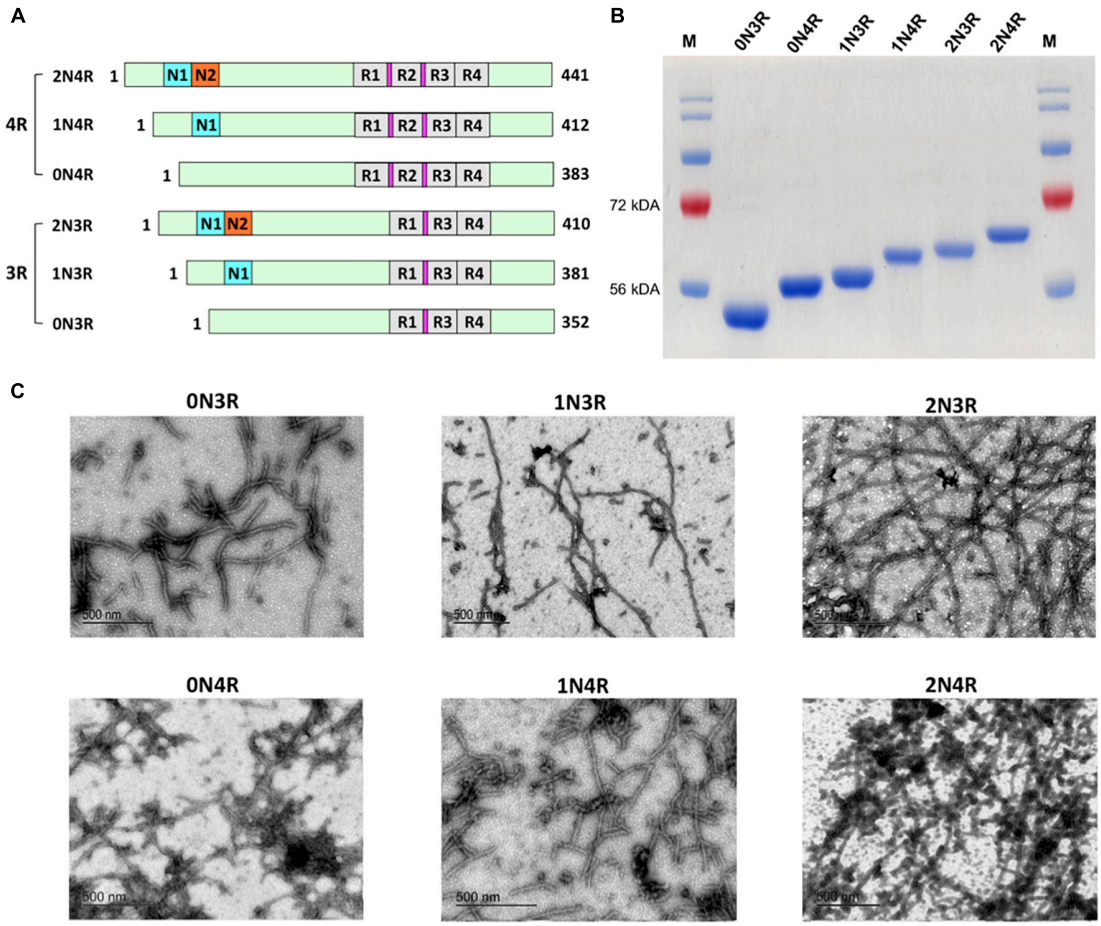

FIGURE 1 | Human tau isoforms. **(A)** Schematic illustration of the alternative spliced six isoforms of human CNS tau. Amino-terminal insert domains (N1 and N2) and carboxy-terminal repeat domains (R1-R4) are shown. Amino acid residue numbers for each isoform are listed. Locations for the hexapeptide sequences (VQIINK in R2 and VQIVYK in R3) are highlighted in magenta. **(B)** SDS-PAGE analysis demonstrated six recombinant human tau isoforms purified to homogeneity. **(C)** TEM images of mature filaments of all six human tau isoform are shown. 30 μM of each tau isoform was prepared in 20 mM Tris pH 7.4 with 0.06 mg/ml heparin and incubated at 37°C for 12 days. Mature tau isoform fibrils were visualized after staining with uranyl acetate.

constructs were designed with a his_6-tag at their carboxy-termini to facilitate protein purification and were verified by DNA sequencing.

Brain Tissue Collection, Handling and Analysis

The autopsy brain samples were collected and diagnosed neuropathologically at Case Western Reserve University Alzheimer's Disease Research Center and Case Human Tissue Procurement Facility. Diagnostic guidelines follow the National Institute on Aging-Alzheimer's Association workgroups (McKhann et al., 2011). All protocols currently in place were to support and facilitate the research in the context of IRB and HIPAA regulations, by articulating and implementing criteria allowing the acquisition, storage and distribution for research use of such data and specimens with or without linkage to personal health identifiers. Postmortem brain tissues for research usage was approved by the Case Western Reserve University's Institutional Review Board (IRB) with informed consent from patients or their families. Additional postmortem control and rare tauopathy brain samples were collected from the Bryan Brain Bank and Biorepository of the Duke University/University of North Carolina Alzheimer's Disease Research Center (Duke/UNC ADRC). All participants were enrolled in the autopsy and brain donation program of the Joseph and Kathleen Price Bryan ADRC as previously described (Hulette et al., 1998). All subjects gave informed consent. All protocols were approved by the Duke University's IRB. Neuropathological evaluation was performed following published guidelines (Cairns et al., 2007; Hyman et al., 2012; McKeith et al., 2017; Nelson et al., 2019). Postmortem brain tissues were homogenized at 10% (w/v) in lysis buffer (10 mM Tris pH 7.4, 150 mM NaCl, 0.5% Nonidet P-40, 0.5% deoxycholate, 5 mM EDTA) with mini Beads Beater or hand-held homogenizer. The brain homogenates were further subjected to centrifugation at 1,000 x g for 3 min at 4°C and the supernatants were collected and stored at -80°C for RT-QuIC assays as seeds or for other analyses such as Western blotting.

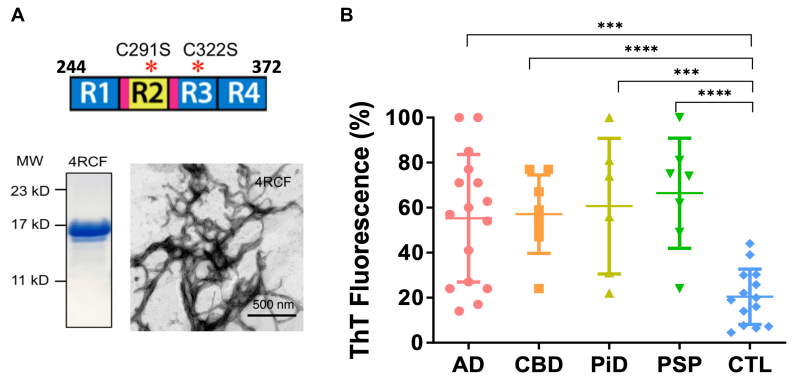

FIGURE 2 | Recombinant truncated tau protein 4RCF and scattered plot of tau-aggregation seeding activity (tau-ASA) of brain tissues from tauopathies. **(A)** Schematic representation of truncated tau protein (upper panel; four repeating segments of 2N4R only, with two cysteine to serine mutations – cysteine free, therefore its name 4RCF; it covers the four-repeating segment of tau by spanning the amino acid sequence from 244 to 372 of the longest isoform 2N4R tau). Locations for the hexapeptide sequences (VQIINK in R2 and VQIVYK in R3) are highlighted in magenta. SDS-PAGE of purified recombinant 4RCF and corresponding 4RCF fibrils transmission electron microscopy (TEM) image are shown in the lower panels. **(B)** Tau-ASA is represented by the percentage of tau ThT fluorescence at the endpoint of brain tissues after real-time quaking-induced conversion analyses (RT-QuIC) assay. Corresponding time-dependent ThT fluorescence kinetic curves are shown in **Supplementary Figure 4**. The brain tissues from Alzheimer's disease (AD) (n = 16), CBD (n = 8), PiD (n = 6), PSP (n = 7) and control (CTL, n = 14) were examined by RT-QuIC assay in the presence of the 4RCF tau substrate. AD: 55.3 ± 28.4 (average ± SD); CBD: 57.1 ± 17.5; PiD: 60.7 ± 30.1; PSP: 66.4 ± 24.5 and CTL: 21.0 ± 12.1. ****$p < 0.0001$; ***$p < 0.0004$.

Demographic Characteristics and Neuropathological Diagnosis of Clinical Patients

Alzheimer's disease (AD) patients, non-AD subjects, PiD, PSP, and CBD rare tauopathy patients are as the following: patient ages (in years ± standard deviation) are 71.9 ± 10.1, 72.4 ± 18.3, 74.2 ± 7.0, 77.9 ± 9.7, and 70.3 ± 10.8 for AD, non-AD control, PiD, PSP and CBD patients, respectively. In the same order of these groups, number of male (%) are 11 (61.1%), 12 (63.2%), 0 (0%), 5 (50%) and 3 (33.3%) respectively, and PMI (Post-Mortem Interval; in hours) are 11.2 ± 10.4, 12.0 ± 7.5, 10.2 ± 5.4, 18.9 ± 15.9, and 16.3 ± 12.7, respectively. For the control cohorts, neuropathological diagnosis include mild amyloid angiopathy, mild or moderate atherosclerosis, infarct or microscopic infarcts, microhemorrorhages, metabolic astrocytosis, argyrophilic grain disease. For most of the control subjects, Aβ-plaque scores A0 or A1, the Braak NFT stage scores B0 or B1, and the CERAD neuritic plaque scores C0 or C1. For AD cohorts, most subjects have Aβ-plaque scores A2 or A3, the Braak NFT stage scores B2 or B3, and the CERAD neuritic plaque scores C2 or C3. Some AD cohorts have comorbid conditions of LBD. Rare tauopathies subjects generally have low Thal phases (0–1), indicating no amyloid plaques or plaques limited to neocortex.

Recombinant Tau Fragment 4RCF and Full Length Human Tau Isoforms Expression and Purification

Plasmids encoding human tau isoforms or truncation mutant 4RCF were transformed into BL21-DE3 E. coli cells. Overnight starter cultures of BL21-DE3 E. coli cells transformed with recombinant tau plasmids were inoculated into multi-liter LB broth at 1:50 dilution and 100 mg/mL ampicillin. Cultures were incubated at 37°C, shaking until OD_{600} reached between 0.5 and 0.6. Tau expression was induced using 1 mM IPTG and continued to grow for an additional 4 h. BL21- DE3 cells containing expressed tau were pelleted and resuspended in 50 mM NaH_2PO_4, pH 8.0 and 300 mM NaCl (sonication lysis buffer) at a concentration of 20 mL/L of culture preparation and sonicated at 60% power in ten 30-s intervals over 10 min. An extra boiling step at 90°C for 20 min was added for all full-length tau isoforms before centrifugation (Barghorn et al., 2005). Cell lysates were centrifuged and supernatant containing the protein was applied to Ni-NTA column equilibrated with sonication lysis buffer. The columns were washed with 30-50 times of bed volumes of column buffer followed by washing buffer (50 mM NaH_2PO_4, pH 8, 300 mM NaCl, and 20 mM imidazole). Recombinant protein was then eluted using elution buffer (50 mM NaH_2PO_4, pH 8, 300 mM NaCl, and 200 mM imidazole). Fractions were tested for protein concentration using 5 μL of protein sample mixed with 10 μL Coommassie Protein Assay reagent (Thermo Scientific). Pooled fractions were concentrated to 4 mL using 10 kD molecular weight cut-off spin columns (Millipore) and filtered using 0.22 μm low-binding Durapore PVDF membrane filters (Millipore). Tau protein was further purified by FPLC using size exclusion Superdex75 and Superdex200 columns (GE Healthcare) in 1X PNE buffer (25 mM PIPES, 150 mM NaCl and 1 mM EDTA at pH 7.0). Purified tau isoforms or tau fragment were evaluated by SDS-PAGE for purity and quantified by BCA protein assays.

Extraction of Paired Helical Filament-Tau From Alzheimer's Disease Brains

Paired Helical Filament (PHF)-tau purification follows established protocols (Goedert et al., 1992; Lee et al., 1999; Guo et al., 2016). Briefly, brain tissues from sporadic AD patients

with abundant tau pathology qualified for AD were used in this study. All cases used were histologically confirmed. For each purification, 10–12 g of frontal cortical gray matter was homogenized using a homogenizer in 9:1 (v/w) of high-salt buffer (10 mM Tris-HCl, pH 7.4, 0.8 M NaCl, 1 mM EDTA, and 2 mM dithiothreitol, with protease inhibitor cocktail, with 0.1% Sarkosyl and 10% sucrose added and centrifuged at 10,000 g for 10 min at 4°C). Pellets were reextracted once or twice using the same buffer conditions as the starting materials, and the supernatants from all two to three initial extractions were filtered and pooled. Additional Sarkosyl was added to the pooled low-speed supernatant to reach 1%. After 1-h nutation at room temperature, samples were centrifuged again at 300,000 g for 60 min at 4°C. The resulted 1% Sarkosyl-insoluble pellets, which contain pathological tau (PHF-tau), were washed once in PBS and then resuspended in PBS (100 μl/g gray matter) by passing through 27-G 0.5-in. needles. The resuspended Sarkosyl-insoluble pellets were further purified by a brief sonication (20 pulses at 0.5 s/pulse) followed by centrifugation at 100,000 *g* for 30 min at 4°C, whereby the majority of protein contaminants were partitioned into the supernatant, with 60–70% of tau remaining in the pellet fraction. The pellets were resuspended in PBS at one fifth to one half of the pre-centrifugation volume, sonicated with 20–60 short pulses (0.5 s/pulse), and spun at 10,000 g for 30 min at 4°C to remove large debris. The final supernatants, which contained enriched AD PHFs, were used in the study and referred to as PHF-tau or AD-tau. The final supernatant fraction was further analyzed by SDS-PAGE, Western blotting, BCA protein assays, and mass spectrometry.

Thioflavin-T Fluorescence Aggregation Kinetic Analysis

Fluorescence experiments were performed using a SpectraMax M5 plate reader (Molecular Devices, Sunnyvale, CA). All kinetic reads were taken at 37°C in non-binding all black clear bottom Greiner 96-well plates covered with optically clear films and stirred for 10 s prior to each reading. ThT fluorescence was measured at 444 nm and 491 nm as excitation and emission wavelengths. Each kinetic assay consisted of final concentrations of 30 μM tau protein, 60 μg/ml heparin, and 10 μM ThT. The amount of time required to reach half maximum ThT intensity ($t_{1/2}$) and inhibition constant (IC_{50}) values for dose response curves were estimated by multiparameter logistic non-linear regression analysis. The transition from the lag-phase to the growth phase was estimated when the first measurable ThT fluorescence/time (slope) value exceeded ≥5 fold of the previous measured slope (i.e., where the quantum leap in ThT RFU is first noticeable).

Sarkosyl-Insoluble Tau Pelleting Assay

Purified recombinant tau (10 μM) and heparin (100 μg/ml) were incubated at 37°C for 48 h in 30 mM Tris-HCl, pH 7.5, containing 20 mM DTT. Aggregated tau was assayed on the basis of 1% Sarkosyl insolubility as described below. Aliquots (10 μl) of assembly mixtures were removed and added to 50 μl of 30 mM Tris-HCl, pH 7.5, containing 1% Sarkosyl, and the mixture was left for 30 min. The mixture was then spun at 150,000 × *g* for 20 min. The supernatant (Sarkosyl-soluble tau) was removed, and the pellet (Sarkosyl-insoluble tau) was resuspended in 20 μl of SDS sample buffer containing 5% 2-mercaptoethanol and subjected to SDS-PAGE. Aggregated tau isoforms were visualized after staining of the gel with Coomassie Brilliant Blue.

Transmission Electron Microscopy Analysis

Transmission electron microscopy (TEM) images were collected as previously described (Velander et al., 2016; Wu et al., 2017). Briefly, 30 μM human tau isoforms were incubated in 20 mM Tris-HCl, pH 7.4 for 10–12 days at 37°C. Prior to imaging, 2 μL of sample were blotted on a 200 mesh formvar-carbon coated grid for 5 min, and stained with uranyl acetate (1%) for 1 min. Both sample and stain solutions were wicked dry (sample dried before addition of stain) by filter paper. Qualitative assessments of the amount of fibrils or oligomers observed were made by taking representative images following a careful survey of each grid. At least 15–20 locations of each grid were observed. TEM was performed on a JEOL-1400 transmission electron microscope (JOEL United States, Inc., Peabody, MA) operated at 120 kV.

Real-Time Quaking-Induced Conversion Analysis

Tau RT-QuIC assays were conducted as previously described with minor modifications (Orru et al., 2017; Saijo et al., 2017; Kraus et al., 2019; Wang et al., 2019). In brief, each recombinant tau isoform was thawed at room temperature and filtered with a 100 kDa spin column filter (Millipore) to remove unwanted tau aggregates. RT-QuIC reaction mix was composed of 10 mM HEPES, 400 mM NaCl, and 10 μM thioflavin T (ThT) and was filtered through a 0.22 μm filter before use. Each tau isoform was slowly and gently added into the RT-QuIC reaction mix at a final concentration of 12 μM. A 98 μl of RT-QuIC reaction mix containing tau isoform was loaded into each well of a 96-well plate (Nunc). The 10% brain homogenates were diluted at 1:200 in a dilution buffer containing 10 mM HEPES and 1.7% 1 × N2 supplement (Gibco) in 1x PBS and centrifuged at 2,000 *g* for 2 min at 4°C. A 2 μl of diluted brain homogenate was added to the 98 μl of RT-QuIC reaction mix in each well with or without 800 μm silica beads (OPS Diagnostics, Lebanon, NJ). The plate was then sealed with a plate sealing tape (Nalgene Nunc International) and incubated at 37°C in a BMG FLUOstar Omega plate reader (BMG Labtech, Cary, NC) with cycles of 1 min shaking (500 rpm orbital) and 1 min rest throughout the incubation time. ThT fluorescence measurements were monitored every 45 min using 450 ± 10 nm excitation and 480 ± 10 nm emission by bottom reading. Four replicate reactions were prepared at the same dilution for each individual sample. The average fluorescence values per sample were calculated using fluorescence values from all four replicate wells and are shown as one trace. The seeding activity was considered to be tau positive if the ThT fluorescence signal exceeded a threshold reading. The threshold

was defined as the average of mean baseline readings for all the negative controls plus four times the standard deviation of those readings.

Western Blotting Analysis

10% brain homogenates were resuspended in 1x Laemmli sample buffer in sample preparation. Standard procedures were followed as previously described (Wu et al., 2021). Briefly, proteins were transferred to PVDF membranes. The membranes were blocked with 5% non-fat dry milk in PBS-T buffer (0.1% Tween-20 in PBS) for 1 h followed by overnight incubation at 4°C with primary antibody. For human tau isoform detection from postmortem AD brains, anti-tau mAb (HT7; ThermoFisher Scientific, Waltham, MA) was used. After three washes with PBS-T buffer, the membrane was incubated with secondary antibody conjugated with HRP for 1 h at room temperature. The membranes were incubated with Amersham ECL reagents (GE Life Sciences) for signal development after PBS-T and PBS washes.

Mass Spectrometric Analysis

Paired helical filament (PHF)-tau extracted from neuropathologically diagnosed AD patient brain cortex tissues were processed using S-Trap protocols as detailed by the manufacturer (ProtiFi) and described elsewhere (Gustin et al., 2022). Peptides (10 μl) were injected onto an Easy-nLC 1200 UPLC equipped with a nanospray C18 column (ES801A). The data acquisition and UPLC method lasted for 126 minutes. The mass spectrometer (ThermoFisher Lumos) was operated with an ion spray voltage of 3.0 kV and the ion transfer tube was maintained at 275 degree Celsius. MS data was collected in profile mode while tandem MS data was collected in centroid mode. Raw data was converted to mascot generic format using Proteome Discoverer 2.2 and then searched using Mascot server 2.6.2. The database used was Homo sapiens combined with the Proteome Discoverer contaminants database along with the reversed decoy. Full detailed are provided in the **Supplementary Material**.

Statistical Analysis

All data are presented as the mean ± S.E.M and the differences were analyzed with unpaired Student's *t*-test as implemented within GraphPad Prism software (version 6.0). $p < 0.05$ were considered significant. Tau RT-QuIC data were plotted and analyzed using GraphPad Prism as well.

RESULTS

Recombinant Full-Length Tau Isoforms and Engineered Tau Fragment 4RCF Are Capable of Forming Protein Fibrils

All tau isoforms and truncation mutant were purified to homogeneity (>90% purity) by Ni-NTA affinity chromatography and additional steps of size exclusion chromatography. Full-size tau isoforms (**Figure 1A**) went through an additional boiling step for enhanced purity (> 95%; **Figure 1B**) (Barghorn et al., 2005). Recombinant human tau isoforms were capable of generating circular oligomers (data not shown) as well as mature fibrils that can be visualized by transmission electron microscopy (TEM; **Figure 1C**). We noticed that it takes a significantly longer time period (typically 10–12 days under typical incubation conditions) to form tau fibrils, in marked contrast to other more amyloidogenic proteins such as amylin, for which it takes only 2–3 days to form mature fibrils under similar buffer conditions (Velander et al., 2016; Wu et al., 2017).

4RCF tau is an engineered, truncated fragment of the longest isoform of tau isoform 2N4R tau, spanning 2N4R amino acid sequence 244-372 (four repeats of 2N4R) and a carboxy-terminal his_6-tag to facilitate purification (**Figure 2A**). Two free cysteine residues C291, C322 were mutated to serine to minimized aberrant inter-molecular crosslinking during expression and purification. Recombinant 4RCF was purified to homogeneity (> 90% purity) and was competent to aggregate and generate protein fibrils (**Figure 2A**). In comparison with full-length 4R-tau isoforms (0N4R, 1N4R, and 2N4R), 4RCF displayed significantly faster aggregation kinetics, reaching ThT fluorescence signal plateau in approximately 1 h (**Supplementary Figure 1**) versus 40–60 h for full-length 4R-tau isoforms (**Figure 3**).

Verification of Tau Isoforms in Paired Helical Filament-Tau Extracted From Postmortem Alzheimer's Disease Brains

To verify the existence of multiple human tau isoforms, we purified enriched PHF-tau (AD tau) from postmortem AD brains, following Sarkosyl extraction-based protocols (Lee et al., 1999; Guo et al., 2016). Enriched PHF-tau was clustered between 45 and 70 kD in migration in SDS-PAGE gel (**Supplementary Figure 2**). These isoforms were confirmed using Western blotting (**Supplementary Figure 2**) with an anti-tau monoclonal antibody (HT7) that targets the conserved PPGQK sequence (corresponding to residues 159-163 in 2N4R). Our Western blotting analysis showed at least three closely clustered bands (**Supplementary Figure 2**), in good agreement with PHF-tau preparations described in the literature (Goedert et al., 1992; Guo et al., 2016). Additional TEM characterization of the native tissues showed circular aggregates and fibril species of assembled tau isoforms as reported in the literature (Guo et al., 2016; data not shown). In an effort to identify human tau isoforms, we performed high resolution mass spectrometric analyses of AD brain extracted PHF-tau via a standard bottom-up analysis of released tryptic peptides. The clustered protein bands from SDS-PAGE gel were excised, underwent trypsin-digestion, and resulting fragments were confirmed as human tau isoforms by mass spectrometry (**Supplementary Figure 3** and **Supplementary Table 1**). High-resolution mass spectrometry verified the presence of multiple human tau isoforms by observing the tau isoform fragments (**Supplementary Table 1**). The results provided unambiguous identification of peptides found in all six isoforms although one cannot provide relative ratios for all six without using labeled standards as there are no prototypic

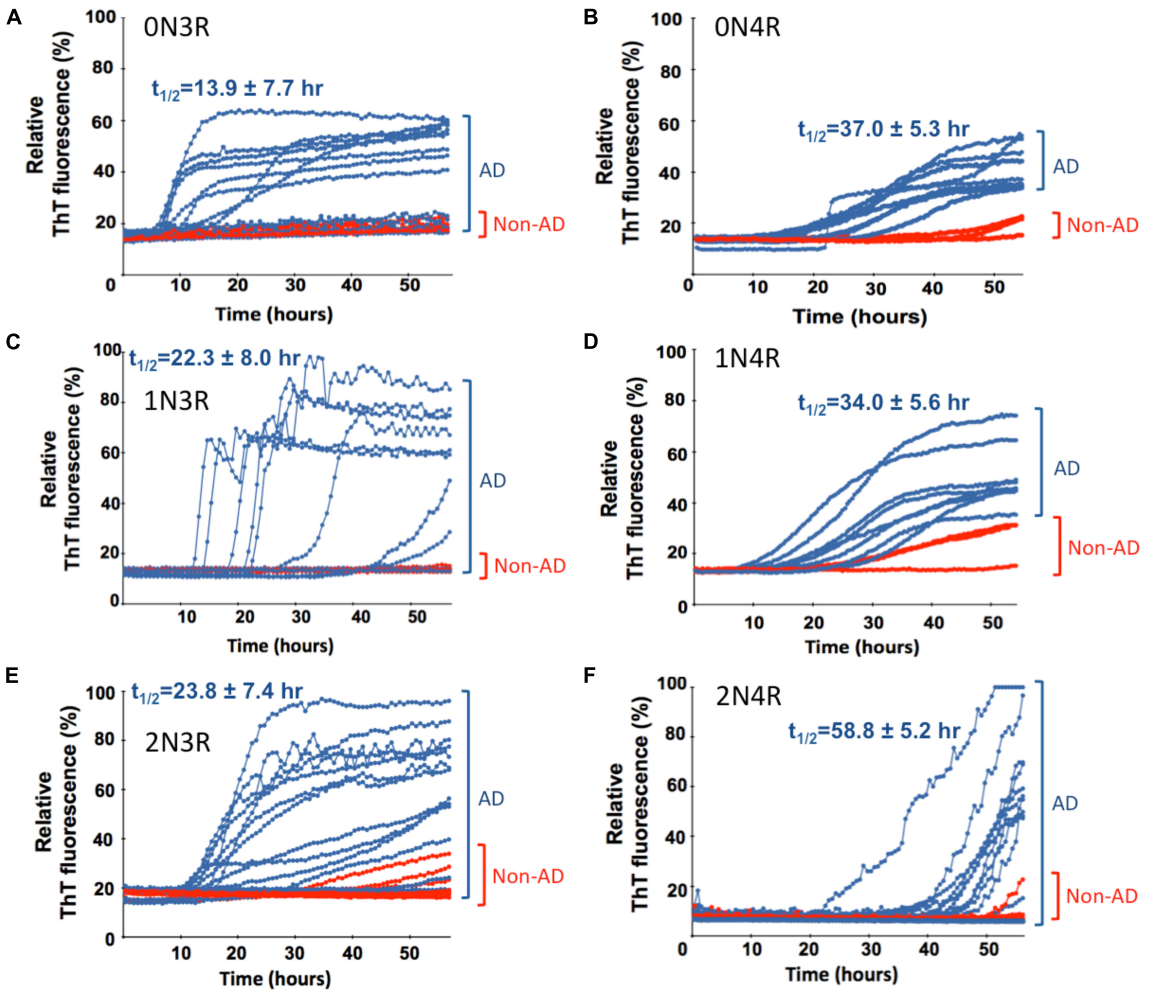

FIGURE 3 | Real-time quaking-induced conversion analyses (RT-QuIC) analysis of seeding activity of misfolded tau from autopsy brain tissues of post-mortem Alzheimer's disease (AD) and non-AD cadavers in the presence of different recombinant tau isoform (labeled) as a substrate. Tau seeding activity of neuropathologically confirmed AD brains was examined by RT-QuIC assays in the presence of six different individual recombinant full-length tau isoforms. For all panels, seeding activities with AD brain homogenate are shown in blue traces and red traces for non-AD cases. Scattered plots, statistical evaluation of seeding activities, and numbers of cases for AD and non-AD control brains are shown in **Figure 4**. Average $t_{1/2}$ values for the seeding traces of misfolded tau from AD brains with individual tau isoform substrate are indicated and related scattered plots and statistical evaluation are shown in **Supplementary Figure 5**.

peptides for any individual isoform (**Supplementary Figure 3** and **Supplementary Table 1**).

4RCF-Tau-Based Real-Time Quaking-Induced Conversion Assay Selectively Detects Misfolded Tau Seeds in the Alzheimer's Disease and Related Tauopathies Brains

Real-time quaking-induced conversion analyses (RT-QuIC) assay has been recently used for detection of seeding activities of misfolded proteins, first for prions and then for αSyn and tau *in vitro* (Atarshi et al., 2008; Orru et al., 2017; Kraus et al., 2019). To differentiate misfolded tau seeds in postmortem tauopathy brains from normal controls, an endpoint RT-QuIC-based tau-aggregation seeding activity (tau-ASA) assay was developed using tau fragment 4RCF as the substrate. 4RCF tau has a similar sequence as K18 tau reported in the literature (von Bergen et al., 2001) but with serine mutations at Cys291 and Cys322 (**Figure 2A**). Such mutations help to avoid protein aggregation during protein expression and purification due to free cysteine mispairing. We examined postmortem brain samples from AD, CBD, PiD, PSP and normal control group by RT-QuIC assays in the presence of 4RCF tau substrate. The concentrations of the substrate and the brain homogenate seeds used for our studies (full-length tau isoform-based RT-QuIC assays included) were determined by our pre-experiments according to recent studies by others (Saijo et al., 2017; Kraus et al., 2019; and Metrick et al., 2020). Specifically, we first conducted the RT-QuIC assays without brain homogenate tau seeds in the presence of different concentrations of recombinant tau substrates but excluded the concentrations that showed self-aggregation during

reactions. Then we did seed titrations with selected tau protein concentration to find the best condition showing no or less spontaneous reaction but high sensitivity for our subsequent studies. Tau-ASA, represented by the percentage of tau ThT fluorescence at the endpoint of brain tissues after RT-QuIC assay, indicated significantly higher levels of misfolded tau seeds from tauopathies brains that included 16 cases of AD, 8 cases of CBD, 6 cases of PiD, and 7 cases of PSP (n = 37 in total) than those from non-tauopathy controls (n = 14) (**Figure 2B**, $P < 0.0001$ or 0.0004). Corresponding time-dependent kinetic profiles of these RT-QuIC assays with 4RCF substrate are shown in **Supplementary Figure 4**. This RT-QuIC-based assay, therefore provided a means to differentiate AD and other tauopathies from normal controls. We did not observe any significant differences about seeding activities with 4RCF substrate among samples from 3R-predominant tauopathy (PiD), 4R-predominant tauopathies (PSP, CBD), and 3R/4R mixed tauopathy (AD). Therefore no 3R/4R sample preference was noticed. RT-QuIC ThT signal profiles were heterogenous and overlapping among AD and different tauopathies, albeit average ThT fluorescene for each disease category was significant elevated than the control cases after 50 h of amplification (**Supplementary Figure 4**).

Full-Length Tau Isoform-Based Real-Time Quaking-Induced Conversion Analyses Assays Selectively Detect Misfolded Tau Seeds in Alzheimer's Disease Brains

To further extend our work and to test the *bona fide* substrates in AD brains, we sought to determine whether various recombinant full-length wild-type human tau isoforms can be converted by the tau aggregate seeds from AD brains. We examined autopsied AD and non-AD brain samples from neuropathologically confirmed cadavers (see Materials and Methods). Since there are six tau isoforms present in the human brain (Goedert et al., 1989; Espinoza et al., 2008), we tested how individual isoforms worked as substrates for the RT-QuIC assay of tau aggregation. The tau seeding activities of brain samples from multiple AD and non-AD patients as seeds in the presence of individual six recombinant tau isoforms are shown in **Figure 3** and related scattered plots and statistical analyses are shown in **Figure 4**. Tau-seeding activities were detected starting at approximately 10-30 h and reached a plateau at about 57 h (or >68 h in the case of 2N4R substrate) in AD samples. In contrast, tau-seeding activities in non-AD samples were significantly lower than that in AD samples at ∼57 h (p = 0.0087 for 0N3R; p = 0.0019 for 1N3R; p = 0.0037 for 2N3R; p = 0.0344 for 0N4R; p = 0.0001 for 2N4R; **Figure 4**). For 1N4R substrate, tau-seeding activities was marginally higher (p = 0.0845) with AD brain homogenates than those with non-AD brain samples. While tau-seeding activities represented by the average ThT fluorescence intensities were significantly higher in AD samples versus non-AD samples, small numbers of false negative cases in the AD sample groups (or end-point overlapping between AD and non-AD in the amplified fluorescent signals) were also observed (**Figures 3**, **4**). Blank controls (tau isoform substrate only and no tissue seeds were added) did not show any seeding activities (data not shown). Based on 10 cases of AD, 2 cases of familiar AD, 2 cases of vascular dementia, and 8 cases of non-AD controls, sensitivity of detection was ranged from 56 to 83.3% and specificity of detection was ranged from 80 to 100% for full-length tau isoform substrates.

3R-Tau Isoforms Have Significantly Faster Aggregation Kinetics Than Each of Their 4R-Tau Counterpart

We further analyzed the time course profile of tau RT-QuIC to extract the kinetics information on seeding activities of the misfolded tau by calculating $t_{1/2}$ (time when the fluorescence signal reaches half maximum of each seeding aggregation curve). Seeding aggregation $t_{1/2}$ was estimated to be 13.9 ± 7.7 h, 22.3 ± 8.0 h, and 23.8 ± 7.4 h for 0N3R, 1N3R, and 2N3R substrates and 37.0 ± 5.3 h, 34.0 ± 5.6 h, and 58.8 ± 5.2 h for 0N4R, 1N4R, and 2N4R isoforms, respectively (**Figure 3**). Full-length 3R-tau substrates exhibited faster seeding kinetics. Pair-wise $t_{1/2}$ comparison of 3R-tau and 4R-tau substrates revealed significantly faster seeding activity kinetics for 3R-tau substrates versus their corresponding 4R-tau counterparts: $p < 0.001$ for 0N3R vs. 0N4R, $p < 0.05$ for 1N3R vs. 1N4R, and $p < 0.0001$ for 2N3R vs. 2N4R (**Supplementary Figure 5**).

To further investigate if such isoform-specific kinetics observed in RT-QuIC seeding activities may be recapitulated in "cleaner" biochemical assays (tau isoforms and buffer only and no ingredients from brain tissues), we performed recombinant tau isoform auto-aggregation assays. Consistent with RT-QuIC seeding assays, all the 3R-tau variants auto-aggregated and reached signal plateaus significantly faster (2–20 h) than those for the 4R isoforms (near or after 40 h of incubation) (**Figures 5A,B**). Pair-wise $t_{1/2}$ comparison of 3R and 4R isoforms mirrored isoform-specific kinetics observed in the RT-QuIC-based postmortem brain tissue seeding assays: 0N3R and 0N4R have $t_{1/2}$s of 1.2 ± 0.4 h and 14.7 ± 3.0 h, respectively, a drastic 12.2-fold change; the 1N3R and 1N4R isoforms have $t_{1/2}$s of 4.3 ± 1.1 h and 17.0 ± 1.6 h, respectively, a 3.9-fold change; and 2N3R and 2N4R have $t_{1/2}$s of 4.2 ± 0.6 h and 8.0 ± 0.3 h, respectively, a 1.9-fold change (**Figure 5B**). These results demonstrated that microtubule repeat segment 2 (R2)-less 3R-tau isoforms form aggregates much faster compared to the R2-bearing 4R-tau isoforms.

In order to further verify our findings, we performed Sarkosyl-insoluble tau pelleting assays to assess tau assembly kinetics (Taniguchi et al., 2005; Aoyagi et al., 2007). To compare the aggregation kinetics of 0N3R and 0N4R tau isoforms, we examined the lag times of fibrillation in the absence or presence of heparin. No Sarkosyl-insoluble tau was observed with either isoform in the absence of heparin (data not shown). Incubation of tau with heparin resulted in an increase of Sarkosyl-insoluble tau in both isoforms (**Figure 5C**). Although 0N4R did not exhibit aggregation until 24 h of incubation, 0N3R tau started to aggregate from 4 h of incubation (highlighted in red boxes in **Figure 5C**) using identical fibril formation conditions, in good agreement with the results from ThT fluorescence kinetic assays (**Figures 5A,B**). Sarkosyl-insoluble tau pelleting assay was not

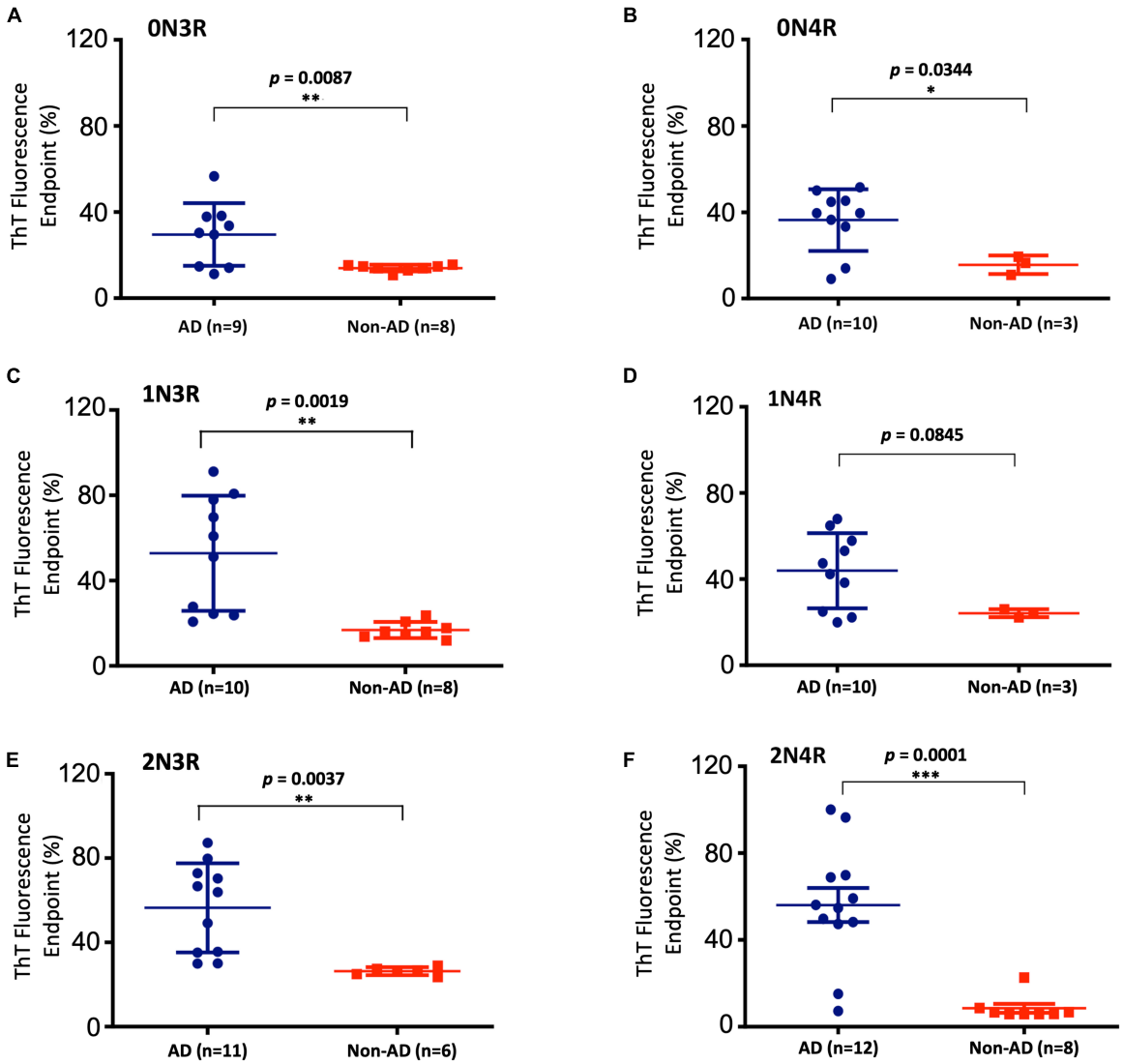

FIGURE 4 | Scattered plot and statistical evaluation of real-time quaking-induced conversion analyses (RT-QuIC) assays of six individual tau isoform (labeled) seeding activities with brain tissues of post-mortem Alzheimer's disease (AD) and non-AD control subjects as described in **Figure 3**. GraphPad Prism 6.0 software was used for statistical analyses. Subject numbers in each group are specified. False negative cases are included. *$p < 0.05$; **$p < 0.01$; ***$p < 0.001$.

sensitive enough to detect the difference between 1N3R/1N4R and 2N3R/2N4R pairs, presumably due to their less pronounced kinetic differences (fold of change) than that of 0N3R/0N4R (data not shown).

DISCUSSION

Applying both concepts and assays derived from prion diseases, we were able to successfully amplify misfolded tau seeds from AD brains using an engineered tau fragment 4RCF, and each of the six individual full-length wild-type tau isoforms as a substrate. There is no reported RT-QuIC study with 4RCF or similar K18 alone as substrate. Previous studies of RT-QuIC seeding assays with other truncated fragments focused on K19 or a longer variant K12 (both are 3R constructs) or mixed fragments (K19 + τ306 or K19 + K18) (Saijo et al., 2017; Kraus et al., 2019; Metrick et al., 2020). Our RT-QuiC assays with 4RCF substrate demonstrated that the four repeating segment alone is capable to amplify misfolded tau seeds from AD and rare tauopathies brains. Separately, to our knowledge, this is the first study reported of selective detection of misfolded tau seeds from AD brains with each of all six full-length tau isoforms as the substrate. In comparison with two recent studies describing ultrasensitive detection of tau aggregate conformer of AD with engineered and significantly shortened tau fragments as substrates (Kraus et al., 2019; Metrick et al., 2020), our study demonstrated such selective detections are also feasible with six full-length human tau isoforms. Non-AD brain samples yielded minimal or significantly lower levels of fluorescent signals

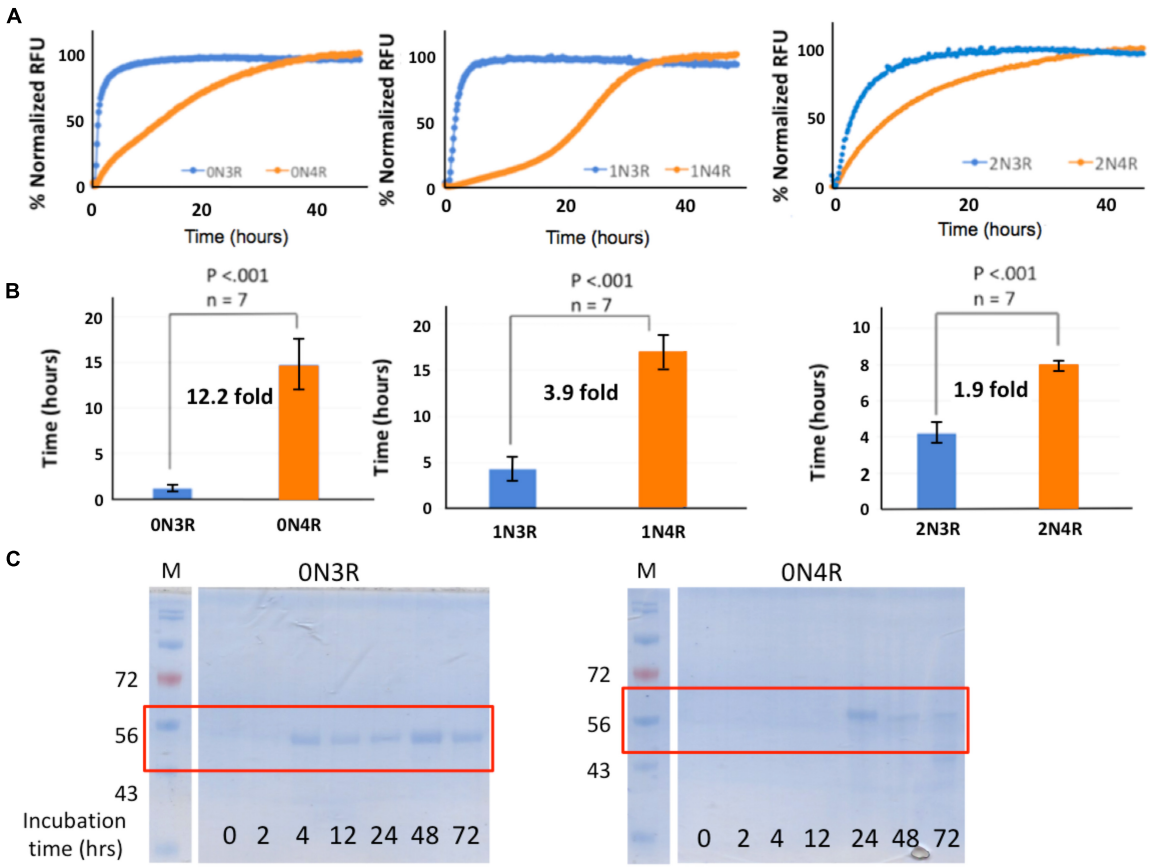

FIGURE 5 | Pair-wise aggregation kinetics comparison of 3R and 4R tau isoforms. **(A, B)** Quantitative analysis of tau isoform aggregation kinetics using ThT fluorescence-based assays. 30 μM of 0N3R or 0N4R (Left Panel), 1N3R or 1N4R (Center Panel), and 2N3R or 2N4R (Right Panel) were incubated in 20 mM Tris pH 7.4 with 0.06 mg/ml of heparin at 37°C for specified time periods. Kinetic fluorescence traces are shown in panel **(A)**. Corresponding $t_{1/2}$ values for each aggregation kinetics curves are shown in panel **(B)**. **(C)** Aggregation kinetics comparison of 0N3R and 0N4R isoforms by Sarkosyl-insoluble tau pelleting assay. 30 μM of 0N3R or 0N4R were incubated in 20 mM Tris pH 7.4 with 0.06 mg/ml of heparin at 37°C for specified time periods. Aggregated tau isoforms (Sarkosyl-insoluble tau) were visualized by SDS-PAGE after Commassie Blue staining.

for aggregation. Because small numbers of false negative cases in the AD sample groups (or end-point overlapping between AD and non-AD in the amplified fluorescent signals) were observed (**Figures 3**, **4**), we interpret this is likely due to the transition between non-AD and AD is a gradual spectrum (AD disease continuum). Different tau strains can be faithfully amplified *in vitro* from tau isolated from different tauopathy brains and that the amplified tau variants retain their strain-dependent pathogenic characteristics (Xu et al., 2021), our full-length tau isoform-based RT-QuIC assays therefore presumably reflect more faithfully the pathological molecular species of AD brains because full-length tau isoforms are the native forms of tau proteins in human brains (Goedert et al., 1992) and hence offer potentially more accurate diagnosis of AD and other tauopathies for future translational applications. It will be interesting in the future to investigate the structural features of the RT-QuIC end products with substrates of either full-length tau isoforms or truncated tau fragments, and compares them with respective tau fibril structures derived from 3R, 4R, and mixed 3R/4R tauopathies for authenticity. All our tau constructs (full-length isoforms and 4RCF) have a his_6-tag at C-terminal of each protein to facilitate purification. Because it is far away from the four repeat segments, key region relevant to aggregation, or other structured segment such as N1 and N2, it is highly unlikely the his-tag will affect tau aggregation properties. We have not tested them experimentally, which is a possible limitation.

Results from our ThT fluorescence assays and orthogonal pelleting assays revealed differential aggregation kinetics of the 3R and 4R isoforms. Pair-wise $t_{1/2}$ rate differences (fold changes; **Figure 5**) may reflect the sequence variations of 0N, 1N and 2N isoforms, specifically the N1 and N2 domains of the tau protein. As the differences between 0N3R/0N4R, 1N3R/1N4R, and 2N3R/2N4R are due to the presence or absence of the microtubule repeat R2 segment, the presence of the R2 repeat, while itself a key aggregation core element, intriguingly slows down the aggregation of the resulting isoforms. Our results are consistent with a recent study reporting that 3R-tau isoforms are more prone to form oligomers than 4R-tau isoforms (Shahpasand-Kroner et al., 2021). However, past work suggested aggregation rate of 3R-tau (or K19) or 4R-tau (or K18) may

be redox condition dependent such as the presence or absence of reducing reagent DTT (Schweers et al., 1995; Barghorn and Mandelkow, 2002; Adams et al., 2010). It is currently unknown why the inclusion of a key aggregation R2 element to the 3R tau isoforms yielded corresponding 4R isoforms with slower aggregation kinetics. The fold increase in $t_{1/2}$ was sequentially reduced from 0N3R/0N4R (12.2 fold) to 1N3R/1N4R (3.9 fold), and to 2N3R/2N4R (1.9 fold) in recombinant tau isoform only aggregation systems (**Figure 5**). Unlike the recombinant tau isoform biochemical systems, there was no decreasing trend in folds with N1/N2 in the RT-QuIC seeding system (2.7-fold for 0N3R/0N4R, 1.5-fold for 1N3R/1N4R, 2.5-fold for 2N3R/2N4R; **Figure 3**). We interpret that pure recombinant tau isoform aggregation assays are "cleaner" biochemical systems and therefore provide better quantitative molecular insights such as domain contributions to tau protein aggregation. RT-QuIC assays, however, are much more heterogenous and less quantitative. It may complement the pure recombinant tau isoform systems and model better for physiological/pathological states. The physiological and/or pathological significance of these kinetic differences in aggregation remained to be determined. We hypothesize that amino-terminal N1 and N2 segments play some novel roles in tau aggregation partly because the differences in $t_{1/2}$ fold of changes may be assigned to the presence or absence of the N1 and N2 segments of the isoforms evaluated. Roles of N1 and N2 remain to be further investigated and this is an interesting future direction.

Previous studies have demonstrated that all six tau isoforms are present in PHF-tau from AD brains. Most of semi-quantitative estimates of tau amount were based on immunodetection of tau isoforms (Goedert et al., 1992; Lee et al., 1999). Yet detailed quantitative measurements of human tau isoforms within NFTs such as PHF-tau are currently not available. Our mass spectrometric analysis of PHF-tau and recent literature (Barthélemy et al., 2019) demonstrated that it is possible to perform target quantifications in normal and diseased samples if isotope-labeled peptide standards with known quantities are spiked in the testing samples and used as external standards. Such quantification may help to address important yet unresolved questions regarding 3R/4R ratio in normal and diseased CNS samples, and how imbalance of 3R/4R ratios among a combination of tau isoforms affects their aggregation and contributes to AD pathogenesis. Recent development in new technology such as ion mobility-mass spectrometry (Young et al., 2014, 2015) may provide powerful new methods and tools to define protein aggregate intermediates in functionally relevant tau isoform strains.

Tau filaments extracted from AD or other tauopathy brains are heavily decorated with posttranslational modifications (PTMs) (Arakhamia et al., 2020; Wesseling et al., 2020). The PTMs include not only high degree of phosphorylation at dozens of sites, but also other PTMs such as acetylation, ubiquitination, methylation etc. Site-specific PTM has been proposed to play important roles in tau filament formation and AD disease progression (Dujardin et al., 2020; Wesseling et al., 2020). Therefore, it is important to investigate the roles individual PTM site plays in tau aggregation as well as their potential utility for selective detection for tauopathy diagnosis. In this regard, there are significant recent advances in the development of site-specific phosphor-tau biomarkers, such as p-tau181 and p-tau217 for blood- or CSF-based AD diagnosis (Blennow et al., 2015; Janelidze et al., 2020; Thijssen et al., 2021; Leuzy et al., 2022). Nevertheless, *in vitro* assembly of recombinant tau may have its own significant utility because recent study showed that filaments grown from recombinant tau can adopt identical structures as those of AD and chronic traumatic encephalopathy (CTE) (Lövestam et al., 2022). The ease of making AD PHFs and CTE tau filaments *in vitro* with recombinant tau proteins opens new avenues for tauopathies research such as understanding the molecular mechanisms of amyloid formation, small molecule drug screening, filament-specific diagnostic ligand development for positron emission tomography, or special binding agent development to couple the protein degradation machinery aiming to degrade toxic tau filaments inside neurons as potential AD therapy.

Multiple cell-based and *in vivo* mice based tau-seeding experiments provided strong evidence that tau protein has essential characteristics of a prion (Guo and Lee, 2011; Guo et al., 2016; Dujardin et al., 2018). Prion-like propagation of tau aggregates may therefore underlie the disease pathogenesis and progression of neurodegenerative tauopathies. Recent groundbreaking cryo-EM structures of tau filaments from patients with AD, PiD, and CBD further provided atomic evidence of different molecular conformers for several distinct neurodegenerative tauopathies (Fitzpatrick et al., 2017; Falcon et al., 2018; Zhang et al., 2020). Utilizing concepts and techniques such as RT-QuIC originally used in prion disease research, we demonstrated "prion-like" tau isoform seeding activities in diseased AD and related tauopathy brains. For future translational applications, it will be interesting to validate in larger number of disease and control cohorts, to get more accurate estimate of detection selectivity and specificity, and to compare systematically with RT-QuIC assays with various truncated or mixed tau fragments for sensitivity. Important basic science questions also remain to be addressed. For examples, whether tau isoform aggregation plays any roles in disease progression in the context of rapid and slow progressive AD patients? Roles of post-translational modifications such as site-specific phosphorylation and acetylation in tau aggregation? New technological advances will certainly facilitate to address many of such important questions.

DATA AVAILABILITY STATEMENT

The datasets presented in this study can be found in online repositories. The names of the repository/repositories and accession number(s) can be found in the article/**Supplementary Material**.

AUTHOR CONTRIBUTIONS

LW and ZW performed experiments and acquired and analyzed the data. SL, NG, DD, MM, and FH assisted with the

experiments. RH and WR designed and collected and analyzed mass spectrometry data. JL participated in the experiments and provided inputs in experimental design. XZ and SS contributed key reagents and clinical diagnosis data. S-HW verified clinical diagnosis, and collected brain tissues and clinical diagnosis data. GB contributed key reagents and provided inputs in experimental design. W-QZ conceived, designed the experiments, collected brain tissues, acquired and analyzed data, and prepared the manuscript. BX conceived, designed the experiments, analyzed the data, and prepared the manuscript. All authors contributed to the revision and editing of the manuscript.

FUNDING

This study was supported in part by grants from the Alzheimer's Association, Biomarkers Across Neurodegenerative Diseases (BAND) Program (BAND-19-614848) (W-QZ and BX), Awards Nos. 16-1 and 18-4 from the Commonwealth of Virginia's Alzheimer's and Related Diseases Research Award Fund (BX and LW), the Commonwealth Health Research Board of Virginia (BX), Diabetes Action Research and Education Foundation (BX), Duke/NCCU CTSI Collaborative Research Award (BX and S-HW), National Institute of Health grants AG061531 (BX), AG067607 (ZW and BX), NS109532 (ZW and W-QZ), NS112010 (ZW and W-QZ), AG051085 (GB), P30 AG062428 (XZ and Case Western Reserve University Alzheimer's Disease Research Center), P30 AG072958 (S-HW and Duke/UNC Alzheimer's Disease Research Center), Owens Family Foundation (GB), and Cure Alzheimer's Fund (GB).

ACKNOWLEDGMENTS

We thank Case Western Reserve University Alzheimer's Disease Research Center, Case Human Tissue Procurement Facility, and the Duke/UNC Alzheimer's Disease Research Center for AD and non-AD brain tissues access. We thank Kathy Lowe at Virginia-Maryland Regional College of Veterinary Medicine for her excellent technical assistance in using transmission electron microscope. We thank Virginia Tech Center for Drug Discovery and BRITE Research Institute of North Carolina Central University for instrument access. We also thank John Ervin at the Bryan Brain Bank and Biorepository at Duke University Medical Center for rare tauopathy and control brain tissue collection.

SUPPLEMENTARY MATERIAL

The Supplementary Material for this article can be found online at: https://www.frontiersin.org/articles/10.3389/fnagi.2022.945875/full#supplementary-material

REFERENCES

Adams, S. J., DeTure, M. A., McBride, M., Dickson, D. W., and Petrucelli, L. (2010). Three repeat isoforms of tau inhibit assembly of four repeat tau filaments. *PLoS One* 5:e10810. doi: 10.1371/journal.pone.0010810

Aoyagi, H., Hasegawa, M., and Tamaoka, A. (2007). Fibrillogenic nuclei composed of P301L mutant tau induce elongation of P301L tau but not wild-type tau. *J. Biol. Chem.* 282, 20309–20318. doi: 10.1074/jbc.M611876200

Arai, T., Ikeda, K., Akiyama, H., Shikamoto, Y., Tsuchiya, K., Yagishita, S., et al. (2001). Distinct isoforms of tau aggregated in neurons and glial cells in brains of patients with Pick's disease, corticobasal degeneration and progressive supranuclear palsy. *Acta Neuropathol.* 101, 167–173.

Arakhamia, T., Lee, C. E., Carlomagno, Y., Duong, D. M., Kundinger, S. R., Wang, K., et al. (2020). Posttranslational modifications mediate the structural diversity of tauopathy strains. *Cell* 180, 633.e12–644.e12.

Atarshi, R., Wilham, J. M., Christensen, L., Hughson, A. G., Moore, R. A., Johnson, L. M., et al. (2008). Simplified ultrasensitive prion detection by recombinant PrP conversion with shaking. *Nat. Methods* 5, 211–212. doi: 10.1038/nmeth0308-211

Barghorn, S., Biernat, J., and Mandelkow, E. (2005). Purification of recombinant tau protein and preparation of Alzheimer-paired helical filaments in vitro. *Methods Mol. Biol.* 299, 35–51. doi: 10.1385/1-59259-874-9:035

Barghorn, S., and Mandelkow, E. (2002). Toward a unified scheme for the aggregation of tau into Alzheimer paired helical filaments. *Biochemistry* 41, 14885–14896. doi: 10.1021/bi026469j

Barthélemy, N. R., Mallipeddi, N., Moiseyev, P., Sato, C., and Bateman, R. J. (2019). Tau phosphorylation rates measured by mass spectrometry differ in the intracellular brain vs. Extracellular cerebrospinal fluid compartments and are differentially affected by Alzheimer's disease. *Front. Aging Neurosci.* 11:121. doi: 10.3389/fnagi.2019.00121

Blennow, K., Dubois, B., Fagan, A. M., Lewczuk, P., de Leon, M. J., and Hampel, H. (2015). Clinical utility of cerebrospinal fluid biomarkers in the diagnosis of early Alzheimer's disease. *Alzheimers Dement.* 11, 58–69.

Bloom, G. S. (2014). Amyloid-β and tau: the trigger and bullet in Alzheimer disease pathogenesis. *JAMA Neurol.* 71, 505–508. doi: 10.1001/jamaneurol.2013.5847

Braak, H., and Braak, E. (1991). Neuropathological staging of Alzheimer-related changes. *Act. Neuropathol.* 82, 239–259.

Cairns, N. J., Bigio, E. H., Mackenzie, I. R., Neumann, M., Lee, V. M., and Hatanpaa, K. J. (2007). Neuropathologic diagnostic and nosologic criteria for frontotemporal lobar degeneration: consensus of the Consortium for frontotemporal lobar degeneration. *Acta Neuropathol.* 114, 5–22. doi: 10.1007/s00401-007-0237-2

Chiti, F., and Dobson, C. M. (2017). Protein misfolding, amyloid formation, and human disease: a summary of progress over the last decade. *Annu. Rev. Biochem.* 86, 27–68. doi: 10.1146/annurev-biochem-061516-045115

Dujardin, S., Bégard, S., Caillierez, R., Lachaud, C., Carrier, S., Lieger, S., et al. (2018). Different tau species lead to heterogeneous tau pathology propagation and misfolding. *Acta Neuropathol. Commun.* 6:132. doi: 10.1186/s40478-018-0637-7

Dujardin, S., Commins, C., Lathuiliere, A., Beerepoot, P., Fernandes, A. R., Kamath, T. V., et al. (2020). Tau molecular diversity contributes to clinical heterogeneity in Alzheimer's disease. *Nat. Med.* 26, 1256–1263.

Espinoza, M., de Silva, R., Dickson, D. W., and Davies, P. (2008). Differential incorporation of tau isoforms in Alzheimer's disease. *J. Alzheimers Dis.* 14, 1–16.

Fairfoul, G., McGuire, L. I., Pal, S., Ironside, J. W., Neumann, J., Christie, S., et al. (2016). Alpha-synuclein RT-QuIC in the CSF of patients with alpha-synucleinopathies. *Ann. Clin. Transl. Neurol.* 3, 812–818.

Falcon, B., Zhang, W., Murzin, A. G., Murshudov, G., Garringer, H. J., Vidal, R., et al. (2018). Structures of filaments from Pick's disease reveal a novel tau protein fold. *Nature* 561, 137–140. doi: 10.1038/s41586-018-0454-y

Fitzpatrick, A. W. P., Falcon, B., He, S., Murzin, A. G., Murshudov, G., Garringer, H. J., et al. (2017). Cryo-EM structures of tau filaments from Alzheimer's disease. *Nature* 547, 185–190.

Gibbons, G. S., Lee, V. M. Y., and Trojanowski, J. Q. (2019). Mechanisms of cell-to-cell transmission of pathological tau: a review. *JAMA Neurol.* 76, 101–108. doi: 10.1001/jamaneurol.2018.2505

Goedert, M. (2020). Tau proteinopathies and the prion concept. *Prog. Mol. Biol. Transl. Sci.* 175, 239–259.

Goedert, M., Ghetti, B., and Spillantini, M. G. (2012). Frontotemporal dementia: implications for understanding Alzheimer disease. *Cold Spring Harb. Perspect. Med.* 2:a006254.

Goedert, M., and Spillantini, M. G. (2017). Propagation of Tau aggregates. *Mol. Brain* 10:18.

Goedert, M., Spillantini, M. G., Cairns, N. J., and Crowther, R. A. (1992). Tau proteins of Alzheimer paired helical filaments: abnormal phosphorylation of all six brain isoforms. *Neuron* 8, 159–168.

Goedert, M., Spillantini, M. G., Jakes, R., Rutherford, D., and Crowther, R. A. (1989). Multiple isoforms of human microtubule-associated protein tau: sequences and localization in neurofibrillary tangles of Alzheimer's disease. *Neuron* 3, 519–526. doi: 10.1016/0896-6273(89)90210-9

Groveman, B. R., Orrù, C. D., Hughson, A. G., Raymond, L. D., Zanusso, G., Ghetti, B., et al. (2018). Rapid and ultra-sensitive quantitation of disease-associated α-synuclein seeds in brain and cerebrospinal fluid by αSyn RT-QuIC. *Acta Neuropathol. Commun.* 6:7.

Guo, J. L., and Lee, V. M. (2011). Seeding of normal Tau by pathological Tau conformers drives pathogenesis of Alzheimer-like tangles. *J. Biol. Chem.* 286, 15317–15331. doi: 10.1074/jbc.M110.209296

Guo, J. L., Narasimhan, S., Changolkar, L., He, Z., Stieber, A., Zhang, B., et al. (2016). Unique pathological tau conformers from Alzheimer's brains transmit tau pathology in nontransgenic mice. *J. Exp. Med.* 213, 2635–2654. doi: 10.1084/jem.20160833

Gustin, A., Navobpour, S., Farrell, K., Martin, K., DuVall, J., Ray, W. K., et al. (2022) Protein SUMOylation is a sex-specific regulator of fear memory formation in the amygdala. *Behav. Brain Res.* 430:113928. doi: 10.1016/j.bbr.2022.113928

Hulette, C. M., Welsh-Bohmer, K. A., Murray, M. G., Saunders, A. M., Mash, D. C., and McIntyre, L. M. (1998). Neuropathological and neuropsychological changes in "normal" aging: evidence for preclinical Alzheimer disease in cognitively normal individuals. *J. Neuropathol. Exp. Neurol.* 57, 1168–1174.

Hyman, B. T., Phelps, C. H., Beach, T. G., Bigio, E. H., Cairns, N. J., Carrillo, M. C., et al. (2012). National Institute on Aging-Alzheimer's Association guidelines for the neuropathologic assessment of Alzheimer's disease. *Alzheimers Dement.* 8, 1–13.

Janelidze, S., Mattsson, N., Palmqvist, S., Smith, R., Beach, T. G., Serrano, G. E., et al. (2020). Plasma P-tau181 in Alzheimer's disease: relationship to other biomarkers, differential diagnosis, neuropathology and longitudinal progression to Alzheimer's dementia. *Nat. Med.* 26, 379–386. doi: 10.1038/s41591-020-0755-1

Kaufman, S. K., Sanders, D. W., Thomas, T. L., Ruchinskas, A. J., Vaquer-Alicea, J., Sharma, A. M., et al. (2016). Tau prion strains dictate patterns of cell pathology, progression rate, and regional vulnerability in vivo. *Neuron* 92, 796–812. doi: 10.1016/j.neuron.2016.09.055

Kraus, A., Saijo, E., Metrick, M. A. II, Newell, K., Sigurdson, C. J., Zanusso, G., et al. (2019). Seeding selectivity and ultrasensitive detection of tau aggregate conformers of Alzheimer disease. *Acta Neuropathol.* 137, 585–598. doi: 10.1007/s00401-018-1947-3

Lee, V. M., Goedert, M., and Trojanowski, J. Q. (2001). Neurodegenerative tauopathies. *Annu. Rev. Neurosci.* 24, 1121–1159.

Lee, V. M., and Trojanowski, J. Q. (2006). Mechanisms of Parkinson's disease linked to pathological alpha-synuclein: new targets for drug discovery. *Neuron* 52, 33–38. doi: 10.1016/j.neuron.2006.09.026

Lee, V. M., Wang, J., and Trojanowski, J. Q. (1999). Purification of paired helical filament tau and normal tau from human brain tissue. *Methods Enzymol.* 309, 81–89.

Leuzy, A., Mattsson-Carlgren, N., Palmqvist, S., Janelidze, S., Dage, J. L., and Hansson, O. (2022). Blood-based biomarkers for Alzheimer's disease. *EMBO Mol. Med.* 14:e14408.

Lövestam, S., Koh, F. A., van Knippenberg, B., Kotecha, A., Murzin, A. G., Goedert, M., et al. (2022). Assembly of recombinant tau into filaments identical to those of Alzheimer's disease and chronic traumatic encephalopathy. *eLife* 11:e76494. doi: 10.7554/eLife.76494

McKeith, I. G., Boeve, B. F., Dickson, D. W., Halliday, G., Taylor, J. P., Weintraub, D., et al. (2017). Diagnosis and management of dementia with Lewy bodies: fourth consensus report of the DLB Consortium. *Neurology* 89, 88–100.

McKhann, G. M., Knopman, D. S., Chertkow, H., Hyman, B. T., Jack, C. R. Jr., Kawas, C. H., et al. (2011). The diagnosis of dementia due to Alzheimer's disease: recommendations from the National Institute on Aging-Alzheimer's Association workgroups on diagnostic guidelines for Alzheimer's disease. *Alzheimers Dement.* 7, 263–269.

Metrick, M. A. II, Ferreira, N. D. C., Saijo, E., Kraus, A., Newell, K., Zanusso, G., et al. (2020). A single ultrasensitive assay for detection and discrimination of tau aggregates of Alzheimer and Pick diseases. *Acta Neuropathol. Commun.* 8:22. doi: 10.1186/s40478-020-0887-z

Moda, F., Gambetti, P., Notari, S., Concha-Marambio, L., Catania, M., Park, K. W., et al. (2014). Prions in the urine of patients with variant Creutzfeldt-Jakob disease. *N. Engl. J. Med.* 371, 530–539.

Nelson, P. T., Alafuzoff, I., Bigio, E. H., Bouras, C., Braak, H., Cairns, N. J., et al. (2012). Correlation of Alzheimer disease neuropathologic changes with cognitive status: a review of the literature. *J. Neuropathol. Exp. Neurol.* 71, 362–381. doi: 10.1097/NEN.0b013e31825018f7

Nelson, P. T., Dickson, D. W., Trojanowski, J. Q., Jack, C. R., Boyle, P. A., Arfanakis, K., et al. (2019). Limbic-predominant age-related TDP-43 encephalopathy (LATE): consensus working group report. *Brain* 142, 1503–1527. doi: 10.1093/brain/awz099

Orru, C. D., Yuan, J., Appleby, B. S., Li, B., Li, Y., Winner, D., et al. (2017). Prion seeding activity and infectivity in skin samples from patients with sporadic Creutzfeldt-Jakob disease. *Sci. Transl. Med.* 9:eaam7785.

Prusiner, S. B. (2013). Biology and genetics of prions causing neurodegeneration. *Annu. Rev. Genet.* 47, 601–623.

Saá, P., Castilla, J., and Soto, C. (2005). Cyclic amplification of protein misfolding and aggregation. *Methods Mol. Biol.* 299, 53–65.

Saijo, E., Ghetti, B., Zanusso, G., Oblak, A., Furman, J. L., Diamond, M. I., et al. (2017). Ultrasensitive and selective detection of 3-repeat tau seeding activity in Pick disease brain and cerebrospinal fluid. *Acta Neuropathol.* 133, 751–765. doi: 10.1007/s00401-017-1692-z

Salvadores, N., Shahnawaz, M., Scarpini, E., Tagliavini, F., and Soto, C. (2014). Detection of misfolded Aβ oligomers for sensitive biochemical diagnosis of Alzheimer's disease. *Cell Rep.* 7, 261–268. doi: 10.1016/j.celrep.2014.02.031

Schweers, O., Mandelkow, E. M., Biernat, J., and Mandelkow, E. (1995). Oxidation of cysteine-322 in the repeat domain of microtubule-associated protein tau controls the in vitro assembly of paired helical filaments. *Proc. Natl. Acad. Sci. U.S.A.* 92, 8463–8467. doi: 10.1073/pnas.92.18.8463

Selkoe, D. J. (2001). Alzheimer's disease: genes, proteins, and therapy. *Physiol. Rev.* 81, 741–766.

Shahnawaz, M., Mukherjee, A., Pritzkow, S., Mendez, N., Rabadia, P., Liu, X., et al. (2020). Discriminating α-synuclein strains in Parkinson's disease and multiple system atrophy. *Nature* 578, 273–277.

Shahnawaz, M., Tokuda, T., Waragai, M., Mendez, N., Ishii, R., Trenkwalder, C., et al. (2017). Development of a biochemical diagnosis of parkinson disease by detection of α-synuclein misfolded aggregates in cerebrospinal fluid. *JAMA Neurol.* 74, 163–172. doi: 10.1001/jamaneurol.2016.4547

Shahpasand-Kroner, H., Portillo, J., Lantz, C., Seidler, P. M., Sarafian, N., Loo, J. A., et al. (2021). Three-repeat and four-repeat tau isoforms form different oligomers. *Protein Sci.* 31, 613–627. doi: 10.1002/pro.4257

Spires-Jones, T. L., and Hyman, B. T. (2014). The intersection of amyloid beta and tau at synapses in Alzheimer's disease. *Neuron* 82, 756–771.

Swanson, E., Breckenridge, L., McMahon, L., Som, S., McConnell, L., and Bloom, G. S. (2017). Extracellular Tau oligomers induce invation of endogenous tau into the somatodendritic compartment and axonal transport dysfunction. *J. Alzheimers Dis.* 58, 803–820. doi: 10.3233/JAD-170168

Taniguchi, S., Suzuki, N., Masuda, M., Hisanaga, S., Iwatsubo, T., Goedert, M., et al. (2005). Inhibition of heparin-induced tau filament formation by phenothiazines, polyphenols, and porphyrins. *J. Biol. Chem.* 280, 7614–7623. doi: 10.1074/jbc.M408714200

Thijssen, E. H., La Joie, R., Strom, A., Fonseca, C., Iaccarino, L., Wolf, A., et al. (2021). Plasma phosphorylated tau 217 and phosphorylated tau 181 as biomarkers in Alzheimer's disease and frontotemporal lobar degeneration: a retrospective diagnostic performance study. *Lancet Neurol.* 20, 739–752. doi: 10.1016/S1474-4422(21)00214-3

Vaquer-Alicea, J., and Diamond, M. I. (2019). Propagation of protein aggregation in neurodegenerative diseases. *Annu. Rev. Biochem.* 88, 785–810.

Vaquer-Alicea, J., Diamond, M. I., and Joachimiak, L. A. (2021). Tau strains shape disease. *Acta Neuropathol.* 142, 57–71.

Velander, P., Wu, L., Ray, W. K., Helm, R. F., and Xu, B. (2016). Amylin amyloid inhibition by flavonoid baicalein: key roles of its vicinal dihydroxyl groups of the catechol moiety. *Biochemistry* 55, 4255–4258. doi: 10.1021/acs.biochem.6b00578

von Bergen, M., Barghorn, S., Li, L., Marx, A., Biernat, J., Mandelkow, E. M., et al. (2001). Mutations of tau protein in frontotemporal dementia promote aggregation of paired helical filaments by enhancing local beta-structure. *J. Biol. Chem.* 276, 48165–48174. doi: 10.1074/jbc.M105196200

Wang, Z., Becker, K., Donadio, V., Siedlak, S., Yuan, J., Rezaee, M., et al. (2020). Skin α-synuclein aggregation seeding activity as a novel biomarker for Parkinson disease. *JAMA Neurol.* 78, 1–11. doi: 10.1001/jamaneurol.2020.3311

Wang, Z., Manca, M., Foutz, A., Martinez, M. C., Raymond, G. J., Race, B., et al. (2019). Early preclinical detection of prions in the skin of prion-infected animals. *Nat. Commun.* 10:247.

Wesseling, H., Mair, W., Kumar, M., Schlaffner, C. N., Tang, S., Beerepoot, P., et al. (2020). Tau PTM profiles identify patient heterogeneity and stages of Alzheimer's disease. *Cell* 183, 1699.e13–1713.e13. doi: 10.1016/j.cell.2020.10.029

Westermark, P., Andersson, A., and Westermark, G. T. (2011). Islet amyloid polypeptide, islet amyloid, and diabetes mellitus. *Physiol. Rev.* 91, 795–826.

Wilcock, G. K., and Esiri, M. M. (1982). Plaques, tangles and dementia. A quantitative study. *J. Neurol. Sci.* 56, 343–356.

Wu, L., Velander, P., Brown, A. M., Wang, Y., Liu, D., Bevan, D. R., et al. (2021). Rosmarinic acid potently detoxifies amylin amyloid and ameliorates diabetic pathology in a transgenic rat model of type 2 diabetes. *ACS Pharmacol. Transl. Sci.* 4, 1322–1337. doi: 10.1021/acsptsci.1c00028

Wu, L., Velander, P., Liu, D., and Xu, B. (2017). Olive component oleuropein promotes β-cell insulin secretion and protects β-cells from amylin amyloid-induced cytotoxicity. *Biochemistry* 56, 5035–5039. doi: 10.1021/acs.biochem.7b00199

Xu, H., O'Reilly, M., Gibbons, G. S., Changolkar, L., McBride, J. D., Riddle, D. M., et al. (2021). In vitro amplification of pathogenic tau conserves disease-specific bioactive characteristics. *Acta Neuropathol.* 141, 193–215. doi: 10.1007/s00401-020-02253-4

Young, L. M., Cao, P., Raleigh, D. P., Ashcroft, A. E., and Radford, S. E. (2014). Ion mobility spectrometry-mass spectrometry defines the oligomeric intermediates in amylin amyloid formation and the mode of action of inhibitors. *J. Am. Chem. Soc.* 136, 660–670. doi: 10.1021/ja406831n

Young, L. M., Saunders, J. C., Mahood, R. A., Revill, C. H., Foster, R. J., Tu, L. H., et al. (2015). Screening and classifying small-molecule inhibitors of amyloid formation using ion mobility spectrometry-mass spectrometry. *Nat. Chem.* 7, 73–81. doi: 10.1038/nchem.2129

Zhang, W., Tarutani, A., Newell, K. L., Murzin, A. G., Matsubara, T., Falcon, B., et al. (2020). Novel tau filament fold in corticobasal degeneration. *Nature* 580, 283–287.

Conflict of Interest: The authors declare that the research was conducted in the absence of any commercial or financial relationships that could be construed as a potential conflict of interest.

Publisher's Note: All claims expressed in this article are solely those of the authors and do not necessarily represent those of their affiliated organizations, or those of the publisher, the editors and the reviewers. Any product that may be evaluated in this article, or claim that may be made by its manufacturer, is not guaranteed or endorsed by the publisher.

frontiers | Frontiers in Aging Neuroscience

TYPE Original Research
PUBLISHED 28 July 2022
DOI 10.3389/fnagi.2022.964336

OPEN ACCESS

EDITED BY
Woon-Man Kung,
Chinese Culture University, Taiwan

REVIEWED BY
Ivan V. Zaletel,
University of Belgrade, Serbia
Shinwoo Kang,
Gachon University, South Korea

*CORRESPONDENCE
Man-Lung Fung
fungml@hku.hk
You-qiang Song
songy@hku.hk
Lee Wei Lim
drlimleewei@gmail.com

†These authors share first authorship

SPECIALTY SECTION
This article was submitted to Alzheimer's Disease and Related Dementias,
a section of the journal
Frontiers in Aging Neuroscience

RECEIVED 08 June 2022
ACCEPTED 28 June 2022
PUBLISHED 28 July 2022

CITATION
Tsui KC, Roy J, Chau SC, Wong KH, Shi L, Poon CH, Wang Y, Strekalova T, Aquili L, Chang RC-C, Fung M-L, Song Y-q and Lim LW (2022) Distribution and inter-regional relationship of amyloid-beta plaque deposition in a 5xFAD mouse model of Alzheimer's disease.
Front. Aging Neurosci. 14:964336.
doi: 10.3389/fnagi.2022.964336

Distribution and inter-regional relationship of amyloid-beta plaque deposition in a 5xFAD mouse model of Alzheimer's disease

Ka Chun Tsui[1†], Jaydeep Roy[1†], Sze Chun Chau[1], Kah Hui Wong[1,2], Lei Shi[1], Chi Him Poon[1], Yingyi Wang[1], Tatyana Strekalova[3,4], Luca Aquili[1,5], Raymond Chuen-Chung Chang[1], Man-Lung Fung[1*], You-qiang Song[1,6*] and Lee Wei Lim[1*]

[1]School of Biomedical Sciences, Li Ka Shing Faculty of Medicine, The University of Hong Kong, Pokfulam, Hong Kong SAR, China, [2]Department of Anatomy, Faculty of Medicine, Universiti Malaya, Kuala Lumpur, Malaysia, [3]Department of Neuroscience, Maastricht University, Maastricht, Netherlands, [4]Department of Normal Physiology and Laboratory of Psychiatric Neurobiology, Sechenov First Moscow State Medical University, Moscow, Russia, [5]Discipline of Psychology, College of Science, Health, Engineering, and Education, Murdoch University, Perth, WA, Australia, [6]The State Key Laboratory of Brain and Cognitive Sciences, The University of Hong Kong, Pokfulam, Hong Kong SAR, China

Alzheimer's disease (AD) is the most common form of dementia. Although previous studies have selectively investigated the localization of amyloid-beta (Aβ) deposition in certain brain regions, a comprehensive characterization of the rostro-caudal distribution of Aβ plaques in the brain and their inter-regional correlation remain unexplored. Our results demonstrated remarkable working and spatial memory deficits in 9-month-old 5xFAD mice compared to wildtype mice. High Aβ plaque load was detected in the somatosensory cortex, piriform cortex, thalamus, and dorsal/ventral hippocampus; moderate levels of Aβ plaques were observed in the motor cortex, orbital cortex, visual cortex, and retrosplenial dysgranular cortex; and low levels of Aβ plaques were located in the amygdala, and the cerebellum; but no Aβ plaques were found in the hypothalamus, raphe nuclei, vestibular nucleus, and cuneate nucleus. Interestingly, the deposition of Aβ plaques was positively associated with brain inter-regions including the prefrontal cortex, somatosensory cortex, medial amygdala, thalamus, and the hippocampus. In conclusion, this study provides a comprehensive morphological profile of Aβ deposition in the brain and its inter-regional correlation. This suggests an association between Aβ plaque deposition and specific brain regions in AD pathogenesis.

KEYWORDS

Alzheimer's disease, amyloid-beta (AB), morphology, neuroanatomy, 5xFAD, dementia

Introduction

Alzheimer's disease (AD) is a neurodegenerative disorder characterized by the deposition of amyloid beta (Aβ) plaques and the aggregation of neurofibrillary tangles (NFTs) caused by the hyperphosphorylated tau protein, and involves mutations in amyloid precursor protein (APP), presenilin 1 (PSEN1), presenilin 2 (PSEN2), and apolipoprotein E (APOE) (Bekris et al., 2010; Iqbal et al., 2010; Poon et al., 2020). Patients with AD generally experience memory deficits, cognitive impairment, psychological changes, and sleep disorders. It is the most common form of dementia and affects over 55 million people worldwide, with healthcare costs estimated at $355 billion US dollars in 2021 (Bature et al., 2017; WHO, 2019). Despite extensive research, there is still no effective treatment on the market mainly due to our limited understanding of AD pathogenesis. The prevailing hypothesis is that the deposition of Aβ plaques causes a cascade of neurotoxic events that result in observable synaptic and neuronal loss with neurotransmission dysfunction, eventually leading to AD symptoms (Kametani and Hasegawa, 2018; Soria Lopez et al., 2019; Wong et al., 2020).

Several transgenic models have been developed to overexpress mutant forms of the amyloid precursor protein to mimic AD pathologies such as Aβ deposition. The transgenic 5xFAD mouse model was developed in 2006 to study late-onset AD. This mouse model consists of five familial AD mutations: Swedish APP mutation (K670N/M671L), Florida APP mutation (I716V), and London APP mutation (V717I), PSEN1 M146L mutation, and the PSEN1 L286V mutation (Poon et al., 2020; Forner et al., 2021). These mutations result in the overproduction of Aβ peptides, leading to observable Aβ deposition in the brain as early as 1.5 months (Poon et al., 2020; Forner et al., 2021) and memory deficits by 4–6 months (Eimer and Vassar, 2013; Poon et al., 2020). Although previous studies have selectively reported the deposition of Aβ plaques in specific brain regions in animal models of AD (Oakley et al., 2006; Rodrigue et al., 2009; Vlassenko et al., 2012; Oh et al., 2018; Kim et al., 2020), a comprehensive investigation which gather all the distribution information of Aβ plaques across the brain has not been conducted. Our study aims to provide a comprehensive distribution profile of the rostro-caudal deposition of Aβ and its inter-regional correlation in adult 5xFAD brain.

Materials and methods

Subjects

Nine-month-old female 5xFAD mice (n = 10) and C57bL/6J wildtype (WT) mice (n = 9) were socially housed in standard cages (4–5 mice per cage) with access of food and water *ad libitum*. The female 5xFAD mouse model was selected based on the sex-biased epidemiological profile and neuropathological development in women compared to men (Bundy et al., 2019; Sil et al., 2022). The mice were kept under a 12-h light/dark cycle under controlled temperature (22 ± 1°C) and humidity (60–70%). The procedures for behavioral testing and euthanasia were approved by the Committee on the Use of Live Animals in Teaching and Research, the University of Hong Kong (No. 4807-18).

Forced alternation Y-maze

The experimental procedure was conducted as previously described to measure working memory function (Melnikova et al., 2006; Yu et al., 2022). In brief, animals were placed in a symmetrical Y-maze (each arm: 35 cm × 35 cm × 35 cm) in dim light condition (30 ± 5 lux). The test consisted of an acquisition phase and a retrieval phase (5 min each). During the acquisition phase, the animal was placed in the start arm and allowed to explore only two arms of the Y maze, with the third arm blocked. The retrieval phase was performed 30 min after the acquisition phase. During the retrieval phase, the animal was placed in the start arm and allowed to explore all three arms. The time spent in the novel arm and the total distance traveled in the retrieval phase was recorded and analyzed using ANY-maze software (Stoelting Co., Wood Dale, IL, United States).

Open field test

The experiment was conducted as previously described to evaluate locomotor function (Lim et al., 2016; Tan et al., 2020b). The test was conducted in an enclosed square arena (40 cm × 40 cm × 40 cm) in dim light condition (30 ± 5 lux). Animals were placed in the middle of the area and allowed to explore freely for 5 min. The total distance traveled was recorded by video and subsequently measured using ANY-maze software (Stoelting Co., Wood Dale, IL, United States).

Morris water maze

This test was conducted to measure the hippocampal-dependent learning and memory function as previously described (Liu et al., 2015; Tan et al., 2020a; Yu et al., 2022). The apparatus consisted of a black circular pool (150 cm × 60 cm) filled with water at 25 ± 1°C. The water in the pool was colored opaque using non-toxic skim milk powder. A circular platform (11 cm diameter) was placed 1 cm below the water surface and 15 cm away from the pool wall. The experiment was conducted in dim light condition (30 ± 5 lux). The spatial acquisition consisted of training phase 1 (day 1–4), and training phase 2 (reversal phase, day 6–7). The spatial acquisition training phase

1 consisted of four trials per day (1 min duration with 90 s interval) for four consecutive days (day 1–4). In the training phase, mice were trained to locate the submerged platform in the black circular pool with randomized starting positions that were equidistant from the submerged platform. If the mice were unable to locate the platform, they were gently guided onto the platform. On day 5, a probe test was carried out 24 h after day 4 to assess long-term memory function. After the probe test, the reversal phase consisted of four consecutive trials (1 min each with 90 s interval) carried out on day 6–7. In the reversal phase, the submerged platform was placed in the opposite quadrant of the water maze and each animal was trained with randomized starting positions. On day 7, another probe test was performed to measure the short-term memory function with the platform removed 90 min after the last trial. All trials were video recorded and the frequency to enter each imaginary quadrant and the time spent in each quadrant were evaluated by ANY-maze software (Stoelting Co., Wood Dale, IL, United States).

Histological study

All animals were anesthetized with overdose of sodium pentobarbital and perfused transcardially with Tyrode solution (0.8% sodium chloride, 0.02% potassium chloride, 0.0005% magnesium chloride hexahydrate, 0.1% sodium bicarbonate, 0.004% sodium phosphate monobasic, and 0.1% glucose) and 4% paraformaldehyde. Brain samples were harvested and post-fixed for 24 h in 4% paraformaldehyde, followed by incubation in 15 and 30% sucrose solutions until brains sank to the bottom. The brains were snap-frozen in liquid nitrogen before storing at -80^{o}C.

The immunohistochemistry procedures were performed as previously described with minor modifications (Lim et al., 2015b; Liu et al., 2015). Brains were sliced into 20-μm coronal sections (Bregma: from 4.3 to −8.0 mm) using a CryoStar NX50 Cryostat (Thermo Fisher Scientific, Waltham, MA, United States). All sections were washed in PBS and incubated with 3% H_2O_2 in 0.01 M phosphate buffered saline and 0.5% Triton X-100 (PBS-T) for 15 min, and then incubated in 1% bovine serum albumin for 15 min. A primary mouse anti-human 4G8 antibody (1:500, Biolegend, CA, United States) was added and sections were incubated at 4^{o}C for 24 h. After rinsing, secondary biotinylated goat anti-mouse antibody (1:500, Vector Laboratories, CA, United States) was added and sections were incubated at room temperature for 90 min, followed by avidin and biotinylated horse radish peroxidase (1:1,000, Vectastain, Vector Laboratories, CA, United States) and further incubated for 2 h. Finally, sections were incubated in 1 mg/mL 3,3′-diaminobenzidene tetrahydrochloride (DAB Substrate Kit; Vector Laboratories, CA, United States) in Tris–HCl with 0.005% H_2O_2 and 8% nickel ammonium sulphate. After dehydration, sections were mounted and cover-slipped with Permount (Thermo Fisher Scientific, Waltham, MA, United States). Color images were acquired under a Zeiss AxioPhot upright microscope (ZEISS, Germany) at 5× magnification.

Evaluation of Aβ plaque deposition in different brain regions

The level of Aβ plaque deposition was qualitatively graded by two independent researchers according to the intensity level (0 = no deposition; 1 = mild; 2 = moderate; 3 = high). The methodology of intensity evaluation was conducted as previously described (Chong et al., 2019). The evaluation was conducted with researchers blind to the experimental design. The inter-rater reliability score was calculated as 93.2%. Representative photomicrographs of each intensity category of Aβ plaque deposition are presented in **Figure 2C**. Mild intensity was described as sparse Aβ deposits, moderate intensity was described as scattered clusters of Aβ deposits, and high intensity was described as dense clusters of Aβ deposits. The Aβ burden (n = 4–6 mice, around 12–48 sections) in each selected regions of interest (ROIs) were quantified using ImageJ (NIH, Bethesda, MD, United States) using the threshold analysis method. In this method, we first use the free hand selection tool to outline the entire region, then the image was divided into two classes of pixels, the foreground Aβ plaque and the background (Schneider et al., 2012).

Correlation matrix and 3D model

Correlational analysis was used to measure the correlation as previously described (Wheeler et al., 2014). Briefly, the Aβ plaque burden was the dependent variable, which was averaged for each ROI. We then calculated the pairwise Pearson correlation coefficients between all ROIs to construct a symmetric correlation matrix. High correlation between pairs were noted when Aβ plaque burden in one region was strongly related to another region. Each Pearson correlation coefficient was displayed on the color-coded correlation matrix using GraphPad Prism 9.0 (GraphPad Software, San Diego, CA, United States). A 3D model was constructed by only considering the strongest inter-regional correlations. To determine the correlation threshold, we only retained correlations with a p-value less than 0.05, corresponding to a network correlation coefficient higher than ± 0.9. The resulting 3D model was visualized in R using the cocoframer package (Lein et al., 2007; Oh et al., 2014).

Statistical analysis

All data analyses were performed in IBM SPSS Statistics 27. The results were reported as the mean ± S.D, unless

otherwise indicated. Kolmogorov-Smirnov test was performed to examine data normality. The Y-maze and OFT results were analyzed by independent samples *t*-test. The Morris Water Maze (MWM) training latency was analyzed by factorial mixed design ANOVA for day 1–7. Inter-reliability analysis was performed to qualitatively assess the reliability of the intensity grading by the two researchers. Finally, Pearson correlation coefficients were calculated to examine the inter-regional correlation of the Aβ plaque deposition.

Results

Spatial and learning memory deficits in 5xFAD mice

In the forced alternation Y-maze test, we found a significant reduction in the time spent in the novel arm [$t_{(16)} = 2.477$, $p = 0.025$] and the frequency to enter the novel arm [$t_{(16)} = 4.291$, $p = 0.001$] in 5xFAD mice compared to the wildtype control (**Figures 1A,B**). In the OFT, we found no difference in the distance moved [$t_{(16)} = 0.445$, $p = 0.662$] between 5xFAD mice and wildtype mice (**Figure 1C**), indicating locomotor function was not impaired. In the MWM, repeated-measures ANOVA revealed significant main effects for day [$F_{(5,75)} = 6.066$, $p < 0.001$], group [$F_{(1,15)} = 12.076$, $p = 0.003$], and their interaction [$F_{(5,15)} = 3.095$, $p = 0.014$] (**Figure 1D**). Interestingly, there was a significant reduction in learning memory with increased escape latency in 5xFAD mice on days 2, 4, and 7 [all $t_{(16-17)} = < -2.452$, $p < 0.025$], but no significant differences were observed on days 1, 3, and 6 [all $t_{(16-17)} = < -1.787$, $p > 0.082$] compared to wildtype mice. In the MWM probe test for long-term memory function, there was a significant decrease in the frequency to enter the target quadrant in 5xFAD mice [$t_{(15)} = 2.722$, $p = 0.016$] compared to wildtype mice, but no significant differences were found for the other quadrants [all $t_{(17)} = 1.085$, $p > 0.293$] (**Figure 1E**). The Mann-Whitney *U* test revealed a significant reduction in the time spent on the platform in 5xFAD mice ($Z = -2.599$, $p = 0.010$) compared to wildtype mice. We found no significant differences in the latency to escape in MWM probe test for short-term memory function [all $t_{(15-17)} = < -1.787$, $p > 0.115$] (**Figure 1F**).

Aβ plaque deposition in different brain regions in 5xFAD mice

Figures 2A,B show schematic diagrams of the sagittal view of photomicrographs corresponding to coronal brain sections at different rostro-caudal levels. **Figure 2C** shows photomicrographs representing intensity levels of Aβ plaque deposition. Representative photomicrographs of coronal brain sections were combined and annotated according to Paxinos and Franklin's mouse brain atlas (Paxinos and Franklin, 2008; **Figures 3–8** and **Supplementary Figures 1–3**). The abbreviations and terms used in this study can be found in the list of abbreviations in **Supplementary Table 1**. Qualitative (inter-reliability rate: 0.93) and quantitative assessments of the intensity level of the Aβ plaque load in various ROIs are summarized in **Table 1** and **Supplementary Table 2**, respectively.

Olfactory-related areas

We found moderate Aβ deposition in the dorsal, external, lateral, medial, posterior, and ventral regions of the anterior olfactory bulb, olfactory ventricle, dorsal region of the tenia tecta, and the navicular nucleus in 5xFAD mice. We also observed mild Aβ deposition in the glomerular layer and granule cell layer of olfactory bulb, olfactory tubercle, ventral region of the tenia tecta, and dorsal transition zone. However, no Aβ deposition was detected in the olfactory nerve (**Figures 3A–C**).

Anterior cortical area

We found high levels of Aβ deposition in anterior cortical areas in 5xFAD mice, including the perirhinal cortex, primary region (6.61 ± 2.82%), barrel field (5.88 ± 1.3%), forelimb region (6.40 ± 2.21%), dysgranular zone, hindlimb region (8.76 ± 3.58%), jaw region, shoulder region, trunk region, upper lip region, and secondary region of the somatosensory cortex, and piriform cortex (6.94 ± 2.00%). We also observed moderate Aβ deposition in the primary motor cortex (3.42 ± 1.27%), secondary motor cortex (2.75 ± 0.71%), prelimbic cortex (1.86 ± 0.69%), infralimbic cortex (1.86 ± 1.26%), dorsal peduncular cortex of the medial prefrontal cortex, area 1 and area 2 of the cingulate cortex, dorsolateral, lateral (2.59 ± 0.83%) and ventral (2.52 ± 0.95%) regions of the orbital cortex, dorsal and ventral (2.38 ± 1.12%) and posterior regions of the agranular insular cortex (5.94 ± 0.9%), and intermediate part of the endopiriform claustrum. In contrast, only mild Aβ deposition was detected in the medial part of orbital cortex, dorsal and ventral regions of the endopiriform claustrum, and dorsal and ventral claustrum (**Figures 3B–4A**).

Basal ganglia

We observed moderate Aβ deposition in the subthalamic nucleus, nucleus accumbens shell, lateral accumbens shell, and zona incerta; whereas mild Aβ deposition was detected in the pars compacta and pars reticulata of substantia nigra, lateral substantia nigra, nucleus accumbens core, ventral pallidum, caudate putamen, globus pallidus, and internal capsule. However, we did not detect Aβ deposition in the dorsal

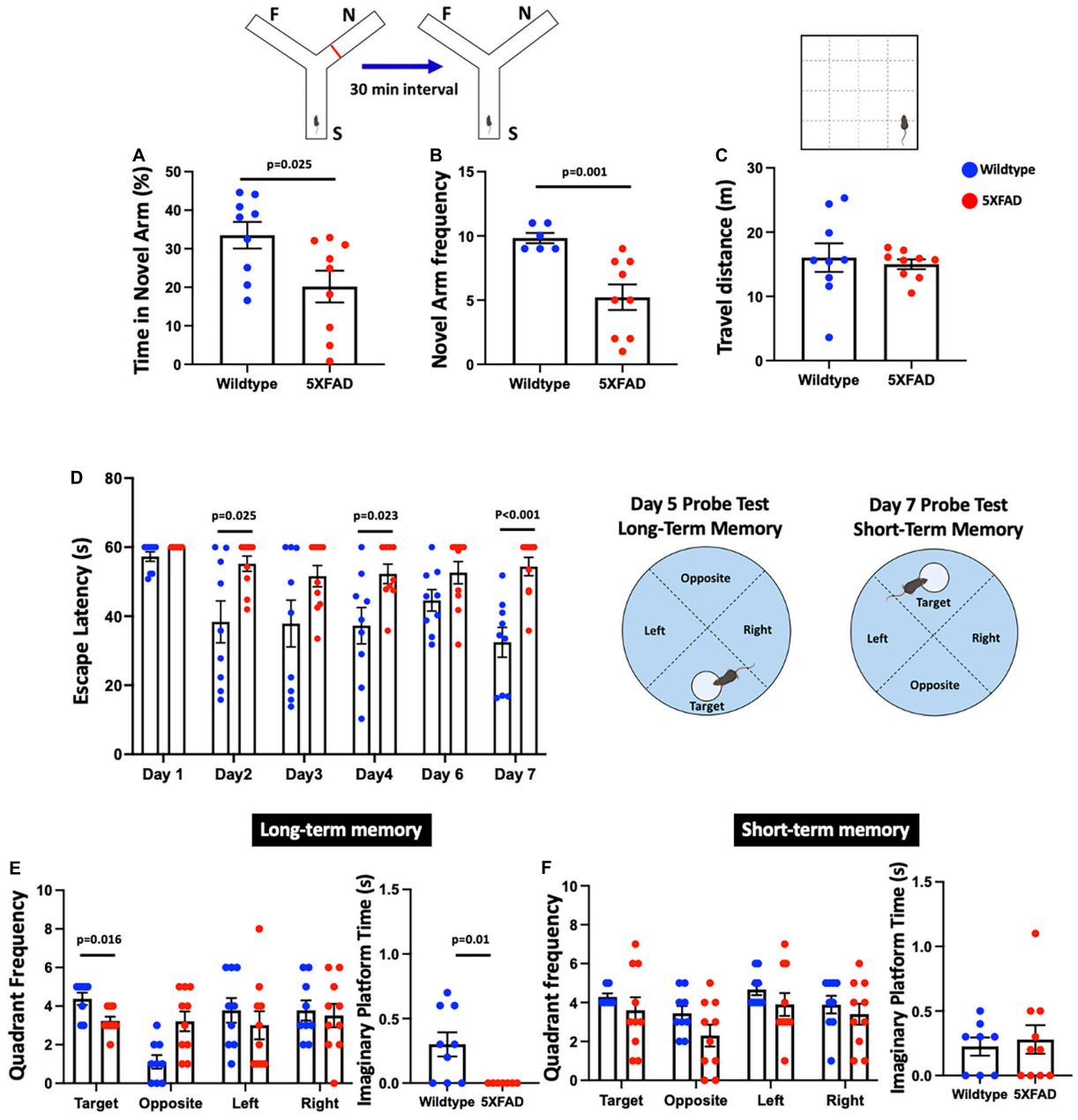

FIGURE 1
A symmetrical Y-maze experiment was conducted with Start Arm (S), Familiar Arm (F), Novel Arm (N). 5xFAD mice showed **(A)** significantly decreased proportion of time spent (%) in the novel arm, **(B)** significantly decreased frequency of visits to the novel arm, **(C)** no significant difference in the distance traveled compared to wildtype mice, **(D)** significantly increased escape latency (s) on days 2, 4, and 7, but no significant differences on days 1, 3, and 6, **(E)** significant decreased frequency to enter the target quadrant and time spent on the platform in the long-term memory probe test, and **(F)** no significant difference in the short-term memory probe test.

and medial regions of the substantia nigra pars compacta, or external capsule (Figures 4A–6B).

Amygdala and bed nucleus of the stria terminalis

We observed moderate Aβ deposition in the anterior cortical amygdaloid area, posterior basolateral amygdaloid nucleus, anterior basolateral amygdaloid nucleus (2.99 ± 0.68%), medial posterior amygdala (2.76 ± 0.98%), medial anterior amygdala (1.22 ± 0.24%), and amygdalopiriform transition area. We also detected mild Aβ deposition in the anterior amygdaloid area, posterior basomedial amygdaloid nucleus, anterior basolateral amygdaloid nucleus, capsular of central amygdaloid nucleus,

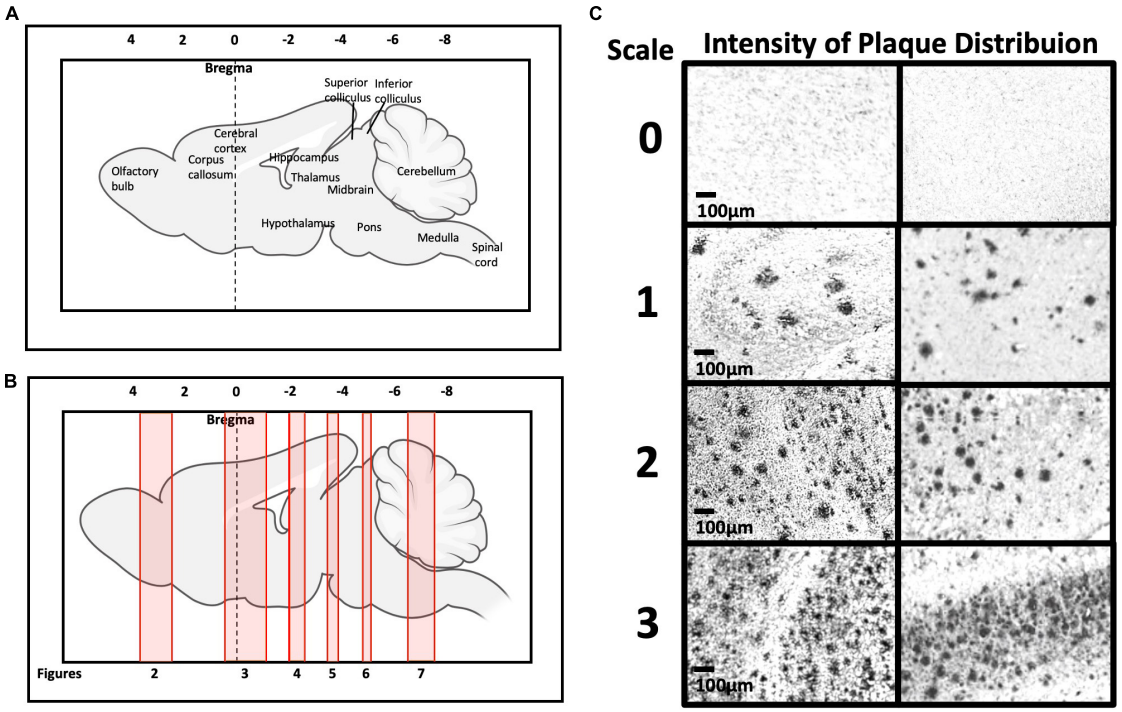

FIGURE 2
(A,B) Representation of brain rostro-caudal levels of Aβ deposition within the respective coronal brain sections depicted in Figures 2–8.
(C) Categorization of Aβ deposition according to the intensity level (0 = no deposition; 1 = mild; 2 = moderate; 3 = high).

extended amygdala, medial amygdala (1.82 ± 0.40%), lateral amygdaloid nucleus, and posteromedial cortical amygdaloid nucleus. However, we found no Aβ deposition in the lateral and medial central amygdaloid or bed nucleus of the stria terminalis (Figures 4B–6B).

Thalamus

We found high levels of Aβ burden in the thalamus of 5xFAD mice, particularly in the posterior thalamic nucleus (6.82 ± 2.78%), ventral posterolateral thalamic nucleus (7.84 ± 3.20%), ventral posteromedial thalamic nucleus (6.26 ± 2.20%), and ventrolateral thalamic nucleus. We observed moderate Aβ deposition in the submedius thalamic nucleus, lateral posterior thalamic nucleus, parafascicular thalamic nucleus, and posterior intralaminar thalamic nucleus. We also detected mild Aβ deposition in the rhomboid thalamic nucleus, mediodorsal thalamic nucleus, subparafascicular thalamic nucleus, and ventral anterior thalamic nucleus. However, we did not detect any Aβ deposition in the anterior and posterior paraventricular thalamic nuclei, paratenial thalamic nucleus, or the reuniens thalamic nucleus (Figures 4B–5B).

Hypothalamus

We did not detect Aβ deposition in the hypothalamus of 5xFAD mice, including the paraventricular hypothalamic nucleus, striohypothalamic nucleus, posterior, dorsal, ventromedial, dorsomedial, central, and ventrolateral regions, shell region, lateral hypothalamus, lateral tuberal region, ventrolateral part of the hypothalamic area, and medial tuberal nucleus (Figures 4B–5B).

Hippocampus

In the dorsal hippocampus of 5xFAD mice, we found high Aβ deposition in dentate gyrus (5.16 ± 1.43%), while moderate Aβ deposition was observed in CA1 (5.56 ± 1.45%), and CA3 (3.69 ± 1.83%) subregions of the dorsal hippocampus. In the ventral hippocampus, high Aβ deposition was shown in dentate gyrus (6.54 ± 2.92%), CA1/2 (8.83 ± 2.76%), CA3 (9.06 ± 2.86%), dorsal, transition area (18.38 ± 0.93%), and ventral subiculum (Figures 4B–6B).

Midbrain

In 5xFAD mice, we detected high Aβ burden in the external cortex of the inferior colliculus (5.19 ± 1.08%), whereas moderate Aβ deposition was found in the pontine reticulotegmental nucleus, paranigral nucleus, and intermediate reticular nucleus. We also observed mild Aβ deposition in the dorsal cortex of inferior colliculus, P1, ventrolateral periaqueductal gray, ventral tegmental area, parainterfascicular nucleus, ventral tegmental decussation, lateral superior olive, dorsal nucleus, subnucleus B, and subnucleus C

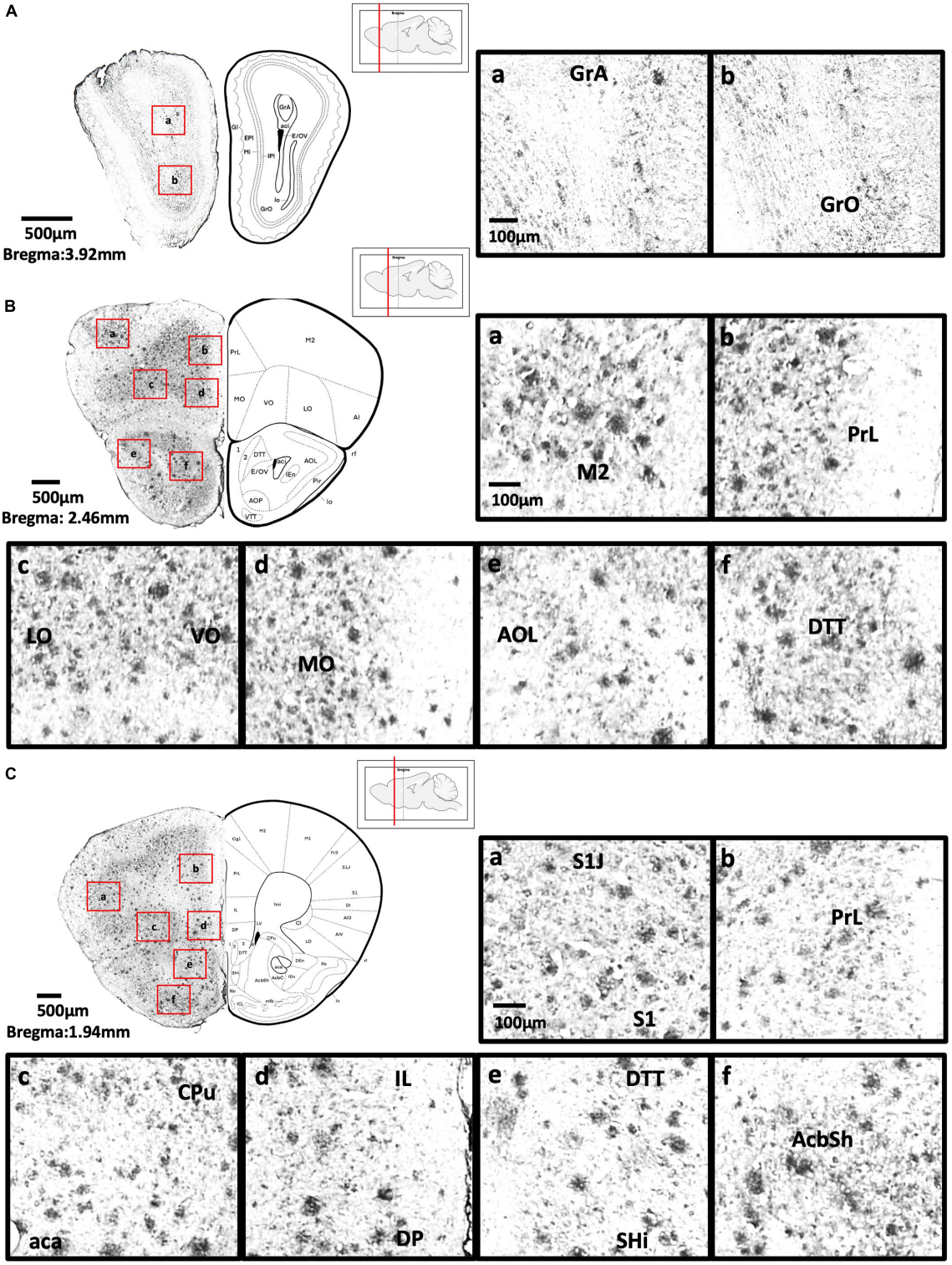

FIGURE 3
(A) Coronal section of olfactory-related areas showing Aβ deposition in the granule cell layer of the accessory olfactory bulb (a) and granule cell layer of the olfactory bulb (b). **(B)** Coronal section of the frontal cortex and olfactory-related areas showing Aβ deposition in the secondary motor cortex (a), prelimbic cortex (b), lateral orbital cortex, ventral orbital cortex (c), medial orbital cortex (d), lateral part of anterior olfactory area (e), and dorsal tenia tecta (f). **(C)** Coronal section through the cerebral cortex showing Aβ deposition in the primary somatosensory cortex, jaw region of the somatosensory cortex (a), prelimbic cortex (b), caudate putamen, anterior part of anterior commissure (c), infralimbic cortex, dorsal peduncular cortex (d), dorsal tenia tecta, septohippocampal nucleus (e), and nucleus accumbens shell (f).

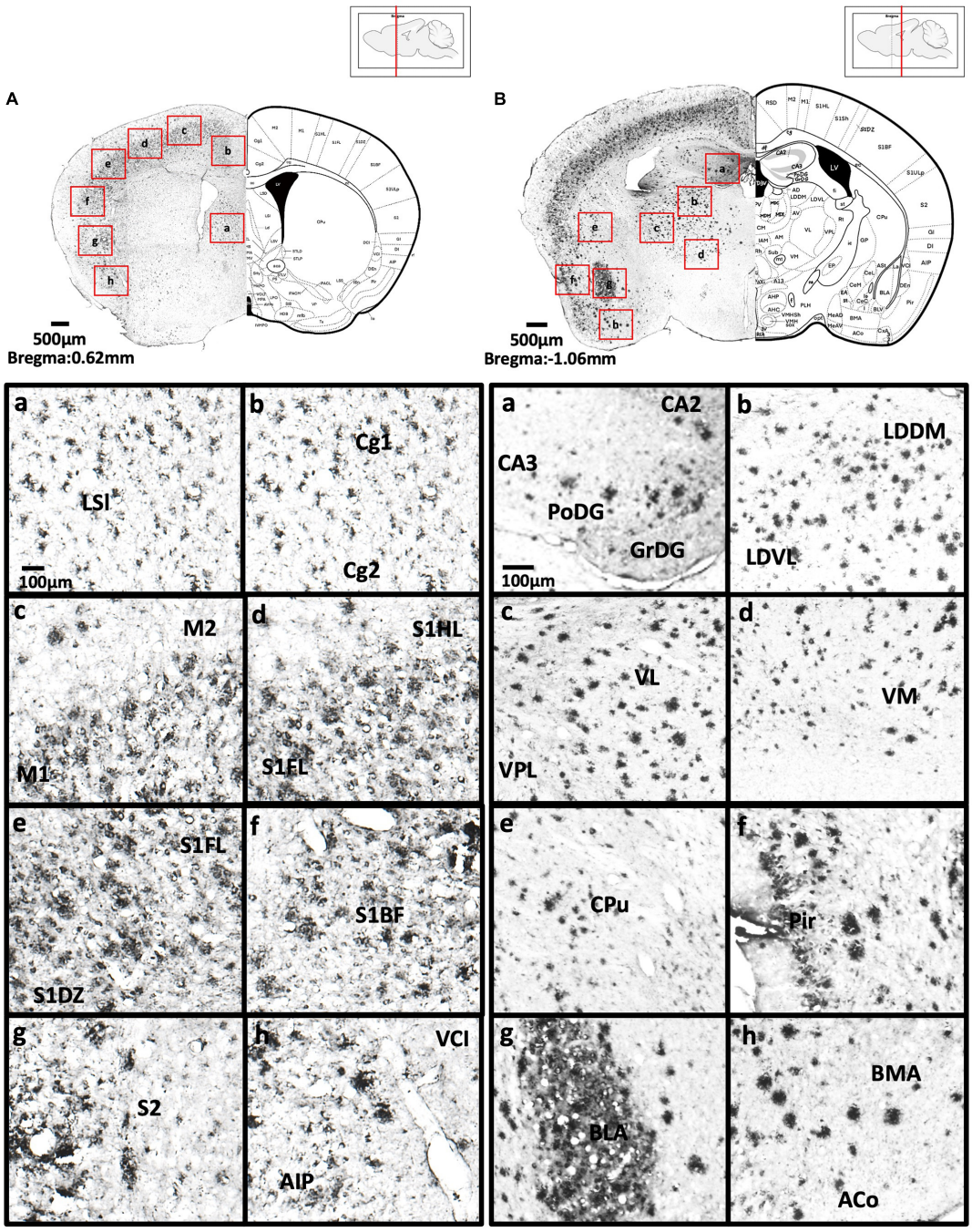

FIGURE 4
(A) Coronal section through the cerebral cortex showing Aβ deposition in the intermediate part of the lateral septal nucleus (a), area 1 and area 2 of the cingulate cortex (b), primary motor cortex and secondary motor cortex (c), hindlimb region and forelimb region of somatosensory cortex (d), forelimb region and dysgranular zone of somatosensory cortex (e), barrel field of the somatosensory cortex (f), secondary somatosensory cortex (g), ventral part of claustrum and posterior agranular insular cortex (h). **(B)** Coronal section through the forebrain showing Aβ deposition in CA2 field, CA3 field and dentate gyrus (a), dorsomedial and ventrolateral areas of the laterodorsal thalamic nucleus (b), ventrolateral thalamic nucleus, ventral posterolateral thalamic nucleus (c), ventromedial thalamic nucleus (d), caudate putamen (e), piriform cortex (f), basolateral amygdaloid nucleus (g), anterior part of the basomedial amygdaloid nucleus, and anterior cortical amygdaloid area (h).

of medial nucleus of the inferior olive, lateral terminal nucleus, supragenual nucleus, and external and rotundus part of the cuneate nucleus. However, we did not detect Aβ deposition in several midbrain regions, including the

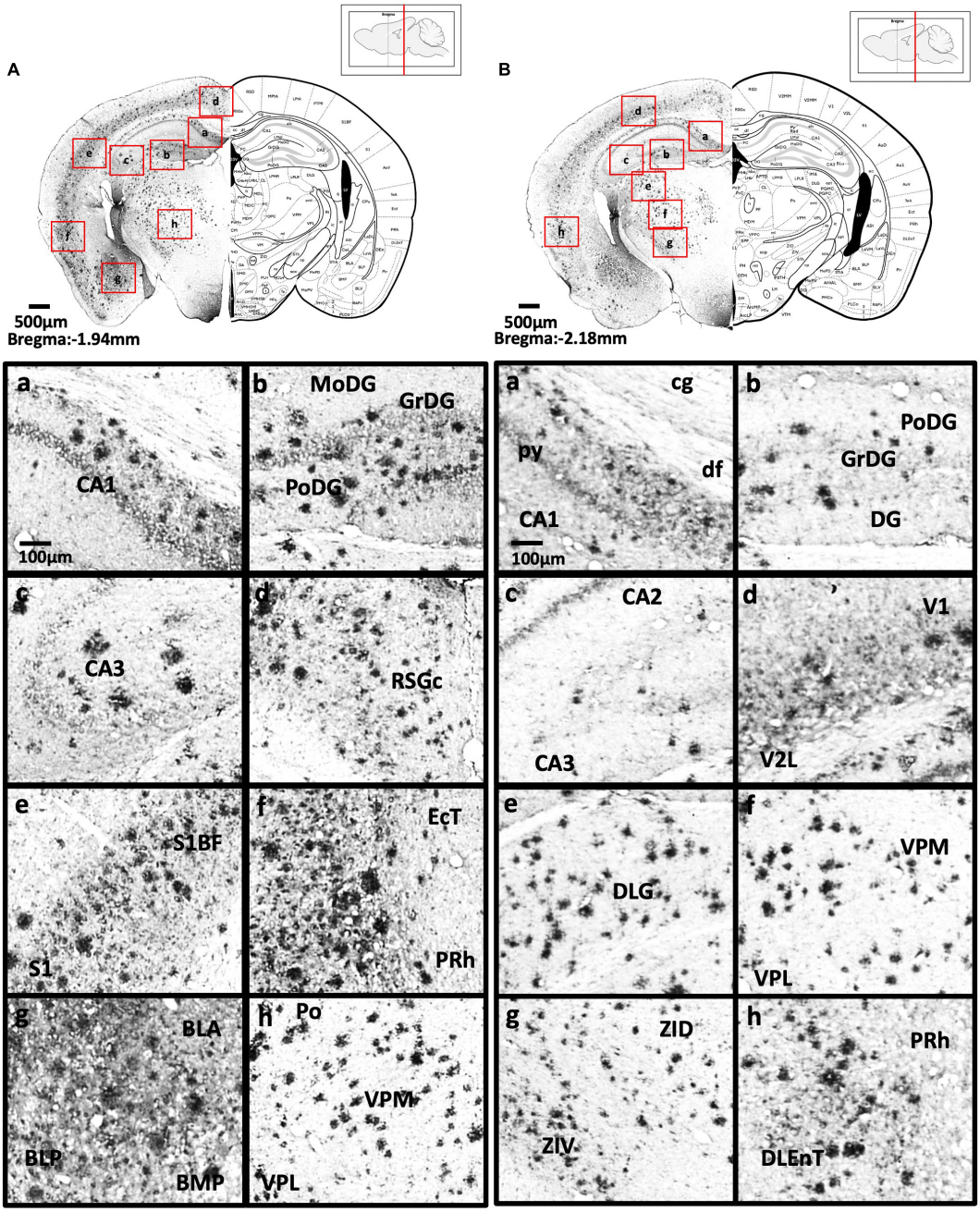

FIGURE 5
(A) Coronal section through the forebrain showing Aβ deposition in CA1 field (a), dentate gyrus (b), CA3 field (c), C region of the retrosplenial granular cortex (d), barrel field of the somatosensory cortex, primary somatosensory cortex (e), ectorhinal cortex, perihinal cortex (f), anterior and posterior basolateral amygdaloid nucleus, posterior basomedial amygdaloid nucleus (g), and posterior, ventral posterolateral and ventral posteromedial thalamus (h). **(B)** Coronal section through the forebrain showing Aβ deposition in the cingulum, pyramidal tract, dorsal fornix and CA1 field (a), dentate gyrus (b), CA2, CA3 (c), primary visual cortex and secondary lateral visual cortex (d), dorsal lateral geniculate nucleus (e), ventral posterolateral and ventral posteromedial thalamus (f), dorsal and ventral part of zona incerta (g), perihinal cortex, and dorsolateral entorhinal cortex (h).

superficial layer, optic nerve layer, brachium, zona layer, intermediate gray layer, intermediate white layer of superior colliculus, dorsal lateral, dorsal medial, and lateral areas of the periaqueductal gray, caudal, dorsal, interfascicular, lateral, and ventral dorsal raphe, median raphe, nucleus of the trapezoid body, gracile nucleus, gracile fasciculus, median accessory nucleus, and cuneate nucleus of the medulla (Figures 6A–7B).

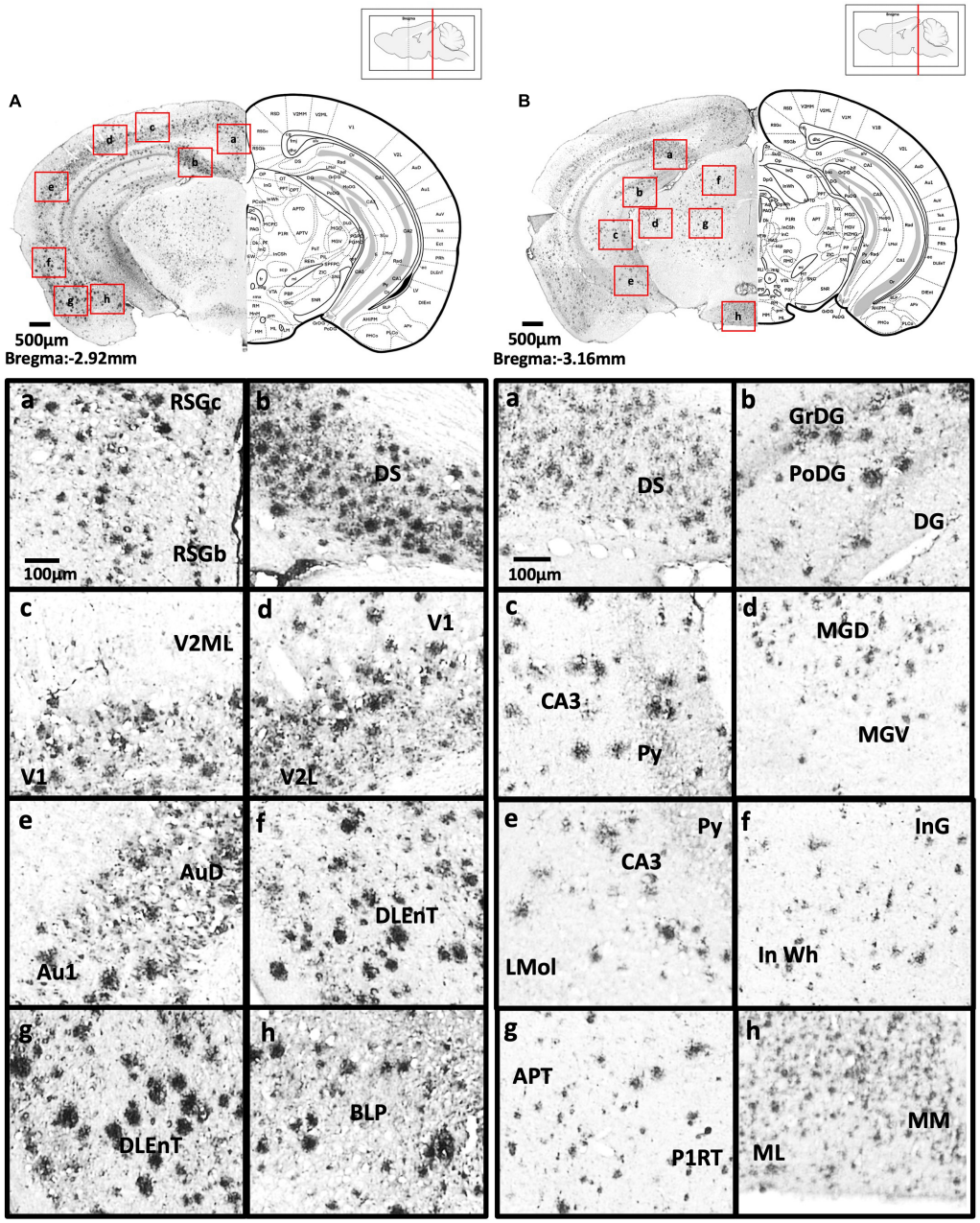

FIGURE 6
(A) Coronal section through the midbrain showing Aβ deposition in the B region and C region of the retrosplenial granular cortex (a), dorsal subiculum (b), primary visual cortex, mediolateral area in the secondary visual cortex (c), primary visual cortex, lateral secondary visual cortex (d), primary auditory cortex, dorsal auditory cortex (e), dorsolateral entorhinal cortex (f), dorsolateral entorhinal cortex (g), and posterior basolateral amygdaloid nucleus (h). **(B)** Coronal section through the midbrain showing Aβ deposition in the dorsal subiculum (a), dentate gyrus (b), CA3 field and pyramidal tract (c), dorsal and ventral medial geniculate nucleus (d), pyramidal tract, CA3 field, and lacunosum molecular layer of the hippocampus (e), intermediate gray layer of the superior colliculus, intermediate white layer of the superior colliculus (f), anterior pretectal nucleus, p1 reticular formation (g), and lateral and medial mammillary nucleus (h).

Posterior cortical areas

In 5xFAD mice, we found high Aβ deposition in the dorsal, dorsolateral, and ventral intermediate entorhinal cortex, as well as binocular and monocular areas of the primary visual cortex. We also observed moderate Aβ deposition in the ectorhinal cortex, medial entorhinal cortex, A, B, and C regions of the retrosplenial granular cortex, retrosplenial dysgrandular cortex (2.3 ± 0.49%), primary visual cortex (2.68 ± 0.81%), lateral (2.7 ± 0.55%), mediolateral, and mediomedial (2.29 ± 0.60%) areas of the secondary visual cortex, primary auditory

cortex (2.18 ± 0.66%), dorsal (1.99 ± 0.63%), and ventral (1.99 ± 0.53%) areas of the secondary auditory cortex, and the temporal association cortex (1.62 ± 0.37%) (**Figures 4B–7B**).

Cerebellum and vestibular nucleus

We observed mild Aβ deposition in the superior cerebellar peduncle, paraflocculus of the cerebellum, superior, and lateral vestibular nuclei of 5xFAD mice (**Figures 8A,B**). However, we did not detect Aβ deposition in lobules 2, 3, 4, and 5 of the cerebellum, crus 1 or crus 2 of the ansiform lobule, medial cerebellar nucleus, middle cerebellar peduncle, simple lobule, interposed cerebellar nucleus, lateral cerebellar nucleus, vestibulocerebellar nucleus, medial vestibular nucleus, magnocellular, and parvicellular areas of the medial vestibular nucleus, or spinal vestibular nucleus.

Spinal cord and other regions

In 5xFAD mice, we detected moderate Aβ deposition in the gelatinous layer, interpolar, caudal, and oral areas of the spinal trigeminal nuclei, and anterior areas of the anterior commissure. We also observed mild Aβ deposition in the central cervical nucleus of the spinal cord, intrabulbar and posterior nerve of the anterior commissure, magnocellular nucleus of the posterior commissure, nucleus of the posterior commissure, and island of Calleja (**Figures 8A,B**). We found no Aβ deposition in the nucleus of solitary tract.

Correlation

We examined the possible inter-regional correlation by determining the Aβ plaque burden in the ROIs and their inter-regional correlations in 36 regions. The correlations are presented in the correlation matrix in **Figure 9A**. Red spots represent strong positive correlation, yellow spots represent no correlation, and blue spots represent strong negative correlation. Distinct red clusters were observed in the medial prefrontal cortex, somatosensory cortex, medial amygdala, thalamus, and hippocampus, which suggest strong relationships among these regions. The 3D model in **Figure 9B** shows the brain regions with correlation coefficients higher than + 0.9.

Discussion

In this study, we showed 9-month-old adult 5xFAD mice had significantly impaired spatial learning and memory functions. These results are in line with the memory deficits found in human AD patients (Eustache et al., 2006). As the cognitive impairments seen in the Y-maze and MWM are related to hippocampal-dependent memory formation (Stackman et al., 2003; Kraeuter et al., 2019; Yu et al., 2022), we next investigated the anatomical localization of Aβ deposition in the hippocampus. We found Aβ deposition was strongly associated with the hippocampus and hippocampal-projected regions, including the medial prefrontal cortex, somatosensory cortex, thalamus, and medial amygdala. Our findings are in line with the results from PET studies and human post-mortem brain studies, which observed Aβ deposition in the hippocampus (Martinez-Pinilla et al., 2016; Shokri-Kojori et al., 2018; D'Haese et al., 2020). In AD, Aβ deposition in the hippocampus results in hippocampal atrophy associated with loss of neurons, eventually leading to the accumulation of astrocytes and other glial cells (Martinez-Pinilla et al., 2016; Palmqvist et al., 2017; Uddin and Lim, 2022). Specifically, we found Aβ plaques were widely distributed throughout the dorsal and ventral hippocampus of 5xFAD mice. However, a study on 12-month-old 3xTg-AD mice found Aβ plaque accumulated only in the subiculum of hippocampus (Javonillo et al., 2021). Interestingly, another study on 4-month-old APP/PS1 mice found Aβ plaque accumulation in the hippocampus was associated with cognitive impairment and synaptic marker loss (Sanchez-Varo et al., 2021). These findings and our results not only demonstrate the differential accumulation of Aβ plaques in different AD mouse models, but also the effects of Aβ deposition on cognitive function. We constructed an inter-regional correlation matrix of Aβ deposition, which revealed strong relationships among the hippocampus, medial prefrontal cortex, somatosensory cortex, medial amygdala, and thalamus. The hippocampus together with the regions projecting from it are involved in the control of memory retrieval and consolidation (Hagena et al., 2016). Therefore, the accumulation of Aβ plaques in the hippocampus might also disrupt the functions of these projected areas, contributing to the cognitive impairments.

The deposition of Aβ in the cerebral cortex in AD patients has been confirmed by many studies using polarization sensitive optical coherence microscopy (PS-OCM), positron emission tomography (PET), and the magnetic resonance imaging (MRI) (Klunk et al., 2004; Davatzikos et al., 2008; Johnson et al., 2012; Baumann et al., 2017). Moreover, a PET scan study in humans revealed that the first region to experience Aβ deposition was the cerebral cortex, particularly the precuneus, medial orbitofrontal, and posterior cingulate cortices (Palmqvist et al., 2017). In 5xFAD mice, Aβ deposition was found to start in the subiculum of the hippocampus and layer V of the cerebral cortex by 2 months of age (Oakley et al., 2006). In our study, the immunostaining not only showed pronounced Aβ deposition throughout the cerebral cortex of 5xFAD mice, but also revealed two distinct Aβ deposition patterns in the cerebral cortices. We detected Aβ deposition in layers 4, 5, and 6a (somatosensory cortex, visual cortex, and auditory cortex) and in layers 1, 2, and 3 (agranular insular cortex and piriform cortex) of 5xFAD mice. Similar findings were observed in previous studies that showed neuronal loss in cortical layers 4 and 5 in APP/PS1 and 5xFAD mice, respectively (Beker et al., 2012; Jawhar et al., 2012; Eimer and Vassar, 2013). In this study, we are first to

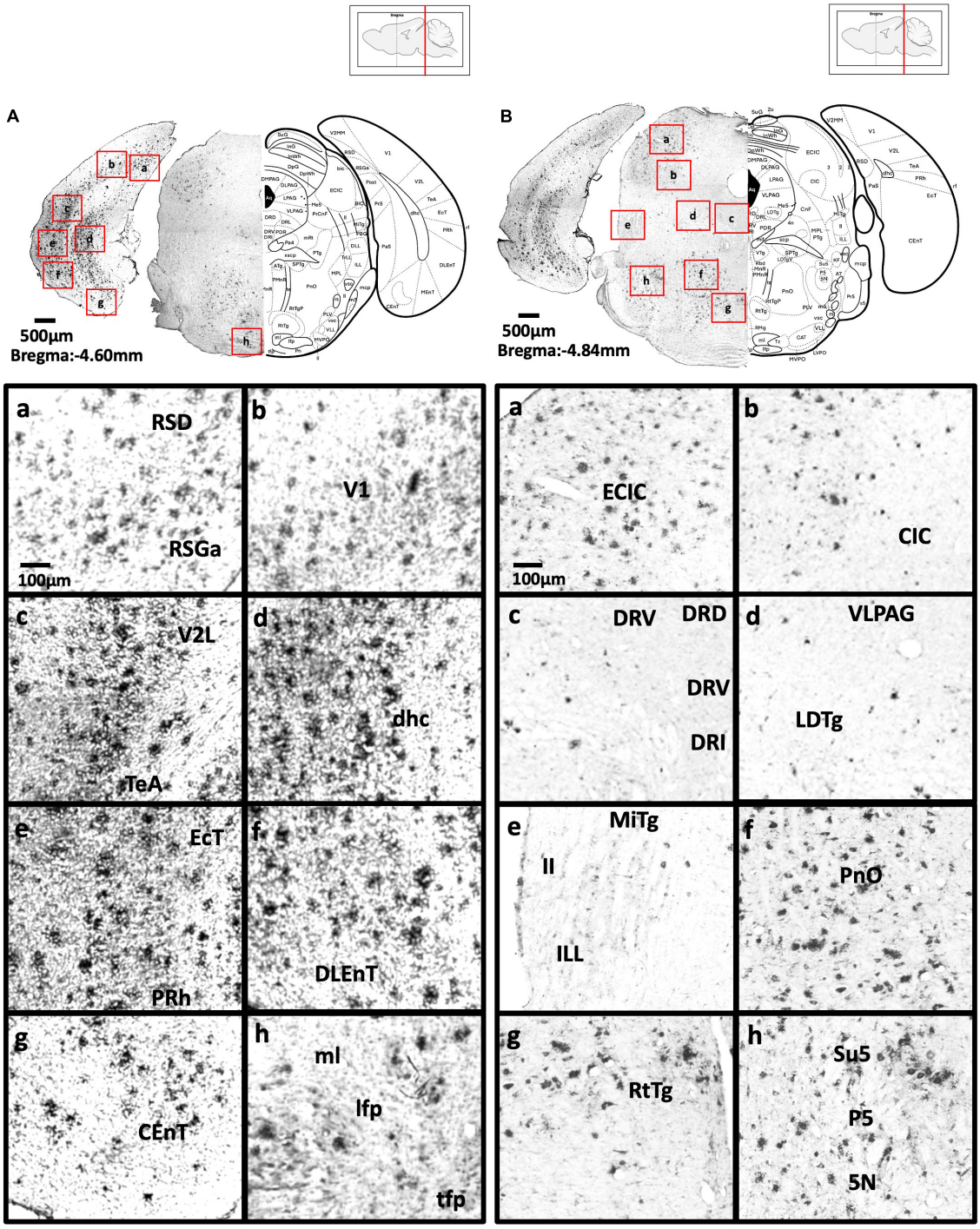

FIGURE 7
(A) Coronal section through the midbrain showing Aβ deposition in the retrosplenial dysgranular cortex, A region of retrosplenial granular cortex (a), primary visual cortex (b), lateral secondary visual cortex (c), dorsal hippocampal commissure (d), ectorhinal cortex, perihinal cortex (e), dorsolateral entorhinal cortex (f), caudomedial entorhinal cortex (g), medial lemniscus, longitudinal fasciculus of nucleus, and transverse fibers of the pons (h). **(B)** Coronal section through the midbrain showing Aβ deposition in the external cortex of the inferior colliculus (a), central nucleus of the inferior colliculus (b), dorsal, ventral, interfascicular, and lateral dorsal raphe (c), ventrolateral periaqueductal gray, laterodorsal tegmental nucleus (d), microcellular tegmental nucleus, lateral lemniscus, intermediate nucleus of the lateral lemniscus (e), oral region of the pontine reticular nucleus (f), reticulotegmental nucleus of the pons (g), supratrigeminal nucleus, peritrigeminal zone, and motor trigeminal nucleus (h).

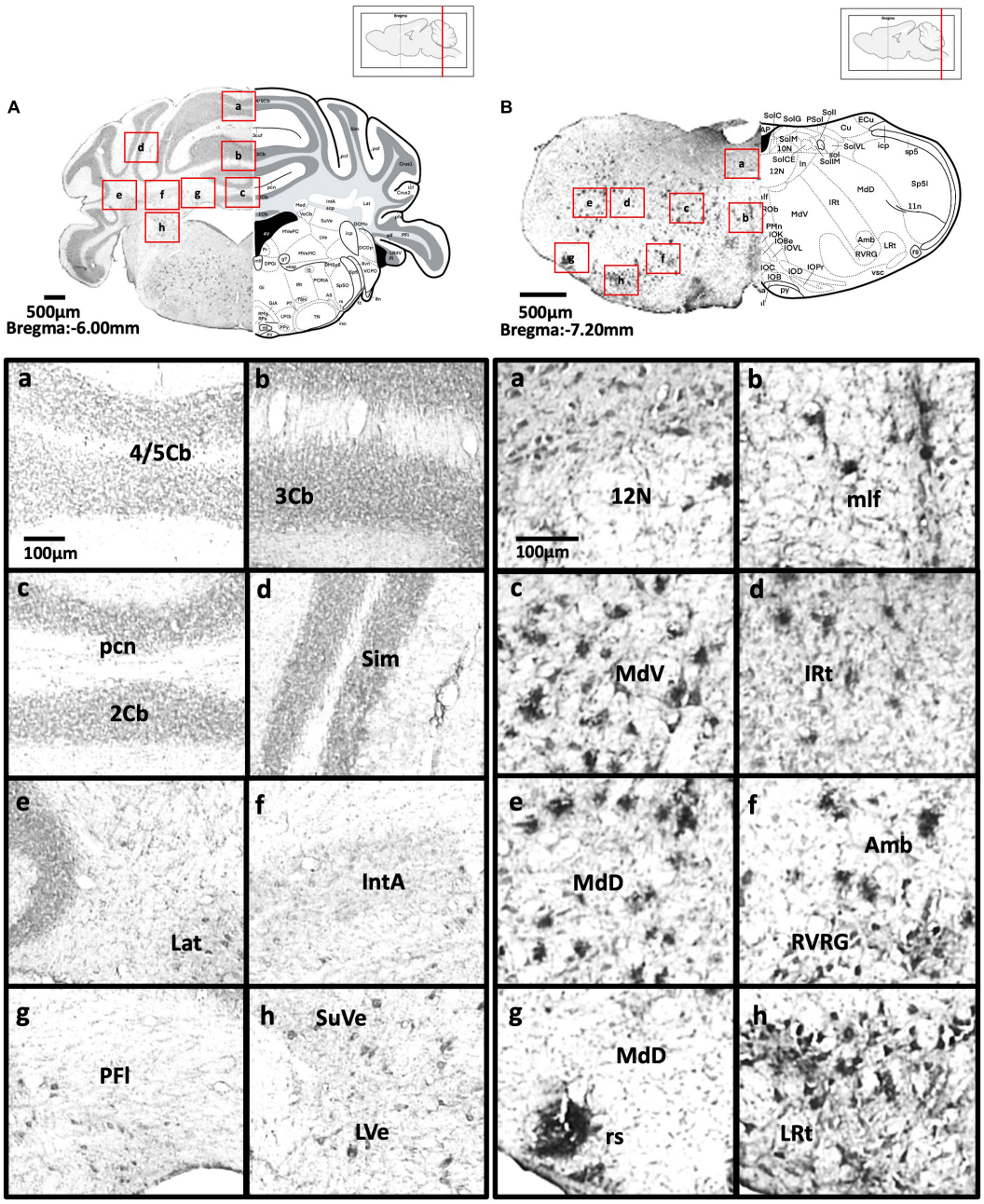

FIGURE 8
(A) Coronal section through the cerebellum and medulla showing Aβ deposition in lobules 4 and 5 of the cerebellar vermis (a), lobule 3 of the cerebellar vermis (b), lobule 2 of the cerebellar vermis and precentral fissure (c), simple lobule (d), lateral cerebellar nucleus (e), anterior interposed cerebellar nucleus (f), paraflocculus (g), superior vestibular nucleus, and lateral vestibular nucleus (h). **(B)** Coronal section through the spinal cord showing Aβ deposition in the hypoglossal nucleus (a), medial longitudinal fasciculus (b), ventral medullary reticular nucleus (c), intermediate reticular nucleus (d), dorsal medullary reticular nucleus (e), ambiguus nucleus and rostral ventral respiratory group (f), rubrospinal tract and dorsal medullary reticular nucleus (g), and lateral reticular nucleus (h).

demonstrate an Aβ deposition pattern in cortical layers 1, 2, and 3 of 5xFAD mice.

In the correlation matrix, the medial prefrontal cortex and somatosensory cortex showed strong correlations with the hippocampus. The cerebral cortex is highly involved in hippocampal-dependent memory formation, given that it receives numerous projections from the hippocampus. The projection from the hippocampus to medial prefrontal cortex regulates social, hippocampal-dependent and fear memory (Lim et al., 2015a; Liu et al., 2015; Tan et al., 2020a, 2021), whereas

10.3389/fnagi.2022.964336

TABLE 1 Quantitative assessment of the average Aβ plaque deposition in the brain of 5xFAD mice.

Brain regions	Plaque burden (%)±S.D
Motor cortex	
Primary Motor Cortex, M1	3.42 ± 1.27
Secondary Motor Cortex, M2	2.75 ± 0.71
Medial prefrontal cortex	
Prelimbic Cortex, PrL	1.86 ± 0.69
Infralimbic Cortex, IL	1.86 ± 1.26
Orbital cortex	
Lateral, LO	2.59 ± 0.83
Ventral, VO	2.52 ± 0.95
Agranular insular cortex	
Ventral/Dorsal, AIV/AID	2.38 ± 1.12
Posterior, AIP	5.94 ± 0.9
Somatosensory cortex	
Primary Region, S1	6.61 ± 2.82
Barrel Field, S1BF	5.88 ± 1.30
Forelimb Region, S1FL	6.40 ± 2.21
Hindlimb Region, S1HL	8.76 ± 3.58
Piriform cortex, Pir	6.94 ± 2.00
Amygdala	
Basolateral, anterior part, BLA	2.99 ± 0.68
Medial, anterior, MeA	1.22 ± 0.24
Medial, posterior, MeP	2.76 ± 0.98
Medial, Me	1.82 ± 0.40
Thalamus	
Posterior, Po	6.82 ± 2.78
Ventral Posterolateral, VPL	7.84 ± 3.20
Ventral Posteromedial, VPM	6.26 ± 2.20
Dorsal hippocampus	
CA1 Subfield, CA1	5.56 ± 1.45
CA3 Subfield, CA3	3.69 ± 1.83
Dentate Gyrus, DG	5.16 ± 1.43
Ventral hippocampus	
Dorsal Subiculum, DS	18.382 ± 0.93
CA1 Subfield, CA1	8.832 ± 2.76
CA3 Subfield, CA3	9.06 ± 2.86
Dentate Gyrus, DG	6.538 ± 2.92
Inferior colliculus	
External Cortex, ECIC	5.19 ± 1.08
Retrosplenial cortex	
Dysgranular, RSD	2.3 ± 0.49
Visual cortex	
Primary, V1	2.68 ± 0.81
Secondary Lateral, V2L	2.70 ± 0.55
Secondary Mediolateral and Mediomedial Area, V2ML+V2MM	2.29 ± 0.60
Auditory cortex	
Primary, Au1	2.18 ± 0.66
Dorsal, AuD	1.99 ± 0.63
Ventral, AuV	1.99 ± 0.53
Temporal association cortex, TeA	1.62 ± 0.37

The plaque burden was measured using the ImageJ threshold method.

the projection from hippocampus to the somatosensory cortex regulates somatosensory responses and the consolidation of human motor memory (Bellistri et al., 2013; Kumar et al., 2019). Moreover, projections from the hippocampus to other cortical areas, such as the retrosplenial cortex, are involved in the retention of recognition memory (Balcerek et al., 2021). The hippocampus also sends navigational signals to visual cortex to induce a visual response, and to the auditory cortex to modulate auditory information and auditory fear conditioning (Xiao et al., 2018; Diamanti et al., 2021). Therefore, Aβ deposition in the hippocampus and cerebral cortex might further increase cognitive impairment.

We observed moderate to mild Aβ deposition in the amygdala, which showed a strong positive correlation with the hippocampus in the correlation matrix. The medial amygdala is involved in innate emotional behavior *via* regulating olfactory information to hypothalamus (Lim et al., 2008; Lim et al., 2009; Keshavarzi et al., 2014). Therefore, Aβ deposition in medial amygdala might lead to altered emotional behavior. On the other hand, the projection from the hippocampus to the amygdala also regulates the formation of long-term memories, particularly significant emotional events (Richter-Levin and Akirav, 2000). Remarkably, human AD patients were shown to have impaired amygdala-dependent memory, in which they failed to exhibit conditioned fear responses to stimuli (Hamann et al., 2002). Consistently, Aβ deposition induced impairment of amygdala-dependent memory in AD animal models, including APPswe/PS1dE9, APP(Ind)/APP(Sw, Ind), and 3xTg-AD transgenic mice (Espana et al., 2010; Lin et al., 2015).

We detected mild Aβ deposition in the pars compacta and pars reticulata of substantia nigra and ventral tegmental area (VTA). These regions also receive projections layer V of the cortex layer V of the cortex from the hippocampus and are involved in hippocampal memory systems (Martig et al., 2009; Kafkas and Montaldi, 2015). The VTA and substantia nigra are two major dopaminergic areas in the brain. The deposition of Aβ in these regions can disrupt dopaminergic-regulated reward memory processing in 3xTg-AD and Tg2576 mouse models (Nobili et al., 2017; Gloria et al., 2021). Moreover, tyrosine hydroxylase cells and dopamine neurons in the VTA and substantia nigra were significantly suppressed in 5xFAD mice (Vorobyov et al., 2019). In human study, there were remarkable reduction of catecholamine and their metabolites (Liu et al., 2011), as well as alteration of dopamine and its receptors in AD patients (Pan et al., 2019).

We are first to show mild Aβ deposition in both the VTA and substantia nigra of 5xFAD mice, which suggests mild Aβ deposition may be sufficient to suppress the dopaminergic system and disrupt memory encoding and memory consolidation processes in 5xFAD mice, although the dopaminergic system could also be affected by other AD pathologies. Our study also demonstrated for the first time mild

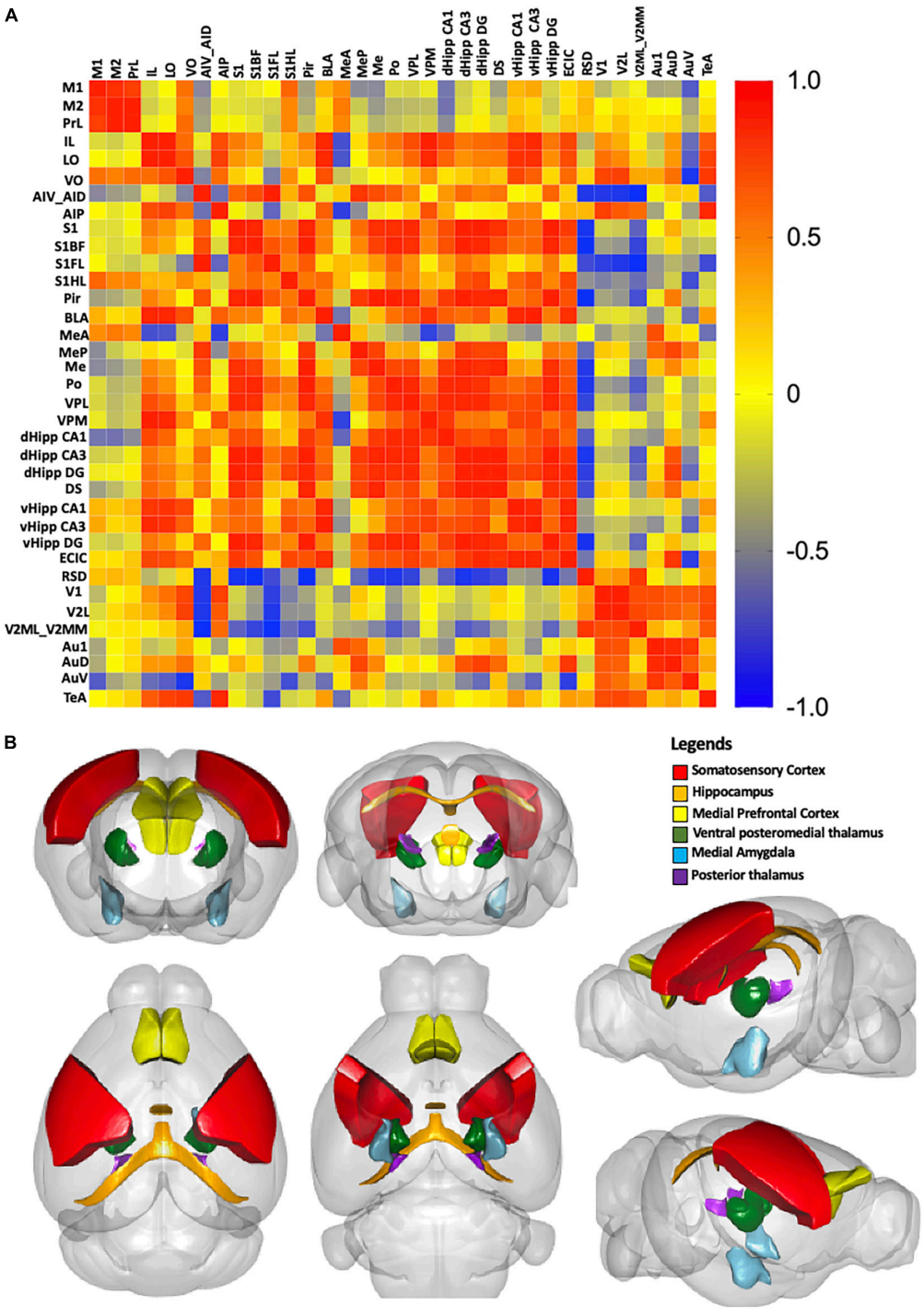

FIGURE 9
(A) Correlation matrix with color scale. A correlation coefficient of 1 represents the maximum positive correlation, whereas, -1 represents the maximum negative correlation. Red indicates 1 and blue indicates -1. **(B)** A 3D model of the strongest correlated regions. Red represents the somatosensory cortex, orange represents the hippocampus, yellow represents the medial prefrontal cortex, darkgreen represents the ventral posteromedial thalamus, and skyblue represents the medial amygdala, purple presents the posterior thalamus.

to moderate Aβ deposition in the nucleus accumbens of 5xFAD mice. The nucleus accumbens is a key regulator of reward and satisfaction, and also receives projections from the hippocampus to mediate decision-making processes (Abela et al., 2015; Salgado and Kaplitt, 2015) and impulsivity (Sesia et al., 2008; Sesia et al., 2010). It was found that Aβ accumulation in

the nucleus accumbens suppressed cholinergic, dopaminergic, and norepinephrine systems in Wistar rats (Preda et al., 2008; Morgese et al., 2015).

We found Aβ deposition in various regions of the thalamus of 5xFAD mice. Deposition of Aβ in thalamus was also reported in post-mortem human AD brain tissues and in AD models by positron emission tomography (Alderson et al., 2017; Frost et al., 2020). The thalamus is connected to the hippocampus to regulate spatial memory, spatial sensory information, and human episodic memory (Burgess et al., 2002; Aggleton et al., 2010; Chan et al., 2017). Therefore, Aβ deposition in the thalamus might contribute to the cognitive impairment in AD (Alderson et al., 2017; Frost et al., 2020).

We did not detect Aβ deposition in the hypothalamus of 5xFAD mice, which is contrary to the report of Aβ deposition in the paraventricular nucleus of the hypothalamus in autopsy brain of AD patients (Ishii and Iadecola, 2015). The hypothalamus contains many nuclear divisions that regulate neuroendocrine systems and serve as the primary coordinator of memory updating (Clarke, 2015; Burdakov and Peleg-Raibstein, 2020). It was reported that AD patients have increased basal cortisol levels, overall insensitivity to glucocorticoid feedback, lowered thyroid hormones, and gradual decline of estrogen and testosterone (Ishii and Iadecola, 2015). The altered glucose metabolism might be one of the possible reasons that caused the absent of Aβ in hypothalamus. A study demonstrated hypothalamus as a primary brain region with metabolic abnormalities in APP/PS1 transgenic mouse (Zheng et al., 2018). A reduced cerebral glucose uptake pattern was observed in 5-month-old 5xFAD mice, and a more significant reduction was observed in the 13-month-old mice. Tharp et al. (2016) showed the correlation between glucose level and Aβ secretion. Therefore, glucose metabolism in the hypothalamus of 5xFAD mice warrants further investigation to justify the lack of Aβ in this region.

Although we observed Aβ deposition throughout the olfactory areas except for the olfactory nerve, the effect of the Aβ deposition on olfactory memory was ambiguous. Two studies suggested that 5xFAD mice retain intact olfactory memory from 3 to 15 months of age without olfactory impairment (Girard et al., 2014; O'Leary et al., 2020), although another study showed that 3-month-old 5xFAD mice did not have full olfactory function (Son et al., 2021). Other studies observed olfactory dysfunction in human AD patients, 3xTg-AD mice, and APPxPS1 mice (Saiz-Sanchez et al., 2013; Franks et al., 2015; Mitrano et al., 2021). Further studies with more stringent behavioral testing are needed to reveal whether Aβ deposition has negative effects on olfactory memory in 5xFAD mice.

We also did not detect Aβ deposition in the periaqueductal gray of 5xFAD mice, which contradicts the findings in a post-mortem AD brain study that observed senile plaques in the periaqueductal gray in 81% of samples (Parvizi et al., 2000). The periaqueductal gray is a major component of brainstem that has pivotal roles in autonomic function, behavior, memory formation, and emotional response to aversive events (Lim et al., 2008; Lim et al., 2010; Temel et al., 2012; Tan et al., 2020b). The absence of Aβ deposition in the periaqueductal gray in 5xFAD mice might represent an inability to recapitulate the Aβ pathological characteristics of human AD.

In summary, the present findings provide comprehensive insights on the rostral-caudal distribution profile of Aβ depositions and their inter-regional correlation in adult 5xFAD mouse brain. Although our study focused on Aβ deposition, other hallmarks of AD (e.g., neurofibrillary tangles, presenilin, and apolipoprotein E) are equally important and will need to be investigated to further enhance translation from animal models to clinical applications.

Data availability statement

The raw data supporting the conclusions of this article will be made available by the authors, without undue reservation.

Ethics statement

The animal study was reviewed and approved by Committee on the Use of Live Animals in Teaching and Research, The University of Hong Kong (No. 4807-18).

Author contributions

TS, YS, MLF, and LWL: conceptualization, funding acquisition, project administration, resources, and supervision. KCT, JR, SCC, and LS: data curation and formal analysis. KCT, JR, SCC, KHW, LS, CHP, YW, TS, LA, RCCC, YS, MLF, and LWL: investigation. KCT, JR, SCC, YS, MLF, and LWL: methodology. KCT, JR, SCC, LA, and KHW: visualization and validation. KCT and LWL: writing–original draft. JR, SCC, KHW, LS, CHP, YW, TS, LA, RCCC, YS, and MLF: writing–review and editing. All authors have read and agreed to the published version of the manuscript.

Funding

This study was supported by Research Grants awarded to LWL, and the Midstream Research Project (MRP/056/21) awarded to YS. This study was also supported by PhytoAPP EU framework (2021-2025, to TS and LWL). The PhytoAPP project has received funding from the the European Union's HORIZON

2020 research and innovation programme under the Marie Skłodowvska-Curie grant agreement 101007642.

Acknowledgments

We would like to thank Mazel Mihardja, Tse Wing Man, Anna Chung Kwan Tse, and Gavin Luu Greaton for their technical assistance on immunohistochemistry and microscopy imaging.

Conflict of interest

The authors declare that the research was conducted in the absence of any commercial or financial relationships that could be construed as a potential conflict of interest.

Publisher's note

Supplementary material

The Supplementary Material for this article can be found online at: https://www.frontiersin.org/articles/10.3389/fnagi.2022.964336/full#supplementary-material

References

Abela, A. R., Duan, Y., and Chudasama, Y. (2015). Hippocampal interplay with the nucleus accumbens is critical for decisions about time. *Eur. J. Neurosci.* 42, 2224–2233. doi: 10.1111/ejn.13009

Aggleton, J. P., O'mara, S. M., Vann, S. D., Wright, N. F., Tsanov, M., and Erichsen, J. T. (2010). Hippocampal-anterior thalamic pathways for memory: uncovering a network of direct and indirect actions. *Eur. J. Neurosci.* 31, 2292–2307. doi: 10.1111/j.1460-9568.2010.07251.x

Alderson, T., Kehoe, E., Maguire, L., Farrell, D., Lawlor, B., Kenny, R. A., et al. (2017). Disrupted thalamus white matter anatomy and posterior default mode network effective connectivity in amnestic mild cognitive impairment. *Front. Aging Neurosci.* 9:370. doi: 10.3389/fnagi.2017.00370

Balcerek, E., Wlodkowska, U., and Czajkowski, R. (2021). Retrosplenial cortex in spatial memory: focus on immediate early genes mapping. *Mol. Brain* 14:172. doi: 10.1186/s13041-021-00880-w

Bature, F., Guinn, B. A., Pang, D., and Pappas, Y. (2017). Signs and symptoms preceding the diagnosis of Alzheimer's disease: a systematic scoping review of literature from 1937 to 2016. *BMJ Open* 7:e015746. doi: 10.1136/bmjopen-2016-015746

Baumann, B., Woehrer, A., Ricken, G., Augustin, M., Mitter, C., Pircher, M., et al. (2017). Visualization of neuritic plaques in Alzheimer's disease by polarization-sensitive optical coherence microscopy. *Sci. Rep.* 7:43477. doi: 10.1038/srep43477

Beker, S., Kellner, V., Kerti, L., and Stern, E. A. (2012). Interaction between amyloid-beta pathology and cortical functional columnar organization. *J. Neurosci.* 32, 11241–11249. doi: 10.1523/JNEUROSCI.2426-12.2012

Bekris, L. M., Yu, C. E., Bird, T. D., and Tsuang, D. W. (2010). Genetics of Alzheimer disease. *J. Geriatr. Psychiatry Neurol.* 23, 213–227.

Bellistri, E., Aguilar, J., Brotons-Mas, J. R., Foffani, G., and De La Prida, L. M. (2013). Basic properties of somatosensory-evoked responses in the dorsal hippocampus of the rat. *J. Physiol.* 591, 2667–2686. doi: 10.1113/jphysiol.2013.251892

Bundy, J. L., Vied, C., Badger, C., and Nowakowski, R. S. (2019). Sex-biased hippocampal pathology in the 5XFAD mouse model of Alzheimer's disease: a multi-omic analysis. *J. Comp. Neurol.* 527, 462–475. doi: 10.1002/cne.24551

Burdakov, D., and Peleg-Raibstein, D. (2020). The hypothalamus as a primary coordinator of memory updating. *Physiol. Behav.* 223:112988. doi: 10.1016/j.physbeh.2020.112988

Burgess, N., Maguire, E. A., and O'keefe, J. (2002). The human hippocampus and spatial and episodic memory. *Neuron* 35, 625–641.

Chan, R. W., Leong, A. T. L., Ho, L. C., Gao, P. P., Wong, E. C., Dong, C. M., et al. (2017). Low-frequency hippocampal-cortical activity drives brain-wide resting-state functional MRI connectivity. *Proc. Natl. Acad. Sci. U.S.A.* 114, E6972–E6981. doi: 10.1073/pnas.1703309114

Chong, P. S., Poon, C. H., Fung, M. L., Guan, L., Steinbusch, H. W. M., Chan, Y. S., et al. (2019). Distribution of neuronal nitric oxide synthase immunoreactivity in adult male Sprague-Dawley rat brain. *Acta Histochem.* 121:151437.

Clarke, I. J. (2015). Hypothalamus as an endocrine organ. *Compr. Physiol.* 5, 217–253.

Davatzikos, C., Resnick, S. M., Wu, X., Parmpi, P., and Clark, C. M. (2008). Individual patient diagnosis of AD and FTD via high-dimensional pattern classification of MRI. *Neuroimage* 41, 1220–1227. doi: 10.1016/j.neuroimage.2008.03.050

D'Haese, P. F., Ranjan, M., Song, A., Haut, M. W., Carpenter, J., Dieb, G., et al. (2020). Beta-amyloid plaque reduction in the hippocampus after focused ultrasound-induced blood-brain barrier opening in Alzheimer's disease. *Front. Hum. Neurosci.* 14:593672. doi: 10.3389/fnhum.2020.593672

Diamanti, E. M., Reddy, C. B., Schroder, S., Muzzu, T., Harris, K. D., Saleem, A. B., et al. (2021). Spatial modulation of visual responses arises in cortex with active navigation. *Elife* 10:e63705.

Eimer, W. A., and Vassar, R. (2013). Neuron loss in the 5XFAD mouse model of Alzheimer's disease correlates with intraneuronal Abeta42 accumulation and caspase-3 activation. *Mol. Neurodegener.* 8:2. doi: 10.1186/1750-1326-8-2

Espana, J., Gimenez-Llort, L., Valero, J., Minano, A., Rabano, A., Rodriguez-Alvarez, J., et al. (2010). Intraneuronal beta-amyloid accumulation in the amygdala enhances fear and anxiety in Alzheimer's disease transgenic mice. *Biol. Psychiatry* 67, 513–521. doi: 10.1016/j.biopsych.2009.06.015

Eustache, F., Giffard, B., Rauchs, G., Chetelat, G., Piolino, P., and Desgranges, B. (2006). [Alzheimer's disease and human memory]. *Rev. Neurol.* 162, 929–939.

Forner, S., Kawauchi, S., Balderrama-Gutierrez, G., Kramar, E. A., Matheos, D. P., Phan, J., et al. (2021). Systematic phenotyping and characterization of the 5xFAD mouse model of Alzheimer's disease. *Sci. Data* 8:270.

Franks, K. H., Chuah, M. I., King, A. E., and Vickers, J. C. (2015). Connectivity of pathology: the olfactory system as a model for network-driven mechanisms of Alzheimer's disease pathogenesis. *Front. Aging Neurosci.* 7:234. doi: 10.3389/fnagi.2015.00234

Frost, G. R., Longo, V., Li, T., Jonas, L. A., Judenhofer, M., Cherry, S., et al. (2020). Hybrid PET/MRI enables high-spatial resolution, quantitative imaging of amyloid plaques in an Alzheimer's disease mouse model. *Sci. Rep.* 10:10379.

Girard, S. D., Jacquet, M., Baranger, K., Migliorati, M., Escoffier, G., Bernard, A., et al. (2014). Onset of hippocampus-dependent memory impairments in 5XFAD transgenic mouse model of Alzheimer's disease. *Hippocampus* 24, 762–772.

Gloria, Y., Ceyzeriat, K., Tsartsalis, S., Millet, P., and Tournier, B. B. (2021). Dopaminergic dysfunction in the 3xTg-AD mice model of Alzheimer's disease. *Sci. Rep.* 11:19412.

Hagena, H., Hansen, N., and Manahan-Vaughan, D. (2016). Beta-adrenergic control of hippocampal function: subserving the choreography of synaptic information storage and memory. *Cereb. Cortex* 26, 1349–1364. doi: 10.1093/cercor/bhv330

Hamann, S., Monarch, E. S., and Goldstein, F. C. (2002). Impaired fear conditioning in Alzheimer's disease. *Neuropsychologia* 40, 1187–1195.

Iqbal, K., Liu, F., Gong, C. X., and Grundke-Iqbal, I. (2010). Tau in Alzheimer disease and related tauopathies. *Curr. Alzheimer Res.* 7, 656–664.

Ishii, M., and Iadecola, C. (2015). Metabolic and non-cognitive manifestations of Alzheimer's disease: the hypothalamus as both culprit and target of pathology. *Cell Metab.* 22, 761–776.

Javonillo, D. I., Tran, K. M., Phan, J., Hingco, E., Kramar, E. A., Da Cunha, C., et al. (2021). Systematic phenotyping and characterization of the 3xTg-AD mouse model of Alzheimer's disease. *Front. Neurosci.* 15:785276. doi: 10.3389/fnins.2021.785276

Jawhar, S., Trawicka, A., Jenneckens, C., Bayer, T. A., and Wirths, O. (2012). Motor deficits, neuron loss, and reduced anxiety coinciding with axonal degeneration and intraneuronal Abeta aggregation in the 5XFAD mouse model of Alzheimer's disease. *Neurobiol. Aging* 33, 196.e129–e140. doi: 10.1016/j.neurobiolaging.2010.05.027

Johnson, K. A., Fox, N. C., Sperling, R. A., and Klunk, W. E. (2012). Brain imaging in Alzheimer disease. *Cold Spring Harb. Perspect. Med.* 2:a006213.

Kafkas, A., and Montaldi, D. (2015). Striatal and midbrain connectivity with the hippocampus selectively boosts memory for contextual novelty. *Hippocampus* 25, 1262–1273. doi: 10.1002/hipo.22434

Kametani, F., and Hasegawa, M. (2018). Reconsideration of amyloid hypothesis and tau hypothesis in Alzheimer's disease. *Front. Neurosci.* 12:25. doi: 10.3389/fnins.2018.00025

Keshavarzi, S., Sullivan, R. K., Ianno, D. J., and Sah, P. (2014). Functional properties and projections of neurons in the medial amygdala. *J. Neurosci.* 34, 8699–8715.

Kim, D. H., Kim, H. A., Han, Y. S., Jeon, W. K., and Han, J. S. (2020). Recognition memory impairments and amyloid-beta deposition of the retrosplenial cortex at the early stage of 5XFAD mice. *Physiol. Behav.* 222:112891. doi: 10.1016/j.physbeh.2020.112891

Klunk, W. E., Engler, H., Nordberg, A., Wang, Y., Blomqvist, G., Holt, D. P., et al. (2004). Imaging brain amyloid in Alzheimer's disease with Pittsburgh compound-B. *Ann. Neurol.* 55, 306–319.

Kraeuter, A. K., Guest, P. C., and Sarnyai, Z. (2019). The Y-maze for assessment of spatial working and reference memory in mice. *Methods Mol. Biol.* 1916, 105–111. doi: 10.1007/978-1-4939-8994-2_10

Kumar, N., Manning, T. F., and Ostry, D. J. (2019). Somatosensory cortex participates in the consolidation of human motor memory. *PLoS Biol.* 17:e3000469. doi: 10.1371/journal.pbio.3000469

Lein, E. S., Hawrylycz, M. J., Ao, N., Ayres, M., Bensinger, A., Bernard, A., et al. (2007). Genome-wide atlas of gene expression in the adult mouse brain. *Nature* 445, 168–176.

Lim, L. W., Blokland, A., Tan, S., Vlamings, R., Sesia, T., Aziz-Mohammadi, M., et al. (2010). Attenuation of fear-like response by escitalopram treatment after electrical stimulation of the midbrain dorsolateral periaqueductal gray. *Exp. Neurol.* 226, 293–300. doi: 10.1016/j.expneurol.2010.08.035

Lim, L. W., Blokland, A., Visser-Vandewalle, V., Vlamings, R., Sesia, T., Steinbusch, H., et al. (2008). High-frequency stimulation of the dorsolateral periaqueductal gray and ventromedial hypothalamus fails to inhibit panic-like behaviour. *Behav. Brain Res.* 193, 197–203. doi: 10.1016/j.bbr.2008.05.020

Lim, L. W., Prickaerts, J., Huguet, G., Kadar, E., Hartung, H., Sharp, T., et al. (2015b). Electrical stimulation alleviates depressive-like behaviors of rats: investigation of brain targets and potential mechanisms. *Transl. Psychiatry* 5:e535. doi: 10.1038/tp.2015.24

Lim, L. W., Janssen, M. L., Kocabicak, E., and Temel, Y. (2015a). The antidepressant effects of ventromedial prefrontal cortex stimulation is associated with neural activation in the medial part of the subthalamic nucleus. *Behav. Brain Res.* 279, 17–21. doi: 10.1016/j.bbr.2014.11.008

Lim, L. W., Shrestha, S., Or, Y. Z., Tan, S. Z., Chung, H. H., Sun, Y., et al. (2016). Tetratricopeptide repeat domain 9A modulates anxiety-like behavior in female mice. *Sci. Rep.* 6:37568.

Lim, L. W., Temel, Y., Visser-Vandewalle, V., Blokland, A., and Steinbusch, H. (2009). Fos immunoreactivity in the rat forebrain induced by electrical stimulation of the dorsolateral periaqueductal gray matter. *J. Chem. Neuroanat.* 38, 83–96.

Lin, T. W., Liu, Y. F., Shih, Y. H., Chen, S. J., Huang, T. Y., Chang, C. Y., et al. (2015). Neurodegeneration in amygdala precedes hippocampus in the APPswe/PS1dE9 mouse model of Alzheimer's disease. *Curr. Alzheimer Res.* 12, 951–963. doi: 10.2174/1567205012666151027124938

Liu, A., Jain, N., Vyas, A., and Lim, L. W. (2015). Ventromedial prefrontal cortex stimulation enhances memory and hippocampal neurogenesis in the middle-aged rats. *Elife* 4:e04803. doi: 10.7554/eLife.04803

Liu, L., Li, Q., Li, N., Ling, J., Liu, R., Wang, Y., et al. (2011). Simultaneous determination of catecholamines and their metabolites related to Alzheimer's disease in human urine. *J. Sep. Sci.* 34, 1198–1204.

Martig, A. K., Jones, G. L., Smith, K. E., and Mizumori, S. J. (2009). Context dependent effects of ventral tegmental area inactivation on spatial working memory. *Behav. Brain Res.* 203, 316–320. doi: 10.1016/j.bbr.2009.05.008

Martinez-Pinilla, E., Ordonez, C., Del Valle, E., Navarro, A., and Tolivia, J. (2016). Regional and gender study of neuronal density in brain during aging and in Alzheimer's disease. *Front. Aging Neurosci.* 8:213. doi: 10.3389/fnagi.2016.00213

Melnikova, T., Savonenko, A., Wang, Q., Liang, X., Hand, T., Wu, L., et al. (2006). Cycloxygenase-2 activity promotes cognitive deficits but not increased amyloid burden in a model of Alzheimer's disease in a sex-dimorphic pattern. *Neuroscience* 141, 1149–1162. doi: 10.1016/j.neuroscience.2006.05.001

Mitrano, D. A., Houle, S. E., Pearce, P., Quintanilla, R. M., Lockhart, B. K., Genovese, B. C., et al. (2021). Olfactory dysfunction in the 3xTg-AD model of Alzheimer's disease. *IBRO Neurosci. Rep.* 10, 51–61.

Morgese, M. G., Colaianna, M., Mhillaj, E., Zotti, M., Schiavone, S., D'antonio, P., et al. (2015). Soluble beta amyloid evokes alteration in brain norepinephrine levels: role of nitric oxide and interleukin-1. *Front. Neurosci.* 9:428. doi: 10.3389/fnins.2015.00428

Nobili, A., Latagliata, E. C., Viscomi, M. T., Cavallucci, V., Cutuli, D., Giacovazzo, G., et al. (2017). Dopamine neuronal loss contributes to memory and reward dysfunction in a model of Alzheimer's disease. *Nat. Commun.* 8:14727. doi: 10.1038/ncomms14727

Oakley, H., Cole, S. L., Logan, S., Maus, E., Shao, P., Craft, J., et al. (2006). Intraneuronal beta-amyloid aggregates, neurodegeneration, and neuron loss in transgenic mice with five familial Alzheimer's disease mutations: potential factors in amyloid plaque formation. *J. Neurosci.* 26, 10129–10140. doi: 10.1523/JNEUROSCI.1202-06.2006

Oh, S. J., Lee, H. J., Kang, K. J., Han, S. J., Lee, Y. J., Lee, K. C., et al. (2018). Early detection of Abeta deposition in the 5xFAD mouse by amyloid PET. *Contrast Media Mol. Imaging* 2018:5272014. doi: 10.1155/2018/5272014

Oh, S. W., Harris, J. A., Ng, L., Winslow, B., Cain, N., Mihalas, S., et al. (2014). A mesoscale connectome of the mouse brain. *Nature* 508, 207–214.

O'Leary, T. P., Stover, K. R., Mantolino, H. M., Darvesh, S., and Brown, R. E. (2020). Intact olfactory memory in the 5xFAD mouse model of Alzheimer's disease from 3 to 15 months of age. *Behav. Brain Res.* 393:112731. doi: 10.1016/j.bbr.2020.112731

Palmqvist, S., Scholl, M., Strandberg, O., Mattsson, N., Stomrud, E., Zetterberg, H., et al. (2017). Earliest accumulation of beta-amyloid occurs within the default-mode network and concurrently affects brain connectivity. *Nat. Commun.* 8:1214. doi: 10.1038/s41467-017-01150-x

Pan, X., Kaminga, A. C., Wen, S. W., Wu, X., Acheampong, K., and Liu, A. (2019). Dopamine and dopamine receptors in Alzheimer's disease: a systematic review and network meta-analysis. *Front. Aging Neurosci.* 11:175. doi: 10.3389/fnagi.2019.00175

Parvizi, J., Van Hoesen, G. W., and Damasio, A. (2000). Selective pathological changes of the periaqueductal gray matter in Alzheimer's disease. *Ann. Neurol.* 48, 344–353.

Paxinos, G., and Franklin, K. B. (2008). *The Mouse Brain in Stereotaxic Coordinates*. Cambridge, MA: Academic Press.

Poon, C. H., Wang, Y., Fung, M. L., Zhang, C., and Lim, L. W. (2020). Rodent models of amyloid-beta feature of Alzheimer's disease: development and potential treatment implications. *Aging Dis.* 11, 1235–1259.

Preda, S., Govoni, S., Lanni, C., Racchi, M., Mura, E., Grilli, M., et al. (2008). Acute beta-amyloid administration disrupts the cholinergic control of dopamine release in the nucleus accumbens. *Neuropsychopharmacology* 33, 1062–1070. doi: 10.1038/sj.npp.1301485

Richter-Levin, G., and Akirav, I. (2000). Amygdala-hippocampus dynamic interaction in relation to memory. *Mol. Neurobiol.* 22, 11–20.

Rodrigue, K. M., Kennedy, K. M., and Park, D. C. (2009). Beta-amyloid deposition and the aging brain. *Neuropsychol. Rev.* 19, 436–450.

Saiz-Sanchez, D., De La Rosa-Prieto, C., Ubeda-Banon, I., and Martinez-Marcos, A. (2013). Interneurons and beta-amyloid in the olfactory bulb, anterior olfactory nucleus and olfactory tubercle in APPxPS1 transgenic mice model of Alzheimer's disease. *Anat. Rec.* 296, 1413–1423. doi: 10.1002/ar.22750

Salgado, S., and Kaplitt, M. G. (2015). The nucleus accumbens: a comprehensive review. *Stereotact. Funct. Neurosurg.* 93, 75–93.

Sanchez-Varo, R., Sanchez-Mejias, E., Fernandez-Valenzuela, J. J., De Castro, V., Mejias-Ortega, M., and Gomez-Arboledas, A. (2021). Plaque-associated oligomeric amyloid-beta drives early synaptotoxicity in APP/PS1 mice hippocampus: ultrastructural pathology analysis. *Front. Neurosci.* 15:752594. doi: 10.3389/fnins.2021.752594

Schneider, C. A., Rasband, W. S., and Eliceiri, K. W. (2012). NIH image to imageJ: 25 years of image analysis. *Nat. Methods* 9, 671–675.

Sesia, T., Bulthuis, V., Tan, S., Lim, L. W., Vlamings, R., Blokland, A., et al. (2010). Deep brain stimulation of the nucleus accumbens shell increases impulsive behavior and tissue levels of dopamine and serotonin. *Exp. Neurol.* 225, 302–309. doi: 10.1016/j.expneurol.2010.06.022

Sesia, T., Temel, Y., Lim, L. W., Blokland, A., Steinbusch, H. W., and Visser-Vandewalle, V. (2008). Deep brain stimulation of the nucleus accumbens core and shell: opposite effects on impulsive action. *Exp. Neurol.* 214, 135–139. doi: 10.1016/j.expneurol.2008.07.015

Shokri-Kojori, E., Wang, G. J., Wiers, C. E., Demiral, S. B., Guo, M., Kim, S. W., et al. (2018). Beta-amyloid accumulation in the human brain after one night of sleep deprivation. *Proc. Natl. Acad. Sci. U.S.A.* 115, 4483–4488. doi: 10.1073/pnas.1721694115

Sil, A., Erfani, A., Lamb, N., Copland, R., Riedel, G., and Platt, B. (2022). Sex differences in behavior and molecular pathology in the 5XFAD model. *J. Alzheimers Dis.* 85, 755–778.

Son, G., Yoo, S. J., Kang, S., Rasheed, A., Jung, D. H., Park, H., et al. (2021). Region-specific amyloid-beta accumulation in the olfactory system influences olfactory sensory neuronal dysfunction in 5xFAD mice. *Alzheimers Res. Ther.* 13:4. doi: 10.1186/s13195-020-00730-2

Soria Lopez, J. A., Gonzalez, H. M., and Leger, G. C. (2019). Alzheimer's disease. *Handb. Clin. Neurol.* 167, 231–255.

Stackman, R. W., Eckenstein, F., Frei, B., Kulhanek, D., Nowlin, J., and Quinn, J. F. (2003). Prevention of age-related spatial memory deficits in a transgenic mouse model of Alzheimer's disease by chronic *Ginkgo biloba* treatment. *Exp. Neurol.* 184, 510–520. doi: 10.1016/s0014-4886(03)00399-6

Tan, S. Z. K., Temel, Y., Chan, A. Y., Mok, A. T. C., Perucho, J. A. U., Blokland, A., et al. (2020b). Serotonergic treatment normalizes midbrain dopaminergic neuron increase after periaqueductal gray stimulation. *Brain Struct. Funct.* 225, 1957–1966. doi: 10.1007/s00429-020-02102-w

Tan, S. Z. K., Neoh, J., Lawrence, A. J., Wu, E. X., and Lim, L. W. (2020a). Prelimbic Cortical stimulation improves spatial memory through distinct patterns of hippocampal gene expression in aged rats. *Neurotherapeutics* 17, 2054–2068. doi: 10.1007/s13311-020-00913-7

Tan, S. Z. K., Poon, C. H., Chan, Y. S., and Lim, L. W. (2021). Prelimbic cortical stimulation disrupts fear memory consolidation through ventral hippocampal dopamine D2 receptors. *Br. J. Pharmacol.* 178, 3587–3601. doi: 10.1111/bph.15505

Temel, Y., Blokland, A., and Lim, L. W. (2012). Deactivation of the parvalbumin-positive interneurons in the hippocampus after fear-like behaviour following electrical stimulation of the dorsolateral periaqueductal gray of rats. *Behav. Brain Res.* 233, 322–325. doi: 10.1016/j.bbr.2012.05.029

Tharp, W. G., Gupta, D., Smith, J., Jones, K. P., Jones, A. M., and Pratley, R. E. (2016). Effects of glucose and insulin on secretion of amyloid-beta by human adipose tissue cells. *Obesity (Silver Spring)* 24, 1471–1479.

Uddin, M. S., and Lim, L. W. (2022). Glial cells in Alzheimer's disease: from neuropathological changes to therapeutic implications. *Ageing Res. Rev.* 78:101622.

Vlassenko, A. G., Benzinger, T. L., and Morris, J. C. (2012). PET amyloid-beta imaging in preclinical Alzheimer's disease. *Biochim. Biophys. Acta* 1822, 370–379.

Vorobyov, V., Bakharev, B., Medvinskaya, N., Nesterova, I., Samokhin, A., Deev, A., et al. (2019). Loss of midbrain dopamine neurons and altered apomorphine EEG effects in the 5xFAD mouse model of Alzheimer's disease. *J. Alzheimers Dis.* 70, 241–256. doi: 10.3233/JAD-181246

Wheeler, A. L., Creed, M. C., Voineskos, A. N., and Nobrega, J. N. (2014). Changes in brain functional connectivity after chronic haloperidol in rats: a network analysis. *Int. J. Neuropsychopharmacol.* 17, 1129–1138. doi: 10.1017/S1461145714000042

WHO (2019). *Risk Reduction of Cognitive Decline and Dementia: WHO Guidelines*. Geneva: WHO.

Wong, K. Y., Roy, J., Fung, M. L., Heng, B. C., Zhang, C., and Lim, L. W. (2020). Relationships between mitochondrial dysfunction and neurotransmission failure in Alzheimer's disease. *Aging Dis.* 11, 1291–1316.

Xiao, C., Liu, Y., Xu, J., Gan, X., and Xiao, Z. (2018). Septal and hippocampal neurons contribute to auditory relay and fear conditioning. *Front. Cell Neurosci.* 12:102. doi: 10.3389/fncel.2018.00102

Yu, W. S., Aquili, L., Wong, K. H., Lo, A. C. Y., Chan, L. L. H., Chan, Y. S., et al. (2022). Transcorneal electrical stimulation enhances cognitive functions in aged and 5XFAD mouse models. *Ann. N. Y. Acad. Sci.* doi: 10.1111/nyas.14850

Zheng, H., Zhou, Q., Du, Y., Li, C., Xu, P., Lin, L., et al. (2018). The hypothalamus as the primary brain region of metabolic abnormalities in APP/PS1 transgenic mouse model of Alzheimer's disease. *Biochim. Biophys. Acta Mol. Basis Dis.* 1864, 263–273. doi: 10.1016/j.bbadis.2017.10.028

frontiers | Frontiers in Aging Neuroscience

TYPE Original Research
PUBLISHED 29 July 2022
DOI 10.3389/fnagi.2022.938071

OPEN ACCESS

EDITED BY
Woon-Man Kung,
Chinese Culture University, Taiwan

REVIEWED BY
Haewon Byeon,
Inje University, South Korea
Eugen Ružický,
Pan-European University, Slovakia
Jose Ramon Saura,
Rey Juan Carlos University, Spain

*CORRESPONDENCE
Zhenhua Liu
liuzhenhua@csu.edu.cn

SPECIALTY SECTION
This article was submitted to Parkinson's Disease and Aging-related Movement Disorders, a section of the journal Frontiers in Aging Neuroscience

RECEIVED 06 May 2022
ACCEPTED 12 July 2022
PUBLISHED 29 July 2022

CITATION
Deng P, Xu K, Zhou X, Xiang Y, Xu Q, Sun Q, Li Y, Yu H, Wu X, Yan X, Guo J, Tang B and Liu Z (2022) Constructing prediction models for excessive daytime sleepiness by nomogram and machine learning: A large Chinese multicenter cohort study. *Front. Aging Neurosci.* 14:938071. doi: 10.3389/fnagi.2022.938071

Constructing prediction models for excessive daytime sleepiness by nomogram and machine learning: A large Chinese multicenter cohort study

Penghui Deng[1,2], Kun Xu[1], Xiaoxia Zhou[1], Yaqin Xiang[1], Qian Xu[1], Qiying Sun[3], Yan Li[4], Haiqing Yu[4], Xinyin Wu[5], Xinxiang Yan[1], Jifeng Guo[1,2,6,7], Beisha Tang[1,2,6,7] and Zhenhua Liu[1,2,6,7]*

[1]Department of Neurology, Xiangya Hospital, Central South University, Changsha, China, [2]National Clinical Research Center for Geriatric Disorders, Xiangya Hospital, Central South University, Changsha, China, [3]Department of Geriatrics, Xiangya Hospital, Central South University, Changsha, China, [4]Research Institute, Hunan Kechuang Information Technology Joint-Stock Co., Ltd., Changsha, China, [5]Department of Epidemiology and Health Statistics, Xiangya School of Public Health, Central South University, Changsha, China, [6]Key Laboratory of Hunan Province in Neurodegenerative Disorders, Central South University, Changsha, China, [7]Hunan Key Laboratory of Medical Genetics, Center for Medical Genetics, School of Life Sciences, Central South University, Changsha, China

Objective: Although risk factors for excessive daytime sleepiness (EDS) have been reported, there are still few cohort-based predictive models for EDS in Parkinson's disease (PD). This 1-year longitudinal study aimed to develop a predictive model of EDS in patients with PD using a nomogram and machine learning (ML).

Materials and methods: A total of 995 patients with PD without EDS were included, and clinical data during the baseline period were recorded, which included basic information as well as motor and non-motor symptoms. One year later, the presence of EDS in this population was re-evaluated. First, the baseline characteristics of patients with PD with or without EDS were analyzed. Furthermore, a Cox proportional risk regression model and XGBoost ML were used to construct a prediction model of EDS in PD.

Results: At the 1-year follow-up, EDS occurred in 260 of 995 patients with PD (26.13%). Baseline features analysis showed that EDS correlated significantly with age, age of onset (AOO), hypertension, freezing of gait (FOG). In the Cox proportional risk regression model, we included high body mass index (BMI), late AOO, low motor score on the 39-item Parkinson's Disease Questionnaire (PDQ-39), low orientation score on the Mini-Mental State Examination (MMSE), and absence of FOG. Kaplan–Meier survival curves showed that the survival prognosis of patients with PD in the high-risk group was significantly worse than that in the low-risk group. XGBoost demonstrated that BMI, AOO, PDQ-39 motor score, MMSE orientation score, and FOG contributed to the

model to different degrees, in decreasing order of importance, and the overall accuracy of the model was 71.86% after testing.

Conclusion: In this study, we showed that risk factors for EDS in patients with PD include high BMI, late AOO, a low motor score of PDQ-39, low orientation score of MMSE, and lack of FOG, and their importance decreased in turn. Our model can predict EDS in PD with relative effectivity and accuracy.

KEYWORDS

excessive daytime sleepiness, nomogram, Parkinson's disease, prediction model, machine learning

Introduction

Parkinson's disease (PD) is a common neurodegenerative disease typically affecting individuals from middle age onward. Its main pathophysiological mechanism is the progressive degeneration of dopaminergic neurons in the substantia nigra of the midbrain and the formation of Lewy bodies in the cytoplasm of the remaining neurons in the substantia nigra. Clinically, the main manifestations are static tremor, bradykinesia, myotonia, and postural gait disorders, which are often accompanied by sleep disorders, olfactory disorders, autonomic nervous system dysfunction, cognitive disorders, and other non-motor symptoms (Bloem et al., 2021).

Sleep disturbance is a common non-motor symptom of PD. This mainly includes excessive daytime sleepiness (EDS), rapid eye movement sleep behavior disorder (RBD), restless leg syndrome (RLS), circadian rhythm sleep disorders, and sleep-disordered breathing (Zuzuarregui and During, 2020). EDS refers to the difficulty in staying awake and alert during the day, leading to pathological sleep or sleepiness, which manifests as inappropriate sleep episodes during the day. This affects the daily life of patients with PD (Suzuki, 2021). Many clinical studies have been conducted on patients with PD with EDS over the years (Maggi et al., 2021; Videovic et al., 2021; Xu Z. et al., 2021; Mehan et al., 2022). However, contributing factors for EDS in PD are controversial and need to be further researched (Bestwick et al., 2021; Xu Z. et al., 2021).

Nomograms create visual models of complex regression equations, facilitating the analysis of making the results of prediction models. Nomograms are gaining increasing attention and application in medical research and clinical practice because of their ease of interpretation and simplicity (Wu et al., 2020; Dong et al., 2021; Liu L. et al., 2021).

The severity of EDS increases with the duration of PD (Tholfsen et al., 2015; Amara et al., 2017; Xu Z. et al., 2021). EDS can seriously affect the quality of life of patients with PD, increase the financial burden to patients and their caregivers, and increase the risk of car accidents (Ueno et al., 2018; Hurt et al., 2019). Therefore, it is crucial to identify EDS and contributing factors in patients with PD and to provide prompt treatment.

Current models can predict some PD symptoms, including freezing of gait (FOG) or RBD (Xu K. et al., 2021). Nonetheless, few studies have constructed models to predict EDS in patients with PD. Our team investigated the prevalence and clinical characteristics of EDS in PD (Xiang et al., 2019) and conducted a longitudinal study with a large cohort to develop a prediction model for EDS in patients with PD. This study (1) analyzed the baseline characteristics of patients with PD with and without EDS, (2) identified risk factors for EDS at 1-year follow-up by Cox regression analysis, and (3) developed an effective and accurate prediction model for EDS in patients with PD using a nomogram and machine learning (ML).

Materials and methods

The study flow chart is shown in **Figure 1**.

Study population

A total of 1,030 patients attending eight movement disorder centers (all 3A hospitals) in China, from January 2018 to December 2020, were recruited. None of these patients had EDS, as determined using the Epworth Sleepiness Scale (ESS; Johns, 1991). The clinical diagnostic criteria of PD used in this study were based on the International Parkinson and Movement Disorder Society (MDS) Clinical Diagnostic Criteria for PD, and the diagnosis was made by two neurologists, including clinically confirmed PD or clinically suspected PD (Postuma et al., 2015). Patients with the following were excluded: (1) chronic wasting diseases including chronic atrophic gastritis, hyperthyroidism, active tuberculosis, renal failure, and anemia with hemoglobin $\leq$60 g/L, (2) other diseases that involve severe drowsiness, such as obstructive sleep apnea (OSA) and hypothyroidism, (3) other

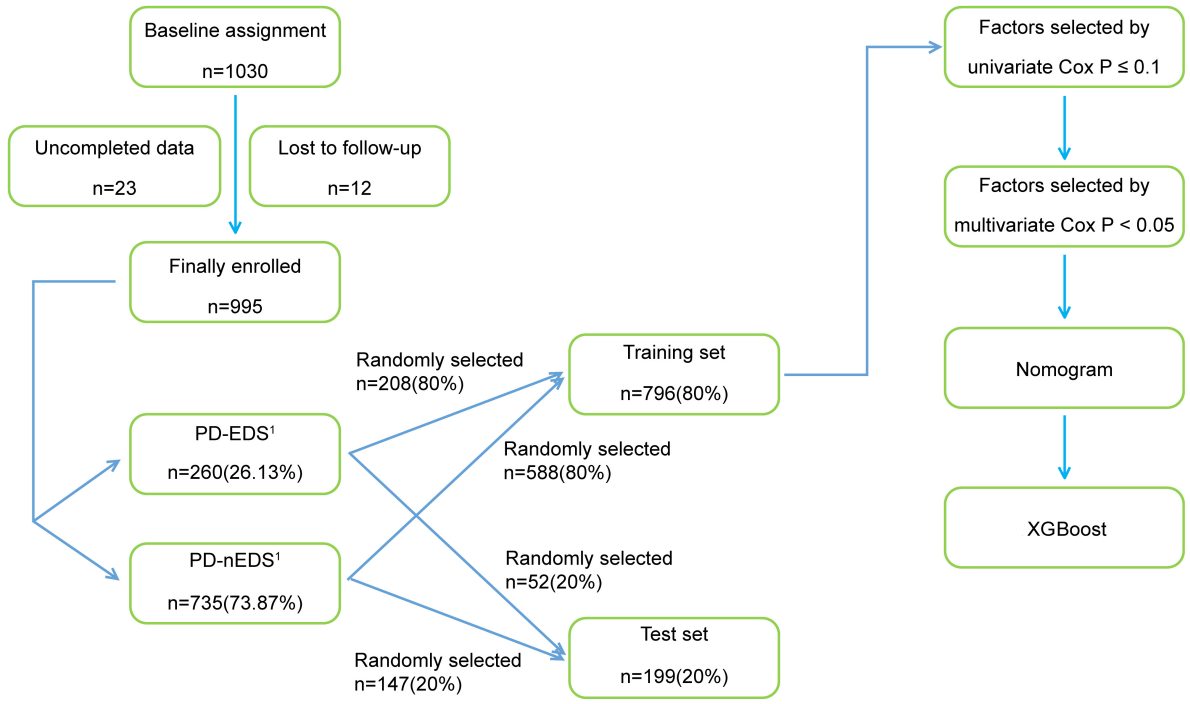

FIGURE 1
The flow chart of the study. PD-EDS[1], patients with PD with EDS after 1 year; PD-nEDS[1], patients with PD without EDS after 1 year; PD, Parkinson's disease; EDS, excessive daytime sleepiness; XGBoost, eXtreme Gradient Boosting.

diseases that may cause drowsiness confirmed by doctors to be associated with the use of medication, such as antihistamine drugs and sedatives, (4) malignant tumors or other serious systemic diseases. Based on these criteria, 995 patients with PD were included in the study. Twenty-three patients who had incomplete data and 12 patients who could not finish the interview were excluded.

This study was approved by the Ethics Committee of Central South University, Xiangya Hospital (202005124). All patients provided written informed consent before entering the study and were registered in the Multicenter Database and Collaborative Network of Parkinson's Disease and Movement Disorders in China (PD-MDCNC).

Independent variables and clinical assessments

The patients' basic information and motor as well as non-motor symptoms were assessed and recorded.

Basic information included demographic characteristics, family history of PD, medical history, lifestyle, environmental factors, age of onset (AOO), disease duration, and levodopa-equivalent daily dose (LEDD; Tomlinson et al., 2015). Demographic data included sex, age, height, weight, and education level. Body mass index (BMI) was defined as weight/height^2 (kg/m^2), and education level was classified as primary school and below or secondary school and above. Medical history included the presence or absence of hypertension, diabetes, hyperlipidemia, heart disease, liver disease, kidney disease, respiratory disease, previous operation, tumor, stroke, traumatic brain injury (disorder of consciousness), encephalitis, epilepsy, hyperthyroidism, and mental illness. Lifestyle data included information on whether the patient smoked or consumed alcohol, coffee, or tea. Environmental factors included a history of exposure to pesticides, occupational solvents, and heavy metals, and carbon monoxide poisoning.

Motor symptoms were evaluated using the Unified Parkinson's Disease Rating Scale (UPDRS) and the Hoehn-Yahr staging scale (H-Y). The UPDRS was used to evaluate overall motor symptoms in patients with PD (Postuma et al., 2015), and the H-Y scale was used to evaluate the severity of the disease (Hoehn and Yahr, 1967). Motor complications such as dyskinesia and wearing-off were diagnosed by clinicians, and their severity was evaluated using the Rush Dyskinesia Rating Scale (RDRS) and the 9-item End-of-dose Wearing-off Questionnaire (WOQ-9), respectively. FOG was evaluated with the New Freezing of Gait Questionnaire (NFOGQ).

The Non-motor Symptom Rating Scale (NMSS; Chaudhuri et al., 2007), Parkinson's Disease Sleep Scale (PDSS), Parkinson Fatigue Scale (PFS), 39-item Parkinson's Disease Questionnaire

TABLE 1 Comparison of basic conditions between the PD-EDS[1] and PD-nEDS[1] groups.

Variable	PD-nEDS[1]	PD-EDS[1]	*P*
Sex, male (n, %)	331 (45.03%)	126 (48.46%)	0.341
Age (years)	59.60 ± 10.12	62.55 ± 9.3	<0.001*
BMI	22.74 ± 3.39	22.78 ± 3.33	0.856
Education level Primary school and below (n, %)	189 (25.71%)	81 (31.15%)	0.104
Hypertension, yes (n, %)	155 (21.09%)	72 (27.69%)	0.032*
Operation history, yes (n, %)	189 (25.71%)	74 (28.46%)	0.413
Smoking, yes (n, %)	160 (21.77%)	52 (20%)	0.597
Drinking alcohol, yes (n, %)	134 (18.23%)	51 (19.62%)	0.643
AOO (years)	53.95 ± 10.61	56.29 ± 10.19	0.002*
Survival time[a] (years)	5.61 ± 3.88	6.22 ± 4.48	0.054
LEDD	480.2 ± 394.18	510.73 ± 376.55	0.322

Survival time[a]: duration of disease plus 1 year.
*$P < 0.05$ (difference statistically significant).
PD-EDS[1], patients with PD with EDS after 1 year; PD-nEDS[1], patients with PD without EDS after 1 year; PD, Parkinson's disease; EDS, excessive daytime sleepiness; BMI, body mass index; AOO, age of onset; LEDD, levodopa equivalent daily dose.

(PDQ-39), Rome III Functional Constipation Diagnostic Criteria, Mini-Mental State Examination (MMSE), Hyposmia Rating Scale (HRS), Hamilton Depression Scale (17-item version), ESS, Rapid Eye Movement Sleep Behavior Disorder Questionnaire-Hong Kong (RBDQ-HK), and Cambridge-Hopkins Questionnaire for restless leg syndrome (CH-RLSq) were used to evaluate the patients' non-motor symptoms. The sleep quality of patients with PD was evaluated with the PDSS (Chaudhuri et al., 2002). The MMSE was used to evaluate whether patients with PD had cognitive dysfunction. Cognitive dysfunction is related to an individual's education level. Among patients with PD with an education level of primary school and below, a total score <20 points was defined as cognitive dysfunction, while for patients with PD with an education level of middle school and above, a total score <24 was defined as cognitive impairment; lower scores denoted more severe cognitive impairment (Aarsland et al., 2001). The Hamilton Depression Scale (17-item version) was used to evaluate depression in patients with PD. A total score of >7 indicated the presence of depression (Hamilton, 1960; Montgomery and Asberg, 1979). The HRS was used to evaluate whether patients with PD had hyposmia. A total score ≤22.5 indicated the presence of hyposmia (Millar Vernetti et al., 2012). The Rome III Functional Constipation Diagnostic Criteria were used to assess whether patients with PD had constipation (Zhou et al., 2019). The PDQ-39 was used to evaluate the quality of life of patients with PD (Peto et al., 1995). The PFS was used to evaluate fatigue in patients with PD (Nillson et al., 2013). The ESS was used to evaluate EDS in patients with PD, and EDS was diagnosed at scores ≥10 (Johns, 1991). The RBDQ-HK was used to evaluate RBD in patients with PD, which could be diagnosed with a score of 18 or higher (Shen et al., 2014). The CH-RLSq was used to evaluate RLS based on the diagnostic criteria in patients with PD (Allen et al., 2009; **Supplementary Table 1**).

The patients' basic information and motor and non-motor symptoms were recorded at baseline, and EDS was assessed again 1 year later. The assessment was conducted by clinicians and researchers and the results of basic information collection with questionnaires and scale assessment were recorded. Prior to the assessment, all researchers were trained to ensure an equal

TABLE 2 Comparison of motor symptoms between the PD-EDS[1] and PD-nEDS[1] groups.

Variable		PD-nEDS[1]	PD-EDS[1]	*P*
Motor subtypes	PIGD-PD (n, %)	374 (50.88%)	141 (54.23%)	0.340
	TD-PD (n, %)	299 (40.68%)	93 (35.77%)	
	Mixed PD (n, %)	62 (8.44%)	26 (10%)	
Wearing-off, yes (n, %)		150 (20.41%)	60 (23.08%)	0.377
FOG, yes (n, %)		146 (19.86%)	72 (27.69%)	0.011*
UPDRS total score (point)		35.45 ± 17.33	43.6 ± 21.74	<0.001*
UPDRS-II score (point)		9.59 ± 4.95	12.13 ± 6.24	<0.001*
UPDRS-III score (point)		22.23 ± 12.27	27.34 ± 15.21	<0.001*
Tremor score (point)		4.09 ± 3.6	4.6 ± 4.4	0.095
Posture gait score (point)		3.54 ± 2.54	4.54 ± 3.11	<0.001*
UPDRS-I score (point)				0.032*
UPDRS-IV-B score (point)				0.020*
UPDRS-IV-C score (point)		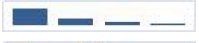	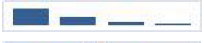	0.038*
H-Y stage				<0.001*

*$P < 0.05$ (difference statistically significant).
PD-EDS[1], patients with PD with EDS after 1 year; PD-nEDS[1], patients with PD without EDS after 1 year; PD, Parkinson's disease; EDS, excessive daytime sleepiness; PIGD-PD, PD with postural instability/gait difficulty; TD-PD, tremor-dominant PD; FOG, freezing of gait; UPDRS, Unified Parkinson's Disease Rating Scale; H-Y, Hoehn–Yahr.

understanding of the scales used for clinical data collection as well as the methodology and wording used.

Statistical analysis

Sample characteristics

Traditional statistical parameters were used for descriptive analyses. In the analysis of inter-group differences, for non-normal variables, particularly unordered categorical variables, the chi-square test was used. The independent-sample *t*-test and non-parametric Mann-Whitney *U* test were used for continuous variables and ordinal categorical variables, respectively. Unordered categorical variables such as FOG are presented as sample number and proportion, and continuous variables such as BMI are expressed as mean ± standard deviation. Ordinal categorical variables such as H-Y stage were plotted using distribution histograms to show the distribution of data among different grades. $P < 0.05$ was considered statistically significant.

The training set and the test set

A stratified random sampling method was used to divide the 995 samples into two independent sets at a ratio of 8:2, namely, a training set and a test set. The training set included 80% (796/995) of the study cohort and was initially used to establish the model. The remaining 20% (199/995) of the samples, the test set, were used along with the training set to adjust and validate the model to optimize its accuracy.

Cox proportional regression risk model

A Cox proportional regression risk model was used to determine the hazard ratio (HRs) of the variables affecting EDS and to construct a model to predict EDS in patients with PD. Some statistically insignificant variables were eliminated by variable preprocessing. We constructed a univariate Cox proportional risk regression model with the remaining variables

TABLE 3 Comparison of non-motor symptoms between the PD-EDS[1] and PD-nEDS[1] groups.

Variable	PD-nEDS[1]	PD-EDS[1]	*P*
Hyposmia, yes (n, %)	263 (35.78%)	109 (41.92%)	0.086
RBD, yes (n, %)	225 (30.61%)	109 (41.92%)	0.001*
Depression, yes (n, %)	170 (23.13%)	76 (29.23%)	0.054
NMSS total score (point)	27.22 ± 20.46	35.06 ± 24.49	<0.001*
NMSS-2 (point)	6.09 ± 5.85	7.91 ± 6.21	<0.001*
NMSS-3 (point)	5.11 ± 7.85	5.48 ± 8.5	0.515
NMSS-5 (point)	2.58 ± 3.26	3.47 ± 4.47	0.004*
NMSS-6 (point)	2.89 ± 3.62	4.46 ± 4.94	<0.001*
NMSS-7 (point)	4.43 ± 5.36	5.7 ± 5.62	0.001*
NMSS-9 (point)	4.43 ± 4.69	5.36 ± 5.28	0.012*
MMSE total score (point)	27.25 ± 3	25.97 ± 4.09	<0.001*
Recall score (point)			<0.001*
Language score (point)			<0.001*
Orientation score (point)			<0.001*
Attention and calculation score (point)			0.019*
PDSS score (point)	123.24 ± 22.76	117.44 ± 27.31	0.002*
PDQ-39 total score (point)	20.64 ± 19.95	27 ± 23.46	<0.001*
Motor score (point)	5.43 ± 7.95	7.53 ± 9.75	0.002*
Activities of daily living score (point)	3.8 ± 4.91	5.06 ± 5.9	0.002*
Emotional well-being score (point)	3.63 ± 5.2	4.36 ± 5.21	0.054
Stigma score (point)	2.95 ± 4.39	3.52 ± 4.79	0.092
Social support score (point)	0.25 ± 1.07	0.35 ± 1.35	0.278
Cognition score (point)	2.13 ± 2.29	2.96 ± 2.44	<0.001*
Communication score (point)	0.77 ± 1.58	1.03 ± 1.91	0.055
Bodily discomfort score (point)	1.67 ± 2.1	2.18 ± 2.18	0.001*

*$P < 0.05$ (difference statistically significant).

PD-EDS[1], patients with PD with EDS after 1 year; PD-nEDS[1], patients with PD without EDS after 1 year; PD, Parkinson's disease; EDS, excessive daytime sleepiness; RBD, rapid eye movement sleep behavior disorder; NMSS, Non-motor Symptom Rating Scale; MMSE, Mini-Mental State Examination; PDSS, Parkinson's Disease Sleep Scale; PDQ-39, 39-Item Parkinson's Disease Questionnaire.

TABLE 4 Univariate Cox proportional risk regression model.

Variable	β-coefficient	HR (95% CI)	*P*
BMI	0.048	1 (1–1.1)	0.009*
Hypertension	0.32	1.4 (1–1.9)	0.035**
AOO	0.9	2.5 (1.8–3.4)	<0.001**
UPDRS-IV-B score	−0.12	0.89 (0.8–0.98)	0.023**
Posture gait score	−0.058	0.94 (0.9–0.99)	0.013**
H-Y stage	−0.18	0.83 (0.69–1)	0.053*
Wearing off	−0.45	0.64 (0.46–0.88)	0.0064**
FOG	−0.46	0.63 (0.46–0.88)	0.006**
MMSE total score	−0.049	0.95 (0.92–0.98)	0.0039**
Orientation score	−0.18	0.84 (0.75–0.93)	0.0012**
Recall score	−0.2	0.82 (0.72–0.94)	0.0037**
Language score	−0.1	0.9 (0.82–1)	0.039**
PDQ-39 total score	−0.0066	0.99 (0.99–1)	0.039**
Motor score	−0.022	0.98 (0.96–0.99)	0.0034**
Activities of daily living score	−0.024	0.98 (0.95–1)	0.062*
Cognition score	0.047	1 (0.99–1.1)	0.091*

*$P < 0.1$; **$P < 0.05$ (difference statistically significant).
BMI, body mass index; AOO, age of onset; UPDRS, Unified Parkinson's Disease Rating Scale; H-Y, Hoehn-Yahr; FOG, freezing of gait; MMSE, Mini-Mental State Examination; PDQ-39, 39-Item Parkinson's Disease Questionnaire; HR, hazard ratio; CI, confidence interval.

in the training set. The variables with $P \leq 0.1$ were screened into the multivariate Cox proportional risk regression model. The forward likelihood ratio (LR) method was used to screen the variables again, and the variables that were finally used to construct the prediction model were obtained. $P < 0.05$ was considered statistically significant. Survival time was set as baseline course plus 1 year. We calculated the prognostic index of each patient according to the multivariate Cox proportional risk regression model. The patients were divided into high- and low-risk groups according to the median of the prognostic index, and KM survival curves were drawn to investigate differences in survival rates according to this index. Then, we visualized the prediction model and drew line graphs, i.e., the nomograms. Finally, the model was validated. The main evaluation indexes included the C-index and time-dependent receiver operating characteristic (td-ROC) curves.

Machine learning

XGBoost, a ML method, is an optimized distributed Gradient Boosting library designed to be efficient, flexible, and portable. XGBoost is a massively parallel Boosting Tree tool, which is currently the fastest and best open-source Boosting Tree toolkit and is more than 10 times faster than the common toolkit (Peng et al., 2021). This study built a nomogram using a training dataset and improved the model by analyzing the test and training datasets using XGBoost. XGBoost uses these datasets to calibrate the model, to analyze the contribution of each variable to the model, and to optimize the model.

Results

Prevalence of excessive daytime sleepiness in the Parkinson's disease population

A total of 995 patients with PD were included. This population had relatively complete baseline clinical data, including basic information and motor and non-motor symptoms. This population had no EDS, as assessed with the ESS, at baseline and was classified as the PD-nEDS^0 group. The population was followed up 1 year later to reassess EDS. Our data showed that, in the PD-nEDS^0 group, there were 260 patients (26.13%) with EDS and 735 patients (73.87%) without EDS, recorded as the PD-EDS^1 and the PD-nEDS^1 groups, respectively.

Baseline clinical characteristics

In the PD-nEDS^0 group, patients with PD were divided into PD-EDS^1 and PD-nEDS^1 groups according to the presence or absence of EDS in the follow-up period. Their baseline data were compared. Some statistically insignificant variables were eliminated through data preprocessing.

Basic information

Compared with the PD-nEDS^1 group, the patients in the PD-EDS^1 group were older ($p < 0.001$) and had a later AOO ($p = 0.002$). Regarding medical history, the PD-EDS^1 group was more likely to have hypertension ($p = 0.032$). There were no statistical differences in sex, BMI, education level, family history of PD, lifestyle, environmental factors, survival time, and LEDD between the groups (Table 1).

Motor symptoms

Compared with the PD-nEDS^1 group, the UPDRS total score ($p < 0.001$), UPDRS-II score ($p < 0.001$), UPDRS-III score ($p < 0.001$), and posture gait score ($p < 0.001$) were higher in the PD-EDS^1 group. Additionally, the PD-EDS^1 group included more patients with FOG ($p = 0.011$). There were significant differences in the UPDRS-I score ($p = 0.032$), UPDRS-IV-B score ($p = 0.020$), UPDRS-IV-C score ($p = 0.038$), and H-Y stage ($p < 0.001$) between the groups. However, there was no significant difference in dyskinesia and wearing-off (Table 2).

Non-motor symptoms

Compared with the PD-nEDS^1 group, NMSS-2 ($p < 0.001$), NMSS-5 ($p = 0.004$), NMSS-6 ($p < 0.001$), NMSS-7 ($p = 0.001$), NMSS-9 ($p = 0.012$) scores, and the NMSS total score ($p < 0.001$) were higher in the PD-EDS^1 group. The PD-EDS^1 group had a lower MMSE total score ($p < 0.001$). For PDQ-39, the PD-EDS^1 group had higher PDQ-39 total

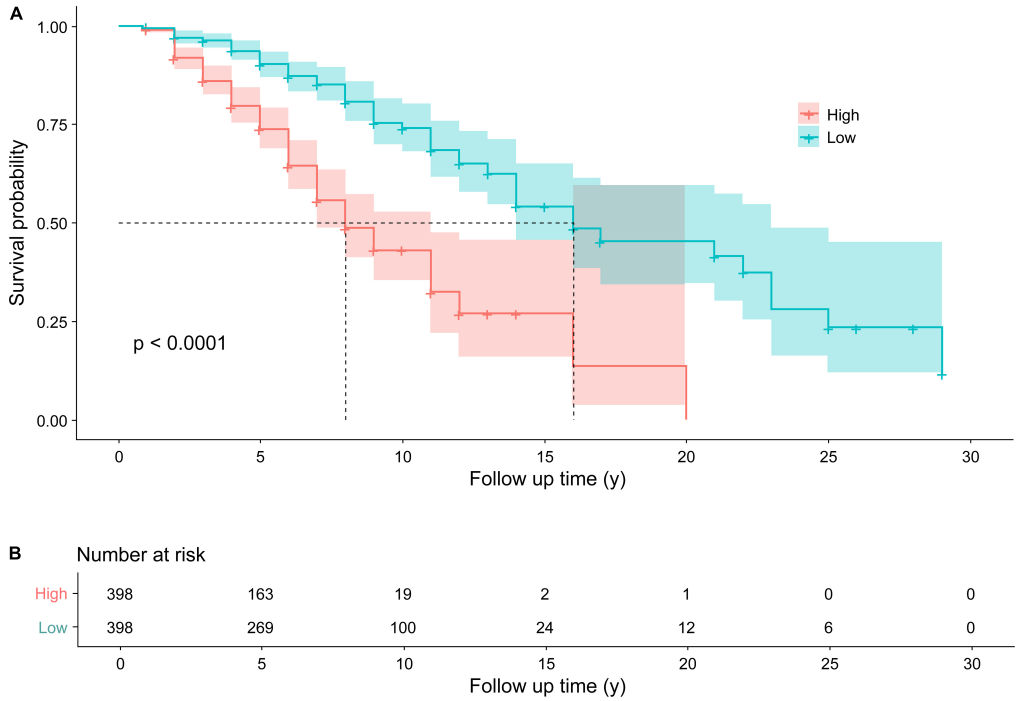

FIGURE 2
Kaplan–Meier survival curves **(A)** for patients with PD with higher and lower risks of EDS. The Kaplan–Meier curves showed a significant difference over time between patients with Parkinson's disease with a higher risk of EDS and those with a lower risk of EDS. Follow up time (y): the time from the diagnosis of PD to the end of follow-up, namely, the course of disease at baseline plus 1 year. Number at risk **(B)** the Number of EDS in patients with PD in the high and low risk groups, respectively. PD, Parkinson's disease; EDS, excessive daytime sleepiness.

($p < 0.001$), motor ($p = 0.002$), activity of daily living ($p = 0.002$), cognition ($p < 0.001$), and bodily discomfort ($p = 0.001$) scores. Additionally, the PD-EDS[1] group included more patients with RBD ($p = 0.001$) and a lower PDSS score ($p = 0.002$). There were significant differences in the scores of orientation ($p < 0.001$), attention and calculation ($p = 0.019$), recall ($p < 0.001$), and language ($p < 0.001$) domains of the MMSE between groups. However, there were no statistically significant differences in the PFS score, constipation, cognitive impairment, hyposmia, RLS, and depression between groups (Table 3).

TABLE 5 Multivariate Cox proportional risk regression model.

Variables	β-coefficient	HR (95% CI)	*P*
BMI	0.047	1.048 (1.009–1.089)	0.015*
AOO	0.051	1.053 (1.038–1.067)	<0.001*
Orientation score	−0.188	0.829 (0.744–0.924)	0.001*
Motor score	−0.024	0.976 (0.96–0.992)	0.004*
FOG	−0.378	0.685 (0.483–0.972)	0.034*

*$P < 0.05$ (difference statistically significant).
BMI, body mass index; AOO, age of onset; FOG, freezing of gait; HR, hazard ratio; CI, confidence interval.

Risk factors for excessive daytime sleepiness and construction of prediction model

Since the construction of a Cox proportional risk regression model is closely related to disease duration, we controlled for this variable and established a univariate Cox proportional risk regression model. The data showed that factors related to EDS in patients with PD included BMI, AOO, UPDRS-IV-B score, posture and gait score, hypertension, MMSE total score, orientation score, recall score, and language score, PDQ-39 total score, and motor score, wearing off, and FOG. The differences between groups were statistically significant (Table 4).

To avoid omitting important variables, we screened for variables with $p \leq 0.1$ and entered these into the multifactor Cox proportional risk regression model. We set the exit value to $p < 0.05$. Finally, five variables were obtained and were included in the Cox regression equation: BMI, AOO, orientation score, motor score, and FOG. The multifactor Cox regression model is expressed as follows:

$$h(t,x) = h_0(x)exp(0.047 \times BMI + 0.051 \times AOO - 0.188 \times orientation\ score - 0.024 \times motor\ score - 0.378 \times FOG)$$

According to the median of the prognosis index, the subjects were divided into the low- and high-risk groups. After plotting the Kaplan–Meier survival curve, we found that the survival prognosis of patients with PD in the high-risk group was significantly worse than that in the low-risk group (**Figure 2**). Additionally, through the analysis of the multifactor Cox proportional risk regression model, we found that the risk factors for EDS in patients with PD were high BMI, late AOO, low motor score, low orientation score, and lack of FOG (**Table 5**). Consequently, we constructed a nomogram (**Figure 3**). We used td-ROC curves to evaluate the predictive ability of the multivariate Cox regression model. We found that the multivariable model had better predictive ability in the training set than did single-factor models. In the training set, the 5-year area under the curve (AUC) of the Cox regression multivariable model was 0.711, the 7-year survival AUC was 0.783, and the 10-year survival AUC was 0.7632 (**Figure 4**). Furthermore, the C-index was 0.685.

Performance of the prediction model based on XGBoost

Using the five variables included in the above Cox multifactor regression model equation, we adopted XGBoost to centralize the data (x) according to the minimum value, which was then scaled according to the range (maximal-minimum value). After processing, the data converged between [0, 1] and the normalized data followed a normal distribution. The equation was as follows:

$$x = (x_i\text{-}min(x_i))/(max(x_i)\text{-}min(x_i))$$

Where model parameters included: (1) the number of trees: 1000; (2) the depth of the tree: 10; (3) the minimum weight of leaf nodes: 1; (4) penalty parameter: 0.1; (5) learning rate: 0.01; and (6) ratio of training/test set: 8:2. BMI, AOO, motor score, orientation score, and FOG contributed to the model to different degrees, and the importance of each variable decreased in that order (**Figure 5**). Finally, the overall accuracy of the model, which indicates the proportion of correctly predicted samples to total predicted samples, was 71.86% after testing. It showed that the model had 71.86% accuracy in predicting whether patients with PD would develop EDS.

Discussion

No previous study has established a longitudinal EDS prediction model with large samples in patients with PD using a nomogram and ML. Our study included 995 patients with PD who were followed up for a 1-year period. We used a nomogram and the XGBoost ML method to establish an effective and relatively accurate prediction model (accuracy of 71.86%) of EDS in PD. Risk factors for EDS in patients with PD identified and included in this model were high BMI, late AOO, low motor score of PDQ-39, low orientation score of MMSE, and lack of FOG, in decreasing order of importance.

In a previous cross-sectional study of 1,221 patients with PD conducted by our team, the prevalence of EDS was 34.07% (Xiang et al., 2019). Many studies have shown that the incidence of EDS in PD increases with longer PD duration (Tholfsen et al., 2015; Amara et al., 2017; Xu Z. et al., 2021). One study found that the incidence of EDS increased from 17% to 23.3% in 2 years (Xu Z. et al., 2021). In our study, a large sample of data was used and EDS occurred 26.13% of patients with PD after 1 year of follow-up. In terms of the ESS score, a study found that the severity of EDS in patients with PD remained stable over a 10-year period (Höglund et al., 2019). Further study is required on whether the incidence of EDS in patients with PD continues to increase and if the severity of EDS worsens over a longer period of time.

The incidence of EDS in patients with PD is closely related to the type, amount, and duration of therapy for PD (Tholfsen et al., 2015). In our cohort, the type of medication was not a confounding factor and had little influence on the predictive ability of the model. The association between hypertension and increased EDS may be due to (1) an underlying sleep disorder; (2) sleep-disordered breathing; (3) higher sympathetic activity caused by sleep deprivation and increasing serum catecholamine levels; (4) changes in the neuroendocrine axis, leading to an increase in serum cortisol levels, which decrease slowly from morning to afternoon (Punjabi and Haponik, 2000).

The analysis of baseline clinical characteristics showed that patients with PD with EDS had more severe motor symptoms with respect to the UPDRS scores, H-Y stage, and FOG, suggesting that EDS is associated with severe neurodegeneration in the ascending system of the brainstem and cholinergic dysfunction in the brainstem (Muller and Bohnen, 2013). The locus coeruleus, pedunculopontine nucleus, tegmental area, and nucleus magnocellularis are important components of the ascending system of the brainstem and regulate sleep and consciousness. The impairment of these areas can lead to the development of sleep disorders, including EDS, RBD, and RLS (Saper et al., 2001; Diederich and McIntyre, 2012). In turn, patients with PD with EDS had more severe non-motor symptoms with respect to RBD and the NMSS, MMSE, PDSS, and PDQ-39 values. The impairment of executive functions, attention, and memory may be due to the degeneration of brain regions that regulate the sleep-wake cycle and corresponding changes in the levels of neurotransmitters (Braak et al., 2004; Emre et al., 2007). Moreover, the autonomic nervous system is controlled by central and peripheral neural networks, and the degeneration of these regions is associated with EDS and PD, accompanied by nocturia and nocturnal sleep disorders, such as RBD and RLS (Kingsbury et al., 2010; Weerkamp et al., 2013).

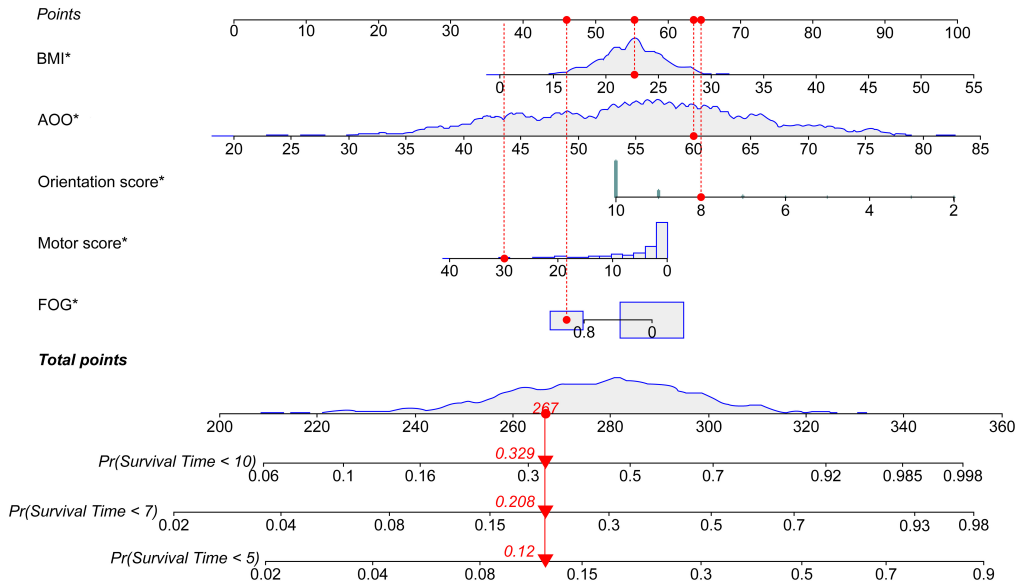

FIGURE 3
Nomogram for survival time with five variables. The nomogram showed that each factor has a score, and the total score is the sum of the scores of each factor, corresponding to the probability of EDS occurring at different survival times. Survival Time: the time from the diagnosis of PD to the end of follow-up, namely, the course of the disease at baseline plus 1 year. PD, Parkinson's disease; EDS, excessive daytime sleepiness; BMI, body mass index; AOO, age of onset; FOG, freezing of gait. *$P < 0.05$.

Nomograms are visual models of complex regression equations, facilitating the analysis of the results of prediction models. Nomograms are gaining increasing attention and application in medical and clinical research, especially that related to coronavirus disease and cancer, because of their ease of interpretation and simplicity (Wu et al., 2020; Dong et al., 2021; Hess, 2021).

Many clinical datasets are inaccurate, limited, cross-sectional, and lack statistical power. These problems are further complicated by the collection of different data types. ML methods learn rules directly from data and apply these rules to make predictions. In addition, these methods improve the integration of data from different models to increase statistical power (Myszczynska et al., 2020). Given its advantages and unique characteristics, ML is widely used in Internet security, data privacy, and medical, clinical, and psychological research (Orrù et al., 2020; Saura et al., 2021a,b).

XGBoost is a flexible decision tree algorithm with a simple structure and high data processing efficiency. It is suitable for large datasets with many variables. In addition, XGBoost can prevent over-fitting and has a high fault tolerance rate. As a result, redundant data do not adversely affect the accuracy of decisions. Random forest algorithms are useful to identify baseline predictors of EDS (Amara et al., 2017). However, these algorithms do not accurately analyze complex datasets and can only be applied to models with specific variables but not to other variables with inconsistent characteristics. Naive Bayes classifiers quickly and reliably find the probability distribution of features but assume that the contribution of each feature is independent, ignoring correlations between features (Orrù et al., 2020). Artificial neural networks have strong generalization and non-linear mapping capabilities, reducing the rate of errors to a certain extent. These networks are used primarily for classification and regression (Orrù et al., 2020). Thus, future studies should combine multiple ML algorithms to improve the accuracy and precision of prediction models (Mei et al., 2021).

Our results showed that patients with PD with high BMI were more likely to have EDS, and BMI had the greatest effect on the prediction efficiency of this model, which is consistent with some previous findings. In a study involving 134 patients with PD, subjective and objective sleepiness were assessed using the ESS and Multiple Sleep Latency Test, respectively (Coche De Cock et al., 2014). Patients with PD with a high BMI were found to have significant subjective and objective sleepiness (Coche De Cock et al., 2014). Additionally, in a study on patients with PD with poor nighttime sleepiness (PNS), the Pittsburgh Sleep Quality Index overall score was positively associated with BMI in patients with PNS as compared to those without (Qin et al., 2020). Our results support this viewpoint since EDS is a sleep disorder.

Furthermore, AOO may be a risk factor for EDS in patients with PD. In our prediction model, the second most important variable was AOO. The older AOO of patients with PD, the higher the risk of EDS. A study for patients with PD in Southwest China found that the prevalence of EDS in patients

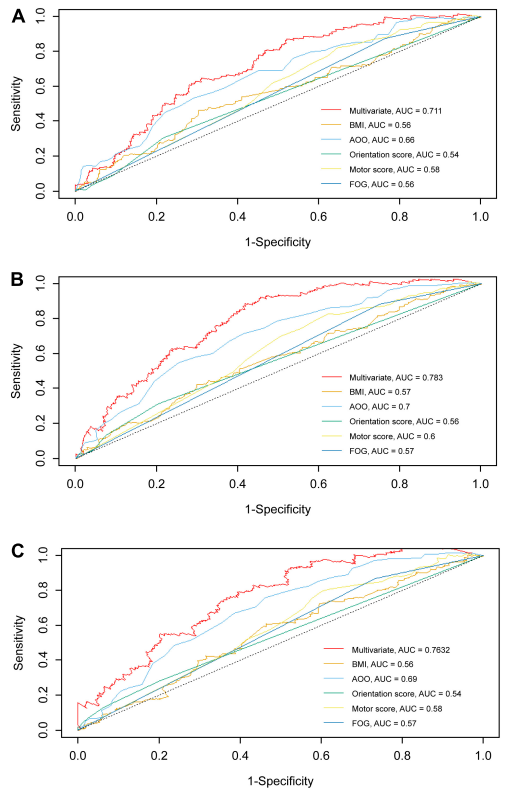

FIGURE 4
td-ROC curves of univariate and multivariate at different survival times in the training set. The td-ROC curves shows that the multivariable model has better predictive ability than other single-factor models in training set. **(A)** td-ROC of 5-year survival; **(B)** td-ROC of 7-year survival; **(C)** td-ROC of 10-year survival. td-ROC, time-dependent receiver operating characteristic; AUC, area under curve; BMI, body mass index; AOO, age of onset; FOG, freezing of gait.

with late-onset PD was higher than that in patients with early-onset PD (Guo et al., 2013). Our research supports this point. Recent studies have found that patients with PD with older AOO are more likely to develop EDS within 1 year after deep brain stimulation (Jung et al., 2020). However, this is controversial, as some studies have shown that the EDS symptoms of patients with PD, including their incidence and severity, are independent of AOO (Amara et al., 2017; Liu M. et al., 2021). Therefore, future research is needed to clarify this controversy.

Many studies have found severe cognitive impairment in patients with PD. A systematic review previously showed that, compared to patients with PD without EDS, those with EDS had more serious overall cognitive dysfunction, executive dysfunction, and processing speed dysfunction, although the groups had similar language ability, memory, and visuospatial ability (Jester et al., 2020). Recently, a study showed that the ESS score of patients with PD was related to cognitive impairment including attention, working memory ability, executive function, memory, and visual space (Goldman et al., 2013). However, patients with PD with EDS are not more likely to have cognitive impairment than patients with PD without EDS (Amara et al., 2017). In the present study, we found that EDS in patients with PD was negatively correlated with the orientation score of the MMSE, which implies that the worse the orientation function of patients with PD, the higher their risk of EDS. This is consistent with some previous results. Although we evaluated patients with cognitive impairment based on their education in combination with MMSE scores, rather than on MMSE scores alone, our data suggested that overall cognitive function in patients with PD may not be significantly associated with EDS.

Previous studies have shown that patients with PD with EDS may have worse quality of life. Patients with PD with EDS have a higher total score or sub-scores in the PDQ-39 (Xiang et al., 2019; Yoo et al., 2019). However, it is worth noting that our study showed that the risk factor for EDS in PD was a lower motor score in the PDQ-39, which implies that the better the quality of life of patients with PD who exercise, the greater the risk of developing EDS in future, which is markedly different from previously reported findings. We could possibly offer an interesting explanation for this: because of the disease characteristics of patients with PD, they tend to objectively exercise less. However, in the process of diagnosis and treatment, doctors often encourage patients to exercise as much as possible because exercise helps control the symptoms and delays the development of the disease. Therefore, patients with a low motor score in the PDQ-39 and good motor function may be more inclined to exercise. However, we should also be aware that PD tends to occur in middle-aged and elderly people. When do active exercise, patients may experience rapid physical decline due to their own aging and disease, often leading to fatigue in this population, which may promote the occurrence of drowsiness and cause EDS. However, more research is needed to confirm this hypothesis.

Few studies have explored the correlation between FOG in patients with PD and EDS. Patients were divided into clinically observed and self-reported FOG in a previous study, which found a significant association with EDS in both groups (Sawada et al., 2019). Furthermore, in a 4-year longitudinal study, it was found that patients with PD with FOG had higher scores on the ESS than did our patients (PD) with a lack of FOG (Banks et al., 2019). However, patients with PD with FOG actually had a lower risk of EDS in our study, contrary to previous study results. FOG may be associated with reduced crosstalk between the frontal cortex and basal ganglia-brainstem circuits. EDS is a non-motor symptom also closely related to neurotransmitter imbalance. Therefore, we hypothesize that FOG and EDS may be related to the reduced crosstalk between these brain regions in patients with PD (Gao et al., 2020).

We built a multi-factor Cox proportional risk regression model. According to the regression coefficient (β) and hazard ratio, among the two positively correlated variables, AOO

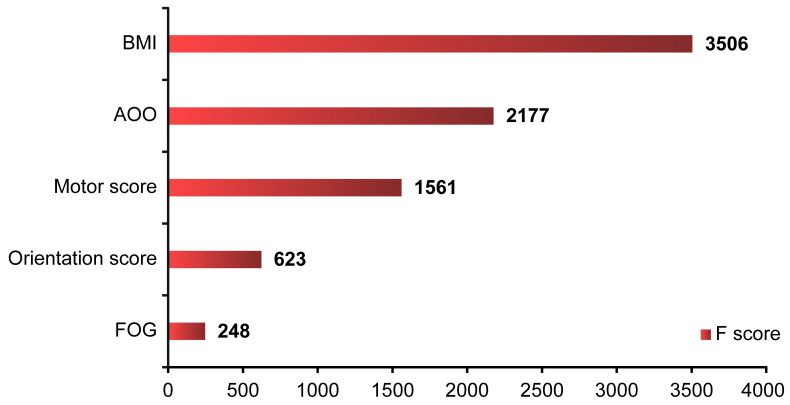

FIGURE 5
XGBoost ML analysis of the importance of each variable. The XGBoost showed that BMI, AOO, motor score, orientation score, and FOG contributed to the model in various degrees, and the importance of each variable decreased in turn. F score: the importance of each factor. XGBoost, eXtreme Gradient Boosting; ML, machine learning; BMI, body mass index; AOO, age of onset; FOG, freezing of gait.

contributed the most to the prediction model. Among the three negatively correlated variables, FOG contributed the most. However, this was not consistent with the contribution of each variable to the final prediction model. A nomogram is a traditional method for preliminarily and intuitively analyzing the meanings of these variables. In fact, there was no conflict. We consider that this study adopted the method of XGBoost, which makes full use of the training and test datasets and tries to build multiple models in internally with the help of powerful computing power and then selects the best model for multiple parameter modification and adjustment to further optimize the model. The prediction model is more effective and accurate than the traditional statistical model and can better reflect the clinical value. We provide a new research method to determine the weight of each variable in the model.

Conclusion

We studied the proportion and clinical features of 995 patients with PD without EDS who developed EDS after 1 year. We established a prediction model for EDS in patients with PD by nomogram and ML of XGBoost. Our data suggested that risk factors for EDS in patients with PD include high BMI, late AOO, low motor score of PDQ-39, low orientation score of MMSE, and lack of FOG, and their importance decreased in turn. The model we developed facilitates effective and relatively accurate prediction of EDS in patients with PD, and the overall accuracy of the model was 71.86%.

Theoretical implications

This study is the first to develop a longitudinal prediction model for EDS using a nomogram and ML in a large cohort with PD. This model provides a basis for the prediction of EDS in patients with PD and a new idea for the prediction of other symptoms, as well as other neurodegenerative diseases. The longitudinal analysis of large datasets increases the reliability and accuracy of the results. Our results complement other previous research results each other and can serve as the basis for understanding the pathogenesis of PD and EDS.

Practical implications

Clinicians can use this nomogram model to predict and to identify EDS, delaying the onset of EDS in patients with PD with early detection and treatment. Then, doctors can carry out targeted propaganda and education for patients according to the predicted results, urge patients to pay attention to their own physical condition consciously, and promote the alleviation of symptoms so that improve the quality of life of patients with PD and reduce the burden of patients and families. Furthermore, the model is visually simple, helping patients understand and accept this condition.

Limitations and future research

This study has limitations. First, the 1-year follow-up period may not be sufficient to assess the influence of the prediction model variables on the outcome measures, leading to representativeness bias. Second, an 11-year follow-up study showed that long naps rather than subjective EDS were a risk factor for PD (Leng et al., 2018). Therefore, future clinical studies should differentiate the groups with long naps and EDS symptoms. Third, although this result helps guide future research, higher accuracy and precision is desirable. Fourth, the ESS has limitations, such as high subjectivity, insufficient comprehensive projects, and unclear boundary of score. Furthermore, this questionnaire does not take into account individual physiological differences, medication use, presence of other sleep disorders, duration and quality of

sleep, time of day for symptoms, and level of patient interest in the condition.

Data availability statement

The data analyzed in this study is subject to the following licenses/restrictions: Data is available from the authors upon reasonable request and with permission of Multicenter Database and Collaborative Network of Parkinson's Disease and Movement Disorders in China. Requests to access these datasets should be directed to PD-MDCNC (http://www.pd-mdcnc.com).

Ethics statement

The studies involving human participants were reviewed and approved by the Ethics Committee of Central South University, Xiangya Hospital. The patients/participants provided their written informed consent to participate in this study.

Author contributions

PD, BT, and JG conceived the study. PD, YL, and HY analyzed and interpreted the data. PD edited the manuscript. PD, KX, XW, JG, BT, and ZL discussed the results. PD, KX, BT, and ZL discussed and revised the manuscript. PD, KX, XZ, YX, QX, QS, XY, JG, BT, and ZL provided clinical data. All authors made some contribution to the manuscript and approved the submitted version for publication.

Funding

This study was supported by the Hunan Innovative Province Construction Project (Grant Nos. 2019SK2335 and 2021SK1010), National Key Research and Development Program of China (Grant Nos. 2021YFC2501204 and 2016YFC306000), National Natural Science Foundation of China (Grant No. 82001359), Scientific Research Project of Hunan Provincial Health Commission (Grant No. 202203074637), and Natural Science Foundation of Hunan Province (Grant No. 2020JJ5929).

Acknowledgments

We thank the patients for participating in this study and the Medical Big Data Division of Hunan Kechuang Information Technology Co., Ltd., for data analysis.

Conflict of interest

YL and HY were employed by the Hunan Kechuang Information Technology Joint-Stock Co., Ltd.

The remaining authors declare that the research was conducted in the absence of any commercial or financial relationships that could be construed as a potential conflict of interest.

Publisher's note

All claims expressed in this article are solely those of the authors and do not necessarily represent those of their affiliated organizations, or those of the publisher, the editors and the reviewers. Any product that may be evaluated in this article, or claim that may be made by its manufacturer, is not guaranteed or endorsed by the publisher.

Supplementary material

The Supplementary Material for this article can be found online at: https://www.frontiersin.org/articles/10.3389/fnagi.2022.938071/full#supplementary-material

References

Aarsland, D., Litvan, I., and Larsen, J. P. (2001). Neuropsychiatric symptoms of patients with progressive supranuclear palsy and Parkinson's disease. *J. Neuropsychiatry Clin. Neurosci.* 13, 42–49. doi: 10.1176/jnp.13.1.42

Allen, R. P., Burchell, B. J., MacDonald, B., Hening, W. A., and Earley, C. J. (2009). Validation of the self-completed cambridge-hopkins questionnaire (CH-RLSq) for ascertainment of restless legs syndrome (RLS) in a population survey. *Sleep Med.* 10, 1097–1100. doi: 10.1016/j.sleep.2008.10.007

Amara, A. W., Chahine, L. M., Caspell-Garcia, C., Long, J. D., Coffey, C., Högl, B., et al. (2017). Longitudinal assessment of excessive daytime sleepiness in early Parkinson's disease. *J. Neurol. Neurosurg. Psychiatry.* 88, 653–662. doi: 10.1136/jnnp-2016-315023

Banks, S. J., Bayram, E., Shan, G., LaBelle, D. R., and Bluett, B. (2019). Non-motor predictors of freezing of gait in Parkinson's disease. *Gait Posture* 68, 311–316. doi: 10.1016/j.gaitpost.2018.12.009

Bestwick, J. P., Auger, S. D., Schrag, A. E., Grosset, D. G., Kanavou, S., Giovannoni, G., et al. (2021). Optimising classification of Parkinson's disease based on motor, olfactory, neuropsychiatric and sleep features. *NPJ Parkinsons Dis.* 7:87. doi: 10.1038/s41531-021-00226-2

Bloem, B. R., Okun, M. S., and Klein, C. (2021). Parkinson's disease. *Lancet* 397, 2284–2303. doi: 10.1016/S0140-6736(21)00218-X

Braak, H., Ghebremedhin, E., Rub, U., Bratzke, H., and Del Tredici, K. (2004). Stages in the development of Parkinson's disease-related pathology. *Cell Tissue Res.* 318, 121–134. doi: 10.1007/s00441-004-0956-9

Chaudhuri, K. R., Pal, S., DiMarco, A., Whately-Smith, C., Bridgman, K., Mathew, R., et al. (2002). The Parkinson's disease sleep scale: a new instrument for assessing sleep and nocturnal disability in Parkinson's disease. *J. Neurol. Neurosurg. Psychiatry* 73, 629–635. doi: 10.1136/jnnp.73.6.629

Chaudhuri, K. R., Martinez-Martin, P., Brown, R. G., Sethi, K., Stocchi, F., Odin, P., et al. (2007). The metric properties of a novel non-motor symptoms scale for Parkinson's disease: results from an international pilot study. *Mov. Disord.* 22, 1901–1911. doi: 10.1002/mds.21596

Coche De Cock, V., Bayard, S., Jaussent, I., Charif, M., Grini, M., Langenier, M. C., et al. (2014). Daytime sleepiness in Parkinson's disease: a reappraisal. *PLoS One* 9:e107278. doi: 10.1371/journal.pone.0107278

Diederich, N. J., and McIntyre, D. J. (2012). Sleep disorders in Parkinson's disease: many causes, few therapeutic options. *J. Neurol. Sci.* 314, 12–19. doi: 10.1016/j.jns.2011.10.025

Dong, Y. M., Sun, J., Li, Y. X., Chen, Q., Liu, Q. Q., Sun, Z., et al. (2021). Development and validation of a nomogram for assessing survival in patients with COVID-19 pneumonia. *Clin. Infect. Dis.* 72, 652–660. doi: 10.1093/cid/ciaa963

Emre, M., Aarsland, D., Brown, R., Burn, D. J., Duyckaerts, C., Mizuno, Y., et al. (2007). Clinical diagnostic criteria for dementia associated with Parkinson's disease. *Mov. Disord.* 22, 1689–1707. doi: 10.1002/mds.21507

Gao, C., Liu, J., Tan, Y., and Chen, S. (2020). Freezing of gait in Parkinson's disease: pathophysiology, risk factors and treatments. *Trans. Neurodegener* 9:12. doi: 10.1186/s40035-020-00191-5

Goldman, J. G., Ghode, R. A., Ouyang, B., Bernard, B., Goetz, C. G., and Stebbins, G. T. (2013). Dissociations among daytime sleepiness, nighttime sleep, and cognitive status in Parkinson's disease. *Parkinsonism Relat. Disord.* 19, 806–811. doi: 10.1016/j.parkreldis.2013.05.006

Guo, X., Song, W., Chen, K., Chen, X., Zheng, Z., Cao, B., et al. (2013). Gender and onset age-related features of non-motor symptoms of patients with Parkinson's disease–a study from Southwest China. *Parkinsonism Relat. Disord.* 19, 961–965. doi: 10.1016/j.parkreldis.2013.06.009

Hamilton, M. (1960). A rating scale for depression. *J. Neurol. Neurosurg. Psychiatry* 23, 56–62. doi: 10.1136/jnnp.23.1.56

Hess, D. R. (2021). A nomogram for use of non-invasive respiratory strategies in COVID-19. *Lancet Digit Health.* 3, e140–e141. doi: 10.1016/S2589-7500(21)00006-6

Hoehn, M. M., and Yahr, M. D. (1967). Parkinsonism: onset, progression and mortality. *Neurology* 17, 427–442. doi: 10.1212/WNL.17.5.427

Höglund, A., Hagell, P., Broman, J. -E., Palhagen, S., Sorjonen, K., and Fredrikson S. (2019). A 10-year follow-up of excessive daytime sleepiness in parkinson's disease. *Parkinsons Dis.* 2019:5708515. doi: 10.1155/2019/5708515

Hurt, C. S., Rixon, L., Chaudhuri, K. R., Moss-Morris, R., Samuel, M., and Brown, R. G. (2019). Barriers to reporting non-motor symptoms to health-care providers in people with Parkinson's. *Parkinsonism Relat Disord.* 64, 220–225. doi: 10.1016/j.parkreldis.2019.04.014

Jester, D. J., Lee, S., Molinari, V., and Volicer, L. (2020). Cognitive deficits in Parkinson's disease with excessive daytime sleepiness: a systematic review. *Aging Mental Health* 24, 1769–1780. doi: 10.1080/13607863.2019.1660852

Johns, M. W. (1991). A new method for measuring daytime sleepiness: the epworth sleepiness scale. *Sleep* 14, 540–545. doi: 10.1093/sleep/14.6.540

Jung, Y. J., Kim, H. J., Lee, W. W., Ehm, G., and Jeon, B. (2020). A 3-year observation of excessive daytime sleepiness after subthalamic deep brain stimulation in patients with Parkinson's disease. *Clin. Neurol. Neurosurg.* 192:105721. doi: 10.1016/j.clineuro.2020.105721

Kingsbury, A. E., Bandopadhyay, R., Silveira-Moriyama, L., Ayling, H., Kallis, C., Sterlacci, W., et al. (2010). Brain stem pathology in Parkinson's disease: an evaluation of the braak staging model. *Mov. Disord.* 25, 2508–2515. doi: 10.1002/mds.23305

Leng, Y., Goldman, S. M., Cawthon, P. M., Stone, K. L., Ancoli-Israel, S., and Yaffe, K. (2018). Excessive daytime sleepiness, objective napping and 11-year risk of Parkinson's disease in older men. *Int. J. Epidemiol.* 47, 1679–1686. doi: 10.1093/ije/dyy098

Liu, L., Xie, J., Wu, W., Chen, H., Li, S., He, H., et al. (2021). A simple nomogram for predicting failure of non-invasive respiratory strategies in adults with COVID-19: a retrospective multicentre study. *Lancet Digit Health.* 3, e166–e174. doi: 10.1016/S2589-7500(20)30316-2

Liu, M., Luo, Y. J., Gu, H. Y., Wang, Y. M., Liu, M. H., Li, K., et al. (2021). Sex and onset-age-related features of excessive daytime sleepiness and night-time sleep in patients with Parkinson's disease. *BMC Neurol.* 21:165.

Maggi, G., Trojano, L., Barone, P., and Santangelo, G. (2021). Sleep disorders and cognitive dysfunctions in Parkinson's disease: a meta-analytic study. *Neuropsychol. Rev.* 31, 643–682. doi: 10.1007/s11065-020-09473-1

Mehan, N., Kumar, M., Bhatt, S., Shankar, R., Kumari, B., Pahwa, R., et al. (2022). THN 102 for excessive daytime sleepiness associated with Parkinson's disease: a phase 2a trial. *Mov. Disord.* 37, 410–415. doi: 10.1002/mds.28840

Mei, J., Desrosiers, C., and Frasnelli, J. (2021). Machine learning for the diagnosis of Parkinson's disease: a review of literature. *Front. Aging Neurosci.* 13:633752. doi: 10.3389/fnagi.2021.633752

Millar Vernetti, P., Perez Lloret, S., Rossi, M., Cerquetti, D., and Merello, M. (2012). Validation of a new scale to assess olfactory dysfunction in patients with Parkinson's disease. *Parkinsonism Relat. Disord.* 18, 358–361. doi: 10.1016/j.parkreldis.2011.12.001

Montgomery, S. A., and Asberg, M. (1979). A new depression scale designed to be sensitive to change. *Br. J. Psychiatry* 134, 382–389. doi: 10.1192/bjp.134.4.382

Muller, M. L., and Bohnen, N. I. (2013). Cholinergic dysfunction in Parkinson's disease. *Curr. Neurol. Neurosci. Rep.* 13:377. doi: 10.1007/s11910-013-0377-9

Myszczynska, M. A., Ojamies, P. N., Lacoste, A. M. B., Neil, D., Saffari, A., Mead, R., et al. (2020). Applications of machine learning to diagnosis and treatment of neurodegenerative diseases. *Nat. Rev. Neurol.* 16, 440–456. doi: 10.1038/s41582-020-0377-8

Nillson, M. H., Bladh, S., and Hagell, P. (2013). Fatigue in Parkinson's disease: measurement properties of a generic and a condition-specific rating scale. *J. Pain Symptom Manag.* 46, 737–746. doi: 10.1016/j.jpainsymman.2012.11.004

Orrù, G., Monaro, M., Conversano, C., Gemignani, A., and Sartori, G. (2020). Machine learning in psychometrics and psychological research. *Front. Psychol.* 10:2970. doi: 10.3389/fpsyg.2019.02970

Peng, L., Chen, Z., Chen, T., Lei, L., Long, Z., Liu, M., et al. (2021). Prediction of the age at onset of spinocerebellar ataxia type 3 with machine learning. *Mov. Disord.* 36, 216–224. doi: 10.1002/mds.28311

Peto, V., Jenkinson, C., Fitzpatrick, R., and Greenhall, R. (1995). The development and validation of a short measure of functioning and well-being for individuals with Parkinson's disease. *Qual. Life. Res.* 4, 241–248. doi: 10.1007/BF02260863

Postuma, R. B., Berg, D., Stern, M., Poewe, W., Olanow, C. W., Oertel, W., et al. (2015). MDS clinical diagnostic criteria for Parkinson's disease. *Mov. Disord.* 30, 1591–1601. doi: 10.1002/mds.26424

Punjabi, N. M., and Haponik, E. (2000). Ask about daytime sleepiness! *J Am Geriatr Soc.* 48, 228–229. doi: 10.1111/j.1532-5415.2000.tb03918.x

Qin, X., Li, X., Chen, G., Chen, X., Shi, M., Liu, X. K., et al. (2020). Clinical features and correlates of poor nighttime sleepiness in patients with Parkinson's disease. *Parkinsons Dis.* 2020:6378673. doi: 10.1155/2020/6378673

Saper, C. B., Chou, T. C., and Scammell, T. E. (2001). The sleep switch: hypothalamic control of sleep and wakefulness. *Trends Neurosci* 24, 726–731. doi: 10.1016/S0166-2236(00)02002-6

Saura, J. R., Ribeiro-Soriano, D., and Palacios-Marqués, D. (2021b). Using data mining techniques to explore security issues in smart living environments in Twitter. *Comput. Commun.* 179, 285–295. doi: 10.1016/j.comcom.2021.08.021

Saura, J. R., Ribeiro-Soriano, D., and Palacios-Marqués, D. (2021a). From user-generated data to data-driven innovation: a research agenda to understand user privacy in digital markets. *Int. J. Inform. Manage.* 60:102331. doi: 10.1016/j.ijinfomgt.2021.102331

Sawada, M., Wada-Isoe, K., Hanajima, R., and Nakashima, K. (2019). Clinical features of freezing of gait in Parkinson's disease patients. *Brain Behav.* 9:e01244. doi: 10.1002/brb3.1244

Shen, S. S., Shen, Y., Xiong, K. P., Chen, J., Mao, C. J., Huang, J. Y., et al. (2014). Validation study of REM sleep behavior disorder questionnaire-hong kong (RBDQ-HK) in east China. *Sleep Med.* 15, 952–958. doi: 10.1016/j.sleep.2014.03.020

Suzuki, K. (2021). Current update on clinically relevant sleep issues in Parkinson's disease: a narrative review. *J. Parkinsons Dis.* 11, 971–992. doi: 10.3233/JPD-202425

Tholfsen, L. K., Larsen, J. P., Schulz, J., Tysnes, O. B., and Gjerstad, M. D. (2015). Development of excessive daytime sleepiness in early Parkinson disease. *Neurology* 85, 162–168. doi: 10.1212/WNL.0000000000001737

Tomlinson, C. L., Stowe, R., Patel, S., Rick, C., Gray, R., and Clarke, C. E. (2015). Systematic review of levodopa dose equivalency reporting in Parkinson's disease. *Mov. Disord.* 25, 2649–2653. doi: 10.1002/mds.23429

Ueno, T., Kon, T., Haga, R., Nishijima, H., and Tomiyama, M. (2018). Motor vehicle accidents in Parkinson's disease: a questionnaire study. *Acta Neurol. Scand.* 137, 218–223. doi: 10.1111/ane.12849

Videovic, A., Amara, A. W., Comella, C., Schweitzer, P. K., Emsellem, H., Liu, K., et al. (2021). Solriamfetol for excessive daytime sleepiness in Parkinson's disease: phase 2 proof-of-concept trial. *Mov. Disord.* 36, 2408–2412. doi: 10.1002/mds.28702

Weerkamp, N. J., Tissingh, G., Poels, P. J., Zuidema, S. U., Munneke, M., Koopmans, R. T., et al. (2013). Nonmotor symptoms in nursing home residents with Parkinson's disease: prevalence and effect on quality of life. *J. Am. Geriatr. Soc.* 61, 1714–1721. doi: 10.1111/jgs.12458

Wu, J., Zhang, H., Li, L., Hu, M., Chen, L., Xu, B., et al. (2020). A nomogram for predicting overall survival in patients with low-grade endometrial stromal sarcoma: a population-based analysis. *Cancer Commun (Lond).* 40, 301–312. doi: 10.1002/cac2.12067

Xiang, Y. Q., Xu, Q., Sun, Q. Y., Wang, Z. Q., Tian, Y., Fang, L. J., et al. (2019). Clinical features and correlates of excessive daytime sleepiness in Parkinson's disease. *Front. Neurol.* 10:121. doi: 10.3389/fneur.2019.00121

Xu, K., Zhou, X. X., He, R. C., Zhou, Z., Liu, Z. H., Xu, Q., et al. (2021). Constructing prediction models for freezing of gait by nomogram and machine learning: a longitudinal study. *Front. Neurol.* 12:684044. doi: 10.3389/fneur.2021.684044

Xu, Z., Anderson, K. N., Saffari, S. E., Lawson, R. A., Chaudhuri, K. R., Brooks, D., et al. (2021). Progression of sleep disturbances in Parkinson's disease: a 5-year longitudinal study. *J. Neurol.* 268, 312–320. doi: 10.1007/s00415-020-10140-x

Yoo, S. W., Kim, J. S., Oh, Y. S., Ryu, D. W., and Lee, K. S. (2019). Excessive daytime sleepiness and its impact on quality of life in de novo Parkinson's disease. *Neurol. Sci.* 40, 1151–1156. doi: 10.1007/s10072-019-03785-8

Zhou, X., Guo, J., Sun, Q., Xu, Q., Pan, H., Yu, R., et al. (2019). Factors associated with dyskinesia in Parkinson's disease in mainland China. *Front. Neurol.* 10:477. doi: 10.3389/fneur.2019.00477

Zuzuarregui, J. R. P., and During, E. H. (2020). Sleep issues in Parkinson's disease and their management (2020). *Neurotherapeutics* 17, 1480–1494.

frontiers | Frontiers in Aging Neuroscience

TYPE Original Research
PUBLISHED 09 August 2022
DOI 10.3389/fnagi.2022.896522

OPEN ACCESS

EDITED BY
Jiehui Jiang,
Shanghai University, China

REVIEWED BY
Mitsuru Shinohara,
National Center for Geriatrics and Gerontology (NCGG), Japan
Yi-Cheng Zhu,
Peking Union Medical College Hospital (CAMS), China

*CORRESPONDENCE
Qi Xu
xuqi@pumc.edu.cn

†These authors have contributed equally to this work and share first authorship

SPECIALTY SECTION
This article was submitted to Alzheimer's Disease and Related Dementias, a section of the journal Frontiers in Aging Neuroscience

RECEIVED 15 March 2022
ACCEPTED 15 July 2022
PUBLISHED 09 August 2022

CITATION
Qiu Y, Sha L, Zhang X, Li G, Zhu W and Xu Q (2022) Induction of *A Disintegrin and Metalloproteinase with Thrombospondin motifs 1* by a rare variant or cognitive activities reduces hippocampal amyloid-β and consequent Alzheimer's disease risk.
Front. Aging Neurosci. 14:896522.
doi: 10.3389/fnagi.2022.896522

Induction of *A Disintegrin and Metalloproteinase with Thrombospondin motifs 1* by a rare variant or cognitive activities reduces hippocampal amyloid-β and consequent Alzheimer's disease risk

Yunjie Qiu[1†], Longze Sha[1,2†], Xiuneng Zhang[1], Guanjun Li[1], Wanwan Zhu[1,2] and Qi Xu[1,2*]

[1]State Key Laboratory of Medical Molecular Biology, School of Basic Medicine Peking Union Medical College, Institute of Basic Medical Sciences Chinese Academy of Medical Sciences, Beijing, China, [2]Neuroscience Center, Chinese Academy of Medical Sciences, Beijing, China

Amyloid-β (Aβ) derived from amyloid precursor protein (APP) hydrolysis is acknowledged as the predominant hallmark of Alzheimer's disease (AD) that especially correlates to genetics and daily activities. In 2019, meta-analysis of AD has discovered five new risk loci among which *A Disintegrin and Metalloproteinase with Thrombospondin motifs 1* (*ADAMTS1*) has been further suggested in 2021 and 2022. To verify the association, we re-sequenced *ADAMTS1* of clinical AD samples and subsequently identified a novel rare variant c.−2067A > C with watchable relevance (whereas the *P*-value was not significant after adjustment). Dual-luciferase assay showed that the variant sharply stimulated *ADAMTS1* expression. In addition, *ADAMTS1* was also clearly induced by pentylenetetrazol-ignited neuronal activity and enriched environment (EE). Inspired by the above findings, we investigated ADAMTS1's role in APP metabolism *in vitro* and *in vivo*. Results showed that ADAMTS1 participated in APP hydrolysis and consequently decreased Aβ generation through inhibiting β-secretase-mediated cleavage. In addition, we also verified that the hippocampal amyloid load of AD mouse model was alleviated by the introduction of *ADAMTS1*, and thus spatial cognition was restored as well. This study revealed the contribution of *ADAMTS1* to the connection of genetic and acquired factors with APP metabolism, and its potential in reducing hippocampal amyloid and consequent risk of AD.

KEYWORDS

***ADAMTS1*, genetic variant, cognitive activities, amyloid precursor protein, amyloid-β, Alzheimer's disease**

Introduction

Alzheimer's disease (AD) is a progressive disorder characterized by cerebral amyloid-β (Aβ) deposition as an early pathological alteration (Jack et al., 2018). Currently, the unbalanced processing of Aβ, finally leading to the formation of amyloid plaques in the brain, is considered to be the initiating event of AD as suggested by available evidence (Jack et al., 2010). This process occurs when individuals are still cognitively normal, as demonstrated by numerous follow-up cohort studies in which Aβ positivity is reached many years before dementia onset (Hanseeuw et al., 2019). The initial Aβ processing may be affected by multiple factors that hereby influence the risk of AD, of which genetics or daily activities may keep individuals retardant or progressive to the amyloid plaque during early life.

Due to the significance of genetic factors, recent studies have focused on identifying associated genes of AD. In 2019, the genome-wide association study implicated 25 risk loci, and positive signals were found in or near genes that encoded proteins participating in amyloid precursor protein (APP) metabolism. Further analysis showed that the up-mentioned variants were associated not only with the early onset autosomal dominant familial AD but also the late-onset type (Kunkle et al., 2019). Moreover, one newly identified locus, *A Disintegrin and Metalloproteinase with Thrombospondin motifs 1* (*ADAMTS1*), has been further suggested in the meta-analysis of AD in 2021 and 2022 (Schwartzentruber et al., 2021; Bellenguez et al., 2022). *ADAMTS1* encodes a zinc metalloprotease belonging to the ADAMTS secretase family (Lemarchant et al., 2013) that functions on extracellular matrix (ECM) hydrolysis (Zhong and Khalil, 2019). ADAMTSs are activated and secreted to hydrolyze substrates, including proteoglycans, collagen, and laminin (Porter et al., 2005). Although ADAMTSs have been studied as hydrolases for decades, the function of the specific member ADAMTS1 in nervous system is still poorly understood. Regarding the adjacency of *ADAMTS1* to *APP* and the role of APP as an ECM component (Beher et al., 1996; Caceres and Brandan, 1997; van der Kant and Goldstein, 2015), we have proposed that ADAMTS1 acts on APP processing and thereby contributes to Aβ generation.

In addition to genetics, cognitive activities may also affect the onset and progression of AD. Numerous longitudinal studies have investigated the relation between cognitive activities and AD progression, suggesting that cognitive enrichment may account for less cognitive decline and AD pathology in old age (Vemuri et al., 2014; Oveisgharan et al., 2020). Moreover, some studies have implied that mice participating in cognitive activities exhibit elevated ECM hydrolase (Murase et al., 2019; Nguyen et al., 2020). Thus, hypothesis that cognitive activities may stimulate associated ECM hydrolase and subsequently function on APP processing ties cognitive enrichment to less AD pathology. However, more evidence is still needed to support the hypothesis, and it is significant to understand the molecular connections of activities to APP processing to reduce the risk of AD.

According to the up-mentioned background, we checked the association of *ADAMTS1* with AD and studied whether *ADAMTS1* was induced by cognitive activities and involved in APP metabolism. To this end, we performed gene re-sequencing using clinical samples, tested the role of neural activities in the induction of *ADAMTS1*, and explored the mechanism of its function on Aβ pathology *in vitro* and *in vivo*. The results demonstrated that a newly identified genetic variant in promoter and cognitive activities both induced *ADAMTS1* expression, which stimulated APP's conversion to a novel product and thus decreased Aβ generation. Our findings identified ADAMTS1 as a novel APP hydrolase that connected the genetics and cognitive activities with hippocampal amyloid processing.

Materials and methods

Clinical samples

Human blood was collected from AD patients (1,152 cases) and control subjects (864 cases) who had given written consent to this study approved by the Institutional Review Board of Chinese Academy of Medical Sciences and Peking Union Medical College (CAMS and PUMC, Beijing, China). Genomic DNA was extracted using Quickgene DNA whole blood kit (DB-L, KURABO, Osaka, Japan) following the manufacturer's instructions.

Re-sequencing

11 pairs of primers were used to amplify the promoter and exon region of *ADAMTS1*, and the PCR products were then subjected to Sanger sequencing. The sequencing data were compared with records of NCBI to search for potential single nucleotide polymorphisms (SNPs). Primers used are shown in **Table 1**.

Dual-luciferase reporter assay

HEK 293T cells were co-transfected with pGL3-Basic (firefly luciferase plasmid) carrying required sequences and pRL-TK (Renilla luciferase plasmid). After 48-h culture, reporter luciferase activity was measured and normalized to Renilla luciferase using Dual-Luciferase Reporter Assay System (E1910, Promega, Madison, United States).

TABLE 1 Primers used in the re-sequencing test.

Region	Primers
Promoter	F: 5′-GTACGGATGGCTTTGCCTTCAAGC-3′
	R: 5′-GTCTCTTGGTTGGCTCCAAGTAG-3′
	F: 5′-CAAGTAAGCAATCTCGCTAGG-3′
	R: 5′-AGCCTGCCAGGAGCTCCTTAG-3′
	F: 5′-AGTCGTCTCTGGTGAAGAGGTG-3′
	R: 5′-CTGAGGCAACGCGGAGATTGGT-3′
Exon 1	F: 5′-TAACAATCCAGAGCAGGCCAACG-3′
	R: 5′-TCTGTCCGCGGACTTATGATCCT-3′
Exon 2	F: 5′-CAGAAGAAATCCTGCTCACACAC-3′
	R: 5′-AGGGTGTGCCTTCACATATG-3′
Exon 3	F: 5′-ATGGTACCAGCTGTGAGACT-3′
	R: 5′-GGATGATATGCAGCAGGTTC-3′
Exon 4	F: 5′-GAGATGGAGTCTCACTCTGTCT-3′
	R: 5′-GACAGGAAGTTATTGATCTGCG-3′
Exon 5	F: 5′-CGCAGATCAATAACTTCCTGTC-3′
	R: 5′-ACCGCACGTTCTCGAACAGTCT-3′
Exon 6/7	F: 5′-GGTGTATCAACGGCAAGTGTGT-3′
	R: 5′-GCAGGCAGTTGCCAATTAATG-3′
Exon 8	F: 5′-CTTAGCTGGAGGAGACATAGGT-3′
	R: 5′-ACTTCGATGTTGGTGGCTCCAGT-3′
Exon 9	F: 5′-AATGGGCCTTTCAACAGGTCTG-3′
	R: 5′-CACCTTACTGATACACCTCACTGG-3′

Animals and drug administration

Wild-type (WT) adult male C57BL/6J mice (7–8 weeks old) were obtained from SPF Biotechnology Co., Ltd. (Beijing, China) and raised together for 2–3 weeks to adapt to the environment before experiments. 5 × FAD lines were maintained by crossing WT mice (C57BL/6J background) with 5 × FAD mice (B6SJL background, #034840-JAX, The Jackson Laboratory, Bar Harbor, United States). Only male mice were used and non-transgenic WT littermate mice served as control. WT and 5 × FAD mice infected with recombinant adeno-associated virus (rAAV)2/9-*hSyn-EGFP* [empty vector (Mock)] or rAAV2/9-*hSyn-ADAMTS1-FLAG* in hippocampus were, respectively, named as WT-Mock, WT-ADAMTS1 (ATS1), 5 × FAD-Mock and 5 × FAD-ATS1. Animals were housed under standard conditions of 22°C and 12-h light/dark cycle with free access to water and food. Animal care and handling were performed according to terms approved by the Institutional Review Board of CAMS and PUMC (Beijing, China).

Drugs were intraperitoneally injected and dose was 55 mg/kg for pentylenetetrazol (PTZ, P6500, Sigma-Aldrich, Shanghai, China) according to Matsu-ura's work with little modification (Matsu-ura et al., 2002) and 400 mg/kg for chloral hydrate (Zemdegs et al., 2019; Cheng et al., 2021) (A600288, Sangon Biotech, Shanghai, China). Each group contained four mice for this analysis.

Enriched environment

Mice in Enriched environment (EE) were housed for 24 h in rat cages measuring 30 cm W × 18 cm H × 46 cm L. Standard nesting, rodent foraging toys, and one running wheel were arranged in the cage. Additionally, metal link chains or small wooden blocks were suspended from the cage roof. Mice housed in normal cages without decorations were considered as control. Each group contained four mice for this analysis.

Immunohistochemistry

Mice deeply anesthetized by pentobarbital sodium (50 mg/kg) were transcardially perfused with PBS. Brains were quickly harvested and fixed in 4% paraformaldehyde for 24 h at 4°C. Then, the tissue was embedded in paraffin and made into 4-μm sections which were deparaffinized by gradient ethanol and subjected to antigen retrieve in citrate buffer.

Sections for Aβ dyeing were blocked by 5% BSA for 1 h at room temperature (RT) and incubated with primary antibodies overnight at 4°C. Next, after three-time washing using PBS buffer, sections were incubated with fluorescent secondary antibodies for 2 h at RT. After another three-time washing using PBS buffer, sections were photographed through upright microscopy (DM6 B, Leica Microsystems, Shanghai, China). Images of 5 × magnification in hippocampus were captured on three sections per animal. Aβ load was evaluated by Image J software 1.52. After a fixed intensity threshold was set using Image J, measurements were performed for positive area covered by Aβ staining on each image. The numbers of animals used for this analysis were seven for 5 × FAD-Mock and six for 5 × FAD-ATS1.

Sections for ADAMTS1 staining were incubated in 3% H_2O_2 for 30 min at RT followed by blocking in 5% BSA for 1 h at RT and incubation with primary antibody overnight at 4°C. Next, after washing using PBS buffer, sections were incubated with HRP-conjugated secondary antibody that reacted with tyramine-coupled fluorescence (B40943, Thermo Fisher Scientific, Waltham, United States). Next, antigen retrieval was performed again to label NeuN, GFAP or iba1. The rest steps were the same as above described.

Antibodies were diluted with PBS buffer containing 1% BSA and listed below: anti-β-amyloid antibody (1:800, RRID:AB_2565328, 803015, BioLegend, San Diego, United States), anti-ADAMTS1 antibody (1:100, RRID:AB_2877879, 12749-1-AP, Proteintech, Wuhan,

China), anti-NeuN antibody (1:500, RRID:AB_2880708, 26975-1-AP, Proteintech, Wuhan, China), anti-GFAP antibody (1:500, RRID:AB_2631098, 12389, Cell Signaling Technology, Danvers, United States), and anti-iba1 antibody (1:200, RRID:AB_2832244, ab178847, Abcam, Cambridge, United Kingdom).

Quantitative real-time polymerase chain reaction

Hippocampal RNA was extracted using TRIzol reagent (15596026, Thermo Fisher Scientific, Waltham, United States) following the manufacturer's protocol. cDNA was then prepared using Transcriptor First Strand cDNA Synthesis Kit (04379012001, Roche, Basel, Switzerland) following the manufacturer's protocol and stored at −20°C until use. Quantitative real-time polymerase chain reaction (qPCR) was performed using real-time PCR System (CFX Connect, Bio-Rad, Hercules, United States). Transcription levels of *Adamts1*, *Fos*, *Npas4,* and *Zif268* were tested using FastStart Essential DNA Green Master mix (06402712001, Roche, Basel, Switzerland). The fold change of mRNA was normalized to *Gapdh* using the $2^{-\Delta\Delta Ct}$ method. Primer sequences are shown in **Table 2**.

TABLE 2 Primers used in qPCR experiments.

Gene	Primers
Adamts1	F: 5′-TGAATGGTGTGAGTGGCGAT-3′
	R: 5′-CCATCAAACATTCCCCGTGT-3′
Arc	F: 5′-GCCAGTCTTGGGCAGCATAG-3′
	R: 5′-GTATGAATCACTGCTGGGGGC-3′
Fos	F: 5′-CGGCAGAAGGGGCAAAGTAG-3′
	R: 5′-AGTTGATCTGTCTCCGCTTGG-3′
Npas4	F: 5′-CTCTGGATGCTGATCGCCTT-3′
	R: 5′-CAGGTGGGTGAGCATGGAAT-3′
Zif268	F: 5′-TATGAGCACCTGACCACAGAGTC-3′
	R: 5′-TAGGTGATGGGAGGCAACCG-3′
Gapdh	F: 5′-CGACTTCAACAGCAACTCCCACTCTTC-3′
	R: 5′-TGGGTGGTCCAGGGTTTCTTACTCCTT-3′

Plasmids construction and transfection

The cDNAs of *ADAMTS1*, *human APP Swedish mutation (swAPP)*, *ADAMTS1-FLAG*, *APP-MYC*, *ARC*, *FOS*, *NPAS4* and *ZIF268* were synthesized by Tsingke Biotechnology Co., Ltd. (Beijing, China) and cloned into the pcDNA3.1 vector. Mutations in *ADAMTS1* (namely, *E402A* and *E402Q*) were generated by overlap extension PCR method and then cloned into pcDNA3.1 vector. NEOFECT DNA-transfection reagent (TF201201, Neofect Biotech, Beijing, China) was used for the transient transfection of plasmids in accordance with the manufacturer's instructions.

Western blot assay

Cells washed with PBS buffer were lysed in CelLytic lysis buffer (C2978, Sigma-Aldrich, Shanghai, China) containing protease inhibitors. Whole proteins were obtained through centrifugation at 12,000 *g* for 15 min at 4°C. Hippocampi acquired from fresh brains were homogenized in 2% SDS buffer and centrifuged for 15 min at 12,000 *g* at 16°C to collect whole proteins. Protein concentration was determined by the bicinchoninic acid method after proper dilution. Then, the protein samples were denatured by mixing with 5 × sample loading buffer and a total of 20-μg protein of each sample was separated by SDS-PAGE and transferred to nitrocellulose membrane by the wet method. Specially, to detect C-terminal fragments of APP (CTFs), samples were mixed with 2 × sample loading buffer (P1325, Solarbio, Beijing, China), separated by Tris-tricine SDS-PAGE (P1320, Solarbio, Beijing, China) and finally transferred to PVDF membrane by the wet method. The membrane was then successively treated by blocking (in TBST buffer containing 5% skim milk for 1 h at RT), incubation with primary antibodies (in TBST buffer containing 5% skim milk overnight at 4°C), washing (three times in TBST buffer), incubation with secondary antibody (in TBST buffer containing 5% skim milk for 1 h at RT), repetitive washing (three times in TBST buffer) and finally developed using ECL reagents (WBULS0500, Millipore, Burlington, United States). The ratio of "target to β-actin" of treated groups was normalized to those of respective control groups and interpreted to fold change (i.e., relative level). Specially, for PTZ experiments, samples from different groups were loaded on the same one gel and thus four replications were separated into four membranes. For each replication, relative levels of different timepoints were normalized to that of PBS group which thus in each membrane was set to "1" without SEM (Suzuki et al., 2012; Sha et al., 2017).

Antibodies were diluted with TBST buffer containing 5% skim milk and listed below: anti-ADAMTS1 antibody for checking ADAMTS1 overexpression in cells and 5 × FAD mice (1:2,000, RRID:AB_11212782, MAB1810, Millipore, Burlington, United States), anti-ADAMTS1 antibody for checking endogenous ADAMTS1 expression in PTZ and EE experiments (1:2,000, ab276133, Abcam, Cambridge, United Kingdom), anti-Arc antibody (1:5,000, RRID:AB_2151832, 16290-1-AP, Proteintech, Wuhan, China), anti-c-fos antibody (1:2,000, RRID:AB_2247211, 2250, Cell Signaling Technology, Danvers, United States), anti-zif268 antibody (1:2,000, RRID:AB_11182923, 22008-1-AP, Proteintech, Wuhan, China), anti-APP antibody (1:20,000, RRID:AB_2289606,

ab32136, Abcam, Cambridge, United Kingdom), anti-sAPP antibody (1:10,000, RRID:AB_94882, MAB348, Millipore, Burlington, United States), anti-sAPPα antibody (1:1,000, RRID:AB_1630819, JP11088, Immuno-Biological Laboratories, Männedorf, Switzerland), anti-sAPPβ-WT antibody (1:1,000, RRID:AB_1630824, JP18957, Immuno-Biological Laboratories, Männedorf, Switzerland), anti-sAPPβ-Swedish antibody (1:1,000, RRID:AB_1630822, JP10321, Immuno-Biological Laboratories, Männedorf, Switzerland), and anti-β-actin antibody (1:100,000, RRID:AB_2223172, 4970, Cell Signaling Technology, Danvers, United States).

Enzyme-linked immunosorbent assay

Concentration of $A\beta_{40}$ and $A\beta_{42}$ was measured using enzyme-linked immunosorbent assay (ELISA) kits following the manufacturer's protocol (KHB3481, KHB3441, Thermo Fisher Scientific, Waltham, United States). Tissue samples were prepared through homogenizing hippocampus in RIPA lysis buffer (R0020, Solarbio, Beijing, China) containing protease inhibitors and centrifugation at 16,000 *g* for 20 min at 4°C, while cell samples were the conditioned medium of 48-h cultured HEK 293T cells co-transfected with *swAPP* and *ADAMTS1* plasmids.

Vector construction and recombinant adeno-associated virus packaging

rAAV was constructed through cloning *ADAMTS1*'s cDNA accompanied by either CMV promoter for primary neuron transfection or *Synapsin* promoter for animal experiments into AAV vector. Next, rAAV2/9-CMV-*ADAMTS1*-3 × *FLAG* and rAAV2/9-CMV-3 × *FLAG* were packaged by OBiO Technology Co., Ltd (Shanghai, China) while rAAV2/9-*hSyn-EGFP* and rAAV2/9-*hSyn-ADAMTS1-FLAG* were packaged by Taitool Bioscience Co., Ltd (Shanghai, China). The final titer of each rAAV was 3–5 × 10^{12} virus genome (V.G.)/mL.

Primary neuronal cultures and chemical treatment

Primary neurons were from E15.5 embryos of ICR mice. Briefly, cerebral cortex was gently separated and digested by 1.5% trypsin at 37°C for 15 min. Suspended cells were harvested and seeded in six-well plates (1.2–1.5 × 10^6 cells/well) pre-coated with poly-D-lysine. Cultures were maintained with Neurobasal Plus medium (A3582901, Thermo Fisher Scientific, Waltham, United States) containing B27 Plus supplement (A3582801, Thermo Fisher Scientific, Waltham, United States) at 37°C in a humidified 5% CO_2 incubator, and half of the medium was replaced regularly. Transfection was performed using rAAV2/9-CMV-*ADAMTS1*-3 × *FLAG* or Mock on days *in vitro* (*DIV*) 7. Specifically, the virus suspension was diluted with Neurobasal Plus medium containing B27 Plus supplement and then 1 × 10^{10} V.G. in total with or without *ADAMTS1* was added into neuron culture; serial dilution of rAAV2/9-CMV-*ADAMTS1*-3 × *FLAG* was also conducted using Neurobasal Plus medium containing B27 Plus supplement and final virus amount for each group was 7.5, 5, 2.5, 1.25, and 0 × 10^9 V.G. in total. Cells were cultured for another 10–12 days before use, and half of the medium was replaced regularly during this period.

Primary neurons on *DIV* 15–17 were treated with ADAM10 inhibitor GI254023X (HY-19956, MCE, New Jersey, United States) or BACE1 inhibitor verubecestat (HY-16759, MCE, New Jersey, United States) which were initially dissolved in DMSO to prepare the stock solution preserved at −20°C (5 mM for GI254023X and 1 mM for verubecestat). Final concentration was set at 20 μM for GI254023X (the final ratio of DMSO was 0.4%) and 1 μM for verubecestat (the final ratio of DMSO was 0.1%) by proper dilution with medium in the culture system. Extracellular medium and neurons were collected 2 d later.

Cellular component separation

Components of HEK 293T cells were separated using cell fractionation kit (SM-005, Invent Biotechnologies, Plymouth, United Kingdom) following the manufacturer's protocol into cytosol, organelles and plasma membrane which were then diluted to equal volume with non-denatured protein solubilization reagent (WA-010, Invent Biotechnologies, Plymouth, United Kingdom).

Co-immunoprecipitation

HEK 293T cells co-transfected with *ADAMTS1-FLAG* and *APP-Myc* were washed with PBS buffer and solubilized in ice-bath by CelLytic lysis buffer (C2978, Sigma-Aldrich, Shanghai, China) containing protease inhibitors. Clear lysates were incubated with primary antibodies overnight at 4°C and then with protein G Agarose beads (11243233001, Roche, Basel, Switzerland) for 2 h at 4°C. After five-time rinse with TBS buffer, immunoprecipitated proteins were recovered from the beads by boiling for 5 min in sample buffer, and then analyzed by immunoblotting.

Antibodies were diluted with TBST buffer containing 5% skim milk and listed below: anti-FLAG tag antibody (1:5,000, RRID:AB_262044, F1804, Sigma-Aldrich, Burlington, United States), anti-Myc tag antibody (1:5,000,

RRID:AB_331783, 2276, Cell Signaling Technology, Danvers, United States) and anti-Na^+/K^+ ATPase antibody (1:5,000, RRID:AB_2227873, 14418-1-AP, Proteintech, Wuhan, China).

Brain stereotaxic injection

Four month-old male 5 × FAD mice were deeply anesthetized and immobilized on a stereotaxic frame. The coordinates of hippocampus were set as $X \pm 2.0$ mm from bregma, Y −2.0 mm from bregma and Z −1.8 mm. 1.0 μL of rAAV suspension (4×10^9 V.G. in total) carrying *ADAMTS1-FLAG* or Mock was then injected into both pieces of hippocampus at 0.2 μL/min and the expression of *ADAMTS1-FLAG* was controlled by *Synapsin* promoter. Syringe was slowly withdrawn 10 min later and mice were kindly housed for 2 months before other tests.

Morris water maze test

Morris water maze was a round, water-filled tub (140 cm in diameter) equipped with cues and an invisible escape platform placed at a fixed spatial location. Mice were consecutively trained 20 times in total (four times per day) in the maze to locate the escape platform with the assistance of cues in 60 s at most, or else they would be manually guided. Their swimming routes and latency time (from release to landing) were recorded. Once getting on the platform, mice were rendered extra 15 s to explore surroundings. Following this training, a probe trial without the escape platform was conducted to record the time mice spent in the platform quadrant. ANYMAZE software 5.11 was utilized for data collection and further analysis. The numbers of animals used in this behavioral analysis were 14 for WT-Mock, 10 for WT-ATS1, 18 for 5 × FAD-Mock, and 14 for 5 × FAD-ATS1.

Statistics

The odd ratios (ORs), 95% confidence intervals, and *P*-values of alleles were calculated by *chi*-squared test to evaluate the association of SNPs with AD. Data were shown as mean ± SEM. Difference was analyzed using GraphPad Prism 6. Unpaired Student's *t*-test or Mann-Whitney *U*-test was used to analyze the significance between two experimental groups and one-way ANOVA or Kruskal-Wallis test was used for multiple comparisons depending on data distribution verified by skewness, kurtosis, and Shapiro-Wilk test (Kim, 2013; Alexander et al., 2017; Ellenberger et al., 2020). Specially, two-way ANOVA was used for animal behavior analysis (Qiu et al., 2007). It was considered as statistically significant when *P*-value was less than 0.05.

Results

A rare variant suggested by its weak association with lower Alzheimer's disease risk stimulated *A Disintegrin and Metalloproteinase with Thrombospondin motifs 1* expression

We performed re-sequencing of promoter and exon regions to assess the association of *ADAMTS1* with AD. As a result, two missense mutations in the exon and five SNPs in the promoter were identified (**Figure 1A**). The SNP at −2067 where adenine was substituted with cytosine (c.−2067A > C, **Figure 1B**) was not reported previously. Statistical analysis suggested that the rare c.−2067A > C [case minor allele frequency (MAF) = 0.00%, control MAF = 0.26%] had a weak association with AD before adjustment (original $P = 0.0166$, false discovery rate-adjusted $P = 0.1162$), indicating a potential protective role of c.−2067A > C against AD.

Since the novel variant located within the promoter, dual-luciferase reporter assay was then performed to explore the effect of c.−2067A > C on gene expression. As illustrated in **Figure 1C**, enhanced luciferase activity was induced by c.−2067A > C (∼50%, $P < 0.0001$, compared with WT group). Thus, individuals carrying c.−2067A > C might have a high transcription level of *ADAMTS1*. Considering the potential negative association of c.-2067A > C with AD, it was suggested that the high-level ADAMTS1 might protect carriers to some extent against the risk of AD.

Activity-related brain activities contributed to the induction of *A Disintegrin and Metalloproteinase with Thrombospondin motifs 1*

The expression pattern of ADAMTS1 in WT mouse hippocampus was examined by labeling ADAMTS1 simultaneously with NeuN, GFAP or iba1. Results presented in **Figure 2** and **Supplementary Figure 1** showed that neurons dominated the expression in CA1, CA3 and dentate gyrus.

In rodent models, neural activities trigger the elimination of ECM surrounding neurons (Nagy et al., 2006; Michaluk et al., 2009), and ADAMTS1, as an ECM hydrolase, acts on the degradation of proteoglycans that constitutes the matrix (Kuno et al., 2000). Considering these two aspects, we next investigated whether *ADAMTS1* expression was related to neuronal activity. PTZ was administrated to WT mice to induce neuronal activation in hippocampus, and subsequent qPCR and western blot revealed that *Adamts1* clearly increased at both mRNA (especially 1 h post injection, $P < 0.001$, compared with PBS group) and protein levels (especially 3 h post injection, $P < 0.01$,

A

Position (from coding region)	m/M	SNP	Case counts	Case MAF	Control counts	Control MAF	χ^2	OR	95% CI	Original *P*-value	FDR adjusted *P*-value
-2067	C/A	-	0/1090	0.00%	4/762	0.26%	5.734	-	-	.0166	.1162
-1824	C/A	rs186337829	10/1078	0.46%	9/745	0.60%	0.336	0.766	0.310-1.894	.5622	.7566
-1754	A/G	rs1036756381	5/1078	0.23%	4/745	0.27%	0.048	0.863	0.231-3.226	.8267	.8267
-1351	A/G	rs181607589	3/1078	0.14%	3/745	0.20%	0.208	0.690	0.139-3.430	.6485	.7566
-647	G/C	rs9974345	7/1067	0.33%	2/730	0.14%	1.270	2.404	0.498-11.610	.2598	.6062
2108	A/G	rs56251528	8/1013	0.39%	2/696	0.14%	1.790	2.762	0.585-13.050	.1809	.6062
2762	T/C	rs1219485538	3/1068	0.14%	3/704	0.21%	0.265	0.658	0.132-3.272	.6065	.7566

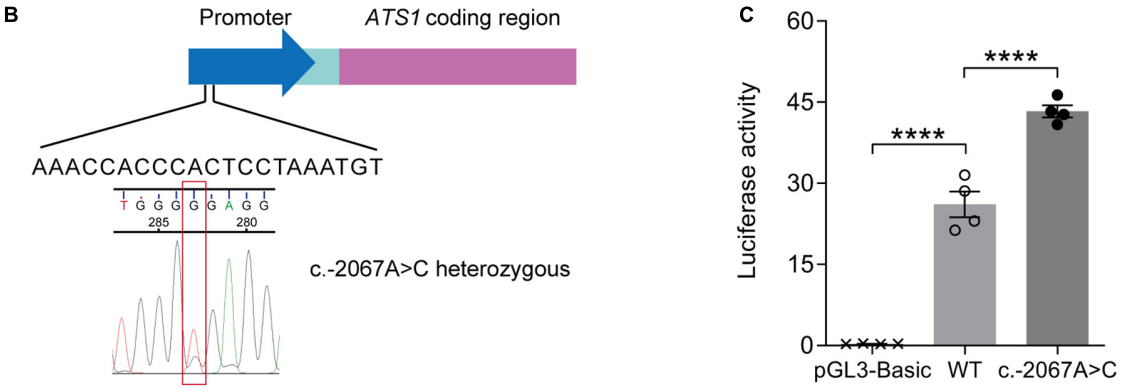

FIGURE 1
A rare variant suggested by its weak association with lower AD risk stimulated *ATS1* expression. **(A)** *ATS1* re-sequencing was conducted using clinical samples from AD patients and healthy aged individuals. Statistical results of SNPs were shown. **(B)** A schematic diagram showing the position of SNP c.−2067A > C in *ATS1*. **(C)** HEK 293T cells transfected with the *ATS1* WT or c.−2067A > C promoter were subjected to dual-luciferase assay. The relative luciferase activity indicated that c.−2067A > C promoted *ATS1* transcription compared with the WT promoter ($n = 4$, $P < 0.0001$, c.−2067A > C vs. WT, one-way ANOVA). ****$P < 0.0001$. Data were expressed as Mean ± SEM. AD, Alzheimer's disease; ATS1, ADAMTS1; CI, confidence interval; FDR, false discovery rate; MAF, minor allele frequency; OR, odds ratio; SNP, single nucleotide polymorphism; WT, wild type.

compared with PBS group) (Figures 3A,B). Furthermore, the PTZ-induced *Adamts1* upregulation was entirely suppressed by chloral hydrate pre-treatment (Figures 3C,D), verifying that the overexpression was triggered by the neuronal activation rather than other effects of PTZ. Additionally, mice raised in EE also held enhanced ADAMTS1 levels (shown in Figures 3E,F, $P < 0.01$, compared with control group). Taken together, the data suggested that the expression of *ADAMTS1* was related to brain activities.

The expression of immediate-early genes (IEGs) identifies neuronal ensembles activated during cognition encoding (Bozon et al., 2003; Plath et al., 2006; Kubik et al., 2007; Lin et al., 2008). Since *Adamts1* expression was regulated by neuronal activity, it was of interest to screen the transcription factor responsible for bridging *ADAMTS1* upregulation and activities. In the current work, several fast-reacting IEGs (zif268, c-fos, Arc and Npas4) were selected because *Adamts1* quickly responded 1-h post-injection. qPCR and western blot results revealed that these genes clearly increased in response to PTZ-induced neuronal activity (Supplementary Figures 2A,B), which had been suggested by previous studies as well (Retchkiman et al., 1996; Flood et al., 2004; Wang et al., 2007; Szyndler et al., 2013; Yun et al., 2013; Reschke et al., 2017; Wu et al., 2017; Shan et al., 2018). Next, *ZIF268*, *ARC*, *FOS*, and *NPAS4* were, respectively, introduced into luciferase system to investigate the managing role of IEGs on *ADAMTS1* expression, and zif268 was shown to have the dominated role (Figure 3G, $P < 0.0001$, compared with respective mock control). Meanwhile, the rare SNP c.-2067A > C identified by re-sequencing obviously enhanced the effects of zif268 on

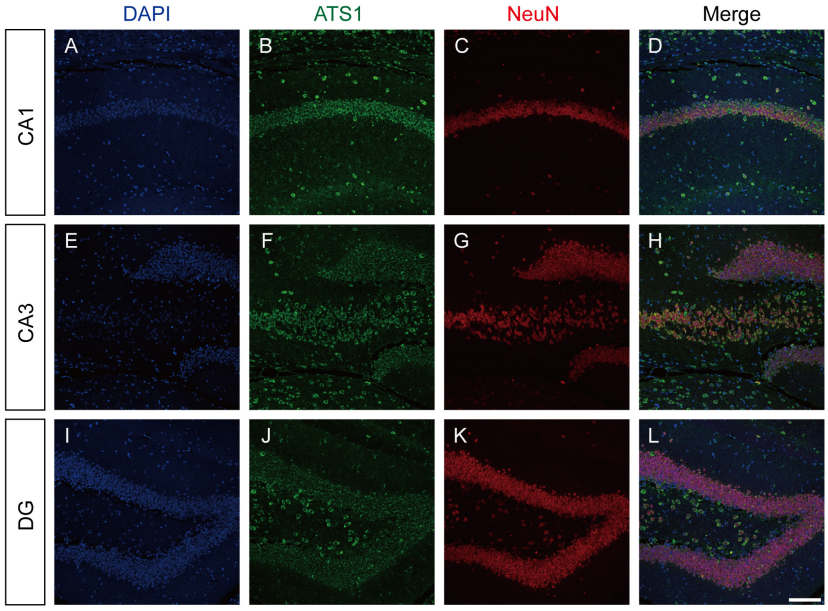

FIGURE 2
ATS1 was mainly expressed in neurons. **(A,E,I)** Nuclei were labeled by DAPI in CA1, CA3, and DG regions. **(B,F,J)** ATS1 was labeled by anti-ATS1 antibody in CA1, CA3, and DG regions. **(C,G,K)** Neurons were labeled by anti-NeuN antibody in CA1, CA3, and DG regions. **(D,H,L)** The merged images of DAPI, ATS1, NeuN revealed that neurons were the predominant source of ATS1. Scale bars, 100 μm. ATS1, ADAMTS1. DG, dentate gyrus.

the promoter activity of *ADAMTS1* (Figure 3G, $P < 0.0001$, compared with WT + zif268). Therefore, the data suggested that the induction of *ADAMTS1* by neural activities might be ascribed to the mediation of IEG zif268.

A Disintegrin and Metalloproteinase with Thrombospondin motifs 1 was involved in amyloid precursor protein metabolism

Previous studies have suggested that APP probably acts as an ECM constituent through the binding of its extracellular domain to ECM components, like heparin sulfate proteoglycans and collagen (Beher et al., 1996; Caceres and Brandan, 1997; van der Kant and Goldstein, 2015). Since *ADAMTS1* is implicated to hold associations with AD (Kunkle et al., 2019) and its product ADAMTS1 exhibits proteolytic activity (Shindo et al., 2000), we investigated whether ADAMTS1 participated in APP metabolism through co-transfecting HEK 293T cells with *swAPP* and *ADAMTS1*. Western blot data showed that the introduction of *ADAMTS1* resulted in a novel APP hydrolysate [about 75–85 kDa, soluble APP fragment cleaved by ADAMTS1 ($sAPP_{ATS1}$)] accompanying traditionally recognized ones (Figure 4A). Moreover, ADAMTS1 expression caused an apparent decrease in sAPPs, CTFs and secreted Aβs simultaneously (Figures 4A,B, $P < 0.01$, compared with mock control). All these results demonstrated preliminarily the involvement of ADAMTS1 in APP proteolytic processing.

To verify the involvement, two types of site-directed mutations were introduced into the active center of ADAMTS1 (Alanine or Glutamine replacing Glutamate, E402A or E402Q) (Rodriguez-Manzaneque et al., 2002). Unsurprisingly, the mutants failed to generate $sAPP_{ATS1}$ and conventional products returned to control level in the E402Q system (Figures 4C,D, $P < 0.05$, compared with ADAMTS1 group). Additionally, as shown in Figure 4E, consistent results were obtained from *ADAMTS1*-infected primary neurons, in which $sAPP_{ATS1}$ appeared and conventional products showed clear attenuation ($P < 0.01$, compared with control group). Meanwhile, with the concentration of rAAV-*ADAMTS1*, the contribution on APP cleavage strengthened (Figure 4F).

Next, we performed co-immunoprecipitation to further illustrate the interaction of APP and ADAMTS1. As shown in Supplementary Figure 3A, the interaction was confirmed reciprocally using ADAMTS1 (FLAG) and APP (Myc) antibodies. Specially, the positive result was only observed in the plasma membrane fraction (Figure 5A). Furthermore, when primary neurons were exposed to the supernatant of *ADAMTS1*-transfected HEK 293T cell culture, the appearance of $sAPP_{ATS1}$ and the sharp decrease of conventional products ($P < 0.05$, compared with mock control) of primary neurons (clearly different from endogenous sAPPs of HEK 293T cells with higher molecular weight (Koch et al., 2012; Supplementary Figure 3B and Figure 5B) were still observed although the

10.3389/fnagi.2022.896522

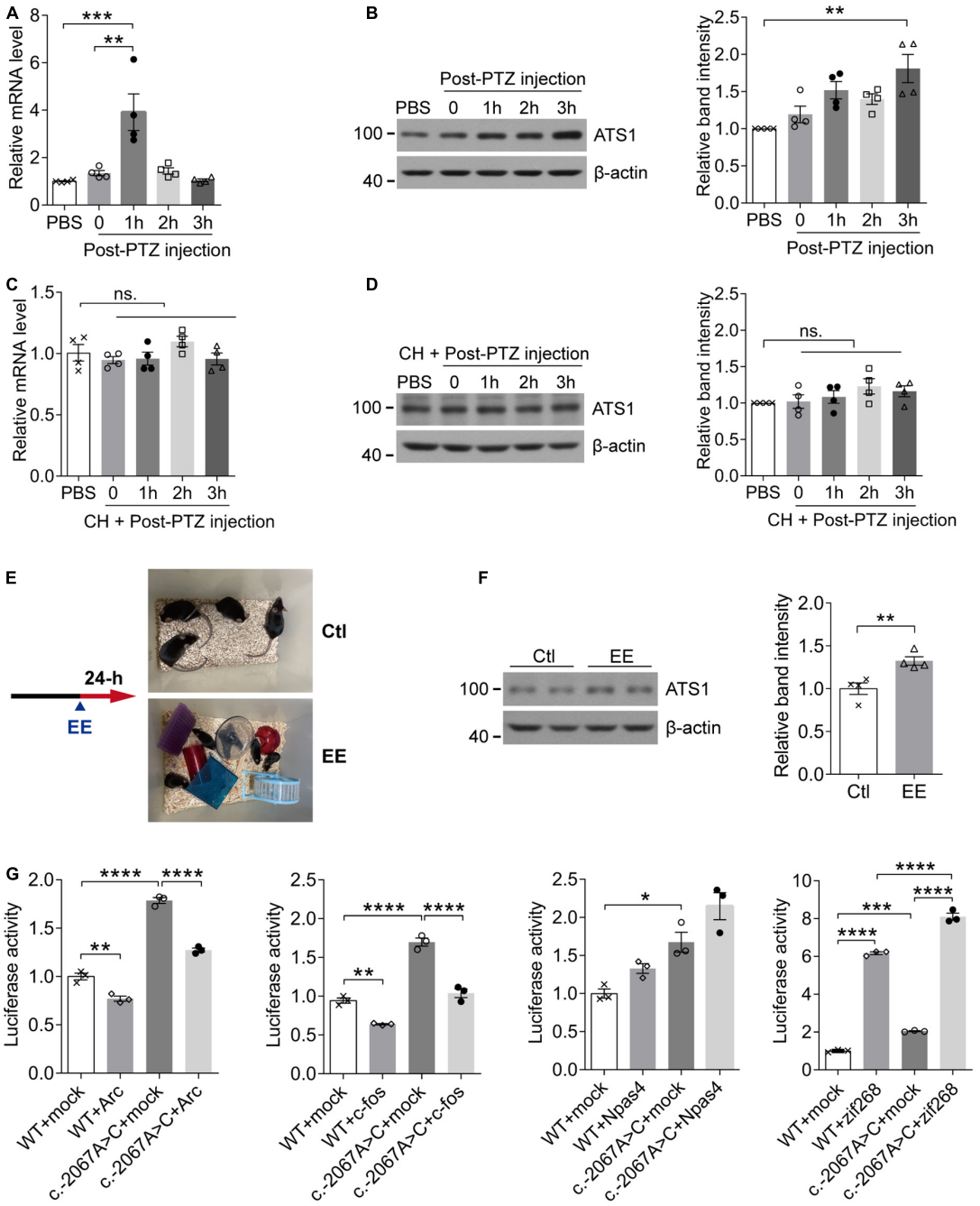

FIGURE 3

The activity-dependent expression pattern of *ATS1* through the potential mediation of zif268. **(A,B)** Ten week-old WT male mice were intraperitoneally injected with PTZ to induce synaptic activation and sacrificed at different timepoints. **(A)** The *Ats1* mRNA was significantly induced 1-h post-injection ($n = 4$, $P < 0.001$, 1 h vs. PBS; $P < 0.01$, 1 h vs. 0, one-way ANOVA). **(B)** Western blot of ATS1 at different timepoints. The relative band intensities showed that ATS1 was obviously upregulated 3-h post-injection ($n = 4$, $P < 0.01$, 3 h vs. PBS, Kruskal-Wallis test). **(C,D)** Ten week-old WT male mice were intraperitoneally injected with CH 30 min before PTZ administration and sacrificed at different timepoints. No significant difference was detected for *Ats1* **(C)** mRNA or **(D)** protein levels when compared with PBS group ($n = 4$, one-way ANOVA). **(E)** Scheme of EE experiments. **(F)** Western blot of ATS1 in hippocampus after 24-h EE-housing. The relative band intensities indicated upregulated expression of ATS1 ($n = 4$, $P < 0.01$, EE vs. Ctl, Student's *t*-test). **(G)** HEK 293T cells transfected with the *ATS1* promoter (WT or c.−2067A > C) and immediate early gene plasmids *ARC*, *FOS*, *NPAS4,* or *ZIF268* were subjected to the dual-luciferase assay. The relative luciferase activity demonstrated that zif268 multiplied *ATS1* promoter activity significantly ($n = 3$, $P < 0.0001$, WT + zif268 vs. WT + mock; $P < 0.0001$, c.−2067A > C + zif268 vs. c.−2067A > C + mock; $P < 0.0001$, c.−2067A > C + zif268 vs. WT + zif268, one-way ANOVA). $^{*}P < 0.05$, $^{**}P < 0.01$, $^{***}P < 0.001$, $^{****}P < 0.0001$. Data were expressed as Mean ± SEM. ATS1, ADAMTS1; CH, chloral hydrate; ns., no significance; Ctl, control; EE, enriched environment; PTZ, pentylenetetrazol; WT, wild type; mock, empty vector.

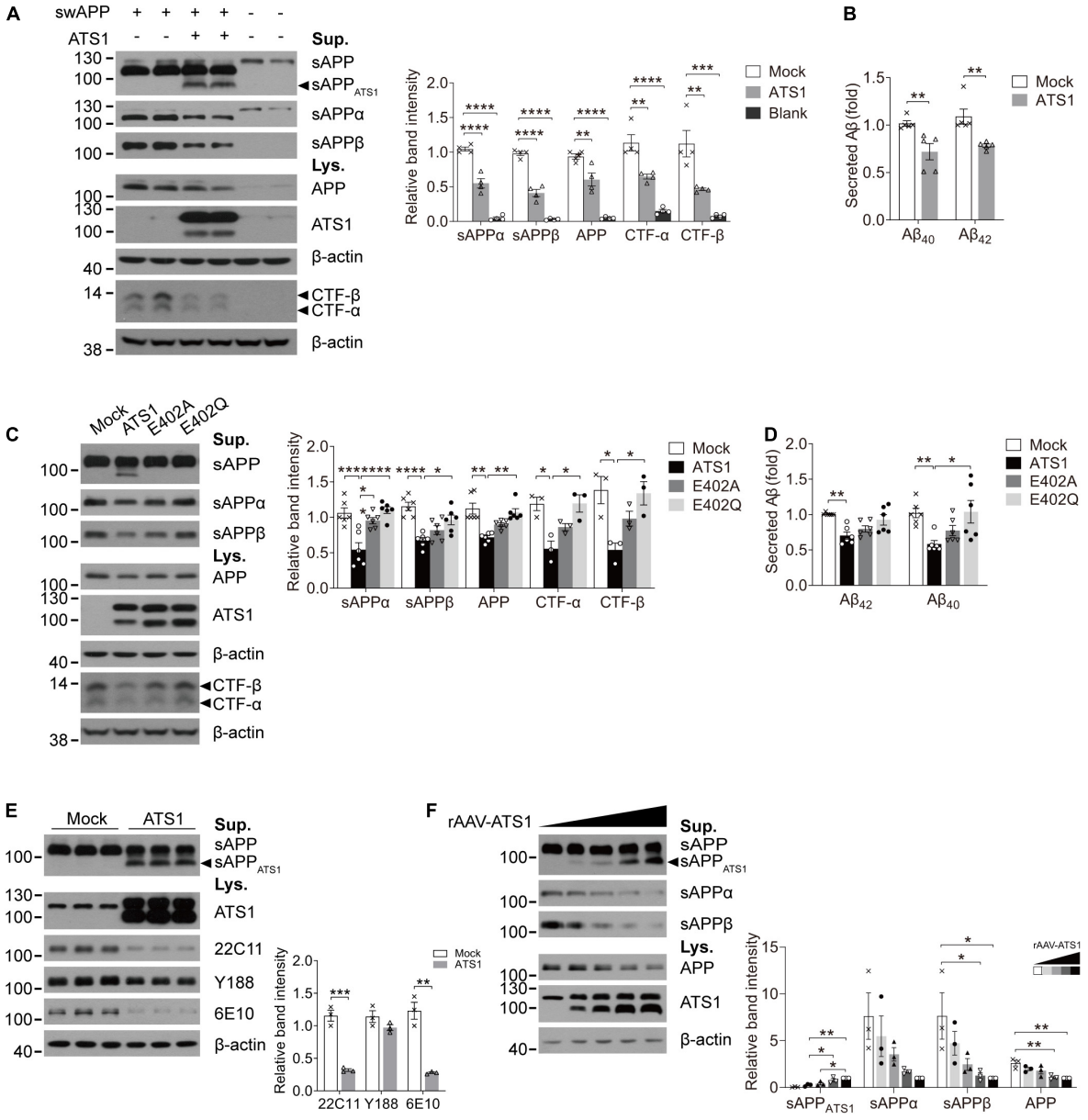

FIGURE 4
ATS1 contributed to APP metabolism and thereby decreased the generation of conventional products. **(A,B)** HEK 293T cells were co-transfected with *swAPP* and *ATS1* plasmids. **(A)** Western blot of APP pathway proteins (sAPP, sAPPα, sAPPβ, APP, and CTFs). A new fragment named sAPP$_{ATS1}$ was observed and the relative band intensities indicated that the conventional cleavage of α and β-secretases was suppressed ($n = 4$, sAPPα, $P < 0.0001$, ATS1 vs. Mock; sAPPβ, $P < 0.0001$, ATS1 vs. Mock; APP, $P < 0.01$, ATS1 vs. Mock; CTF-α, $P < 0.01$, ATS1 vs. Mock; CTF-β, $P < 0.01$, ATS1 vs. Mock, one-way ANOVA). **(B)** ELISA quantification revealed a reduction in Aβ$_{40}$ and Aβ$_{42}$ in the conditioned medium ($n = 5$, Aβ$_{40}$, $P < 0.01$, ATS1 vs. Mock; Aβ$_{42}$, $P < 0.01$, ATS1 vs. Mock, Mann-Whitney *U*-test). **(C,D)** Two types of *ATS1* mutants with site-directed mutations at the active center and *swAPP* were transfected into HEK 293T cells. **(C)** Western blot of APP pathway proteins (sAPP, sAPPα, sAPPβ, APP, and CTFs). The new fragment sAPP$_{ATS1}$ disappeared and the relative band intensities demonstrated that conventional products returned to control level in the E402Q system ($n = 6$, sAPPα, $P < 0.001$, ATS1 vs. Mock, $P < 0.0001$, E402Q vs. ATS1; sAPPβ, $P < 0.0001$, ATS1 vs. Mock, $P < 0.05$, E402Q vs. ATS1; APP, $P < 0.01$, ATS1 vs. Mock, $P < 0.01$, E402Q vs. ATS1; $n = 3$, CTF-α, $P < 0.05$, ATS1 vs. Mock, $P < 0.05$, E402Q vs. ATS1; CTF-β, $P < 0.05$, ATS1 vs. Mock, $P < 0.05$, E402Q vs. ATS1, one-way ANOVA or Kruskal-Wallis test). Specially, the CTFs were examined as verification and thus three replicates were conducted on Tris-tricine SDS-PAGE. **(D)** ELISA quantification showed the recovery of Aβ in E402Q conditioned medium when compared with ATS1 group ($n = 6$, Aβ$_{40}$, $P < 0.01$, ATS1 vs. Mock, $P < 0.05$, E402Q vs. ATS1; Aβ$_{42}$, $P < 0.01$, ATS1 vs. Mock, Kruskal-Wallis test). **(E)** Primary neurons were infected with rAAV-*ATS1* or Mock. Western blot was performed to analyze APP using three different antibodies. The relative band intensities showed that APP cleavage by ATS1 was identified by two antibodies ($n = 3$, 22C11, $P < 0.001$, ATS1 vs. Mock; 6E10, $P < 0.01$, ATS1 vs. Mock, Student's *t*-test). **(F)** Primary neurons were infected with serially diluted rAAV-*ATS1*. Western blot showed that the contribution of ATS1 to APP cleavage strengthened with the concentration of rAAV-*ATS1* ($n = 3$, one-way ANOVA). Data were expressed as Mean ± SEM. *$P < 0.05$, **$P < 0.01$, ***$P < 0.001$, ****$P < 0.0001$. ATS1, ADAMTS1; Lys., lysates; Sup., supernatant; swAPP, human APP Swedish mutation; Mock, empty vector.

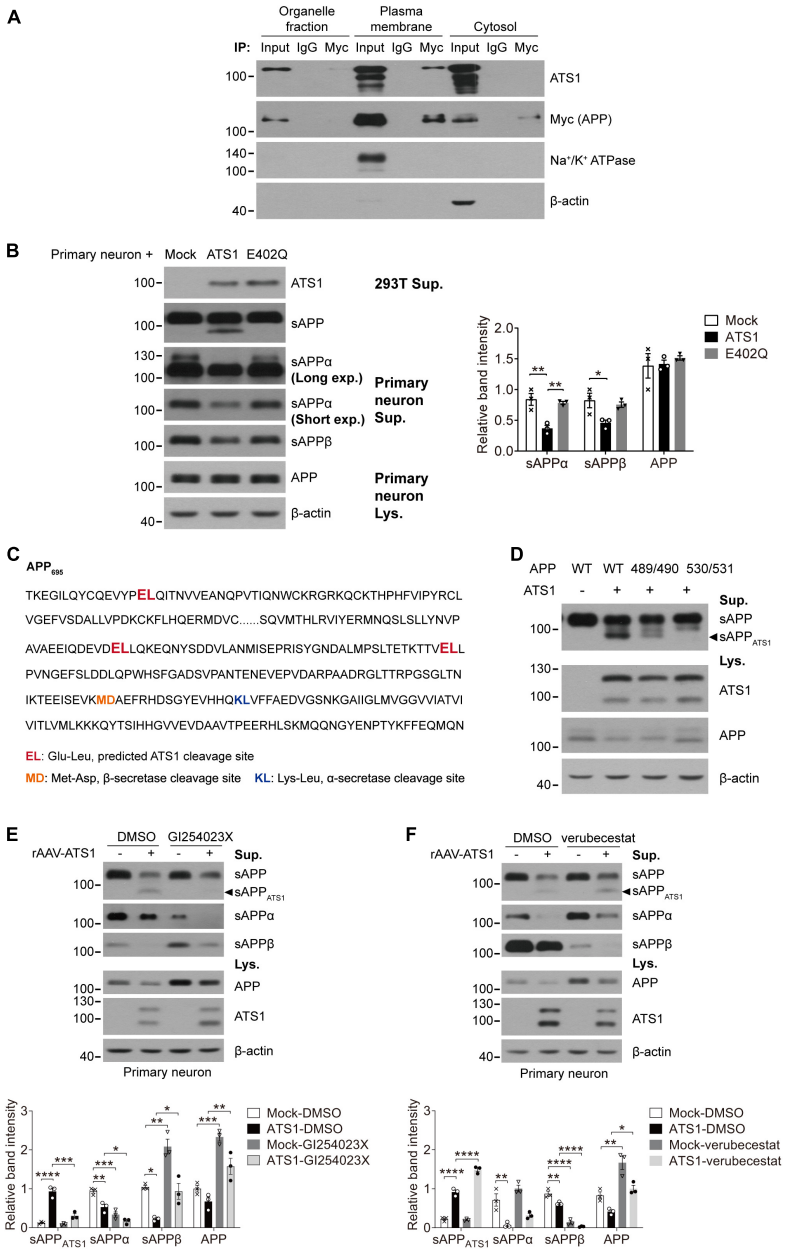

FIGURE 5

ATS1 hydrolyzed APP in plasma membrane at E530/L531 site and competed with BACE1. **(A)** HEK 293T cells transfected with *APP* and *ATS1* were subjected to cellular component separation and subsequent co-immunoprecipitation using Myc tag (APP) antibody. Western blot showed that the interaction of ATS1 and APP mainly occurred at the plasma membrane (labeled by Na^+/K^+ ATPase). **(B)** Primary neurons were treated with conditioned medium from HEK 293T cells transfected with mock, *ATS1* or *E402Q* mutant and subjected to western blot of APP pathway proteins sAPP, sAPPα, sAPPβ, and APP. The relative band intensities of cleavage products were shown. Primary neurons exposed to the supernatant of *ATS1*-transfected HEK 293T cell culture produced $sAPP_{ATS1}$ and exhibited reduced levels of conventional products when compared with mock control or *E402Q*-transfected group ($n = 3$, sAPPα, $P < 0.01$, ATS1 vs. Mock, $P < 0.01$, E402Q vs. ATS1; sAPPβ, $P < 0.05$, ATS1 vs. Mock, one-way ANOVA). Moreover, long exposure time resulted in the detection of endogenous sAPPα of HEK 293T cells with lower protein level but higher molecular weight. **(C)** Predicted ATS1 cleavage sites were shown (emphasized in red), and the latter two sites E489/L490 and E530/L531 within amino acids 420–580 of APP_{695} were selected as the potential targets of ATS1. **(D)** HEK 293T cells were transfected with APP mutants holding A489/A490 or A530/A531. Western blot analysis showed that $sAPP_{ATS1}$ was erased in A530/A531 group. **(E,F)** Primary neurons infected with rAAV-*ATS1* were treated with ADAM10 inhibitor GI254023X (20 μM) or BACE1 inhibitor verubecestat (1 μM) for 48 h. Western blot of APP pathway proteins ($sAPP_{ATS1}$, sAPPα, sAPPβ, and APP) was shown. The relative band intensities of $sAPP_{ATS1}$ revealed the potential competition between ATS1 and BACE1 [**(E)** $n = 3$, $sAPP_{ATS1}$, $P < 0.001$, ATS1-GI254023X vs. ATS1-DMSO, one-way ANOVA; **(F)** $n = 3$, $sAPP_{ATS1}$, $P < 0.0001$, ATS1-verubecestat vs. ATS1-DMSO, one-way ANOVA]. $^*P < 0.05$, $^{**}P < 0.01$, $^{***}P < 0.001$, $^{****}P < 0.0001$. Data were expressed as Mean ± SEM. ATS1, ADAMTS1; IP, immunoprecipitation; Lys., lysates; Sup., supernatant; Mock, empty vector; Long exp., long exposure time; Short exp., short exposure time; WT, wild type; 489/490, A489/A490; 530/531, A530/A531.

full-length APP showed no obvious variations (Figure 5B). This phenomenon did not happen when the supernatant was from cells containing the E402Q mutation (Figure 5B), suggesting that ADAMTS1 was a secretase.

It has been reported that ADAMTS1 cleaves the covalent bond between Glutamate and Leucine (Rodriguez-Manzaneque et al., 2002; Westling et al., 2002). We screened the APP sequence and found three Glu-Leu sites (Figure 5C, emphasized in red). As the molecular mass of $sAPP_{ATS1}$ was about 75–85 kDa, the latter two Glu-Leu sites (E489/L490 and E530/L531, Figure 5C) within amino acids 420–580 of APP_{695} were selected as potential targets of ADAMTS1. By exposing APP_{695} mutants A489/A490 and A530/A531 to *ADAMTS1*-containing HEK 293T cells, the absence of $sAPP_{ATS1}$ fragments in conditioned medium suggested that the cleavage site might be E530/L531 (Figure 5D). Additionally, the $sAPP_{ATS1}$ fragments in A489/A490 also showed a decline, but full-length APP in cell lysate held the same level as WT control (Figure 5D). It was speculated that the mutation within E489/L490 might cause some modest structural modification of APP and thus partially limit ADAMTS1's cleavage. However, further investigations should still be conducted using purified APP mutant and ADAMTS1 protein to verify the exact cleavage site.

While investigating protease inhibitors affecting ADAMTS1, we observed that the ADAM10 inhibitor GI254023X contributed to the downregulation of $sAPP_{ATS1}$ (Supplementary Figure 3C and Figure 5E, $P < 0.05$, compared with DMSO group), and BACE1 inhibitor verubecestat resulted in accumulated $sAPP_{ATS1}$ in HEK 293T cells and primary neurons (Supplementary Figure 3D and Figure 5F, $P < 0.001$, compared with DMSO group). Collectively, the data indicated that ADAMTS1 and BACE1 competed for the same substrate.

The cognition of 5 × FAD mice was alleviated by hippocampal high-level *A Disintegrin and Metalloproteinase with Thrombospondin motifs 1* through the attenuation of amyloid load

Given that ADAMTS1 affected APP metabolism and reduced Aβ, we explored whether high-level ADAMTS1 improved the cognitive performance of 5 × FAD mice. To this end, the stereotaxic injection and subsequent Morris water maze test were performed (Figure 6A). The expression of *ADAMTS1-FLAG* was validated in Figure 6B. After 5 days of training, 5 × FAD mice without *ADAMTS1* still spent much more time (approximately 40 s) on locating the platform (Figures 6C,D, $P < 0.05$, compared with other groups) than those expressing *ADAMTS1*. Moreover, in the probe trial, *ADAMTS1*-transfected mice exhibited an apparent upward trend in the probability of finding the correct quadrant (Figure 6E). These results suggested that ADAMTS1 brought improvement to the cognitive functions of 5 × FAD mice.

Aβ-related proteins in 5 × FAD mice with and without *ADAMTS1* were examined to further explore the underlying mechanism of cognitive improvement. As shown in Figure 6F, consistent results were obtained from *in vivo* studies: $sAPP_{ATS1}$ appeared and full-length APP showed clear downregulation. Moreover, the further check on conventional sAPPs and CTFs demonstrated that the β-cleavage in 5 × FAD mice significantly reduced and meanwhile APP hydrolysates resulted from α-secretase also exhibited downward trends (Figures 6F,G). Additionally, the western blot result of CTF_{ATS1} illustrated its accumulation which corresponded to that of $sAPP_{ATS1}$ (Figure 6G).

Moreover, the amyloid burden was also mitigated by ADAMTS1 expression, which was revealed by the decreased Aβ-positive area in hippocampus expressing *ADAMTS1* (Figure 6H). In addition, a sharp reduction in Aβs was also certified by ELISA data (Figure 6I, compared with mock control), further confirming the effects of ADAMTS1 on Aβ lessening.

Discussion

In this study, we first identified that a rare SNP c.–2067A > C of *ADAMTS1* potentially correlated with a reduced risk of AD, and that the novel variant and cognitive activities could significantly stimulate *ADAMTS1* expression. Further functional studies demonstrated that elevated ADAMTS1 transferred APP metabolism thus leading to reduced soluble Aβ generation. Moreover, the spatial cognition of AD mice was notably alleviated in the Morris water maze test through the reduction of Aβ plaques.

The progressive AD is now regarded as the leading cause of dementia and is partially driven by genetics. Previous GWAS has identified a large number of susceptibility loci for AD, like SNP "rs75932628" coding R47H substitution of TREM2 (Guerreiro et al., 2013; Jonsson et al., 2013). The R47H variant results in function-lost protein, although it possesses an extremely low MAF (Yeh et al., 2016; Song et al., 2017). Similar pattern seemed to be present here, that was, though the rare variant c.–2067A > C at *ADAMTS1* promoter had an MAF of 0.26%, it triggered enhanced fundamental transcription of *ADAMTS1*. However, given the limitation of sample size in identifying rare variants, the correlation of c.–2067A > C with AD still requires larger-scale cohort for further analysis.

In the past decade, nearly no monoclonal antibody targeting Aβ has succeeded in clinical trials, which raises the debates about Aβ's central role in AD. However, the amyloid hypothesis

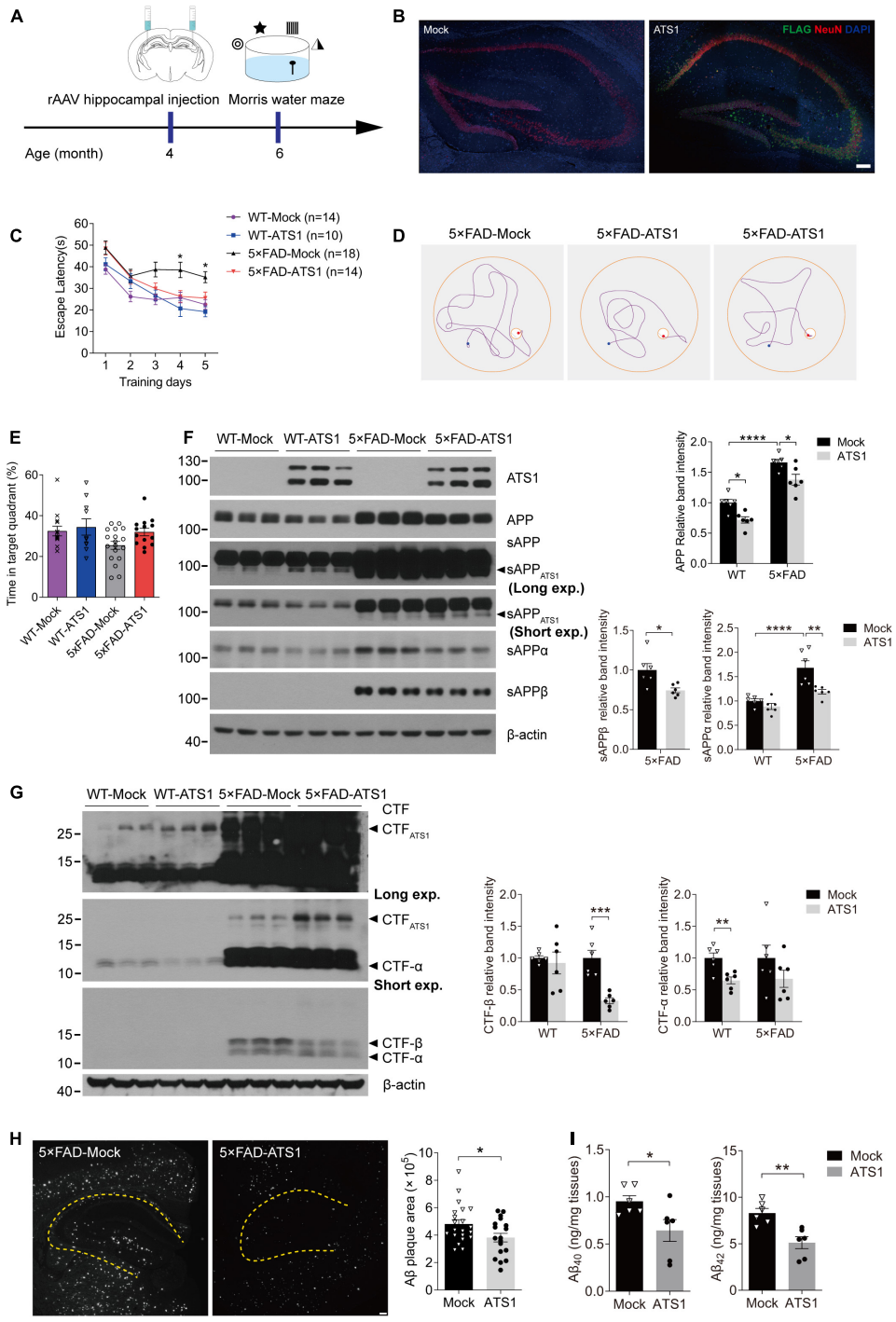

FIGURE 6

High-level ATS1 in hippocampus attenuated amyloid load of 5 × FAD mice and improved the cognitive behavior. **(A)** Scheme of rAAV injection and Morris water maze test performed on 5 × FAD mice. **(B)** Expression of rAAV-*ATS1-FLAG* and Mock. Nuclei (by DAPI), ATS1 (by FLAG), neuron (by NeuN) were labeled in hippocampus. Scale bars, 100 μm. (**C–E**) Morris water maze tests were performed on WT and 5 × FAD mice 2 months after injection of rAAV ($n = 14$ for WT-Mock, $n = 10$ for WT-ATS1, $n = 18$ for 5 × FAD-Mock and $n = 14$ for 5 × FAD-ATS1). **(C)** The escape latency was recorded during the 5-day training, showing that 5 × FAD mice with ATS1 spent less time during the learning trial when compared with mock control [DAY 4, $P < 0.05$, 5 × FAD-ATS1 vs. 5 × FAD-Mock; DAY 5, $P < 0.05$, 5 × FAD-ATS1 vs. 5 × FAD-Mock. Two-way repeated measures ANOVA, day × group $F(3, 52) = 1.153$, $P > 0.05$, no significant interaction; group $F(3, 52) = 16.820$, $P < 0.0001$]. **(D)** Representative navigation routes of 5 × FAD-Mock and 5 × FAD-ATS1 mice to the hidden platform during the last day of training. **(E)** The probe trial was performed 24 h after the last trial of hidden platform task, and the percentage of searching time in the target quadrant indicated that

(Continued)

FIGURE 6
ATS1-transfected mice exhibited an apparent upward trend in the probability of finding the target quadrant (Kruskal-Wallis test). **(F)** Western blot of APP pathway proteins in WT and 5 × FAD mice infected with rAAV-*ATS1-FLAG* or Mock was shown. The relative band intensities showed reduced APP and sAPPβ levels in ATS1 group when compared with respective mock control and sAPPα also exhibited a downward trend ($n = 6$, APP in WT, $P < 0.05$, ATS1 vs. Mock; APP in 5 × FAD, $P < 0.05$, ATS1 vs. Mock; sAPPα in 5 × FAD, $P < 0.01$, ATS1 vs. Mock; sAPPβ in 5 × FAD, $P < 0.05$, ATS1 vs. Mock, one-way ANOVA or Student's *t*-test). **(G)** Western blot of CTFs in WT and 5 × FAD mice infected with rAAV-*ATS1-FLAG* or Mock was shown. The relative band intensities revealed the accumulation of CTF_{ATS1} and reduced CTFs levels in ATS1 group when compared with respective mock control ($n = 6$, CTF-β in 5 × FAD, $P < 0.001$, ATS1 vs. Mock; CTF-α in WT, $P < 0.01$, ATS1 vs. Mock, Student's *t*-test). **(H)** Immunofluorescence showing Aβ plaques in the hippocampus. Scale bar, 100 μm. Quantification of the surface area of Aβ plaques demonstrated the mitigated pathology by *ATS1* overexpression ($n = 7$ for 5 × FAD-Mock and $n = 6$ for 5 × FAD-ATS1, $P < 0.05$, ATS1 vs. Mock, Student's *t*-test). **(I)** ELISA quantification of $Aβ_{40}$ and $Aβ_{42}$ in hippocampus lysates from 6-month-old mice certified the reduction of total Aβs caused by ATS1 ($n = 6$, $Aβ_{40}$, $P < 0.05$, ATS1 vs. Mock; $Aβ_{42}$, $P < 0.01$, ATS1 vs. Mock, Student's *t*-test). $^{*}P < 0.05$, $^{**}P < 0.01$, $^{***}P < 0.001$, $^{****}P < 0.0001$. Data were expressed as Mean ± SEM. ATS1, ADAMTS1; WT, wild type; Long exp., long exposure time; Short exp., short exposure time.

refers to a continuous process lasting for 15–20 years before the onset of clinical symptoms (Rowe et al., 2010; Zhao et al., 2020), and thereby AD may begin much long before the so-called "early clinical stage" (Brookmeyer et al., 2018). This delay may lead to the pathogenic deposition of Aβ plaques in patients' brains and consequent failure of antibody treatment. Considering the involvement of ADAMTS1 in APP metabolism, its relatively higher protein level resulted from the genetic variant or enriched cognitive activities might make carriers benefit during the early life.

Disrupting the process of APP cleavage to reduce Aβ generation represents an approach to delay AD. Based on this, BACE1 inhibitors have been developed. However, BACE1 has substrates other than APP, such as Jagged 1 (Hu et al., 2013), neuregulin 1 (Savonenko et al., 2008), and seizure-related protein 6 (Pigoni et al., 2016), and BACE1 cleavage is essential for their physiological functions. Thus, the clinical potential of current BACE1 inhibitors is largely limited due to numerous side effects through suppressing the cleavage of untargeted substrates. Therefore, competing with BACE1 for APP processing may serve as an attractive alternative. After ADAMTS1 cleavage at E530/L531, the CTF_{ATS1} (531–695 amino acids) still contained BACE1 site. However, the observed reduction of Aβ and CTF-β indicated that BACE1 could not further process CTF_{ATS1}, suggesting that this fragment might not have accessible spatial structure for BACE1. On the other hand, previous studies have indicated that BACE1 primarily hydrolyzes APP within endosomes (Sannerud et al., 2011; Buggia-Prevot et al., 2013) and the internalization of APP from plasma membrane to endosomes is essential for BACE1 cleavage (Shahani et al., 2015; Yi et al., 2021). Considering the fractionation results that APP-ADAMTS1 interaction mainly occurred on plasma membranes, the binding of APP to ADAMTS1 might inhibit its transport and consequently block BACE1 cleavage.

When cells were treated with ADAM10 inhibitor, the decrease in $sAPP_{ATS1}$ indicated limited cleavage of APP by ADAMTS1. Previous studies have shown that ADAMTS1 and ADAM10 own common tissue inhibitor TIMP-3 of which N-terminal residue blocks the active site of enzyme (Baker et al., 2002; Murphy and Nagase, 2008). Thus, the use of GI254023X might simultaneously inhibit ADAMTS1 while acting on ADAM10 cleavage. Additionally, ADAMTS1 and ADAM10 belong to ADAM family who has both disintegrin and zinc endopeptidases domains (Brocker et al., 2009), which implies that they may function on ECM and adhesion molecules (Greening et al., 2015; Shimoda et al., 2021) by similar approach. Therefore, these two enzymes might compete resulting in reduced α-cleavage in ADAMTS1-overexpressed condition.

Actually, cognitive functions are affected by multiple factors including aging, education, and cognitive activities (Phillips, 2017; Yu et al., 2020). Numerous studies focusing on cognitive reserve have shown the retardant beneficial effects of an active lifestyle on cognitive decline in the elderly (Wilson et al., 2002, 2007). Recent clinical data have also repeatedly emphasized that frequent stimuli on cognition of the elderly may delay the onset of AD by as long as 5 years (Wilson et al., 2021). However, the underlying mechanism through which cognitive activities and cognitive functions are bridged remains unclear. As to experimental mice, cognitive activities can be performed in the so-called EE where mice receive physical, cognitive, and social stimulation. We found that ADAMTS1 was clearly upregulated by EE-housing, which verified the speculation that *ADAMTS1* was induced as a result of neuronal activities involved in cognitive events. Moreover, our findings demonstrated that the promoter activity of *ADAMTS1* was clearly induced by IEG zif268. This result suggested the correlation between gene expression and IEG-associated stimulus. Accumulated studies have also reported that zif268 expression is sensitive to specific learning paradigms such as spatial memory, object recognition memory and so on. Deficiency of zif268 severely damages the cognitive performance in different behavioral tests (Gallo et al., 2018). Moreover, it is reported that a mouse model suffering from neurodegenerative disease in long-term EE shows notably attenuated progression and ameliorated amyloid load (Lazarov et al., 2005; Hu et al., 2010). Considering all the above results, we speculated that zif268 played a key role in the bridge of cognitive

activities and *ADAMTS1* expression, and in this way delayed the disease progression.

In summary, based on the association of *ADAMTS1* with AD implied by GWAS, our work illuminated for the first time the significant role of ADAMTS1 as an APP hydrolase that connected both genetic susceptibility and acquired activities with amyloid processing, which might be instructive on further understanding the complex pathogenesis of AD.

Data availability statement

The original contributions presented in the study are included in the article/**Supplementary material**, further inquiries can be directed to the corresponding author/s.

Ethics statement

The studies involving human participants were reviewed and approved by the Institutional Review Board of Chinese Academy of Medical Sciences and Peking Union Medical College. The patients/participants provided their written informed consent to participate in this study. The animal study was reviewed and approved by the Institutional Review Board of Chinese Academy of Medical Sciences and Peking Union Medical College.

Author contributions

QX and LS designed the research. YQ, XZ, and GL performed the experiments. WZ performed statistics. YQ wrote the manuscript. All authors contributed to the article and approved the submitted version.

Funding

This work was supported by research grants from the National Key Research and Development Program of China (2020YFA0804502), the Ministry of Science and Technology of the People's Republic of China (2021ZD0203001, 2022ZD0211700, 2021ZD0200600, and 2021ZD0202000), the National Natural Science Foundation of China (81930104, 82171447, and 81871011), the CAMS Innovation Fund for Medical Sciences (2021-I2M-1-020), and the Science and Technology Program of Guangdong (2018B030334001).

Conflict of interest

The authors declare that the research was conducted in the absence of any commercial or financial relationships that could be construed as a potential conflict of interest.

The reviewer Y-CZ declared a shared parent affiliation with the authors to the handling editor at the time of review.

Publisher's note

All claims expressed in this article are solely those of the authors and do not necessarily represent those of their affiliated organizations, or those of the publisher, the editors and the reviewers. Any product that may be evaluated in this article, or claim that may be made by its manufacturer, is not guaranteed or endorsed by the publisher.

Supplementary material

The Supplementary Material for this article can be found online at: https://www.frontiersin.org/articles/10.3389/fnagi.2022.896522/full#supplementary-material

References

Alexander, D. S., Alfonso, M. L., Cao, C., and Wright, A. R. (2017). Do Maternal Caregiver Perceptions of Childhood Obesity Risk Factors and Obesity Complications Predict Support for Prevention Initiatives Among African Americans? *Matern. Child. Health J.* 21, 1522–1530. doi: 10.1007/s10995-017-2277-0

Baker, A. H., Edwards, D. R., and Murphy, G. (2002). Metalloproteinase inhibitors: Biological actions and therapeutic opportunities. *J. Cell Sci.* 115, 3719–3727. doi: 10.1242/jcs.00063

Beher, D., Hesse, L., Masters, C. L., and Multhaup, G. (1996). Regulation of amyloid protein precursor (APP) binding to collagen and mapping of the binding sites on APP and collagen type I. *J. Biol. Chem,* 271, 1613–1620. doi: 10.1074/jbc.271.3.1613

Bellenguez, C., Kucukali, F., Jansen, I. E., Kleineidam, L., Moreno-Grau, S., Amin, N., et al. (2022). New insights into the genetic etiology of Alzheimer's disease and related dementias. *Nat. Genet.* 54, 412–436. doi: 10.1038/s41588-022-01024-z

Bozon, B., Davis, S., and Laroche, S. (2003). A requirement for the immediate early gene zif268 in reconsolidation of recognition memory after retrieval. *Neuron* 40, 695–701. doi: 10.1016/s0896-6273(03)00674-3

Brocker, C. N., Vasiliou, V., and Nebert, D. W. (2009). Evolutionary divergence and functions of the ADAM and ADAMTS gene families. *Hum. Genom.* 4, 43–55. doi: 10.1186/1479-7364-4-1-43

Brookmeyer, R., Abdalla, N., Kawas, C. H., and Corrada, M. M. (2018). Forecasting the prevalence of preclinical and clinical Alzheimer's disease in the United States. *Alzheimers Dement.* 14, 121–129. doi: 10.1016/j.jalz.2017.10.009

Buggia-Prevot, V., Fernandez, C. G., Udayar, V., Vetrivel, K. S., Elie, A., Roseman, J., et al. (2013). A function for EHD family proteins in

unidirectional retrograde dendritic transport of BACE1 and Alzheimer's disease Abeta production. *Cell Rep.* 5, 1552–1563. doi: 10.1016/j.celrep.2013.12.006

Caceres, J., and Brandan, E. (1997). Interaction between Alzheimer's disease beta A4 precursor protein (APP) and the extracellular matrix: Evidence for the participation of heparan sulfate proteoglycans. *J. Cell. Biochem.* 65, 145–158. doi: 10.1002/(sici)1097-4644(199705)65:2<145::aid-jcb2<3.0.co;2-u

Cheng, Z., Yang, W., Li, B., and Cui, R. (2021). KLF4 Exerts Sedative Effects in Pentobarbital-Treated Mice. *J. Mol. Neurosci.* 71, 596–606. doi: 10.1007/s12031-020-01680-y

Ellenberger, L., Oberle, F., Lorenzetti, S., Frey, W. O., Snedeker, J. G., and Sporri, J. (2020). Dynamic knee valgus in competitive alpine skiers: Observation from youth to elite and influence of biological maturation. *Scand. J. Med. Sci. Sports* 30, 1212–1220. doi: 10.1111/sms.13657

Flood, W. D., Moyer, R. W., Tsykin, A., Sutherland, G. R., and Koblar, S. A. (2004). Nxf and Fbxo33: Novel seizure-responsive genes in mice. *Eur. J. Neurosci.* 20, 1819–1826. doi: 10.1111/j.1460-9568.2004.03646.x

Gallo, F. T., Katche, C., Morici, J. F., Medina, J. H., and Weisstaub, N. V. (2018). Immediate Early Genes. Memory and Psychiatric Disorders: Focus on c-Fos, Egr1 and Arc. *Front. Behav. Neurosci.* 12:79. doi: 10.3389/fnbeh.2018.00079

Greening, D. W., Gopal, S. K., Mathias, R. A., Liu, L., Sheng, J., Zhu, H. J., et al. (2015). Emerging roles of exosomes during epithelial-mesenchymal transition and cancer progression. *Semin. Cell Dev. Biol.* 40, 60–71. doi: 10.1016/j.semcdb.2015.02.008

Guerreiro, R., Wojtas, A., Bras, J., Carrasquillo, M., Rogaeva, E., Majounie, E., et al. (2013). TREM2 variants in Alzheimer's disease. *N. Engl. J. Med.* 368, 117–127. doi: 10.1056/NEJMoa1211851

Hanseeuw, B. J., Betensky, R. A., Jacobs, H. I. L., Schultz, A. P., Sepulcre, J., Becker, J. A., et al. (2019). Association of Amyloid and Tau With Cognition in Preclinical Alzheimer Disease: A Longitudinal Study. *JAMA Neurol.* 76, 915–924. doi: 10.1001/jamaneurol.2019.1424

Hu, X., He, W., Luo, X., Tsubota, K. E., and Yan, R. (2013). BACE1 regulates hippocampal astrogenesis via the Jagged1-Notch pathway. *Cell Rep.* 4, 40–49. doi: 10.1016/j.celrep.2013.06.005

Hu, Y. S., Xu, P., Pigino, G., Brady, S. T., Larson, J., and Lazarov, O. (2010). Complex environment experience rescues impaired neurogenesis, enhances synaptic plasticity, and attenuates neuropathology in familial Alzheimer's disease-linked APPswe/PS1DeltaE9 mice. *FASEB. J.* 24, 1667–1681. doi: 10.1096/fj.09-136945

Jack, C. R. Jr., Bennett, D. A., Blennow, K., Carrillo, M. C., Dunn, B., Haeberlein, S. B., et al. (2018). NIA-AA Research Framework: Toward a biological definition of Alzheimer's disease. *Alzheimers Dement.* 14, 535–562. doi: 10.1016/j.jalz.2018.02.018

Jack, C. R. Jr., Knopman, D. S., Jagust, W. J., Shaw, L. M., Aisen, P. S., Weiner, M. W., et al. (2010). Hypothetical model of dynamic biomarkers of the Alzheimer's pathological cascade. *Lancet Neurol.* 9, 119–128. doi: 10.1016/S1474-4422(09)70299-6

Jonsson, T., Stefansson, H., Steinberg, S., Jonsdottir, I., Jonsson, P. V., Snaedal, J., et al. (2013). Variant of TREM2 associated with the risk of Alzheimer's disease. *N. Engl. J. Med.* 368, 107–116. doi: 10.1056/NEJMoa1211103

Kim, H. Y. (2013). Statistical notes for clinical researchers: Assessing normal distribution (2) using skewness and kurtosis. *Restor. Dent. Endod.* 38, 52–54. doi: 10.5395/rde.2013.38.1.52

Koch, P., Tamboli, I. Y., Mertens, J., Wunderlich, P., Ladewig, J., Stuber, K., et al. (2012). Presenilin-1 L166P mutant human pluripotent stem cell-derived neurons exhibit partial loss of gamma-secretase activity in endogenous amyloid-beta generation. *Am. J. Pathol.* 180, 2404–2416. doi: 10.1016/j.ajpath.2012.02.012

Kubik, S., Miyashita, T., and Guzowski, J. F. (2007). Using immediate-early genes to map hippocampal subregional functions. *Learn. Mem.* 14, 758–770. doi: 10.1101/lm.698107

Kunkle, B. W., Grenier-Boley, B., Sims, R., Bis, J. C., Damotte, V., Naj, A. C., et al. (2019). Genetic meta-analysis of diagnosed Alzheimer's disease identifies new risk loci and implicates Abeta, tau, immunity and lipid processing. *Nat. Genet.* 51, 414–430. doi: 10.1038/s41588-019-0358-2

Kuno, K., Okada, Y., Kawashima, H., Nakamura, H., Miyasaka, M., Ohno, H., et al. (2000). ADAMTS-1 cleaves a cartilage proteoglycan, aggrecan. *FEBS Lett.* 478, 241–245. doi: 10.1016/s0014-5793(00)01854-8

Lazarov, O., Robinson, J., Tang, Y. P., Hairston, I. S., Korade-Mirnics, Z., Lee, V. M., et al. (2005). Environmental enrichment reduces Abeta levels and amyloid deposition in transgenic mice. *Cell* 120, 701–713. doi: 10.1016/j.cell.2005.01.015

Lemarchant, S., Pruvost, M., Montaner, J., Emery, E., Vivien, D., Kanninen, K., et al. (2013). ADAMTS proteoglycanases in the physiological and pathological central nervous system. *J. Neuroinflamm.* 10:133. doi: 10.1186/1742-2094-10-133

Lin, Y., Bloodgood, B. L., Hauser, J. L., Lapan, A. D., Koon, A. C., Kim, T. K., et al. (2008). Activity-dependent regulation of inhibitory synapse development by Npas4. *Nature* 455, 1198–1204. doi: 10.1038/nature07319

Matsu-ura, T., Konishi, Y., Aoki, T., Naranjo, J. R., Mikoshiba, K., and Tamura, T. A. (2002). Seizure-mediated neuronal activation induces DREAM gene expression in the mouse brain. *Brain Res. Mol. Brain Res.* 109, 198–206. doi: 10.1016/s0169-328x(02)00562-4

Michaluk, P., Mikasova, L., Groc, L., Frischknecht, R., Choquet, D., and Kaczmarek, L. (2009). Matrix metalloproteinase-9 controls NMDA receptor surface diffusion through integrin beta1 signaling. *J. Neurosci.* 29, 6007–6012. doi: 10.1523/JNEUROSCI.5346-08.2009

Murase, S., Winkowski, D., Liu, J., Kanold, P. O., and Quinlan, E. M. (2019). Homeostatic regulation of perisynaptic matrix metalloproteinase 9 (MMP9) activity in the amblyopic visual cortex. *Elife* 8:e52503. doi: 10.7554/eLife.52503

Murphy, G., and Nagase, H. (2008). Reappraising metalloproteinases in rheumatoid arthritis and osteoarthritis: Destruction or repair? *Nat. Clin. Pract. Rheumatol.* 4, 128–135. doi: 10.1038/ncprheum0727

Nagy, V., Bozdagi, O., Matynia, A., Balcerzyk, M., Okulski, P., Dzwonek, J., et al. (2006). Matrix metalloproteinase-9 is required for hippocampal late-phase long-term potentiation and memory. *J. Neurosci.* 26, 1923–1934. doi: 10.1523/JNEUROSCI.4359-05.2006

Nguyen, P. T., Dorman, L. C., Pan, S., Vainchtein, I. D., Han, R. T., Nakao-Inoue, H., et al. (2020). Microglial Remodeling of the Extracellular Matrix Promotes Synapse Plasticity. *Cell* 38:e315. doi: 10.1016/j.cell.2020.05.050

Oveisgharan, S., Wilson, R. S., Yu, L., Schneider, J. A., and Bennett, D. A. (2020). Association of Early-Life Cognitive Enrichment With Alzheimer Disease Pathological Changes and Cognitive Decline. *JAMA Neurol.* 77, 1217–1224. doi: 10.1001/jamaneurol.2020.1941

Phillips, C. (2017). Lifestyle Modulators of Neuroplasticity: How Physical Activity, Mental Engagement, and Diet Promote Cognitive Health during Aging. *Neural Plast.* 2017:3589271. doi: 10.1155/2017/3589271

Pigoni, M., Wanngren, J., Kuhn, P. H., Munro, K. M., Gunnersen, J. M., Takeshima, H., et al. (2016). Seizure protein 6 and its homolog seizure 6-like protein are physiological substrates of BACE1 in neurons. *Mol. Neurodegener.* 11:67. doi: 10.1186/s13024-016-0134-z

Plath, N., Ohana, O., Dammermann, B., Errington, M. L., Schmitz, D., Gross, C., et al. (2006). Arc/Arg3.1 is essential for the consolidation of synaptic plasticity and memories. *Neuron* 52, 437–444. doi: 10.1016/j.neuron.2006.08.024

Porter, S., Clark, I. M., Kevorkian, L., and Edwards, D. R. (2005). The ADAMTS metalloproteinases. *Biochem. J.* 386(Pt 1), 15–27. doi: 10.1042/BJ20040424

Qiu, H., Jin, G. Q., Jin, R. F., and Zhao, W. K. (2007). [Analysis of variance of repeated data measured by water maze with SPSS]. *Zhong Xi Yi Jie He Xue Bao* 5, 101–105. doi: 10.3736/jcim20070121

Reschke, C. R., Silva, L. F. A., Norwood, B. A., Senthilkumar, K., Morris, G., Sanz-Rodriguez, A., et al. (2017). Potent Anti-seizure Effects of Locked Nucleic Acid Antagomirs Targeting miR-134 in Multiple Mouse and Rat Models of Epilepsy. *Mol. Ther. Nucleic Acids* 6, 45–56. doi: 10.1016/j.omtn.2016.11.002

Retchkiman, I., Fischer, B., Platt, D., and Wagner, A. P. (1996). Seizure induced C-Fos mRNA in the rat brain: Comparison between young and aging animals. *Neurobiol. Aging* 17, 41–44. doi: 10.1016/0197-4580(95)02022-5

Rodriguez-Manzaneque, J. C., Westling, J., Thai, S. N., Luque, A., Knauper, V., Murphy, G., et al. (2002). ADAMTS1 cleaves aggrecan at multiple sites and is differentially inhibited by metalloproteinase inhibitors. *Biochem. Biophys. Res. Commun.* 293, 501–508. doi: 10.1016/S0006-291X(02)00254-1

Rowe, C. C., Ellis, K. A., Rimajova, M., Bourgeat, P., Pike, K. E., Jones, G., et al. (2010). Amyloid imaging results from the Australian Imaging. Biomarkers and Lifestyle (AIBL) study of aging. *Neurobiol. Aging* 31, 1275–1283. doi: 10.1016/j.neurobiolaging.2010.04.007

Sannerud, R., Declerck, I., Peric, A., Raemaekers, T., Menendez, G., Zhou, L., et al. (2011). ADP ribosylation factor 6 (ARF6) controls amyloid precursor protein (APP) processing by mediating the endosomal sorting of BACE1. *Proc. Natl. Acad. Sci. U.S.A* 108, E559–E568. doi: 10.1073/pnas.1100745108

Savonenko, A. V., Melnikova, T., Laird, F. M., Stewart, K. A., Price, D. L., and Wong, P. C. (2008). Alteration of BACE1-dependent NRG1/ErbB4 signaling and

schizophrenia-like phenotypes in BACE1-null mice. *Proc. Natl. Acad. Sci. U.S.A* 105, 5585–5590. doi: 10.1073/pnas.0710373105

Schwartzentruber, J., Cooper, S., Liu, J. Z., Barrio-Hernandez, I., Bello, E., Kumasaka, N., et al. (2021). Genome-wide meta-analysis, fine-mapping and integrative prioritization implicate new Alzheimer's disease risk genes. *Nat. Genet.* 53, 392–402. doi: 10.1038/s41588-020-00776-w

Sha, L., Wang, X., Li, J., Shi, X., Wu, L., Shen, Y., et al. (2017). Pharmacologic inhibition of Hsp90 to prevent GLT-1 degradation as an effective therapy for epilepsy. *J. Exp. Med.* 214, 547–563. doi: 10.1084/jem.20160667

Shahani, N., Seshadri, S., Jaaro-Peled, H., Ishizuka, K., Hirota-Tsuyada, Y., Wang, Q., et al. (2015). DISC1 regulates trafficking and processing of APP and Abeta generation. *Mol. Psychiatry* 20, 874–879. doi: 10.1038/mp.2014.100

Shan, W., Nagai, T., Tanaka, M., Itoh, N., Furukawa-Hibi, Y., Nabeshima, T., et al. (2018). Neuronal PAS domain protein 4 (Npas4) controls neuronal homeostasis in pentylenetetrazole-induced epilepsy through the induction of Homer1a. *J. Neurochem.* 145, 19–33. doi: 10.1111/jnc.14274

Shimoda, M., Ohtsuka, T., Okada, Y., and Kanai, Y. (2021). Stromal metalloproteinases: Crucial contributors to the tumor microenvironment. *Pathol. Int.* 71, 1–14. doi: 10.1111/pin.13033

Shindo, T., Kurihara, H., Kuno, K., Yokoyama, H., Wada, T., Kurihara, Y., et al. (2000). ADAMTS-1: A metalloproteinase-disintegrin essential for normal growth, fertility, and organ morphology and function. *J. Clin. Invest.* 105, 1345–1352. doi: 10.1172/JCI8635

Song, W., Hooli, B., Mullin, K., Jin, S. C., Cella, M., Ulland, T. K., et al. (2017). Alzheimer's disease-associated TREM2 variants exhibit either decreased or increased ligand-dependent activation. *Alzheimers Dement.* 13, 381–387. doi: 10.1016/j.jalz.2016.07.004

Suzuki, K., Hayashi, Y., Nakahara, S., Kumazaki, H., Prox, J., Horiuchi, K., et al. (2012). Activity-dependent proteolytic cleavage of neuroligin-1. *Neuron* 76, 410–422. doi: 10.1016/j.neuron.2012.10.003

Szyndler, J., Maciejak, P., Wislowska-Stanek, A., Lehner, M., and Plaznik, A. (2013). Changes in the Egr1 and Arc expression in brain structures of pentylenetetrazole-kindled rats. *Pharmacol. Rep.* 65, 368–378. doi: 10.1016/s1734-1140(13)71012-0

van der Kant, R., and Goldstein, L. S. (2015). Cellular functions of the amyloid precursor protein from development to dementia. *Dev. Cell* 32, 502–515. doi: 10.1016/j.devcel.2015.01.022

Vemuri, P., Lesnick, T. G., Przybelski, S. A., Machulda, M., Knopman, D. S., Mielke, M. M., et al. (2014). Association of lifetime intellectual enrichment with cognitive decline in the older population. *JAMA Neurol.* 71, 1017–1024. doi: 10.1001/jamaneurol.2014.963

Wang, Y., Greenwood, J. S., Calcagnotto, M. E., Kirsch, H. E., Barbaro, N. M., and Baraban, S. C. (2007). Neocortical hyperexcitability in a human case of tuberous sclerosis complex and mice lacking neuronal expression of TSC1. *Ann. Neurol.* 61, 139–152. doi: 10.1002/ana.21058

Westling, J., Fosang, A. J., Last, K., Thompson, V. P., Tomkinson, K. N., Hebert, T., et al. (2002). ADAMTS4 cleaves at the aggrecanase site (Glu373-Ala374) and secondarily at the matrix metalloproteinase site (Asn341-Phe342) in the aggrecan interglobular domain. *J. Biol. Chem.* 277, 16059–16066. doi: 10.1074/jbc.M108607200

Wilson, R. S., Mendes, De Leon, C. F., Barnes, L. L., Schneider, J. A., Bienias, J. L., et al. (2002). Participation in cognitively stimulating activities and risk of incident Alzheimer disease. *JAMA* 287, 742–748. doi: 10.1001/jama.287.6.742

Wilson, R. S., Scherr, P. A., Schneider, J. A., Tang, Y., and Bennett, D. A. (2007). Relation of cognitive activity to risk of developing Alzheimer disease. *Neurology* 69, 1911–1920. doi: 10.1212/01.wnl.0000271087.67782.cb

Wilson, R. S., Wang, T., Yu, L., Grodstein, F., Bennett, D. A., and Boyle, P. A. (2021). Cognitive Activity and Onset Age of Incident Alzheimer Disease Dementia. *Neurology* 97:e922–e929. doi: 10.1212/WNL.0000000000012388

Wu, Y. E., Pan, L., Zuo, Y., Li, X., and Hong, W. (2017). Detecting Activated Cell Populations Using Single-Cell RNA-Seq. *Neuron* 31:e316. doi: 10.1016/j.neuron.2017.09.026

Yeh, F. L., Wang, Y., Tom, I., Gonzalez, L. C., and Sheng, M. (2016). TREM2 Binds to Apolipoproteins. Including APOE and CLU/APOJ, and Thereby Facilitates Uptake of Amyloid-Beta by Microglia. *Neuron* 91, 328–340. doi: 10.1016/j.neuron.2016.06.015

Yi, C., Goh, K. Y., Wong, L. W., Ramanujan, A., Tanaka, K., Sajikumar, S., et al. (2021). Inactive variants of death receptor p75(NTR) reduce Alzheimer's neuropathology by interfering with APP internalization. *EMBO. J.* 40:e104450. doi: 10.15252/embj.2020104450

Yu, J. T., Xu, W., Tan, C. C., Andrieu, S., Suckling, J., Evangelou, E., et al. (2020). Evidence-based prevention of Alzheimer's disease: Systematic review and meta-analysis of 243 observational prospective studies and 153 randomised controlled trials. *J. Neurol. Neurosurg. Psychiatry* 91, 1201–1209. doi: 10.1136/jnnp-2019-321913

Yun, J., Nagai, T., Furukawa-Hibi, Y., Kuroda, K., Kaibuchi, K., Greenberg, M. E., et al. (2013). Neuronal Per Arnt Sim (PAS) domain protein 4 (NPAS4) regulates neurite outgrowth and phosphorylation of synapsin I. *J. Biol. Chem.* 288, 2655–2664. doi: 10.1074/jbc.M112.413310

Zemdegs, J., Martin, H., Pintana, H., Bullich, S., Manta, S., Marques, M. A., et al. (2019). Metformin Promotes Anxiolytic and Antidepressant-Like Responses in Insulin-Resistant Mice by Decreasing Circulating Branched-Chain Amino Acids. *J. Neurosci.* 39, 5935–5948. doi: 10.1523/JNEUROSCI.2904-18.2019

Zhao, J., Liu, X., Xia, W., Zhang, Y., and Wang, C. (2020). Targeting Amyloidogenic Processing of APP in Alzheimer's Disease. *Front. Mol. Neurosci.* 13:137. doi: 10.3389/fnmol.2020.00137

Zhong, S., and Khalil, R. A. (2019). A Disintegrin and Metalloproteinase (ADAM) and ADAM with thrombospondin motifs (ADAMTS) family in vascular biology and disease. *Biochem. Pharmacol.* 164, 188–204. doi: 10.1016/j.bcp.2019.03.033

frontiers | Frontiers in Aging Neuroscience

TYPE Systematic Review
PUBLISHED 18 August 2022
DOI 10.3389/fnagi.2022.952181

OPEN ACCESS

EDITED BY
Chih-Yu Hsu,
Fujian University of Technology, China

REVIEWED BY
Jing Jiang,
Beijing University of Chinese Medicine, China
Chao-Qun Yan,
Beijing University of Chinese Medicine, China
Ling Zhao,
Chengdu University of Traditional Chinese Medicine, China
Yanjun Du,
Hubei University of Chinese Medicine, China

*CORRESPONDENCE
Wenxuan Jian
jianwenxuan@gzucm.edu.cn
Jinghu Li
17367074323@163.com
Min Li
doctorlimin@gzucm.edu.cn

SPECIALTY SECTION
This article was submitted to Alzheimer's Disease and Related Dementias, a section of the journal Frontiers in Aging Neuroscience

RECEIVED 24 May 2022
ACCEPTED 14 July 2022
PUBLISHED 18 August 2022

CITATION
Li G, Shi Y, Zhang L, Yang C, Wan T, Lv H, Jian W, Li J and Li M (2022) Efficacy of acupuncture in animal models of vascular dementia: A systematic review and network meta-analysis.
Front. Aging Neurosci. 14:952181.
doi: 10.3389/fnagi.2022.952181

Efficacy of acupuncture in animal models of vascular dementia: A systematic review and network meta-analysis

Guangyao Li[1,2], Yuling Shi[3], Lu Zhang[1], Chuanghui Yang[1], Ting Wan[4], Hang Lv[5], Wenxuan Jian[2]*, Jinghu Li[6]* and Min Li[1]*

[1]Medical College of Acupuncture Moxibustion and Rehabilitation, Guangzhou University of Chinese Medicine, Guangzhou, China, [2]Science and Technology Innovation Center, Guangzhou University of Chinese Medicine, Guangzhou, China, [3]The Second Affiliated Hospital, Guangzhou University of Chinese Medicine (Guangdong Hospital of Traditional Chinese Medicine), Guangzhou, China, [4]The First Affiliated Hospital, Guangzhou University of Chinese Medicine, Guangzhou, China, [5]Nanfang Hospital, Southern Medical University, Guangzhou, China, [6]Department of Massage, The Third Affiliated Hospital of Zhejiang Chinese Medical University, Hangzhou, China

Background and purpose: Acupuncture is widely used in clinical practice for the treatment of vascular diseases. However, the protocol, efficacy, and mechanism of acupuncture in animal models of vascular dementia are still controversial. Based on the above problems, we initiated this comprehensive study.

Methods: To analyze the literatures included in this study, 4 databases were searched and the SYRCLE's Risk of bias tool was employed. To perform the subgroup analysis of different acupuncture methods and the Review Manager 5.3 was applied. Meanwhile, the pairwise and network meta-analysis were conducted using Addis 1.16.8. The outcomes included escape latency, number of crossings, time spent in the target quadrant, and swimming speed.

Results: Forty-two studies with a total of 1,486 animals were included in this meta-analysis. According to the results from subgroup analysis, GV20 + ST36 (Baihui + bilateral Zusanli) combined with 14-day manual acupuncture can obtain best improvement of the rats cognitive function among all acupuncture regimens (MD: −23.41; 95%CI: −26.66, −20.15; $I^2 = 0\%$; $P < 0.001$). The heterogeneity of other acupuncture treatments was significantly higher than that of GV20 + ST36, because the treatment courses were not uniform. Pair-wise and network comparisons are highly consistent. The major results of the network meta-analysis were as follows, In comparison to the impaired group, the acupuncture group showed significantly reduced escape latency (MD: −25.87; 95%CI: −30.75, −21.12), increased number of original platform crossings (MD: 2.63; 95%CI: 1.94, 3.34) and time spent in the target quadrant (MD: 7.88; 95%CI: 4.25, 11.44). The overall results of the network meta-analysis are as follows: the normal and sham-operated groups performed the best, followed by medicine and acupuncture, while no effect was found in the impaired group treated with non-acupoint and palliative.

Conclusions: Acupuncture significantly improves cognitive function in rats with vascular dementia. Compared to other acupuncture plans, (GV20 + ST36, MA) and 14 -day manual acupuncture can be used to obtain better results. The main mechanism of acupuncture in the treatment of vascular dementia is reduced oxidative stress, neuronal inflammation, and apoptosis, as well as the increased synaptic plasticity and neurotransmitters.

Systematic review registration: https://inplasy.com/inplasy-2021-11-0036/, identifier: INPLASY2021110036.

KEYWORDS

acupuncture, vascular dementia, animal studies, network meta-analysis, morris water maze, acupuncture protocol, acupuncture mechanism

Introduction

Vascular dementia (VD) is a syndrome of cognitive dysfunction caused by hypoperfusion disorders in brain regions, such as ischemic stroke and hemorrhagic stroke (O'Brien and Thomas, 2015). There are more than 50 million people worldwide suffering from dementia, and 33% of all dementia cases are vascular dementia (VD), making it the first most common form of dementia except for Alzheimer's disease (AD) (Smith, 2017). When the complexity of tasks in our daily life increasing, VD patients will have a decline in thinking and cognitive function, moreover, some patients will suffer from mental and emotional abnormalities, including forgetfulness, depression, and anxiety (Kuring et al., 2018). As a result, severe VD will cause serious impact on the quality of patients life and their family members, as well as increase heavy burden on society (Cui et al., 2019). In recent years, with the accelerating of the global population aging, VD has become one of the major public health challenges of the 21st century, which deserves more attention (Grande et al., 2020).

Currently, VD lacks a consensus treatment plan. The most widely used drugs in clinical practice include cholinesterase inhibitors, N-methyl-D-aspartate receptor (NMDA) antagonists, and calcium antagonists (Farooq et al., 2017; Battle et al., 2021). The first two classes of drugs were approved by the US Food and Drug Administration (FDA) for the treatment of AD, mainly including donepezil, rivastigmine, galantamine and memantine. These drugs can only produce a transient relief of cognitive dysfunction in mild, moderate or a few patients with severe VD, and they cannot reverse or cure the disease. Additionally, all of them have side effects, such as diarrhea, nausea, and vomiting (Sun, 2018). Calcium antagonists can selectively act on smooth muscle cells of cerebral blood vessels, effectively eliminate cerebral vascular spasm, dilate blood vessels, and increase blood flow, so they are widely used for the treatment of ischemic neurological injury (Lin et al., 2019; Carlson et al., 2020). However, patients are also subjected to side effects such as blood pressure drop and hepatitis while taking nimodipine tablets (St-Onge et al., 2017). Therefore, green and effective methods for VD treatment and therapy is urgently needed.

Acupuncture is the most widely used traditional and complementary medicine, it was used in 113 countries worldwide, and was commonly performed to treat disorders of the motor, nervous, digestive, endocrine, and reproductive systems (Zhang et al., 2022). Recent studies have found that acupuncture showed very clear efficacy in the treatment of VD (Lu et al., 2022). With the deepening of animal studies, a large amount of evidences showed that acupuncture can effectively treat cognitive dysfunction in animals through multiple targets or pathways (Ye et al., 2017a). Ma et al. (2020) conducted an Magnetic Resonance Imaging (MRI)imaging-based acupuncture study, which found that the combination of GV20 + ST36 significantly attenuated the loss of myelin basic proteins and obviously reduced Interleukin-1β (IL-1β), Interleukin-6 (IL-6), and Ionized calcium bindingadaptor molecule-1 (Iba-1) by improving the perfusion and integrity of white matter. A quantitative proteomic study Isobaric Tags for Relative and Absolute Quantitation (iTRAQ) performed by Yang et al. (2018a) showed that most Differentially Expressed Proteins (DEPs) were associated with oxidative stress, apoptosis, and synaptic function, additionally, the proteins associated with acupuncture effects were also significantly involved in these three cellular processes. The results of this study showed that acupuncture reduced Reactive Oxygen Species (ROS) production, increased neuronal cell survival, and improved Long-term Potential (LTP) in VD rats (Yang et al., 2018a).

As an important body of preclinical evidence, animal experiments play an irreplaceable role in improving the efficiency of clinical treatment. Only a direct comparative study of acupuncture in the treatment of VD has been conducted so far, but many key factors such as acupuncture combinations, acupuncture methods, courses of treatment, and treatment mechanisms have not been involved. Additionally, this study was done 5 years ago (Zhang et al., 2018). Thus, more comprehensive and new studies are needed. In fact, systematic

review of animal experiments can increase the probability of successful clinical trials, reduce the producibility of clinical studies, and clarify the underlying mechanisms of acupuncture. In this study, the Bayesian network meta-analysis model was used to comprehensively compare the therapeutic effects of acupuncture, medicine, non-acupoint, and other interventions (Kruschke, 2021). Subgroup analysis was also performed to analyze points, methods and courses of acupuncture. Finally, the mechanism of acupuncture was summarized and sublimated. The conclusions of this research can provide a reference for animal research of acupuncture.

Materials and methods

Search strategy

This meta-analysis was conducted according to the PRISMA 2020 statement: an updated guidelines for reporting systematic reviews (Page et al., 2021). Data searching, extraction, and analysis were performed according to our previously published protocol (https://inplasy.com/inplasy-2021-11-0036/; INPLASY2021110036). Two authors (GY Li and YL Shi) independently searched the databases of Pubmed, Embase, Web of science (including Medline). The search time is limited to the establishment of the database until April 2022. The search terms are: acupuncture, electroacupuncture, acupoint, vascular dementia, infarct dementia, vascular cognitive impairment. Each search word are used alone or in combination.

Inclusion and exclusion criteria

Inclusion criteria

Subjects: animals (rats, mice).

Interventions: Acupuncture.

Comparison: Normal group (Gn), Sham-operated group (Gs), Impaired group (Gi), acupuncture group (Ga), Non-acupoint group (Gna), Medicine group (Gm). Among them, Ga can be divided into Manual Acupuncture (MA) and Electroacupuncture (EA) in subgroup analysis.

Outcome: Morris water maze, including primary outcomes: Escape latency of each group in the hidden platform trial (Escape latency), Number of crossing over the former platform location (Number of crossings). Secondary outcomes: Time spent in the target quadrant, Swimming speed to reach the hidden platform in the hidden platform trial (swimming speed).

Exclusion criteria

(1) Non-vascular dementia studies.
(2) Non-randomized controlled design of experimental studies on animals.
(3) Non-acupuncture studies.
(4) Studies of acupuncture combined with drug therapy or acupuncture compared to herbal medicine.
(5) Reviews and conference.
(6) The study did not have the outcome of the water maze.
(7) Duplicate and data-identical studies.

Data extraction

Two authors (YL Shi and L Zhang) independently extracted data from articles that met the inclusion criteria. Extraction included the following: TABLE I: ① Name of first author and year of publication ② animal species, sex, age, weight ③ Modeling method ④ Rest time after modeling ⑤ Interventions ⑥ Drug dose ⑦ Outcomes. TABLE II: ① Name of first author and year of publication ② Acupuncture methods ③ Acupuncture points ④ non-acupoints location ⑤ Time of each acupuncture treatment ⑥ Total course of treatment.

If different frequencies of acupuncture appear in the article, the data with the highest frequency is extracted. When the main data is missing from the included literature or it is presented graphically, we will try to contact the authors to obtain the original data. If the author does not reply, the values in the figure are scanned by the GetData Graph Digitizer 2.26 software (Wang R. et al., 2021).

Risk of bias

Two investigators (YL Shi and L Zhang) independently assessed the risk of bias for each included study using the SYRCLE's Risk of Bias tool, which included the following: selection bias (sequence generation, baseline characteristics and allocation concealment), performance bias (random housing and blinding), detection bias (random outcome assessment and blinding), attrition bias (incomplete outcome data), reporting bias (selective outcome reporting), other sources of bias (Hooijmans et al., 2014). If disagreements are encountered, they will be resolved through discussions with a third author.

Statistical analysis

Pair-wise Meta-Analysis: Direct comparisons between interventions were calculated using the Pair-wise Meta-analysis panel of Addis 1.16.8, under the premise of a random effects model based on the D-L method.

Subgroup analysis: Review Manager 5.3 was used to conduct subgroup analysis of different acupoint combinations, acupuncture methods and treatment courses in the acupuncture group, and explore the efficacy differences between the acupuncture group and the impaired group. When

heterogeneity occurs, sensitivity analysis is performed to find the source.

Network Meta-Analysis: The results of continuous variables were expressed as mean differences (MD) and 95% CI according to the type of the variable. The network diagrams were drawn using Stata 14, and network meta-analysis was performed using Addis 1.16.8. Addis' model analysis included "consistency" and "inconsistency". Consistency models can assess the size of effect sizes between interventions and can also calculate the rankings between groups of interventions. When the 95% CI of the results did not contain 0, it indicated that the comparison between interventions was statistically significant ($P < 0.05$).

Node split models: The Node split models is a method for judging whether direct and indirect comparison are consistent. $P > 0.05$, indicating consistency between direct and indirect comparison between interventions, using the consistency model. $P < 0.05$, indicating inconsistency between direct and indirect comparison between interventions, using the inconsistency model. If the outcome indicators cannot be tested for Node split models, the inconsistency model is directly used for analysis. The Potential Scale Reduction Factor (PSRF) evaluates the convergence of the model. If the PSRF value is close to 1, the model has good convergence and the results are stable and reliable. If PSRF < 1.2, it is considered acceptable.

Results

Screening process

According to the search strategy set by two researchers, the researchers retrieved a total of 959 literatures from databases. We summarized the retrieved literature and eliminated duplicates, First screen, by reading title and abstract, then delete non-VD, non-randomized controlled animal studies, non-acupuncture, acupuncture combined with other therapy studies, conference papers, reviews. In the second screening, by reading the full text, the research without behavioral indicators, the research on non-water maze indicators and the research on data similarity were excluded, and finally quantitative and qualitative analysis was carried out (Supplementary Figure 1).

Study characteristics

Fourty-two articles were included in this meta-analysis, including 30 in English (Wang et al., 2004, 2015; Shao et al., 2008; Wei et al., 2011; Zhao et al., 2011; Zhu et al., 2012, 2013, 2018; Feng et al., 2013; Yang et al., 2014, 2018b, 2020; Zhang et al., 2014; Li et al., 2015, 2016; Han et al., 2017; Lin et al., 2017; Liu et al., 2017; Ye et al., 2017b; Du et al., 2018; He et al., 2018; Su et al., 2019; Ma et al., 2020; Wang L. et al., 2020; Wang Z. et al., 2020; Zheng et al., 2020; Cao et al., 2021; Pan et al., 2021; Wang H. L. et al., 2021; Bu et al., 2022) and 12 in Chinese (Li and Lai, 2007; Lin and Wang, 2008; Niu et al., 2009; Tian et al., 2015; Jiang et al., 2017; Zhang et al., 2017; Yang et al., 2019; Gao et al., 2020; Guo et al., 2020; Li et al., 2021; Chen et al., 2022; Xu and Zhang, 2022). The publication year of the article was from June 2004 to April 2022. The research was carried out in China, with a total of 1486 animals. The details are as follows (Supplementary Tables 1, 2).

Methods of surgical modeling: There are 4 surgical modeling methods involved in this study, including 23 articles in the literature using bilateral common carotid artery occlusion (2VO) (Lin and Wang, 2008; Wei et al., 2011; Zhu et al., 2012, 2013, 2018; Yang et al., 2014, 2018b, 2019, 2020; Wang et al., 2015; Li et al., 2016, 2021; Han et al., 2017; Ye et al., 2017b; Gao et al., 2020; Guo et al., 2020; Ma et al., 2020; Wang L. et al., 2020; Cao et al., 2021; Pan et al., 2021; Chen et al., 2022; Xu and Zhang, 2022), 8 articles in the literature using 4-vessel occlusion (4VO) (Wang et al., 2004; Li and Lai, 2007; Shao et al., 2008; Niu et al., 2009; Tian et al., 2015; Jiang et al., 2017; Zhang et al., 2017; Bu et al., 2022), 3 articles in the literature using embolic occlusion (EO) (Zhao et al., 2011; Zhang et al., 2014; Li et al., 2015), and 8 articles in the literature using middle cerebral artery occlusion (MCAO) (Feng et al., 2013; Lin et al., 2017; Liu et al., 2017; He et al., 2018; Su et al., 2019; Wang Z. et al., 2020; Zheng et al., 2020; Wang H. L. et al., 2021). Among them, 24 articles clearly stated the total number of the models and the number of successful models (Wang et al., 2004; Li and Lai, 2007; Lin and Wang, 2008; Shao et al., 2008; Wei et al., 2011; Feng et al., 2013; Zhu et al., 2013; Li et al., 2016, 2021; Han et al., 2017; Jiang et al., 2017; Lin et al., 2017; Liu et al., 2017; Ye et al., 2017b; Zhang et al., 2017; Du et al., 2018; He et al., 2018; Yang et al., 2018b, 2019, 2020; Su et al., 2019; Gao et al., 2020; Guo et al., 2020; Ma et al., 2020; Wang L. et al., 2020; Wang Z. et al., 2020; Zheng et al., 2020; Cao et al., 2021; Wang H. L. et al., 2021; Bu et al., 2022; Chen et al., 2022). According to statistics, MCAO had the highest success rate, no difference between 2VO and EO, and the lowest 4VO (Figures 1A,B).

Interventions: Including normal rats, sham-operated, impaired model, acupuncture, non-acupoint, and medicine.

Outcomes: All literatures have escape latency as an important outcome in the water maze, of which 23 included the number of original platform crossings (Wang et al., 2004; Li and Lai, 2007; Shao et al., 2008; Niu et al., 2009; Wei et al., 2011; Feng et al., 2013; Zhang et al., 2014, 2017; Tian et al., 2015; Jiang et al., 2017; Lin et al., 2017; Liu et al., 2017; He et al., 2018; Su et al., 2019; Yang et al., 2019; Gao et al., 2020; Guo et al., 2020; Ma et al., 2020; Wang Z. et al., 2020; Pan et al., 2021; Wang H. L. et al., 2021; Bu et al., 2022; Xu and Zhang, 2022), 11 literatures (Lin and Wang, 2008; Li et al., 2016; Han et al., 2017; Ye et al., 2017b; Zhu et al., 2018; Ma et al., 2020; Yang et al., 2020; Zheng et al., 2020; Cao et al., 2021; Pan et al., 2021; Xu and Zhang, 2022) calculated the time spent in target quadrant, and 7 literatures (Li et al., 2015; Wang et al., 2015; Liu et al., 2017; Yang et al., 2018b,

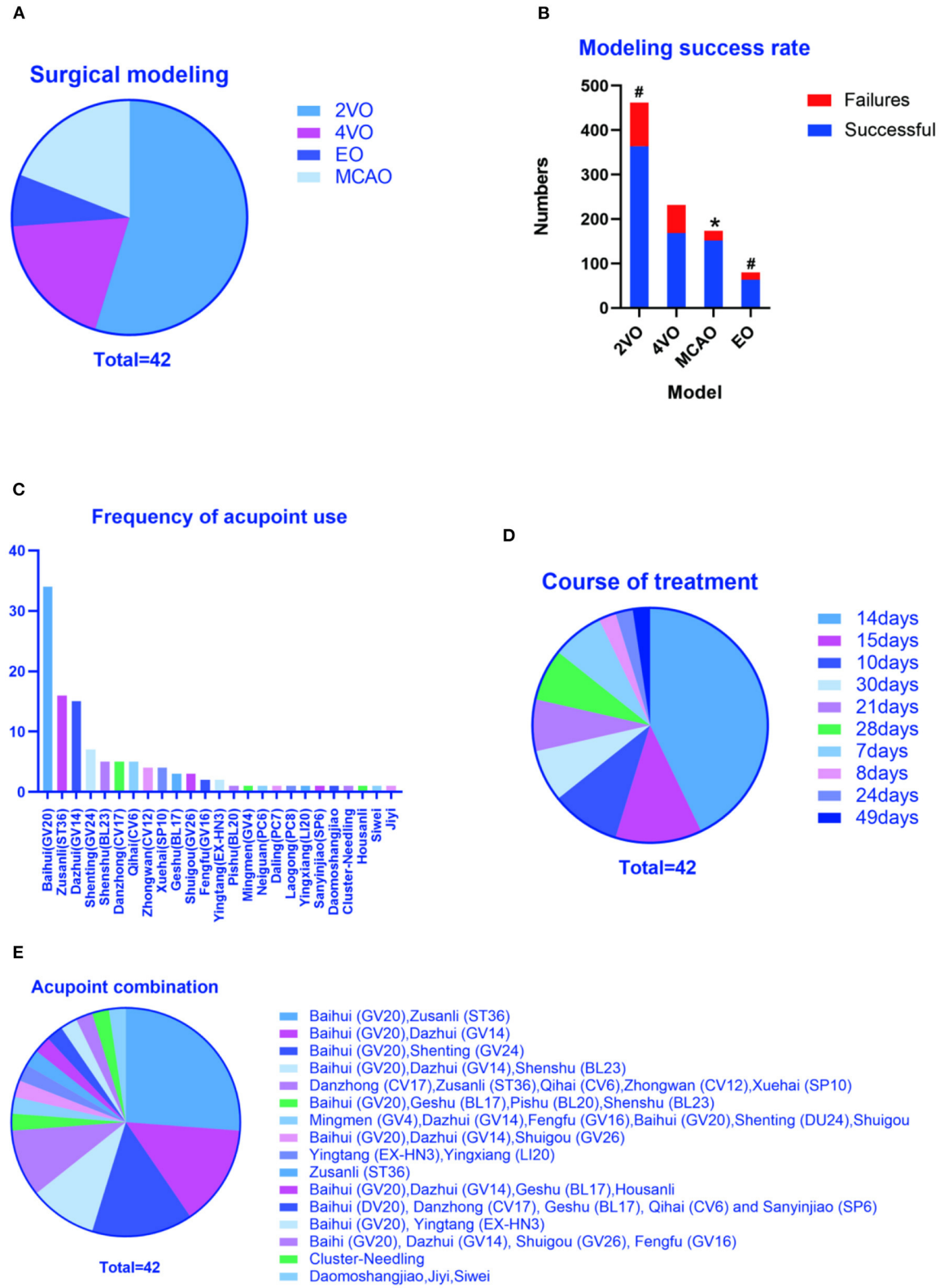

FIGURE 1
Study characteristics. **(A)** Methods of surgical modeling, **(B)** Total number of modeling and the number of successful modeling, **(C)** Frequency of acupoint use, **(D)** Total course of treatment, **(E)** Frequency of acupoint combination. 2VO, Two - Vessel Occlusion or Bilateral Common Carotid Artery Occlusion; 4VO, Four-Vessel Occlusion; MCAO, Middle Cerebral Artery Occlusion; EO, Embolic occlusion, $^{*}P < 0.05$ (Modeling success rate of MCAO VS 2VO, EO and 4VO, MCAO had the highest success rate). $^{\#}P < 0.05$ (Modeling success rate of 2VO VS 4VO and EO VS 4VO, no difference between 2VO and EO, and the lowest is 4VO).

2020; Wang L. et al., 2020; Wang Z. et al., 2020) calculated the swimming speed.

Acupuncture methods: two types were included, manual acupuncture (MA) (Zhao et al., 2011; Yang et al., 2014, 2018b, 2019, 2020; Li et al., 2015, 2016, 2021; Tian et al., 2015; Wang et al., 2015; Ye et al., 2017b; Du et al., 2018; Zhu et al., 2018; Su et al., 2019; Gao et al., 2020; Ma et al., 2020; Wang L. et al., 2020; Cao et al., 2021; Pan et al., 2021; Xu and Zhang, 2022) and electroacupuncture (EA) (Wang et al., 2004; Li and Lai, 2007; Lin and Wang, 2008; Shao et al., 2008; Niu et al., 2009; Wei et al., 2011; Zhu et al., 2012, 2013; Feng et al., 2013; Han et al., 2017; Jiang et al., 2017; Liu et al., 2017; Zhang et al., 2017; He et al., 2018; Guo et al., 2020; Wang Z. et al., 2020; Zheng et al., 2020; Wang H. L. et al., 2021; Bu et al., 2022; Chen et al., 2022).

Frequency of acupoint use and frequency of acupoint combination: All literature clearly pointed out acupuncture points. According to statistics, Baihui (GV20) (Wang et al., 2004, 2015; Li and Lai, 2007; Lin and Wang, 2008; Shao et al., 2008; Wei et al., 2011; Zhu et al., 2012, 2013, 2018; Feng et al., 2013; Li et al., 2016, 2021; Han et al., 2017; Jiang et al., 2017; Lin et al., 2017; Liu et al., 2017; Ye et al., 2017b; Zhang et al., 2017; Du et al., 2018; He et al., 2018; Yang et al., 2018b, 2019, 2020; Su et al., 2019; Gao et al., 2020; Guo et al., 2020; Ma et al., 2020; Wang L. et al., 2020; Wang Z. et al., 2020; Zheng et al., 2020; Cao et al., 2021; Bu et al., 2022; Chen et al., 2022), bilateral Zusanli (ST36) (Zhao et al., 2011; Zhang et al., 2014; Li et al., 2015, 2016, 2021; Wang et al., 2015; Ye et al., 2017b; Du et al., 2018; Yang et al., 2018b, 2020; Zhu et al., 2018; Ma et al., 2020; Wang L. et al., 2020; Cao et al., 2021; Pan et al., 2021; Xu and Zhang, 2022) and Dazhui (GV14) (Wang et al., 2004; Li and Lai, 2007; Lin and Wang, 2008; Shao et al., 2008; Wei et al., 2011; Zhu et al., 2012, 2013; Han et al., 2017; Jiang et al., 2017; Zhang et al., 2017; Su et al., 2019; Yang et al., 2019; Gao et al., 2020; Guo et al., 2020; Chen et al., 2022) were used the most frequently (Figure 1C). According to the analysis of the acupoint combinations in the article, the combination of Baihui + bilateral Zusanli (GV20+ST36) (Wang et al., 2015; Li et al., 2016, 2021; Ye et al., 2017b; Du et al., 2018; Yang et al., 2018b, 2020; Zhu et al., 2018; Ma et al., 2020; Wang L. et al., 2020; Cao et al., 2021), Baihui + Dazhui (GV20+GV14) (Wang et al., 2004; Li and Lai, 2007; Wei et al., 2011; Han et al., 2017; Jiang et al., 2017; Zhang et al., 2017) and Baihui + Shenting (GV20+GV24) (Feng et al., 2013; Lin et al., 2017; Liu et al., 2017; He et al., 2018; Wang Z. et al., 2020; Wang H. L. et al., 2021) is the most frequently used, respectively 26.19, 14.29, and 14.29% (Figure 1E).

Non-acupoint: Fifteen studies in the literature used sham acupuncture or non-acupoint studies. eight of them (Zhao et al., 2011; Li et al., 2015, 2016, 2021; Ye et al., 2017b; Du et al., 2018; Yang et al., 2018b; Ma et al., 2020) selected in the bilateral hypochondrium, 10 mm above the iliac crest as a sham acupuncture point, three of them (Wang et al., 2015; Zhu et al., 2018; Wang Z. et al., 2020) selected 2 cm higher to the anterior superior spine. Two article (Zhang et al., 2014; Pan et al., 2021) 2 articles selected in the hypochondrium, 3 mm above the iliac crest. One article (Lin and Wang, 2008) selected at the thoracoabdominal junction of the first and second lumbar vertebrae. One article (Bu et al., 2022) located on the meridian route, and did not belong to the traditional 14 meridians.

The time of each acupuncture treatment and the total course of treatment: 41 literatures specified the time of each acupuncture treatment, and 1 literature (Li et al., 2021) did not specify. The main time is 30 min (31.71%) (Feng et al., 2013; Tian et al., 2015; Han et al., 2017; Jiang et al., 2017; Lin et al., 2017; Liu et al., 2017; He et al., 2018; Yang et al., 2019; Gao et al., 2020; Wang Z. et al., 2020; Wang H. L. et al., 2021; Bu et al., 2022; Chen et al., 2022), 20 min (21.95%) (Wang et al., 2004; Li and Lai, 2007; Lin and Wang, 2008; Shao et al., 2008; Wei et al., 2011; Zhu et al., 2012, 2013; Zhang et al., 2017; Su et al., 2019), 30 S (21.95%) (Zhao et al., 2011; Zhang et al., 2014; Li et al., 2015, 2016; Ye et al., 2017b; Du et al., 2018; Yang et al., 2018b; Pan et al., 2021; Xu and Zhang, 2022) and 10 min (17.07%) (Niu et al., 2009; Zhu et al., 2018; Wang L. et al., 2020; Yang et al., 2020; Zheng et al., 2020; Cao et al., 2021). All literatures indicated the duration of the entire treatment course, namely 14 days (42.86%) (Li et al., 2015, 2016; Wang et al., 2015; Ye et al., 2017b; Du et al., 2018; Yang et al., 2018b, 2019, 2020; Zhu et al., 2018; Gao et al., 2020; Guo et al., 2020; Ma et al., 2020; Wang L. et al., 2020; Wang Z. et al., 2020; Zheng et al., 2020; Cao et al., 2021; Pan et al., 2021; Lu et al., 2022), 15 days (11.90%) (Wang et al., 2004; Li and Lai, 2007; Shao et al., 2008; Su et al., 2019; Xu and Zhang, 2022), 10 days (9.52%) (Wei et al., 2011; Feng et al., 2013; Tian et al., 2015; Jiang et al., 2017) (Figure 1D).

Risk of bias

The overall quality of the included literatures was medium. According to the SYRCLE risk assessment tool, the evaluation results were as follows: all the literatures mentioned random allocation, of which 8 literatures (Li and Lai, 2007; Lin and Wang, 2008; Jiang et al., 2017; Zhang et al., 2017; Yang et al., 2019; Gao et al., 2020; Guo et al., 2020; Ma et al., 2020) clearly informed the randomization method. All the papers are balanced at baseline, but none of them mentioned allocation concealment. None of the studies indicated whether the animals were randomly housed, but 36 papers specified the housing environment, and the remaining 6 papers unspecified (Wang et al., 2004; Li and Lai, 2007; Lin and Wang, 2008; Niu et al., 2009; Zhu et al., 2013; Su et al., 2019). This study was an acupuncture study, the operator could not be blinded during treatment. All animals in the 30 studies were evaluated for outcome evaluation, but 12 studies (Lin and Wang, 2008; Shao et al., 2008; Niu et al., 2009; Zhu et al., 2012; Zhang et al., 2014; Li et al., 2016; Han et al., 2017; Liu et al., 2017; Ye et al., 2017b; Wang L. et al., 2020; Wang Z. et al., 2020; Yang et al., 2020)

selected some animals for evaluation without specifying whether they were randomly selected. In terms of outcome statistics, 2 articles in the literature explicitly mentioned blinding (Li et al., 2015; Cao et al., 2021), 2 articles in the literature (Shao et al., 2008; Zhu et al., 2013) were counted by the first author, and the remaining 38 articles did not mention statistical blinding. The results of the data for the entire literatures were completed and no selective reporting was evaluated. In terms of other biases, 19 articles in the literature (Li and Lai, 2007; Lin and Wang, 2008; Zhao et al., 2011; Yang et al., 2014; Zhang et al., 2014, 2017; Tian et al., 2015; Jiang et al., 2017; Liu et al., 2017; He et al., 2018; Su et al., 2019; Gao et al., 2020; Ma et al., 2020; Wang Z. et al., 2020; Li et al., 2021; Pan et al., 2021; Wang H. L. et al., 2021; Bu et al., 2022; Chen et al., 2022) had no other biases, and the remaining 23 (Wang et al., 2004, 2015; Shao et al., 2008; Niu et al., 2009; Wei et al., 2011; Zhu et al., 2012, 2013, 2018; Feng et al., 2013; Li et al., 2015, 2016; Han et al., 2017; Lin et al., 2017; Ye et al., 2017b; Du et al., 2018; Yang et al., 2018b, 2019, 2020; Su et al., 2019; Guo et al., 2020; Wang L. et al., 2020; Cao et al., 2021; Xu and Zhang, 2022) did not mention the number of successful surgical modeling or the rest time after modeling (Supplementary Figures 2, 3).

Pair-wise meta-analysis

We compared the escape latency, the number of crossing, and the time spent in the target quadrant. some of the results were the same: Ga was better than Gi and Gna, Ga was worse than Gs and Gn, Gi was worse than Gs and Gn, and Gna was worse than Gs. We compared the swimming speed of VD rats, except that Gn was significant compared to Gna, the rest of the comparisons did not reach the level of significance (Supplementary Table 3).

Subgroup analysis

Escape latency is the most important indicator in the water maze. We performed subgroup analysis on this outcome according to different acupoint combinations, acupuncture methods, and treatment courses.

Escape latency: The statistical results of 42 studies showed that Ga could significantly shorten the escape latency compared to Gi (MD: −25.78; 95%CI: −29.20, −22.37; I^2 = 96%). Subgroup analysis was performed according to different acupoint combinations, acupuncture methods and courses of treatment, GV20 + ST36 (MA) (Wang et al., 2015; Li et al., 2016, 2021; Ye et al., 2017b; Du et al., 2018; Yang et al., 2018b, 2020; Zhu et al., 2018; Ma et al., 2020; Wang L. et al., 2020; Cao et al., 2021) (MD: −23.41; 95% CI: −26.66, −20.16; I^2 = 0%), no heterogeneity within the group. GV20 + GV14 (EA) (Wang et al., 2004; Li and Lai, 2007; Wei et al., 2011; Han et al., 2017; Jiang et al., 2017; Zhang et al., 2017) (MD: −27.54; 95%CI: −36.29, −18.79; I^2 = 97%), with greater heterogeneity within the group. GV20+GV24 (EA) (Feng et al., 2013; Lin et al., 2017; Liu et al., 2017; He et al., 2018; Wang Z. et al., 2020; Wang H. L. et al., 2021) (MD: −24.18; 95%CI: −30.49, −17.87; I^2 = 86%), with greater heterogeneity within the group. GV20 + GV14 + BL23 (EA) (Lin and Wang, 2008; Zhu et al., 2012, 2013; Chen et al., 2022) (MD: −13.26; 95%CI: −16.82, −9.70; I^2 = 3%), no heterogeneity within the group. CV6 + CV12 + CV17 + ST36 + SP10 (MA) (Zhao et al., 2011; Zhang et al., 2014; Pan et al., 2021; Xu and Zhang, 2022) (MD: −9.99; 95%CI: −13.98, −6.00; I^2 = 75%), with mediun heterogeneity within the group. Other Acupoints (MA or EA) (Shao et al., 2008; Niu et al., 2009; Yang et al., 2014, 2019; Li et al., 2015; Tian et al., 2015; He et al., 2018; Su et al., 2019; Gao et al., 2020; Guo et al., 2020; Zheng et al., 2020; Bu et al., 2022) (MD: −39.62; 95%CI: −51.05, −28.19; I^2 = 97%), with greater heterogeneity within the group (Supplementary Figure 4).

Sensitivity analysis was performed for the heterogeneity within the group of GV20 + GV14 (EA) (Wang et al., 2004; Li and Lai, 2007; Wei et al., 2011; Han et al., 2017; Jiang et al., 2017; Zhang et al., 2017) and Other Acupoints (MA or EA) (Shao et al., 2008; Niu et al., 2009; Yang et al., 2014, 2019; Li et al., 2015; Tian et al., 2015; He et al., 2018; Su et al., 2019; Gao et al., 2020; Guo et al., 2020; Zheng et al., 2020; Bu et al., 2022). Deletion of any study did not remove heterogeneity, but the results were still the same as before, the reason for the heterogeneity may be the course of treatment caused by inconsistency. The heterogeneity of GV20 + GV24 (EA) (Feng et al., 2013; Lin et al., 2017; Liu et al., 2017; He et al., 2018; Wang Z. et al., 2020; Wang H. L. et al., 2021) was caused by He et al. (2018), whose postoperative rest period was 7 days, which was longer than the rest of the literature. The heterogeneity of CV6 + CV12 + CV17 + ST36 + SP10 (MA) (Zhao et al., 2011; Zhang et al., 2014; Pan et al., 2021; Xu and Zhang, 2022) was caused by Zhao et al. (2011) or Xu and Zhang (2022), and their treatments were different. Statistical results showed that GV20 + ST36 (MA) (Wang et al., 2015; Li et al., 2016, 2021; Ye et al., 2017b; Du et al., 2018; Yang et al., 2018b, 2020; Zhu et al., 2018; Ma et al., 2020; Wang L. et al., 2020; Cao et al., 2021) was better than other subgroups in terms of heterogeneity and Z value. The duration of this combination of treatment was 14 days, and MA was used uniformly as an acupuncture method.

Network meta-analysis results

We performed a network meta-analysis of escape latency, number of crossings, time spent in target quadrant, and swimming speed under various interventions (Figure 2). Escape latency, number of original crossings, and the time spent in target were tested using the node-split model to evaluate the consistency between direct and indirect comparisons. The

results showed that $P > 0.05$, PSRF = 1.0, and the results were analyzed using the consistency model (Supplementary Figure 5). The Node Split model cannot be used to test swimming speed. To ensure the objectivity of the results, the inconsistency model is used directly for analysis, and the PSRF value is 1.0. The results are stable and reliable.

Escape latency

Forty-two studies with a total of 1,486 animals, 6 interventions framed NMA for escape latency, and the results were as follows: Ga was superior to Gi and Gna, and Ga was inferior to Gn and Gs. Gi was inferior to Gm, Gn, Gna, and Gs. Gm was better than Gna. Gn was better than Gna. Gna was less than Gs. $P < 0.05$ for all the above results (Table 1A).

The probability of escape latency in the treatment of VD under multiple interventions was ranked as follows: Gn (90%), Gs (65%), Gm (46%), Ga (78%), Gna (99%), Gi (99%) (Figure 3A).

Number of crossing

Twenty-three studies (Wang et al., 2004; Li and Lai, 2007; Shao et al., 2008; Niu et al., 2009; Wei et al., 2011; Feng et al., 2013; Zhang et al., 2014, 2017; Tian et al., 2015; Jiang et al., 2017; Liu et al., 2017; He et al., 2018; Su et al., 2019; Yang et al., 2019; Gao et al., 2020; Guo et al., 2020; Ma et al., 2020; Wang Z. et al., 2020; Pan et al., 2021; Wang H. L. et al., 2021; Bu et al., 2022; Xu and Zhang, 2022) with a total of 848 animals and 6 interventions fromed the NMA with the following results: Ga was superior to Gi and Ga was inferior to Gn and Gs. Gi was less than Gm, Gn, Gna, and Gs. Gm was less than Gs. Gna was less than Gs. $P < 0.05$ for all the above results (Table 1B).

The original platform crossing times for the treatment of VD under various interventions were ranked from superior to inferior probability: Gs (52%), Gn (48%), Ga (52%), Gm (44%), Gna (82%), Gi (99%) (Figure 3B).

Time spent in the target quadrant

Eleven studies (Lin and Wang, 2008; Li et al., 2016; Han et al., 2017; Ye et al., 2017b; Zhu et al., 2018; Ma et al., 2020; Yang et al., 2020; Zheng et al., 2020; Cao et al., 2021; Pan et al., 2021; Xu and Zhang, 2022) with a total of 377 animals and five interventions formed the NMA and the results were as follows: Ga was superior to Gi and Gna, and Ga was inferior to Gn and Gs. Gi was inferior to Gn and Gs. Gn was better than Gna. Gna was less than Gs. $P < 0.05$ for all the above results (Table 1C).

The time spent in the target quadrant for the treatment of VD under various interventions were ranked from superior to inferior probability: Gn (85%), Gs (85%), Ga (99%), Gna (55%), Gi (55%) (Supplementary Figure 6).

Swimming speed

Seven studies (Li et al., 2015; Wang et al., 2015; Liu et al., 2017; Yang et al., 2018b, 2020; Wang L. et al., 2020; Wang Z. et al., 2020) with a total of 252 animals, 5 interventions formed the NMA, the results of the network meta-analysis of swimming speed are shown in the table, there is no difference between Ga, Gi, Gn, Gna, and Gs (Table 1D).

Potential mechanism of acupuncture improving cognitive dysfunction in VD rats

Acupuncture improves cognitive dysfunction in VD rats with multi-target characteristics, mainly in: reducing oxidative stress (Wang et al., 2004, 2015; Zhu et al., 2013; Zhang et al., 2014; Li et al., 2016, 2021; Du et al., 2018; Yang et al., 2018b; Su et al., 2019), neuronal inflammation (Li and Lai, 2007; Han et al., 2017; Liu et al., 2017; Ma et al., 2020; Wang L. et al., 2020; Cao et al., 2021; Pan et al., 2021; Bu et al., 2022; Chen et al., 2022; Xu and Zhang, 2022), and apoptosis (Feng et al., 2013; Tian et al., 2015; Zhang et al., 2017; Zhu et al., 2018; Guo et al., 2020; Wang H. L. et al., 2021), increasing synaptic plasticity (Wei et al., 2011; Zhu et al., 2012; Lin et al., 2017; Ye et al., 2017b; Wang Z. et al., 2020; Zheng et al., 2020), neurotransmitter (Lin and Wang, 2008; Shao et al., 2008; Wei et al., 2011; Yang et al., 2014, 2019; Jiang et al., 2017; Ye et al., 2017b; He et al., 2018), and neuron numbers (Li et al., 2015), improving Vascular function (Gao et al., 2020) and glucose metabolism (Zhao et al., 2011), etc. One article (Yang et al., 2020) in all the studies explored the differences in the efficacy of different acupuncture frequencies, but no specific mechanism was involved.

Discussion

Main findings guiding animal experiments

Data for this meta-analysis came from 42 animal studies of acupuncture in the treatment of vascular dementia. The included studies were carried out with reference to the control design, with a total of 1,486 animals. We evaluated the included literature with reference to the SYRCLE animal research evaluation criteria (Hooijmans et al., 2014), and the results were that 17 (Zhao et al., 2011; Yang et al., 2014; Li et al., 2015, 2021; Tian et al., 2015; Jiang et al., 2017; Liu et al., 2017; Zhang et al., 2017; He et al., 2018; Gao et al., 2020; Ma et al., 2020; Zheng et al., 2020; Cao et al., 2021; Pan et al., 2021; Wang H. L. et al., 2021; Bu et al., 2022; Chen et al., 2022) quality were good, 22 (Wang et al., 2004, 2015; Li and Lai, 2007; Lin and Wang, 2008; Wei et al., 2011; Zhu et al., 2012, 2018; Feng et al.,

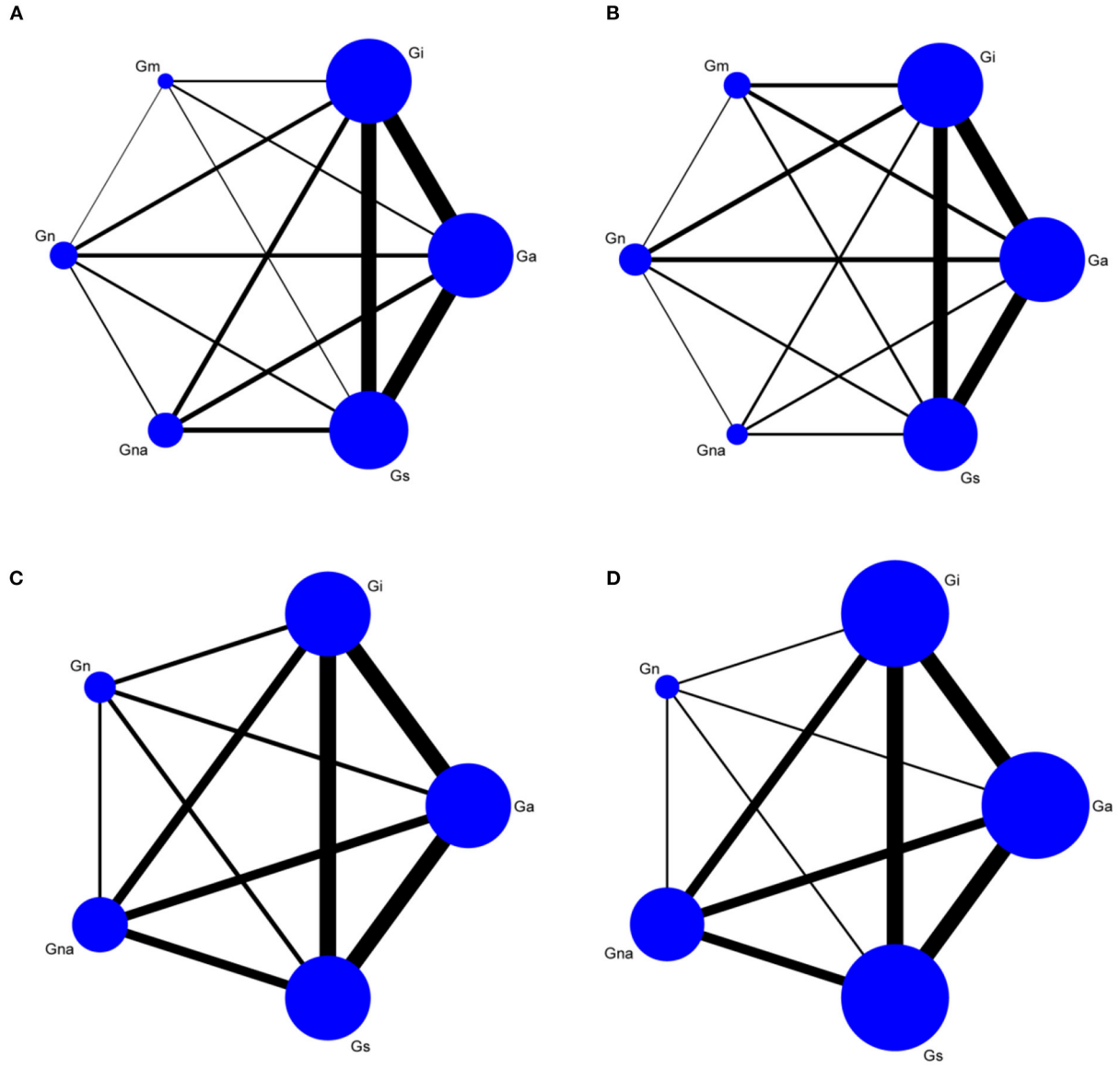

FIGURE 2
Network graph of morris water maze. Escape latency **(A)**, Number of crossings **(B)**, Time spent in target quadrant **(C)**, Swimming speed **(D)**. Gn, Normal group; Gs, Sham-operated group; Gi, Impaired group; Ga, acupuncture group; Gna, Non-acupoint group; Gm, Medicine group.

2013; Zhang et al., 2014; Li et al., 2016; Han et al., 2017; Lin et al., 2017; Ye et al., 2017b; Du et al., 2018; Yang et al., 2018b, 2019, 2020; Su et al., 2019; Guo et al., 2020; Wang Z. et al., 2020; Xu and Zhang, 2022) were moderate, and 3 (Shao et al., 2008; Niu et al., 2009; Zhu et al., 2013) were of low quality. We analyze the characteristics of the included literature. This study includes 4 surgical modeling methods: 2VO, 4VO, EO, and MCAO. This study found that the success rate of MCAO surgical modeling was higher than that of 2VO, EO and 4VO, but different surgical methods could create VD models. Animals have different rest periods after surgery, with a minimum 2 h (Feng et al., 2013; Wang H. L. et al., 2021), which we think may have an impact on the recovery of the animal's body. The duration of treatment in the included literature is different, of which 14 days (Li et al., 2015, 2016; Wang et al., 2015; Ye et al., 2017b; Du et al., 2018; Yang et al., 2018b, 2019, 2020; Zhu et al., 2018; Gao et al., 2020; Guo et al., 2020; Ma et al., 2020; Wang L. et al., 2020; Wang Z. et al., 2020; Zheng et al., 2020; Cao et al., 2021; Pan et al., 2021; Lu et al., 2022) occupy the most, followed by 15 days (Wang et al., 2004; Li and Lai, 2007; Shao et al., 2008; Su et al., 2019; Xu and Zhang, 2022) and 10 days (Wei et al., 2011; Feng et al., 2013; Tian et al., 2015; Jiang et al.,

TABLE 1 Network meta-analysis of MWM.

(A) Escape latency

Ga					
−25.87 (−30.75, −21.12)	Gi				
4.35 (−6.32, 14.48)	30.09 (19.58, 40.46)	Gm			
13.73 (5.76, 21.88)	39.58 (31.44, 47.53)	9.60 (−2.51, 21.54)	Gn		
−15.73 (−23.30, −8.15)	10.16 (2.59, 17.66)	−19.99 (−32.00, −7.53)	−29.40 (−39.26, −19.82)	Gna	
6.79 (1.92, 11.69)	32.68 (27.80, 37.61)	2.58 (−7.88, 13.19)	−6.92 (−15.18, 1.34)	22.54 (15.14, 29.90)	Gs

(B) Number of crossings

Ga					
2.63 (1.94, 3.34)	Gi				
0.09 (−1.09, 1.32)	−2.54 (−3.73, −1.32)	Gm			
−1.29 (−2.41, −0.17)	−3.91 (−5.05, −2.81)	−1.39 (−2.87, 0.09)	Gn		
1.03 (−0.36, 2.41)	−1.61 (−3.01, −0.21)	0.93 (−0.80, 2.65)	2.32 (0.70, 3.92)	Gna	
−1.31 (−2.04, −0.57)	−3.95 (−4.69, −3.20)	−1.41 (−2.70, −0.18)	−0.03 (−1.22, 1.15)	−2.34 (−3.75, −0.93)	Gs

(C) Time spent in the target quadrant

Ga				
7.92 (4.45, 11.48)	Gi			
−8.42 (−14.52, −2.65)	−16.35 (−22.26, −10.64)	Gn		
7.68 (3.35, 12.23)	−0.25 (−4.54, 4.18)	16.13 (9.79, 22.44)	Gna	
−5.36 (−9.03, −1.74)	−13.29 (−16.88, −9.69)	3.09 (−2.80, 9.03)	−13.03 (−17.48, −8.53)	Gs

(D) Swimming speed

Ga				
0.20 (−1.22, 1.71)	Gi			
1.87 (−0.76, 4.24)	1.58 (−0.75, 4.07)	Gn		
0.11 (−1.38, 1.52)	−0.34 (−1.90, 1.06)	−2.08 (−4.55, 0.42)	Gna	
0.24 (−1.51, 1.81)	−0.05 (−1.65, 1.52)	−1.74 (−4.66, 0.55)	0.18 (−1.35, 1.82)	Gs

Treatments, Efficacy (MD [95% Crl]), $P < 0.05$; Efficacy (MD [95% Crl]), $P > 0.05$. Gn, Normal group; Gs, Sham-operated group; Gi, Impaired group; Ga, acupuncture group; Gna, Non-acupoint group; Gm. Medicine group.

2017). Jiang et al. counts the effects of different treatment days on the curative effect (Jiang et al., 2017). We also believe that the duration of treatment is also one of the important factors to consider.

The results of the network and pair-wise meta-analysis were highly consistent, that is, in terms of escape latency and the number of original platform crossings, Gn and Gs have the best curative effect, followed by Ga and Gm (no significant difference between the them), and finally Gna and Gi. In improving the time spent in the target quadrant, Gn and Gs had the best effect, followed by Ga and finally Gna and Gi. In terms of swimming speed, there were no significant differences between almost all groups.

A small part of the results we have obtained are somewhat different between direct comparison and indirect comparison. After careful investigation, we found that the difference in outcomes was mainly due to the Gna intervention. Therefore, we think that the specific location of Gna needs to be carefully selected, and maybe Gna also has some therapeutic effects, which may be one of the reasons for the difference.

The rats in the normal group and the sham-operated group had the best cognitive function

The rats in the normal group not received any intervention. The rats in the sham operation group were operated with the separation of the carotid artery and vagus nerve after the skin of the neck was incised and the carotid artery was not ligated. There were no significant differences in the performance of the morris water maze between the two groups of rats, so the absence of carotid artery ligation did not affect the cognitive ability of the rats. The measurement of the water maze reflects mainly the ability of learning and memory, and the anatomical positions related to these abilities are located primarily in the hippocampus and cortex (Washida et al., 2019).

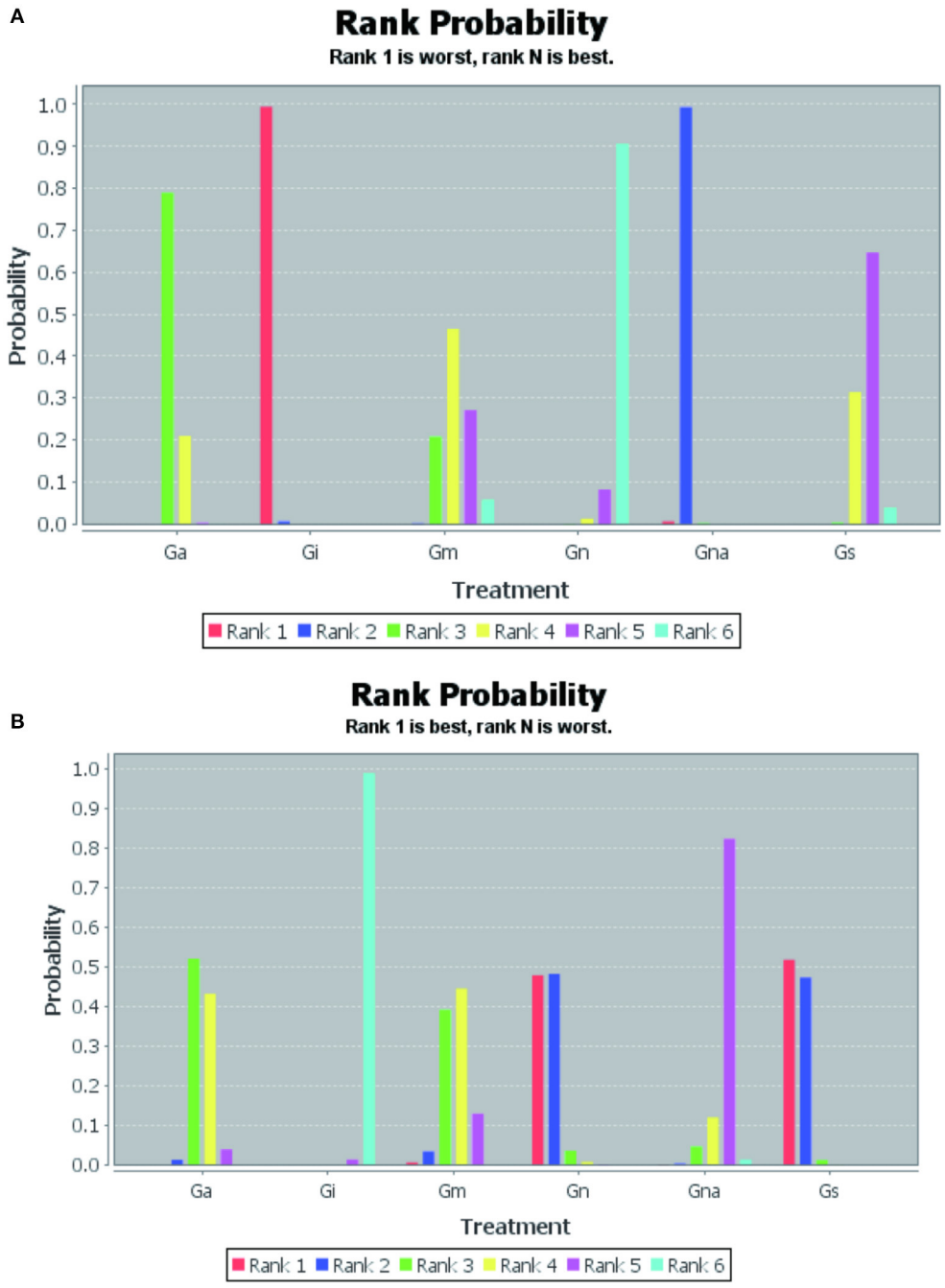

FIGURE 3
Rank probability of interventions. Escape latency **(A)**, Number of crossings **(B).** Gn, Normal group; Gs, Sham-operated group; Gi, Impaired group; Ga, acupuncture group; Gna, Non-acupoint group; Gm, Medicine group.

Acupuncture can significantly improve the cognition in VD rats

Acupuncture has been widely used in the fields of nervous system, digestive system, and rehabilitation treatment. It is one of the important alternative therapies today (Lu et al., 2022). Acupuncture plays an important role in the treatment of vascular dementia. The acupuncture points, methods, and courses of treatment were considered ad the important factors for the efficacy of acupuncture. This study conducted a subgroup analysis of these three factors. The results from the subgroup analysis of acupuncture points selection indicated that the

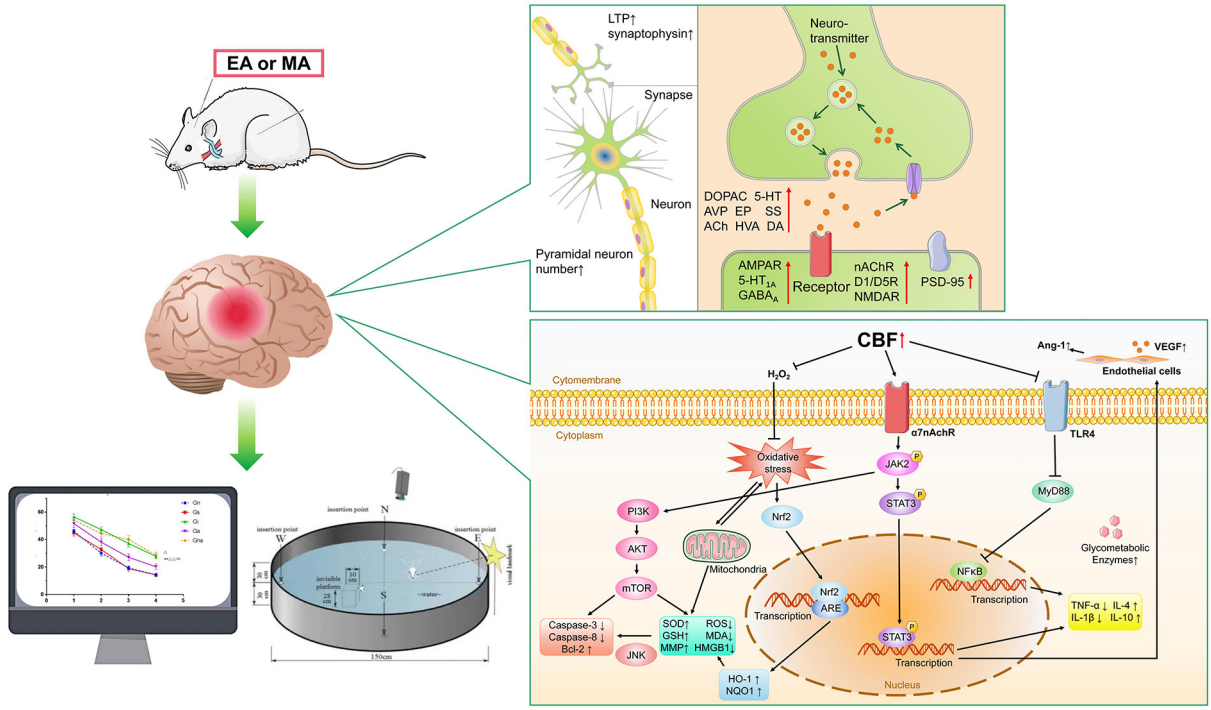

FIGURE 4
The main mechanism of acupuncture in animal models of VD. EA, electroacupuncture; MA, manual acupuncture. Synapse function: LTP (Long-term Potential), AVP (arginine vasopressin), β-EP (β-endorphine), SS (somatostatin), ACh (acetylcholine), HVA (homovanillic acid), DA (dopamine), DOPAC (Dihydroxyphenylaceticacid), 5-HT (5-hydroxytryptamine),EP (Epinephrine), nAChR (Nicotinic-Acetylcholine receptor), D1/D5R (dopamine 1/ dopamine5 receptor), NMDAR (N-methyl-D-aspartate receptor), AMPAR (α-amino-3-hydroxy-5-methyl-4-isoxazole propionic acid receptor), $GABA_AR$ (γ-amino-butyric acid type A receptor), $5\text{-}HT_{1A}R$ (postsynaptic serotonin (1A) receptors), PSD-95 (postsynaptic density-95). signal pathways: CBF (cerebral blood flow), Ang-1 (Angiopoietin-1), VEGF (vascular endothelial growth factor), TLR4 (Toll Like Receptor 4), MyD88 (myeloid differentiation factor 88), NF-κB (nuclear factor-kappa B), α7nAChR (alpha-7 nicotinic acetylcholine receptor), JAK2 (Janus Kinase 2), STAT3 (Signal Transducer and Activator of Transcription 3), TNF-α (Tumor Necrosis Factor-α), IL-4 (interleukin 4), IL-10 (interleukin 10), IL-1β (interleukin 1β), Nrf2 (Nuclear factor erythroid2-related factor2), ARE (antioxidant response element), HO-1 (heme oxygenase), NQO1 (NADP (H) quinone oxidoreductase), ROS (reactive oxygen species), MDA (Malon-dialdehyde), SOD (superoxide dismutase), GSH (glutathione), HMGB1 (mobility group protein B1), MMP (mitochondrial membrane potential), PI3K (phosphatidylinositol 3-kinase), AKT (protein kinase B), mTOR (mammalian target of rapamycin), Bcl-2 (B-cell lymphoma-2), JNK (c-Jun N-terminal kinase).

heterogeneity and effective size of the combination of GV20 + ST36 (Baihui+Zusanli, MA, 14 days) (Wang et al., 2015; Li et al., 2016, 2021; Ye et al., 2017b; Du et al., 2018; Yang et al., 2018b, 2020; Zhu et al., 2018; Ma et al., 2020; Wang L. et al., 2020; Cao et al., 2021) were better than those of other combinations of acupuncture points. It has been found that GV20 could regulate cerebral blood flow in the ischemic region and promote nerve regeneration in the central nervous system (Chavez et al., 2017). Electroacupuncture in ST36 can activate the spinal sympathetic reflex and drive the vagal-adrenal axis through nerve endings to achieve anti-inflammatory effects (Liu et al., 2021). In the literatures we included, Ye et al. (2017b) conducted a study on the difference of three combinations efficacy, such as GV20 + ST36, GV20 + GV24, and ST36 + SP10, and the results showed that GV20 + ST36 performed better than other combinations in the detection of the morris water maze. The reason why GV20 + ST36 has better efficacy than other combinations is considered to be that GV20 is an important acupuncture point in the head. During oblique puncturing, the brain tissue stimulated by the needle tip is an important regulatory center for rat behavior, through which signals of acupuncture stimulation can be transmitted to the meninges, brainstem nucleus, or hippocampus. ST36 belongs to the acupuncture points of the hindlimb, with riched muscles in the lower extremities and more sensitive nerve conduction than in the chest and abdomen. Combining the acupuncture points at the upper and lower ends can better send signals back to the brain, thus increasing cerebral blood flow and improving cognition in rats. Yang et al. (2020) conducted a study using different treatment frequencies and stimulation amounts, and the results showed that high stimulation amounts could promote the recovery of cognitive ability in rats. compared to the rats received low stimulation amounts. In the literatures included in this study, GV20 + ST36 basically stimulated for consecutive 30s, with Angle < 90, Frequency > 120. However, the choice of wave type and frequency of electroacupuncture acupoint

combination treatment were inconsistent, and the current is basically 1–3 mA, plus the inconsistent course of treatment, resulting in bias. Therefore, we recommend the use of the combination of GV20 + ST36 manual acupuncture with a higher frequency of treatment when conducting animal research on acupuncture for VD.

In conclusion, this study showed that acupuncture has a clear neuroprotective effect in VD animal models. The mechanism of acupuncture on VD is summarized as follows: (1) Reduction of the oxidative stress (Wang et al., 2004, 2015; Zhu et al., 2013; Zhang et al., 2014; Li et al., 2016, 2021; Du et al., 2018; Yang et al., 2018b; Su et al., 2019), The oxidative stress which caused by chronic cerebrospinal hypoperfusion (CCH) was considered as a major factor in the underlying mechanism of VD, and brain damage induced by oxidative stress is a key step leading to cognitive deficits (Han et al., 2020). Acupuncture can reverse mitochondrial damage and reduce ROS, MDA and HMGB1, increase MMP, SOD, GSH, up-regulate ChAT and 14-3-3e, and down-regulate AChE and S100B activity. This series of effects were mainly caused by the activation of PI3K/AKT and Nrf2/HO-1 pathways. (2) Reduction of neuronal inflammation (Li and Lai, 2007; Han et al., 2017; Liu et al., 2017; Ma et al., 2020; Wang L. et al., 2020; Cao et al., 2021; Pan et al., 2021; Bu et al., 2022; Chen et al., 2022; Xu and Zhang, 2022). Cellular inflammation is one of the most important pathological mechanisms of VD, and is also involved in the development of other pathological mechanisms (Zhang et al., 2020). Acupuncture decreased IL-1β, IL-2, IL-6, TNF-α, INF-γ, MIP-2, iNOS, COX-2, Iba-1 levels and increased IL-4, IL-10 levels through α7nAChR/JAK2/STAT3 or TLR4/MyD88/NF-kB pathways. (3) Reduced apoptosis (Feng et al., 2013; Tian et al., 2015; Zhang et al., 2017; Zhu et al., 2018; Guo et al., 2020; Wang H. L. et al., 2021). Chronic cerebral hypoperfusion induces the expression and activation of inflammatory vesicle components in different regions of the brain and promotes the activation of apoptotic pathways. Cell survival requires regulation by a series of proteins associated with apoptosis (Poh et al., 2021). Acupuncture improved the cognition in VD rats by initiating the PI3K/AKT/mTOR or Trx-1/P-ASK/P-P38/P-JNK channel, increasing the expression of Bcl-2 protein, decreasing the protein levels of BAX, FAX, P53, Caspase 3, Caspase 8, and Aβ1-40. (4) Increased neurotransmitters (Lin and Wang, 2008; Shao et al., 2008; Niu et al., 2009; Yang et al., 2014, 2019; Jiang et al., 2017; He et al., 2018). Brain neurotransmitters are chemicals that help transmit signals from one nerve cell to another. Neurotransmitters are part of the core mechanism expressed by all neurons, and their content is closely related to cognitive ability (Spitzer, 2012). Acupuncture stimulations can increase the secretion of DOPAC, 5-HT, AVP, EP, SS, ACh, HVA, DA and some neurochemicals in VD rats, thereby increasing the level of neurotransmitter release. (5) Increased synaptic plasticity (Wei et al., 2011; Zhu et al., 2012; Lin et al., 2017; Ye et al., 2017b; Wang Z. et al., 2020; Zheng et al., 2020). Synaptic plasticity is a property of the tunable strength of connections between nerve cells, and synaptic plasticity has long been recognized as the neurobiological basis of cognition (Alkadhi, 2021). As an important determinant of synaptic plasticity, LTP plays a critical role in memory formation (Ye et al., 2017b). Acupuncture not only increased synaptic plasticity by upregulating LTP and increasing the amount of synaptophysin, but also increased the nACh, D1/D5, NMDA, $5HT_{1A}$, AMPA, $GABA_A$ receptors. (6) Increased neuronal cells (Li et al., 2015). Neurons are the most basic structural and functional units in the nervous system. They are limited in number and difficult to recover once damaged. Acupuncture can increase the number of pyramidal neurons to improve synaptic function. (7) Improved vascular function (Gao et al., 2020). Vascular endothelial growth factor (VEGF) and angiogenin-1 (Ang-1) play an important role in angiogenesis. They can enhance vascular permeability through different receptors and maintain the integrity of the vascular lumen (Apte et al., 2019). Acupuncture can promote the repair of cerebral ischemia-reperfusion injury by upregulating VEGF and Ang-1. (8) Increased sugar metabolizing enzymes (Zhao et al., 2011). For brain cells, glucose metabolism is an important energy source. Glucose metabolism is closely related to enzymes (Zhang et al., 2021). Acupuncture increased the activities of hexokinase, pyruvate kinase, and glucose 6 phosphate dehydrogenase, thus affecting the energy metabolism system (Figure 4).

Medicine can significantly improve cognition in VD rats, and there is no significant difference compared to acupuncture

The cholinesterase inhibitors such as donepezil, modulators of the NMDA receptor such as memantine, and calcium antagonists such as nimodipine were most commonly used for the treatment of VD currently (Sun, 2018). However, all the literatures included in this study using nimodipine tablets only, and no literature using donepezil for the treatment of VD meets the inclusion criteria. This ensures the uniformity of the drugs. This study showed that the efficacy of nimodipine is comparable to that of acupuncture. The mechanism of drug taking effect is also the same with that of acupuncture. This proves from another aspect that acupuncture is feasible as a therapy for VD.

The key factors of the drug include the dose, duration of use, and time to begin taking the drug (Battle et al., 2021). The dose of the drugs in the literature included in this study are mainly 12 mg/kg, but the treatment course of the medication has not been unified, mainly 14 days and 20 days. Therefore, we believed that the bias may be caused by the irregular medications. The correct time is closely associated with the recovery of the disease. Sometimes, taking the medicine too early may not have formed VD, and taking the medicine too late may miss the peak of

disease development (Mijajlović et al., 2017). The literatures included in this study started the medication 7–15 days after modeling, and this imbalance may also be the cause of bias.

To promote the development of medical evidence for VD, researchers can conduct an appropriate animal study of donepezil vs. acupuncture in the treatment of VD, start drug treatment at an appropriate time, and take a full course of medication, providing an objective and diversified basis for clinicians to choose.

The non-acupoints had little effect on the cognitive improvement of VD rats, which was similar to the model group

Non-acupoints are a common control method for acupuncture therapy, and its purpose is to highlight the specificity of acupuncture points. Usually, non-acupoints is selected at a position away from the spine and common acupoints, and the frequency and method of sham acupuncture should be consistent with the acupuncture group. This meta-analysis included 15 studies using sham acupuncture or non-acupoint studies. Additionally, based on this research analysis, the bilateral hypochondrium, 10 mm above the iliac crest was mainly selected as the acupuncture points in the control groups. (Ma et al., 2020) speculated that the effect of sham acupuncture is not good, mainly because (1) Due to their distance from the main nerve, stimulation signals from non-acupoints may not reach the central nervous system successfully (2) Signals are transmitted to the brain or spinal cord from non-acupoint acupuncture. However, they may not be effective acupoints for cognitive dysfunction (non-specific effects).

The results of this meta-analysis showed that the effect of non-acupoints was not statistically different from that of the impaired group and was inferior to the other groups. To highlight the specificity of the point of acupuncture, we believed that the bilateral hypochondrium, 10 mm above the iliac crest can be selected as the acupuncture points in the sham intervention group.

Palliative therapy in the model group did not significantly improve the cognition of VD rats

The impaired group was treated with palliative therapy, that is, after surgical modeling, they maintained the same feeding and grasping as the rest of the interventions, but no drugs and acupuncture were given. The surgical modeling methods involved in this study include 2VO, 4VO, EO, and MCAO. The statistical results show that MCAO has the highest success rate, followed by 2VO and EO, and 4VO the lowest. All the methods can successfully shape VD animal models. MCAO is used mainly for modeling ischemic stroke, and the remaining three methods are used mainly for the establishment of chronic ischemia models. Therefore, we paid more focus on the differences of VD rats recovery capacity after successful modeling with different modeling methods. The recovery ability of VD rats is mainly associated to the operation method and the postoperative rest time. 4VO is a modeling method that has a greater effect on rat trauma and death, and the recovery difficulty of this method should be greater than that of 2VO, EO, and MCAO (Ganesana and Venton, 2021). Tuo et al. (2021) found that 8-week to 3-month resting after modeling, cerebral blood flow in rats could restore to normal. However, some studies suggested that the cognitive ability of rats was impaired at 4 weeks after 2VO modeling and the most serious damage was found at 20 weeks (Liu et al., 2005). Unfortunately, we investigated the specificity of acupuncture in this present study, while more in-depth discussions were conducted for the rest after modeling. This is also the next step for our team.

The results of this meta-analysis showed that the model group had the worst effect. We recommend choosing 2VO to create a VD rat model. After the modeling operation, postoperative rest and drug intervention time should be strictly mastered, which can better reflect the pathological characteristics of VD.

Strengths and weaknesses

Advantage

This meta-analysis was performed based on the analysis under the Bayesian Markov Chain Monte Carlo framework. The Bayesian method refers to the posterior probability, which is more realistic and the estimated value is more accurate (Hu et al., 2020). This study is the first network meta-analysis of acupuncture treatment of VD animal models. We comprehensively analyzed various factors of acupuncture efficacy which included in the characteristics of the literature, and provide evidence-based medicine for future animal studies for acupuncture methods. The ultimate goal of all animal researches on acupuncture is to serve the clinic. According to the conclusion from this meta-analysis, the effect mechanism of head acupoints and some acupuncture points is comprehensively summarized. In this way, it may end the VD treatment predicament and improve the effect of clinical treatment, and bring new hope for VD patients.

Limitations

No study is perfect and this meta-analysis has inherent shortcomings. First, the difference between the syndrome differentiation and treatment followed by Chinese medicine in clinic and the generalized modeling method of animal research

was an unavoidable drawback. Second, many literatures were not included in this analysis due to the strict literature inclusion criteria initially established. Third, the literatures included in this study were all carried out in China, resulting in an insufficient original literature for some interventions. Finally, the morris water maze was used as the outcome in this study, and some electron microscopy and light microscopy results were lacking. These shortcomings will partially bias the results of this analysis.

Looking to the future

Evidence-based medicine research will never stop and good animal systematic review research should be linked to clinical practice. In the future, first of all, we will continue to conduct researches on diseases that conform to TCM syndromes combined with VD animal models, organically combine animal experiments with clinical experiments, and refer to each other to promote the transformation between preclinical evidence and clinical evidence. Second, the inclusion criteria will be reestablished and a comprehensive analysis will be performed on the amount of acupuncture stimulation, electron and light microscopy results, as well as the physical and chemical indicators. Finally, we hope that there will be more standardized, large-sample, high-quality animal studies in the future to verify the conclusions of this meta-analysis, provide more reliable reference for acupuncture clinicians, and efficiently reduce the physical and mental burden of VD patients.

Conclusions

The results of this comprehensive network meta-analysis revealed that medication and acupuncture significantly altered outcomes of the Morris water maze in VD rats, while non-acupuncture and palliative care in the impaired group did not show efficacy. When conducting the experimental study for the treatment of VD rats with acupuncture, the acupuncture treatment plan of GV20 + ST36, MA, 14 days treatment can be used to obtain better results. In addition, this study provided multiple beneficial mechanisms about how acupuncture protects neurons in experimental VD, including antioxidative stress, reduction of neuroinflammation, inhibition of apoptosis, and increase in neurotransmitters, synaptic plasticity, and neuronal number. Our findings provide new information on animal studies of VD and contribute to the selection of protocols for acupuncture treatment of VD in animal experiments.

Data availability statement

The original contributions presented in the study are included in the article/Supplementary materials, further inquiries can be directed to the corresponding author/s.

Author contributions

WJ, JL, and ML designed the study and revised the manuscript for important intellectual content. YS, LZ, and TW acquired the data. CY and HL analyzed and interpreted the data. GL drafted the manuscript. All authors read and approved the final manuscript.

Funding

This research was supported by two National Natural Science Foundation of China Youth Fund Projects (82104757 and 82004450).

Acknowledgments

We thank Science and Technology Innovation Center of Guangzhou University of Chinese Medicine, for searching for abstracts and articles related to this study.

Conflict of interest

The authors declare that the research was conducted in the absence of any commercial or financial relationships that could be construed as a potential conflict of interest.

Publisher's note

Supplementary material

The Supplementary Material for this article can be found online at: https://www.frontiersin.org/articles/10.3389/fnagi.2022.952181/full#supplementary-material

References

Alkadhi, K. A. (2021). NMDA receptor-independent LTP in mammalian nervous system. *Prog. Neurobiol.* 200, 101986. doi: 10.1016/j.pneurobio.2020.101986

Apte, R. S., Chen, D. S., and Ferrara, N. (2019). VEGF in signaling and disease: beyond discovery and development. *Cell.* 176, 1248–1264. doi: 10.1016/j.cell.2019.01.021

Battle, C. E., Abdul-Rahim, A. H., Shenkin, S. D., Hewitt, J., and Quinn, T. J. (2021). Cholinesterase inhibitors for vascular dementia and other vascular cognitive impairments: a network meta-analysis. *Cochrane Database Syst. Rev.* 2, D13306. doi: 10.1002/14651858.CD013306.pub2

Bu, Y., Li, W. S., Lin, J., Wei, Y. W., Sun, Q. Y., and Zhu, S. J., et al. (2022). Electroacupuncture attenuates Immune-Inflammatory response in hippocampus of rats with vascular dementia by inhibiting TLR4/MyD88 signaling pathway. *Chin. J. Integr. Med.* 28, 153–161. doi: 10.1007/s11655-021-3350-5

Cao, Y., Wang, L., Lin, L. T., Wang, X. R., Ma, S. M., and Yang, N. N., et al. (2021). Acupuncture attenuates cognitive deficits through α7nAChR mediated anti-inflammatory pathway in chronic cerebral hypoperfusion rats. *Life Sci.* 266, 118732. doi: 10.1016/j.lfs.2020.118732

Carlson, A. P., Hänggi, D., Macdonald, R. L., and Shuttleworth, C. W. (2020). Nimodipine reappraised: an old drug with a future. *Curr. Neuropharmacol.* 18, 65–82. doi: 10.2174/1570159X17666190927113021

Chavez, L. M., Huang, S. S., MacDonald, I., Lin, J. G., Lee, Y. C., and Chen, Y. H. (2017). Mechanisms of acupuncture therapy in ischemic stroke rehabilitation: a literature review of basic studies. *Int. J. Mol. Sci.* 18, 2270.. doi: 10.3390/ijms18112270

Chen, D. F., Zhang, H., Xie, J. Y., Deng, C., Qiu, R. R., and Xu, Y. Y., et al. (2022). Effect of electroacupuncture on gut microbiota and serum IL-1β and IL-18 in rats with vascular dementia based on principle of "curing brain disorders by treating intestines". *Zhen Ci Yan Jiu*. 47, 216–223. doi: 10.13702/j.1000-0607.20210766

Cui, S., Chen, N., Yang, M., Guo, J., Zhou, M., and Zhu, C., et al. (2019). Cerebrolysin for vascular dementia. *Cochrane Database Syst. Rev.* 11, CD008900. doi: 10.1002/14651858.CD008900.pub3

Du, S. Q, Wang, X. R., Zhu, W., Ye, Y., Yang, J. W., and Ma, S. M., et al. (2018). Acupuncture inhibits TXNIP-associated oxidative stress and inflammation to attenuate cognitive impairment in vascular dementia rats. *CNS Neurosci. Ther.* 24, 39–46. doi: 10.1111/cns.12773

Farooq, M. U., Min, J., Goshgarian, C., and Gorelick, P. B. (2017). Pharmacotherapy for vascular cognitive impairment. *CNS Drugs*. 31, 759–776. doi: 10.1007/s40263-017-0459-3

Feng, X., Yang, S., Liu, J., Huang, J., Peng, J., and Lin, J., et al. (2013). Electroacupuncture ameliorates cognitive impairment through inhibition of NF-κB-mediated neuronal cell apoptosis in cerebral ischemia-reperfusion injured rats. *Mol. Med. Rep.* 7, 1516–1522. doi: 10.3892/mmr.2013.1392

Ganesana, M., and Venton, B. J. (2021). Spontaneous, transient adenosine release is not enhanced in the CA1 region of hippocampus during severe ischemia models. . *J. Neurochem.* 159, 887–900. doi: 10.1111/jnc.15496

Gao, Y. L., Tian, H. M., Chen, C. T., Chen, X. Y., He, H. L., and Zheng, H. E., et al. (2020). [Effect of acupuncture technique of Tiaoxin Tongdu on learning-memory ability and expressions of hippocampal VEGF and Ang-1 in rats with vascular dementia]. *Zhongguo Zhen Jiu*. 40, 1108–1112. doi: 10.13703/j.0255-2930.20190821-0008

Grande, G., Qiu, C., and Fratiglioni, L. (2020). Prevention of dementia in an ageing world: evidence and biological rationale. *Ageing Res. Rev.* 64, 101045. doi: 10.1016/j.arr.2020.101045

Guo, F., Zhang, S. Z., Chen, S. Y., Zhang, C., Zhang, X. Q., and Gao, F., et al. (2020). [Electroacupuncture improved learning-memory ability by reducing hippocampal apoptosis and suppressing JNK signaling in rats with vascular dementia]. *Zhen Ci Yan Jiu*. 45, 21–26. doi: 10.13702/j.1000-0607.1905126

Han, B., Jiang, W., Liu, H., Wang, J., Zheng, K., and Cui, P., et al. (2020). Upregulation of neuronal PGC-1α ameliorates cognitive impairment induced by chronic cerebral hypoperfusion. *Theranostics*. 10, 2832–2848. doi: 10.7150/thno.37119

Han, D., Liu, Z., Wang, G., Zhang, Y., and Wu, Z. (2017). Electroacupuncture improves cognitive deficits through increasing regional cerebral blood flow and alleviating inflammation in CCI rats. *Evid Based Complement Alternat Med*. 2017, 5173168. doi: 10.1155/2017/5173168

He, J., Zhao, C., Liu, W., Huang, J., Liang, S., and Chen, L., et al. (2018). Neurochemical changes in the hippocampus and prefrontal cortex associated with electroacupuncture for learning and memory impairment. *Int. J. Mol. Med.* 41, 709–716. doi: 10.3892/ijmm.2017.3287

Hooijmans, C. R., Rovers, M. M., de Vries, R. B., Leenaars, M., Ritskes-Hoitinga, M., and Langendam, M. W. (2014). SYRCLE's risk of bias tool for animal studies. *BMC Med. Res. Methodol.* 14, 43. doi: 10.1186/1471-2288-14-43

Hu, D., O'Connor, A. M., Wang, C., Sargeant, J. M., and Winder, C. B. (2020). How to conduct a bayesian network Meta-Analysis. *Front Vet Sci*. 7, 271. doi: 10.3389/fvets.2020.00271

Jiang, L. G., Zhang, H. W., Zhang, Z., and Shao, Y. (2017). [Influence of electroacupuncture stimulation with different intensities and therapeutic intervals on learning-memory ability and expression of aβ 1-40 and arginine vasopressin genes in the hippocampal CA 1 region in VD rats]. *Zhen Ci Yan Jiu*. 42, 20–24.

Kruschke, J. K. (2021). Bayesian analysis reporting guidelines. *Nat. Hum. Behav.* 5, 1282–1291. doi: 10.1038/s41562-021-01177-7

Kuring, J. K., Mathias, J. L., and Ward, L. (2018). Prevalence of depression, anxiety and PTSD in people with dementia: a systematic review and Meta-Analysis. *Neuropsychol. Rev.* 28, 393–416. doi: 10.1007/s11065-018-9396-2

Li, F., Yan, C. Q., Lin, L. T., Li, H., Zeng, X. H., and Liu, Y., et al. (2015). Acupuncture attenuates cognitive deficits and increases pyramidal neuron number in hippocampal CA1 area of vascular dementia rats. *BMC Complement Altern. Med*. 15, 133. doi: 10.1186/s12906-015-0656-x

Li, H., Liu, Y., Lin, L. T., Wang, X. R., Du SQ, and Yan, C. Q., et al. (2016). Acupuncture reversed hippocampal mitochondrial dysfunction in vascular dementia rats. *Neurochem. Int.* 92, 35–42. doi: 10.1016/j.neuint.2015.12.001

Li, L. C., Li, X. Y., and Du XH. (2021). [Acupuncture improves cognitive function of vascular dementia rats by regulating PI3K/Akt/mTOR pathway]. *Zhen Ci Yan Jiu*. 46, 851–856. doi: 10.13702/j.1000-0607.200844

Li, W., and Lai, X. S. (2007). [Changes of interleukin-1beta and TNF-alpha contents in the hippocampus and the interventional effect of electroacupuncture in vascular dementia rats]. *Zhen Ci Yan Jiu*. 32, 34–37.

Lin, R., Li, X., Liu, W., Chen, W., Yu, K., and Zhao, C., et al. (2017). Electro-acupuncture ameliorates cognitive impairment via improvement of brain-derived neurotropic factor-mediated hippocampal synaptic plasticity in cerebral ischemia-reperfusion injured rats. *Exp. Ther. Med.* 14, 2373–2379. doi: 10.3892/etm.2017.4750

Lin, R. J., Klein-Fedyshin, M., and Rosen, C. A. (2019). Nimodipine improves vocal fold and facial motion recovery after injury: a systematic review and meta-analysis. *Laryngoscope* 129, 943–951. doi: 10.1002/lary.27530

Lin, S. J., and Wang, W. (2008). [Effect of electroacupuncture on NMDAR-2 B mRNA expression in hippocampal tissue in vascular dementia rats]. *Zhen Ci Yan Jiu*. 33, 301–305.

Liu, H. X., Zhang, J. J., Zheng, P., and Zhang, Y. (2005). Altered expression of MAP-2, GAP-43, and synaptophysin in the hippocampus of rats with chronic cerebral hypoperfusion correlates with cognitive impairment. *Brain Res Mol Brain Res*. 139, 169–177. doi: 10.1016/j.molbrainres.2005.05.014

Liu, J., Li, C., Peng, H., Yu, K., Tao, J., and Lin, R., et al. (2017). Electroacupuncture attenuates learning and memory impairment via activation of α7nAChR-mediated anti-inflammatory activity in focal cerebral ischemia/reperfusion injured rats. *Exp. Ther. Med.* 14, 939–946. doi: 10.3892/etm.2017.4622

Liu, S., Wang, Z., Su, Y., Qi, L., Yang, W., and Fu, M., et al. (2021). A neuroanatomical basis for electroacupuncture to drive the vagal-adrenal axis. *Nature* 598, 641–645. doi: 10.1038/s41586-021-04001-4

Lu, L., Zhang, Y., Tang, X., Ge, S., Wen, H., and Zeng, J., et al. (2022). Evidence on acupuncture therapies is underused in clinical practice and health policy. *BMJ* 376, e67475. doi: 10.1136/bmj-2021-067475

Ma, S. M., Wang, L., Su, X. T., Yang, N. N., Huang, J., and Lin, L. L., et al. (2020). Acupuncture improves white matter perfusion and integrity in rat model of vascular dementia: an MRI-Based imaging study. *Front. Aging Neurosci.* 12, 582904. doi: 10.3389/fnagi.2020.582904

Mijajlović, M. D., Pavlović, A., Brainin, M., Heiss, W. D., Quinn, T. J., and Ihle-Hansen, H. B., et al. (2017). Post-stroke dementia - a comprehensive review. *BMC Med.* 15, 11. doi: 10.1186/s12916-017-0779-7

Niu, W. M., Liu, Z. B., Yang, X. H., Niu, X. M., and Wang, Y. (2009). [Effect of "Xiusanzhen" on learning-memory ability and hippocampal somatostatin and arginine vesopressin contents in vascular dementia rats]. *Zhen Ci Yan Jiu*. 34, 106–109.

O'Brien, J. T., and Thomas, A. (2015). Vascular dementia. *Lancet* 386, 1698–1706. doi: 10.1016/S0140-6736(15)00463-8

Page, M. J., McKenzie, J. E., Bossuyt, P. M., Boutron, I., Hoffmann, T. C., and Mulrow, C. D., et al. (2021). The PRISMA 2020 statement: an updated guideline for reporting systematic reviews. *BMJ* 372, 71. doi: 10.1136/bmj.n71

Pan, P., Ma, Z., Zhang, Z., Ling, Z., Wang, Y., and Liu, Q., et al. (2021). Acupuncture can regulate the peripheral immune cell spectrum and inflammatory environment of the vascular dementia rat, and improve the cognitive dysfunction of the rats. *Front. Aging Neurosci.* 13, 706834. doi: 10.3389/fnagi.2021.706834

Poh, L., Fann, D. Y., Wong, P., Lim, H. M., Foo, S. L., and Kang, S. W., et al. (2021). AIM2 inflammasome mediates hallmark neuropathological alterations and cognitive impairment in a mouse model of vascular dementia. *Mol. Psychiatry*. 26, 4544–4560. doi: 10.1038/s41380-020-00971-5

Shao, Y., Fu, Y., Qiu, L., Yan, B., Lai, X. S., and Tang, C. Z. (2008). Electropuncture influences on learning, memory, and neuropeptide expression in a rat model of vascular dementia. *Neural. Regen. Res.* 3, 267–271.

Smith, E. E. (2017). Clinical presentations and epidemiology of vascular dementia. *Clin Sci (Lond)*. 131, 1059–1068. doi: 10.1042/CS20160607

Spitzer, N. C. (2012). Activity-dependent neurotransmitter respecification. *Nat. Rev. Neurosci.* 13, 94–106. doi: 10.1038/nrn3154

St-Onge, M., Anseeuw, K., Cantrell, F. L., Gilchrist, I. C., Hantson, P., and Bailey, B., et al. (2017). Experts consensus recommendations for the management of calcium channel blocker poisoning in adults. *Crit. Care Med.* 45, e306–e315. doi: 10.1097/CCM.0000000000002087

Su, X., Wu, Z., Mai, F., Fan, Z., Du S, and Qian, H., et al. (2019). 'Governor vessel-unblocking and mind-regulating' acupuncture therapy ameliorates cognitive dysfunction in a rat model of middle cerebral artery occlusion. *Int. J. Mol. Med.* 43, 221–232. doi: 10.3892/ijmm.2018.3981

Sun, M. K. (2018). Potential therapeutics for vascular cognitive impairment and dementia. *Curr. Neuropharmacol.* 16, 1036–1044. doi: 10.2174/1570159X15666171016164734

Tian, W. J., Huang, L. N., Wang, R. H., An, J. M., and Zhang, M. (2015). [Effects of scalp-acupuncture on astrocyte apoptosis in hippocampal CA 1 region in rats with vascular dementia]. *Zhen Ci Yan Jiu*. 40, 6–12

Tuo, Q. Z., Zou, J. J., and Lei, P. (2021). Rodent models of vascular cognitive impairment. *J. Mol. Neurosci.* 71, 1–12. doi: 10.1007/s12031-020-01733-2

Wang, H. L., Liu, F. L., Li, R. Q., Wan, M. Y., Li, J. Y., and Shi, J., et al. (2021). Electroacupuncture improves learning and memory functions in a rat cerebral ischemia/reperfusion injury model through PI3K/Akt signaling pathway activation. *Neural. Regen. Res.* 16, 1011–1016. doi: 10.4103/1673-5374.300454

Wang, L., Tang, C., and Lai, X. (2004). Effects of electroacupuncture on learning, memory and formation system of free radicals in brain tissues of vascular dementia model rats. *J. Tradit. Chin. Med.* 24, 140–143.

Wang, L., Yang, J. W., Lin, L. T., Huang, J., Wang, X. R., and Su, X. T., et al. (2020). Acupuncture attenuates inflammation in microglia of vascular dementia rats by inhibiting miR-93-Mediated TLR4/MyD88/NF-κB signaling pathway. *Oxid. Med. Cell. Longev.* 2020, 8253904. doi: 10.1155/2020/8253904

Wang, R., Yao, Q., Chen, W., Gao, F., Li, P., and Wu, J., et al. (2021). Stem cell therapy for Crohn's disease: systematic review and meta-analysis of preclinical and clinical studies. *Stem Cell Res. Ther.* 12, 463. doi: 10.1186/s13287-021-02533-0

Wang, X. R., Shi, G. X., Yang, J. W., Yan, C. Q., Lin, L. T., and Du SQ, et al. (2015). Acupuncture ameliorates cognitive impairment and hippocampus neuronal loss in experimental vascular dementia through Nrf2-mediated antioxidant response. *Free Radic. Biol. Med.* 89, 1077–1084. doi: 10.1016/j.freeradbiomed.2015.10.426

Wang, Z., Lin, B., Liu, W., Peng, H., Song, C., and Huang, J., et al. (2020). Electroacupuncture ameliorates learning and memory deficits via hippocampal 5-HT1A receptors and the PKA signaling pathway in rats with ischemic stroke. *Metab. Brain Dis.* 35, 549–558. doi: 10.1007/s11011-019-00489-y

Washida, K., Hattori, Y., and Ihara, M. (2019). Animal models of chronic cerebral hypoperfusion: from mouse to primate. *Int. J. Mol. Sci.* 20, 6176. doi: 10.3390/ijms20246176

Wei, D., Jia, X., Yin, X., and Jiang, W. (2011). Effects of electroacupuncture versus nimodipine on long-term potentiation and synaptophysin expression in a rat model of vascular dementia. *Neural Regen. Res.* 6, 2357

Xu, P., and Zhang, X. Z. (2022). [Acupuncture for improving neuroinflammation in vascular dementia rats by regulating Th1/Th2 cells balance in peripheral blood]. *Zhongguo Zhen Jiu*. 42, 407–412. doi: 10.13703/j.0255-2930.20210330-k000

Yang, J., Litscher, G., Li, H., Guo, W., Liang, Z., and Zhang, T., et al. (2014). The effect of scalp point cluster-needling on learning and memory function and neurotransmitter levels in rats with vascular dementia. *Evid Based Complement Alternat Med.* 2014, 294103. doi: 10.1155/2014/294103

Yang, J. W., Wang, X. R., Zhang, M., Xiao, L. Y., Zhu, W., and Ji, C. S., et al. (2018a). Acupuncture as a multifunctional neuroprotective therapy ameliorates cognitive impairment in a rat model of vascular dementia: a quantitative iTRAQ proteomics study. *CNS Neurosci. Ther.* 24, 1264–1274. doi: 10.1111/cns.13063

Yang, J. W., Wang, X. R., Zhang, M., Xiao, L. Y., Zhu, W., and Ji, C. S., et al. (2018b). Acupuncture as a multifunctional neuroprotective therapy ameliorates cognitive impairment in a rat model of vascular dementia: a quantitative iTRAQ proteomics study. *CNS Neurosci. Ther.* 24, 1264–1274.

Yang, N. N., Ma, S. M., Yang, J. W., Li, T. R., and Liu, C. Z. (2020). Standardizing therapeutic parameters of acupuncture in vascular dementia rats. *Brain Behav.* 10, e1781. doi: 10.1002/brb3.1781

Yang, X. B., Wang, J. H., An, H. Q., Liu, D. L., Guan, S. M., and Cui, D. N., et al. (2019). [Warming-promotion needling improves learning-memory ability by up-regulating expression of hippocampal nicotinic acetylcholine receptor subunit in rats with vascular dementia]. *Zhen Ci Yan Jiu*. 44, 709–714. doi: 10.13702/j.1000-0607.190202

Ye, Y., Li, H., Yang, J. W., Wang, X. R., Shi, G. X., and Yan, C. Q., et al. (2017b). Acupuncture attenuated vascular Dementia-Induced hippocampal Long-Term potentiation impairments via activation of D1/D5 receptors. *Stroke* 48, 1044–1051. doi: 10.1161/STROKEAHA.116.014696

Ye, Y., Zhu, W., Wang, X. R., Yang, J. W., Xiao, L. Y., and Liu, Y., et al. (2017a). Mechanisms of acupuncture on vascular dementia-A review of animal studies. *Neurochem. Int.* 107, 204–210. doi: 10.1016/j.neuint.2016.12.001

Zhang, L. Y., Pan, J., Mamtilahun, M., Zhu, Y., Wang, L., and Venkatesh, A., et al. (2020). Microglia exacerbate white matter injury via complement C3/C3aR pathway after hypoperfusion. *Theranostics* 10, 74–90. doi: 10.7150/thno.35841

Zhang, S., Lachance, B. B., Mattson, M. P., and Jia, X. (2021). Glucose metabolic crosstalk and regulation in brain function and diseases. *Prog. Neurobiol.* 204, 102089. doi: 10.1016/j.pneurobio.2021.102089

Zhang, X., Wu, B., Nie, K., Jia, Y., and Yu, J. (2014). Effects of acupuncture on declined cerebral blood flow, impaired mitochondrial respiratory function and oxidative stress in multi-infarct dementia rats. *Neurochem. Int.* 65, 23–29. doi: 10.1016/j.neuint.2013.12.004

Zhang, Y. Q., Lu, L., Xu, N., Tang, X., Shi, X., and Carrasco-Labra, A., et al. (2022). Increasing the usefulness of acupuncture guideline recommendations. *BMJ* 376, e70533. doi: 10.1136/bmj-2022-070533

Zhang, Z., Yang, J., Sun, Q., and Shao, Y. (2017). Effects of electroacupuncture treatment of different intensities on learning-memory function and expression of β-amyloid protein 1-40 in hippocampus CA1 region in rats with vascular dementia. *Chin. J. Cerebrovascular Dis.* 331, 321–32.

Zhang, Z. Y., Liu, Z., Deng, H. H., and Chen, Q. (2018). Effects of acupuncture on vascular dementia (VD) animal models: a systematic review and meta-analysis. *BMC Complement Altern. Med.* 18, 302. doi: 10.1186/s12906-018-2345-z

Zhao, L., Shen, P., Han, Y., Zhang, X., Nie, K., and Cheng, H., et al. (2011). Effects of acupuncture on glycometabolic enzymes in multi-infarct dementia rats. *Neurochem. Res.* 36, 693–700. doi: 10.1007/s11064-010-0378-x

Zheng, Y., Qin, Z., Tsoi, B., Shen, J., and Zhang, Z. J. (2020). Electroacupuncture on trigeminal Nerve-Innervated acupoints ameliorates poststroke cognitive impairment in rats with middle cerebral artery occlusion: involvement of neuroprotection and synaptic plasticity. *Neural Plast.* 2020, 8818328. doi: 10.1155/2020/8818328

Zhu, W., Wang, X. R., Du, S. Q, Yan, C. Q., Yang, N. N., and Lin, L. L., et al. (2018). Anti-oxidative and anti-apoptotic effects of acupuncture: role of thioredoxin-1 in the hippocampus of vascular dementia rats. *Neuroscience* 379, 281–291. doi: 10.1016/j.neuroscience.2018.03.029

Zhu, Y., Wang, X., Ye, X., Gao, C., and Wang, W. (2012). Effects of electroacupuncture on the expression of p70 ribosomal protein S6 kinase and ribosomal protein S6 in the hippocampus of rats with vascular dementia. *Neural Regen. Res.* 7, 207–211. doi: 10.3969/j.issn.1673-5374.2012.03.009

Zhu, Y., Zeng, Y., Wang, X., and Ye, X. (2013). Effect of electroacupuncture on the expression of mTOR and eIF4E in hippocampus of rats with vascular dementia. *Neurol. Sci.* 34, 1093–1097. doi: 10.1007/s10072-012-1209-4

frontiers | Frontiers in Aging Neuroscience

TYPE Original Research
PUBLISHED 24 August 2022
DOI 10.3389/fnagi.2022.998255

OPEN ACCESS

EDITED BY
Woon-Man Kung,
Chinese Culture University, Taiwan

REVIEWED BY
Chengjie Mao,
Second Affiliated Hospital of Soochow University, China
Cheng-Yu Wei,
Chang Bing Show Chwan Memorial Hospital, Taiwan

*CORRESPONDENCE
Feng-Tao Liu
liufengtao@fudan.edu.cn
Yu-Jie Yang
yujieyang1015@me.com

†These authors have contributed equally to this work

SPECIALTY SECTION
This article was submitted to Parkinson's Disease and Aging-related Movement Disorders, a section of the journal Frontiers in Aging Neuroscience

RECEIVED 19 July 2022
ACCEPTED 03 August 2022
PUBLISHED 24 August 2022

CITATION
Chen M-J, Lu J-Y, Li X-Y, Jiao F-Y, Zuo C-T, Wang J, Liu F-T and Yang Y-J (2022) Striatal dopaminergic lesions contributed to the disease severity in progressive supranuclear palsy. *Front. Aging Neurosci.* 14:998255. doi: 10.3389/fnagi.2022.998255

Striatal dopaminergic lesions contributed to the disease severity in progressive supranuclear palsy

Ming-Jia Chen[1†], Jia-Ying Lu[2†], Xin-Yi Li[1], Fang-Yang Jiao[2], Chuan-Tao Zuo[2,3], Jian Wang[1], Feng-Tao Liu[1,*] and Yu-Jie Yang[1,4*] for the Progressive Supranuclear Palsy Neuroimage Initiative (PSPNI)

[1]Department of Neurology, National Research Center for Aging and Medicine, National Center for Neurological Disorders, and State Key Laboratory of Medical Neurobiology, Huashan Hospital, Fudan University, Shanghai, China, [2]PET Center, National Center for Neurological Disorders, and National Clinical Research Center for Aging and Medicine, Huashan Hospital, Fudan University, Shanghai, China, [3]Human Phenome Institute, Fudan University, Shanghai, China, [4]Key Laboratory of Arrhythmias, Ministry of Education, Department of Medical Genetics, Shanghai East Hospital, School of Medicine, Tonji University, Shanghai, China

Background: Reduced dopamine transporter (DAT) binding in the striatum has been reported in patients with progressive supranuclear palsy (PSP). However, the relationship between striatal dopaminergic lesions and the disease severity of PSP remains to be explored.

Objective: To investigate the contributions of striatal dopaminergic lesions to the disease severity of PSP.

Methods: One hundred patients with clinically diagnosed PSP were consecutively enrolled in this study. The disease severity was systemically assessed using the PSP rating scale (PSPrs), and the dopaminergic lesions were assessed using the ^{11}C-N-2-carbomethoxy-3-(4-fluorophenyl)-tropane positron emission tomography (^{11}C-CFT PET) imaging. To explore the correlations between striatal DAT bindings and the disease severity, both the region-wise and voxel-wise analysis were adopted. Partial correlations and multiple linear regressions were performed to investigate the contribution of striatal dopaminergic lesions to the disease severity in PSP.

Results: Sixty-three patients of PSP with Richardson's syndrome (PSP-RS) and 37 patients with PSP-non-RS were finally included. The disease severity in PSP-RS was much heavier than that in the PSP-non-RS. The DAT bindings in the caudate and anterior putamen correlated significantly with the PSPrs total scores, mainly in the domains of history, mentation, bulbar, and ocular motor symptoms. The striatal DAT bindings (caudate) contributed significantly

to the disease severity of PSP, independent of the motor, cognition, emotion and behavioral dysfunctions.

Conclusion: Our study highlighted the independent contribution of striatal dopaminergic lesions to the disease severity in PSP.

KEYWORDS

dopamine transporter, position emission tomography, caudate, progressive supranuclear palsy, disease severity

Introduction

Progressive supranuclear palsy (PSP) is a rare, adult-onset neurodegenerative disease, with typical clinical manifestations including impaired ocular mobility, postural instability, akinesia, and neuro-psychological impairments (Höglinger et al., 2017). The disorder severely impacts the life quality and shortens life span (Schrag et al., 1999; Nath et al., 2001). Unfortunately, there is only symptomatic treatment with mild and unsustainable efficacy available (Coughlin and Litvan, 2020). To develop effective therapies, it is of extremely high necessity to explore the factors contributing to the disease severity in PSP.

Previously, researchers have explored variable factors related to the disease severity in PSP. In cerebrospinal fluid (CSF), the levels of neurofilament light chain (Rojas et al., 2018), phosphorylated tau 181 (Rojas et al., 2018), amyloid beta 42 (Schirinzi et al., 2018) were associated with disease severity in PSP. With regard to imaging features, the bindings of several tau tracers in the midbrain were related with the disease severity of PSP (Kepe et al., 2013; Brendel et al., 2017; Perez-Soriano et al., 2017; Schirinzi et al., 2018; Malpetti et al., 2021). Additionally, other tracers to index microglial activation (Malpetti et al., 2021), synapse loss (Holland et al., 2020) and glucose metabolism (Zwergal et al., 2011), were also investigated in PSP patients.

As an atypical Parkinsonism, the dopaminergic lesions in striatum have been widely reported in PSP (Jin et al., 2013; Whitwell et al., 2017; Yoo et al., 2018; Chen et al., 2022). Compared with other tracers, the dopamine transporter (DAT) tracer represents the functional state of the dopaminergic system. The dopaminergic system plays important roles in motor control, motivation, reward, cognitive function, maternal, and reproductive behaviors (Klein et al., 2019). It's widely accepted that dopaminergic dysfunction correlates closely with disease severity in Parkinson's disease (Liu et al., 2018) and atypical Parkinsonism like Multiple System Atrophy (Lee et al., 2021). Given that severely decreased DAT bindings were found in both PSP-RS and PSP-non-RS subtypes (Chen et al., 2022) and the contribution of the dopaminergic lesions to the disease severity in PSP has never been explored before, we conducted this cross-sectional study aiming to explore the contribution of dopaminergic lesions to the disease severity in PSP, with the DAT positron emission tomography (PET) imaging in a relatively large PSP cohort with various subtypes.

Materials and methods

Participants

From January 1, 2018 to March 31, 2021, 100 patients with clinically diagnosed PSP were consecutively enrolled in this DAT PET imaging study. The diagnosis was made and reviewed by three movement disorder specialists according to the Movement Disorder Society Diagnostic Criteria (Höglinger et al., 2017). The study was approved by the Ethics Committee of Huashan Hospital and all subjects provided informed written consent before entering this study in accordance with the Declaration of Helsinki.

Clinical assessments

The demographic characteristics of patients, including the age, sex, education, age at onset, disease duration, and levodopa equivalent daily dosage (LEDD) were systemically collected. After withdrawal of anti-parkinsonian drugs for at least 12 h, the evaluation of the PSP rating scale (PSPrs) and the motor section of the MDS unified Parkinson's disease rating scale (MDS UPDRS-III) was made by two experienced specialists in movement disorders, reflecting the disease severity and motor dysfunctions in PSP patients, with higher scores representing more severe symptoms. Global cognition function was assessed using Mini-mental state examination (MMSE), with higher scores representing better cognitive function. Frontal behavioral abnormalities were assessed by frontal behavioral inventory (FBI), with higher scores indicating more severe abnormality. The symptoms of depression were evaluated using geriatric

depression scale (GDS), with higher scores indicating greater disability.

^{11}C-CFT PET imaging and data analysis

All participants received ^{11}C-N-2-carbomethoxy-3-(4-fluorophenyl)-tropane (^{11}C-CFT) PET examination on a Siemens PET/CT (Biograph 64 HD, Siemens, Germany) in a quiet and dimly lit room, within 1 month of clinical assessments. A low dose computed tomography (CT) was performed first for attenuation correction. ^{11}C-CFT PET scan was performed from the 60 to 80 min after intravenous injection of 350–400 MBq of ^{11}C-CFT, and reconstructed with the ordered subset expectation maximization method.

Image data were preprocessed using the Statistical Parametric Mapping (SPM) 8 software (Wellcome Department of Imaging Neuroscience, Institute of Neurology, London, United Kingdom) and subsequently processed with the ScAnVP software, version 7.0 (Center for Neuroscience, the Feinstein Institute for Medical Research, Manhasset, NY, United States) implemented in Matlab 8.4 (Mathworks Inc., Sherborn, MA, United States). Individual scans were spatially normalized into the Montreal Neurological Institute (MNI) brain space using an internal template (Bu et al., 2018). The spatially normalized PET image was then smoothed using an 8 mm full width at half maximum (FWHM) Gaussian kernel to increase signal-to-noise ratio.

Two analytical approaches were employed to explore the relationship between striatal dopaminergic lesions and disease severity. First, regional analysis was performed. The previously defined volume of interest (VOI) atlas in MNI space identifying manually with reference to the corresponding structural MR images (Bu et al., 2018) was used for semi-quantification. Tracer bindings were calculated in 7 VOIs, consisting of bilateral caudate, bilateral anterior putamen, bilateral posterior putamen (Oh et al., 2012), and occipital area. Using the occipital area as the reference region, striatal-to-occipital ratios (SORs), defined as (striatal VOI—occipital VOI)/occipital VOI were quantified for each hemisphere, and then averaged across hemispheres. Partial correlations were performed between PSPrs scores and striatal DAT binding, adjusted for sex, age at onset, and duration of the disease. The second analytical approach was voxel-wise analysis, to assess specific voxel-level correlations with PSPRrs after adjustment for sex, age at onset, and disease duration. To conduct this analysis, the preprocessed ^{11}C-CFT PET images were first divided by the corresponding value in the occipital area to obtain the SOR maps. Then multiple regression model in SPM8 was used to explore the correlation. Due to hypothesis-driven confirmatory nature, an uncorrected voxel threshold at $P < 0.01$ was applied with an extent threshold of $>$ 1-fold the expected voxels per cluster estimated in SPM.

Statistical analysis

Potential differences between groups regarding demographic characteristics were investigated. For continuous variables, Kolmogorov–Smirnov test was performed, to investigate the normality. Independent *t*-test was performed for data of normalized distribution, and Mann–Whitney U test was performed for data of non-normalized distribution. Pearson's chi-squared test was performed for categorical data. Partial correlations were performed, adjusted for sex, age at onset, and duration of the disease. Multiple linear regression analysis was also performed to explore the predictors of disease severity. We used SPSS (version 26.0, IBM, Armonk, NY, United States) for statistical analysis and $P < 0.05$ was considered statistically significant.

Results

Demographic characteristics and clinical information

In the 100 patients with PSP finally included, 63 cases (63.0%) were classified as PSP with Richardson's syndrome (PSP-RS), and 37 cases (37.9%) as PSP-non-Richardson's syndrome (PSP-non-RS), including 19 cases as PSP with predominant parkinsonism (PSP-P) and 18 cases as PSP with progressive gait freezing (PSP-PGF). The patients with PSP-RS took shorter disease duration ($P < 0.01$), higher disease severity as assessed by PSPrs scores (total score, $P < 0.05$; history score, $P < 0.05$; ocular motor scores, $P < 0.05$), and higher neuropsychological symptoms by FBI scores ($P < 0.05$) and GDS scores ($P < 0.01$), than those with PSP-non-RS. No significant difference was detected between PSP-RS and PSP-non-RS in terms of age, age at onset, sex, education, LEDD, MDS UPDRS III, or MMSE. In terms of the striatal DAT bindings, similar lesions were detected between the groups of PSP-RS and PSP-non-RS. The detailed information could be found in **Table 1** and **Supplementary Table 1**.

Factors correlating with progressive supranuclear palsy rating scale scores

In the region-wise analysis, the scores of MDS UPDRS III ($r = 0.74$, $P < 0.001$), MMSE ($r = -0.66$, $P < 0.001$), FBI ($r = 0.66$, $P < 0.001$), and GDS ($r = 0.50$, $P < 0.001$) correlated well with PSPrs total scores. The average DAT binding in the caudate ($r = -0.36$, $P < 0.001$) and anterior putamen ($r = -0.29$, $P < 0.01$), but not in the posterior putamen ($r = -0.17$, $P = 0.22$), correlated significantly with the PSPrs total scores in all patients with PSP (pooled), as shown in **Figure 1**. Similar

TABLE 1 Demographic characteristics and clinical information.

Variable	PSP (pooled) $n = 100$	PSP-RS $n = 63$	PSP-non-RS $n = 37$	*P*
Sex (male/female)	62/38	36/27	26/11	0.192
Age (years)	65.92 ± 7.59	65.94 ± 7.31	65.89 ± 8.15	0.978
Age at onset (years)	62.59 ± 7.82	63.33 ± 7.64	61.32 ± 8.05	0.216
Duration (months)	34.50 (21.00, 69.75)	31.00 (19.00, 48.00)	52.00 (24.00, 86.00)	0.007
Education (years)	9.00 (6.00, 12.13)	9.00 (6.00, 14.00)	11.00 (7.00, 12.00)	0.645
LEDD	403.41 ± 327.98	400.16 ± 343.34	408.94 ± 304.57	0.898
PSPrs total score	31.00 ± 15.04 28.50 (19.25, 39.00)	33.52 ± 15.67 31.00 (22.00, 40.00)	26.70 ± 13.01 24.00 (16.00, 35.50)	0.028
PSPrs I	6.00 (3.25, 9.00)	8.00 (4.00, 9.00)	5.00 (3.00, 7.00)	0.011
PSPrs II	2.00 (0.00, 4.00)	2.00 (1.00, 3.00)	2.00 (0.00, 5.00)	0.499
PSPrs III	2.00 (1.00, 3.00)	2.00 (1.00, 4.00)	2.00 (1.00, 3.00)	0.125
PSPrs IV	6.00 (4.00, 9.00)	7.00 (5.00, 9.00)	5.00 (2.00, 8.00)	0.022
PSPrs V	4.00 (3.00, 6.00)	4.00 (3.00, 7.00)	4.00 (3.00, 6.00)	0.631
PSPrs VI	7.00 (5.00, 10,75)	7.00 (6.00, 11.00)	6.00 (5.00, 9.50)	0.134
MDS UPDRS III	41.00 (29.75, 51.00)	42.00 (30.50, 51.00)	38.00 (29.00, 52.00)	0.692
MMSE	26.00 (21.00, 28.00)	26.00 (21.00, 28.00)	27.00 (23.00, 28.00)	0.517
FBI	16.00 ± 11.16	17.89 ± 12.01	12.97 ± 8.99	0.046
GDS	10.00 (6.00, 18.00)	12.00 (8.00, 20.00)	7.00 (4.50, 13.00)	0.005
Average DAT bindings				
Caudate	0.73 ± 0.33	0.72 ± 0.35	0.74 ± 0.31	0.861
Anterior Putamen	0.83 ± 0.36	0.83 ± 0.37	0.82 ± 0.35	0.915
Posterior Putamen	0.49 ± 0.23	0.49 ± 0.22	0.49 ± 0.25	0.580

For continuous variables, independent *t*-test was performed for data of normalized distribution, given as mean ± standard deviation and Mann–Whitney U test was performed for data of non-normalized distribution, given as medium (interquartile range). Pearson's chi-squared test was performed for categorical data. PSP-RS, PSP-Richardson's syndrome; LEDD, levodopa equivalent daily dosage; PSPrs, PSP rating scale; UPDRS, unified Parkinson's disease rating scale; MMSE, Mini-Mental State Examination; FBI, frontal behavioral inventory; GDS, geriatric depression scale.

correlations were also found in the subtypes of PSP-RS and PSP-non-RS (Supplementary Table 2). In the voxel-wise analysis, a significant correlation of the DAT binding in the anterior striatum (caudate and anterior putamen, $P < 0.01$) were further validated to correlate with the PSPrs total scores (Figure 2 and Supplementary Table 3).

In the further analysis with the scores of different domains in PSPrs, the DAT bindings in caudate and anterior putamen correlated well with the scores in history (I), mentation (II), bulbar function (III) and ocular mobility domains (IV) ($P < 0.01$). Meanwhile, only a weak correlation was found between the DAT binding in posterior putamen and the ocular motor dysfunctions (IV) ($r = -0.22$, $P < 0.05$). No correlation was detected between those dopaminergic lesions and the dysfunctions in limb motor (V), gait and midline (VI) (Table 2). Similar results could also be identified in the subtypes of PSP-RS and PSP-non-RS (Supplementary Table 4).

Contributors to the disease severity of progressive supranuclear palsy

Given the tight association between DAT binding in the caudate and anterior putamen ($r = 0.96$, $P < 0.001$), only DAT binding in the caudate, which correlated closer with disease severity in terms of PSPrs total scores was introduced in the multiple linear regression model. It's found that the variables of MDS UPDRS III ($\beta = 0.395$, $P < 0.001$), MMSE ($\beta = -0.223$, $P < 0.01$), FBI ($\beta = 0.223$, $P < 0.01$), DAT binding in the caudate ($\beta = -0.217$, $p < 0.001$), and GDS ($\beta = 0.173$, $P < 0.01$) contributed to the disease severity as assessed by PSPrs total scores (Table 3). In the PSP-RS group, higher MDS UPDRSIII scores ($\beta = 0.401$, $P < 0.001$), higher GDS scores ($\beta = 0.274$, $P < 0.01$), lower MMSE scores ($\beta = -0.227$, $P < 0.05$), and lower DAT binding in the caudate ($\beta = -0.222$, $P < 0.05$) were associated with higher PSPrs total scores. While in the PSP-non-RS group, higher FBI scores ($\beta = 0.369$, $P < 0.01$), higher MDS UPDRSIII scores ($\beta = 0.333$, $P < 0.01$) and lower DAT binding in the caudate ($\beta = -0.267$, $P < 0.05$) were related to higher PSPrs total scores (Supplementary Table 5).

Discussion

As we know, this is the first study exploring the contribution of the striatal dopaminergic dysfunctions, assessed by ^{11}C-CFT PET, to the disease severity of PSP. Firstly, the disease severity in patients with PSP-RS was

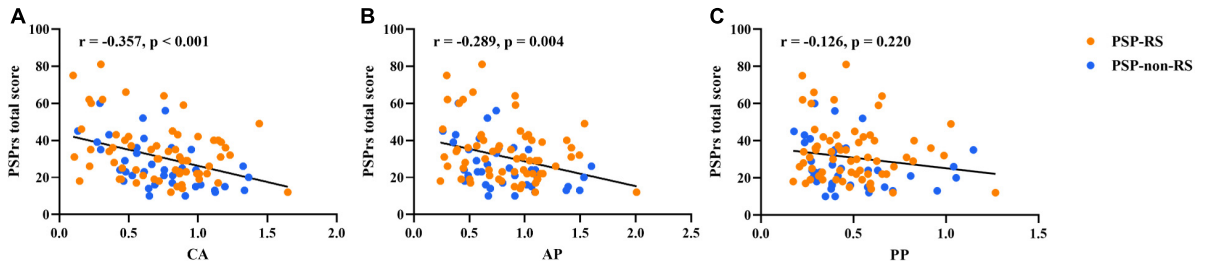

FIGURE 1
Partial correlations between regional DAT bindings [**(A)** caudate; **(B)** anterior putamen; **(C)** posterior putamen] and progressive supranuclear palsy rating scale (PSPrs) total scores in PSP (pooled), adjusted for sex, age at onset, and disease duration. Orange points, values in the PSP-RS group. Blue points, values in the PSP-non-RS group.

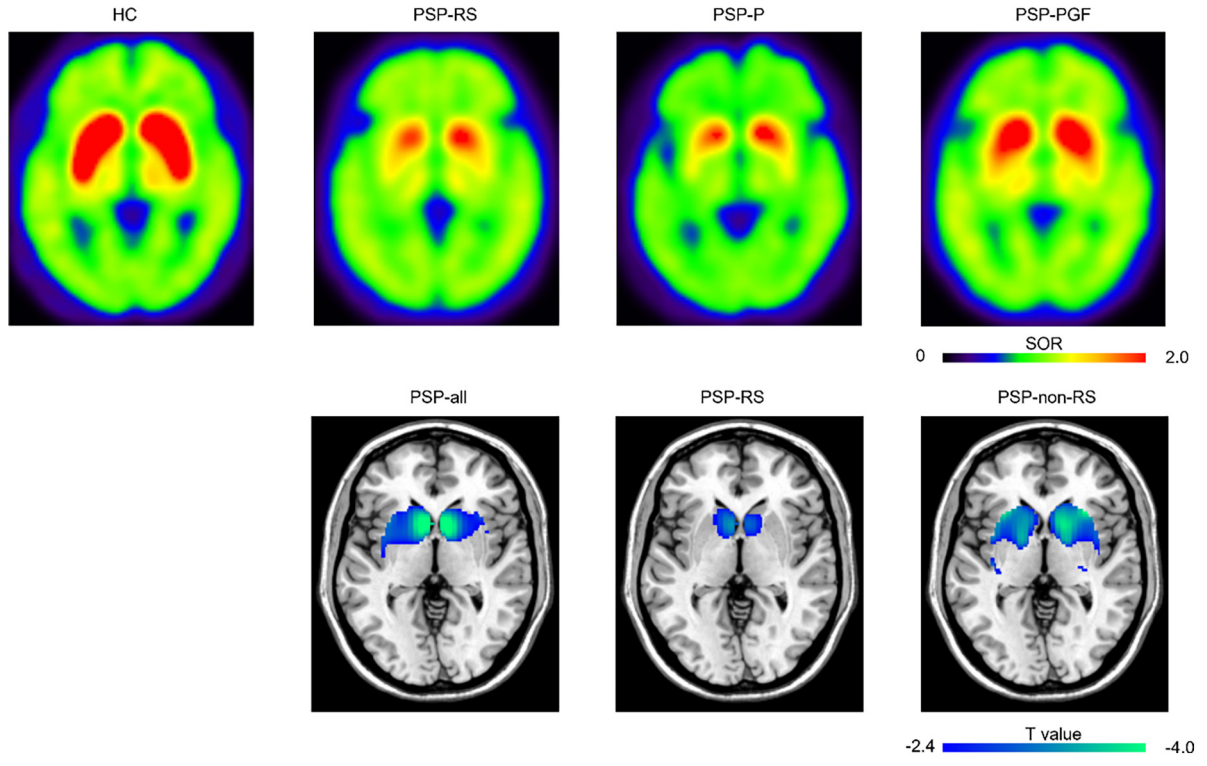

FIGURE 2
Representative ^{11}C-CFT PET images and regions "survived" after the voxel-wise correlations between progressive supranuclear palsy rating scale (PSPrs) total score and DAT bindings. The top row presented the representative ^{11}C-CFT PET images for healthy control and different subtypes of PSP. HC, male, 62 years old; PSP-RS, female, 61 years old, 9 months disease duration, PSPrs total score 42; PSP-P, male, 58 years old, 76 months disease duration, PSPrs total score 41; PSP-PGF, male, 77 years old, 82 months disease duration, PSPrs total score 36. The bottom row displayed the DAT bindings in specific regions showing significant negative correlations with PSPrs total score at $P < 0.01$ (uncorrected). HC, healthy control; SOR, striatal-to-occipital ratio.

higher than that in PSP-non-RS. Secondly, the disease severity of PSP correlated significantly with the DAT bindings in the caudate and anterior putamen, both in the PSP (pooled) and different PSP subtypes; mainly in the domains of history, mentation, bulbar, and ocular motor symptoms. Last but not least, the DAT bindings in caudate contributed to the disease severity of PSP, independent of the clinical severities of motor, cognition, emotion, and behavioral dysfunctions.

We reported that the patients with PSP-RS took a much more severe disease severity as assessed by PSPrs, especially in the domains of history (I) and ocular mobility (IV). Our findings could be supported by previous studies showing that PSPrs total scores and ocular motor scores (Choi et al., 2021)

TABLE 2 Partial correlations between PSPrs subscores and DAT binding in PSP (pooled).

		Caudate	Anterior putamen	Posterior putamen
PSPrs I	*r*	−0.363	−0.297	−0.141
	P	< 0.001	0.003	0.170
PSPrs II	*r*	−0.357	−0.288	−0.114
	P	< 0.001	0.004	0.267
PSPrs III	*r*	−0.372	−0.306	−0.153
	P	< 0.001	0.002	0.134
PSPrs IV	*r*	−0.359	−0.325	−0.220
	P	< 0.001	0.001	0.030
PSPrs V	*R*	−0.139	−0.092	0.007
	P	0.173	0.369	0.942
PSPrs VI	*r*	−0.162	−0.133	−0.038
	P	0.113	0.195	0.712

Partial correlation coefficients were performed, adjusted for sex, age at onset, disease duration.

TABLE 3 Multiple linear regressions predicting PSPrs total scores in PSP (pooled).

	β	*P*	R^2
Age at onset	0.039	0.516	0.747
Duration	−0.024	0.721	
Sex	0.013	0.819	
Subtype	−0.099	0.113	
MDS UPDRS III	0.395	< 0.001	
MMSE	−0.223	0.004	
FBI	0.223	0.006	
GDS	0.173	0.008	
Caudate	−0.217	< 0.001	

β, standardized beta-coefficient; UPDRS, unified Parkinson's disease rating scale; MMSE, Mini-Mental State Examination; FBI, frontal behavioral inventory; GDS, geriatric depression scale.

were relatively higher in PSP-RS patients than that in PSP-P and PSP-PGF, without differences in history, bulbar, limb motor, and gait/midline domains among three subtypes (Horta-Barba et al., 2021).

Severe dopaminergic lesions in the striatum were common in PSP, as shown in the DAT PET imaging (Yoo et al., 2018; Chen et al., 2022). For the first time, we reported the striatal dopaminergic dysfunctions in caudate and anterior putamen contributed to the disease severity in PSP, but not in posterior putamen. We previously reported that the lesions in posterior putamen were more prominent than caudate in PSP, reflecting specific degenerative patterns in Parkinsonism (Chen et al., 2022). Pathologically, dopaminergic projections to the striatum were from different parts of substantial nigra, with putamen from ventral part and caudate from dorsal part (Fearnley and Lees, 1991). In PSP, the ventral part of substantial nigra sustained greatest neuron degeneration (Fearnley and Lees, 1991), and the severe "floor-effect" may account for the irrelevant correlation between the DAT bindings in posterior putamen and the PSPrs total scores (Martin et al., 2008).

The contribution of dopaminergic lesions in striatum varies among different domains in the disease severity of PSP. Here, we reported the DAT binding was associated with the impairments in the domains of history (I), mentation (II), bulbar (III), and ocular motor (IV) in PSP. These domain-related correlations may be due to the involvement of dopaminergic projections in the frontostriatal-nigra circuitry regulating motor and cognitive function (Aarts et al., 2011). Previous studies supported the striatal DAT bindings related to cognitive impairments in PSP (Yoo et al., 2018). However, there was no correlation between the dopaminergic lesions and the dysfunctions in limb motor (V), gait and midline (VI). Interestingly, the items of limb motor subdomain were all eliminated in the recently modified PSPrs, due to low sensitivity to disease change (items 18, 19, 22) or failure of capturing severe disease milestones (items 20, 21, 23) (Grötsch et al., 2021). In terms of the freezing of gait and repeated falls, Cabeleira et al. (2019) reported the impairments in gait kinematics and postural control were not related to dopaminergic lesions in patients with mild and moderate PD, suggesting the involvement of some non-dopaminergic pathways. Further studies should explore the involvement of other neurotransmitters, such as acetylcholine, serotonin, norepinephrine (Maillet et al., 2012) and choline (Karachi et al., 2010; Bohnen and Albin, 2011; Rochester et al., 2012; Bohnen et al., 2013) in PSP.

So far as we know, this is the first study exploring the contributions of dopaminergic lesions to the disease severity of PSP, based on a relatively large cohort. Although our findings suggested that striatal dopaminergic lesions contributed to the disease severity in PSP, the contribution strength was only mild or moderate. This could be supported by the partial and unsustainable response to levodopa in PSP (Lopez et al., 2016).

Notably, as we suggested that DAT binding contributed to disease severity in PSP, the different disease severity but similar DAT binding between the PSP-RS and PSP-non-RS groups to some extent seemed not rational. We assumed it may be not only because dopaminergic dysfunction was one of the contributing factors to disease severity in PSP, but also because its contribution was only mild or moderate in intensity. However, several limitations should be admitted here. First, our cases were enrolled by clinical diagnosis without neuropathologic verification. The misdiagnosis could not be completely ruled out. Second, the threshold we set at the SPM analysis was relatively weak that could be accepted only for the confirmative nature of the analysis. Finally, this was a cross-sectional study performed in a single center, and the center-bias should be admitted and taken with caution. Further study with expanded participants in multiple centers and longitudinal follow-up should be expected.

Conclusion

Our study highlighted the independent contribution of striatal dopaminergic lesions to the disease severity in PSP, inspiring the further therapeutic explorations covering the dopaminergic pathways.

Data availability statement

The raw data supporting the conclusions of this article will be made available by the authors, without undue reservation.

Ethics statement

The studies involving human participants were reviewed and approved by the Human Studies Institutional Review Board, Huashan Hospital, Fudan University. The patients/participants provided their written informed consent to participate in this study. Written informed consent was obtained from the individual(s) for the publication of any potentially identifiable images or data included in this article.

Author contributions

JW and C-TZ provided the data. M-JC, J-YL, and X-YL analyzed the data. M-JC, J-YL, and F-YJ wrote the manuscript. Y-JY and F-TL supervised the work and revised the manuscript. All authors contributed to the article and approved the submitted version.

Funding

Y-JY has received funds (No. 82101952) from the National Natural Science Foundation of China. F-TL has received funds (Nos. 82171252 and 81701250) from the National Natural Science Foundation of China. JW has received grants from the Shanghai Municipal Science and Technology Major Project (Nos. 2018SHZDZX01 and 21S31902200) and the ZHANGJIANG LAB, a grant from National Health Commission of PRC (Pro20211231084249000238), and grants from the National Natural Science Foundation of China (Nos. 82171421 and 91949118). C-TZ has received grants (Nos. 82021002, 81971641 and 81671239) from the National Natural Science Foundation of China; Research project of Shanghai Health Commission (No. 2020YJZX0111); Clinical Research Plan of SHDC (No. SHDC2020CR1038B); and Science and Technology Innovation 2030 Major Project (No. 2022ZD0211600).

Acknowledgments

We would like to thank all the patients participating in this study.

Conflict of interest

The authors declare that the research was conducted in the absence of any commercial or financial relationships that could be construed as a potential conflict of interest.

Publisher's note

Supplementary material

The Supplementary Material for this article can be found online at: https://www.frontiersin.org/articles/10.3389/fnagi.2022.998255/full#supplementary-material

References

Aarts, E., van Holstein, M., and Cools, R. (2011). Striatal dopamine and the interface between motivation and cognition. *Front. Psychol.* 2:163. doi: 10.3389/fpsyg.2011.00163

Bohnen, N. I., and Albin, R. L. (2011). The cholinergic system and Parkinson disease. *Behav. Brain Res.* 221, 564–573. doi: 10.1016/j.bbr.2009.12.048

Bohnen, N. I., Frey, K. A., Studenski, S., Kotagal, V., Koeppe, R. A., Scott, P. J., et al. (2013). Gait speed in Parkinson disease correlates with cholinergic degeneration. *Neurology* 81, 1611–1616. doi: 10.1212/WNL.0b013e3182a9f558

Brendel, M., Schönecker, S., Höglinger, G., Lindner, S., Havla, J., Blautzik, J., et al. (2017). [(18)F]-THK5351 PET correlates with topology and symptom severity in progressive supranuclear palsy. *Front. Aging Neurosci.* 9:440. doi: 10.3389/fnagi.2017.00440

Bu, L. L., Liu, F. T., Jiang, C. F., Guo, S. S., Yu, H., Zuo, C. T., et al. (2018). Patterns of dopamine transporter imaging in subtypes of multiple system atrophy. *Acta Neurol. Scand.* 138, 170–176. doi: 10.1111/ane.12932

Cabeleira, M. E. P., Pagnussat, A. S., do Pinho, A. S., Asquidamini, A. C. D., Freire, A. B., Pereira, B. T., et al. (2019). Impairments in gait kinematics and postural control may not correlate with dopamine transporter depletion in individuals with mild to moderate Parkinson's disease. *Eur. J. Neurosci.* 49, 1640–1648. doi: 10.1111/ejn.14328

Chen, Q. S., Li, X. Y., Li, L., Lu, J. Y., Sun, Y. M., Liu, F. T., et al. (2022). Dopamine transporter imaging in progressive supranuclear palsy: Severe but nonspecific to subtypes. *Acta Neurol. Scand.* 46, 237–245. doi: 10.1111/ane.13653

Choi, J. H., Kim, H., Shin, J. H., Lee, J. Y., Kim, H. J., Kim, J. M., et al. (2021). Eye movements and association with regional brain atrophy in clinical subtypes of progressive supranuclear palsy. *J. Neurol.* 268, 967–977. doi: 10.1007/s00415-020-10230-w

Coughlin, D. G., and Litvan, I. (2020). Progressive supranuclear palsy: Advances in diagnosis and management. *Parkinsonism Relat. Disord.* 73, 105–116. doi: 10.1016/j.parkreldis.2020.04.014

Fearnley, J. M., and Lees, A. J. (1991). Ageing and Parkinson's disease: Substantia nigra regional selectivity. *Brain* 114(Pt 5), 2283–2301. doi: 10.1093/brain/114.5.2283

Grötsch, M. T., Respondek, G., Colosimo, C., Compta, Y., Corvol, J. C., Ferreira, J., et al. (2021). A modified progressive supranuclear palsy rating scale. *Mov. Disord.* 36, 1203–1215. doi: 10.1002/mds.28470

Höglinger, G. U., Respondek, G., Stamelou, M., Kurz, C., Josephs, K. A., Lang, A. E., et al. (2017). Clinical diagnosis of progressive supranuclear palsy: The movement disorder society criteria. *Mov. Disord.* 32, 853–864. doi: 10.1002/mds.26987

Holland, N., Jones, P. S., Savulich, G., Wiggins, J. K., Hong, Y. T., Fryer, T. D., et al. (2020). synaptic loss in primary tauopathies revealed by [(11) C]UCB-J positron emission tomography. *Mov. Disord.* 35, 1834–1842. doi: 10.1002/mds.28188

Horta-Barba, A., Pagonabarraga, J., Martínez-Horta, S., Busteed, L., Pascual-Sedano, B., Illán-Gala, I., et al. (2021). Cognitive and behavioral profile of progressive supranuclear palsy and its phenotypes. *J. Neurol.* 268, 3400–3408. doi: 10.1007/s00415-021-10511-y

Jin, S., Oh, M., Oh, S. J., Oh, J. S., Lee, S. J., Chung, S. J., et al. (2013). Differential diagnosis of parkinsonism using dual-phase F-18 FP-CIT PET imaging. *Nucl. Med. Mol. Imaging* 47, 44–51. doi: 10.1007/s13139-012-0182-4

Karachi, C., Grabli, D., Bernard, F. A., Tandé, D., Wattiez, N., Belaid, H., et al. (2010). Cholinergic mesencephalic neurons are involved in gait and postural disorders in Parkinson disease. *J. Clin. Invest.* 120, 2745–2754. doi: 10.1172/jci42642

Kepe, V., Bordelon, Y., Boxer, A., Huang, S. C., Liu, J., Thiede, F. C., et al. (2013). PET imaging of neuropathology in tauopathies: Progressive supranuclear palsy. *J. Alzheimers Dis.* 36, 145–153. doi: 10.3233/jad-130032

Klein, M. O., Battagello, D. S., Cardoso, A. R., Hauser, D. N., Bittencourt, J. C., and Correa, R. G. (2019). Dopamine: Functions, signaling, and association with neurological diseases. *Cell. Mol. Neurobiol.* 39, 31–59. doi: 10.1007/s10571-018-0632-3

Lee, R., Shin, J. H., Choi, H., Kim, H. J., Cheon, G. J., and Jeon, B. (2021). Variability of FP-CIT PET patterns associated with clinical features of multiple system atrophy. *Neurology* 96, e1663–e1671. doi: 10.1212/wnl.0000000000011634

Liu, F. T., Ge, J. J., Wu, J. J., Wu, P., Ma, Y., Zuo, C. T., et al. (2018). Clinical, dopaminergic, and metabolic correlations in Parkinson disease: A dual-tracer pet study. *Clin. Nucl. Med.* 43, 562–571. doi: 10.1097/rlu.0000000000002148

Lopez, G., Bayulkem, K., and Hallett, M. (2016). Progressive supranuclear palsy (PSP): Richardson syndrome and other PSP variants. *Acta Neurol. Scand.* 134, 242–249. doi: 10.1111/ane.12546

Maillet, A., Pollak, P., and Debû, B. (2012). Imaging gait disorders in parkinsonism: A review. *J. Neurol. Neurosurg. Psychiatry* 83, 986–993. doi: 10.1136/jnnp-2012-302461

Malpetti, M., Passamonti, L., Jones, P. S., Street, D., Rittman, T., Fryer, T. D., et al. (2021). Neuroinflammation predicts disease progression in progressive supranuclear palsy. *J. Neurol. Neurosurg. Psychiatry* 92, 769–775. doi: 10.1136/jnnp-2020-325549

Martin, W. R., Wieler, M., Stoessl, A. J., and Schulzer, M. (2008). Dihydrotetrabenazine positron emission tomography imaging in early, untreated Parkinson's disease. *Ann. Neurol.* 63, 388–394. doi: 10.1002/ana.21320

Nath, U., Ben-Shlomo, Y., Thomson, R. G., Morris, H. R., Wood, N. W., Lees, A. J., et al. (2001). The prevalence of progressive supranuclear palsy (Steele-Richardson-Olszewski syndrome) in the UK. *Brain* 124(Pt 7), 1438–1449. doi: 10.1093/brain/124.7.1438

Oh, M., Kim, J. S., Kim, J. Y., Shin, K. H., Park, S. H., Kim, H. O., et al. (2012). Subregional patterns of preferential striatal dopamine transporter loss differ in Parkinson disease, progressive supranuclear palsy, and multiple-system atrophy. *J. Nucl. Med.* 53, 399–406. doi: 10.2967/jnumed.111.095224

Perez-Soriano, A., Arena, J. E., Dinelle, K., Miao, Q., McKenzie, J., Neilson, N., et al. (2017). PBB3 imaging in Parkinsonian disorders: Evidence for binding to tau and other proteins. *Mov. Disord.* 32, 1016–1024. doi: 10.1002/mds.27029

Rochester, L., Yarnall, A. J., Baker, M. R., David, R. V., Lord, S., Galna, B., et al. (2012). Cholinergic dysfunction contributes to gait disturbance in early Parkinson's disease. *Brain* 135(Pt 9), 2779–2788. doi: 10.1093/brain/aws207

Rojas, J. C., Bang, J., Lobach, I. V., Tsai, R. M., Rabinovici, G. D., Miller, B. L., et al. (2018). CSF neurofilament light chain and phosphorylated tau 181 predict disease progression in PSP. *Neurology* 90, e273–e281. doi: 10.1212/wnl.0000000000004859

Schirinzi, T., Sancesario, G. M., Di Lazzaro, G., Scalise, S., Colona, V. L., Imbriani, P., et al. (2018). Clinical value of CSF amyloid-beta-42 and tau proteins in progressive supranuclear palsy. *J. Neural Transm. (Vienna)* 125, 1373–1379. doi: 10.1007/s00702-018-1893-1

Schrag, A., Ben-Shlomo, Y., and Quinn, N. P. (1999). Prevalence of progressive supranuclear palsy and multiple system atrophy: A cross-sectional study. *Lancet* 354, 1771–1775. doi: 10.1016/s0140-6736(99)04137-9

Whitwell, J. L., Höglinger, G. U., Antonini, A., Bordelon, Y., Boxer, A. L., Colosimo, C., et al. (2017). Radiological biomarkers for diagnosis in PSP: Where are we and where do we need to be? *Mov. Disord.* 32, 955–971. doi: 10.1002/mds.27038

Yoo, H. S., Chung, S. J., Kim, S. J., Oh, J. S., Kim, J. S., Ye, B. S., et al. (2018). The role of 18F-FP-CIT PET in differentiation of progressive supranuclear palsy and frontotemporal dementia in the early stage. *Eur. J. Nucl. Med. Mol. Imaging* 45, 1585–1595. doi: 10.1007/s00259-018-4019-y

Zwergal, A., la Fougère, C., Lorenzl, S., Rominger, A., Xiong, G., Deutschenbaur, L., et al. (2011). Postural imbalance and falls in PSP correlate with functional pathology of the thalamus. *Neurology* 77, 101–109. doi: 10.1212/WNL.0b013e318223c79d

frontiers | Frontiers in Aging Neuroscience

TYPE Original Research
PUBLISHED 26 August 2022
DOI 10.3389/fnagi.2022.935652

OPEN ACCESS

EDITED BY
Jiehui Jiang,
Shanghai University, China

REVIEWED BY
Jong-Min Kim,
Seoul National University Bundang Hospital, South Korea
Peter Mukli,
University of Oklahoma Health Sciences Center, United States
Etsuko Imabayashi,
National Institute for Quantum Science and Technology, Japan

*CORRESPONDENCE
Pai-Yi Chiu
paiyibox@gmail.com

SPECIALTY SECTION
This article was submitted to Alzheimer's Disease and Related Dementias, a section of the journal Frontiers in Aging Neuroscience

RECEIVED 04 May 2022
ACCEPTED 10 August 2022
PUBLISHED 26 August 2022

CITATION
Chen T-Y, Chan P-C, Tsai C-F, Wei C-Y and Chiu P-Y (2022) White matter hyperintensities in dementia with Lewy bodies are associated with poorer cognitive function and higher dementia stages.
Front. Aging Neurosci. 14:935652.
doi: 10.3389/fnagi.2022.935652

White matter hyperintensities in dementia with Lewy bodies are associated with poorer cognitive function and higher dementia stages

Tai-Yi Chen[1], Po-Chi Chan[2], Ching-Fang Tsai[3], Cheng-Yu Wei[4] and Pai-Yi Chiu[2,5]*

[1]Department of Radiology, Show Chwan Memorial Hospital, Changhua, Taiwan, [2]Department of Neurology, Show Chwan Memorial Hospital, Changhua, Taiwan, [3]Tainan Sin-Lau Hospital, The Presbyterian Church in Taiwan, Tainan, Taiwan, [4]Department of Neurology, Chang Bing Show Chwan Memorial Hospital, Changhua, Taiwan, [5]Department of Applied Mathematics, Tunghai University, Taichung, Taiwan

Purpose: White matter hyperintensities (WMHs) are frequently found in elderly individuals with or without dementia. However, the association between WMHs and clinical presentations of dementia with Lewy bodies (DLB) has rarely been studied.

Methods: We conducted a retrospective analysis of patients with DLB registered in a dementia database. WMHs were rated visually using the Fazekas scale, and its associated factors including dementia severity, cognitive functions, neuropsychiatric symptoms, and core clinical features were compared among different Fazekas scores. Domains in the Clinical Dementia Rating (CDR), Cognitive abilities Screening Instruments (CASI), and Neuropsychiatric Inventory (NPI) were compared among different Fazekas groups after adjusting for age, sex, education, and disease duration.

Results: Among the 449 patients, 76, 207, 110, and 56 had Fazekas score of 0, 1, 2, and 3, respectively. There was a positive association between dementia severity and WMHs severity, and the mean sums of boxes of the Clinical Dementia Rating (CDR-SB) were 5.9, 7.8, 9.5, and 11.2 (f = 16.84, $p < 0.001$) for the Fazekas scale scores 0, 1, 2, and 3, respectively. There was a negative association between cognitive performance and WMHs severity, and the mean CASI were 57.7, 45.4, 4.06, and 33.4 (f = 14.22, $p < 0.001$) for the Fazekas scale scores 0, 1, 2, and 3, respectively. However, WMHs were not associated with the core clinical features of DLB. After adjustment, all cognitive domains in CDR increased as the Fazekas score increased. In addition, performance on all cognitive domains in CASI decreased as the Fazekas score increased (all $p < 0.001$). Among neuropsychiatric symptoms, delusions, euphoria, apathy, aberrant motor behavior, and sleep disorders were significantly worse in the

higher Fazekas groups compared to those in the group with Fazekas score of 0 after adjustment.

Conclusion: WMHs in DLB might contribute to deterioration of cognitive function, neuropsychiatric symptoms, and dementia stages. However, core clinical features were not significantly influenced by WMHs in DLB.

KEYWORDS

white matter hyperintensities, dementia with Lewy bodies, Fazekas, cognitive, sums of boxes of the clinical dementia rating, cognitive abilities screening instruments

Introduction

White matter hyperintensities (WMHs) resulting from chronic ischemia associated with cerebral small vessel disease are frequently detected on magnetic resonance imaging (MRI) in elderly individuals (Prins et al., 2004). WMHs predict an increased risk of stroke, dementia, and death; therefore, detailed screening for risk factors of stroke and dementia should be performed if WMHs were identified (Debette and Markus, 2010). The histopathology of WMHs is various. The tissue damages range from slight disentanglement of the matrix to myelin and axonal loss (Prins and Scheltens, 2015; Wardlaw et al., 2015). In a previous study, WMHs were more frequent in patients with dementia than in patients with normal cognition (Sarro et al., 2016) and were strongly associated with cognitive dysfunction, especially in processing speed or executive functions (de Groot et al., 2000; Prins et al., 2004; Burton et al., 2006; Defrancesco et al., 2013). In patients with mild cognitive impairment (MCI), low scores in orientation and verbal delayed recall were predictors of progression from MCI to Alzheimer's disease (AD) (Defrancesco et al., 2013). WMHs can be used to predict an increased risk of dementia (Wolf et al., 2000; van Straaten et al., 2008; Brickman et al., 2012; Kamagata et al., 2013) and a high WMHs burden may result in imminent progression from MCI to dementia (de Groot et al., 2000).

Previous studies have focused on the association between WMHs and cerebrovascular disease or dementia due to AD (Wolf et al., 2000; Defrancesco et al., 2013; Taylor et al., 2017). However, the association or influence of WMHs burden on the clinical manifestation or progression of dementia with Lewy bodies (DLB) has less been studied. DLB is the second most common degenerative dementia, accounting for 0–26.3% of hospital- or population-based dementia cases (Zaccai et al., 2005). In a previous study, patients with DLB presented with fewer WMHs than those with vascular dementia (Barber et al., 1999; Ihara et al., 2010), while those with DLB and AD showed more severe WMHs than patients with Parkinson's disease (PD) with dementia (Joki et al., 2018). According to a previous study, WMHs in AD and DLB may be determined by similar processes and periventricular hyperintensities, but not deep WMHs, independently correlate with advancing age and increasing ventricular dilatation (Barber et al., 2000). However, studies investigating the contribution of WMHs or its associated factors in DLB have shown greater occipital WMHs in patients with DLB than in those with AD (Watson et al., 2012; Nedelska et al., 2015; Sarro et al., 2016). In addition, another study has reported an inverse relationship between small vessel disease scores and the severity of Lewy pathology in patients with Lewy body disease (LBD) (Ghebremedhin et al., 2010). There was an increased severity of WMHs on MRI, but not neuropathology, in DLB and Parkinson's disease (PD) with dementia compared to PD without dementia and age-matched controls (Hijazi et al., 2022).

Some studies have reported an association between cognitive function and WMHs in patients with PD or DLB. One study showed a significant correlation between WMHs and Mini-Mental State Examination and verbal fluency scores in the AD group, but not in the DLB group (Oppedal et al., 2012). Another found a significant association between increased total WMHs volume and worse performance in executive function, memory, and language (Vesely and Rektor, 2016).

The Fazekas scale is a simple visual rating tool for clinical assessment of WMHs in normal aging and dementia (Fazekas et al., 1987). To investigate the factors associated with WMHs in patients with DLB, the Fazekas scale was used in a relatively large sample size of patients with DLB. The important clinical features, cognitive performance, motor dysfunction including gait disturbance, neuropsychiatric symptoms, medication, and vascular risk factors (VRFs) were analyzed and compared between the high and low Fazekas groups. Based on the current evidence, we hypothesized that higher WMHs should have higher dementia severity, WMHs in DLB might contribute to more cognitive and motor dysfunction, and worse neuropsychiatric symptoms.

Materials and methods

Database

This retrospective study included patients aged more than 59 years old with probable DLB registered in the dementia database of the Show Chwan Health Care System. Registration is currently ongoing in three hospitals in Taiwan. The Committee for Medical Research Ethics of Show Chwan Memorial Hospital reviewed the project, and the Data Inspectorate approved it (SCMH_IRB No: IRB1081006). The following information was extracted from this database and used in this study:

(1) Diagnosis of dementia (major neurocognitive disorder) according to the criteria for primary degenerative dementia in the fifth edition of the Diagnostic and Statistical Manual of Mental Disorders. Diagnosis of DLB according to the revised consensus criteria for probable or possible DLB developed by the fourth report of the DLB consortium (McKeith et al., 2017).

(2) Age, sex, education, dementia severity according to the Clinical Dementia Rating Scale (CDR) and CDR-SB, such as memory, orientation, judgment, community affairs, home hobbies, and personal care (Morris, 1997), and motor severity assessed using the motor score (UPDRS-m) and gait sub-score (UPDRS-gait) of the Unified Parkinson's Disease Rating Scale (UPDRS) (Ballard et al., 1997; Movement Disorder Society Task Force on Rating Scales for Parkinson's, 2003) at the time of entry.

(3) Clinical features of DLB, including fluctuation in cognition, parkinsonism, visual hallucinations (VH), rapid eye movement sleep behavior disorder (RBD), and abnormal dopamine transporter imaging in partial participants (McKeith et al., 2017). To acquire a detailed clinical history, all participants were asked to complete a registration form, including a detailed history registration questionnaire, named the History-based Artificial Intelligent Clinical Dementia Diagnostic System (HAICDDS) (Lin et al., 2018; Chiu et al., 2019; Wang et al., 2020). Prior to starting the study, we trained 12 neuropsychologists in three centers, and reliability tests for HAICDDS and neuropsychological tests were performed after training. The HAICDDS is a structured questionnaire used for the diagnosis of core clinical features of DLB. It includes 6 domains on fluctuation, 7 domains on parkinsonism, 2 domains on VH, and 4 domains on RBD. Fluctuations were diagnosed when a mayo fluctuation composite score of $>$ 2 and a clinical history of fluctuation in cognition were present; VH were diagnosed when a clinical history of recurrent well-formed, complex, and detailed VH was present. Parkinsonism was diagnosed when at least two of the following were present: bradykinesia, rigidity, tremor, and postural instability; RBD was diagnosed when the minimum criteria for RBD according to the International Classification of Sleep Disorders were met (American Academy of Sleep Medicine, 2005).

(4) Cognitive performance assessed using the Chinese version of the Cognitive Abilities Screening Instrument (CASI) with the following domains: remote memory, recent memory, attention, mental manipulation, orientation, abstract thinking, language, drawing, and verbal fluency (Teng et al., 1994). Montreal Cognitive Assessment (MoCA) includes the following domains: visuospatial/executive, naming, attention, language, abstraction, memory, and orientation (Nasreddine et al., 2005; Kasten et al., 2010). Activities of daily living (ADL) assessed using the ADL scale embedded in the HAICDDS questionnaire (HAIADL) (Hung et al., 2021).

(5) Composite scores of the neuropsychiatric symptoms in the 12-item version of the NPI, such as delusions, hallucinations, agitation, depression, anxiety, euphoria, apathy, disinhibition, irritation, aberrant motor behavior, night behavior, and eating/appetite behavior. They were monitored according to observations in the past month (Cummings et al., 1994).

(6) Information on clinically relevant vascular risk comorbidities including hypertension, diabetes, hyperlipidemia, coronary artery disease, arrhythmia, congestive heart failure, and cerebrovascular disease (history of stroke or the diagnosis of vascular encephalopathy in brain imaging).

(7). MRI and WMHs ratings: MRI was performed using one of the four MRI scans currently used in the three centers (one 1.5 T Ingenia, Philips Healthcare, Best, the Netherlands, one 1.5 T Avanto, Siemens Medical Solutions, Erlangen, Germany, one 1.5 T Optima 450W, GE Healthcare, Milwaukee, Wisconsin, United States; and one 1.5 T Signa EXCITE-HD, GE Healthcare, Milwaukee, Wisconsin, United States). They were obtained at first clinical workup. The Fazekas scale (Fazekas et al., 1987) was used to determine the severity of WMHs. A total Fazekas WMH score, usually ranging from 0 to 6, was obtained by summing the periventricular (PVWM) and deep white matter (DWM) scores. In this study, to simplify the categories, we combined the periventricular and DWM scores and reduced the categories to 0–3. If PVWM and DWM scores were different, higher ones were selected for categorizing. Protocols include axial DWI (*b*-value 0, 1,000 s/mm^2) and ADC map, axial FLAIR (TE: 110 ms, TR: 9,000 ms, Flip angle (FA): 90, inversion time: 2,400 ms, FOV: 14 $\times$ 23 cm, slice thickness: 5 mm), axial T1WI (TE: 13 ms, TR: 450 ms, FA: 90, FOV: 14 $\times$ 23 cm, slice thickness: 5 mm), axial T2WI (TE: 85 ms, TR: 5,000 ms, FA: 90, FOV: 14 $\times$ 23 cm, slice thickness: 5 mm), axial SWI (3D-MRA TOF without contrast), sagittal 3D-T1 SPGR (fast spoiled gradient-recalled echo), and coronal T2WI (TE: 85 ms, TR: 3,500 ms, FA: 150, FOV: 20 $\times$ 20 cm, SL: 3 mm). The key sequence for evaluating the severity of WMHs is axial FLAIR sequence. Before the starting of the study, 36 patients were tested by one neuroradiologist (TY Chen) and one neurologist (PY Chiu) and the reproducibility was studied using the interrater reliability analysis with a high intra-class correlation coefficient of 0.927.

(8) Striatal background ratio and caudate putamen ratio (CPR) were assessed using Tc-99m Trodat-1 SPECT and

analyzed semi-quantitatively (Huang et al., 2012). Dopamine transporter imaging is one of the indicative biomarkers; therefore, some participants received 99m Trodat-1 SPECT or cerebral perfusion SPECT to obtain more accurate diagnosis. The procedure of the dopamine transporter imaging is as the following: A dose of 25 mCi of [99 mTc] TRODAT-1 was injected intravenously into each patient. The binding to dopamine transporter was assessed 4 h after injection by SPECT. A rotating three-headed gamma camera with fan-beam collimator (Multi SPECT 3, Siemens, Germany) and a commercially available computer system were used for data acquisition and processing. Data were collected for 120 projections (360° rotation) in a 128 × 128 matrix. The acquisition time was 40 s per projection. Attenuation correction was performed in the selected transverse slices according to a modified Chang's method. In-plane resolution of the reconstructed images was 8.5 mm FWHM, and slice thickness was approximately 6 mm.

Data analysis

The Chinese version of SPSS 22.0 for Windows (IBM, SPSS Inc., Chicago) was used for statistical analyses. Background characteristics, clinical features, VRFs, current medication usage, performance on different cognitive domains, and manifestation of neuropsychiatric symptoms of patients with DLB in different Fazekas groups were compared. Comparison of characteristics included age, education level, global dementia severity according to the CDR and CDR-SB, results of cognitive tests including subscale scores of the CASI and MoCA, and subscale scores of the neuropsychiatric symptoms according to the NPI. One-way ANOVA with either Bonferroni or Dunnett T3 *post hoc* analysis was according to the homogeneity of variance. Sex, clinical features of DLB, VRFs, and current medication usage were analyzed using the chi-square test with Bonferroni correction. The motor scores of the UPDRS and findings of dopamine transporter imaging performed using Tc-99m Trodat-1 SPECT were analyzed among the partial participants (36, 86, 42, and 22 cases with Fazekas 0, 1, 2, and 3, respectively). Domains in the CDR including a supplementary domain of language (HAICDDS-Language, Lin et al., 2018), CASI, and NPI were compared using multivariate logistic regression among different Fazekas group after adjusting for age, sex, education, and disease duration. Odds ratio (OR) of the higher Fazekas groups were compared to that of the group with Fazekas score of 0.

Results

The registration period for this study was from September 2015 to August 2020. During this period, we registered 9,607 individuals with either normal cognition (n = 2,131), MCI (n = 2,485), or dementia (n = 4,269) in a hospital-based cohort. In the dementia group, 1,841 (47.1%) patients had probable AD, 449 (10.5%) patients had DLB, 1,979 (43.4%) patients had other subtypes of dementia or undetermined dementia. Among patients with DLB, 76, 207, 110, and 56 patients had Fazekas scale scores of 0, 1, 2, and 3, respectively (**Table 1**). A comparison of ages among the four Fazekas subgroups revealed no significant association, and the mean age was 78.6, 79.5, 80.8, and 80.5 for the Fazekas scale scores of 0, 1, 2, and 3, respectively. The sex disparity, education, and disease duration were not significantly different among the four Fazekas subgroups, either. However, there was a positive association between dementia severity and WMH severity, and the mean CDR-SB were 5.9, 7.8, 9.5, and 11.2 (f = 16.84, $p < 0.001$) for the Fazekas scale scores 0, 1, 2, and 3, respectively. There was a negative association between cognitive performance and WMH severity, and the mean CASI were 57.7, 45.4, 4.06, and 33.4 (f = 14.22, $p < 0.001$) for the Fazekas scale scores 0, 1, 2, and 3, respectively. In addition, there was a negative association between ADL function and WMH severity, and the mean HAIADL were 11.0, 14.7, 17.8, and 2.3 (f = 17.02, $p < 0.001$) for the Fazekas scale scores 0, 1, 2, and 3, respectively. Poorer motor and gait functions according to UPDRS-m (f = 4.81, p = 0.003) and UPDRS-gait (f = 4.50, p = 0.004) were found only in the Fazekas 3. The CPR according to Tc-99m Trodat-1 SPECT was significantly higher in the lower Fazekas subgroups (Fazekas 0 and 1) compared to those in the higher Fazekas groups (Fazekas 2 and 3).

Comparisons of core clinical features for the diagnosis of DLB, VRFs, and current medications among different Fazekas groups are summarized in **Table 2**. Among all participants, frequencies of core clinical features including fluctuation in cognition, VH, parkinsonism, and RBD were 67.3, 43.2, 87.5, and 45.9%, respectively. Frequency of abnormal dopamine transporter imaging was 82.3% (153 with abnormal finding within 186 participants that performed dopamine transporter imaging). Comparison of these important diagnostic features for DLB were not significantly different among the Fazekas groups. Comparisons of VRFs and current medications usage among different Fazekas groups demonstrated that no significant difference among groups after Bonferroni correction except for CVD was higher in the Fazekas 3 group compared to those in the Fazekas 0 or 1 groups (f = 14.40, p = 0.002).

Figure 1 demonstrated a comparison of domains in CDR among different Fazekas groups and showed positive correlations of domains including memory, orientation, judgment, community affairs, home hobbies, personal care, and language with all $p < 0.001$. After adjustment for age, sex, education, and disease duration, all cognitive domains increased as the Fazekas score increased. After adjustment, compared to Fazekas 0 in memory, the ORs were 1.38, 1.81, and

TABLE 1 Comparison of demographical characteristics among different Fazekas groups.

	Fazekas 0 (F0) Mean (SD, range)	Fazekas 1 (F1) Mean (SD, range)	Fazekas 2 (F2) Mean (SD, range)	Fazekas 3 (F3) Mean (SD, range)	F/X^2	*p*	*Post hoc*
N	76	207	110	56			
Age, year	78.6 (5.1, 66–93)	79.5 (6.7, 60–97)	80.8 (6.8, 61–95)	80.5 (7.3, 60–97)	2.01	NS	
Female, *n*	31 (40.8)	100 (48.3)	52 (47.3)	31 (55.4)	2.81	NS	
Education, year	4.7 (4.0, 0–16)	4.1 (4.3, 0–18)	3.4 (3.9, 0–14)	3.5 (4.2, 0–16)	1.64	NS	
Duration, year	1.9 (1.9, 0.2–10.0)	2.3 (2.5, 0.2–13.0)	2.0 (2.3, 0.2–15.0)	2.8 (3.3, 0.3–16.0)	1.99	NS	
CDR	1.0 (0.7, 0.5–3.0)	1.3 (0.8, 0.5–3.0)	1.6 (0.9, 0.5–3.0)	1.8 (0.7, 0.5–3.0)	13.34	<0.001	F0 < F1 < F2 = F3
CDR-SB	5.9 (4.3, 0.5–17.0)	7.8 (4.8, 0.5–18.0)	9.5 (5.1, 1.0–18.0)	11.2 (4.0, 1.0–18.0)	16.84	<0.001	F0 < F1 < F2 = F3
MoCA	10.9 (6.5, 0–24)	7.5 (6.0, 0–28)	6.3 (5.1, 0–19)	5.2 (4.8, 0–22)	13.20	<0.001	F0 > F1 > F3
CASI	57.7 (21.8, 0–93)	45.4 (23.2, 0–94)	40.6 (22.9, 0–82)	33.4 (21.4, 0–79)	14.22	<0.001	F0 > F1 > F3
HAIADL	11.0 (7.8, 2–31)	14.7 (8.3, 2–31)	17.8 (8.4, 2–31)	20.3 (8.0, 2–31)	17.02	<0.011	F0 < F1 < F2 = F3
NPI	9.7 (9.1, 0–41)	14.1 (15.2, 0–101)	15.2 (13.7, 0–90)	17.4 (14.5, 0–72)	3.84	0.010	F0 < F1 = F2 = F3
UPDRS-m	27.2 (12.6, 2–56)	34.2 (19.6, 5–84)	33.4 (21.1, 0–91)	47.4 (18.6, 9–84)	4.81	0.003	F0 = F1 = F2 < F3
UPDRS-gait	1.4 (1.1, 0–4)	1.6 (1.1, 0–4)	1.8 (1.3, 0–4)	2.1 (1.3, 0–4)	4.50	0.004	F0 = F1 = F2 < F3
PVWM, 0/1/2/3	76/0/0/0	2/205/0/0	0/8/102/0	0/0/2/53	1247.5	<0.001	F0 < F1 < F2 < F3
DWM, 0/1/2/3	76/0/0/0	4/203/0/0	1/16/93/0	0/1/4/50	1146.1	<0.001	F0 < F1 < F2 < F3
Cortical MB, *n* (%)	5 (6.6)	14 (6.8)	19 (17.1)	18 (32.7)	31.46	<0.001	F0 = F1 < F2 < F3
Subcortical MB, *n* (%)	9 (11.8)	19 (9.2)	21 (18.9)	17 (30.9)	18.63	<0.001	F0 = F1 < F2 < F3
SBR	1.2 (0.4, 0.2–1.8)	1.2 (0.5, 0.0–2.3)	1.1 (0.4, 0.2–2.2)	1.0 (0.5, 0.0–2.0)	1.11	NS	
CPR	1.7 (0.2, 1.3–2.3)	1.7 (0.3, 1.1–2.4)	1.50 (0.3, 1.0–2.2)	1.5 (0.3, 1.1–2.1)	4.44	0.005	F0 = F1 < F2 = F3

N, Number of cases; Fazekas, Fazekas scale for white matter hyperintensities; NS, Non-significance. Duration, Disease duration; CDR, Clinical Dementia Rating scale; CDR-SB, sum of boxes of the CDR; MoCA, Montreal Cognitive Assessment; CASI, Cognitive Abilities Screening Instrument; HAIADL, History-based Artificial Intelligence Activities of Daily Living scale; NPI, total score of 12-domain Neuropsychiatric Inventory; UPDRS-m, motor score of the Unified Parkinson's Disease Rating Scale; UPDRS-gait, gait sub-score of the UPDRS-m; PVWM, periventricular white matter score in Fazekas; DWM, deep white matter score in Fazekas; MB, microbleeds; SBR, Striatal background ratio in Tc-99m Trodat-1 SPECT among 36, 86, 42, and 22 cases with Fazekas 0, 1, 2, and 3, respectively; CPR, caudate putamen ratio in Tc-99m Trodat-1 SPECT among 36, 86, 42, and 22 cases with Fazekas 0, 1, 2, and 3, respectively.

TABLE 2 Comparison of clinical features, vascular risk factors, and current medication usage among different Fazekas groups.

	Fazekas 0 (F0) *n* (%)	Fazekas 1 (F1) *n* (%)	Fazekas 2 (F2) *n* (%)	Fazekas 3 (F3) *n* (%)	X^2	*P*	Bonferroni correction
n	76	207	110	56			
Clinical features							
Fluctuation	50 (65.8)	131 (63.9)	75 (58.2)	45 (80.4)	5.53	NS	
VH	25 (32.9)	88 (42.5)	52 (47.3)	29 (51.8)	5.76	NS	
Parkinsonism	70 (92.1)	186 (89.9)	89 (80.9)	48 (85.7)	7.07	NS	
RBD	37 (48.7)	101 (48.8)	50 (45.5)	18 (32.1)	5.21	NS	
DaTabN	28 (77.8)	69 (80.2)	39 (92.9)	17 (77.3)	4.35	NS	
Vascular risk factors							
CVD	4 (5.3)	21 (10.1)	19 (17.3)	14 (25.0)	14.40	0.002	F0 < F3; F1 < F3
Hypertension	27 (35.5)	93 (45.8)	59 (55.1)	27 (50.9)	7.31	NS	
Diabetes	19 (25.0)	53 (26.1)	29 (27.1)	9 (17.0)	2.20	NS	
Hyperlipidemia	6 (7.9)	38 (18.7)	14 (13.1)	8 (15.1)	5.51	NS	
Heart diseases	15 (19.7)	37 (18.2)	18 (16.8)	8 (15.1)	0.56	NS	
Current medication							
Anti-dementia drugs	7 (9.2)	30 (14.5)	13 (11.8)	9 (16.1)	1.95	NS	
Anti-Parkinson drugs	19 (25.0)	39 (18.8)	13 (11.8)	11 (19.6)	5.49	NS	
Antiplatelets	13 (17.1)	40 (19.3)	18 (16.4)	11 (19.6)	3.84	NS	
Antipsychotics	6 (7.9)	27 (13.0)	11 (10.0)	10 (17.9)	3.66	NS	

NS, Non-significance; VH, visual hallucinations; RBD, REM sleep behavior disorder; DaTabN, abnormal dopamine transporter imaging in Tc-99m Trodat-1 SPECT among 36, 86, 42, and 22 cases with Fazekas 0, 1, 2, and 3, respectively; CVD, cerebrovascular disease or transient ischemic attack according to clinical history or MRI imaging; Heart diseases including carotid artery disease, congestive heart failure, and arrhythmia.

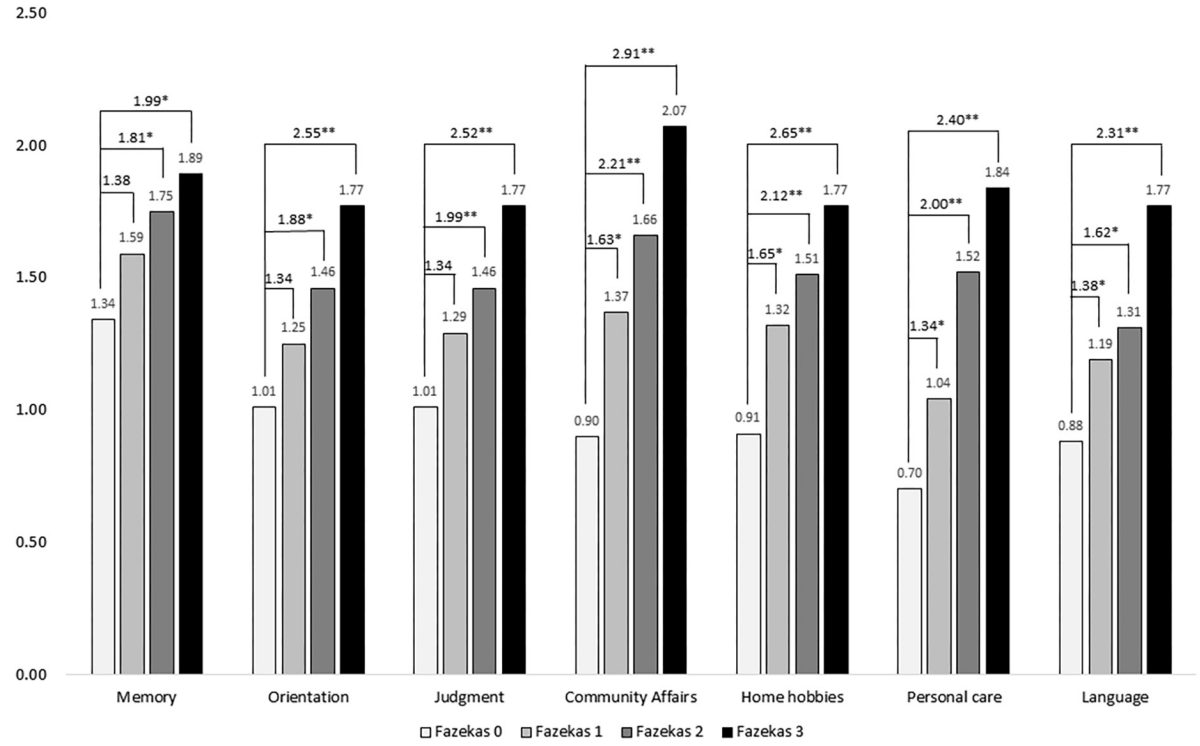

FIGURE 1
Comparison of scores of boxes of the Clinical Dementia Rating (CDR-SB) among different Fazekas groups adjusted for age, sex, education, and disease duration. ORs were compared to Fazekas score of 0. *$p < 0.05$; **$p < 0.001$.

1.99 in Fazekas 1, 2, and 3, respectively. In orientation, the ORs were 1.34, 1.88, and 2.55 in Fazekas 1, 2, and 3, respectively. In judgment, the ORs were 1.34, 1.99, and 2.52 in Fazekas 1, 2, and 3, respectively. In community affairs, the ORs were 1.63, 2.61, and 2.91 in Fazekas 1, 2, and 3, respectively. In home hobbies, the ORs were 1.65, 2.12, and 2.65 in Fazekas 1, 2, and 3, respectively. In personal care, the ORs were 1.34, 2.00, and 2.40 in Fazekas 1, 2, and 3, respectively. In language, the ORs were 1.38, 1.62, and 2.31 in Fazekas 1, 2, and 3, respectively.

Figure 2 demonstrated a comparison of cognitive domains of the CASI among different Fazekas groups and showed positive correlations of domains including remote memory, recent memory, attention, mental manipulation, orientation, abstract thinking, language, drawing, and verbal fluency with all $p < 0.001$. Performance on all cognitive domains decreased as the Fazekas score increased. After adjustment, in remote memory, the ORs were 0.83, 0.82, and 0.78 in Fazekas 1, 2, and 3, respectively. In recent memory, the ORs were 0.93, 0.86, and 0.82 in Fazekas 1, 2, and 3, respectively. In attention, the ORs were 0.93, 0.82, and 0.92 in Fazekas 1, 2, and 3, respectively. In orientation, the ORs were 0.90, 0.85, and 0.82 in Fazekas 1, 2, and 3, respectively. In mental manipulation, the ORs were 0.83, 0.85, and 0.67 in Fazekas 1, 2, and 3, respectively. In abstract thinking, the ORs were 0.84, 0.79, and 0.75 in Fazekas 1, 2, and 3, respectively. In language, the ORs were 0.90, 0.85, and 0.82 in Fazekas 1, 2, and 3, respectively. In drawing, the ORs were 0.90, 0.91, and 0.81 in Fazekas 1, 2, and 3, respectively. In verbal fluency, the ORs were 0.95, 0.89, and 0.80 in Fazekas 1, 2, and 3, respectively.

Figure 3 shows a comparison of composite scores of neuropsychiatric symptoms in the NPI among different Fazekas groups. Among them, delusions, euphoria, apathy, aberrant motor behavior, and sleep disorders were significantly worse in the higher Fazekas (2 or 3) groups compared to those in the group with Fazekas score of 0 after adjustment. In delusions, the ORs were 1.6, 2.0, and 2.0 in Fazekas 1, 2, and 3, respectively. In euphoria, the ORs were 0.8, 3.8, and 3.3 in Fazekas 1, 2, and 3, respectively. In apathy, the ORs were 1.5, 2.2, and 2.1 in Fazekas 1, 2, and 3, respectively. In sleep disorders, the ORs were 1.0, 1.1, and 1.1 in Fazekas 1, 2, and 3, respectively.

Discussion

Our study reports some important findings. First, the age, sex disparity, education, and disease duration in this study were not significantly different among the four Fazekas subgroups; however, WMHs were positively correlated with dementia severity and negatively correlated with cognitive

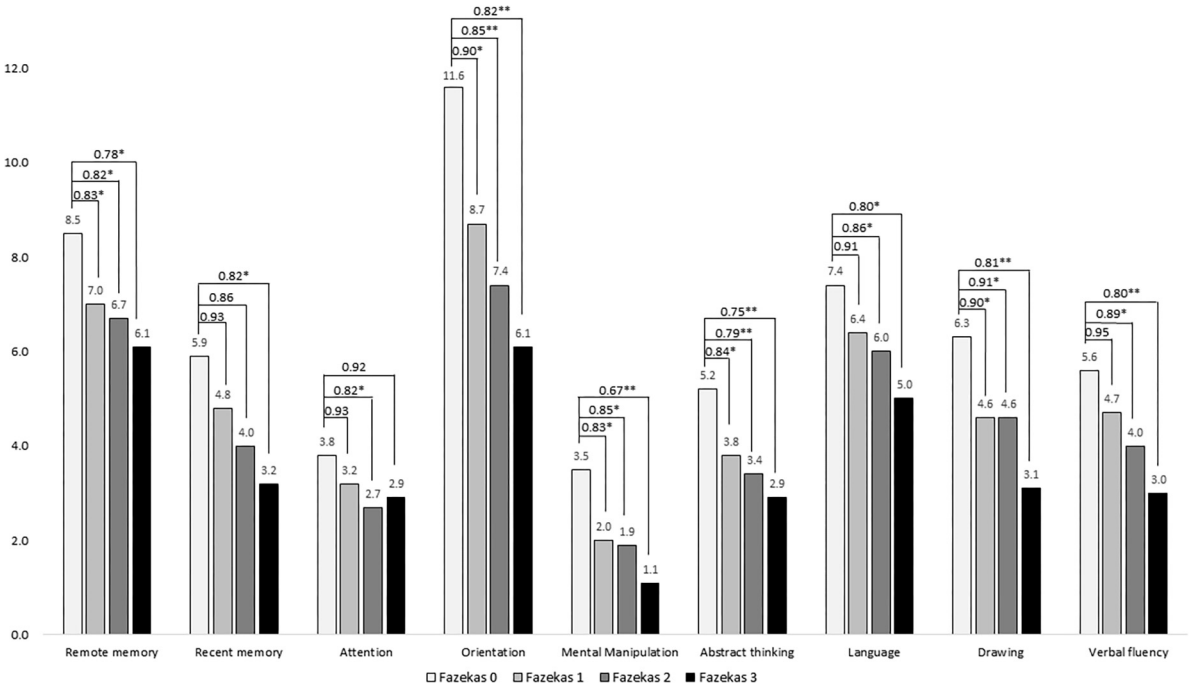

FIGURE 2
Comparison of cognitive domains of the CASI among different Fazekas groups adjusted for age, sex, education, and disease duration. ORs were compared to Fazekas score of 0. *$p < 0.05$; **$p < 0.001$.

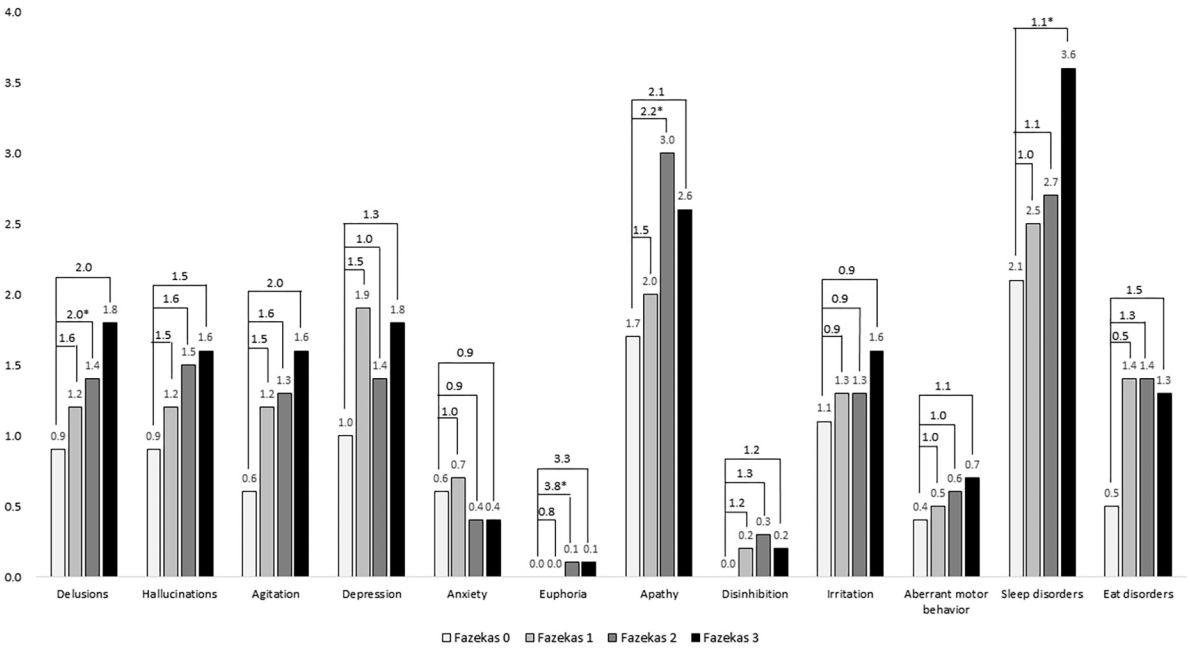

FIGURE 3
Comparison of composite scores of neuropsychiatric symptoms in the NPI among different Fazekas groups adjusted for age, sex, education, and disease duration. ORs were compared to Fazekas score of 0. *$p < 0.05$.

performance and ADL function which are consistent with the results of most previous studies on WMHs and dementia (Prins et al., 2004; Sarro et al., 2016). Dopamine transporter imaging is one of the indicative biomarkers for the diagnosis of DLB. In this study, there is no difference in the SBR (striatal background ratio) among different Fazekas groups; however, the CPR is significantly lower in the higher Fazekas groups (Fazekas 2 and 3) indicating a worse cognitive function instead of motor function in the higher Fazekas groups compared to the lower Fazekas groups (Fazekas 0 and 1). This is also compatible with clinical findings of higher dementia severity and lower cognitive performance in the higher Fazekas groups.

Second, we found that there was no significant association between WMHs and core clinical features for the diagnosis of DLB including fluctuation, VH, parkinsonism, and RBD. However, significantly poorer motor and gait functions according to motor and gait sub-scores found in the Fazekas 3 indicated a potential contribution of severe WMHs to motor dysfunction in DLB. In addition, most of the VRFs and current medication usage were not different among Fazekas groups, either. These results suggest that cerebral or systemic vascular factors contribute less to the emergence of the clinical presentation in DLB. However, in this study, we found a positive association between WMHs and CVD (5.3, 10.1, 17.3, and 25.3% for the Fazekas scale scores of 0, 1, 2, 3, respectively) after Bonferroni correction. This finding is also consistent with the evidence of an inverse relationship between small vessel disease and the severity of cerebral vascular pathology in patients with vascular dementia (Barber et al., 1999; Ihara et al., 2010).

Third, although cognitive screening tests (such as the CASI and MoCA) were used to study the association between cognitive function and WMHs. After adjustment for age, sex, education, and disease duration, patients with DLB and higher Fazekas scale scores had poorer cognitive functions in all domains of CASI including remote memory, recent memory, attention, mental manipulation, orientation, abstract thinking, language, drawing, and verbal fluency than those with lower Fazekas scale scores. Based on the consensus criteria, cognitive deficits in the domains of executive function, visuospatial function, and attention are considered essential for the diagnosis of DLB (McKeith et al., 2017). Therefore, in this study, most cognitive domains in which WMHs contributed to the clinical presentation of DLB were not only the essential cognitive features (visuospatial function, attention, mental manipulation, abstract thinking, and verbal fluency) for the diagnosis of DLB but were also some other cognitive features (orientation, language, remote memory, and recent memory). The poor performance of the higher Fazekas groups could be attributed to the additional effects of WMHs on cognitive dysfunction in the patients with DLB.

Finally, when studying the association between WMHs and neuropsychiatric features in DLB, we found that among neuropsychiatric symptoms, delusions, euphoria, apathy, aberrant motor behavior, and sleep disorders were significantly worse in the higher Fazekas groups compared to those in the group with the Fazekas score of 0 after adjustment. This finding suggests that WMHs might have partial contribution to the neuropsychiatric manifestation of DLB. For example, according to the previous studies and consensus criteria, sleep disorders are striking features of DLB (Yamane et al., 2011; Chiu et al., 2017; McKeith et al., 2017). These findings also support the previous findings that WMHs cannot be considered as mere incidental findings, at least in patients who show severe lesions (Pantoni et al., 2007).

This study has some limitations. First, it was conducted in three hospitals in Taiwan. Therefore, the study findings may not be generalizable to all patients with DLB. Second, the comparison of the associated factors between the high and low Fazekas groups was cross-sectional. Therefore, causal relationships between the factors and dementia could not be ascertained. Third, the current study did not compare DLB with non-synucleinopathy disease; therefore, both contribution of synucleinopathy to deterioration of cognition and interaction of synucleinopathy with WMH were not able to be well demonstrated. In addition, this study did not include the CHIPS score for analysis. According to the previous studies, cholinergic function decline was not only found in the patients with AD, but was also noticed in the patients with Lewy body dementia including DLB and PDD (Francis and Perry, 2007). Fourth, the identification of RBD or DLB type VH is relatively strict in our cohort. Therefore, the prevalence of DLB core clinical features in our cohort was relatively lower. We considered a relatively strict evaluation of core clinical features and neuropsychiatric symptoms to guarantee a better discrimination of DLB from AD. Lastly, only 41.4% study participants had undergone dopamine transporter uptake imaging; this may have resulted in a lower diagnostic rate of probable DLB in this study.

Conclusion

In conclusion, we evaluated WMHs using brain MRI in a relatively large sample of patients with DLB and performed multi-dimensional analysis of the associated factors of WMHs in DLB according to different Fazekas scale scores. Compared to the lower Fazekas group, the higher Fazekas groups had more severe stages of dementia, poorer cognitive function and ADL, and more severe sleep disorders. There was no significant association between WMHs and core clinical features for the diagnosis of DLB including fluctuation, VH, parkinsonism, and RBD. This cohort will be prospectively followed up for the influence of WMHs on the progression of clinical manifestations of DLB.

Data availability statement

The original contributions presented in this study are included in the article/supplementary material, further inquiries can be directed to the corresponding author/s.

Ethics statement

The studies involving human participants were reviewed and approved by the Show Chwan Memorial Hospital. Written informed consent for participation was not required for this study in accordance with the national legislation and the institutional requirements.

Author contributions

P-YC: conception and study design. C-FT and P-YC: statistical analysis. T-YC: drafting the manuscript work. T-YC, P-CC, and P-YC: revising the manuscript. All authors: data collection and acquisition, interpretation of results, and approval of final version.

Acknowledgments

We would like to thank Dr. Hsing-Ju Wu at the Research Assistant Center of the Show Chwan Memorial Hospital for editing the manuscript.

Conflict of interest

The authors declare that the research was conducted in the absence of any commercial or financial relationships that could be construed as a potential conflict of interest.

Publisher's note

References

American Academy of Sleep Medicine (2005). *International Classification of Sleep Disorders: Diagnostic and Coding Manual*. Westchester, IL: American Academy of Sleep Medicine.

Ballard, C., McKeith, I., Burn, D., Harrison, R., O'Brien, J., Lowery, K., et al. (1997). The UPDRS scale as a means of identifying extrapyramidal signs in patients suffering from dementia with Lewy bodies. *Acta Neurol. Scand.* 96, 366–371. doi: 10.1111/j.1600-0404.1997.tb00299.x

Barber, R., Gholkar, A., Scheltens, P., Ballard, C., McKeith, I. G., and O'Brien, J. T. (2000). MRI volumetric correlates of white matter lesions in dementia with Lewy bodies and Alzheimer's disease. *Int. J. Geriatr. Psychiatry* 15, 911–916.

Barber, R., Scheltens, P., Gholkar, A., Ballard, C., McKeith, I., Ince, P., et al. (1999). White matter lesions on magnetic resonance imaging in dementia with Lewy bodies, Alzheimer's disease, vascular dementia, and normal aging. *J. Neurol. Neurosurg. Psychiatry* 67, 66–72. doi: 10.1136/jnnp.67.1.66

Brickman, A. M., Provenzano, F. A., Muraskin, J., Manly, J. J., Blum, S., Apa, Z., et al. (2012). Regional white matter hyperintensity volume, not hippocampal atrophy, predicts incident Alzheimer disease in the community. *Arch. Neurol.* 69, 1621–1627. doi: 10.1001/archneurol.2012.1527

Burton, E. J., McKeith, I. G., Burn, D. J., Firbank, M. J., and O'Brien, J. T. (2006). Progression of white matter hyperintensities in Alzheimer disease, dementia with lewy bodies, and Parkinson disease dementia: a comparison with normal aging. *Am. J. Geriat.r Psychiatry* 14, 842–849. doi: 10.1097/01.JGP.0000236596.56982.1c

Chiu, P. Y., Wang, C. W., Tsai, C. T., Li, S. H., Lin, C. L., and Lai, T. J. (2017). Depression in dementia with Lewy bodies: a comparison with Alzheimer's disease. *PLoS One* 12:e0179399. doi: 10.1371/journal.pone.0179399

Chiu, P. Y., Wei, C. Y., and Hung, G. U. (2019). Preliminary study of the history-based artificial intelligent clinical dementia diagnostic system. *Show Chwan Med. J.* 18, 18–27.

Cummings, J. L., Mega, M., Gray, K., Rosenberg-Thompson, S., Carusi, D. A., and Gornbein, J. (1994). The Neuropsychiatric Inventory: comprehensive assessment of psychopathology in dementia. *Neurology* 44, 2308–2314. doi: 10.1212/wnl.44.12.2308

de Groot, J. C., de Leeuw, F. E., Oudkerk, M., van Gijn, J., Hofman, A., Jolles, J., et al. (2000). Cerebral white matter lesions and cognitive function: the rotterdam scan study. *Ann. Neurol.* 47, 145–151.

Debette, S., and Markus, H. S. (2010). The clinical importance of white matter hyperintensities on brain magnetic resonance imaging: systematic review and meta-analysis. *BMJ* 341:c3666. doi: 10.1136/bmj.c3666

Defrancesco, M., Marksteiner, J., Deisenhammer, E., Kemmler, G., Djurdjevic, T., and Schocke, M. (2013). Impact of white matter lesions and cognitive deficits on conversion from mild cognitive impairment to Alzheimer's disease. *J. Alzheimers Dis.* 34, 665–672. doi: 10.3233/JAD-122095

Fazekas, F., Chawluk, J. B., Alavi, A., Hurtig, H. I., and Zimmerman, R. A. (1987). MR signal abnormalities at 1.5 T in Alzheimer's dementia and normal aging. *AJR Am. J. Roentgenol.* 149, 351–356. doi: 10.2214/ajr.149.2.351

Francis, P. T., and Perry, E. K. (2007). Cholinergic and other neurotransmitter mechanisms in Parkinson's disease, Parkinson's disease dementia, and dementia with Lewy bodies. *Move. Disord.* 22, S351–S357. doi: 10.1002/mds.21683

Ghebremedhin, E., Rosenberger, A., Rub, U., Vuksic, M., Berhe, T., Bickeboller, H., et al. (2010). Inverse relationship between cerebrovascular lesions and severity of lewy body pathology in patients with lewy body diseases. *J. Neuropathol. Exp. Neurol.* 69, 442–448. doi: 10.1097/NEN.0b013e3181d88e63

Hijazi, Z., Yassi, N., O'Brien, J. T., and Watson, R. (2022). The influence of cerebrovascular disease in dementia with Lewy bodies and Parkinson's disease dementia. *Eur. J. Neurol.* 29, 1254–1265. doi: 10.1111/ene.15211

Huang, C. C., Yen, T. C., and Lu, C. S. (2012). "Dopamine Transporter Imaging for Distinguishing Between Idiopathic Parkinson's Disease and Secondary Parkinsonism," in *Neuroimaging - Clinical Applications*, ed. P. Bright (London: IntechOpen), 401–422.

Hung, C. H., Hung, G. U., Wei, C. Y., Tzeng, R. C., and Chiu, P. Y. (2021). Function-based dementia severity assessment for vascular cognitive impairment. *J. Formos. Med. Assoc.* 120, 533–541. doi: 10.1016/j.jfma.2020.07.001

Ihara, M., Polvikoski, T. M., Hall, R., Slade, J. Y., Perry, R. H., Oakley, A. E., et al. (2010). Quantification of myelin loss in frontal lobe white matter in vascular dementia, Alzheimer's disease, and dementia with Lewy bodies. *Acta Neuropathol.* 119, 579–589. doi: 10.1007/s00401-009-0635-8

Joki, H., Higashiyama, Y., Nakae, Y., Kugimoto, C., Doi, H., Kimura, K., et al. (2018). White matter hyperintensities on MRI in dementia with Lewy bodies, Parkinson's disease with dementia, and Alzheimer's disease. *J. Neurol. Sci.* 385, 99–104. doi: 10.1016/j.jns.2017.12.018

Kamagata, K., Motoi, Y., Tomiyama, H., Abe, O., Ito, K., Shimoji, K., et al. (2013). Relationship between cognitive impairment and white-matter alteration in Parkinson's disease with dementia: tract-based spatial statistics and tract-specific analysis. *Eur. Radiol.* 23, 1946–1955. doi: 10.1007/s00330-013-2775-4

Kasten, M., Bruggemann, N., Schmidt, A., and Klein, C. (2010). Validity of the MoCA and MMSE in the detection of MCI and dementia in Parkinson disease. *Neurology* 75, 478–479. doi: 10.1212/WNL.0b013e3181e7948a

Lin, C. M., Hung, G. U., Wei, C. Y., Tzeng, R. C., and Chiu, P. Y. (2018). An Informant-based simple questionnaire for language assessment in neurodegenerative disorders. *Dement. Geriatr. Cogn. Disord.* 46, 207–216. doi: 10.1159/000493540

McKeith, I. G., Boeve, B. F., Dickson, D. W., Halliday, G., Taylor, J. P., Weintraub, D., et al. (2017). Diagnosis and management of dementia with lewy bodies: fourth consensus report of the DLB Consortium. *Neurology* 89, 88–100. doi: 10.1212/WNL.0000000000004058

Morris, J. C. (1997). Clinical dementia rating: a reliable and valid diagnostic and staging measure for dementia of the Alzheimer type. *Int. Psychogeriatr.* 9, 173–176.

Movement Disorder Society Task Force on Rating Scales for Parkinson's (2003). The Unified Parkinson's Disease Rating Scale (UPDRS): status and recommendations. *Mov. Disord.* 18, 738–750. doi: 10.1002/mds.10473

Nasreddine, Z. S., Phillips, N. A., Bedirian, V., Charbonneau, S., Whitehead, V., Collin, I., et al. (2005). The montreal cognitive assessment, MoCA: a brief screening tool for mild cognitive impairment. *J. Am. Geriatr. Soc.* 53, 695–699. doi: 10.1111/j.1532-5415.2005.53221.x

Nedelska, Z., Schwarz, C. G., Boeve, B. F., Lowe, V. J., Reid, R. I., Przybelski, S. A., et al. (2015). White matter integrity in dementia with Lewy bodies: a voxel-based analysis of diffusion tensor imaging. *Neurobiol. Aging* 36, 2010–2017. doi: 10.1016/j.neurobiolaging.2015.03.007

Oppedal, K., Aarsland, D., Firbank, M. J., Sonnesyn, H., Tysnes, O. B., O'Brien, J. T., et al. (2012). White matter hyperintensities in mild lewy body dementia. *Dement. Geriatr. Cogn. Dis. Extra* 2, 481–495. doi: 10.1159/000343480

Pantoni, L., Poggesi, A., and Inzitari, D. (2007). The relation between white-matter lesions and cognition. *Curr. Opin. Neurol.* 20, 390–397. doi: 10.1097/WCO.0b013e328172d661

Prins, N. D., and Scheltens, P. (2015). White matter hyperintensities, cognitive impairment and dementia: an update. *Nat. Rev. Neurol.* 11, 157–165. doi: 10.1038/nrneurol.2015.10

Prins, N. D., van Dijk, E. J., den Heijer, T., Vermeer, S. E., Koudstaal, P. J., Oudkerk, M., et al. (2004). Cerebral white matter lesions and the risk of dementia. *Arch. Neurol.* 61, 1531–1534. doi: 10.1001/archneur.61.10.1531

Sarro, L., Schwarz, C., Graff-Radford, J., Tosakulwong, N., Reid, R. I., Przybelski, S., et al. (2016). An investigation of cerebrovascular lesions in dementia with Lewy bodies compared to Alzheimer's disease. *Alzheimers Dement.* 13:86.

Taylor, A. N. W., Kambeitz-Ilankovic, L., Gesierich, B., Simon-Vermot, L., Franzmeier, N., Araque Caballero, M. A., et al. (2017). Tract-specific white matter hyperintensities disrupt neural network function in Alzheimer's disease. *Alzheimers Dement* 13, 225–235. doi: 10.1016/j.jalz.2016.06.2358

Teng, E. L., Hasegawa, K., Homma, A., Imai, Y., Larson, E., Graves, A., et al. (1994). The Cognitive Abilities Screening Instrument (CASI): a practical test for cross-cultural epidemiological studies of dementia. *Int. Psychogeriatr.* 6, 45–58. doi: 10.1017/s1041610294001602

van Straaten, E. C., Harvey, D., Scheltens, P., Barkhof, F., Petersen, R. C., Thal, L. J., et al. (2008). Periventricular white matter hyperintensities increase the likelihood of progression from amnestic mild cognitive impairment to dementia. *J. Neurol.* 255, 1302–1308. doi: 10.1007/s00415-008-0874-y

Vesely, B., and Rektor, I. (2016). The contribution of white matter lesions (WML) to Parkinson's disease cognitive impairment symptoms: a critical review of the literature. *Parkinsonism Relat. Disord.* 22, S166–S170. doi: 10.1016/j.parkreldis.2015.09.019

Wang, C. T., Hung, G. U., Wei, C. Y., Tzeng, R. C., and Chiu, P. Y. (2020). An informant-based simple questionnaire for visuospatial dysfunction assessment in dementia. *Front. Neurosci.* 14:44. doi: 10.3389/fnins.2020.00044

Wardlaw, J. M., Valdes Hernandez, M. C., and Munoz-Maniega, S. (2015). What are white matter hyperintensities made of? Relevance to vascular cognitive impairment. *J. Am. Heart Assoc.* 4:001140. doi: 10.1161/JAHA.114.001140

Watson, R., Blamire, A. M., Colloby, S. J., Wood, J. S., Barber, R., He, J., et al. (2012). Characterizing dementia with Lewy bodies by means of diffusion tensor imaging. *Neurology* 79, 906–914. doi: 10.1212/WNL.0b013e318266fc51

Wolf, H., Ecke, G. M., Bettin, S., Dietrich, J., and Gertz, H. J. (2000). Do white matter changes contribute to the subsequent development of dementia in patients with mild cognitive impairment? A longitudinal study. *Int. J. Geriatr. Psychiatry* 15, 803–812. doi: 10.1002/1099-1166(200009)15:9<803::aid-gps190>3.0.co;2-w

Yamane, Y., Sakai, K., and Maeda, K. (2011). Dementia with lewy bodies is associated with higher scores on the geriatric depression scale than is Alzheimer's disease. *Psychogeriatrics* 11, 157–165. doi: 10.1111/j.1479-8301.2011.00368.x

Zaccai, J., McCracken, C., and Brayne, C. (2005). A systematic review of prevalence and incidence studies of dementia with Lewy bodies. *Age Ageing* 34, 561–566. doi: 10.1093/ageing/afi190

frontiers | Frontiers in Aging Neuroscience

TYPE Methods
PUBLISHED 07 September 2022
DOI 10.3389/fnagi.2022.984894

OPEN ACCESS

EDITED BY
Chih-Yu Hsu,
Fujian University of Technology, China

REVIEWED BY
Yu-hai Li,
Central China Normal University, China
King Lee,
Dalhousie University, Canada
Jerry Lv,
The Chinese University of Hong Kong, Hong Kong SAR, China

*CORRESPONDENCE
Zu-hai Zhang
zuhai_zhang@outlook.com

SPECIALTY SECTION
This article was submitted to Alzheimer's Disease and Related Dementias, a section of the journal Frontiers in Aging Neuroscience

RECEIVED 02 July 2022
ACCEPTED 11 August 2022
PUBLISHED 07 September 2022

CITATION
Zhao M, Li J, Xiang L, Zhang Z-h and Peng S-L (2022) A diagnosis model of dementia *via* machine learning. *Front. Aging Neurosci.* 14:984894. doi: 10.3389/fnagi.2022.984894

A diagnosis model of dementia *via* machine learning

Ming Zhao[1], Jie Li[1], Liuqing Xiang[1], Zu-hai Zhang[2]* and Sheng-Lung Peng[3]

[1]School of Computer Science, Yangtze University, Jingzhou, China, [2]Department of Ophthalmology, The First Affiliated Hospital of Yangtze University, Jingzhou, China, [3]Department of Creative Technologies and Product Design, National Taipei University of Business, Taipei, Taiwan

As the aging population poses serious challenges to families and societies, the issue of dementia has also received increasing attention. Dementia detection often requires a series of complex tests and lengthy questionnaires, which are time-consuming. In order to solve this problem, this article aims at the diagnosis method of questionnaire survey, hoping to establish a diagnosis model to help doctors make a diagnosis through machine learning method, and use feature selection method to select important questions to reduce the number of questions in the questionnaire, so as to reduce medical and time costs. In this article, Clinical Dementia Rating (CDR) is used as the data source, and various methods are used for modeling and feature selection, so as to combine similar attributes in the data set, reduce the categories, and finally use the confusion matrix to judge the effect. The experimental results show that the model established by the bagging method has the best effect, and the accuracy rate can reach 80% of the true diagnosis rate; in terms of feature selection, the principal component analysis (PCA) has the best effect compared with other methods.

KEYWORDS

dementia, machine learning, bagging, principal component analysis, diagnosis model

Introduction

In recent years, China has slowly entered a deeply aging society, with the elderly accounting for 14% of the total population. By 2033, China will enter a super-aging society with 22% of the elderly population. Then around 2060, the proportion of aging will reach 35%, which means that by 2060, 1 in 3 Chinese will be over 65 years old. In an aging society, the health care of the elderly has become an important issue, in which dementia clearly occupies a very important position. Alzheimer's disease is the most common type of dementia, accounting for approximately 70% of all dementias (GBD 2019 Dementia Forecasting Collaborators, 2022). For dementia, the earlier it is detected, the earlier treatment can be initiated. But as the population continues to age and the number of people with dementia continues to increase, dementia screening has become an urgent problem.

Since the beginning of the 20th century, machine learning has made remarkable achievements in various fields. The combination of machine learning and the medical

field is particularly remarkable. Especially in the severe epidemic period, the use of machine learning methods can help doctors to quickly identify lung CT images and make a diagnosis (Elaziz et al., 2020; Prakash et al., 2020; Afshar et al., 2021; Aboghazalah et al., 2022; Das et al., 2022; Elkamouny and Ghantous, 2022; Shiri et al., 2022; Sun et al., 2022). There are also many studies and applications of machine learning in dementia, researchers also summarize many applications of machine learning and deep learning in dementia (Ahmed et al., 2018; Miah et al., 2021). Alashwal et al. (2019) found patterns in patients that were difficult for medical practitioners to spot by using clustering methods in unsupervised learning in machine learning, and identified several features of the transition from early to late stages of dementia. Alexiou et al. (2017) used a Bayesian model to predict early dementia, and used the model to correlate and evaluate biomarkers to output predicted probabilities. Alickovic and Subasi (2019) used histograms to convert brain images into feature vectors, and passed these features into classifiers constructed by machine learning methods such as random forests to achieve automatic detection of Alzheimer's disease. An et al. (2020) used an ensemble learning method to build a dementia classification model, and the obtained model was better than any single algorithm. Ansari et al. (2019) used a deep learning network to analyze the EEG (Electroencephalogram) features of the incoming network. At the end of the network, a random forest classifier was used to classify the output, and the final detection accuracy could reach 77%. Bloch and Friedrich (2019) used volumetric features from multiple magnetic resonance imaging (MRI) scans to classify Alzheimer's disease, and the resulting best model had a test classification accuracy of 75.49%.

The above-mentioned methods basically analyze pathological images, which require the elderly to go to the hospital for some professional examinations to obtain relevant data, which is time-consuming and labor-intensive. And in recent years, affected by the epidemic, people usually do not go to the hospital before they have obvious symptoms. Therefore, this article aims to use a questionnaire to conduct a preliminary examination of dementia, and use machine learning methods to establish a dementia diagnosis model. Prior to this, Trambaiolli et al. (2011), Williams et al. (2013), Broman et al. (2022), and Khan et al. (2022) have used machine learning combined with some questionnaires to detect and classify dementia. Based on these studies, this article optimizes some questionnaire questions by cooperating with clinicians, using a variety of machines. Learning methods to model and extract features, so as to combine similar attributes in the data set, reduce the number of questions in the questionnaire, and achieve rapid screening of dementia.

The rest of this article is arranged as follows:

Section "Related work" introduces dementia and related knowledge of machine learning that will be used in this article. In section "Experiment and analysis," experiment and analysis of experimental results will be explained. In section "Conclusion and future work," summary and prospects of the research will be given.

Related work

In this section, we will explain the theory and terminology used in the article, including an explanation of dementia-related terms, an introduction to machine learning, and the algorithms used in this research.

Dementia

The most common type of dementia is Alzheimer's disease in the elderly. The typical initial symptom is memory impairment. The patient forgets what has just happened (poor short-term memory), while memory from older times (long-term memory) is relatively unaffected in the early stages of the disease. Dementia affects language skills, comprehension, motor skills, short-term memory, ability to identify everyday objects, reaction time, personality, executive ability, and problem-solving skills. Even if there are no signs of mental decline, delusions are common (15–56% of Alzheimer's types), such as doubting that the person in the mirror is someone else.

Symptoms of dementia also include changes in personality or behavior. Many patients with a final diagnosis of dementia had intense confusional symptoms early in their hospitalization. Older adults may also have symptoms of mental changes due to other medications, surgery, infections, lack of sleep, an abnormal diet, dehydration, changing places, or a personal crisis. Because most patients with dementia may have symptoms of insanity. Although the symptoms of confusion may be alleviated by close care, improvement of living environment and diet; Psychiatric drugs can also help stabilize mood, reduce hallucinations and delusions, or control impulse. But at present, drugs have not been able to slow down brain degeneration. Dementia patients are often accompanied by depression, and it is best to be diagnosed and treated by professionals.

Mild cognitive impairment

The definition of mild cognitive impairment (MCI) is as follows:

(1) Subjective memory impairment.
(2) Objective memory impairment.
(3) Poor memory compared with people of the same age and education level.
(4) Normal cognition and daily life function.
(5) Not dementia, has not reached the degree of dementia.

Clinical dementia rating

The Clinical Dementia Rating (CDR) is mainly aimed at patients with Alzheimer's disease. By asking their caregivers, an overall assessment of daily living and cognitive function is carried out to define the severity of the disorder. CDR contains six projects: Memory (M), Orientation (O), judgment-problem-solving (J), Community affairs (C), Home hobbies (H), and Personal care (P), with five severity levels from 0 to 3: 0 stands for normal Health, 0.5 for suspected or Mild impairment, 1 for Mild dementia, 2 for Moderate dementia, 3 represents Severe dementia. The evaluator observed the patient's current performance, and based upon the information provided by the caregiver, took memory as the main item score, and sense of orientation, judgment and problem-solving, community affairs, home and hobbies and personal care as the secondary items scores, and then calculated the CDR score according to the rules. Among them, the Normal category, although it represents normal in this article, the patients who had gone to the hospital for treatment more or less have problems with memory, so the Normal here does not mean that the patients really have no problems, but it is analyzed in this scale is normal. The CDR used in this article is a revised version of the collaborating doctors after years of clinical experience, and the questions are shown in **Table 1**.

Very early dementia screening scale (AD-8)

The Early Dementia Screening Scale (AD-8) is a simple tool for screening dementia. It was invented by Washington University and put forward in 2005. It can screen out very mild dementia symptoms and is widely used in the world. The scale contains eight questions. The long-term caregiver observes the individual's long-term changes and fills in the answer, or the individual can fill in the answer by themselves. The scoring method is to fill in "yes, there is a change" and get 1 point, and fill in "no, there is no change" and get 0 point. If the long-term caregiver cannot assess the individual condition, fill in "I don't know," then this question will not be scored. If the total score is greater than or equal to 2 points, the subject needs to go to the hospital for further evaluation. The problems of the AD-8 scale are shown in **Table 2**.

Machine learning

Machine learning is a multi-field interdisciplinary subject involving probability theory, statistics, approximation theory, convex analysis, algorithm complexity theory and other disciplines. It specializes in how computers simulate or realize human learning behaviors to acquire new knowledge or skills, and to reorganize existing knowledge structures to continuously improve their performance. In the current era of big data, machine learning is mainly used to find rules from data and build models, and then use the models to predict unknown data. When the input data is larger, the model continuously adjusts to make more accurate predictions.

The machine learning methods used in this article include Bagging and C4.5 decision tree. The C4.5 decision tree is an extension and optimization of the ID3 algorithm, which introduces improvements such as information gain rate. The algorithm mentioned above will be briefly explained below.

ID3

ID3 is a decision tree algorithm whose structure is based on information theory proposed by Shannon. In information theory, entropy represents the expected value of a random variable, and in the ID3 algorithm, it is a pointer that determines the importance of the variable. The following is an introduction to the entropy algorithm in ID3:

Calculation of data volume before test

$$\text{info}\,(T) \;=\; -\sum_{i=1}^{m} \frac{\text{freq}(C_i, T)}{|T|} \log_2\left(\frac{\text{freq}(C_i, T)}{|T|}\right) \qquad (1)$$

T: A collection.

$|T|$: The amount of data in the set T.

C_i: Categories in the set, $i \;=\; 1,2,\ldots,m$ (m: number of categories)

freq(C_i, T): The number of categories of data in the set T.

Calculation of data volume after test

$$\text{info}_X\,(T) \;=\; \sum_{i=1}^{p} \frac{|T_i|}{|T|} \text{info}\,(T_i) \qquad (2)$$

T_i : Subset of T set after testing against variable X, $i \;=\; 1,2,\ldots,p$, $X \in \{X_1, X_2, \ldots, X_p\}$

The algorithm of ID3 is developed based on the concept of information theory. The decision of nodes is determined by information gain, and the concept is that the amount of data before the test is subtracted from the amount of data after the test.

$$\text{Gain}\,(X) \;=\; \text{info}\,(T) \;-\; \text{info}_X(T) \qquad (3)$$

C4.5 decision tree

The C4.5 algorithm is a classic algorithm for generating decision trees, and it is an extension and optimization of the ID3 algorithm. The C4.5 algorithm has improved the ID3 algorithm. The main improvements are as follows:

(1) Using the information gain rate to select the partition features overcomes the deficiency of the information gain selection, but the information gain rate has a preference for the attributes with a small number of possible values.
(2) Ability to handle discrete and continuous attribute types, that is, to discretize continuous attributes.

TABLE 1 Questions in the clinical dementia rating.

Question number	Question content	Options	
M01	Are cognitive functions (e.g., memory, thinking, and judgment) significantly worse than before?	Yes	No
M02	Do you forget the name of your spouse or children?	Yes	No
M03	Has cognitive decline affected daily life, social interaction and work?	Yes	No
M04	Do the symptoms of cognitive function fluctuate greatly, or even get worse within a day?	Yes	No
M05	Do you often lose things?	Yes	Never or occasionally
M06	Do you often forget what you said recently?	Yes	Never or occasionally
M07	Do you find it difficult to learn how to use tools and equipment?	Yes	No
M08	Do you often forget what happened recently?	Yes	Never or occasionally
M09	Do you ask the same questions or say the same things over and over again?	Yes	No
M10	Will you cherish the past (often mention the past)?	Yes	No
M12	Do you forget familiar things (such as place of origin, address, and occupation)?	Yes	No
O02	Will you forget the correct year and month?	Yes	No
O03	Is it difficult to remember when to date?	Yes	No
O05	Do you get lost in familiar surroundings, such as near your home?	Yes	No
O06	Can't figure out where you are?	Yes	No
O07	Do you often mistake your son for your husband and your daughter for your sister?	Yes	Never or occasionally
J01	Do you often behave inappropriately when dealing with advance and retreat (such as attending weddings and funerals of friends and relatives)?	Yes	No
J02	Does judgment often have difficulty? (e.g., falling into a trap, a scam, and buying inappropriate gifts)	Yes	Never or occasionally
J03	Is it difficult to handle complex finances (banking, paying bills, writing checks)?	Yes	No
J04	Do you feel that your work ability or professional skills have deteriorated?	Yes	No
J05	Will it be difficult to deal with big and small affairs inside and outside the home?	Yes	No
J06	Is it obviously more difficult to operate daily necessities than before? (e.g., using a telephone, a remote control, or a microwave oven, etc.)	Yes	No
C01	Go shopping (go out shopping to buy gifts and vegetables, etc.)	Complete by oneself	Every time you go shopping, you need someone to accompany you or you won't buy it at all.
C02	Money handling capacity	Normal	Can handle routine purchases, but needs help dealing with banks or cannot handle money
C03	The ability to use the phone, such as making or receiving calls	Normal	Can only answer the phone, but can't dial the phone or completely need help
C04	Cooking food (or preparing a table of dishes such as cooking, ordering or cooking)	Normal	Need someone else to cook, set or order the meal
C05	Household maintenance (simple housework such as housekeeping, cleaning)	Normal	All household chores need help from others
C06	Laundry (or handling personal correspondence such as mailing and receiving)	Normal	Completely dependent on others
C07	Outings (ride or ride, drive to destination)	Normal	Need assistance or escort
C08	Self-medication	Normal	Self-administration or not self-administration if the amount of medication to be taken is prepared in advance
C09	Difficulty in the above activities, the patient is due to physical or mobility impairment	Yes	No

(Continued)

TABLE 1 (Continued)

Question number	Question content	Options				
H01	Are you still engaged in routine activities? (For example, walking, chanting Buddha, going to temples, worshipping, praying, and going to church, etc.) or common hobbies or interests? (For example, dancing, playing cards, mahjong, karaoke, mallet, etc., ball, playing with grandchildren, etc.)	As usual.	A little less	A lot less	Almost no	Not at all, in my room all day
P01	Eating	At a reasonable time, you can eat your immediate food with chopsticks		Need someone to help put on and take off eating aids or only eat with a spoon		Inability to self-feed or take too long
P02	Transfer between wheelchair and bed	Can be completed independently	Need a little help or verbal instruction		Able to sit up from bed on their own, but still needs help when moving	You can only sit up when others help you
P03	Personal hygiene		Able to wash face, wash hands, brush teeth and comb hair independently			Need help from others
P04	To the restroom	Can go to the toilet and be self-assembled, and will not stain clothes		Need to help keep balance, tidy clothes or use toilet paper		Need help from others
P05	Bath		Can be done independently			Need help from others
P06	Walk up and down stairs	Can be done independently		Need a little help or verbal guidance		Unable to go up and down stairs
P07	Put on and take off clothes	Clothes, shoes and accessories that can be put on and taken off by oneself		With the help of others, you can complete more than half of the movements by yourself		Need help from others
P08	Walk more than 50 m on the flat ground	Can walk independently	Need a little support or guidance		Can't walk, but can operate the wheelchair independently	Need help from others
P09	Stool control	No incontinence and self-administration of suppositories		Occasional incontinence or needing help using suppositories		Need to be handled by others
P10	Urinary control	No urinary incontinence day or night		Occasional incontinence or need help		Need to be handled by others

(3) Ability to handle training data with missing attribute values.
(4) Pruning in the process of constructing the tree.

And the information gain ratio is calculated as follows:

$$\text{Gain Ratio}\,(X) = \frac{\text{Gain}(X)}{\text{Splitinfo}(X)} \tag{4}$$

Among them

$$\text{Splitinfo}\,(X) = \sum_{i=1}^{m} \frac{|T_i|}{|T|} \log_2\left(\frac{|T_i|}{|T|}\right) \tag{5}$$

Bagging

Bagging (Bootstrap Aggregating) is a kind of ensemble learning. The ensemble algorithm is a method of combining multiple weak classifiers into strong classifiers in a certain

TABLE 2 The problems of the AD-8 scale.

Question	Yes, there is a change (1 point)	No, no change (0 points)	Don't know (no credit)
1. Difficulty in judgment: e.g., falling into a trap or scam, making a bad financial decision, and buying a gift that is inappropriate for the recipient			
2. Decreased interest in activities and hobbies			
3. Repeat the same questions, stories, and statements			
4. Difficulty learning how to use tools, equipment, and gadgets. For example: TV, stereo, remote control, air conditioner, washing machine, water heater, microwave oven, etc.			
5. Forget the correct month and year			
6. Difficulty dealing with complex finances. For example: personal or family balance of payments, bills of payment, income tax, etc.			
7. Difficulty remembering appointment times			
8. Has persistent thinking and memory problems			
Total			

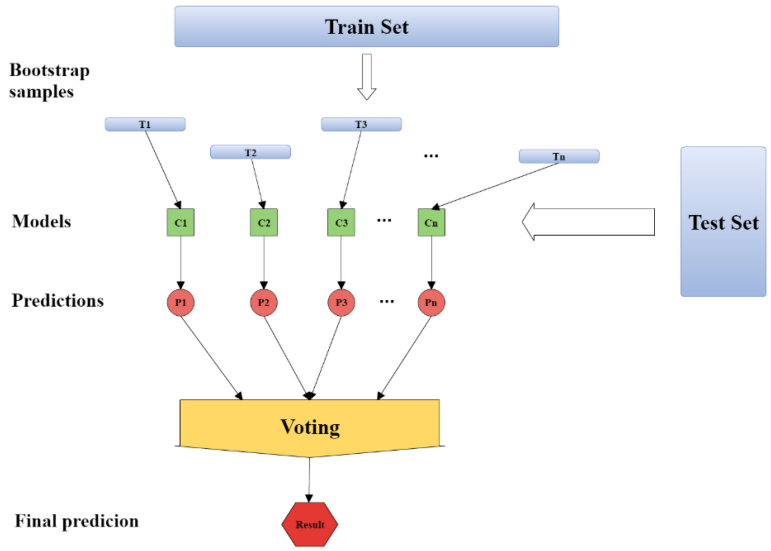

FIGURE 1
The process of Bagging algorithm.

combination. First, 60% of the data set is used as the training set, and 40% of the data set is used as the test set. About 60% of the data is randomly and repeatedly extracted from the training set to establish T_n sets of training data, and the T_n sets of training data are used. Build C_n models from the training data, substitute the data from the test set into C_n groups of models to get P_n answers, and finally get the results by voting or averaging for the n answers. The process of Bagging algorithm is shown in Figure 1.

Principal components analysis

One of the main directions of research in this article is to reduce the number of questions in the questionnaire, which can be understood as reducing the number of features. This article will use three methods to measure the importance of each problem, namely information gain, information gain ratio, and PCA. Among them, the information gain and the information gain ratio have been introduced in the previous introduction of C4.5. Therefore, in this part, we will introduce PCA.

Principal component analysis is a very effective way to reduce dimensions. When analyzing data, it is often necessary to deal with a number of interrelated variables, transform interrelated variables into independent linear combinations, and explain the whole data structure with a few variables.

Assume that the original data X consists of the following:

$$X = \begin{array}{c} X_1\ X_2\ \ldots\ X_P \\ \left[\begin{array}{ccc} x_{11} & x_{12} & \ldots x_{1p} \\ x_{21} & x_{22} & \ldots x_{2p} \\ x_{31} & x_{32} & \ldots x_{3p} \\ \vdots & \vdots & \vdots \\ x_{n1} & x_{n2} & x_{np} \end{array}\right]_{n \times p} \end{array} \quad (6)$$

p is the number of variables, n is the number of samples, $X_1, X_2, \ldots, X_P$ are variables; The calculation process of the main components is divided into the following steps

(1) Data standardization

$$X_i^* = \frac{\left(X_i - \overline{X_i}\right)}{\sigma_{X_i}}, i = 1, 2, \ldots., p-1, p \quad (7)$$

Where X_i^* is the standardized data, $\overline{X_i} = \frac{1}{n}\sum_{j=1}^{n} x_{ij}$ is the average of X_i, $\sigma_{X_i} = \sqrt{\frac{1}{n}\sum_{j=1}^{n}\left(x_{ij} - \overline{X_i}\right)^2}$ is the standard deviation of X_i.

(2) Calculate the correlation coefficient matrix between variables.

$$R = \begin{pmatrix} r_{11} & r_{12} & \ldots & r_{1p} \\ r_{21} & r_{22} & \ldots & r_{2p} \\ \vdots & \vdots & \ldots & \vdots \\ r_{p1} & r_{p2} & & r_{pp} \end{pmatrix} \quad (8)$$

$$r_{ij} = \frac{\left(X_i^*\right)^T X_j^*}{(n-1)}, i, j = 1, 2, \ldots, p \quad (9)$$

TABLE 3 Attributes of data set A.

Date	07/09/2015–14/04/2017	
Total people		1,565
Sex	Male	656
	Female	909
Age	23–103	
	Age ≤ 65	293
	65 < Age ≤ 75	422
	Age 76	845
Education level	0–19 years	
	Primary school level (1–6 years)	1178
	Secondary school level (7–12 years)	288
	Advanced level (12–20 years)	99

R is the correlation coefficient matrix, and r_{ij} is the correlation coefficient.

(3) Calculate eigenvalues and eigenvectors

Substitute the correlation coefficient matrix into the characteristic equation, and solve the p eigenvalues $\lambda 1, \lambda 2, \lambda 3, \ldots, \lambda_P$, and $\lambda 1 > \lambda\lambda 2 > \lambda 3 > \ldots > \lambda_P \geq 0$.

$$\det(R - \lambda I) = 0 \quad (10)$$

where R is the correlation coefficient matrix, λ is the eigenvalue, and I is the identity matrix. Use $\lambda 1, \lambda 2, \lambda 3, \ldots, \lambda_p$ to calculate the corresponding eigenvectors $V_1, V_2, V_3, \ldots, V_p$.

(4) Select the number of principal component variables

Observe the cumulative ratio. In the experimental process, if the cumulative ratio is above 0.8, the effect is very good.

Experiment and analysis

Data set and experimental environment

The software used in this article is weka, version 3.8.1, and its full name is waikato environment for knowledge analysis. This software is a machine learning software written in Java, which integrates a large number of algorithms and has the characteristics of simple operation and powerful functions.

The data set is the diagnostic information collected from the hospital, which includes the patient's gender, age, education level, problems, and diagnosis results. Here we call it Data A for short. Table 3 shows the date, total number, gender, age, and education level of Data A. The date is from 07/09/2015 to 14/04/2017. There are 1,565 people, and the number of female patients is larger than that of male patients. There were only 293 patients below the age of 65, and only 422 between the ages of 65 and 75. However, the number of people above the age of 75 increased sharply to 845. It can be found that the number of people at primary school level was the largest, reaching 1,178. The higher the level of education, the lower the number of patients. Data A contains 42 questions and diagnosis results. There are five categories of diagnosis results. Table 4 shows the number of people in each category. The answers to 33 questions are 0, 1, and the answers to 6 questions are 0, 1, 2, and 2.

TABLE 4 Diagnostic results.

State	Number of people
Normal	83
Uncertain dementia	397
Mild dementia	347
Moderate dementia	493
Severe dementia	246

TABLE 5 Average and standard deviation of the problem.

Question	Options	Mean	Standard deviation	Question	Options	Mean	Standard deviation
M01	0, 1	0.9016	0.29795	C01	0, 1	0.47476	0.49952
M02	0, 1	0.26965	0.44392	C02	0, 1	0.55783	0.4968
M03	0, 1	0.56805	0.49551	C03	0, 1	0.45176	0.49783
M04	0, 1	0.16294	0.36943	C04	0, 1	0.4901	0.50006
M05	0, 1	0.70032	0.45826	C05	0, 1	0.4377	0.49626
M06	0, 1	0.70671	0.45542	C06	0, 1	0.46454	0.4989
M07	0, 1	0.75655	0.4293	C07	0, 1	0.54633	0.49801
M08	0, 1	0.64153	0.4797	C08	0, 1	0.58275	0.49326
M09	0, 1	0.6492	0.47737	C09	0, 1	0.05304	0.22418
M10	0, 1	0.43387	0.49577	H01	0, 1, 2, 3, 5	1.65367	1.61955
M12	0, 1	0.26518	0.44157	P01	0, 1, 2	1.51757	0.73494
O02	0, 1	0.60511	0.48898	P02	0, 1, 2, 3	2.10032	1.25089
O03	0, 1	0.59617	0.49082	P03	0, 1	0.72077	0.44877
O05	0, 1	0.39233	0.48843	P04	0, 1, 2	1.36422	0.86284
O06	0, 1	0.32204	0.46741	P05	0, 1	0.59105	0.4918
O07	0, 1	0.1623	0.36884	P06	0, 1, 2	1.22812	0.91714
J01	0, 1	0.15911	0.36589	P07	0, 1, 2	1.37444	0.83121
J02	0, 1	0.57444	0.49459	P08	0, 1, 2, 3	2.09265	1.24585
J03	0, 1	0.56358	0.4961	P09	0, 1, 2	1.41406	0.837
J04	0, 1	0.56805	0.49551	P10	0, 1, 2	1.3623	0.83696
J05	0, 1	0.46837	0.49916				
J06	0, 1	0.4262	0.49468				

The answers to 1 question are 0, 1, 2, 3, and the answers to 1 question are 0, 1, 2, 3, 5. Table 5 illustrates the mean and standard deviation of the 42 questions in Data A.

In order to verify the accuracy of the method, this article uses a confusion matrix to test the accuracy of the model (see Figure 2). It can judge whether the predicted value matches the actual value. The characteristic is that the classified category can be clearly seen.

The meaning of each item in the figure is explained as follows:

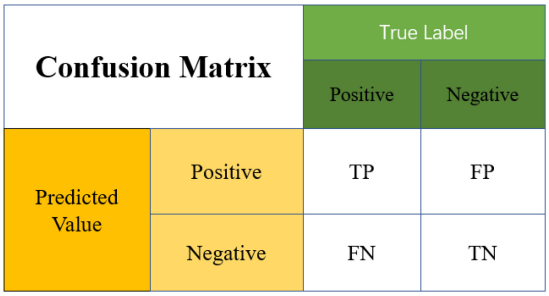

FIGURE 2
Confusion matrix diagram.

True-Positive (TP): The predicted value is Positive, and the actual value is also judged to be Positive.

False-Negative (FN): The predicted value is Negative, but the actual value is judged to be Positive.

False-Positive (FP): The predicted value is Positive, but the actual value is judged to be Negative.

True-Negative (TN): The predicted value is Negative, and the actual value is also judged as Negative.

Through this figure, its performance can be tested according to the following indicators, and it is hoped that the test algorithm can obtain the highest accuracy and true positive rate (TPR):

$$Accuracy = \frac{TP + TN}{\mathrm{TP} + \mathrm{TN} + \mathrm{FN} + \mathrm{FP}}, TPR = \frac{TP}{\mathrm{TP} + \mathrm{FN}} \quad (11)$$

Algorithm comparison

In addition to the questions and results, Data A also includes gender, age, and education level. Here we only take all 42 different questions and results for analysis. The results are not calculated according to the CDR formula, but are re-diagnosed by physicians referring to the CDR questionnaire, and there are five result categories. In this part we substitute Data Set B into both algorithms and use the confusion matrix to see the effect. We combine the categories with similar attributes,

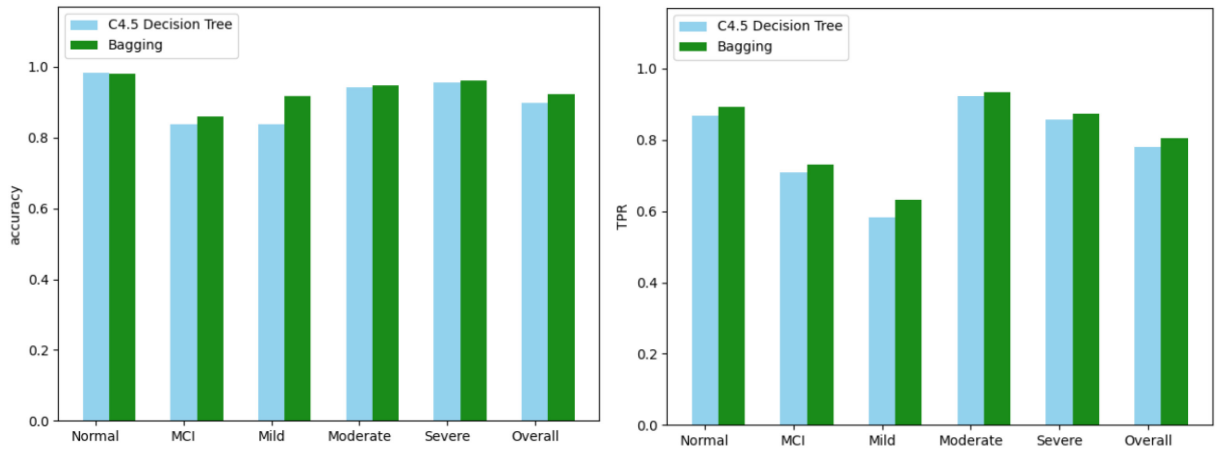

FIGURE 3
Comparison results of two algorithms.

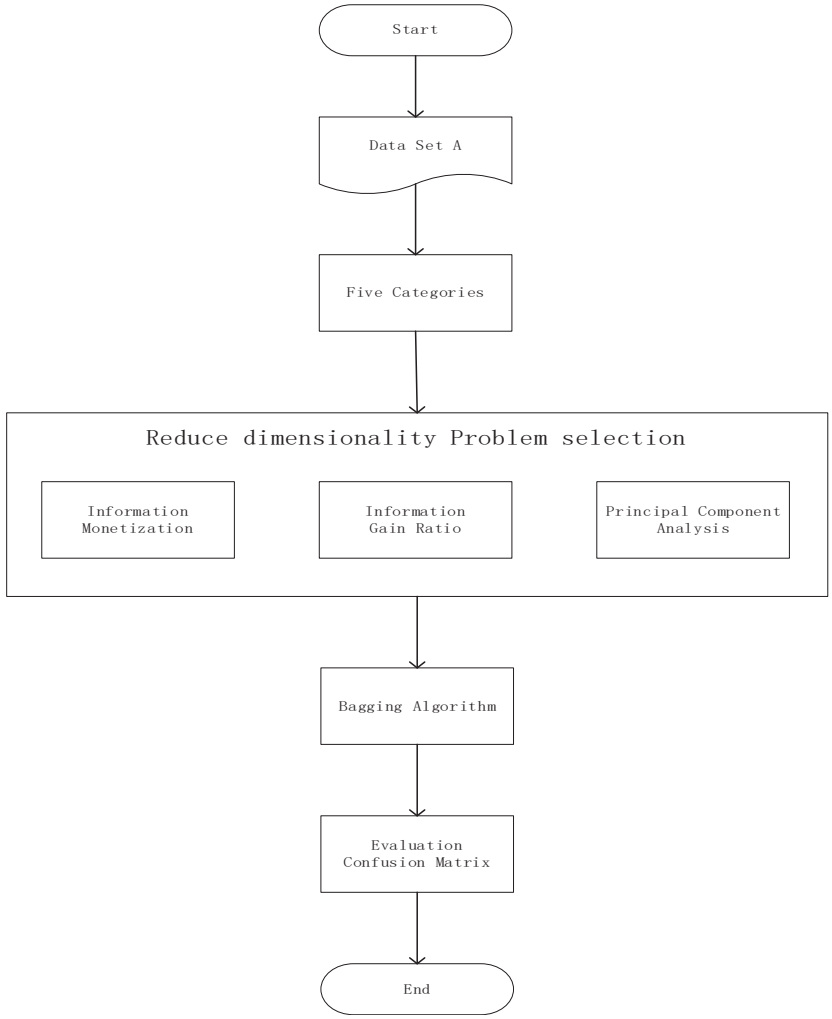

FIGURE 4
Flow chart of principal component extraction experiment.

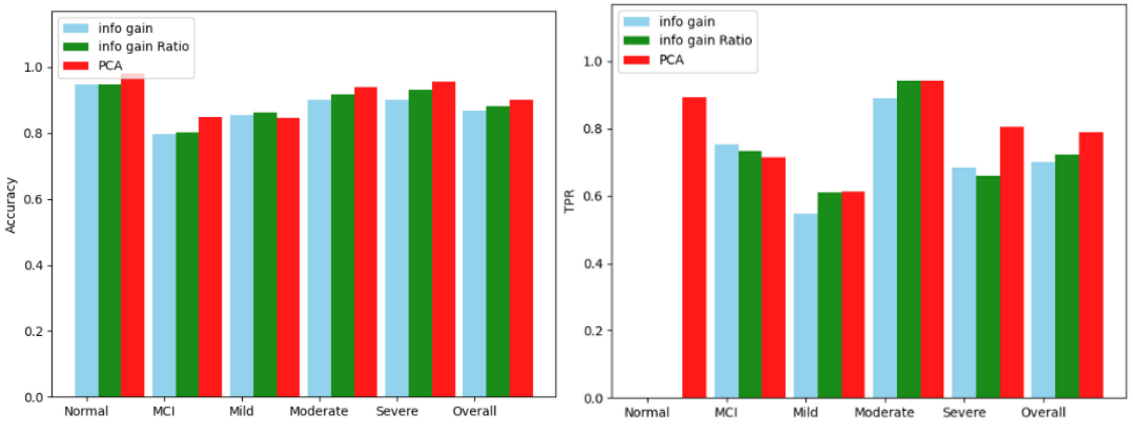

FIGURE 5
Comparison results for 19 questions.

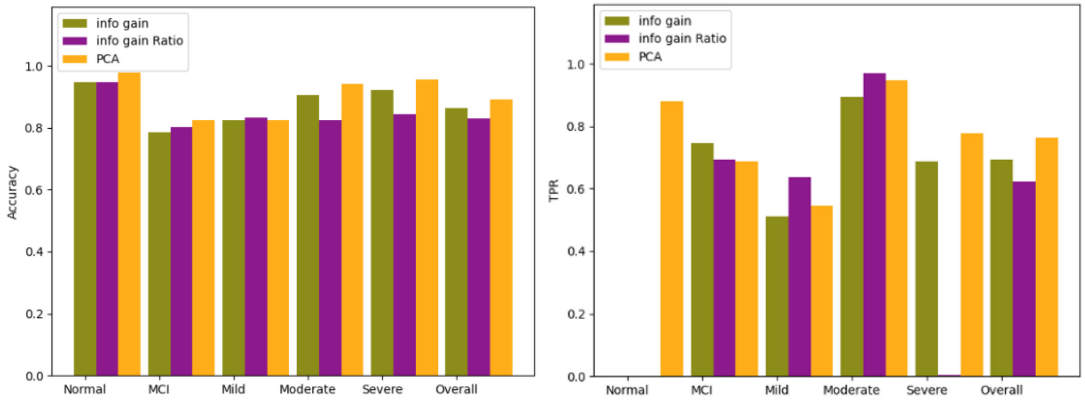

FIGURE 6
Comparison results for 14 questions.

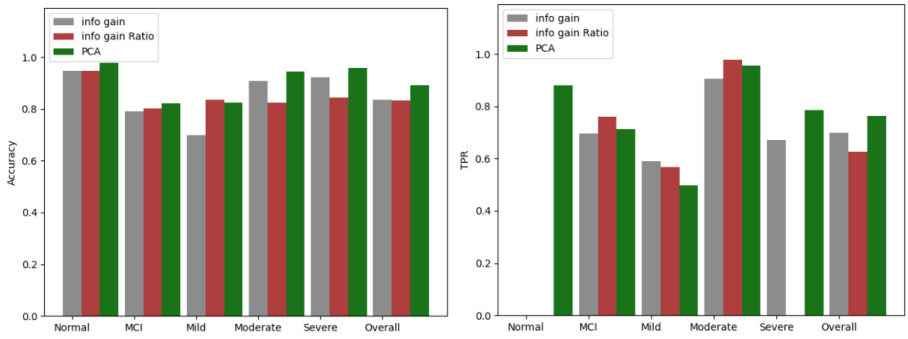

FIGURE 7
Comparison results for 12 questions.

reduce the categories, and use the confusion matrix to check the effect again. We choose C4.5 decision tree and Bagging to calculate, and use confusion matrix to calculate the accuracy and TPR of each category. Figure 3 shows the comparison results of the two algorithms.

Decision scale analysis

Comparison of three algorithms

In this part, we choose three algorithms (information gain, gain ratio, and PCA) to get the importance of 42 questions, and then delete the questions based on them, and watch the effect with the confusion matrix. Then, we choose the best algorithm and compare the eight questions selected with the eight questions in AD-8. The flow chart is shown in Figure 4.

The three screening methods individually pick out the questions with the highest scores, substitute the questions into the Bagging algorithm, and then use the confusion matrix to test the accuracy of each category. According to the number of variables in PCA, the number of questions is selected and compared four times, which is 19 questions, 14 questions, 12 questions, and 9 questions. The comparison results of the three algorithms are shown in Figures 5–8.

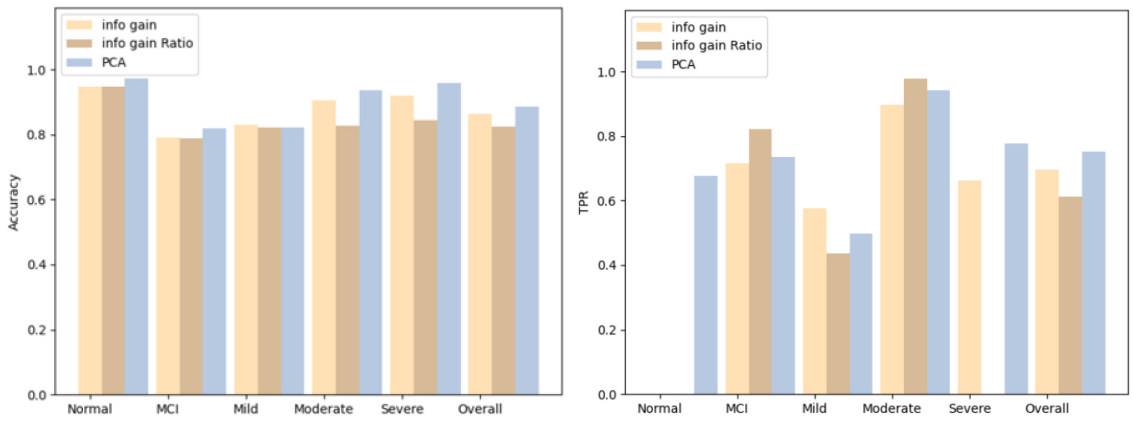

FIGURE 8
Comparison results for 9 questions.

TABLE 6 Eight questions screened by PCA.

Algorithm	Question number							
PCA	M01	M05	M09	O07	J01	J02	C06	H01
AD-8	M01	M09	O02	O03	J02	J03	J06	H01

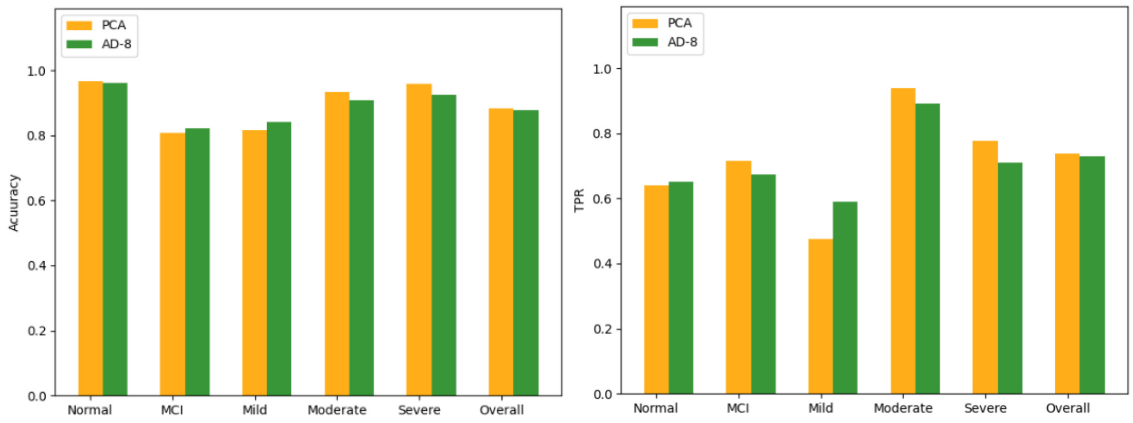

FIGURE 9
Comparison of PCA and AD-8 results.

Comparison with AD-8

In the CDR there are eight questions that are very similar to the AD-8, and in the AD-8 the answer is "yes, changed" or "no, no change," while in the CDR the answer is quite different. Pick out the problems similar to AD-8 from the CDR, and then use the eight problems screened out by PCA to input them into the Bagging algorithm, and then use the confusion matrix for comparison. The eight problems selected are shown in **Table 6**. See **Figure 9** for a comparison of the results, showing that both have the same degree of accuracy.

Conclusion and future work

In the experimental part, it can be seen that the effect of the Bagging algorithm is the best, and the accuracy is above 80%. In the Normal category, although the C4.5 decision tree has a higher accuracy than Bagging, in TPR, Bagging is better than the decision tree, and TPR is what we value more. In the selection of important features, the effect of PCA is better than that of information profit or information profit ratio, especially in the Normal category, the TPR of information profit or information profit ratio is 0, both of which will be all Normal misidentification is unacceptable to us. And compared with AD-8, the effect of PCA in the five categories is also better.

Although medical databases are widely used now, the data on dementia is very scarce. It is hoped that in the future, a database will be established to collect a large amount of dementia data. The more data, the better the model there will be, to help patients understand their own situation and seek medical treatment earlier. In addition, we also hope to expand the fields for collecting data in medical databases. The more data there are, the more extensive the research topics will be, and the personal data of patients should be removed. And these data is used only for research purposes. In addition, more kinds of algorithms can be used in the future, be it fuzzy logic or neural network, or even deep learning algorithms. There will be a combination of categories and a way to deal with imbalanced data, and there should be different results.

Data availability statement

The raw data supporting the conclusions of this article will be made available by the authors, without undue reservation.

Author contributions

Z-HZ: resources. LX: supervision. MZ: funding acquisition. JL: writing—original draft preparation. MZ and S-LP: writing—review and editing. All authors have read and agreed to the published version of the manuscript.

Funding

This research was funded by the Hubei Provincial Department of Education: 21D031.

Conflict of interest

The authors declare that the research was conducted in the absence of any commercial or financial relationships that could be construed as a potential conflict of interest.

Publisher's note

All claims expressed in this article are solely those of the authors and do not necessarily represent those of their affiliated organizations, or those of the publisher, the editors and the reviewers. Any product that may be evaluated in this article, or claim that may be made by its manufacturer, is not guaranteed or endorsed by the publisher.

References

Aboghazalah, M., El Kafrawy, P. M., and Torkey, H. (2022). Using X-ray Image Processing Techniques to Improve Pneumonia Diagnosis based on Machine Learning Algorithms. *Menouf. J. Electr. Engin. Res.* 31, 47–54. doi: 10.21608/mjeer.2022.218823

Afshar, P., Heidarian, S., and Enshaei, N. (2021). COVID-CT-MD, COVID-19 computed tomography scan dataset applicable in machine learning and deep learning. *Scientific Data* 8, 1–8. doi: 10.1038/s41597-021-00900-3

Ahmed, M. R., Zhang, Y., and Feng, Z. (2018). Neuroimaging and machine learning for dementia diagnosis: recent advancements and future prospects. *IEEE Rev. Biomed. Engin.* 12, 19–33. doi: 10.1109/RBME.2018.2886237

Alashwal, H., Halaby, M. E., Crouse, J. J., Abdalla, A., and Moustafa, A. A. (2019). The Application of Unsupervised Clustering Methods to Alzheimer's Disease. *Front. Comput. Neurosci.* 13:31. doi: 10.3389/fncom.2019.00031

Alexiou, A., Mantzavinos, V. D., Greig, N. H., and Kamal, M. A. (2017). A Bayesian Model for the Prediction and Early Diagnosis of Alzheimer's Disease. *Front. Aging Neurosci.* 9:77. doi: 10.3389/fnagi.2017.00077

Alickovic, E., and Subasi, A. (2019). "Automatic Detection of Alzheimer Disease Based on Histogram and Random Forest," in *International Conference opn medical Imaging and Biological Engineering, CMBEBIH 2019. CMBEBIH 2019. IFMBE Proceedings*, Vol. 73, (Cham: Springer), doi: 10.1007/978-3-030-17971-7_14

An, N., Ding, H., Yang, J., Au, R., and Ang, T. F. A. (2020). Deep ensemble learning for Alzheimer's disease classification. *J. Biomed. Inform.* 105, 103411. doi: 10.1016/j.jbi.2020.103411

Ansari, A. H., Cherian, P. J., Caicedo, A., Naulaers, G., De Vos, M., and Van Huffel, S. (2019). Neonatal Seizure Detection Using Deep Convolutional Neural Networks. *Int. J. Neural Syst.* 29:1850011. doi: 10.1142/S0129065718500119

Bloch, L., and Friedrich, C. M. (2019). "Classification of Alzheimer's Disease using volumetric features of multiple MRI scans," in *2019 41st Annual International Conference of the IEEE Engineering in Medicine and Biology Society (EMBC)*, (Germany: EMBC), 2396–2401. doi: 10.1109/EMBC.2019.8857188

Broman, S., O'Hara, E., and Ali, M. L. (2022). "A Machine Learning Approach for the Early Detection of Dementia," in *IEEE International IOT, Electronics and Mechatronics Conference (IEMTRONICS)*, (Netherland: IEEE), 1–6. doi: 10.1109/IEMTRONICS55184.2022.9795717

Das, S., Pradhan, S. K., Mishra, S., et al. (2022). "A Machine Learning based Approach for Detection of Pneumonia by Analyzing Chest X-Ray Images," in *9th International Conference on Computing for Sustainable Global Development (INDIACom)*, (Netherland: IEEE), 177–183. doi: 10.23919/INDIACom54597.2022.9763203

Elaziz, M. A., Hosny, K. M., and Salah, A. (2020). New machine learning method for image-based diagnosis of COVID-19. *PLoS One* 15:e0235187. doi: 10.1371/journal.pone.0235187

Elkamouny, M., and Ghantous, M. (2022). "Pneumonia Classification for Covid-19 Based on Machine Learning," in *2nd International Mobile, Intelligent, and Ubiquitous Computing Conference (MIUCC)*, (Netherland: IEEE), 135–140. doi: 10.1109/MIUCC55081.2022.9781796

GBD 2019 Dementia Forecasting Collaborators (2022). Estimation of the global prevalence of dementia in 2019 and forecasted prevalence in 2050: an analysis for the Global Burden of Disease Study 2019. *Lancet Publ. Health* 7, e105–e125. doi: 10.1016/S2468-2667(21)00249-8

Khan, A., Zubair, S., and Khan, S. (2022). A systematic analysis of assorted machine learning classifiers to assess their potential in accurate prediction of dementia. *Arab Gulf Jo. Scientif. Res.* 40, 2–24. doi: 10.1108/AGJSR-04-2022-0029

Miah, Y., Prima, C. N. E., and Seema, S. J. (2021). "Performance comparison of machine learning techniques in identifying dementia from open access clinical datasets," in *Advances on Smart and Soft Computing. Advances in Intelligent Systems and Computing*, Vol. 1188, eds F. Saeed, T. Al-Hadhrami, F. Mohammed, and E. Mohammed (Singapore: Springer), doi: 10.1007/978-981-15-6048-4_8

Prakash, K. B., Imambi, S. S., and Ismail, M. (2020). Analysis, prediction and evaluation of covid-19 datasets using machine learning algorithms. *Int. J.* 8, 2199–2204. doi: 10.30534/ijeter/2020/117852020

Shiri, I., Mostafaei, S., and Avval, A. H. (2022). High-Dimensional Multinomial Multiclass Severity Scoring of COVID-19 Pneumonia Using CT Radiomics Features and Machine Learning Algorithms. *medRxiv* [Preprint] doi: 10.1101/2022.04.27.22274369

Sun, X., Douiri, A., and Gulliford, M. (2022). Applying machine learning algorithms to electronic health records to predict pneumonia after respiratory tract infection. *J. Clin. Epidemiol.* 145, 154–163. doi: 10.1016/j.jclinepi.2022.01.009

Trambaiolli, L. R., Lorena, A. C., Fraga, F. J., Kanda, P. A., Anghinah, R., and Nitrini, R. (2011). Improving Alzheimer's Disease Diagnosis with Machine Learning Techniques. *Clin. EEG Neurosci.* 42, 160–165.

Williams, J. A., Weakley, A., Cook, D. J., and Schmitter-Edgecombe, M. (2013). "Machine Learning Techniques for Diagnostic Differentiation of Mild Cognitive Impairment and Dementia," in *Proceeding of Workshops at the Twenty-Seventh AAAI Conference on Artificial Intelligence (AAAI-13)*, (Washington, USA), 71–76.

frontiers | Frontiers in Aging Neuroscience

TYPE Original Research
PUBLISHED 12 September 2022
DOI 10.3389/fnagi.2022.973068

OPEN ACCESS

EDITED BY
Woon-Man Kung,
Chinese Culture University, Taiwan

REVIEWED BY
Heather M. Wilkins,
University of Kansas Medical Center Research Institute, United States
Mervyn Maze,
University of California, San Francisco, United States

*CORRESPONDENCE
Gordon Tin Chun Wong
gordon@hku.hk
Chunxia Huang
huangchunxia@ahmu.edu.cn

†These authors have contributed equally to this work and share first authorship

SPECIALTY SECTION
This article was submitted to Neurocognitive Aging and Behavior, a section of the journal Frontiers in Aging Neuroscience

RECEIVED 19 June 2022
ACCEPTED 16 August 2022
PUBLISHED 12 September 2022

CITATION
Lu W, Tang S, Li A, Huang Q, Dou M, Zhang Y, Hu X, Chang RCC, Wong GTC and Huang C (2022) The role of PKC/PKR in aging, Alzheimer's disease, and perioperative neurocognitive disorders. *Front. Aging Neurosci.* 14:973068. doi: 10.3389/fnagi.2022.973068

The role of PKC/PKR in aging, Alzheimer's disease, and perioperative neurocognitive disorders

Wenping Lu[1,2,3†], Sailan Tang[1,2,3†], Ao Li[4], Qiuyue Huang[4], Mengyun Dou[1], Ye Zhang[1,2], Xianwen Hu[1,2], Raymond Chuen Chung Chang[5,6], Gordon Tin Chun Wong[7*] and Chunxia Huang[1,2*]

[1]Department of Anesthesiology, The Second Affiliated Hospital of Anhui Medical University, Hefei, China, [2]Key Laboratory of Anesthesiology and Perioperative Medicine of Anhui Higher Education Institutes, Anhui Medical University, Hefei, China, [3]Scientific Research and Experiment Center of the Second Affilliated Hospital of Anhui Medical University, Hefei, China, [4]The Second Clinical Medical College of Anhui Medical University, Hefei, China, [5]Laboratory of Neurodegenerative Diseases, School of Biomedical Sciences, LKS Faculty of Medicine, The University of Hong Kong, Pokfulam, Hong Kong SAR, China, [6]State Key Laboratory of Brain and Cognitive Sciences, The University of Hong Kong, Pokfulam, Hong Kong SAR, China, [7]Department of Anaesthesiology, LKS Faculty of Medicine, The University of Hong Kong, Pokfulam, Hong Kong SAR, China

Background: The incidence of perioperative neurocognitive disorders (PNDs) is reportedly higher in older patients. Mitochondrial and synaptic dysfunctions have consistently been demonstrated in models of aging and neurodegenerative diseases; nonetheless, their role in PND is not well understood.

Methods: The Morris water maze and elevated plus maze tests were used to assess the learning and memory abilities of both C57BL/6 and 3×Tg-AD mice of different ages (8 and 18 months). PND was induced by laparotomy in C57BL/6 mice and 3×Tg-AD mice (8 months old). Markers associated with neuroinflammation, mitochondrial function, synaptic function, and autophagy were assessed postoperatively. The roles of protein kinase C (PKC) and double-stranded RNA-dependent protein kinase (PKR) were further demonstrated by using PKC-sensitive inhibitor bisindolylmaleimide X (BIMX) or $PKR^{-/-}$ mice.

Results: Significant cognitive impairment was accompanied by mitochondrial dysfunction and autophagy inactivation in both aged C57BL/6 and 3×Tg-AD mice. Laparotomy induced a significant neuroinflammatory response and synaptic protein loss in the hippocampus. Cognitive and neuropathological changes induced by aging or laparotomy were further exacerbated in 3×Tg-AD mice. Deficits in postoperative cognition, hippocampal mitochondria, autophagy, and synapse were significantly attenuated after pharmacological inhibition of PKC or genetic deletion of PKR.

Conclusions: Our findings suggest similar pathogenic features in aging, Alzheimer's disease, and PND, including altered mitochondrial homeostasis and autophagy dysregulation. In addition, laparotomy may exacerbate cognitive deficits associated with distinct neuronal inflammation,

mitochondrial dysfunction, and neuronal loss independent of genetic background. The dysregulation of PKC/PKR activity may participate in the pathogenesis of these neurodegenerative diseases.

KEYWORDS

perioperative neurocognitive disorders, autophagy, protein kinase C, double-stranded RNA (dsRNA)-dependent protein kinase, laparotomy

Introduction

For over half a century, it has been observed that some patients experience impairment in memory, attention, action, and perception after surgery, a condition previously known as postoperative cognitive dysfunction (POCD) but now termed perioperative neurocognitive disorder (PND). A systematic review of 274 studies has reported that the overall postoperative incidence at 1–3 months is around 29.0% (Borchers et al., 2021). It is well established that delayed neurocognitive recovery can have a long-term impact on daily living function and even mortality (Schwarz et al., 2013). A study reported that the incidence of dementia was 30.8%, and detectable cognitive impairment was 30.8% in elderly patients after coronary artery bypass graft at 7.5 years postoperatively. Patients with detectable impairment at 3 and 12 months postoperatively had increased mortality (Evered L.A. et al., 2016). Due to the pathological similarities between PND and Alzheimer's disease (AD), Aβ, tau, and neuroinflammation have been considered predictors of the development of PND (Evered L. et al., 2016). Interestingly, in the absence of clinically detectable AD symptoms, patients with AD neuropathology may be more susceptible to a postoperative cognitive decline (Evered L. et al., 2016).

The protein kinase C (PKC) family of serine/threonine kinases regulates diverse cellular functions for cell survival, proliferation, and death. Human PKC isoforms include PKCα, β, δ, ε, γ, and ζ, and imbalances in their expression and activities have been implicated in the pathophysiology of AD, diabetes, and cancers (Newton, 2018). In the central nervous system (CNS), these enzymes play critical roles in learning and memory, among other important functions (Sun and Alkon, 2014). Although the activation of some PKC isoforms, such as PKCα and ε, has been shown to regulate nonamyloidogenic pathways and Aβ degradation, it is unclear whether other PKC isoforms are involved in β-amyloid precursor protein (APP) processing and the pathogenesis of AD. In this regard, PKCδ reportedly governs cellular homeostatic responses, such as autophagy and apoptosis, against hypoxic stress through PKCδ/JNK1-mediated signaling pathways (Chen et al., 2009). PKCδ also plays an important role in exacerbating AD pathogenesis and may be a potential therapeutic target in AD. Importantly, in a transgenic AD mouse model, inhibition of PKCδ by rottlerin has been shown to markedly reduce the expression of β-site APP-cleaving enzyme I (BACE1, a novel aspartyl protease in Aβ genesis), Aβ levels, and plaque formation and improves cognitive deficits (Du et al., 2018).

Double-stranded RNA-dependent protein serine/threonine kinase (PKR) is a ubiquitous eukaryotic initiation factor 2α kinase that inhibits translation involving memory formation and consolidation. Current evidence suggests that PKR accumulates in the brain and cerebrospinal fluid in patients with AD and mild cognitive impairment, leading to TNFα and IL1-β production (Hugon et al., 2017). In addition, PKR contributes to inflammatory and immune dysfunction through mitogen-activated protein kinases, interferon regulatory factor 3, nuclear factor κB, apoptosis, and autophagy pathways (Kang and Tang, 2012). In a previous study, we demonstrated that PKR signaling participates in the development of PND with defective mitophagy in aged mice (Wang et al., 2022).

Given that PKC and PKR are implicated in the pathogenesis of Alzheimer's disease and advanced age is a risk factor for both AD and PND, we hypothesized that age-related changes in PKC and PKR activities are involved in the development of PND and may account for the increased susceptibility of the elderly. We used wild-type transgenic AD mice to compare age-related changes in PKC/PKR expression and mitochondrial function. Finally, we demonstrated the restorative effects of PKC inhibition PKR knockout on postoperative cognitive changes.

Abbreviations: PND, perioperative neurocognitive disorder; POCD, postoperative cognitive dysfunction; AD, Alzheimer's disease; PKC, protein kinase C; CNS, central nervous system; PKR, double-stranded RNA (dsRNA)-dependent protein kinase; APP, β-amyloid precursor protein; OCT, optimal cutting temperature; MCP-1, monocyte chemoattractant protein-1; ROS, reactive oxygen species; DHE, dihydroethidium; BIMX, bisindolylmaleimide X; MWM, Morris water maze; TFEB, transcription factor EB; E2, endogenous estradiol; PI3K phosphatidylinositol 3-kinase; ERK, extracellular signal-regulated kinase; PKA, protein kinase A.

Materials and methods

Animals

Male C57BL/6 mice, 3×Tg-AD mice (triple transgenic B6; 129-*Psen*^{1tm1Mpm} Tg (APPSwe, tauP301L)1Lfa/J), and PKR$^{-/-}$

mice were obtained from the Laboratory Animal Unit of Anhui Medical University and the University of Hong Kong. All experimental protocols and animal handling procedures were approved by the Faculty Committee on the Use of Live Animals in Teaching and Research at The University of Hong Kong (CULATR Ref. No. 3437-14) and the Ethics Committee for the use of experimental animals in Anhui Medical University (reference number LLSC20190765; date of approval 26/10/2019). The animals were randomly divided into specific groups depending on the protocols. The mice were bred and housed in a temperature- and humidity-controlled room. All animals had free access to food and water. Acclimatization for 1 week was completed before experiments. All behavioral tests were conducted from 09:00 to 12:00 P.M.

Laparotomy

Bisindolylmaleimide X (hydrochloride) (BIMX) (Sigma, USA), a selective PKC inhibitor, was administered intraperitoneally at 30 min before laparotomy for the treatment groups. A laparotomy was performed under sevoflurane (Sevorane^{TM}, Abbott, Switzerland) anesthesia, induced *via* a rodent inhalation anesthesia apparatus (Harvard, USA), as previously described (Huang et al., 2018). The intestine was exposed through a longitudinal midline incision and rubbed vigorously for 30 s. After 1-min exposure, it was replaced in the abdominal cavity. Following sterile chromic gut sutures (4-0, PS-2; Ethicon, USA), the animals were returned to their cage for recovery. The entire procedure was completed within 15 min, and anesthesia was discontinued immediately after performing the last stitch. The control mice were exposed to sevoflurane only for 15 min.

Morris water maze test

To assess allocentric navigational abilities, the Morris water maze (MWM) test was performed from postoperative days 6–12. This test required a circular tank (35 cm in depth with a diameter of 120 cm) containing a floating platform (7 cm high), conspicuous visual cues, and a video recording system (Debut Professional, NCH Software, Australia). The pool was divided into four quadrants, each with a specific visual cue. The platform was stabilized in the middle of one quadrant 0.7 cm below the water. The entire test consisted of a hidden platform training spanning over 6 days and the probe test without the platform. In each trial during training, the mice were randomly placed into each quadrant to search for the invisible platform. If the animal failed to reach the platform by itself within 60 s, it would be guided to the platform for a 20-s stay. The probe test was performed 24 h after the last training trial. The animals were placed in the opposite quadrant for 60 s. Finally, the learning curve was calculated by the accumulated escape latency in the training phase, and the number of platform crossings was used to assess spatial memory in the probe test.

Elevated plus maze test

This test was used to evaluate the changes in anxiety-related behaviors in the mice. To assess the spontaneous activity and anxiety, an elevated plus maze test was performed on postoperative day 13. The apparatus consisted of two open and closed arms of the same size (35 cm length, 5 cm width, 15 cm height) and a central square connecting the arms. The apparatus was placed at a height of 40 cm from the ground (RWD Life Science, China). The animals were allowed to move freely in the elevated cross maze for 10 min, and their movements were recorded with a video camera. The number of crossings and time spent in the open arm were analyzed by PanLab Smart 3 software (Harvard, USA).

Y-maze test

To assess the hippocampal-dependent spatial learning capacity, a modified Y-maze test was used (Huang et al., 2018). The device consisted of two black arms capable of delivering electric shocks at 2 Hz for 10s (40 $\pm$ 5 V) and one shock-free compartment. After habituation, each mouse was placed in one of the black compartments to assess spontaneous alternating behavior, and electric shocks were applied until it entered the shock-free compartment and stayed there for 30 s, which was then deemed a correct choice. Successful training was made with nine continuous correct choices. Each mouse was tested 10 times for the validation trial, following the same procedures as in the training trial. The number of incorrect choices and the time taken to enter the shock-free compartment (latency) were recorded.

Transmission electron microscopy

The mice were killed 24 h after the elevated plus maze test. The hippocampi were sectioned (1 mm^3) and fixed overnight in 2.5% glutaraldehyde at 4°C. After rinsing in PBS for 6 h at 4°C, the sections were post-fixed in 1% osmium tetroxide for 1 h at 4°C. Then, the sections were dehydrated with alcohol. After incubation in propylene oxide and epoxy resin for 2 h at room temperature, the sections were embedded in epoxy resin to obtain ultrathin sections (70 nm thick, Leica UC-7 microtome). The area and diameter of mitochondria (10,000×) were analyzed using ImageJ software (National Institutes of Health, USA). The number of mitochondria autophagy bodies (10,000×) was

observed in at least 10 visual fields (including intact neuronal bodies) by using a JEM1400 electron microscope (JEOL, Japan).

SDS-PAGE and western blot analysis

After transcardial perfusion, the left cerebral hemisphere was immediately frozen and embedded in an optimal cutting temperature (OCT) compound for further sectioning. The hippocampal tissues were dissected from the right hemisphere, and protein extracts were stored at −80°C. Whole-protein lysates were extracted using RIPA buffer containing protease and phosphatase inhibitors (Roche, Germany). The mitochondria and cytoplasmic fractions were collected using a mitochondria isolation kit (MITOISO1, Sigma, USA). The synaptosomal and cytosolic fractions were freshly prepared using Syn-PER^{TM} Synaptic Protein Extraction Reagent (Thermo Fisher Scientific, USA) plus protease and phosphatase inhibitors (Roche, USA), following the manufacturer's instructions.

Total lysates or cellular compartment fractions were subjected to 10 to 15% polyacrylamide gel electrophoresis and transferred onto PVDF membranes, as described previously (Huang et al., 2018). After blocking with 5% non-fat milk for 1 h at room temperature, the membranes were incubated overnight at 4°C with specific primary antibodies including Bax, Bcl-2, cleaved caspase 3, Pink1, Parkin, p62, LC3B, PKR, p-PKR, PKC, p-PKC, p-eif2α, eif2α (Cell Signaling Technology, USA), BDNF (Santa Cruz Biotechnology), and OXPHOS (Abcam, USA). After incubation with horseradish peroxidase-conjugated secondary antibodies (DAKO, Denmark) for 2 h at room temperature, the immunoreactive band signal intensity was subsequently visualized by chemiluminescence (SuperSignal^{TM} West Femto Maximum Sensitivity Substrate) (Thermo Fisher Scientific, USA). All immunoblots were normalized with β-actin or GAPDH (Sigma-Aldrich, USA) antibodies. The intensities of chemiluminescent bands were measured by ImageJ software (National Institutes of Health, USA).

RNA isolation and real-time PCR

Total RNA from hippocampi and livers were extracted using Tri Reagent® (MRC, USA) and purified using an Ambion® DNA-free^{TM} DNA Removal Kit (Invitrogen, USA). After reverse transcription using a PrimeScript^{TM} Master Mix Kit (TAKARA, Japan), PCR was performed using an SYBR® Premix Ex Taq^{TM} II Kit (TAKARA, Japan). The amplification conditions of IL-1β, IL-6, and IL-8 were previously described in the literature (Huang et al., 2018). In addition, monocyte chemoattractant protein-1 (MCP-1) was also detected by using the StepOnePlus^{TM} Real-Time PCR System (Applied Biosystems, USA) with the following sequence: F: 5′-TGCTGTCTCAGCCAGATGCAGTTA-3′, R: 5′-TACAGC TTCTTTGGGACACCTGCT-3′. The relative levels of cytokines were normalized to the endogenous reference glyceraldehyde-3-phosphate dehydrogenase (GAPDH) using the $2^{-\Delta\Delta Ct}$ method.

Dihydroethidium and JC-1 assay

To detect the level of reactive oxygen species (ROS), fresh frozen sections of the hippocampus were labeled with a dihydroethidium (DHE) fluorescence probe. Following activation in methanol for 20 min, 15-μm-thick sections were incubated with 10 μM DHE dye (Thermo Fisher Scientific, USA) for 20 min at 37°C. The images were then captured using a confocal microscope by excitation at 568 nm (Carl Zeiss LSM 900, Germany).

To assess for any changes in mitochondrial membrane potential, 5 μg of fresh mitochondrial proteins were incubated with a JC-1 dye (1 μg/ml, Thermo Fisher Scientific, USA) for 20 min at 37°C. The fluorescence intensity ratio of 525 nm/488 nm was measured by using a CLARIOstar instrument (BMG LabTech, Thermo Fisher Scientific, USA).

Immunofluorescence staining and apoptosis assay

For immunofluorescence staining, 12-μm-thick coronal frozen sections were obtained from OCT embedded blocks (from−1.46 mm to−2.46 mm posterior to bregma). To block non-specific antibody binding, 10% normal goat serum was used after antigen retrieval with citrate buffer (0.01 M, pH 6.0) at 90°C for 15 min. Specific primary antibodies were applied at 4°C overnight as follows: IBA1 (Wako, Japan), GFAP (Sigma-Aldrich, USA), CD68 (Serotec, USA), cleaved caspase 3 (Cell Signaling Technology, USA), PSD95, and synaptophysin (Synaptic System, Germany). The sections were then incubated with specific Alexa Fluor 568 or 488 secondary antibodies (Invitrogen, USA) for 2 h at room temperature.

Apoptosis was detected using the TdT-mediated dUTP nick-end labeling (TUNEL) technique (*In Situ* Cell Death Detection Kit TMR red, Roche, USA). The nuclei were labeled with 4'-6-diamidino-2-phenylindole (DAPI) (3 μM, Sigma-Aldrich, USA). Photographs were observed under a laser scanning confocal fluorescent microscope (5×, 20×, and 40× oil immersion objectives) (Carl Zeiss LSM 900, Germany). *Z*-stack images were acquired at 1,024 × 1,024 resolution. All quantitative analyses were performed on at least three images acquired from three serial sections per animal.

Statistical analyses

Using the statistic software GraphPad Prism 9.0 (Graph Pad Software Inc., USA), data from the Morris water maze were analyzed using a two-way analysis of variance (ANOVA), followed by the Tukey's *post hoc* test for repeated measures. Other data, such as elevated plus maze test, relative mRNA levels of cytokines, normalized band intensities in Western blot, and quantification of immunoreactivity, were analyzed by one-way ANOVA, followed by the Tukey's *post hoc* test or *t*-test. The normality of the data and homogeneity of group variances were assessed using the D'Agostino–Pearson omnibus normality test, Shapiro–Wilk normality test, and Kolmogorov–Smirnov test. A P-value < 0.05 was statistically significant.

Results

Mitochondrial characteristics, PKR and PKC activities, and cognitive performances during aging in both wild-type and 3×Tg-AD mice

To assess age-related neuropathological changes, we first examined ultrastructural characteristics of neuronal mitochondria using a transmission electron microscope (Figure 1A). In both wild-type or 3×Tg-AD mice, the mitochondrial number, area, and diameter were significantly decreased in 18-month-old mice compared with their younger counterparts (mitochondrial number, 12.1 ± 3.2 vs. 8.7 ± 1.6 in wild-type mice, 10.2 ± 2.2 vs 8.3 ± 1.9 in 3×Tg-AD mice; mitochondrial area, 0.38 ± 0.24 μm^2 vs. 0.28 ± 0.18 μm^2 in wild-type mice, 0.32 ± 0.23 vs. 0.21 ± 0.13 μm^2 in 3×Tg-AD mice; mitochondrial diameter, 0.74 ± 0.29 vs. 0.64 ± 0.23 μm in wild-type mice, 0.63 ± 0.25 vs. 0.52 ± 0.18 μm in 3×Tg-AD mice; Figures 1B–D). Levels of autophagy were reduced in the hippocampus during aging in both strains, as indicated by the significantly decreased expressions of autophagy-related proteins, including LC3, P62, Pink1, and Parkin. These protein levels were lower in 3×Tg-AD mice than in wild-type mice (Figure 1E). There were also changes in the activities of PKR and PKC during aging. Increased activity of PKR and Eif2α in terms of phosphorylation was observed in the hippocampus in both wild-type and 3×Tg-AD mice. With respect to the different isoforms, there was an enhancement in PKCδ and suppression in PKCα activity during aging in wild-type mice and 3×Tg-AD mice (Figure 1F).

The Morris water maze (MWM) test was then performed to evaluate the functional impact of aging on spatial learning and memory. In consecutive training sessions, the mice with different genetic backgrounds successfully located the submerged platform, as indicated by the significant decrease in escape latency (Figure 2A, $P_{time} < 0.0001$). Aged mice from both strains consistently demonstrated longer latency than the middle-aged mice (Figure 2A). The difference between the Wt and 3×Tg-AD mice was observed in the second and third training sessions. In the probe test, the aged mice spent more time locating the submerged platform (11.85 ± 2.53 vs. 23.53 ± 3.27 s in wild-type mice, 15.97 ± 3.57 vs. 31.66 ± 2.38 s in 3×Tg-AD mice; Figures 2B,C) and performed fewer crossings in the target quadrant (3.4 ± 1.4 vs. 1.9 ± 1.1 in wild-type mice, 3.4 ± 1.4 vs. 1.2 ± 0.4 in 3×Tg-AD mice; Figure 2D). One-way ANOVA showed significant differences among the groups in the escape latency and representative swimming route and number of crossings in the target quadrant. A similar performance in recall memory between the two strains of the same age further indicated that spatial memory deficits might be age-related.

To assess the anxiety response, an elevated plus maze test was performed 24 h after the probe test of MWM. Compared with the middle-aged mice, there were consistent decreases in the number of entries and time spent in the open arms in the Wt and 3×Tg-AD aged mice (Figures 2E–G). These data suggested that anxiety existed during aging, particularly in the aged 3×Tg-AD mice.

Laparotomy-induced inflammation and cognitive impairment in wild-type and 3×Tg-AD mice

Peripheral inflammation and neuroinflammation were observed 24 h postoperatively with increases in the mRNA levels of pro-inflammatory cytokines in the liver (Supplementary Figure S1A) and hippocampus (Figure 3A), respectively. The neuroinflammatory response was still present on postoperative day 14, as indicated by the activation of $Iba1^+$ microglia and $GFAP^+$ astrocytes, as well as $CD68^+$ macrophages observed in the hippocampus (Supplementary Figures S1B,C). Meanwhile, disruption in the intestinal lining and synapses after laparotomy was observed in both strains (Figures 3B,C). There was obvious evidence of apoptosis with a significant increase in Bax (1.49-fold of Wt-Ctrl in wild-type mice, 1.50-fold of 3×Tg-Ctrl in 3×Tg-AD mice) and decrease in Bcl2 (0.86-fold of Wt-Ctrl in wild-type mice, 0.89-fold of 3×Tg-Ctrl in 3×Tg-AD mice) in the hippocampi, and predominant localization of $TUNEL^+$ and cleaved caspase 3^+ cells in the hippocampal CA3 region in both strains following laparotomy (Figure 3D, Supplementary Figure S2).

All mice successfully acquired spatial learning abilities during the MWM training sessions, although postoperative 3×Tg-AD mice required more time to locate the submerged platform on the first training day. However, the significantly longer escape latency seen on the fifth and sixth training sessions suggested that surgery consistently impaired spatial learning in both wild-type and 3×Tg-AD mice (Figure 4A).

10.3389/fnagi.2022.973068

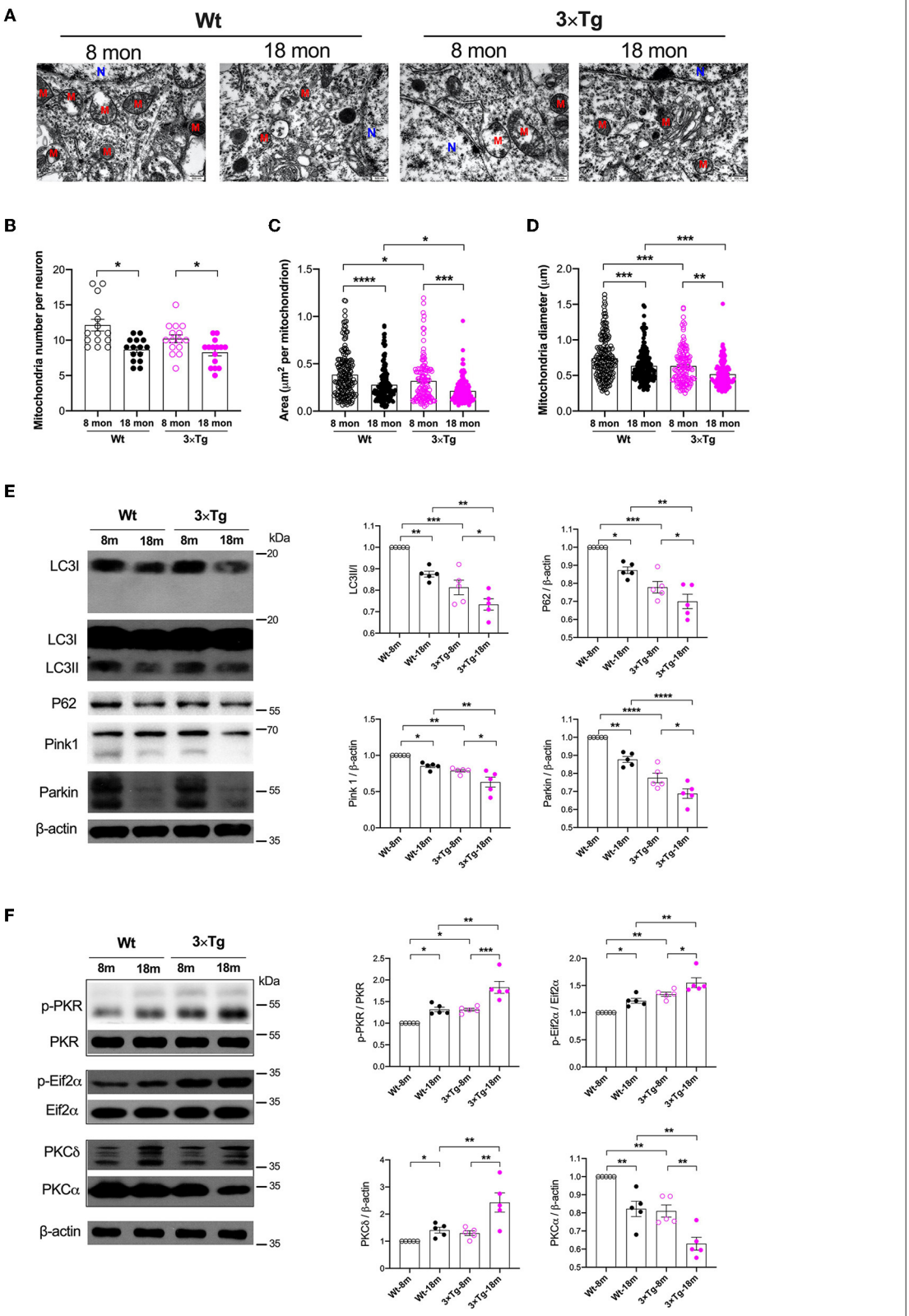

FIGURE 1
Variations of mitochondria and autophagy during aging in the wild-type and 3×Tg AD mice. **(A)** Representative electron microscopy photographs of mitochondria in the hippocampal neurons in different ages of wild-type and transgenic AD mice (N, nucleus; M, mitochondria; scale bar = 500 nm). **(B–D)** Quantification of mitochondrial number, area, and diameter in the hippocampal tissues from two strains of mice by

(Continued)

FIGURE 1 (Continued)
electron microscopy, n = 182, 160, 138, 121 mitochondria from 15 neurons in five mice per group. **(B)**: $F_{(3,56)} = 8.787$, $P < 0.0001$, $n = 15$; **(C)**: $F_{(3,597)} = 18.49$, $P < 0.0001$, $n = 121–182$; **(D)**: $F_{(3,597)} = 20.05$, $P < 0.0001$, $n = 121–182$. **(E)** In wild-type and 3×Tg AD mice, the relative expressions of autophagy-related proteins in the hippocampi were quantified by Western blotting analysis. LC3: $F_{(3,16)} = 24.74$, $P < 0.0001$; P62: $F_{(3,16)} = 22.62$, $P < 0.0001$; Pink1: $F_{(3,16)} = 17.26$, $P < 0.0001$; Parkin: $F_{(3,16)} = 43.14$, $P < 0.0001$. **(F)** Quantitative analysis of the relative expression of PKR, Eif2α, PKCδ, and PKCα in the hippocampal tissues in two strains of mice at different ages. p-PKR/PKR: $F_{(3,16)} = 20.58$, $P < 0.0001$; p-Eif2α/Eif2α: $F_{(3,16)} = 18.22$, $P < 0.0001$; PKCδ: $F_{(3,16)} = 10.51$, $P = 0.0005$; PKCα: $F_{(3,16)} = 21.72$, $P < 0.0001$. Wt, wild-type mice; 3×Tg, triple transgenic mice. Data are presented as mean ± SEM and were analyzed using one-way ANOVA using Tukey's *post hoc* test, $n = 5$, $^{*}P < 0.05$, $^{**}P < 0.01$, $^{***}P < 0.001$, $^{****}P < 0.0001$.

During the probe test, the longer escape latency (12.98 ± 3.29 vs. 17.56 ± 6.23 s in wild-type mice, 19.04 ± 3.31 vs. 22.46 ± 6.07 s in 3×Tg-AD mice) and a reduced number of crossings (3.3 ± 1.5 vs. 1.7 ± 0.8 in wild-type mice, 3.6 ± 1.2 vs. 1.3 ± 1.0 in 3×Tg-AD mice) further indicated that surgery could induce memory deficits in both mice strains (Figures 4B–D). The impact of laparotomy on memory in 3×Tg-AD mice was also determined in the Y-maze test. Compared with sevoflurane anesthesia alone, more errors and longer escape latency were observed on postoperative days 1 and 14 in the adult 3×Tg-AD mice. In addition to the body weight loss during the early postoperative period, more errors were observed in the aged 3×Tg-AD mice, rather than a longer escape latency (Supplementary Figure S3). In the elevated plus maze test, anxiety was only presented in postoperative mice, indicated by fewer entries in the open arms (48.81 ± 11.34 vs. 39.93 ± 10.78% in wild-type mice, 43.50 ± 10.95 vs. 17.97 ± 15.27% in 3×Tg-AD mice Figures 4E–G).

Laparotomy-induced autophagy-dependent PKC activation

In addition to inducing neuroinflammation, laparotomy can significantly impact mitochondria and autophagy. Consistent with our previous study (Wang et al., 2022), laparotomy caused neuronal oxidative stress in the 3×Tg-AD mice, with significant elevation of ROS, and reduction in the mitochondrial membrane potential (1.053 ± 0.046 vs. 0.793 ± 0.064 in wild-type mice, 0.826 ± 0.106 vs. 0.624 ± 0.040 in 3×Tg-AD mice) and activity of the mitochondrial complexes. In this respect, complexes I, IV, II, and III were significantly decreased after laparotomy in the 3×Tg-AD mice compared with wild-type mice (Figures 5A–C). There were decreases in mitochondrial complex activity in the intact 3×Tg-AD mice compared with the wild-type mice.

At the same time, laparotomy caused consistent decreases in autophagy-related proteins, such as LC3, P62, Pink1, and Parkin, in the hippocampus of both wild-type and 3×Tg-AD mice, especially in the 3×Tg-AD mice (Figure 5D). Compared with the control group, the increased activities in PKR/Eif2α and variations of PKC were significantly expressed in the hippocampus in both strains of mice, with these changes being more pronounced in the postoperative 3×Tg-AD mice (Figure 5E).

Pharmacological inhibition of PKC with BIMX resulted in significantly increased expression of autophagy-related proteins after laparotomy (Figure 6A). There were also distinct increases in synaptic proteins such as PSD95 (1.375-fold of Lap), synapsin 1 (1.976-fold of Lap), and synaptophysin (1.309-fold of Lap) in the synaptosome fractions in the hippocampal CA3 region (Figures 6B,C). Furthermore, neuronal apoptosis was attenuated by BIMX, with significant decreases in Bax and cleaved caspase-3 expression (Supplementary Figure S4). The activities of PKR/Eif2α and PKCδ were also decreased with an increase in PKCα in the hippocampi of the 3×Tg-AD mice (Figure 6D).

Laparotomy-induced autophagy-dependent PKR activation

To further investigate the role of PKR in the neuropathological changes induced by laparotomy, the $PKR^{-/-}$ mice were subjected to laparotomy under sevoflurane anesthesia. The disruption in the intestinal lining, increases in hippocampal ROS, and the impairment of mitochondrial membrane potentiation seen postoperatively in wild-type and AD mice were not observed in the $PKR^{-/-}$ mice (Figures 7A–C). The decreases in synaptic proteins (PSD95, synapsin 1, and synaptophysin) and autophagy-related proteins (LC3, P62, Pink1, and Parkin) observed in the wild-type and AD mice were not present after genomic silencing of PKR (Figures 7D,E, Supplementary Figure S6). Furthermore, PKR/Eif2α and PKC activities were not changed in the postoperative $PKR^{-/-}$ mice (Figure 7F). Finally, the $PKR^{-/-}$ mice that underwent laparotomy and control mice exhibited a comparable escape latency during the MWM test (Supplementary Figure S7).

Discussion

It is well established that clinically older patients and those with preexisting cognitive impairment are more susceptible to developing PND. In this respect, it has been shown that in patients aged 60 years or older undergoing elective total hip

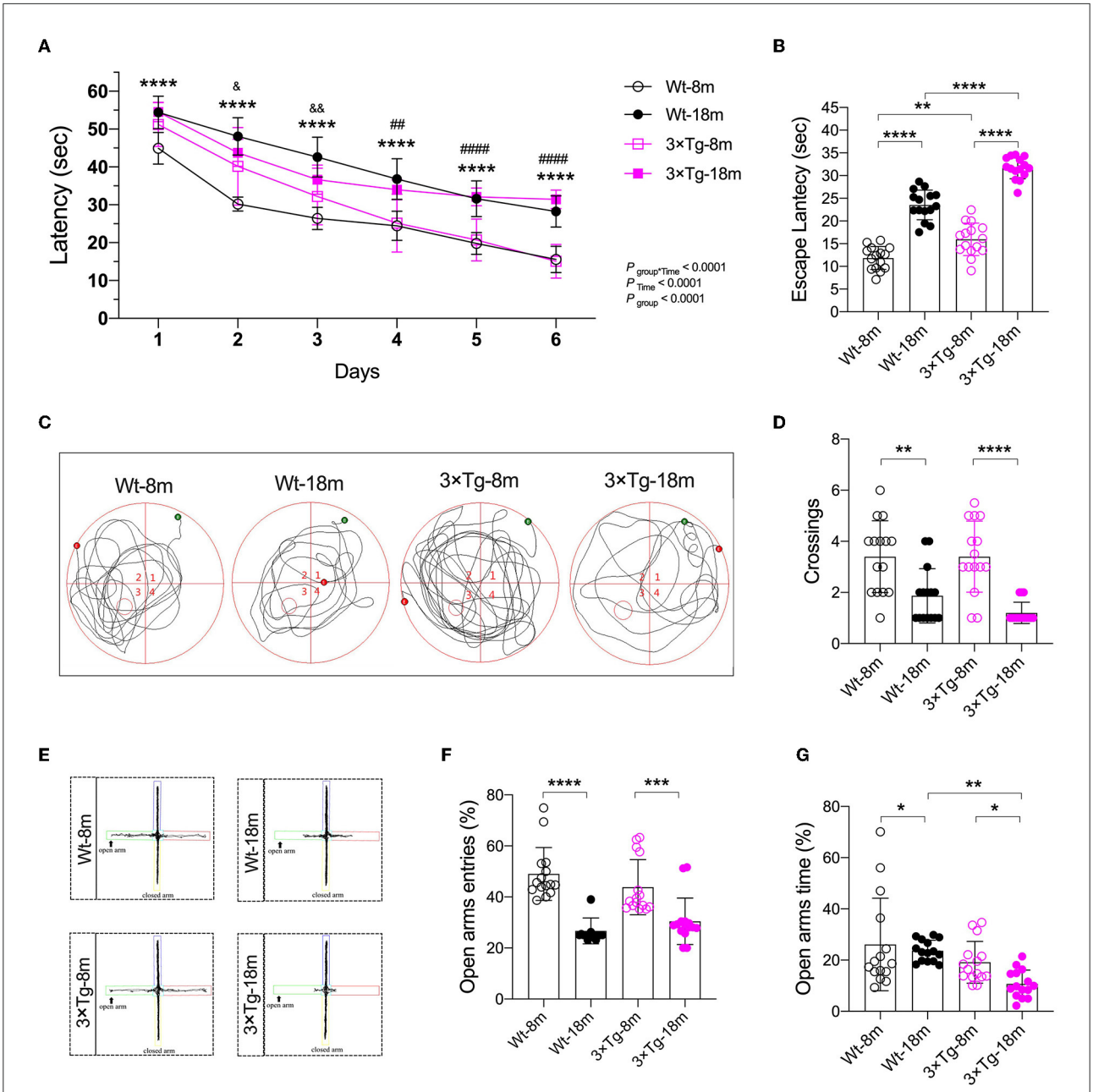

FIGURE 2
Cognitive impairment during aging in the wild-type and 3×Tg AD mice. **(A)** In the Morris water maze (MWM) test, a learning curve was made after consecutive training. Escape latencies were analyzed using a two-way ANOVA using Tukey's *post hoc* test, $n = 15$, $F_{(15,280)} = 7.493$. $^{****}P < 0.0001$, Wt-18 m vs. Wt-8m; $^{\#\#}P < 0.05$, $^{\#\#\#\#}P < 0.0001$, 3×Tg-18 m vs. 3×Tg-8 m; $^{\&}P < 0.05$, $^{\&\&}P < 0.01$, 3×Tg-18 m vs Wt-18 m. **(B–D)** Escape latency [$F_{(3, 56)} = 129.2$, $P < 0.001$], representative swimming route, and number of crossings [$F_{(3, 56)} = 14.25$, $P < 0.001$] in the target quadrant were made in the probe test of the MWM test. Data were analyzed with one-way ANOVA using Tukey's *post hoc* test, $n = 15$. **(E–G)** In the elevated plus maze (EPM) test, representative moving route, the number of entries $F_{(3, 56)} = 20.43$, ($P < 0.0001$), and stay duration [$F_{(3, 56)} = 6.277$, $P = 0.0010$] in the open arm were recorded. Wt, wild-type mice; 3×Tg, triple transgenic mice. Data are presented as mean ± SEM, n = 15, $^{*}P < 0.05$, $^{**}P < 0.01$, $^{***}P < 0.001$, $^{****}P < 0.0001$.

replacement, a low CSF $A\beta_{1-42}$ may be a significant predictor of PND at 3 months postoperatively (Evered L. et al., 2016). Advanced age may independently affect cognition by reducing PKCα/ε expression mediated by PKC/HuD/BDNF signaling, leading to alterations in inhibitory synaptic transmission and reduced mushroom spine synapses (Hongpaisan et al., 2013). Using murine models of Alzheimer's disease and perioperative neurocognitive disorders, we compared the neuropathological

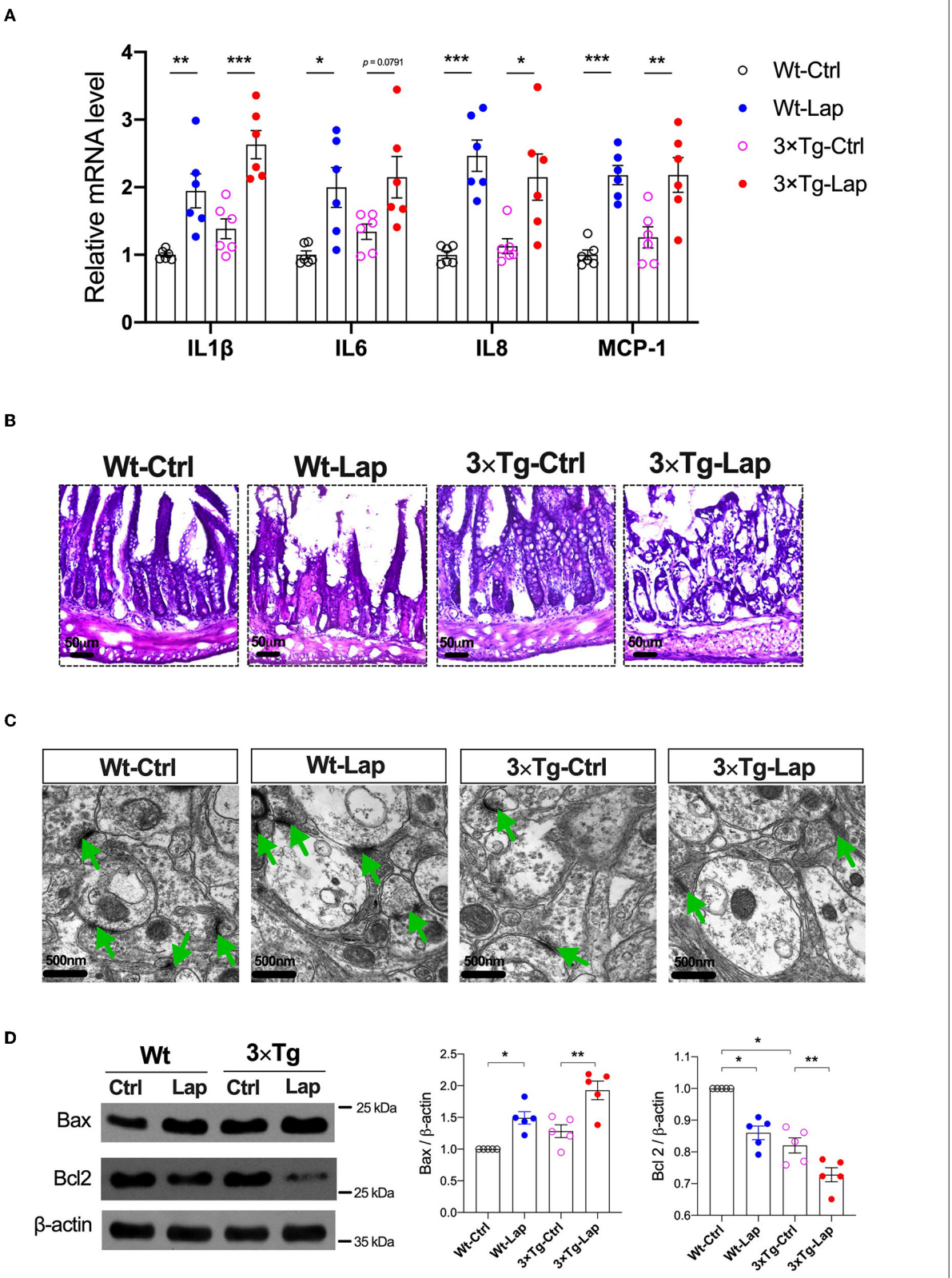

FIGURE 3
Laparotomy caused similar inflammatory responses in the periphery and hippocampus in both wild-type and 3×Tg AD mice. **(A)** Relative mRNA level of pro-inflammatory cytokines at postoperative 24 h in the hippocampi. IL-1β: $F_{(3,20)} = 15.60$, $P < 0.0001$; IL-6: $F_{(3,20)} = 5.97$, $P = 0.0044$; IL-8: $F_{(3,20)} = 11.57$, $P = 0.0001$; MCP-1: $F_{(3,20)} = 13.18$, $P < 0.0001$. **(B)** Morphological changes of acini and base of the intestine in postoperative
(Continued)

FIGURE 3 (Continued)
14 days by using H&E staining. Representative pictures were obtained from three independent experiments. **(C)** Representative ultrastructure of the hippocampal neuronal synapse using transmission electron microscopy following laparotomy in both wild-type and 3×Tg AD mice. **(D)** Protein expressions of apoptotic proteins, Bax, and Bcl2 in the hippocampi were determined by Western blot analysis. Bax: $F_{(3,16)} = 14.79$, $P < 0.0001$; BCL2: $F_{(3,16)} = 33.36$, $P < 0.0001$. Wt, wild-type mice; 3×Tg, triple transgenic mice; Ctrl, control; Lap, laparotomy. Data are presented as mean ± SEM and were analyzed using one-way ANOVA using Tukey's *post hoc* test, $^{*}P < 0.05$, $^{**}P < 0.01$, $^{***}P < 0.001$.

characteristics of these two conditions in the mice of different ages. In addition to the inflammatory changes in the periphery and central nervous system, mitochondrial dysfunction, defective autophagy, synaptic dysfunction, and neuronal apoptosis were documented. Importantly, the unique roles of PKC/PKR in these changes were examined.

Our study substantiated the adverse impact of aging on cognitive impairment in the wild-type and 3×Tg-AD mice. Similar to 3-month-old young wild-type mice with better learning ability compared with APPswe/PS1dE9 mice (Jiang et al., 2018), aged wild-type mice (18 months old) also required a shorter time to find the hidden platform than the aged 3×Tg-AD mice in the Morris water maze test. Aging significantly impacts cognition levels after surgery. Another study demonstrated that aged mice (19 months old) and young surgical mice exhibited comparable cognitive performance in the Barnes maze test (Lai et al., 2021). In animals, it has been shown that PND could be triggered by neuroinflammation in peripheral surgery models such as left carotid artery exposure (Lai et al., 2021) and laparotomy (Huang et al., 2018). In the wild-type and 3×Tg-AD mice of the same age, laparotomy induced PND with significant intestinal disruption and glial activation. However, although partial hepatectomy significantly exacerbated cognitive deficits in the APPswe/PS1dE9 transgenic mice (Jiang et al., 2018), laparotomy failed to replicate this finding in the middle-aged 3×Tg-AD mice in our study (Figure 4).

It is widely acknowledged that autophagy is initiated to restore neurotransmitter release, synaptic plasticity, and neuronal survival (Limanaqi et al., 2021). As a specialized form of autophagy, defective mitophagy is critical in the development and progression of AD, according to cross-species analyses of both transgenic animal models and human patients with AD (Swerdlow et al., 2014; Kerr et al., 2017). In this study, we provided compelling evidence that advanced age and surgery are associated with mitochondrial dysfunction and defective autophagy in both wild-type and 3×Tg-AD mice. Laparotomy had a greater impact on the mitochondria and autophagy in the 3×Tg-AD mice than in the wild-type mice. In AD, multiple mitophagy and autophagy pathways related to AD mitochondrial cascade hypothesis have been documented (Lazarou et al., 2015; Menzies et al., 2015; Kerr et al., 2017). Current evidence suggests that both Pink1 (Du et al., 2017) and Parkin (Khandelwal et al., 2011) improve mitochondrial functions and eliminate intracellular Aβ. Importantly, the regulation of autophagy depends on the activity of PKC in association with the P13K/Akt/mTOR signaling pathway (Harris et al., 2020). Although PKCs are particularly sensitive to redox stress (Giorgi et al., 2010), lysosomal activities are increased through the PKC–transcription factor EB (TFEB) axis even under nutrient-rich conditions (Li et al., 2016). To eliminate nonfunctional protein aggregations, autophagy activators can induce autophagy *via* the PRKC/PKC–TFEB pathway in cellular models of Parkinson's disease and Huntingdon disease (Kataura et al., 2021).

In aged mice, activation of PKC has been shown to reverse age-related neuropathological changes in the hippocampal neurons to regenerate memory comparable to young rats (Hongpaisan et al., 2013). Indeed, in the AD brain, levels of PKC, its receptors, activity, and associated phosphatases are decreased (Harris et al., 2020). Aβ has been shown to directly reduce PKC protein levels and activity and attenuate kinase translocation to the cell membrane in AD brains (Wang et al., 1994) and in *in vitro* studies (Lee et al., 2004). During APP processing, different PKC isoforms act on different cleavage sites to induce both amyloidogenic and nonamyloidogenic cleavages (Lanni et al., 2004; Galvao et al., 2019). Studies on AD have shown that PKC activation has a positive impact on amyloid pathology, enhancing the secretion of the α-secretase product sAPPα and reducing Aβ40 (Etcheberrigaray et al., 2004) and tau pathology (Isagawa et al., 2000). On the other hand, inhibition of PKC and NOX can strongly attenuate the direct neurotoxicity of Aβ and the effects on lysosomal and mitochondrial functions in the hippocampal neurons (Li and Jiang, 2018). We found consistent increases in PKCδ expression in the wild-type and 3×Tg-AD mice with either aging or laparotomy. The increases in PKCδ were reinforced in the 3×Tg-AD mice following laparotomy. The inhibition of PKC by BIMX dramatically attenuated the effects of laparotomy on autophagy and mitochondrial functions.

PKCα is one of the three highly penetrant variants in the PRKCA gene, identified by whole-genome sequencing of 1345 individuals from 410 families with late-onset AD (Alfonso et al., 2016). Intriguingly, an AD-associated mutation in PKCα permits enhanced agonist-dependent signaling *via* evading the cell homeostatic downregulation of constitutively active PKCα in AD (Callender et al., 2018). Interestingly, PKCα contributes to tau phosphorylation in the early stages of frontotemporal lobar degeneration (Fujita et al., 2018) and synaptogenesis. Moreover, the actions of Aβ on synapses are reportedly mediated by PKCα through scaffold interactions (Alfonso et al., 2016).

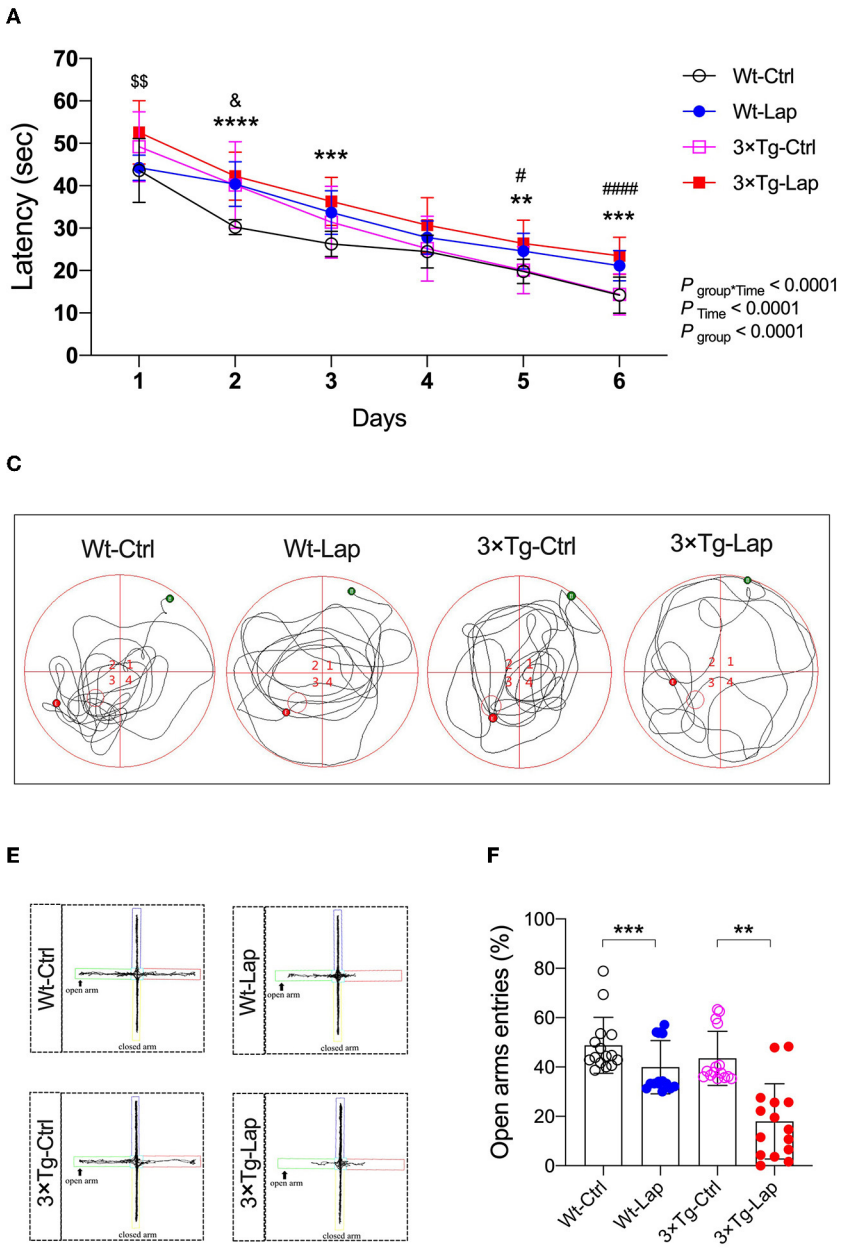

FIGURE 4
Laparotomy induced cognitive impairment in both wild-type and 3×Tg AD mice. **(A)** In the wild-type and AD mice without or with laparotomy, the learning ability of spatial acquisition was made during the training session in the MWM test. $F_{(15,280)} = 4.066$. $^{**}P < 0.01$, $^{***}P < 0.001$, $^{****}P < 0.0001$, Wt-Lap vs. Wt-Ctrl; $^{\#}P < 0.05$, $^{\#\#\#\#}P < 0.0001$, 3×Tg-Lap vs. 3×Tg-Ctrl; $^{\&}P < 0.05$, 3×Tg-Ctrl vs. Wt-Ctrl; $^{\$\$}P < 0.01$, 3×Tg-Lap vs. Wt-Lap. **(B–D)** On postoperative day 12 after laparotomy, escape latency [$F_{(3,56)} = 9.531$, $P < 0.0001$], representative swimming route, and number of crossings [$F_{(3,56)} = 14.03$, $P < 0.0001$] were recorded in the probe test of the MWM test. **(E–G)** In the EPM test, representative moving tracks, the number of entries [$F_{(3,56)} = 18.44$, $P < 0.0001$] and time spent [$F_{(3,56)} = 2.098$, $P = 0.1108$] in the open arm were summarized. Wt, wild-type mice; 3×Tg, triple transgenic mice; Ctrl, control; Lap, laparotomy. Data are present as mean ± SEM and were analyzed using one-way ANOVA using Tukey's *post hoc* test, $n = 15$, $^{*}P < 0.05$, $^{**}P < 0.01$, $^{***}P < 0.001$, $^{****}P < 0.0001$.

In the initial stages of AD, accumulated intracellular amyloid-beta oligomer causes functional spreading of hyperexcitability through a synaptic-driven mechanism, which is PKC-dependent (Fernandez-Perez et al., 2021). Significant suppression of PKCα activity was observed in the wild-type and 3×Tg-AD mice in the aged or postsurgical hippocampus. This suppressive effect induced by laparotomy was enhanced in the 3×Tg-AD mice. The decrease in synaptic proteins following

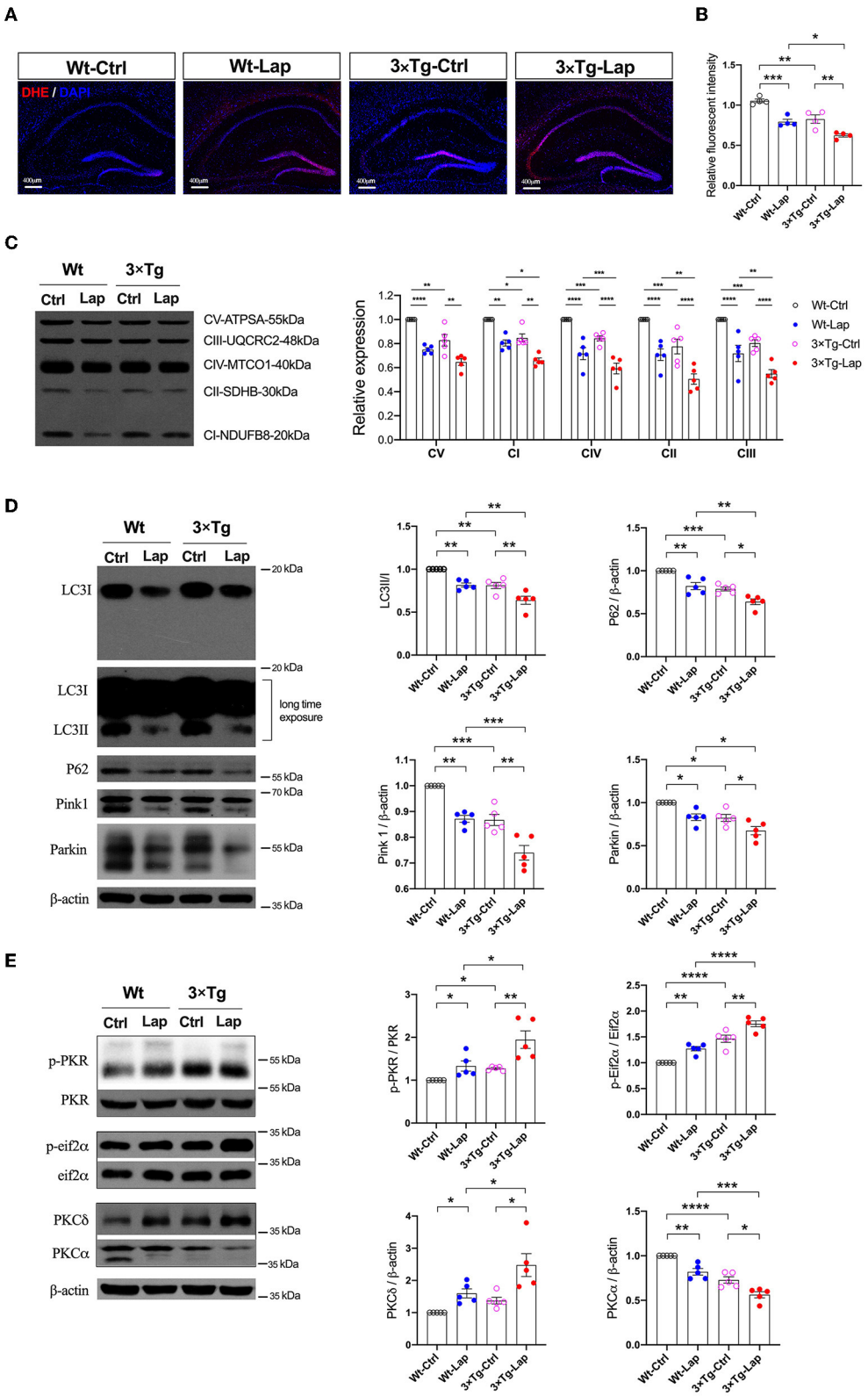

FIGURE 5
Laparotomy impaired mitochondria mediated by the activation of PKR. **(A)** To evaluate the oxidative stress in the CNS, DHE staining was used in the entire hippocampal region following laparotomy in two strains of animals. Representative pictures were obtained from three independent experiments. **(B)** Mitochondria membrane potentiation was determined by JC-1 assay in the isolated mitochondria fractions in the hippocampi.
(Continued)

FIGURE 5 (Continued)
$F_{(3,12)} = 26.14$, $P < 0.0001$. **(C)** After laparotomy, the expression of the mitochondria OXPHOS complex was detected by Western blot analysis in the hippocampi. CV:$F_{(3,16)} = 27.28$, $P < 0.0001$; CI: $F_{(3,16)} = 35.95$, $P < 0.0001$; CIV:$F_{(3,16)} = 24.85$, $P < 0.0001$; CII:$F_{(3,16)} = 20.70$, $P < 0.0001$; CIII:$F_{(3,16)} = 21.64$, $P < 0.0001$. **(D)** Western blots of autophagy-related proteins, including LC3, P62, Pink1, and Parkin, in the hippocampus following laparotomy in the middle-aged wild-type and 3×Tg AD mice. **(E)** Activities of PKR and PKC in the hippocampus induced by laparotomy in both wild-type and 3×Tg AD mice. Wt, wild-type mice; 3×Tg, triple transgenic mice; Ctrl, control; Lap, laparotomy. Data are presented as mean ± SEM and were analyzed using one-way ANOVA using Tukey's *post hoc* test, $^{*}P < 0.05$, $^{**}P < 0.01$, $^{***}P < 0.001$, $^{****}P < 0.0001$.

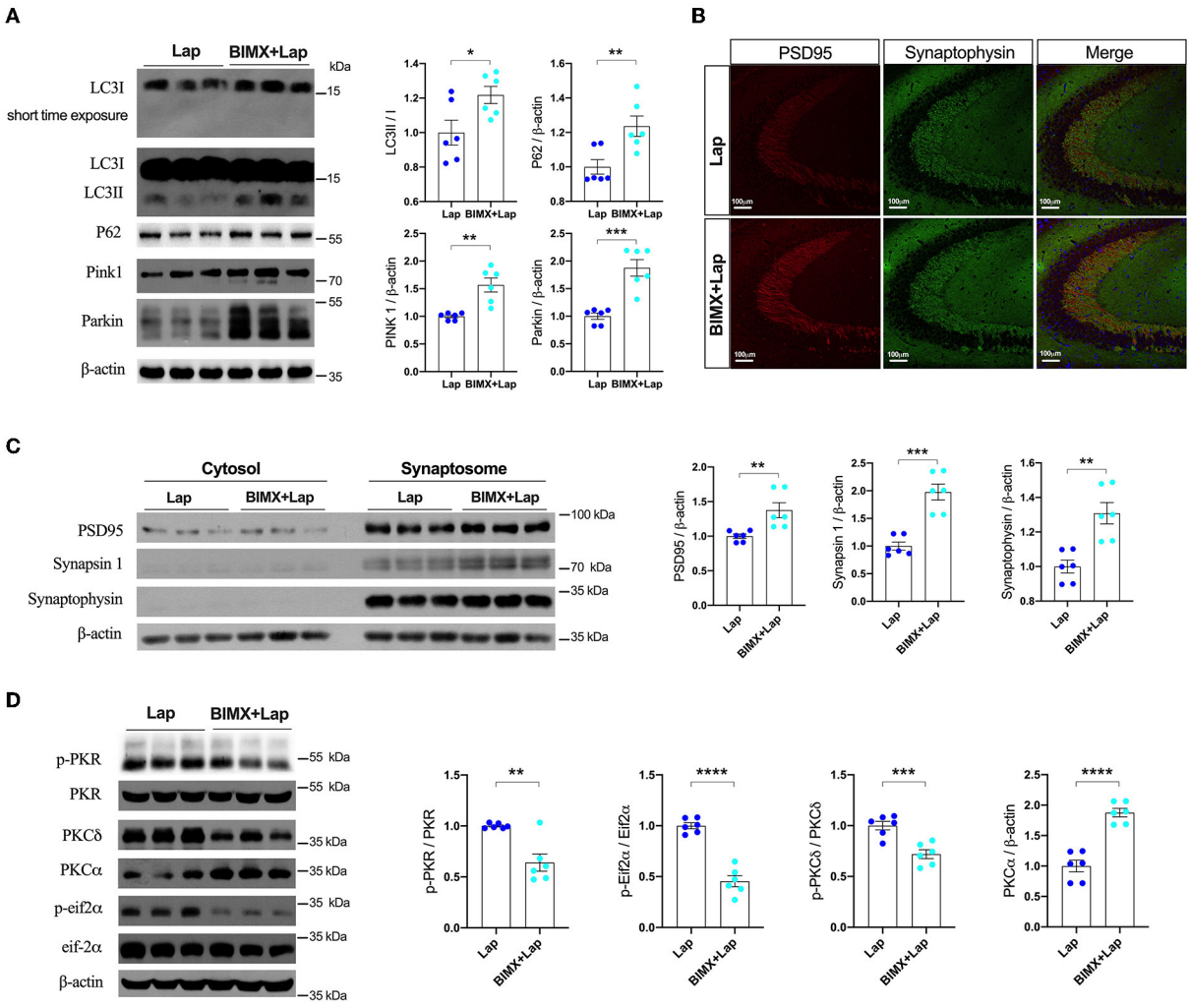

FIGURE 6
Inhibition of PKC attenuated deficits of autophagy and synapse in middle-aged wild-type mice. **(A)** Autophagy protein expressions without or with PKC inhibitor (BIMX) following laparotomy in the wild-type mice. **(B)** Spread of synaptic proteins, including PSD95 and synaptophysin, was observed using immunofluorescent staining in the cornu ammonis (CA) 3 hippocampal region after laparotomy. **(C)** Synaptic protein expressions in the cytosol and synaptosome in postoperative hippocampi without or with BIMX using Western blot analysis. **(D)** Activities of PKR with pharmacological inhibition of PKC in middle-aged wild-type mice after laparotomy. Wt, wild type; Ctrl, control; Lap, laparotomy. Data are presented as mean ± SEM and were analyzed using one-way ANOVA using Tukey's *post hoc* test, $^{*}P < 0.05$, $^{**}P < 0.01$, $^{***}P < 0.001$, $^{****}P < 0.0001$.

laparotomy was successfully rescued by the inhibition of PKC with BIMX.

PKR is a pro-apoptotic kinase that inhibits protein translation that has been implicated in several molecular pathways that lead to AD brain lesions and disturbed memory formation and consolidation (Hugon et al., 2017). PKR is also required for autophagy stimulation and accumulation (Ogolla et al., 2013). Given that significant elevations in total

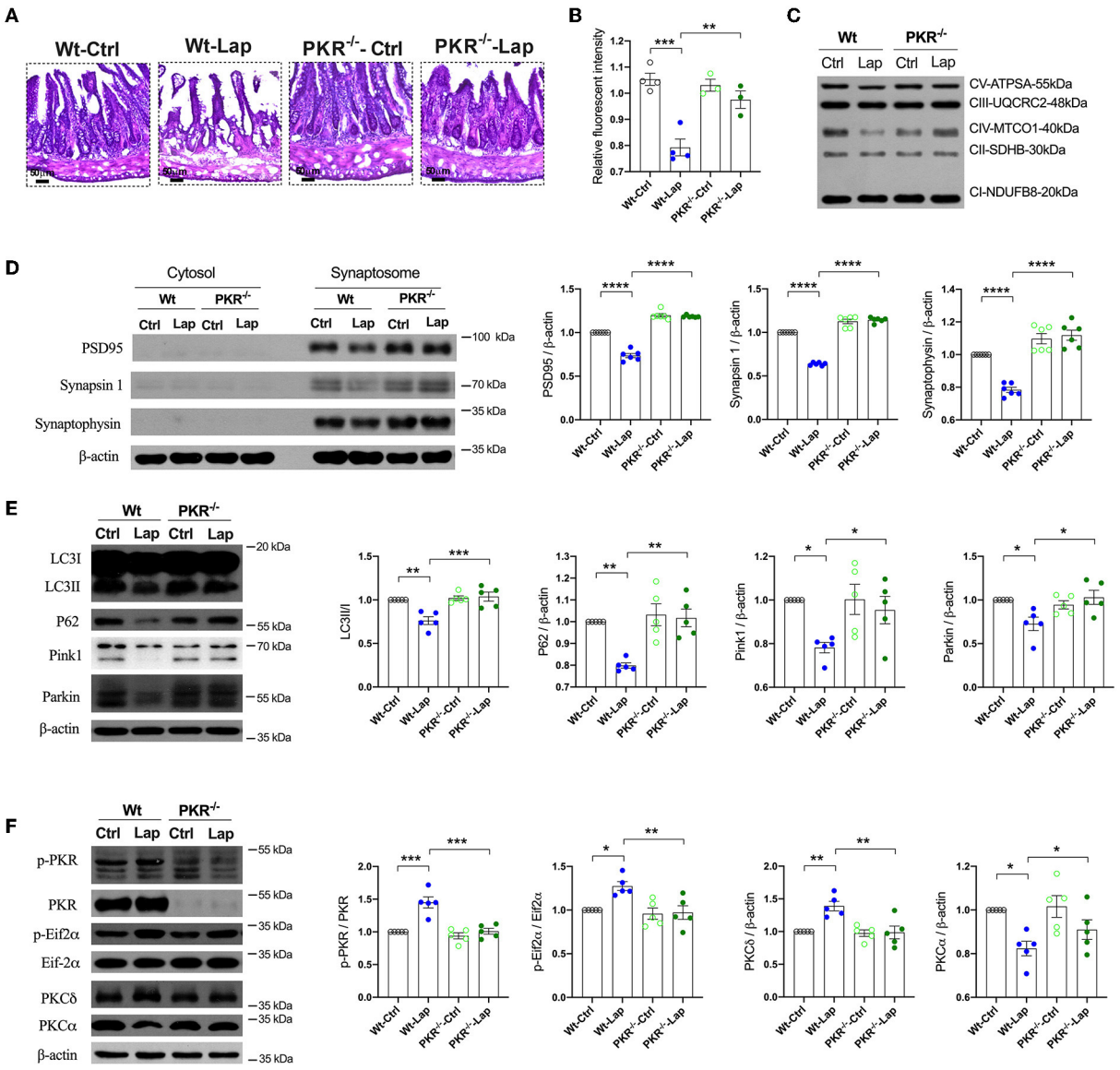

FIGURE 7
Pathological signatures induced by laparotomy were determined by PKR activity. **(A)** Representative morphological changes of the intestine by H&E staining following laparotomy in the wild-type and PKR$^{-/-}$ mice. **(B)** Mitochondria membrane potentiation was detected by JC-1 assay in the isolated mitochondria fractions. $F_{(3,10)} = 18.96$, $P = 0.0002$. **(C)** Representative Western blots of the mitochondria OXPHOS complex in the hippocampi after laparotomy in the wild-type and PKR$^{-/-}$ mice. **(D)** Western blots of synaptic proteins in the isolated synaptosome from postoperative hippocampi in the wild-type and PKR$^{-/-}$ mice. **(E)** Relative expressions of autophagy proteins, LC3B: $F_{(3,16)} = 12.58$, $P = 0.0002$; P62: $F_{(3,16)} = 21.14$, $P < 0.0001$; Pink1: $F_{(3,16)} = 17.26$, $P < 0.0001$; Parkin: $F_{(3,16)} = 43.14$, $P < 0.0001$. **(F)** Relative activities of PKC induced by laparotomy in the wild-type and PKR$^{-/-}$ mice. Wt, wild type; Ctrl, control; Lap, laparotomy. Data are presented as mean ± SEM and were analyzed using one-way ANOVA using Tukey's *post hoc* test, $^{*}P < 0.05$, $^{**}P < 0.01$, $^{***}P < 0.001$, $^{****}P < 0.0001$.

PKR and p-PKR concentrations have been documented in AD and amnestic mild cognitive impairment subjects, the assessment of T-PKR and p-PKR in cerebrospinal fluid could be used to diagnose AD (Mouton-Liger et al., 2012). A study reported that the cognitive scores of 299 participants exhibited a significant negative relationship with the protein expressions of IRS1, JNK, and PKR in their neocortex. These proteins are also significantly associated with the pathological brain signatures in'patients with Alzheimer's disease (Taga et al., 2017). Moreover, in AD animal models, either β-amyloid oligomers or AD-associated toxins initiate the elevation of phosphorylated Eif2α, neuronal insulin receptor substrate inhibition, synapse loss, and cognition impairment through activating PKR (Lourenco et al., 2013). Furthermore,

PKR initially facilitated tau hyperphosphorylation, which is independent of PKR-mediated downstream activation of GSK-3β or neuroinflammation in AD and other tauopathies (Reimer et al., 2021). In our previous study, PKR activation positively regulated autophagy and tau phosphorylation in PND induced by laparotomy in aged wild-type mice (Wang et al., 2022). Therefore, significant improvement in cognitive deficits was achieved when PKR activity was suppressed with a selective PKR inhibitor (SAR439883). Meanwhile, there were prominent decreases in synaptic protein loss, pro-inflammatory cytokine accumulation, and neurodegeneration in AD experimental mice with ApoE4 overexpression or intracerebroventricular Aβ-injection (Lopez-Grancha et al., 2021). When PKR activity was silenced by using a genomic approach, such as double-mutant 5×FAD with $PKR^{-/-}$, 9-month-old mice displayed significant improvements in memory consolidation and a series of neuropathological changes in the brain as compared to 5×FAD mice, including decreases in amyloid accumulation, BACE1 expression, neuronal apoptosis, neurodegeneration markers, and synaptic alterations, as well as a neuroinflammatory burden. This finding further corroborates the indispensable contribution of PKR to microglia-induced neuronal death in neuron-glial cocultures after LPS stimulation (Tible et al., 2019). In this study, we substantiated the role of PKR in aging and PND in 3×Tg-AD mice. There were significant increases in PKR activity by phosphorylation in the hippocampus. However, neuropathological variations induced by laparotomy were not observed in $PKR^{-/-}$ mice.

A major limitation of this study is that we did not examine the effect of gender. It is well established that estradiol induces gene transcription and rapid membrane signaling mediated by three receptors, including estrogen receptor-alpha (ERα), estrogen receptor-beta (ERβ), and a recently characterized G-protein-coupled estrogen receptor. Moreover, studies using receptor-specific agonists have shown that all three receptors rapidly activate kinase signaling and have complex dose-dependent influences on memory (Bean et al., 2014). The binding of endogenous estradiol (E2) and ERs affects hippocampal learning and memory function by activating various cell signaling kinases, such as phosphatidylinositol 3-kinase (PI3K), extracellular signal-regulated kinase (ERK), protein kinase A (PKA), and PKC (Fan et al., 2010). In a transgenic model of Alzheimer's disease, female mice exhibited more extensive amyloid lesions, but not tau lesions (Rae and Brown, 2015). Mortality in 3×Tg-AD mice appeared as early as 12 months since tau lesions developed at 9-12 months. 3×Tg-AD male mice exhibited earlier mortality than female mice. Accordingly, tau pathology may be more aggressive in male than in female mice (Hirata-Fukae et al., 2008; Rae and Brown, 2015). Although the prevalence of the disease is higher in female mice, neuroimmunoendocrine factors may cause early mortality in male mice. The higher vulnerability of the neuroimmunoendocrine network in male mice could result in a higher susceptibility to deleterious effects of aging and be responsible for the increased morbidity and mortality observed in 3×Tg-AD male mice (Clinton et al., 2007; Gimenez-Llort et al., 2008). In this study, only male mice were used to exclude the influence on E2 on the areas of focus. Nonetheless, future studies should compare the effect of gender on these findings.

Conclusions

Aging, AD, and PND appear to share similar pathogenic mechanisms, including altered mitochondrial homeostasis and neuroinflammation. Laparotomy consistently caused cognitive deficits accompanied by peripheral and neuronal inflammation, mitochondrial dysfunction, synaptic proteins, and neuronal loss in wild-type and 3×Tg-AD mice. The inhibition of PKC and PKR may be the key to developing new drug candidates for aging, AD, and PND therapy.

Data availability statement

The datasets presented in this study can be found in online repositories. The names of the repository/repositories and accession number(s) can be found in the article/Supplementary material.

Ethics statement

All experimental protocols and animal handling procedures were approved by the Faculty Committee on the Use of Live Animals in Teaching and Research in The University of Hong Kong (CULATR Ref. No. 3437-14) and the Ethics Committee for the use of experimental animals in Anhui Medical University (reference number LLSC 20190765; date of approval 26/10/2019).

Author contributions

WL and ST performed the experiments and data acquisitions. AL, QH, and MD contributed to the interpretation of data. YZ, XH, and RC helped prepare the manuscript. GW contributed to the experimental design and manuscript preparation. CH designed the study, performed data analysis, and prepared the manuscript. All authors contributed to the article and approved the submitted version.

Funding

This study was supported by the National Natural Science Foundation of China [Grant Number 81801050], Basic and

Clinical Cooperative Research Promotion Plan of Anhui Medical University [Grant Number 2019xkjT026], Scientific Research Platform Base Construction and Promotion Project of Anhui Medical University [Grant Number 2020xkjT060], and NSFC Incubation Project of the Second Hospital of Anhui Medical University [Grant Number 2019GQFY14]. The experiments carried out in Hong Kong on PKR were supported by General Research Fund 17123217 to RC.

Acknowledgments

We thank the technical support from the Center for Scientific Research of Anhui Medical University and the Faculty Core Facility, The University of Hong Kong.

Conflict of interest

The authors declare that the research was conducted in the absence of any commercial or financial relationships that could be construed as a potential conflict of interest.

Publisher's note

All claims expressed in this article are solely those of the authors and do not necessarily represent those of their affiliated organizations, or those of the publisher, the editors and the reviewers. Any product that may be evaluated in this article, or claim that may be made by its manufacturer, is not guaranteed or endorsed by the publisher.

Supplementary material

The Supplementary Material for this article can be found online at: https://www.frontiersin.org/articles/10.3389/fnagi.2022.973068/full#supplementary-material

References

Alfonso, S. I., Callender, J. A., Hooli, B., Antal, C. E., Mullin, K., Sherman, M. A., et al. (2016). Gain-of-function mutations in protein kinase Calpha (PKCalpha) may promote synaptic defects in Alzheimer's disease. *Sci Signal* 9, ra47. doi: 10.1126/scisignal.aaf6209

Bean, L. A., Ianov, L., and Foster, T. C. (2014). Estrogen receptors, the hippocampus, and memory. *Neuroscientist*. 20, 534–545. doi: 10.1177/1073858413519865

Borchers, F., Spies, C. D., Feinkohl, I., Brockhaus, W. R., Kraft, A., Kozma, P., et al. (2021). Methodology of measuring postoperative cognitive dysfunction: a systematic review. *Br. J. Anaesth*. 126, 1119–1127. doi: 10.1016/j.bja.2021.01.035

Callender, J. A., Yang, Y., Lorden, G., Stephenson, N. L., Jones, A. C., Brognard, J., et al. (2018). Protein kinase Calpha gain-of-function variant in Alzheimer's disease displays enhanced catalysis by a mechanism that evades down-regulation. *Proc. Natl. Acad. Sci. USA*. 115, E5497–E5505. doi: 10.1073/pnas.1805046115

Chen, J. L., Lin, H. H., Kim, K. J., Lin, A., Ou, J. H., and Ann, D. K. (2009). PKC delta signaling: a dual role in regulating hypoxic stress-induced autophagy and apoptosis. *Autophagy*. 5, 244–246. doi: 10.4161/auto.5.2.7549

Clinton, L. K., Billings, L. M., Green, K. N., Caccamo, A., Ngo, J., Oddo, S., et al. (2007). Age-dependent sexual dimorphism in cognition and stress response in the 3xTg-AD mice. *Neurobiol. Dis*. 28, 76–82. doi: 10.1016/j.nbd.2007.06.013

Du, F., Yu, Q., Yan, S., Hu, G., Lue, L. F., Walker, D. G., et al. (2017). PINK1 signalling rescues amyloid pathology and mitochondrial dysfunction in Alzheimer's disease. *Brain*. 140, 3233–3251. doi: 10.1093/brain/awx258

Du, Y., Zhao, Y., Li, C., Zheng, Q., Tian, J., Li, Z., et al. (2018). Inhibition of PKCdelta reduces amyloid-beta levels and reverses Alzheimer disease phenotypes. *J. Exp. Med*. 215, 1665–1677. doi: 10.1084/jem.20171193

Etcheberrigaray, R., Tan, M., Dewachter, I., Kuiperi, C., Van der Auwera, I., Wera, S., et al. (2004). Therapeutic effects of PKC activators in Alzheimer's disease transgenic mice. *Proc. Natl. Acad. Sci. USA*. 101, 11141–11146. doi: 10.1073/pnas.0403921101

Evered, L., Silbert, B., Scott, D. A., Ames, D., Maruff, P., and Blennow, K. (2016). Cerebrospinal fluid biomarker for alzheimer disease predicts postoperative cognitive dysfunction. *Anesthesiology*. 124, 353–361. doi: 10.1097/ALN.0000000000000953

Evered, L. A., Silbert, B. S., Scott, D. A., Maruff, P., and Ames, D. (2016). Prevalence of dementia 7.5 years after coronary artery bypass graft surgery. *Anesthesiology*. 125, 62–71. doi: 10.1097/ALN.0000000000001143

Fan, L., Zhao, Z., Orr, P. T., Chambers, C. H., Lewis, M. C., and Frick, K. M. (2010). Estradiol-induced object memory consolidation in middle-aged female mice requires dorsal hippocampal extracellular signal-regulated kinase and phosphatidylinositol 3-kinase activation. *J. Neurosci*. 30, 4390–4400. doi: 10.1523/JNEUROSCI.4333-09.2010

Fernandez-Perez, E. J., Munoz, B., Bascunan, D. A., Peters, C., Riffo-Lepe, N. O., Espinoza, M. P., et al. (2021). Synaptic dysregulation and hyperexcitability induced by intracellular amyloid beta oligomers. *Aging cell 20, e*13455. doi: 10.1111/acel.13455

Fujita, K., Chen, X., Homma, H., Tagawa, K., Amano, M., Saito, A., et al. (2018). Targeting Tyro3 ameliorates a model of PGRN-mutant FTLD-TDP via tau-mediated synaptic pathology. *Nat. Commun*. 9, 433. doi: 10.1038/s41467-018-02821-z

Galvao, F. Jr., Grokoski, K. C., da Silva, B. B., Lamers, M. L., and Siqueira, I. R. (2019). The amyloid precursor protein (APP) processing as a biological link between Alzheimer's disease and cancer. *Ageing Res. Rev*. 49, 83–91. doi: 10.1016/j.arr.2018.11.007

Gimenez-Llort, L., Arranz, L., Mate, I., and De la Fuente, M. (2008). Gender-specific neuroimmunoendocrine aging in a triple-transgenic 3xTg-AD mouse model for Alzheimer's disease and its relation with longevity. *Neuroimmunomodulation*. 15, 331–343. doi: 10.1159/000156475

Giorgi, C., Agnoletto, C., Baldini, C., Bononi, A., Bonora, M., Marchi, S., et al. (2010). Redox control of protein kinase C: cell- and disease-specific aspects. *Antioxid. Redox Signal*. 13, 1051–1085. doi: 10.1089/ars.2009.2825

Harris, M., El Hindy, M., Usmari-Moraes, M., Hudd, F., Shafei, M., Dong, M., et al. (2020). BCAT-induced autophagy regulates Abeta load through an interdependence of redox state and PKC phosphorylation-implications in Alzheimer's disease. *Free Radic. Biol. Med*. 152, 755–766. doi: 10.1016/j.freeradbiomed.2020.01.019

Hirata-Fukae, C., Li, H. F., Hoe, H. S., Gray, A. J., Minami, S. S., Hamada, K., et al. (2008). Females exhibit more extensive amyloid, but not tau, pathology in an Alzheimer transgenic model. *Brain Res*. 1216, 92–103. doi: 10.1016/j.brainres.2008.03.079

Hongpaisan, J., Xu, C., Sen, A., Nelson, T. J., and Alkon, D. L. (2013). PKC activation during training restores mushroom spine synapses and memory in the aged rat. *Neurobiol. Dis*. 55, 44–62. doi: 10.1016/j.nbd.2013.03.012

Huang, C., Irwin, M. G., Wong, G. T. C., and Chang, R. C. C. (2018). Evidence of the impact of systemic inflammation on neuroinflammation from a non-bacterial endotoxin animal model. *J. Neuroinflammation*. 15, 147. doi: 10.1186/s12974-018-1163-z

Hugon, J., Mouton-Liger, F., Dumurgier, J., and Paquet, C. (2017). PKR involvement in Alzheimer's disease. *Alzheimers. Res. Ther*. 9, 83. doi: 10.1186/s13195-017-0308-0

Isagawa, T., Mukai, H., Oishi, K., Taniguchi, T., Hasegawa, H., Kawamata, T., et al. (2000). Dual effects of PKNalpha and protein kinase C on phosphorylation of tau protein by glycogen synthase kinase-3beta. *Biochem. Biophys. Res. Commun*. 273, 209–212. doi: 10.1006/bbrc.2000.2926

Jiang, Y., Li, Z., Ma, H., Cao, X., Liu, F., Tian, A., et al. (2018). Upregulation of TREM2 Ameliorates Neuroinflammatory Responses and Improves Cognitive Deficits Triggered by Surgical Trauma in Appswe/PS1dE9 Mice. *Cell. Physiol. Biochem*. 46, 1398–1411. doi: 10.1159/000489155

Kang, R., and Tang, D. (2012). PKR-dependent inflammatory signals. *Sci. Signal*. 5, pe47. doi: 10.1126/scisignal.2003511

Kataura, T., Tashiro, E., Nishikawa, S., Shibahara, K., Muraoka, Y., Miura, M., et al. (2021). A chemical genomics-aggrephagy integrated method studying functional analysis of autophagy inducers. *Autophagy*. 17, 1856–1872. doi: 10.1080/15548627.2020.1794590

Kerr, J. S., Adriaanse, B. A., Greig, N. H., Mattson, M. P., Cader, M. Z., Bohr, V. A., et al. (2017). Mitophagy and Alzheimer's disease: cellular and molecular mechanisms. *Trends Neurosci*. 40, 151–166. doi: 10.1016/j.tins.2017.01.002

Khandelwal, P. J., Herman, A. M., Hoe, H. S., Rebeck, G. W., and Moussa, C. E. (2011). Parkin mediates beclin-dependent autophagic clearance of defective mitochondria and ubiquitinated Abeta in AD models. *Hum. Mol. Genet*. 20, 2091–2102. doi: 10.1093/hmg/ddr091

Lai, Z., Shan, W., Li, J., Min, J., Zeng, X., and Zuo, Z. (2021). *Appropriate exercise level attenuates gut dysbiosis and valeric acid increase to improve neuroplasticity and cognitive function after surgery in mice. Mol Psychiatry*. 26, 7167–7187. doi: 10.1038/s41380-021-01291-y

Lanni, C., Mazzucchelli, M., Porrello, E., Govoni, S., and Racchi, M. (2004). Differential involvement of protein kinase C alpha and epsilon in the regulated secretion of soluble amyloid precursor protein. *Eur. J. Biochem*. 271, 3068–3075. doi: 10.1111/j.1432-1033.2004.04240.x

Lazarou, M., Sliter, D. A., Kane, L. A., Sarraf, S. A., Wang, C., Burman, J. L., et al. (2015). The ubiquitin kinase PINK1 recruits autophagy receptors to induce mitophagy. *Nature*. 524, 309–314. doi: 10.1038/nature14893

Lee, W., Boo, J. H., Jung, M. W., Park, S. D., Kim, Y. H., Kim, S. U., et al. (2004). Amyloid beta peptide directly inhibits PKC activation. *Mol. Cell. Neurosci*. 26, 222–231. doi: 10.1016/j.mcn.2003.10.020

Li, X., and Jiang, L. H. (2018). Multiple molecular mechanisms form a positive feedback loop driving amyloid beta42 peptide-induced neurotoxicity via activation of the TRPM2 channel in hippocampal neurons. *Cell Death Dis*. 9, 195. doi: 10.1038/s41419-018-0270-1

Li, Y., Xu, M., Ding, X., Yan, C., Song, Z., Chen, L., et al. (2016). Protein kinase C controls lysosome biogenesis independently of mTORC1. *Nat. Cell Biol*. 18, 1065–1077. doi: 10.1038/ncb3407

Limanaqi, F., Busceti, C. L., Celli, R., Biagioni, F., and Fornai, F. (2021). Autophagy as a gateway for the effects of methamphetamine: From neurotransmitter release and synaptic plasticity to psychiatric and neurodegenerative disorders. *Prog. Neurobiol*. 204, 102112. doi: 10.1016/j.pneurobio.2021.102112

Lopez-Grancha, M., Bernardelli, P., Moindrot, N., Genet, E., Vincent, C., Roudieres, V., et al. (2021). A novel selective PKR inhibitor restores cognitive deficits and neurodegeneration in Alzheimer disease experimental models. *J. Pharmacol. Exp. Ther*. 378, 262–275. doi: 10.1124/jpet.121.000590

Lourenco, M. V., Clarke, J. R., Frozza, R. L., Bomfim, T. R., Forny-Germano, L., Batista, A. F., et al. (2013). TNF-alpha mediates PKR-dependent memory impairment and brain IRS-1 inhibition induced by Alzheimer's beta-amyloid oligomers in mice and monkeys. *Cell Metab*. 18, 831–843. doi: 10.1016/j.cmet.2013.11.002

Menzies, F. M., Fleming, A., and Rubinsztein, D. C. (2015). Compromised autophagy and neurodegenerative diseases. *Nat. Rev. Neurosci*. 16, 345–357. doi: 10.1038/nrn3961

Mouton-Liger, F., Paquet, C., Dumurgier, J., Lapalus, P., Gray, F., Laplanche, J. L., et al. (2012). Increased cerebrospinal fluid levels of double-stranded RNA-dependant protein kinase in Alzheimer's disease. *Biol. Psychiatry*. 71, 829–835. doi: 10.1016/j.biopsych.2011.11.031

Newton, A. C. (2018). Protein kinase C: perfectly balanced. *Crit. Rev. Biochem. Mol. Biol*. 53, 208–230. doi: 10.1080/10409238.2018.1442408

Ogolla, P. S., Portillo, J. A., White, C. L., Patel, K., Lamb, B., Sen, G. C., et al. (2013). The protein kinase double-stranded RNA-dependent (PKR) enhances protection against disease cause by a non-viral pathogen. *PLoS Pathog*. 9, e1003557. doi: 10.1371/journal.ppat.1003557

Rae, E. A., and Brown, R. E. (2015). The problem of genotype and sex differences in life expectancy in transgenic AD mice. *Neurosci. Biobehav. Rev*. 57, 238–251. doi: 10.1016/j.neubiorev.2015.09.002

Reimer, L., Betzer, C., Kofoed, R. H., Volbracht, C., Fog, K., Kurhade, C., et al. (2021). PKR kinase directly regulates tau expression and Alzheimer's disease-related tau phosphorylation. *Brain Pathol*. 31, 103–119. doi: 10.1111/bpa.12883

Schwarz, N., Kastaun, S., Schoenburg, M., Kaps, M., and Gerriets, T. (2013). Subjective impairment after cardiac surgeries: the relevance of postoperative cognitive decline in daily living. *Eur. J. Cardiothorac. Surg*. 43, e162–166. doi: 10.1093/ejcts/ezt078

Sun, M. K., and Alkon, D. L. (2014). The "memory kinases": roles of PKC isoforms in signal processing and memory formation. *Prog. Mol. Biol. Transl. Sci*. 122, 31–59. doi: 10.1016/B978-0-12-420170-5.00002-7

Swerdlow, R. H., Burns, J. M., and Khan, S. M. (2014). The Alzheimer's disease mitochondrial cascade hypothesis: progress and perspectives. *Biochim. Biophys. Acta*. 1842, 1219–1231. doi: 10.1016/j.bbadis.2013.09.010

Taga, M., Minett, T., Classey, J., Matthews, F. E., Brayne, C., Ince, P. G., et al. (2017). Metaflammasome components in the human brain: a role in dementia with Alzheimer's pathology? *Brain Pathol*. 27, 266–275. doi: 10.1111/bpa.12388

Tible, M., Mouton Liger, F., Schmitt, J., Giralt, A., Farid, K., Thomasseau, S., et al. (2019). PKR knockout in the 5xFAD model of Alzheimer's disease reveals beneficial effects on spatial memory and brain lesions. *Aging Cell*. 18, e12887. doi: 10.1111/acel.12887

Wang, H. Y., Pisano, M. R., and Friedman, E. (1994). Attenuated protein kinase C activity and translocation in Alzheimer's disease brain. *Neurobiol. Aging*. 15, 293–298. doi: 10.1016/0197-4580(94)90023-X

Wang, J., Zhu, S., Lu, W., Li, A., Zhou, Y., Chen, Y., et al. (2022). Varenicline improved laparotomy-induced cognitive impairment by restoring mitophagy in aged mice. *Eur. J. Pharmacol*. 916, 174524. doi: 10.1016/j.ejphar.2021.174524

frontiers | Frontiers in Aging Neuroscience

TYPE Original Research
PUBLISHED 20 September 2022
DOI 10.3389/fnagi.2022.932354

OPEN ACCESS

EDITED BY
Chih-Yu Hsu,
Fujian University of Technology, China

REVIEWED BY
Sergio Santos,
UiT The Arctic University of Norway, Norway
Johannes Rheinlaender,
University of Tübingen, Germany
Daniele Passeri,
Sapienza University of Rome, Italy
Gregory Barshtein,
The Hebrew University of Jerusalem, Israel

*CORRESPONDENCE
Gabriele Ciasca
gabriele.ciasca@unicatt.it
Carlo Masullo
carlo.masullo@unicatt.it

†These authors have contributed equally to this work

‡These authors share senior authorship

SPECIALTY SECTION
This article was submitted to Alzheimer's Disease and Related Dementias, a section of the journal Frontiers in Aging Neuroscience

RECEIVED 29 April 2022
ACCEPTED 10 August 2022
PUBLISHED 20 September 2022

CITATION
Nardini M, Ciasca G, Lauria A, Rossi C, Di Giacinto F, Romanò S, Di Santo R, Papi M, Palmieri V, Perini G, Basile U, Alcaro FD, Di Stasio E, Bizzarro A, Masullo C and De Spirito M (2022) Sensing red blood cell nano-mechanics: Toward a novel blood biomarker for Alzheimer's disease.
Front. Aging Neurosci. 14:932354.
doi: 10.3389/fnagi.2022.932354

Sensing red blood cell nano-mechanics: Toward a novel blood biomarker for Alzheimer's disease

Matteo Nardini[1,2†], Gabriele Ciasca[1,2*†], Alessandra Lauria[3], Cristina Rossi[4], Flavio Di Giacinto[1,2], Sabrina Romanò[1,2], Riccardo Di Santo[2], Massimiliano Papi[1,2], Valentina Palmieri[1,5], Giordano Perini[1,2], Umberto Basile[4], Francesca D. Alcaro[4], Enrico Di Stasio[4], Alessandra Bizzarro[6], Carlo Masullo[1,7*‡] and Marco De Spirito[1,2‡]

[1]Dipartimento di Neuroscienze, Sezione di Fisica, Università Cattolica del Sacro Cuore, Rome, Italy, [2]Fondazione Policlinico Universitario Agostino Gemelli IRCCS, Rome, Italy, [3]Unitá Operativa Complessa Neuroriabilitazione ad Alta Intensitá, Fondazione Policlinico Universitario A. Gemelli IRCCS, Rome, Italy, [4]Department of Laboratory Diagnostic and Infectious Diseases, Fondazione Policlinico Universitario Agostino Gemelli IRCCS, Rome, Italy, [5]Istituto dei Sistemi Complessi (ISC), Consiglio Nazionale delle Ricerche (CNR), Rome, Italy, [6]Unitáa Operativa Complessa Continuità assistenziale, Fondazione Policlinico Universitario A. Gemelli IRCCS, Rome, Italy, [7]Sezione di Neurologia, Dipartimento di Neuroscienze, Università Cattolica del Sacro Cuore, Rome, Italy

Red blood cells (RBCs) are characterized by a remarkable elasticity, which allows them to undergo very large deformation when passing through small vessels and capillaries. This extreme deformability is altered in various clinical conditions, suggesting that the analysis of red blood cell (RBC) mechanics has potential applications in the search for non-invasive and cost-effective blood biomarkers. Here, we provide a comparative study of the mechanical response of RBCs in patients with Alzheimer's disease (AD) and healthy subjects. For this purpose, RBC viscoelastic response was investigated using atomic force microscopy (AFM) in the force spectroscopy mode. Two types of analyses were performed: (i) a conventional analysis of AFM force–distance (FD) curves, which allowed us to retrieve the apparent Young's modulus, E; and (ii) a more in-depth analysis of time-dependent relaxation curves in the framework of the standard linear solid (SLS) model, which allowed us to estimate cell viscosity and elasticity, independently. Our data demonstrate that, while conventional analysis of AFM FD curves fails in distinguishing the two groups, the mechanical parameters obtained with the SLS model show a very good classification ability. The diagnostic performance of mechanical parameters was assessed using receiving operator characteristic (ROC) curves, showing very large areas under the curves (AUC) for selected biomarkers (AUC $>$ 0.9). Taken all together, the data presented here demonstrate that RBC mechanics

are significantly altered in AD, also highlighting the key role played by viscous forces. These RBC abnormalities in AD, which include both a modified elasticity and viscosity, could be considered a potential source of plasmatic biomarkers in the field of liquid biopsy to be used in combination with more established indicators of the pathology.

KEYWORDS

Alzheimer's disease, biomarker, liquid biopsy, AFM, mechanics, red blood cells

Introduction

Currently, Alzheimer's disease (AD) diagnostics rely on cognitive testing supported by additional biomarkers, which include cerebrospinal fluid Aβ42, total and phosphorylated full-length-tau or its truncated form, positron emission tomography (PET) of brain amyloid deposition and glucose metabolism, and brain atrophy on MRI (Cross et al., 2007; Battisti et al., 2012; Okamura et al., 2014; Brier et al., 2016; Florenzano et al., 2017; Wojsiat et al., 2017). Although considerable progress has been made in demonstrating how these biomarkers relate to the pathophysiology of AD (Jack et al., 2013), the search and validation of cost-effective and less invasive biomarkers, contributing to the early diagnosis of AD and the prediction of disease progression, are highly demanded (Snyder et al., 2014). In this context, blood biomarkers are specifically desirable because they reduce costs, and minimize the risk and the discomfort for the patients, thus stimulating the development of novel high-throughput screening methods.

Two classes of biomarkers can be distinguished in blood: circulating molecules and cell-based biomarkers (Wojsiat et al., 2017). The latter class has recently attracted a lot of attention, especially for what concerns red blood cells (RBCs), because of their easy and large accessibility. In this context, it has been demonstrated that 15% of RBCs in patients with AD showed an elongated shape, associated with the presence of alterations in the RBC membrane architecture (Mohanty et al., 2010). Moreover, a large body of evidence pointed out an association between RBCs and Aβ-peptides in patients with AD, which negatively affects cell integrity, functionality, and adhesion properties, thus contributing to cerebral hypoperfusion, favoring vascular damages, and eventually facilitating AD (van Oijen et al., 2006; Nakagawa et al., 2011; Kiko et al., 2012; Lucas and Rifkind, 2013). The association between Aβ and RBCs is not only involved in functional impairments of erythrocytes but also induces detectable shape and structural changes in the RBC morphology and membrane roughness, as recently demonstrated by Carelli-Alinovi et al. (2019). This experimental evidence highlights the occurrence of biochemical and morphological alterations of RBCs obtained from patients with AD in comparison with control subjects, suggesting that such alterations could be a potential source of blood biomarkers.

However, in the last two decades, it has been shown that both morphological and biochemical changes are deeply connected to a modification of the mechanical properties of cells and tissues, stimulating a significant research effort toward the identification and validation of novel mechanical biomarkers of pathologies (Suresh et al., 2005; Suresh, 2007; Cross et al., 2008; Shieh, 2011; Swaminathan et al., 2011; Ethier and Simmons, 2013; Choi et al., 2014; Van Zwieten et al., 2014; Minelli et al., 2017, 2018; Pichiecchio et al., 2018; Carelli-Alinovi et al., 2019). This is particularly true for RBCs for which mechanical deformability is a key characteristic. RBCs, indeed, need to undergo multiple deformations, when traveling through small blood vessels and organs (Dao et al., 2003; Ciasca et al., 2015). This remarkable deformability is closely related to RBC membrane structure, primarily consisting of a phospholipid bilayer with an underlying two-dimensional network of spectrin molecules. There is growing evidence that this extreme deformability is significantly altered in several pathological conditions, such as diabetes mellitus, essential hypertension, arteriosclerosis, and coronary artery, hereditary spherocytosis, thalassemia, G6PD deficiency, sickle cell disease, and that such alteration contributes to enhancing the flow resistance of blood (Barnes et al., 1977; Cooper et al., 1977; Brown et al., 2005; Lekka et al., 2005; Dulińska et al., 2006; Maciaszek and Lykotrafitis, 2011; Pretorius, 2013; Tomaiuolo, 2014; Ciasca et al., 2015). On the one hand, RBC modifications occur at the cellular level, on the other hand, they are closely related to changes in the molecular composition and organization of the cell that, in their turn, occur at the nanoscale level. This has made it necessary to develop quantitative tools able to probe RBC biomechanical changes at the nanometer and piconewton scales. In this context, atomic force microscopy (AFM) is an extremely powerful technique as it permits probing cells, tissues, and molecules at the nanoscale level in nearly physiological conditions (Cappella and Dietler, 1999; Kuznetsova et al., 2007; Montis et al., 2020; Ridolfi et al., 2020; Romanò et al., 2020; Di Santo et al., 2021). In this study, we investigate the viscoelastic properties of RBCs obtained from patients with AD, intending to search and validate possible blood biomarkers of

the pathology that can be used for diagnostic applications as well as for therapy monitoring. For this purpose, we compared conventional AFM analysis with the Sneddon model with a more detailed analysis based on the application of the standard linear solid (SLS) model.

Materials and methods

Atomic force microscopy measurements: Patients' recruitment, sample preparation, and data analysis

We observed a total of 53 blood samples from patients diagnosed with AD (26 subjects) and healthy controls (27 subjects). Patients with AD were selected by clinical and neuropsychological evaluation showing a diffuse cognitive impairment and were classified as probable AD according to the standardized clinical diagnostic criteria (McKhann et al., 2011). Patients with AD at the time of blood sampling were not treated with acetylcholinesterase (AchE) inhibitors or antiplatelet drugs. Prior measurements samples were centrifuged to separate serum from blood and red blood cells were deposited on a poly-L-lysine coated Petri dish. Force mapping measurements were performed at room temperature and in physiological solution (0.9% NaCl, Fresenius Kabi), using a JPK Nano Wizard II (JPK Instruments, Berlin, Germany) atomic force microscope equipped with silicon cantilevers with conical tip [MIKROMASCH CSC38 (Sofia, Bulgaria), nominal spring constant 0.03 N/m]. The cantilever spring constant was determined before each measurement by thermal calibration. We acquired a map of 64 force–distance (FD) curves and a map of 64 force–relaxation (FR) curves for each RBC for an average of 10 RBCs per sample. Each map covered the whole RBC surface and a portion of the unoccupied Petri surface. The latter region was eliminated before data analysis. Indentation curves were acquired using an indentation force of 2 nN at 5 μm/s indentation speed and were analyzed using the Sneddon model:

$$F(\delta) = \frac{2E\, tan(\alpha)}{\pi\,(1-\nu^2)}\delta^2 \qquad (1)$$

where E accounts for the apparent Young's modulus, υ for the Poisson ratio, and δ for the indentation depth. The Poisson ratio was set at 0.5 to account for material incompressibility. Representative FD curves, together with the best fit of Eq. 1 to data, are shown in **Figures 1A,B**. The term apparent Young's modulus (referred to as E in the following) accounts for the fact that, for sharp tips, E depends on both, the scanner velocity during indentation and the indentation depth. An indentation depth of 0.5 microns has been selected to analyze the data, as most of the measured FD curves displayed a parabolic behavior up to this threshold value, in agreement with Eq. 1. However, we note that this indentation depth exceeds the 10% threshold on the overall sample thickness (**Figure 1C**) and therefore, we might have induced an overestimation of the measured E-values, which could complicate the comparison with other AFM studies exploiting different experimental conditions or AFM set-ups. However, we believe that this overestimation is not affecting the comparison between the two groups, as the measured RBCs' thickness is not significantly different in patients with AD and controls (**Figure 1C**).

The behavior of Young's modulus E as a function of the indentation speed in the range 1–20 μm/s was also investigated to assess the relevance of dissipative contributions in the determination of E (two representative curves are shown in **Figures 1D–F**). This analysis is extremely time-consuming and therefore it has been carried out on a reduced number of cells obtained from a small subset of the recruited subjects. For this purpose, 50 × 50 μm elasticity maps have been acquired (two representative images are shown in **Figure 1D**). The application of Eq. 1 relies on the assumption that the sample behaves like an elastic body. Biological samples rarely verify this assumption leading to well-known problems in the determination of E. To overcome this limitation, we acquired specifically designed time-dependent force–relaxation curves. These measurements were performed on a subset of the recruited subjects. Specifically, a total of 16 patients and 20 controls were subjected to this type of analysis. According to Rianna and Radmacher (2017), we studied cell mechanics with the SLS model, a theoretical framework that describes the sample as a linear combination of two elastic springs (k_1 and k_2) and a viscous damping element, f (**Figure 1G**). An additional elastic spring, k_c, accounts for the cantilever contribution (**Figure 1G**). The following variables were defined: the cantilever position Z, deflection d, and the sample indentation δ (**Figure 1G**). It is worth stressing that δ cannot be measured directly, but it is obtained from the knowledge of Z and d. For these variables, the following relationship can be established: $\triangle Z = d + \delta \rightarrow \delta = \triangle Z - \delta$ (**Figure 1G**). At the contact point, immediately before indenting the sample, we can set $\triangle Z = d_0 = \delta_0 = 0$ (**Figure 2**), as the cantilever is not deflected, the sample is not indented, and the $Z = 0$ position can be chosen arbitrarily (**Figure 2**). During the approach and indentation phase, we exploited a high indentation speed (35 μm/s) to avoid possible sample relaxation during indentation, before the target force is reached (point a, **Figure 2**). In this abrupt indentation phase, it can be assumed that the viscous dashpot has had no time to respond and, thus, the sample in the point a behaves like the parallel between k_1 and k_2. A dwell phase at constant height is then imposed, where the piezoelectric extension remains constant and the sample is allowed to relax (**Figure 2**). During this phase, $\triangle Z = cost \rightarrow \dot{\delta} + -\dot{d}$ and the following time-dependent differential equation can be written:

$$k_c d + \frac{f}{k_1}\left(k_c \dot{d}\right) = k_2\delta + f\frac{(k_1+k_2)}{k_1}\dot{\delta} \qquad (2)$$

where k_c is the cantilever elastic constant, as measured with the thermal calibration method. In the constant height mode ($\Delta Z = cost \rightarrow \dot{\delta} = -\dot{d}$), Eq. 2 can be written as $d(t) = \frac{k_2}{(k_2+k_c)}\Delta Z - \tau_c \dot{d}$, and solved as follows:

$$d(t) - Ae^{-\frac{t}{\tau_c}} + d_b \quad (3)$$

with $\tau_c = \frac{f(k_1+k_2+k_c)}{k_1(k_c+k_2)}$, $A = \left(d_a - \frac{k_2}{(k_c+k_2)} \cdot \Delta Z\right)$ and $d_b = \frac{k_2}{(k_c+k_2)} \cdot \Delta Z$, where d_a and d_b are the cantilever deflections at points a and b (Figures 1F,G). The parameters A, τ_c and d_b can be retrieved fitting the measured FR curves with Eq. 3 and used to calculate k_1, k_2, and f. Unfortunately, these quantities depend on ΔZ and d_a, which are affected by a large experimental error in our set-up. To overcome this limitation, a height step is applied to the cantilever when the first relaxation is completed, retracting the tip of a known quantity J, as indicated in Figure 2. Being a pure elastic body, the cantilever instantly follows this variation, while the cell initially maintains its deformed state and then relaxes until a new equilibrium in point c is reached (Figures 1E–G). In the new equilibrium point c, the following equation can be written: $k_c d_c = k_2(\Delta Z - J - d_c)$, where d_c is the measured deflection. Similarly, in point a, we can write $k_c d_a = (k_1 + k_2)(\Delta Z - d_a)$. Combining the latter five equations, we can get rid of ΔZ and d_a, thus finding a mathematical expression for the SLS parameters (Eq. 4):

$$\begin{cases} k_1 = \frac{A(k_c+k_2)k_2}{(k_c d_b - k_2 A)} \\ k_2 = \frac{k_c(d_b - d_c)}{(J + d_c - d_b)} \\ f = \tau_c \frac{k_1(k_c+k_2)}{(k_1+k_2+k_c)} \end{cases} \quad (4)$$

Laboratory parameters

Clinical chemistry assay are highly automated and tests performed are closely monitored and quality controlled. The specimens are on serum or plasma analysis with techniques such as spectrophotometry and immunoassays to measure the concentration of substances (glucose, lipids, enzymes, electrolytes, hormones, proteins, and metabolic products) present in human blood. A complete blood count test measures several components and features of blood (amount of red blood cells, white blood cells, and platelets). The cytometric methods include cell size, cell count, and cell morphology.

Statistical analysis

Statistical analyses were performed using the software package R (3.5.2 release) (R Development Core Team, 2016). Biomarkers were tested for normality by a visual inspection of the Q–Q plot followed by a Shapiro–Wilk test. It was found that selected biomarkers show some degree of deviation from normality; therefore, an unpaired two-samples Wilcoxon Test was used for group comparison. Analysis of covariance was used to account for covariates such as age (Table 1). The diagnostic accuracy of selected biomarkers in discriminating between the two groups was assessed by logistic regression and ROC curves. Logistic regression is executed using the function *glm* from the stats R package to extract probabilities from the fitted models, either with a single biomarker or with several biomarkers used in combination. A backward stepwise logistic regression was used to select, among biochemical and biomechanical parameters, the most effective subset of biomarkers for discriminating the two groups. For this purpose, Akaike's Information Criterion (AIC) was exploited. ROC curves and AUC values were calculated using the R package *pROC*. Correlation between variables was evaluated by linear regression analysis and by calculating Spearman's correlation coefficients. The strength of correlation was judged using correlation coefficients of >0.70 as strong correlation, 0.30–0.70 as moderate correlation, and <0.3 as weak correlation (Napodano et al., 2021).

Results

In Figures 1A,B, two representative FD curves acquired on an RBC obtained from a control subject and an AD patient are reported, respectively. A qualitative analysis of Figures 1A,B does not show marked differences between the two curves. However, a single-point measure cannot be considered representative of the biomechanical response of the whole cell. Therefore, we decided to probe the local response of each cell acquiring different FD curves at different positions over the cell surface. The Sneddon model (Eq. 1) was fitted to the experimental curves (black dashed lines in Figures 1A,B) to obtain the effective Young's modulus, E. FD curves were fitted up to an indentation depth of 0.5 μm (black continuous lines in

TABLE 1 ANCOVA table for the variables k_1, k_2, and f reported in Figure 2.

	Df	Sum sq	Mean sq	*F*	*P*
k1					
Age	1	3.43E-07	3.43E-07	3.766	0.061159
Group	1	1.41E-06	1.41E-06	15.477	0.000421
Residuals	32	2.92E-06	9.12E-08		
k2					
Age	1	9.79E-07	9.79E-07	1.412	0.24351
Group	1	5.71E-06	5.71E-06	8.231	0.00724
Residuals	32	2.22E-05	6.94E-07		
f					
Age	1	1.01E-06	1.01E-06	6.253	0.017713
Group	1	2.49E-06	2.49E-06	15.445	0.000426
Residuals	32	5.15E-06	1.61E-07		

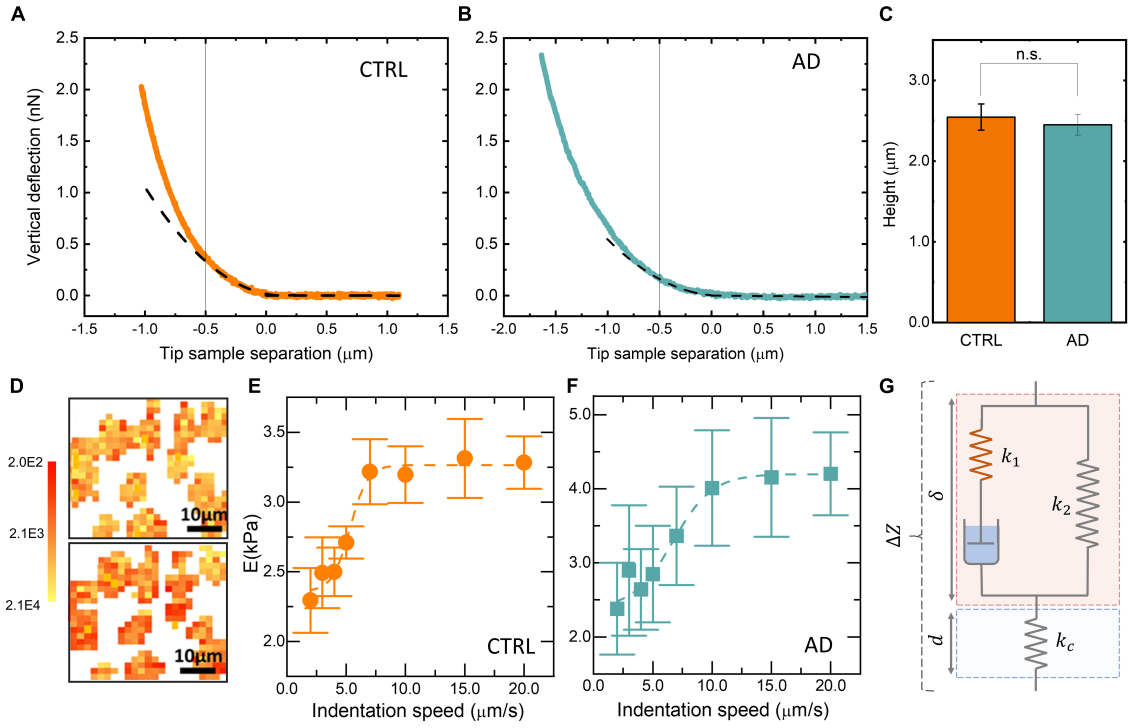

FIGURE 1
Representative force–distance (FD) approach curve acquired on a red blood cell (RBC) obtained from a control subject **(A)** and an Alzheimer's disease (AD) patient **(B)**. Average RBC height in liquid environment **(C)**. Two representative RBC maps acquired at 20 μm/s (**D**, upper panel) and 5 μm/s (**D**, lower panel). Average Young's modulus E as a function of the indentation speed for a control subject **(E)** and a patient with AD **(F)**. Schematic view of the standard linear solid (SLS) model **(G)**.

Figures 1A,B). This indentation range was chosen as the great majority of the analyzed curves showed the expected parabolic behavior up to this threshold. The experimental consequences of this choice are commented on in the Section "Discussion." The representative fitting curves were prolonged up to 1 μm for visualization purposes. The mean *E*-value for each recruited subject was calculated by averaging the results obtained on all the measured cells. In Figure 1C, the average height of RBCs in liquid is shown for the two groups. Data are reported as mean ± SEM. No statistically significant differences are highlighted between the two groups. In most of the AFM studies exploiting Sneddon's model or similar ones, the basic assumption is that the sample has a purely elastic behavior; hence dissipative forces are neglected, and Young's modulus is treated as unaffected by probe dynamics. We checked for this assumption by measuring the average Young's modulus E as a function of the cantilever speed during indentation in the range of 1–20 μm/s. The analysis was conducted over eight 50 × 50 μm maps. Two representative E maps acquired on a control subject at different indentation rates, v = 20 μm/s (Figure 1D, upper panel) and v = 5 μm/s (Figure 1D, lower panel) are reported. The same color scale was used for the two maps (Figure 1D, left). One can notice that the upper figure appears to be systematically brighter than the lower one in any location, pointing out a global stiffening of RBCs while increasing the indentation speed. In Figure 1E, a representative curve of the average Young's modulus E as a function of the indentation rate is reported for a typical control subject. Data are shown as mean ± SEM. A sigmoidal curve was fitted to the data (dashed orange line). Increasing the scanner velocity, we observe a monotonous increase in E, which starts from approximately 2.3 kPa up to reaching a plateau value of 3.3 kPa at approximately 10 μm/s. The same analysis is carried out on a selected AD patient (Figure 1F), showing behavior that resembles the one reported in Figure 1E: we again observe a monotonous increase of E from approximately 2.3 kPa up to a plateau value of 4.25 kPa at approximately 15 μm/s. The reported sigmoidal behaviors are qualitatively in agreement with the SLS model, which is a mathematical way to evaluate the deformation properties of a sample as a linear combination of an elastic term (k_1) and Maxwell's arm, composed of an elastic element (k_2) and a viscous dashpot (f) in series with each other (Figure 1G). It can be demonstrated that, according to this model, the sample reaction force at a very low indentation speed is dominated by elastic contributions. In the intermediate range, viscosity contributes to a non-linear increase of the reaction force, until it reaches a plateau at high speed. The qualitative agreement between the described trend and the data shown in

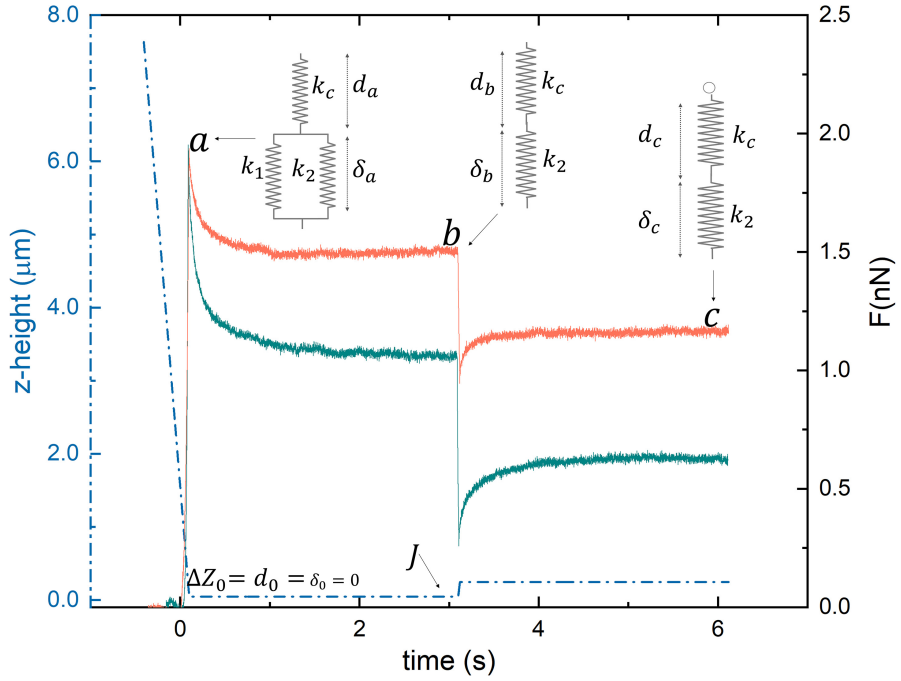

FIGURE 2
Two representative loading/unloading time-dependent relaxation curves acquired on a healthy (orange) and pathological (cyan) subject.

Figures 1E,F demonstrate that RBCs do not have a purely elastic behavior. Conversely, their biomechanical response appears to be dependent on dissipative forces and viscous contributions (Leo et al., 2020). To measure viscous and elastic terms, separately, we acquired AFM time-dependent relaxation curves, as explained in the Section "Materials and methods." For this purpose, we used a slightly modified version of the model proposed in Rianna and Radmacher (2016, 2017). In **Figure 2**, two representative FR curves are shown for a control subject and an AD patient, respectively. At variance with the typical FD curves (**Figures 1A,B**), where a clear difference between AD and control subjects was not observed, the two time-dependent curves appear different. To quantify this difference, we analyzed data using Eqs 2–4, which allowed us to retrieve the SLS parameters, namely, the damping element *f*, and the two elastic springs k_1 and k_2. Similarly to the conventional FD curves, a single-point measure is not representative of the biomechanical response of the whole cell; therefore, we acquired different time-dependent curves in different locations of the cell, and we averaged the results obtained on all the measured cells (on average 10 cells/subject). A box plot analysis of the average *E*-values calculated fitting Eq. 1 to conventional FD curves is shown in **Figure 3A** for control and pathological subjects. An unpaired two-samples Wilcoxon test was used to compare AD and control subjects, pointing out the absence of statistically significant differences between the two groups ($p = 0.9878$). In **Figures 3B–D**, a box plot analysis of the mechanical parameters obtained with the SLS model was shown. Additionally, a similar analysis is shown in **Supplementary Figure 1** for τ_c. Statistically significant *p*-values were obtained for all the SLS parameters (**Figures 3B–D**), namely, the damping element *f* ($p = 9.1e\text{-}6$) and the elastic terms k_1 ($p = 0.00097$) and k_2 ($p = 0.0013$). In this regard, a caveat is necessary as the two groups are not age-matched. Therefore, we performed an analysis of covariance (ANCOVA) analysis to decouple differences due to age. The results of this analysis show that the group membership is highly significant for all three variables, even if age is taken into account as a covariate. These findings suggest that, while the effective Young's modulus E cannot be used to distinguish the two groups in our experimental conditions, SLS parameters are potentially useful for the development of novel mechanical biomarkers of the pathology. In the next section, we briefly commented on the possibility of using *E*-values obtained at higher indentation speeds to distinguish the two groups. ROC curves—a widely used statistical technique to evaluate and compare diagnostic tools (Hoo et al., 2017; Caputo et al., 2021; Di Santo et al., 2022)—were exploited to assess the performance of the four mechanical parameters (**Figure 4A**). ROC curves are two-dimensional graphs in which sensitivity, also referred to as the True Positive (TP) rate, is plotted against 1–specificity, which is the false positive (FP) rate (Metz, 1978). As specificity ranges between 0 and 1, ROC curves might be also reported in terms of sensitivity as a function of specificity, inverting the x-axis. In the present paper, the latter notation is used. The diagonal line

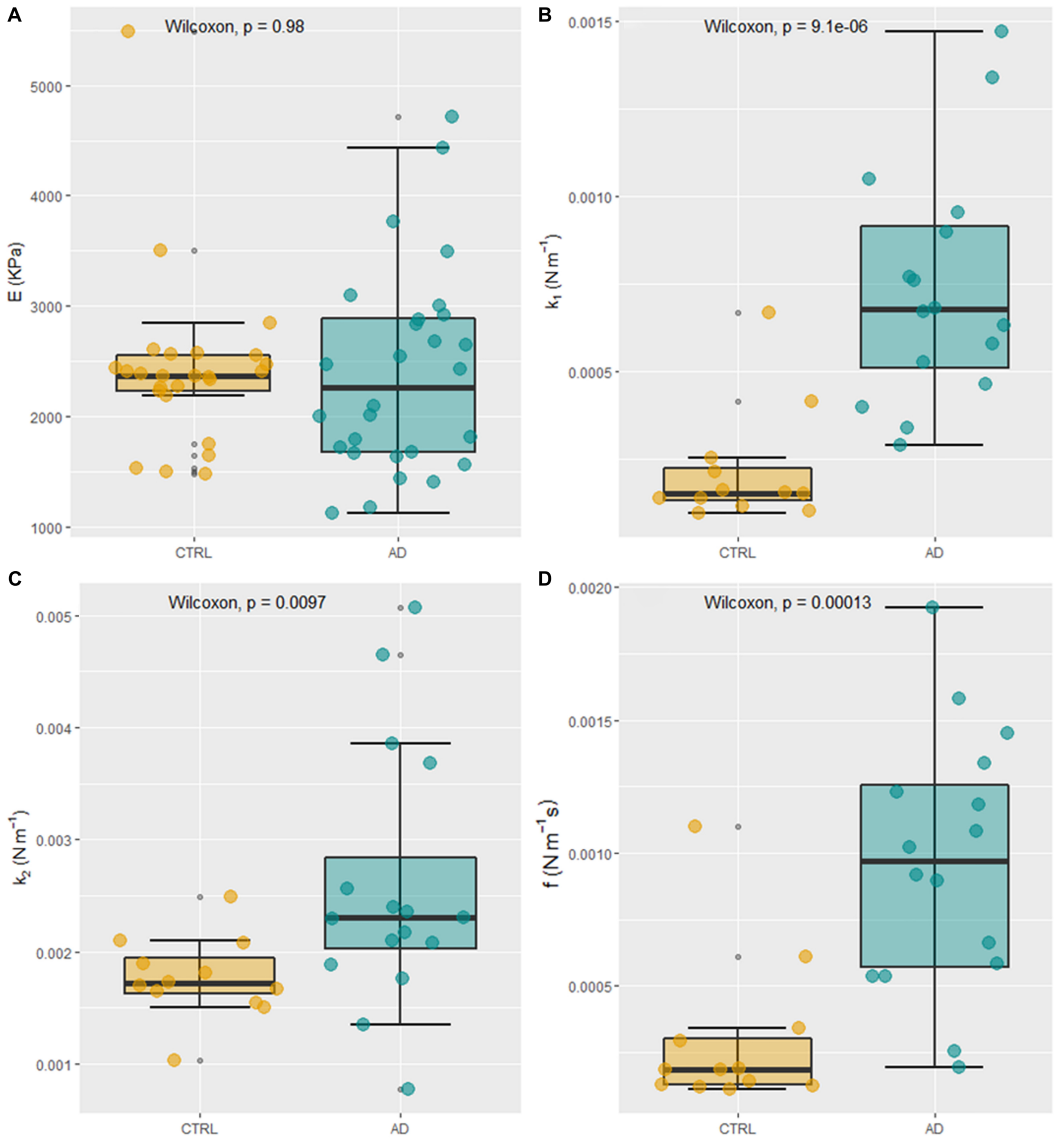

FIGURE 3
Box plot analysis of average *E*-values for control and pathological subjects **(A)**. Box plot analysis of mechanical parameters obtained from the standard linear solid (SLS) model **(B–D)**.

represents the y = x bisector, which is the expected performance for a completely random classifier. ROC curves of the three SLS parameters rapidly increase for low values of the x-axis, showing that *f*, k_1, and k_2 are effective in distinguishing between the two groups. Conversely, Young's modulus E fails in discriminating between control subjects and patients with AD. A widely used statistical metric for the quantitative evaluation of a ROC curve is the so-called area under the curve (AUC). By definition, AUC values lie in the range 0–1, where 1 corresponds to an ideal classifier and 0.5 to a completely random classifier; in general, the higher the AUC value, the better the classifier performance. As expected, large AUCs were measured for the three SLS parameters, namely, 0.88 (95% CI: 0.78–0.99) for *f*, 0.87 (95% CI: 0.76–0.99) for k_1, and 0.80 (95% CI: 0.63–0.96) for k_2. Young's modulus E shows an AUC of 0.5 (95% CI: 0.34–0.67), which highlights its poor ability to discriminate between the two groups. To improve the effectiveness of the model shown in Figure 3B, we performed a stepwise logistic regression including all the measured biomechanical (E, k_1, k_2, *f*) parameters and several RBC indices routinely measured in blood tests, namely, erythrocyte sedimentation rate (ESR), RBC count, mean corpuscular volume (MCV), mean corpuscular hemoglobin (MCH), hemoglobin (Hb), and mean corpuscular hemoglobin concentration (MCHC). For this purpose, first, the complete model was obtained and then a stepwise backward selection was performed to highlight the most relevant subset

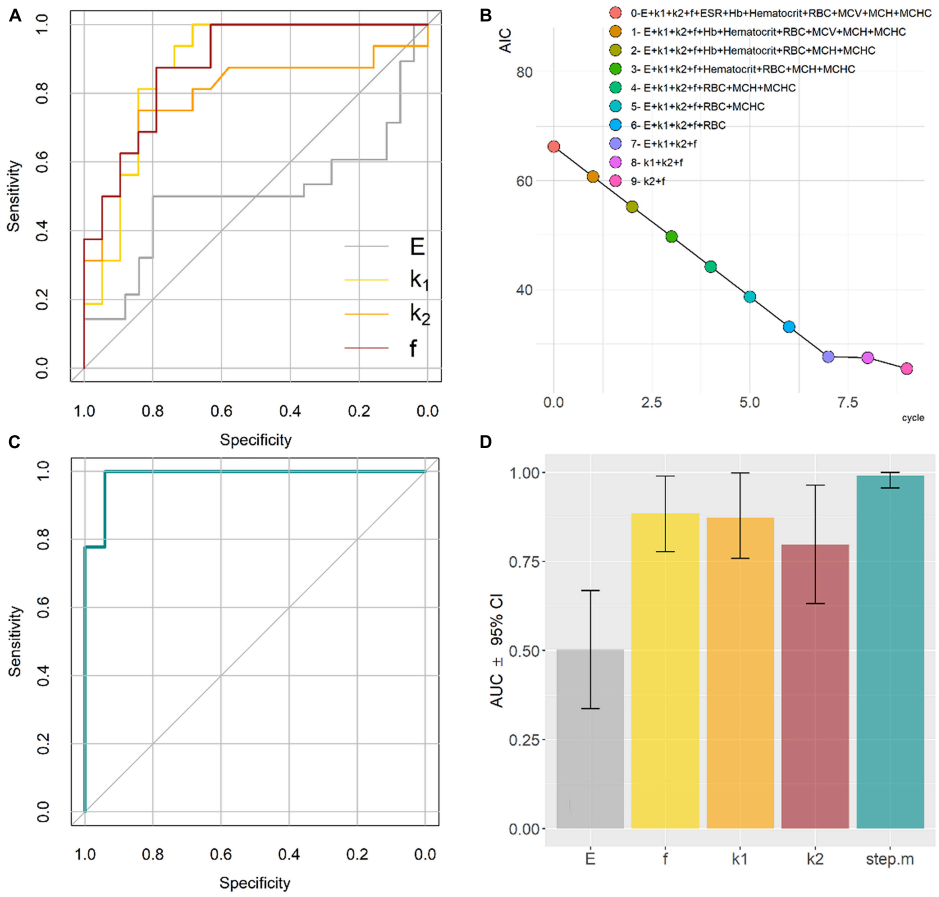

FIGURE 4
Receiving operator characteristic (ROC) curves for the four selected mechanical biomarkers **(A)**; Evolution of the Akaike's Information Criterion (AIC) during a stepwise logistic regression performed on all the measured mechanical and biochemical parameters **(B)**; ROC curve calculated using the selected variables f and k2 **(C)**; Areas under the curves (AUC) values for the four mechanical parameters and the stepwise model **(D)**.

of parameters that minimize AIC. Given the modest number of data points and to keep the model as simple as possible, we used the following information criterion that strongly penalizes large models with many parameters (n): $AIC = 2k - 2\ln(\tilde{L})$, where $k = \ln(n)$ and $\tilde{L}$ are the maximum value of the likelihood function for the model. The computed AIC value for each cycle of the stepwise regression procedure is shown in Figure 4B, showing the progressive removal of the less effective biomarkers. Notably, as shown in the figure, the procedure selects f and k_2, while it discards all the biochemical parameters together with the effective Young's modulus E and k_1. In Figure 4C, we show the corresponding ROC curve for the selected model, which includes f and k_2 and shows a very large AUC, 0.99 (95% CI: 0.96–1.00). The computed AUC values, together with the corresponding 95% CI, are summarized in Figure 4D.

To investigate a more in-depth relationship between mechanical and biochemical parameters together with the results of neurological tests on patients with AD, we performed a correlational analysis between the two groups of variables. A biomarker correlation map is shown in Figure 5A for control subjects (white background) and patients with AD (gray background). The two maps report only the statistically significant correlations (significance level 0.05). In control subjects, a strong negative correlation $\rho = -0.72$ ($p = 0.0008$) was observed for the variables MCV and k_1 and moderate negative correlations were observed for Hb/k_1 $\rho = -0.50$ ($p = 0.036$), MCHC/f $\rho = -0.50$ ($p = 0.034$), TBIL/k_2 $\rho = -0.58$ ($p = 0.018$), and ALP/k_1 $\rho = -0.55$ ($p = 0.028$). In patients with AD, a moderate positive correlation of $\rho = 0.66$ ($p = 0.00018$) is observed for the concentration of reactive oxygen species (ROS) and E, and a strong negative correlation of $\rho = -1.0$ ($p = 0.0072$) was observed for Fe/k_2. No other relevant correlations are shown. For the sake of completeness, in Figure 5B, we report the corresponding scatterplots, which were analyzed according to a linear model (this analysis was conducted only on the datasets which did not show marked deviation from normality).

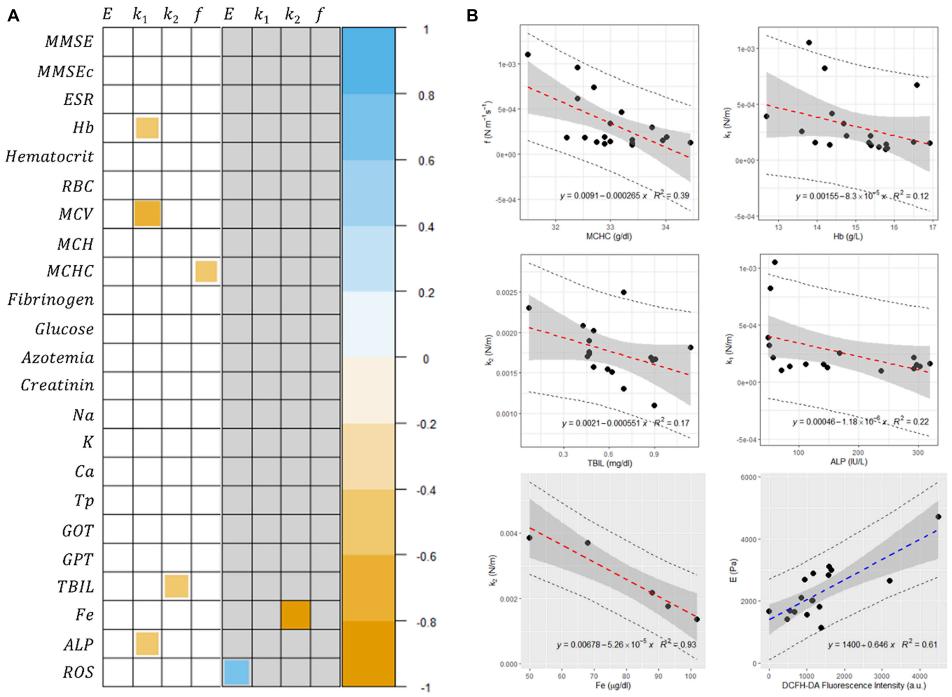

FIGURE 5
(A) Spearman correlation matrix between selected hematological parameters and mechanical biomarkers. Correlation maps are shown separately for control subjects (white background) and patients with Alzheimer's disease (AD) (gray background). The two maps show only the statistically significant correlations (significance level 0.05). **(B)** Scatter plots showing the relationship between selected variables together with the corresponding linear regression analysis.

Discussion

In the last decades, a large body of evidence has emerged that—along with biochemical and genetic cues—mechanical stimuli are critical regulators in human physiology, as well as fundamental players in the onset and the progression of many pathological states (Kumar and Weaver, 2009; Lu et al., 2011; Van Zwieten et al., 2014; Ciasca et al., 2016a, 2019; Vielmuth et al., 2016; Weaver, 2017; Perini et al., 2019; De-Giorgio et al., 2020; Di Giacinto et al., 2020; Mazzini et al., 2020). A wide range of diseases that bring patients to the doctor's office can be, indeed, associated with significant alterations in the mechanical properties of cells, tissues, and organs. Mechanical deformability is also a major characteristic of RBCs, as they need to undergo large deformations when passing through small vessels and capillaries. Such extreme deformability is deeply altered in pathological conditions and inflammatory diseases (MacIaszek et al., 2011; Buys et al., 2013; Pretorius, 2013; Pretorius and Kell, 2014; Pretorius et al., 2015). In this context, the quantitative analysis of the biomechanical response of RBCs has potentially wide applications in diagnostics.

Here we presented a comparative AFM study of the mechanical properties of RBCs extracted from patients with AD and healthy control subjects. The study is aimed to identify possible mechanical biomarkers of the pathology directly from the blood, which could be exploited for diagnostic purposes and therapy monitoring.

For this purpose, two types of analyses were exploited. First, we performed a conventional analysis of AFM FD curves with the Sneddon model, which allowed us to retrieve the apparent Young's modulus E of cells. E is one of the most widely used parameters to probe RBC stiffness in different pathological conditions. However, in this case, no statistically significant differences were found between the two groups (**Figure 3A**), as further confirmed by a ROC curve analysis (**Figure 4A**), showing that E has extremely poor classification abilities. This finding is in close agreement with the results of Bester et al. (2013), which first compared the biomechanical properties of RBCs extracted from control subjects and patients with AD, showing no significant differences among the elastic modulus values in the two groups (Ethier and Simmons, 2013). Interestingly, they found a significant increase in Young's modulus of hyperferritinemic AD subjects compared to healthy and normoferritinemic AD ones, providing further evidence of the strong relation between AD, and ferritin levels and its metal content (De Sole et al., 2013). Many studies investigating the biomechanical properties of RBC rely only on the analysis of conventional FD curves with the Hertz model, the Sneddon model, or similar ones. In this regard, a caveat is necessary.

These analyses implicitly assume that the sample behaves like an elastic body. This assumption cannot be considered strictly valid in our case, as shown in **Figures 1D–F**, where the apparent Young's modulus E shows a sigmoidal dependence on the indentation speed. The analysis is carried out on two representative subjects randomly selected within the recruited population. Therefore, the comparison between the two curves cannot be used to draw a statistically relevant conclusion on the mechanical behavior of RBCs in the two groups. Nonetheless, this comparison is interesting as it suggests that the effective Young's modulus E measured at 20 μm/s might be more effective in highlighting differences between the two groups, a hypothesis that deserves a more in-depth investigation in a dedicated paper. The E behavior shown in **Figures 1D–F** indicates that viscous forces contribute relevantly to RBC biomechanics and, thus, need to be included in the analysis of force spectroscopy measurements. Since the loading rate is not constant during the acquisition of FD curves on a soft sample, due to the change in the tip-sample contact area, extending the Sneddon model (or similar ones) to effectively include viscous effects is a hard and non-trivial task. An alternative way of estimating the contribution of dissipative forces in AFM experiments is to measure the percentage of energy dissipated during indentation, also referred to as hysteresis (H). Unfortunately, H does not provide a quantitative measure of sample viscosity, but rather a semi-quantitative estimation of dissipative contributions (Suresh, 2007; Cross et al., 2008; Ciasca et al., 2016b; Kulkarni et al., 2019).

To overcome these limitations and to measure the viscoelastic properties of cells and polymeric materials with AFM, several approaches have been proposed and tested (Ngan et al., 2005; Passeri et al., 2009; Moreno-Flores et al., 2010; Cartagena and Raman, 2014; Rianna and Radmacher, 2016, 2017; Heydarian et al., 2020; Zhang et al., 2020). In the present paper, we employed a slightly modified version of a model developed by Rianna and Radmacher (2016, 2017), as discussed in the Section "Materials and methods". In their paper, the authors designed a specific sequence of time-dependent force–relaxation curves, which easily allows decoupling of viscous and elastic contributions in the framework of the SLS model. Interestingly, and at variance with Young's modulus E, a statistically significant difference between patients with AD and control subjects was found for all the biomechanical parameters obtained with the SLS models (**Figures 3B–D**). Very often RBCs extracted from pathological subjects are reported to be simply stiffer than the ones obtained from healthy controls, based on Young's modulus value obtained from the analysis of FD curves with Hertz's model. This widely observed effect is likely to be due, not only to a change in RBC elastic properties—mainly associated with cytoskeletal alterations—but also to a change in cell viscosity that can be ascribed, among other factors, to the plasma membrane or hemoglobin modifications. These two effects can contribute in a complex fashion to the measured *E*-values obtained from FD curves, in some cases producing a detectable difference between the apparent cell stiffness in healthy and pathological erythrocytes, in some other cases—this one included—masking the actual impairment of cell mechanical properties. In the latter case, decoupling viscous and elastic terms is an effective strategy in the search for novel mechanical biomarkers of the pathology, as confirmed by the large AUC values obtained for the SLS parameters in **Figure 4D**.

This paper fits in the research areas related to the search and the validation of novel cell-based plasma biomarkers, which are highly desirable because of the reduced discomfort for patients, the generally low cost, and scalability to large screening for early diagnosis and prevention. At present, a wide panel of hematological and biochemical markers is routinely measured in diagnostics. To investigate more in-depth the relationship between the mechanical parameters presented in this paper and more established clinical parameters, we performed a correlation analysis between these two classes of blood indicators. Interestingly, few correlations were found between biochemical and mechanical parameters in the pathological group, suggesting that RBC biomechanics can be considered as a rather independent source of clinical information and, thus, can be used in combination with more established blood markers to get a comprehensive view of the patient's clinical conditions. A second notable result is the presence of a moderate correlation between selected mechanical parameters and RBC indices, including MCV, MCH, and MCHC in the control group. Similar correlations were recently observed in the paper of Von Tempelhoff et al. (2016), studying a group of apparently healthy women. Our results show that the damping parameter f is significantly correlated only with the mean corpuscular hemoglobin concentration in healthy subjects. This result was expected as the hemoglobin concentration and its biochemical properties primarily determine intracellular fluid viscosity (Connes et al., 2014). Interestingly, we also detected the presence of moderate correlation between selected mechanical and hepatic parameters in the control group, namely, alkaline phosphatase (ALP) and total bilirubin. This result is particularly interesting and deserves a more in-depth study as it strengthens the link between the presence of a possible alteration in hepatic microcirculation and the impairment of the RBC mechanical properties.

Ultimately, we investigated the presence of correlations between the investigated mechanical parameters and the results of the Mini-Mental State Examination (MMSE), a neurological test extensively used in clinical and research settings to measure the cognitive impairment of patients (Tombaugh and McIntyre, 1992). This investigation aimed to assess whether the mechanical parameters could be used as a quantitative measure of the progression of the pathology. The MMSE corrected for patients' age (MMSEc) was also investigated for the same reason. Unfortunately, none of the studied mechanical parameters shows any significant correlation with the MMSE score, indicating that RBC biomechanics as measured in this setting cannot be used to develop a

quantitative biomarker of disease progression, an issue that can be regarded as a limitation hindering the applicability of the investigated markers. Moreover, it is also important to stress further limitations of the proposed technique. First, it is well-known that RBC nano-mechanics is highly sensitive to the inflammatory environment, which characterizes many clinical conditions other than AD, e.g., diabetes (Pretorius and Kell, 2014). Therefore, RBC mechanical properties cannot be considered specific markers of AD, but rather additional diagnostic parameters that have to be used in combination with more established clinical indicators to improve diagnostic specificity and sensitivity. Additionally, AFM is a time-consuming technique in terms of measurement time and data analysis and often requires specialized personnel with a physical background. Fortunately, these limitations can be overcome by using high-speed (HS-) AFM and machine learning for data analysis (Nievergelt et al., 2015; Wang et al., 2016; Dufrêne et al., 2017; Sokolov et al., 2018; Casuso et al., 2020; Dokukin and Dokukina, 2020; Ridolfi et al., 2020; Chandrashekar et al., 2022; Nguyen and Liu, 2022). To conclude, a further limitation of our work consists in the use of single exponential decays for fitting time-dependent curves such as those reported in **Figure 2**. We adopted this choice to keep the model as simple as possible so that data could be fitted automatically with homemade software, but a fitting function composed of multiple exponential decays ($\geq$2) would be more appropriate than a single exponential decay. Therefore, similar to *E*-values, the SLS parameters here presented should be considered effective parameters, and special care must be paid when comparing their absolute value with similar values obtained with more complex models. Nevertheless, we believe that the mentioned simplification is not negatively affecting the diagnostic potential of our quantitative markers, as far as the same protocol is used for all the recruited subjects, irrespectively of the group membership.

Conclusion

In order to pass through the microcirculation, RBCs need to undergo extensive deformations and recover their original shape. On the one hand, this extreme deformability is altered by various pathological conditions; on the other hand, an altered RBC deformability can have major effects on blood flow, leading to pathological implications. In this scenario, the investigation of the viscoelastic response of RBCs by AFM is highly effective to unveil subtle alterations of their deformability under pathological conditions. By using AFM in the force spectroscopy mode, we compared the biomechanical properties of RBC obtained from healthy donors and patients with AD, to search for novel blood biomarkers of the pathology. Our results show that Young's modulus E, obtained with a conventional analysis of FD curves, fails in discriminating between control subjects and patients with AD. This is likely since this analysis relies on the assumption that the investigated cell has a purely elastic behavior. Such an assumption is rarely verified in soft and biological samples and, very often, the interplay of elastic and viscous contributions affects the determination of E in a complex fashion. To overcome this limitation, we applied a more in-depth analysis, which combines time-dependent force–relaxation curves with the SLS model, a general theoretical framework that allows describing the sample as a linear combination of elastic and viscous terms. Interestingly, the SLS parameters, namely, the damping term f and the elastic springs k_1 and k_2, are significantly different in the two classes of subjects, as further confirmed by the corresponding ROC curves with very large AUC values. A correlational analysis between mechanical parameters and biochemical ones was also performed. This analysis showed the presence of few mild correlations between the two classes of parameters, pointing out that RBC biomechanics is a potentially independent source of valuable clinical information. Taken all together, our results highlight the presence of significant abnormalities in the biomechanics of RBCs obtained from patients with AD, whose detection and quantification can positively influence the search for novel blood biomarkers of AD useful for diagnosis and therapy monitoring.

Data availability statement

The data are available from the authors upon reasonable request.

Ethics statement

The studies involving human participants were reviewed and approved by Ethical Committee of Università Cattolica del Sacro Cuore (protocol code no. 22237/19). The patients/participants provided their written informed consent to participate in this study.

Author contributions

All authors have contributed substantially to the manuscript and have read and agreed to the published version of the manuscript.

Acknowledgments

The center of light and electron microscopy of the Catholic University of the Sacred Heart of Rome (LABCEMI) facility is gratefully acknowledged and also acknowledged the journal fee will be paid by Universitá Cattolica (linea D. 3.1.).

Conflict of interest

The authors declare that the research was conducted in the absence of any commercial or financial relationships that could be construed as a potential conflict of interest.

Publisher's note

All claims expressed in this article are solely those of the authors and do not necessarily represent those of their affiliated organizations, or those of the publisher, the editors and the reviewers. Any product that may be evaluated in this article, or claim that may be made by its manufacturer, is not guaranteed or endorsed by the publisher.

Supplementary material

The Supplementary Material for this article can be found online at: https://www.frontiersin.org/articles/10.3389/fnagi.2022.932354/full#supplementary-material

SUPPLEMENTARY FIGURE 1
Box plot analysis of τ_C in the two groups.

References

Barnes, A. J., Locke, P., Scudder, P. R., Dormandy, T. L., Dormandy, J. A., and Slack, J. (1977). Is hyperviscosity a treatable component of diabetic microcirculatory disease? *Lancet* 2, 789–791. doi: 10.1016/s0140-6736(77)90724-3

Battisti, A., Ciasca, G., Grottesi, A., Bianconi, A., and Tenenbaum, A. (2012). Temporary secondary structures in tau, an intrinsically disordered protein. *Mol. Simul.* 38, 525–533. doi: 10.1080/08927022.2011.633347

Bester, J., Buys, A. V., Lipinski, B., Kell, D. B., and Pretorius, E. (2013). High ferritin levels have major effects on the morphology of erythrocytes in Alzheimer's disease. *Front. Aging Neurosci.* 5:88. doi: 10.3389/fnagi.2013.00088

Brier, M. R., Gordon, B., Friedrichsen, K., McCarthy, J., Stern, A., Christensen, J., et al. (2016). Tau and Ab imaging, CSF measures, and cognition in Alzheimer's disease. *Sci. Transl. Med.* 8:338ra66. doi: 10.1126/scitranslmed.aaf2362

Brown, C. D., Ghali, H. S., Zhao, Z., Thomas, L. L., and Friedman, E. A. (2005). Association of reduced red blood cell deformability and diabetic nephropathy. *Kidney Int.* 67, 295–300. doi: 10.1111/j.1523-1755.2005.00082.x

Buys, A. V., Van Rooy, M. J., Soma, P., Van Papendorp, D., Lipinski, B., and Pretorius, E. (2013). Changes in red blood cell membrane structure in type 2 diabetes: A scanning electron and atomic force microscopy study. *Cardiovasc. Diabetol.* 12, 1–25. doi: 10.1186/1475-2840-12-25

Cappella, B., and Dietler, G. (1999). Force-distance curves by atomic force microscopy. *Surf. Sci. Rep.* 34, 1–3,5–104. doi: 10.1016/S0167-5729(99)00003-5

Caputo, D., Digiacomo, L., Cascone, C., Pozzi, D., Palchetti, S., Di Santo, R., et al. (2021). Synergistic analysis of protein corona and haemoglobin levels detects pancreatic cancer. *Cancers (Basel)* 13:93. doi: 10.3390/cancers13010093

Carelli-Alinovi, C., Dinarelli, S., Sampaolese, B., Misiti, F., and Girasole, M. (2019). Morphological changes induced in erythrocyte by amyloid beta peptide and glucose depletion: A combined atomic force microscopy and biochemical study. *Biochim. Biophys. Acta Biomembr.* 1861, 236–244. doi: 10.1016/j.bbamem.2018.07.009

Cartagena, A., and Raman, A. (2014). Local viscoelastic properties of live cells investigated using dynamic and quasi-static atomic force microscopy methods. *Biophys. J.* 106, 1033–1043. doi: 10.1016/j.bpj.2013.12.037

Casuso, I., Redondo-Morata, L., and Rico, F. (2020). Biological physics by high-speed atomic force microscopy. *Philos. Trans. R. Soc. A* 378:20190604. doi: 10.1098/rsta.2019.0604

Chandrashekar, A., Belardinelli, P., Bessa, M. A., Staufer, U., and Alijani, F. (2022). Quantifying nanoscale forces using machine learning in dynamic atomic force microscopy. *Nanoscale Adv.* 4, 2134–2143. doi: 10.1039/d2na00011c

Choi, S.-Y., Jeong, W. K., Kim, Y., Kim, J., Kim, T. Y., and Sohn, J. H. (2014). Shear-wave elastography: A noninvasive tool for monitoring changing hepatic venous pressure gradients in patients with cirrhosis. *Radiology* 273, 917–926. doi: 10.1148/radiol.14140008

Ciasca, G., Pagliei, V., Minelli, E., Palermo, F., Nardini, M., Pastore, V., et al. (2019). Nanomechanical mapping helps explain differences in outcomes of eye microsurgery: A comparative study of macular pathologies. *PLoS One* 14, e0220571. doi: 10.1371/journal.pone.0220571

Ciasca, G., Papi, M., Di Claudio, S., Chiarpotto, M., Palmieri, V., Maulucci, G., et al. (2015). Mapping viscoelastic properties of healthy and pathological red blood cells at the nanoscale level. *Nanoscale* 7:17030–17037. doi: 10.1039/c5nr03145a

Ciasca, G., Papi, M., Minelli, E., Palmieri, V., and De Spirito, M. (2016a). Changes in cellular mechanical properties during onset or progression of colorectal cancer. *World J. Gastroenterol.* 22, 7203–7215. doi: 10.3748/wjg.v22.i32.7203

Ciasca, G., Sassun, T. E., Minelli, E., Antonelli, M., Papi, M., Santoro, A., et al. (2016b). Nano-mechanical signature of brain tumours. *Nanoscale* 8, 19629–19643. doi: 10.1039/c6nr06840e

Connes, P., Lamarre, Y., Waltz, X., Ballas, S. K., Lemonne, N., Etienne-Julan, M., et al. (2014). Haemolysis and abnormal haemorheology in sickle cell anaemia. *Br. J. Haematol.* 165, 564–572. doi: 10.1111/bjh.12786

Cooper, R. A., Durocher, J. R., and Leslie, M. H. (1977). Decreased fluidity of red cell membrane lipids in abetalipoproteinemia. *J. Clin. Invest.* 60, 115–121. doi: 10.1172/JCI108747

Cross, S. E., Jin, Y. S., Rao, J., and Gimzewski, J. K. (2007). Nanomechanical analysis of cells from cancer patients. *Nat. Nanotechnol.* 4, 72–73. doi: 10.1038/nnano.2009.036

Cross, S. E., Jin, Y. S., Tondre, J., Wong, R., Rao, J. Y., and Gimzewski, J. K. (2008). AFM-based analysis of human metastatic cancer cells. *Nanotechnology* 19, 1–8. doi: 10.1088/0957-4484/19/38/384003

Dao, M., Lim, C. T., and Suresh, S. (2003). Mechanics of the human red blood cell deformed by optical tweezers. *J. Mech. Phys. Solids* 53, 2259–2280. doi: 10.1016/j.jmps.2003.09.019

De Sole, P., Rossi, C., Chiarpotto, M., Ciasca, G., Bocca, B., Alimonti, A., et al. (2013). Possible relationship between Al/ferritin complex and Alzheimer's disease. *Clin. Biochem.* 46, 89–93. doi: 10.1016/j.clinbiochem.2012.10.023

De-Giorgio, F., Ciasca, G., D'Amico, R., Trombatore, P., D'Angelo, A., Rinaldi, P., et al. (2020). An evaluation of the objectivity and reproducibility of shear wave elastography in estimating the post-mortem interval: A tissue biomechanical perspective. *Int. J. Legal Med.* 134, 1939–1948. doi: 10.1007/s00414-020-02370-5

Di Giacinto, F., Tartaglione, L., Nardini, M., Mazzini, A., Romanò, S., Rizzo, G. E., et al. (2020). Searching for the mechanical fingerprint of pre-diabetes in T1DM: A case report study. *Front. Bioeng. Biotechnol.* 8:569978. doi: 10.3389/fbioe.2020.569978

Di Santo, R., Romanò, S., Mazzini, A., Jovanović, S., Nocca, G., Campi, G., et al. (2021). Recent advances in the label-free characterization of exosomes for cancer liquid biopsy: From scattering and spectroscopy to nanoindentation and nanodevices. *Nanomaterials* 11:1476. doi: 10.3390/nano11061476

Di Santo, R., Vaccaro, M., Romanò, S., Di Giacinto, F., Papi, M., Rapaccini, G. L., et al. (2022). Machine learning-assisted FTIR analysis of circulating extracellular vesicles for cancer liquid biopsy. *J. Pers. Med.* 12:949. doi: 10.3390/jpm12060949

Dokukin, M., and Dokukina, I. (2020). Application of ensemble machine learning methods to multidimensional AFM data sets. *Procedia Comput. Sci.* 169, 763–766. doi: 10.1016/j.procs.2020.02.168

Dufrêne, Y. F., Ando, T., Garcia, R., Alsteens, D., Martinez-Martin, D., Engel, A., et al. (2017). Imaging modes of atomic force microscopy for application in molecular and cell biology. *Nat. Nanotechnol.* 12, 295–307. doi: 10.1038/nnano.2017.45

Dulińska, I., Targosz, M., Strojny, W., Lekka, M., Czuba, P., Balwierz, W., et al. (2006). Stiffness of normal and pathological erythrocytes studied by means of atomic force microscopy. *J. Biochem. Biophys. Methods* 66, 1–11. doi: 10.1016/j.jbbm.2005.11.003

Ethier, C. R., and Simmons, C. A. (2013). *Introductory biomechanics: From cells to organisms*. Cambridge: Cambridge University Press.

Florenzano, F., Veronica, C., Ciasca, G., Ciotti, M. T., Pittaluga, A., Olivero, G., et al. (2017). Extracellular truncated tau causes early presynaptic dysfunction associated with Alzheimer's disease and other tauopathies. *Oncotarget* 8, 64745–64778. doi: 10.18632/oncotarget.17371

Heydarian, A., Milani, D., and Moein Fatemi, S. M. (2020). An investigation of the viscoelastic behavior of MCF-10A and MCF-7 cells. *Biochem. Biophys. Res. Commun.* 20, 432–436. doi: 10.1016/j.bbrc.2020.06.010

Hoo, Z. H., Candlish, J., and Teare, D. (2017). What is an ROC curve? *Emerg. Med. J.* 34, 357–359. doi: 10.1136/emermed-2017-206735

Jack, C. R., Knopman, D. S., Jagust, W. J., Petersen, R. C., Weiner, M. W., Aisen, P. S., et al. (2013). Tracking pathophysiological processes in Alzheimer's disease: An updated hypothetical model of dynamic biomarkers. *Lancet Neurol.* 12, 207–216. doi: 10.1016/S1474-4422(12)70291-0

Kiko, T., Nakagawa, K., Satoh, A., Tsuduki, T., Furukawa, K., Arai, H., et al. (2012). Amyloid β levels in human red blood cells. *PLoS One* 7:e49620. doi: 10.1371/journal.pone.0049620

Kulkarni, T., Tam, A., Mukhopadhyay, D., and Bhattacharya, S. (2019). AFM study: Cell cycle and probe geometry influences nanomechanical characterization of Panc1 cells. *Biochim. Biophys. Acta Gen. Subj.* 1863, 802–812. doi: 10.1016/j.bbagen.2019.02.006

Kumar, S., and Weaver, V. M. (2009). Mechanics, malignancy, and metastasis: The force journey of a tumor cell. *Cancer Metastasis Rev.* 28, 113–127. doi: 10.1007/s10555-008-9173-4

Kuznetsova, T. G., Starodubtseva, M. N., Yegorenkov, N. I., Chizhik, S. A., and Zhdanov, R. I. (2007). Atomic force microscopy probing of cell elasticity. *Micron* 38, 824–833. doi: 10.1016/j.micron.2007.06.011

Lekka, M., Fornal, M., Pyka-Fościak, G., Lebed, K., Wizner, B., Grodzicki, T., et al. (2005). Erythrocyte stiffness probed using atomic force microscope. *Biorheology* 42, 307–317.

Leo, M., Di Giacinto, F., Nardini, M., Mazzini, A., Rossi, C., Porceddu, E., et al. (2020). Erythrocyte viscoelastic recovery after liver transplantation in a cirrhotic patient affected by spur cell anaemia. *J. Microsc.* 280, 287–296. doi: 10.1111/jmi.12958

Lu, P., Takai, K., Weaver, V. M., and Werb, Z. (2011). Extracellular matrix degradation and remodeling in development and disease. *Cold Spring Harb. Perspect. Biol.* 3:a005058. doi: 10.1101/cshperspect.a005058

Lucas, H. R., and Rifkind, J. M. (2013). Considering the vascular hypothesis of Alzheimer's disease: Effect of copper associated amyloid on red blood cells. *Adv. Exp. Med. Biol.* 765, 131–138. doi: 10.1007/978-1-4614-4989-8_19

Maciaszek, J. L., and Lykotrafitis, G. (2011). Sickle cell trait human erythrocytes are significantly stiffer than normal. *J. Biomech.* 44, 657–661. doi: 10.1016/j.jbiomech.2010.11.008

MacIaszek, J. L., Andemariam, B., and Lykotrafitis, G. (2011). Microelasticity of red blood cells in sickle cell disease. *J. Strain Anal. Eng. Des.* 44, 657–661. doi: 10.1177/0309324711398809

Mazzini, A., Palermo, F., Pagliei, V., Romanò, S., Papi, M., Zimatore, G., et al. (2020). A time-dependent study of nano-mechanical and ultrastructural properties of internal limiting membrane under ocriplasmin treatment. *J. Mech. Behav. Biomed. Mater.* 110:103853. doi: 10.1016/j.jmbbm.2020.103853

McKhann, G. M., Knopman, D. S., Chertkow, H., Hyman, B. T., Jack, C. R., Kawas, C. H., et al. (2011). The diagnosis of dementia due to Alzheimer's disease: Recommendations from the National Institute on Aging-Alzheimer's Association workgroups on diagnostic guidelines for Alzheimer's disease. *Alzheimers Dement.* 7, 263–269. doi: 10.1016/j.jalz.2011.03.005

Metz, C. E. (1978). Basic principles of ROC analysis. *Semin. Nucl. Med.* 8, 283–298. doi: 10.1016/S0001-2998(78)80014-2

Minelli, E., Ciasca, G., Sassun, T. E., Antonelli, M., Palmieri, V., Papi, M., et al. (2017). A fully-automated neural network analysis of AFM force-distance curves for cancer tissue diagnosis. *Appl. Phys. Lett.* 111:143701. doi: 10.1063/1.4996300

Minelli, E., Sassun, T. E., Papi, M., Palmieri, V., Palermo, F., Perini, G., et al. (2018). Nanoscale mechanics of brain abscess: An Atomic Force Microscopy study. *Micron* 113, 34–40. doi: 10.1016/j.micron.2018.06.012

Mohanty, J. G., Shukla, H. D., Williamson, J. D., Launer, L. J., Saxena, S., and Rifkind, J. M. (2010). Alterations in the red blood cell membrane proteome in Alzheimer's subjects reflect disease-related changes and provide insight into altered cell morphology. *Proteome Sci.* 8:11. doi: 10.1186/1477-5956-8-11

Montis, C., Salvatore, A., Valle, F., Paolini, L., Carlà, F., Bergese, P., et al. (2020). Biogenic supported lipid bilayers as a tool to investigate nano-bio interfaces. *J. Colloid Interface Sci.* 570, 340–349. doi: 10.1016/j.jcis.2020.03.014

Moreno-Flores, S., Benitez, R., Vivanco, M. D. M., and Toca-Herrera, J. L. (2010). Stress relaxation and creep on living cells with the atomic force microscope: A means to calculate elastic moduli and viscosities of cell components. *Nanotechnology* 21:445101. doi: 10.1088/0957-4484/21/44/445101

Nakagawa, K., Kiko, T., Kuriwada, S., Miyazawa, T., Kimura, F., and Miyazawa, T. (2011). Amyloid β induces adhesion of erythrocytes to endothelial cells and affects endothelial viability and functionality. *Biosci. Biotechnol. Biochem.* 75, 2030–2033. doi: 10.1271/bbb.110318

Napodano, C., Callà, C., Fiorita, A., Marino, M., Taddei, E., Di Cesare, T., et al. (2021). Salivary biomarkers in COVID-19 patients: Towards a wide-scale test for monitoring disease activity. *J. Pers. Med.* 11:385. doi: 10.3390/jpm11050385

Ngan, A. H. W., Wang, H. T., Tang, B., and Sze, K. Y. (2005). Correcting power-law viscoelastic effects in elastic modulus measurement using depth-sensing indentation. *Int. J. Solids Struct.* 42, 1831–1846. doi: 10.1016/j.ijsolstr.2004.07.018

Nguyen, L. T. P., and Liu, B. H. (2022). Machine learning approach for reducing uncertainty in AFM nanomechanical measurements through selection of appropriate contact model. *Eur. J. Mech.* 94:104579. doi: 10.1016/j.euromechsol.2022.104579

Nievergelt, A. P., Erickson, B. W., Hosseini, N., Adams, J. D., and Fantner, G. E. (2015). Studying biological membranes with extended range high-speed atomic force microscopy. *Sci. Rep.* 5:11987. doi: 10.1038/srep11987

Okamura, N., Harada, R., Furumoto, S., Arai, H., Yanai, K., and Kudo, Y. (2014). Tau PET imaging in Alzheimer's disease. *Curr. Neurol. Neurosci. Rep.* 14:500. doi: 10.1007/s11910-014-0500-6

Passeri, D., Bettucci, A., Biagioni, A., Rossi, M., Alippi, A., Tamburri, E., et al. (2009). Indentation modulus and hardness of viscoelastic thin films by atomic force microscopy: A case study. *Ultramicroscopy* 109, 1417–1427. doi: 10.1016/j.ultramic.2009.07.008

Perini, G., Ciasca, G., Minelli, E., Papi, M., Palmieri, V., Maulucci, G., et al. (2019). Dynamic structural determinants underlie the neurotoxicity of the N-terminal tau 26-44 peptide in Alzheimer's disease and other human tauopathies. *Int. J. Biol. Macromol.* 141, 278–289. doi: 10.1016/j.ijbiomac.2019.08.220

Pichiecchio, A., Alessandrino, F., Bortolotto, C., Cerica, A., Rosti, C., Raciti, M. V., et al. (2018). Muscle ultrasound elastography and MRI in preschool children with Duchenne muscular dystrophy. *Neuromuscul. Disord.* 28, 476–483. doi: 10.1016/j.nmd.2018.02.007

Pretorius, E. (2013). The adaptability of red blood cells. *Cardiovasc. Diabetol.* 12, 63. doi: 10.1186/1475-2840-12-63

Pretorius, E., and Kell, D. B. (2014). Diagnostic morphology: Biophysical indicators for iron-driven inflammatory diseases. *Integr. Biol. (United Kingdom)* 6, 486–510. doi: 10.1039/c4ib00025k

Pretorius, E., Bester, J., Vermeulen, N., Alummoottil, S., Soma, P., Buys, A. V., et al. (2015). Poorly controlled type 2 diabetes is accompanied by significant morphological and ultrastructural changes in both erythrocytes and in thrombingenerated fibrin: Implications for diagnostics. *Cardiovasc. Diabetol.* 14, 30. doi: 10.1186/s12933-015-0192-5

R Development Core Team (2016). *A Language and Environment for Statistical Computing*. Vienna: R Foundation for Statistical Computing.

Rianna, C., and Radmacher, M. (2016). "Cell mechanics as a marker for diseases: Biomedical applications of AFM," in *Proceedings of the AIP Conference Proceedings*, Vol. 1760, p. 020057. doi: 10.1063/1.4960276

Rianna, C., and Radmacher, M. (2017). Comparison of viscoelastic properties of cancer and normal thyroid cells on different stiffness substrates. *Eur. Biophys. J.* 46, 309–324. doi: 10.1007/s00249-016-1168-4

Ridolfi, A., Brucale, M., Montis, C., Caselli, L., Paolini, L., Borup, A., et al. (2020). AFM-based high-throughput nanomechanical screening of single extracellular vesicles. *Anal. Chem.* 92, 10274–10282. doi: 10.1021/acs.analch

Romanò, S., Di Giacinto, F., Primiano, A., Mazzini, A., Panzetta, C., Papi, M., et al. (2020). Fourier transform infrared spectroscopy as a useful tool for the automated classification of cancer cell-derived exosomes obtained under different culture conditions. *Anal. Chim. Acta* 1140, 219–227. doi: 10.1016/j.aca.2020.09.037

Shieh, A. C. (2011). Biomechanical forces shape the tumor microenvironment. *Ann. Biomed. Eng.* 39, 1379–1389. doi: 10.1007/s10439-011-0252-2

Snyder, H. M., Carrillo, M. C., Grodstein, F., Henriksen, K., Jeromin, A., Lovestone, S., et al. (2014). Developing novel blood-based biomarkers for Alzheimer's disease. *Alzheimers Dement.* 10, 109–114. doi: 10.1016/j.jalz.2013.10.007

Sokolov, I., Dokukin, M. E., Kalaparthi, V., Miljkovic, M., Wang, A., Seigne, J. D., et al. (2018). Noninvasive diagnostic imaging using machine-learning analysis of nanoresolution images of cell surfaces: Detection of bladder cancer. *Proc. Natl. Acad. Sci. U.S.A.* 115, 12920–12925. doi: 10.1073/pnas.1816459115

Suresh, S. (2007). Biomechanics and biophysics of cancer cells. *Acta Mater.* 55, 3989–4014. doi: 10.1016/j.actamat.2007.04.022

Suresh, S., Spatz, J., Mills, J. P., Micoulet, A., Dao, M., Lim, C. T., et al. (2005). Connections between single-cell biomechanics and human disease states: Gastrointestinal cancer and malaria. *Acta Biomater.* 1, 15–30. doi: 10.1016/j.actbio.2004.09.001

Swaminathan, V., Mythreye, K., Tim O'Brien, E., Berchuck, A., Blobe, G. C., and Superfine, R. (2011). Mechanical stiffness grades metastatic potential in patient tumor cells and in cancer cell lines. *Cancer Res.* 71, 5075–5080. doi: 10.1158/0008-5472.CAN-11-0247

Tomaiuolo, G. (2014). Biomechanical properties of red blood cells in health and disease towards microfluidics. *Biomicrofluidics* 8:e051501. doi: 10.1063/1.4895755

Tombaugh, T. N., and McIntyre, N. J. (1992). The mini-mental state examination: A comprehensive review. *J. Am. Geriatr. Soc.* 40, 922–935. doi: 10.1111/j.1532-5415.1992.tb01992.x

van Oijen, M., Hofman, A., Soares, H. D., Koudstaal, P. J., and Breteler, M. M. (2006). Plasma Aβ1-40 and Aβ1-42 and the risk of dementia: A prospective case-cohort study. *Lancet Neurol.* 5, 655–660.

Van Zwieten, R. W., Puttini, S., Lekka, M., Witz, G., Gicquel-Zouida, E., Richard, I., et al. (2014). Assessing dystrophies and other muscle diseases at the nanometer scale by atomic force microscopy. *Nanomedicine* 9, 393–406. doi: 10.2217/NNM.12.215

Vielmuth, F., Schumann, R. G., Spindler, V., Wolf, A., Scheler, R., Mayer, W. J., et al. (2016). Biomechanical properties of the internal limiting membrane after intravitreal ocriplasmin treatment. *Ophthalmologica* 235, 233–240. doi: 10.1159/000444508

Von Tempelhoff, G. F., Schelkunov, O., Demirhan, A., Tsikouras, P., Rath, W., Velten, E., et al. (2016). Correlation between blood rheological properties and red blood cell indices(MCH, MCV, MCHC) in healthy women. *Clin. Hemorheol. Microcirc.* 62, 45–54. doi: 10.3233/CH-151944

Wang, A., Vijayraghavan, K., Solgaard, O., and Butte, M. J. (2016). Fast stiffness mapping of cells using high-bandwidth atomic force microscopy. *ACS Nano* 10, 257–264. doi: 10.1021/acsnano.5b03959

Weaver, V. M. (2017). Cell and tissue mechanics: The new cell biology frontier. *Mol. Biol. Cell* 28, 1815–1818. doi: 10.1091/mbc.e17-05-0320

Wojsiat, J., Laskowska-Kaszub, K., Mietelska-Porowska, A., and Wojda, U. (2017). Search for Alzheimer's disease biomarkers in blood cells: Hypotheses-driven approach. *Biomark. Med.* 11, 917–931. doi: 10.2217/bmm-2017-0041

Zhang, H., Guo, Y., Zhou, Y., Zhu, H., Wu, P., Wang, K., et al. (2020). Fluidity and elasticity form a concise set of viscoelastic biomarkers for breast cancer diagnosis based on Kelvin–Voigt fractional derivative modeling. *Biomech. Model. Mechanobiol.* 19, 2163–2177. doi: 10.1007/s10237-020-01330-7

frontiers | Frontiers in Molecular Neuroscience

TYPE Review
PUBLISHED 06 October 2022
DOI 10.3389/fnmol.2022.1011225

OPEN ACCESS

EDITED BY
Jiehui Jiang,
Shanghai University, China

REVIEWED BY
Francesca Massenzio,
Università di Bologna, Italy
Sun Young Park,
Pusan National University, South Korea

*CORRESPONDENCE
Avnesh S. Thakor
asthakor@stanford.edu

SPECIALTY SECTION
This article was submitted to Brain Disease Mechanisms, a section of the journal Frontiers in Molecular Neuroscience

RECEIVED 04 August 2022
ACCEPTED 20 September 2022
PUBLISHED 06 October 2022

CITATION
Regmi S, Liu DD, Shen M, Kevadiya BD, Ganguly A, Primavera R, Chetty S, Yarani R and Thakor AS (2022) Mesenchymal stromal cells for the treatment of Alzheimer's disease: Strategies and limitations. *Front. Mol. Neurosci.* 15:1011225. doi: 10.3389/fnmol.2022.1011225

Mesenchymal stromal cells for the treatment of Alzheimer's disease: Strategies and limitations

Shobha Regmi, Daniel Dan Liu, Michelle Shen, Bhavesh D. Kevadiya, Abantika Ganguly, Rosita Primavera, Shashank Chetty, Reza Yarani and Avnesh S. Thakor*

Department of Radiology, Interventional Radiology Innovation at Stanford (IRIS), Stanford University, Palo Alto, CA, United States

Alzheimer's disease (AD) is a major cause of age-related dementia and is characterized by progressive brain damage that gradually destroys memory and the ability to learn, which ultimately leads to the decline of a patient's ability to perform daily activities. Although some of the pharmacological treatments of AD are available for symptomatic relief, they are not able to limit the progression of AD and have several side effects. Mesenchymal stem/stromal cells (MSCs) could be a potential therapeutic option for treating AD due to their immunomodulatory, anti-inflammatory, regenerative, antioxidant, anti-apoptotic, and neuroprotective effects. MSCs not only secret neuroprotective and anti-inflammatory factors to promote the survival of neurons, but they also transfer functional mitochondria and miRNAs to boost their bioenergetic profile as well as improve microglial clearance of accumulated protein aggregates. This review focuses on different clinical and preclinical studies using MSC as a therapy for treating AD, their outcomes, limitations and the strategies to potentiate their clinical translation.

KEYWORDS

mesenchymal stromal cells, mesenchymal stem cells, Alzheimer's disease, microglia, neurons, neuroprotection

Introduction

Alzheimer's disease

Alzheimer's disease (AD) is a neurodegenerative disease and the leading cause of age-associated dementia. It is the eighth leading cause of death in the United States and affects approximately 6.2 million people while accounting for about $305 billion in healthcare costs annually (Wong, 2020). AD is characterized by progressive brain damage that slowly destroys memory and the ability to learn, which eventually

hinders patients in performing daily activities. Studies have identified three stages of AD progression: preclinical stage, mild cognitive impairment stage and dementia stage (No author list, 2021). The preclinical stage is of varied duration in which patients demonstrate no observable clinical symptoms but begin to exhibit early pathophysiological signs of AD, such as elevated amyloid-beta (Aβ) peptide and a reduction in glucose metabolism in the brain (No author list, 2021). However, while the brain can compensate for these early AD pathologies for an extent of time, the mild cognitive impairment stage is inevitably expressed as the disease progresses. Approximately one-third of patients with mild cognitive impairment then advance into the dementia stage within 5 years of symptom onset (No author list, 2021).

Alzheimer's disease can be stratified into two main types: early onset and late-onset AD. Late-onset AD, which is mostly comprised of sporadic AD, is typically diagnosed at age 65 and older, and accounts for about 90% of the total AD cases (Reitz et al., 2020). On the other hand, early onset AD accounts for 5–10% of AD cases and is typically diagnosed before the age of 65 (Reitz et al., 2020). While most AD cases are sporadic, approximately 1% of cases are familial, meaning that the patient inherited AD-inducing genetic mutations from their parents (van der Flier et al., 2011). These familial cases usually manifest as early onset AD and are commonly associated with genetic mutations in amyloid precursor protein (APP), presenilin 1 (PS1), and presenilin 2 (PS2) (Swerdlow, 2007; van der Flier et al., 2011).

Pathophysiology

Although the precise pathophysiology of AD remains inconclusive, the progressive accumulation of Aβ plaques and neurofibrillary tangles (NFTs), which are aggregates of hyperphosphorylated tau protein, have been identified as the primary hallmark of AD. The extracellular deposition of Aβ plaques and the intracellular formation of NFTs leads to synapse loss, dystrophic neurites, microgliosis, and astrogliosis, all of which contribute to AD-associated brain atrophy (Pini et al., 2016). Interestingly, the formation of Aβ plaques is spatially and temporally separated from NFTs (Busche et al., 2019). The aggregation of Aβ plaques is an early event in the AD trajectory and is observed in the preclinical stage, while the accumulation of NFTs occurs at a timepoint closer to the later stages of AD, when neuronal dysfunction and degeneration has begun to induce clinical symptoms (He et al., 2018). Moreover, Aβ plaque accumulation initiates in the neocortex and progresses into deeper brain regions, while NFT accumulation initiates in the medial temporal lobe and spreads outward toward the Aβ-rich neocortex (Busche et al., 2019).

In AD, neuronal loss is found to be focal, predominantly in the cortex and hippocampus regions. Thus, it has been suggested that the coexistence of Aβ plaques and NFTs correlates with AD-driven behavioral symptoms such as memory loss and impaired cognitive abilities. The onset of these symptoms are likely a result of synapse loss, failure to maintain axon and dendrite functions, as well as extensive neuronal damage and death in the cortex and hippocampal regions (Bloom, 2014). Therefore, the transition from the asymptomatic preclinical stage into symptomatic stages of AD may be associated with the propagation of tau pathology into the Aβ plaque-rich cortex, suggesting a collaborative interaction between the two aggregates toward AD progression (Busche et al., 2019).

The aggregation of misfolded proteins, such as Aβ plaques and NFTs, is involved in the pathophysiology of various neurodegenerative diseases. Chaperone proteins, which influence protein folding, can contribute to both AD protection and advancement. For instance, heat shock proteins (HSPs), mainly HSP70 and HSP90, have been described as chaperone proteins that play critical roles in neurodegenerative diseases (Martin-Pena et al., 2018; Gupta et al., 2020). While HSP70 facilitates the clearing and refolding of misfolded proteins in AD, HSP90 stabilizes the misfolded proteins, leading to augmentation of Aβ aggregation and neurodegeneration (Gupta et al., 2020). Based on this hypothesis, HSP70 inducers and HSP90 inhibitors may have therapeutic potential in clearing tau and Aβ aggregates (Gupta et al., 2020).

Genetic mutations account for familial AD cases. Mutations in APP, PS1, and PS2 alter normal APP processing and produce the neurotoxic Aβ oligomer that gives rise to Aβ-induced neurotoxicity and aggregation of Aβ plagues (Benilova et al., 2012). However, Aβ pathology is not the sole determinant of AD pathology, since disease onset is accompanied by the formation of NFTs in neurons. These intracellular aggregates are composed of hyperphosphorylated tau proteins and are associated with impaired microtubular cytoskeleton formation, synapse loss, and neurodegeneration (Alonso et al., 1996; Guillozet et al., 2003).

The interconnection between Aβ and tau pathology is demonstrated by the synergistic and correlative nature of amyloidosis and tau hyperphosphorylation, which are also interrelated in the induction of neural toxicity (Busche et al., 2019; Griner et al., 2019; Tripathi and Khan, 2020). An example of Aβ and tau interaction occurs in the mitochondria. Studies have shown that APP can be targeted to the mitochondria, and this mitochondria localization of APP correlates with AD adversity and only occurs in pathogenic brain areas of AD patients (Lin and Beal, 2006). The aggregated APP gets processed into the accumulative Aβ peptide by active γ-secretase complex, which leads to Aβ presence in the mitochondria. Aβ presence in the mitochondria then generates hyperphosphorylated tau proteins by interacting with mitochondrial Drp1 protein, which, in turn, disrupts microtubule function and induces neural toxicity (Manczak et al., 2011; Manczak and Reddy, 2012). Mitochondrial Aβ can also interact with Aβ–binding alcohol dehydrogenase (ABAD),

leading to mitochondrial dysfunction and the production of reactive oxygen species (ROS) (Lin and Beal, 2006).

The main consequence of mitochondrial dysfunction, ROS accumulation and increased oxidative stress, serve as the major factors involved in AD pathogenesis. Postmortem studies in AD brains have found evidence of oxidative stress in the form of lipid peroxidation, DNA, RNA, and protein oxidation, and decreased antioxidant enzymes (Marcus et al., 1998; Pratico, 2008). This evidence supports the oxidative stress hypothesis as a significant mechanism of AD-induced neurodegeneration and neuron death (Marcus et al., 1998; Pratico, 2008). In fact, both Aβ aggregation and tau hyperphosphorylation can directly increase oxidative stress, since Aβ can act as an oxidant while hyperphosphorylated tau induces neuroinflammation and the consequent microglial ROS production (Nunomura et al., 2006; Alavi Naini and Soussi-Yanicostas, 2015; Cheignon et al., 2018).

Interestingly, postmortem analysis of AD brains from 20 AD patients also identified breakdown of the blood-brain barrier (BBB) (Nelson et al., 2016), likely due to pericyte detachment and degradation that is also observed during AD pathology. The loss of pericytes contribute to reduced BBB and dysregulated BBB transport, which increases the amount of vascular infiltrate entering the brain. Since soluble Aβ peptide is regularly transported across the BBB under normal physiological conditions, the disruption of BBB transport alters the balance between the efflux and influx of Aβ peptides, thereby contributing to reduced Aβ clearance, increased Aβ burden, and the formation of extracellular Aβ plaques in the brain (Deane et al., 2009). Downregulated glucose transport to the brain during AD progression also accelerates BBB breakdown and Aβ pathology, since the loss of glucose contributes to an energy deficiency that induces neuron necrosis and the resulting neuroinflammation (Nelson et al., 2016; Montagne et al., 2017).

Breakdown of the BBB leads to capillary leakage, which fosters neuronal death and injury *via* the accumulation of vascular-origin neurotoxic products in the brain. These neurotoxic products include RBC-derived hemoglobin, immunoglobulins, fibrinogen, thrombin, and plasminogen. Free Fe^{2+} from the vasculature can cause further ROS generation, and an increase in oxidative stress. In addition, the entry of albumin from the vasculature to the brain can inhibit blood flow, which contributes to ischemia or hypoxia-induced edema (Zlokovic, 2011). The BBB breakdown enhances neuroinflammation by enabling neutrophils and other immune cells to enter the brain (Zenaro et al., 2015). Enhanced neuroinflammation fosters neurotoxicity by producing ROS from activated immune cells, which causes synapse loss and neuronal damage and ultimately death (Schain and Kreisl, 2017). However, not all neuroinflammation is neurotoxic, and transient neuroinflammation and mobilization of blood-borne myeloid cells to the CNS during early stages of neural damage can have a neuroprotective effect. Alleviation of cognitive symptoms in an AD mouse model has been achieved by blockade of programmed cell death receptor 1 (PD-1/PD-L1), which induces a systemic immune response and enhances recruitment of monocyte-derived macrophages to the brain (Rosenzweig et al., 2019). However, even though immune enhancement achieved by checkpoint blockade has the potential to alleviate both Aβ and tau pathologies in some cases of AD, PD-1 blockade in another study failed to increase the infiltration of monocyte-derived macrophages into the brain and was unable to alter the Aβ burden (Baruch et al., 2016; Latta-Mahieu et al., 2018; Rosenzweig et al., 2019). Thus, additional neuroimmunology mechanisms and treatment options should be considered better to elucidate the role of neuroinflammation in AD pathology.

Current treatment approaches

There are currently two major approaches to AD intervention: symptomatic treatment, and disease-modifying therapy. These interventions are mainly recognized as pharmacological or cellular treatments.

Pharmacological treatments

Pharmacological AD treatment mainly utilizes psychotropic drugs that aim to alleviate behavioral and cognitive AD symptoms such as dementia. For instance, acetylcholinesterase (AChE) inhibitors, responsible for increasing the expression and half-life of the acetylcholine neurotransmitter, have been used to improve AD-induced cognitive function. AChE inhibitors such as rivastigmine, galantamine and donepezil, and NMDA-receptor antagonists like memantine, have been approved by the FDA for AD treatment (Alzheimer's Association, 2019). However, these drugs are not able to limit the progression of AD and have several side effects. Thus, there is need for development of a molecule that can target multiple factors involved in AD.

Recently, therapies utilizing APP inhibitors, ROS inhibitors, anti-inflammatory, and anti-tau factors have been proposed as potential treatments for AD (Scarpini et al., 2003; Cummings et al., 2019; Xie et al., 2020). However, their efficacy remains uncertain, since some of them are still undergoing clinical trials while others have failed to demonstrate therapeutic efficacy in clinical settings. Recently, a monoclonal antibody targeted against Aβ (aducanumab) was approved for treating AD in the United States; however, the approval was highly controversial due to a lack of evidence that the drug is effective (Rabinovici, 2021).

Cell therapy

In contrast to the symptom-oriented approach of pharmacological therapies, cell therapy aims to target the origin of AD pathologies by replacing lost neurons, clearing toxic aggregates, stimulating neuronal precursors, and enhancing neuroprotection (Si and Wang, 2021). Cell therapy typically utilize stem cells, chosen for their multilineage differentiation and self-renewal capacities. Under the umbrella of the cell

therapies are two main therapeutic strategies. The first seeks to directly supply new neurons *via* engraftment and differentiation of transplanted stem cells (i.e., cell replacement therapy). The second relies on the transplanted cells' ability to release soluble factors that indirectly stimulate endogenous neural regeneration or promote neuroprotection. Various pre-clinical research and clinical trials have been conducted to determine the therapeutic efficacy of stem cell-based therapies for intractable neurodegenerative diseases like AD.

Different types of stem cells have been utilized for cell therapy in AD. Cell replacement therapies rely on transplanted cells engrafting and differentiating into neuronal fates, and thus must use competent cells to give rise to neurons. These include induced pluripotent stem cells (iPS), embryonic stem cells (ES), and neural stem cells (NSCs). However, ES and iPS cells have inherent risks of teratoma formation and immune rejection. Additionally, transplanted cells would have to demonstrate robust engraftment and site-appropriate neuronal differentiation and synaptic integration, which has not been achieved. Due to these difficulties, some have given up on direct engraftment of stem cells and have turned instead to the ability of adult stem cells to stimulate endogenous neural regeneration *via* paracrine effects. Mesenchymal stem/stromal cells (MSCs) have been a popular platform for cell therapy in general. While they are not competent to give rise to neural cell types by themselves, they have been described to have anti-inflammatory and immunomodulatory properties. Preclinical studies have reported the therapeutic efficacy of MSC-based therapies, and several clinical trials have explored the potential of clinically translating these therapies.

Characteristics of mesenchymal stem/stromal cells

When they were first discovered, MSCs were recognized as a subcomponent of the bone marrow (BM) cell population. They were defined by the International Society of Cellular Therapy (ISCT) as adherent fibroblastic cells that can differentiate into osteocytes, chondrocytes, and adipocytes (Dominici et al., 2006). In addition, MSCs express cell surface markers such as CD105, CD73, and CD90, and do not express CD45, CD19, CD11b, and HLA-DR surface molecules (Dominici et al., 2006; Maleki et al., 2014). MSCs cannot be characterized by the expression of a single, specific marker, and they behave differently under different conditions like hypoxia and inflammation. The metabolic profile, secretomes, and proteome of MSCs may also vary based on their origin, culture conditions and microenvironment. These environment and origin-based variations make it challenging to identify and characterize MSCs, and the criteria provided by ISCT might not be enough for the proper characterization of MSCs (Maleki et al., 2014). Indeed, it is generally agreed that MSCs are not a coherent cell type, but rather a mix of various stem, progenitor, and mature cell types. Despite these issues, MSCs have remained popular for cellular therapy research, as they are easy to obtain and expand *in vitro*.

Applications of mesenchymal stem/stromal cells and mesenchymal stem/stromal cell-derived therapeutics

Mesenchymal stem/stromal cells have been established as an important platform for cell therapy for treating various injuries and illnesses. Several clinical trials have been conducted to assess the therapeutic efficacy of MSC-derived therapies for a variety of diseases, but only 9 hMSC-based products have acquired legal approval for clinical application. In South Korea, Cellgram AMI, Cartistem, Cupistem, and Neuronata-R have been approved for the treatment of myocardial infarction, cartilage defects, Crohn's diseases and amyotrophic lateral sclerosis, respectively. Similarly, Prochymal, an intravenous formulation of mesenchymal stem cells, has been approved in Canada, New Zealand, and Australia while TEMCELLS has been approved in Japan for the treatment of acute graft versus host disease (GVHD). Recently, STEMIRAC and Stempeucel have been approved for the treatment of spinal cord injury and Buerger's disease-induced critical limb ischemia, respectively (Lopez-Beas et al., 2020). Some of these commercial MSC-based therapeutics have shown beneficial effects whereas the results of a few other products have not been published yet.

Therapeutic potential of mesenchymal stem/stromal cells for AD treatment

Neurodegenerative diseases, like AD, are characterized by abnormal protein aggregation leading to neuroinflammation and neuronal cell damage. The neuronal loss leads to synaptic dysfunction that fosters clinical symptoms such as memory, cognitive, and behavioral impediments (No author list, 2021). MSC-based therapies have been investigated as a cell therapy for AD due the paracrine ability of MSCs to secrete growth factors, anti-inflammatory proteins, membrane receptors, and microRNAs (miRNA) that aid in the reduction of neuronal loss by blocking apoptosis and increasing neurogenesis, synaptogenesis, and angiogenesis (Nooshabadi et al., 2018).

Mesenchymal stem/stromal cells are commonly derived from bone marrow and adipose tissues, and are capable of secreting factors that promote recruitment, proliferation and differentiation of other neural stem cells. Their role as an antioxidant coupled with their anti-apoptotic effects foster the inhibition of neuronal cell death, and secrets growth factors,

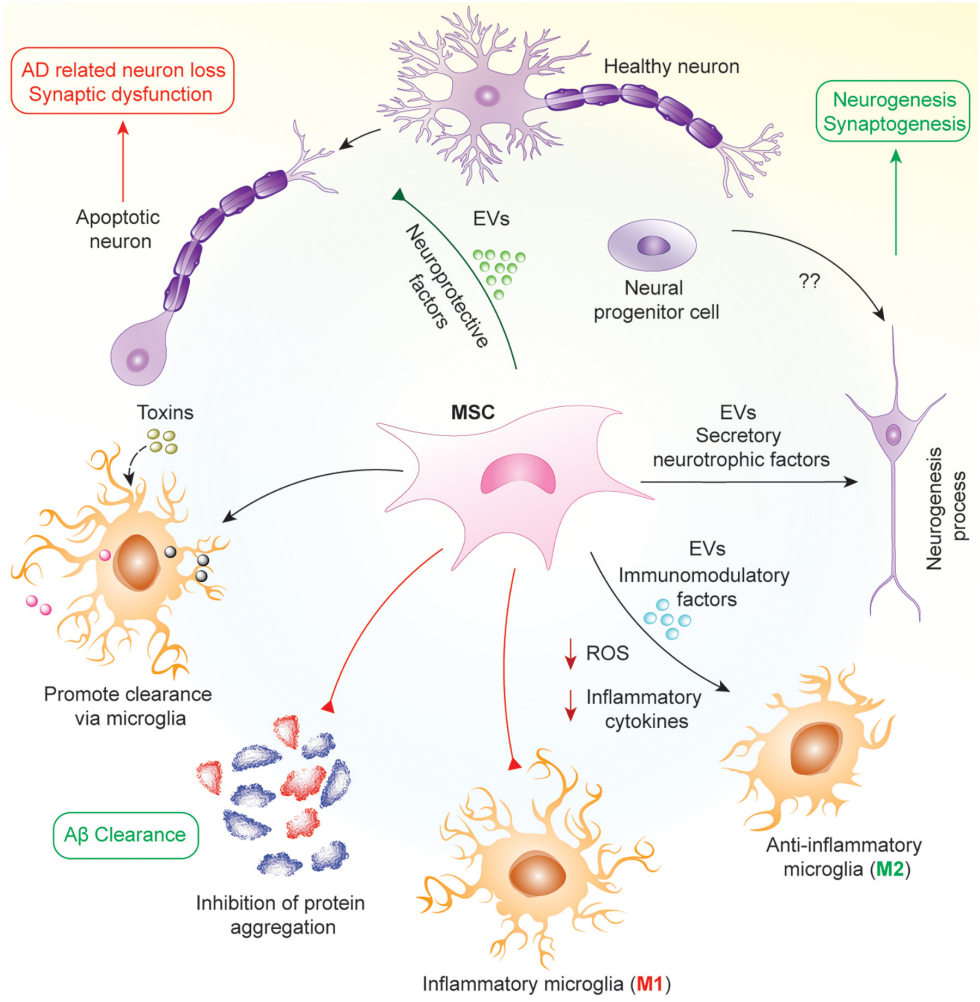

FIGURE 1
Mechanism of protective effects of MSCs in AD. In AD, neuronal loss and synaptic dysfunction occur due to the apoptosis of neurons by accumulating different proteins such as Aβ and hyperphosphorylated tau. MSCs work in pleiotropic mechanisms in this pathology to attenuate AD *via* secretion of various neuroprotective and neurotrophic factors such as VEGF, GDNF, BDNF, and several miRNAs in soluble or insoluble form as EVs. As a result, MSCs help in the clearance of aggregated proteins by increasing microglial phagocytosis, reprogramming microglia into anti-inflammatory phenotype, attenuating oxidative stress and neuronal apoptosis, and promoting neurogenesis from neural progenitor cells.

such as brain-derived neurotrophic factor (BDNF) and glial cell line-derived neurotrophic factor (GDNF), to promote neurogenesis *via* the stimulation of neural progenitor cells (Harris et al., 2012; Van Velthoven et al., 2012; Reza-Zaldivar et al., 2018). In addition, MSCs exert immunomodulatory effects by inhibiting the activation of inflammatory microglia (M1) and promoting the activation of the anti-inflammatory microglia (M2) to prevent further tissue damage induced by chronic neuroinflammation. MSCs also accelerate the accumulation of microglia around Aβ deposits to promote Aβ clearance, and studies have revealed that MSCs can enhance activation of autophagy, which might be responsible for lysosomal clearance of Aβ plaques (Shin et al., 2014; Yokokawa et al., 2019; **Figure 1**).

In early stage AD, there is aggregation of Aβ and inefficient clearance of these aggregates resulting in the formation of amyloid plaques. In mid-stage AD, there is the formation of neuro-fibrillary tangles and neuronal cell death due to these aggregates. Finally, in late-stage AD, there is inflammation and oxidative stress mediated by reactive microglia. Hence, the mechanism by which MSCs work will be dependent on the stage of the disease in which they are being used. In early and mid-stages, MSCs will work to inhibit Aβ generation and promote its effective clearance, alter APP processing, decrease tau phosphorylation and increase proteasomal activity resulting in reduced accumulation of ubiquitin-conjugated proteins (Lee et al., 2017; Mendonça et al., 2019; Neves et al., 2021). In later stages, their effects will be more geared toward

microglial reprograming, reducing the number of reactive microglia in the brain and promoting anti-inflammatory/anti-oxidant strategies (Cui et al., 2017; Zhao et al., 2018; Peruzzaro et al., 2019). Furthermore, MSCs have also been shown to promote microglia and autophagy mediated clearance of protein aggregates including Aβ (Kim et al., 2012; Shin et al., 2014; Yokokawa et al., 2019). Throughout all stages of AD, MSCs are able to protect neurons from cell death *via* secretion of different neuroprotective factors, growth factors and, mitochondrial transfer (Cui et al., 2017; Wang et al., 2018; Zhang et al., 2020). Hence, MSCs have multiple effects based on the disease condition, with their activity determined by the surrounding microenvironment in which they finally reside following their administration.

As stated earlier, the anti-inflammatory, immunomodulatory, and neuro-regenerative aspects of MSCs highlight them as potential therapeutics for AD. The therapeutic potential of MSCs has been suggested by various studies, in which intravenous injection of placenta-derived MSCs in Aβ-infused mice significantly inhibited neuroinflammation while improving cognitive function (Yun et al., 2013). The intravenous delivery of human umbilical cord mesenchymal stem cells (UC-MSCs) in transgenic AD mice (Tg2576) inhibited oxidative stress while fostering neuro-repair and neurogenesis (Cui et al., 2017). The therapeutic effect of UC-MSC engraftment was enhanced when UC-MSCs were treated with resveratrol, which is an activator that has been suggested to rejuvenate and improve the survival and differentiation of resident stem cells (Gorbunov et al., 2012; Wang et al., 2018). In addition, Aβ accumulation was significantly decreased by UC-MSC infusion (Lykhmus et al., 2019). Aβ deposition in the hippocampus and cortex regions of APP/PS1 mice was reduced after intra-carotid arterial injection of UC-MSCs, which is also associated with improved cognitive function *in vivo* (Boutajangout et al., 2017).

In addition to UC-MSCs, those from other sites of origin have also demonstrated therapeutic efficacy for AD. For instance, stereotactic injection of amniotic MSCs into bilateral hippocampi of APP/PS1 mice significantly stimulated microglial activation and phagocytic activity, resulting in Aβ clearance, neurogenesis and cognitive improvement (Zheng et al., 2017). Intracerebral injection of menstrual blood-derived MSCs correlates with reduced BACE1 (β-APP cleaving enzyme 1) and β-CTF in the cortex and hippocampus of APP/PS1 mice, suggesting an inhibition of β-secretase activity that diminished the formation of Aβ plagues (Zhao et al., 2018). Preclinical studies on the effectiveness of MSC-derived treatments in AD are listed in **Table 1**.

Despite the effectiveness of MSC-based therapies in preclinical studies, they have largely failed to be clinically translated. Although MSC therapies are feasible, safe, and well tolerated when delivered into the brain *via* stereotactic injection, a recent clinical trial found minimal therapeutic improvements in a 24-month follow-up period (Kim H. J. et al., 2015). Nevertheless, this phase 1 study paved way for further evaluation of MSC therapies in larger cohorts with long-term follow-up, and many clinical trials are currently being conducted in AD patients. In another clinical trial, a single dose I.V. injection of MSCs showed improvement in inflammation and neurocognitive function compared to a placebo (Oliva et al., 2021; Brody et al., 2022; **Table 2**). The dose of MSCs *via* stereotactic injection into the hippocampus was 3-to-33 times less than the clinical trial with I.V. injection. Both of these clinical trials support the potential of MSCs in treating AD. However, the variation in doses, MSCs source, disease onset time, route of delivery, and small study population hinder any definitive conclusions. Nevertheless, local injection of MSCs might be an effective strategy in decreasing the dose of MSCs being used for therapy due to minimal loss in the systemic circulation.

Impact of mesenchymal stem/stromal cells on neurons and neural progenitor cells

Mesenchymal stem/stromal cells are involved in neuroprotection *via* the secretion of anti-inflammatory cytokines and anti-apoptotic, angiogenic, and neurotrophic factors. Direct contact between primary neurons and MSCs is believed to enhance the long-term survival of neurons and may play a vital role in neuronal maturation and differentiation (Scuteri et al., 2006). Furthermore, MSCs have been shown to prevent oxidative stress in neurons as well as Aβ/tau-induced toxicity by clearing Aβ or tau *via* autophagy activation, increasing proteasome activity and promoting microglial phagocytosis (Yan et al., 2014b; Lee et al., 2017; Zhao et al., 2018; Neves et al., 2021; Santamaria et al., 2021). It had been postulated that MSCs could transdifferentiate into neuron-like cells, which would serve as an asset in AD therapies (Yang et al., 2013). The differentiation of MSCs into a neuronal lineage is still controversial, even though some research shows the ability of MSCs to differentiate into neural-like cells (Scuteri et al., 2011a; Divya et al., 2012; Jeong et al., 2013; Feng et al., 2014; Haragopal et al., 2015; Joe et al., 2015; Hernández et al., 2020; Zhou et al., 2020). Interestingly, a study by Lu et al. showed morphological and immunocytochemical changes in MSCs after their exposure to a medium for neuronal induction and differentiation, which they attributed to not be the consequence of true neuronal differentiation but rather a biological response to chemical stress (Lu et al., 2004). In another study, it was shown that newly generated neuronal cells regained their MSC morphology as soon as the neuronal induction therapy stopped, indicating that this change is reversible in many instances (Lukomska et al., 2019). Other studies have also

TABLE 1 Application of MSCs for Alzheimer's disease in preclinical models.

Source	Dose	Route	Animal model	Major targets	Results	Reference
Human placental MSCs	1×10^5, 5×10^5, and 1×10^6	I.V.	$A\beta_{1-42}$ infused mouse	APP, BACE1, Aβ, β-secretase, and γ-secretase activity	Improved cognitive function (MWM); decreased Aβ, APP, and BACE levels; decreased astrocyte and microglia area; decreased expression of iNOS, COX2; decreased hippocampal apoptosis; increased hippocampal neurogenesis (DCX^+)	Yun et al., 2013
Human UC-MSCs	1×10^6	I.V.	STZ-induced rats	Reactive microglia	Improved cognitive function (BMT, OFT, and MBT); restored hippocampal volume and neuron density; no restoration of hippocampal neurogenesis (DCX^+); no change in astrocyte or microglia area; the decreased proportion of reactive microglia (by morphology); modestly increased expression of some synaptic proteins (SYT1, SYP, and GAD65).	Villar et al., 2020
Rat AD-MSCs primed with melatonin (MT)	1×10^6	I.V.	Aβ-injected rat model	Aβ clearance	Improved cognitive function (NORT, OFT, EPM, PAL, and MWM), melatonin priming further improved performance on some tests (NORT, MWM, and PAL); decreased Aβ deposits; decreased microglial density.	Nasiri et al., 2019
Human UC-MSCs	2×10^6	I.V.	Tg2576 mice	Oxidative stress	Improved cognitive function (MWM); no change in hippocampal Aβ; decreased oxidative stress; increased expression of BDNF, Sirt1, and SYN in the hippocampus.	Cui et al., 2017
Human UC-MSCs, plus oral administration of resveratrol	1×10^6 administered every 2 weeks for 2 months	I.V.	Tg2576 mice	Oxidative stress and senescence	Increased hippocampal engraftment with resveratrol (3-fold); improved cognitive function (MWM); decreased hippocampal apoptosis; increased hippocampal neurogenesis (Nestin+/βIII $tubulin^+$) and neuron density; increased expression of BDNF, NGF, NT-3, and Sirt1 in the hippocampus; effects generally enhanced with resveratrol.	Wang et al., 2018
Human UC-MSCs, mouse placental MSCs	1×10^6	I.V.	LPS-induced mice	nicotinic acetylcholine receptors, Aβ accumulation, mitochondria	Improved cognitive function (NORT); decreased Aβ levels; qualitatively increased numbers of microglia and astrocytes.	Lykhmus et al., 2019
Human amniotic MSCs	1×10^6	Intracerebral (bilateral hippocampus)	APP/PS1 mice	Aβ plague clearance	Improved cognitive function (MWM); reduced Aβ deposits; increased microglia area and activation ($ED1^+$); decreased expression of TNF-α, IL-1β, increased expression of IL-10, TGF-β in the brain; increased expression of IDE, NEP, BDNF; increased hippocampal neurogenesis (DCX^+, $BrdU^+/NeuN^+$); increased dendritic spine density in cortical and hippocampal neurons.	Zheng et al., 2017
CM of rat AD-MSCs cultured in hypoxic condition	200 μL CM administered eight times at 1-day intervals	Intraperitoneal	Intra-hippocampal $A\beta_{1-40}$ injected rats	Neurotrophic and anti-inflammatory factors	Improved cognitive function (MWM and NORT); increased hippocampal neuron density; decreased hippocampal Aβ deposits; decreased expression of TLR2, TLR4, IL-1β, and TNF-α	Mehrabadi et al., 2020
Human UC-MSCs	1×10^6	I.V. and I.C.V.	Intra-hippocampal $A\beta_{1-42}$ injected rats	Promoting cholinergic function of neurons	Marginally improved homing to hippocampus with magnetic guidance (non-significant); improved cognitive function (PAL and MWM); increased expression of AChE and ChAT in the hippocampus; effects increased with magnetic guidance.	Hour et al., 2020
Rat BM-MSCs	3×10^5	I.V.	APP/PS1 mice	Microglia and oxidative stress	Marginally improved cognitive function (MWM); decreased oxidative stress (EPR imaging); decreased Aβ deposits; marginally decreased soluble Aβ but no change in insoluble Aβ; decreased microglia area in cortex; marginal increase in number of associated microglia per Aβ plaque; increased proportion of $CD14^+$ microglia.	Yokokawa et al., 2019

(Continued)

TABLE 1 (Continued)

Source	Dose	Route	Animal model	Major targets	Results	Reference
MSCs, MSC-derived EVs (host species and tissue of origin not reported)	1×10^6 or 10 μg exosomes	Intracerebral (bilateral hippocampus)	Intra-hippocampal $A\beta_{1-42}$ injected mice	Neurons and neuro-regeneration	Improved cognitive function (MWM and NORT); increased SVZ neurogenesis ($PSA\text{-}NCAM^+/DCX^+$); comparable results between MSCs and MSC-derived EVs.	Reza-Zaldivar et al., 2019
Human UC-MSCs	5×10^5	Intra-arterial (carotid) with BBB opening (mannitol)	APP/PS1 mice	Aβ burden	Improved motor function (rotarod) and cognitive function (NORT); decreased Aβ deposits in motor cortex and hippocampus; no change in astrocyte area; decreased microglia area.	Boutajangout et al., 2017
Human UC-MSCs	2×10^6	I.V.	APP/PS1 mice	Aβ and neuroinflammation	Improved cognitive function (MWM); decreased Aβ deposits; increased microglia area on day one but decreased microglia area on day four; increased IL-10, decreased IL-1β, and TNF-α.	Xie et al., 2016
Human UC-MSCs, primed with Aβ	1×10^5	I.C.V.	5XFAD mice	TGF-β mediated neuroprotection and Aβ clearance	Reduced cell death; reduced Aβ deposition; more significant effect in primed MSCs.	Park et al., 2021
Human UC-MSCs	1×10^5	I.C.V.	5XFAD mice	GAL-3-mediated inhibition of GSK-3β targeting tau	Improved cognitive function (OFT, T-maze); decreased tau hyperphosphorylation, possibly through GAL-3-mediated inhibition of GSK-3β	Lim et al., 2020
Human UC-MSCs	1×10^5, administered once, or three times at 4-week intervals	Intrathecal	APP/PS1 mice	Aβ mediated neuronal loss	Increased hippocampal neurogenesis ($SOX2^+GFAP^+$ and $NeuN^+$); reduced Aβ levels, possibly through GDF-15	Kim H. J. et al., 2015
Human UC-MSCs	1×10^5	I.C.V.	5XFAD mice	TSP-1 mediated neuroprotection	Alleviation of hippocampal synapse loss, possibly through TSP-1	Kim et al., 2018b
Rat BM-MSCs	1×10^5	I.C.V.	APP/PS1 mice	miR-146a targeting astrocytes for improving synaptogenesis	Improved cognitive function (MWM), no change in hippocampal Aβ deposition, neuron count, or synapse density, a slight decrease in activated microglia, and decreased TNF-α possibly through miR-146a-mediated suppression of NF-κB.	Nakano et al., 2020
Human BM-MSCs	2×10^6	I.V.	APP/PS1 mice	Aβ-mediated inflammation	Improved cognitive function (MWM); decreased Aβ and BACE, increased A2M levels in brain; decreased serum IL-1, IL-2, TNF-α, and IFN-γ.	Wei et al., 2018
Mouse BM-MSCs	1×10^6	I.V.	APP/PS1/Tau 3×Tg mice	Migration of MSCs to brain	Higher MSC migration to brain in AD mice (0.31%) compared to control mice (0.21%), but extremely low in both cases	Park et al., 2018
Mouse BM-MSCs	1×10^6	I.V.	APP/PS1 mice	Aβ pathology	No change in Aβ plaque numbers; slight reduction in plaque size in hippocampus but not cortex; slight decrease in microglia count in the cortex; reduced microglia size; decreased expression of TNF-α, IL-6, MCP-1, and NGF in brain, though not consistent by region; no change in expression of IL-10, CCR5, BDNF, VEGF, and IFN-γ.	Naaldijk et al., 2017
CM of mouse BM-MSCs primed with AD mouse brain homogenate	CM of 1×10^6 cells cultured for 24 h, single or repeated dose	I.V. or intranasal	APP/PS1	Aβ-mediated inflammation and neuronal loss	Improved memory function (NORT); decreased Aβ deposits; decreased microglia and astrocyte area; decreased astrocytic TNF-α expression; increased neuron density in cortex (+10%) and hippocampus (+25%); decreased hippocampal atrophy; increased survival (+45%)	Santamaria et al., 2021
EVs derived from cytokine-primed human BM-MSCs	1.5×10^{10} EVs (30 μg), administered twice at 18-h interval	Intranasal	APP/PS1/Tau 3×Tg mice	Aβ mediated activation of reactive microglia	Reduced microglia density, size, and activation ($CD68^+$); increased dendritic spine density in cortical and hippocampal neurons.	Losurdo et al., 2020

(Continued)

TABLE 1 (Continued)

Source	Dose	Route	Animal model	Major targets	Results	Reference
RVG-tagged EVs derived from mouse BM-MSCs	5×10^{11} EVs	I.V.	APP/PS1 mice	Improving migration to brain for anti-inflammatory effect	Improved homing to the brain; decreased Aβ deposits; decreased astrocyte area; improved cognitive function (MWM); decreased expression of TNF-α, IL-1β, and IL-6, increased expression of IL-4, IL-10, and IL-13 in the brain.	Cui et al., 2019
Mouse BM-MSCs overexpressing CX3CL1 and Wnt3a	4×10^5	I.C.V.	APP/PS1 mice	Aβ, synaptic loss and neurodegeneration and neuroinflammation	With CX3CL1 overexpression: decreased microglia frequency, decreased TNF-α and increased IL-10 expression in brain, increased expression of synaptic proteins (PSD95 and SYP) in cortex and hippocampus, no increase in cognitive function (MWM); with CX3CL1 and Wnt3a overexpression: increased cognitive function (MWM), increased neurogenesis in hippocampus ($SOX2^+Ki67^+$ and DCX^+), increased phosphorylation of PI3K, Akt, and GSK3β (ser9)	Li et al., 2020
Mouse BM-MSCs overexpressing VEGF	1×10^6	I.C.V.	APP/PS1 mice	Aβ mediated neuroinflammation	Improve hippocampal neovascularization, diminish senile plaques, inhibit inflammation, and rescue behavioral and cognitive functions as compared to control MSCs	Garcia et al., 2014
Human menstrual blood-derived MSCs	1×10^5	Intracerebral (bilateral hippocampus)	APP/PS1 mice	Tau and Aβ mediated neuroinflammation	Improved cognitive function (MWM); decreased Aβ plaque area and tau hyperphosphorylation; decreased expression of β-CTF, BACE1, increased expression of IDE, NEP in the brain; increased microglial area and shift toward alternative phenotype.	Zhao et al., 2018
AD-MSCs	1×10^5	stereotaxic surgery	APP/PS1 mice	Aβ mediated oxidative stress	Inhibition of oxidative stress and promotion of neurogenesis in hippocampus,	Yan et al., 2014b
Rat AD-MSCs	1×10^5	Intracerebral (bilateral hippocampus)	APP/PS1 mice	Aβ mediated oxidative stress	Slightly improved memory function (NORT); decreased oxidative stress; increased neurogenesis ($BrdU^+/DCX^+$ cells) in hippocampus and SVZ.	
Human UC-MSCs	2×10^5	Intracerebral (left hippocampus)	5XFAD mice	Proteasome activity	Increased proteasome activity *via* AgRP, reduced accumulation of ubiquitin-conjugated proteins.	Lee et al., 2017
Mouse BM-MSCs	1×10^6	I.V., single or quadruple dose	APP/PS1/Tau 3×Tg mice	Tau and Aβ mediated neuroinflammation	Decreased neuroinflammation, altered APP processing, no decrease in Aβ plaques, decrease in tau phosphorylation	Neves et al., 2021

Unless otherwise noted, results describing microglia and astrocytes refer to positive staining for Iba1 and GFAP. BMT, Barnes maze test; EMT, elevated plus maze; I.C.V., intracerebroventricular; I.V., intravenous; MBT, marble burying test; MWM, Morris Water Maze; NORT, novel object recognition task; OFT, open field test; PAL, passive avoidance learning; CM, condition media; ADMSC, adipose derived mesenchymal stem cells; BM-MSC, bone marrow derived mesenchymal stem cells.

shown a beneficial interaction between MSCs and NSCs in promoting neurogenesis (i.e., differentiation, proliferation and survival of NSCs), neuroprotection as well as facilitating the differentiation of MSCs to neural cells (Alexanian, 2005; Oh et al., 2011; Haragopal et al., 2015; Ju et al., 2015; Kim D. H. et al., 2015). Hence, the co-transplantation of NSCs and MSCs. or transplantation of NSCs-primed MSCs. could be an effective strategy for neuroregeneration and neuroprotection.

Neuroprotective effect of mesenchymal stem/stromal cells on co-cultured neurons

Co-culturing MSCs with primary rat cortical neurons has been shown to protect neurons from apoptosis and enhance their survival (Scuteri et al., 2011b; Scheibe et al., 2012). MSC-co-cultured neurons demonstrated no signs of degeneration and survived 60 days or more, while primary neuronal cultures without MSC exposure experienced cellular death in a few days (Scuteri et al., 2011b). This MSC-induced neuroprotection and promotion of long-term neuron survival was suggested to be the result of downregulated matrix metalloproteinase (MMP) activity and the fostering of neuronal maturation (Scuteri et al., 2006, 2011b).

Co-culture of MSCs with hippocampal neurons in a transwell system protected neurons from Aβ-induced oxidative stress and prevented the synapse loss that is typically associated with Aβ exposure (de Godoy et al., 2018). This protective effect was speculated to be a consequence of MSC-mediated Aβ clearance (de Godoy et al., 2018). The study further reported that MSCs are capable of internalizing fibrillary Aβ and neurotoxic Aβ oligomers without

TABLE 2 Use of MSCs in Alzheimer's disease in different clinical trials.

Source	Dose	Route	Study phase	Participants	Results	Study location	Clinical trial.gov ID
Lomecel-B (allogeneic BM-MSCs)	2×10^7, or 1×10^8 cells	I.V.	Phase1a, randomized, placebo-controlled study	33	Safe and well tolerated, effective in increasing anti-inflammatory and pro-vascular biomarker in serum, improve neurocognition and quality of life in treated patients compared to placebo	United States	(NCT02600130) (Oliva et al., 2021; Brody et al., 2022)
Autologous ADMSCs	2×10^8 cells (9 times at 2 weeks intervals)	I.V.	1/2, randomized, double-blind, placebo-controlled study	21	–	United States	NCT03117738
Autologous ADMSCs	2×10^8 cells (4 times at 2 weeks intervals)	I.V.	1/2a, open-label, non-randomized study	24	Withdrawn due to COVID-19 pandemic	United States	NCT04228666
Allogeneic BM-MSCs	Placebo or 1.5×10^6cells/kg body weight	I.V.	2a, randomized, single-blind, placebo-controlled, crossover, multicenter study	40	–	United States	NCT02833792
Allogeneic UC-MSCs	1×10^7 or 3×10^7 cells administered 3 times at 4-week intervals	I.C.V.	1/2a, double-blind, single-center study	45	–	South Korea	NCT02054208 NCT03172117
Allogeneic human UC-MSCs	Placebo or 2×10^7 cells, administered 8 times at 2-week intervals	I.V.	1/2, randomized, double-blind, placebo-controlled, multicenter study	16	–	China	NCT02672306
Allogeneic UC-MSCs	Placebo, 3×10^6, or 6×10^6 cells per brain	Intra hippocampus bilaterally and right precuneus	Phase 1, open-label, single-center study	9	Feasible, safe, and well-tolerate with no effect on AD pathophysiology.	South Korea	NCT01297218 NCT01696591 (Kim H. J. et al., 2015)
Autologous human ADMSCs	N/A	N/A	N/A	1	–	United States	NCT04855955
Allogeneic human UC-MSCs	1×10^8 cells, administered 4 times at 13-week intervals	I.V.	1, prospective open-label study	6	–	United States	NCT04040348
Allogeneic human ADMSC-derived EVs	5, 10, or 20 μg EVs, administered twice a week for 12 weeks	Nasal drip infusion	1/2, open-label, single-center study	9	–	China	NCT04388982
Human P-MSCs	Placebo or 2×10^8 cells, 1–2 times at 4-week interval	I.V.	1/2a, randomized, double-blind, placebo-controlled study	24	–	South Korea	NCT02899091
Autologous ADMSCs	Placebo or 2×10^8 cells, administered 4 times at 4-week intervals	I.V.	2b, randomized, double-blind study	80	–	United States	NCT04482413
Allogeneic human UC-MSCs	2×10^7 cells, administered 8 times at 2-week intervals	I.V.	1/2, open-label, single-center study	30	–	China	NCT01547689

10.3389/fnmol.2022.1011225

compromising their own viability, proliferation and ROS levels, and that the internalized Aβ oligomers and fibrils then undergo endosomal and lysosomal clearance (de Godoy et al., 2018). This MSC-induced autophagy and lysosomal clearance correlates with neuroprotection *in vivo* and *in vitro* and insinuates a connection between MSCs and microglial activation (Shin et al., 2014). For instance, when LPS-stimulated microglia and dopaminergic neurons were co-cultured with MSCs, the anti-inflammatory and clearance-inducing effects of MSC led to a decrease in LPS-induced damage and suppression of dopaminergic neuronal loss (Kim et al., 2009).

Role of mesenchymal stem/stromal cell-secreted neuroprotective factors

Mesenchymal stem/stromal cell-induced neuron survival and neuroprotection have been suggested to be a result of various MSC-secreted factors. For instance, thrombospondin-1 secreted by UC-MSCs has been shown to rescue synaptic dysfunction induced by Aβ deposition in hippocampal neurons *via* the upregulation of neuroligin-1 (NLGN1) and the voltage-activated Ca2+ channel subunit α2δ-1, both of which are involved in glutamatergic synapses and mediation of long-term potentiation (Kim et al., 2018b). In addition, MSCs have been shown to secrete BDNF growth factor to upregulate AKT phosphorylation while downregulating p38 phosphorylation in order to protect neurons against trophic factor withdrawal and ROS exposure (Wilkins et al., 2009). BDNF-overexpressing hMSCs have been shown to have an augmented neuroprotective effect (Scheper et al., 2019).

Other MSC-secreted neuroprotective factors include the antioxidant enzyme superoxide dismutase 3 (SOD3) and agouti-related peptide (AgRP) (Kemp et al., 2010). Inflammatory cytokines, specifically tumor necrosis factor alpha (TNF-α) and interferon-gamma (IFN-γ), can induce MSCs to secrete SOD3, thereby reducing the build-up of excess superoxide and enhancing neuronal and axonal survival *in vitro* (Kemp et al., 2010). Pretreating MSCs with the antioxidant tanshinone has been reported to reduce neuroinflammation and suppress ROS in rats with Aβ-induced neuroinflammation (Huang et al., 2019). In another study, when SH-SY5Y neuroblastoma cells were co-cultured with MSCs, the ubiquitin proteasomal system was significantly upregulated in a dose-dependent manner based on the concentration of the MSC-secreted cytokine AgRP (Lee et al., 2017). This upregulation in proteasome activity fosters the formation of autolysosomes, which propels the clearance of abnormal protein aggregates, enhances neuron survival and reduces cognitive impairment in AD (Lee et al., 2017).

Neuroprotective effects of mesenchymal stem/stromal cell-secreted extracellular vesicles

The neuroprotective effect of MSCs is also exerted by secreted extracellular vesicles (EVs), which deliver antioxidant catalase and other MSC-derived factors (de Godoy et al., 2018). miRNA-21 derived from MSC-secreted exosomes has been shown to inhibit neuron apoptosis by downregulating the expression of phosphatase and tensin homolog (PTEN) and programmed cell death protein 4 (PDCD4) in rats with spinal cord injury (Kang et al., 2019). Interestingly, the secretome of MSCs varies based on the time that the conditioned media (CM) is collected, exerting different effects on neurons and glial cells. The CM collected during earlier time points (24 h) enhanced neuron viability while CM collected at later time points (96 h) contributed to higher glial viability (Ribeiro et al., 2011), though the factors responsible for this difference were not determined. Exosomal miR-21 from MSCs have been shown to not only inhibit neuronal apoptosis but also improve the cognition and memory in transgenic APP/PS1 mice, thereby reducing Aβ deposition and downregulating pro-inflammatory cytokines. This effect was further improved with exosomes from hypoxia pre-conditioned MSCs (Cui et al., 2018). miR-146a in BM-MSC derived exosomes decreased NF-kB in astrocytes thereby restoring their function, which, in turn, promoted synaptogenesis and improved cognitive function (Nakano et al., 2020). Recently, BM-MSC derived EVs exhibited a protective effect on hippocampal neurons by decreasing amyloid beta deposition and reducing inflammatory cytokines in an amyloid beta-induced rat model of AD; these effects were deeded to be mediated by miR-29c-3p which was shown to activate the Wnt/β-catenin pathway (Sha et al., 2021). In another study, miR-29b overexpressed exosomes from MSCs reduced neuronal cell death and the pathology of Aβ in a rat model of AD while also showing improvement in spatial learning and memory (Jahangard et al., 2020). Similarly, miR-455-3p from BM-MSCs also ameliorated neuronal injury in the hippocampus (Gan and Ouyang, 2022).

Role of mesenchymal stem/stromal cells on microglia

Microglia are the resident phagocytic immune cells of the central nervous system (CNS). They are involved in immune surveillance, pathogen defense, and maintenance of homeostasis in the brain (Li and Barres, 2018). Microglia are also crucial for the development of the brain and play a critical role in neurogenesis, myelin turnover, and the modeling and pruning of synaptic architecture and network (Li and Barres, 2018).

Under normal brain physiology, microglia are responsible for the clearance and degradation of extracellular Aβ, which they recognize through microglial integrin receptors and recruitment of several enzymes such as the pro-inflammatory matrix metalloproteinases (MMPs) to restrict the formation of Aβ plaques (Konnecke and Bechmann, 2013; Doens and Fernandez, 2014; Hansen et al., 2018). However, in AD pathology, the accumulation of Aβ aggregates and other chemokines released from injured neurons prolongs the activation of microglia, which can lead to chronic neuroinflammation and subsequent accumulation of ROS (Leng and Edison, 2021). Activated microglia are characterized by elevated expressions of CD86, CD40 and Iba-1, and are also responsible for secretion of inflammatory cytokines and chemokines to recruit peripheral immune cells into the brain (Leng and Edison, 2021). However, while transient neuroinflammation is beneficial for neurogenesis and aggregate clearance, excessive or chronic neuroinflammation that fails to resolve itself can worsen AD symptoms due to ROS generation, necrosis, and collateral tissue damage in the brain (DiSabato et al., 2016; Schain and Kreisl, 2017; Yong et al., 2019). Thus, microglial activation plays a critical role in AD pathology and has been proposed as a target for AD therapy (Solito and Sastre, 2012; Siskova and Tremblay, 2013).

Mesenchymal stem/stromal cells have been proposed as mediators of AD therapy by targeting microglia due to their immunomodulatory effects. As a result, interactions between MSCs and microglia have been studied extensively in the context of neurological diseases. Intraparenchymal MSC transplantation in rats with traumatic brain injury has been shown to improve fine motor function, an effect the authors attribute to MSCs shifting microglia from a classical inflammation (CD86) to an alternative inflammation state (CD163) (Peruzzaro et al., 2019). MSCs transplanted in AD mice have been reported to reduce microglial production of pro-inflammatory factors TNF-α, IL-1β, iNOS, and COX-2, and upregulate the expression of Aβ-degrading enzymes such as insulin-degrading enzyme (IDE) and neprilysin (NEP) (Zhao et al., 2018). This led to an improved clearance of abnormal protein aggregates, including Aβ plaques and hyperphosphorylated tau, without causing chronic neuroinflammation (Zhao et al., 2018).

Interestingly, studies suggest that MSCs have the ability to reprogram microglia into an "M2-like" phenotype that is characterized by an increase in phagocytic activity and a reduction in neuroinflammation. In fact, MSCs induce a mixed microglial phenotype that is CD206-high, Arg1-high, CD86-high, IL-10-high, MCP-1/CCL2-high, PGE2-high, IL-1β-moderate, TNF-α-low, and NALP-3-low (Hegyi et al., 2014). Thus, it has been speculated that the therapeutic effect of MSCs in AD pathology is related to their ability to alter microglia cells from the inflammatory, neurotoxic phenotype to a neuroprotective, anti-inflammatory phenotype that fosters neuro-regeneration and repair (Hegyi et al., 2014).

Impact of mesenchymal stem/stromal cell-secreted factors on microglia

The therapeutic benefits and tissue repair observed in MSC transplantation has been associated with their ability to modulate the functional behavior of cells in the brain *via* paracrine mechanisms associated with MSC-secreted cytokines, growth factors, chemokines, and EVs (Gnecchi et al., 2016). For instance, human UC-MSCs secrete soluble intercellular adhesion molecule-1 (sICAM-1) after co-culturing with BV2 microglia which, in turn, diminish accumulation of Aβ plaques (Kim et al., 2012). Release of sICAM-1 increased after Aβ induction in the BV2 microglia, and an up-regulation of NEP enzyme was observed in co-cultured microglia as compared to those that were not exposed to MSCs (Kim et al., 2012). sICAM-1 also interrupts CD40/CD40L activity, thereby reducing pro-inflammatory signaling and enhancing microglial phagocytosis for Aβ and tau deposits (Kim et al., 2012). In addition, MSCs also up-regulate the expression of CD14, an important receptor for Aβ uptake, in microglia to facilitate microglial internalization and clearance of Aβ deposits, both *in vitro* and *in vivo* (Yokokawa et al., 2019). Growth differentiation factor-15 (GDF-15) secreted by UC-MSCs has also been associated with enhanced BV2 microglial Aβ clearance, *in vitro* and *in vivo*, through the upregulation of IDE (Kim et al., 2018a).

The ability of MSCs to regulate microglia activation also relies on its secreted paracrine factors. For instance, transwell co-culture of MSCs and LPS-stimulated microglia attenuated the activation of microglia with increased IL-6, IL-10, and TGF-β expressions, and reduced NO and TNF-α production (Kim et al., 2009). MSC-secreted CX3CL1 also exerts a regulatory effect on microglia by inhibiting expression of TNF-α, inducible nitric oxide synthase (iNOS), and ROS (Giunti et al., 2012). This enables an alternate microglial activation that enhances microglial phagocytic capacity without the onset of neurotoxic, chronic neuroinflammation, thereby reducing cellular damage and apoptosis (Giunti et al., 2012). Thus, it has been suggested that the ability of MSCs to improve microglial phagocytic activity under the anti-inflammatory, neuroprotective phenotype is dependent on the secretion of CX3CL1 (Giunti et al., 2012). While MSCs induce functional changes to microglia, they do not appear to promote microglial proliferation (Giunti et al., 2012). In fact, studies suggest that MSCs actually exhibit anti-proliferative effect toward BV2 microglia by reducing TNF-α expression, increasing the percentage of BV2 microglia that are under G0/G1 cell cycle arrest even in the face of LPS stimulation (Jose et al., 2014). **Table 3** summarize different studies showing the effect of MSCs

TABLE 3 Studies exploring factors governing the neuroprotective/immunomodulatory effect of MSCs.

Source	Microglia cell type	Factors secreted	Effect of MSCs on microglia	References
hUC-MSCs	BV2 mouse microglia	sICAM	Enhanced NEP expression, reduced CD40 expression, increased microglial Aβ clearance	Kim et al., 2012
Rat MSCs	Rat primary microglia	TGF-β	Enhanced anti-inflammatory phenotype and phagocytic activity of microglia is mediated *via* TGF-β signaling	Noh et al., 2016
Mouse BM-MSCs	BV2 mouse microglia	TSG-6	Inhibited pro-inflammatory factors in TSG-6 dependent mechanism where NF-κB and MAPK signaling are inhibited in LPS-induced microglia	Liu et al., 2014
UC-MSCs	BV2 mouse microglia	GDF-15	Increased in insulin-degrading enzyme expression in microglia- mediated Aβ clearance *via* GDF-15 secretion from MSCs	Kim et al., 2018a
BM-MSCs	BV2 mouse microglia	Soluble CCL5	Promoted alternative activation of microglia and reduced in Aβ *via* neprilysin and interleukin-4 from alternatively activated microglia	Lee et al., 2012
Human amniotic-derived MSCs	BV2 mouse microglia	Nitric oxide	Decrease viability, migration of microglia and promoted anti-inflammatory phenotype of microglia	Yan et al., 2014a

in modulating microglia for decreasing neuroinflammation and neuroprotection.

Limitations of mesenchymal stem/stromal cells for the treatment of Alzheimer's disease

The therapeutic efficacy of MSC-based therapies depends on a variety of factors, including a homogenous cell population, the source of MSCs, the optimal dose of transplanted cells, time of transplantation, and suitable route for cell delivery. However, an optimal protocol for the isolation, characterization, and expansion of MSCs remains poorly characterized, and there is an unmet need to determine the appropriate dose, route and time for MSC transplantation. The occurrence of immune responses, especially from allogeneic transplantations of cells, also complicates the application of MSC therapies. While some clinical trials reported evidence of therapeutic efficacy, many studies failed to observe clinical improvement after MSC therapy. In addition to the above-mentioned variables, the lack of homing of MSCs to brain is another hurdle in the treatment of neurodegenerative diseases as blood-brain barrier (BBB) also increases the difficulty of MSC delivery to the brain.

Strategies to overcome limitations

Facilitating mesenchymal stem/stromal cell delivery to the brain

Although MSCs possess some homing capacity to sites of injury, very few intravenously injected cells successfully migrate to the target site, and the majority end up entrapped in the lung microvasculature instead of the brain (Ullah et al., 2019). The BBB is another major limiting factor that compromises the delivery of therapeutics, including MSCs, into the brain for treatment of neurodegenerative diseases (Hour et al., 2020). As a result, several studies have attempted to bypass the BBB by delivering MSCs *via* intraparenchymal or intracerebroventricular routes (Ma et al., 2013; Zheng et al., 2017; Zhao et al., 2018; Reza-Zaldivar et al., 2019). Delivering MSCs *via* the intrathecal route has also been identified as a less invasive delivery route, since it does not require brain surgery (Kim et al., 2020).

Focused ultrasound is another technology that has been leveraged to improve MSC homing (Liu et al., 2020). Application of focused ultrasound to the brain transiently ruptures the capillary lining of the BBB and supports delivery of therapeutic molecules into the brain through increased capillary permeability. Focused ultrasound application has also been shown to upregulate intercellular adhesion molecules (ICAMs), stromal cell-derived factor 1α (SDF-1α), monocyte chemotactic protein 1 (MCP-1), matrix metalloproteinase 9 (MMP9), and immune cell trophic factors that contribute to transient BBB opening and tropism of MSCs to the brain (Kovacs et al., 2017; Yang et al., 2019). Preclinical studies in rats have demonstrated that focused ultrasound to the hippocampus increases local expression of vascular cell adhesion molecule 1 (VCAM-1) and ICAM-1, and results in a more than 2-fold increase in the number of MSCs found in the sonicated region following intravenous infusion (Lee et al., 2020). Focused ultrasound has also been combined with contrast agents such as microbubbles to enhance BBB permeabilization. In response to ultrasound, microbubbles cavitate and locally exert various physical forces, a technique known as ultrasound-mediated microbubble destruction. In a rat model of brain ischemia, ultrasound-mediated microbubble destruction has been shown to increase

the number of intravenously infused MSCs found in the brain parenchyma by 2.3-fold (Cui et al., 2020). The increased MSC homing appeared to correlate with greater recovery of neurological function, though the ultrasound-only control, which would be necessary to make this conclusion, was not included.

Magnetic targeting has also been investigated for improving MSC delivery to the brain. By labeling MSCs with superparamagnetic nanoparticles, they can be guided to the brain using external magnets. One such study found that magnetic targeting of intravenously infused MSCs improved their migration into the brains of AD rats, to levels comparable to those of intracerebroventricularly injected MSCs (Hour et al., 2020). Magnetic targeting also appeared to improve certain measures of cognitive function as well as expression of cholinergic signaling molecules.

Genetic modification of mesenchymal stem/stromal cells

Studies have explored various genetic modifications of MSCs to enhancing their function or survival. For instance, MSCs overexpressing CX3CL1 have been shown to attenuate synaptic loss and the levels of pro-inflammatory cytokines in APP/PS1 transgenic AD mice (Li et al., 2020). While CX3CL1 overexpression alone did not lead to cognitive improvement, transplantation of MSCs overexpressing both CX3CL1 and Wnt3a successfully fostered hippocampal neurogenesis, improved cognitive function, and reduced microglia neurotoxicity (Li et al., 2020). In the same mouse model, MSCs overexpressing VEGF have been shown to improve hippocampal neovascularization, diminish senile plaques, inhibit inflammation, and rescue behavioral and cognitive functions as compared to control MSCs (Garcia et al., 2014).

Studies have revealed that microRNA-modified MSCs may play a beneficial role in treatment of neurodegenerative diseases like AD (Liu et al., 2015; Han et al., 2018). For instance, MSCs overexpressing BDNF have been shown to promote neuron survival when they are co-cultured with primary neurons isolated from APP/PS1 mice (Song et al., 2015). It was revealed that MSCs express low levels of Brn-4 protein despite the high expression of the transcription factor Brn-4 mRNA due to the presence of miR-937, which inhibits the translation of Brn-4 mRNA (Liu et al., 2015). However, bone marrow MSCs induced to express the antisense of miR-937 (as-miR-937) successfully suppressed miR-937 to increase expression of transcription factor Brn-4, which in turn increased BDNF protein levels and significantly enhanced the therapeutic effect of MSCs in the APP/PS1 mice (Liu et al., 2015). Additionally, MSCs overexpressing as-miR-937 had reduced Aβ accumulation, and enhanced cognitive function (Liu et al., 2015).

It has been observed that MSCs exposed to Aβ express early apoptosis and increased levels of the apoptosis mediating protease caspase 3, along with a decrease in levels of the microRNA let-7f-5p (Han et al., 2018). Upregulation of let-7f-5p countered the Aβ-induced apoptosis in MSCs by decreasing the levels of caspase-3, thereby prolonging MSC retention in the brain (Han et al., 2018). Elevation of let-7f-5p also reduced Aβ-induced cytotoxicity and enhanced survival of engrafted MSCs by targeting caspase-3 (Han et al., 2018).

Glucagon-like peptide-1 (GLP-1) has also been suggested to protect neurons from Aβ-mediated toxicity by preventing neuronal apoptosis, oxidative injury, and the generation and accumulation of Aβ deposits from APP (Perry and Greig, 2002). One study has shown that intracerebroventricular transplantation of GLP-1 overexpressing MSCs into AD mice reduced Aβ deposition and a downregulated microglial and astrocytic immunoreactivity in the brain (Klinge et al., 2011), though the reductions were moderate.

Priming of mesenchymal stem/stromal cells

Priming MSCs with cytokines, hypoxia, nutrition deficiency, and various small molecules has been conducted to enhance the therapeutic efficacy and long-term survival of MSCs. For instance, pre-treating gingiva-derived MSCs (G-MSCs) with cannabidiol (CBD) modified the transcriptional profile of these MSCs to downregulate expression of proteins that are potentially involved in tau phosphorylation and Aβ production while upregulating genes involved in Aβ clearance and degradation (Libro et al., 2016). CBD-treated G-MSCs exhibited a downregulation of β- and γ-secretases which are usually responsible for Aβ production, and an upregulation of α-secretases which are responsible for the normal cleavage of APP (Libro et al., 2016). CBD treatment also upregulated the expressions of HSPs (HSP70s and HSP90s) and ubiquitin-conjugating enzymes, which enhances the clearance of aberrant proteins associated with AD pathology, such as Aβ plaques and neurofibrillary tangles. CBD was also found to bind to the vanilloid receptor 1 (TRPV1) to promote PI3K/Akt signaling and inhibit GSK3β, the latter of which is believed to be responsible for tau hyperphosphorylation. In another study, pre-treating MSCs with melatonin improved survival of transplanted adipose tissue-derived MSCs (ADMSCs) and better preserved the cognitive, learning, and memory functions in Aβ-treated AD rats (Nasiri et al., 2019). The number of activated microglia was also significantly decreased in melatonin-pre-treated ADMSCs group, and Aβ clearance

was increased relative to untreated ADMSCs (Nasiri et al., 2019).

Extracellular vesicles as cell-free therapy

The primary mechanism of action for MSC-based therapies is believed to be their paracrine activities *via* release of various secretory factors to facilitate tissue repair and immunomodulation. Due to this, many groups are investigating cell-free therapies based on MSC-derived EVs which have been shown to be sufficient for inhibiting apoptosis and reducing neuroinflammation (de Godoy et al., 2018; Kang et al., 2019). Conditioned media (CM) collected from different types of MSCs have been shown to reduce cognitive impairment in AD mice (Mita et al., 2015).

The use of MSC-derived EVs confers several advantages, including low immunogenicity, higher safety profile, ease of injection, and enhanced ability to trespass biological barriers. These attributes circumvent complications such as tumor formation, immune rejection, and undesired entrapment in the lung microvasculature. Moreover, MSC-derived EVs express the same set of membrane receptors and surface markers as MSCs, which may allow them to retain some of the homing capabilities possessed by their parent MSCs (Grange et al., 2014).

Mesenchymal stem/stromal cell-secreted EVs have demonstrated therapeutic efficacy in several AD studies. For instance, treating neural stem cells derived from the Tg2576 AD mouse model with ADMSC-derived EVs successfully reduced Aβ levels and neuronal apoptosis while fostering neuronal growth *in vitro* (Lee et al., 2018). It has been demonstrated that AD-MSC-derived EVs carry enzymatically active NEP and successfully degrade secreted and intracellular Aβ levels in Aβ-overexpressing neuroblastoma cells (Katsuda et al., 2013). Interestingly, the Aβ inhibition of these AD-MSC-derived EVs exceeded that of BM-MSCs (Katsuda et al., 2013). UC-MSC-derived EVs have also been shown to ameliorate cognitive dysfunction and neuroinflammation by modulating microglia activation in a mouse AD model (Ding et al., 2018).

Extracellular vesicles secreted from 3D-cultured MSCs seem to demonstrate higher therapeutic effect in several studies relative to those derived from 2D-cultured MSCs. 3D-cultured MSCs produced higher yield of EVs, and these EVs exhibited improved efficiency in delivering their contents to neurons (Haraszti et al., 2018). EVs secreted from UC-MSCs cultured in 3D graphene scaffold have been shown to differentially express hundreds of miRNAs compared to those collected from 2D-cultured UC-MSCs, and were enriched for several genes relevant to AD therapy such as HSP90, NEP, and IDE (Yang et al., 2020). These differences highlight the large variation in EV functional properties depending on the culture conditions, which will be a crucial factor to consider for successful clinical translation.

Conclusion and future implications

Mesenchymal stem/stromal cells have been extensively investigated as a therapeutic strategy for treating neurodegenerative diseases such as AD. However, while preclinical studies have demonstrated some therapeutic potential of MSC-based therapies, several limitations mentioned above have hindered their effectiveness in clinical trials. Since intravenously administration of MSCs results in majority being trapped in the microvasculature of the lungs, finding a path of delivery that enables efficient MSC delivery and homing to the brain remains a challenge. In order to foster MSC migration to the brain and improve clinical therapeutic efficacy, studies have explored applications such as focused ultrasound, genetic modification, MSC conditioning, and local delivery of MSC into the brain. In addition to MSC-based cell therapy, cell free therapy based on MSC-derived EVs has also demonstrated potential in the treatment of AD.

As we have seen in this review, much of the preclinical literatures investigating MSCs for AD therapy have utilized widely different AD animal models, MSC sources, culture conditions and administration routes; while the reported therapeutic effects often attain statistical significance but are yet to be established in clinics. Nevertheless, the mechanistic understanding of how MSCs might ameliorate AD pathology still remains to be proven. The potential future of MSC-based therapy for AD hinges on a thorough scientific inquiry and mechanistic insight into the interaction between MSCs and neural cells, followed by rigorous preclinical studies that evaluate clinically meaningful endpoints. Majority of clinical trials have not lived up to their potential despite having good pre-clinical data due to limited consideration in pathological variability corresponding to different stages of the disease and its resulting impact on therapeutic effect of MSC-based therapies. Hence, well defined pre-clinical study protocols will be essential for effective clinical translation of novel therapeutics. Indeed, this can include testing specific animal models with therapeutic interventions mapped to specific stages of the disease. Furthermore, the actual therapeutic candidate should be controlled and evaluated for at the pre-clinical stage, in terms of its source, dose and route of administration. These specific parameters should then not be changed to ensure that the clinical translation is optimal less likely to fail. Finally, given that each patient will have their own unique physiology and microenvironment, modulation of the brain tissue at target sites may in fact help to ensure consistent and reproducible regenerative and protective responses. Without this groundwork, it is highly possible that clinical trials will continue to generate disappointing results.

Author contributions

SR and AST contributed to conceptualization. SR, MS, and DDL contributed to writing the review. SR, MS, DDL, AG, RP, SC, RY, and AST contributed to editing and review. BDK contributed to preparing the figures. AST contributed to supervision. All authors contributed to the article and approved the submitted version.

Funding

This study was supported by the Radiology Research Fund for Alzheimer's disease at Stanford University.

Conflict of interest

The authors declare that the research was conducted in the absence of any commercial or financial relationships that could be construed as a potential conflict of interest.

Publisher's note

All claims expressed in this article are solely those of the authors and do not necessarily represent those of their affiliated organizations, or those of the publisher, the editors and the reviewers. Any product that may be evaluated in this article, or claim that may be made by its manufacturer, is not guaranteed or endorsed by the publisher.

References

Alavi Naini, S. M., and Soussi-Yanicostas, N. (2015). Tau Hyperphosphorylation and oxidative stress, a critical vicious circle in neurodegenerative tauopathies? *Oxid. Med. Cell Longev.* 2015:151979. doi: 10.1155/2015/151979

Alexanian, A. R. (2005). Neural stem cells induce bone-marrow-derived mesenchymal stem cells to generate neural stem-like cells via juxtacrine and paracrine interactions. *Exp. Cell Res.* 310, 383–391. doi: 10.1016/j.yexcr.2005.08.015

Alonso, A. C., Grundke-Iqbal, I., and Iqbal, K. (1996). Alzheimer's disease hyperphosphorylated tau sequesters normal tau into tangles of filaments and disassembles microtubules. *Nat. Med.* 2, 783–787. doi: 10.1038/nm0796-783

Alzheimer's Association (2019). 2019 Alzheimer's disease facts and figures. *Alzheimer Dement* 15, 321–387. doi: 10.1016/j.jalz.2019.01.010

Baruch, K., Deczkowska, A., Rosenzweig, N., Tsitsou-Kampeli, A., Sharif, A. M., Matcovitch-Natan, O., et al. (2016). PD-1 immune checkpoint blockade reduces pathology and improves memory in mouse models of Alzheimer's disease. *Nat. Med.* 22:135. doi: 10.1038/nm.4022

Benilova, I., Karran, E., and De Strooper, B. (2012). The toxic Abeta oligomer and Alzheimer's disease: An emperor in need of clothes. *Nat. Neurosci.* 15, 349–357. doi: 10.1038/nn.3028

Bloom, G. S. (2014). Amyloid-beta and tau: The trigger and bullet in Alzheimer disease pathogenesis. *JAMA Neurol.* 71, 505–508. doi: 10.1001/jamaneurol.2013.5847

Boutajangout, A., Noorwali, A., Atta, H., and Wisniewski, T. (2017). Human umbilical cord stem cell xenografts improve cognitive decline and reduce the amyloid burden in a mouse model of Alzheimer's Disease. *Curr. Alzheimer Res.* 14, 104–111. doi: 10.2174/1567205013666161004151416

Brody, M., Agronin, M., Herskowitz, B. J., Bookheimer, S. Y., Small, G. W., Hitchinson, B., et al. (2022). Results and insights from a phase I clinical trial of Lomecel-B for Alzheimer's disease. *Alzheimers Dement.* 2022, 1–13. doi: 10.1002/alz.12651

Busche, M. A., Wegmann, S., Dujardin, S., Commins, C., Schiantarelli, J., Klickstein, N., et al. (2019). Tau impairs neural circuits, dominating amyloid-beta effects, in Alzheimer models in vivo. *Nat. Neurosci.* 22, 57–64. doi: 10.1038/s41593-018-0289-8

Cheignon, C., Tomas, M., Bonnefont-Rousselot, D., Faller, P., Hureau, C., and Collin, F. (2018). Oxidative stress and the amyloid beta peptide in Alzheimer's disease. *Redox Biol.* 14, 450–464. doi: 10.1016/j.redox.2017.10.014

Cui, G. H., Guo, H. D., Li, H., Zhai, Y., Gong, Z. B., Wu, J., et al. (2019). RVG-modified exosomes derived from mesenchymal stem cells rescue memory deficits by regulating inflammatory responses in a mouse model of Alzheimer's disease. *Immun. Ageing* 16:10. doi: 10.1186/s12979-019-0150-2

Cui, G. H., Wu, J., Mou, F. F., Xie, W. H., Wang, F. B., Wang, Q. L., et al. (2018). Exosomes derived from hypoxia-preconditioned mesenchymal stromal cells ameliorate cognitive decline by rescuing synaptic dysfunction and regulating inflammatory responses in APP/PS1 mice. *FASEB J.* 32, 654–668. doi: 10.1096/fj.201700600R

Cui, H., Zhu, Q., Xie, Q., Liu, Z., Gao, Y., He, Y., et al. (2020). Low intensity ultrasound targeted microbubble destruction assists MSCs delivery and improves neural function in brain ischaemic rats. *J. Drug Target* 28, 320–329. doi: 10.1080/1061186X.2019.1656724

Cui, Y., Ma, S., Zhang, C., Cao, W., Liu, M., Li, D., et al. (2017). Human umbilical cord mesenchymal stem cells transplantation improves cognitive function in Alzheimer's disease mice by decreasing oxidative stress and promoting hippocampal neurogenesis. *Behav. Brain Res.* 320, 291–301. doi: 10.1016/j.bbr.2016.12.021

Cummings, J., Lee, G., Ritter, A., Sabbagh, M., and Zhong, K. (2019). Alzheimer's disease drug development pipeline: 2019. *Alzheimers Dement (N Y)* 5, 272–293. doi: 10.1016/j.trci.2019.05.008

de Godoy, M. A., Saraiva, L. M., De Carvalho, L. R. P., Vasconcelos-Dos-Santos, A., Beiral, H. J. V., Ramos, A. B., et al. (2018). Mesenchymal stem cells and cell-derived extracellular vesicles protect hippocampal neurons from oxidative stress and synapse damage induced by amyloid-beta oligomers. *J. Biol. Chem.* 293, 1957–1975. doi: 10.1074/jbc.M117.807180

Deane, R., Bell, R. D., Sagare, A., and Zlokovic, B. V. (2009). Clearance of amyloid-beta peptide across the blood-brain barrier: Implication for therapies in Alzheimer's disease. *CNS Neurol. Disord Drug Targets* 8, 16–30. doi: 10.2174/187152709787601867

Ding, M., Shen, Y., Wang, P., Xie, Z., Xu, S., Zhu, Z., et al. (2018). Exosomes isolated from human umbilical cord mesenchymal stem cells alleviate neuroinflammation and reduce amyloid-beta deposition by modulating microglial activation in Alzheimer's Disease. *Neurochem. Res.* 43, 2165–2177. doi: 10.1007/s11064-018-2641-5

DiSabato, D. J., Quan, N., and Godbout, J. P. (2016). Neuroinflammation: The devil is in the details. *J. Neurochem.* 139 Suppl 2, 136–153. doi: 10.1111/jnc.13607

Divya, M. S., Roshin, G. E., Divya, T. S., Rasheed, V. A., Santhoshkumar, T. R., Elizabeth, K. E., et al. (2012). Umbilical cord blood-derived mesenchymal stem cells consist of a unique population of progenitors co-expressing mesenchymal stem cell and neuronal markers capable of instantaneous neuronal differentiation. *Stem Cell Res. Ther.* 3:57. doi: 10.1186/scrt148

Doens, D., and Fernandez, P. L. (2014). Microglia receptors and their implications in the response to amyloid beta for Alzheimer's disease pathogenesis. *J. Neuroinflammation* 11:48. doi: 10.1186/1742-2094-11-48

Dominici, M., Le Blanc, K., Mueller, I., Slaper-Cortenbach, I., Marini, F., Krause, D., et al. (2006). Minimal criteria for defining multipotent mesenchymal stromal cells. The International society for cellular therapy position statement. *Cytotherapy* 8, 315–317. doi: 10.1080/14653240600855905

Feng, N., Han, Q., Li, J., Wang, S., Li, H., Yao, X., et al. (2014). Generation of highly purified neural stem cells from human adipose-derived mesenchymal

stem cells by Sox1 activation. *Stem Cells Dev.* 23, 515–529. doi: 10.1089/scd.2013.0263

Gan, C., and Ouyang, F. (2022). Exosomes released from bone-marrow stem cells ameliorate hippocampal neuronal injury through transferring miR-455-3p. *J. Stroke Cerebrovasc. Dis.* 31:106142. doi: 10.1016/j.jstrokecerebrovasdis.2021.106142

Garcia, K. O., Ornellas, F. L., Martin, P. K., Patti, C. L., Mello, L. E., Frussa-Filho, R., et al. (2014). Therapeutic effects of the transplantation of VEGF overexpressing bone marrow mesenchymal stem cells in the hippocampus of murine model of Alzheimer's disease. *Front. Aging Neurosci.* 6:30. doi: 10.3389/fnagi.2014.00030

Giunti, D., Parodi, B., Usai, C., Vergani, L., Casazza, S., Bruzzone, S., et al. (2012). Mesenchymal stem cells shape microglia effector functions through the release of CX3CL1. *Stem Cells* 30, 2044–2053. doi: 10.1002/stem.1174

Gnecchi, M., Danieli, P., Malpasso, G., and Ciuffreda, M. C. (2016). Paracrine mechanisms of mesenchymal stem cells in tissue repair. *Methods Mol. Biol.* 1416, 123–146. doi: 10.1007/978-1-4939-3584-0_7

Gorbunov, N., Petrovski, G., Gurusamy, N., Ray, D., Kim, D. H., and Das, D. K. (2012). Regeneration of infarcted myocardium with resveratrol-modified cardiac stem cells. *J. Cell Mol. Med.* 16:174–184. doi: 10.1111/j.1582-4934.2011.01281.x

Grange, C., Tapparo, M., Bruno, S., Chatterjee, D., Quesenberry, P. J., Tetta, C., et al. (2014). Biodistribution of mesenchymal stem cell-derived extracellular vesicles in a model of acute kidney injury monitored by optical imaging. *Int. J. Mol. Med.* 33, 1055–1063. doi: 10.3892/ijmm.2014.1663

Griner, S. L., Seidler, P., Bowler, J., Murray, K. A., Yang, T. P., Sahay, S., et al. (2019). Structure-based inhibitors of amyloid beta core suggest a common interface with tau. *Elife* 8:e46924. doi: 10.7554/eLife.46924

Guillozet, A. L., Weintraub, S., Mash, D. C., and Mesulam, M. M. (2003). Neurofibrillary tangles, amyloid, and memory in aging and mild cognitive impairment. *Arch. Neurol.* 60, 729–736. doi: 10.1001/archneur.60.5.729

Gupta, A., Bansal, A., and Hashimoto-Torii, K. (2020). HSP70 and HSP90 in neurodegenerative diseases. *Neurosci. Lett.* 716:134678. doi: 10.1016/j.neulet.2019.134678

Han, L., Zhou, Y., Zhang, R., Wu, K., Lu, Y., Li, Y., et al. (2018). MicroRNA Let-7f-5p Promotes bone marrow mesenchymal stem cells survival by targeting Caspase-3 in Alzheimer Disease Model. *Front. Neurosci.* 12:333. doi: 10.3389/fnins.2018.00333

Hansen, D. V., Hanson, J. E., and Sheng, M. (2018). Microglia in Alzheimer's disease. *J. Cell Biol.* 217, 459–472. doi: 10.1083/jcb.201709069

Haragopal, H., Yu, D., Zeng, X., Kim, S. W., Han, I. B., Ropper, A. E., et al. (2015). Stemness enhancement of human neural stem cells following bone marrow MSC coculture. *Cell Transplant.* 24, 645–659. doi: 10.3727/096368915X687561

Haraszti, R. A., Miller, R., Stoppato, M., Sere, Y. Y., Coles, A., Didiot, M.-C., et al. (2018). Exosomes produced from 3D Cultures of MSCs by tangential flow filtration show higher yield and improved activity. *Mol. Ther.* 26, 2838–2847. doi: 10.1016/j.ymthe.2018.09.015

Harris, V. K., Faroqui, R., Vyshkina, T., and Sadiq, S. A. (2012). Characterization of autologous mesenchymal stem cell-derived neural progenitors as a feasible source of stem cells for central nervous system applications in multiple sclerosis. *Stem Cells Transl. Med.* 1, 536–547. doi: 10.5966/sctm.2012-0015

He, Z., Guo, J. L., Mcbride, J. D., Narasimhan, S., Kim, H., Changolkar, L., et al. (2018). Amyloid-beta plaques enhance Alzheimer's brain tau-seeded pathologies by facilitating neuritic plaque tau aggregation. *Nat. Med.* 24, 29–38. doi: 10.1038/nm.4443

Hegyi, B., Környei, Z., Ferenczi, S., Fekete, R., Kudlik, G., Kovács, K. J., et al. (2014). Regulation of mouse microglia activation and effector functions by bone marrow-derived mesenchymal stem cells. *Stem Cells Dev.* 23, 2600–2612. doi: 10.1089/scd.2014.0088

Hernández, R., Jiménez-Luna, C., Perales-Adán, J., Perazzoli, G., Melguizo, C., and Prados, J. (2020). Differentiation of human mesenchymal stem cells towards neuronal lineage: Clinical trials in nervous system disorders. *Biomol. Ther (Seoul)* 28, 34–44. doi: 10.4062/biomolther.2019.065

Hour, F. Q., Moghadam, A. J., Shakeri-Zadeh, A., Bakhtiyari, M., Shabani, R., and Mehdizadeh, M. (2020). Magnetic targeted delivery of the SPIONs-labeled mesenchymal stem cells derived from human Wharton's jelly in Alzheimer's rat models. *J. Control Release* 321, 430–441. doi: 10.1016/j.jconrel.2020.02.035

Huang, N., Li, Y., Zhou, Y., Zhou, Y., Feng, F., Shi, S., et al. (2019). Neuroprotective effect of tanshinone IIA-incubated mesenchymal stem cells on Aβ25-35-induced neuroinflammation. *Behav. Brain Res.* 365, 48–55. doi: 10.1016/j.bbr.2019.03.001

Jahangard, Y., Monfared, H., Moradi, A., Zare, M., Mirnajafi-Zadeh, J., and Mowla, S. J. (2020). Therapeutic effects of transplanted exosomes containing miR-29b to a rat model of Alzheimer's Disease. *Front. Neurosci.* 14:564. doi: 10.3389/fnins.2020.00564

Jeong, S. G., Ohn, T., Kim, S. H., and Cho, G. W. (2013). Valproic acid promotes neuronal differentiation by induction of neuroprogenitors in human bone-marrow mesenchymal stromal cells. *Neurosci. Lett.* 554, 22–27. doi: 10.1016/j.neulet.2013.08.059

Joe, I. S., Jeong, S. G., and Cho, G. W. (2015). Resveratrol-induced SIRT1 activation promotes neuronal differentiation of human bone marrow mesenchymal stem cells. *Neurosci. Lett.* 584, 97–102. doi: 10.1016/j.neulet.2014.10.024

Jose, S., Tan, S. W., Ooi, Y. Y., Ramasamy, R., and Vidyadaran, S. (2014). Mesenchymal stem cells exert anti-proliferative effect on lipopolysaccharide-stimulated BV2 microglia by reducing tumour necrosis factor-α levels. *J. Neuroinflammation* 11:149. doi: 10.1186/s12974-014-0149-8

Ju, R., Zeng, W., Wu, R., and Feng, Z. (2015). Interaction between neural stem cells and bone marrow derived-mesenchymal stem cells during differentiation. *Biomed. Rep.* 3, 242–246. doi: 10.3892/br.2014.405

Kang, J., Li, Z., Zhi, Z., Wang, S., and Xu, G. (2019). MiR-21 derived from the exosomes of MSCs regulates the death and differentiation of neurons in patients with spinal cord injury. *Gene Ther.* 26, 491–503. doi: 10.1038/s41434-019-0101-8

Katsuda, T., Tsuchiya, R., Kosaka, N., Yoshioka, Y., Takagaki, K., Oki, K., et al. (2013). Human adipose tissue-derived mesenchymal stem cells secrete functional neprilysin-bound exosomes. *Sci. Rep.* 3:1197. doi: 10.1038/srep01197

Kemp, K., Gray, E., Mallam, E., Scolding, N., and Wilkins, A. (2010). Inflammatory cytokine induced regulation of superoxide dismutase 3 expression by human mesenchymal stem cells. *Stem Cell Rev. Rep.* 6, 548–559. doi: 10.1007/s12015-010-9178-6

Kim, D. H., Lee, D., Chang, E. H., Kim, J. H., Hwang, J. W., Kim, J.-Y., et al. (2015). GDF-15 secreted from human umbilical cord blood mesenchymal stem cells delivered through the cerebrospinal fluid promotes hippocampal neurogenesis and synaptic activity in an Alzheimer's disease model. *Stem Cells Dev.* 24, 2378–2390. doi: 10.1089/scd.2014.0487

Kim, D. H., Lee, D., Lim, H., Choi, S. J., Oh, W., Yang, Y. S., et al. (2018a). Effect of growth differentiation factor-15 secreted by human umbilical cord blood-derived mesenchymal stem cells on amyloid beta levels in in vitro and in vivo models of Alzheimer's disease. *Biochem. Biophys. Res. Commun.* 504, 933–940. doi: 10.1016/j.bbrc.2018.09.012

Kim, D. H., Lim, H., Lee, D., Choi, S. J., Oh, W., Yang, Y. S., et al. (2018b). Thrombospondin-1 secreted by human umbilical cord blood-derived mesenchymal stem cells rescues neurons from synaptic dysfunction in Alzheimer's disease model. *Sci. Rep.* 8:354. doi: 10.1038/s41598-017-18542-0

Kim, H. J., Seo, S. W., Chang, J. W., Lee, J. I., Kim, C. H., Chin, J., et al. (2015). Stereotactic brain injection of human umbilical cord blood mesenchymal stem cells in patients with Alzheimer's disease dementia: A phase 1 clinical trial. *Alzheimers Dement (N Y)* 1, 95–102. doi: 10.1016/j.trci.2015.06.007

Kim, H., Na, D. L., Lee, N. K., Kim, A. R., Lee, S., and Jang, H. (2020). Intrathecal injection in a rat model: A potential route to deliver human wharton's jelly-derived mesenchymal stem cells into the brain. *Int. J. Mol. Med. Sci.* 21:1272. doi: 10.3390/ijms21041272

Kim, J. Y., Kim, D. H., Kim, J. H., Lee, D., Jeon, H. B., Kwon, S. J., et al. (2012). Soluble intracellular adhesion molecule-1 secreted by human umbilical cord blood-derived mesenchymal stem cell reduces amyloid-β plaques. *Cell Death Differ.* 19, 680–691. doi: 10.1038/cdd.2011.140

Kim, Y. J., Park, H. J., Lee, G., Bang, O. Y., Ahn, Y. H., Joe, E., et al. (2009). Neuroprotective effects of human mesenchymal stem cells on dopaminergic neurons through anti-inflammatory action. *Glia* 57, 13–23. doi: 10.1002/glia.20731

Klinge, P. M., Harmening, K., Miller, M. C., Heile, A., Wallrapp, C., Geigle, P., et al. (2011). Encapsulated native and glucagon-like peptide-1 transfected human mesenchymal stem cells in a transgenic mouse model of Alzheimer's disease. *Neurosci. Lett.* 497, 6–10. doi: 10.1016/j.neulet.2011.03.092

Konnecke, H., and Bechmann, I. (2013). The role of microglia and matrix metalloproteinases involvement in neuroinflammation and gliomas. *Clin. Dev. Immunol.* 2013:914104. doi: 10.1155/2013/914104

Kovacs, Z. I., Kim, S., Jikaria, N., Qureshi, F., Milo, B., Lewis, B. K., et al. (2017). Disrupting the blood-brain barrier by focused ultrasound induces sterile inflammation. *Proc. Natl. Acad. Sci. U.S.A.* 114, E75–E84. doi: 10.1073/pnas.1614777114

Latta-Mahieu, M., Elmer, B., Bretteville, A., Wang, Y., Lopez-Grancha, M., Goniot, P., et al. (2018). Systemic immune-checkpoint blockade with anti-PD1 antibodies does not alter cerebral amyloid−β burden in several amyloid transgenic mouse models. *Glia* 66, 492–504. doi: 10.1002/glia.23260

Lee, J. K., Schuchman, E. H., Jin, H. K., and Bae, J.-S. (2012). Soluble CCL5 derived from bone marrow-derived mesenchymal stem cells and activated by Amyloid β Ameliorates Alzheimer's Disease in mice by recruiting bone marrow-induced microglia immune responses. *Stem Cells* 30, 1544–1555. doi: 10.1002/stem.1125

Lee, J., Chang, W. S., Shin, J., Seo, Y., Kong, C., Song, B.-W., et al. (2020). Non-invasively enhanced intracranial transplantation of mesenchymal stem cells using focused ultrasound mediated by overexpression of cell-adhesion molecules. *Stem Cell Res.* 43:101726. doi: 10.1016/j.scr.2020.101726

Lee, M., Ban, J.-J., Yang, S., Im, W., and Kim, M. (2018). The exosome of adipose-derived stem cells reduces β-amyloid pathology and apoptosis of neuronal cells derived from the transgenic mouse model of Alzheimer's disease. *Brain Res.* 1691, 87–93. doi: 10.1016/j.brainres.2018.03.034

Lee, N. K., Park, S. E., Kwon, S. J., Shim, S., Byeon, Y., Kim, J. H., et al. (2017). Agouti related peptide secreted via human mesenchymal stem cells upregulates proteasome activity in an Alzheimer's Disease Model. *Sci. Rep.* 7:39340. doi: 10.1038/srep39340

Leng, F., and Edison, P. (2021). Neuroinflammation and microglial activation in Alzheimer disease: Where do we go from here? *Nat. Rev. Neurol.* 17, 157–172. doi: 10.1038/s41582-020-00435-y

Li, A., Zhao, J., Fan, C., Zhu, L., Huang, C., Li, Q., et al. (2020). Delivery of exogenous proteins by mesenchymal stem cells attenuates early memory deficits in a murine model of Alzheimer's disease. *Neurobiol. Aging* 86, 81–91. doi: 10.1016/j.neurobiolaging.2019.10.012

Li, Q., and Barres, B. A. (2018). Microglia and macrophages in brain homeostasis and disease. *Nat. Rev. Immunol.* 18, 225–242. doi: 10.1038/nri.2017.125

Libro, R., Diomede, F., Scionti, D., Piattelli, A., Grassi, G., Pollastro, F., et al. (2016). Cannabidiol modulates the expression of Alzheimer's Disease-related genes in mesenchymal stem cells. *Int. J. Mol. Sci.* 18:26. doi: 10.3390/ijms18010026

Lim, H., Lee, D., Choi, W. K., Choi, S. J., Oh, W., and Kim, D. H. (2020). Galectin-3 secreted by human umbilical cord blood-derived mesenchymal stem cells reduces aberrant tau phosphorylation in an Alzheimer Disease Model. *Stem Cells Int.* 2020:8878412. doi: 10.1155/2020/8878412

Lin, M. T., and Beal, M. F. (2006). Alzheimer's APP mangles mitochondria. *Nat. Med.* 12, 1241–1243. doi: 10.1038/nm1106-1241

Liu, D. D., Ullah, M., Concepcion, W., Dahl, J. J., and Thakor, A. S. (2020). The role of ultrasound in enhancing mesenchymal stromal cell-based therapies. *Stem Cells Transl. Med.* 9, 850–866. doi: 10.1002/sctm.19-0391

Liu, Y., Zhang, R., Yan, K., Chen, F., Huang, W., Lv, B., et al. (2014). Mesenchymal stem cells inhibit lipopolysaccharide-induced inflammatory responses of BV2 microglial cells through TSG-6. *J. Neuroinflammation* 11:135. doi: 10.1186/1742-2094-11-135

Liu, Z., Wang, C., Wang, X., and Xu, S. (2015). Therapeutic effects of transplantation of As-MiR-937-Expressing mesenchymal stem cells in murine model of Alzheimer's Disease. *Cell Physiol. Biochem.* 37, 321–330. doi: 10.1159/000430356

Lopez-Beas, J., Guadix, J. A., Clares, B., Soriano-Ruiz, J. L., Zugaza, J. L., and Gálvez-Martín, P. (2020). An overview of international regulatory frameworks for mesenchymal stromal cell-based medicinal products: From laboratory to patient. *Med. Res. Rev.* 40, 1315–1334. doi: 10.1002/med.21659

Losurdo, M., Pedrazzoli, M., D'agostino, C., Elia, C. A., Massenzio, F., Lonati, E., et al. (2020). Intranasal delivery of mesenchymal stem cell-derived extracellular vesicles exerts immunomodulatory and neuroprotective effects in a 3xTg model of Alzheimer's disease. *Stem Cells Transl. Med.* 9, 1068–1084. doi: 10.1002/sctm.19-0327

Lu, P., Blesch, A., and Tuszynski, M. H. (2004). Induction of bone marrow stromal cells to neurons: Differentiation, transdifferentiation, or artifact? *J. Neurosci. Res.* 77, 174–191. doi: 10.1002/jnr.20148

Lukomska, B., Stanaszek, L., Zuba-Surma, E., Legosz, P., Sarzynska, S., and Drela, K. (2019). Challenges and controversies in human mesenchymal stem cell therapy. *Stem Cells Int.* 2019:9628536. doi: 10.1155/2019/9628536

Lykhmus, O., Koval, L., Voytenko, L., Uspenska, K., Komisarenko, S., Deryabina, O., et al. (2019). Intravenously injected mesenchymal stem cells penetrate the brain and treat inflammation-induced brain damage and memory impairment in mice. *Front. Pharmacol.* 10:355. doi: 10.3389/fphar.2019.00355

Ma, T., Gong, K., Ao, Q., Yan, Y., Song, B., Huang, H., et al. (2013). Intracerebral transplantation of adipose-derived mesenchymal stem cells alternatively activates microglia and ameliorates neuropathological deficits in Alzheimer's Disease Mice. *Cell Transplant.* 22, 113–126. doi: 10.3727/096368913X672181

Maleki, M., Ghanbarvand, F., Reza Behvarz, M., Ejtemaei, M., and Ghadirkhomi, E. (2014). Comparison of mesenchymal stem cell markers in multiple human adult stem cells. *Int. J. Stem Cells* 7, 118–126. doi: 10.15283/ijsc.2014.7.2.118

Manczak, M., and Reddy, P. H. (2012). Abnormal interaction between the mitochondrial fission protein Drp1 and hyperphosphorylated tau in Alzheimer's disease neurons: Implications for mitochondrial dysfunction and neuronal damage. *Hum. Mol. Genet.* 21, 2538–2547. doi: 10.1093/hmg/dds072

Manczak, M., Calkins, M. J., and Reddy, P. H. (2011). Impaired mitochondrial dynamics and abnormal interaction of amyloid beta with mitochondrial protein Drp1 in neurons from patients with Alzheimer's disease: Implications for neuronal damage. *Hum. Mol. Genet.* 20, 2495–2509. doi: 10.1093/hmg/ddr139

Marcus, D. L., Thomas, C., Rodriguez, C., Simberkoff, K., Tsai, J. S., Strafaci, J. A., et al. (1998). Increased peroxidation and reduced antioxidant enzyme activity in Alzheimer's Disease. *Exp. Neurol.* 150, 40–44. doi: 10.1006/exnr.1997.6750

Martin-Pena, A., Rincon-Limas, D. E., and Fernandez-Funez, P. (2018). Engineered Hsp70 chaperones prevent Abeta42-induced memory impairments in a Drosophila model of Alzheimer's disease. *Sci. Rep.* 8:9915. doi: 10.1038/s41598-018-28341-w

Mehrabadi, S., Motevaseli, E., Sadr, S. S., and Moradbeygi, K. (2020). Hypoxic-conditioned medium from adipose tissue mesenchymal stem cells improved neuroinflammation through alternation of toll like receptor (TLR) 2 and TLR4 expression in model of Alzheimer's disease rats. *Behav. Brain Res.* 379:112362. doi: 10.1016/j.bbr.2019.112362

Mendonça, C. F., Kuras, M., Nogueira, F. C. S., Plá, I., Hortobágyi, T., Csiba, L., et al. (2019). Proteomic signatures of brain regions affected by tau pathology in early and late stages of Alzheimer's disease. *Neurobiol. Dis.* 130:104509. doi: 10.1016/j.nbd.2019.104509

Mita, T., Furukawa-Hibi, Y., Takeuchi, H., Hattori, H., Yamada, K., Hibi, H., et al. (2015). Conditioned medium from the stem cells of human dental pulp improves cognitive function in a mouse model of Alzheimer's disease. *Behav. Brain Res.* 293, 189–197. doi: 10.1016/j.bbr.2015.07.043

Montagne, A., Zhao, Z., and Zlokovic, B. V. (2017). Alzheimer's disease: A matter of blood-brain barrier dysfunction? *J. Exp. Med.* 214, 3151–3169. doi: 10.1084/jem.20171406

Naaldijk, Y., Jäger, C., Fabian, C., Leovsky, C., Blüher, A., Rudolph, L., et al. (2017). Effect of systemic transplantation of bone marrow-derived mesenchymal stem cells on neuropathology markers in APP/PS1 Alzheimer mice. *Neuropathol. Appl. Neurobiol.* 43, 299–314. doi: 10.1111/nan.12319

Nakano, M., Kubota, K., Kobayashi, E., Chikenji, T. S., Saito, Y., Konari, N., et al. (2020). Bone marrow-derived mesenchymal stem cells improve cognitive impairment in an Alzheimer's disease model by increasing the expression of microRNA-146a in hippocampus. *Sci. Rep.* 10:10772. doi: 10.1038/s41598-020-67460-1

Nasiri, E., Alizadeh, A., Roushandeh, A. M., Gazor, R., Hashemi-Firouzi, N., and Golipoor, Z. (2019). Melatonin-pretreated adipose-derived mesenchymal stem cells efficeintly improved learning, memory, and cognition in an animal model of Alzheimer's disease. *Metab. Brain Dis.* 34, 1131–1143. doi: 10.1007/s11011-019-00421-4

Nelson, A. R., Sweeney, M. D., Sagare, A. P., and Zlokovic, B. V. (2016). Neurovascular dysfunction and neurodegeneration in dementia and Alzheimer's disease. *Biochim. Biophys. Acta* 1862, 887–900. doi: 10.1016/j.bbadis.2015.12.016

Neves, A. F., Camargo, C., Premer, C., Hare, J. M., Baumel, B. S., and Pinto, M. (2021). Intravenous administration of mesenchymal stem cells reduces Tau phosphorylation and inflammation in the 3xTg-AD mouse model of Alzheimer's disease. *Exp. Neurol.* 341:113706. doi: 10.1016/j.expneurol.2021.113706

No author list. (2021). 2021 Alzheimer's disease facts and figures. *Alzheimer's Dement* 17, 327–406. doi: 10.1002/alz.12328

Noh, M. Y., Lim, S. M., Oh, K.-W., Cho, K.-A., Park, J., Kim, K.-S., et al. (2016). Mesenchymal stem cells modulate the functional properties of microglia via TGF−β secretion. *Stem Cells Transl. Med.* 5, 1538–1549. doi: 10.5966/sctm.2015-0217

Nooshabadi, V. T., Mardpour, S., Yousefi-Ahmadipour, A., Allahverdi, A., Izadpanah, M., Daneshimehr, F., et al. (2018). The extracellular vesicles-derived from mesenchymal stromal cells: A new therapeutic option in regenerative medicine. *J. Cell Biochem.* 119, 8048–8073. doi: 10.1002/jcb.26726

Nunomura, A., Castellani, R. J., Zhu, X., Moreira, P. I., Perry, G., and Smith, M. A. (2006). Involvement of Oxidative Stress in Alzheimer Disease. *J. Neuropathol. Exp. Neurol.* 65, 631–641. doi: 10.1097/01.jnen.0000228136.58062.bf

Oh, J. S., Kim, K. N., An, S. S., Pennant, W. A., Kim, H. J., Gwak, S. J., et al. (2011). Cotransplantation of mouse neural stem cells (mNSCs) with adipose

tissue-derived mesenchymal stem cells improves mNSC survival in a rat spinal cord injury model. *Cell Transplant.* 20, 837–849. doi: 10.3727/096368910X539083

Oliva, A. A. Jr., Brody, M., Agronin, M., Herskowitz, B., Bookheimer, S. Y., Hitchinson, B., et al. (2021). Safety and efficacy of Lomecel-B in patients with mild Alzheimer's disease: Results of a double-blinded, randomized, placebo-controlled phase 1 clinical trial. *Alzheimers Dement* 17, e057581. doi: 10.1002/alz.057581

Park, B. N., Lim, T. S., Yoon, J. K., and An, Y. S. (2018). In vivo tracking of intravenously injected mesenchymal stem cells in an Alzheimer's animal model. *Cell Transplant.* 27, 1203–1209. doi: 10.1177/0963689718788067

Park, S. E., Kim, H. S., Kwon, S. J., Kim, M. J., Choi, S. J., Oh, S. Y., et al. (2021). Exposure of mesenchymal stem cells to an Alzheimer's Disease environment enhances therapeutic effects. *Stem Cells Int.* 2021:6660186. doi: 10.1155/2021/6660186

Perry, T., and Greig, N. H. (2002). The glucagon-like peptides: A new genre in therapeutic targets for intervention in Alzheimer's disease. *J. Alzheimers Dis.* 4, 487–496. doi: 10.3233/JAD-2002-4605

Peruzzaro, S. T., Andrews, M. M. M., Al-Gharaibeh, A., Pupiec, O., Resk, M., Story, D., et al. (2019). Transplantation of mesenchymal stem cells genetically engineered to overexpress interleukin-10 promotes alternative inflammatory response in rat model of traumatic brain injury. *J. Neuroinflammation* 16:2. doi: 10.1186/s12974-018-1383-2

Pini, L., Pievani, M., Bocchetta, M., Altomare, D., Bosco, P., Cavedo, E., et al. (2016). Brain atrophy in Alzheimer's Disease and aging. *Ageing Res. Rev.* 30, 25–48. doi: 10.1016/j.arr.2016.01.002

Pratico, D. (2008). Oxidative stress hypothesis in Alzheimer's disease: A reappraisal. *Trends Pharmacol. Sci.* 29, 609–615. doi: 10.1016/j.tips.2008.09.001

Rabinovici, G. D. (2021). Controversy and Progress in Alzheimer's Disease — FDA Approval of Aducanumab. *N. Engl. J. Med.* 385, 771–774. doi: 10.1056/NEJMp2111320

Reitz, C., Rogaeva, E., and Beecham, G. W. (2020). Late-onset vs nonmendelian early-onset Alzheimer disease: A distinction without a difference? *Neurol. Genet.* 6:e512. doi: 10.1212/NXG.0000000000000512

Reza-Zaldivar, E. E., Hernández-Sapiéns, M. A., Gutiérrez-Mercado, Y. K., Sandoval-Ávila, S., Gomez-Pinedo, U., Márquez-Aguirre, A. L., et al. (2019). Mesenchymal stem cell-derived exosomes promote neurogenesis and cognitive function recovery in a mouse model of Alzheimer's disease. *Neural. Regen. Res.* 14, 1626–1634. doi: 10.4103/1673-5374.255978

Reza-Zaldivar, E. E., Hernández-Sapiéns, M. A., Minjarez, B., Gutiérrez-Mercado, Y. K., Márquez-Aguirre, A. L., and Canales-Aguirre, A. A. (2018). Potential effects of MSC-derived exosomes in neuroplasticity in Alzheimer's disease. *Front. Cell Neurosci.* 12:317. doi: 10.3389/fncel.2018.00317

Ribeiro, C., Salgado, A., Fraga, J., Silva, N., Reis, R., and Sousa, N. (2011). The secretome of bone marrow mesenchymal stem cells-conditioned media varies with time and drives a distinct effect on mature neurons and glial cells (primary cultures). *J. Regen. Med. Tissue Eng.* 5, 668–672. doi: 10.1002/term.365

Rosenzweig, N., Dvir-Szternfeld, R., Tsitsou-Kampeli, A., Keren-Shaul, H., Ben-Yehuda, H., Weill-Raynal, P., et al. (2019). PD-1/PD-L1 checkpoint blockade harnesses monocyte-derived macrophages to combat cognitive impairment in a tauopathy mouse model. *Nat. Commun.* 10, 1–15. doi: 10.1038/s41467-019-08352-5

Santamaria, G., Brandi, E., Vitola, P., Grandi, F., Ferrara, G., Pischiutta, F., et al. (2021). Intranasal delivery of mesenchymal stem cell secretome repairs the brain of Alzheimer's mice. *Cell Death Differ.* 28, 203–218. doi: 10.1038/s41418-020-0592-2

Scarpini, E., Schelterns, P., and Feldman, H. (2003). Treatment of Alzheimer's disease; current status and new perspectives. *Lancet Neurol.* 2, 539–547. doi: 10.1016/S1474-4422(03)00502-7

Schain, M., and Kreisl, W. C. (2017). Neuroinflammation in neurodegenerative disorders-a review. *Curr. Neurol. Neurosci. Rep.* 17:25. doi: 10.1007/s11910-017-0733-2

Scheibe, F., Klein, O., Klose, J., and Priller, J. (2012). Mesenchymal stromal cells rescue cortical neurons from apoptotic cell death in an in vitro model of cerebral ischemia. *Cell Mol. Neurobiol.* 32, 567–576. doi: 10.1007/s10571-012-9798-2

Scheper, V., Schwieger, J., Hamm, A., Lenarz, T., and Hoffmann, A. (2019). BDNF-overexpressing human mesenchymal stem cells mediate increased neuronal protection in vitro. *J. Neurosci. Res.* 97, 1414–1429. doi: 10.1002/jnr.24488

Scuteri, A., Cassetti, A., and Tredici, G. (2006). Adult mesenchymal stem cells rescue dorsal root ganglia neurons from dying. *Brain Res.* 1116, 75–81. doi: 10.1016/j.brainres.2006.07.127

Scuteri, A., Miloso, M., Foudah, D., Orciani, M., Cavaletti, G., and Tredici, G. (2011a). Mesenchymal stem cells neuronal differentiation ability: A real perspective for nervous system repair? *Curr. Stem Cell Res. Ther.* 6, 82–92. doi: 10.2174/157488811795495486

Scuteri, A., Ravasi, M., Pasini, S., Bossi, M., and Tredici, G. (2011b). Mesenchymal stem cells support dorsal root ganglion neurons survival by inhibiting the metalloproteinase pathway. *Neuroscience* 172, 12–19. doi: 10.1016/j.neuroscience.2010.10.065

Sha, S., Shen, X., Cao, Y., and Qu, L. (2021). Mesenchymal stem cells-derived extracellular vesicles ameliorate Alzheimer's disease in rat models via the microRNA-29c-3p/BACE1 axis and the Wnt/β-catenin pathway. *Aging (Albany NY)* 13, 15285–15306. doi: 10.18632/aging.203088

Shin, J. Y., Park, H. J., Kim, H. N., Oh, S. H., Bae, J.-S., Ha, H.-J., et al. (2014). Mesenchymal stem cells enhance autophagy and increase β-amyloid clearance in Alzheimer disease models. *Autophagy* 10, 32–44. doi: 10.4161/auto.26508

Si, Z., and Wang, X. (2021). Stem Cell Therapies in Alzheimer's Disease: Applications for disease modeling. *J. Pharmacol. Exp. Ther.* 377, 207–217. doi: 10.1124/jpet.120.000324

Siskova, Z., and Tremblay, M. -È (2013). Microglia and Synapse: Interactions in health and neurodegeneration. *Neural plasticity* 2013, 425845. doi: 10.1155/2013/425845

Solito, E., and Sastre, M. (2012). Microglia Function in Alzheimer's Disease. *Front. Pharmacol.* 3:14. doi: 10.3389/fphar.2012.00014

Song, M. S., Learman, C. R., Ahn, K. C., Baker, G. B., Kippe, J., Field, E. M., et al. (2015). In vitro validation of effects of BDNF-expressing mesenchymal stem cells on neurodegeneration in primary cultured neurons of APP/PS1 mice. *Neuroscience* 307, 37–50. doi: 10.1016/j.neuroscience.2015.08.011

Swerdlow, R. H. (2007). Pathogenesis of Alzheimer's disease. *Clin. Interv. Aging* 2, 347–359.

Tripathi, T., and Khan, H. (2020). Direct Interaction between the beta-Amyloid Core and Tau Facilitates Cross-Seeding: A Novel Target for Therapeutic Intervention. *Biochemistry* 59, 341–342. doi: 10.1021/acs.biochem.9b01087

Ullah, M., Liu, D. D., and Thakor, A. S. (2019). Mesenchymal stromal cell homing: Mechanisms and strategies for improvement. *iScience* 15, 421–438. doi: 10.1016/j.isci.2019.05.004

van der Flier, W. M., Pijnenburg, Y. A., Fox, N. C., and Scheltens, P. (2011). Early-onset versus late-onset Alzheimer's disease: The case of the missing APOE varepsilon4 allele. *Lancet Neurol.* 10, 280–288. doi: 10.1016/S1474-4422(10)70306-9

Van Velthoven, C. T., Kavelaars, A., and Heijnen, C. J. (2012). Mesenchymal stem cells as a treatment for neonatal ischemic brain damage. *Pediatr. Res.* 71, 474–481. doi: 10.1038/pr.2011.64

Villar, M. F. Z., Hanotte, J. L., Pardo, J., Morel, G. R., Mazzolini, G., García, M. G., et al. (2020). Mesenchymal stem cells therapy improved the streptozotocin-induced behavioral and hippocampal impairment in rats. *Mol. Neurobiol.* 57, 600–615. doi: 10.1007/s12035-019-01729-z

Wang, X., Ma, S., Yang, B., Huang, T., Meng, N., Xu, L., et al. (2018). Resveratrol promotes hUC-MSCs engraftment and neural repair in a mouse model of Alzheimer's disease. *Behav. Brain Res.* 339, 297–304. doi: 10.1016/j.bbr.2017.10.032

Wei, Y., Xie, Z., Bi, J., and Zhu, Z. (2018). Anti-inflammatory effects of bone marrow mesenchymal stem cells on mice with Alzheimer's disease. *Exp. Ther. Med.* 16, 5015–5020. doi: 10.3892/etm.2018.6857

Wilkins, A., Kemp, K., Ginty, M., Hares, K., Mallam, E., and Scolding, N. (2009). Human bone marrow-derived mesenchymal stem cells secrete brain-derived neurotrophic factor which promotes neuronal survival in vitro. *Stem Cell Res.* 3, 63–70. doi: 10.1016/j.scr.2009.02.006

Wong, W. (2020). Economic burden of Alzheimer disease and managed care considerations. *Am. J. Manag. Care* 26, S177–S183. doi: 10.37765/ajmc.2020.88482

Xie, J., Liang, R., Wang, Y., Huang, J., Cao, X., and Niu, B. (2020). Progress in Target Drug Molecules for Alzheimer's Disease. *Curr. Top Med. Chem.* 20, 4–36. doi: 10.2174/1568026619666191203113745

Xie, Z. H., Liu, Z., Zhang, X. R., Yang, H., Wei, L. F., Wang, Y., et al. (2016). Wharton's Jelly-derived mesenchymal stem cells alleviate memory deficits and reduce amyloid-beta deposition in an APP/PS1 transgenic mouse model. *Clin. Exp. Med.* 16, 89–98. doi: 10.1007/s10238-015-0375-0

Yan, K., Zhang, R., Chen, L., Chen, F., Liu, Y., Peng, L., et al. (2014a). Nitric oxide-mediated immunosuppressive effect of human amniotic membrane-derived mesenchymal stem cells on the viability and migration of microglia. *Brain Res.* 1590, 1–9. doi: 10.1016/j.brainres.2014.05.041

Yan, Y., Ma, T., Gong, K., Ao, Q., Zhang, X., and Gong, Y. (2014b). Adipose-derived mesenchymal stem cell transplantation promotes adult neurogenesis in

the brains of Alzheimer's disease mice. *Neural. Regen. Res.* 9, 798–805. doi: 10.4103/1673-5374.131596

Yang, C., Li, Y., Du, M., and Chen, Z. (2019). Recent advances in ultrasound-triggered therapy. *J. Drug Target* 27, 33–50. doi: 10.1080/1061186X.2018.1464012

Yang, H., Xie, Z. H., Wei, L. F., Yang, H. N., Yang, S. N., Zhu, Z. Y., et al. (2013). Human umbilical cord mesenchymal stem cell-derived neuron-like cells rescue memory deficits and reduce amyloid-beta deposition in an AβPP/PS1 transgenic mouse model. *Stem Cell Res. Ther.* 4:76. doi: 10.1186/scrt227

Yang, L., Zhai, Y., Hao, Y., Zhu, Z., and Cheng, G. (2020). The regulatory functionality of exosomes derived from hUMSCs in 3D Culture for Alzheimer's Disease Therapy. *Small* 16:1906273. doi: 10.1002/smll.201906273

Yokokawa, K., Iwahara, N., Hisahara, S., Emoto, M. C., Saito, T., Suzuki, H., et al. (2019). Transplantation of mesenchymal stem cells improves Amyloid-β pathology by modifying microglial function and suppressing oxidative stress. *J. Alzheimers Dis.* 72, 867–884.

Yong, H. Y. F., Rawji, K. S., Ghorbani, S., Xue, M., and Yong, V. W. (2019). The benefits of neuroinflammation for the repair of the injured central nervous system. *Cell Mol. Immunol.* 16, 540–546. doi: 10.1038/s41423-019-0223-3

Yun, H., Kim, H., Park, K., Shin, J., Kang, A., Il Lee, K., et al. (2013). Placenta-derived mesenchymal stem cells improve memory dysfunction in an A β 1–42-infused mouse model of Alzheimer's disease. *Cell Death Dis.* 4, e958–e958. doi: 10.1038/cddis.2013.490

Zenaro, E., Pietronigro, E., Della Bianca, V., Piacentino, G., Marongiu, L., Budui, S., et al. (2015). Neutrophils promote Alzheimer's disease-like pathology and cognitive decline via LFA-1 integrin. *Nat. Med.* 21, 880–886. doi: 10.1038/nm.3913

Zhang, Z., Sheng, H., Liao, L., Xu, C., Zhang, A., Yang, Y., et al. (2020). Mesenchymal stem cell-conditioned medium improves mitochondrial dysfunction and suppresses apoptosis in okadaic acid-Treated SH-SY5Y Cells by extracellular vesicle mitochondrial transfer. *J. Alzheimers Dis.* 78, 1161–1176. doi: 10.3233/JAD-200686

Zhao, Y., Chen, X., Wu, Y., Wang, Y., Li, Y., and Xiang, C. (2018). Transplantation of human menstrual blood-derived mesenchymal stem cells alleviates Alzheimer's Disease-Like Pathology in APP/PS1 Transgenic Mice. *Front. Mol. Neurosci.* 11:140. doi: 10.3389/fnmol.2018.00140

Zheng, X.-Y., Wan, Q.-Q., Zheng, C.-Y., Zhou, H.-L., Dong, X.-Y., Deng, Q.-S., et al. (2017). Amniotic mesenchymal stem cells decrease Aβ deposition and improve memory in APP/PS1 transgenic mice. *Neurochem. Res.* 42, 2191–2207. doi: 10.1007/s11064-017-2226-8

Zhou, L. N., Wang, J. C., Zilundu, P. L. M., Wang, Y. Q., Guo, W. P., Zhang, S. X., et al. (2020). A comparison of the use of adipose-derived and bone marrow-derived stem cells for peripheral nerve regeneration in vitro and in vivo. *Stem Cell Res. Ther.* 11:153. doi: 10.1186/s13287-020-01661-3

Zlokovic, B. V. (2011). Neurovascular pathways to neurodegeneration in Alzheimer's disease and other disorders. *Nat. Rev. Neurosci.* 12, 723–738. doi: 10.1038/nrn3114

frontiers | Frontiers in Aging Neuroscience

TYPE Original Research
PUBLISHED 06 October 2022
DOI 10.3389/fnagi.2022.1010765

OPEN ACCESS

EDITED BY
Woon-Man Kung,
Chinese Culture University, Taiwan

REVIEWED BY
Katharina Glomb,
Charité Medical University of Berlin, Germany
Murat Ozgoren,
Near East University, Cyprus

*CORRESPONDENCE
Elvira Khachatryan
elvira.khachatryan@ugent.be

SPECIALTY SECTION
This article was submitted to Alzheimer's Disease and Related Dementias, a section of the journal Frontiers in Aging Neuroscience

RECEIVED 03 August 2022
ACCEPTED 20 September 2022
PUBLISHED 06 October 2022

CITATION
Khachatryan E, Wittevrongel B, Reinartz M, Dauwe I, Carrette E, Meurs A, Van Roost D, Boon P and Van Hulle MM (2022) Cognitive tasks propagate the neural entrainment in response to a visual 40 Hz stimulation in humans.
Front. Aging Neurosci. 14:1010765.
doi: 10.3389/fnagi.2022.1010765

Cognitive tasks propagate the neural entrainment in response to a visual 40 Hz stimulation in humans

Elvira Khachatryan[1,2,3]*, Benjamin Wittevrongel[3,4], Mariska Reinartz[4,5], Ine Dauwe[1], Evelien Carrette[1], Alfred Meurs[1], Dirk Van Roost[6], Paul Boon[1] and Marc M. Van Hulle[3,4]

[1]Department of Neurology, Ghent University Hospital, Ghent, Belgium, [2]Department of Neurology, General Hospital Maria Middelares, Ghent, Belgium, [3]Department of Neuroscience, Laboratory for Neuro- and Psychophysiology, KU Leuven, Leuven, Belgium, [4]Leuven Brain Institute (LBI), Leuven, Belgium, [5]Department of Neuroscience, Laboratory for Cognitive Neurology, KU Leuven, Leuven, Belgium, [6]Department of Neurosurgery, Ghent University Hospital, Ghent, Belgium

Introduction: Alzheimer's disease is one of the great challenges in the coming decades, and despite great efforts, a widely effective disease-modifying therapy in humans remains elusive. One particular promising non-pharmacological therapy that has received increased attention in recent years is based on the Gamma ENtrainment Using Sensory stimulation (GENUS), a high-frequency neural response elicited by a visual and/or auditory stimulus at 40 Hz. While this has shown to be effective in animal models, studies on human participants have reported varying success. The current work hypothesizes that the varying success in humans is due to differences in cognitive workload during the GENUS sessions.

Methods: We recruited a cohort of 15 participants who underwent a scalp-EEG recording as well as one epilepsy patient who was implanted with 50 subdural surface electrodes over temporo-occipital and temporo-basal cortex and 14 depth contacts that targeted the hippocampus and insula. All participants completed several GENUS sessions, in each of which a different cognitive task was performed.

Results: We found that the inclusion of a cognitive task during the GENUS session not only has a positive effect on the strength and extent of the gamma entrainment, but also promotes the propagation of gamma entrainment to additional neural areas including deep ones such as hippocampus which were not recruited when no cognitive task was required from the participants. The latter is of particular interest given that the hippocampal complex is considered to be one of the primary targets for AD therapies.

Discussion: This work introduces a possible improvement strategy for GENUS therapy that might contribute to increasing the efficacy of the therapy or shortening the time needed for the positive outcome.

KEYWORDS

electroencephalography (EEG), electrocorticography (ECoG), Gamma ENtrainment Using Sensory stimulation (GENUS), cognitive decline, cognitive task

1. Introduction

Alzheimer disease's (AD) is a progressive, life-shortening condition characterized by a gradual decline in cognitive abilities, eventually leading to dementia (Breijyeh and Karaman, 2020; Knopman et al., 2021). The risk for AD-development dramatically increases with age as, according to the Alzheimer's Association report, more than 30% of the population aged above 85 live with AD (Hebert et al., 2013; Association, 2020). Given the globally aging population and the suffering that the disease causes the patients and their caregivers, the social and economic burden associated with AD will progressively grow.

Despite considerable efforts, research toward therapeutic disease-modifying strategies for AD have, so far, not been widely successful. The vast majority of these efforts is built upon the amyloid hypothesis which states that the disease evolves as a result of amyloid accumulation and, subsequent accumulation of more non-specific proteins, such as total and phosphorylated tau, that cause neural injury resulting in neurodegeneration and cognitive decline (Sperling et al., 2011; Jack et al., 2018). Several pharmaceutical therapies aimed at improving amyloid clearance have been developed but reported little success (Breijyeh and Karaman, 2020). Also, Aducanumab, the first ever FDA-approved disease-modifying therapy for AD, despite showing great promise, yields contradictory results (Mullard, 2021).

In recent years, a new therapeutic technique has been described based on "Gamma ENtrainment Using Sensory stimuli" (GENUS; Iaccarino et al., 2016; Adaikkan and Tsai, 2020). This technique presents the subject with sensory (visual and/or auditory) stimulation at a frequency of 40 Hz and elicits neural gamma activations. It has shown promising outcomes in mouse models of AD, where reduced amyloid production and improved clearance in hippocampus and prefrontal cortex, as well as improved recognition and visuospatial memory (Adaikkan et al., 2019; Martorell et al., 2019), have been described following a GENUS "therapy" of 1 h daily sessions over the course of one to several weeks.

According to the *in vivo* studies GENUS stimulation activates microglia, down-regulates the expression of inflammatory proteins therefore having an anti-inflammatory effect as well as modulates synaptic plasticity (Guan et al., 2022). Visual 40 hz stimulation alleviates the cell loss in V1, CA1 cingulate cortex and somatosensory cortex in mice AD-model. TMS with 40 Hz shown to enhance gamma band power in a number of areas including left parietotemporal cortex and in this way improves condition and executive function in AD patients. It was shown also improves connectivity between posterior cingulate cortex and precuneus (Adaikkan and Tsai, 2020; Guan et al., 2022).

However, GENUS studies in humans have, so far, not shown conclusive results (Ismail et al., 2018; Sharpe et al., 2020). While some studies have described improved cognition with a decline in cortical atrophy and strengthening of the default mode network in patients with mild-AD (Chan et al., 2021), and an improved mood and memory in healthy participants (Sharpe et al., 2020), others were unable to observe any change in amyloid accumulation after a 10-day therapy (Ismail et al., 2018).

It is currently unclear why the outcomes of gamma entrainment therapy in humans are inconclusive. The authors of previously mentioned negative report (Ismail et al., 2018), which used 10-day therapies of visual entrainment, suggested that a longer therapy would be required for positive outcomes. While successful reports indeed adapted longer therapies [4 weeks (Sharpe et al., 2020) to 3 months (Chan et al., 2021)], the entrainment-evoking stimulation also differed across the studies [visual (Park et al., 2020), auditory (Sharpe et al., 2020), or audiovisual (Chan et al., 2021)], rendering a direct comparison not trivial.

Another suggestion relates to the activities performed during the therapy. It has been recently shown in mice (Park et al., 2020) that physical exercise during the gamma entrainment therapy (over the course of 4 weeks) reduces amyloid and tau-levels to a greater degree compared to visual stimulation or exercise alone, and in this way improves spatial learning, working and long-term memory. In previous human studies, the activities of the patients enrolled in the therapies have not been well-described. EEG in response to 40 Hz stimulation was also not recorded in all studies (for example Ismail et al., 2018; Sharpe et al., 2020; Chan et al., 2021) making it in some cases difficult to assure that the entrainment actually occurred. These factors render it hard to distill a clear conclusion about the effect of cognitive or physical activity during the entrainment therapy.

With the current study, we aim to investigate the latter issue and deepen our understanding of the exact conditions required for improved gamma entrainment. To this end, we adopted a visual gamma entrainment paradigm (i.e., a 40 Hz flickering stimulation) and combined it with simple visual and non-visual tasks. We captured the evoked entrainment and its spreading in the brain using scalp- and intracranial electroencephalography (EEG) in young cognitively-healthy participants.

Based on previous frequency tagging studies (Silberstein et al., 2001; Toffanin et al., 2009), we hypothesize that the combination of 40 Hz flickering with a cognitive task would evoke a stronger and more widespread entrainment compared to a non-task setting. This cortical spreading is important as traditional visual steady-state responses are believed to be limited to the early visual cortices (Wittevrongel et al., 2018), while entrainment therapies mostly target hippocampal amyloid buildup. Furthermore, given that the visual task requires an interaction with the stimulation paradigm, we hypothesize that it will evoke a stronger (and/or more widespread) entrainment compared to a non-visual cognitive task of similar complexity.

In case our hypothesis holds, and addition of a simple cognitive task during entrainment therapy contributes to its spreading across the cortex or its strengthening, it might open the door for more efficient non-pharmacological and non-invasive gamma entrainment therapies for Alzheimer's disease in humans.

2. Results

To investigate the effect of cognitive tasks on the gamma entrainment, we developed a paradigm that presents a visual flicker to 16 participants while we recorded their neural responses using scalp-EEG (15 participants) or invasive-EEG (1 participant). The eye movements and fixation was recorded using eye-tracking. Each of the participants completed four sessions each 5 min long, during each of which a visual flickering was presented (Figure 1): 3 sessions of 40 Hz regular [R] flickering and 1 session of irregular [I] flickering using concatenated single periods of frequencies randomly sampled between 30 and 50 Hz. Two out of three R-sessions were combined with a cognitive task—one with mental counting [RC] and one with visual attention (oddball paradigm) [RO]. The remaining R- and I-conditions were coupled with a resting state, i.e., no-task conditions (RN and IN). In addition to these conditions, the 15 participants that underwent scalp-EEG recordings (62 active Ag/AgCl electrodes) were also presented with an irregular flickering combined with a visual attention task (IO condition), and 14 of these participants also completed an attention task without visual flicker [O]. For a detailed description of the experimental paradigm and the analysis methods, we refer the reader to the Section 4.

2.1. Cognitive tasks strengthen the gamma entrainment and contribute to its cortical spreading

2.1.1. Eye-tracking

The eyetracking results showed that subjects were continuously attending the stimulation device during all stimulation conditions with the average deviation of $1.7 \pm 0.17^{\circ}$ in horizontal axis and $1.3 \pm 0.47^{\circ}$ in vertical axis, while the stimulation device spanned 8.3° visual angle.

2.1.2. Scalp EEG

First, the spectral content of the neural responses was obtained using the Fourier transform (frequency resolution of 0.033 Hz). All conditions in which a regular visual flicker was presented exhibit a clear peak at 40 Hz in the spectrum (i.e., the gamma entrainment) while the irregular conditions do not (Figure 2). Noteworthy, the irregular condition that was paired with a task, similar to the irregular-no task condition, did not evoke a change in the 40 Hz amplitude. This suggests that the task *per se* is not responsible for a change in the frequency-of-interest. Given these negative results and in order to keep the message clear, we will discuss only the results on the regular flickering in the remainder of this manuscript. Supplementary Figure S1 further shows the time-frequency spectrum on two representative electrodes, clearly showing the effect of the stimulation on the recorded signals.

The extent of the entrainment elicited by the different conditions is further quantified using the signal-to-noise ratio (SNR), which represents the prominence of the 40 Hz amplitude response with respect to the surrounding frequencies (i.e., baseline). Figure 3 shows the difference in scalp topography between each pair of the regular conditions averaged across subjects, effectively showing the spreading of the gamma entrainment over the scalp. Note that electrode with a significant difference are indicates with thicker dots. As quantitative illustration, Table 1 lists the median SNRs and their 95% confidence intervals (CI) for each stimulation condition across all subjects on electrodes O2 and Cz.

The non-parametric Kruskal-Wallis test shows a significant effect of stimulation condition (RN, RO, RC, IN, and IO) on the SNR at nearly all electrode sites (e.g., on electrode O2, $\chi^2 = 810.14$, $p < 0.0001$; on electrode Cz, $\chi^2 = 736.92$, $p < 0.0001$ and on electrode Fz, $\chi^2 = 480.96$, $p < 0.0001$). When comparing only the three regular conditions using the same method, a large number of electrodes showed a significant effect of cognitive task on the measured SNR, this time mainly at parieto-central and centro-frontal locations. Further pairwise comparison using the Kruskal-Wallis test with FDR correction for p-values showed a significant difference between mainly both task conditions and no-task condition (all $p < 0.05$, Figure 3 for the spatial distribution of the difference). Figure 3 suggests that the inclusion of a cognitive task during the sensory stimulus (conditions RC and RO) spreads the effect of the gamma entrainment over a larger cortical area, as nearly all non-occipital scalp electrodes exhibit a significant increase in SNR compared to the non-task (RN) setting (e.g., for electrode CP1, $\chi^2 = 12.37$, $p = 0.0004$ between RO and RN and, $\chi^2 = 16.62$, $p = 0.000046$ between RC and RN conditions). In contrary to what was expected, the difference between the two task conditions (i.e., RO and RC) was considerably less pronounced and limited to only electrode C1.

In addition to the previous group-level analysis, we further investigated our data on a single-subject level. We adopted the cluster-based permutation test (Maris and Oostenveld, 2007) to statistically quantify the spreading of the gamma entrainment (reflected in an increased SNR compared to the non-task setting) for each subject individually. This method considers not only the temporal properties of EEG signal but also the spatial distribution of the effect and does so using a data-driven approach. This allows us to perform a

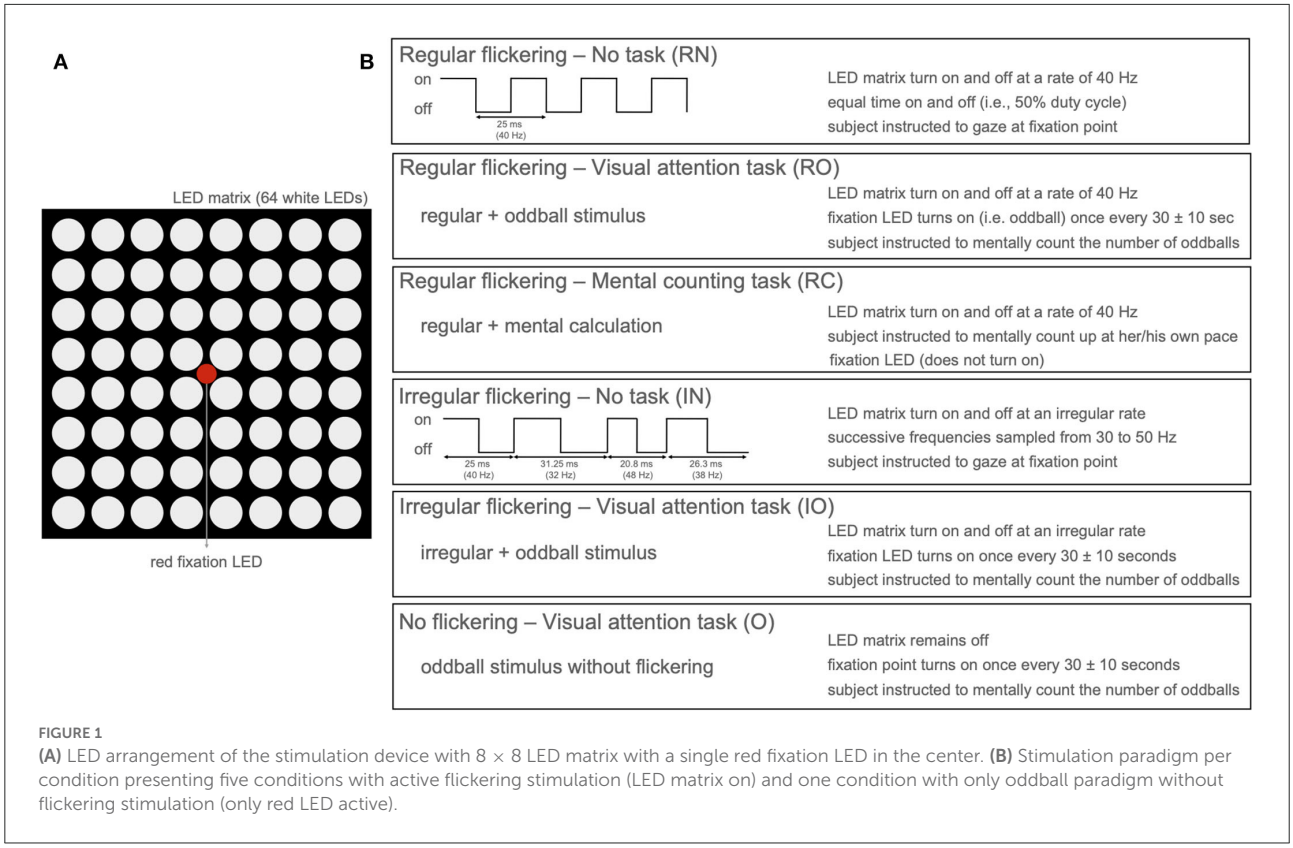

FIGURE 1
(A) LED arrangement of the stimulation device with 8 × 8 LED matrix with a single red fixation LED in the center. **(B)** Stimulation paradigm per condition presenting five conditions with active flickering stimulation (LED matrix on) and one condition with only oddball paradigm without flickering stimulation (only red LED active).

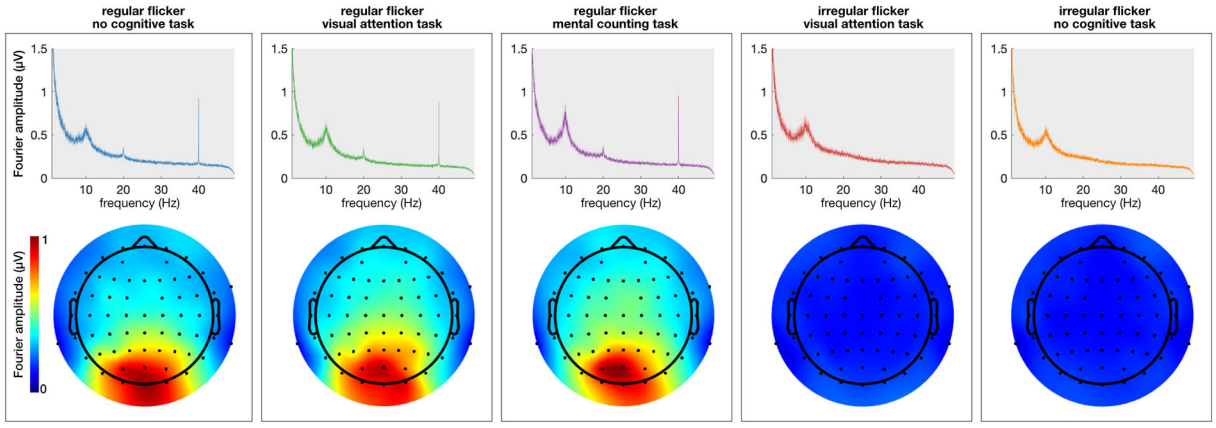

FIGURE 2
Average (across subjects) frequency spectrum showing gamma entrainment for each of every five stimulation conditions. The **(top)** panel shows the amplitude of the 40 Hz frequency in the frequency spectrum presented in μV and the **(bottom)** panels show the spatial distribution of 40 Hz across the scalp. As one can see, unlike regular stimulation conditions, there is no increase in 40 Hz amplitude in irregular stimulation conditions. As to spatial distribution of the entrainment, as expected, it was the most prominent in the occipital area of the scalp for all regular conditions.

rigorous statistical comparison while simultaneously preserving the power of our study. The irregular conditions did not show a significantly higher gamma entrainment in any of the subjects. This is expected as these conditions do not satisfy the stationarity criteria to elicit a steady-state neural response. To further corroborate, we compared the two irregular conditions and again obtained practically no significant clusters. When comparing the regular no-task (RN) and visual attention (RO)

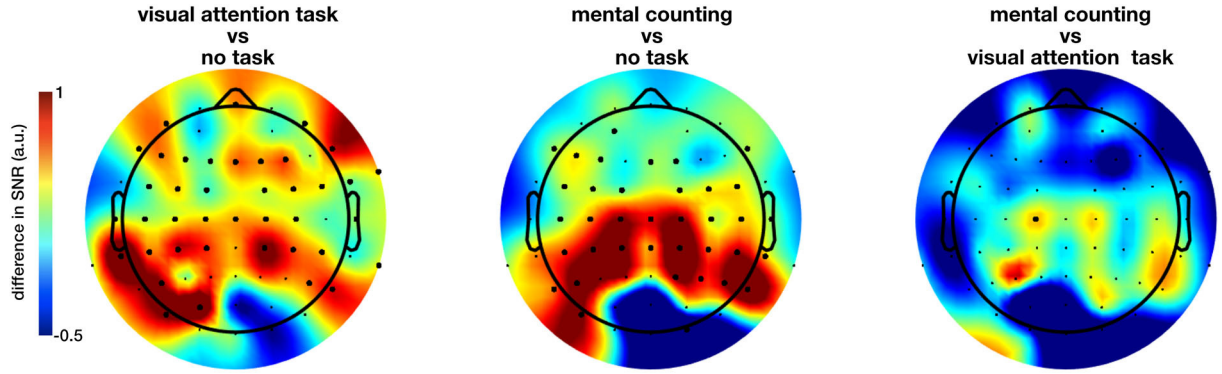

FIGURE 3
Difference in the gamma entrainment signal-to-noise ratios (ΔSNR) of regular-flickering conditions across subjects. The electrodes at which a statistical significance between conditions is detected are marked with thick dots. The significant difference between conditions with and without cognitive task are always in the anterior regions with visual task being more spread to the centro-frontal areas and non-visual task to the parietocentral regions. Furthermore, even though not statistically significant, one can see that the no-task condition consistently evokes stronger entrainment in the occipital regions in comparison with task conditions.

TABLE 1 Median SNR and 95% confidence interval for each stimulation condition at two representative electrodes.

	Regular flickering			Irregular flickering	
	No task	Visual attention task	Mental counting task	No task	Visual attention task
O2	7.55 (6.77–8.48)	7.04 (6.04–7.96)	5.96 (4.98–6.77)	0.95 (0.9–1.04)	1 (0.9–1.07)
Cz	3.1 (2.88–3.43)	3.68 (3.38–3.95)	3.96 (3.73–4.26)	0.96 (0.85–1.03)	0.88 (0.79–0.93)

conditions, 12 out of 15 subjects had at least one statistically significant cluster (median $p = 0.0005$) exhibiting a higher SNR for the RO condition with an average number of 25.5 electrodes per cluster (ranging between 4 and 48 electrodes). This suggests a more widespread effect of the gamma entrainment with the addition of a visual attention task. Similarly, when comparing the mental counting (RC) and no-task (RN) conditions, 10 out of 15 subjects exhibited at least one significant cluster (median $p = 0.0005$) of wider/stronger SNR for the mental counting task, with an average of 26.7 electrodes per cluster (ranging between 3 and 49 electrodes). Finally, when comparing the RO and RC conditions, 12 out of 15 subjects presented clusters (median $p = 0.0047$) where the activation for RC was higher than for RO, with on average 14.75 electrodes per cluster ranging between 4 and 36 electrodes. The difference between the two cognitive task conditions seems to suggest that the topography of the spreading depends on the type of task instructed to the participants. Figure 4 summarizes these results by showing the number of subjects that exhibited a significant effect for each scalp electrode (i.e., for how many subjects that each electrode was included in a significant cluster). This figure shows that, while there is a considerable degree of variability in spreading across subjects, a general trend toward an anterior inclusion is clearly noticeable. Furthermore, it becomes clear that the mental counting task seems more restricted to the central scalp area while the visual attention task also involves the frontal areas.

2.2. Cognitive tasks propagate the gamma entrainment to the hippocampus and insula

2.2.1. Intracranial EEG

While the results of the scalp-EEG cohort are promising, the evidence is indirect as scalp signals lack the spatial fidelity to make strong claims about cortical involvements. In an effort to corroborate the propagation of the gamma entrainment through the brain with the addition of a cognitive task, we recruited one epilepsy patient who was temporarily implanted with subdural and depth electrodes (63 contacts in total, Figures 5C,D) and repeated the same experiment, albeit with a reduced number of conditions (RN, RO, RC, and IN) in order to adhere to the clinical constraints (see Section 4 for a detailed description). Similar to the scalp-EEG cohort, we extracted frequency spectrum for each condition (frequency resolution of 0.033 Hz; see Figures 5A,B for example spectra at two locations)

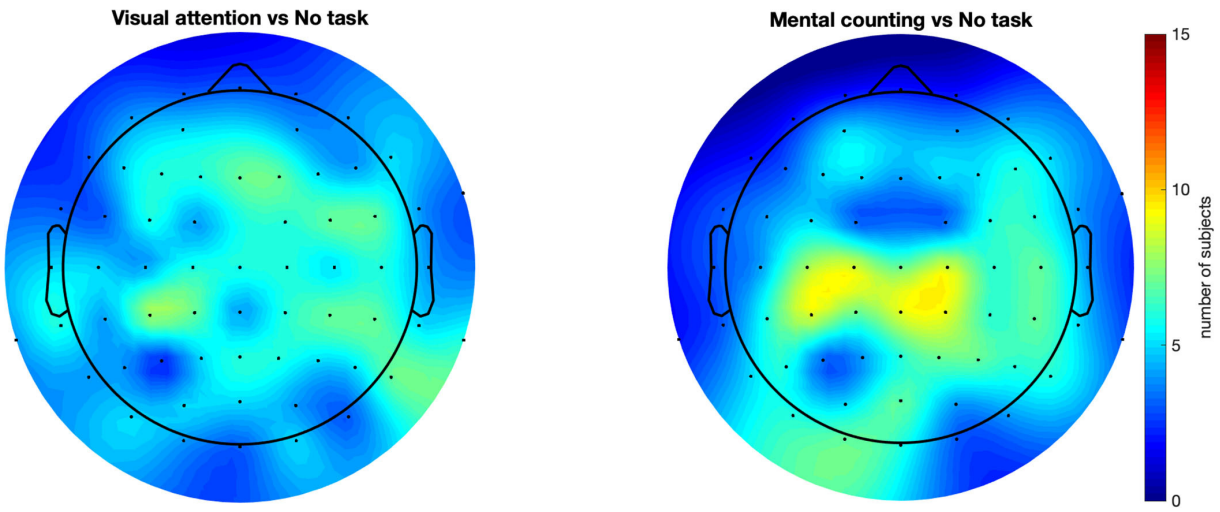

FIGURE 4
Scalp plots representing for how many subjects each electrode was included in a statistically significant cluster. All compared conditions had regular flickering. This figure suggests a consistency in the results across subjects, showing that majority of the subjects had an anterior propagation of the entrainment with introducing a cognitive task. These results also strengthen the observation in Figure 3 (the spatial distribution for task-conditions), but in this case in a single subject case basis.

and calculated the SNR of the 40 Hz component (i.e., the gamma entrainment) for each electrode individually.

The Kruskal-Wallis test revealed a significant effect of stimulation condition on gamma entrainment (Figures 5C,D) on five out of six electrodes implanted in the right hippocampus (e.g., for electrode RHD1, $p < 0.00001$), in four out of eight insular (ROD and RID) electrodes (e.g., on electrode RID1, $p = 0.00017$), in 6 out of 32 electrodes implanted over the right posterior temporal lobe (e.g., on electrode RTG8, $p = 0.004$), in 9 out of 10 electrodes implanted in the right occipital cortex (e.g., on electrode RGO1, $p < 0.00001$) and in six out of eight electrodes implanted in the right anterior lateral and basal temporal cortex (e.g., on electrode RSA4, $p = 0.0006$). This suggests that multiple brain areas, also outside the visual cortex, exhibit gamma entrainment when stimulated visually.

Further multiple comparison with the Wilcoxon rank-sum test (Supplementary Figure S2) and with FDR-correction shows a significant difference in the extent of gamma entrainment between the no-task and cognitive task conditions at hippocampal electrode RHD1 ($p = 0.0026$ between RN and RO and, $p = 0.003$ between RN and RC; Figure 5E). More importantly, no significant difference between regular and irregular no-task conditions was found at this electrode ($p = 0.27$), and the median SNR of both conditions is close to 1 suggesting that the visual stimulation alone has no effect on these neural areas. In contrast, the most superficial contact on the hippocampal probe (RHD6), which is not located within the hippocampal structure, does show a significant effect of gamma stimulation ($p = 0.0006$ between RN and IN conditions) but does not show a difference between regular conditions with and without a cognitive task ($p = 0.25$ between RN and RO; $p = 0.84$ between RN and RC and; $p = 0.16$ between RO and RC, analysis is not shown). For the insular electrodes, the main significant difference is observed between the regular no-task (RN) and visual attention (RO) conditions (e.g., for electrode RID2, $p < 0.00001$) and between the visual attention (RO) and mental counting (RC) conditions (e.g., for electrode RID1, $p = 0.016$). The right posterior temporal lobe is barely involved in the entrainment, while the majority of electrodes implanted over the right occipital cortex (Figure 5F) show significant differences across the stimulation conditions. At the latter locations, in addition to the expected absence of gamma entrainment for the irregular visual flickering (i.e., SNR close to 1), a significantly stronger gamma entrainment is observed for both cognitive task conditions compared to the no-task condition (e.g., $p < 0.00001$ on electrode RGO2, and, $p < 0.00005$ on electrode RGO4 for RO and RC conditions, respectively) and between two conditions with a cognitive task (e.g., on electrode RGO4, $p < 0.00001$ between RO and RC). On the right anterior temporal cortex, the main significant difference is noted between the no-task (RN) and both cognitive task conditions (e.g., on electrode RSA4, $p = 0.0015$ and $p = 0.0036$, for visual attention and for mental counting, respectively). Our results show that different brain areas react differently to the 40Hz flickering stimulation and the presence of a cognitive task influences the propagation of the entrainment.

10.3389/fnagi.2022.1010765

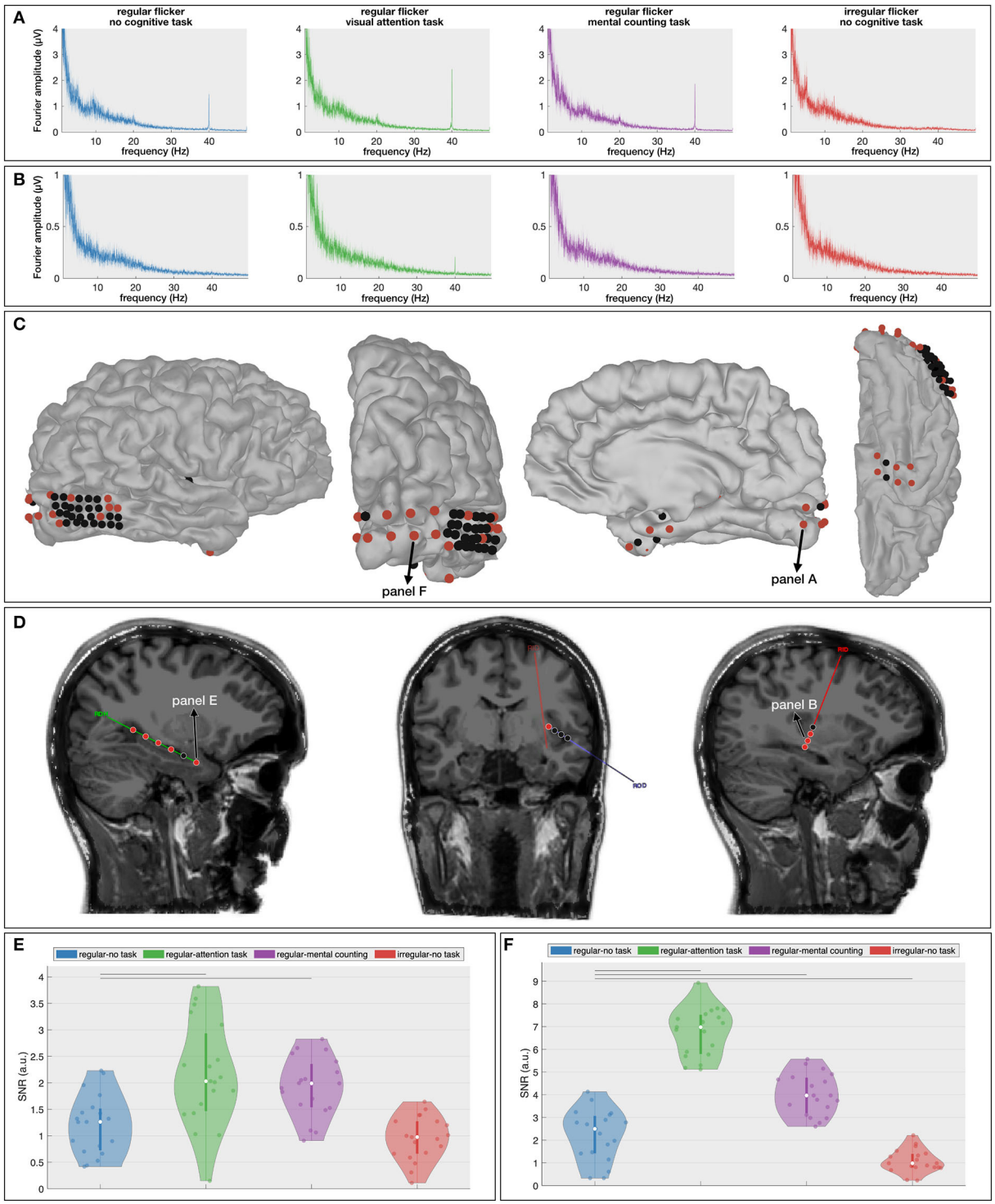

FIGURE 5
Intracranial results. **(A,B)** Frequency spectra for the four presented conditions at one cortical [**(A)**, primary visual cortex] and one depth [**(B)**, insular cortex] contact. These spectra show the increased gamma entrainment when the subject is instructed to perform a cognitive task during the visual stimulation. **(C,D)** Localization of the cortical **(C)** and depth **(D)** contacts. Electrodes that exhibit a significant difference in gamma entrainment across the four conditions using Kruskall-Wallis test are indicated in red. **(D,E)** Signal-to-noise ratio (SNR) boxplots in response to the four stimulation conditions for one hippocampal contact **(E)** and one occipital electrode **(F)**. Note that their locations are marked in **(C,D)**. The horizontal lines above the boxplots indicate the pairs that exhibit a statistically significant difference with no-task condition (Wilcoxon rank-sum test with FDR correction).

2.3. Unlike regular flickering, the irregular flickering negatively influences the attention processing

In a final analysis, in addition to the regular and irregular conditions with a visual attention task (RO and IO, respectively), we included the neural responses to the visual attention task without visual flickering (O). Here, we investigated the effect of flickering (regular and irregular) on the P300 Event-Related Potential (ERP; Soltani and Knight, 2000). As the P300 is one of the most commonly investigated ERP components in the context of memory, attention, and engagement (Datta et al., 2007), investigating its properties when combined with the visual flickering stimulation would allow us to judge effect of the flickering stimulation on the engagement processes in the brain. We expect to obtain a larger P300 response for oddball combined with regular flickering given that it would positively affect the engagement in comparison with oddball stimulation with combined with irregular flickering. One subject from the EEG cohort did not perform the O-condition and was hence excluded from this analysis. For each of the remaining 14 subjects, we extracted the P300 component for the RO-, IO-, and O-conditions as the maximal amplitude and its peak latency of the average response to the oddball stimulus (i.e., the red LED, see methods section) in the time window between 200 and 600 ms. The Kruskal-Wallis test with condition as independent factor showed a significant effect of condition on the P300 amplitude on a limited number of electrodes in the occipito-parieto-central (PO7, PO3, POz, PO8, P2, P6, CP5, CP4, CP6) areas (e.g., for electrode POz, $\chi^2 = 10.92$, $p = 0.0043$; for electrode P2, $\chi^2 = 9.33$, $p = 0.0094$, and for electrode CP4, $\chi^2 = 6.1$, $p < 0.05$) (Figure 6A). A further multiple comparison with the Wilcoxon rank-sum test and FDR correction for multiple comparison shows that this effect is mainly driven by a significantly smaller P300 peak amplitude for the IO condition compared to the O condition, which is consistent for several neighboring parieto-occipital electrodes (e.g., on electrode POz, $Z = 3.23$, $p = 0.0037$). For the other two comparisons, merely few (≤ 3) scattered electrodes exhibited a significant difference, rendering this difference less reliable. Figure 6B shows the scalp distribution of the mentioned effects. The thick dots on the scalp-plots represent the significant difference between the pairs of conditions. The Kruskal-Wallis test showed a significant effect of condition on the P300 peak-latency (Figure 6C) at 31 scalp electrodes (out of 62; e.g., for electrode Pz, $\chi^2 = 9.51$, $p = 0.0086$; for electrode POz, $\chi^2 = 12.76$, $p = 0.0017$). Further multiple comparison with the Wilcoxon rank-sum test and FDR correction for multiple comparison confirms the observation that this effect is mainly driven by a significantly shorter latency for the O condition (e.g., for electrode POz, $Z = 3.31$, $p = 0.0028$ with IO and $Z = 2.76$, $p = 0.0086$ for RO).

3. Discussion

In an effort to contribute to the development of more effective non-pharmacological therapies for AD, the current study aimed at deepen our understanding on how the therapy based on cortical gamma entrainment induced by visual stimulation can be improved. We showed that the inclusion of a simple cognitive task while gazing at a flickering 40 Hz stimulation not only results in an enhanced gamma entrainment but also propagates it to additional neural areas on which it can potentially have a sparing effect. We presented evidence from a scalp-EEG cohort, and furthermore corroborated these results using direct intracranial recordings. The latter additionally showed that in the presence of a cognitive task, the gamma entrainment effect is not only noticeable at the cortical surface but also in deep brain areas such as the hippocampus and insula. Entrainment of these deeper regions is of particular importance since those are believed to be among the first ones to be affected by AD, and therefore serve as primary targets for many AD-therapies (Mu and Gage, 2011). Despite this being an exciting observation, it is important to mention that these results do not imply the observed increased entrainment would have a larger effect on amyloid clearance or cognitive decline *per se*. Further studies are needed to tackle these issues.

One of the striking observations in the current study is that the hippocampus reacted similarly to both visual and non-visual cognitive tasks, while barely reacting to the gamma entrainment stimulation without a task. This could be explained by its involvement in memory processing rather than in processing the visual aspect of the stimulation (Bird and Burgess, 2008), which corroborates the importance of including a task during GENUS therapy and clearly reporting this to be able to aggregate the different reports in a future review study. Even though promising, we need to note that these results were obtained from a single subject. A follow-up study with inclusion of multiple intracranial recordings is required to generalize these results. Furthermore, it is important to remember that the data is obtained from a patient with epilepsy that was implanted with intracranial electrodes for clinical reasons. Thus, the brain response from this patient would not necessarily fully correspond to the response from a general population or patients with AD. Even though this is a serious concern but this is at this point the only way of recording intracranial human data within ethical norms.

It has been previously shown (Park et al., 2020) that visual gamma entrainment therapy can improve amyloid clearance in mouse models of AD, but studies with human participants were inconclusive with regard to the efficacy of the GENUS therapies. Importantly, none of the previous human studies considered the effect of the subject's mental activity during the therapy, which we showed here to have a significant impact. Given this, we recommend that further studies disclose whether

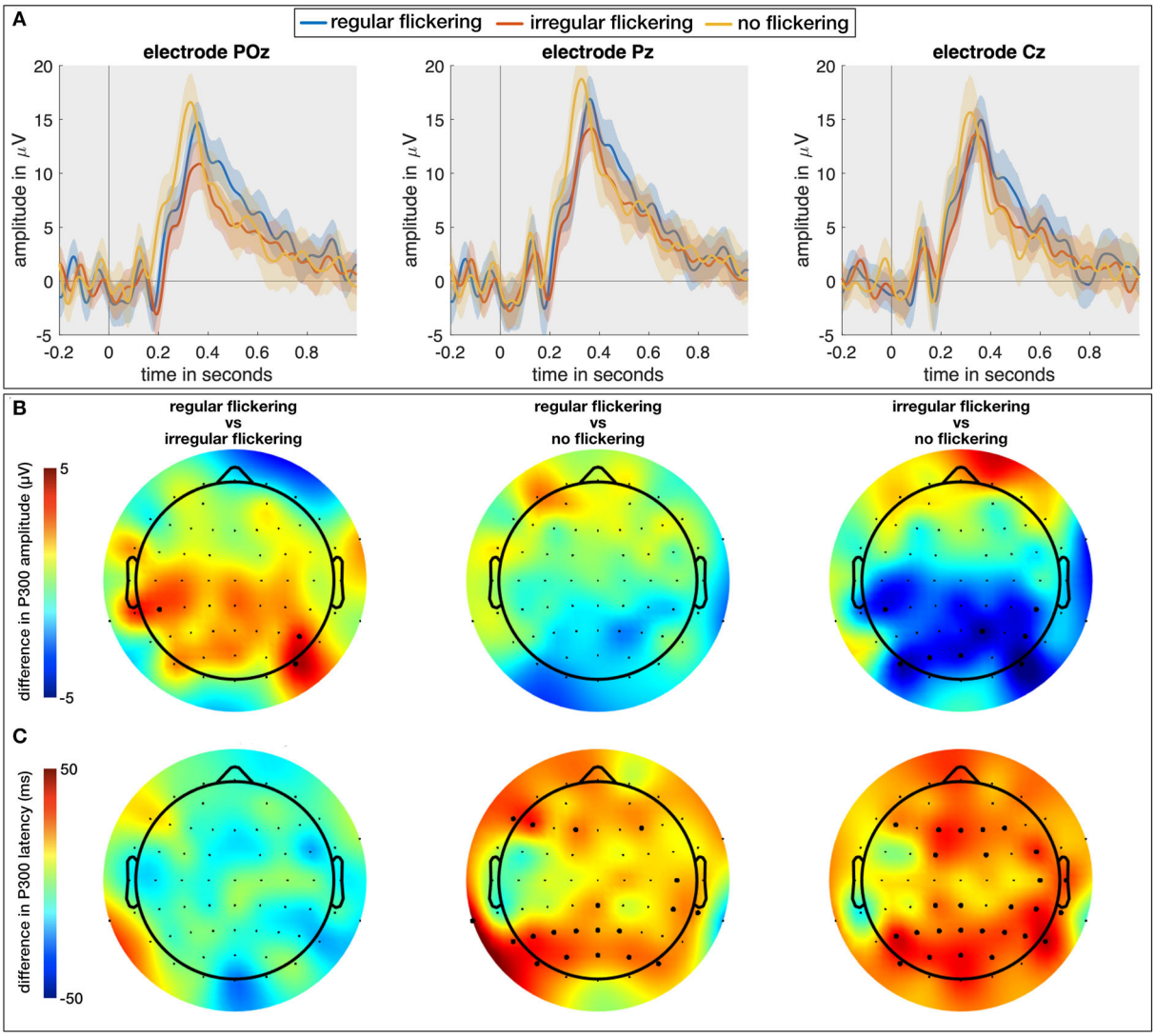

FIGURE 6
(A) The temporal plots (ERPs) in response to regular-oddball, irregular-oddball, and no-flickering-oddball conditions on electrodes POz, Pz, and Cz. Shaded area indicates 95% confidence interval, full-line is the average across the subjects. **(B)** Difference between P300 peak amplitudes [max between 200 and 600 ms (in μV)] between groups accounting for multiple comparisons (three groups). The largest difference was observed between irregular- and no-flicker conditions with no-flicker condition exhibiting the largest P300 amplitude on several electrodes. **(C)** Scalp plots for differences between P300 peak latencies across three groups accounted for multiple comparisons. The P300 response to flickering stimulus (both regular and irregular) was delayed in comparison to no-flickering stimulus. The electrodes indicating a statistically significant difference in **(B,C)** are presented with thick dots.

the participants were instructed to perform a cognitive task during the therapy, and specify the exact type of task in order to assess their effect on potential amyloid clearance in AD patients. The type of task can be important as also in the present work, we showed that the effect of mental counting seems more restricted to centro-parietal areas for most subjects while the gamma entrainment propagated more frontally during a visual attention task.

The analysis of the oddball data showed that regular flickering does not affect the amplitude of the P300-ERP evoked in response to visual attention task while the irregular flickering considerably decreased it in the parietal region. As the P300 component is assumed to reflect attention and engagement (Datta et al., 2007), this finding suggests that regular flickering does not influence these processes while irregular flickering considerably disrupts them. The increased latency for both regular and irregular flickering conditions suggests that an increased workload for both conditions. As irregular flickering is rarely used in studies, additional studies will be needed to corroborate this hypothesis.

In our previous ECoG study, using flickering stimulation between 10 and 15 Hz (Wittevrongel et al., 2018), we observed steady-state responses at the stimulus frequency that were confined to the primary visual cortex (V1) with no spreading to the associative visual cortex (V2). In contrast, in the current study, we observed a more widespread entrainment in the occipital cortex (i.e., beyond V1), even for the control condition without a cognitive task (as in aforementioned study). This seems to suggest that visual gamma entrainment fundamentally differs from the steady-state responses induced by lower stimulation frequencies, which is in line with theories stating that steady-state responses to higher frequencies have a different cortical distribution compared to those elicited by lower frequencies (Vialatte et al., 2010; Wu, 2016). A recent paper (Cimenser et al., 2021) suggests that the lower frequencies in the gamma range propagate to the larger scalp areas compared to the higher frequencies (including 40 Hz). The authors of this paper however, did not use a task and it is still not clear whether the propagation of the entrainment in combination with a task is different in 40 Hz stimulation from other gamma frequencies. Even though it will be undoubtedly interesting to investigate if such propagation is specific to 40 Hz stimulation or general to higher frequencies, it is out of scope of the current study.

While the current work presents compelling evidence that gamma entrainment benefits from a cognitive task, it remains to be seen whether it also promotes improvements in amyloid clearance in AD patients. If the efficacy of the therapy correlates with the strength/propagation of the entrainment, then the introduction of an additional mental task can help to shorten the currently conducted entrainment sessions in order to reach a predefined desired effect. This, together with a safe (He et al., 2021) and less taxing flickering stimulation procedure that is currently underway (Carstensen et al., 2020; Figueiro and Leggett, 2021), would make the non-invasive and non-pharmacological GENUS therapy more attractive and user-friendly. It is worth mentioning that the therapy if and when available with target the MCI or even earlier stages of disease considering the effect of any experimental disease-modifying therapy in the later stages of AD doomed to a failure due to irreversibility of neuronal damage in this stage. Furthermore, the integration of the stimulation in the daily life (e.g., as a background for ipad) would make the more user-friendly and less tiring.

4. Methods and materials

4.1. Subjects

Fifteen healthy young volunteers (10 female, ages between 21 and 35 years old, 13 right handed, on average 20 years of education) with normal or corrected-to-normal vision participated in the experiment. The healthy participants did not report any current or previous neurological or psychiatric condition. Additionally, one female patient with refractory epilepsy (24 years old, right handed, 16 years of education) was recruited for this study. Implantation of intracranial EEG (electrocorticography and stereo-EEG electrodes) was done in the scope of the patient's clinical workup with the purpose to locate and further remove the epileptogenic zone. The experiment was conducted while the patient was being monitored at the center for epilepsy monitoring at Gent University Hospital. Before participating, the healthy volunteers and the patient were informed about the purpose of the experiment, the procedure and how the data will be used (GDPR). They all read and signed the informed consent form prior approved by the ethical committees of Leuven (healthy subjects) and Gent (patient) University Hospitals.

4.2. Stimulation device

The stimulation device (Figure 1A) consisted of an 8 × 8 LED matrix (FND-588XW4SM00BW35, Forge, UK) controlled by an Arduino Uno microcontroller. The LED matrix was embedded in a white plastic enclosure, to diffuse the light emitted by the LEDs over a surface of 8 × 8 cm, and was suspended by a mounting arm whose height could be adjusted to match the position of the subject. In the center, a small red LED was mounted which was used for oddball stimulation (i.e., the visual attention task, see further) and also served as a fixation point for all sessions.

4.3. Experimental procedure

During the experiment, both healthy controls and the patient were sitting at a distance of 55 cm from the stimulation device. Background light was slightly dimmed during the experiment. The subjects experienced a light intensity ranging between 225 and 250 lumen when the stimulation device was on compared to the environmental luminosity (between 125 and 140 lumen) when it was off. In total, six experimental conditions (Figure 1B) were developed: Regular flickering-No task (RN), Regular flickering-Visual attention task (oddball, RO), Regular flickering-Mental counting task (RC), Irregular flickering-No task (IN), Irregular flickering-Visual attention task (oddball, IO), and No flickering-Visual attention task (oddball, O). Fourteen out of 15 healthy participants completed all six experimental conditions, while the remaining participant did not perform the O condition. The patient completed four conditions (no IO and O, due to practical constraints). Each condition was presented once for five consecutive minutes, and

the total experiment, including the EEG set-up and breaks, was completed within 60–90 min. In the RN condition, a regular 40 Hz stimulation was presented, which consisted of a square-wave pattern with a 50% duty cycle (Figure 1B). During the IN condition an irregular stimulation pattern was presented that was created by appending single periods of square-wave patterns (50% duty cycle) of random integer frequencies between 30 and 50 Hz. The same luminosity was used for both conditions. Participants were requested to gaze at the fixation point (Figure 1A) and to refrain from thinking about anything specific in order to avoid unintentional cognitive activity. In the RO and IO conditions, the regular and irregular stimulation, respectively, was complemented with an oddball stimulation during which the red fixation LED would light up for 250 ms using a jittered interstimulus interval of 30 ± 10 s (Figure 1B). For both conditions, participants were instructed to mentally count the number of oddball occurrences. During the RC condition, the regular 40 Hz stimulation was presented and participants were asked to gaze at the fixation LED while mentally counting up at their own pace as long as the stimulation was on. Note that, contrary to RO and IO conditions, the fixation LED did not light up in this condition. The purpose of this condition was to determine whether there are differences in visual attention during the execution of two cognitive tasks of similar complexity (i.e., counting up or counting the oddballs) would influence the gamma entrainment and its propagation through the brain. Additionally, for the scalp-EEG cohort only, a pure oddball condition (O) was presented where only the fixation LED would light up for 250 ms with a jittered interstimulus interval of 30 ± 10 s during 5 min while no surrounding flickering was present. Similar to the previous oddball conditions, the subjects were instructed to mentally count the occurrences of the oddball. All conditions were presented in pseudo-randomized order and never more than two of the same type of condition (regular or irregular flickering) were presented consecutively. Each condition was initiated by the researcher pressing a button connected to the microcontroller. In between conditions, the participants were asked to take a short break. For both the healthy subjects and the patient, the attendance to the stimulation was monitored in real-time using an eye-tracker (EyeLink 1000 Plus for healthy participants and a Tobii Pro device for the patient). Stimulus presentation was controlled *via* an Arduino microcontroller (Arduino IDE software, version 1.8.16). For the healthy group, the triggers to EEG, signaling the beginning and end of the flickering stimulation, as well as the beginning and end of the oddball presentation were sent *via* a StimTracker device (Cedric, USA). For the patient, this was done *via* MATLAB, 2017 using the serial cable connecting the laptop that controlled the stimulation and the EEG acquisition device.

4.4. Scalp and intracranial EEG data acquisition

4.4.1. Scalp EEG

From the group of healthy subjects, scalp EEG was acquired continuously using 62 active Ag/AgCl electrodes evenly distributed over the scalp at locations following the international 10/20 system. The ground and reference electrodes were placed at AFz and FCz locations, respectively. A drop of conductive gel was applied to each electrode to ensure optimal contact between the electrodes and the subject's scalp. The impedance was kept below 5 kΩ throughout the recordings. EEG data was acquired at a sampling rate of 1 kHz using Synamps RT device (Compumedics Europe, Germany) and stored on a laptop for further analysis.

4.4.2. Intracranial EEG

The patient was implanted with subdural grids covering the right occipital (grid 5 × 2 = 10 contacts), posterior temporal (grid 8 × 4 = 32 contacts) and, anterior and basal temporal (2 strips of 1 × 4 contacts) cortices (Figure 5), and three depth electrodes targeting the hippocampus (6 contacts) and insula (2 × 4 contacts) on the right side. The stereo-EEG contacts in hippocampus had size of 5 mm with 10 mm inter-contact spacing, in insula, they had size of 2 mm with 5 mm inter-contact spacing, the electrodes of the grids and strips had size of 3 mm with a center-to-center distance of 10 mm. In addition, 21 scalp-EEG electrodes were evenly distributed over the scalp at locations following the international 10/20 system. Both intracranial and scalp-EEG were recorded continuously using SD LTM 64 Express devices (Micromed, Italy) operating at a sampling rate of 256 Hz. Reference electrodes were placed on both mastoids. The intracranial electrodes were localized as described in our previous studies (Khachatryan et al., 2019; Hnazaee et al., 2020; Wittevrongel et al., 2020): from the pre-implantation MRI scan of the participants, a cortical reconstruction and volumetric segmentation was performed using the FreeSurfer image analysis suite (version 6.0; Fischl, 2012). The FreeSurfer output was then loaded into Brainstorm (Tadel et al., 2011) and co-registered with a post-implant CT using the SPM12 (Penny et al., 2011) extension. The coordinates of the implanted electrodes were then manually obtained from the artifacts in the CT scan and projected on the cortical surface. The obtained electrode locations were then verified by a neurologist based on the intra-operative images, if available. All cortical visualizations were done using the Brainstorm toolbox (Tadel et al., 2011) and custom Matlab (R2019a) scripts.

4.5. Data analysis

4.5.1. Preprocessing

Five-minute epochs were extracted locked to the onset of each condition and a notch filter was applied to remove the 50 Hz interference from the powerline.

4.5.2. Power spectrum

The frequency spectrum at each (scalp and intracranial) EEG channel in response to each experimental condition was extracted by cutting the 5 min epoch into 50% overlapping 30 s segments, obtaining the Fourier transform of each segment, and averaging their spectra. The described procedure results in a frequency resolution of 0.033 Hz.

4.5.3. Signal-to-noise ratio

To quantify the extent of the gamma entrainment relative to the background activity, the experimental conditions were compared using the signal-to-noise ratio (SNR) of the neural response at 40 Hz. The SNR was obtained as the ratio of the (Fourier) amplitude at 40 Hz and the average of the amplitudes in the range from 38 to 42 Hz, excluding 40 Hz. Note that a SNR equal to 1 indicates that the 40 Hz amplitude does not stand out from the background activity.

4.5.4. Oddball analysis

The scalp-EEG data from the oddball conditions was offline re-referenced to the average of the mastoid electrodes (TP9 and TP10) and filtered between 0.5 and 15 Hz using a 4th order zero-phase Butterworth filter. Next, the EEG recording was cut into epochs starting from 200 ms before until 1,000 ms after the onset of each oddball stimulus. The epochs were baselined to the average of the 200 ms pre-onset signal. The epochs for which the maximal amplitude exceeded $\pm 100\ \mu V$ were rejected as they were considered artifactual. As a measure of the P300 event related potentials (ERP) we took the maximal positive amplitude between 200 and 600 ms post-onset (i.e., peak amplitude) as well as its latency relative to the stimulus onset.

4.5.5. Eye-tracking data

The subjects' gaze during the sessions was monitored using eye-tracking of the left eye. For each session, we first cleaned the artifacts in the eye-tracking signal that originated from eye blinks. Eye blinks were determined online by the Eyelink software and stored as timestamped messages in the offline data file. We then determined the standard deviation of the remaining gaze signal (i.e., after eye blink removal) in both horizontal and vertical axis.

4.6. Statistics

For the descriptive statistics, we used the median SNR across subjects and calculated its 95% confidence interval (CI) using a bootstrapping procedure with 1,000 samples selected with replacement. In order to eliminate the effect of outliers on the obtained results we opted for non-parametric statistical testing on SNR evaluation, which, even though less powerful, is less prone to the biases of outliers. The SNRs, initially across all five conditions (RN, RO, RC, IN, and IO) and afterwards across the regular conditions (RN, RO, and RC) separately, were compared using the non-parametric Kruskal-Wallis test, where experimental conditions served as independent variable and SNR on each channel as dependent variables. Then, a multiple comparison across the regular conditions with the same Kruskal-Wallis test was performed, using the false discovery rate (FDR) correction (Benjamini Yoav, 1995) for multiple comparison. The spread of activation for SNRs for each subject was compared across experimental conditions using a cluster-based permutation test (Maris and Oostenveld, 2007) using the Matlab-based Fieldtrip toolbox (Oostenveld et al., 2011) to find spatial clusters that exhibit a significant difference in response to stimulation groups. We used a Monte-Carlo method to perform a significance probability mapping using the one-tailed independent *t*-test and max-sum as cluster statistics. At least two neighboring electrodes had to pass the significance threshold of 0.05 for it to be considered a cluster. The number of permutations was set to 2,000. The significance threshold was set to 0.05 for all conditions and subjects. The effect of the type of flickering (i.e., regular, irregular or no flickering) on the P300-ERP was assessed using a Kruskal-Wallis non-parametric test with condition (O, RO, and IO) as independent variable and peak amplitude/latency of the P300 on each electrode as a dependent variable. Further multiple comparison between these conditions was done using the same Kruskal-Wallis test with FDR-correction for *p*-values. The effect of condition (four conditions) on the intracranial data was assessed using the Kruskal-Wallis non-parametric test, and further multiple comparison was performed using a non-parametric Wilcoxon rank-sum test with FDR-corrections for multiple comparisons. For all analyses, the threshold for statistical significance was kept at 0.05.

Data availability statement

The datasets presented in this article are not readily available because of the sensitive nature of intracranial patient data. Requests to access the datasets should be directed to corresponding author: elvira.khachatryan@ugent.be for scalp-EEG data and to EC, evelien.carrette@uzgent.be for intracranial data.

Ethics statement

The studies involving human participants were reviewed and approved by Ethische Commissie Onderzoek, UZ Leuven and Commissie voor Medische Ethiek, UZ Gent. The patients/participants provided their written informed consent to participate in this study.

Author contributions

EK, BW, and MV conceptualized the study. EK and BW developed the paradigm and analyzed the data. BW implemented the paradigm. EK, MR, EC, PB, AM, ID, and DV recruited the participants and collected the data. All authors participated in writing the manuscript. All authors contributed to the article and approved the submitted version.

Funding

The work has been performed while EK and BW were employed by KU Leuven. MV was supported by research grants received from the European Union's Horizon 2020 research and innovation programme under grant agreement No. 857375, the special research fund of the KU Leuven (C24/18/098), the Belgian Fund for Scientific Research—Flanders (G088314N, G0A0914N, G0A4118N, and G0A4321N), the Inter-university Attraction Poles Programme—Belgian Science Policy (IUAP P7/11), and the Hercules Foundation (AKUL 043).

Acknowledgments

The authors would like to thank prof. Rik Vandenberghe for fruitful discussions leading to this article.

Conflict of interest

The authors declare that the research was conducted in the absence of any commercial or financial relationships that could be construed as a potential conflict of interest.

Publisher's note

Supplementary material

The Supplementary Material for this article can be found online at: https://www.frontiersin.org/articles/10.3389/fnagi.2022.1010765/full#supplementary-material

References

Adaikkan, C., Middleton, S. J., Marco, A., Pao, P.-C., Mathys, H., Kim, D. N.-W., et al. (2019). Gamma entrainment binds higher-order brain regions and offers neuroprotection. *Neuron* 102, 929–943. doi: 10.1016/j.neuron.2019.04.011

Adaikkan, C., and Tsai, L.-H. (2020). Gamma entrainment: impact on neurocircuits, glia, and therapeutic opportunities. *Trends Neurosci.* 43, 24–41. doi: 10.1016/j.tins.2019.11.001

Alzheimer's Association (2020). 2020 Alzheimer's disease facts and figures. *Alzheimers Dement.* 16, 391–460. doi: 10.1002/alz.12068

Benjamini Yoav, H. Y. (1995). Controlling the false discovery rate: a practical and powerful approach to multiple testing. *J. R. Stat. Soc.* 57, 289–300. doi: 10.1111/j.2517-6161.1995.tb02031.x

Bird, C. M., and Burgess, N. (2008). The hippocampus and memory: insights from spatial processing. *Nat. Rev. Neurosci.* 9, 182–194. doi: 10.1038/nrn2335

Breijyeh, Z., and Karaman, R. (2020). Comprehensive review on Alzheimer's disease: causes and treatment. *Molecules* 25:5789. doi: 10.3390/molecules25245789

Carstensen, M. S., Lindén, J., Nguyen, N. M., Hansen, H. E., Carrillo, G. M. F., Hansen, L. S., et al. (2020). "40 Hz invisible spectral flicker and its potential use in Alzheimer's light therapy treatment," in *Mechanisms of Photobiomodulation Therapy XV, Vol. 11221*, San Francisco, 47–58. doi: 10.1117/12.2544338

Chan, D., Suk, H.-J., Jackson, B., Milman, N. P., Stark, D., Klerman, E. B., et al. (2021). 40 Hz sensory stimulation induces gamma entrainment and affects brain structure, sleep and cognition in patients with Alzheimer's dementia. *medRxiv*. 1–3. doi: 10.1101/2021.03.01.21252717

Cimenser, A., Hempel, E., Travers, T., Strozewski, N., Martin, K., Malchano, Z., et al. (2021). Sensory-evoked 40-hz gamma oscillation improves sleep and daily living activities in Alzheimer's disease patients. *Front. Syst. Neurosci.* 15:746859. doi: 10.3389/fnsys.2021.746859

Datta, A., Cusack, R., Hawkins, K., Heutink, J., Rorden, C., Robertson, I. H., et al. (2007). The p300 as a marker of waning attention and error propensity. *Comput. Intell. Neurosci.* 2007:93968. doi: 10.1155/2007/93968

Figueiro, M. G., and Leggett, S. (2021). Intermittent light exposures in humans: a case for dual entrainment in the treatment of Alzheimer's disease. *Front. Neurol.* 12:625698. doi: 10.3389/fneur.2021.625698

Fischl, B. (2012). Freesurfer. *Neuroimage* 62, 774–781. doi: 10.1016/j.neuroimage.2012.01.021

Guan, A., Wang, S., Huang, A., Qiu, C., Li, Y., Li, X., et al. (2022). The role of gamma oscillations in central nervous system diseases: mechanism and treatment. *Front. Cell. Neurosci.* 16:962957. doi: 10.3389/fncel.2022.962957

He, Q., Colon-Motas, K. M., Pybus, A. F., Piendel, L., Seppa, J. K., Walker, M. L., et al. (2021). A feasibility trial of gamma sensory flicker for patients with prodromal Alzheimer's disease. *Alzheimer's Dementia* 7:e12178. doi: 10.1002/trc2.12178

Hebert, L. E., Weuve, J., Scherr, P. A., and Evans, D. A. (2013). Alzheimer disease in the United States (2010-2050) estimated using the 2010 census. *Neurology* 80, 1778–1783. doi: 10.1212/WNL.0b013e31828726f5

Hnazaee, M. F., Wittevrongel, B., Khachatryan, E., Libert, A., Carrette, E., Dauwe, I., et al. (2020). Localization of deep brain activity with scalp

and subdural EEG. *NeuroImage* 223:117344. doi: 10.1016/j.neuroimage.2020.117344

Iaccarino, H. F., Singer, A. C., Martorell, A. J., Rudenko, A., Gao, F., Gillingham, T. Z., et al. (2016). Gamma frequency entrainment attenuates amyloid load and modifies microglia. *Nature* 540, 230–235. doi: 10.1038/nature20587

Ismail, R., Hansen, A. K., Parbo, P., Brændgaard, H., Gottrup, H., Brooks, D. J., et al. (2018). The effect of 40-hz light therapy on amyloid load in patients with prodromal and clinical Alzheimer's disease. *Int. J. Alzheimer's Dis*. 2018:6852303. doi: 10.1155/2018/6852303

Jack Jr, C. R., Bennett, D. A., Blennow, K., Carrillo, M. C., Dunn, B., Haeberlein, S. B., et al. (2018). Nia-AA research framework: toward a biological definition of Alzheimer's disease. *Alzheimer's Dement*. 14, 535–562. doi: 10.1016/j.jalz.2018.02.018

Khachatryan, E., Wittevrongel, B., Hnazaee, M. F., Carrette, E., Dauwe, I., Meurs, A., et al. (2019). Semantic and perceptual priming activate partially overlapping brain networks as revealed by direct cortical recordings in humans. *NeuroImage* 203:116204. doi: 10.1016/j.neuroimage.2019.116204

Knopman, D. S., Amieva, H., Petersen, R. C., Chételat, G., Holtzman, D. M., Hyman, B. T., et al. (2021). Alzheimer disease. *Nat. Rev. Dis. Primers*, 7, 1–21. doi: 10.1038/s41572-021-00269-y

Maris, E., and Oostenveld, R. (2007). Nonparametric statistical testing of EEG-and MEG-data. *J. Neurosci. Methods* 164, 177–190. doi: 10.1016/j.jneumeth.2007.03.024

Martorell, A. J., Paulson, A. L., Suk, H.-J., Abdurrob, F., Drummond, G. T., Guan, W., et al. (2019). Multi-sensory gamma stimulation ameliorates Alzheimer's-associated pathology and improves cognition. *Cell* 177, 256–271. doi: 10.1016/j.cell.2019.02.014

MATLAB (2017). *Version 2017b*. Natick, MA: The MathWorks Inc.

Mu, Y., and Gage, F. H. (2011). Adult hippocampal neurogenesis and its role in Alzheimer's disease. *Mol. Neurodegener*. 6, 1–9. doi: 10.1186/1750-1326-6-85

Mullard, A. (2021). Controversial Alzheimer's drug approval could affect other diseases. *Nature* 595, 162–163. doi: 10.1038/d41586-021-01763-9

Oostenveld, R., Fries, P., Maris, E., and Schoffelen, J.-M. (2011). Fieldtrip: open source software for advanced analysis of MEG, EEG, and invasive electrophysiological data. *Comput. Intell. Neurosci*. 2011:156869. doi: 10.1155/2011/156869

Park, S.-S., Park, H.-S., Kim, C.-J., Kang, H.-S., Kim, D.-H., Baek, S.-S., et al. (2020). Physical exercise during exposure to 40-hz light flicker improves cognitivefunctions in the 3XTG mouse model of Alzheimer's disease. *Alzheimer's Res. Ther*. 12, 1–15. doi: 10.1186/s13195-020-00631-4

Penny, W. D., Friston, K. J., Ashburner, J. T., Kiebel, S. J., and Nichols, T. E. (2011). *Statistical Parametric Mapping: The Analysis of Functional Brain Images*. London: Elsevier.

Sharpe, R. L., Mahmud, M., Kaiser, M. S., and Chen, J. (2020). Gamma entrainment frequency affects mood, memory and cognition: an exploratory pilot study. *Brain Informatics* 7, 1–12. doi: 10.1186/s40708-020-00119-9

Silberstein, R. B., Nunez, P. L., Pipingas, A., Harris, P., and Danieli, F. (2001). Steady state visually evoked potential (SSVEP) topography in a graded working memory task. *Int. J. Psychophysiol*. 42, 219–232. doi: 10.1016/S0167-8760(01)00167-2

Soltani, M., and Knight, R. T. (2000). Neural origins of the p300. *Crit. Rev. Neurobiol*. 14, 199–224. doi: 10.1615/CritRevNeurobiol.v14.i3-4.20

Sperling, R. A., Aisen, P. S., Beckett, L. A., Bennett, D. A., Craft, S., Fagan, A. M., et al. (2011). Toward defining the preclinical stages of Alzheimer's disease: recommendations from the national institute on aging-Alzheimer's association workgroups on diagnostic guidelines for Alzheimer's disease. *Alzheimer's Dement*. 7, 280–292. doi: 10.1016/j.jalz.2011.03.003

Tadel, F., Baillet, S., Mosher, J. C., Pantazis, D., and Leahy, R. M. (2011). Brainstorm: a user-friendly application for MEG/EEG analysis. *Comput. Intell. Neurosci*. 2011:879716. doi: 10.1155/2011/879716

Toffanin, P., de Jong, R., Johnson, A., and Martens, S. (2009). Using frequency tagging to quantify attentional deployment in a visual divided attention task. *Int. J. Psychophysiol*. 72, 289–298. doi: 10.1016/j.ijpsycho.2009.01.006

Vialatte, F.-B., Maurice, M., Dauwels, J., and Cichocki, A. (2010). Steady-state visually evoked potentials: focus on essential paradigms and future perspectives. *Prog. Neurobiol*. 90, 418–438. doi: 10.1016/j.pneurobio.2009.11.005

Wittevrongel, B., Khachatryan, E., Carrette, E., Boon, P., Meurs, A., Van Roost, D., et al. (2020). High-gamma oscillations precede visual steady-state responses: a human electrocorticography study. *Hum. Brain Mapp*. 41, 5341–5355. doi: 10.1002/hbm.25196

Wittevrongel, B., Khachatryan, E., Hnazaee, M. F., Carrette, E., De Taeye, L., Meurs, A., et al. (2018). Representation of steady-state visual evoked potentials elicited by luminance flicker in human occipital cortex: an electrocorticography study. *Neuroimage* 175, 315–326. doi: 10.1016/j.neuroimage.2018.04.006

Wu, Z. (2016). Physical connections between different SSVEP neural networks. *Sci. Rep*. 6, 1–9. doi: 10.1038/srep22801

frontiers | Frontiers in Aging Neuroscience

TYPE Systematic Review
PUBLISHED 09 November 2022
DOI 10.3389/fnagi.2022.1036315

OPEN ACCESS

EDITED BY
Woon-Man Kung,
Chinese Culture University, Taiwan

REVIEWED BY
Heather M. Wilkins,
University of Kansas Medical Center Research Institute, United States
Saheem Ahmad,
University of Hail, Saudi Arabia

*CORRESPONDENCE
Yanhui Lu
luyanhui@bjmu.edu.cn

†These authors have contributed equally to this work and share first authorship

SPECIALTY SECTION
This article was submitted to Alzheimer's Disease and Related Dementias, a section of the journal Frontiers in Aging Neuroscience

RECEIVED 04 September 2022
ACCEPTED 17 October 2022
PUBLISHED 09 November 2022

CITATION
Song Y, Du Y, An Y, Zheng J and Lu Y (2022) A systematic review and meta-analysis of cognitive and behavioral tests in rodents treated with different doses of D-ribose. *Front. Aging Neurosci.* 14:1036315. doi: 10.3389/fnagi.2022.1036315

A systematic review and meta-analysis of cognitive and behavioral tests in rodents treated with different doses of D-ribose

Ying Song[1†], Yage Du[1†], Yu An[2], Jie Zheng[1] and Yanhui Lu[1*]

[1]School of Nursing, Peking University, Beijing, China, [2]Department of Endocrinology, Beijing Chaoyang Hospital, Beijing, China

Background: D-ribose is an aldehyde sugar and a necessary component of all living cells. Numerous reports have focused on D-ribose intervention in animal models to assess the negative effects of D-ribose on cognition. However, the results across these studies are inconsistent and the doses and actual effects of D-ribose on cognition remain unclear. This systematic review aimed to evaluate the effect of D-ribose on cognition in rodents.

Methods: The articles from PubMed, Embase, Sciverse Scopus, Web of Science, the Chinese National Knowledge Infrastructure, SinoMed, Wanfang, and Cqvip databases were screened. The results from the abstract on cognitive-related behavioral tests and biochemical markers from the included articles were extracted and the reporting quality was assessed.

Results: A total of eight trials involving 289 rodents met the eligibility criteria, and both low- and high-dose groups were included. Meta-analyses of these studies showed that D-ribose could cause a significant decrease in the number of platform crossings (standardized mean difference [SMD]: −0.80; 95% CI: −1.14, −0.46; $p < 0.00001$), percentage of distance traversed in the target quadrant (SMD: −1.20; 95% CI: −1.47, −0.92; $p < 0.00001$), percentage of time spent in the target quadrant (SMD: −0.93; 95% CI: −1.18, −0.68; $p < 0.00001$), and prolonged escape latency (SMD: 0.41; 95% CI: 0.16, 0.65; $p = 0.001$) in the Morris water maze test. Moreover, D-ribose intervention increased the levels of advanced glycation end products (AGEs) in the brain (SMD: 0.49; 95% CI: 0.34, 0.63; $p < 0.00001$) and blood (SMD: 0.50; 95% CI: 0.08, 0.92; $p = 0.02$). Subsequently, subgroup analysis for the dose of D-ribose intervention revealed that high doses injured cognitive function more significantly than low D-ribose doses.

Conclusion: D-ribose treatment caused cognitive impairment, and cognition deteriorated with increasing dose. Furthermore, the increase in AGEs in the blood and brain confirmed that D-ribose may be involved in cognitive impairment through non-enzymatic glycosylation resulting in the

generation of AGEs. These findings provide a new research idea for unveiling basic mechanisms and prospective therapeutic targets for the prevention and treatment of patients with cognitive impairment.

KEYWORDS

D-ribose, rodent, cognition, behavioral test, meta-analysis

Introduction

Alzheimer's disease (AD) is the most common type of dementia, accounting for 60–80% of all reported cases (Yankner, 1996; Abramov and Duchen, 2005). AD is a progressive neurodegenerative disease characterized by cognitive deficits, irreversibly destroying memory, language, thinking, and other important mental skills (Devadhasan et al., 2011; Ashraf et al., 2015, 2018; Lee et al., 2017). The estimates from the World Health Organization suggest that approximately 50 million individuals suffered from AD, with nearly 10 million new cases being added annually. Globally, the number of elderly is increasing rapidly, making AD a critical public health concern in the 21st century (Dartigues, 2009; Scheltens et al., 2021). According to the Alzheimer Report 2022, the overall global cost of dementia treatment is more than US$800 billion. Jia et al. (2018) estimated that the cost was US$957.56 billion in 2015 and is expected to rise to US$2.54 trillion in 2030, and US$9.12 trillion in 2050. The public health system is also heavily burdened by AD (Alzheimers Dementia, 2021). However, specific risk factors and mechanisms underlying AD remain unclear.

D-ribose is an aldehyde sugar present in all living cells and plays significant biological roles (Akhter et al., 2016; Li et al., 2021). It is a component of RNA and adenosine triphosphate (ATP) and a synthetic material for nucleotide coenzymes and vitamin B2 (Broom et al., 1964; Keller et al., 1988; Wei et al., 2012). It can be synthesized endogenously from glucose through the pentose phosphate pathway and exogenously from riboflavin-rich foods like fruits and vegetables (Mauser et al., 1985; Dhanoa and Housner, 2007). Serum D-ribose level in humans is 0.02 mM in healthy people, and 0.01–0.1 mM in the cerebrospinal fluid (Seuffer, 1977; Cai et al., 2005). In the case of metabolic diseases, including diabetes mellitus, the serum and urinary D-ribose levels are elevated, resulting in the dysregulation of D-ribose metabolism. Evidence shows that dysregulated D-ribose metabolism causes several neurodegenerative diseases such as AD.

As a reactive sugar, D-ribose can bind to protein or lipid molecules for non-enzymatic glycation, resulting in the production of advanced glycation end products (AGEs) (Wei et al., 2012; Akhter et al., 2014; Siddiqui et al., 2018). Reports show that AGEs are involved in the pathogenesis of aging, diabetes, and neurodegenerative diseases (Akhter et al., 2013, 2015). Moreover, AGEs are neurotoxic in cultured neurons, and their precursors, including methylglyoxal and glyoxal, also promote intracellular aggregation of amyloid-beta carboxy-terminal fragments and cytotoxicity (Takeuchi et al., 2000; Woltjer et al., 2003). An animal study also reported that D-ribose accelerated the formation of AGEs in astrocytes, ultimately activating the NF-κB pathway in the brain and causing cognitive impairment (Han et al., 2014). Chen et al. (2019b) showed that the synthesis of hepatic triglycerides is significantly influenced by D-ribose, which in turn affects hepatocellular steatosis and cognitive functions.

Animal experiments show that D-ribose impairs the spatial learning and memory of mice. For example, Han et al. (2014) demonstrated that high concentrations of D-ribose led to cognitive losses in mice. Notably, not all studies suggest that D-ribose significantly affects spatial learning and memory, especially those using low-dose D-ribose intervention. For example, Han et al. (2011) found that low concentrations of D-ribose showed no effects on spatial cognition. The inconsistent results might be due to the differences in the intervention doses of D-ribose. To date, D-ribose and its role in cognition remain unclear. Therefore, we systematically reviewed and analyzed the available evidence to clarify the actual effects of D-ribose and its differential doses on cognition.

Methods

Literature search and screen

A literature search on the effects of D-ribose on cognitive dysfunction was performed using the search term, "ribose," in combination with "Cognitive Dysfunction, Cognition Disorders, Dementia, AD, Cognitive Impairment, Mild Cognitive Impairment, Mild Neurocognitive Disorder, Cognitive Decline, and Memory deficits," in PubMed, Embase, Sciverse Scopus, Web of Science, the Chinese National Knowledge Infrastructure (CNKI), SinoMed, Wanfang, and Cqvip databases for studies published from database creation up to January 2022. In the

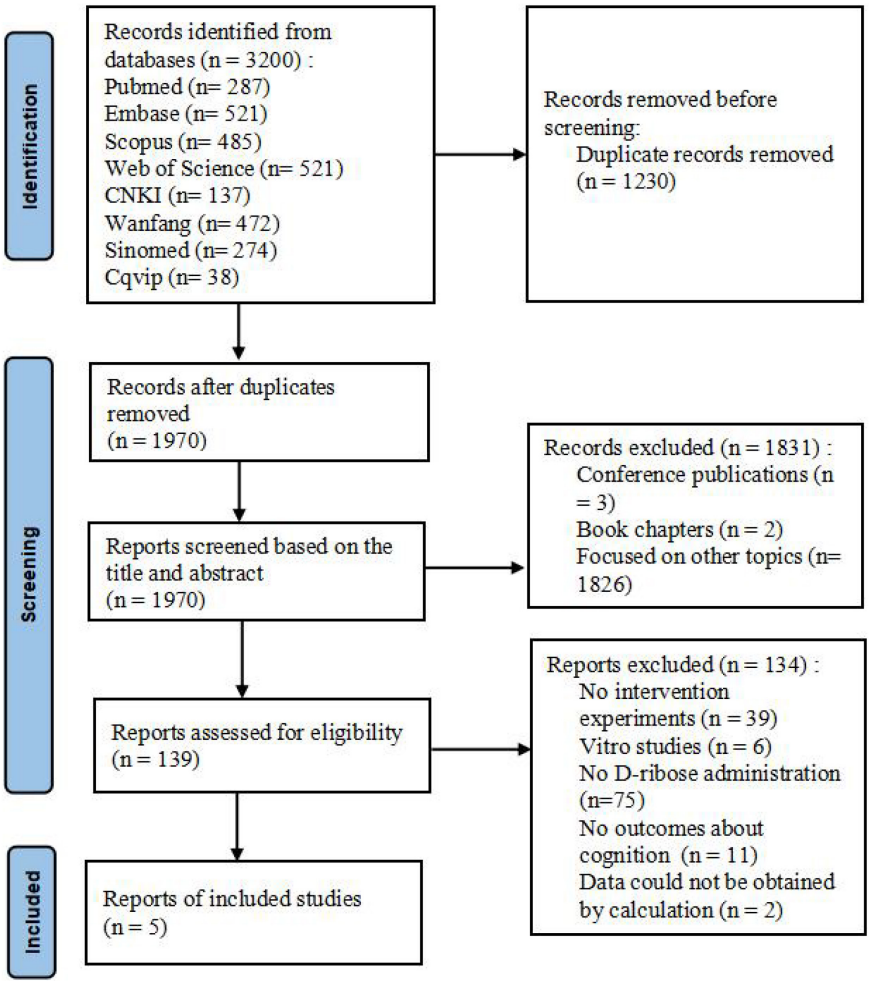

FIGURE 1
Prisma flowchart depicting the article selection process.

beginning, no filters were applied for the search, including language, publication date, dose of administration, route of administration, and duration of administration. Two reviewers (SY and YD) examined the papers to ensure that they met the inclusion criteria for the meta-analysis. A third member (YL) was consulted in case of a disagreement.

Eligibility criteria

The systematic review was limited to published studies, i.e., random assignment of rodents to treatment groups. An intact design with at least one healthy control group of rodents treated with vehicle (saline, phosphate-buffered saline, or a similar solution) and at least an experimental group of rodents treated with D-ribose was an inclusion criterion. All the included studies reported at least one measure of learning and memory after the intervention. Studies with incomplete data in the published text or Supplementary material, or in cases of D-ribose administered with other components, were excluded.

Quality assessment and data extraction

The Animal Research: Reporting *in vivo* Experiments (ARRIVE) guidelines checklist 2.0 including 21 entries was used to assess the quality of each study (Percie et al., 2020). Two reviewers (SY and YD) independently extracted the data in a standardized format suited for animal study design from the reports that met the inclusion criteria. The items recorded were as follows: fundamental information (name of the author, year of publication, and nation); animals (animal species, age, weight, gender, and sample size); study design (dose, route, and duration of D-ribose manipulation); and measurement outcomes (behavioral test results such as those of the Morris

TABLE 1 Characteristics of the included studies.

References	Country/ Region	Animals						Intervention	
		Species	Age	Weight	Gender	Sample size		Way	Dose	Duration (day)
						Intervention group	Control group			
Xu et al., 2021	China	C57BL/6J mice	8–10 weeks	\	Male	Low-dose $n = 15$ high-dose $n = 22$	$n = 22$	Intraperitoneal injection	Low-dose 0.4 g/kg/day High-dose 4 g/kg/day	28
Wu et al., 2019	China	Sprague Dawley rats	8 weeks	\	Male	$n = 10$	$n = 10$	Tail intravenous injection	0.025 g/kg/day	30
Han et al., 2011	China	C57BL/6J mice	8–10 weeks	\	Male	Low-dose $n = 12$ high-dose $n = 12$	$n = 12$	Intraperitoneal injection	Low-dose 0.2 g/kg/day High-dose 2 g/kg/day	30
Wu et al., 2015	China	C57BL/6J mice	8 weeks	\	Male	Low-dose $n = 12$ high-dose $n = 12$	$n = 12$	Gavage administration	Low-dose 0.375 g/kg/day High-dose 3.75 g/kg/day	180
Han et al., 2014	China	C57BL/6J mice	8–10 weeks	\	Male	$n = 12$	$n = 12$	Intraperitoneal injection	First dose 0.4 g/kg/day Second dose 0.8 g/kg/day Third dose 1.6 g/kg/day Forth dose 3.2 g/kg/day	10

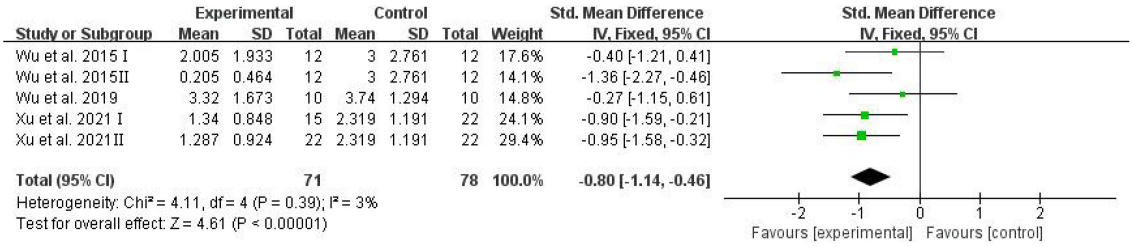

FIGURE 2
Forest plot of the number of platforms crossing in the Morris water maze test.

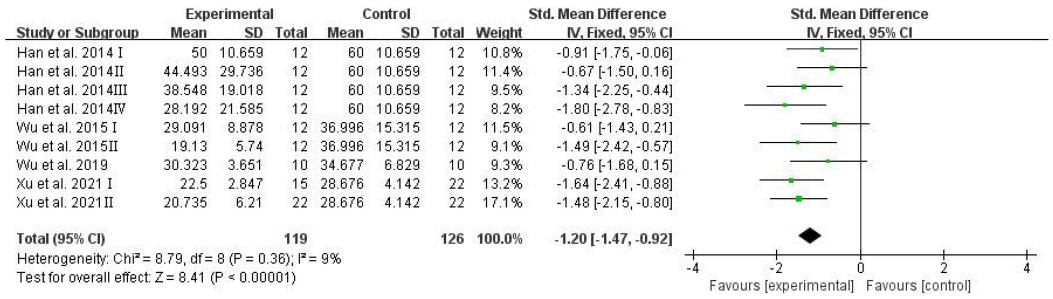

FIGURE 3
Forest plot of the percentage of distance in target quadrant in the Morris water maze test.

water maze test and biochemistry such as AGEs). If data were not obtained in a table or in text, the Web Plot Digitizer software to extract data from images was used to obtain these from the published figures (Drevon et al., 2017). For studies that compared the results of groups treated with different D-ribose doses with those of a single control group, the data from the latter were utilized in each of the dose intervention meta-analyses. The mean score and standard deviation [SD] were extracted for the meta-analysis. If an error was presented as a standard error [SE] or a 95% CI, the formula provided in the Cochrane Handbook was used to convert it into SD values.

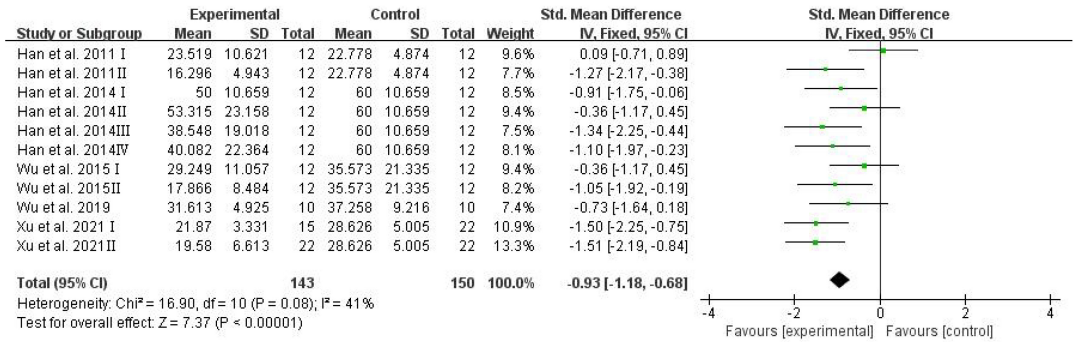

FIGURE 4
Forest plot of the percentage of time in target quadrant in the Morris water maze test.

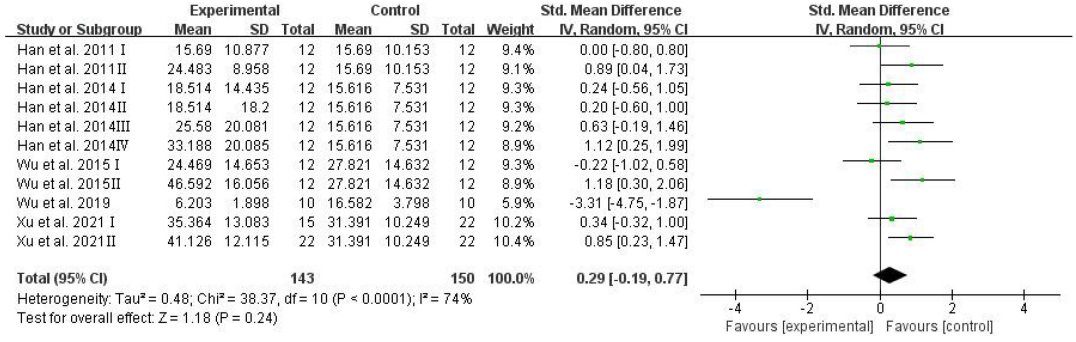

FIGURE 5
Forest plot of the escape latency in the Morris water maze test.

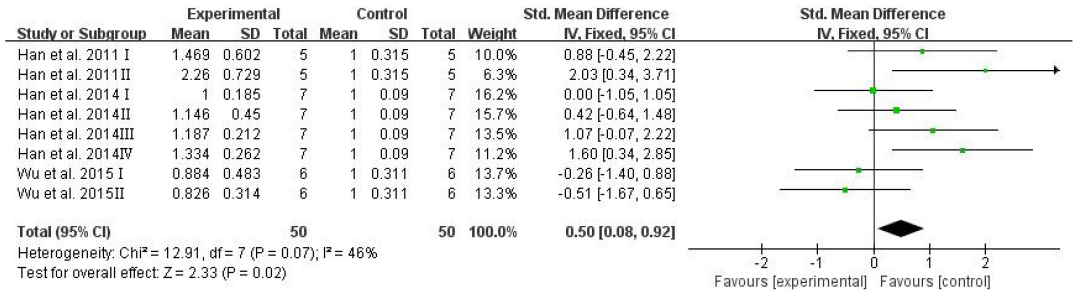

FIGURE 6
Forest plot of the serum AGEs.

Statistical analysis

Data were analyzed using the Review Manager (version 5.4, The Nordic Cochrane Centre, The Cochrane Collaboration, Copenhagen, Denmark). According to the Cochrane Handbook for Systematic Reviews of Interventions, the standardized mean difference (SMD) corresponding to the difference of the means of the two groups and 95% CIs as our effect size of interest was used to estimate the effect of D-ribose treatment on cognitive outcomes (García-Bonilla et al., 2012). The I^2 statistic was used to assess heterogeneity, reflecting the percentage variance between trials for low (<50%) and high (≥50%) heterogeneity values. A random effect model was used when heterogeneity was more than 50%, and a fixed effect model was employed when heterogeneity was less than 50% (Borenstein et al., 2010). A value of $\alpha = 0.05$ was considered statistically significant. Subgroup analysis was conducted for the dose of D-ribose treatment (low dose: <1 g/kg/day vs. high dose: ≥2 g/kg/day). To assess

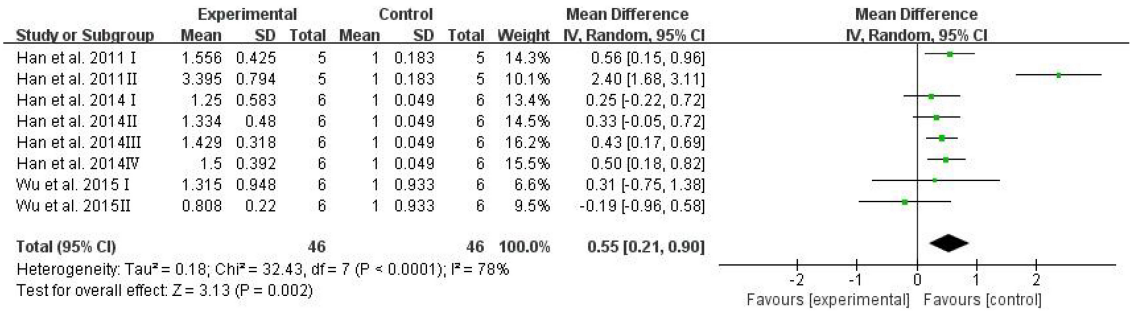

FIGURE 7
Forest plot of the brain AGEs.

the possible causes for heterogeneity in case of a significant difference ($I^2 \geq 50\%$), sensitivity analysis was performed by removing the included data points one by one to see whether the changes had any impact on the combined result estimate.

Results

Study selection and inclusion

A total of 3,200 reports were identified including 287 from PubMed, 521 from Embase, 485 from Scopus, 986 from Web of Science, 137 from CNKI, 472 from Wanfang, 274 from SinoMed, and 38 from Cqvip. Subsequently, 1,970 records were retained after all the searches were pooled and duplicates were deleted. After construing all the titles and abstracts, 1,831 records were found to be irrelevant (the majority of these were excluded as they were conference publications or studies focused on other topics). After reading the full text of the remaining 139 records, 5 studies met the predefined eligibility criteria. Non-consensus on the inclusion of these articles was not applicable. The representation of the article selection process is shown in **Figure 1**.

Study characteristics

Most of the included studies were published in the last decade, and 2 were published in the past 3 years. Among the 5 studies included, C57BL/6J mice were used in 4 reports, while Sprague Dawley rats were used in the remaining one. All the male rodent models were 8–10 weeks old and no study reported the animal weights.

For the D-ribose treatment, the most frequently selected duration was 30 days (2 studies), followed by 10 days (1 study), 28 days (1 study), and 180 days (1 study). Intraperitoneal injection was the most commonly used route for D-ribose administration, except for two studies, which employed intravenous tail injection and gavage administration, respectively. Among the total of 11 experimental groups in the 5 studies, 6 used a dose of less than 1 g/kg/day; 4 employed a dose of more than 2 g/kg/day, and 1 used a dose of 1.6 g/kg/day according to administration protocol. The specific characteristics of the included studies are shown in **Table 1**.

Study quality

In the ARRIVE guidelines for assessing the quality of studies, all showed the four items, comprising the title, objectives, experimental outcomes, and estimated outcomes. For the experimental procedure, although most studies mentioned, "What was done, how it was done, and what was used" and "When and how often," only two studies detailed "Why (provided the rationale for procedures)." All studies presented the sample size but they did not explain how the sample size was estimated. The specific results of the quality assessment were shown in **Table 2**.

Meta-analysis of study outcomes

Morris water maze test

All studies described the effects of D-ribose on cognition in the Morris water maze test, and these studies were included in the meta-analysis. Three studies reported the number of platform crossings; four studies reported the percentage of the distance traversed in the target quadrant; five studies reported the percentage of time spent in the target quadrant, and all studies reported the escape latency.

The number of platform crossings, the percentage of the distance traversed in the target quadrant, and the percentage of time spent in the target quadrant were counted and analyzed by RevMan in trials to test memory functions (Vorhees and Williams, 2006). Meta-analysis indicated that D-ribose reduced the number of platform crossings (**Figure 2**; SMD: −0.80; 95% CI: −1.14, −0.46; $p < 0.00001$) with less heterogeneity

TABLE 2 Reporting the quality of the included studies.

Study	ARRIVE guideline																													
	Introduction				Methods														Results				Discussion							
	Title	Abstract	Background	Objectives	Ethical statement	Study design	Experimental procedure	Experimental animals	Housing/Husbandry	Sample size	Allocating animals to experimental groups	Experimental outcomes	Statistical methods	Baseline data	Numbers analyzed	Outcomes and estimation	Adverse events	Interpretation/Scientific implications	Generalizability/Translation	Funding
Ke Xu et al.	F	P	F	F	F	F	P	P	F	N	A	P	F	F	F	N	A	F	N	F	N	F	F	N	F	F	F	F	F	F
Beibei Wu et al.	F	P	F	F	F	F	P	P	F	N	A	P	F	F	F	N	A	F	N	F	N	F	F	N	F	F	F	F	P	F
Chanshuai Han et al.	F	F	F	P	F	F	P	P	F	N	N	P	F	F	F	N	N	F	N	F	N	F	F	N	F	F	F	F	F	F
Beibei Wu et al.	F	F	F	F	F	F	P	P	F	N	N	P	F	F	F	N	N	F	N	F	N	F	F	N	F	F	F	F	N	F
C Han et al.	F	P	F	N	F	F	P	P	F	N	N	P	F	F	F	N	N	F	N	F	N	F	F	N	F	F	F	F	P	F

ARRIVE, animal research: Reporting *in vivo* experiments; F, fully reported; P, partially reported; N, not reported; NA, not applicable.

among studies (I^2 = 3%). Moreover, in a total of 245 animals, the meta-analysis showed less percentage of the distance traversed in the target quadrant in the D-ribose-treated group as compared to the control group, with an SMD of −1.20, suggesting less heterogeneity (**Figure 3**; 95% CI: −1.47, −0.92; $p < 0.00001$; I^2 = 9%). The D-ribose group showed a substantially decreased percentage of time spent in the target quadrant relative to the control group (**Figure 4**; SMD: −0.93; 95% CI: −1.18, −0.68; $p < 0.00001$). Evidence of low heterogeneity among studies was found (I^2 = 41%). The heterogeneity in the sensitivity analysis obviously declined after excluding the data in the low-dose group in the study reported by Han et al. (2011) (I^2 = 9%).

The escape latency was assessed and analyzed by RevMan in trials to test spatial learning ability (Vorhees and Williams, 2006). Meta-analysis revealed that D-ribose intervention had no significant effects on escape latency (**Figure 5**; SMD: 0.29; 95% CI: −0.19, 0.77; p = 0.24).

Levels of advanced glycation end products

Advanced glycation end products have been investigated extensively owing to their involvement in cognitive diseases such as AD (Vlassara et al., 1994; Dukic-Stefanovic et al., 2001). Serum AGEs were adopted as an outcome in three studies, and the analysis showed the effects of D-ribose in significantly elevating AGEs in mouse blood (**Figure 6**; SMD: 0.50; 95% CI: 0.08, 0.92; p = 0.02); the heterogeneity in the studies was acceptable (I^2 = 46%), and the results remained unaffected after sensitivity analysis.

The brain AGEs were adopted as an outcome in three studies, and D-ribose intervention significantly increased the levels of AGEs in the mouse brain (**Figure 7**; SMD: 0.55; 95% CI: 0.21, 0.90; p = 0.002). However, there was significant heterogeneity among the studies (I^2 = 78%). The heterogeneity in the sensitivity analysis completely disappeared after excluding the data of the high-dose group in the study reported by Han et al. (2011) (I^2 = 0%).

Subgroup analysis

To further investigate the potential influence of dose on the effects of D-ribose on cognition and assess the source of heterogeneity, a subgroup analysis was conducted based on the dose of D-ribose intervention (low dose: <1 g/kg/day vs. high dose: ≥2 g/kg/day).

After the D-ribose intervention, the number of platform crossings reduced remarkably in both groups of D-ribose intervention, and the group with a high intervention dose had a larger effect size (SMD = −1.08; 95% CI: −1.60, −0.57; $p < 0.0001$) as compared to the group with a low administration of D-ribose dose (SMD = −0.58; 95% CI: −1.03, −0.13; p = 0.01). Similarly, regarding the percentage of

TABLE 3 Results of subgroup analysis.

Results	Subgroups	Estimate mean (95% CI)	Heterogeneity	Studies (n)	Comparisons (n)
The number of platform crossing	High dose	SMD = −1.08; 95% CI: −1.60, −0.57	I^2 = 0%; p = 0.46	34	34
	Low dose	SMD = −0.58; 95% CI: −1.03,-0.13	I^2 = 0%; p = 0.48	34	44
The percentage of distance in target quadrant	High dose	SMD = −1.56; 95% CI:-2.03,-1.08	I^2 = 0%; p = 0.85	46	46
	Low dose	SMD = −0.95; 95% CI: −1.32, −0.58	I^2 = 9%;p = 0.35	61	68
The percentage of time in target quadrant	High dose	SMD = −1.27; 95% CI:-1.68,-0.87	I^2 = 0%; p = 0.83	58	58
	Low dose	SMD = −0.64; 95% CI: −0.97, −0.31	I^2 = 48%;p = 0.09	73	80
The escape latency	High dose	SMD = 0.98; 95% CI: 0.59,1.37	I^2 = 0%; p = 0.92	58	58
	Low dose	SMD = −0.29; 95% CI: −1.01, 0.43	I^2 = 77%;p = 0.0005	73	80
Serum AGEs	High dose	SMD = 0.27; 95% CI:0.10,0.44	I^2 = 86%; p = 0.0008	18	18
	Low dose	SMD = 0.03; 95% CI: −0.10, 0.16	I^2 = 2%;p = 0.38	25	25
Brain AGEs	High dose	SMD = 0.69; 95% CI:0.42,0.96	I^2 = 93%; p < 0.00001	17	17
	Low dose	SMD = 0.39; 95% CI: 0.15, 0.62	I^2 = 0%;p = 0.78	23	23

the distance traversed and time spent in the target quadrant, the effect was more pronounced in the group with a high D-ribose dose intervention (distance: SMD = −1.56; 95% CI: −2.03, −1.08; p < 0.00001; time: SMD = −1.27; 95% CI: −1.68, −0.87; p < 0.00001). In addition, D-ribose intervention showed no significant influence on escape latency. However, the subgroup analysis revealed that the escape latency increased significantly in the group with a high D-ribose dose intervention (SMD = 0.98; 95% CI: 0.59, 1.37; p < 0.00001), while the group with a low D-ribose dose intervention did not affect the escape latency in rodents (SMD = −0.29; 95% CI: −1.01, 0.43; p = 0.44).

The specific results of the subgroup analysis are shown in Table 3. Subgroup analysis showed that the levels of serum AGEs increased markedly in the group with a high D-ribose dose intervention (SMD = 0.27; 95% CI: 0.10, 0.44; p = 0.002), while there was no significant difference in the group with a low D-ribose dose intervention as compared to the controls (SMD = 0.03; 95% CI: −0.10, 0.16; p = 0.60). Moreover, the brain AGEs reduced significantly in both groups; however, a larger effect size was found in the group with a high D-ribose dose (SMD = 0.69; 95% CI: 0.42, 0.96; p < 0.00001) as compared to the group with a low D-ribose dose intervention (SMD = 0.39; 95% CI: 0.15, 0.62; p = 0.001).

Discussion

Metabolic disorder of ribose is associated with adverse effects on cognition (Siddiqui et al., 2018). Although studies focused on D-ribose intervention show inconsistent findings, no systematic review of D-ribose on cognitive alterations has been published. We examined animal studies to assess the effects of D-ribose on cognition through a systematic review and meta-analysis of the impact of differential D-ribose doses on cognition.

D-ribose treatment caused cognitive impairment, and the cognition deteriorated with increasing dose. We assessed the effects of different doses of D-ribose on cognitive changes in mice and rats according to the results of the Morris water maze, the number of platform crossings, the percentage of the distance traversed in the target quadrant, and the percentage of time spent in the target quadrant to test memory function and escape latency to assess spatial learning abilities. The meta-analysis revealed that D-ribose intervention produced a significant impairment in the spatial learning task but not in the spatial memory task. We verified that D-ribose caused cognitive impairment, consistent with previous studies, which suggest that metabolic disorders due to D-ribose are a possible risk factor for age-related neurodegenerative disorders such as AD (Zhu et al., 2022). Lyu et al. (2019) found that D-ribose levels in patients with AD were considerably higher than those in age-matched controls with normal cognition. A cross-sectional study reported that T2DM-MCI patients had higher serum concentrations of D-ribose and were correlated negatively with the MoCA score (Lu et al., 2021).

In addition, our subgroup analysis revealed that the group with a high D-ribose dose intervention injured cognitive function more significantly than the group with a low D-ribose dose intervention. It was clear that the impaired spatial memory ability was more prominent in the high-dose group than the low-dose D-ribose-treated group. D-ribose at a low dose did not cause a decline in the spatial learning ability in rodents, and only D-ribose at a high dose led to a significant decrease in the spatial learning ability. For the increase in brain AGEs, D-ribose at a high dose had a stronger impact relative to the low-dose D-ribose group. Moreover, only a high dose of D-ribose but not a low dose led to the rise in AGEs in serum. These outcomes clearly suggested cognitive detriment due to D-ribose at a high dose.

Sensitivity analysis explained most of the heterogeneity. In terms of the significant reduction of heterogeneity in the percentage of time spent in the target quadrant, contrary results were found in the study of Han et al. (2011), whereby

a low dose of D-ribose was used. Similarly, the obvious reduction of heterogeneity in the latency was attributed to the results reported by Wu et al. (2019) which were contrary to other studies. Regarding the brain AGEs, sensitivity analysis revealed the source of heterogeneity which may be attributed to differences in dose, sample size, and eligibility criteria (Garcia-Alamino et al., 2017).

In the included studies, the rodents used were all male. Population-based studies suggest that gender may affect cognitive impairment (Au et al., 2017; Tang et al., 2019; C Silva et al., 2022). Nonetheless, owing to hormonal secretion, physical fitness, and other factors, males are usually selected as experimental subjects in animal studies (Schaeffer, 2018). Hence, future research is needed to further address these gender-based differences. As for sample size, due to ethical and economic reasons, a sample size calculation is not necessary for each experiment, and at least 7–10 animals are utilized per group in most animal studies (Festing, 2018; Ricci et al., 2020). The sample size can be further calculated based on power analysis, precision analysis, and other methods in future studies.

Evidence suggests that D-ribose is involved in the generation of free oxygen radicals, glycation, protein aggregation, AGEs, and age-related neurodegenerative illnesses (Chen et al., 2009, 2017, 2019a; Batkulwar et al., 2018). According to cell-based experiments, D-ribose interacts with proteins and produces AGEs. Furthermore, the expression of the receptor of advanced glycation end products (RAGE) is linked to AGE elevation caused by ribosylation in both astrocytoma cells and astrocytes, resulting in RAGE-dependent NF-κB activation and astrocyte stimulation, further impairing the spatial learning and memory (Han et al., 2014). Our analysis of AGEs is consistent with the conclusions reported previously, i.e., ribose-induced cognitive impairment may be related to AGEs produced by non-enzymatic glycosylation of D-ribose (Chen et al., 2010; Wei et al., 2012). These findings suggested that D-ribose-induced non-enzymatic glycosylation may play a role in the pathogenesis of cognitive impairment. However, the mechanisms underlying D-ribose-mediated cognitive impairment remain unclear, and these should be further investigated in the future.

Limitations

This review, however, has some limitations, including a relatively small total sample size and the number of included studies. Furthermore, poor reporting quality increased the likelihood of bias and reduced the validity of the findings. To validate the harm caused by D-ribose in cognitive impairment and comprehensively study the underlying mechanisms, more precise and rigorous experiments with high sample sizes are warranted.

Conclusion

We summarized the effects of D-ribose intervention with different doses based on cognitive and behavioral tests and found that D-ribose was related to learning and memory functions. Our findings indicate that D-ribose intervention causes cognitive impairment, and cognition deteriorated with increasing dose. Furthermore, the increase in AGEs in the blood and brain confirmed that D-ribose may be involved in cognitive impairment through glycosylation, resulting in the generation of AGEs. These provide a new research direction for unveiling basic mechanisms and prospective therapeutic targets for the prevention and treatment of cognitive impairment in these patients.

Data availability statement

The raw data supporting the conclusions of this article will be made available by the authors, without undue reservation.

Author contributions

YS and YD completed the data analysis and wrote the manuscript. JZ contributed to the data analysis. YL and YA supervised the project. All authors reviewed and approved the submitted version.

Funding

This research was supported by grants from National Natural Science Foundation of China (82003456) and the Fundamental Research Funds for the Central Universities.

Conflict of interest

The authors declare that the research was conducted in the absence of any commercial or financial relationships that could be construed as a potential conflict of interest.

Publisher's note

All claims expressed in this article are solely those of the authors and do not necessarily represent those of their affiliated organizations, or those of the publisher, the editors and the reviewers. Any product that may be evaluated in this article, or claim that may be made by its manufacturer, is not guaranteed or endorsed by the publisher.

References

Abramov, A. Y., and Duchen, M. R. (2005). The role of an astrocytic NADPH oxidas e in the neurotoxicity of amyloid beta peptides. *Philos. Trans. R. Soc. Lond. B Biol. Sci.* 360, 2309–2314. doi: 10.1098/rstb.2005.1766

Akhter, F., Khan, M. S., Alatar, A. A., Faisal, M., and Ahmad, S. (2016). Antigenic role of the adaptive immune response to d-ribose glycated LDL in diabetes, atherosclerosis and diabetes atherosclerotic patients. *Life Sci.* 151, 139–146. doi: 10.1016/j.lfs.2016.02.013

Akhter, F., Khan, M. S., and Ahmad, S. (2015). Acquired immunogenicity of calf thymus DNA and LDL modified by D-ribose: a comparative study. *Int. J. Biol. Macromol.* 72, 1222–1227. doi: 10.1016/j.ijbiomac.2014.10.034

Akhter, F., Khan, M. S., Singh, S., and Ahmad, S. (2014). An immunohistochemical analysis to validate the rationale behind the enhanced immunogenicity of D-ribosylated low density lipo-protein. *PLoS One* 9:e113144. doi: 10.1371/journal.pone.0113144

Akhter, F., Salman Khan, M., Shahab, U., Moinuddin, and Ahmad, S. (2013). Bio-physical characterization of ribose induced glycation: a mechanistic study on DNA perturbations. *Int. J. Biol. Macromol.* 58, 206–210. doi: 10.1016/j.ijbiomac.2013.03.036

Alzheimers Dementia, (2021). 2021 Alzheimer's disease facts and figures. *Alzheimers Dement.* 17, 327–406. doi: 10.1002/alz.12328

Ashraf, G. M., Tabrez, S., Jabir, N. R., Firoz, C. K., Ahmad, S., Hassan, I., et al. (2015). An overview on global trends in nanotechnological approaches for Alzheimer therapy. *Curr. Drug Metab.* 16, 719–727. doi: 10.2174/1389200216081511071257 57

Ashraf, J. M., Ansari, M. A., Fatma, S., Abdullah, S. M. S., Iqbal, J., Madkhali, A., et al. (2018). Inhibiting effect of zinc oxide nanoparticles on advanced glycation products and oxidative modifications: A potential tool to counteract oxidative stress in neurodegenerative diseases. *Mol. Neurobiol.* 55, 7438–7452. doi: 10.1007/s12035-018-0935-x

Au, B., Dale-McGrath, S., and Tierney, M. C. (2017). Sex differences in the prevalence and incidence of mild cognitive impairment: A meta-analysis. *Ageing Res. Rev.* 35, 176–199.

Batkulwar, K., Godbole, R., Banarjee, R., Kassaar, O., Williams, R. J., and Kulkarni, M. J. (2018). Advanced glycation end products modulate amyloidogenic APP processing and tau phosphorylation: A mechanistic link between glycation and the development of Alzheimer's disease. *ACS Chem. Neurosci.* 9, 988–1000. doi: 10.1021/acschemneuro.7b00410

Borenstein, M., Hedges, L. V., Higgins, J. P., and Rothstein, H. R. (2010). A basic introduction to fixed-effect and random-effects models for meta-analysis. *Res. Synth. Methods* 1, 97–111. doi: 10.1002/jrsm.12

Broom, A. D., Townsend, L. B., Jones, J. W., and Robins, R. K. (1964). Purine nucleosides.6. Further methylation studies of naturally occurring purine nucleosides. *Biochemistry* 3, 494–500.

C Silva, T., Zhang, W., Young, J. I., Gomez, L., Schmidt, M. A., Varma, A., et al. (2022). Distinct sex-specific DNA methylation differences in Alzheimer's disease. *Alzheimers Res. Ther.* 14:133. doi: 10.1186/s13195-022-01070-z

Cai, Y., Liu, J., Shi, Y., Liang, L., and Mou, S. (2005). Determination of several sugars in serum by high-performance anion-exchange chromatography with pulsed amperometric detection. *J. Chromatogr. A* 1085, 98–103. doi: 10.1016/j.chroma.2004.11.100

Chen, L., Wei, Y., Wang, X., and He, R. (2009). D-Ribosylated Tau forms globular aggregates with high cytotoxicity. *Cell. Mol. Life Sci.* 66, 2559–2571. doi: 10.1007/s00018-009-0058-7

Chen, L., Wei, Y., Wang, X., and He, R. (2010). Ribosylation rapidly induces alpha-synuclein to form highly cytotoxic molten globules of advanced glycation end products. *PLoS One* 5:e9052. doi: 10.1371/journal.pone.0009052

Chen, X., Su, T., Chen, Y., He, Y., Liu, Y., Xu, Y., et al. (2017). d-Ribose as a Contributor to Glycated Haemoglobin. *EBioMedicine* 25, 143–153. doi: 10.1016/j.ebiom.2017.10.001

Chen, Y., Yu, L., Wei, Y., Long, Y., Xu, Y., He, T., et al. (2019b). D-ribose increases triglyceride via upregulation of DGAT in the liver. *Sci. China Life Sci.* 62, 858–861. doi: 10.1007/s11427-019-9542-2

Chen, Y., Yu, L., Wang, Y., Wei, Y., Xu, Y., He, T., et al. (2019a). d-Ribose contributes to the glycation of serum protein. *Biochim. Biophys. Acta Mol. Basis Dis.* 1865, 2285–2292. doi: 10.1016/j.bbadis.2019.05.005

Dartigues, J. F. (2009). Alzheimer's disease: a global challenge for the 21st century. *Lancet Neurol.* 8, 1082–1083.

Devadhasan, J. P., Kim, S., and An, J. (2011). Fish-on-a-chip: a sensitive detection microfluidic system for Alzheimer's disease. *J. Biomed. Sci.* 18:33. doi: 10.1186/1423-0127-18-33

Dhanoa, T. S., and Housner, J. A. (2007). Ribose: more than a simple sugar? *Curr. Sports Med. Rep.* 6, 254–257.

Drevon, D., Fursa, S. R., and Malcolm, A. L. (2017). Intercoder reliability and validity of webplotdigitizer in extracting graphed data. *Behav. Modif.* 41, 323–339. doi: 10.1177/0145445516673998

Dukic-Stefanovic, S., Schinzel, R., Riederer, P., and Münch, G. (2001). AGES in brain ageing: AGE-inhibitors as neuroprotective and anti-dementia drugs? *Biogerontology* 2, 19–34. doi: 10.1023/a:1010052800347

Festing, M. F. (2018). On determining sample size in experiments involving laboratory animals. *Lab. Anim.* 52, 341–350.

Garcia-Alamino, J. M., Bankhead, C., Heneghan, C., Pidduck, N., and Perera, R. (2017). Impact of heterogeneity and effect size on the estimation of the optimal information size: analysis of recently published meta-analyses. *BMJ Open* 7:e015888. doi: 10.1136/bmjopen-2017-015888

García-Bonilla, L., Campos, M., Giralt, D., Salat, D., Chacón, P., Hernández-Guillamon, M., et al. (2012). Evidence for the efficacy of statins in animal stroke models: A meta-analysis. *J. Neurochem.* 122, 233–243.

Han, C., Lu, Y., Wei, Y., Liu, Y., and He, R. (2011). D-ribose induces cellular protein glycation and impairs mouse spatial cognition. *PLoS One* 6:e24623. doi: 10.1371/journal.pone.0024623

Han, C., Lu, Y., Wei, Y., Wu, B., Liu, Y., He, R., et al. (2014). D-ribosylation induces cognitive impairment through RAGE-dependent astrocytic inflammation. *Cell Death Dis.* 5:e1117. doi: 10.1038/cddis.2014.89

Jia, J., Wei, C., Chen, S., Li, F., Tang, Y., Qin, W., et al. (2018). The cost of Alzheimer's disease in China and re-estimation of costs worldwide. *Alzheimers Dement.* 14, 483–491. doi: 10.1016/j.jalz.2017.12.006

Keller, P. J., Le Van, Q., Kim, S. U., Bown, D. H., Chen, H. C., Kohnle, A., et al. (1988). Biosynthesis of riboflavin: mechanism of formation of the ribitylamino linkage. *Biochemistry* 27, 1117–1120. doi: 10.1021/bi00404a006

Lee, D., Lee, W.-S., Lim, S., Kim, Y. K., Jung, H.-Y., Das, S., et al. (2017). A guanidine-appended scyllo-inositol derivative AAD-66 enhances brain delivery and ameliorates Alzheimer's phenotypes. *Sci. Rep.* 7:14125. doi: 10.1038/s41598-017-14559-7

Li, S., Wang, J., Xiao, Y., Zhang, L., Fang, J., Yang, N., et al. (2021). D-ribose: Potential clinical applications in congestive heart failure and diabetes, and its complications (Review). *Exp. Ther. Med.* 21:496. doi: 10.3892/etm.2021.9927

Lu, Y., Jiang, H., Zhang, H., Li, R., Zhang, Q., Luo, D., et al. (2021). Serum oxidized low density lipoprotein serves as a mediator for the inverse relationship between serum D-ribose and cognitive performance in type 2 diabetic patients. *Free Radic. Biol. Med.* 171, 91–98. doi: 10.1016/j.freeradbiomed.2021.05.015

Lyu, J., Yu, L. X., He, Y. G., Wei, Y., and Rong-Qiao, H. (2019). A Brief Study of the Correlation of Urine D-ribose with MMSE Scores of Patients with Alzheimer's Disease and Cognitively Normal Participants. *Am. J. Urol. Res.* 4, 18–23.

Mauser, M., Hoffmeister, H. M., Nienaber, C., and Schaper, W. (1985). Influence of ribose, adenosine, and "AICAR" on the rate of myocardial adenosine triphosphate synthesis during reperfusion after coronary artery occlusion in the dog. *Circ. Res.* 56, 220–230. doi: 10.1161/01.res.56.2.220

Percie, D. S. N., Hurst, V., Ahluwalia, A., Alam, S., Avey, M. T., Baker, M., et al. (2020). The ARRIVE guidelines 2.0: Updated guidelines for reporting animal research. *PLoS Biol.* 18:e3000410. doi: 10.1371/journal.pbio.3000410

Ricci, C., Baumgartner, J., Malan, L., and Smuts, C. M. (2020). Determining sample size adequacy for animal model studies in nutrition research: limits and ethical challenges of ordinary power calculation procedures. *Int. J. Food Sci. Nutr.* 71, 256–264. doi: 10.1080/09637486.2019.1646714

Schaeffer, L. R. (2018). Necessary changes to improve animal models. *J. Anim. Breed Genet.* 135, 124–131.

Scheltens, P., Blennow, K., Breteler, M. M., de Strooper, B., Frisoni, G. B., Salloway, S., et al. (2021). Alzheimer's disease. *Lancet* 397, 1577–1590.

Seuffer, R. (1977). [A new method for the determination of sugars in cerebrospinal fluid (author's transl)]. *J. Clin. Chem. Clin. Biochem.* 15, 663–668.

Siddiqui, Z., Ishtikhar, M., Moinuddin, and Ahmad, S. (2018). d-Ribose induced glycoxidative insult to hemoglobin protein: An approach to spot its structural perturbations. *Int. J. Biol. Macromol.* 112, 134–147.

Takeuchi, M., Bucala, R., Suzuki, T., Ohkubo, T., Yamazaki, M., Koike, T., et al. (2000). Neurotoxicity of advanced glycation end-products for cultured cortical neurons. *J. Neuropathol. Exp. Neurol.* 59, 1094–1105.

Tang, F., Chi, I., and Dong, X. (2019). Sex differences in the prevalence and incidence of cognitive impairment: Does immigration matter? *J. Am. Geriatr. Soc.* 67, S513–S518.

Vlassara, H., Bucala, R., and Striker, L. (1994). Pathogenic effects of advanced glycosylation: Biochemical, biologic, and clinical implications for diabetes and aging. *Lab. Invest.* 70, 138–151.

Vorhees, C. V., and Williams, M. T. (2006). Morris water maze: Procedures for assessing spatial and related forms of learning and memory. *Nat. Protoc.* 1, 848–858.

Wei, Y., Han, C. S., Zhou, J., Liu, Y., Chen, L., and He, R. Q. (2012). D-ribose in glycation and protein aggregation. *Biochim. Biophys. Acta* 1820, 488–494.

Woltjer, R. L., Maezawa, I., Ou, J. J., Montine, K. S., and Montine, T. J. (2003). Advanced glycation endproduct precursor alters intracellular amyloid-beta/A beta PP carboxy-terminal fragment aggregation and cytotoxicity. *J. Alzheimers Dis.* 5, 467–476.

Wu, B., Wei, Y., Wang, Y., Su, T., Zhou, L., Liu, Y., et al. (2015). Gavage of D-Ribose induces ASS-like deposits, Tau hyperphosphorylation as well as memory loss and anxiety-like behavior in mice. *Oncotarget* 6, 34128–34142.

Wu, B., Wang, Y., Shi, C., Chen, Y., Yu, L., Li, J., et al. (2019). Ribosylation-derived advanced glycation end products induce tau hyperphosphorylation through brain-derived neurotrophic factor reduction. *J. Alzheimers Dis.* 71, 291–305.

Xu, K., Wang, M., Zhou, W., Pu, J., Wang, H., and Xie, P. (2021). Chronic D-ribose and D-mannose overload induce depressive/anxiety-like behavior and spatial memory impairment in mice. *Transl. Psychiatry* 11:90. doi: 10.1038/s41398-020-01126-4

Yankner, B. A. (1996). Mechanisms of neuronal degeneration in Alzheimer's disease. *Neuron* 16, 921–932.

Zhu, X., Zhao, C., Liu, J., Qin, F., Xiong, Z., and Zhao, L. (2022). Urine D-ribose levels correlate with cognitive function in community-dwelling older adults. *BMC Geriatr.* 22:693. doi: 10.1186/s12877-022-03288-w

frontiers | Frontiers in Aging Neuroscience

TYPE Original Research
PUBLISHED 11 November 2022
DOI 10.3389/fnagi.2022.1040293

OPEN ACCESS

EDITED BY
Woon-Man Kung,
Chinese Culture University, Taiwan

REVIEWED BY
Robert Fekete,
New York Medical College,
United States
Yafu Yin,
Shanghai Jiao Tong University School of Medicine, China

*CORRESPONDENCE
Zhenhua Liu
liuzhenhua@csu.edu.cn
Lifang Lei
Lei_lifang@qq.com

†These authors have contributed equally to this work and share first authorship

SPECIALTY SECTION
This article was submitted to Parkinson's Disease and Aging-related Movement Disorders, a section of the journal Frontiers in Aging Neuroscience

RECEIVED 09 September 2022
ACCEPTED 27 October 2022
PUBLISHED 11 November 2022

CITATION
Zhou Z, Zhou X, Xiang Y, Zhao Y, Pan H, Wu J, Xu Q, Chen Y, Sun Q, Wu X, Zhu J, Wu X, Li J, Yan X, Guo J, Tang B, Lei L and Liu Z (2022) Subtyping of early-onset Parkinson's disease using cluster analysis: A large cohort study.
Front. Aging Neurosci. 14:1040293.
doi: 10.3389/fnagi.2022.1040293

Subtyping of early-onset Parkinson's disease using cluster analysis: A large cohort study

Zhou Zhou[1,2†], Xiaoxia Zhou[1†], Yaqin Xiang[1], Yuwen Zhao[1], Hongxu Pan[1], Juan Wu[1], Qian Xu[1], Yase Chen[1], Qiying Sun[2,3], Xinyin Wu[4], Jianping Zhu[5], Xuehong Wu[5], Jianhua Li[6], Xinxiang Yan[1,3], Jifeng Guo[1,3,7], Beisha Tang[1,3,7], Lifang Lei[8*] and Zhenhua Liu[1,3,7*] for Parkinson's Disease, and Movement Disorders Multicenter Database and Collaborative Network in China (PD-MDCNC)

[1]Department of Neurology, Xiangya Hospital, Central South University, Changsha, China, [2]Department of Geriatrics, Xiangya Hospital, Central South University, Changsha, China, [3]National Clinical Research Center for Geriatric Disorders, Xiangya Hospital, Central South University, Changsha, China, [4]Department of Epidemiology and Health Statistics, Xiangya School of Public Health, Central South University, Changsha, China, [5]Hunan KeY Health Technology Co., Ltd., Changsha, China, [6]Hunan Creator Information Technology Co., Ltd., Changsha, China, [7]Key Laboratory of Hunan Province in Neurodegenerative Disorders, Central South University, Changsha, China, [8]Department of Neurology, The Third Xiangya Hospital, Central South University, Changsha, China

Background: Increasing evidence suggests that early-onset Parkinson's disease (EOPD) is heterogeneous in its clinical presentation and progression. Defining subtypes of EOPD is needed to better understand underlying mechanisms, predict disease course, and eventually design more efficient personalized management strategies.

Objective: To identify clinical subtypes of EOPD, assess the clinical characteristics of each EOPD subtype, and compare the progression between EOPD subtypes.

Materials and methods: A total of 1,217 patients were enrolled from a large EOPD cohort of the Parkinson's Disease & Movement Disorders Multicenter Database and Collaborative Network in China (PD-MDCNC) between January 2017 and September 2021. A comprehensive spectrum of motor and non-motor features were assessed at baseline. Cluster analysis was performed using data on demographics, motor symptoms and signs, and other non-motor manifestations. In 454 out of total patients were reassessed after a mean follow-up time of 1.5 years to compare progression between different subtypes.

Results: Three subtypes were defined: mild motor and non-motor dysfunction/slow progression, intermediate and severe motor and non-motor dysfunction/malignant. Compared to patients with mild subtype, patients with the severe subtype were more likely to have rapid eye movement sleep behavior disorder, wearing-off, and dyskinesia, after adjusting for age and

disease duration at baseline, and showed a more rapid progression in Unified Parkinson's Disease Rating Scale (UPDRS) total score (P = 0.002), UPDRS part II (P = 0.014), and III (P = 0.001) scores, Hoehn and Yahr stage (P = 0.001), and Parkinson's disease questionnaire-39 item version score (P = 0.012) at prospective follow-up.

Conclusion: We identified three different clinical subtypes (mild, intermediate, and severe) using cluster analysis in a large EOPD cohort for the first time, which is important for tailoring therapy to individuals with EOPD.

KEYWORDS

early-onset Parkinson's disease, heterogeneous, subtype, PD-MDCNC, cluster analysis

Introduction

Parkinson's disease (PD) is the second most common neurodegenerative movement disorder characterized by typical motor symptoms and many less visible non-motor symptoms (NMSs; Poewe et al., 2017; Bloem et al., 2021). It is characterized pathologically by dopaminergic neuronal loss in the substantia nigra pars compacta and intracellular inclusions containing α-synuclein aggregates (Armstrong and Okun, 2020; Liu et al., 2022; Zhou et al., 2022). PD is a progressive and complex neurological disorder with heterogeneous symptomatology (Jafari et al., 2020; Bloem et al., 2021). Although PD is an age-related disease that typically appears after the age of 65 years, the age of onset for approximately 10% of affected individuals is younger than 50 years, referring to early-onset PD (EOPD; Zhang et al., 2005; Schrag and Schott, 2006; Poewe et al., 2017; Niemann and Jankovic, 2019). Patients with EOPD have relatively high clinical heterogeneity and a longer disease course and typically develop motor fluctuations and dyskinesias earlier, which vary dramatically in its clinical manifestations and prognosis (Pagano et al., 2016; Schirinzi et al., 2020). Thus, EOPD requires more personalized treatment and long-term management.

Several previous studies have used cluster analysis to define clinical PD subtypes based on motor severity, motor complications, some non-motor features, and demographic characteristics (Fereshtehnejad et al., 2015; Lawton et al., 2018; De Pablo-Fernández et al., 2019; Belvisi et al., 2021; Brendel et al., 2021; Mestre et al., 2021). Growing evidences have shown that there are distinct subtypes of PD with diverging trends of progression (Qian and Huang, 2019; Hendricks and Khasawneh, 2021; Mestre et al., 2021). However, all previous cluster analyses were limited to patients with PD, and an EOPD cluster analysis was not available. With some patients with EOPD following a relatively benign course and others progressing rapidly to disability, subtyping EOPD is required. It is essential to perform cluster analysis based on deep phenotyping, followed by prospective validation of subtypes. Defining different subcategories of EOPD is key to better understand its underlying disease mechanisms, predict its disease course, and subsequently design more efficient personalized management strategies (Qian and Huang, 2019).

This study aimed to (1) identify clinical EOPD subtypes using cluster analysis based on a comprehensive baseline dataset, (2) assess the clinical characteristics of each EOPD subtype, and (3) compare disease progression between different EOPD subtypes.

Materials and methods

Participants

Participants were enrolled from a large EOPD cohort of the Parkinson's Disease & Movement Disorders Multicenter Database and Collaborative Network in China (PD-MDCNC) between January 2017 and September 2021. The clinical diagnosis of PD was confirmed by at least two neurological specialists according to the Movement Disorder Society Clinical Diagnostic Criteria for Parkinson's Disease (Postuma et al., 2015), including diagnoses of either clinically established or probable PD. The exclusion criteria were as follows: (1) familial history, (2) missing data $\geq$ 10%, and (3) diagnosis of other causes of parkinsonism on baseline or follow-up assessments. The clinical data of all participants were stored in the PD-MDCNC.[1] Written informed consent was obtained from all the participants. This study was approved by the Ethics Committee of Xiangya Hospital and was conducted in accordance with the ethical guidelines of the Declaration of Helsinki.

1 http://www.pd-mdcnc.com

Clinical assessment

All participants underwent comprehensive and standardized clinical assessments. Before conducting the assessment, all researchers were trained to ensure an equal understanding of the scales used and the methods and phrasing for clinical data collection. Demographic information and clinical characteristics were collected, as described in our previous study (Zhao et al., 2020; Zhou et al., 2022). Clinical examinations of motor symptoms were performed based on the Unified Parkinson's Disease Rating Scale (UPDRS) and Hoehn and Yahr (H&Y) stages, defining motor subtypes as either tremor dominant, postural instability/gait difficulty or indeterminate group. Motor complications, such as dyskinesia and wearing-off were diagnosed by clinicians, and the severities of dyskinesia and wearing-off were evaluated by UPDRS part IV-A and 9-item End-of-dose Wearing-off Questionnaire (WOQ-9), respectively. Freezing of gait (FOG) was evaluated using New Freezing of Gait Questionnaire (NFOGQ).

In addition to motor symptoms, we evaluated a broad range of NMSs based on the NMSS, the Scale for Outcomes in Parkinson's Disease for Autonomic Dysfunction (SCOPA-AUT), Mini-Mental State Examination (MMSE), Rapid Eye Movement Sleep Behavior Disorder Questionnaire-Hong Kong (RBDQ-HK), Epworth Sleepiness Scale (ESS), Parkinson's Disease Sleep Scale (PDSS), Hyposmia Rating Scale (HRS), Functional Constipation Diagnostic Criteria Rome III, and Hamilton Depression Scale (HAMD-17). Quality of life was assessed using the Parkinson's disease questionnaire-39 item version (PDQ-39). Details regarding the clinical scales were provided in our previous study (Zhou et al., 2022). Patients with illiteracy, primary education, and above junior education were identified as having cognitive impairment when the MMSE scores were below 17, 20, and 24 points, respectively. Hyposmia was defined as a total HRS score less than 22.5. Rapid eye movement sleep behavior disorder (RBD) was defined as a total RBDQ-HK scale score no less than 18. Excessive daytime sleepiness (EDS) was defined as a total ESS score higher than 10. Depression was defined as a total HAMD-17 score higher than 7. The levodopa equivalent daily dose (LEDD) was calculated based on a commonly used method (Tomlinson et al., 2010).

After a mean follow-up period of 1.5 years, the same patients were reassessed on the same variables as the baseline.

Database

Our team established the PD-MDCNC, a comprehensive yet flexible, user friendly, secure, and easily accessible database. And we launched the Chinese Early-Onset Parkinson's Disease Registry (CEOPDR), which is a large and longitudinal study designed to assess clinical features, genetic architecture, imaging, and biologic markers of EOPD progression in China. All study data will be integrated in the CEOPDR study database through the PD-MDCNC.

Data preprocessing

We conducted standardization to eliminate the influence of various dimensions by scaling the variables to zero mean and unit variance. Correlation analysis was performed between the two variables. When the calculated coefficient was greater than 0.98, only one feature was retained. Finally, the analysis did not exclude any factors. To address high-dimensional and multicollinearity problems, we used principal component analysis (PCA). PCA was performed using the Python software (version 3.6).

Cluster analysis

All data downloaded from the PD-MDCNC database were analyzed using R version 4.1.2.[2] Agglomerative hierarchical clustering, K-means clustering, and spectral clustering analyses were synchronously performed. We computed the Calinski–Harabasz score to estimate the optimal clustering methods. Ultimately, agglomerative hierarchical clustering was performed because of the higher Calinski–Harabasz score and better-balanced data distribution (**Supplementary Tables 1**, **2**). Visualization of the final hierarchical cluster solution was performed using Python software (version 3.6) (**Supplementary Figure 1**). A flowchart of data-driven clustering is shown in **Supplementary Figure 2**.

Statistical analyses

For the analysis of cross-sectional data, continuous variables were analyzed using one-way analysis of variance or non-parametric tests. Categorical variables were analyzed using the chi-squared test. Comparison of the baseline demography and clinical features between the three statistical clusters was also applied, adjusting for age and disease duration (continuous variables were analyzed by linear regression, and categorical variables were analyzed by logistic regression model).

We used general linear models (GLMs) for a comprehensive longitudinal comparison of the progression of the three subtypes. In each GLM, change of clinical characteristics was defined as the dependent variable. To reduce the regression toward the mean bias, the analysis was adjusted by the follow-up duration and baseline values of the clinical factors (Vickers and Altman, 2001; Fereshtehnejad et al., 2017). Statistical significance was defined as $P < 0.05$. All data were analyzed

2 https://www.r-project.org

using the IBM SPSS Statistics version 23.0 (IBM Corp., Armonk, NY, USA).

Results

Overview

A total of 1,217 patients with EOPD were included in this study. The mean age was 50.54 ± 6.82 years, 53.66% were male patients, and the mean age at onset was 44.12 ± 5.54 years, with an average disease duration of 6.34 ± 5.22 years. The mean UPDRS part I, II, III, and total scores were 2.28 ± 1.98, 10.98 ± 6.56, 25.42 ± 15.73, and 40.58 ± 23.25, respectively. Among the entire study population, RBD and dementia were found in 322 (26.46%) and 103 (8.46%) patients, respectively, at baseline. **Supplementary Table 3** summarizes the baseline clinical characteristics of the patients.

Cluster results and baseline characteristics in different clusters

The following 25 variables were included in the final clustering solution: age, age at onset, sex, duration, body mass index, LEDD, UPDRS total score, UPDRS part I–III scores, NMSS score, PDSS score, SCOPA-AUT score, PDQ-39 score, H&Y stage score, motor subtypes, dyskinesia, wearing-off, FOG, RBD, depression, EDS, dementia, hyposmia, and constipation (**Supplementary Table 3**). As illustrated in **Supplementary Figure 1** (visualization of the final hierarchical cluster solution in the EOPD cohort), cluster analysis revealed three distinct clusters of patients with EOPD. Detailed characteristics of the three clusters are listed in **Table 1**. We also demonstrated the discriminative power of these features using the heatmap shown in **Figure 1**. We observed evident baseline differences in motor and non-motor manifestations among clusters, with clinically important effect sizes.

The first cluster of 533 patients (cluster I, termed mild motor and non-motor dysfunction based on baseline features) was characterized by a low frequency of RBD, wearing-off, and dyskinesia and mild motor and NMSs. Motor symptoms/signs were relatively mild, with the lowest mean UPDRS part II and, III and total scores ($P < 0.05$). The H&Y stage of the patients was relatively mild. RBD [109 (20.45%) patients], wearing-off [104 (19.51%) patients], and dyskinesia [69 (12.95%) patients] were uncommon. Autonomic symptoms were generally mild (5.75 ± 5.35 in the SCOPA-AUT scale, $P = 0.013$). Moreover, the average LEDD was lower in cluster I than in clusters II and III ($P < 0.001$).

At the other extreme, the third cluster of 172 patients (cluster III, termed severe motor and non-motor dysfunction based on baseline features) was characterized by a high frequency of RBD, wearing-off and dyskinesia and more severe motor and NMSs. Motor symptoms/signs were relatively severe, with the highest mean UPDRS part II and, III and total scores ($P < 0.05$). The H&Y stage score were also relatively worse. RBD [70 (40.70%) patients], wearing-off [81 (47.09%) patients], and dyskinesia [60 (34.88%) patients] were more common in cluster III than in clusters I and II ($P < 0.05$). Autonomic symptoms were the most severe (8.72 ± 6.95 in the SCOPA-AUT scale, $P = 0.013$). Moreover, the average LEDD was significantly higher in cluster III than in clusters I and II ($P < 0.001$).

The patients in cluster II (512 patients with the subtype of intermediate EOPD) had intermediate motor and NMSs between clusters I and III. The UPDRS part II, III, and total scores were intermediate. The H&Y stage of the patients was relatively moderate. RBD (143 [27.93%] patients), wearing-off (148 [28.91%] patients) and dyskinesia (103 [20.12%] patients) were moderately frequent.

Disease progression in different clusters

After a mean duration of 1.5 years, follow-up data were available for 454 patients (**Table 2** and **Figure 2**). Patients in cluster III had a dramatically worse prognosis, with a more rapid progression in the UPDRS total ($P = 0.009$), UPDRS part II ($P = 0.035$), UPDRS part III ($P = 0.004$), H&Y stage ($P = 0.006$), and PDQ-39 ($P = 0.037$) scores. The intermediate cluster had a medium progression rate, which was slightly higher than that of cluster I.

Results from the GLM adjusted for baseline values and follow-up duration showed that compared to the cluster I, the cluster III subtypes had significantly greater progression in UPDRS total score (7.44 units more increase in compared to the mild subtype), UPDRS part II score (1.67 points more decline), UPDRS part III score (5.63 points more decline), H&Y stage score (0.31 points more decline), and PDQ-39 score (7.63 points more decline), which demonstrated the worst prognosis of all groups. Similar hierarchical progression was also observed in several non-motor features, namely, NMSS (1.92 points faster in cluster II, 5.00 points faster in cluster III), SCOPA-AUT (0.51 and 0.56 points faster), RBDQ-HK (0.25 and 2.69 points faster), ESS (0.82 and 1.44 points faster), HRS (−0.02 and −0.05 points faster), and HAMD (0.17 and 0.17 points faster) scores. Nevertheless, all showed no statistical significance.

However, the rate of progression was not statistically different between clusters I and II. As illustrated in **Figure 2**, the faster slope of progression in cluster III was most observed for the UPDRS total, UPDRS part III, and PDQ-39 scores. Based on this prognostic information, we updated the terminology of cluster III to severe motor and non-motor dysfunction/malignant and that of cluster I to mild motor and non-motor dysfunction/slow progression, leaving

TABLE 1 Comparison of the baseline demography and clinical features between the three clusters of EOPD cohort based on hierarchical clustering solution.

Characteristic	Cluster*			*P*-value	Adjusted *P*-value**	Multiple comparisons***
	I (*n* = 533)	II (*n* = 512)	III (*n* = 172)			
Age	49.54 ± 6.59	50.67 ± 6.86	53.22 ± 6.70	< 0.001	–	–
Gender ratio (male,%)	52.16	53.52	58.72	0.323	0.158	–
BMI	22.66 ± 3.01	22.54 ± 3.16	22.51 ± 2.77	0.715	0.880	–
Age at onset	44.24 ± 5.77	44.13 ± 5.32	43.76 ± 5.49	0.325	0.413	-
Disease duration	5.20 ± 4.83	6.48 ± 5.14	9.44 ± 5.30	< 0.001	–	–
LEDD	124.40 ± 85.88	367.62 ± 74.17	766.12 ± 197.62	< **0.001**	< **0.001**	**All comparisons**
UPDRS part I	2.08 ± 1.88	2.31 ± 2.02	2.82 ± 2.03	< 0.001	0.140	–
UPDRS part II	9.92 ± 5.78	10.89 ± 6.63	14.52 ± 7.41	< **0.001**	< **0.001**	I **vs.** III, II **vs.** III
UPDRS part III	23.31 ± 14.16	25.44 ± 15.78	31.89 ± 18.29	< **0.001**	**0.034**	I **vs.** III
UPDRS total score	36.76 ± 20.71	40.54 ± 23.48	52.49 ± 25.96	< **0.001**	**0.001**	I **vs.** III, II **vs.** III
TD/Indeterminate/PIGD (%)	27.02/19.89/53.09	27.54/16.80/55.66	20.35/13.95/65.70	0.051	–	–
H&Y	1.97 ± 0.83	2.15 ± 0.87	2.58 ± 0.88	< **0.001**	**0.001**	I **vs.** III, II **vs.** III
Dyskinesia (%)[a]	12.95	20.12	34.88	< **0.001**	**0.001**	**All comparisons**
Wearing-off (%)[b]	19.51	28.91	47.09	< **0.001**	< **0.001**	**All comparisons**
FOG (%)[c]	23.08	26.95	40.12	< 0.001	0.352	–
NMSS	27.71 ± 26.12	31.94 ± 28.59	39.26 ± 27.19	< 0.001	0.165	–
PDSS	121.75 ± 26.82	119.76 ± 25.78	111.04 ± 26.35	< 0.001	0.099	–
SCOPA-AUT	5.75 ± 5.35	6.42 ± 6.02	8.72 ± 6.95	< **0.001**	**0.013**	I **vs.** III, II **vs.** III
PDQ-39	24.95 ± 22.65	27.53 ± 25.70	37.73 ± 26.53	< 0.001	0.051	–
Dementia (%)[d]	5.63	10.74	10.47	0.007	0.052	–
RBD (%)[e]	20.45	27.93	40.70	< **0.001**	**0.029**	I **vs.** III
EDS (%)[f]	22.89	25.37	32.56	0.038	0.503	–
Hyposmia (%)[g]	31.71	34.18	38.95	0,210	0.947	–
Depression (%)[h]	24.58	27.54	36.05	0.014	0.156	–
Constipation (%)[i]	16.28	18.95	24.55	0.055	0.978	–

*Quantitative data were expressed as mean ± SD, categorical variables were expressed as percentages, unless otherwise indicated. **Adjusted *P*-value were performed between subtypes comparisons by multivariable linear or logistic regression (controlled for baseline age and duration of disease). ***Multiple comparisons were performed among the three subtypes if adjusted *P*-value was less than 0.05. Significant *P*-values are indicated in bold. [a−i]Evaluated, respectively by UPDRS part IV-A, WOQ-9, the 9-item End-of-dose Wearing-off Questionnaire; NFOGQ, New Freezing of Gait Questionnaire; MMSE, Mini-Mental State Examination; RBDQ-HK, Rapid Eye Movement Sleep Behavior Disorder Questionnaire-Hong Kong; ESS, Epworth Sleepiness Scale; HRS, Hyposmia Rating Scale; HAMD-17, Hamilton Depression Scale and Rome III criteria; EOPD, Early-onset Parkinson's Disease; BMI, Body Mass Index; LEDD, Levodopa Equivalent Daily Dose; UPDRS, Unified Parkinson's disease Rating Scale; TD, Tremor-Dominant; PIGD, Postural Instability and Gait Difficulty; H&Y, Hoehn and Yahr; FOG, freezing of gait; NMSS, Non-Motor Symptoms Scale; PDSS, Parkinson's Disease Sleep Scale; SCOPA-AUT, the Scale for Outcomes in Parkinson Disease for Autonomic Dysfunction; PDQ-39, Parkinson's disease questionnaire-39 item version; RBD, Rapid Eye Movement Sleep Behavior Disorder; EDS, excessive daytime sleepiness.

cluster II terminology unchanged (i.e., intermediate). The data distribution of all clusters and the prevalence of clinical symptoms at baseline and follow-up are shown in Supplementary Figures 3, 4, respectively.

Discussion

To the best of our knowledge, this is the first study to explore the classification of patients with EOPD with a longitudinal large-sample cohort in a comprehensive database on a broad spectrum of motor and non-motor characteristics. Our study found that the most critical determinants of EOPD subtype and prognosis were motor and some NMSs, especially the UPDRS total score, motor complications, RBD, and autonomic dysfunction. Three subtypes were identified: mild motor and non-motor dysfunction/slow progression (cluster I), intermediate (cluster II) and severe motor and non-motor dysfunction/malignant (cluster III). Identification of these subtypes at baseline helps predict prognosis.

Evidence suggests that early-onset Parkinson's disease is clinically heterogeneous; however, cluster studies of clinical subtypes in patients with EOPD remain scarce. We compared different clustering solutions in our EOPD cohort and selected the best solution to compare the baseline differences and disease progression among the clusters. As expected, baseline differences in motor and NMSs were observed among the clusters. The mild subtype represents patients with EOPD who have mild motor and non-motor manifestations, and RBD and motor complications might be present but are milder than those

TABLE 2 Longitudinal changes in clinical motor and non-motor outcomes in three different clinical phenotypes of EOPD at follow-up.

Outcome	Phenotype			Total *P*-value	*P*-value
	I (*n* = 216)	II (*n* = 181)	III (*n* = 57)		
UPDRS total score					
t2-t1	0.50 (17.04)	2.38 (16.11)	5.82 (18.65)	**0.009**	–
β adjusted coefficient (95% CI)	0*	2.24 (−0.95 to 5.43)	7.44 (2.67 to 12.20)	–	P_{II} = **0.168**, P_{III} = **0.002**
UPDRS part I score					
t2-t1	0.06 (2.06)	0.05 (2.08)	0.49 (2.46)	0.079	–
β adjusted coefficient (95% CI)	0*	0.13 (−0.24 to 0.50)	0.64 (0.08 to 1.19)	–	P_{II} = 0.489, P_{III} = 0.024
UPDRS part II score					
t2-t1	0.21 (4.30)	0.83 (4.76)	1.21 (5.18)	**0.035**	–
β adjusted coefficient (95% CI)	0*	0.67 (−0.21 to 1.55)	1.67 (0.34 to 2.99)	–	P_{II} = **0.136**, P_{III} = **0.014**
UPDRS part III score					
t2-t1	−0.72 (12.45)	1.31 (12.36)	3.53 (13.77)	**0.004**	–
β adjusted coefficient (95% CI)	0*	2.08 (−0.23 to 4.39)	5.63 (2.19 to 9.06)	–	P_{II} = **0.078**, P_{III} = **0.001**
H&Y					
t2-t1	0.21 (0.73)	0.19 (0.74)	0.30 (0.67)	**0.006**	–
β adjusted coefficient (95% CI)	0*	0.05 (−0.071 to 0.18)	0.31 (0.123 to 0.50)	–	P_{II} = **0.391**, P_{III} = **0.001**
NMSS					
t2-t1	0.61 (24.03)	0.91 (23.97)	3.49 (31.08)	0.335	–
β adjusted coefficient (95% CI)	0*	1.92 (−2.76 to 6.60)	5.00 (−1.86 to 11.88)	–	P_{II} = 0.420, P_{III} = 0.153
PDSS					
t2-t1	−4.27 (27.89)	−3.33 (28.65)	−4.69 (27.66)	0.866	–
β adjusted coefficient (95% CI)	0*	0.48 (−4.98 to 5.95)	−1.72 (−9.66 to 6.21)	–	P_{II} = 0.862, P_{III} = 0.670
SCOPA-AUT					
t2-t1	1.38 (5.82)	1.54 (6.15)	1.85 (5.11)	0.707	–
β adjusted coefficient (95% CI)	0*	0.51 (−0.79 to 1.81)	0.56 (−1.49 to 2.61)	–	P_{II} = 0.443, P_{III} = 0.589
PDQ-39					
t2-t1	−1.10 (19.92)	1.47 (22.10)	4.07 (23.59)	**0.037**	–
β adjusted coefficient (95% CI)	0*	2.48 (−1.49 to 6.46)	7.63 (1.70 to 13.55)	–	P_{II} = **0.220**, P_{III} = **0.012**
MMSE					
t2-t1	0.17 (2.17)	0.32 (2.40)	−0.30 (2.17)	0.249	–
β adjusted coefficient (95% CI)	0*	0.00 (−0.42 to 0.43)	−0.52 (−1.15 to 0.12)	–	P_{II} = 0.988, P_{III} = 0.114
RBDQ-HK					
t2-t1	1.53 (11.51)	1.45 (12.78)	2.56 (16.21)	0.355	–
β adjusted coefficient (95% CI)	0*	0.25 (−2.27 to 2.772)	2.69 (−1.04 to 6.43)	–	P_{II} = 0.846, P_{III} = 0.157
ESS					
t2-t1	−0.07 (6.03)	0.08 (6.55)	1.22 (5.84)	0.156	–
β adjusted coefficient (95% CI)	0*	0.82 (−0.31 to 1.96)	1.44 (−0.25 to 3.13)	–	P_{II} = 0.156, P_{III} = 0.095
HRS					
t2-t1	−1.28 (4.62)	−1.12 (4.77)	−1.40 (5.66)	0.998	–
β adjusted coefficient (95% CI)	0*	−0.02 (−0.98 to 0.94)	−0.05 (−1.44 to 1.35)	–	P_{II} = 0.968, P_{III} = 0.947
HAMD					
t2-t1	0.54 (5.85)	0.34 (4.80)	1.06 (6.81)	0.945	–
β adjusted coefficient (95% CI)	0*	0.17 (−0.88 to 1.21)	0.17 (−1.39 to 1.72)	–	P_{II} = 0.752, P_{III} = 0.834

All presented values are mean (standard deviation), unless otherwise specified. In each general linear models, change of clinical characteristics was defined as the dependent variable, and was adjusted by the follow-up duration and baseline value of clinical factors. *Reference group. Significant *P*-values are indicated in bold. EOPD, Early-onset Parkinson's Disease; UPDRS, Unified Parkinson's Disease Rating Scale; H&Y, Hoehn and Yahr; NMSS, Non-Motor Symptoms Scale; PDSS, Parkinson's Disease Sleep Scale; SCOPA-AUT, the scale for outcomes in Parkinson's Disease for Autonomic Dysfunction; PDQ-39, Parkinson's disease questionnaire-39 item version; MMSE, Mini Mental State Examination; RBDQ-HK, Rapid Eye Movement Sleep Behavior Disorder Questionnaire-Hong Kong; ESS, Epworth Sleepiness Scale; HRS, Hyposmia Rating Scale; HAMD, Hamilton Depression Scale.

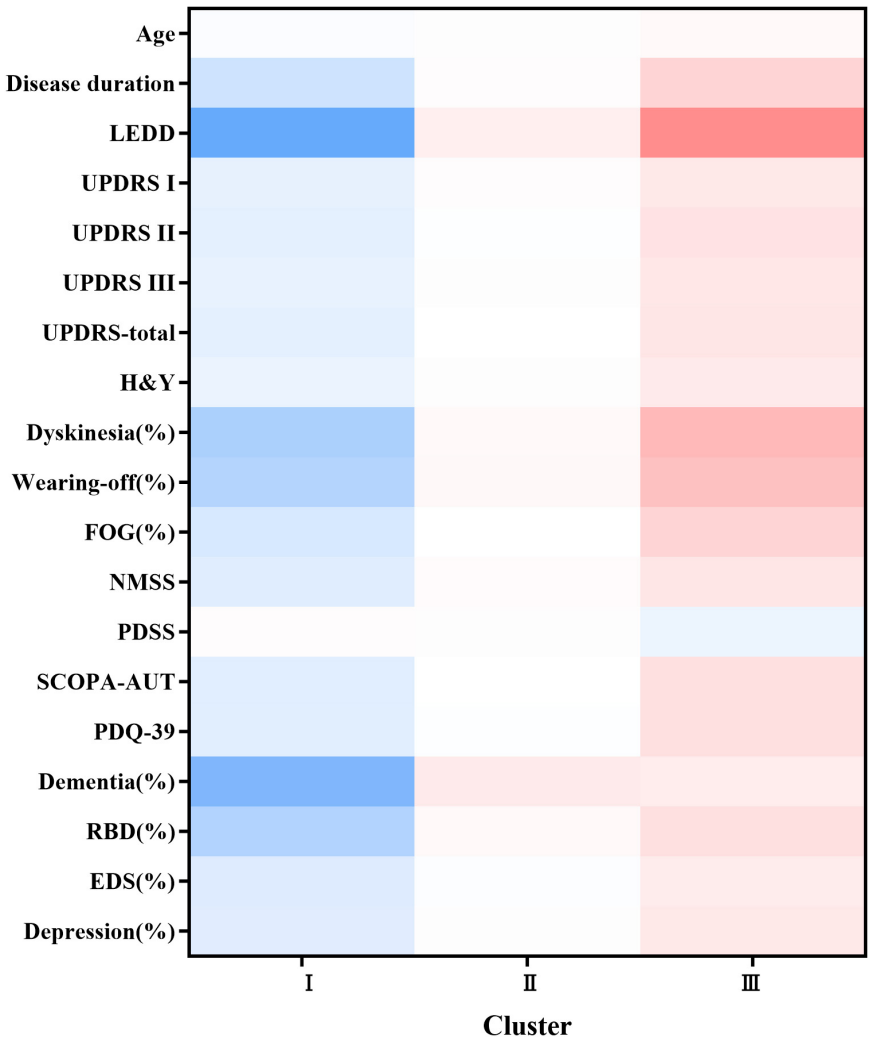

FIGURE 1
Heatmap of the three subtypes at baseline. The figure was depicted according to the mean values or percentages of subtypes. The red color represented a more severe deficit and the blue color referred to a less severe symptom. The darker the figure described, the larger difference were shown among the subtypes. Variables with *P* value <0.05 are shown. LEDD, Levodopa Equivalent Daily Dose; UPDRS, Unified Parkinson's disease Rating Scale; H&Y, Hoehn and Yahr; FOG, freezing of gait; NMSS, Non-Motor Symptoms Scale; PDSS, Parkinson's Disease Sleep Scale; SCOPA-AUT, the Scale for Outcomes in Parkinson's Disease for Autonomic Dysfunction; PDQ-39, Parkinson's disease questionnaire-39 item version; RBD, Rapid Eye Movement Sleep Behavior Disorder; EDS, excessive daytime sleepiness.

present in cluster III. These patients had the most favorable disease course, with the least worsening of the UPDRS total score after 1.5 years. In contrast, the severe subtype had a high frequency of RBD, wearing-off, and dyskinesia at baseline. These patients also exhibited more severe motor and autonomic symptoms. This subtype showed the most rapid and malignant progression rate in terms of the UPDRS total, UPDRS part II, UPDRS part III, H&Y stage, and PDQ-39 total scores. Between these two extremes, the intermediate subtype was defined as having intermediate motor and NMSs. This subtype showed a moderate progression rate, which was slightly higher than that in cluster I. Our results further confirmed the clinical heterogeneity of EOPD. Defining EOPD subtypes contributes to a better understanding of the underlying mechanisms of EOPD, predicts the disease course of EOPD, and leads to tailored treatment strategies (Hendricks and Khasawneh, 2021).

A heterogeneous clinical presentation and prognosis of patients with PD is increasingly recognized; in a recent longitudinal study, the presence of RBD, cognitive impairment, and autonomic dysfunction were the best predictors of a diffuse/malignant phenotype of PD (Fereshtehnejad et al., 2015). In our study, patients with the severe subtype also showed a higher propensity for RBD and more worsened autonomic disturbance, in agreement with previous studies (Fereshtehnejad et al., 2015, 2017). Previous study (Fereshtehnejad et al., 2015, 2017; Udow et al., 2016; Jozwiak et al., 2017) also

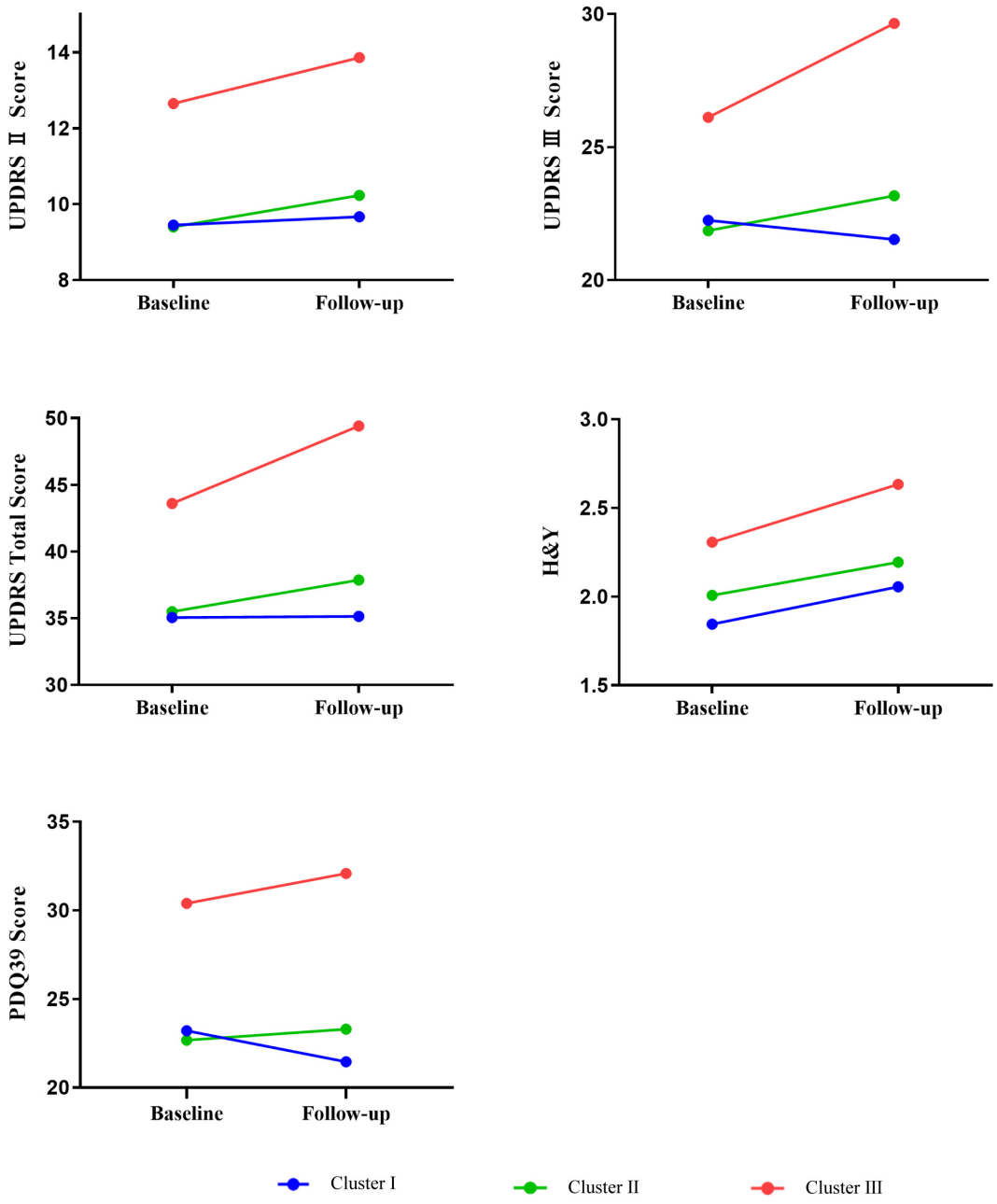

FIGURE 2
Longitudinal changes in outcomes of interest in different phenotypes of EOPD at follow-up. In each general linear models, change of clinical characteristics was defined as the dependent variable, and was adjusted by the follow-up duration and baseline value of clinical factors. Mean follow-up duration in the entire population = 1.5 years. UPDRS, Unified Parkinson's disease Rating Scale; H&Y, Hoehn and Yahr; PDQ-39, Parkinson's disease questionnaire-39 item version.

found that these NMSs often coincided, suggesting a common neurobiological factor (Udow et al., 2016). Reduced noradrenergic function in PD was associated with the presence of RBD and autonomic dysfunction and noradrenergic impairment may contribute to the high prevalence of these NMSs in PD (Sommerauer et al., 2018). In addition, compared to patients with mild and intermediate EOPD subtypes, patients with severe EOPD subtype had more severe motor symptoms and higher frequency of motor complications in our study, which are consistent with the results of other similar studies in PD (van Rooden et al., 2011; Belvisi et al., 2021), and severe motor and non-motor dysfunction/malignant subtype may indicate a relatively diffuse neurodegenerative process. Different from the results of other cohort studies, our study further

highlights the importance of motor complications as drivers of EOPD subtyping and prognosis.

The mechanism underlying the EOPD subtype differences remains unclear. Studies have indicated that genetic, environmental factors, gene-environment interactions, or all of these factors may play an important role in the pathogenesis of EOPD. There is accumulating evidence indicating that different genotypes of EOPD may lead to distinct clinical characteristics and rate of progression. For example, EOPD with *PRKN*, *PINK1*, or *DJ-1* mutations are characterized by good response to L-dopa treatment, dystonia and dyskinesia being relatively common, cognitive decline relatively uncommon and a slower deterioration of the disease when compared with idiopathic PD (Kasten et al., 2018; Lin et al., 2019; Zhao et al., 2020; Sun et al., 2021). Patients of EOPD with *SNCA* mutations show asymmetric onset, good responsiveness for L-dopa in initial time, early motor complications, rapid progression and worse cognitive impairment (Trinh et al., 2018; Chen et al., 2020; Zhao et al., 2020). Potential explanations of subtype differences include different PD-associated protein dysfunctions (Quinn et al., 2020; Mencke et al., 2021; Menozzi and Schapira, 2021), different accumulation rates of pathogenic alpha-synuclein (Lawton et al., 2022), different trajectories of pathology progression (De Pablo-Fernández et al., 2019) or possibly even different compensatory capacities in the neural circuits (Palermo et al., 2020; Wang et al., 2022). Future studies should focus on understanding the underlying disease pathophysiology that drives these different clinical clusters in EOPD and their subsequent progression.

This study has some limitations. Our cluster analysis solution classified EOPD based on clinical presentation only, and additional variables (i.e., genetics, neuroimaging markers, and other biomarkers) may be able to further refine the clusters. Secondly, our study has the heterogeneity of clinical data collection and quality from different investigators. Nevertheless, to retain the consistency and quality of the data as much as possible, all the researchers involved in the study received standardized and unified training. Thirdly, the follow-up data are incomplete, and the reasons of causing this are varied. For example, the follow-up time of some patients with EOPD has not been reached, and the impact of COVID-19 containment measures. Moreover, the prognostic value and applicability of our recommended EOPD subtyping method should be confirmed in other cohorts.

In summary, we developed three clinical EOPD subtypes based on the cluster analysis of a large EOPD cohort. Motor symptoms, motor complications, and NMSs were distinguished among the clusters, some of which were verified in follow-up data. These findings improve our understanding of EOPD heterogeneity. Exploring EOPD subtypes will shed light on precision medicine and develop more effective approaches for clinical trials and treatment strategies for patients with EOPD in the future.

Conclusion

We identified three different clinical subtypes (mild, intermediate, and severe) using cluster analysis in a large EOPD cohort for the first time, which is important for tailoring therapy to individuals with EOPD.

Data availability statement

The raw data supporting the conclusions of this article will be made available by the authors, without undue reservation.

Ethics statement

The studies involving human participants were reviewed and approved by the Ethics Committee of Xiangya Hospital of Central South University. The patients/participants provided their written informed consent to participate in this study.

Author contributions

ZZ and XZ: research project conception, organization, execution, statistical analysis design and execution of the study, patients' enrollment and follow up, and writing of the first manuscript draft. YX, YZ, HP, and JW: research project execution and patients' enrollment and follow up. QX, YC, QS, XY, JG, and BT: research project organization, execution, and manuscript review and critique. XYW, JZ, XHW, and JL: statistical analysis design, execution, review and critique of the study, and manuscript review and critique. LL and ZL: research project conception, organization, execution, and manuscript review and critique. All authors contributed to the article and approved the submitted version for publication.

Funding

This study was supported by the Hunan Innovative Province Construction Project (Grant Nos. 2019SK2335 and 2021SK1010), Natural Science Foundation of Hunan Province (Grant Nos. 2022JJ40843 and 2020JJ5929), National Key Research and Development Program of China (Grant Nos. 2021YFC2501204 and 2016YFC306000), National Natural Science Foundation of China (Grant No. 82001359), and Scientific Research Project of Hunan Provincial Health Commission (Grant No. 202203074637).

Acknowledgments

We thank all subjects for their participation, all investigators for their efforts and support in this study. We also thank Editage (www.editage.cn) for English language editing.

Conflict of interest

Authors JZ and XHW were employees of Hunan KeY Health Technology Co., Ltd. Author JL was employee of Hunan Creator Information Technology Co., Ltd.

The remaining authors declare that the research was conducted in the absence of any commercial or financial relationships that could be construed as a potential conflict of interest.

Publisher's note

Supplementary material

The Supplementary Material for this article can be found online at: https://www.frontiersin.org/articles/10.3389/fnagi.2022.1040293/full#supplementary-material

References

Armstrong, M. J., and Okun, M. S. (2020). Diagnosis and treatment of parkinson disease: A review. *JAMA* 323, 548–560. doi: 10.1001/jama.2019.22360

Belvisi, D., Fabbrini, A., De Bartolo, M. I., Costanzo, M., Manzo, N., Fabbrini, G., et al. (2021). The pathophysiological correlates of Parkinson's disease clinical subtypes. *Mov. Disord.* 36, 370–379. doi: 10.1002/mds.28321

Bloem, B. R., Okun, M. S., and Klein, C. (2021). Parkinson's disease. *Lancet* 397, 2284–2303. doi: 10.1016/s0140-6736(21)00218-x

Brendel, M., Su, C., Hou, Y., Henchcliffe, C., and Wang, F. (2021). Comprehensive subtyping of Parkinson's disease patients with similarity fusion: A case study with BioFIND data. *NPJ Parkinsons Dis.* 7:83. doi: 10.1038/s41531-021-00228-0

Chen, Y., Gu, X., Ou, R., Zhang, L., Hou, Y., Liu, K., et al. (2020). Evaluating the role of SNCA, LRRK2, and GBA in Chinese patients with early-onset Parkinson's disease. *Mov. Disord.* 35, 2046–2055. doi: 10.1002/mds.28191

De Pablo-Fernández, E., Lees, A. J., Holton, J. L., and Warner, T. T. (2019). Prognosis and neuropathologic correlation of clinical subtypes of Parkinson disease. *JAMA Neurol.* 76, 470–479. doi: 10.1001/jamaneurol.2018.4377

Fereshtehnejad, S. M., Romenets, S. R., Anang, J. B., Latreille, V., Gagnon, J. F., and Postuma, R. B. (2015). New clinical subtypes of parkinson disease and their longitudinal progression: A prospective cohort comparison with other phenotypes. *JAMA Neurol.* 72, 863–873. doi: 10.1001/jamaneurol.2015.0703

Fereshtehnejad, S. M., Zeighami, Y., Dagher, A., and Postuma, R. B. (2017). Clinical criteria for subtyping Parkinson's disease: Biomarkers and longitudinal progression. *Brain* 140, 1959–1976. doi: 10.1093/brain/awx118

Hendricks, R. M., and Khasawneh, M. T. (2021). A systematic review of Parkinson's disease cluster analysis research. *Aging Dis.* 12, 1567–1586. doi: 10.14336/ad.2021.0519

Jafari, Z., Kolb, B. E., and Mohajerani, M. H. (2020). Auditory dysfunction in Parkinson's disease. *Mov. Disord.* 35, 537–550. doi: 10.1002/mds.28000

Jozwiak, N., Postuma, R. B., Montplaisir, J., Latreille, V., Panisset, M., Chouinard, S., et al. (2017). REM sleep behavior disorder and cognitive impairment in Parkinson's disease. *Sleep* 40:zsx101. doi: 10.1093/sleep/zsx101

Kasten, M., Hartmann, C., Hampf, J., Schaake, S., Westenberger, A., Vollstedt, E. J., et al. (2018). Genotype-phenotype relations for the Parkinson's disease genes Parkin, PINK1, DJ1: MDSGene systematic review. *Mov. Disord.* 33, 730–741. doi: 10.1002/mds.27352

Lawton, M., Ben-Shlomo, Y., May, M. T., Baig, F., Barber, T. R., Klein, J. C., et al. (2018). Developing and validating Parkinson's disease subtypes and their motor and cognitive progression. *J. Neurol. Neurosurg. Psychiatry* 89, 1279–1287. doi: 10.1136/jnnp-2018-318337

Lawton, M., Tan, M. M., Ben-Shlomo, Y., Baig, F., Barber, T., Klein, J. C., et al. (2022). Genetics of validated Parkinson's disease subtypes in the Oxford discovery and tracking Parkinson's cohorts. *J. Neurol. Neurosurg. Psychiatry* 93, 952–959. doi: 10.1136/jnnp-2021-327376

Lin, C. H., Chen, P. L., Tai, C. H., Lin, H. I., Chen, C. S., Chen, M. L., et al. (2019). A clinical and genetic study of early-onset and familial parkinsonism in taiwan: An integrated approach combining gene dosage analysis and next-generation sequencing. *Mov. Disord.* 34, 506–515. doi: 10.1002/mds.27633

Liu, Z., Yang, N., Dong, J., Tian, W., Chang, L., Ma, J., et al. (2022). Deficiency in endocannabinoid synthase DAGLB contributes to early onset Parkinsonism and murine nigral dopaminergic neuron dysfunction. *Nat. Commun.* 13:3490. doi: 10.1038/s41467-022-31168-9

Mencke, P., Boussaad, I., Romano, C. D., Kitami, T., Linster, C. L., and Krüger, R. (2021). The role of DJ-1 in cellular metabolism and pathophysiological implications for Parkinson's disease. *Cells* 10:347. doi: 10.3390/cells10020347

Menozzi, E., and Schapira, A. H. V. (2021). Exploring the genotype-phenotype correlation in GBA-Parkinson disease: Clinical aspects, biomarkers, and potential modifiers. *Front. Neurol.* 12:694764. doi: 10.3389/fneur.2021.694764

Mestre, T. A., Fereshtehnejad, S. M., Berg, D., Bohnen, N. I., Dujardin, K., Erro, R., et al. (2021). Parkinson's disease subtypes: Critical appraisal and recommendations. *J. Parkinsons Dis.* 11, 395–404. doi: 10.3233/jpd-202472

Niemann, N., and Jankovic, J. (2019). Juvenile parkinsonism: Differential diagnosis, genetics, and treatment. *Parkinsonism Relat. Disord.* 67, 74–89. doi: 10.1016/j.parkreldis.2019.06.025

Pagano, G., Ferrara, N., Brooks, D. J., and Pavese, N. (2016). Age at onset and Parkinson disease phenotype. *Neurology* 86, 1400–1407. doi: 10.1212/wnl.0000000000002461

Palermo, G., Giannoni, S., Frosini, D., Morganti, R., Volterrani, D., Bonuccelli, U., et al. (2020). Dopamine transporter, age, and motor complications in Parkinson's disease: A clinical and single-photon emission computed tomography study. *Mov. Disord.* 35, 1028–1036. doi: 10.1002/mds.28008

Poewe, W., Seppi, K., Tanner, C. M., Halliday, G. M., Brundin, P., Volkmann, J., et al. (2017). Parkinson disease. *Nat. Rev. Dis. Primers* 3:17013. doi: 10.1038/nrdp.2017.13

Postuma, R. B., Berg, D., Stern, M., Poewe, W., Olanow, C. W., Oertel, W., et al. (2015). MDS clinical diagnostic criteria for Parkinson's disease. *Mov. Disord.* 30, 1591–1601. doi: 10.1002/mds.26424

Qian, E., and Huang, Y. (2019). Subtyping of Parkinson's disease–Where are we up to? *Aging Dis.* 10, 1130–1139. doi: 10.14336/ad.2019.0112

Quinn, P. M. J., Moreira, P. I., Ambrósio, A. F., and Alves, C. H. (2020). PINK1/PARKIN signalling in neurodegeneration and neuroinflammation. *Acta Neuropathol. Commun.* 8:189. doi: 10.1186/s40478-020-01062-w

Schirinzi, T., Di Lazzaro, G., Sancesario, G. M., Summa, S., Petrucci, S., Colona, V. L., et al. (2020). Young-onset and late-onset Parkinson's disease exhibit a

different profile of fluid biomarkers and clinical features. *Neurobiol. Aging* 90, 119–124. doi: 10.1016/j.neurobiolaging.2020.02.012

Schrag, A., and Schott, J. M. (2006). Epidemiological, clinical, and genetic characteristics of early-onset parkinsonism. *Lancet Neurol.* 5, 355–363. doi: 10.1016/s1474-4422(06)70411-2

Sommerauer, M., Fedorova, T. D., Hansen, A. K., Knudsen, K., Otto, M., Jeppesen, J., et al. (2018). Evaluation of the noradrenergic system in Parkinson's disease: An 11C-MeNER PET and neuromelanin MRI study. *Brain* 141, 496–504. doi: 10.1093/brain/awx348

Sun, Y. M., Yu, H. L., Zhou, X. Y., Xiong, W. X., Luo, S. S., Chen, C., et al. (2021). Disease progression in patients with parkin-related Parkinson's disease in a longitudinal cohort. *Mov. Disord.* 36, 442–448. doi: 10.1002/mds.28349

Tomlinson, C. L., Stowe, R., Patel, S., Rick, C., Gray, R., and Clarke, C. E. (2010). Systematic review of levodopa dose equivalency reporting in Parkinson's disease. *Mov. Disord.* 25, 2649–2653. doi: 10.1002/mds.23429

Trinh, J., Zeldenrust, F. M. J., Huang, J., Kasten, M., Schaake, S., Petkovic, S., et al. (2018). Genotype-phenotype relations for the Parkinson's disease genes SNCA, LRRK2, VPS35: MDSGene systematic review. *Mov. Disord.* 33, 1857–1870. doi: 10.1002/mds.27527

Udow, S. J., Robertson, A. D., MacIntosh, B. J., Espay, A. J., Rowe, J. B., Lang, A. E., et al. (2016). 'Under pressure': Is there a link between orthostatic hypotension and cognitive impairment in α-synucleinopathies? *J. Neurol. Neurosurg. Psychiatry* 87, 1311–1321. doi: 10.1136/jnnp-2016-314123

van Rooden, S. M., Colas, F., Martínez-Martín, P., Visser, M., Verbaan, D., Marinus, J., et al. (2011). Clinical subtypes of Parkinson's disease. *Mov. Disord.* 26, 51–58. doi: 10.1002/mds.23346

Vickers, A. J., and Altman, D. G. (2001). Statistics notes: Analysing controlled trials with baseline and follow up measurements. *BMJ* 323, 1123–1124. doi: 10.1136/bmj.323.7321.1123

Wang, L., Wu, P., Brown, P., Zhang, W., Liu, F., Han, Y., et al. (2022). Association of structural measurements of brain reserve with motor progression in patients with Parkinson disease. *Neurology*. doi: 10.1212/wnl.0000000000200814 [Epub ahead of print].

Zhang, Z. X., Roman, G. C., Hong, Z., Wu, C. B., Qu, Q. M., Huang, J. B., et al. (2005). Parkinson's disease in China: Prevalence in Beijing, Xian, and Shanghai. *Lancet* 365, 595–597. doi: 10.1016/s0140-6736(05)17909-4

Zhao, Y., Qin, L., Pan, H., Liu, Z., Jiang, L., He, Y., et al. (2020). The role of genetics in Parkinson's disease: A large cohort study in Chinese mainland population. *Brain* 143, 2220–2234. doi: 10.1093/brain/awaa167

Zhou, X., Liu, Z., Zhou, X., Xiang, Y., Zhou, Z., Zhao, Y., et al. (2022). The Chinese Parkinson's disease registry (CPDR): Study design and baseline patient characteristics. *Mov. Disord.* 37, 1335–1345. doi: 10.1002/mds.29037

frontiers | Frontiers in Aging Neuroscience

TYPE Original Research
PUBLISHED 16 December 2022
DOI 10.3389/fnagi.2022.1061096

OPEN ACCESS

EDITED BY
Woon-Man Kung,
Chinese Culture University,
Taiwan

REVIEWED BY
Zhenhua Liu,
Central South University,
China
Federico Verde,
Italian Auxological Institute (IRCCS),
Italy

*CORRESPONDENCE
Lan Tan
dr.tanlan@163.com

†These authors have contributed equally to this work

SPECIALTY SECTION
This article was submitted to Alzheimer's Disease and Related Dementias, a section of the journal Frontiers in Aging Neuroscience

RECEIVED 04 October 2022
ACCEPTED 24 November 2022
PUBLISHED 16 December 2022

CITATION
Sheng Z-H, Ma L-Z, Liu J-Y, Ou Y-N, Zhao B, Ma Y-H and Tan L (2022) Cerebrospinal fluid neurofilament dynamic profiles predict cognitive progression in individuals with *de novo* Parkinson's disease. *Front. Aging Neurosci.* 14:1061096. doi: 10.3389/fnagi.2022.1061096

Cerebrospinal fluid neurofilament dynamic profiles predict cognitive progression in individuals with *de novo* Parkinson's disease

Ze-Hu Sheng†, Ling-Zhi Ma†, Jia-Yao Liu†, Ya-Nan Ou, Bing Zhao, Ya-Hui Ma and Lan Tan*

Department of Neurology, Qingdao Municipal Hospital, Qingdao University, Qingdao, China

Background: Neurofilament light chain protein (NfL) in cerebrospinal fluid (CSF) reflects the severity of neurodegeneration, with its altered concentrations discovered in Parkinson's disease (PD) and Parkinson's disease dementia (PD-D).

Objective: To determine whether CSF NfL, a promising biomarker of neuronal/axonal damage, can be used to monitor cognitive progression in *de novo* Parkinson's disease and predict future cognitive decline.

Methods: A total of 259 people were recruited in this study, including 85 healthy controls (HC) and 174 neonatal PD patients from the Parkinson's Progression Markers Initiative (PPMI). Multiple linear regression and linear mixed effects models were used to examine the associations of baseline/longitudinal CSF NfL with cognitive decline and other CSF biomarkers. Kaplan–Meier analysis and log-rank test were used to compare the cumulative probability risk of cognition progression during the follow-up. Multivariate cox regression was used to detect cognitive progression in *de novo* PD.

Results: We found PD patients with mild cognitive impairment (PD-MCI) was higher than with normal cognition (PD-NC) in terms of CSF NfL baseline levels (p=0.003) and longitudinal increase rate (p=0.034). Both baseline CSF NfL and its rate of change predicted measurable cognitive decline in *de novo* PD (MoCA, β=−0.010, p=0.011; β=−0.0002, p<0.001, respectively). The predictive effects in *de novo* PD patients aged >65, male, ill-educated (<13years) and without carrying Apolipoprotein E $\varepsilon 4$ (*APOE* $\varepsilon 4$) seemed to be more obvious and reflected in more domains investigated. We also observed that CSF NfL levels predicted progression in *de novo* PD patients with different cognitive diagnosis and amyloid status. After an average follow-up of 6.66±2.54years, higher concentration above the median of baseline CSF NfL was associated with a future high risk of PD with dementia (adjusted HR 2.82, 95% CI: 1.11–7.20, p=0.030).

Conclusion: Our results indicated that CSF NfL is a promising prognostic predictor of PD, and its concentration and dynamics can monitor the severity and progression of cognitive decline in *de novo* PD patients.

KEYWORDS

cerebrospinal fluid, neurofilament light, Parkinson's progression markers initiative, cognitive decline, Parkinson's disease

Introduction

Parkinson's disease (PD) secondary to basal ganglia dysfunction is a complex ailment in terms of epidemiology, pathology, genetics, clinical expression, and therapy (Kalia and Lang, 2015). Due to an aging population, the number individuals afflicted with this second most common neurodegenerative disease is anticipated to double in 20 years (Mehta and Adler, 2016). Approximately 15–40% of PD patients with mild cognitive impairment (PD-MCI) can be offered a diagnosis when motor symptoms are observed. In patients with PD, cognitive decline has been recognized as a factor that further worsens a patient's prognosis, as compared to other disease-related non-motor symptoms (Mollenhauer et al., 2014). Meanwhile, the incidence of PD with dementia (PD-D) ranges within 24 to 31%, and rises to 80% in a 20-year duration (Aarsland et al., 2005b; Song et al., 2011; Leaver and Poston, 2015). The lack of great approaches to predict the time frame of disease progression possibly contributes to poor prognosis and serious economic burden to PD patients (Findley et al., 2003). Therefore, it is of utmost importance to investigate whether certain biomarkers in cerebrospinal fluid (CSF) can predict or monitor the extent of cognitive deterioration in PD patients (Hall et al., 2015).

Neuroaxonal degeneration is a significant pathological mechanism that generates permanent disability in neurological disorders (Ng et al., 2020). Neurofilament light (NfL) is an enriched cytoskeletal protein exclusively expressed by central and peripheral neurons; it is also released to CSF after axonal injury and neurodegeneration (Bridel et al., 2019). CSF NfL provides a sensitive measurement for the identification of neuroaxonal damage, as well as the extent of this damage (Khalil et al., 2018). Recent studies have found that CSF NfL concentration is significantly elevated in PD-MCI and PD-D patients in comparison to healthy controls (HC; Hall et al., 2012; Lerche et al., 2020). Nonetheless, whether this increase in concentration presents in early PD patients with cognitive decline remains uncertain. Longitudinal data of CSF biomarkers in PD population is rare, and comprehensive longitudinal models for cognitive prediction are deficient in past research studies. It is essential to critically discuss and further explore the predictive value of CSF NfL to validate whether this effect exists in independent PD cohorts.

Considering CSF NfL as a promising biomarker in neurodegenerative diseases, we hypothesize that its concentration and dynamic analysis may possibly predict cognitive progression and detect related pathological changes in *de novo* PD patients. In the present research, we investigated the associations of CSF NfL with cognitive progression on different aspects and CSF biomarkers through cross-sectional and longitudinal analyses based on different diagnostic groups of studied population from the Parkinson's Progression Markers Initiative (PPMI) database (2011).

Materials and methods

Participants from PPMI

We obtained the data from the PPMI database on February 27, 2022.[1] The PPMI is an international multi-center, ongoing, observational, longitudinal study that aims to identify biomarkers of PD progression and thus accelerate clinical trials and development of therapies (Marek et al., 2011). PD population included must be ≥30 years when diagnosed; have an asymmetric resting tremor or asymmetric bradykinesia or two of bradykinesia, resting tremor and rigidity within two years after diagnosis of PD (Hoehn-Yahr Stage I or II at Baseline; Lewis et al., 2005; Selikhova et al., 2009; Eggers et al., 2012); be untreated for PD especially not using drugs that might impact dopamine transporter imaging and CSF composition; have no dementia as determined by the investigator. Longitudinal review of the diagnosis conducted by researchers aims to prevent misdiagnosis. PD subjects should be excluded from follow-up if suspected as PSP or MSA. Pregnant, lactating women or planning pregnancy during the course are also not included. HC could be enrolled if they had no significant neurologic disorder, Montreal Cognitive Assessment (MoCA) > 26 and first-degree relatives without PD (2011). Both PD subjects and HC were assessed in clinical and CSF biomarkers study. In our research, participants were obliged to have baseline CSF NfL data and at least one more additional monitoring CSF NfL in later visit. As a result, CSF NfL concentration was measured at baseline (BL), 0.5, 1, 2, 3 and 4 years, and 1,166 data were collected altogether.

1 http://www.ppmi-info.org, clinicaltrials.gov: NCT01141023.

After the first CSF NfL collected, Longitudinal follow-up analyzed of other 4 CSF biomarkers and 6 clinical assessments (Supplementary Table 1).

Analyses of CSF biomarkers

Details about collection and analyses for CSF biomarkers can be read in the PPMI biologics manual (Kang et al., 2013). Roche NTK was used to quantify CSF NfL on a cobas e411 analyzer at Covance Greenfield laboratories (Translational Biomarker Solutions, Indiana; Bartl et al., 2021). Likewise, above-mentioned sandwich immunoassay was used to measure CSF total α-synuclein (α-syn) by Bio-Legend (San Diego, CA; Kang et al., 2016). CSF amyloid-β_{42} ($A\beta_{42}$), total tau (T-tau), and phosphorylated tau (P-tau) were measured by electrochemiluminescence (ECL) method on a completely automated cobas e601 analyzer (Shaw et al., 2018).

Clinical assessment measures

As reported elsewhere, various cognitive function evaluations have been performed for each clinical visit in the PPMI study (Kang et al., 2013). Since the system of cognitive disorder in PD is highly variable in its scope and intensity involving various filed, only using MoCA or MMSE as a screening instrument is not comprehensive enough (Caviness, 2007).We selected the following 6 cognitive function tests in different areas: MoCA for global cognition, Hopkins Verbal Learning Test for episodic memory, Wechsler Memory Scale third edition Letter-Number Sequencing test (LNS) for verbal working memory, Symbol Digit Modalities Test (SDMT) for processing speed-attention, Semantic Fluency Test for language, Benton Judgment of Line Orientation Score (BJLO) for visuospatial function (Kang et al., 2013; Schrag et al., 2017). Considering MoCA is a suitably accurate, brief instrument with adequate specificity and sensitivity of psychometric properties when screening degrees of cognition in PD (Dalrymple-Alford et al., 2010). In addition to evidence of detecting PD-MCI or PD-D (Hendershott et al., 2017), MoCA has been verified in several language superior to the standardized MMSE in several PD cohort studies (Chou et al., 2010). Cognitive status of study population was defined according to MDS level I guideline: MoCA score was <22 defined as PD-D, PD-MCI if MoCA score was 22–26, finally population scored MoCA >26 defined as PD patients with normal cognition (PD-NC; Hoops et al., 2009; Litvan et al., 2012; Chahine et al., 2016).

Statistical analyses

We used the R (version 4.1.0) to perform statistical analyses. Comparisons of demographic, clinical assessments and CSF biomarkers were made between HC, PD-NC and PD-MCI. Chi-square tests with continuity correction were used for categorical variables; Student's *t*-tests or Wilcoxon rank-sum tests were used for continuous variables. Shapiro–Wilk tests were used to check normal distribution and Bartlett tests of homogeneity were used for variances. Differences in characteristics between groups were analyzed using the one-way ANOVA or Kruskal-Wallis with Dunn *post hoc* tests. CSF NfL levels did not distribute normally ($p < 0.05$). To be proximity of normal distribution, we used log10-transformed method (Supplementary Figure 1). Then other needed indicators in our study were applied with same normalization method. We excluded 7 participants in reference to outliers which were defined as mean value ±3 SD to eliminate the influence of extreme values. Multiple linear regression model was used to examine the association of CSF NfL baseline concentration with data of other CSF biomarkers and cognitive assessments. Meanwhile, multiple linear mixed-effects (LME) model was used to calculate random slope and intercepts terms modeling CSF NfL longitudinal rate. Prediction of other cognitive measurements using baseline concentration or change rate of CSF NfL was also tested by the multiple LME model. We evaluated models with median of NfL baseline levels or longitudinal change rate. Low CSF Aβ and elevated tau (T-tau and P-tau) levels had been shown to predict progression of cognitive decline specifically in cognitive impairment and Alzheimer's disease (AD; Diniz et al., 2008). We selected the transforming formula (Shaw et al., 2019) which has been proved credible and used in previous studies (Kang et al., 2016; Irwin et al., 2020), to shift Elecsys values to equivalent values of AlzBio3 [$x = (\text{CSF } A\beta_{42} + 251.55)/3.74$] to reduce the bias caused by difference of CSF $A\beta_{42}$ levels between PPMI and AD cohorts (Stewart et al., 2019), and considered cut off value <250 pg/ml of corresponding AlzBio3 (Shaw et al., 2018) to distinguish amyloid positivity (A+) or amyloid negativity (A−). Kaplan–Meier curves were used to compare the cumulative probability risk of cognitive progression in the follow-up among different groups. Besides multivariate cox regression model was used to analysis the association between CSF NfL and the occurrence of conversion to the PD-D during the follow-up. We then added 'medical comorbidities' as a covariate in multiple linear regression, linear mixed effects and multivariate cox regression models to conduct sensitivity analyses.

The covariates of all regression and LME analyses were age, gender, educated years, Apolipoprotein E ε4 (*APOE ε4*) carrier status, and disease duration, and the significance threshold was set at $p < 0.05$. All *de novo* PD patients were classified by age (<56, 56–65, >65), gender, educated years (≥13, <13), *APOE ε4* carrier status to investigate the associations between CSF NfL and various cognitive indicators.

Results

Study participants

Included participants consisted of cognitively intact HC (n = 85), PD-NC (n = 116) and PD-MCI (*n* = 58; Table 1).

TABLE 1 Baseline clinical information and NfL concentration of participants in this study.

Characteristics	HC ($n = 85$)	PD-NC ($n = 116$)	PD-MCI ($n = 58$)	*P*
Age (y)	62.31 ± 10.14	59.00 ± 9.69	63.75 ± 9.72	**0.005**
Gender (Female/Male)	28/57	38/78	20/38	0.972
Education (y)	16.14 ± 2.55	16.29 ± 2.44	15.76 ± 2.68	0.308
APOE ε4 carriers (%)	22 (25.9)	33 ± 28.4	15 ± 25.9	0.712
$A\beta_{42}$ (pg/mL)	1019.89 ± 439.97	931.02 ± 368.54	909.22 ± 393.35	0.322
T-tau (pg/mL)	190.66 ± 67.39	169.48 ± 48.72	173.95 ± 60.35	0.113
P-tau (pg/mL)	16.82 ± 6.63	14.52 ± 4.67	15.02 ± 5.89	0.058
α-syn (pg/mL)	1649.29 ± 646.94	1500.39 ± 559.36	1580.20 ± 671.16	0.271
NfL (pg/mL)	97.94 ± 43.29	91.33 ± 46.07	119.89 ± 65.35	**0.009**
Montreal Cognitive Assessment	28.13 ± 1.08	28.26 ± 1.03	24.71 ± 1.39	**<0.001**
HVLT Total Recall	48.60 ± 10.71	47.84 ± 9.94	43.29 ± 9.39	**0.007**
HVLT Delayed Recall	47.45 ± 12.55	47.49 ± 10.05	41.67 ± 10.77	**0.002**
HVLT Retention	48.12 ± 12.68	48.35 ± 9.88	45.71 ± 13.58	0.122
HVLT Recognition Discrimination	47.14 ± 12.43	47.41 ± 10.39	42.31 ± 12.16	**0.011**
Benton Judgment of Line Orientation Score	12.19 ± 2.96	12.84 ± 2.50	11.97 ± 3.11	0.170
Letter Number Sequencing	11.76 ± 2.93	11.80 ± 2.47	10.81 ± 2.49	0.072
Semantic Fluency Test	51.25 ± 10.36	53.38 ± 9.14	47.07 ± 9.43	**<0.001**
Symbol Digit Modality Test	48.55 ± 10.86	46.18 ± 8.40	44.38 ± 9.48	0.079

NfL, Neurofilament light; HC, Healthy controls; PD, Parkinson's disease; PD-NC, PD patients with normal cognition; PD-MCI, PD patients with mild cognitive impairment; APOE, Apolipoprotein E; $A\beta_{42}$, Amyloid-β_{42}; T-tau, Total tau; P-tau, Phosphorylated tau; α-syn, α-synuclein; HVLT, Hopkins Verbal Learning Test; values are mean ± standard deviation (SD), or n or n (% of the group).

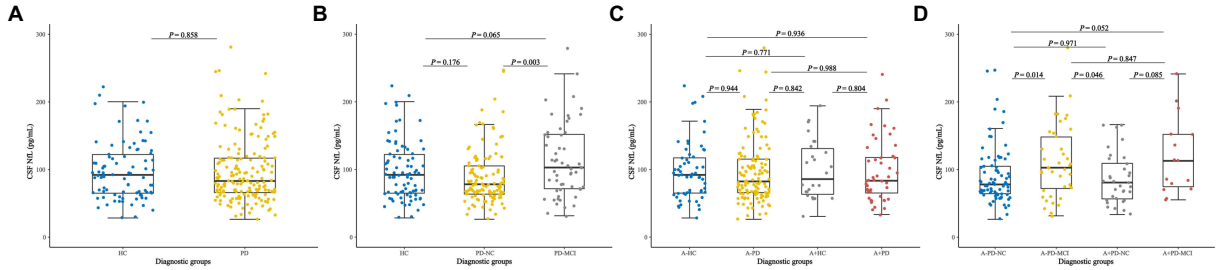

FIGURE 1
Baseline CSF NfL concentration of **(A)** Healthy controls and patients with *de novo* PD. **(B)** HC and *de novo* PD patients with different cognitive status. **(C)** HC and *de novo* PD patients in different amyloid status. **(D)** HC and *de novo* PD patients with different cognitive status in different amyloid status. CSF, cerebrospinal fluid; NfL, neurofilament light; HC, Healthy controls; PD, Parkinson's disease; PD-NC, PD patients with normal cognition; PD-MCI, PD patients with mild cognitive impairment; A, Amyloid.

There were no significant differences in sex, educated years and *APOE ε4* allele status between HC, PD-NC and PD-MCI, which was closely similar to the previous studies of PPMI cohort (Kang et al., 2016). As expected, cognitive performance differed in three populations (MoCA, $p < 0.001$; HVLT Total Recall, $p = 0.007$; HVLT Delayed Recall, $p = 0.002$; HVLT Recognition Discrimination, $p = 0.011$; Semantic Fluency Test, $p < 0.001$). Age and CSF NfL levels were significantly different between three groups, meanwhile age positively correlated with CSF NfL in each group (HC: $\beta = 2.2983$, $p < 0.001$; PD-NC: $\beta = 2.3492$, $p < 0.001$; PD-MCI: $\beta = 3.5410$, $p < 0.001$; Supplementary Figure 2) which was also consistent with reported study (Lerche et al., 2020; Fagan et al., 2021).

Cross-sectional analyses of CSF NfL baseline concentration

No significant differences of baseline CSF NfL levels were found between *de novo* PD patients and HC (Figure 1A). NfL concentration was higher in PD-MCI (119.89 pg/ml) than PD-NC (91.33 pg/ml; $p = 0.003$; Figure 1B). Considering the acknowledged cut-point in AD, we cross-sectionally investigated HC, PD-NC and

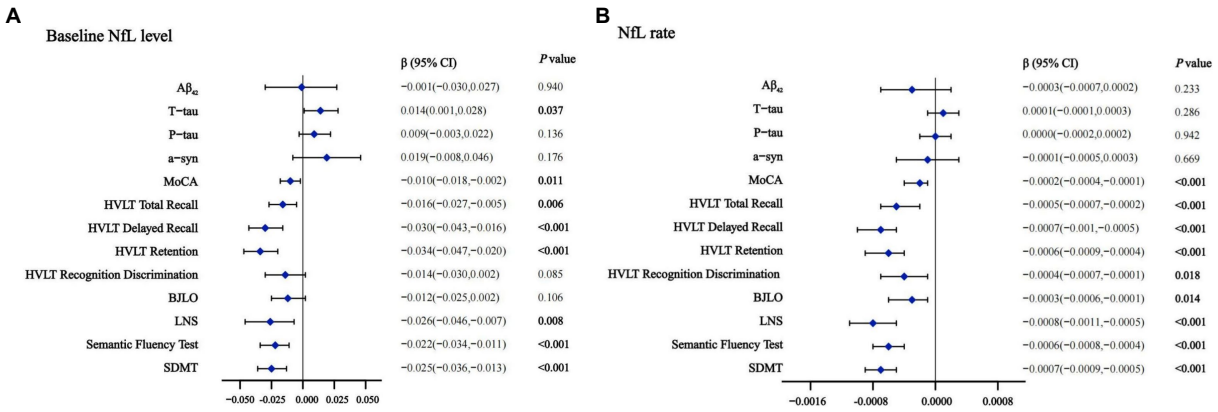

FIGURE 2
Effects of baseline NfL **(A)** and NfL accumulation rate **(B)** on CSF biomarkers and cognition measurements in linear mixed-effects analysis among PD participants. Adjusted for age, gender, educated years, *APOE ε4* carrier status and duration. CSF, cerebrospinal fluid; NfL, neurofilament light; PD, Parkinson's disease; $A\beta_{42}$, Amyloid-β_{42}; T-tau, Total tau; P-tau, Phosphorylated tau; α-syn, α-synuclein; MoCA, Montreal Cognitive Assessment; HVLT, Hopkins Verbal Learning Test; BJLO, Benton Judgment of Line Orientation Score; LNS, Letter Number Sequencing; SDMT, Symbol Digit Modality Test.

PD-MCI at baseline with presumed amyloid-positivity (Yarnall et al., 2014). Relative of low CSF $A\beta_{42}$ in pathology of amyloidosis (A+) in PD group (28.16%) and HC group (30.59%) had no differences in CSF NfL baseline concentration between A + and A-groups (Figure 1C). However, CSF NfL levels were significantly higher in the A-PD-MCI (119.90 pg/ml) compared to A-PD-NC (90.46 pg/ml; $p = 0.014$). We also found difference in NfL concentration between A-PD-MCI (119.90 pg/ml) and A + PD-NC (93.44 pg/ml; $p = 0.046$; Figure 1D).

After considered and adjusted age, gender, educated years, *APOE ε4* carrying status, and PD duration, we found the significant correlations between CSF NfL levels and cognition severity (MoCA, $\beta = -0.031$, $p = 0.045$) in *de novo* PD patients.

Prediction and CSF NfL baseline concentration in *de novo* PD patients

To exploratorily analyze the prediction using CSF NfL in early PD cognitive decline according to reported discovery (Lerche et al., 2020; Oosterveld et al., 2020; Aamodt et al., 2021), we hypothesize that upregulation of CSF NfL will associate with cognitive progression in several domains. In PD population, higher CSF NfL baseline concentration predicted faster decline in global cognition (MOCA, $\beta = -0.010$, $p = 0.011$), episodic memory (HVLT Total Recall, $\beta = -0.016$, $p = 0.006$; HVLT Delayed Recall, $\beta = -0.030$, $p < 0.001$; HVLT Retention, $\beta = -0.034$, $p < 0.001$), verbal working memory (LNS, $\beta = -0.026$, $p = 0.008$), language (Semantic Fluency Test, $\beta = -0.022$, $p < 0.001$) and processing speed-attention (SDMT, $\beta = -0.025$, $p < 0.001$; Figure 2A). Compared with the low NfL Concentration below the median, higher CSF NfL Concentration above the median can predict decline in most of investigated cognitive domains except visuospatial functioning (Supplementary Table 3).

Results of Kaplan–Meier analysis displays a remarkable decline of MoCA score, and log-rank test has statistical significance ($p < 0.001$; Figure 3A). In addition, 34 of 174 PD patients (16.28%) had transition to PD-D during a mean follow-up period of 6.66 ± 2.54 years. Cox proportional-hazards models were used to estimate the conversion risk from PD patients with non-dementia to PD-D (Supplementary Table 4). PD individuals with higher CSF NfL levels above the median added an increased risk of conversion to PD-D compared with the subjects in low CSF NfL concentrations below the median (HR = 2.82, 95% CI: 1.11–7.20, $p = 0.030$).

CSF NfL baseline concentration and other CSF biomarkers

Cross-sectionally Significant associations were observed between baseline NfL and other CSF biomarkers both in the HC (T-tau, $\beta = 0.484$, $p < 0.001$; P-tau, $\beta = 0.540$, $p < 0.001$; α-syn, $\beta = 0.506$, $p < 0.001$) and PD patients (T-tau, $\beta = 0.247$, $p < 0.001$; P-tau, $\beta = 0.256$, $p < 0.001$; α-syn, $\beta = 0.192$, $p = 0.013$; Aβ42, $\beta = 0.182$, $p = 0.027$). In PD-NC and PD-MCI group, CSF NfL levels were also significantly associated with CSF T-tau and P-tau too (Supplementary Table 2). Baseline NfL levels also predicted the longitudinal increase of CSF T-tau ($\beta = 0.014$, $p = 0.037$) by the multiple LME models (Figure 2A). Additionally, the associations were pronounced between higher baseline NfL concentration above the median (T-tau, $\beta = 0.007$, $p = 0.013$; P-tau, $\beta = 0.005$, $p = 0.037$; Supplementary Table 3).

Longitudinal change in CSF NfL

The Longitudinal profile of CSF NfL was further examined from baseline in PD population and HC by using LME models.

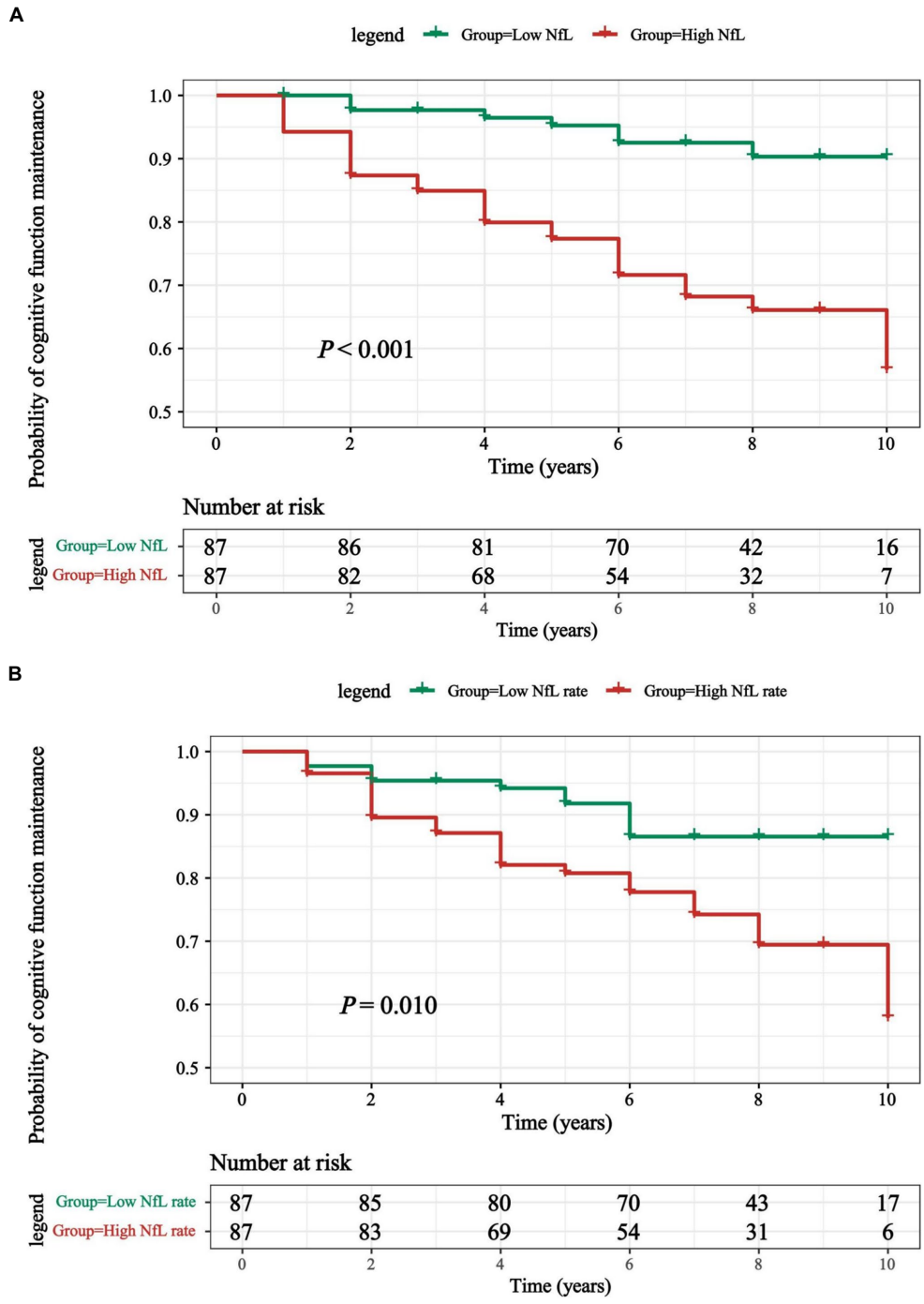

FIGURE 3
(A) Kaplan-Meier curves were used to compare the cumulative probability risk of cognitive progression in the follow-up among participants which were divided into 2 groups by the median of CSF NfL levels. **(B)** Kaplan-Meier curves were used to compare the cumulative probability risk of cognitive progression in the follow-up among participants which were divided into 2 groups by the median of CSF NfL change rate. Kaplan–Meier curve for conversion from *de novo* PD patients converted to PD-D during 9-years follow-up. PD, Parkinson's disease; PD-D, Parkinson's disease with dementia; NfL, neurofilament light.

The NfL change rate was slightly above zero in *de novo* PD patients (0.60 pg/ml/a, Figure 4A). CSF NfL concentration increased significantly with higher rate in PD-MCI (5.67 pg/ml/a) than PD-NC (−1.94 pg/ml per year; $p = 0.034$; Figure 4B). There were no significant differences of CSF NfL rate between *de novo* PD patients and HC in different amyloid status (Figure 4C). Finally, A+ PD-MCI (16.02 pg/ml per year) increased faster with highest NfL growth than both A+ PD-NC (−0.86 pg/ml per year;

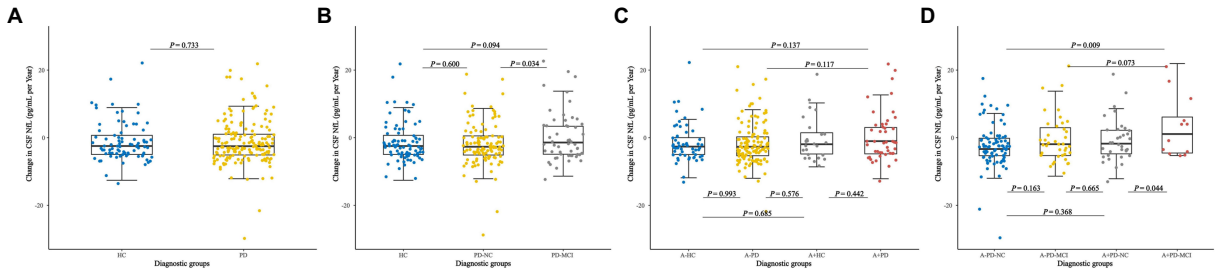

FIGURE 4
Longitudinal changes in CSF NfL of **(A)** Healthy controls and patients with *de novo* PD. **(B)** HC and *de novo* PD patients with different cognitive status. **(C)** HC and *de novo* PD patients in different amyloid status. **(D)** HC and *de novo* PD patients with different cognitive status in different amyloid status. CSF, cerebrospinal fluid; NfL, neurofilament light; HC, Healthy controls; PD, Parkinson's disease; PD-NC, PD patients with normal cognition; PD-MCI, PD patients with mild cognitive impairment; A, Amyloid.

$p = 0.044$) and A-PD-NC (−2.39 pg/ml per year; $p = 0.009$; Figure 4D).

Prediction and CSF NfL change rate in *de novo* PD patients

Analyses of cognitive decline using CSF NfL change rate demonstrated that 4 years longitudinally increased CSF NfL concentration was correlated with cognitive performance significantly. We observed higher increasing CSF NfL rate predicted faster worsening in global cognition (MOCA, $\beta = -0.0002$, $p < 0.001$) in episodic memory (HVLT Total Recall, $\beta = -0.0005$, $p < 0.001$; HVLT Delayed Recall, $\beta = -0.0007$, $p < 0.001$; HVLT Retention, $\beta = -0.0006$, $p < 0.001$; HVLT Recognition Discrimination, $\beta = -0.0004$, $p = 0.018$), visuospatial functioning (BJLO, $\beta = -0.0003$, $p = 0.014$), verbal working memory (LNS, $\beta = -0.0008$, $p < 0.001$), language (Semantic Fluency Test, $\beta = -0.0006$, $p < 0.001$), and processing speed-attention (SDMT, $\beta = -0.0007$, $p < 0.001$; Figure 2B). Compared with the low NfL rate below the median higher change rate of NfL above the median can predict a decline in most of investigated cognitive domains except visuospatial functioning. No significant associations were observed between longitudinal CSF NfL and other CSF biomarkers (Supplementary Table 3).

Although no correlation between CSF NfL change rate and the risk of PD-D transformation according to Cox proportional-hazards models was found (Supplementary Table 4), the results of Kaplan–Meier analysis and log rank test demonstrated that differences existed comparing two groups divided by median of NfL change rates ($p = 0.010$; Figure 3B).

Subgroup analyses

In *de novo* PD patients aged >65, male, ill-educated (<13 years) and without carrying *APOE ε4*, we found the predictive effects of CSF NfL baseline concentration and longitudinal rate on cognitive decline appeared to be more remarkable and comprehensive. (Supplementary Tables 5–8). In PD-NC, NfL baseline concentration and longitudinal rate predicted cognitive decline in episodic memory and verbal working memory. In PD-MCI, NfL baseline concentration and longitudinal rate predicted cognitive decline in episodic memory, language and processing speed-attention. (Supplementary Table 9). In A-PD group, predictive effects of NfL baseline levels and longitudinal rate were observed not only on cognitive decline in episodic memory, language and processing speed-attention but also on increase of CSF T-tau and P-tau. In A + PD group, the NfL baseline levels and longitudinal rate showed significant predictive effects on cognitive decline in global cognition, verbal working memory, language and processing speed-attention (Supplementary Table 10).

Sensitivity analyses

After adjusting for medical comorbidities, the results were consistent with the previous fingings (Supplementary Tables 11–13), consolidating the predictive value of CSF NFL on cognition.

Discussion

This study involves a well-designed longitudinal cohort of *de novo* PD patients to comprehensively investigate the predictive value of cerebrospinal fluid NfL linked to various indicators of cognitive decline. The analyses demonstrated the following: (1) PD-MCI was significantly higher than PD-NC in terms of CSF NfL baseline concentration and longitudinal change rate; (2) CSF NfL predicted the longitudinal cognitive progression of *de novo* PD patients and successfully marked conversion to cognitive impairment beforehand; and (3) The predictive effects of CSF NfL baseline concentration and the cognitive decline change rate among *de novo* PD male patients aged >65 who were ill-educated and without *APOE ε4* carrier status seemed to be more obvious.

We found cross-sectional correlation between CSF NfL concentration and global cognition in PD patients, which fit a reported study (Lerche et al., 2020). In the PD group, we employed LME models to predict disease time frame and cognitive progression. The results showed that the CSF NfL change rate predicted greater decline in six investigated domains over an average of 6.66 years follow-up. Moreover, baseline NfL concentration can also predict these cognitive domains except for visuospatial functioning. Differing from a previous study that reported an increase in CSF NfL levels with cognitive dysfunction without marking conversion to cognitive impairment (Lerche et al., 2020), a higher CSF NfL concentration above the median added risk of conversion to the PD-D in our study. However, this outcome was consistent with another cohort study (Bäckström et al., 2015), and provides the possibility of CSF NfL dictating predictive values for general early cognitive decline in PD. NfL levels might be impacted by medical comorbidities that are common among elders, complicating its utility as a biomarker. Although multiple sclerosis, neurodegenerative dementia, stroke, amyotrophic lateral sclerosis (Khalil et al., 2018), orthostatic hypotension (Park et al., 2021), hearing disorder (Park et al., 2016; Han et al., 2018), depression and anxiety disorders (Tauil et al., 2021), diabetes (Thota et al., 2022), psoriasis (Nowowiejska et al., 2022), transient ischemic attack (TIA; De Marchis et al., 2018) and sleep disorder (Jennum et al., 2017; Lysen et al., 2020; Targa et al., 2021) might impact NfL levels, we still found consistent results after adjusting for medical comorbidities. CSF NfL can purposefully play the role of a future candidate for CSF biomarkers when cognitive disorder risk is estimated among patients with PD (Hoops et al., 2009).

Substantial existing biological heterogeneity and pathological evidence underlie the clinical features (cognitive impairment) of Parkinson's disease (Chen-Plotkin et al., 2018). The etiology of PD cognitive disorder is complex with several pathological mechanisms (Aarsland et al., 2017). There are a few cohort studies that systematically investigated longitudinal changes in the CSF biomarkers of PD patients. A previous study confirmed the correlation between CSF NfL concentration, CSF $A\beta_{42}$, and T-tau levels in PD (Aamodt et al., 2021). We further examined the relationship between CSF NfL and AD-related CSF biomarkers. CSF T-tau is presumed to be correlated with cognitive impairment in PD (Ritchie et al., 2017; Schrag et al., 2017). In our research, CSF T-tau and P-tau levels were cross-sectionally correlated with CSF NfL. We found that NfL concentration can predict the increase of CSF T-tau. Results from several autopsy studies demonstrated that limbic and neocortical Lewy body depositions were major determinants of cognitive decline in PD (Braak et al., 2005; Aarsland et al., 2005a). Nevertheless, other studies favor the cortical Aβ deposition theory (Ballard et al., 2006; Sabbagh et al., 2009; Alves et al., 2014). A recent review showed that the coexistence of amyloid and tau pathology can facilitate the process of α-synuclein aggregation, which results in an increase of insoluble fibrils representing the core of intraneuronal Lewy bodies and Lewy neurites. This process will boost a microglial reaction through inflammatory mediators, which subsequently attract peripheral immune cells within the CNS (Parnetti et al., 2019). Parallel to these pathological changes, more CSF Nfl is released.

Correlations between CSF NfL, cognitive decline, and AD-related CSF biomarkers in this study showed that these CSF biomarkers may partially share underlying processes in PD. Although anomalous CSF $A\beta_{42}$ and tau were only detected in 6.5% of PD patients at the first diagnosis, autopsy exhibited the pathological change of AD in 60 to 80% of PD patients (Marek et al., 2018). Considered that AD type changes may contribute to PD-D, CSF Aβ42 has been shown to reliably predict the risk of cognitive impairment in PD patients (Parnetti et al., 2019), especially in verbal memory, processing speed, and visual memory (Leverenz et al., 2011; Alves et al., 2014; Yarnall et al., 2014). Therefore, A+ cut off value recognized in AD were selected to reflect the AD-related CSF profiles of enrolled patients (Shaw et al., 2018). In reference to the reputable AD cut point, approximately 1/3 of PD subjects exhibited low CSF $A\beta_{42}$ pathologically, which indicates a positivity status of amyloid. These findings are consistent with two reported studies and one autopsy involving end-stage PD patients (Irwin et al., 2012, 2020; Ma et al., 2021). Moreover, AD patients with amyloidosis+ showed a significant association between reduced gray matter density in AD vulnerable regions and increased NfL concentrations in CSF (Kang et al., 2021). In our research, the significantly higher increase rate of NfL in A + PD-MCI, as compared to A-PD-NC was evidence that supports the assertion that dynamic CSF NfL in *de novo* PD may be consistent with AD pathological process (Olsson et al., 2019). It is also possible that amyloid deposition alone, independent of tau pathology, can hasten the development of PD cognitive impairment (Lin and Wu, 2015; Oosterveld et al., 2020). NfL was discovered in the hippocampus of PD-D patients through autopsy, but not discovered in PD-NC (Arai et al., 1992). Another explanation is that NfL leading to PD cognitive disorder is independent of Aβ pathology theory (Kovacs et al., 2017). Further research should be performed to clarify related biological and pathological mechanisms of cognitive disorder in early-stage PD.

Furthermore, CSF NfL concentration in *de novo* PD was reported to be positively correlated with age, which is consistent with studies (Bridel et al., 2019; Lerche et al., 2020; Fagan et al., 2021). There were differences in the predictive effects of NfL baseline levels/change rate on cognitive decline in PD through subgroup analyses that considered age, gender, educated years, and *APOE ε4* carrier status, respectively. Further research is required to study the interactions between these factors and CSF NfL with cognitive decline in *de novo* PD patients.

The following are the strengths of this study: (1) Enrolled PD population was newly diagnosed within a 7.4-month period as compared to more than 2 years in other studies (Lerche et al., 2020; Oosterveld et al., 2020); (2) Cross-sectional and longitudinal

study designs were used; and (3) More sophisticated cognitive assessments were performed overall, rendering the prediction for conversion to dementia in PD more reasonable and reliable.

However, a few limitations of our study should be noted. First, missing values of follow-up in this longitudinal cohort inevitably influenced the reliability of our results. Second, whether there is an interaction or intermediation between NfL and Tau on the cognitive progress of PD patients remains unclear due to lack of suitable cut-off point to classify CSF tau. Third, we referenced medical history as a confounding factor and conducted sensitivity analyses, but the medication history was not enough to talk about the drug affect. Besides, quantity of CSF $A\beta_{42}$ in our research was too little to back the transforming formula of CSF $A\beta_{42}$ levels up with Gaussian Mixture Modelling statistics. In addition, all analyses are based on CSF protein measurements, which are not adequately accurate as compared to PET imaging data for cerebral neurodegeneration. Last but not the least, sampling of CSF NfL is an invasive procedure, and may not be obtained from all patients.

Collectively, CSF NfL can be considered as a valuable biomarker to monitor the severity of cognitive progression in *de novo* PD. Baseline levels and the change rate of CSF NfL can predict future cognitive decline in many domains. In addition, higher CSF NfL concentration tends to represent a higher risk of conversion to PD-D in *de novo* PD patients. Dynamic changes of NfL measurements may assist in identifying this risk of rapid cognitive decline for subsequent modification of therapy in future clinical trials.

Data availability statement

The original contributions presented in the study are included in the article/Supplementary materials, further inquiries can be directed to the corresponding author.

Ethics statement

The studies involving human participants were reviewed and approved by Parkinson's Progression Markers Initiative. The patients/participants provided their written informed consent to participate in this study.

Author contributions

Z-HS: design, execution, analysis, writing, and review and critique. L-ZM: design, execution, analysis, and review and critique. J-YL: design, analysis, and review and critique. Y-NO: analysis, review and critique. BZ: analysis, review and critique. Y-HM: analysis, review and critique. LT: design, analysis, review and critique, and financial support. All authors contributed to the article and approved the submitted version.

Funding

This study was supported by grants from the National Natural Science Foundation of China (81971032, 82001133, and 81901121).

Acknowledgments

Parkinson's Progression Markers Initiative (a public–private partnership) is funded by the Michael J Fox Foundation for Parkinson's Research and funding partners, including AbbVie, Allergan, Avid Radiopharmaceuticals, Biogen, Bio-Legend, Bristol-Myers Squibb, Celgene, Denali, GE Health care, Genentech, GlaxoSmithKline, Lilly, Lundbeck, Merck, Meso-Scale Discovery, Pfizer, Piramal, Prevail Therapeutics, Roche, Sanofi Genzyme, Servier, Takeda, Teva, UCB, Verily, Voyager Therapeutics, and Golub Capital.

Conflict of interest

The authors declare that the research was conducted in the absence of any commercial or financial relationships that could be construed as a potential conflict of interest.

Publisher's note

Supplementary material

The Supplementary material for this article can be found online at: https://www.frontiersin.org/articles/10.3389/fnagi.2022.1061096/full#supplementary-material

References

Aamodt, W. W., Waligorska, T., Shen, J., Tropea, T. F., Siderowf, A., Weintraub, D., et al. (2021). Neurofilament light chain as a biomarker for cognitive decline in Parkinson disease. *Mov. Disord.* 36, 2945–2950. doi: 10.1002/mds.28779

Aarsland, D., Creese, B., Politis, M., Chaudhuri, K. R., Ffytche, D. H., Weintraub, D., et al. (2017). Cognitive decline in Parkinson disease. *Nat. Rev. Neurol.* 13, 217–231. doi: 10.1038/nrneurol.2017.27

Aarsland, D., Perry, R., Brown, A., Larsen, J. P., and Ballard, C. (2005a). Neuropathology of dementia in Parkinson's disease: a prospective, community-based study. *Ann. Neurol.* 58, 773–776. doi: 10.1002/ana.20635

Aarsland, D., Zaccai, J., and Brayne, C. (2005b). A systematic review of prevalence studies of dementia in Parkinson's disease. *Mov. Disord.* 20, 1255–1263. doi: 10.1002/mds.20527

Alves, G., Lange, J., Blennow, K., Zetterberg, H., Andreasson, U., Førland, M. G., et al. (2014). CSF Aβ42 predicts early-onset dementia in Parkinson disease. *Neurology* 82, 1784–1790. doi: 10.1212/wnl.0000000000000425

Arai, H., Schmidt, M. L., Lee, V. M., Hurtig, H. I., Greenberg, B. D., Adler, C. H., et al. (1992). Epitope analysis of senile plaque components in the hippocampus of patients with Parkinson's disease. *Neurology* 42, 1315–1322. doi: 10.1212/wnl.42.7.1315

Bäckström, D. C., Eriksson Domellöf, M., Linder, J., Olsson, B., Öhrfelt, A., Trupp, M., et al. (2015). Cerebrospinal fluid patterns and the risk of future dementia in early, incident Parkinson disease. *JAMA Neurol.* 72, 1175–1182. doi: 10.1001/jamaneurol.2015.1449

Ballard, C., Ziabreva, I., Perry, R., Larsen, J. P., O'Brien, J., McKeith, I., et al. (2006). Differences in neuropathologic characteristics across the Lewy body dementia spectrum. *Neurology* 67, 1931–1934. doi: 10.1212/01.wnl.0000249130.63615.cc

Bartl, M., Dakna, M., Galasko, D., Hutten, S. J., Foroud, T., Quan, M., et al. (2021). Biomarkers of neurodegeneration and glial activation validated in Alzheimer's disease assessed in longitudinal cerebrospinal fluid samples of Parkinson's disease. *PLoS One* 16:e0257372. doi: 10.1371/journal.pone.0257372

Braak, H., Rüb, U., Jansen Steur, E. N., Del Tredici, K., and de Vos, R. A. (2005). Cognitive status correlates with neuropathologic stage in Parkinson disease. *Neurology* 64, 1404–1410. doi: 10.1212/01.Wnl.0000158422.41380.82

Bridel, C., van Wieringen, W. N., Zetterberg, H., Tijms, B. M., Teunissen, C. E., Alvarez-Cermeño, J. C., et al. (2019). Diagnostic value of cerebrospinal fluid neurofilament light protein in neurology: a systematic review and meta-analysis. *JAMA Neurol.* 76, 1035–1048. doi: 10.1001/jamaneurol.2019.1534

Caviness, J. N. (2007). Parkinsonism & related disorders. Myoclonus. *Parkinsonism Relat. Disord.* 13, S375–S384. doi: 10.1016/s1353-8020(08)70033-6

Chahine, L. M., Xie, S. X., Simuni, T., Tran, B., Postuma, R., Amara, A., et al. (2016). Longitudinal changes in cognition in early Parkinson's disease patients with REM sleep behavior disorder. *Parkinsonism Relat. Disord.* 27, 102–106. doi: 10.1016/j.parkreldis.2016.03.006

Chen-Plotkin, A. S., Albin, R., Alcalay, R., Babcock, D., Bajaj, V., Bowman, D., et al. (2018). Finding useful biomarkers for Parkinson's disease. *Sci. Transl. Med.* 10:eaam6003. doi: 10.1126/scitranslmed.aam6003

Chou, K. L., Amick, M. M., Brandt, J., Camicioli, R., Frei, K., Gitelman, D., et al. (2010). A recommended scale for cognitive screening in clinical trials of Parkinson's disease. *Mov. Disord.* 25, 2501–2507. doi: 10.1002/mds.23362

Dalrymple-Alford, J. C., MacAskill, M. R., Nakas, C. T., Livingston, L., Graham, C., Crucian, G. P., et al. (2010). The MoCA: well-suited screen for cognitive impairment in Parkinson disease. *Neurology* 75, 1717–1725. doi: 10.1212/WNL.0b013e3181fc29c9

De Marchis, G. M., Katan, M., Barro, C., Fladt, J., Traenka, C., Seiffge, D. J., et al. (2018). Serum neurofilament light chain in patients with acute cerebrovascular events. *Eur. J. Neurol.* 25, 562–568. doi: 10.1111/ene.13554

Diniz, B. S., Pinto Júnior, J. A., and Forlenza, O. V. (2008). Do CSF total tau, phosphorylated tau, and beta-amyloid 42 help to predict progression of mild cognitive impairment to Alzheimer's disease? A systematic review and meta-analysis of the literature. *World J. Biol. Psychiatry* 9, 172–182. doi: 10.1080/15622970701535502

Eggers, C., Pedrosa, D. J., Kahraman, D., Maier, F., Lewis, C. J., Fink, G. R., et al. (2012). Parkinson subtypes progress differently in clinical course and imaging pattern. *PLoS One* 7:e46813. doi: 10.1371/journal.pone.0046813

Fagan, A. M., Henson, R. L., Li, Y., Boerwinkle, A. H., Xiong, C., Bateman, R. J., et al. (2021). Comparison of CSF biomarkers in down syndrome and autosomal dominant Alzheimer's disease: a cross-sectional study. *Lancet Neurol.* 20, 615–626. doi: 10.1016/s1474-4422(21)00139-3

Findley, L., Aujla, M., Bain, P. G., Baker, M., Beech, C., Bowman, C., et al. (2003). Direct economic impact of Parkinson's disease: a research survey in the United Kingdom. *Mov. Disord.* 18, 1139–1145. doi: 10.1002/mds.10507

Hall, S., Öhrfelt, A., Constantinescu, R., Andreasson, U., Surova, Y., Bostrom, F., et al. (2012). Accuracy of a panel of 5 cerebrospinal fluid biomarkers in the differential diagnosis of patients with dementia and/or parkinsonian disorders. *Arch. Neurol.* 69, 1445–1452. doi: 10.1001/archneurol.2012.1654

Hall, S., Surova, Y., Öhrfelt, A., Zetterberg, H., Lindqvist, D., and Hansson, O. (2015). CSF biomarkers and clinical progression of Parkinson disease. *Neurology* 84, 57–63. doi: 10.1212/wnl.0000000000001098

Han, J. J., Lee, H. S., and Park, M. H. (2018). Neuroplastic change of cytoskeleton in inferior colliculus after auditory deafferentation. *Hear. Res.* 367, 207–212. doi: 10.1016/j.heares.2018.06.010

Hendershott, T. R., Zhu, D., Llanes, S., and Poston, K. L. (2017). Domain-specific accuracy of the Montreal cognitive assessment subsections in Parkinson's disease. *Parkinsonism Relat. Disord.* 38, 31–34. doi: 10.1016/j.parkreldis.2017.02.008

Hoops, S., Nazem, S., Siderowf, A. D., Duda, J. E., Xie, S. X., Stern, M. B., et al. (2009). Validity of the MoCA and MMSE in the detection of MCI and dementia in Parkinson disease. *Neurology* 73, 1738–1745. doi: 10.1212/WNL.0b013e3181c34b47

Irwin, D. J., Fedler, J., Coffey, C. S., Caspell-Garcia, C., Kang, J. H., Simuni, T., et al. (2020). Evolution of Alzheimer's disease cerebrospinal fluid biomarkers in early Parkinson's disease. *Ann. Neurol.* 88, 574–587. doi: 10.1002/ana.25811

Irwin, D. J., White, M. T., Toledo, J. B., Xie, S. X., Robinson, J. L., Van Deerlin, V., et al. (2012). Neuropathologic substrates of Parkinson disease dementia. *Ann. Neurol.* 72, 587–598. doi: 10.1002/ana.23659

Jennum, P. J., Østergaard Pedersen, L., Czarna Bahl, J. M., Modvig, S., Fog, K., Holm, A., et al. (2017). Cerebrospinal fluid biomarkers of neurodegeneration are decreased or normal in narcolepsy. *Sleep* 40:zsw006. doi: 10.1093/sleep/zsw006

Kalia, L. V., and Lang, A. E. (2015). Parkinson's disease. *Lancet* 386, 896–912. doi: 10.1016/s0140-6736(14)61393-3

Kang, M. S., Aliaga, A. A., Shin, M., Mathotaarachchi, S., Benedet, A. L., Pascoal, T. A., et al. (2021). Amyloid-beta modulates the association between neurofilament light chain and brain atrophy in Alzheimer's disease. *Mol. Psychiatry* 26, 5989–6001. doi: 10.1038/s41380-020-0818-1

Kang, J. H., Irwin, D. J., Chen-Plotkin, A. S., Siderowf, A., Caspell, C., Coffey, C. S., et al. (2013). Association of cerebrospinal fluid β-amyloid 1-42, T-tau, P-tau181, and α-synuclein levels with clinical features of drug-naive patients with early Parkinson disease. *JAMA Neurol.* 70, 1277–1287. doi: 10.1001/jamaneurol.2013.3861

Kang, J. H., Mollenhauer, B., Coffey, C. S., Toledo, J. B., Weintraub, D., Galasko, D. R., et al. (2016). CSF biomarkers associated with disease heterogeneity in early Parkinson's disease: the Parkinson's progression markers initiative study. *Acta Neuropathol.* 131, 935–949. doi: 10.1007/s00401-016-1552-2

Khalil, M., Teunissen, C. E., Otto, M., Piehl, F., Sormani, M. P., Gattringer, T., et al. (2018). Neurofilaments as biomarkers in neurological disorders. *Nat. Rev. Neurol.* 14, 577–589. doi: 10.1038/s41582-018-0058-z

Kovacs, G. G., Andreasson, U., Liman, V., Regelsberger, G., Lutz, M. I., Danics, K., et al. (2017). Plasma and cerebrospinal fluid tau and neurofilament concentrations in rapidly progressive neurological syndromes: a neuropathology-based cohort. *Eur. J. Neurol.* 24, 1326–1e77. doi: 10.1111/ene.13389

Leaver, K., and Poston, K. L. (2015). Do CSF biomarkers predict progression to cognitive impairment in Parkinson's disease patients? A systematic review. *Neuropsychol. Rev.* 25, 411–423. doi: 10.1007/s11065-015-9307-8

Lerche, S., Wurster, I., Röben, B., Zimmermann, M., Machetanz, G., Wiethoff, S., et al. (2020). CSF NFL in a longitudinally assessed PD cohort: age effects and cognitive trajectories. *Mov. Disord.* 35, 1138–1144. doi: 10.1002/mds.28056

Leverenz, J. B., Watson, G. S., Shofer, J., Zabetian, C. P., Zhang, J., and Montine, T. J. (2011). Cerebrospinal fluid biomarkers and cognitive performance in non-demented patients with Parkinson's disease. *Parkinsonism Relat. Disord.* 17, 61–64. doi: 10.1016/j.parkreldis.2010.10.003

Lewis, S. J., Foltynie, T., Blackwell, A. D., Robbins, T. W., Owen, A. M., and Barker, R. A. (2005). Heterogeneity of Parkinson's disease in the early clinical stages using a data driven approach. *J. Neurol. Neurosurg. Psychiatry* 76, 343–348. doi: 10.1136/jnnp.2003.033530

Lin, C. H., and Wu, R. M. (2015). Biomarkers of cognitive decline in Parkinson's disease. *Parkinsonism Relat. Disord.* 21, 431–443. doi: 10.1016/j.parkreldis.2015.02.010

Litvan, I., Goldman, J. G., Tröster, A. I., Schmand, B. A., Weintraub, D., Petersen, R. C., et al. (2012). Diagnostic criteria for mild cognitive impairment in Parkinson's disease: Movement Disorder Society Task Force guidelines. *Mov. Disord.* 27, 349–356. doi: 10.1002/mds.24893

Lysen, T. S., Ikram, M. A., Ghanbari, M., and Luik, A. I. (2020). Sleep, 24-h activity rhythms, and plasma markers of neurodegenerative disease. *Sci. Rep.* 10:20691. doi: 10.1038/s41598-020-77830-4

Ma, L. Z., Zhang, C., Wang, H., Ma, Y. H., Shen, X. N., Wang, J., et al. (2021). Serum neurofilament dynamics predicts cognitive progression in de novo Parkinson's disease. *J. Parkinsons Dis.* 11, 1117–1127. doi: 10.3233/jpd-212535

Marek, K., Chowdhury, S., Siderowf, A., Lasch, S., Coffey, C. S., Caspell-Garcia, C., et al. (2018). The Parkinson's progression markers initiative (PPMI) – establishing a PD biomarker cohort. *Ann. Clin. Transl. Neurol.* 5, 1460–1477. doi: 10.1002/acn3.644

Marek, K., Jennings, D., Lasch, S., Siderowf, A., Tanner, C., Simuni, T., et al. (2011). The Parkinson progression marker initiative (PPMI). *Prog. Neurobiol.* 95, 629–635. doi: 10.1016/j.pneurobio.2011.09.005

Mehta, S. H., and Adler, C. H. (2016). Advances in biomarker research in Parkinson's disease. *Curr. Neurol. Neurosci. Rep.* 16:7. doi: 10.1007/s11910-015-0607-4

Mollenhauer, B., Rochester, L., Chen-Plotkin, A., and Brooks, D. (2014). What can biomarkers tell us about cognition in Parkinson's disease? *Mov. Disord.* 29, 622–633. doi: 10.1002/mds.25846

Ng, A. S. L., Tan, Y. J., Yong, A. C. W., Saffari, S. E., Lu, Z., Ng, E. Y., et al. (2020). Utility of plasma Neurofilament light as a diagnostic and prognostic biomarker of the postural instability gait disorder motor subtype in early Parkinson's disease. *Mol. Neurodegener.* 15:33. doi: 10.1186/s13024-020-00385-5

Nowowiejska, J., Baran, A., Hermanowicz, J. M., Sieklucka, B., Krahel, J. A., Kiluk, P., et al. (2022). Fatty acid-binding protein 7 (FABP-7), glutamic acid and Neurofilament Light Chain (NFL) as potential markers of neurodegenerative disorders in psoriatic patients-a pilot study. *J. Clin. Med.* 11:2430. doi: 10.3390/jcm11092430

Olsson, B., Portelius, E., Cullen, N. C., Sandelius, Å., Zetterberg, H., Andreasson, U., et al. (2019). Association of cerebrospinal fluid neurofilament light protein levels with cognition in patients with dementia, motor neuron disease, and movement disorders. *JAMA Neurol.* 76, 318–325. doi: 10.1001/jamaneurol.2018.3746

Oosterveld, L. P., Kuiper, T. I., Majbour, N. K., Verberk, I. M. W., van Dijk, K. D., Twisk, J. W. R., et al. (2020). CSF biomarkers reflecting protein pathology and axonal degeneration are associated with memory, attentional, and executive functioning in early-stage Parkinson's disease. *Int. J. Mol. Sci.* 21:8519. doi: 10.3390/ijms21228519

Park, M. H., Jang, J. H., Song, J. J., Lee, H. S., and Oh, S. H. (2016). Neurofilament heavy chain expression and neuroplasticity in rat auditory cortex after unilateral and bilateral deafness. *Hear. Res.* 339, 155–160. doi: 10.1016/j.heares.2016.07.010

Park, D. G., Kim, J. W., An, Y. S., Chang, J., and Yoon, J. H. (2021). Plasma neurofilament light chain level and orthostatic hypotension in early Parkinson's disease. *J. Neural Transm.* 128, 1853–1861. doi: 10.1007/s00702-021-02423-y

Parnetti, L., Gaetani, L., Eusebi, P., Paciotti, S., Hansson, O., El-Agnaf, O., et al. (2019). CSF and blood biomarkers for Parkinson's disease. *Lancet Neurol.* 18, 573–586. doi: 10.1016/s1474-4422(19)30024-9

Ritchie, C., Smailagic, N., Noel-Storr, A. H., Ukoumunne, O., Ladds, E. C., and Martin, S. (2017). CSF tau and the CSF tau/ABeta ratio for the diagnosis of Alzheimer's disease dementia and other dementias in people with mild cognitive impairment (MCI). *Cochrane Database Syst. Rev.* 2017:Cd010803. doi: 10.1002/14651858.CD010803.pub2

Sabbagh, M. N., Adler, C. H., Lahti, T. J., Connor, D. J., Vedders, L., Peterson, L. K., et al. (2009). Parkinson disease with dementia: comparing patients with and without Alzheimer pathology. *Alzheimer Dis. Assoc. Disord.* 23, 295–297. doi: 10.1097/WAD.0b013e31819c5ef4

Schrag, A., Siddiqui, U. F., Anastasiou, Z., Weintraub, D., and Schott, J. M. (2017). Clinical variables and biomarkers in prediction of cognitive impairment in patients with newly diagnosed Parkinson's disease: a cohort study. *Lancet Neurol.* 16, 66–75. doi: 10.1016/s1474-4422(16)30328-3

Selikhova, M., Williams, D. R., Kempster, P. A., Holton, J. L., Revesz, T., and Lees, A. J. (2009). A clinico-pathological study of subtypes in Parkinson's disease. *Brain* 132, 2947–2957. doi: 10.1093/brain/awp234

Shaw, L. M., Hansson, O., Manuilova, E., Masters, C. L., Doecke, J. D., Li, Q. X., et al. (2019). Method comparison study of the Elecsys® β-amyloid (1-42) CSF assay versus comparator assays and LC-MS/MS. *Clin. Biochem.* 72, 7–14. doi: 10.1016/j.clinbiochem.2019.05.006

Shaw, L. M., Waligorska, T., Fields, L., Korecka, M., Figurski, M., Trojanowski, J. Q., et al. (2018). Derivation of cutoffs for the Elecsys(®) amyloid β (1-42) assay in Alzheimer's disease. *Alzheimers Dement.* 10, 698–705. doi: 10.1016/j.dadm.2018.07.002

Song, S. K., Lee, J. E., Park, H. J., Sohn, Y. H., Lee, J. D., and Lee, P. H. (2011). The pattern of cortical atrophy in patients with Parkinson's disease according to cognitive status. *Mov. Disord.* 26, 289–296. doi: 10.1002/mds.23477

Stewart, T., Shi, M., Mehrotra, A., Aro, P., Soltys, D., Kerr, K. F., et al. (2019). Impact of pre-analytical differences on biomarkers in the ADNI and PPMI studies: implications in the era of classifying disease based on biomarkers. *J. Alzheimers Dis.* 69, 263–276. doi: 10.3233/jad-190069

Targa, A., Dakterzada, F., Benítez, I., López, R., Pujol, M., Dalmases, M., et al. (2021). Decrease in sleep depth is associated with higher cerebrospinal fluid neurofilament light levels in patients with Alzheimer's disease. *Sleep* 44:zsaa147. doi: 10.1093/sleep/zsaa147

Tauil, C. B., Rocha-Lima, A. D., Ferrari, B. B., Silva, F. M. D., Machado, L. A., Ramari, C., et al. (2021). Depression and anxiety disorders in patients with multiple sclerosis: association with neurodegeneration and neurofilaments. *Braz. J. Med. Biol. Res.* 54:e10428. doi: 10.1590/1414-431x202010428

Thota, R. N., Chatterjee, P., Pedrini, S., Hone, E., Ferguson, J. J. A., Garg, M. L., et al. (2022). Association of plasma neurofilament light chain with glycaemic control and insulin resistance in middle-aged adults. *Front. Endocrinol.* 13:915449. doi: 10.3389/fendo.2022.915449

Yarnall, A. J., Breen, D. P., Duncan, G. W., Khoo, T. K., Coleman, S. Y., Firbank, M. J., et al. (2014). Characterizing mild cognitive impairment in incident Parkinson disease: the ICICLE-PD study. *Neurology* 82, 308–316. doi: 10.1212/wnl.0000000000000066

frontiers | Frontiers in Aging Neuroscience

TYPE Original Research
PUBLISHED 19 December 2022
DOI 10.3389/fnagi.2022.956273

OPEN ACCESS

EDITED BY
Woon-Man Kung,
Chinese Culture University, Taiwan

REVIEWED BY
Cuili Wang,
Peking University,
China
Antonio Hernández-Mendo,
University of Malaga,
Spain

*CORRESPONDENCE
Guohua Zheng
✉zhenggh@sumhs.edu.cn

SPECIALTY SECTION
This article was submitted to Neurocognitive Aging and Behavior, a section of the journal Frontiers in Aging Neuroscience

RECEIVED 30 May 2022
ACCEPTED 29 November 2022
PUBLISHED 19 December 2022

CITATION
Wan M, Xia R, Lin H, Ye Y, Qiu P and Zheng G (2022) Baduanjin exercise modulates the hippocampal subregion structure in community-dwelling older adults with cognitive frailty. *Front. Aging Neurosci.* 14:956273. doi: 10.3389/fnagi.2022.956273

Baduanjin exercise modulates the hippocampal subregion structure in community-dwelling older adults with cognitive frailty

Mingyue Wan[1,2,3], Rui Xia[3,4], Huiying Lin[3], Yu Ye[3], Pingting Qiu[3] and Guohua Zheng[2]*

[1]School of Rehabilitation Sciences, Southern Medical University, Guangzhou, China, [2]College of Nursing and Health Management, Shanghai University of Medicine and Health Sciences, Shanghai, China, [3]College of Rehabilitation Medicine, Fujian University of Traditional Chinese Medicine, Fuzhou, China, [4]Department of Rehabilitation, Shenzhen Bao 'an District People's Hospital, Shenzhen, China

Background: Regular Baduanjin exercise intervention was proven to be beneficial in improving the cognitive ability and physical performance of older adults with different health conditions but was unclear to influence the structural plasticity of the hippocampus. This study aimed to explore the modulation of hippocampal subregions as a mechanism by which Baduanjin exercise improves cognitive frailty in older adults.

Methods: A total of 102 community-dwelling older adults with cognitive frailty were recruited and randomly allocated to the Baduanjin exercise training group and usual physical activity control group. The participants in the Baduanjin exercise training group participated in a 24-week Baduanjin exercise intervention program with an exercise frequency of 60 min per day, 3days per week. Cognitive ability and physical frailty were assessed, and MRI scans were performed on all participants at baseline and after 24 weeks of intervention. The structural MRI data were processed with MRIConvert (version 2.0 Rev. 235) and FreeSurfer (version 6.0.0) software. Data analyses were performed using the independent sample *t* tests/Mann–Whitney *U* tests with the Bonferroni correction, mixed linear model, correlation, or mediation analysis by the SPSS 24.0 software (IBM Corp, Armonk, NY, United States).

Results: After 24 weeks of intervention, a statistically significant increase was found for the Montreal Cognitive Assessment (MoCA) scores (p=0.002) with a large effect size (Cohen's d=0.94) and the significant interaction effect ($P_{goupxtime}$<0.05), Memory Quotient (MQ) scores (p=0.019) with a medium effect size (Cohen's d=0.688) and the significant interaction effect ($P_{goupxtime}$<0.05), and other parameters of WMS-RC test including pictures (p=0.042), recognition (p=0.017), and association (p=0.045) test with a medium effect size (Cohens' d=0.592, 0.703, and 0.581) for the Baduanjin training group, while significant decrease for the Edmonton Frailty Scale (EFS) score (p=0.022), with a medium effect size (Cohen's d=−0.659) and the significant interaction effect ($P_{goupxtime}$<0.05) for the Baduanjin training group. The differences in the left parasubiculum, Hippocampal Amygdala Transition Area (HATA), right Cornu Ammonis Subfield 1 (CA1) and presubiculum volumes from baseline to

24 weeks after intervention in the Baduanjin training group were significantly greater than those in the control group ($p<0.05/12$). Further analysis showed that the changes in right CA1 volume were positively correlated with the changes in MoCA and MQ scores ($r=0.510$, $p=0.015$; $r=0.484$, $p=0.022$;), the changes in right presubiculum and left parasubiculum volumes were positively correlated with the changes in MQ ($r=0.435$, $p=0.043$) and picture test scores ($r=0.509$, $p=0.016$), respectively, and the changes in left parasubiculum and HATA volumes were negatively correlated with the changes in EFS scores ($r=-0.534$, $p=0.011$; $r=-0.575$, $p=0.005$) in the Baduanjin training group, even after adjusting for age, sex, years of education and marital status; furthermore, the volume changes in left parasubiculum and left HATA significantly mediated the Baduanjin exercise training-induced decrease in the EFS scores ($\beta=0.376$, 95% CI 0.024~0.947; $\beta=0.484$, 95% CI 0.091~0.995); the changes of left parasubiculum and right CA1 significantly mediated the Baduanjin exercise training-induced increase in the picture and MO scores ($\beta=-0.83$, 95% CI-1.95~−0.002; $\beta=-2.44$, 95% CI-5.99~−0.32).

Conclusion: A 24-week Baduanjin exercise intervention effectively improved cognitive ability and reduced physical frailty in community-dwelling older adults with cognitive frailty, and the mechanism might be associated with modulating the structural plasticity of the hippocampal subregion.

KEYWORDS

Baduanjin, cognitive frailty, hippocampal subregion, structural plasticity, MRI

Introduction

Cognitive frailty (*CF*) refers to a state characterized by the presence of both physical frailty and cognitive impairment in nondemented older adults (Buchman and Bennett, 2013), and is associated with increased risk of dysfunction, deterioration of quality of life, hospitalization, mortality, dementia and neurocognitive impairment (Panza et al., 2018). Although the underlying mechanism of *CF* remains unclear, a direct link has been proposed between brain pathology and cognitive frailty. An increasing number of studies have demonstrated the association of structural brain changes with the pathogenesis of cognitive frailty (Sugimoto et al., 2022). Current evidences showed the hippocampus or its subregion played an important role in memory consolidation as well as in energy intake, behaviors and mood regulation, therefore associated with cognitive and body function (Davidson et al., 2007; Bettio et al., 2017). For example, a study reported that hippocampal subfields including cornu ammonis 1 (CA1), CA2/3 and CA4 were significantly covaried with grey matter volume in older adults with cognitive impairment compared to the normal controls (Wang et al., 2018). Another study also found that the larger left parahippocampal gyrus and right hippocampus volumes were associated with the higher physical activity ability (Domingos et al., 2021). In our previous studies, we found a significant decrease in the volume of subcortical nuclei (composing of hippocampus, thalamus, caudate, putamen, pallor and amygdala) in the *CF* older adults (Wan et al., 2020). Then we further found a significant atrophy of six hippocampal subregions in *CF* older adults, including the left presubiculum, left parasubiculum, left molecular layer of the hippocampus proper (molecular layer of the HP), left HATA, right presubiculum, and right cornu ammonis subfield 1 (CA1; Wan et al., 2020). Therefore, changes in hippocampal subregion structure might play an important role in the pathogenesis of cognitive frailty.

Physical activity or regular exercise has been deemed an effective intervention for reducing physical frailty and increasing cognitive ability (Bherer et al., 2013; Angulo et al., 2020), and therefore should be a promising approach for improving cognitive frailty (Liu et al., 2018). For example, the community-based exercise program (i.e., a kind of exercise mode for community-dwelling older adults including multi-component exercise training with a low-moderate intensity) was effective in improving quality of life and physical frailty of community-dwelling older adults (Julien, 2021), while the aerobic, resistance or multicomponent exercise was proved to increase the cognitive function in older adults with or without cognitive impairment (Lee, 2020; Venegas-Sanabria et al., 2022). Moreover, converging evidences also suggest that the cognitive and physical performance improvement of exercise intervention may be brought about by enhanced structural network integrity of the human brain (Pani et al., 2021; Won et al., 2021; Huang et al., 2022). As one of the most popular traditional mind–body exercises in China, Baduanjin exercise consists of eight movements with low-medium intensity and is

characterized by symmetrical body postures and movements, breathing control, a meditative state of mind, and mental focus (Koh, 1982). Different from other types of physical exercise, Baduanjin emphasizes the mindfulness and breathing integration practice by cultivating *qi* (a vital energy based on traditional Chinese medicine) to improve physical, mental and cognitive health, and is recommended for older adults in China (Zheng et al., 2016; Tao et al., 2017; Zou et al., 2017). Our previous study found that regular Baduanjin intervention could increase the connection of resting function between the bilateral hippocampus and prefrontal lobe, and effectively prevent the decline of memory in the process of aging (Tao et al., 2016). This study aimed to explore the mechanism related to the central nervous system by which Baduanjin improves cognitive frailty in older adults from the perspective of the hippocampal subregions.

Materials and methods

Study design

This study was designed as a randomized controlled trial and has been registered in the China clinical trial registration center with the registration number ChiCTR1800020341.[1] This trial was approved by the Medical Ethics Committee of the Second People's Hospital of Fujian Province (approval number 2018-KL015). More details about the study design were described in previous published protocol (Xia et al., 2020).

Participants

Participants were recruited from three communities (Niushan, Wenquan and Wufeng communities) in Fuzhou city, China. Eligible participants met the following criteria: cognitive frailty with mild cognitive impairment [Fuzhou Version Montreal Cognitive Assessment (MoCA) $\leq$26 points]; physical frailty (EFS $\geq$ 5 points), absence of dementia (Global Deterioration Scale (GDS) level of II or III); aged 60 years or older; no regular exercise in the past half a year; and signed informed consent. Those with a history of mental illness (such as personality disorder, schizophrenia, etc.), depression (Beck Depression Scale $>$10 points), severe aphasia and visual impairment, severe organ failure, cerebral hemorrhage, cerebral infarction, history of coronary heart disease, musculoskeletal system diseases and other sports contraindications, hypertension and uncontrollable blood pressure (systolic blood pressure greater than 160 mmHg or diastolic blood pressure greater than 100 mmHg); metal implants (such as pacemakers, fixed metal dentures, etc.) and other conditions that were not suitable for MRI scanning, history of alcohol or drug abuse, or participation in other clinical trials were excluded.

Intervention

A total of 102 eligible participants were enrolled, and were randomly allocated into the Baduanjin training group or the control group with equal ratio. Participants in the Baduanjin group participated in Baduanjin training for 24 weeks, three times a week. Each training session lasted for 60 min, including 15 min of warm-up, 40 min of Baduanjin training, and 5 min of cool down. Health education on nutrition and diet related knowledge for the elderly was conducted every 4 weeks (at least 30 min per session). Baduanjin training was implemented in the Niushan, Wenquan and Wufeng communities with 15–20 participants from each community. Professional coaches of Fujian University of Traditional Chinese Medicine were responsible for leading Baduanjin practice. Participants in the control group did not receive any specific exercise training except for the same health education on nutrition and diet as the Baduanjin exercise training group. They were asked to maintain their original activity habits.

Cognitive and physical frailty assessment

Global cognitive function was assessed by using the Fuzhou version of the Montreal Cognitive Assessment (MoCA), which includes several cognitive domain dimensions (Fang et al., 2017) such as visuospatial, executive function, naming, memory, attention, language, abstraction, and orientation. The total score is 30, and a higher score indicates better global cognitive function. Memory was assessed using the Wechsler Memory Scale-Revised, Chinese version (WMS-RC). The MQ was the total score of WMS-RC which calculated according to age (Elwood, 1991). Higher MQ score denoted better memory. The WMS-RC was a set of memory tests that could detect impairment of long-term, short-term, and transient memory. Long-term memory includes counting 1–100, counting 100–1, accumulate subtests; short-term memory includes recognition, pictures, regenerate, association, touch and understand subtests; transient memory includes recite numbers subtests. Physical frailty was assessed by using the Chinese version of the Edmonton frail scale (EFS) with a total of 17 points, and high scores denoted a serious degree of frailty (Rolfson et al., 2006). All measures were conducted by blinded assessors at baseline and after intervention.

Basic information acquisition

Basic information included demographic characteristics such as age, gender, marital status, years of education were collected, while cognitive deterioration and depressive symptoms were assessed by the recruiters using the self-designed questionnaire,

1 http://www.chictr.org.cn/index.aspx

the Global Deterioration Scale and Beck Depression Scale, respectively.

MRI data acquisition

All participants underwent structural MRI at baseline and after intervention using a Siemens Prisma 3.0 T MRI system (Siemens Medical System, Erlangen, Germany) at the Rehabilitation Hospital Affiliated with FJTCM. The parameters of the structural MRI were as follows: repetition time (TR) = 2,300 ms, echo time (TE) = 2.27 ms, flip angle = 8°, slice thickness = 1.0 mm, field of view (FOV) = 250 × 250 mm, matrix = 256× 256, voxel size = 0.98 × 0.98 × 1 mm^3, and number of slices = 160.

Image processing

MRIConvert (version 2.0 Rev. 235) and FreeSurfer (version 6.0.0) software were used to preprocess the structural MRI data. Image processing was divided into the following steps: (1) image format conversion: MRIConvert software was used to convert the structure MRI data from the DICOM to the NIFTI format; (2) image quality inspection: each subject's image was checked for artifacts, lesions and other abnormalities and unqualified images were excluded; (3) direction adjustment: the image direction for each subject was adjusted consistently; (4) image segmentation: gray matter, white matter, subcortical nucleus, surface of white matter and cerebrospinal fluid were segmented by using the consistent segmentation method; (5) obtaining of deformation relation: obtaining curvature deformation relation from individual structure image to standard space; (6) spatial standardization: the individual level indicators are registered into the standard space by using the upper generated deformation relationship; and (7) smoothing: differences between individuals were reduced after standardization and the signal-to-noise ratio was improved.

The volume of the hippocampus in the subcortical nucleus segmentation file for each subject was extracted by using FreeSurfer 6.0.0 software, and the hippocampus and amygdala were segmented at the same time. The joint segmentation of the two areas ensured that the structures would not overlap or have a gap between them, making the results more accurate (Saygin et al., 2017). According to the official website for FreeSurfer,[2] each subject's hippocampus was divided into 19 regions according to the segmentation template of the hippocampus and then combined into the following areas: hippocampal tail, subiculum, cornu ammonis 1 (CA1), hippocampal fissure, presubiculum, parasubiculum, molecular layer of the HP, granule cell layer and molecular layer of the dentate gyrus (GC-ML-DG), CA2/3, CA4, hippocampal fimbria, and hippocampal amygdala transition area (HATA; Iglesias et al., 2015). CA2 was always included in CA3.

Data analysis

The data were analyzed by using SPSS 24.0 software (IBM Corp, Armonk, NY, United States), and $p < 0.05$ was considered significant. Independent sample t tests or Mann–Whitney U tests were used to compare the quantitative data from the two groups; Chi square tests were used to compare the categorical data of the two groups. Between-group effect size for cognitive and physical frailty outcomes were calculated using Cohen's d, in which effect sizes of 0.2, 0.5, and 0.8 were considered small, medium, and large effects, respectively. The mixed linear model with the fixed effect was used to analyze the interaction effect of group by time for the cognitive and physical frailty variables between two groups. To examine the robustness of results on Baduanjin exercise for cognitive frailty outcomes, we conducted sensitivity analysis by including data from participants who were lost follow-up, and the missing data were filled in using the multiple imputation method.

Bonferroni correction was used in the analysis of hippocampal subregion volume, and $p < 0.05/12$ was considered significance. To explore whether Baduanjin could improve cognitive frailty by changing the plasticity of the hippocampal subregions, we analyzed the correlation between the changes in hippocampal subregion volume and the changes in cognitive and physical frailty, with sex, age, marital status, and years of education as covariates. Moreover, we also analyzed the mediation effect of changes of hippocampal subregions in the relationship between intervention and cognitive frailty measurement by using the SPSS-PROCESS v3.5 software.

Results

Figure 1 shows the flow diagram of participants recruitment, randomization and follow up. A total of 102 eligible participants performed the baseline characteristics assessment and were randomly allocated into the groups. Of 102 participants, 73 were willing to perform MRI scans (37 in the Baduanjin group and 36 in the control group), and 50 of them completed the post-intervention assessment and the second MRI scans (26 in the Baduanjin group and 24 in the control group). Finally, 50 participants who completed two MRI scan were included in the analysis. For the Baduanjin exercise training group, some participants did not complete all training plans due to the limitation of bad weather and personal reasons. Even so the adherence rate was still up to 81.3%. The comparison on baseline characteristics of participants who completed two MRI scan between two groups are presented in Table 1. No significant differences were observed in basic demographic data between the two groups,

2 http://www.freesurfer.net/swiki/HippocampalSubfieldsAndNucleiOfAmygdala

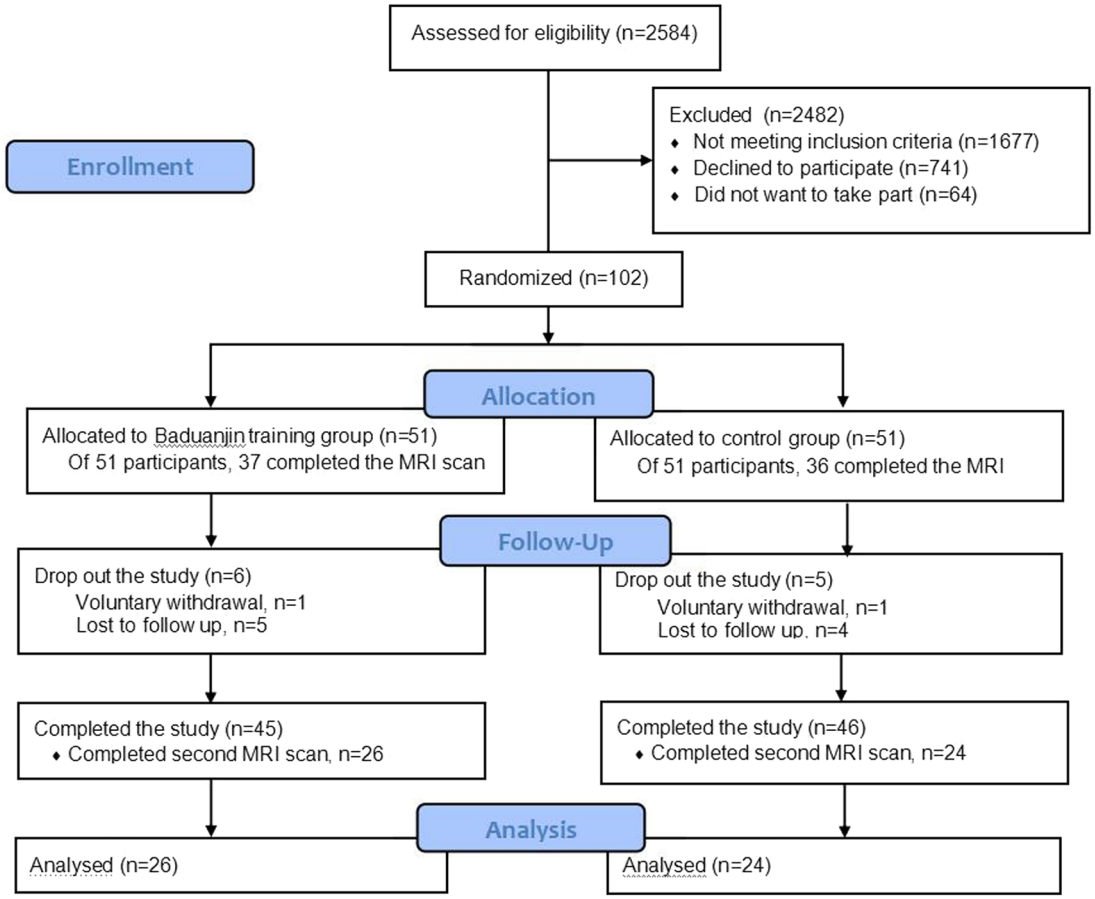

FIGURE 1
Research flow diagram.

TABLE 1 Comparison of baseline characteristics between two groups [ratio/ $\bar{X} \pm S$ / M (P_{25}~P_{75})].

Characteristics	BDJ (n=26)	CON (n=24)	$t/Z/\chi^2$	P
Age (year)	67.31 ± 5.58	64.71 ± 5.07	−1.843	0.065
Gender (male/female) (n)	9/17	12/12	1.213	0.271
marital status(married/widowed) (n)	25/1	24/0	–	1
BMI (kg/m^2)	23.47 ± 2.28	24.45 ± 3.28	−1.230	0.225
Average years of education (year)	11.58 ± 2.79	10.25 ± 2.92	−1.609	0.108
Beck Depression Scale Index*	3.5 (1.75 ~ 5)	3.5 (3 ~ 5)	0.426	0.670
Global deterioration scale(II/III)(n)	17/9	19/5	1.176	0.278

BDJ, Baduanjin exercise group; CON, control group. BMI, body mass index. *Data were performed by Mann–Whitney U tests.

including age, sex, marital status, body mass index (BMI), years of education, global deterioration scale level and Beck depression scale score.

To observe the variability on baseline characteristics between 50 participants who completed two MRI scan and 73 participants who were willing to perform MRI scan and all 102 participants, we conducted the comparison on baseline characteristics between two groups among three data sets, and those results were substantively unchanged in three data sets. The comparison on baseline characteristics between two groups among three data sets are presented in Supplementary Table 1.

Changes in cognitive ability and physical frailty

Comparison (according to the PP analysis model) on changes of cognitive ability and physical frailty from 24-week intervention

to baseline between two groups who completed two MRI scan are presented in Table 2. There was no significant difference between the two groups in terms of MoCA, WMS-RC test (both total and subtest scores) and EFS scores at baseline. After 24 weeks of the Baduanjin intervention, the independent sample *t* test or Mann–Whitney *U* test showed: the average scores of MoCA and MQ test in the Baduanjin exercise group were significantly higher than them in the control group with a medium to large effect size ($p = 0.002$ and 0.019; Cohen's $d = 0.94$ and 0.688), and the EFS scores in Baduanjin exercise group were significantly lower than that in the control group with a medium effect size ($p = 0.022$; Cohen's $d = -0.659$); For parameters of WMS-RC test, the scores of pictures, recognition, and association test in the Baduanjin exercise group were significantly higher than them in the control groups with medium effect sizes ($p = 0.042$, 0.017, and 0.045; Cohens' $d = 0.592$, 0.703, and 0.581); no significant difference between groups were found in other parameters such as counting 100–1, counting 1–100, accumulate, regenerate, touch, understand, and recite number. The linear mixed model analysis showed the significant interaction effect (group × time) in MoCA, EFS scores, MQ, and counting 1–100 scores, indicating that Baduanjin exercise intervention has a differential treatment effect compared with the control group.

To examine the robustness of effect on Baduanjin exercise for cognitive frailty outcomes, we conducted sensitivity analysis by including data from participants who were lost follow-up (ITT analysis model), and the results are presented in Table 3. Two analysis models yielded equivalent significant findings for the

TABLE 2 Comparison of cognitive ability and physical frailty between groups at baseline and after 24 weeks intervention.

Variables	Groups	N	Baseline		After 24 weeks intervention			Group×time interaction *P*
			$\bar{X} \pm S$ / *M* (P_{25}~P_{75})	*P*	$\bar{X} \pm S$ / *M* (P_{25}~P_{75})	*P*	Cohen' d	
MoCA (scores)	BDJ	26	22.50 ± 2.40	0.799	25.31 ± 2.41	**0.002**	0.940	**0.004**
	CON	24	21.88 ± 3.60		22.58 ± 3.35			
WMS-RC test (scores)								
MQ (scores)	BDJ	26	92.69 ± 13.02	0.270	102.92 ± 11.77	**0.019**	0.688	**0.026**
	CON	24	88.25 ± 15.11		93.71 ± 14.96			
Counting 1-100 (scores)	BDJ	26	7.81 ± 2.64	0.582	9.27 ± 1.87	0.235	0.349	0.015
	CON	24	8.25 ± 15.11		8.33 ± 3.34			
Counting 100-1 (scores)	BDJ	26	9.50 (6.50 ~ 11.25)	0.837	10.00 (7.00 ~ 12.00)	0.630	−0.008	0.565
	CON	24	10.00 (8.00 ~ 11.00)		11.00 (8.25 ~ 12.00)			
Accumulate (scores)	BDJ	26	10.00 (8.00 ~ 11.00)	0.896	10.00 (8.00 ~ 11.00)	1.000	0.000	0.855
	CON	24	8.25 (10.00 ~ 10.75)		9.00 (10.00 ~ 11.00)			
Pictures (scores)	BDJ	26	8.00 ± 2.67	0.955	9.81 ± 2.21	**0.042**	0.592	0.160
	CON	24	7.96 ± 2.56		8.50 ± 2.21			
Recognition (scores)	BDJ	26	8.88 ± 2.86	0.159	9.00 ± 2.84	**0.017**	0.703	0.500
	CON	24	7.58 ± 3.56		6.96 ± 2.97			
Regenerate (scores)	BDJ	26	7.00 ± 2.70	0.408	7.62 ± 2.58	0.590	0.154	0.823
	CON	24	6.38 ± 2.58		7.17 ± 3.25			
Association (scores)	BDJ	26	4.54 ± 3.43	0.205	6.23 ± 3.50	**0.045**	0.581	0.369
	CON	24	3.33 ± 3.19		4.25 ± 3.30			
Touch (scores)	BDJ	26	7.00 (6.00 ~ 7.25)	0.289	8.00 (7.00 ~ 8.00)	0.281	0.170	0.764
	CON	24	6.00 (6.00 ~ 8.00)		7.00 (6.00 ~ 8.00)			
Understand (scores)	BDJ	26	6.23 ± 1.99	0.359	7.27 ± 2.97	0.263	0.195	0.898
	CON	24	5.63 ± 2.62		6.75 ± 2.29			
Recite numbers (scores)	BDJ	26	8.27 ± 3.24	0.529	8.88 ± 3.41	0.495	0.155	0.766
	CON	24	7.71 ± 2.99		8.08 ± 2.04			
EFS (scores)	BDJ	26	5.46 ± 0.65	0.469	3.38 ± 1.33	**0.022**	−0.659	**0.016**
	CON	24	5.33 ± 0.57		4.33 ± 1.55			

BDJ, Baduanjin exercise group; CON, control group; MoCA, Montreal Cognitive Assessment; WMS-RC test, Wechsler Memory Scale-Revised, Chinese version; MQ, Memory Quotient; EFS, Edmonton Frailty Scale. Bold type *p* value represented significant.

TABLE 3 Comparison of cognitive ability and physical frailty between groups at baseline and after 24 weeks intervention.

Variables	Groups	N	Baseline		After 24 weeks intervention			Group×time interaction *P*
			$\bar{X} \pm S$	*P*	$\bar{X} \pm S$	*P*	Cohen' d	
MoCA (scores)	BDJ	37	22.59 ± 2.34	0.216	24.97 ± 2.57	**0.001**	0.793	**0.002**
	CON	36	21.67 ± 3.85		21.97 ± 4.72			
WMS-RC test (scores)								
MQ (scores)	BDJ	37	91.73 ± 13.06	0.155	100.97 ± 12.01	**0.025**	0.535	0.270
	CON	36	86.67 ± 16.86		93.56 ± 15.54			
Counting 1-100 (scores)	BDJ	37	7.76 ± 2.59	0.633	8.81 ± 2.42	0.506	0.157	0.151
	CON	36	8.08 ± 3.20		8.33 ± 3.58			
Counting 100-1 (scores)	BDJ	37	8.57 ± 3.44	0.692	9.46 ± 3.01	0.827	−0.051	0.385
	CON	36	8.22 ± 3.96		9.61 ± 2.88			
Accumulate (scores)	BDJ	37	9.03 ± 2.79	0.379	10.30 ± 2.25	0.174	0.321	0.946
	CON	36	8.33 ± 3.83		9.56 ± 2.37			
Pictures (scores)	BDJ	37	8.24 ± 2.58	0.419	9.70 ± 2.13	**0.025**	0.536	0.355
	CON	36	7.75 ± 2.61		8.56 ± 2.14			
Recognition (scores)	BDJ	37	8.70 ± 3.20	0.279	8.70 ± 3.02	0.059	0.449	0.598
	CON	36	7.86 ± 3.38		7.39 ± 2.83			
Regenerate (scores)	BDJ	37	7.05 ± 2.53	0.206	7.62 ± 2.41	0.783	0.065	0.366
	CON	36	6.25 ± 2.85		7.44 ± 3.05			
Association (scores)	BDJ	37	4.16 ± 3.17	0.118	6.14 ± 3.42	**0.011**	0.615	0.201
	CON	36	3.03 ± 2.94		4.06 ± 3.35			
Touch (scores)	BDJ	37	6.70 ± 2.05	0.421	7.35 ± 0.92	0.238	0.279	0.785
	CON	36	6.33 ± 1.84		6.83 ± 2.48			
Understand (scores)	BDJ	37	6.08 ± 1.99	0.312	7.22 ± 2.83	0.428	0.187	0.910
	CON	36	5.56 ± 2.41		6.75 ± 2.10			
Recite numbers (scores)	BDJ	37	8.38 ± 3.24	0.291	9.03 ± 3.06	0.112	0.376	0.759
	CON	36	7.56 ± 3.36		8.00 ± 2.34			
EFS (scores)	BDJ	37	5.38 ± 0.59	0.619	3.45 ± 1.43	**0.006**	−0.669	**0.006**
	CON	36	5.47 ± 0.97		4.50 ± 1.70			

BDJ, Baduanjin exercise group; CON, control group; MoCA, Montreal Cognitive Assessment; WMS-RC test, Wechsler Memory Scale-Revised, Chinese version; MQ, Memory Quotient; EFS, Edmonton Frailty Scale. Bold type *P* value represented significant.

MoCA, EFS, and MQ, pictures and association of WMS-RC test though the Cohen's *d* values of MoCA and MQ in the ITT model were a little lower than them in the PP model. Recognition parameter of WMS-RC test between two comparison groups was significant ($p = 0.017$) in the PP model but not in the ITT model ($p = 0.059$).

Changes in hippocampal subregions and the correlation with changes in cognitive or physical function

After 24 weeks of intervention, the change in hippocampal subregion volume before and after intervention was compared between the two groups. The volumes of the left parasubiculum, HATA, right CA1 and presubiculum in the Baduanjin group were significantly increased after intervention, and the volume changes were significantly higher than those in the control group after Bonferroni correction ($p < 0.05/12$; Table 4; Figures 2,3). After adjusting for the influence of sex, age, marital status and years of education, a correlation analysis between the changes in the volumes of the above 4 hippocampal subregions and the changes in cognitive frailty showed that the change in the volume of the right CA1 region in the Baduanjin training group was positively correlated with the change in the MoCA score ($r = 0.510$, $p = 0.015$); the change in the volume of the left parasubiculum and HATA was negatively correlated with the change in the EFS score ($r = -0.534$, $p = 0.011$; $r = -0.575$, $p = 0.005$); the change in the volume of the right CA1 and right presubiculum was positively correlated with the change in the MQ score ($r = 0.484$, $p = 0.022$;

TABLE 4 Comparison of the volume change between the two groups (unit: mm^3).

	BDJ (n=26)	CON (n=24)	t	P
Hippocampal tail (left)	1.57 ± 30.55	−2.21 ± 21.29	0.503	0.617
Subiculum (left)	5.05 ± 11.61	−5.35 ± 11.69	0.093	0.926
CA1 (left)	−7.31 ± 30.27	−9.71 ± 19.94	0.328	0.744
Hippocampal fissure (left)	1.01 ± 10.80	−3.45 ± 13.07	1.319	0.193
Presubiculum (left)	−3.89 ± 16.92	−5.64 ± 13.87	0.398	0.692
Parasubiculum (left)	2.72 ± 6.06	−2.60 ± 5.37	3.275	**0.002**
Molecular layer of the HP (left)	−6.08 ± 20.75	−8.17 ± 14.15	0.413	0.682
GC-ML-DG (left)	−2.09 ± 11.89	−3.73 ± 10.58	0.512	0.611
CA3 (left)	−1.39 ± 9.62	−1.39 ± 10.02	0.002	0.999
CA4 (left)	−1.20 ± 9.57	−2.60 ± 9.91	0.505	0.616
Hippocampal fimbria (left)	−2.39 ± 9.74	−0.78 ± 8.29	−0.624	0.536
HATA (left)	2.90 ± 4.62	−0.57 ± 3.45	2.996	**0.004**
Total hippocampus (left)	−21.19 ± 94.41	−42.14 ± 71.72	0.878	0.384
Hippocampal tail (right)	0.17 ± 23.25	7.58 ± 19.77	−1.209	0.233
Subiculum (right)	−1.35 ± 10.97	3.73 ± 7.96	−1.860	0.069
CA1 (right)	2.07 ± 11.47	−9.67 ± 13.96	3.261	**0.002**
Hippocampal fissure (right)	1.93 ± 11.15	−3.09 ± 9.35	1.719	0.092
Presubiculum (right)	4.40 ± 8.90	−5.86 ± 13.81	3.149	**0.003**
Parasubiculum (right)	0.98 ± 5.34	0.05 ± 4.71	0.651	0.518
Molecular layer of the HP (right)	−1.36 ± 13.39	−0.34 ± 11.58	−0.287	0.775
GC-ML-DG (right)	−0.69 ± 11.79	0.95 ± 9.56	−0.536	0.595
CA3 (right)	1.17 ± 11.13	0.16 ± 11.83	0.310	0.758
CA4 (right)	−0.60 ± 10.80	1.11 ± 9.12	−0.600	0.551
Hippocampal fimbria (right)	−2.14 ± 7.28	0.80 ± 7.46	−1.409	0.165
HATA (right)	0.32 ± 4.38	−1.09 ± 3.21	1.287	0.204
Total hippocampus (right)	4.91 ± 72.62	3.22 ± 59.17	0.089	0.929

BDJ, Baduanjin exercise group; CON, control group; CA, Cornu Ammonis Subfield; GC-ML-DG, Granule Cell Layer and Molecular Layer of the Dentate Gyrus; HATA, Hippocampal Amygdala Transition Area; Bold type p value represented significant.

r = 0.435, p = 0.043); and change in left parasubiculum volume was positively correlated with change in the picture subtest scores (r = 0.509, p = 0.016; Table 5; Figure 4).

To investigate hippocampal subregions as a potential mediator of Baduanjin exercise training improving cognitive frailty, we performed a mediation analysis using the significant volume changes of hippocampal subregions (i.e., left parasubiculum, left HATA, right CA1, or right presubiculum) as a mediator between groups and the significant scores changes of cognitive or physical frailty measures (MoCA, MQ, or pictures). The analysis results showed the volume changes in left parasubiculum and left HATA mediated the Baduanjin exercise training-induced decrease in the EFS scores with a significant indirect effect (β = 0.376, 95% CI 0.024 ~ 0.947; β = 0.484, 95% CI 0.091 ~ 0.995); the changes of left parasubiculum and right CA1 mediated the Baduanjin exercise training-induced increase in the picture and MO scores with the significant indirect effects (β = −0.83, 95% CI-1.95 ~ −0.002; β = −2.44, 95% CI-5.99 ~ −0.32; Figure 5).

Discussion

This study investigated the changes in hippocampal subregion volumes and cognitive frailty after a 24-week Baduanjin exercise intervention. After 24 weeks of regular Baduanjin intervention, both analysis models (the PP and ITT analysis) showed that the MoCA, MQ, and EFS scores of participants in the Baduanjin exercise training group were significantly improved compared to those in the control group, with a medium to large effect size and significant group by time interaction effect. The MRI data showed that the volume reduction of four hippocampal subregions including the left parasubiculum, left HATA, right CA1 and right presubiculum in the Baduanjin training group was significantly lower than that in the control group. Furthermore, in the Baduanjin training group, the volume change in the left parasubiculum was positively correlated with the change in MQ score and negatively correlated with the change in the EFS index; the volume change in the left HATA was negatively correlated with

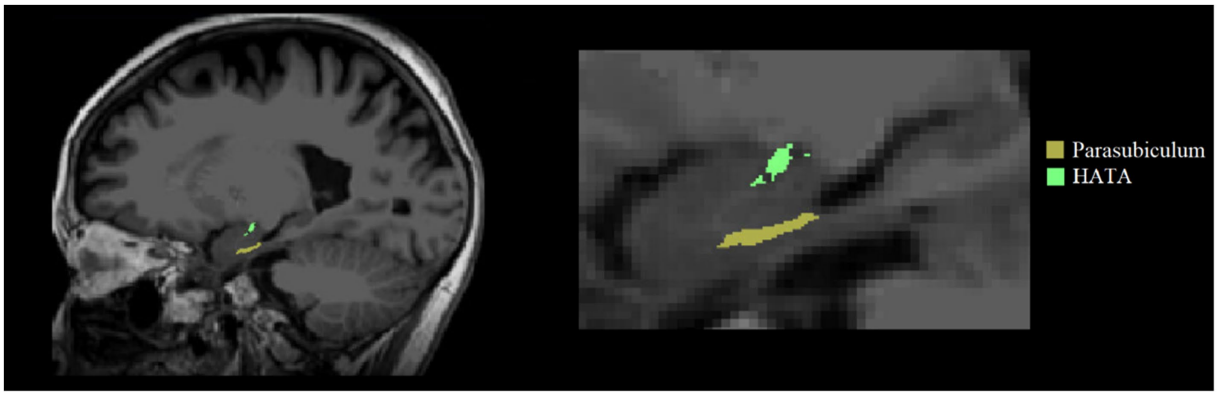

FIGURE 2
Left two hippocampal subregions with significant volume changes after intervention.

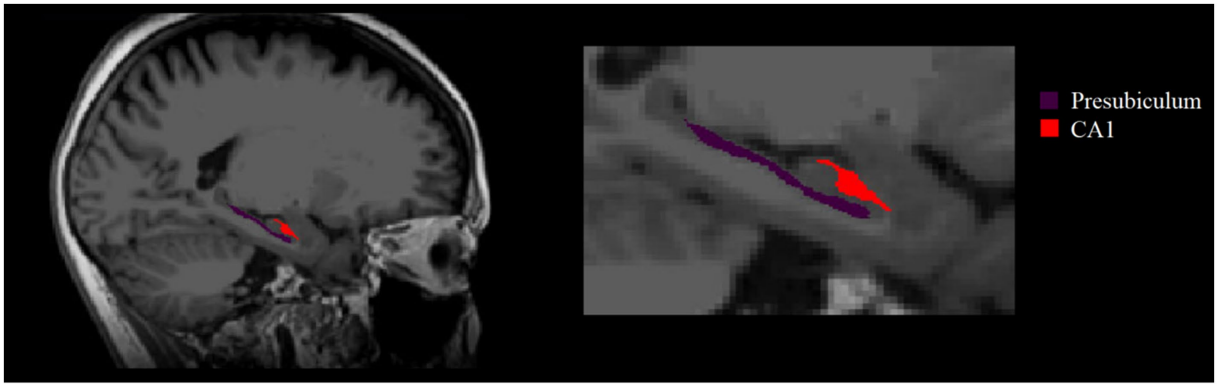

FIGURE 3
Right two hippocampal subregions with significant volume changes after intervention.

TABLE 5 Correlation between the volume changes of hippocampal subregion and changes of cognitive ability and physical frailty in Baduanjin group (*n*=26).

	Left parasubiculum		Left HATA		Right CA1		Right presubiculum	
	r	*P*	*r*	*P*	*r*	*P*	*r*	*P*
MoCA	0.032	0.888	0.068	0.764	0.510	**0.015**	0.347	0.113
MQ	0.084	0.709	0.203	0.366	0.484	**0.022**	0.435	**0.043**
Pictures	0.509	**0.016**	0.266	0.232	−0.145	0.520	0.255	0.253
Recognition	−0.029	0.897	0.221	0.323	0.419	0.053	0.157	0.485
Association	−0.115	0.611	−0.123	0.585	0.285	0.198	0.123	0.584
EFS	−0.534	**0.011**	−0.575	**0.005**	−0.151	0.501	−0.323	0.142

Gender, age, marital status and years of education were used as covariates for partial correlation analysis. Bold type *P* value represented significant. MoCA, Montreal Cognitive Assessment; MQ, Memory Quotient; EFS, Edmonton Frailty Scale. Bold type *P* value represented significant.

the change in the EFS index; the volume change in the right CA1 was positively correlated with the change in the MoCA and MQ score; and the volume change in the right presubiculum was positively correlated with the change in MQ score. The mediation analysis showed the volume changes in left parasubiculum and left HATA significantly mediated the Baduanjin exercise training-induced decrease in the EFS scores; the changes of left parasubiculum and right CA1 significantly mediated the Baduanjin exercise training-induced increase in the picture and MO scores. The findings in this study suggest that regular

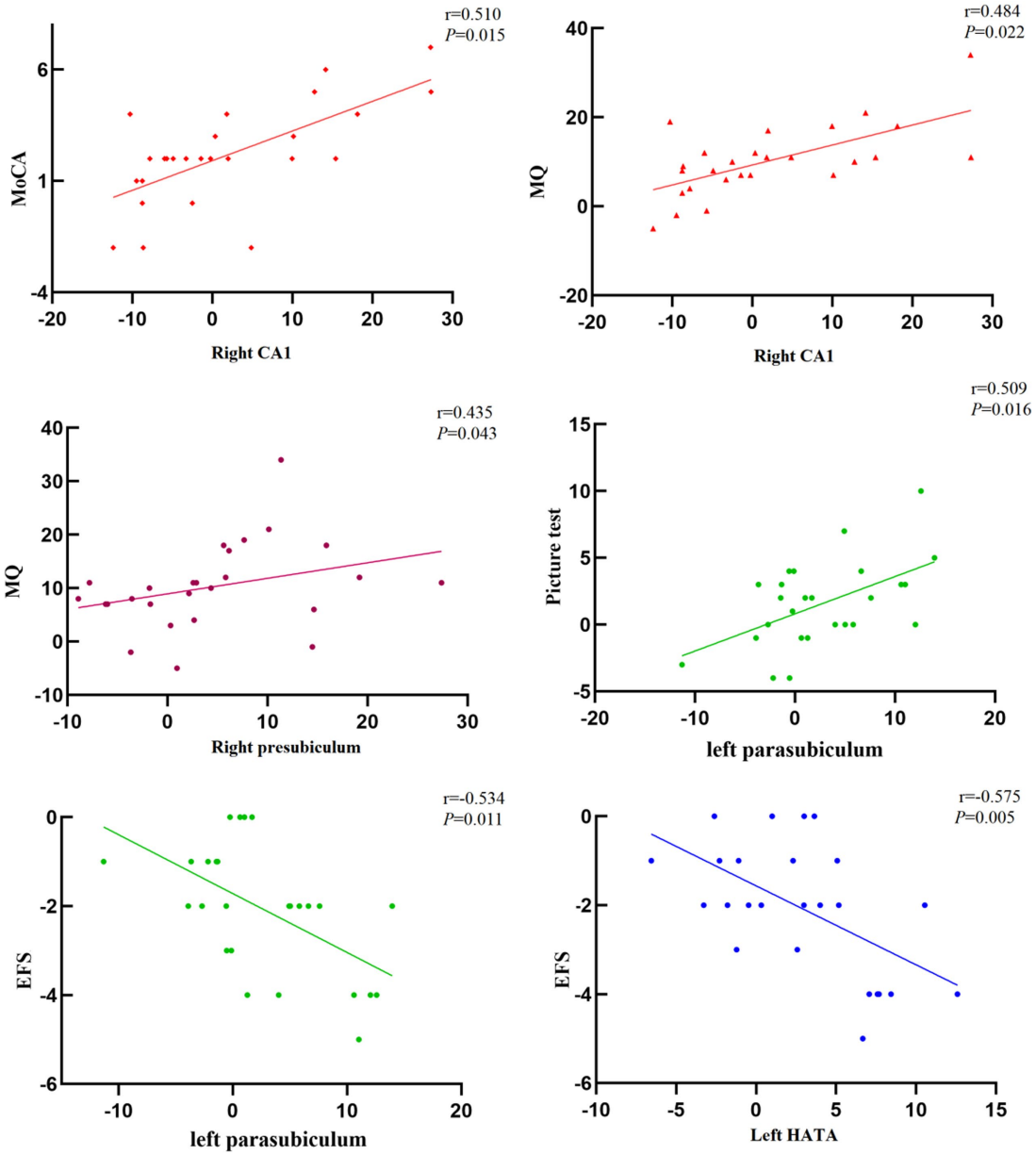

FIGURE 4
Correlation between the volume change of hippocampal subregion and cognitive frailty in Baduanjin group (n=26).

Baduanjin intervention might improve the cognitive ability and physical frailty of community-dwelling older adults with cognitive frailty by modulating the plasticity of some hippocampal subregions.

Baduanjin is a mind–body exercise based on traditional Chinese medicine. A systematic review showed that Baduanjin exercise was safe and effective in enhancing the overall cognitive function and memory of middle-aged and older adults (Wang et al., 2021). One study also found that a 6-month Baduanjin training intervention had a positive effect on increasing brain gray matter in the temporal, frontal, parietal, medial occipital, cingulate and angular gyrus, and improving cognitive function in older adults with MCI. Furthermore, the increase in the right medial temporal gyrus was significantly correlated with the improvement in cognitive function (Zheng et al., 2021). Another study reported that Baduanjin training could change the functional connection of the dorsal attention network in patients with MCI and improve their attention (Xia et al., 2019). Current findings showed that the 24-week Baduanjin exercise intervention significantly improved global cognitive ability, memory, and physical frailty in community-dwelling older adults with cognitive frailty and significantly reduced the atrophy of some hippocampal subregions. These findings further support previous studies and suggest a potential

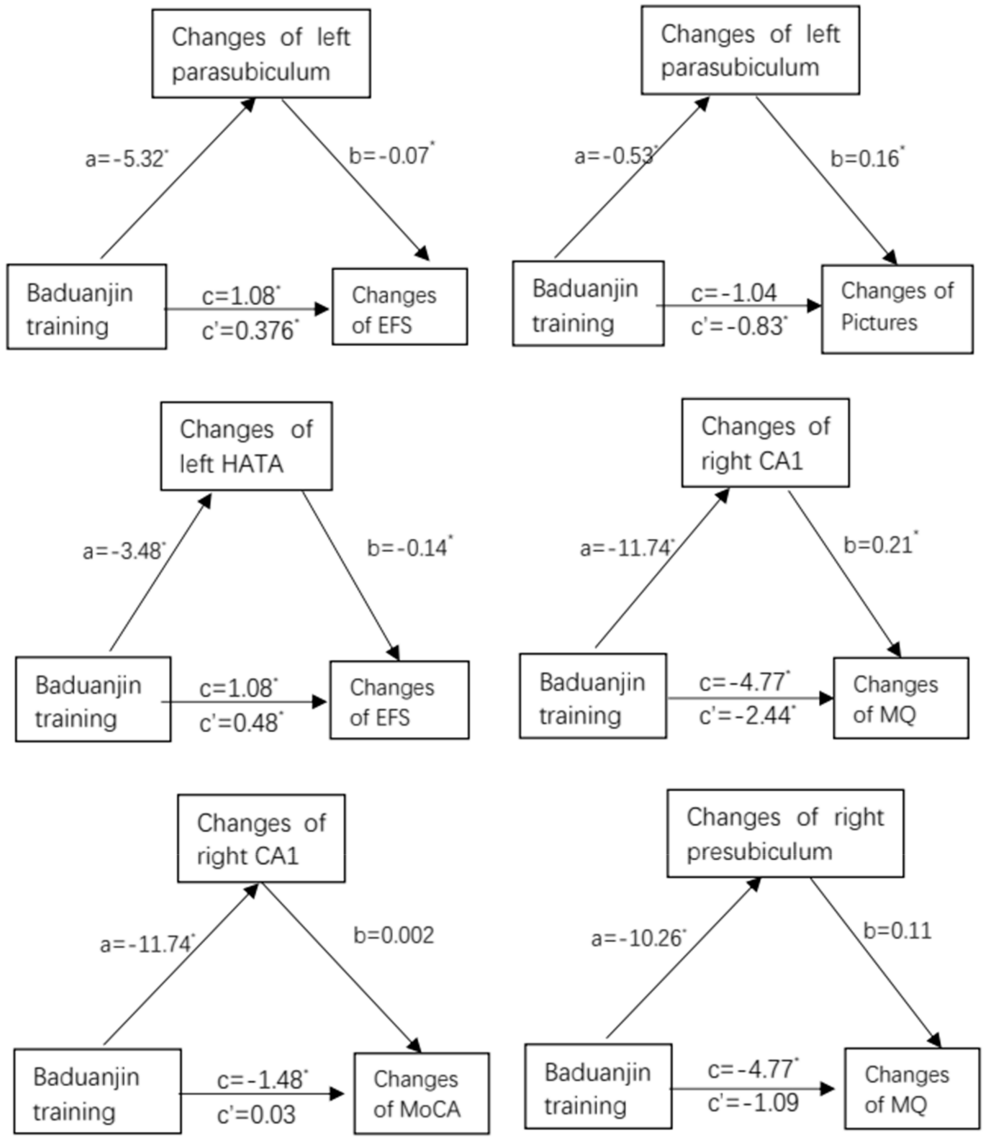

FIGURE 5
Mediation analysis: path diagram depicting mediation model 4, testing whether changes in changes in hippocampal subregion volume (left parasubiculum, left HATA, right CA1, or right presubiculum) mediate the effect of Baduanjin training intervention vs. control (no specific exercise intervention) on improvement in cognition (MoCA, MQ, or pictures) or physical frailty (EFS). MoCA, Montreal Cognitive Assessment; MQ, Memory Quotient; EFS, Edmonton Frailty Scale; CA1, Cornu Ammonis Subfield 1; HATA, Hippocampal Amygdala Transition Area. a, b, c′ and c are unstandardized path coefficients, and *<0.05. a-path represent effect of Baduanjin training over hippocampal subregions (left parasubiculum, left HATA, right CA1, or right presubiculum); b-path represent effect of hippocampal subregions over cognition (MoCA, MQ, or pictures) or physical frailty (EFS); c′-path represent indirect effect of Baduanjin training over cognition (MoCA, MQ, or pictures) or physical frailty (EFS); and c-path represent total effect of Baduanjin training over cognition (MoCA, MQ, or pictures) or physical frailty (EFS).

mechanism by which Baduanjin exercise improves cognitive frailty.

The CA1 subregion of the hippocampus functions in the separation of spatial coding and recall processes by processing spatial and temporal memory at the same time as an independent neural network in the process of memory coding (Eichenbaum, 2017; Tanaka et al., 2018) and plays a special role in encoding episodic memory information (Schlichting et al., 2014). Existing studies have shown that exercise can affect the structural plasticity of the CA1 region and improve cognitive function (Woodward et al., 2018). The present study also found that 24 weeks of Baduanjin exercise intervention can improve the cognitive and physical function of older adults with cognitive frailty and reverse the decrease in CA1 volume. Other studies suggest that running may induce hippocampal neurogenesis and synaptic plasticity by increasing the complexity and number of dendritic spines in the dentate gyrus, CA1 and entorhinal cortex (Opendak and Gould, 2015). A systematic review revealed that mind–body exercise modulated brain structure and functional connectivity mainly in the hippocampus/medial temporal lobe, as well as the cognitive

control and default mode networks, which might underlie the beneficial effects of such exercises on the health of individuals (Zhang et al., 2021).

The presubiculum of the hippocampus is a part of the subiculum, which is the transition region from the parahippocampus to the hippocampus. Studies have shown that smaller hippocampal and presubiculum volumes could predict the conversion of Parkinson's patients to dementia, while the hippocampal, presubiculum and parasubiculum volumes of Parkinson's patients with dementia were significantly decreased, and the decrease in these volumes was positively correlated with the decrease in cognitive ability (Low et al., 2019). Another study also found that from the early stage of Alzheimer's disease, the subiculum and presubiculum of the hippocampus have atrophied (Carlesimo et al., 2015). Therefore, structural changes in the presubiculum might play an important role in predicting cognitive impairment. Our study showed that Baduanjin could slow the volume decrease of the right presubiculum, and there was a positive correlation between the right presubiculum and MQ score ($r = 0.435$). The volume of the presubiculum is positively correlated with the ability of observation, which could also prevent the decline of memory and enhance its persistence (Barry et al., 2021).

The parasubiculum is a small, narrow structure located between the presubiculum and medial entorhinal cortex, which is responsible for spatial navigation and memory (Sammons et al., 2019). Atrophy of the parasubiculum was only observed in older adults with Alzheimer's disease; thus, researchers believe that a significant decrease in the volume of the parasubiculum may be a potential biomarker of dementia (Zheng et al., 2018). Additionally, atrophy of the parasubiculum may affect the integrity of the hippocampal-amygdala network, which is the basis of information processing; therefore, it may play a key role in cognitive processes (Foo et al., 2017). Animal experiments also found that the parasubiculum may be more involved in real-time spatial information processing than in long-term information storage (Tang et al., 2016). The results of the present study showed that there was a positive correlation between short-term memory test results and parasubiculum volume ($r = 0.509$). This suggests that the integrity of the parasubiculum structure may be closely related to the function of immediate spatial information processing.

Hippocampal amygdala transition area anatomically connects the hippocampus to the amygdala and has a regulatory effect on muscle atrophy. It has been reported that the HATA of amyotrophic lateral sclerosis (ALS) patients with central amyotrophic and myasthenic lesions presents significant atrophy (Christidi et al., 2019). The hippocampal input to the amygdala originates from the CA and mainly projects to the amygdala area, the accessory nucleus of the amygdala and the ventral basal nucleus through the HATA and contains immature neuronal populations, which may be the cellular mechanism behind the plasticity of context learning and emotional memory (Fudge et al., 2012). Our results showed that 24 weeks of Baduanjin exercise intervention may reduce physical frailty and increase the HATA volume. Furthermore, there was a significant negative correlation between HATA and EFS score ($r = -0.575$), which means that a smaller HATA volume indicates a frailer individual. Our findings suggest that the mechanism by which Baduanjin improves the physical frailty of older adults with cognitive frailty might be associated with an increase in the HATA volume.

In terms of other hippocampal subregions. CA3 and CA4 play the important role in the encoding of new spatial information with short-term memory (Kesner, 2007). The GC-ML-DG mainly receives cortical input from the entorhinal cortex and projects to CA3 pyramidal cells, also is a key brain region associated with the stress response, pathology of depression, and antidepressant response (Tuncdemir et al., 2019). The subiculum has functional properties seemingly independent from the rest of the hippocampus, and has a substantial contribution to interregional communication and behavioral performance (Matsumoto et al., 2019). Hippocampal fimbria, as a structural bridge between the hippocampus and other brain regions, is key to hippocampus preserving memory (Chauhan et al., 2021). Hippocampal fissure, also called the hippocampal sulcus, is a kind of narrow furrow to separate the gyri of brain (Humphrey, 1967); and its width may negatively related to the atrophy of the hippocampal subfields (Li et al., 2018). Growing evidence indicates that physical exercise could profoundly increase hippocampal neurogenesis, by altering neurochemistry and function of newly generated neurons (Pereira et al., 2007; Lafenetre et al., 2011; Farioli-Vecchioli and Tirone, 2015; Ma et al., 2017; Firth et al., 2018). In our present trial, we did not find a 24-week Baduanjin exercise training had a significant effect in improving structures of those hippocampal subregions including CA3, CA4, Subiculum, hippocampal fissure, and, hippocampal fimbria. A recent study reported that the exercise type is an important factor affecting the effects of exercise on the hippocampus (Tsuchida et al., 2022). Another possible reason results from the small samples of our current trial. Therefore future studies with a larger samples is need to further determine the relation of Baduanjin exercise intervention with those hippocampal subregions.

Limitations

Some limitations of this study should be recognized. First, we used hippocampal subregion analysis to explore the possible mechanism by which Baduanjin improves cognitive frailty. Instead of analyzing the problem from the perspective of the whole brain, it only focuses on the hippocampus. Second, because some older adults who participated in the study did not correctly report their metal implantation conditions at enrollment or were unwilling to perform the MRI scan at baseline assessment, leading to a reduction in the MRI sample size. We compared the baseline characteristics between two groups among three data sets, in which contained all 102 participants, 73 participants who were willing to do MRI scan, and 50 participants who completed two

MRI scan, respectively, and the results showed little variability among three data sets and good balance between two groups for each data set. In addition, we also analyzed effect of Baduanjin exercise intervention on cognitive ability and physical frailty outcomes using two analysis models, and the findings were equivalent. Even so, the attrition bias was possible unavoidable due to unknow confounders. In future research, the sample size should be expanded to improve the stability of the results. Third, this study only focuses on the hippocampal subregions and those hippocampal subregions that showed no significant changes were not discussed. Future studies are needed to further explore more brain structures. Fourth, considering the difficult of recruitment and study to be conducted, this study did not use another experimental control group with another exercise type to determine the effect of Baduanjin different from other exercise type. Finally, EFS is a frailty assessment tool (including cognition, social support, mood indicators other than physical indicators), therefore it has a limitation on accurately assessing physical frailty characterized by the vulnerability of strength, endurance, and physiological functions. Therefore, those findings of this trial should be explained cautiously. Future study should compare Baduanjin training with other exercise type to identify its exclusive effect. In addition, participants in the control group of this study did not to receive any specific exercise intervention (maintain their original life habit), which would result in ethical implications.

Conclusion

The 24-week Baduanjin exercise intervention effectively improved the cognitive ability and reduced the physical frailty of community-dwelling older adults with cognitive frailty and slowed the atrophy of hippocampal subregions, including the left parasubiculum, left HATA, right CA1 and right presubiculum. The mechanism by which Baduanjin improves cognitive frailty of older adults may be associated with changes in the structural plasticity of hippocampal subregions. This results also provide potential theoretical support for the application of Baduanjin exercise to intervene the cognitive frailty of community-dwelling older adults.

Data availability statement

The original contributions presented in the study are included in the article/Supplementary material, further inquiries can be directed to the corresponding author.

Ethics statement

The studies involving human participants were reviewed and approved by Second People's Hospital Affiliated to Fujian University of Traditional Chinese Medicine. The patients/participants provided their written informed consent to participate in this study.

Author contributions

GZ designed this study and responsible for coordinating and monitoring the process. MW and RX wrote the manuscript. HL, YY, and PQ manage maintenance and data analysis. All authors contributed to the article and approved the submitted version.

Funding

This study was supported by the National Natural Science Foundation of China (http://www.nsfc.gov.cn, No. 82074510) and GuangDong Basic and Applied Basic Research Foundation (2021A1515110764).

Acknowledgments

We thank the participants from the community and the staff of the Rehabilitation Hospital Affiliated to Fujian University of Traditional Chinese Medicine and the Second People's Hospital Affiliated to Fujian University of Traditional Chinese Medicine.

Conflict of interest

The authors declare that the research was conducted in the absence of any commercial or financial relationships that could be construed as a potential conflict of interest.

Publisher's note

Supplementary material

The Supplementary material for this article can be found online at: https://www.frontiersin.org/articles/10.3389/fnagi.2022.956273/full#supplementary-material

References

Angulo, J., El Assar, M., Álvarez-Bustos, A., and Rodríguez-Mañas, L. (2020). Physical activity and exercise: strategies to manage frailty. *Redox Biol.* 35:101513. doi: 10.1016/j.redox.2020.101513

Barry, D. N., Clark, I. A., and Maguire, E. A. (2021). The relationship between hippocampal subfield volumes and autobiographical memory persistence[J]. *Hippocampus* 31, 362–374. doi: 10.1002/hipo.23293

Bettio, L. E. B., Rajendran, L., and Gil-Mohapel, J. (2017). The effects of aging in the hippocampus and cognitive decline. *Neurosci. Biobehav. Rev.* 79:5. doi: 10.1016/j.neubiorev.2017.04.030

Bherer, L., Erickson, K. I., and Liu-Ambrose, T. (2013). A review of the effects of physical activity and exercise on cognitive and brain functions in older adults. *J. Aging Res.* 2013:657508. doi: 10.1155/2013/197326

Buchman, A. S., and Bennett, D. A. (2013). Cognitive frailty[J]. *J. Nutr. Health Aging* 17, 738–739. doi: 10.1007/s12603-013-0397-9

Carlesimo, G. A., Piras, F., Orfei, M. D., Iorio, M., Caltagirone, C., and Spalletta, G. (2015). Atrophy of presubiculum and subiculum is the earliest hippocampal anatomical marker of Alzheimer's disease[J]. *Alzheimers Dement (Amst.)* 1, 24–32. doi: 10.1016/j.dadm.2014.12.001

Chauhan, P., Jethwa, K., Rathawa, A., Chauhan, G., and Mehra, S. (2021). "The anatomy of the hippocampus," in *Cerebral Ischemia*. ed. R. Pluta (Brisbane (AU): Exon Publications) doi: 10.36255/exonpublications.cerebralischemia.2021.hippocampus

Christidi, F., Karavasilis, E., Rentzos, M., Velonakis, G., Zouvelou, V., Xirou, S., et al. (2019). Hippocampal pathology in amyotrophic lateral sclerosis: selective vulnerability of subfields and their associated projections[J]. *Neurobiol. Aging* 84, 178–188. doi: 10.1016/j.neurobiolaging.2019.07.019

Davidson, T. L., Kanoski, S. E., Schier, L. A., Clegg, D. J., and Benoit, S. C. (2007). A potential role for the hippocampus in energy intake and body weight regulation. *Curr. Opin. Pharmacol.* 7, 613–616.

Domingos, C., Picó-Pérez, M., Magalhães, R., Moreira, M., Sousa, N., Pêgo, J. M., et al. (2021). Free-living physical activity measured with a wearable device is associated with larger hippocampus volume and greater functional connectivity in healthy older adults: an observational, cross-sectional study in northern Portugal. *Front. Aging Neurosci.* 13:729060. doi: 10.3389/fnagi.2021.729060

Eichenbaum, H. (2017). On the integration of space, time, and memory[J]. *Neuron* 95, 1007–1018. doi: 10.1016/j.neuron.2017.06.036

Elwood, R. W. (1991). The Wechsler memory scale-revised: psychometric characteristics and clinical application[J]. *Neuropsychol. Rev.* 2, 179–201. doi: 10.1007/BF01109053

Fang, Y., Tao, Q., Zhou, X., Chen, S., Huang, J., Jiang, Y., et al. (2017). Patient and family member factors influencing outcomes of poststroke inpatient rehabilitation[J]. *Arch. Phys. Med. Rehabil.* 98, 249–255.e2. doi: 10.1016/j.apmr.2016.07.005

Farioli-Vecchioli, S., and Tirone, F. (2015). Control of the cell cycle in adult neurogenesis and its relation with physical exercise. *Brain Plast.* 1, 41–54.

Firth, J., Stubbs, B., Vancampfort, D., et al. (2018). Effect of aerobic exercise on hippocampal volume in humans: a systematic review and meta-analysis. *NeuroImage* 1, 230–238.

Foo, H., Mak, E., Chander, R. J., Ng, A., Au, W. L., Sitoh, Y. Y., et al. (2017). Associations of hippocampal subfields in the progression of cognitive decline related to Parkinson's disease[J]. *Neuroimage Clin.* 14, 37–42. doi: 10.1016/j.nicl.2016.12.008

Fudge, J. L., DeCampo, D. M., and Becoats, K. T. (2012). Revisiting the hippocampal–amygdala pathway in primates: association with immature-appearing neurons[J]. *Neuroscience* 212, 104–119. doi: 10.1016/j.neuroscience.2012.03.040

Huang, X., Zhao, X., Cai, Y., and Wan, Q. (2022). The cerebral changes induced by exercise interventions in people with mild cognitive impairment and Alzheimer's disease: a systematic review. *Arch. Gerontol. Geriatr.* 98:104547. doi: 10.1016/j.archger.2021.104547

Humphrey, T. (1967). The development of the human hippocampal fissure. *J. Anat.* 101, 655–676.

Iglesias, J. E., Augustinack, J. C., Nguyen, K., Player, C. M., Player, A., Wright, M., et al. (2015). A computational atlas of the hippocampal formation using ex vivo, ultra-high resolution MRI: application to adaptive segmentation of in vivo MRI[J]. *NeuroImage* 115, 117–137. doi: 10.1016/j.neuroimage.2015.04.042

Julien, V. (2021). le Bruchec Solenn, Bernat Valérie et al. frailty and quality of life, the benefits of physical activity for the elderly.[J]. *Geriatr. Psychol. Neuropsychiatr. Vieil.* 10

Kesner, R. P. (2007). Behavioral functions of the CA3 subregion of the hippocampus. *Learn. Mem.* 14, 771–781.

Koh, T. C. (1982). Baduanjin—an ancient Chinese exercise. *Am. J. Chin. Med.* 10, 14–21.

Lafenetre, P., Leske, O., Wahle, P., et al. (2011). The beneficial effects of physical activity on impaired adult neurogenesis and cognitive performance. *Front. Neurosci.* 12:51.

Lee, J. (2020). Effects of aerobic and resistance exercise interventions on cognitive and physiologic adaptations for older adults with mild cognitive impairment: a systematic review and meta-analysis of randomized control trials. *Int. J. Environ. Res. Public Health* 17:9216.

Li, Y., Yan, J., Zhu, X., Zhu, Y., Qin, J., Zhang, N., et al. (2018). Increased hippocampal fissure width is a sensitive indicator of rat hippocampal atrophy. *Brain Res. Bull.* 137, 91–97. doi: 10.1016/j.brainresbull.2017.11.014

Liu, Z., Hsu, F. C., Trombetti, A., King, A. C., Liu, C. K., Manini, T. M., et al. (2018). Effect of 24-month physical activity on cognitive frailty and the role of inflammation: the LIFE randomized clinical trial. *BMC Med.* 16:185. doi: 10.1186/s12916-018-1174-8

Low, A., Foo, H., Yong, T. T., Tan, L. C. S., and Kandiah, N. (2019). Hippocampal subfield atrophy of CA1 and subicular structures predict progression to dementia in idiopathic Parkinson's disease[J]. *J. Neurol. Neurosurg. Psychiatry* 90, 681–687. doi: 10.1136/jnnp-2018-319592

Ma, C. L., Ma, X. T., Wang, J. J., Liu, H., Chen, Y. F., and Yang, Y. (2017). Physical exercise induces hippocampal neurogenesis and prevents cognitive decline. *Behav. Brain Res.* 317, 332–339. doi: 10.1016/j.bbr.2016.09.067

Matsumoto, N., Kitanishi, T., and Mizuseki, K. (2019). The subiculum: unique hippocampal hub and more. *Neurosci. Res.* 143, 1–12.

Opendak, M., and Gould, E. (2015). Adult neurogenesis: a substrate for experience-dependent change[J]. *Trends Cogn. Sci.* 19, 151–161. doi: 10.1016/j.tics.2015.01.001

Pani, J., Reitlo, L. S., Evensmoen, H. R., Lydersen, S., Wisløff, U., Stensvold, D., et al. (2021). Effect of 5 years of exercise intervention at different intensities on brain structure in older adults from the general population: a generation 100 substudy. *Clin. Interv. Aging* 16, 1485–1501. doi: 10.2147/CIA.S318679

Panza, F., Lozupone, M., Solfrizzi, V., Sardone, R., Dibello, V., di Lena, L., et al. (2018). Different cognitive frailty models and health-and cognitive-related outcomes in older age: from epidemiology to prevention[J]. *J. Alzheimers Dis.* 62, 993–1012. doi: 10.3233/JAD-170963

Pereira, A. C., Huddleston, D. E., Brickman, A. M., Sosunov, A. A., Hen, R., McKhann, G. M., et al. (2007). An in vivo correlate of exercise-induced neurogenesis in the adult dentate gyrus. *Proc. Natl. Acad. Sci. U. S. A.* 104, 5638–5643. doi: 10.1073/pnas.0611721104

Rolfson, D. B., Majumdar, S. R., Tsuyuki, R. T., Tahir, A., and Rockwood, K. (2006). Validity and reliability of the Edmonton frail scale[J]. *Age Ageing* 35, 526–529. doi: 10.1093/ageing/afl041

Sammons, R. P., Parthier, D., Stumpf, A., and Schmitz, D. (2019). Electrophysiological and molecular characterization of the *Parasubiculum*[J]. *J. Neurosci.* 39, 8860–8876. doi: 10.1523/JNEUROSCI.0796-19.2019

Saygin, Z. M., Kliemann, D., Iglesias, J. E., van der Kouwe, A., Boyd, E., Reuter, M., et al. (2017). High-resolution magnetic resonance imaging reveals nuclei of the human amygdala: manual segmentation to automatic atlas[J]. *NeuroImage* 155, 370–382. doi: 10.1016/j.neuroimage.2017.04.046

Schlichting, M. L., Zeithamova, D., and Preston, A. R. (2014). CA1 subfield contributions to memory integration and inference[J]. *Hippocampus* 24, 1248–1260. doi: 10.1002/hipo.22310

Sugimoto, T., Arai, H., and Sakurai, T. (2022). An update on cognitive frailty: its definition, impact, associated factors and underlying mechanisms, and interventions. *Geriatr. Gerontol. Int.* 22, 99–109. doi: 10.1111/ggi.14322

Tanaka, K. Z., He, H., Tomar, A., Niisato, K., Huang, A. J. Y., and McHugh, T. J. (2018). The hippocampal engram maps experience but not place[J]. *Science* 361, 392–397. doi: 10.1126/science.aat5397

Tang, Q., Burgalossi, A., Ebbesen, C. L., Sanguinetti-Scheck, J. I., Schmidt, H., Tukker, J. J., et al. (2016). Functional architecture of the rat Parasubiculum[J]. *J. Neurosci.* 36, 2289–2301. doi: 10.1523/JNEUROSCI.3749-15.2016

Tao, J., Liu, J., Egorova, N., Chen, X., Sun, S., Xue, X., et al. (2016). Increased hippocampus-medial prefrontal cortex resting-state functional connectivity and memory function after tai chi Chuan practice in elder adults[J]. *Front. Aging Neurosci.* 8:25. doi: 10.3389/fnagi.2016.00025

Tao, J., Liu, J., Liu, W., Huang, J., Xue, X., Chen, X., et al. (2017). Tai chi Chuan and Baduanjin increase Grey matter volume in older adults: a brain imaging study[J]. *J. Alzheimers Dis.* 60, 389–400. doi: 10.3233/JAD-170477

Tsuchida, R., Yamaguchi, T., Funabashi, D., et al. (2022). Exercise type influences the effect of an acute bout of exercise on hippocampal neuronal activation in mice. *Neurosci. Lett.* 13:136707

Tuncdemir, S. N., Lacefield, C. O., and Hen, R. (2019). Contributions of adult neurogenesis to dentate gyrus network activity and computations. *Behav. Brain Res.* 18:112112

Venegas-Sanabria, L. C., Cavero-Redondo, I., Martínez-Vizcaino, V., Cano-Gutierrez, C. A., and Álvarez-Bueno, C. (2022). Effect of multicomponent exercise in cognitive impairment: a systematic review and meta-analysis. *BMC Geriatr.* 22:617.

Wan, M., Xia, R., Lin, H., Qiu, P., He, J., Ye, Y., et al. (2020). Volumetric and diffusion abnormalities in subcortical nuclei of older adults with cognitive frailty[J]. *Front. Aging Neurosci.* 12:202. doi: 10.3389/fnagi.2020.00202

Wan, M., Ye, Y., Lin, H., Xu, Y., Liang, S., Xia, R., et al. (2020). Deviations in hippocampal subregion in older adults with cognitive frailty[J]. *Front. Aging Neurosci.* 12:615852. doi: 10.3389/fnagi.2020.615852

Wang, X., Yu, Y., Zhao, W., Li, Q., Li, X., Li, S., et al. (2018). Altered whole-brain structural covariance of the hippocampal subfields in subcortical vascular mild cognitive impairment and amnestic mild cognitive impairment patients[J]. *Front. Neurol.* 9:342. doi: 10.3389/fneur.2018.00342

Wang, X., Wu, J., Ye, M., Wang, L., and Zheng, G. (2021). Effect of Baduanjin exercise on the cognitive function of middle-aged and older adults: a systematic review and meta-analysis.[J]. *Complement. Ther. Med.* 59:102727. doi: 10.1016/j.ctim.2021.102727

Won, J., Callow, D. D., Pena, G. S., Gogniat, M. A., Kommula, Y., Arnold-Nedimala, N. A., et al. (2021). Evidence for exercise-related plasticity in functional and structural neural network connectivity. *Neurosci. Biobehav. Rev.* 131, 923–940. doi: 10.1016/j.neubiorev.2021.10.013

Woodward, M. L., Gicas, K. M., Warburton, D. E., White, R. F., Rauscher, A., Leonova, O., et al. (2018). Hippocampal volume and vasculature before and after exercise in treatment-resistant schizophrenia[J]. *Schizophr. Res.* 202, 158–165. doi: 10.1016/j.schres.2018.06.054

Xia, R., Qiu, P., Lin, H., Ye, B., Wan, M., Li, M., et al. (2019). The effect of traditional Chinese mind-body exercise (Baduanjin) and brisk walking on the dorsal attention network in older adults with mild cognitive impairment.[J]. *Front. Psychol.* 10:2075. doi: 10.3389/fpsyg.2019.02075

Xia, R., Wan, M., Lin, H., Qiu, P., Ye, Y., He, J., et al. (2020). Effects of a traditional Chinese mind-body exercise, Baduanjin, on the physical and cognitive functions in the community of older adults with cognitive frailty: study protocol for a randomised controlled trial[J]. *BMJ Open* 10:e34965. doi: 10.1136/bmjopen-2019-034965

Zhang, X., Zong, B., Zhao, W., and Li, L. (2021). Effects of mind-body exercise on brain structure and function: a systematic review on MRI studies[J]. *Brain Sci.* 11:205. doi: 10.3390/brainsci11020205

Zheng, F., Cui, D., Zhang, L., Zhang, S., Zhao, Y., Liu, X., et al. (2018). The volume of hippocampal subfields in relation to decline of memory recall across the adult lifespan[J]. *Front. Aging Neurosci.* 10:320. doi: 10.3389/fnagi.2018.00320

Zheng, G., Huang, M., Li, S., Li, M., Xia, R., Zhou, W., et al. (2016). Effect of Baduanjin exercise on cognitive function in older adults with mild cognitive impairment: study protocol for a randomised controlled trial[J]. *BMJ Open* 6:e10602. doi: 10.1136/bmjopen-2015-010602

Zheng, G., Ye, B., Xia, R., Qiu, P., Li, M., Zheng, Y., et al. (2021). Traditional Chinese mind-body exercise Baduanjin modulate Gray matter and cognitive function in older adults with mild cognitive impairment: a brain imaging study.[J]. *Brain Plast.* 7, 131–142. doi: 10.3233/BPL-210121

Zou, L., SasaKi, J., Wang, H., Xiao, Z., Fang, Q., and Zhang, M. (2017). A systematic review and meta-analysis of Baduanjin qigong for health benefits: randomized controlled trials[J]. *Evid. Based Complement. Alternat. Med.* 2017, 4548706–4548717. doi: 10.1155/2017/4548706

frontiers | Frontiers in Pharmacology

TYPE Review
PUBLISHED 22 December 2022
DOI 10.3389/fphar.2022.1094351

OPEN ACCESS

EDITED BY
Woon-Man Kung,
Chinese Culture University, Taiwan

REVIEWED BY
Yoana Rabanal,
University of Castilla-La Mancha, Spain
Chengfu Su,
Henan University of Chinese Medicine, China

*CORRESPONDENCE
T. Tamilanban,
tamilant@srmist.edu.in
Gobinath Ramachawolran,
r.gobinath@rcsiucd.edu.my
Ling Shing Wong,
lingshing.wong@newinti.edu.my
Mahendran Sekar,
mahendransekar@unikl.edu.my

†These authors have contributed equally to this work

SPECIALTY SECTION
This article was submitted to Neuropharmacology, a section of the journal Frontiers in Pharmacology

RECEIVED 10 November 2022
ACCEPTED 12 December 2022
PUBLISHED 22 December 2022

CITATION
Subramanian A, Tamilanban T, Alsayari A, Ramachawolran G, Wong LS, Sekar M, Gan SH, Subramaniyan V, Chinni SV, Izzati Mat Rani NN, Suryadevara N and Wahab S (2022), Trilateral association of autophagy, mTOR and Alzheimer's disease: Potential pathway in the development for Alzheimer's disease therapy. *Front. Pharmacol.* 13:1094351. doi: 10.3389/fphar.2022.1094351

Trilateral association of autophagy, mTOR and Alzheimer's disease: Potential pathway in the development for Alzheimer's disease therapy

Arunkumar Subramanian[1†], T. Tamilanban[1*†], Abdulrhman Alsayari[2,3], Gobinath Ramachawolran[4*], Ling Shing Wong[5*], Mahendran Sekar[6*†], Siew Hua Gan[7], Vetriselvan Subramaniyan[8], Suresh V. Chinni[9,10], Nur Najihah Izzati Mat Rani[11], Nagaraja Suryadevara[8] and Shadma Wahab[2,3]

[1]Department of Pharmacology, SRM College of Pharmacy, SRM Institute of Science and Technology, Chengalpattu, Tamilnadu, India, [2]Department of Pharmacognosy, College of Pharmacy, King Khalid University, Abha, Saudi Arabia, [3]Complementary and Alternative Medicine Unit, King Khalid University, Abha, Saudi Arabia, [4]Department of Foundation, RCSI & UCD Malaysia Campus, Georgetown, Pulau Pinang, Malaysia, [5]Faculty of Health and Life Sciences, INTI International University, Nilai, Malaysia, [6]Department of Pharmaceutical Chemistry, Faculty of Pharmacy and Health Sciences, Royal College of Medicine Perak, Universiti Kuala Lumpur, Ipoh, Perak, Malaysia, [7]School of Pharmacy, Monash University Malaysia, Bandar Sunway, Selangor, Malaysia, [8]Faculty of Medicine, Bioscience and Nursing, MAHSA University, Bandar Saujana Putra, Selangor, Malaysia, [9]Department of Biochemistry, Faculty of Medicine, Bioscience, and Nursing, MAHSA University, Bandar Saujana Putra, Selangor, Malaysia, [10]Department of Periodontics, Saveetha Dental College and Hospitals, Saveetha Institute of Medical and Technical Sciences, Chennai, India, [11]Faculty of Pharmacy and Health Sciences, Royal College of Medicine Perak, Universiti Kuala Lumpur, Ipoh, Perak, Malaysia

The primary and considerable weakening event affecting elderly individuals is age-dependent cognitive decline and dementia. Alzheimer's disease (AD) is the chief cause of progressive dementia, and it is characterized by irreparable loss of cognitive abilities, forming senile plaques having Amyloid Beta (Aβ) aggregates and neurofibrillary tangles with considerable amounts of tau in affected hippocampus and cortex regions of human brains. AD affects millions of people worldwide, and the count is showing an increasing trend. Therefore, it is crucial to understand the underlying mechanisms at molecular levels to generate novel insights into the pathogenesis of AD and other cognitive deficits. A growing body of evidence elicits the regulatory relationship between the mammalian target of rapamycin (mTOR) signaling pathway and AD. In addition, the role of autophagy, a systematic degradation, and recycling of cellular components like accumulated proteins and damaged organelles in AD, is also pivotal. The present review describes different mechanisms and signaling regulations highlighting the trilateral association of autophagy, the mTOR pathway, and AD with a description of inhibiting drugs/molecules of mTOR, a strategic target in AD. Downregulation of mTOR signaling triggers autophagy activation, degrading the misfolded proteins and preventing the further accumulation of misfolded proteins that inhibit the progression of AD.

10.3389/fphar.2022.1094351

Other target mechanisms such as autophagosome maturation, and autophagy-lysosomal pathway, may initiate a faulty autophagy process resulting in senile plaques due to defective lysosomal acidification and alteration in lysosomal pH. Hence, the strong link between mTOR and autophagy can be explored further as a potential mechanism for AD therapy.

KEYWORDS

Alzheimer's disease, mTOR pathway, dementia, autophagy, tau protein

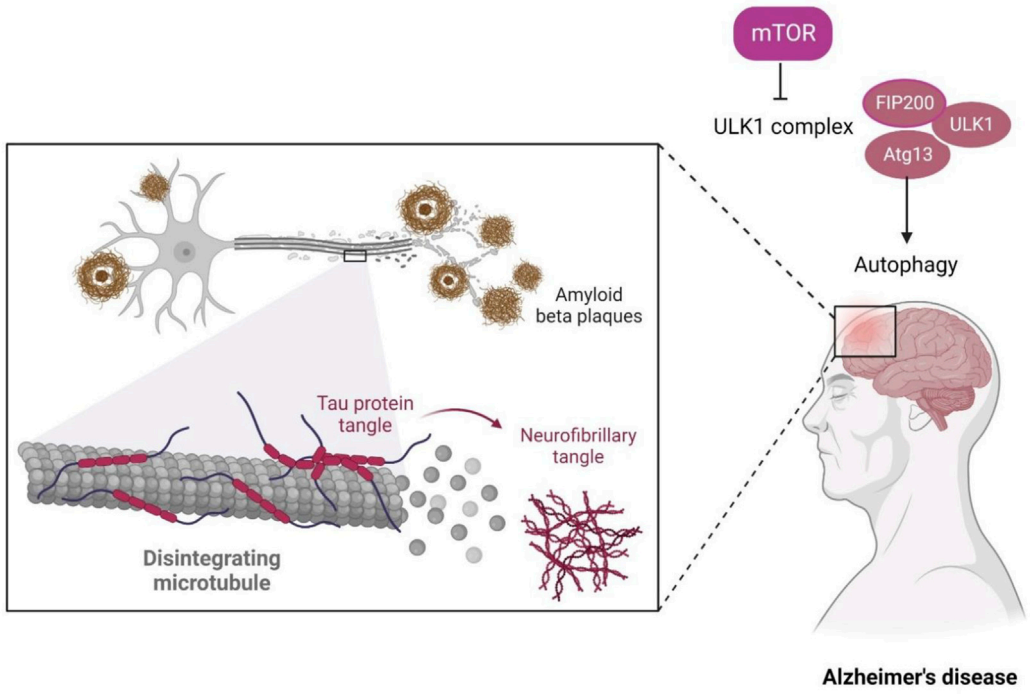

GRAPHICAL ABSTRACT

1 Introduction

Many individuals above 65 years of age tend to suffer from a general progressive neurodegenerative disorder called Alzheimer's disease (AD) (Scheltens et al., 2016). The disorder includes the formation of amyloid-β peptide (Aβ) aggregates as a result of proteolytic processing of the amyloid precursor protein (APP) and, to date, has no effective treatment (Oddo et al., 2006). Age is the prime risk factor for the progression of AD, the prevalent type of dementia spreading across the world, where 40 million individuals are affected (Selkoe and Hardy, 2016), and the count is expected to triple by 2050 (Galvan and Hart, 2016).

In terms of genetics, AD-inherited patients show the presence of a mutated amyloid precursor protein (APP) gene with an autosomal dominant trait and mutated presenilin genes. Clinically, AD is also illustrated by cognitive impairment, overproduction of Aβ aggregates, and tau protein's hyper-phosphorylation in many basic research studies. AD is a gradually progressive neurodegenerative disease prominently consisting of 1) neuritic senile plaques and neurofibrillary tangles (NFT) (Figure 1) 2) shrinkage of the hippocampus region, resulting in the accumulation of Aβ aggregates in the medial temporal lobe, and 3) neocortical structures of the affected human brain (De-Paula et al., 2012).

AD, an essential type of dementia, mainly affects various brain functions like behavior, thinking, and memory. These symptoms, in due course, increase the worsening of daily activities. Memory is lost when 1) crucial meetings are

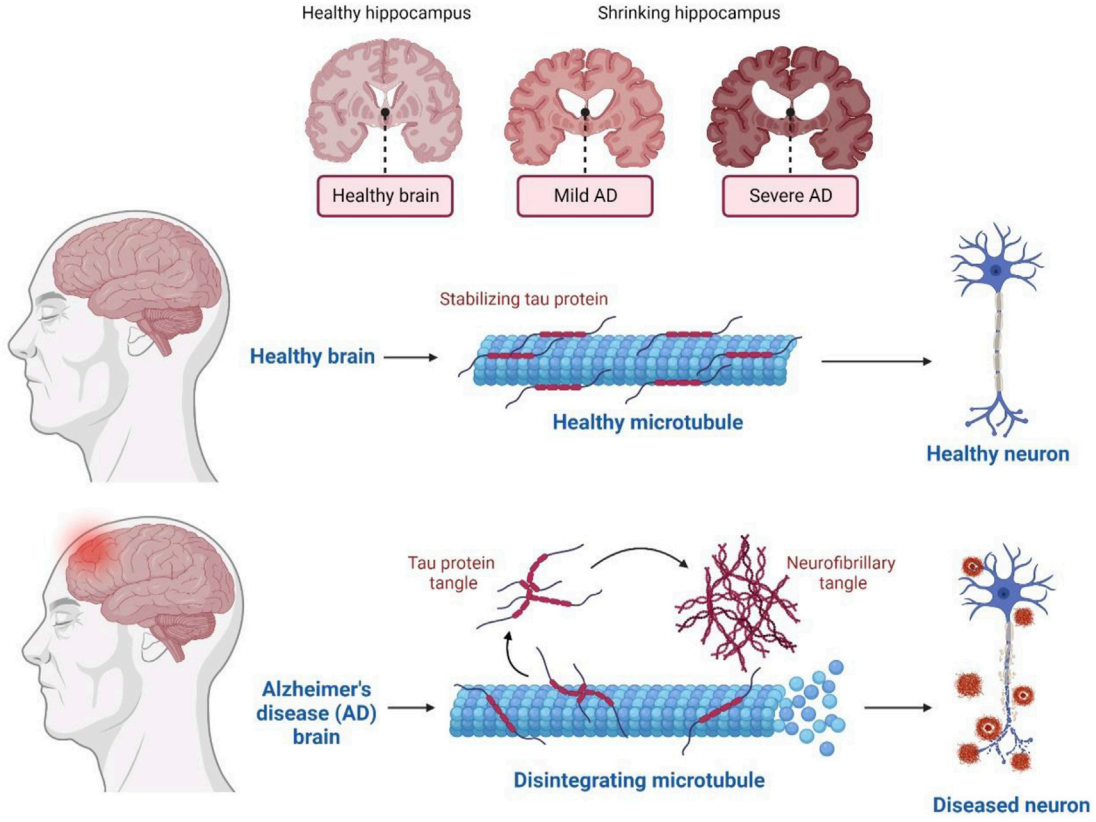

FIGURE 1
Physiological structure in Healthy and AD human Brain.

forgotten, 2) familiar tasks such as cooking, driving, writing, and speaking are disoriented, and 3) varied mood swings and withdrawal from relations and family happens (Breijyeh and Karaman, 2020). In addition, many risk factors are correlated with AD, making it a multifactorial disease (Figure 2).

Autophagy, defined as "self-eating," is a self and systematic degradable process occurring within the cell for recycling cellular components like protein aggregates, misfolded proteins, and unwanted cell organelles (Glick et al., 2010; Fornai and Puglisi-Allegra, 2021). Recent studies on AD mainly focus on autophagy's contribution to its pathology (Leidal et al., 2018; Aman et al., 2021; Pang et al., 2022). Like other cells, neurons can gather toxic substances/organelles during senescence and require autophagy activation to maintain cell homeostasis (Mariño et al., 2011).

A recent study reported that autophagy-related genes, namely ATG18, ATG8a, and ATG1 in *Drosophila melanogaster* insect model, are down-regulated with age and neuron dysfunction (Zhang et al., 2013). The autophagic flux represents the complete dynamic steps of autophagy including autophagosome formation, maturation, fusion with lysosomes, and subsequent breakdown, followed by the release of macromolecules back into the cytosol (Klionsky, 2008). The autophagy pathway includes releasing various factors, proteins, and signaling molecules. It is associated with other signaling pathways like adenosine monophosphate protein kinase (AMPK), Mammalian target of rapamycin (mTOR), and insulin signaling. The pictorial representation of the autophagy pathway in *Homo sapiens* retrieved from the Kyoto Encyclopedia of Genes and Genomes (KEGG) pathway database is shown in Figure 3 (Kanehisa, 2000).

AD worsens with aging, expressing its symptoms and affecting many brain functions, among which cognitive dysfunction (loss of synapses) and memory loss are prominent (Scheltens et al., 2016). In AD, extracellular senile plaques have amyloid beta particles and intraneural NFT, constituting the major part of aggregated MAPT/Tau protein (Loera-Valencia et al., 2019). The focus on the defects of autophagic flux in AD will not only update the current monitoring methods but also provide visions for developing autophagy-related therapeutics for treating the disease. Through the mTOR signaling, beta-amyloid (Aβ) peptides are accumulated by altering APP metabolism and upregulating β and γ secretases while the mTOR inhibits autophagy function.

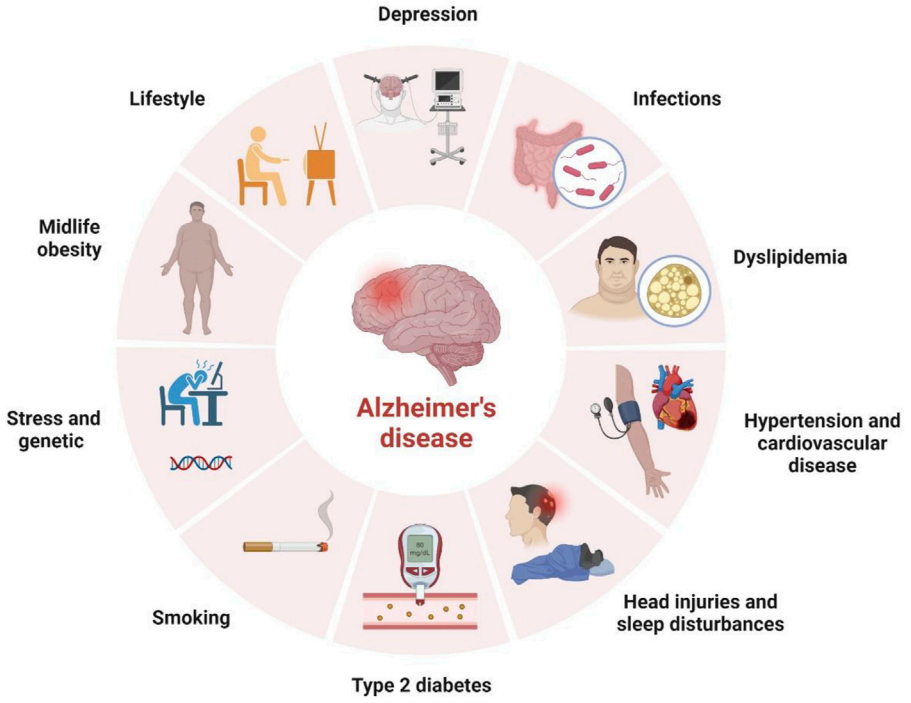

FIGURE 2
Risk factors of Alzheimer's Disease.

Moreover, dysregulation of mTOR is allied with many human diseases, like cancer and neurological and metabolic diseases (Chong et al., 2010; Dazert and Hall, 2011; Meng et al., 2013), with more focus now shown on mTOR's role in the AD's pathology.

The mTOR is a member of the phosphoinositide-3-kinase-related family with conserved Ser/Thr protein kinase and can respond to environmental stimuli like nutrient concentration, energy state, and growth factors (Yoon, 2017). mTOR is significant for cell growth, metabolism, proliferation, protein translation, and autophagy. Several studies on AD pathology are supported by ample evidence, stressing the association between AD and mTOR signaling (Wang et al., 2014a). The present review is on the divergent mechanistic regulations of autophagy and mTOR proteins, the available inhibitors for mTOR, and how all these combined factors apply to AD's treatment.

2 The role of autophagy in Alzheimer's disease

Autophagy is a highly conserved pathway for degrading long-lived intracellular proteins, protein aggregates, and organelles (e.g., mitochondrial) *via* lysosomes to maintain homeostasis under physiological conditions (Dikic and Elazar, 2018). Many studies have reported that altered autophagy is directly related to multiple chronic diseases, including AD. Inducing autophagy may therefore result in the removal of Aβ accumulations (Zhang et al., 2022) providing a beneficial effect in preclinical AD models, indicating that autophagy is a reliable tool for developing therapeutic compounds for AD treatment (Figure 4). Moreover, chaperone-mediated autophagy and mitophagy have also been associated with AD (Cuervo and Wong, 2014; Kerr et al., 2017).

The body of scientific evidence suggests the impact of defective mitophagy in the aggregation of faulty autophagosomal vacuoles. Calcium ion imbalance, altered pH, and increased oxidative stress play an important role in this faulty mitochondrial dysfunction mechanism leading to AD progression (Nixon et al., 2008; Nixon, 2013; Medina et al., 2015). Ashrafi et al. (2015) claimed the involvement of PINK1 and PARK2 genes in mitochondrial health maintenance. Mutations occurring in these genes may result in an impaired mitophagy process leading to the clustering of defective autophagosomal vacuoles (Ashrafi and Schwarz, 2015). Another study proposed that mutations in the PSEN1 gene might induce an altered autophagy/mitophagy pathway. This mutation can lead to reduced lysosomal hydrolase activity accelerating the lysosome alkalization resulting in AD (Coffey et al., 2014).

Alteration of the autophagy-lysosome pathway contributes to APP (Torres et al., 2012) and APP-CTFb degradation, overall

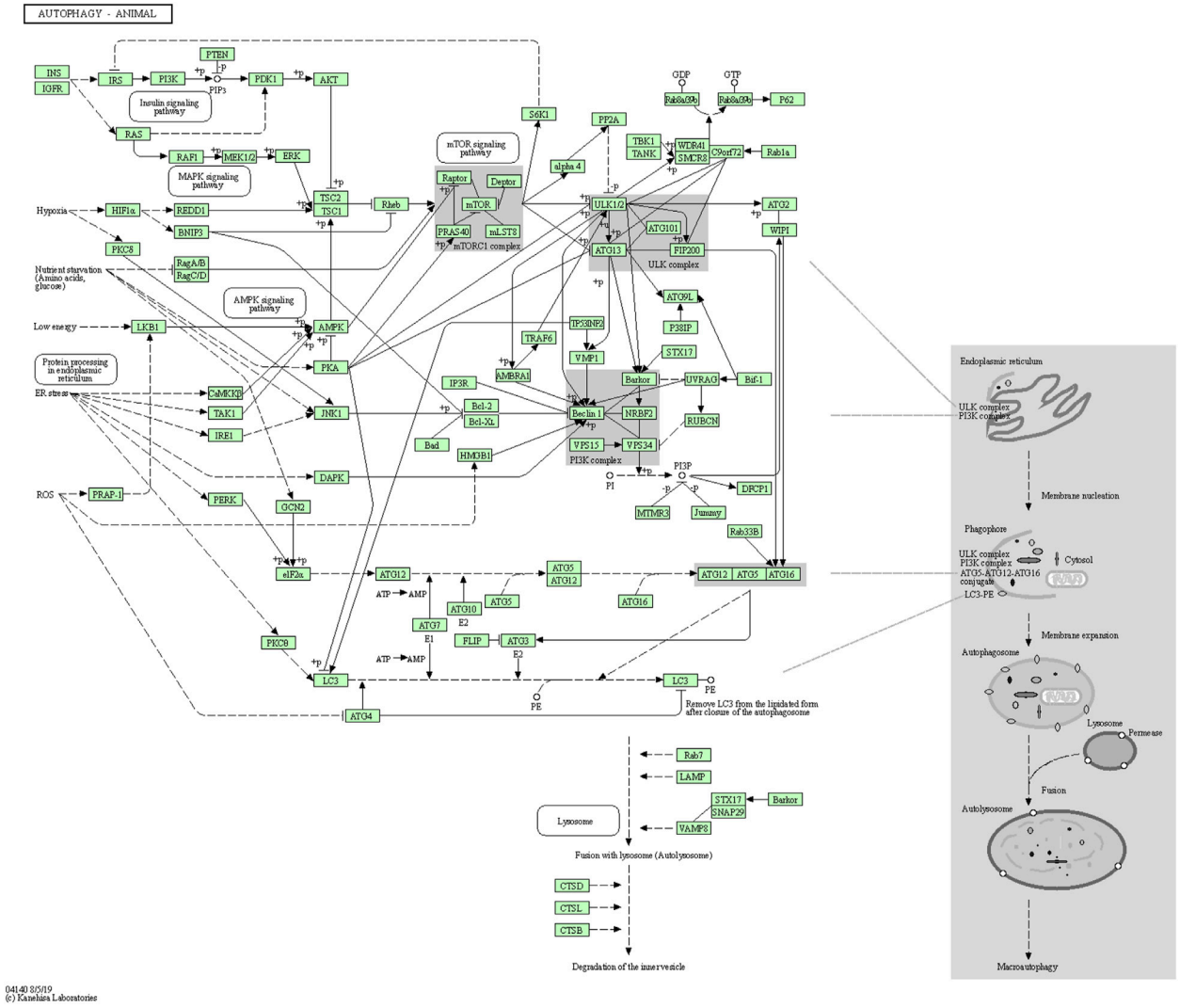

FIGURE 3
Autophagy pathway (KEGG Id: hsa04140), highlighting its association with the mTOR signaling pathway.

leading to Aβ aggregate formation. This step also eventually inhibits MAPT/tau aggregates degradation (Inoue et al., 2012) which further induces neurodegeneration. Autophagy is critical in regulating inflammation, where autophagy inducers can also cause glial cells' autophagy *via* neuron cross-talks (Zhang et al., 2022). Characterization of autophagy-lysosomes impairment in various AD stages, molecules, and genetic types may also pave the way to generate avenues for novel therapeutics.

In another *in vitro* model study, the overexpression of let-7b promoted Aβ1-40 to trigger the phosphatidylinositol-3-kinase (PI3K)/AKT/mTOR pathway in neuroblastoma (SK-N-SH) cells, subsequently inhibiting autophagy and promoting apoptosis (Ji et al., 2006). Some evidence also emphasizes that uncontrolled Aβ accumulations generated more neurotoxicity and progression of AD (Tomiyama et al., 1996). Investigation on Aβ neurotoxicity usually represents SK-N-SH cells and Aβ1-40 as the AD's cell models (Muñoz and Inestrosa, 1999), thus suggesting that age-induced reduction in autophagy-related gene expression is interlinked with AD in the later stages (Pang et al., 2022). In AD cells, the removal of abnormal protein aggregates can be achieved by utilizing autophagy mechanisms (Metcalf et al., 2012).

Lysosomal acidification and the dysregulation of the V-ATPase complex are common metabolic interruptions associated with AD (Ward et al., 2016) (Colacurcio and Nixon, 2016). But, recent study findings reveal the defective acidification of autolysosomes may induce faulty autophagic build-up of Aβ in neurons (Lee et al., 2022). Therefore, autophagy-stimulating agents/drugs, like mTOR inhibition, remain a potential therapeutic agent for AD without altering the autophagy-lysosomal pathway.

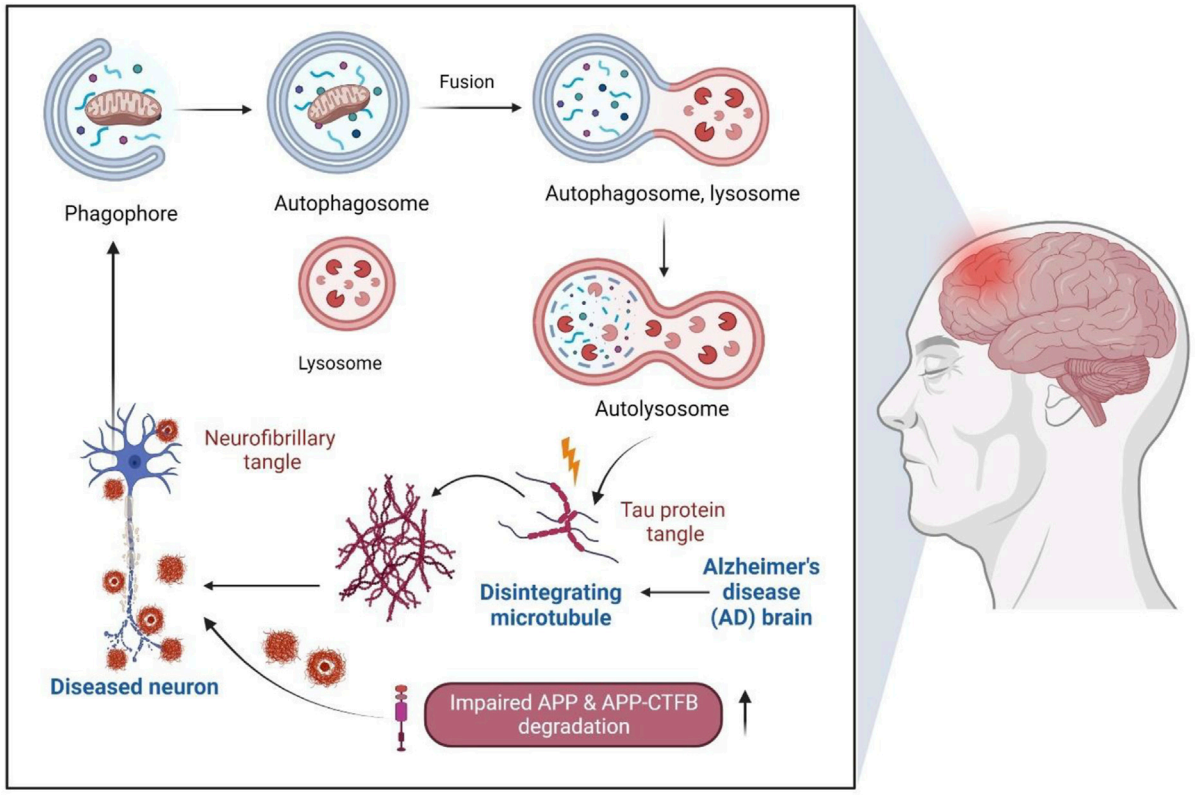

FIGURE 4
Dysfunction of autophagy-lysosome pathway in AD

3 Dysregulation of mTOR pathway in AD conditions

mTOR is a 289-kD Ser/Thr multidomain protein with an FKBP12 binding and kinase domain which controls many physiological processes. mTOR coordinates the upstream signaling components such as glycogen synthase kinase 3 (GSK-3), growth factors, insulin, AMPK, and PI-3K/Akt (Ferrer et al., 2002; Griffin et al., 2005; Kaper et al., 2006; Gouras, 2013). AD pathogenesis depends on both the down- and upstream regions of mTOR signaling (Cai et al., 2015). Several research studies have highlighted the dysregulation of the mTOR pathway in other diseases like cancer and diabetes (Hsieh and Edlind, 2014) (Habib and Liang, 2014), cardiovascular disease (Chong et al., 2011; Yang and Ming, 2012), aging (Gharibi et al., 2014; Yang et al., 2014), neurodegenerative diseases (Jiang et al., 2013; Sarkar, 2013) as well as obesity (Martínez-Martínez et al., 2014). In fact, some reports stated that mTOR activation contributes to AD progression and interferes with the clinical manifestation and AD pathology (Paccalin et al., 2006; Ma et al., 2010).

Hyperactivated mTOR, the able cause of AD, is regulated with various upstream signaling cascades like GSK3, AMPK (PI3-K)/Akt, and IGF-1. It is also observed that many diseases like mitochondrial dysfunction, auto-immunity, and cancer affect these pathways, causing uncontrolled stimulation of mTOR and leading to tau protein hyperphosphorylation. The phenomenon leads to the formation of NFTs and paired helical filaments (PHFs), the characteristic symptom of AD. Additionally, Aβ plaques are also formed due to the direct inhibition of autophagy by mTOR activation, which induces tau protein hyperphosphorylation and mTOR activities, thus enhancing the advancement of AD (Mueed et al., 2019).

Furthermore, it was reported that mitochondrial and nuclear DNA oxidation in AD brains occur with increased levels of 8-oxo-2-dehydroguaninie, 5-hydroxyuracil, and 8-hydroxyadenine in temporal, frontal, and parietal lobes of AD brains (Santos et al., 2012; Perluigi et al., 2021). Likewise, in hippocampus regions of AD brains, heavy levels of 8-hydroxyguanine were also reported (Lovell and Markesbery, 2007; Siman et al., 2015) investigated the selective expression and toxicity of diseased tau by a viral vector approach in the mouse lateral perforant pathway to understanding the activity of rapamycin and its neuroprotective effect. Rapamycin was found to simultaneously inhibit mTOR protein kinase and stimulates autophagy (Siman et al., 2015). The study's qualitative and

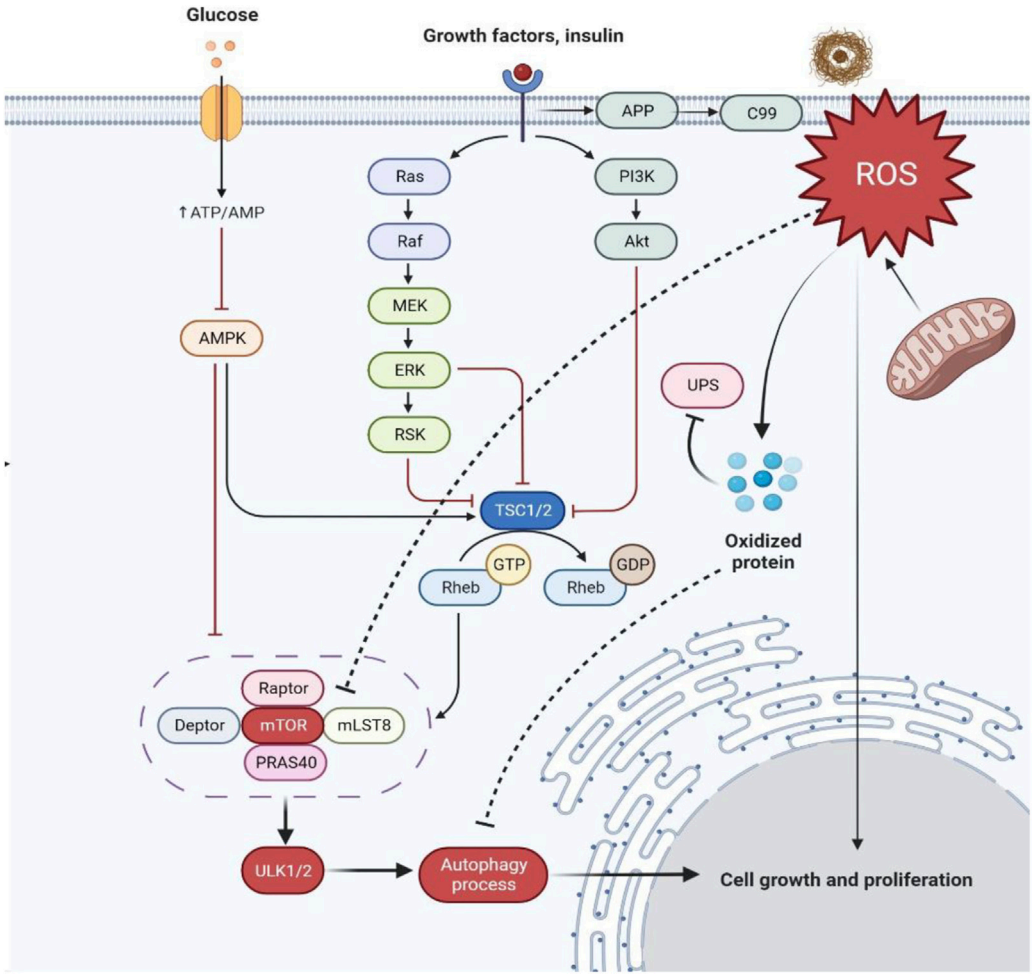

FIGURE 5
Schematic representation of hyperactivation of mTOR in AD dysregulating insulin signaling and producing more oxidized proteins. Abbreviations: APP, Amyloid precursor protein; ROS, Reactive oxygen species; UPS, Ubiquitin-proteasome system; P13K, Phosphatidylinositol 3-kinase; Akt, Ak strain transforming; Ras, Rat sarcoma; Raf, Rapidly accelerated fibrosarcoma; MEK, Mitogen-activated protein kinase; ERK, Extracellular signal-regulated kinase; RSK, Ribosomal S6 kinase; TSC1/2, Tuberous sclerosis proteins 1/2; GTP, Rheb, Ras homolog enriched in the brain; GDP, Guanosine diphosphate; mTOR, Mammalian target of rapamycin; mLST8, Mammalian lethal with SEC13 protein eight; PRAS40, Proline-rich AKT substrate of 40 kDa; ULK1/2, Unc-51 like autophagy activating kinase; AMPK, AMP-activated protein kinase; ATP/AMP, Adenosine triphosphate/adenosine monophosphate.

quantitative histological findings and morphometric methods revealed a significant reduction in the disease's symptomatic effects of tau in the perforant pathway upon chronic systematic rapamycin treatment. Henceforth, the progression in the early stages of AD can be addressed by lowering the tau toxicity effect (Figure 5).

Under controlled conditions, decreased levels of free radical or reactive oxygen species (ROS) and Aβ aggregates coordinate stress responses like ubiquitin protease system (UPS), autophagy, and unfolded protein response (UPR) and remove damaged cell organelles and other compounds. Under diseased conditions, ROS are overproduced for the control of protein quality leading to the formation of more oxidized proteins because of protein dysfunction and also leading to the dysregulation of insulin signaling (Tramutola et al., 2015; Höhn et al., 2020).

4 Trilateral association between autophagy, mTOR signaling, and Alzheimer's disease

During the persistent circumstance of AD pathology, the mechanistic target of rapamycin complex (mTORC1) regulation is lost, resulting in aggregate formation inside the cell. Indeed, the levels of eukaryotic Initiative Factor 4E (eIF4E) (Li et al., 2005), phosphorylated eukaryotic translation initiation factor 4E-binding

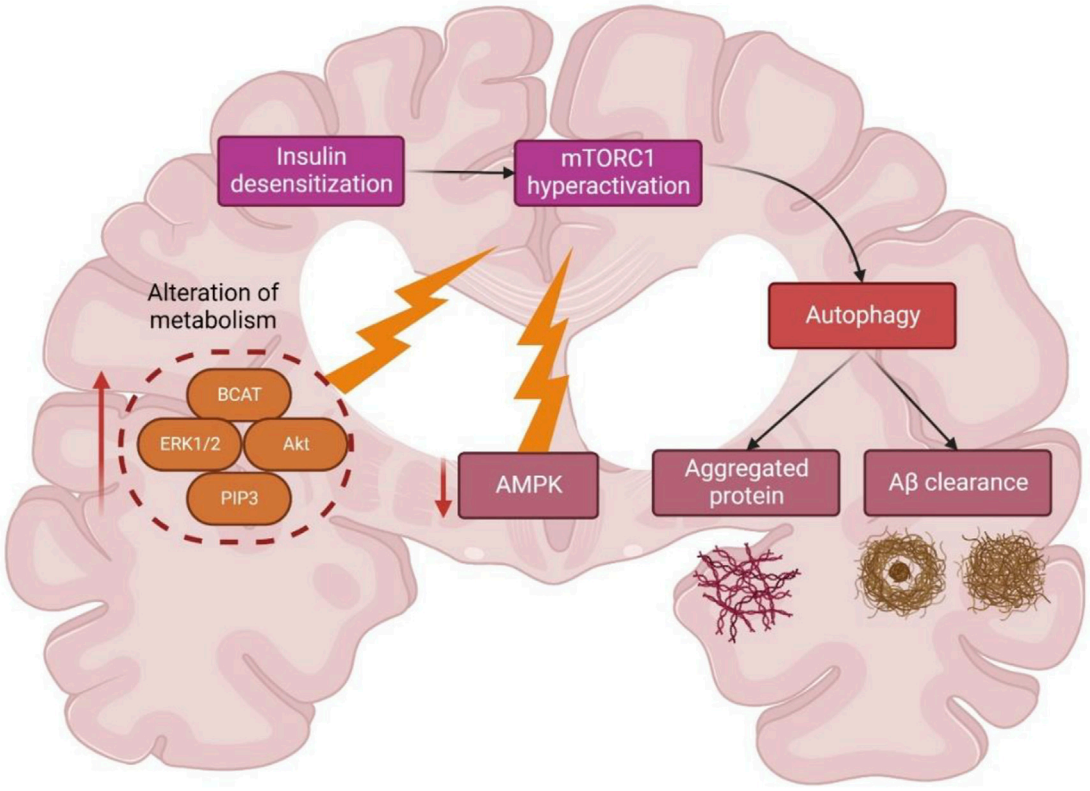

FIGURE 6
Schematic representation of different metabolic regulations of autophagy and mTOR in Alzheimer's disease. Abbreviations: BCAT, Branched-chain amino acid aminotransferase; ERK1/2; extracellular signal-regulated kinase 1/2; Akt, Ak strain transforming; PIP3, Phosphatidylinositol (3,4,5)-trisphosphate; AMPK, AMP-activated protein kinase; mTORC1, mammalian target of rapamycin complex 1.

protein 1 (4EBP1) (Li et al., 2005), ribosomal protein S6 kinase beta-1 (p70S6K) (Sun et al., 2013), Akt activation (Griffin et al., 2005) and mTOR phosphorylation (at Ser248) are considerably increased in AD-affected brains. These alterations correlate with Braak staging and tau pathology resulting in protein translation disorder. The cognitive decline during AD and mTOR hyperactivation co-exists (Caccamo et al., 2010; Sun et al., 2013). In addition, the levels of phosphate and tensin homologue (PTEN) immunoreactive neurons are decreased in the temporal cortex and hippocampus regions of AD-affected brains showing a negative correlation with senile plaque and NFT formations (Griffin et al., 2005).

The PI3K/Akt signaling is attenuated by PTEN, followed by the dephosphorylation of phosphatidylinositol-3,4,5-triphosphate (PIP3), resulting in the Akt signal hyper-activation to trigger the mTORC1 activity further. This phenomenon leads to the inhibition of autophagy, contributing to Aβ clearance. However, the chances of insulin desensitization need to be checked, which further interrupts Akt activation, as reported in the post-mortem AD brain (Shafei et al., 2017).

Insulin activation of mTORC1 triggers the extracellular signal-regulated kinases $(ERK)_{1/2}$ pathway, which is upregulated in AD brain and cell models (Morales-Corraliza et al., 2016). During AD, Aβ aggregates worsened mTORC1 signaling due to 40 kDa proline-rich Akt substrate phosphorylation (PRAS40), leading to mTORC1 activity enhancement and autophagy inhibition (Caccamo et al., 2011; Tramutola et al., 2015) (Figure 6). A study (Caccamo et al., 2010) showed the significance of future targets for neuron health regulation by using drug molecules like rapamycin which can inhibit mTOR and induce autophagy by alleviating the accumulation of Aβ peptides. Nevertheless, the mTORC1 upstream region is interlinked with other mechanisms like glucose metabolism, insulin resistance, and AD pathology, thus complicating further studies (Shafei et al., 2017).

In the brains affected with AD, autophagy's function is altered, leading to the deposition of many toxic proteins. There are many genes, factors, and mechanisms interlinked with the autophagy pathway, which include neuro-

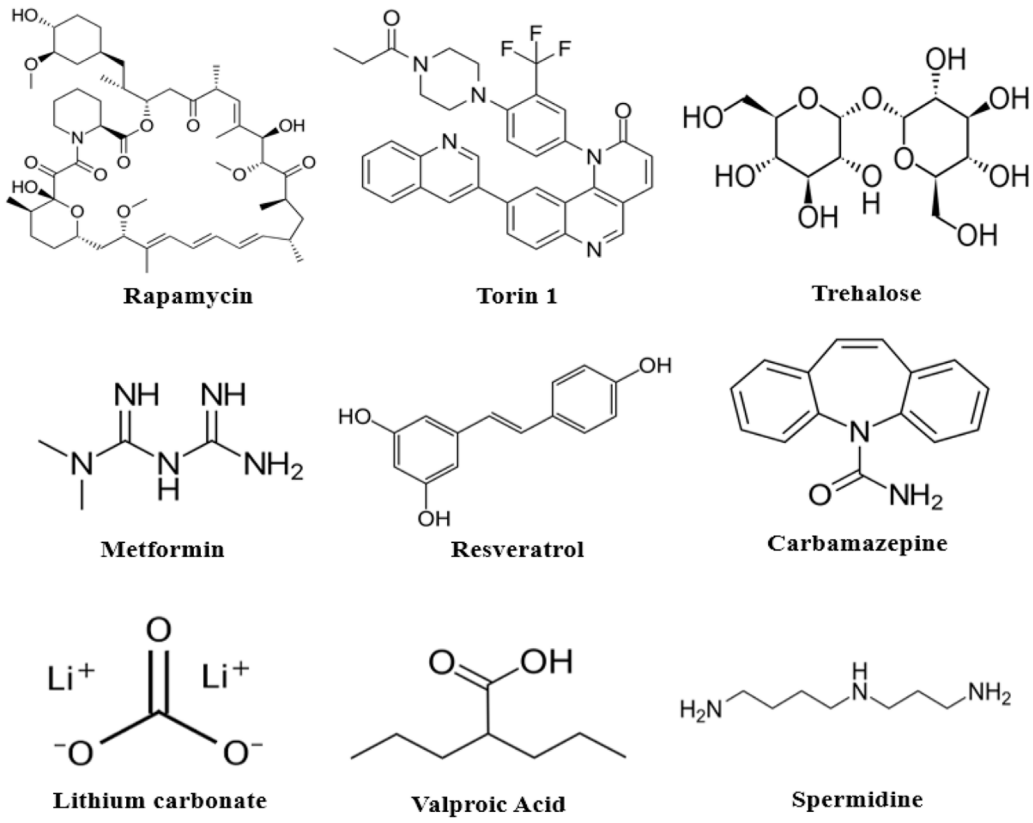

FIGURE 7
Chemical structures of some autophagy-inducing agents.

inflammation, mTOR signaling, the endocannabinoid system, and UCHL1, UBQLN1, SNCA, PSEN1, MAPT, ITPR1, GFAP, FOXO1, CTSD, CLU, CDK5, BECN1, BCL2, ATG7 signaling pathways (Uddin et al., 2018).

Many autophagy inducers or mTOR inhibitors are used for AD treatment. However, there are several autophagy-inducing agents which require validation. For instance, primary mTORC1 inhibitors termed rapalogs are effective in AD models, while secondary compounds like torins have not been verified. The mTORC1 activity will be blocked by these molecules, like ATP-competitive kinase inhibitors (Zheng and Jiang, 2015). The alteration of cell signaling concerning the mTOR pathway may protect neurons and pose a new approach for neurodegenerative disorders.

Most molecules like calpeptin, minoxidil, and BH3 mimetics, which are autophagy-independent and mTOR-dependent, were not examined in AD models (Sarkar, 2013) (Levine et al., 2015) (Pierzynowska et al., 2018). Henceforward, the studies on the mechanism of autophagy induction by these molecules and the side effects are becoming more relevant for AD treatment (Schmukler and Pinkas-Kramarski, 2020).

4.1 Drugs that can suppress/inhibit mTOR

AD has become a globally reported disease with 24 million victims, and the cases are expected to quadruple in due course over the years. Despite the worldwide prevalence, only two types of drug molecules, namely N-methyl D-aspartate (NMDA) antagonists and cholinesterase enzyme inhibitors, have been approved for AD treatment.

Treatment strategies for AD include the use of symptomatic agents such as cholinesterase inhibitors (e.g., donepezil and rivastigmine), disease-modifying therapeutics (e.g., aducanumab and gantenerumab), disease-modifying agents (e.g., lithium and riluzole), chaperone proteins (HSPs), vacuolar sorting protein 35 and several other extracts from natural products (Breijyeh and Karaman, 2020). Many drugs are designed with the function of activating autophagic flux and inhibiting mTOR signaling for AD diagnosis. In recent years, many studies revealed that rapamycin has neuroprotective activity and can act as a pro-autophagy molecule in animal and cell models (Kaeberlein and Galvan, 2019). The toxic nature of various amyloidogenic peptides responds to rapamycin treatment in

TABLE 1 List of some Autophagy inducers/activators that may be useful in AD.

Autophagy inducer	Chemical formula	Inducing pathway	Clinical sign/Nature of the molecule
Rapamycin	$C_{51}H_{79}NO_{13}$	Direct inhibition of mTORC1	Immunosuppressant, anti-fungal, anti-cancer
Metformin	$C_4H_{11}N_5$	Activation of AMPK	Anti-diabetic
Torin1	$C_{35}H_{28}F_3N_5O_2$	Blockade of ATP binding site on mTOR	Anti-cancer
Trehalose	$C_{12}H_{22}O_{11}$	Activation of AMPK	Antioxidant
Resveratrol	$C_{14}H_{12}O_3$	Activation of AMPK; upregulation of ATGs expression	Antioxidant
Lithium carbonate	Li_2CO_3	Inhibition of GSK-3β; Inhibition of the phosphoinositide cycle	Mood stabilizer
Valproic acid	$C_8H_{16}O_2$	Inhibition of the phosphoinositide cycle; inhibition of GSK-3β	Anti-epileptic, mood stabilizer
Spermidine	$C_7H_{19}N_3$	Prevention of beclin 1 cleavage; upregulation of ATGs expression; inhibition of EP300	Natural polyamine
Carbamazepine	$C_{15}H_{12}N_2O$	Inhibition of phosphoinositide cycle; inhibition of GSK-3β	Analgesic, anti-epileptic, mood stabilizer
Apelin	$C_{266}H_{427}N_{95}O_{71}S_2$	Inhibition of the phosphoinositide cycle	Peptide
Tramadol	$C_{16}H_{25}NO_2$	Inhibition of the phosphoinositide cycle	Opioid analgesic
Gemfibrozil	$C_{15}H_{22}O_3$	Inhibition of the phosphoinositide cycle	Fibrate
Salidroside	$C_{14}H_{20}O_7$	Activation of AMPK	Natural glycoside
β-asarone	$C_{12}H_{16}O_3$	Akt—mTOR inhibition	Natural phenylpropanoid
Curcumin	$C_{21}H_{20}O_6$	Inhibition of phosphoinositide/Akt pathway	Antioxidant, Natural polyphenol
Cubebene	$C_{15}H_{24}$	Inhibition of phosphoinositide/Akt pathway	Natural sesquiterpene

neuron cell cultures (Boland et al., 2008; Spilman et al., 2010). Similar positive results were observed in other animal models with parameters like aging, protein misfolding, neurotoxicity, and inheritance leading to neurodegeneration (Malagelada et al., 2010).

Several studies on amyotrophic lateral sclerosis (ALS)-affected patients with lithium conveyed positive results in clinical trials (Fornai et al., 2008), and also, recently, the efficiency of rapamycin in AD-affected patients was validated in randomized placebo-controlled Phase-II clinical trials (Mandrioli et al., 2018). Autophagy, i.e., autophagic flux and its modulation, needs 1) complicated and multifaceted signaling, 2) integration coupling of environmental conditions, and 3) functional cell communications that include differentiation, proliferation, and cytoplasmic homeostasis (Thellung et al., 2019).

Rapamycin, a member of the macrolide class, and its analogs, generally known as rapalogs, are meant for the inhibition of mTOR signaling. The said first-generation mTOR inhibitors like everolimus, rapamycin and temsirolimus bind to the 12-kDa FK506 binding protein (FKBP-12) outside the ATP binding pocket and inhibit the mTORC1 kinase activity, keeping mTORC2 unaltered (Ballou and Lin, 2008).

The drugs acting as autophagy activators can be a novel approach for neural protection by reducing the toxicity levels of misfolded proteins (Thellung et al., 2019). In general, all neurodegenerative disorders show similar pathogenic mechanisms like autophagic flux impairment losing the ability to degrade the neurotoxic oligomers of wrongly folded proteins. Nevertheless, the autophagy process can be pharmacologically activated by hindering the enzymatic activity of mTORC1. Consequently, its autophagy suppressing activity, found in the physiological condition, is lost. Similarly, rapamycin is the first drug that acts pharmacologically by enhancing autophagy inducing neuroprotection, and offering the clearance of oligomers. This step necessitates disease-modifying strategies to trigger the development of new compounds and also the modification of existing drug molecules for better pro-autophagic potentiality.

The rapalogs and rapamycin act as autophagy inducers by stabilizing raptor-mTOR connectivity and inhibiting mTOR stimulation (Lamming et al., 2013). Torin1 and dactolisib can also inhibit mTOR signaling. Other compounds that activate AMPK signaling, like trehalose, metformin, and resveratrol, promote mTOR inactivation and are AMPK-dependent (Figure 7). Furthermore, compounds such as Apelins (Jiang et al., 2020), Tramadol (Soltani et al., 2020), Curcumin (Wang

et al., 2014b; Zhu and Bu, 2017), Cubebene (Li et al., 2019), Gemfibrozil (Luo et al., 2020), β-asarone (Wang et al., 2020) and Salidroside (Rong et al., 2020) promote inhibition of mTOR *via* inhibition of phosphoinositide/Akt pathway.

4.2 Validation of the role of autophagy induction in Alzheimer's disease: Concepts and queries

One of the key considerations in assessing the effect of autophagy induction on AD prevention is that the chemical molecules are non-specific and, therefore, may affect other processes in the cell. Henceforth, to verify and understand the effects and treatment modes of the molecules, the autophagy-inducing agent enhancing autophagy in AD must be demonstrated, on which the therapeutic effect of the said molecule relies on.

Table 1 lists several autophagy inducers and their mechanism of autophagy induction, which acts *via* the direct or indirect inhibition of mTOR (Heras-Sandoval et al., 2020). Few other drugs/molecules were also claimed to induce autophagy, but they may trigger defective autophagy process by modifying the autophagosome formation, autophagosome maturation, and the autophagy-lysosomal pathway *via* faulty lysosomal acidification (Uddin et al., 2019). Another critical challenge is whether the autophagy inducers virtually influence all AD types and whether it must be applied to populations based on the disease stage and the patient genetic history.

Overall, since the combined hypothesis on molecular mechanisms of neuron destruction in various neurodegenerative disorders includes autophagy pathway malfunction leading to oligomer aggregation, analysis of the utilization of pro-autophagic drugs will validate this role further, even in AD conditions. Specifically, existing and novel compounds are under preclinical and clinical trials for the induction of autophagy through oligomer clearance. Besides, many existing drugs will have off-target effects. Hence, there remains the necessity for developing novel assays for detecting autophagic flux in clinical trials of animal and human models.

5 Conclusion

Despite the collection of huge data in the current review on the role of autophagy in AD treatment, the proper functioning of autophagy and the mechanical induction of autophagy by drug compounds is decisive for aging and neurons in a natural way. The defect in the autophagic mechanism of neurons is one of the projecting factors that generate neurodegenerative disorders like AD. Although its therapeutic effect requires further validation studies, and since autophagy is mainly affected in AD, autophagy remains a primary innovation as a new therapeutic target in the form of autophagy inducers.

The Aβ and tau protein metabolism pathways, mTOR signaling, and autophagy's role are significant, including mediating effects in neuro-inflammation and endo-cannabinoid systems, and are tremendously influenced by the autophagy process acting as intermediating agents during AD conditions. Therefore, therapeutic approaches targeting the autophagy mechanism would pave the way for expanding novel strategies for AD management. The new approaches should include therapeutics that inhibit mTOR signaling and induce autophagy without altering the other interconnected mechanisms.

Author contributions

Writing—original draft: AS, TT, GR, LSW, and MS; Conceptualisation: AS, TT, GR, LSW, and MS; Supervision: AS, TT, GR, LSW, and MS; Resources: AS, TT, AA, GR, LSW, MS, SHG, VS, SVC, NNIMR, NS and SW; Data curation: AS, TT, AA, GR, LSW, MS, SHG, VS, SVC, NNIMR, NS and SW; Writing—review and editing: AS, TT, AA, GR, LSW, MS, SHG, VS, SVC, NNIMR, NS and SW. All authors have read and agreed to the published version of the manuscript.

Acknowledgments

The authors appreciation to the Deanship of Scientific Research at King Khalid University for funding this work through Large Groups Project under grant number (RGP.2/58/43). All the authors of this manuscript extend their appreciation to their respective Departments/Universities for successful completion of this study. The figures in this manuscript were created with the support of https://biorender.com under a paid subscription.

Conflict of interest

The authors declare that the research was conducted in the absence of any commercial or financial relationships that could be construed as a potential conflict of interest.

Publisher's note

References

Aman, Y., Schmauck-Medina, T., Hansen, M., Morimoto, R. I., Simon, A. K., Bjedov, I., et al. (2021). Autophagy in healthy aging and disease. *Nat. Aging* 1, 634–650. doi:10.1038/s43587-021-00098-4

Ashrafi, G., and Schwarz, T. L. (2015). PINK1- and PARK2-mediated local mitophagy in distal neuronal axons. *Autophagy* 11, 187–189. doi:10.1080/15548627.2014.996021

Ballou, L. M., and Lin, R. Z. (2008). Rapamycin and mTOR kinase inhibitors. *J. Chem. Biol.* 1, 27–36. doi:10.1007/s12154-008-0003-5

Boland, B., Kumar, A., Lee, S., Platt, F. M., Wegiel, J., Yu, W. H., et al. (2008). Autophagy induction and autophagosome clearance in neurons: Relationship to autophagic pathology in Alzheimer's disease. *J. Neurosci.* 28, 6926–6937. doi:10.1523/JNEUROSCI.0800-08.2008

Breijyeh, Z., and Karaman, R. (2020). Comprehensive review on Alzheimer's disease: Causes and treatment. *Molecules* 25, 5789. doi:10.3390/molecules25245789

Caccamo, A., Majumder, S., Richardson, A., Strong, R., and Oddo, S. (2010). Molecular interplay between mammalian target of rapamycin (mTOR), amyloid-beta, and tau: Effects on cognitive impairments. *J. Biol. Chem.* 285, 13107–13120. doi:10.1074/jbc.M110.100420

Caccamo, A., Maldonado, M. A., Majumder, S., Medina, D. X., Holbein, W., Magrí, A., et al. (2011). Naturally secreted amyloid-β increases mammalian target of rapamycin (mTOR) activity via a PRAS40-mediated mechanism. *J. Biol. Chem.* 286, 8924–8932. doi:10.1074/jbc.M110.180638

Cai, Z., Zhou, Y., Xiao, M., Yan, L.-J., and He, W. (2015). Activation of mTOR: A culprit of alzheimer& rsquo;s disease? *Neuropsychiatr. Dis. Treat.* 1015, 1015–1030. doi:10.2147/NDT.S75717

Chong, Z. Z., Shang, Y. C., and Maiese, K. (2011). Cardiovascular disease and mTOR signaling. *Trends cardiovasc. Med.* 21, 151–155. doi:10.1016/j.tcm.2012.04.005

Chong, Z. Z., Shang, Y. C., Zhang, L., Wang, S., and Maiese, K. (2010). Mammalian target of rapamycin: Hitting the bull's-eye for neurological disorders. *Oxid. Med. Cell. Longev.* 3, 374–391. doi:10.4161/oxim.3.6.14787

Coffey, E. E., Beckel, J. M., Laties, A. M., and Mitchell, C. H. (2014). Lysosomal alkalization and dysfunction in human fibroblasts with the Alzheimer's disease-linked presenilin 1 A246E mutation can be reversed with cAMP. *Neuroscience* 263, 111–124. doi:10.1016/j.neuroscience.2014.01.001

Colacurcio, D. J., and Nixon, R. A. (2016). Disorders of lysosomal acidification—the emerging role of v-ATPase in aging and neurodegenerative disease. *Ageing Res. Rev.* 32, 75–88. doi:10.1016/j.arr.2016.05.004

Cuervo, A. M., and Wong, E. (2014). Chaperone-mediated autophagy: Roles in disease and aging. *Cell Res.* 24, 92–104. doi:10.1038/cr.2013.153

Dazert, E., and Hall, M. N. (2011). mTOR signaling in disease. *Curr. Opin. Cell Biol.* 23, 744–755. doi:10.1016/j.ceb.2011.09.003

De-Paula, V. J., Radanovic, M., Diniz, B. S., and Forlenza, O. V. (2012). *Alzheimer's Dis.*, 329–352. doi:10.1007/978-94-007-5416-4_14

Dikic, I., and Elazar, Z. (2018). Mechanism and medical implications of mammalian autophagy. *Nat. Rev. Mol. Cell Biol.* 19, 349–364. doi:10.1038/s41580-018-0003-4

Ferrer, I., Barrachina, M., and Puig, B. (2002). Glycogen synthase kinase-3 is associated with neuronal and glial hyperphosphorylated tau deposits in Alzheimer's disease, Pick's disease, progressive supranuclear palsy and corticobasal degeneration. *Acta Neuropathol.* 104, 583–591. doi:10.1007/s00401-002-0587-8

Fornai, F., Longone, P., Cafaro, L., Kastsiuchenka, O., Ferrucci, M., Manca, M. L., et al. (2008). Lithium delays progression of amyotrophic lateral sclerosis. *Proc. Natl. Acad. Sci.* 105, 2052–2057. doi:10.1073/pnas.0708022105

Fornai, F., and Puglisi-Allegra, S. (2021). Autophagy status as a gateway for stress-induced catecholamine interplay in neurodegeneration. *Neurosci. Biobehav. Rev.* 123, 238–256. doi:10.1016/j.neubiorev.2021.01.015

Galvan, V., and Hart, M. J. (2016). Vascular mTOR-dependent mechanisms linking the control of aging to Alzheimer's disease. *Biochim. Biophys. Acta - Mol. Basis Dis.* 1862, 992–1007. doi:10.1016/j.bbadis.2015.11.010

Gharibi, B., Farzadi, S., Ghuman, M., and Hughes, F. J. (2014). Inhibition of akt/mTOR attenuates age-related changes in mesenchymal stem cells. *Stem Cells* 32, 2256–2266. doi:10.1002/stem.1709

Glick, D., Barth, S., and Macleod, K. F. (2010). Autophagy: Cellular and molecular mechanisms. *J. Pathol.* 221, 3–12. doi:10.1002/path.2697

Gouras, G. K. (2013). mTOR: at the crossroads of aging, chaperones, and Alzheimer's disease. *J. Neurochem.* 124, 747–748. doi:10.1111/jnc.12098

Griffin, R. J., Moloney, A., Kelliher, M., Johnston, J. A., Ravid, R., Dockery, P., et al. (2005). Activation of Akt/PKB, increased phosphorylation of Akt substrates and loss and altered distribution of Akt and PTEN are features of Alzheimer's disease pathology. *J. Neurochem.* 93, 105–117. doi:10.1111/j.1471-4159.2004.02949.x

Habib, S. L., and Liang, S. (2014). Hyperactivation of Akt/mTOR and deficiency in tuberin increased the oxidative DNA damage in kidney cancer patients with diabetes. *Oncotarget* 5, 2542–2550. doi:10.18632/oncotarget.1833

Heras-Sandoval, D., Pérez-Rojas, J. M., and Pedraza-Chaverri, J. (2020). Novel compounds for the modulation of mTOR and autophagy to treat neurodegenerative diseases. *Cell. Signal.* 65, 109442. doi:10.1016/j.cellsig.2019.109442

Höhn, A., Tramutola, A., and Cascella, R. (2020). Proteostasis failure in neurodegenerative diseases: Focus on oxidative stress. *Oxid. Med. Cell. Longev.* 2020, 5497046. doi:10.1155/2020/5497046

Hsieh, A., and Edlind, M. (2014). PI3K-AKT-mTOR signaling in prostate cancer progression and androgen deprivation therapy resistance. *Asian J. Androl.* 16, 378–386. doi:10.4103/1008-682X.122876

Inoue, K., Rispoli, J., Kaphzan, H., Klann, E., Chen, E. I., Kim, J., et al. (2012). Macroautophagy deficiency mediates age-dependent neurodegeneration through a phospho-tau pathway. *Mol. Neurodegener.* 7, 48. doi:10.1186/1750-1326-7-48

Ji, Z.-S., Müllendorff, K., Cheng, I. H., Miranda, R. D., Huang, Y., and Mahley, R. W. (2006). Reactivity of apolipoprotein E4 and amyloid beta peptide: Lysosomal stability and neurodegeneration. *J. Biol. Chem.* 281, 2683–2692. doi:10.1074/jbc.M506646200

Jiang, T.-F., Zhang, Y.-J., Zhou, H.-Y., Wang, H.-M., Tian, L.-P., Liu, J., et al. (2013). Curcumin ameliorates the neurodegenerative pathology in A53T α-synuclein cell model of Parkinson's disease through the downregulation of mTOR/p70S6K signaling and the recovery of macroautophagy. *J. Neuroimmune Pharmacol.* 8, 356–369. doi:10.1007/s11481-012-9431-7

Jiang, W., Zhao, P., and Zhang, X. (2020). Apelin promotes ECM synthesis by enhancing autophagy flux via TFEB in human degenerative NP cells under oxidative stress. *Biomed. Res. Int.* 2020, 4897170–4897178. doi:10.1155/2020/4897170

Kaeberlein, M., and Galvan, V. (2019). Rapamycin and Alzheimer's disease: Time for a clinical trial? *Sci. Transl. Med.* 11, eaar4289. doi:10.1126/scitranslmed.aar4289

Kanehisa, M., and Goto, S. (2000). Kegg: Kyoto Encyclopedia of genes and Genomes. *Nucleic Acids Res.* 28, 27–30. doi:10.1093/nar/28.1.27

Kaper, F., Dornhoefer, N., and Giaccia, A. J. (2006). Mutations in the PI3K/PTEN/TSC2 pathway contribute to mammalian target of rapamycin activity and increased translation under hypoxic conditions. *Cancer Res.* 66, 1561–1569. doi:10.1158/0008-5472.CAN-05-3375

Kerr, J. S., Adriaanse, B. A., Greig, N. H., Mattson, M. P., Cader, M. Z., Bohr, V. A., et al. (2017). Mitophagy and Alzheimer's disease: Cellular and molecular mechanisms. *Trends Neurosci.* 40, 151–166. doi:10.1016/j.tins.2017.01.002

Klionsky, D. J. (2008). Autophagy revisited: A conversation with christian de Duve. *Autophagy* 4, 740–743. doi:10.4161/auto.6398

Lamming, D. W., Ye, L., Sabatini, D. M., and Baur, J. A. (2013). Rapalogs and mTOR inhibitors as anti-aging therapeutics. *J. Clin. Invest.* 123, 980–989. doi:10.1172/JCI64099

Lee, J.-H., Yang, D.-S., Goulbourne, C. N., Im, E., Stavrides, P., Pensalfini, A., et al. (2022). Faulty autolysosome acidification in Alzheimer's disease mouse models induces autophagic build-up of Aβ in neurons, yielding senile plaques. *Nat. Neurosci.* 25, 688–701. doi:10.1038/s41593-022-01084-8

Leidal, A. M., Levine, B., and Debnath, J. (2018). Autophagy and the cell biology of age-related disease. *Nat. Cell Biol.* 20, 1338–1348. doi:10.1038/s41556-018-0235-8

Levine, B., Packer, M., and Codogno, P. (2015). Development of autophagy inducers in clinical medicine. *J. Clin. Invest.* 125, 14–24. doi:10.1172/JCI73938

Li, X., Alafuzoff, I., Soininen, H., Winblad, B., and Pei, J.-J. (2005). Levels of mTOR and its downstream targets 4E-BP1, eEF2, and eEF2 kinase in relationships with tau in Alzheimer's disease brain. *FEBS J.* 272, 4211–4220. doi:10.1111/j.1742-4658.2005.04833.x

Li, X., Song, J., and Dong, R. (2019). Cubeben induces autophagy via PI3K-AKT-mTOR pathway to protect primary neurons against amyloid beta in Alzheimer's disease. *Cytotechnology* 71, 679–686. doi:10.1007/s10616-019-00313-6

Loera-Valencia, R., Cedazo-Minguez, A., Kenigsberg, P. A., Page, G., Duarte, A. I., Giusti, P., et al. (2019). Current and emerging avenues for Alzheimer's disease drug targets. *J. Intern. Med.* 286, 398–437. doi:10.1111/joim.12959

Lovell, M. A., and Markesbery, W. R. (2007). Oxidative DNA damage in mild cognitive impairment and late-stage Alzheimer's disease. *Nucleic Acids Res.* 35, 7497–7504. doi:10.1093/nar/gkm821

Luo, R., Su, L.-Y., Li, G., Yang, J., Liu, Q., Yang, L.-X., et al. (2020). Activation of PPARA-mediated autophagy reduces Alzheimer disease-like pathology and cognitive decline in a murine model. *Autophagy* 16, 52–69. doi:10.1080/15548627.2019.1596488

Ma, T., Hoeffer, C. A., Capetillo-Zarate, E., Yu, F., Wong, H., Lin, M. T., et al. (2010). Dysregulation of the mTOR pathway mediates impairment of synaptic plasticity in a mouse model of Alzheimer's disease. *PLoS One* 5, e12845. doi:10.1371/journal.pone.0012845

Malagelada, C., Jin, Z. H., Jackson-Lewis, V., Przedborski, S., and Greene, L. A. (2010). Rapamycin protects against neuron death in *in vitro* and*in vivo* models of Parkinson's disease. *J. Neurosci.* 30, 1166–1175. doi:10.1523/JNEUROSCI.3944-09.2010

Mandrioli, J., D'Amico, R., Zucchi, E., Gessani, A., Fini, N., Fasano, A., et al. (2018). Rapamycin treatment for amyotrophic lateral sclerosis: Protocol for a phase II randomized, double-blind, placebo-controlled, multicenter, clinical trial (RAP-ALS trial). *Med. Baltim.* 97, e11119. doi:10.1097/MD.0000000000011119

Mariño, G., Madeo, F., and Kroemer, G. (2011). Autophagy for tissue homeostasis and neuroprotection. *Curr. Opin. Cell Biol.* 23, 198–206. doi:10.1016/j.ceb.2010.10.001

Martínez-Martínez, E., Jurado-López, R., Valero-Muñoz, M., Bartolomé, M. V., Ballesteros, S., Luaces, M., et al. (2014). Leptin induces cardiac fibrosis through galectin-3, mTOR and oxidative stress: Potential role in obesity. *J. Hypertens.* 32, 1104–1114. doi:10.1097/HJH.0000000000000149

Medina, D. L., Di Paola, S., Peluso, I., Armani, A., De Stefani, D., Venditti, R., et al. (2015). Lysosomal calcium signalling regulates autophagy through calcineurin and TFEB. *Nat. Cell Biol.* 17, 288–299. doi:10.1038/ncb3114

Meng, X.-F., Yu, J.-T., Song, J.-H., Chi, S., and Tan, L. (2013). Role of the mTOR signaling pathway in epilepsy. *J. Neurol. Sci.* 332, 4–15. doi:10.1016/j.jns.2013.05.029

Metcalf, D. J., García-Arencibia, M., Hochfeld, W. E., and Rubinsztein, D. C. (2012). Autophagy and misfolded proteins in neurodegeneration. *Exp. Neurol.* 238, 22–28. doi:10.1016/j.expneurol.2010.11.003

Morales-Corraliza, J., Wong, H., Mazzella, M. J., Che, S., Lee, S. H., Petkova, E., et al. (2016). Brain-wide insulin resistance, tau phosphorylation changes, and hippocampal neprilysin and amyloid-β alterations in a monkey model of type 1 diabetes. *J. Neurosci.* 36, 4248–4258. doi:10.1523/JNEUROSCI.4640-14.2016

Mueed, Z., Tandon, P., Maurya, S. K., Deval, R., Kamal, M. A., and Poddar, N. K. (2019). Tau and mTOR: The hotspots for multifarious diseases in Alzheimer's development. *Front. Neurosci.* 12, 1017. doi:10.3389/fnins.2018.01017

Muñoz, F. J., and Inestrosa, N. C. (1999). Neurotoxicity of acetylcholinesterase amyloid beta-peptide aggregates is dependent on the type of Abeta peptide and the AChE concentration present in the complexes. *FEBS Lett.* 450, 205–209. doi:10.1016/S0014-5793(99)00468-8

Nixon, R. A. (2013). The role of autophagy in neurodegenerative disease. *Nat. Med.* 19, 983–997. doi:10.1038/nm.3232

Nixon, R. A., Yang, D.-S., and Lee, J.-H. (2008). Neurodegenerative lysosomal disorders: A continuum from development to late age. *Autophagy* 4, 590–599. doi:10.4161/auto.6259

Oddo, S., Caccamo, A., Smith, I. F., Green, K. N., and LaFerla, F. M. (2006). A dynamic relationship between intracellular and extracellular pools of Abeta. *Am. J. Pathol.* 168, 184–194. doi:10.2353/ajpath.2006.050593

Paccalin, M., Pain-Barc, S., Pluchon, C., Paul, C., Besson, M.-N., Carret-Rebillat, A.-S., et al. (2006). Activated mTOR and PKR kinases in lymphocytes correlate with memory and cognitive decline in Alzheimer's disease. *Dement. Geriatr. Cogn. Disord.* 22, 320–326. doi:10.1159/000095562

Pang, Y., Lin, W., Zhan, L., Zhang, J., Zhang, S., Jin, H., et al. (2022). Inhibiting autophagy pathway of PI3K/AKT/mTOR promotes apoptosis in SK-N-sh cell model of Alzheimer's disease. *J. Healthc. Eng.* 2022, 6069682. doi:10.1155/2022/6069682

Perluigi, M., Di Domenico, F., Barone, E., and Butterfield, D. A. (2021). mTOR in Alzheimer disease and its earlier stages: Links to oxidative damage in the progression of this dementing disorder. *Free Radic. Biol. Med.* 169, 382–396. doi:10.1016/j.freeradbiomed.2021.04.025

Pierzynowska, K., Gaffke, L., Cyske, Z., Puchalski, M., Rintz, E., Bartkowski, M., et al. (2018). Autophagy stimulation as a promising approach in treatment of neurodegenerative diseases. *Metab. Brain Dis.* 33, 989–1008. doi:10.1007/s11011-018-0214-6

Rong, L., Li, Z., Leng, X., Li, H., Ma, Y., Chen, Y., et al. (2020). Salidroside induces apoptosis and protective autophagy in human gastric cancer AGS cells through the PI3K/Akt/mTOR pathway. *Biomed. Pharmacother.* 122, 109726. doi:10.1016/j.biopha.2019.109726

Santos, R. X., Correia, S. C., Zhu, X., Lee, H.-G., Petersen, R. B., Nunomura, A., et al. (2012). Nuclear and mitochondrial DNA oxidation in Alzheimer's disease. *Free Radic. Res.* 46, 565–576. doi:10.3109/10715762.2011.648188

Sarkar, S. (2013). Regulation of autophagy by mTOR-dependent and mTOR-independent pathways: Autophagy dysfunction in neurodegenerative diseases and therapeutic application of autophagy enhancers. *Biochem. Soc. Trans.* 41, 1103–1130. doi:10.1042/BST20130134

Scheltens, P., Blennow, K., Breteler, M. M. B., de Strooper, B., Frisoni, G. B., Salloway, S., et al. (2016). Alzheimer's disease. *Lancet* 388, 505–517. doi:10.1016/S0140-6736(15)01124-1

Schmukler, E., and Pinkas-Kramarski, R. (2020). Autophagy induction in the treatment of Alzheimer's disease. *Drug Dev. Res.* 81, 184–193. doi:10.1002/ddr.21605

Selkoe, D. J., and Hardy, J. (2016). The amyloid hypothesis of Alzheimer's disease at 25 years. *EMBO Mol. Med.* 8, 595–608. doi:10.15252/emmm.201606210

Shafei, M. A., Harris, M., and Conway, M. E. (2017). Divergent metabolic regulation of autophagy and mTORC1—early events in Alzheimer's disease? *Front. Aging Neurosci.* 9, 173. doi:10.3389/fnagi.2017.00173

Siman, R., Cocca, R., and Dong, Y. (2015). The mTOR inhibitor rapamycin mitigates perforant pathway neurodegeneration and synapse loss in a mouse model of early-stage alzheimer-type tauopathy. *PLoS One* 10, e0142340. doi:10.1371/journal.pone.0142340

Soltani, R., Boroujeni, M. E., Aghajanpour, F., Khatmi, A., Ezi, S., Mirbehbahani, S. H., et al. (2020). Tramadol exposure upregulated apoptosis, inflammation and autophagy in PC12 cells and rat's striatum: An *in vitro- in vivo* approach. *J. Chem. Neuroanat.* 109, 101820. doi:10.1016/j.jchemneu.2020.101820

Spilman, P., Podlutskaya, N., Hart, M. J., Debnath, J., Gorostiza, O., Bredesen, D., et al. (2010). Inhibition of mTOR by rapamycin abolishes cognitive deficits and reduces amyloid-β levels in a mouse model of Alzheimer's disease. *PLoS One* 5, e9979. doi:10.1371/journal.pone.0009979

Sun, Y.-X., Ji, X., Mao, X., Xie, L., Jia, J., Galvan, V., et al. (2013). Differential activation of mTOR complex 1 signaling in human brain with mild to severe Alzheimer's disease. *J. Alzheimer's Dis.* 38, 437–444. doi:10.3233/JAD-131124

Thellung, S., Corsaro, A., Nizzari, M., Barbieri, F., and Florio, T. (2019). Autophagy activator drugs: A new opportunity in neuroprotection from misfolded protein toxicity. *Int. J. Mol. Sci.* 20, 901. doi:10.3390/ijms20040901

Tomiyama, T., Shoji, A., Kataoka, K., Suwa, Y., Asano, S., Kaneko, H., et al. (1996). Inhibition of amyloid beta protein aggregation and neurotoxicity by rifampicin. Its possible function as a hydroxyl radical scavenger. *J. Biol. Chem.* 271, 6839–6844. doi:10.1074/jbc.271.12.6839

Torres, M., Jimenez, S., Sanchez-Varo, R., Navarro, V., Trujillo-Estrada, L., Sanchez-Mejias, E., et al. (2012). Defective lysosomal proteolysis and axonal transport are early pathogenic events that worsen with age leading to increased APP metabolism and synaptic Abeta in transgenic APP/PS1 hippocampus. *Mol. Neurodegener.* 7, 59. doi:10.1186/1750-1326-7-59

Tramutola, A., Triplett, J. C., Di Domenico, F., Niedowicz, D. M., Murphy, M. P., Coccia, R., et al. (2015). Alteration of mTOR signaling occurs early in the progression of alzheimer disease (AD): Analysis of brain from subjects with pre-clinical AD, amnestic mild cognitive impairment and late-stage AD. *J. Neurochem.* 133, 739–749. doi:10.1111/jnc.13037

Uddin, M. S., Mamun, A. Al, Labu, Z. K., Hidalgo-Lanussa, O., Barreto, G. E., and Ashraf, G. M. (2019). Autophagic dysfunction in Alzheimer's disease: Cellular and molecular mechanistic approaches to halt Alzheimer's pathogenesis. *J. Cell. Physiol.* 234, 8094–8112. doi:10.1002/jcp.27588

Uddin, M. S., Stachowiak, A., Mamun, A. Al, Tzvetkov, N. T., Takeda, S., Atanasov, A. G., et al. (2018). Autophagy and Alzheimer's disease: From molecular mechanisms to therapeutic implications. *Front. Aging Neurosci.* 10, 04. doi:10.3389/fnagi.2018.00004

Wang, C., Yu, J.-T., Miao, D., Wu, Z.-C., Tan, M.-S., and Tan, L. (2014a). Targeting the mTOR signaling network for Alzheimer's disease therapy. *Mol. Neurobiol.* 49, 120–135. doi:10.1007/s12035-013-8505-8

Wang, C., Zhang, X., Teng, Z., Zhang, T., and Li, Y. (2014b). Downregulation of PI3K/Akt/mTOR signaling pathway in curcumin-induced autophagy in APP/PS1 double transgenic mice. *Eur. J. Pharmacol.* 740, 312–320. doi:10.1016/j.ejphar.2014.06.051

Wang, N., Wang, H., Li, L., Li, Y., and Zhang, R. (2020). β-Asarone inhibits amyloid-β by promoting autophagy in a cell model of Alzheimer's disease. *Front. Pharmacol.* 10, 1529. doi:10.3389/fphar.2019.01529

Ward, C., Martinez-Lopez, N., Otten, E. G., Carroll, B., Maetzel, D., Singh, R., et al. (2016). Autophagy, lipophagy and lysosomal lipid storage disorders. *Biochim. Biophys. Acta - Mol. Cell Biol. Lipids* 1861, 269–284. doi:10.1016/j.bbalip.2016.01.006

Yang, F., Chu, X., Yin, M., Liu, X., Yuan, H., Niu, Y., et al. (2014). mTOR and autophagy in normal brain aging and caloric restriction ameliorating age-related cognition deficits. *Behav. Brain Res.* 264, 82–90. doi:10.1016/j.bbr.2014.02.005

Yang, Z., and Ming, X.-F. (2012). mTOR signalling: the molecular interface connecting metabolic stress, aging and cardiovascular diseases. *Obes. Rev.* 13, 58–68. doi:10.1111/j.1467-789X.2012.01038.x

Yoon, M.-S. (2017). The role of mammalian target of rapamycin (mTOR) in insulin signaling. *Nutrients* 9, 1176. doi:10.3390/nu9111176

Zhang, W., Xu, C., Sun, J., Shen, H.-M., Wang, J., and Yang, C. (2022). Impairment of the autophagy–lysosomal pathway in Alzheimer's diseases: Pathogenic mechanisms and therapeutic potential. *Acta Pharm. Sin. B* 12, 1019–1040. doi:10.1016/j.apsb.2022.01.008

Zhang, X., Chen, S., Huang, K., and Le, W. (2013). Why should autophagic flux be assessed? *Acta Pharmacol. Sin.* 34, 595–599. doi:10.1038/aps.2012.184

Zheng, Y., and Jiang, Y. (2015). mTOR inhibitors at a glance. *Mol. Cell. Pharmacol.* 7, 15–20. doi:10.4255/mcpharmacol.15.02

Zhu, Y., and Bu, S. (2017). Curcumin induces autophagy, apoptosis, and cell cycle arrest in human pancreatic cancer cells. *Evidence-Based Complement. Altern. Med.* 2017, 5787218. doi:10.1155/2017/5787218

Glossary

AD Alzheimer's Disease
APP Amyloid Precursor Protein
NFTs Neurofibrillary Tangles
mTOR Mechanistic Target of Rapamycin
mTORC1 Mechanistic Target of Rapamycin Complex
UCHL-1 Ubiquitin C-Terminal hydrolase L1
UBQLN1 Ubiquitin-1
SNCA Alpha Synuclein gene
PSEN1 Presenilin-1
MAPT Microtubule Associated Protein tau
ITPR1 Inositol 1,4,5-triphosphate receptor type-I
GFAP Glial Fibrillary Acidic Protein
FOXO1 Forkhead Box Protein O1
CTSD Cathepsin D
CLU Clusterin
CDK5 Cyclin dependent kinase 5
BECN1 Beclin-1
BCL 2 B-Cell lymphoma 2
ATGs Autophagy-related genes
AMPK AMP-activated Protein Kinase
APPCTF C-terminal Fragments of Amyloid Precursor Protein
PI3K Phosphatidyl Inositol 3 Kinase
AKT Serine/Threonine kinase
PHFs Paired Helical Filament
ROS Reactive Oxygen Species
UPS Ubiquitin Protease System
UPR Unfolded Protein Response
EIF4E Eukaryotic Initiative Factor 4E
Ebp1 ErbB3-Binding Protein
P70s6k Ribosomal Protein S6 Kinase beta-1
PTEN Phosphate and Tensin Homologue
FKBP FK506 Binding Protein
ATP Adenosine Triphosphate
GSK3β Glycogen Synthase Kinase 3 Beta
PARK2 Parkin 2
PINK1 PTEN induced putative kinase 1

frontiers | Frontiers in Aging Neuroscience

TYPE Original Research
PUBLISHED 04 January 2023
DOI 10.3389/fnagi.2022.1071520

OPEN ACCESS

EDITED BY
Jiehui Jiang,
Shanghai University,
China

REVIEWED BY
Luyao Wang,
Shanghai University,
China
Wanli W. Smith,
Johns Hopkins Medicine,
United States

*CORRESPONDENCE
Zenglin Cai
✉ caizengling@hotmail.com
Nizhuan Wang
✉ wangnizhuan1120@gmail.com

†These authors have contributed equally to this work

SPECIALTY SECTION
This article was submitted to Parkinson's Disease and Aging-related Movement Disorders, a section of the journal Frontiers in Aging Neuroscience

RECEIVED 16 October 2022
ACCEPTED 12 December 2022
PUBLISHED 04 January 2023

CITATION
Du S, Wang Y, Li G, Wei H, Yan H, Li X, Wu Y, Zhu J, Wang Y, Cai Z and Wang N (2023) Olfactory functional covariance connectivity in Parkinson's disease: Evidence from a Chinese population. *Front. Aging Neurosci.* 14:1071520. doi: 10.3389/fnagi.2022.1071520

Olfactory functional covariance connectivity in Parkinson's disease: Evidence from a Chinese population

Shouyun Du[1†], Yiqing Wang[2,3†], Guodong Li[1†], Hongyu Wei[2†], Hongjie Yan[4†], Xiaojing Li[2], Yijie Wu[2], Jianbing Zhu[5], Yi Wang[5], Zenglin Cai[2,3*] and Nizhuan Wang[6*]

[1]Department of Neurology, Guanyun County People's Hospital, Lianyungang, China, [2]Department of Neurology, The Affiliated Suzhou Hospital of Nanjing University Medical School, Suzhou, China, [3]Department of Neurology, Suzhou Science & Technology Town Hospital, Gusu School, Nanjing Medical University, Suzhou, China, [4]Department of Neurology, Affiliated Lianyungang Hospital of Xuzhou Medical University, Lianyungang, China, [5]Department of Radiology, The Affiliated Suzhou Hospital of Nanjing University Medical School, Suzhou, China, [6]School of Biomedical Engineering, ShanghaiTech University, Shanghai, China

Introduction: Central anosmia is a potential marker of the prodrome and progression of Parkinson's disease (PD). Resting-state functional magnetic resonance imaging studies have shown that olfactory dysfunction is related to abnormal changes in central olfactory-related structures in patients with early PD.

Methods: This study, which was conducted at Guanyun People's Hospital, analyzed the resting-state functional magnetic resonance data using the functional covariance connection strength method to decode the functional connectivity between the white–gray matter in a Chinese population comprising 14 patients with PD and 13 controls.

Results: The following correlations were observed in patients with PD: specific gray matter areas related to smell (i.e., the brainstem, right cerebellum, right temporal fusiform cortex, bilateral superior temporal gyrus, right Insula, left frontal pole and right superior parietal lobule) had abnormal connections with white matter fiber bundles (i.e., the left posterior thalamic radiation, bilateral posterior corona radiata, bilateral superior corona radiata and right superior longitudinal fasciculus); the connection between the brainstem [region of interest (ROI) 1] and right cerebellum (ROI2) showed a strong correlation. Right posterior corona radiation (ROI11) showed a strong correlation with part 2 of the Unified Parkinson's Disease Rating Scale, and right superior longitudinal fasciculus (ROI14) showed a strong correlation with parts 1, 2, and 3 of the Unified Parkinson's Disease Rating Scale and Hoehn and Yahr Scale.

Discussion: The characteristics of olfactory-related brain networks can be potentially used as neuroimaging biomarkers for characterizing PD states. In the future, dynamic testing of olfactory function may help improve the accuracy and specificity of olfactory dysfunction in the diagnosis of neurodegenerative diseases.

KEYWORDS

Parkinson's disease, functional covariance connectivity, resting-state fMRI, gray matter, white matter, olfactory function

1. Introduction

Recently, resting-state functional magnetic resonance imaging (fMRI) has found widespread application for the analysis of various stages of Parkinson's disease (PD). fMRI analysis for PD encompasses regional homogeneity (ReHo; Zang et al., 2004), amplitude of low-frequency fluctuation (ALFF; Han et al., 2011), and functional connectivity (Olde Dubbelink et al., 2014). Independent component analysis of resting-state fMRI can identify several specific brain networks in the awake and resting states, such as the default mode, salience, and executive control networks, which have been widely investigated in a variety of neurodegenerative diseases, including PD (Wang and Weiming, 2012; Wang et al., 2013, 2015, 2016a,b; Pellegrino et al., 2016; Chang et al., 2017; Shi et al., 2017; Xiong et al., 2021).

Central anosmia may be a potential marker of the prodrome and disease progression in PD and Alzheimer's disease (AD; Turetsky et al., 2009; Zou et al., 2015). In 2017, Fjaeldstad et al (Fjaeldstad et al., 2017) developed a new method of structural olfactory connectivity fingerprinting to study two functional and structural maps of the olfactory cortical network and constructed a combined map containing the expected structural connectivity, which can be used as a potential neuroimaging biomarker of early structural connectivity changes in diseases such as PD. In 2021, we developed a new spectral contrast mapping method to decode brain activity at the voxel level, and analyzed 15 patients with severe hyposmia, 15 patients with no/mild hyposmia, and 15 healthy controls. Patients with severe or no/mild hyposmia presented with prominent differences in the vermis, cerebellum, and insula, while patients with severe hyposmia showed differences in the frontal, parietal, and temporal lobe gyri compared to the healthy control group (Yu et al., 2021).

Although some progress has been made in brain structural and fMRI studies for PD, the changes in the connectivity of the white matter and gray matter related to the olfactory system have received little attention. Mounting evidence shows that the blood-oxygen-level-dependent imaging (BOLD) signal in the white matter undergoes stimulus-related synchronous changes in response to olfactory and other related stimuli, and the signal changes in white matter pathway possess specificity (Ding et al., 2018). White-gray matter functional covariance connectivity can explore differences between brain functions. For example, Chen et al. used a white-gray matter functional connectivity approach to explore brain function in autistic and normal children (Chen et al., 2021). The ALFF of resting-state fMRI signals reflects the intensity of regional spontaneous brain activity (Zou et al., 2008), and there is a specific frequency distribution of amplitude low-frequency BOLD fluctuations in gray matter and white matter (Peer et al., 2017). We adopted a new ALFF-based functional covariance connectivity method for gray and white matter to explore PD-associated imaging markers. Our previous study showed that (Wang et al., 2022) the functional covariance connection strength (FCS) values of the dorsolateral prefrontal cortex of the right hemisphere and superior corona radiata of the left hemisphere are independent risk factors for PD, which may be helpful to explore the early pathogenesis of PD. Thus, we hypothesized that the olfactory-related gray–white matter connectivity information of patients with PD would be specific. This study aimed to analyzed the resting-state functional magnetic resonance data using the FCS method to decode the functional connectivity between the white–gray matter in a Chinese population.

2. Materials and methods

2.1. Participants

This study enrolled 14 patients with primary PD admitted to Guanyun County People's Hospital between June 2020 and June 2022. All patients with PD were diagnosed by two chief neurologists. The inclusion criteria were as follows: (1) patients diagnosed with PD according to the Movement Disorder Society's clinical diagnostic criteria for PD (Postuma et al., 2015), (2) the diagnosis was consistent with the findings of clinical examination and complete scale and imaging evaluations, and (3) patients who provided written informed consent. The exclusion criteria were as follows: (1) patients whose Parkinson's symptoms were caused by definite infection, trauma, overdose of drugs, poisoning and other factors in the past; (2) patients with a past history of intracranial nucleus destruction surgery, deep brain electrical stimulation implantation, transcranial magnetic stimulation (TMS), and other treatments; (3) patients with severe heart failure, respiratory failure, renal insufficiency, and other diseases; (4) patients diagnosed with psychiatric diseases (such as anxiety disorder, depression, etc.); (5) patients with stroke (lesion diameter > 20 mm), intracranial space occupying lesions, and other diseases; and (6) patients with other conditions deemed unsuitable for research. At the same time, 15 age-and sex-matched normal controls [healthy control (HC) group] were recruited. The normal controls provided written informed consent and did not meet the exclusion criteria. This study was approved by the Ethics Committee of Suzhou Science and Technology Town Hospital.

2.2. Clinical assessment measures

Demographic and clinical information such as sex, age at admission, age at onset, first symptom (tremor or rigidity), disease duration, and other data of all patients with PD were collected by one neurologist. All the different domains and the entirety of the Movement Disorder Society Unified Parkinson's Disease Rating Scale [including part I (non-motor experiences of daily living), part II (motor aspects of daily living), part III (motor examination), and part IV (motor complications)] and the Hoehn and Yahr Scale were used to evaluate disease severity. All patients were evaluated by trained clinicians.

2.3. MRI acquisition

Patients underwent imaging with a 1.5-T MRI System (OPTIMA MR360; GE, Milwaukee, WI). T1-sequences were acquired using the following scanning parameters: three-dimensional magnetization-prepared rapid gradient echo sequences, repetition time (TR) = 1904.26 ms, echo time (TE) = 28.20 ms, inversion time (TI) =750.00 ms, thickness = 5 mm, flip angle (FA) = 90°, matrix size = 288 × 224, and 32 sagittal slices. Resting-state fMRI was performed with the following parameters: TR =3,000 s, TE = 40 ms, TI = 0.00 ms, 32 transverse slices, layer spacing = 5 mm, thickness = 3 mm, matrix size = 64 × 64, and FA = 90°. The total resting-state fMRI scanning time was 384 s. fMRI scanning was conducted in darkness, and participants were given clear instructions to relax, close their eyes and not fall asleep during MR acquisition in the resting state (confirmed immediately after the experiment). Earplugs were used to reduce scanner noise and cushions were used to minimize head movement.

2.4. Preprocessing of fMRI data

The resting-state fMRI data were preprocessed according to our previous research (Wang et al., 2022) using DPABI (http://rfmri.org/dpabi; Yan et al., 2016), which is based on Statistical Parametric Mapping (SPM12; https://www.fil.ion.ucl.ac.uk/spm/) and the Resting-State fMRI Data Analysis Toolkit (REST, Song et al., 2011; http://www.restfmri.net). The default method selected for this study is called "New Segment + DARTEL" in SPM8. The Friston 24 parameter model was selected to adjust for the effect of head movement. We used Peer et al.'s method (Peer et al., 2017) to filter the band of gray matter, whose fMRI image signal was 0.01–0.1 Hz, while that of the white matter was 0.01–0.15 Hz. The resultant images were spatially normalized to the Montreal Neurological Institute echo-planar imaging template using default settings and resampling to $3 \times 3 \times 3\ mm^3$ voxels, and smoothed with a Gaussian kernel of $4 \times 4 \times 4\ mm^3$.

We adopted the white matter and gray matter masks in MRIcroN as the group mask.[1] Individual mapping distinguishes gray matter from white matter in the group mask to avoid voxels that overlap between the two. In this study, the matrix dot product operation in MATLAB was used to remove the mixed signals from the images.[2] The signals of the non-white matter and non-gray matter were set to zero in the ALFF atlas. ALFF maps of gray matter and white matter were obtained for each participant (Wang et al., 2022). We performed a one-way ANOVA on the four groups of ALFF profiles obtained as shown in Figure 1. All image operations were performed over an area measuring $61 \times 73 \times 61\ mm^3$.

1 https://www.nitrc.org/projects/mricron

2 https://ww2.mathworks.cn/

The FCS value was calculated for each participant (Wang et al., 2022). Drawing on the definition of structural covariance linkage (Eisenberg et al., 2015), the functional covariance connection was defined as the Pearson correlation coefficient between the ALFF values of two voxels for all participants, and was calculated using the following formula:

$$r = \frac{1}{N-1}\sum_{i=1}^{N}\left(\frac{X_i - \bar{X}}{S_X}\right)\left(\frac{Y_i - \bar{Y}}{S_Y}\right) = \frac{1}{N-1}\sum_{i=1}^{N} Z_{Xi}Z_{Yi}, \quad (1)$$

where N is the number of participants, $\bar{X}$ and $\bar{Y}$ are the mean values of the data X and Y, and S is the sample standard deviation. The Pearson correlation coefficient (r) between the data series X and Y can be represented as the normalized inner product of standard scores (z-scores). We use the product ($Z_{Xi}Z_{Yi}$) of the z-score of each individual (i) as a measure of the strength of the individual's functional connection. The FCS is the product of the standard scores of each pair of voxels. The FCS can be used to measure the strength of the functional covariance of each pair of voxels (Eisenberg et al., 2015; Chen et al., 2021).

2.5. Obtaining regions of interest

We obtained a voxel-based $67{,}541 \times 1{,}632$ functional covariance connection matrix (67,541 represents the number of gray matter voxels, and 1,632 represents the number of white matter voxels) for each participant. This study tested whether each gray–white matter connection differed significantly between the PD and HC groups by comparing the functional covariance contribution values using t-tests, whose significance was set at $p < 0.00005$. Areas with differences in gray matter–white matter connection relative to the controls were considered as regions of interest (ROIs).

2.6. Correlation analysis of ROI and Parkinson's scale

The functional connections between the gray and white matter of the whole brain were constructed. The functional gray–white matter connection with $p < 0.00005$ was denoted as a brain area with a significant difference. The DPABI V6.1 ROI signal extractor tool was used to extract the signal value of this area with the coordinates as the origin and a radius of 3 mm to analyze the correlation between the nine gray matter brain areas.16 spherical ROIs were drawn. We analyzed the correlation of the nine brain regions, to obtain the correlation coefficient and map them. Thereafter, the respective correlations between the signal values of the nine ROIs and the subscores of each domain of the Unified Parkinson's Scale were plotted and analyzed.

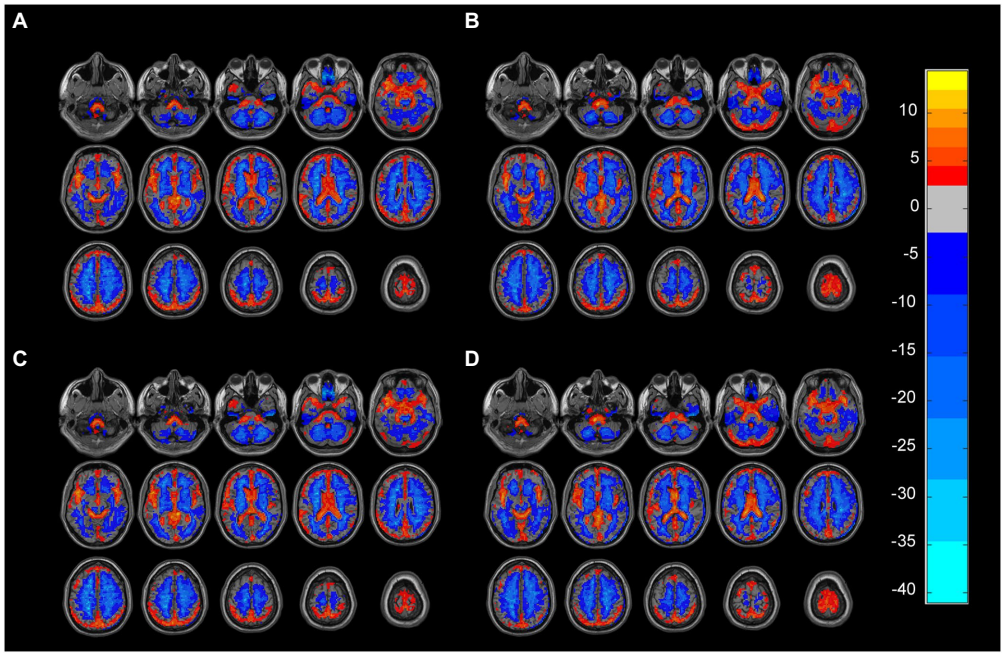

FIGURE 1
(A) Gray matter ALFF mapping of PD group (One-sample *t*-test, FDR, $p<0.05$). **(B)** Gray matter ALFF mapping of HC group (One-sample *t*-test, FDR, $p<0.05$). **(C)** White matter ALFF mapping in the PD group (One-sample *t*-test, FDR, $p<0.05$). **(D)** White matter ALFF mapping in the PD group (One-sample *t*-test, FDR, $p<0.05$). ALFF: amplitude of low-frequency fluctuations, PD: Parkinsons's disease, HC: healthy control.

TABLE 1 Baseline data.

Clinical characteristics	Patients with Parkinson's disease	Healthy controls	*p* Value
All patients	14	13	
Sex			0.252
Women	6 (40%)	9 (60%)	
Men	8 (66.7%)	4 (33.3%)	
Age ± SD	67.2 ± 10.1	69.9 ± 6.4	0.081

3. Results

3.1. Demographic comparison between the two groups

Initially, 18 patients with PD were included in this study, of which 4 were excluded from the statistical analysis due to considerable head movement and poor image data quality, while 5 participants from the control group were not included in the statistical analysis for the same reasons. Finally, 14 patients with PD (8 men, 6 women; mean age, 67.2 ± 10.1 years; range, 46–80 years) who had not received anti-Parkinsonian medication or were taking only levodopa (L-DOPA) and 13 HCs (4 men, 9 women; age, 69.9 ± 6.4 years; range, 61–79 years) were enrolled in the study. There were no significant differences in sex and age between the two groups ($p < 0.05$; Table 1). All participants were right-handed.

3.2. Abnormal functional covariance connections for the HC and PD groups

We analyzed the voxel-based 67,541 × 1,632 functional covariance connection matrix, where 67,541 represents the number of gray matter voxels and 1,632 represents the number of white matter voxels. Subsequently, FCS analysis revealed that 13 × 11 functional covariance connections differed significantly between the PD and control groups (Figure 2).

3.3. Analysis of cerebral gray matter ROIs

The FCS of 13 gray matter areas in the PD group differed from that of the control group (Table 2). They were mainly located in the brainstem, right cerebellum, right temporal fusiform cortex, bilateral superior temporal gyrus, right Insula, left frontal pole, and right superior parietal lobule (Table 3; Figure 3).

3.4. Analysis of white matter ROIs

The FCS of 11 white matter areas in the PD group differed from that of the control group (Table 4). They were mainly located

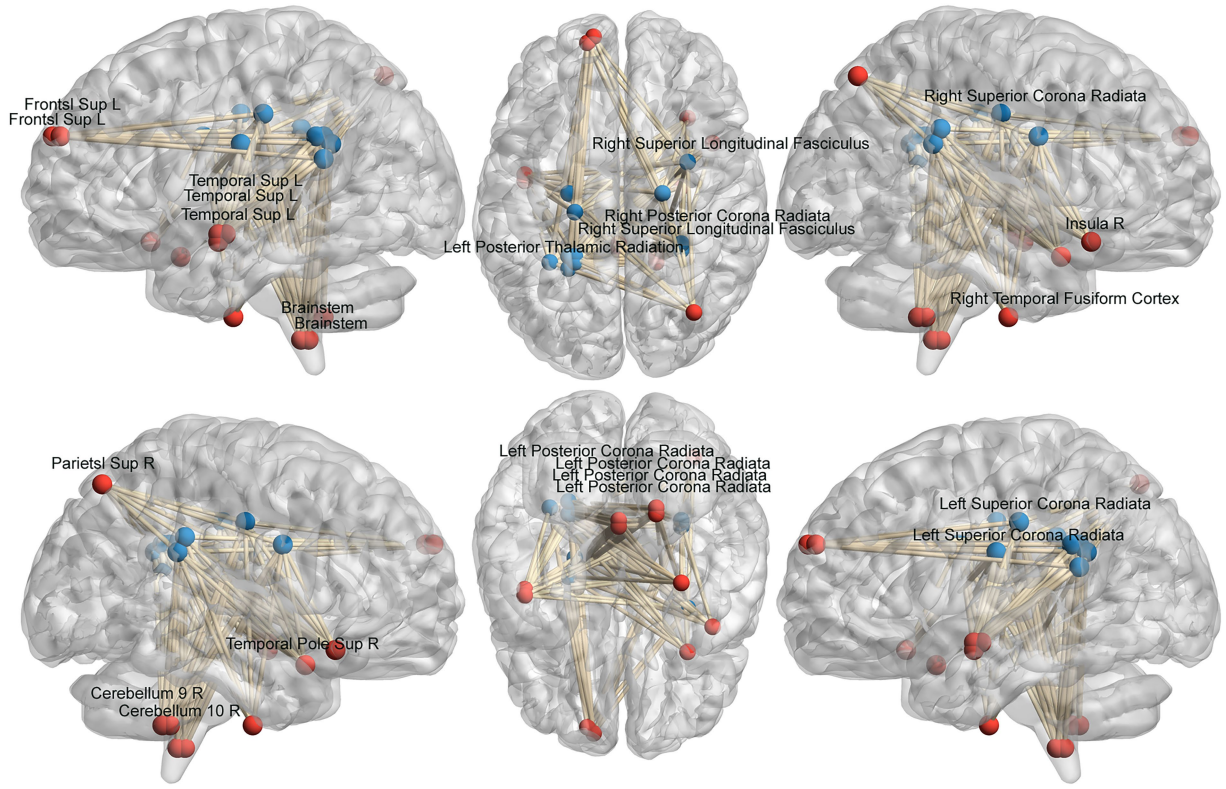

FIGURE 2
Schematic diagram of the abnormal functional covariance connections between 13 gray matter voxels and 11 white matter voxels identified by FCS analysis for the PD and HC groups. The red balls represent gray matter voxels, and the blue balls are the white matter voxels. PD: Parkinsons's disease, HC: healthy control.

TABLE 2 Gray matter brain areas with significant differences between the PD and control groups based on anatomical automatic labeling.

Coordinates			Anatomical automatic labeling
X	Y	Z	
0	−42	−54	Brainstem
0	−39	−54	Brainstem
18	−48	−45	Cerebellum_9_R
18	−45	−45	Cerebellum_10_R
30	−12	−45	Right Temporal Fusiform Cortex
45	9	−21	Temporal_Pole_Sup_R
−45	−6	−15	Temporal_Sup_L
33	21	−15	Insula_R
−45	−9	−12	Temporal_Sup_L
−45	−6	−12	Temporal_Sup_L
−15	57	27	Frontal_Sup_L
−12	60	27	Frontal_Sup_L
36	−72	51	Parietal_Sup_R

X, Y, and Z represent the spatial coordinates in the Montreal Neurological Institute space. R, right; L, left; Sup, superior; PD, Parkinson's disease.

in the left posterior thalamic radiation, bilateral posterior corona radiata, bilateral superior corona radiata, and right superior longitudinal fasciculus (Table 3; Figure 4).

3.5. ALFF analysis based on cerebral gray matter

We analyzed the ALFF of 16 regions of interest. The ALFF of the normal group was generally higher than that of the PD group, and the ALFF of the insular brain region (ROI6) of the HC group was lower than that of the PD group. Significantly lower ALFF values were found in the left posterior thalamic radiation, bilateral posterior corona radiata and right superior longitudinal fasciculus than in the normal group (Figure 5). We analyzed the 8 gray matter region of interest correlation matrices and the 8 white matter region of interest correlation matrices separately, and found a strong correlation between the connection of the brainstem (ROI1) and right cerebellum (ROI2; Figure 6). We also analyzed the direct relationship between the region of interest and the Unified Parkinson's Disease Rating Scale in the case group. We found that right posterior corona radiation (ROI11) showed a strong correlation with part 2 of the Unified Parkinson's Disease

TABLE 3 ROI with significant differences in the PD and control groups.

Coordinates			Cluster Size	Labeling	Name
X	Y	Z			
−1	−41	−54	2	ROI1	Brainstem
17	−46	−45	2	ROI2	Right Cerebellum
30	−12	−45	1	ROI3	Right Temporal Fusiform Cortex
45	9	−21	1	ROI4	Right Temporal Pole: Superior Temporal Gyrus
−45	−7	−12	3	ROI5	Left Superior Temporal Gyrus
33	21	−15	1	ROI6	Right Insula
−14	59	27	2	ROI7	Left Frontal Pole
36	−72	51	1	ROI8	Right Superior Parietal Lobule
−33	−48	18	1	ROI9	Left Posterior Thalamic Radiation
−24	−47	26	4	ROI10	Left Posterior Corona Radiata
30	−42	24	1	ROI11	Right Posterior Corona Radiata
−24	−15	24	1	ROI12	Left Superior Corona Radiata
33	0	27	1	ROI13	Right Superior Longitudinal Fasciculus
30	−39	30	1	ROI14	Right Superior Longitudinal Fasciculus
−21	−24	36	1	ROI15	Left Superior Corona Radiata
21	−15	36	1	ROI16	Right Superior Corona Radiata

X, Y, and Z represent the spatial coordinates in the Montreal Neurological Institute space. ROI, region of interest; PD, Parkinson's disease.

Rating Scale, and right superior longitudinal fasciculus (ROI14) showed a strong correlation with parts 1, 2, and 3 of the Unified Parkinson's Disease Rating Scale and Hoehn and Yahr Scale under the control of age and gender (Figure 7).

4. Discussion

Numerous neurodegenerative diseases are associated with the aging process, including the two most common ones, i.e., PD and AD. The establishment of biomarkers to improve early risk identification is essential for early treatment aimed at delaying or hindering the pathological process. Alterations in olfactory function are considered to be early biomarkers of neurodegenerative diseases (Dan et al., 2021). Olfactory dysfunction occurs in 90% of early PD and 85% of early AD cases, rendering it an attractive biomarker for the early diagnosis of these diseases. Olfactory decline is one of the principal early symptoms of PD. Mounting clinical and pathological data indicate that the dysfunction of the olfactory cortex may be responsible for the impairment of olfactory processing observed in PD. However, there is no clear evidence to establish a direct correlation between the changes in brain metabolism and hyposmia in PD (Baba et al., 2011).

The non-invasive nature and cost-effectiveness of olfactory function assessment make it extremely enticing option for the prediction and diagnosis of neurodegenerative diseases, because early diagnosis is essential for implementing interventions when the brain pathology is relatively closer to normal. Simple olfactory tests can effectively detect olfactory dysfunction in the two most common neurodegenerative diseases (Velayudhan et al., 2015; Morley et al., 2018), and help differentiate patients from normal individuals and patients with some similar characteristics but different etiopathologies (Duff et al., 2002). However, in some cases, olfactory testing alone may not be sufficient to determine certain specific diseases (Mesholam et al., 1998).

Olfactory testing should be used in conjunction with other disease-specific phenotypic tests to ensure accurate disease prediction and diagnosis. The combination of olfactory testing and dopamine transporter imaging predicted that 67% patients with prodromal PD underwent conversion to PD within 4 years (Jennings et al., 2017). Chen et al. showed that hyposmia and hyperechogenicity of the substantia nigra are important risk indicators for PD, and the combination of the two can improve the diagnostic specificity of patients with PD and those with primary tremor (Chen et al., 2012). The use of the L-DOPA challenge in combination with olfactory testing can improve the diagnostic sensitivity for early PD with mild movement disorder (Terroba Chambi et al., 2017).

Our previous research with a public database showed that (Wang et al., 2022) the dorsolateral prefrontal, anterior entorhinal cortex, and fronto-orbital cortices in the gray matter had abnormal connectivity with the posterior corona radiata and superior corona radiata in the white matter of patients with Parkinson's

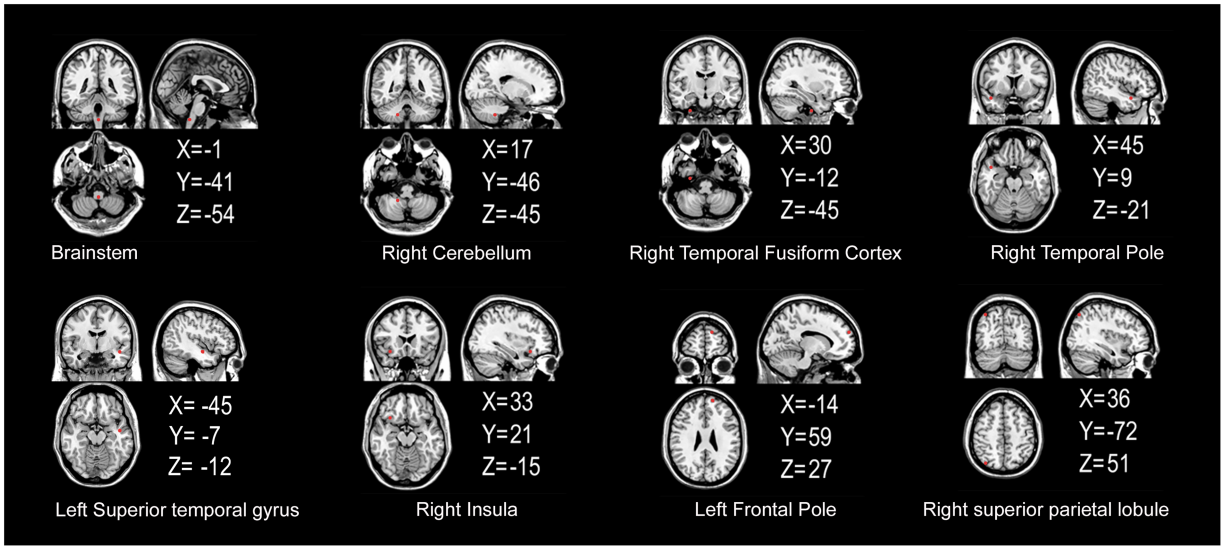

FIGURE 3
Gray matter areas with abnormal functional covariance connections. The areas marked in red represent the gray matter areas, where the FCS is statistically different between the PD and HC groups (two sample *T*-test, $p<0.00005$). X, Y, and Z refer to the coordinate axes in the Montreal Neurological Institute space. PD: Parkinsons's disease, HC: healthy control, FCS: functional covariance connection strength.

hyposmia. The FCS of the right dorsolateral prefrontal cortex and white matter, and the covariance connection strength of the left superior corona radiata and gray matter function possess potential diagnostic value. To verify these findings, the current study analyzed the functional magnetic resonance data of 14 patients with Parkinson's disease and 13 normal controls. The FCS of 16 region of interest (ROIs) in the PD group differed from that of the control group (Figure 7). The FCS of the posterior thalamic radiation, posterior corona radiata, anterior corona radiata, and white matter area of the superior longitudinal bundle were different. Correlation matrix analysis based on ALFF showed that the connection between the brainstem (ROI1) and right cerebellum (ROI2; Figure 6). In the partial correlation analysis, right posterior corona radiation (ROI11) showed a strong correlation with part 2 of the Unified Parkinson's Disease Rating Scale, and right superior longitudinal fasciculus (ROI14) showed a strong correlation with parts 1, 2, and 3 of the Unified Parkinson's Disease Rating Scale and Hoehn and Yahr Scale (Figure 7). The ROI7 of our current study matched fronto-orbital cortices found in previous studies in terms of spatial location. This further validates our previous finding that Parkinson's hyposmia is altered in a specific brain region that is associated with the prefrontal orbital cortex (Wang et al., 2022). Right posterior corona radiation (ROI11) is consistent with the posterior corona radiata reported in our previous study. Our previous study considered Parkinson's disease olfactory-related brain regions with ROI11. The present finding that ROI14 is closely associated with multiple Parkinson's disease clinical scales and that this brain region predicts disease severity has clinical significance. In addition, these targeted locations and functional connectivity could potentially provide some cues for the PD treatment in view of occupational therapy (Foster et al., 2021) and occupational neuroscience (Yan et al., 2016; Shi et al., 2017; Shi et al., 2017; Wang et al., 2017, 2018; Wu et al., 2020).

Neuroimaging studies have provided several potential biomarkers for research on neurodegenerative diseases. Measurement of the ALFF of the BOLD signal can effectively reflect local spontaneous neuronal activity (Zuo and Xing, 2014; Cao et al., 2022) with high repeatability and reliability, facilitating its application as an indicator of functional differences in a single region (Zuo et al., 2019). Wang et al. (2020) used ALFF measurement of resting-state fMRI data to investigate the alterations in ALFF in patients with PD. They found that the ALFF was reduced in the left cerebellum, right anterior cuneiform lobe, and left posterior central/supramarginal gyrus (PostC) in patients with PD, and a greater decrease in the ALFF was observed in the left pallidum and anterior central gyrus/PostC, and the left caudate nucleus/putamen showed a positive correlation with the disease course, similar to some results of the current study. Zhang et al. (2022) found that chronic hypoxia can lead to extensive cognitive impairment, in addition to a significant reduction in the ROI density of the left olfactory cortex, right medial superior orbitofrontal gyrus, bilateral insular lobes, left globus pallidus and temporal lobe. These findings also support the idea that changes in orbitofrontal gyrus brain function may be a promising imaging marker in Parkinson's disease, consistent with our idea.

A systematic review of neurodegenerative changes on MRI in patients with olfactory impairment, mild cognitive impairment (MCI) or dementia found that (Yi et al., 2022) 17 (71%) of 24 studies reported changes in hippocampal volume, and 14 reported the correlation between hippocampal volume and olfactory performance. Two of four prospective studies (50%) reported the

potential value of baseline hippocampal volume as a marker of dementia transformation in MCI. Of the 24 studies that reported the findings of olfactory fMRI, 5 (21%) emphasized the role of olfactory fMRI in identifying individuals with early cognitive decline. Donoshita et al. (2021) used 7-T fMRI to assess olfactory function in the human brain, and found that olfactory stimulation mainly activated the piriform cortex and orbitofrontal cortex, except the amygdala. The subjective odor intensity was significantly related to the average fMRI signal of the piriform cortex. The value of the frontal orbital cortex as a neuroimaging marker in Parkinson's disease was again discovered on a high-resolution magnetic resonance scanner.

TABLE 4 White matter brain areas with significant differences between the PD and control groups based on the John Hopkins University-White Matter atlas.

Coordinates			Brain region
X	Y	Z	
−33	−48	18	Left Posterior Thalamic Radiation
−24	−51	24	Left Posterior Corona Radiata
30	−42	24	Right Posterior Corona Radiata
−24	−15	24	Left Superior Corona Radiata
−21	−48	27	Left Posterior Corona Radiata
−21	−45	27	Left Posterior Corona Radiata
−24	−45	27	Left Posterior Corona Radiata
33	0	27	Right Superior Longitudinal Fasciculus
30	−39	30	Right Superior Longitudinal Fasciculus
−21	−24	36	Left Superior Corona Radiata
21	−15	36	Right Superior Corona Radiata

X, Y, and Z represent the spatial coordinates in the Montreal Neurological Institute space.

Although some progress has been made in the study of brain structure and functional magnetic resonance in PD in recent years, few researchers have focused on the relationship of the changes in white–gray matter connectivity with olfactory function. Increasing evidence shows that the BOLD signal in white matter undergoes stimulus-related synchronous changes in response to olfactory and other related stimuli, and the signal changes in white matter pathways in the brain show clear specificity (Ding et al., 2018). We used the white–gray matter FCS method to devise a new approach to study the early changes in olfactory network connectivity in neurodegenerative diseases. This method can be used to detect changes in the brain regions associated with olfactory function in patients with neurodegenerative diseases, including PD. We found that specific brain regions (viz. the brainstem, right cerebellum, right fusiform gyrus, right temporal pole, lower part of the left superior temporal gyrus, right insular lobe, upper part of the left superior temporal gyrus, left frontal pole, and right superior parietal gyrus) have special connections with white matter fiber bundles (posterior thalamic radiation,

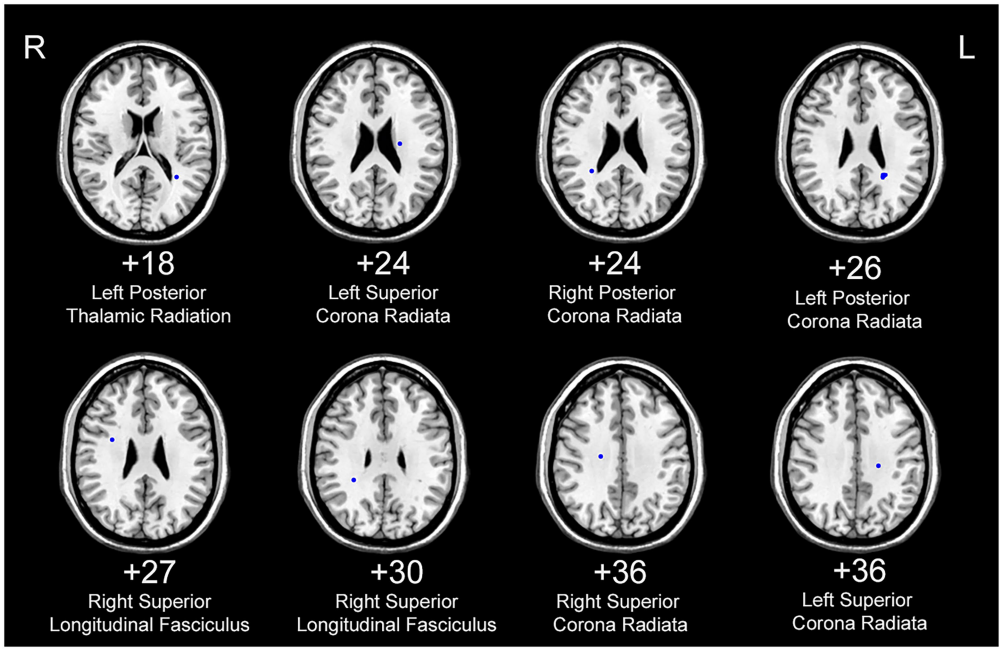

FIGURE 4
White matter areas with abnormal functional covariance connections. The areas marked in blue are the white matter areas, where the FCS is statistically different between the PD and HC groups (two sample *T*-test, $p<0.00005$). The white figure depicts the cross-section level (Montreal Neurological Institute space). R: right side; L: left side. PD: Parkinsons's disease, HC: healthy control.

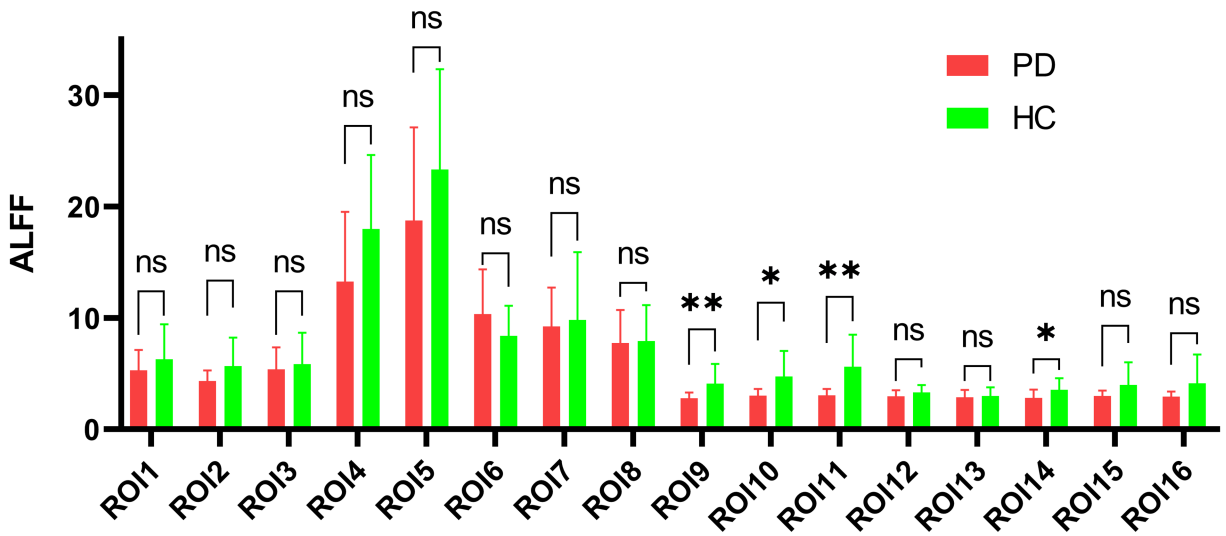

FIGURE 5
Amplitude comparison diagram of low-frequency fluctuation. ROI: region of interest, ALFF: amplitude of low-frequency fluctuations, PD: Parkinson's disease group, HC: normal control group, ns: no significance, *$p < 0.05$, **$p < 0.01$.

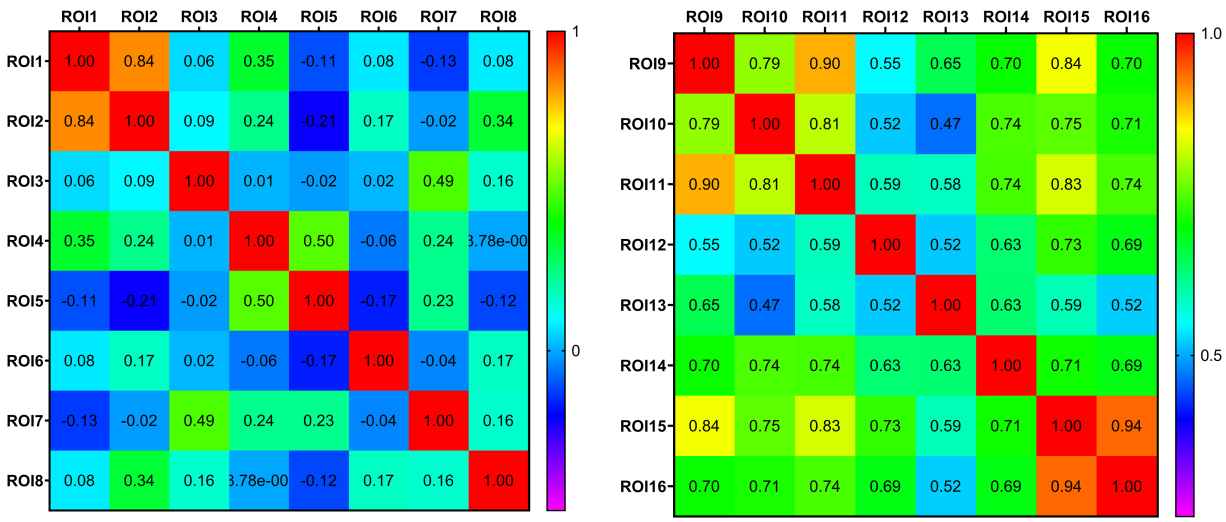

FIGURE 6
Thermodynamic diagram of the connectivity matrix of region of interest. Each row and column in the matrix corresponds to different region of interest. The value at the intersection of the rows and columns represents the correlation coefficient of the functional connection of the corresponding brain regions. Positive values represent a positive correlation and negative values represent a negative correlation. The larger the value, the closer the functional connection.

posterior corona radiata, anterior corona radiata, and superior longitudinal bundle) in patients with PD. The frontal orbital cortex may be the brain area affected by specific brain function changes in Parkinson's hyposmia. This indicates that the characteristics of olfactory-related brain networks can be used as potential neuroimaging biomarkers for the changes in early structural connectivity in PD.

5. Limitations of this study and future prospects

This is the first clinical study to use the FCS method to study the connectivity between the white and gray matter to elucidate the changes in olfactory network connectivity in PD. Since all MRI equipment used in this test were 1.5-T scanners, there were certain

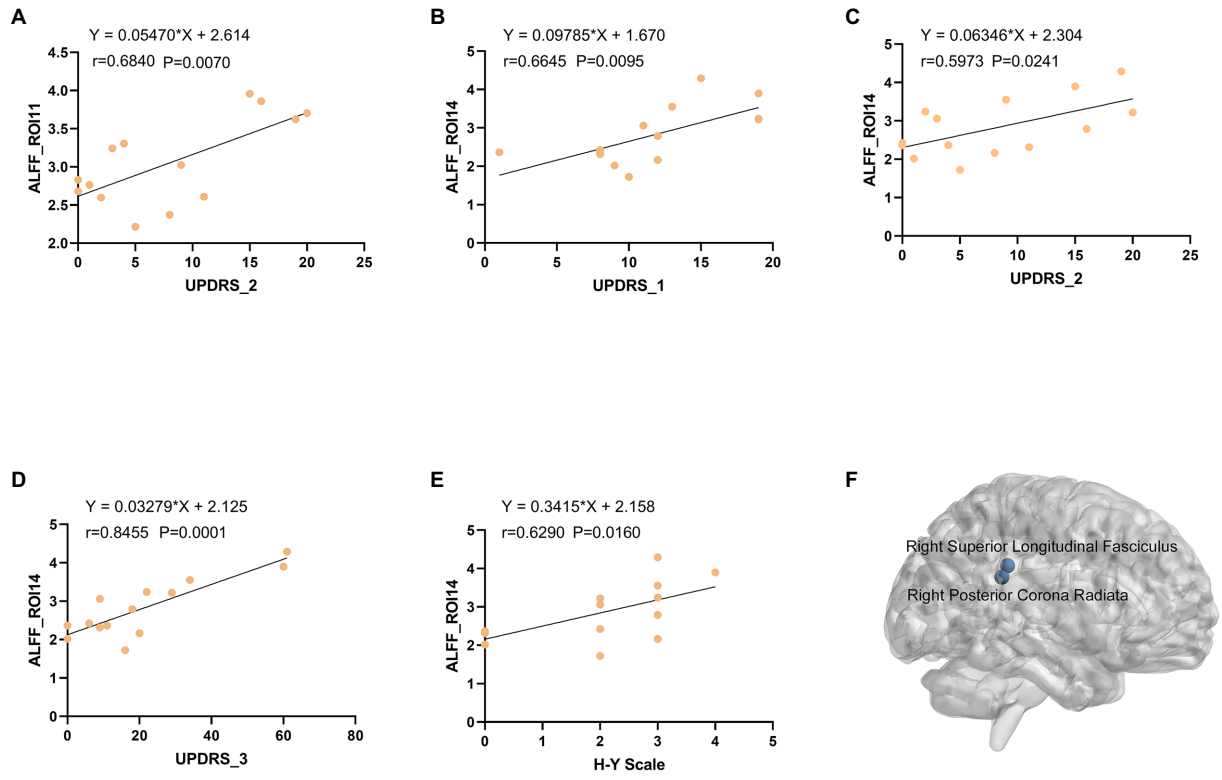

FIGURE 7
(A) The ALFF values of right ROI11 were positively correlated with UPDRS-2 (r=0.5946, p=0.0249). **(B)** The ALFF values of left ROI14 were positively correlated with UPDRS-1 (r=0.5768, p=0.0308). **(C)** The ALFF values of left ROI14 were positively correlated with UPDRS-2 (r=0.5768, p=0.0308). **(D)** The ALFF values of left ROI14 were positively correlated with UPDRS-3 (r=0.5768, p=0.0308). **(E)** The ALFF values of left ROI14 were positively correlated with H-Y Scale (r=0.5768, p=0.0308). **(F)** Three-dimensional map of the Right Posterior Corona Radiata (ROI11) and Right Superior Longitudinal Fasciculus (ROI14) brain regions. ALFF: amplitude of low-frequency fluctuations, ROI: region of interest, UPDRS: Unified Parkinson Disease Scale, H-Y Scale: Hoehn and Yahr Scale.

limitations in image clarity and other parameters. Moreover, the sample population was small, the clinical data were not detailed, and comprehensive neuropsychological evaluation was not performed, which hindered the exploration of specific PD dysfunction. In the near future, we endeavor to use 3-T (even 5 or 7-T) high-resolution MRI scanning combined with olfactory testing and comprehensive neuropsychological assessment to gather a large sample, and subsequently, in the later stage, we will use new task states and multimodal techniques to further study olfactory network function of patients with PD. Future studies should combine specific olfactory testing and other biomarkers to perform comprehensive evaluations of olfactory function.

6. Conclusion

Central anosmia is a potential marker of the early prodrome and progression of PD. Resting-state fMRI studies have shown that the impairment of olfactory function in patients with early PD is related to abnormal changes in olfactory-related central structures. Our results found abnormal connections between specific gray matter areas (frontal cortex) related to olfaction and white matter fiber bundles (posterior corona radiata, anterior corona radiata) in Chinese patients with PD, and ALFF values were found in specific white matter brain regions [Right posterior corona radiation (ROI11) and superior longitudinal fasciculus (ROI14)] to predict disease severity, indicating that the characteristics of olfaction-related brain networks can be used as potential neuroimaging biomarkers of connectivity structure changes in PD. In the future, combining dynamic observation of olfactory function with other disease-specific diagnostic tests may help improve the accuracy and specificity of olfactory dysfunction in the diagnosis of neurodegenerative diseases.

Data availability statement

The original contributions presented in the study are included in the article/supplementary material, further inquiries can be directed to the corresponding authors.

Ethics statement

The studies involving human participants were reviewed and approved by the Ethics Committee of Suzhou Science and Technology Town Hospital. The patients/participants provided their written informed consent to participate in this study.

Author contributions

ZC and NW played a critical role in conceptualizing this study. YqW, HW, SD, and GL collected and analyzed all data. YqW and HY contributed to writing the first draft of the paper. XL, YjW, JZ, and YW prepared the manuscript. All authors provided critical feedback on the manuscript. All authors have read and approved the submitted manuscript.

Funding

This work was supported by the National Natural Science Foundation of China (No. 82001160), Special Project for Diagnosis and Treatment of Key Clinical Diseases in Suzhou (No. LCZX202029), Suzhou City Medical Device and New Medicine Clinical Trial Institutional Capacity Improvement Project (No. SLT202001), Suzhou Science and Technology Development Plan (No. SS2019048), Scientific research project of Gusu School, Nanjing Medical University (No. GSKY20210240), Research Projects on Aging Health of Lianyungang City (No. L202201), and Project of Huaguoshan Mountain Talent Plan—Doctors for Innovation and Entrepreneurship.

Acknowledgments

We would like to thank all the patients for their participation in this project. We would also like to express our profound appreciation for the reviewers' insightful comments, which have improved the quality of this manuscript. Finally, we would like to thank Editage (www.editage.cn) for English language editing.

Conflict of interest

The authors declare that the research was conducted in the absence of any commercial or financial relationships that could be construed as a potential conflict of interest.

Publisher's note

References

Baba, T., Takeda, A., Kikuchi, A., Nishio, Y., Hosokai, Y., Hirayama, K., et al. (2011). Association of olfactory dysfunction and brain. Metabolism in Parkinson's disease. *Mov. Disord.* 26, 621–628. doi: 10.1002/mds.23602

Cao, K., Pang, H., Yu, H., Li, Y., Guo, M., Liu, Y., et al. (2022). Identifying and validating subtypes of Parkinson's disease based on multimodal MRI data via hierarchical clustering analysis. *Front. Hum. Neurosci.* 16:919081. doi: 10.3389/fnhum.2022.919081

Chang, Y. T., Lu, C. H., Wu, M. K., Hsu, S. W., Huang, C. W., Chang, W. N., et al. (2017). Salience network and depressive severities in Parkinson's disease with mild cognitive impairment: a structural covariance network analysis. *Front. Aging Neurosci.* 9:417. doi: 10.3389/fnagi.2017.00417

Chen, H., Long, J., Yang, S., and He, B. (2021). Atypical functional covariance connectivity between gray and white matter in children with autism spectrum disorder. *Autism Res.* 14, 464–472. doi: 10.1002/aur.2435

Chen, W., Tan, Y. Y., Hu, Y. Y., Zhan, W. W., Wu, L., Lou, Y., et al. (2012). Combination of olfactory test and substantia nigra transcranial sonopraphy in the differential diagnosis of Parkinson's disease: a pilot study from China. *Transl. Neurodegener.* 1:25. doi: 10.1186/2047-9158-1-25

Dan, X., Wechter, N., Gray, S., Mohanty, J. G., Croteau, D. L., and Bohr, V. A. (2021). Olfactory dysfunction in aging and neurodegenerative diseases. *Ageing Res. Rev.* 70:101416. doi: 10.1016/j.arr.2021.101416

Ding, Z., Huang, Y., Bailey, S. K., Gao, Y., Cutting, L. E., Rogers, B. P., et al. (2018). Detection of synchronous brain activity in white matter tracts at rest and under functional loading. *Proc. Natl. Acad. Sci. U. S. A.* 115, 595–600. doi: 10.1073/pnas.1711567115

Donoshita, Y., Choi, U. S., Ban, H., and Kida, I. (2021). Assessment of olfactory information in the human brain using 7-tesla functional magnetic resonance imaging. *NeuroImage* 236:118212. doi: 10.1016/j.neuroimage.2021.118212

Duff, K., Mccaffrey, R. J., and Solomon, G. S. (2002). The pocket smell test: successfully discriminating probable Alzheimer's dementia from vascular dementia and major depression. *J. Neuropsychiatr. Clin. Neurosci.* 14, 197–201. doi: 10.1176/jnp.14.2.197

Eisenberg, I. W., Wallace, G. L., Kenworthy, L., Gotts, S. J., and Martin, A. (2015). Insistence on sameness relates to increased covariance of gray matter structure in autism spectrum disorder. *Mol. Autism.* 6:54. doi: 10.1186/s13229-015-0047-7

Fjaeldstad, A., Fernandes, H. M., Van Hartevelt, T. J., Gleesborg, C., Moller, A., Ovesen, T., et al. (2017). Brain fingerprints of olfaction: a novel structural method for assessing olfactory cortical networks in health and disease. *Sci. Rep.* 7:42534. doi: 10.1038/srep42534

Foster, E. R., Carson, L. G., Archer, J., and Hunter, E. G. (2021). Occupational therapy interventions for instrumental activities of daily living for adults with parkinson's disease: A systematic review. *Am J Occup Ther* 75, 7503190030p1–7503190030p24. doi: 10.5014/ajot.2021.046581

Han, Y., Wang, J., Zhao, Z., Min, B., Lu, J., Li, K., et al. (2011). Frequency-dependent changes in the amplitude of low-frequency fluctuations in amnestic mild cognitive impairment: a resting-state fMRI study. *NeuroImage* 55, 287–295. doi: 10.1016/j.neuroimage.2010.11.059

Jennings, D., Siderowf, A., Stern, M., Seibyl, J., Eberly, S., Oakes, D., et al. (2017). Conversion to Parkinson disease in the PARS Hyposmic and dopamine transporter-deficit prodromal cohort. *JAMA Neurol.* 74, 933–940. doi: 10.1001/jamaneurol.2017.0985

Mesholam, R. I., Moberg, P. J., Mahr, R. N., and Doty, R. L. (1998). Olfaction in neurodegenerative disease: a meta-analysis of olfactory functioning in Alzheimer's and Parkinson's diseases. *Arch. Neurol.* 55, 84–90. doi: 10.1001/archneur.55.1.84

Morley, J. F., Cohen, A., Silveira-Moriyama, L., Lees, A. J., Williams, D. R., Katzenschlager, R., et al. (2018). Optimizing olfactory testing for the diagnosis of

Parkinson's disease: item analysis of the university of Pennsylvania smell identification test. *NPJ Parkinsons Dis.* 4:2. doi: 10.1038/s41531-017-0039-8

Olde Dubbelink, K. T., Schoonheim, M. M., Deijen, J. B., Twisk, J. W., Barkhof, F., and Berendse, H. W. (2014). Functional connectivity and cognitive decline over 3 years in Parkinson disease. *Neurology* 83, 2046–2053. doi: 10.1212/WNL.0000000000001020

Peer, M., Nitzan, M., Bick, A. S., Levin, N., and Arzy, S. (2017). Evidence for functional networks within the human Brain's white matter. *J. Neurosci.* 37, 6394–6407. doi: 10.1523/JNEUROSCI.3872-16.2017

Pellegrino, R., Hähner, A., Bojanowski, V., Hummel, C., Gerber, J., and Hummel, T. (2016). Olfactory function in patients with hyposmia compared to healthy subjects - an fMRI study. *Rhinology* 54, 374–381. doi: 10.4193/Rhino16.098

Postuma, R. B., Berg, D., Stern, M., Poewe, W., Olanow, C. W., Oertel, W., et al. (2015). MDS clinical diagnostic criteria for Parkinson's disease. *Mov. Disord.* 30, 1591–1601. doi: 10.1002/mds.26424

Shi, Y., Zeng, W., and Wang, N. (2017). SCGICAR: spatial concatenation based group ICA with reference for fMRI data analysis. *Comput. Methods Prog. Biomed.* 148, 137–151. doi: 10.1016/j.cmpb.2017.07.001

Song, X. W., Dong, Z. Y., Long, X. Y., Li, S. F., Zuo, X. N., Zhu, C. Z., et al. (2011). REST: a toolkit for resting-state functional magnetic resonance imaging data processing. *PLoS One* 6:e25031. doi: 10.1371/journal.pone.0025031

Terroba Chambi, C., Rossi, M., Bril, A., Vernetti, P. M., Cerquetti, D., Cammarota, A., et al. (2017). Diagnostic value of combined acute levodopa challenge and olfactory testing to predict Parkinson's disease. *Mov. Disord. Clin. Pract.* 4, 824–828. doi: 10.1002/mdc3.12517

Turetsky, B. I., Hahn, C. G., Borgmann-Winter, K., and Moberg, P. J. (2009). Scents and nonsense: olfactory dysfunction in schizophrenia. *Schizophr. Bull.* 35, 1117–1131. doi: 10.1093/schbul/sbp111

Velayudhan, L., Gasper, A., Pritchard, M., Baillon, S., Messer, C., and Proitsi, P. (2015). Pattern of smell identification impairment in Alzheimer's disease. *J. Alzheimers Dis.* 46, 381–387. doi: 10.3233/JAD-142838

Wang, Z., Liu, Y., Ruan, X., Li, Y., Li, E., Zhang, G., et al. (2020). Aberrant amplitude of low-frequency fluctuations in different frequency bands in patients with Parkinson's disease. *Front. Aging Neurosci.* 12:576682. doi: 10.3389/fnagi.2020.576682

Wang, Y., Wei, H., Du, S., Yan, H., Li, X., Wu, Y., et al. (2022). Functional covariance connectivity of gray and white matter in olfactory-related brain regions in Parkinson's disease. *Front. Neurosci.* 16:853061. doi: 10.3389/fnins.2022.853061

Wang, N., Wu, H., Xu, M., Yang, Y., Chang, C., Zeng, W., et al. (2018). Occupational functional plasticity revealed by brain entropy: A resting-state fMRI study of seafarers. *Hum Brain Mapp* 39, 2997–3004. doi: 10.1002/hbm.24055

Wang, N., Zeng, W., and Chen, L. (2013). SACICA: a sparse approximation coefficient-based ICA model for functional magnetic resonance imaging data analysis. *J. Neurosci. Methods* 216, 49–61. doi: 10.1016/j.jneumeth.2013.03.014

Wang, N., Zeng, W., and Chen, D. (2016a). A novel sparse dictionary learning separation (SDLS) model with adaptive dictionary mutual incoherence constraint for fMRI data analysis. *IEEE Trans. Biomed. Eng.* 63, 2376–2389. doi: 10.1109/TBME.2016.2533722

Wang, N., Zeng, W., Chen, D., Yin, J., and Chen, L. (2016b). A novel brain networks enhancement model (BNEM) for BOLD fMRI data analysis with highly spatial reproducibility. *IEEE J. Biomed. Health Inform.* 20, 1107–1119. doi: 10.1109/JBHI.2015.2439685

Wang, N., Zeng, W., Shi, Y., Ren, T., Jing, Y., Yin, J., et al. (2015). WASICA: an effective wavelet-shrinkage based ICA model for brain fMRI data analysis. *J. Neurosci. Methods* 246, 75–96. doi: 10.1016/j.jneumeth.2015.03.011

Wang, N., Zeng, W., Shi, Y., and Yan, H. (2017). Brain functional plasticity driven by career experience: A resting-state fMRI study of the seafarer. *Front Psychol* 8:1786. doi: 10.3389/fpsyg.2017.01786

Wang, N., and Weiming, Z. (2012). A combination model of ICA and sparsity prior with respect to fMRI signal analysis. *Front. Comput. Neurosci.* 6:14. doi: 10.3389/conf.fncom.2012.55.00014

Wu, H., Yan, H., Yang, Y., Xu, M., Shi, Y., Zeng, W., et al. (2020). Occupational neuroplasticity in the human brain: A critical review and meta-analysis of neuroimaging studies. *Front Hum Neurosci* 14:215. doi: 10.3389/fnhum.2020.00215

Xiong, Y., Yu, Q., He, S., Tang, H., Liu, K., and Wang, N. (2021). "Comparison of Picard versions for analyzing functional magnetic resonance imaging data", in *Proceedings of the 2021 International Conference on Bioinformatics and Intelligent Computing. (Harbin, China: Association for Computing Machinery)*. doi: 10.1145/3448748.3448818

Yan, C. G., Wang, X. D., Zuo, X. N., and Zang, Y. F. (2016). DPABI: Data Processing & Analysis for (resting-state) brain imaging. *Neuroinformatics* 14, 339–351. doi: 10.1007/s12021-016-9299-4

Yi, J. S., Hura, N., Roxbury, C. R., and Lin, S. Y. (2022). Magnetic resonance imaging findings among individuals with olfactory and cognitive impairment. *Laryngoscope* 132, 177–187. doi: 10.1002/lary.29812

Yu, Q., Cai, Z., Li, C., Xiong, Y., Yang, Y., He, S., et al. (2021). A novel Spectrum contrast mapping method for functional magnetic resonance imaging data analysis. *Front. Hum. Neurosci.* 15:739668. doi: 10.3389/fnhum.2021.739668

Zang, Y., Jiang, T., Lu, Y., He, Y., and Tian, L. (2004). Regional homogeneity approach to fMRI data analysis. *NeuroImage* 22, 394–400. doi: 10.1016/j.neuroimage.2003.12.030

Zhang, Y. Q., Zhang, W. J., Liu, J. H., and Ji, W. Z. (2022). Effects of chronic hypoxic environment on cognitive function and neuroimaging measures in a high-altitude population. *Front. Aging Neurosci.* 14:788322. doi: 10.3389/fnagi.2022.788322

Zou, L. Q., Geng, F. L., Liu, W. H., Wei, X. H., Jiang, X. Q., Wang, Y., et al. (2015). The neural basis of olfactory function and its relationship with anhedonia in individuals with schizotypy: an exploratory study. *Psychiatry Res.* 234, 202–207. doi: 10.1016/j.pscychresns.2015.09.011

Zou, Q. H., Zhu, C. Z., Yang, Y., Zuo, X. N., Long, X. Y., Cao, Q. J., et al. (2008). An improved approach to detection of amplitude of low-frequency fluctuation (ALFF) for resting-state fMRI: fractional ALFF. *J. Neurosci. Methods* 172, 137–141. doi: 10.1016/j.jneumeth.2008.04.012

Zuo, X. N., and Xing, X. X. (2014). Test-retest reliabilities of resting-state FMRI measurements in human brain functional connectomics: a systems neuroscience perspective. *Neurosci. Biobehav. Rev.* 45, 100–118. doi: 10.1016/j.neubiorev.2014.05.009

Zuo, X. N., Xu, T., and Milham, M. P. (2019). Harnessing reliability for neuroscience research. *Nat. Hum. Behav.* 3, 768–771. doi: 10.1038/s41562-019-0655-x

frontiers | Frontiers in Aging Neuroscience

TYPE Original Research
PUBLISHED 05 January 2023
DOI 10.3389/fnagi.2022.1105019

OPEN ACCESS

EDITED BY
Jiehui Jiang,
Shanghai University,
China

REVIEWED BY
Haigang Ren,
Soochow University,
China
Anubhuti Dixit,
Amity University,
India

*CORRESPONDENCE
Hong Jiang
✉ jianghong73868@126.com

SPECIALTY SECTION
This article was submitted to Parkinson's Disease and Aging-related Movement Disorders, a section of the journal Frontiers in Aging Neuroscience

RECEIVED 22 November 2022
ACCEPTED 16 December 2022
PUBLISHED 05 January 2023

CITATION
Chen D, Wan L, Chen Z, Yuan X, Liu M, Tang Z, Fu Y, Zhu S, Zhang X, Qiu R, Tang B and Jiang H (2023) Serum vitamin levels in multiple system atrophy: A case-control study.
Front. Aging Neurosci. 14:1105019.
doi: 10.3389/fnagi.2022.1105019

Serum vitamin levels in multiple system atrophy: A case-control study

Daji Chen[1], Linlin Wan[1,2,3,4], Zhao Chen[1,2,4,5], Xinrong Yuan[1], Mingjie Liu[1], Zhichao Tang[1], You Fu[1], Sudan Zhu[1], Xuewei Zhang[6], Rong Qiu[7], Beisha Tang[1,2,4,5] and Hong Jiang[1,2,4,5,8,9]*

[1]Department of Neurology, Xiangya Hospital, Central South University, Changsha, China, [2]Key Laboratory of Hunan Province in Neurodegenerative Disorders, Central South University, Changsha, China, [3]Department of Radiology, Xiangya Hospital, Central South University, Changsha, China, [4]Hunan International Scientific and Technological Cooperation Base of Neurodegenerative and Neurogenetic Diseases, Changsha, China, [5]National Clinical Research Center for Geriatric Disorders, Xiangya Hospital, Central South University, Changsha, China, [6]Health Management Center, Xiangya Hospital, Central South University, Changsha, China, [7]School of Computer Science and Engineering, Central South University, Changsha, China, [8]School of Basic Medical Science, Central South University, Changsha, China, [9]National International Collaborative Research Center for Medical Metabolomics, Central South University, Changsha, China

Aim: There is increasing evidence suggesting that vitamins may play important roles in the pathogenesis of multiple system atrophy (MSA). The purpose of this study was to detect the changes of serum vitamin levels and investigate their correlation with disease severity in MSA patients.

Methods: In this cross-sectional study, 244 MSA patients, 200 Parkinson's disease (PD) patients and 244 age-gender matched healthy controls were recruited. Serum vitamin levels were measured, including vitamin A, B1, B2, B9 (folate), B12, C, D, and E. Relevant clinical scales were used to assess the disease severity of MSA patients.

Results: Compared with the healthy controls, decreased serum folate levels and increased serum vitamin A and C levels were detected in MSA patients. Similar differences were also observed in the gender-based subgroup analysis. There were no differences detected between MSA and PD patients. In MSA patients, significant correlation was found between vitamin A, folate, or vitamin C and relevant clinical scales or laboratory findings. In addition, ROC analysis showed potential diagnostic value of the combination of vitamin A, folate, and vitamin C in distinguishing MSA patients from healthy controls.

Conclusion: There were significant changes in the blood vitamin spectrums of MSA patients, suggesting that dysregulation of vitamins homeostasis might play an important role in the pathogenesis of MSA.

KEYWORDS

multiple system atrophy, vitamins, Parkinson's disease, pathogenesis, biomarker

1. Introduction

Multiple system atrophy (MSA) is a rare but fatal neurodegenerative disease characterized by variable combination of progressive autonomic dysfunction, Parkinson's symptoms, cerebellar ataxia, and pyramidal tract dysfunction, with a mean survival time being 6–10 years from symptom onset (Wenning et al., 2013; Coon et al., 2015; Foubert-Samier et al., 2020). Varied clinical presentations are the results of different pathologies including striatonigral, olivopontocerebellar, and central autonomic degeneration. Clinically, MSA is mainly divided into two subtypes, the parkinsonism subtype (MSA-P) and the cerebellar subtype (MSA-C), according to the predominant motor symptom or the onset sign (Krismer and Wenning, 2017; Poewe et al., 2022). The prominent pathological feature of MSA is oligodendroglia cytoplasmic inclusions (GCIs) mainly composed of α-synuclein (Ahmed et al., 2012; Koga et al., 2021), which is also the essential histologic hallmark for diagnosis of definite MSA (Gilman et al., 2008). MSA imposes an immense burden on patients and families. However, little is known about therapies for MSA due to the insufficient understanding of both the etiological factors and the pathological mechanisms influencing disease progression (Fanciulli and Wenning, 2015). Clinical diagnosis is also quite challenging because of significant overlap of clinical symptoms with other movement disorders, particularly Parkinson's disease (PD) and other parkinsonian disorders (Stankovic et al., 2019). Therefore, reliable biomarkers are crucial for both diagnosis and treatments of patients.

Vitamins are a group of essential organic compounds playing important roles in the regulation of metabolism, growth and development, as well as maintenance of life (de Vries Jasmijn et al., 2018). There is abundant evidence that kinds of vitamins levels in blood varied across individuals with neurodegenerative disease (Blasko et al., 2021; Schulz et al., 2021; Rahnemayan et al., 2022). Numerous studies have been performed to explore the association between vitamins and the risk of PD as well as the role of vitamin supplementation in the prevention and treatment of PD (Lehmann et al., 2017; Schirinzi et al., 2019; Christine et al., 2020; Zhong et al., 2022). Recent metabolomic studies of cerebrospinal fluid indicated that some kinds of vitamins were associated with age and neurodegenerative diseases (Hwangbo et al., 2022a,b). Since MSA shares neuropathogenesis similarities with PD, the exact roles of vitamins in MSA remain to be investigated. Although several studies have analyzed the alternation of vitamins in MSA, the findings in relative small size were controversial (Chen et al., 2015; Zhang et al., 2015; Guo et al., 2017), making it necessary to validate the association of vitamins with MSA in the larger cohorts.

Our study enrolled the largest MSA cohort so far, and investigated the difference of serum vitamin spectrums among MSA patients, PD patients and healthy controls (HC). Furthermore, we evaluated the correlations between serum levels of different vitamins and disease severity in MSA patients. Our study aimed to explore the dysregulation of vitamins homeostasis in MSA patients, as well as their potentials as biomarkers for MSA.

2. Materials and methods

2.1. Patients and study design

A hospital-based case control study was performed in the Xiangya Hospital of Central South University. 244 MSA patients and 200 PD patients were enrolled from Department of Neurology of Xiangya Hospital between March 2017 and October 2021. Patients with MSA were divided into two subtypes (MSA-P and MSA-C) according to the consensus criteria for the clinical diagnosis of both probable and possible MSA which was established in 2008 (Gilman et al., 2008). The patients with PD fulfilled the MDS Clinical Diagnostic Criteria for Parkinson's Disease, respectively (Postuma et al., 2015). Additionally, we recruited 244 gender-age matched healthy control subjects from the Physical Examination Center of the same hospital. Exclusion criteria were as follows: (1) gastrointestinal disorders or gastrointestinal surgery impairing vitamin absorption; (2) pernicious anemia; (3) alcohol abuse or alcohol dependence; (4) other neurodegenerative diseases; and (5) the use of proton pump inhibitors, H2 antagonists, or vitamin supplements. This study was approved by the Ethics Committee of the Xiangya Hospital of Central South University. All subjects agreed and signed informed consent.

2.2. Measurement of serum vitamins

Fasting peripheral venous blood was collected from subjects. Then, the serum levels of vitamins (including vitamin A, B1, B2, B9 (folate), B12, C, D, and E) were examined in the Clinical Laboratory of Xiangya hospital by electrochemistry method (LK3000V, Lanbiao, Tianjin, China).

2.3. Clinical investigations

A thorough neurological examination was performed on all subjects by two experienced neurologists. Among them, 124 MSA patients were evaluated through clinical scales including the Unified MSA Rating Scale (UMSARS), Hoehn and Yahr Parkinson's disease staging scheme (H&Y stage), Scales for Outcomes in Parkinson's Disease-Autonomic (SCOPA-AUT), Mini-Mental State Examination (MMSE) and Frontal Assessment Battery (FAB). UMSARS included four parts (I. Activities of Daily Living; II. Motor Examination Scale; III. Orthostatic hypotension; and IV. Disability Scale) and total UMSARS score was the sum of parts I and II. Hoehn and Yahr Parkinson's disease staging scheme (H&Y stage) was used to assess overall disease severity (Wenning et al., 2004). The Scales for Outcomes in PD-Autonomic (SCOPA-AUT) questionnaire was used to evaluate the autonomic dysfunction, which covered six different autonomic domains: gastrointestinal, urinary, cardiovascular, thermoregulatory, pupillomotor, and sexual domains (Damon-Perrière et al., 2012). Wexner score was used to evaluate the anal incontinence and constipation specifically. The Frontal

Assessment Battery (FAB) score and Mini-Mental State Examination (MMSE) score was used to assess global cognition. In addition, urine residue and serum homocysteine (HCY) levels were also recorded.

2.4. Statistical analysis

Continuous data were presented as mean ± standard deviation (SD). Normality assumptions were verified by the Shapiro–Wilk test, and homogeneity of variances were checked by the Levene test. All categorical variables, such as gender and subtype, were presented as percentages.

When the data conformed to the normal distribution, Student's t test and one-way analysis of variance (ANOVA) were used for comparison among groups. For non-parametric data, Mann–Whitney *U* test and Kruskal–Wallis test were conducted for comparison among two or more groups, respectively. Bonferroni's *post hoc* analysis was performed for multiple testing and protection against a false positive error. Categorical variables were analyzed using a chi-square test. In subgroup analysis, binary logistic regression model was used to access the odds ratio (OR) and adjust for covariates such as age and gender. Correlations between the clinical characteristics and serum vitamin levels were performed using Spearman's rank correlation. The diagnostic accuracy of different vitamins and their combination for MSA was calculated by receiver operating characteristic (ROC) curves. A value of $p < 0.05$ was considered to be statistically significant. All statistical analyses were performed through SPSS 26.0 (IBM Corp., New York, NY, United States) and GraphPad Prism 9.0(GraphPad Software, Inc.).

3. Results

3.1. Characteristics of subjects

Table 1 presented the demographic features and serum vitamin levels of the subjects. This cross-sectional study enrolled 244 MSA [145 males (59.4%) and 99 females (40.6%)], 200 PD patients [113 males (56.5%) and 87 females (43.5%)], and 244 healthy subjects [145 males (59.4%) and 99 females (40.6%)]. The median age of MSA, PD, and healthy controls was 56 (51–63), 56 (52–63), and 55 (52–62), respectively (Table 1). No significant differences were detected in terms of age and gender between MSA patients, PD patients, and healthy subjects. The clinical characteristics of 124 MSA patients were summarized in Table 2, in which the subjects were classified into two subtypes, including 36 MSA-P patients and 88 MSA-C patients.

3.2. Comparisons of vitamin levels among three groups

There were significant differences in serum vitamin A, B9, B12, and C levels among the MSA, PD and healthy control groups (Table 1; Figure 1). Pairwise comparisons by Bonferroni's *post hoc* analysis demonstrated that serum vitamin A ($p < 0.001$) and C ($p < 0.001$) in MSA patients were significantly higher than healthy subjects (Table 1), while serum vitamin B9 in MSA was lower than healthy subjects ($p < 0.001$; Table 1). However, for vitamin B12 levels, no significance was identified between MSA and controls, nor that between MSA and PD, while vitamin B12 levels in PD patients were

TABLE 1 Characteristics of the three participant cohorts.

	MSA (mean±SD)	PD (mean±SD)	Control (mean±SD)	χ^2值	*p*-Value	P_1	P_2	P_3
Number	244	200	244					
Gender				0.501	0.779[a]			
Male (%)	145 (59.4)	113 (56.5)	145 (59.4)					
Female (%)	99 (40.6)	87 (43.5)	99 (40.6)					
Age	56.56 ± 7.55	57.26 ± 7.82	56.06 ± 8.13	3.37	0.185[b]			
Vitamin A (μmol/L)	2.55 ± 0.69	2.48 ± 0.57	2.26 ± 0.16	32.6	<0.001[b]	0.738[c]	<0.001[c]	<0.001[c]
Vitamin B1(nmol/L)	126.78 ± 20.15	125.44 ± 21.27	127.66 ± 14.08	0.719	0.698[b]			
Vitamin B2 (μg/L)	8.00 ± 1.34	8.13 ± 1.42	7.98 ± 1.06	1.94	0.380[b]			
Vitamin B9 (μg/L)	9.74 ± 5.71	10.17 ± 6.09	15.06 ± 5.25	123	<0.001[b]	0.502[c]	<0.001[c]	<0.001[c]
Vitamin B12 (ng/L)	507.98 ± 339.80	488.00 ± 388.81	504.41 ± 217.30	16.1	<0.001[b]	0.181[c]	0.083[c]	<0.001[c]
Vitamin C (μmol/L)	32.12 ± 8.78	32.58 ± 9.50	28.58 ± 6.48	27.5	<0.001[b]	0.968[c]	<0.001[c]	<0.001[c]
Vitamin D (nmol/L)	87.39 ± 28.10	86.59 ± 24.18	87.65 ± 15.56	5.51	0.064[b]			
Vitamin E (μg/ml)	7.05 ± 1.22	6.99 ± 1.23	7.04 ± 0.82	2.70	0.259[b]			

SD, standard deviation; MSA, Multiple System Atrophy; PD, Parkinson's disease; P_1, comparison between MSA and PD; P_2, comparison between MSA and HC; P_3, comparison between PD and HC.

[a]Chi-square test.

[b]Kruskal–Wallis test.

[c]Bonferroni's *post hoc* analysis.

TABLE 2 Demographic, clinical parameters in MSA, MSA-P, and MSA-C patients.

	MSA-ALL	MSA-P	MSA-C
Number	124	36	88
Gender (*n*)			
Male (%)	75	19	56
Female (%)	49	17	32
Age (years)	55.96 ± 7.29	57.86 ± 7.01	55.18 ± 7.30
Age of onset (years)	53.49 ± 7.15	55.00 ± 6.91	52.87 ± 7.19
Disease during (years)	2.47 ± 1.21	2.86 ± 1.29	2.31 ± 1.14
UMSARS (total)	38.23 ± 15.04	44.44 ± 13.75	35.68 ± 14.88
UMSARS I	19.36 ± 7.44	21.42 ± 6.45	18.52 ± 7.68
UMSARS II	18.86 ± 8.47	23.03 ± 8.37	17.76 ± 7.95
UMSARS IV	2.61 ± 1.05	2.61 ± 0.93	2.61 ± 1.11
H&Y	3.51 ± 0.91	3.25 ± 0.96	3.67 ± 0.86
SCOPA-AUT	19.90 ± 8.75	24.25 ± 7.5	17.41 ± 8.49
Digestive	4.92 ± 3.57	6.26 ± 3.64	4.19 ± 3.35
Urinary	7.87 ± 4.34	9.69 ± 3.25	6.82 ± 4.57
Cardiovascular	2.00 ± 1.16	2.17 ± 1.10	1.92 ± 1.20
Thermoregulatory	1.95 ± 1.44	2.53 ± 1.81	1.56 ± 1.00
Pupillomotor	0.19 ± 0.71	0.33 ± 0.68	0.56 ± 0.91
Sexual	5.52 ± 1.22	5.62 ± 1.08	5.46 ± 1.32
Wexner score	6.00 ± 4.26	6.85 ± 4.01	5.56 ± 4.36
MMSE	25.44 ± 3.66	25.45 ± 3.62	25.44 ± 3.70
FAB	11.28 ± 3.64	10.83 ± 3.99	11.53 ± 3.46
Hcy	13.12 ± 3.82	12.99 ± 3.14	13.19 ± 4.20
Urine residue	93.12 ± 136.91	120.74 ± 179.08	81.47 ± 114.35

MSA-ALL, whole MSA cohort; MSA-P, MSA parkinsonism subtype; MSA-C, cerebellar subtype; UMSARS, Unified Multiple system atrophy Rating Scale; PDSS, PD Sleep Scale; H&Y, the modified Hoehn and Yahr staging scale; SCOPA-AUT, the Scales for Outcomes in PD-Autonomic questionnaire; MMSE, mini-mental state examination; FAB, The Frontal Assessment Battery score.

significantly lower than healthy subjects ($p < 0.001$; Table 1; Figure 1). Our results showed no significant differences in the vitamin A, B9, and C levels between MSA and PD patients by Bonferroni's *post hoc* analysis. In addition, there was no significant difference in serum levels of vitamin B1, B2, B6, D, and E among MSA patients, PD patients, and healthy subjects (Table 1; Figure 1).

In the subgroup analysis according to gender, similar results retained between MSA patients and healthy subjects (Supplementary Table 1; Figure 2). The vitamin A levels in both male and female subgroup-analysis differed significantly between two groups ($p = 0.000$ for males, $p = 0.024$ for females). Meanwhile, the vitamin C levels exhibited an upward trend in MSA patients than healthy subjects ($p = 0.001$ for males, $p = 0.010$ for females). In addition, regardless of male or female, vitamin B9 levels showed a reduction in MSA patients compared with healthy subjects ($p < 0.001$ for both males and females,). Vitamin B1, B6, B12, D, and E levels did not present any differences in the subgroups (Supplementary Table 1). We also investigated the difference between two subtypes of MSA. Given that age is not equal between the two subgroups, binary logistic regression was utilized to adjust age and gender. The result revealed no significant difference in serum levels of vitamins between two subgroups (Supplementary Table 2).

3.3. Correlations between vitamin levels and clinical assessing scales

Spearman's correlation analysis was performed in 124 MSA patients to evaluate the correlations between the clinical characteristics and serum vitamin levels (Table 3; Supplementary Table 3). A significant correlation was observed between serum vitamin A and SCOPA-AUT pupillomotor subdomain ($r_s = -0.356$, $p = 0.01$). Meanwhile, the serum vitamin B9 levels were found to be negatively correlated with UMSARS IV, H&Y stages, and HCY ($r_s = -0.290$ [$p = 0.001$], -0.365 [$p = 0.11$], and -0.297 [$p = 016$], respectively). Additionally, our data showed that serum vitamin C levels positively correlated with SCOPA-AUT thermoregulatory subdomain ($r_s = 0.339$, $p = 0.028$). Besides, vitamin D negatively correlated with urine residue. Vitamin B12 positively correlated with age and age of onset. However, the association between vitamin B12 and age of onset showed no significance after adjusting for age. In addition to such findings, no significant correlations were found between vitamins and remaining clinical characteristics (Figure 3).

3.4. The ROC analysis of vitamins in the diagnosis of MSA

Receiver operating characteristic curve (ROC) analysis was conducted to assess the ability of serum vitamins to distinguish between MSA patients and healthy controls. The ROC of vitamin A analysis demonstrated that an area under the curve (AUC) value was 0.6291 (95% CI: 0.5769 to 0.6813, $p < 0.001$, Figure 4A), with a sensitivity of 95% and specificity of 40%. The AUC of vitamin B9 was 0.7653 (95% CI: 0.7229 to 0.8077, $p < 0.001$, Figure 4B), with a sensitivity of 73% and specificity of 72%. The AUC of serum vitamin C was 0.6236 (95% CI: 0.5732 to 0.6739, $p < 0.001$, Figure 4C), with a sensitivity of 74% and specificity of 55%. Furthermore, the optimal ROC curve was provided by the combination of vitamin A, B9, and C for discrimination between MSA patients and healthy controls, of which the AUC was 0.8143 (95% CI: 0.7762 to 0.8523, $p < 0.001$, Figure 4D), with a sensitivity of 81% and specificity of 70%.

4. Discussion

Our study included the largest-sample MSA cohorts till now and investigated the variation of serum vitamin levels and their correlation with disease severity in MSA patients.

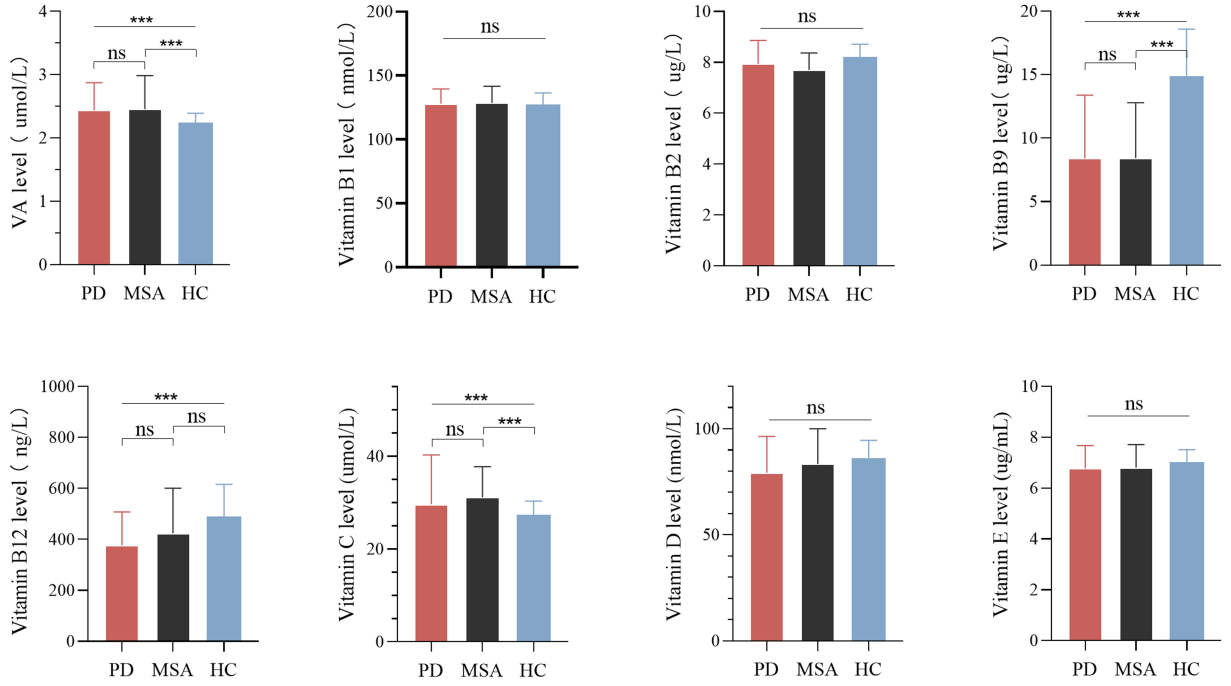

FIGURE 1
Levels of different vitamins in patients with multiple system atrophy (MSA), Parkinson's disease (PD), and healthy controls (HC). Multiple comparisons were corrected with Bonferroni correction. ns: non-significant. ***p<0.001.

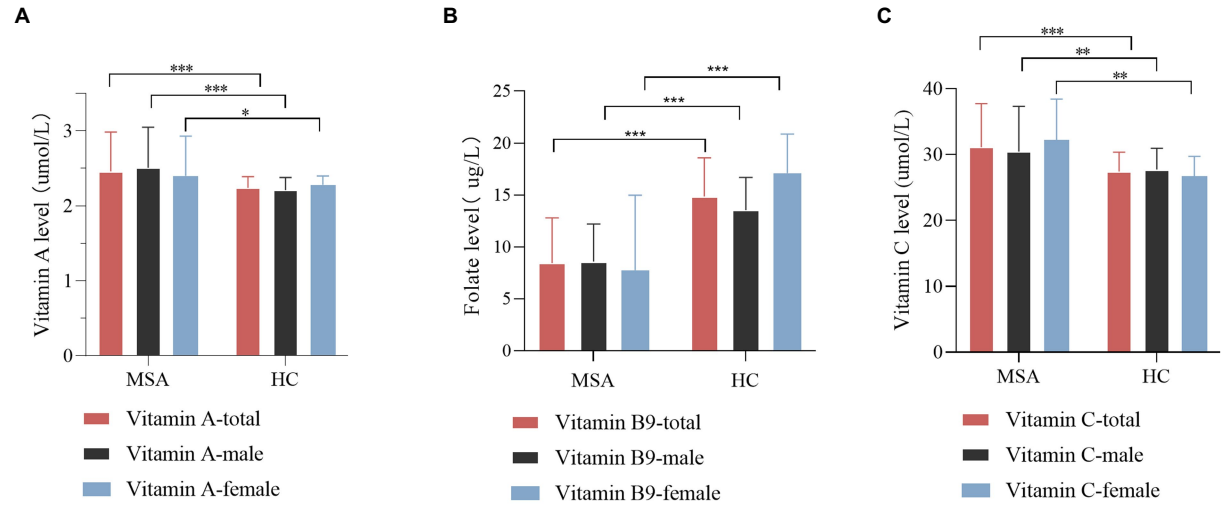

FIGURE 2
Comparison of vitamin A, B9, and C levels between MSA patients and healthy control (HC), according to gender. **(A)** Comparison of vitamin A level between control and MSA groups. MSA (male) vs. control (male), ***p<0.001; MSA (female) vs. control (female), *p=0.024. **(B)** Comparison of vitamin B9 level between control and MSA groups. MSA (male) vs. control (male), ***p<0.001; MSA (female) vs. control (female), ***p<0.001. **(C)** Comparison of vitamin C levels between control and MSA groups. MSA (male) vs. control (male), **p=0.001; MSA (female) vs. control (female), **p=0.001.

We found the decreased vitamin B9 and increased vitamin A and C levels in MSA patients compared with healthy controls, no matter in male or female. Besides, vitamin A, B9, and C were found to be significantly correlated with motor, pupillomotor, and thermoregulatory dysfunction, respectively. Moreover, the ROC curve analysis demonstrated that the combination of vitamin A, B9, and C could help to discriminate MSA patients from healthy subjects. As far as we know, this study was the most comprehensive research to investigate the changes of the serum vitamins levels in MSA patients, further highlighting the role of vitamins homeostasis dysregulation in MSA pathogenesis.

TABLE 3 Correlations between vitamin A, B9, and C with clinical characteristics of multiple system atrophy (MSA).

Variable	Vitamin A		Vitamin B9		Vitamin C	
	r_s	p	r_s	p	r_s	p
Age	−0.035	0.583	0.053	0.413	0.077	0.229
Age of onset	−0.030	0.637	0.058	0.365	0.068	0.289
Disease duration	−0.033	0.607	−0.030	0.637	0.063	0.329
UMSARS (total)	0.011	0.911	−0.089	0.325	−0.037	0.680
UMSARS I	−0.004	0.964	−0.101	0.261	−0.053	0.562
UMSARS II	0.024	0.795	−0.069	0.446	−0.020	0.823
UMSARS IV	0.057	0.536	−0.290**	0.001	−0.140	0.125
H&Y	0.084	0.570	−0.365*	0.011	−0.025	0.867
SCOPA-AUT	0.048	0.677	0.064	0.582	−0.015	0.897
Digestive	−0.082	0.437	0.050	0.639	0.132	0.209
Urinary	0.099	0.377	0.154	0.171	−0.080	0.480
Cardiovascular	−0.032	0.817	0.113	0.412	−0.078	0.573
Thermoregulatory	0.011	0.943	0.100	0.528	0.339*	0.028
Pupillomotor	−0.356**	0.001	−0.018	0.870	0.124	0.254
Sexual	−0.014	0.904	−0.003	0.980	−0.036	0.762
Wexner score	0.052	0.614	−0.060	0.561	0.042	0.682
MMSE	0.085	0.397	−0.084	0.402	−0.099	0.323
FAB	−0.190	0.083	0.097	0.379	−0.084	0.447
HCY	−0.019	0.879	−0.297*	0.016	0.007	0.953
Urine residue	0.026	0.804	0.074	0.480	0.051	0.626

r_s, Spearman's rank correlation coefficient; UMSARS, Unified Multiple system atrophy Rating Scale; PDSS, PD Sleep Scale; H&Y, the modified Hoehn and Yahr staging scale; SCOPA-AUT: the Scales for Outcomes in PD-Autonomic; MMSE, mini-mental state examination; FAB, The Frontal Assessment Battery score; HCY, homocysteine.
*$p < 0.05$; **$p < 0.01$.

The limited understanding of the etiology hindered the development of diagnostic and treatment for MSA. Given that the main biological characteristic is the presence of intracellular aggregates of α-syn, MSA and PD are often thought to share similar pathogenesis (Koga et al., 2021). We noted that several studies have indicated that inflammatory responses and oxidative stress played a significant role in the neurodegenerative cascade leading to neurodegenerative diseases (Wyss-Coray and Mucke, 2002; Rebec et al., 2006; Sekiyama et al., 2012; Zhu et al., 2016) There was also evidence that many kinds of vitamins had a close relationship with the occurrence and development of AD and PD (Peterson et al., 2013; Lehmann et al., 2017; Christine et al., 2018; Nourhashemi et al., 2018). What attracted our attention was whether those vitamins were also involved in the pathogenesis of MSA, as well as their relationship with the disease severity.

Vitamin A was involved in several important homeostatic processes, such as cell differentiation, antioxidant activity, inflammation, and neuronal plasticity. The role of vitamin A and its derivatives in the pathogenesis of neurodegenerative diseases, as well as the potentials as therapeutic targets, has drawn attention for years (Eichele, 1997; Clark et al., 2020; Marie et al., 2021). Our study demonstrated a significantly increased vitamin A levels in MSA patients compared with healthy controls, which might due to the compensatory reactions for the dysregulated processes above in MSA. Vitamin C was another elevated vitamin in MSA, contrast to the alteration of serum vitamin C levels in previous studies in PD (Ide et al., 2015; Barmaki et al., 2021). However, it was also reported that serum vitamin C level was found increased in AD patients compared with healthy people (Liu et al., 2022). Oxidative stress was increasingly supposed to be a critical epigenetic factor for neurodegenerative disease and contributed to the aggregation of α-synuclein (Macedo et al., 2015). Vitamin C had a strong capacity for antioxidant and free radical scavenging in serum, central nervous system and other tissues. The elevated serum levels of vitamin A and C further implied that oxidative stress might play an important role in the pathogenesis of the MSA. Further analysis in the sub-group by gender indicated that the alteration of serum levels in the patient with MSA had no relationship with gender.

Interestingly, we observed significantly decreased serum vitamin B9 levels in MSA patients compared with healthy people, while no difference was found in serum vitamin B12 levels between two groups. Consistent results were also obtained in gender-based subgroup analysis. It was known that both vitamin B12 and folate were required in the remethylation of homocysteine (HCY), which was involved in the pathogenesis of neurodegenerative disease *via* mediating inflammation response

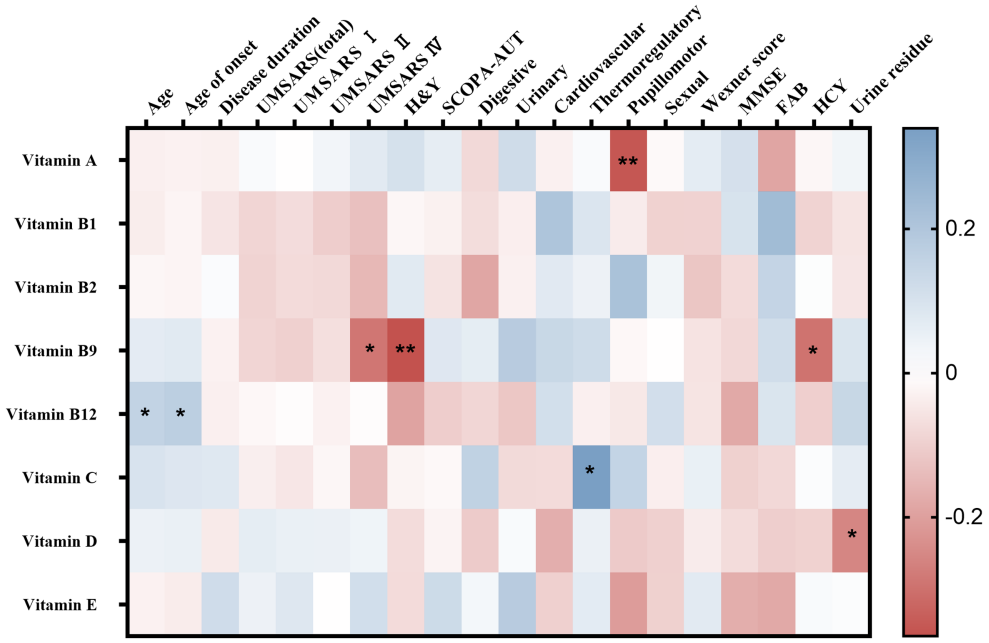

FIGURE 3
Heatmap for correlation analysis between different vitamins and clinical characteristics of multiple system atrophy (MSA). UMSARS, the Unified MSA Rating Scale; H&Y, Hoehn and Yahr Parkinson's disease staging scheme; SCOPA-AUT, the Scales for Outcomes in PD-Autonomic questionnaire; MMSE, Mini-Mental State Examination score; FAB, Frontal Assessment Battery score. *p<0.05; **p<0.01.

(Seshadri et al., 2002). Increased serum HCY levels were observed in MSA patients compared with healthy subjects in previous studies (Chen et al., 2015; Guo et al., 2017; Zhong et al., 2022). The decreased vitamin B9 levels might contribute to the neuroinflammation in MSA, which was further validated through the negative correlation between folate and HCY levels. We also observed decreased serum vitamin B9 levels in PD patients compared with healthy controls, which was consistent with the previous meta-analysis result (Shen, 2015; Dong and Wu, 2020). It was proposed that folate deficit might results from the gastrointestinal dysfunction and gut microbial metabolic disorder (Rosario et al., 2021). Similar outcomes were also reported in AD and ALS studies that found decreased serum vitamin B9 level in patients compared with healthy controls (Wang et al., 2020; Liu et al., 2022). The mechanisms of vitamin B9 reduction in MSA was worth exploring. Since the human body could not synthesize folate, exogenously folate supply was necessary. Rosario et al. (2021) found that folate deficit in PD might result from gastrointestinal dysfunction and gut microbial metabolic disorder. The study showed that folate biosynthesis decreased in a state of gastrointestinal dysfunction. Meanwhile, personalized metabolic modeling revealed the microbial contribution to folate deficiency (Rosario et al., 2021). In MSA, the gastrointestinal function was also an important symptom (Sakakibara, 2021). Besides, increasing studies found the presence of gut microbial imbalance in MSA patients, which might serve important roles in MSA pathogenesis. (Tan et al., 2018; Wan et al., 2019). Thus, the gastrointestinal dysfunction and gut microbial dysbiosis might account for the vitamin B9 deficiency in MSA. Overall, the role of vitamin B9 in the pathogenesis of MSA and the potential to treat consequent metabolic and clinical complications warrant more thoroughly investigation.

As for the correlation with clinical scales, vitamin B9 showed negative correlations with UPDRS IV and H&Y scores, indicating that vitamin B9 might influence motor symptoms in MSA patients. Li et al. (2021) demonstrated that serum vitamin B9 and B12 levels were critical factors influencing the motor performance status in PD, where increased serum vitamin B9 level negatively correlated with moderate motor impairment. In addition, our data indicated that serum vitamin A levels were negatively correlated with pupillomotor dysfunction of SCOPA-AUT while vitamin C levels were positively correlated with thermoregulatory dysfunction of SCOPA-AUT scores. Our results suggested that vitamin B9 might have a more prominent influence on motor function of MSA while vitamin A and C were mainly associated with autonomic dysfunction. These results revealed the correlations of vitamins with disease severity of MSA and further implied the critical roles of vitamins in the pathogenic mechanisms of MSA.

ROC curve analysis was performed to assess the ability of serum vitamin A, B9, and C to distinguish MSA patients from HCs. vitamin B9 showed the most reliable diagnostic ability, followed by vitamin A and C. Moreover, our data demonstrated that the combination of vitamin A, B9, and C could provide more reliable discrimination between MSA and healthy controls than any vitamin alone, which might facilitate clinical practice. Notably, the results of the ROC curve analysis did not endorse accurate identification due to the overlap among MSA, PD, and other related diseases, further validation in the larger cohorts were necessary.

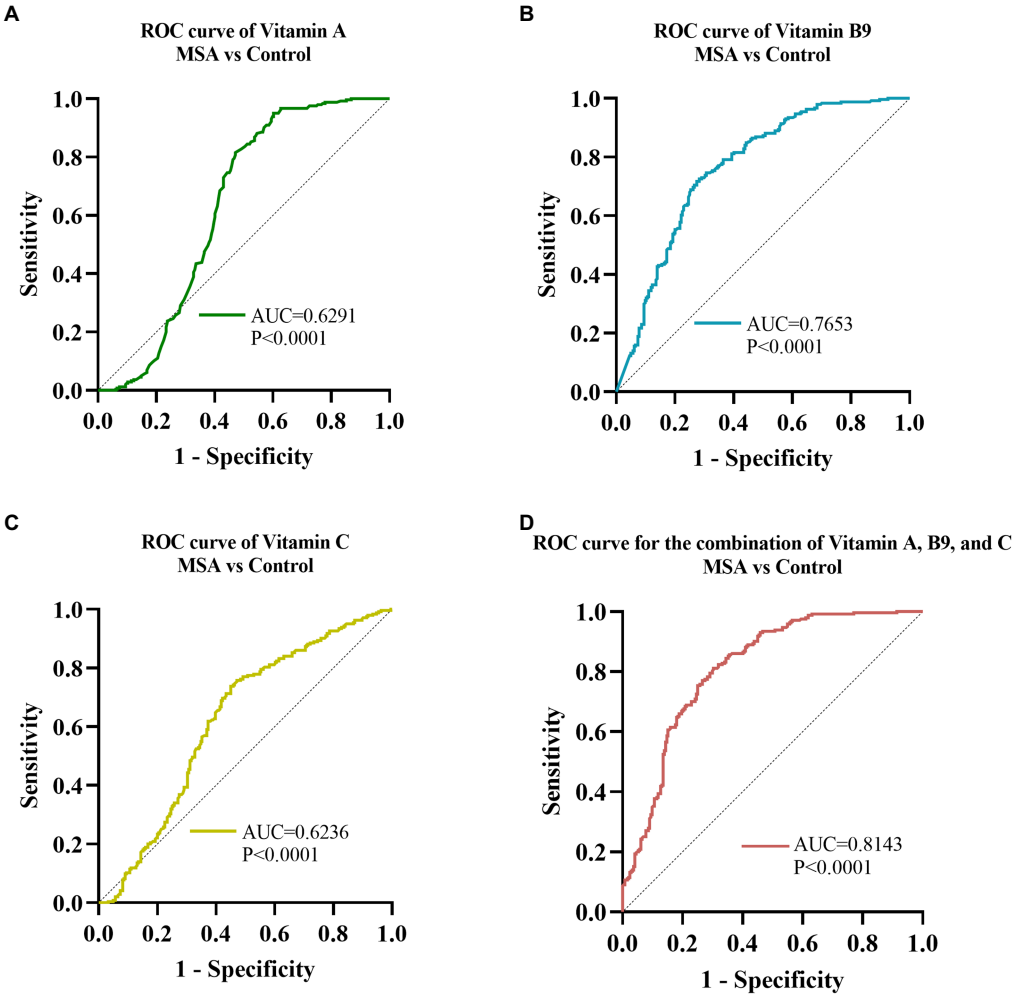

FIGURE 4
ROC curves to evaluate the utility of serum levels of vitamin for the discrimination of MSA patients from healthy controls. The AUC of ROC curves for **(A)** vitamin A, **(B)** vitamin B9, and **(C)** vitamin C were 0.6291 (95% CI: 0.5769 to 0.6813, $p<0.0001$), 0.7653 (95% CI: 0.7229 to 0.8077, $p<0.001$), and 0.6236 (95% CI: 0.5732 to 0.6739, $p<0.0001$), respectively. The AUC of **(D)** combination of vitamin A, B9, and C was 0.8143 (95% CI: 0.7762 to 0.8523, $p<0.001$).

The variation between MSA patients and healthy controls provided compromised evidence regarding the involvement of vitamins in the occurrence and development of MSA. Several studies indirectly suggested that vitamins may be useful in the treatment of MSA. *In vitro* experiments indicated that vitamin A could potently destabilize preformed alpha-synuclein fibrils, which suggested that vitamin A might be useful in the treatment and prevention of MSA (Ono and Yamada, 2007). McCarter et al. (2020) found that low vitamin B12 levels were associated with shorter survival in MSA, implying the potential role as a modifiable survival factor of vitamin B12 for MSA. In addition, a systematic review found supplementation of folate had the potential to reduce the high homocysteine concentrations and other clinical complications in Parkinson's disease (Boelens Keun et al., 2021). Noticeably, few study provided reliable clinical evidence and demonstrated clear effectiveness for vitamins in MSA, and strict randomized clinical trials were necessary in the future to validate the benefits of vitamin supplementation in MSA patients.

Some limitations of the study warrant consideration. Firstly, our study was cross-sectional research and the longitudinal dynamics of serum vitamins levels, as well as the effects on the disease progression, were needed to be further explored in the longitudinal study. Then, the difference of serum vitamins levels between MSA and other easily-confused diseases, such as PSP (Progressive Supranuclear Palsy), and SAOA (Sporadic Adult-Onset Ataxia). remained to be further investigated. Thus, the future longitudinal cohort study including more diseases mimicking MSA are needed to uncover the dysregulation of vitamins homeostasis in MSA pathogenesis thoroughly. Moreover, we did not collect detailed dietary and economical information of the participants in this retrospective study. However, all subjects were from south-central China, who might have similar dietary patterns. Besides, we excluded those who were overweight or malnourished, as well as taking vitamin supplements. In the following studies, we will collect the detailed dietary and economic data through related questionnaires to further validated our conclusions.

In conclusion, based on the case-control study in the largest MSA cohort so far, we revealed the significant changes in the blood vitamin spectrums of MSA patients, suggesting the pivotal role of dysregulation of vitamins homeostasis in the pathogenesis of MSA. The present study showed that several vitamins level were altered and associated with the severity of disease in MSA patients, demonstrating a potential value for disease diagnosis and surveillance. Our data also provided supports for clinical guidance on vitamin supplements of MSA patients. Further validations and explorations in the longitudinal cohorts consisting of more disease mimicking MSA were necessary.

Data availability statement

The original contributions presented in the study are included in the article/Supplementary material; further inquiries can be directed to the corresponding author.

Ethics statement

The studies involving human participants were reviewed and approved by the Ethics Committee of the Xiangya Hospital of Central South University. The patients/participants provided their written informed consent to participate in this study.

Author contributions

DC and LW designed the study. DC analyzed data and wrote original draft. DC, XY, ML, and XZ contributed to the data acquisition of vitamin levels. ZT, XY, DC, YF, and SZ collected clinical data. LW, ZC, RQ, BT, and HJ supervised the process and edited the manuscript. All authors contributed to the article and approved the submitted version.

Funding

This study was funded by the National Key R&D Program of China (No. 2021YFA0805200 to HJ), the National Natural Science Foundation of China (No. 81974176 and No. 82171254 to HJ; No. 81901169 to ZC; No. 81901305 to CW; No. 82201411 to L He), the Innovation Research Group Project of Natural Science Foundation of Hunan Province (No. 2020JJ1008 to HJ), the Science and Technology Innovation Group of Hunan Province (No. 2020RC4043 to HJ), the Scientific Research Foundation of Health Commission of Hunan Province (No. B2019183 to HJ), the Key Research and Development Program of Hunan Province (Nos. 2020SK2064 and 2018SK2092 to HJ), the Innovative Research and Development Program of Development and Reform Commission of Hunan Province to HJ, the Natural Science Foundation of Hunan Province (Nos. 2022JJ20094 and 2021JJ40974 to ZC; No. 2020JJ5925 to CW; No. 2022JJ40783 to L He), the Central South University Research Programme of Advanced Interdisciplinary Study (No. 2023QYJC010 to HJ), the Project Program of National Clinical Research Center for Geriatric Disorders (Xiangya Hospital, Nos. 2020LNJJ12 and XYYYJSTG-05 to HJ), the Science and Technology Innovation Program of Hunan Province (2022RC1027 to ZC).

Acknowledgments

The authors thank L He and CR Wang for giving financial support for this study. In addition, the authors are grateful to all patients and healthy individuals who participated in the study.

Conflict of interest

The authors declare that the research was conducted in the absence of any commercial or financial relationships that could be construed as a potential conflict of interest.

Publisher's note

Supplementary material

The supplementary material for this article can be found online at: https://www.frontiersin.org/articles/10.3389/fnagi.2022.1105019/full#supplementary-material

References

Ahmed, Z., Asi, Y. T., Sailer, A., Lees, A. J., Houlden, H., Revesz, T., et al. (2012). The neuropathology, pathophysiology and genetics of multiple system atrophy. *Neuropathol. Appl. Neurobiol.* 38, 4–24. doi: 10.1111/j.1365-2990.2011.01234.x

Barmaki, H., Morovati, A., Eydivandi, Z., Jafari Naleshkenani, F., Saedi, S., Musavi, H., et al. (2021). The association between serum oxidative stress indexes and pathogenesis of Parkinson's disease in the northwest of Iran. *Iran. J. Public Health* 50, 606–615. doi: 10.18502/ijph.v50i3.5621

Blasko, I., Defrancesco, M., Oberacher, H., Loacker, L., Kemmler, G., Marksteiner, J., et al. (2021). Plasma phosphatidylcholines and vitamin B12/folate levels are possible prognostic biomarkers for progression of Alzheimer's disease. *Exp. Gerontol.* 147:111264. doi: 10.1016/j.exger.2021.111264

Boelens Keun, J. T., Arnoldussen, I. A., Vriend, C., and van de Rest, O. (2021). Dietary approaches to improve efficacy and control side effects of levodopa therapy in Parkinson's disease: a systematic review. *Adv. Nutr.* 12, 2265–2287. doi: 10.1093/advances/nmab060

Chen, D., Wei, X., Zou, J., Wang, R., Liu, X., Xu, X., et al. (2015). Contra-directional expression of serum homocysteine and uric acid as important biomarkers of multiple system atrophy severity: a cross-sectional study. *Front. Cell. Neurosci.* 9:247. doi: 10.3389/fncel.2015.00247

Christine, C. W., Auinger, P., Joslin, A., Yelpaala, Y., and Green, R. (2018). Vitamin B12 and homocysteine levels predict different outcomes in early Parkinson's disease. *Mov. Disord.* 33, 762–770. doi: 10.1002/mds.27301

Christine, C. W., Auinger, P., Saleh, N., Tian, M., Bottiglieri, T., Arning, E., et al. (2020). Relationship of cerebrospinal fluid vitamin B12 status markers with Parkinson's disease progression. *Mov. Disord.* 35, 1466–1471. doi: 10.1002/mds.28073

Clark, J. N., Whiting, A., and McCaffery, P. (2020). Retinoic acid receptor-targeted drugs in neurodegenerative disease. *Expert Opin. Drug Metab. Toxicol.* 16, 1097–1108. doi: 10.1080/17425255.2020.1811232

Coon, E. A., Sletten, D. M., Suarez, M. D., Mandrekar, J. N., Ahlskog, J. E., Bower, J. H., et al. (2015). Clinical features and autonomic testing predict survival in multiple system atrophy. *Brain J. Neurol.* 138, 3623–3631. doi: 10.1093/brain/awv274

Damon-Perrière, N., Foubert-Samier, A., De Cock, V. C., Gerdelat-Mas, A., Debs, R., Pavy-Le Traon, A., et al. (2012). Assessment of the Scopa-Aut questionnaire in multiple system atrophy: relation to UMSARS scores and progression over time. *Parkinsonism Relat. Disord.* 18, 612–615. doi: 10.1016/j.parkreldis.2011.12.009

de Vries Jasmijn, Y., Pundir, S., McKenzie, E., Keijer, J., and Kussmann, M. (2018). Maternal circulating vitamin status and colostrum vitamin composition in healthy lactating women-a systematic approach. *Nutrients* 10:687. doi: 10.3390/nu10060687

Dong, B., and Wu, R. (2020). Plasma homocysteine, folate and vitamin B12 levels in Parkinson's disease in China: a meta-analysis. *Clin. Neurol. Neurosurg.* 188:105587. doi: 10.1016/j.clineuro.2019.105587

Eichele, G. (1997). Retinoids: from hindbrain patterning to Parkinson disease. *Trends Genet.* 13, 343–345. doi: 10.1016/s0168-9525(97)01218-3

Fanciulli, A., and Wenning, G. K. (2015). Multiple-system atrophy. *N. Engl. J. Med.* 372, 249–263. doi: 10.1056/NEJMra1311488

Foubert-Samier, A., Pavy-Le Traon, A., Guillet, F., Le-Goff, M., Helmer, C., Tison, F., et al. (2020). Disease progression and prognostic factors in multiple system atrophy: a prospective cohort study. *Neurobiol. Dis.* 139:104813. doi: 10.1016/j.nbd.2020.104813

Gilman, S., Wenning, G. K., Low, P. A., Brooks, D. J., Mathias, C. J., Trojanowski, J. Q., et al. (2008). Second consensus statement on the diagnosis of multiple system atrophy. *Neurology* 71, 670–676. doi: 10.1212/01.wnl.0000324625.00404.15

Guo, Y., Zhuang, X.-D., Xian, W.-B., Wu, L.-L., Huang, Z.-N., Hu, X., et al. (2017). Serum klotho, vitamin D, and homocysteine in combination predict the outcomes of Chinese patients with multiple system atrophy. *CNS Neurosci. Ther.* 23, 657–666. doi: 10.1111/cns.12711

Hwangbo, N., Zhang, X., Raftery, D., Gu, H., Hu, S. C., Montine, T. J., et al. (2022b). Predictive modeling of Alzheimer's and Parkinson's disease using metabolomic and lipidomic profiles from cerebrospinal fluid. *Metabolites* 12:277. doi: 10.3390/metabo12040277

Hwangbo, N., Zhang, X., Raftery, D., Gu, H., Hu, S. C., Montine, T. J., et al. (2022a). A metabolomic aging clock using human cerebrospinal fluid. *J. Gerontol. A Biol. Sci. Med. Sci.* 77, 744–754. doi: 10.1093/gerona/glab212

Ide, K., Yamada, H., Umegaki, K., Mizuno, K., Kawakami, N., Hagiwara, Y., et al. (2015). Lymphocyte vitamin C levels as potential biomarker for progression of Parkinson's disease. *Nutrition* 31, 406–408. doi: 10.1016/j.nut.2014.08.001

Koga, S., Sekiya, H., Kondru, N., Ross, O. A., and Dickson, D. W. (2021). Neuropathology and molecular diagnosis of Synucleinopathies. *Mol. Neurodegener.* 16:83. doi: 10.1186/s13024-021-00501-z

Krismer, F., and Wenning, G. K. (2017). Multiple system atrophy: insights into a rare and debilitating movement disorder. *Nat. Rev. Neurol.* 13, 232–243. doi: 10.1038/nrneurol.2017.26

Lehmann, S., Loh, S. H. Y., and Martins, L. M. (2017). Enhancing NAD salvage metabolism is neuroprotective in a PINK1 model of Parkinson's disease. *Biol. Open* 6, 141–147. doi: 10.1242/bio.022186

Li, S., Zhang, Q., Gao, Y., Nie, K., Liang, Y., Zhang, Y., et al. (2021). Serum folate, vitamin B12 levels, and systemic immune-inflammation index correlate with motor performance in Parkinson's disease: a cross-sectional study. *Front. Neurol.* 12:665075. doi: 10.3389/fneur.2021.665075

Liu, X. X., Wu, P. F., Liu, Y. Z., Jiang, Y. L., Wan, M. D., Xiao, X. W., et al. (2022). Association between serum vitamins and the risk of Alzheimer's disease in Chinese population. *J. Alzheimers Dis.* 85, 829–836. doi: 10.3233/jad-215104

Macedo, D., Tavares, L., McDougall, G. J., Vicente Miranda, H., Stewart, D., Ferreira, R. B., et al. (2015). (poly) phenols protect from α-synuclein toxicity by reducing oxidative stress and promoting autophagy. *Hum. Mol. Genet.* 24, 1717–1732. doi: 10.1093/hmg/ddu585

Marie, A., Darricau, M., Touyarot, K., Parr-Brownlie, L. C., and Bosch-Bouju, C. (2021). Role and mechanism of vitamin a metabolism in the pathophysiology of Parkinson's disease. *J. Parkinsons Dis.* 11, 949–970. doi: 10.3233/jpd-212671

McCarter, S. J., Coon, E. A., Savica, R., St Louis, E. K., Bower, J. H., Benarroch, E. E., et al. (2020). Lower vitamin B12 level at multiple system atrophy diagnosis is associated with shorter survival. *Mov. Disord.* 35, 1462–1466. doi: 10.1002/mds.28070

Nourhashemi, F., Hooper, C., Cantet, C., Féart, C., Gennero, I., Payoux, P., et al. (2018). Cross-sectional associations of plasma vitamin D with cerebral β-amyloid in older adults at risk of dementia. *Alzheimers Res. Ther.* 10:43. doi: 10.1186/s13195-018-0371-1

Ono, K., and Yamada, M. (2007). Vitamin a potently destabilizes preformed alpha-synuclein fibrils in vitro: implications for Lewy body diseases. *Neurobiol. Dis.* 25, 446–454. doi: 10.1016/j.nbd.2006.10.010

Peterson, A. L., Murchison, C., Zabetian, C., Leverenz, J. B., Watson, G. S., Montine, T., et al. (2013). Memory, mood, and vitamin D in persons with Parkinson's disease. *J. Parkinsons Dis.* 3, 547–555. doi: 10.3233/JPD-130206

Poewe, W., Stankovic, I., Halliday, G., Meissner, W. G., Wenning, G. K., Pellecchia, M. T., et al. (2022). Multiple system atrophy. *Nat. Rev. Dis. Primers.* 8:56. doi: 10.1038/s41572-022-00382-6

Postuma, R. B., Berg, D., Stern, M., Poewe, W., Olanow, C. W., Oertel, W., et al. (2015). MDS clinical diagnostic criteria for Parkinson's disease. *Mov. Disord.* 30, 1591–1601. doi: 10.1002/mds.26424

Rahnemayan, S., Ahari, S. G., Rikhtegar, R., Riyahifar, S., and Sanaie, S. (2022). An umbrella review of systematic reviews with meta-analysis on the role of vitamins in Parkinson's disease. *Acta Neurol. Belg.* doi: 10.1007/s13760-022-02055-3 [Epub ahead of print]

Rebec, G. V., Conroy, S. K., and Barton, S. J. (2006). Hyperactive striatal neurons in symptomatic Huntington R6/2 mice: variations with behavioral state and repeated ascorbate treatment. *Neuroscience* 137, 327–336. doi: 10.1016/j.neuroscience.2005.08.062

Rosario, D., Bidkhori, G., Lee, S., Bedarf, J., Hildebrand, F., Le Chatelier, E., et al. (2021). Systematic analysis of gut microbiome reveals the role of bacterial folate and homocysteine metabolism in Parkinson's disease. *Cell Rep.* 34:108807. doi: 10.1016/j.celrep.2021.108807

Sakakibara, R. (2021). Gastrointestinal dysfunction in movement disorders. *Neurol. Sci.* 42, 1355–1365. doi: 10.1007/s10072-021-05041-4

Schirinzi, T., Martella, G., Imbriani, P., Di Lazzaro, G., Franco, D., Colona, V. L., et al. (2019). Dietary vitamin E as a protective factor for Parkinson's disease: clinical and experimental evidence. *Front. Neurol.* 10:148. doi: 10.3389/fneur.2019.00148

Schulz, I., Kruse, N., Gera, R. G., Kremer, T., Cedarbaum, J., Barbour, R., et al. (2021). Systematic assessment of 10 biomarker candidates focusing on α-Synuclein-related disorders. *Mov. Disord.* 36, 2874–2887. doi: 10.1002/mds.28738

Sekiyama, K., Sugama, S., Fujita, M., Sekigawa, A., Takamatsu, Y., Waragai, M., et al. (2012). Neuroinflammation in Parkinson's disease and related disorders: a lesson from genetically manipulated mouse models of α-Synucleinopathies. *Parkinsons Dis.* 2012:271732. doi: 10.1155/2012/271732

Seshadri, S., Beiser, A., Selhub, J., Jacques, P. F., Rosenberg, I. H., D'Agostino, R. B., et al. (2002). Plasma homocysteine as a risk factor for dementia and Alzheimer's disease. *N. Engl. J. Med.* 346, 476–483. doi: 10.1056/NEJMoa011613

Shen, L. (2015). Associations between B vitamins and Parkinson's disease. *Nutrients* 7, 7197–7208. doi: 10.3390/nu7095333

Stankovic, I., Quinn, N., Vignatelli, L., Antonini, A., Berg, D., Coon, E., et al. (2019). A critique of the second consensus criteria for multiple system atrophy. *Mov. Disord.* 34, 975–984. doi: 10.1002/mds.27701

Tan, A. H., Chong, C. W., Song, S. L., Teh, C. S. J., Yap, I. K. S., Loke, M. F., et al. (2018). Altered gut microbiome and metabolome in patients with multiple system atrophy. *Mov. Disord.* 33, 174–176. doi: 10.1002/mds.27203

Wan, L., Zhou, X., Wang, C., Chen, Z., Peng, H., Hou, X., et al. (2019). Alterations of the gut microbiota in multiple system atrophy patients. *Front. Neurosci.* 13:1102. doi: 10.3389/fnins.2019.01102

Wang, M., Liu, Z., Sun, W., Yuan, Y., Jiao, B., Zhang, X., et al. (2020). Association between vitamins and amyotrophic lateral sclerosis: a center-based survey in mainland China. *Front. Neurol.* 11:488. doi: 10.3389/fneur.2020.00488

Wenning, G. K., Geser, F., Krismer, F., Seppi, K., Duerr, S., Boesch, S., et al. (2013). The natural history of multiple system atrophy: a prospective European cohort study. *Lancet Neurol.* 12, 264–274. doi: 10.1016/S1474-4422(12)70327-7

Wenning, G. K., Tison, F., Seppi, K., Sampaio, C., Diem, A., Yekhlef, F., et al. (2004). Development and validation of the unified multiple system atrophy rating scale (UMSARS). *Mov. Disord.* 19, 1391–1402. doi: 10.1002/mds.20255

Wyss-Coray, T., and Mucke, L. (2002). Inflammation in neurodegenerative disease--a double-edged sword. *Neuron* 35, 419–432. doi: 10.1016/s0896-6273(02)00794-8

Zhang, S., Shi, C., Mao, C., Song, B., Hou, H., Wu, J., et al. (2015). Plasma homocysteine, vitamin B12 and folate levels in multiple system atrophy: a case-control study. *PLoS One* 10:e0136468. doi: 10.1371/journal.pone.0136468

Zhong, M., Zhu, S., Gu, R., Wang, Y., Jiang, Y., Bai, Y., et al. (2022). Elevation of plasma homocysteine and minor hallucinations in Parkinson's disease: a cross-sectional study. *Behav. Neurol.* 2022:4797861. doi: 10.1155/2022/4797861

Zhu, M., Li, B., Ma, X., Huang, C., Wu, R., Zhu, W., et al. (2016). Folic acid protected neural cells against aluminum-Maltolate-induced apoptosis by preventing miR-19 downregulation. *Neurochem. Res.* 41, 2110–2118. doi: 10.1007/s11064-016-1926-9

frontiers | Frontiers in Aging Neuroscience

TYPE Original Research
PUBLISHED 11 January 2023
DOI 10.3389/fnagi.2022.1066331

OPEN ACCESS

EDITED BY
Kuangyu Shi,
University of Bern,
Switzerland

REVIEWED BY
Susanna Nuvoli,
University of Sassari,
Italy
Takayasu Mishima,
Fukuoka University,
Japan

*CORRESPONDENCE
Qiang Guan
✉ guanqianglu@126.com
Lingjing Jin
✉ lingjingjin@tongji.edu.cn

†These authors have contributed equally to this work and share first authorship

SPECIALTY SECTION
This article was submitted to Parkinson's Disease and Aging-related Movement Disorders, a section of the journal Frontiers in Aging Neuroscience

RECEIVED 10 October 2022
ACCEPTED 22 December 2022
PUBLISHED 11 January 2023

CITATION
Li S, Yue L, Chen S, Wu Z, Zhang J, Hong R, Xie L, Peng K, Wang C, Lin A, Jin L and Guan Q (2023) High clinical diagnostic accuracy of combined salivary gland and myocardial metaiodobenzylguanidine scintigraphy in the diagnosis of Parkinson's disease.
Front. Aging Neurosci. 14:1066331.
doi: 10.3389/fnagi.2022.1066331

High clinical diagnostic accuracy of combined salivary gland and myocardial metaiodobenzylguanidine scintigraphy in the diagnosis of Parkinson's disease

Shuangfang Li[1,2†], Lei Yue[1†], Shuzhen Chen[3], Zhuang Wu[1], Jingxing Zhang[1], Ronghua Hong[1], Ludi Xie[1], Kangwen Peng[1], Chenghong Wang[3], Ao Lin[1], Lingjing Jin[1,2,4]* and Qiang Guan[1]*

[1]Neurotoxin Research Center of Key Laboratory of Spine and Spinal Cord Injury Repair and Regeneration of Ministry of Education, Department of Neurology, Tongji Hospital, School of Medicine, Tongji University, Shanghai, China, [2]Department of Neurology and Neurological Rehabilitation, Shanghai YangZhi Rehabilitation Hospital (Shanghai Sunshine Rehabilitation Center), School of Medicine, Tongji University, Shanghai, China, [3]Department of Nuclear Medicine, Tongji Hospital, School of Medicine, Tongji University, Shanghai, China, [4]Shanghai Clinical Research Center for Aging and Medicine, Shanghai, China

Background: Decreased myocardial uptake of ^{131}I-metaiodobenzylguanidine (MIBG) is known to be an important feature to diagnose Parkinson's disease (PD). However, the diagnosis accuracy of myocardial MIBG scintigraphy alone is often unsatisfying. Recent studies have found that the MIBG uptake of the major salivary glands was reduced in PD patients as well.

Purpose: To evaluate the diagnostic value of major salivary gland MIBG scintigraphy in PD, and explore the potential role of myocardial MIBG scintigraphy combined with salivary gland MIBG scintigraphy in distinguishing PD from non-PD (NPD).

Methods: Thirty-seven subjects were performed with ^{131}I-MIBG scintigraphy. They were classified into the PD group (N=18) and the NPD group (N=19), based on clinical diagnostic criteria, DAT PET and ^{18}F-FDG PET imaging findings. Images of salivary glands and myocardium were outlined to calculated the MIBG uptake ratios.

Results: The combination of left parotid and left submandibular gland early images had a good performance in distinguishing PD from NPD, with sensitivity, specificity, and accuracy of 50.00, 94.74, and 72.37%, respectively. Combining the major salivary gland and myocardial scintigraphy results in the early period showed a good diagnostic value with AUC, sensitivity and specificity of 0.877, 77.78, and 94.74%, respectively. Meanwhile, in the delayed period yield an excellent diagnostic value with AUC, sensitivity and specificity of 0.904, 88.89, and 84.21%, respectively.

Conclusion: ^{131}I-MIBG salivary gland scintigraphy assisted in the diagnosis and differential diagnosis of PD. The combination of major salivary gland and myocardial ^{131}I-MIBG scintigraphy further increased the accuracy of PD diagnosis.

KEYWORDS

Parkinson's disease, parkinsonism, salivary glands, MIBG scintigraphy, diagnosis

1. Introduction

Parkinson's disease (PD) is a common progressive neurological illness with insidious onset and slow progression (De Rijk et al., 1997). As no biomarkers are available, the diagnosis of PD is mainly based on clinical criteria but the accuracy is limited, especially in the early stages because of lacking typical clinical signs and symptoms (Adler et al., 2014). Similar motor symptoms, such as resting tremor or bradykinesia, occur in atypical parkinsonian syndromes (APS), vascular parkinsonism (VaP) and essential tremor (ET) (Lees et al., 2009). However, the prognosis of these diseases is completely different, and therefore, improving diagnostic accuracy is very important for the choice of a therapeutic approach.

PD is characterized by abnormal deposition of α-synuclein aggregates forming intraneuronal Lewy bodies and Lewy neurites, which are found in many regions of the central nervous system and peripheral tissues, such as the heart, salivary glands and gut (Den Hartog Jager and Bethlem, 1960; Beach et al., 2010; Del Tredici et al., 2010; Tsukita et al., 2019). Degeneration of the cardiac sympathetic system due to abnormal aggregation of α-synuclein has been used to diagnose PD by means of metaiodobenzylguanidine (MIBG) scintigraphy (Orimo et al., 2008). The new clinical diagnostic criteria for PD proposed by the International Parkinson and Movement Disorder Society (MDS) in 2015 used cardiac sympathetic denervation on MIBG scintigraphy as a supportive criterion (Postuma et al., 2015). Many studies have reported that myocardial MIBG uptake decreases in PD patients with disease progression (Spiegel et al., 2005; Ryu et al., 2019), and myocardial MIBG scintigraphy is significant in the differential diagnosis of PD and other forms of parkinsonism, such as multiple system atrophy (MSA), progressive supranuclear palsy (PSP), corticobasal degeneration (CBD), vascular parkinsonism, etc., and in the discrimination from healthy people (Satoh et al., 1999; Orimo et al., 2012; Treglia et al., 2012). However, the diagnostic value of this test can be affected when PD patients experience concurrent damage to the cardiac muscle, such as ischemic heart disease, myocardiopathy, and congestive heart failure (Braune, 2001; Jacobson et al., 2010).

Recent studies have found that the sympathetic nerves to the salivary glands are also damaged, and MIBG scintigraphy of the major salivary glands has shown reduced uptake in PD patients (Haqparwar et al., 2017; Campo et al., 2019; Schepici et al., 2020). Normal MIBG uptake in healthy people and patients with PSP, MSA, and CBD is consistent with myocardial MIBG scintigraphy (Haqparwar et al., 2017; Schubert et al., 2019). Therefore, we speculate that salivary gland MIBG scintigraphy may have some clinical value and can improve the diagnostic value of myocardial MIBG scintigraphy when used in combination in PD patients. In previous studies, planar whole-body images were mostly collected, and the regions of interest (ROIs) in the relevant parts were delineated to calculate the radioactive uptake ratio. Concomitantly, in planar images, lung uptake or liver uptake superimposed on cardiac uptake may cause false-negative and false-positive results (Oh et al., 2015). Tomographic images are superior imaging techniques for the evaluation of specific organ activity (Fukuoka et al., 2011). In our study, single photon emission computed tomography (SPECT/CT) images were used to further evaluate the salivary glands and cardiac sympathetic denervation.

Accordingly, the present study aims to (1) evaluate the diagnostic value of major salivary gland ^{131}I-MIBG scintigraphy in PD patients; and (2) explore the potential role of ^{131}I-MIBG myocardial scintigraphy in conjunction with ^{131}I-MIBG salivary glands scintigraphy in distinguishing PD patients from non-PD (NPD) patients.

2. Materials and methods

2.1. Participants

The study involved 31 patients who visited the outpatient clinic of the Neurological Department of Tongji Hospital Affiliated to Tongji University from April 2017 to October 2019. The patients chiefly complained of one or more parkinsonian symptoms, including bradykinesia, rigidity or resting tremor. All patients were subjected to a comprehensive clinical evaluation and examination conducted by specialists in movement disorders, and were followed up over a course of 3 to 4 years. Those who met the MDS clinical diagnostic criteria for Parkinson's disease were diagnosed with clinically definite PD (Postuma et al., 2015), and the myocardial MIBG scintigraphy results were not used as a supportive diagnostic criterion. Others with clinically relevant symptoms of parkinsonian syndrome, but without a diagnosis of clinically definite and possible PD or who did not match the

dopamine transporter (DAT) and ^{18}F-fluorodeoxyglucose (^{18}F-FDG) positron emission tomography (PET) imaging findings of PD patients were classified as NPD by 2 independent neurologists. Referring to a similar diagnostic flow in previous studies (Ishibashi et al., 2010; Stathaki et al., 2020), patients with unclassified Parkinsonian syndrome were included in the NPD group after excluding PD diagnosis. Moreover, considering that this study is an exploration of diagnostic methods, only comparing PD patients with other parkinsonian syndrome or healthy control group will reduce the accuracy of diagnostic tests (Sackett and Haynes, 2002; Rutjes et al., 2006). Therefore, the control group of this study includes patients with Parkinsonian syndrome whose symptoms are easily confused with Parkinson's disease clinically and some healthy people. We recruited 6 healthy subjects into the NPD group. Motor symptoms were evaluated using the MDS sponsored revision of the Unified Parkinson's Disease Rating Scale part III (MDS-UPDRS III) (Goetz et al., 2008), and the Hoehn and Yahr (H&Y) scale.

The exclusion criteria for the study included an individual history of salivary glands disease, heart disease, diabetes, hypothyroidism or peripheral neuropathy. None of the patients were on specific medications that would interfere with MIBG uptake, such as calcium antagonists, tricyclic antidepressant medications, labetalol, and ephedrine hydrochloride. ^{131}I-MIBG scintigraphy was performed for all subjects.

The Ethics Committee of Tongji Hospital approved the present research (IRB 2018-LCYJ-009-XZ-181105) and the registration number is ChiCTR1800015757. All participants signed written informed consent before the research. All the research procedures were performed according to Helsinki declaration.

2.2. ^{131}I-MIBG scintigraphy

To block the thyroid gland, all subjects were administered compound iodine solution starting 3 days prior to imaging. On the day of imaging, an intravenous injection of ^{131}I-MIBG with a radioactivity of 111 MBq was given. SPECT/CT images of the major salivary glands and the heart were obtained at 30 min for the early images and at 4 h for the delayed images after the injection on a dual-head gamma camera and multidetector (16-row) spiral CT (Precedence SPECT/CT; Philips Healthcare, Amsterdam, Netherlands). The spiral CT examination from head to thorax was performed with the parameters of 100 mAs, 120 keV, and 5-mm section width. SPECT followed a CT scan from head to thorax with a 15% energy window centred on a 364-keV photopeak. Acquisition parameters for SPECT included a 64 × 64 matrix with 64 frames (15 s/frame) over 360°. SPECT data were reconstructed using Astonish methods incorporating photon attenuation correction based on the X-ray transmission map and scatter correction through AutoSPECT+ software. Then the reconstructed SPECT data and CT data were fused and analysed on an EBW workstation, providing the transverse, sagittal, and coronal slices of SPECT, CT, and fused SPECT/CT data.

2.3. Imaging analysis

For quantification of the relative organ uptake of ^{131}I-MIBG, the left ventricular wall, parotid glands and submandibular glandswere contoured manually three times on the fusion images of transverse slices using an ROI technique(Figure 1). A rectangular ROI of the neck subcutaneous tissueand served as the background activity. The mean radioactive values of the left ventricular wall, parotid glands, submandibular glands and background activity were calculated. Care was taken to exclude blood in the ventricle. The radioactive value ratio of the heart to the neck subcutaneous tissue(H/N), and the ratio of the major salivary glands to the neck subcutaneous tissue(P/N or S/N) in the early and delayed periods were calculated. Regarding the P/N and S/N indices, values for the salivary glands on the left and right were used for the analysis.

2.4. Statistical analysis

The statistical analyses were performed using SPSS software (IBM SPSS Statistics, version 20, IBM, Corp., Armonk, New York, United States). The normality of the data distribution was estimated by the Shapiro–Wilk test. Differences in the quantitative indices between PD and NPD groups were compared using the Mann–Whitney *U* test or independent sample *t* test. *p* values of <0.05 (two-sided) were considered statistically significant. Figures were produced by GraphPad Prism software (GraphPad Prism Version 8.0, GraphPad software, San Diego, CA, United States).

3. Results

According to the clinical diagnosis and evaluation, 18 patients (12 men and 6 women; age range: 42–76 years, mean age ± SD: 57.61 ± 11.09 years) were diagnosed with PD, and 19 patients (7 men and 12 women; age range: 47–78 years, mean age ± SD: 63.95 ± 8.61 years) were classified into NPD group, including 8 MSA patients, 1 PSP patient, 1 VaP patient, 6 healthy individuals and 3 patients for whom the diagnosis could not be defined despite follow-up for at least 3 years. The MDS-UPDRS III score was 42.61 ± 12.20 points (mean ± SD) in PD patients. The distributions of age and sex did not differ between the two groups. Characters and the MIBG uptake ratios of all subjects are given in Supplementary Tables 1, 2.

The salivary gland and myocardial MIBG uptake ratios in the two groups are showed in Table 1. Both in the early and delayed images, the MIBG uptake in the bilateral parotid glands and submandibular glands in the PD group was obviously lower than that in the NPD group. In the early images, the left parotid gland, the left and right submandibular gland MIBG uptake ratios in the PD patients were significantly lower (L-P/N, $p < 0.05$; L-S/N, $p < 0.05$; R-S/N, $p < 0.05$). The MIBG uptake ratio for the left submandibular gland was also significantly decreased in the

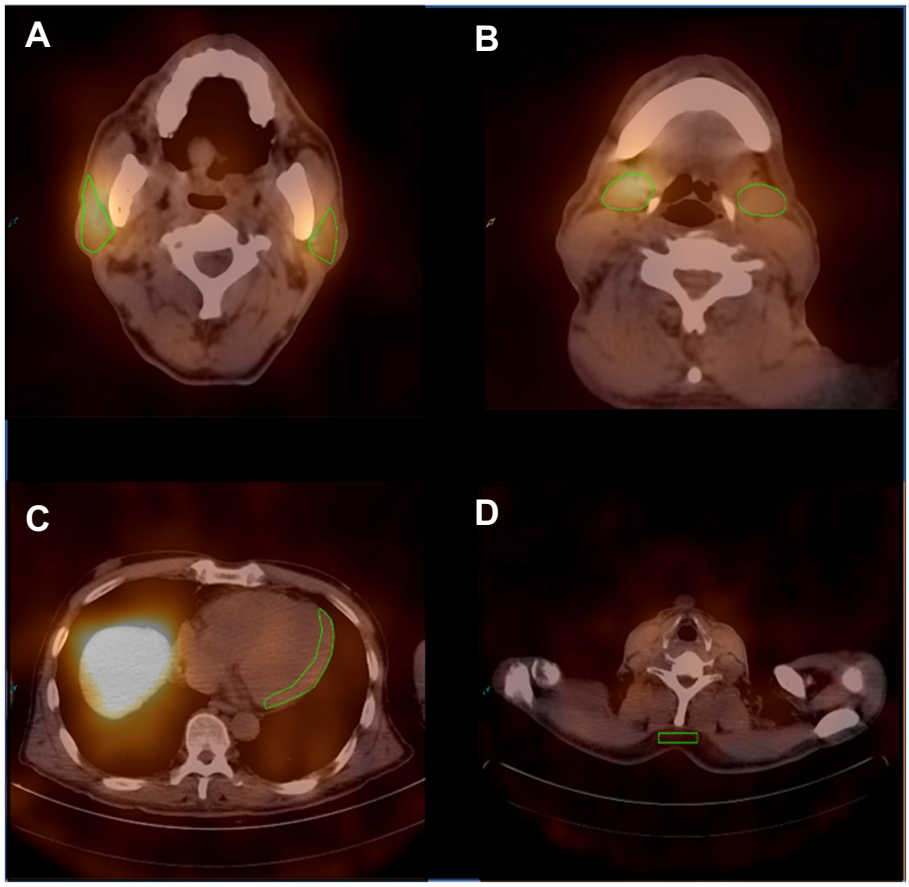

FIGURE 1
Representative ROIs of MIBG scintigraphy. **(A)** The ROIs of the bilateral parotid glands. **(B)** The ROIs of the bilateral submandibular glands. **(C)** The ROI of the left ventricular wall. **(D)** The ROI of the neck subcutaneous tissue.

delayed images (L-S/N, $p < 0.05$). Regarding myocardial MIBG scintigraphy, the differences were more pronounced between the two groups, both in the early and delayed periods, compared to salivary glands images.

Table 2 shows the results of the ROC curve analysis as an indicator of the diagnostic abilies of salivary gland and myocardial MIBG values. The OCVs were L-P/N: 4.63, L-S/N: 4.47, R-S/N:6.47, and H/N:3.49 in the early images and L-S/N: 6.99, and H/N: 3.57 in the delayed images.

In the early salivary gland MIBG scintigraphy, the left parotid gland had a better diagnostic ability; the AUC value was 0.734 (95% CI: 0.567–0.900, $p < 0.05$), the sensitivity was 66.67% and the specificity was 76.68%. The AUC value with the left submandibular gland was 0.703 in the delayed images, greater than 0.5 (95% CI: 0.532–0.875, $p < 0.05$), and the sensitivity and specificity were 88.89 and 52.63%, respectively. The MIBG uptake ratios for major salivary glands and ROC curves in the discrimination of PD from NPD are shown in Figure 2.

Similarly, myocardial MIBG scintigraphy exhibited better AUC values for distinguishing PD from NPD in both the early and delayed images. At the OCVs for the myocardial MIBG uptake ratios from early and delayed images, the AUCs were 0.868 (95% CI: 0.567–0.900, $p < 0.001$) and 0.857 (95% CI: 0.719–0.995, $p < 0.001$), the sensitivities were 72.22 and 88.89%, and the specificities were 94.74 and 84.21%, respectively. Figure 3 shows the relevant analysis results.

With the MIBG imaging of salivary glands and myocardium at both periods, we screened out the regions with significant differences in the comparative analysis between the two groups, and performed ROC curve analysis for a diagnosis based on all logical combinations. Among all the multiple indicators of the combination of major salivary glands or the combination of salivary glands and myocardium, we concluded that the best AUC was 0.947 (95% CI: 0.872–1, $p < 0.001$), the sensitivity and specificity were 83.33 and 100% respectively, and the accuracy was 91.67%, which was obtained when we combined all the meaningful indicators in the early and delayed phase imaging. We found that the largest AUC was also obtained when combining indicators other than the early L-P/N, resulting in a sensitivity and specificity of 88.89 and 94.74% (AUC = 0.947, 95% CI: 0.869–1, $p < 0.001$) respectively, and an accuracy of 91.82%. Considering that this approach can provide a more comprehensive diagnosis in practical

clinical applications, we selected the best indicators for diagnosis from the early combinations and from the combinations in the delayed period, to use a combination of fewer indicators while achieving relatively higher diagnostic value. By comparing the area under the ROC curve, we found that the combination of data from the major salivary glands did not yield good diagnostic value with an optimal sensitivity and specificity of 50.00 and 94.74% respectively, in early imaging. The accuracy was 72.37% (AUC = 0.731, 95% CI: 0.568–0.894, $p = 0.0062$), for the combination of L-P/N and L-S/N in the early phase. When the L-P/N in major salivary glands and cardiac indicators were combined in early imaging, we obtained the most appropriate sensitivity, specificity and accuracy, which were 77.78, 94.74, and 86.26%, respectively, (AUC = 0.877, 95% CI: 0.763–0.991, $p < 0.001$).

However, in the delayed images, the combination of L-S/N and H/N yielded an AUC of 0.904 (95% CI: 0.789–1, $p < 0.001$), which resulted in a sensitivity of 88.89%, a specificity of 84.21% and an accuracy of 86.55%. Combining only the myocardial MIBG imaging indicators, we obtained the best sensitivity, specificity and accuracy, 72.22, 94.74, and 83.48%, respectively, with an AUC = 0.865 (95% CI: 0.742–0.989, $p < 0.001$). Figure 4 shows the combined diagnostic ROC curves of several optimal combinations.

TABLE 1 Differences of salivary gland and myocardial MIBG scintigraphy results in PD and NPD.

	PD	NPD	*P* value
Early P/N			
L-P/N	4.74 ± 2.38	6.01 ± 1.88	**0.014***
R-P/N	5.57 ± 2.28	6.70 ± 1.81	0.103
Early S/N			
L-S/N	4.84 ± 1.76	6.18 ± 1.76	**0.022***
R-S/N	5.24 ± 2.04	6.27 ± 1.54	**0.034***
Early H/N	3.37 ± 1.46	6.01 ± 1.80	**<0.001*****
Delayed P/N			
L-P/N	6.01 ± 2.06	7.18 ± 2.51	0.118
R-P/N	6.64 ± 2.00	7.77 ± 2.75	0.258
Delayed S/N			
L-S/N	5.36 ± 2.04	7.04 ± 2.54	**0.034***
R-S/N	5.69 ± 1.90	6.71 ± 1.69	0.070
Delayed H/N	2.89 ± 2.33	5.22 ± 1.76	**<0.001*****

Bold font means significant results; Data are means ± SD; PD, Parkinson's disease; NPD, other Parkinsonian syndrome and healthy control; L, left side; R, right side; P/N, the ratio of the parotid glands to the neck subcutaneous tissue; S/N, the ratio of the submandibular glands to the neck subcutaneous tissue; H/N, the ratio of the heart to the neck subcutaneous tissue. *$P < 0.05$, ***$P < 0.001$.

4. Discussion

To our knowledge, this study is the first to use ^{131}I-MIBG SPECT/CT imaging for detecting the uptake of sympathetic nerve in major salivary glands and myocardium simultaneously in PD patients. In particular, the ROIs were outlined on the tomographic images. Alhough a few studies have evaluated the sensitivity and specificity of MIBG imaging of the major salivary glands in diagnosing PD, they utilized planar imaging to delineate ROI to quantify the relevant indicators. One study reported that MIBG SPECT had a significantly higher diagnostic performance for PD than planar images (Oh et al., 2015). Furthermore, we collected images at 30 min and 4 h after contrast injection to obtain relevatnt data on the parotid and submandibular glands and myocardium. No study has applied these quantitative indicators together to diagnose PD, including the differential diagnosis of PD and other parkinsonian syndromes. This approach reduces the examination cost and radiation exposure, and also saves time for the patients, especially when compared with previous studies on the diagnosis of PD by combining multiple imaging methods (Sudmeyer et al., 2011; Stathaki et al., 2020).

TABLE 2 Measures of diagnostic accuracy of salivary gland and myocardial MIBG scintigraphy in differentiating PD and NPD.

	AUC	OCV	95% CI	Sensitivity (%)	Specificity (%)	Accuracy (%)
Early L-P/N	**0.734**	4.63	0.567–0.900	66.67	76.68	71.68
Early R-P/N	0.678	5.62	0.502–0.855	66.67	68.42	67.55
Early L-S/N	**0.719**	4.47	0.552–0.886	55.56	84.21	69.89
Early R-S/N	**0.703**	6.47	0.528–0.878	83.33	57.89	70.61
Early H/N	**0.868**	3.49	0.746–0.991	72.22	94.74	83.48
Delayed L-P/N	0.652	4.98	0.471–0.834	55.56	84.21	69.89
Delayed R-P/N	0.610	8.33	0.425–0.794	88.89	36.84	62.87
Delayed L-S/N	**0.703**	6.99	0.532–0.875	88.89	52.63	70.76
Delayed R-S/N	0.674	5.90	0.495–0.853	66.67	68.42	67.55
Delayed H/N	**0.857**	3.57	0.719–0.995	88.89	84.21	86.55

Bold font means significant results; AUC, area under the receiver operating characteristic curve; OCV, the optimal cutoff values; CI, the confidence interval; L, left side; R, right side; P/N, the ratio of the parotid glands to the neck subcutaneous tissue; S/N, the ratio of the submandibular glands to the neck subcutaneous tissue; H/N, the ratio of the heart to the neck subcutaneous tissue.

10.3389/fnagi.2022.1066331

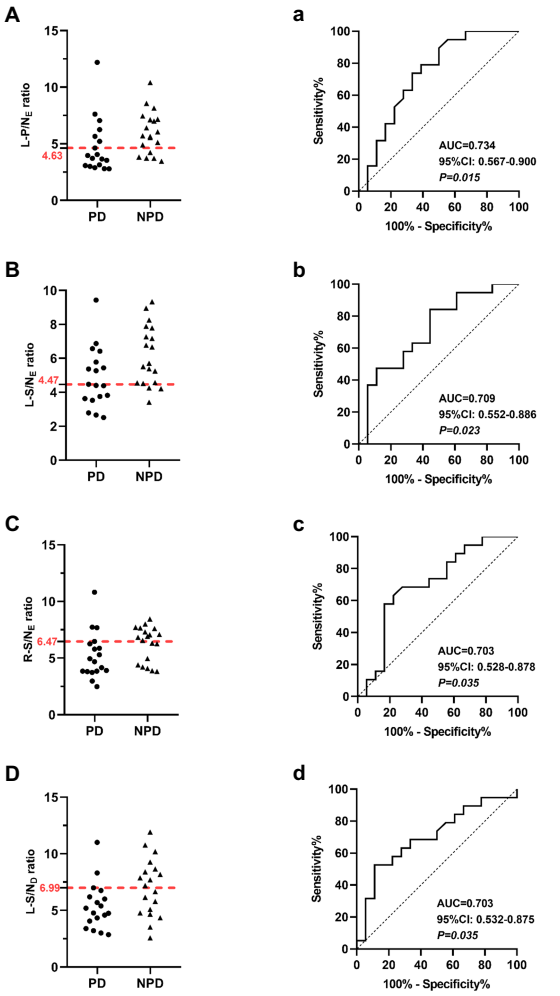

FIGURE 2
Scatter diagrams show salivary gland MIBG scintigraphy results in the differentiation of PD and NPD. **(A)** The left parotid gland uptake ratio in early images. **(B)** The left submandibular gland uptake ratio in early images. **(C)** The right submandibular gland uptake ratio in early images. **(D)** The left submandibular gland uptake ratio in delayed images. The red dotted line indicates a cutoff value that yields the most appropriate sensitivity and specificity. Receiver Operating Characteristic (ROC) analysis showing sensitivity and specificity of the left parotid gland uptake ratio **(a)** the left submandibular gland uptake ratio **(b)** the right submandibular gland uptake ratio **(c)** in early images, and the left submandibular gland uptake ratio in delayed images **(d)** used to differentiate patients between PD and NPD.

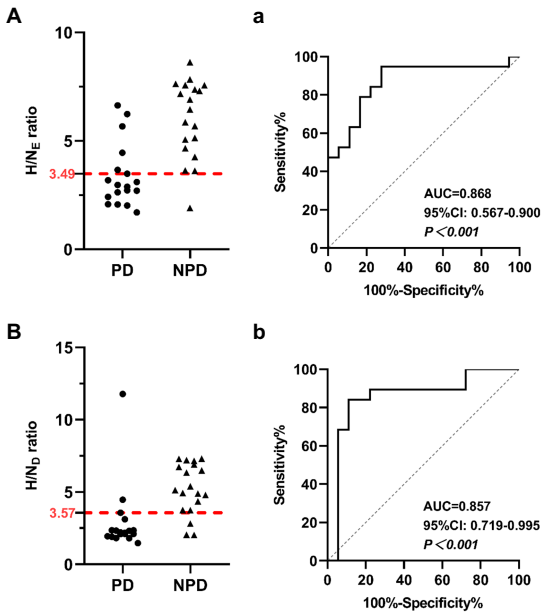

FIGURE 3
Scatter diagrams show myocardial MIBG scintigraphy results in the differentiation of PD and NPD. **(A)** The heart uptake ratio in early images. **(B)** The heart uptake ratio in delayed images. The red dotted line indicates a cutoff value that yields the most appropriate sensitivity and specificity. Receiver Operating Characteristic (ROC) analysis showing sensitivity and specificity of the heart uptake ratio in early images **(a)** and the delayed images **(b)** used to differentiate patients between PD and NPD.

MIBG is a guanethidine analog that shares the same uptake and storage mechanism as noradrenaline (Spiegel et al., 2005). The ^{131}I and ^{123}I-labeled MIBG are used in the same principle for myocardial scintigraphy, the latter has relatively good imaging quality, but the short half-life and inconvenient storage of ^{123}I-MIBG limit its clinical application. In China, some scholars have made relevant studies on patients with PD, MSA and ET using ^{131}I-MIBG myocardial scintigraphy, and proved that ^{131}I-MIBG myocardial scintigraphy is helpful in the diagnosis and differential diagnosis of PD (Yang et al., 2017). Our study mainly investigated the complementary role of ^{131}I-MIBG major salivary gland and myocardial scintigraphy in the differential diagnosis of parkinsonism, and observed that the combined approach can improve the diagnostic accuracy.

It has been reported that MIBG uptake in the parotid and submandibular glands decreased to different degrees in PD patients during delayed imaging, which is largely normal in MSA patients, PSP patients and healthy subjects (Haqparwar et al., 2017; Soboll et al., 2018; Schubert et al., 2019). This is consistent with our research. In our study, MIBG uptake in the PD group was also significantly lower than that in the NPD group in the early imaging. In particular, the left parotid gland images in the early period and the left submandibular gland images in the delayed period had better specificity and sensitivity in distinguishing the two groups. In view of the small number of patients included in this study and the few previous studies on salivary gland MIBG scintigraphy in PD patients, we cannot determine whether the difference in salivary gland uptake ratio between the left and right sides is related to the side of onset or the side with severe clinical symptoms. However, it is clear that the uptake of salivary glands in early period is related to the MDS-UPDRS III (Supplementary Table 3). In other words, with the aggravation of motor symptoms, the MIBG uptake of salivary glands decreases more significantly.

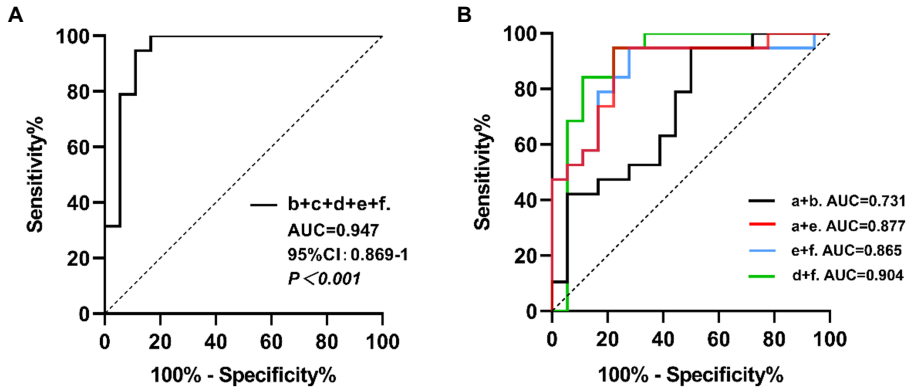

FIGURE 4
The ROC curves for the combined MIBG scintigraphy uptake ratio. **a**: the left parotid gland uptake ratio in early images; **b**: the left submandibular gland uptake ratio in early images; **c**: the right submandibular gland uptake ratio in early images; **d**: the left submandibular gland uptake ratio in delayed images; **e**: the heart uptake ratio in early images; **f**: the heart uptake ratio in delayed images. **(A)** The b+c+d+e+f combined, AUC=0.947, 95% CI: 0.869–1, $p < 0.001$. **(B)** The a+b combined, AUC=0.731, 95% CI: 0.568–0.894, $p=0.0062$; the a+e combined, AUC=0.877, 95% CI: 0.763–0.991, $p<0.001$; the e+f combined, AUC=0.865, 95% CI: 0.742–0.989, $p<0.001$; the d+f combined, AUC=0.904, 95% CI: 0.789–1, $p<0.001$.

However, the sensitivity and specificity of major salivary gland MIBG scintigraphy were still relatively low when compared with those of myocardial MIBG scintigraphy. But the combination of diseases common in elderly populations, such as ischemic heart disease and congestive heart failure will also have an impact on the results of myocardial MIBG scintigraphy in PD patients. Therefore, salivary gland MIBG scintigraphy has more important significance as a supplement to myocardial MIBG scintigraphy. The optimal combination of salivary glands was the combination of the left parotid and left submandibular glands in early imaging, with a sensitivity and specificity of 50.00 and 94.74%, respectively, and an accuracy of 72.37%. High specificity has important implications for the clinical exclusion of PD.

The results of salivary gland MIBG scintigraphy can still be used as an important reference, although its sensitivity and specificity were not sufficient to distinguish PD from NPD alone. Because previous studies has confirmed that it is inaccurate to use myocardial MIBG scintigraphy to diagnose PD when patients had heart diseases (Braune, 2001; Jacobson et al., 2010). So, salivary glands MIBG scintigraphy could be used as an important reference index.

In addition to ischemic heart disease, there are several factors that interfere with the use of myocardial MIBG scintigraphy to diagnose PD, such as normal MIBG uptake in some early PD patients. Among the recruited PD patients, 2 PD patients with H&Y stage 1 also had normal myocardial MIBG uptake. Furthermore, myocardial MIBG uptake in some MSA patients was similar to PD patients (Kollensperger et al., 2007; Iwabuchi et al., 2021). In our research results, compared with myocardial MIBG scintigraphy alone, combined scintigraphy improved the sensitivity and specificity of diagnosis, which can reduce the influence of the above factors on the diagnostic value of MIBG imaging to a certain extent.

To facilitate clinical application in the future, we wanted to minimize the number of examinations for patients as much as possible, that is, select only early or delayed image acquisition after contrast agent injection. Therefore in our analysis, we found that combining the left parotid gland and myocardial scintigraphy results in early imaging increased the sensitivity without sacrificing specificity and improved accuracy compared to myocardial scintigraphy alone. When combining the left submandibular gland and myocardial scintigraphy results in delayed imaging, the AUC improved, while the sensitivity and specificity were not reduced. To determine which method is more meaningful, further research is needed. This also provides evidence for major salivary gland MIBG scintigraphy as a supplementary diagnostic basis in Parkinson's-related disease diagnoses. In this case, imaging of the salivary glands can assist in the diagnosis of PD without repeated examination. Because we injected the contrast agent only once, but could simultaneously collect MIBG images of both the salivary glands and myocardium using SPECT/CT.

However, there are some limitations of our study. First, given that our patients were recruited from a single centre, the sample size was relatively small, and our results might be limited by specific institutional factors. Second, each diagnosis was not pathologically confirmed. Finally, limited local actual conditions, we choose ^{131}-MIBG for scintigraphy, while ^{123}-MIBG has been widely used for myocardial scintigraphy in previous studies due to its clearer imaging. If the actual conditions permit, using ^{123}I-MIBG imaging may make the diagnostic value of MIBG scintigraphy higher.

In addition, artificial intelligence technology includes machine learning such as e classification and regression tree (CART), support vector machines (SVM) and random forest (RF) classifier, plays a certain role in assisting to determine the cutoff values and further diagnosing Parkinson's syndrome by combing MIBG scintigraphy, and its effectiveness has been well demonstraed in previous studies(Nuvoli et al., 2017, 2020; Iwabuchi et al., 2021). Besides, some studies have applied deep learning to DAT PET and FDG PET scans to analyze multiple regions as well as their correlation, which proved that it was helpful for the early diagnosis

of Parkinson's disease (Wu et al., 2022; Zhao et al., 2022). In future studies, we can also refer to the above methods to simultaneously analyze MIBG uptake in sympathetic distributed organs including salivary glands and heart from SPECT/CT imaging, so as to improve the combined multiorgan MIBG imaging for the differential diagnosis of Parkinson's disease. At the same time, combined with demographic, clinical data and other indicators to further improve the diagnostic accuracy. In a word, we still need to improve methods to enhance diagnostic performance.

5. Conclusion

The sympathetic nerves that innervate the parotid and submandibular glands are damaged in PD patients, mainly manifested by decreased MIBG uptake compared to NPD patients. ^{131}I-MIBG salivary gland scintigraphy has certain clinical diagnostic value in the diagnosis and differential diagnosis of PD, especially when PD patients suffer from heart disease and it provides a complementary method. It is important that the combination of ^{131}I-MIBG major salivary gland and myocardium scintigraphy improves the accuracy of PD diagnosis and appears to be a feasible method in practical clinical applications.

Data availability statement

The raw data supporting the conclusions of this article will be made available by the authors, without undue reservation.

Ethics statement

Written informed consent was obtained from the individual(s) for the publication of any potentially identifiable images or data included in this article.

Author contributions

QG and LJ designed the research and revised the manuscript. SL drafted the manuscript. SL and LY performed the research, collected and analyzed data. ZW and RH revised the manuscript. SC and CW helped in images acquisition and data analysis. JZ, LX, KP, and AL contributed to data collection and analysis. All authors have read and approved the final version of manuscript for publication.

Funding

This study was supported by the National Natural Science Foundation of China (Grant number. 81974198); the Fundamental Research Funds for the Central Universities (Grant number. 22120180511); Clinical Technology Innovation Project of Shanghai Shenkang Hospital Development Center (Grant number. SHDC12018X08); and Key Projects Clinical Research Cultivation Project of Tongji Hospital (Grant number. ITJ(ZD)1810).

Acknowledgments

We thank all participants in this research for their understanding, support and participation.

Conflict of interest

The authors declare that the research was conducted in the absence of any commercial or financial relationships that could be construed as a potential conflict of interest.

Publisher's note

All claims expressed in this article are solely those of the authors and do not necessarily represent those of their affiliated organizations, or those of the publisher, the editors and the reviewers. Any product that may be evaluated in this article, or claim that may be made by its manufacturer, is not guaranteed or endorsed by the publisher.

Supplementary material

The Supplementary material for this article can be found online at: https://www.frontiersin.org/articles/10.3389/fnagi.2022.1066331/full#supplementary-material

References

Adler, C. H., Beach, T. G., Hentz, J. G., Shill, H. A., Caviness, J. N., Driver-Dunckley, E., et al. (2014). Low clinical diagnostic accuracy of early vs advanced Parkinson disease: clinicopathologic study. *Neurology* 83, 406–412. doi: 10.1212/WNL.0000000000000641

Beach, T. G., Adler, C. H., Sue, L. I., Vedders, L., Lue, L., White Iii, C. L., et al. (2010). Multi-organ distribution of phosphorylated alpha-synuclein histopathology in subjects with Lewy body disorders. *Acta Neuropathol.* 119, 689–702. doi: 10.1007/s00401-010-0664-3

Braune, S. (2001). The role of cardiac metaiodobenzylguanidine uptake in the differential diagnosis of parkinsonian syndromes. *Clin. Auton. Res.* 11, 351–355. doi: 10.1007/BF02292766

Campo, F., Carletti, R., Fusconi, M., Pellicano, C., Pontieri, F. E., Di Gioia, C. R., et al. (2019). Alpha-synuclein in salivary gland as biomarker for Parkinson's disease. *Rev. Neurosci.* 30, 455–462. doi: 10.1515/revneuro-2018-0064

de Rijk, M. C., Rocca, W. A., Anderson, D. W., Melcon, M. O., Breteler, M. M. B., and Maraganore, D. M. (1997). A population perspective on diagnostic criteria for Parkinson's disease. *Neurology* 48, 1277–1281. doi: 10.1212/wnl.48.5.1277

Del Tredici, K., Hawkes, C. H., Ghebremedhin, E., and Braak, H. (2010). Lewy pathology in the submandibular gland of individuals with incidental Lewy body disease and sporadic Parkinson's disease. *Acta Neuropathol.* 119, 703–713. doi: 10.1007/s00401-010-0665-2

Den Hartog Jager, W. A., and Bethlem, J. (1960). The distribution of Lewy bodies in the central and autonomic nervous systems in idiopathic paralysis agitans. *J. Neurol. Neurosurg. Psychiatry* 23, 283–290. doi: 10.1136/jnnp.23.4.283

Fukuoka, M., Taki, J., Mochizuki, T., and Kinuya, S. (2011). Comparison of diagnostic value of I-123 MIBG and high-dose I-131 MIBG scintigraphy including incremental value of SPECT/CT over planar image in patients with malignant pheochromocytoma/paraganglioma and neuroblastoma. *Clin. Nucl. Med.* 36, 1–7. doi: 10.1097/RLU.0b013e3181feeb5e

Goetz, C. G., Tilley, B. C., Shaftman, S. R., Stebbins, G. T., Fahn, S., Martinez-Martin, P., et al. (2008). Movement Disorder Society-sponsored revision of the unified Parkinson's disease rating scale (MDS-UPDRS): scale presentation and clinimetric testing results. *Mov. Disord.* 23, 2129–2170. doi: 10.1002/mds.22340

Haqparwar, J., Pepe, A., Fassbender, K., Dillmann, U., Ezziddin, S., Schaefer, A., et al. (2017). Reduced MIBG accumulation of the parotid and submandibular glands in idiopathic Parkinson's disease. *Parkinsonism Relat. Disord.* 34, 26–30. doi: 10.1016/j.parkreldis.2016.10.011

Ishibashi, K., Saito, Y., Murayama, S., Kanemaru, K., Oda, K., Ishiwata, K., et al. (2010). Validation of cardiac (123)I-MIBG scintigraphy in patients with Parkinson's disease who were diagnosed with dopamine PET. *Eur. J. Nucl. Med. Mol. Imaging* 37, 3–11. doi: 10.1007/s00259-009-1202-1

Iwabuchi, Y., Kameyama, M., Matsusaka, Y., Narimatsu, H., Hashimoto, M., Seki, M., et al. (2021). A diagnostic strategy for Parkinsonian syndromes using quantitative indices of DAT SPECT and MIBG scintigraphy: an investigation using the classification and regression tree analysis. *Eur. J. Nucl. Med. Mol. Imaging* 48, 1833–1841. doi: 10.1007/s00259-020-05168-0

Jacobson, A. F., Senior, R., Cerqueira, M. D., Wong, N. D., Thomas, G. S., Lopez, V. A., et al. (2010). Myocardial iodine-123 meta-iodobenzylguanidine imaging and cardiac events in heart failure. Results of the prospective ADMIRE-HF (AdreView myocardial imaging for risk evaluation in heart failure) study. *J. Am. Coll. Cardiol.* 55, 2212–2221. doi: 10.1016/j.jacc.2010.01.014

Kollensperger, M., Seppi, K., Liener, C., Boesch, S., Heute, D., Mair, K. J., et al. (2007). Diffusion weighted imaging best discriminates PD from MSA-P: a comparison with tilt table testing and heart MIBG scintigraphy. *Mov. Disord.* 22, 1771–1776. doi: 10.1002/mds.21614

Lees, A. J., Hardy, J., Fau-Revesz, T., and Revesz, T. (2009). Parkinson's disease. *Lancet* 373, 2055–2066. doi: 10.1016/S0140-6736(09)60492-X

Nuvoli, S., Spanu, A., Fravolini, M. L., Bianconi, F., Cascianelli, S., Madeddu, G., et al. (2020). [(123)I]Metaiodobenzylguanidine (MIBG) cardiac scintigraphy and automated classification techniques in Parkinsonian disorders. *Mol. Imaging Biol.* 22, 703–710. doi: 10.1007/s11307-019-01406-6

Nuvoli, S., Spanu, A., Piras, M. R., Nieddu, A., Mulas, A., Rocchitta, G., et al. (2017). 123I-ioflupane brain SPECT and 123I-MIBG cardiac planar scintigraphy combined use in uncertain parkinsonian disorders. *Medicine* 96:e6967. doi: 10.1097/MD.0000000000006967

Oh, J. K., Choi, E. K., Song, I. U., Kim, J. S., and Chung, Y. A. (2015). Comparison of I-123 MIBG planar imaging and SPECT for the detection of decreased heart uptake in Parkinson disease. *J. Neural Transm.* 122, 1421–1427. doi: 10.1007/s00702-015-1409-1

Orimo, S., Suzuki, M., Inaba, A., and Mizusawa, H. (2012). 123I-MIBG myocardial scintigraphy for differentiating Parkinson's disease from other neurodegenerative parkinsonism: a systematic review and meta-analysis. *Parkinsonism Relat. Disord.* 18, 494–500. doi: 10.1016/j.parkreldis.2012.01.009

Orimo, S., Uchihara, T., Nakamura, A., Mori, F., Kakita, A., Wakabayashi, K., et al. (2008). Axonal alpha-synuclein aggregates herald centripetal degeneration of cardiac sympathetic nerve in Parkinson's disease. *Brain* 131, 642–650. doi: 10.1093/brain/awm302

Postuma, R. B., Berg, D., Stern, M., Poewe, W., Olanow, C. W., Oertel, W., et al. (2015). MDS clinical diagnostic criteria for Parkinson's disease. *Mov. Disord.* 30, 1591–1601. doi: 10.1002/mds.26424

Rutjes, A. W., Reitsma, J. B., di Nisio, M., Smidt, N., van Rijn, J. C., and Bossuyt, P. M. M. (2006). Evidence of bias and variation in diagnostic accuracy studies. *CMAJ* 174, 469–476. doi: 10.1503/cmaj.050090

Ryu, D. W., Kim, J. S., Lee, J. E., Oh, Y. S., Yoo, S. W., Yoo, I. R., et al. (2019). Initial versus follow-up sequential myocardial 123I-MIBG scintigraphy to discriminate Parkinson disease from atypical Parkinsonian syndromes. *Clin. Nucl. Med.* 44, 282–288. doi: 10.1097/RLU.0000000000002424

Sackett, D. L., and Haynes, R. B. (2002). The architecture of diagnostic research. *BMJ* 324, 539–541. doi: 10.1136/bmj.324.7336.539

Satoh, A., Serita, T., Seto, M., Tomita, I., Satoh, H., Iwanaga, K., et al. (1999). Loss of 123I-MIBG uptake by the heart in Parkinson's disease: assessment of cardiac sympathetic denervation and diagnostic value. *J. Nucl. Med.* 40, 371–375. PMID: 10086697

Schepici, G., Silvestro, S., Trubiani, O., Bramanti, P., and Mazzon, E. (2020). Salivary biomarkers: future approaches for early diagnosis of neurodegenerative diseases. *Brain Sci.* 10:245. doi: 10.3390/brainsci10040245

Schubert, E., Dogan, S., Dillmann, U., Schaefer-Schuler, A., Fassbender, K., Ezziddin, S., et al. (2019). MIBG scintigraphy of the major salivary glands in progressive supranuclear palsy and corticobasal degeneration. *Parkinsonism Relat. Disord.* 66, 247–248. doi: 10.1016/j.parkreldis.2019.07.003

Soboll, L., Leppert, D., Dillmann, U., Schaefer-Schuler, A., Fassbender, K., Ezziddin, S., et al. (2018). MIBG scintigraphy of the major salivary glands in multiple system atrophy. *Parkinsonism Relat. Disord.* 53, 112–114. doi: 10.1016/j.parkreldis.2018.04.034

Spiegel, J., Mollers, M. O., Jost, W. H., Fuss, G., Samnick, S., Dillmann, U., et al. (2005). FP-CIT and MIBG scintigraphy in early Parkinson's disease. *Mov. Disord.* 20, 552–561. doi: 10.1002/mds.20369

Stathaki, M., Koukouraki, S., Simos, P., Boura, I., Papadaki, E., Bourogianni, O., et al. (2020). Is there any clinical value of adding 123I-Metaiodobenzylguanidine myocardial scintigraphy to 123I-Ioflupane (DaTscan) in the differential diagnosis of parkinsonism? *Clin. Nucl. Med.* 45, 588–593. doi: 10.1097/RLU.0000000000003098

Sudmeyer, M., Antke, C., Zizek, T., Beu, M., Nikolaus, S., Wojtecki, L., et al. (2011). Diagnostic accuracy of combined FP-CIT, IBZM, and MIBG scintigraphy in the differential diagnosis of degenerative parkinsonism: a multidimensional statistical approach. *J. Nucl. Med.* 52, 733–740. doi: 10.2967/jnumed.110.086959

Treglia, G., Cason, E., Stefanelli, A., Cocciolillo, F., Di Giuda, D., Fagioli, G., et al. (2012). MIBG scintigraphy in differential diagnosis of parkinsonism: a meta-analysis. *Clin. Auton. Res.* 22, 43–55. doi: 10.1007/s10286-011-0135-5

Tsukita, K., Sakamaki-Tsukita, H., Tanaka, K., Suenaga, T., and Takahashi, R. (2019). Value of in vivo α-synuclein deposits in Parkinson's disease: a systematic review and meta-analysis. *Mov. Disord.* 34, 1452–1463. doi: 10.1002/mds.27794

Wu, P., Zhao, Y., Wu, J., Brendel, M., Lu, J., Ge, J., et al. (2022). Differential diagnosis of parkinsonism based on deep metabolic imaging indices. *J. Nucl. Med.* 63, 1741–1747. doi: 10.2967/jnumed.121.263029

Yang, T., Wang, L., Li, Y., Cheng, M., Jiao, J., Wang, Q., et al. (2017). (131) I-MIBG myocardial scintigraphy for differentiation of Parkinson's disease from multiple system atrophy or essential tremor in Chinese population. *J. Neurol. Sci.* 373, 48–51. doi: 10.1016/j.jns.2016.12.006

Zhao, Y., Wu, P., Wu, J., Brendel, M., Lu, J., Ge, J., et al. (2022). Decoding the dopamine transporter imaging for the differential diagnosis of parkinsonism using deep learning. *Eur. J. Nucl. Med. Mol. Imaging* 49, 2798–2811. doi: 10.1007/s00259-022-05804-x

frontiers | Frontiers in Aging Neuroscience

TYPE Study Protocol
PUBLISHED 19 January 2023
DOI 10.3389/fnagi.2022.1041076

OPEN ACCESS

EDITED BY
Jiehui Jiang,
Shanghai University,
China

REVIEWED BY
Can Sheng,
Capital Medical University,
China
Dean Wu,
Taipei Medical University,
Taiwan

*CORRESPONDENCE
Chun-Pai Yang
✉ neuralyung@gmail.com
Cheng-Yu Wei
✉ yuyu@seed.net.tw

†These authors have contributed equally to this work

SPECIALTY SECTION
This article was submitted to Alzheimer's Disease and Related Dementias, a section of the journal Frontiers in Aging Neuroscience

RECEIVED 10 September 2022
ACCEPTED 23 December 2022
PUBLISHED 19 January 2023

CITATION
Lin T-H, Yang C-C, Lee S-Y, Chang C-M, Tsai I-J, Wei C-Y and Yang C-P (2023) The effect of bright light therapy in migraine patients with sleep disturbance: A prospective, observational cohort study protocol.
Front. Aging Neurosci. 14:1041076.
doi: 10.3389/fnagi.2022.1041076

The effect of bright light therapy in migraine patients with sleep disturbance: A prospective, observational cohort study protocol

Tsung-Hsing Lin[1†], Cheng-Chia Yang[2†], Shih-Yu Lee[3,4], Ching-Mao Chang[5,6,7], I-Ju Tsai[8], Cheng-Yu Wei[9,10*] and Chun-Pai Yang[8,11*]

[1]Department of Emergency Medicine, Kuang Tien General Hospital, Taichung, Taiwan, [2]Department of Healthcare Administration, Asia University, Taichung, Taiwan, [3]Biotechnology Health and Innovation Research Center, Hungkuang University, Taichung, Taiwan, [4]College of Nursing, Hungkuang University, Taichung, Taiwan, [5]Center for Traditional Medicine, Taipei Veterans General Hospital, Taipei, Taiwan, [6]Faculty of Medicine, National Yang Ming Chiao Tung University, Taipei, Taiwan, [7]Institute of Traditional Medicine, National Yang Ming Chiao Tung University, Taipei, Taiwan, [8]Department of Neurology, Kuang Tien General Hospital, Taichung, Taiwan, [9]Department of Exercise and Health Promotion, College of Kinesiology and Health, Chinese Culture University, Taipei, Taiwan, [10]Department of Neurology, Chang Bing Show Chwan Memorial Hospital, Changhua, Taiwan, [11]Ph.D. Program in Translational Medicine, National Chung Hsing University, Taichung, Taiwan

Background: Migraine is a common disabling disorder, and its substantial burden is associated with a considerable negative impact on the patients' quality of life. Moreover, aging patients with migraine have more cognitive complaints. Additionally, the elderly are more likely to have sleep disturbances, which may also predict the risk of incident dementia. Migraines are reported to be closely associated with sleep and circadian rhythms. Sleep disturbance is a well-known trigger for migraine episodes; moreover, shift work or jet lag reportedly triggers some migraines. The hypothalamus is thought to be the migraine generator; sleep and circadian activity rhythm are also controlled by the hypothalamus. Evidence suggests an influence of both sleep and circadian system on migraine. Previously, light therapy has been show to stabilize sleep architecture and further improve insomnia related to circadian rhythm disorders. However, the beneficial effect of light therapy on migraine with sleep disturbance has not yet been determined. We aim to explore the effects of light therapy for migraine combined with sleep disturbance.

Methods and analysis: This project is a 2-year, randomized, double-blind, placebo-controlled clinical trial. The study design includes a 4-week monitoring period (baseline and pretest), a 4-week treatment period, and a posttest. The study participants will undergo assessments on headache frequency and severity and subjective and objective (wrist actigraphy and polysomnography) sleep disturbances, and quality of life and a series of blood tests for serum biomarkers.

Discussion: This study will establish evidence-based alternative medicine for the preventive effect of bright light therapy in migraine patients with

sleep disturbances. Moreover, our data will be useful to comprehend the biochemical mechanism of light therapy in migraine prevention.

Clinical Trial Registration: ClinicalTrials.gov, identifier NCT04890691.

KEYWORDS

migraine, light therapy, circadian rhythms, PSG, neuropeptides, wrist actigraph

Introduction

Over 1 billion people experience migraine, with approximately three times as many women as men suffering (Ashina et al., 2021a,b). The incidence of migraine in Taiwan is 9.3%, with the most common age group being young adults aged 35–55 years, and the ratio of women to men being approximately 3:1 (Wang et al., 2000). Migraine is one of the five most disabling and most burdensome conditions in women (Stovner et al., 2007; Steiner et al., 2018). Generally, if migraine is undertreated, it not only causes extreme discomfort to patients, but also reduces their quality of life (QOL) and work productivity, increases absenteeism, and places a significant burden on the healthcare system (Burstein et al., 2015). Additionally, migraine patients also have many comorbidities, including mental illnesses (e.g., depression, anxiety), sleep disorders, and pain in other body parts. Migraine patients often complain of lack of sleep before and during a migraine attack, whereas good sleep is helpful for migraines. Lack of sleep is often cited as one of the causes of migraine. Apart from the lack of sleep triggering migraines, too much sleep or circadian rhythm disturbances, such as shift interference, can also trigger migraine attacks (Vgontzas and Pavlovic, 2018). These phenomena suggest that migraines are not only related to sleep but also sleep rhythm disorders. The hypothalamus in the brain is responsible for circadian rhythm and sleep, and it is confirmed as the migraine generator (Burstein et al., 2015); thus, we hypothesized that day and night rhythm regulation or stabilization can reduce migraine attacks.

Although the link between migraine and sleep has been documented for decades, its physiological mechanism is still unclear. Migraine exhibits menstrual and circadian rhythms, and individuals with migraine may have a defect in chronobiologic synchronizing systems (Silberstein, 2008). Women seem more vulnerable to the effects of sleep disturbances than men because of both physiological and psychosocial factors. For example, shifting of hormone levels, including those occurring with puberty, menstruation, and perimenopause, may modulate circadian rhythms among women (Brandes, 2006), and may be responsible for substantive changes in the nature of women's sleep. Circadian rhythms affect sleep and wakefulness in humans, and exposure to sunlight helps stabilize and regularize the circadian rhythms (Lindskov et al., 2022).

Migraine is caused by the activation of the trigeminovascular system, resulting in the release of pain-producing nerve-inflaming substances around the nerves and blood vessels in the head and neck (Burstein et al., 2015). Migraine is reportedly initiated at the same location as the center that controls the circadian rhythm, the hypothalamus, which may explain why sleep disturbances are both a precipitating factor and common comorbidity in migraine (Baksa et al., 2019; Tiseo et al., 2020). The pathogenesis of migraine is extremely complex, and the "trigeminovascular theory" is the main theory currently recognized (Noseda and Burstein, 2013). This theory holds that activation of trigeminal nerve endings from around the meningeal blood vessels causes localized nerve inflammation, which mainly includes the following two neuropeptides: calcitonin gene-related peptide (CGRP) and pituitary adenylate-cyclase-activating polypeptide (PACAP). These two peptides will further cause the activation of the trigeminal nucleus and stimulate the cerebral cortex to produce headaches (Amin et al., 2016; American Headache Society, 2019).

One of the main treatment methods of migraine is to reduce the triggering factors, and sleep disturbance is among the common triggering factors of migraine. However, few sleep interventions have been used to reduce the frequency and severity of migraine attacks. Bright light therapy (BLT) can reportedly improve nighttime sleepiness due to circadian rhythm or neuro-psychiatric disorders and sleep duration and reduce daytime sleepiness (Burkhalter et al., 2015; Faulkner et al., 2019); however, the effect of BLT in migraine patients with sleep disturbance is uncertain. Particularly, light has been viewed as a trigger for migraine, but a recent review reported that migraine patients are not photophobic to all wavebands of the light spectrum (Artemenko et al., 2022). Thus, light therapy should be an innovative approach. Additionally, the mechanism of the link between sleep disturbance and migraine is still not clearly understood, and understanding the pathological mechanism is helpful for future clinical care and further research. Therefore, we aim to examine a BLT intervention designed to reduce migraine in women by improving the sleep and circadian activity rhythms. Subsequently, we will test a BLT intervention as part of the sleep hygiene bundle designed to reduce migraine attacks in women by improving sleep and circadian activity rhythms.

Objectives

The specific goals of this prospective study are to (1) compare the effects of BLT (green light and sleep hygiene) with an attention control treatment (placebo light and sleep hygiene) on selected sleep variables [total nocturnal sleep time, wake after sleep onset

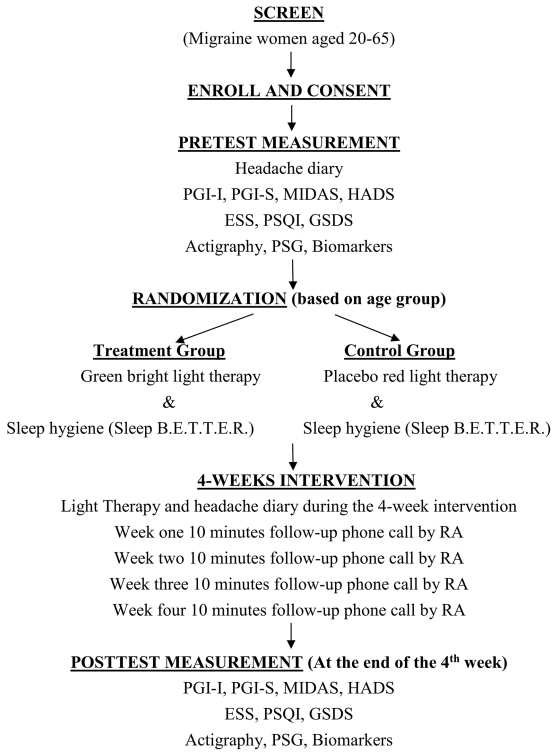

FIGURE 1
Randomized pretest–posttest design.

(WASO), sleep efficiency, daytime sleepiness], migraine conditions (frequency and severity), and QOL (mental health) from baseline to 1 month after beginning the intervention; and (2) explore the light therapy's molecular and biochemical effects on migraine prevention.

Materials and methods

Study design

This parallel, randomized, double-blind, placebo-controlled clinical trial will be conducted at a teaching hospital in the middle part of Taiwan. The sample will consist of 60 women diagnosed with migraine and sleep disorders. After a 1:1 random assignment, 30 women will be assigned to light therapy and sleep hygiene education, and the other 30 women will be assigned to placebo light and sleep hygiene education for a 4-week clinical trial (Figure 1).

Inclusion and exclusion criteria

The inclusion criteria are as follows: diagnosed with migraine according to the International Classification of Headache Disorder 3rd edition (ICHD-3); aged 20–65 years; with sleep disorders (PSQI >5 points); willing to participate in activity monitoring (wrist recorder) during the day and night for 9 consecutive weeks, and one night in the sleep room for polysomnography, totaling to two time periods (before and after treatment); willingness to have blood drawn twice; not allergic to metals (a contraindication to wearing wrist actigraph); and not currently participating in other interventional trials.

The exclusion criteria are as follows: non-migraine headaches (e.g., tension-type or secondary headaches, among others); major head trauma in the past; alcoholism within 1 year; (4) pregnant or breastfeeding women; (5) cannot cooperate with the test progress; (6) allergic to light; and (7) taking beta-blockers, antiepileptic drugs, calcium ion blockers, antidepressants, onabotulinumtoxinA, CGRP monoclonal antibody, and hormone preparations in the past month.

Interventions

Our study has a two-component intervention package, including a 30-min daily BLT (green and red lights for the treatment and control groups, respectively) and a sleep hygiene educational package for 4 weeks. The bright light visor (Feel Bright Light Model 100, Physician Engineered Products, Fryeburg, ME) will be used for the treatment group; however, the visor delivers blue–green light, thus we blocked the blue light and remind the participants to use the green light to prevent potential damage to eyes, especially the elderly. The unit weighs approximately 1.7 ounces, is comfortable to wear, and is powered by a rechargeable battery, allowing participants to move freely for their daily work. Participants will undergo 30 min of BLT within an hour of waking up for 4 weeks. A red-light visor (Physician Engineered Products, Fryeburg, ME), an attention control strategy, that does not have any therapeutic effect will be used for the control group. Both groups will receive a sleep hygiene educational booklet.

Sleep hygiene is fundamental to improving sleep and is considered an important intervention to promote sleep (McCurry et al., 2004). Sleep B.E.T.T.E.R. will be included in this educational package. This booklet includes information on normal sleep and promoting the homeostatic drive for sleep using the following six basic guidelines: bedroom environment, regular daily exercise, reducing tension and stress, time trying to sleep, eating and drinking, and maintaining regular day–night rhythms.

Participant recruitment

A research assistant (RA) under a neurologist's supervision will screen the visiting log at the research site's migraine clinic to identify potential participants. Then, the RA will approach the women and describe the study. The opportunity will be given to the women to privately consider the project, and a later contact will be made to answer questions and enroll the women interested in participating.

TABLE 1 Measurement schedule.

	Baseline	Treatment and data collection timepoints			
Timepoint	Pretest	1st week	2nd week	3rd week	4th week
Enrolment					
Eligibility screening	X				
Informed consent	X				
Demographics	X				
Medical records	X				
MEASUREMENTS					
4-week headache diary	X X X X	X	X	X	X
PGI-I	X				X
PGI-S	X				X
MIDAS	X				X
HADS	X				X
ESS	X				X
PSQI	X				X
GSDS	X				X
7-day wrist actigraphy	X				X
7-day sleep diary	X				X
Overnight PSG	X				X
Blood sample	X				X
Weekly phone call		X	X	X	X

PGI-I, Patient Global Impression of Improvement; PGI-S, Patient Global Impression of Severity; MIDAS, Migraine Disability Assessment; HADS, Hospital Anxiety and Depression Scale; ESS, Epworth Sleepiness Scale; PSQI, Pittsburgh Sleep Quality Questionnaire; GSDS, General Sleep Disturbance Scale; PSG, Polysomnography.

Data collection

Apart from the demographic form, psychometric sound instruments will be used in the study, which are described below (Table 1).

Headache diaries

This diary includes headache days, duration, intensity, frequency, location, characteristics, use of pain medication, accompanying symptoms and triggers, among others. Each diary covers 28 days.

Detection of headache-related scales

Patient Global Impression of Improvement (PGI-I) is an assessment to measure disease improvement (Guy, 1993). PGI of Severity (PGI-S) will be used to measure the severity of migraine (Guy, 1993). The Migraine Disability Assessment (MIDAS) (Stewart et al., 1999) will be used to assess migraine-related disabilities in different areas of life in the past 3 months.

The hospital anxiety and depression scale

This will be used to evaluate the depression and anxiety of chronic migraine patients (Zigmond and Snaith, 1983). Cut-off points are ≥ 10 and ≥ 13 for depression and anxiety, respectively.

Epworth sleepiness scale

The study participant's daytime sleepiness will be measured with ESS (Johns, 1991).

Pittsburgh sleep quality questionnaire

This records the sleep status of the past month, including the following six sub-items: sleep quality, sleep onset time, sleep hours, sleep efficiency, sleep disturbance, use of sleep medication, and daytime activity. It will be filled in by self-assessment, with a total score of > 5 indicating poor sleep quality (Buysse et al., 1989).

General sleep disturbance scale

This questionnaire utilizes a weekly sleep rating scale of 0–7, which includes 21 items related to frequency, in the past week, quality of sleep, quantity of sleep, fatigue and wakefulness at work, and use of sleep-promoting substances (Lee, 1992; Lee and DeJoseph, 1992; Lee, 2007).

Wrist actigraphy (Mini Motionlogger Actigraphy, AMI, Ardsley, NY)

A lightweight watch-lime motion sensor monitor will be used to collect objective sleep data, including total nocturnal and day sleep time (TST), WASO, and circadian activity rhythms for 7 consecutive days. Various investigators in the past have demonstrated a very high correlation ($r = 0.93$–0.99) between the two measures of total sleep time during the night and measures of wakefulness using the sleep polysomnography (PSG) (Jean-Louis et al., 1996; Ancoli-Israel et al., 1997).

Polysomnography

In addition to the wrist actigraphy data, an overnight sleep visit will be required to collect the objective sleep data.

Physiological indicators

A blood sample will be collected to measure CGRP and PACAP.

Data management

The following information will be obtained from each subject: demographics, 4-week headache data (pre and posttreatment), pre and posttreatment outcome variables (PGI-I, PGI-S, MIDAS, HADS, PSQI, and GSDS), selected physiological indicators (PSG, CGRP, and PACAP), and pre and posttreatment 7-day wrist actigraphy data (TST, WASO, circadian activity rhythm). The physiological analysis will be performed in the hospital's laboratory using established laboratory protocols for specimen processing and analysis. Assay preparation will be performed following the manufacturer's instructions. The sleep data obtained

with the watch will be analyzed by using the Action 4 software, and the PSG will be analyzed by using the Crystal software.

Data analysis

All data analyzes will be conducted using the intent-to-treat principle. When considering the results of multiple comparisons, the Bonferroni correction will be used to correct the significance level. Pre and posttest, the related scales of the experimental and control groups, such as the headache diary, PGI-I, PGI-S, MIDAS, HADS, PSQI, ESS, GSDS, and PSG, wrist actigraphy, and blood test analysis, will be expressed as mean ± standard deviation.

The above-mentioned scales and blood test values of the pre and posttreatment assessments of each patient will be tested with the Sign test to identify any difference before and after the test. Finally, the generalized estimating equation model will be used to evaluate whether the experimental group significantly had reduced pain frequency and severity and improved sleep than the control group to understand the effect of light therapy on migraine.

Ethical considerations

The study was approved by the Institutional Review Board of Kuang Tien General Hospital (KTGH21002) and registered in the ClinicalTrials.gov (NCT4890691).

Participation in research is voluntary. Completing the data booklets may result in some discomfort as women will reflect on the answers that they will provide; they will be reminded that they may stop at any time. Women wearing the bright light visor may have a slight chance of developing a headache similar to exposure to natural sunlight; if so, participants will be instructed to use the 8,000 lux instead of 12,000 lux. During the weekly follow-up phone call, participants will be asked if they have any unusual symptoms. If yes, this will be discussed with the Co-PI, who is a neurologist, and, if any adverse symptoms are noted, the participant will be requested to discontinue the light treatment. All participants may choose to terminate their participation at any time without incurring any adverse consequences.

Discussion

Although there have been considerable advances in the treatment of migraine in the last decade, migraine remains one of the debilitating chronic pain conditions and many patients continue to experience substantial pain and disability, despite taking multiple drugs. Patient and clinician interests in non-pharmacological treatments remain strong (Robbins, 2021).

Migraine and sleep have drawn great attention due to their strong, bidirectional, and complex clinical relationship (Tiseo, Vacca, Felbush, Filimonova, Gai, Glazyrina, Hubalek, Marchenko, Overeem, Piroso, Tkachev, Martelletti, Sacco and European Headache Federation School of Advanced 2020). The hypothalamus involved in homeostatic regulation, including pain processing and sleep–wake cycle regulation, is also a key integrator of circadian entrainment to light and has emerged as a key brain area in migraine (Schulte and May, 2016). Although clinical evidence has shown that light therapy can stabilize sleep architecture, its beneficial effects in migraine patients with sleep disturbance remain to be elucidated.

To date, few studies have tested an intervention designed to prevent migraine by improving sleep. This protocol provides a detailed overview of the design and implementation of a randomized, double-blind, placebo-controlled clinical trial comparing the effects between green light for the treatment group and red light for the control group in migraine patients with sleep disturbance. It is anticipated that this study will provide preliminary support for the use of light therapy in conjunction with sleep hygiene intervention for reducing women's migraine attacks by improving sleep. This study will provide the basis for further development of nonpharmaceutical interventions for sleep to prevent migraine attacks in various populations and will have direct clinical applicability by adding an important primary intervention for the clinical care of migraine patients.

Ethics statement

The studies involving human participants were reviewed and approved by Institutional Review Board of Kuang Tien General Hospital (KTGH21002). The patients/participants provided their written informed consent to participate in this study.

Author contributions

T-HL, C-CY, S-YL, and C-PY were responsible for the study concept and research design, and study design modification. T-HL, C-CY, S-YL, C-MC, and C-PY were also responsible for drafting and revising the manuscript. C-MC, C-YW, and C-PY modified the study design and revised the manuscript. T-HL, C-CY, S-YL, C-MC, C-YW, and C-PY contributed to the collection, analysis, and interpretation of data and revision of the manuscript. All authors have read and approved the final version of the manuscript.

Funding

This study was supported by Hungkuang University and Kuang Tien General Hospital (HK-KTOH-110-03), Taichung, Taiwan.

Conflict of interest

The authors declare that the research was conducted in the absence of any commercial or financial relationships that could be construed as a potential conflict of interest.

Publisher's note

References

American Headache Society (2019). The American headache society position statement on integrating new migraine treatments into clinical practice. *Headache* 59, 1–18. doi: 10.1111/head.13456.

Amin, F. M., Hougaard, A., Magon, S., Asghar, M. S., Ahmad, N. N., Rostrup, E., et al. (2016). Change in brain network connectivity during PACAP38-induced migraine attacks: a resting-state functional MRI study. *Neurology* 86, 180–187. doi: 10.1212/WNL.0000000000002261

Ancoli-Israel, S., Clopton, P., Klauber, M. R., Fell, R., and Mason, W. (1997). Use of wrist activity for monitoring sleep/wake in demented nursing-home patients. *Sleep* 20, 24–27. doi: 10.1093/sleep/20.1.24

Artemenko, A. R., Filatova, E., Vorobyeva, Y. D., Do, T. P., Ashina, M., and Danilov, A. B. (2022). Migraine and light: a narrative review. *Headache* 62, 4–10. doi: 10.1111/head.14250

Ashina, M., Amin, F. M., Kokturk, P., Cohen, J. M., Konings, M., Tassorelli, C., et al. (2021a). PEARL study protocol: a real-world study of fremanezumab effectiveness in patients with chronic or episodic migraine. *Pain Manage.* 11, 647–654. doi: 10.2217/pmt-2021-0015

Ashina, M., Katsarava, Z., Do, T. P., Buse, D. C., Pozo-Rosich, P., Ozge, A., et al. (2021b). Migraine: epidemiology and systems of care. *Lancet* 17, 1485–1495. doi: 10.1016/S0140-6736(20)32160-7

Baksa, D., Gecse, K., Kumar, S., Toth, Z., Gal, Z., Gonda, X., et al. (2019). Circadian variation of migraine attack onset: a review of clinical studies. *Biomed. Res. Int.* 2019:4616417. doi: 10.1155/2019/4616417

Brandes, J. L. (2006). The influence of estrogen on migraine: a systematic review. *JAMA* 295, 1824–1830. doi: 10.1001/jama.295.15.1824

Burkhalter, H., Wirz-Justice, A., Denhaerynck, K., Fehr, T., Steiger, J., Venzin, R. M., et al. (2015). The effect of bright light therapy on sleep and circadian rhythms in renal transplant recipients: a pilot randomized, multicentre wait-list controlled trial. *Transpl. Int.* 28, 59–70. doi: 10.1111/tri.12443

Burstein, R., Noseda, R., and Borsook, D. (2015). Migraine: multiple processes, complex pathophysiology. *J. Neurosci.* 29, 6619–6629. doi: 10.1523/JNEUROSCI.0373-15.2015

Buysse, D. J., Reynolds, C. F. 3rd, Monk, T. H., Berman, S. R., and Kupfer, D. J. (1989). The Pittsburgh sleep quality index: a new instrument for psychiatric practice and research. *Psychiatry Res.* 28, 193–213. doi: 10.1016/0165-1781(89)90047-4

Faulkner, S. M., Bee, P. E., Meyer, N., Dijk, D. J., and Drake, R. J. (2019). Light therapies to improve sleep in intrinsic circadian rhythm sleep disorders and neuropsychiatric illness: a systematic review and meta-analysis. *Sleep Med. Rev.* 46, 108–123. doi: 10.1016/j.smrv.2019.04.012

Guy, W. (1993). *ECDEU Assessment Manual for Psychopharmacology*. US Department of Health Education, and Welfare Public Health Service, Alcohol, Drug, Abuse, and Mental Health Administration, National Institute of Mental Health Psychopharmacology Research Branch, Division of Extramural Research Programs.

Jean-Louis, G., von Gizycki, H., Zizi, F., Fookson, J., Spielman, A., Nunes, J., et al. (1996). Determination of sleep and wakefulness with the actigraph data analysis software (ADAS). *Sleep* 19, 739–743.

Johns, M. W. (1991). A new method for measuring daytime sleepiness: the Epworth sleepiness scale. *Sleep* 14, 540–545. doi: 10.1093/sleep/14.6.540

Lee, K. A. (1992). Self-reported sleep disturbances in employed women. *Sleep* 15, 493–498. doi: 10.1093/sleep/15.6.493

Lee, S. Y. (2007). Validating the general sleep disturbance scale among Chinese American parents with hospitalized infants. *J. Transcult. Nurs.* 18, 111–117. doi: 10.1177/1043659606298502

Lee, K. A., and DeJoseph, J. F. (1992). Sleep disturbances, vitality, and fatigue among a select group of employed childbearing women. *Birth* 19, 208–213. doi: 10.1111/j.1523-536X.1992.tb00404.x

Lindskov, F. O., Iversen, H. K., and West, A. S. (2022). Clinical outcomes of light therapy in hospitalized patients - a systematic review. *Chronobiol. Int.* 39, 299–310. doi: 10.1080/07420528.2021.1993240

McCurry, S. M., Logsdon, R. G., Vitiello, M. V., and Teri, L. (2004). Treatment of sleep and nighttime disturbances in Alzheimer's disease: a behavior management approach. *Sleep Med.* 5, 373–377. doi: 10.1016/j.sleep.2003.11.003

Noseda, R., and Burstein, R. (2013). Migraine pathophysiology: anatomy of the trigeminovascular pathway and associated neurological symptoms, CSD, sensitization and modulation of pain. *Pain* 154, S44–S53. doi: 10.1016/j.pain.2013.07.021

Robbins, M. S. (2021). Diagnosis and Management of Headache: a review. *JAMA* 11, 1874–1885. doi: 10.1001/jama.2021.1640

Schulte, L. H., and May, A. (2016). The migraine generator revisited: continuous scanning of the migraine cycle over 30 days and three spontaneous attacks. *Brain* 139, 1987–1993. doi: 10.1093/brain/aww097

Silberstein, S. D. (2008). Recent developments in migraine. *Lancet* 372, 1369–1371. doi: 10.1016/S0140-6736(08)61569-X

Steiner, T. J., Stovner, L. J., Vos, T., Jensen, R., and Katsarava, Z. (2018). Migraine is first cause of disability in under 50s: will health politicians now take notice? *J. Headache Pain* 19:17. doi: 10.1186/s10194-018-0846-2

Stewart, W. F., Lipton, R. B., Kolodner, K., Liberman, J., and Sawyer, J. (1999). Reliability of the migraine disability assessment score in a population-based sample of headache sufferers. *Cephalalgia* 19, 107–114. doi: 10.1046/j.1468-2982.1999.019002107.x

Stovner, L., Hagen, K., Jensen, R., Katsarava, Z., Lipton, R., Scher, A., et al. (2007). The global burden of headache: a documentation of headache prevalence and disability worldwide. *Cephalalgia* 27, 193–210. doi: 10.1111/j.1468-2982.2007.01288.x

Tiseo, C., Vacca, A., Felbush, A., Filimonova, T., Gai, A., Glazyrina, T., et al. (2020). Migraine and sleep disorders: a systematic review. *J. Headache Pain* 21:126. doi: 10.1186/s10194-020-01192-5

Vgontzas, A., and Pavlovic, J. M. (2018). Sleep disorders and migraine: review of literature and potential pathophysiology mechanisms. *Headache* 58, 1030–1039. doi: 10.1111/head.13358

Wang, S. J., Fuh, J. L., Young, Y. H., Lu, S. R., and Shia, B. C. (2000). Prevalence of migraine in Taipei, Taiwan: a population-based survey. *Cephalalgia* 20, 566–572. doi: 10.1046/j.1468-2982.2000.00085.x

Zigmond, A. S., and Snaith, R. P. (1983). The hospital anxiety and depression scale. *Acta Psychiatr. Scand.* 67, 361–370. doi: 10.1111/j.1600-0447.1983.tb09716.x

frontiers | Frontiers in Aging Neuroscience

TYPE Original Research
PUBLISHED 22 February 2023
DOI 10.3389/fnagi.2023.1088829

OPEN ACCESS

EDITED BY
Jiehui Jiang,
Shanghai University, China

REVIEWED BY
Zhentao Zhang,
Renmin Hospital of Wuhan University, China
Shu-Wei Richard Sun,
Loma Linda University, United States

*CORRESPONDENCE
Lu Shen
shenlu@csu.edu.cn
Dongcui Wang
wangdongcui_bme@csu.edu.cn

†These authors have contributed equally to this work and share first authorship

SPECIALTY SECTION
This article was submitted to Alzheimer's Disease and Related Dementias, a section of the journal Frontiers in Aging Neuroscience

RECEIVED 03 November 2022
ACCEPTED 06 February 2023
PUBLISHED 22 February 2023

CITATION
Hao X, Zhang W, Jiao B, Yang Q, Zhang X, Chen R, Wang X, Xiao X, Zhu Y, Liao W, Wang D and Shen L (2023) Correlation between retinal structure and brain multimodal magnetic resonance imaging in patients with Alzheimer's disease. *Front. Aging Neurosci.* 15:1088829. doi: 10.3389/fnagi.2023.1088829

Correlation between retinal structure and brain multimodal magnetic resonance imaging in patients with Alzheimer's disease

Xiaoli Hao[1†], Weiwei Zhang[2†], Bin Jiao[1,3,4,5,6], Qijie Yang[1], Xinyue Zhang[1], Ruiting Chen[2], Xin Wang[1], Xuewen Xiao[1], Yuan Zhu[1], Weihua Liao[2], Dongcui Wang[2*] and Lu Shen[1,3,4,5,6,7*]

[1]Department of Neurology, Xiangya Hospital of Central South University, Changsha, China, [2]Department of Radiology, Xiangya Hospital of Central South University, Changsha, China, [3]National Clinical Research Center for Geriatric Disorders, Central South University, Changsha, China, [4]Engineering Research Center of Hunan Province in Cognitive Impairment Disorders, Central South University, Changsha, China, [5]Hunan International Scientific and Technological Cooperation Base of Neurodegenerative and Neurogenetic Diseases, Changsha, China, [6]Key Laboratory of Hunan Province in Neurodegenerative Disorders, Central South University, Changsha, China, [7]Key Laboratory of Organ Injury, Aging and Regenerative Medicine of Hunan Province, Changsha, China

Background: The retina imaging and brain magnetic resonance imaging (MRI) can both reflect early changes in Alzheimer's disease (AD) and may serve as potential biomarker for early diagnosis, but their correlation and the internal mechanism of retinal structural changes remain unclear. This study aimed to explore the possible correlation between retinal structure and visual pathway, brain structure, intrinsic activity changes in AD patients, as well as to build a classification model to identify AD patients.

Methods: In the study, 49 AD patients and 48 healthy controls (HCs) were enrolled. Retinal images were obtained by optical coherence tomography (OCT). Multimodal MRI sequences of all subjects were collected. Spearman correlation analysis and multiple linear regression models were used to assess the correlation between OCT parameters and multimodal MRI findings. The diagnostic value of combination of retinal imaging and brain multimodal MRI was assessed by performing a receiver operating characteristic (ROC) curve.

Results: Compared with HCs, retinal thickness and multimodal MRI findings of AD patients were significantly altered ($p < 0.05$). Significant correlations were presented between the fractional anisotropy (FA) value of optic tract and mean retinal thickness, macular volume, macular ganglion cell layer (GCL) thickness, inner plexiform layer (IPL) thickness in AD patients ($p < 0.01$). The fractional amplitude of low frequency fluctuations (fALFF) value of primary visual cortex (V1) was correlated with temporal quadrant peripapillary retinal nerve fiber layer (pRNFL) thickness ($p < 0.05$). The model combining thickness of GCL and temporal quadrant pRNFL, volume of hippocampus and lateral geniculate nucleus, and age showed the best performance to identify AD patients [area under the curve (AUC) = 0.936, sensitivity = 89.1%, specificity = 87.0%].

Conclusion: Our study demonstrated that retinal structure change was related to the loss of integrity of white matter fiber tracts in the visual pathway and the

decreased LGN volume and functional metabolism of V1 in AD patients. Trans-synaptic axonal retrograde lesions may be the underlying mechanism. Combining retinal imaging and multimodal MRI may provide new insight into the mechanism of retinal structural changes in AD and may serve as new target for early auxiliary diagnosis of AD.

KEYWORDS

Alzheimer's disease, retina, visual pathway, multimodal magnetic resonance imaging, biomarker

Introduction

Alzheimer's disease (AD) is the most common type of senile dementia and is characterized by a progressive deterioration of cognitive function over time (Ge et al., 2021). The pathology of AD is featured by extracellular amyloid plaques formed by the aggregation of amyloid-β (Aβ) and neuronal fibrillary tangles (NFT) formed by abnormally phosphorylated tau. Studies have demonstrated that the pathological changes of AD precede the onset of clinical symptoms 15–20 years (Drew, 2018). Therefore, early diagnosis of AD is particularly important in order to achieve early intervention and treatment. Currently, Aβ and tau proteins are mainly quantified by positron emission tomography (PET) or cerebrospinal fluid (CSF) (Arvanitakis et al., 2019; Jiao et al., 2021). However, these tests are invasive and expensive, pending the discovery of new universally applicable early diagnostic markers.

The retina shares similar neurobiology of neuronal cells and microvasculature with those in central nervous system (CNS), thus, changes in retina structure and function may serve as a window to access the changes in CNS (Liao et al., 2021; Zhang et al., 2022). In recent years, a number of clinical studies have shown that AD patients have functional visual defects and anatomical changes in retinal structure. In fact, about 58% patients develop visual problems before the initial symptoms of AD, such as impaired visual acuity, color perception, contrast sensitivity, and visual field (Mendez et al., 1990; Mendola et al., 1995; Chiquita et al., 2019). Optical coherence tomography (OCT) is a non-invasive technique for cross-sectional imaging of the internal structure of the retina, primarily to visualize morphological changes in the retina and to show retinal layering. Studies using OCT technology have demonstrated that the thickness of the peripapillary retinal nerve fiber layer (pRNFL) and macular ganglion cell layer (GCL) in patients with early AD and mild cognitive impairment (MCI) are significantly reduced (Criscuolo et al., 2018). Recent studies found that retinal thickness correlated with concentrations of AD biomarkers in CSF and PET-Aβ uptake values (Golzan et al., 2017; Santangelo et al., 2020). Moreover, after taking curcumin, deposition of Aβ protein can be detected in the retina of patients with AD by non-invasive fluorescence imaging techniques (Koronyo et al., 2017). Accumulation of tau protein in the retina of AD mice was observed before the onset of symptoms (Chiasseu et al., 2017). Our team's previous study also found that the retinal thickness reduced significantly in AD patients, which was correlated with the concentration of Aβ and tau in CSF (Wang X. et al., 2022). These above studies indicate that changes in retinal structure may serve as an early diagnostic biomarker for AD. However, the retinal structural changes are not specific to AD (Cheung et al., 2021; Snyder et al., 2021), their diagnostic and prognostic values in AD are still under debate.

Multimodal magnetic resonance imaging (MRI), dividing as structural imaging and functional imaging, reflect the structure and intrinsic activity of the brain (Zhou et al., 2021). Previous studies found that volumes of hippocampus were reduced in AD (Mu and Gage, 2011). Hippocampal atrophy can also distinguish AD patients from healthy controls and those who will convert from MCI to AD from non-converters (Teipel et al., 2015; Wang H. et al., 2022). In addition, recent study observed the degeneration of lateral geniculate nucleus (LGN) in AD patients (Erskine et al., 2016). Hippocampal atrophy and LGN degeneration may act as early changes in the progenesis of AD, but their relationship with retinal structure remains vague. Diffusion tensor imaging (DTI) is based on water diffusion within the brain that can detect early white matter microstructure changes. After software post-processing, DTI can visualize the visual pathways. The diffusion metrics of DTI include fractional anisotropy (FA), mean diffusivity (MD), radial Diffusivity (RD), and axial diffusivity (DA) (Bosch et al., 2012; Zhang et al., 2014). The loss of nerve fibers and neurotrophic tissue atrophy lead to the decrease of FA and the increase of MD, which are generally considered as indicators of axonal damage (Altıntaş et al., 2017). A study on the relationship between the integrity of whole brain white matter and the thickness of retinal layers in early AD patients found that the FA value of whole brain white matter fiber tracts was positively correlated with the thickness of inner nuclear layer (INL) (Alves et al., 2019). Nevertheless, the study did not separate the FA values of the visual pathways independently, and no association between FA values and thickness of GCL or pRNFL was observed.

Despite functional imaging has not yet been established for routine clinical use, studies confirm that most AD patients have irreversible pathological changes in the brain prior to the appearance of structural abnormalities, and functional changes may precede structural abnormalities (Wang et al., 2013). In recent years, blood oxygen level-dependent (BOLD) functional MRI (fMRI) has been introduced into the field of early AD research (Wierenga and Bondi, 2007). Resting-state fMRI (rs-fMRI) is a new functional imaging technique that indirectly reflects neuronal activity by measuring BOLD signals. In which, fractional amplitude of low frequency fluctuations (fALFF) can reflect spontaneous neuronal activity in brain regions and physiological state of the brain (Xi et al., 2012). Weiler et al. (2014) found that ALFF was

reduced in the temporal region of MCI patients and in the posterior cingulate gyrus of mild AD patients. These data manifest functional deficits of certain brain regions in early AD patients. At present, there is still a lack of research on the correlation between retinal structure and brain activity changes in AD patients.

Previous studies have attributed visual deficits in AD patients to degenerative damage in the primary visual cortex (V1) (Mendez et al., 1990; Leuba and Kraftsik, 1994; Armstrong, 1996; Jorge et al., 2020), but several recent studies have shown that visual cortex is relatively unaffected by Aβ and Tau protein pathology (Frisoni et al., 2010; Coppola et al., 2015). This indicates that visual deficits cannot simply be explained by visual cortex dysfunction, implying that other mechanisms may exist that contribute to visual problems in AD patients.

Although retinal structural changes and brain MRI have been explored as possible biomarkers for the early diagnosis of AD, their correlation and the internal mechanism of retinal structural changes remain elusive. Besides, the retinal structural changes are not specific to AD. To fill these gaps in knowledge, we combined OCT and multimodal MRI techniques to explore the possible correlation between retinal structure and visual pathway, brain structure, intrinsic activity changes in AD patients, as well as to evaluate their ability to auxiliary diagnose AD.

Materials and methods

Participants

The study included 49 AD patients and 48 healthy controls (HCs) matched by age, gender from the Department of Neurology at Xiangya Hospital of Central South University, between March 2020 and May 2022. The subjects were between 50 and 80 years of age, and the AD patients met the diagnostic criteria of "probable AD" in the 2011 edition of the National Institute on Aging and Alzheimer's Association (NIA-AA) guidelines (McKhann et al., 2011). The exclusion criteria of the study were as follows: (1) Best-corrected visual acuity (BCVA) >6.00 D or with astigmatism >3.00 D, and (3) intraocular pressure (IOP) >21 mmHg. All participants were free of other neurologic, psychiatric disorders, and systemic diseases that may affect retina (such as diabetes mellitus and uncontrolled hypertension), as well as ocular diseases (including cataract, glaucoma, uveitis, epiretinal membrane, age-related macular degeneration, macular hole, eye trauma, and any eye surgery). The Ethics Committee of Xiangya Hospital of Central South University approved this study, and all subjects signed written informed consent.

General data collection

General information was collected on all subjects, including name, age, gender, years of education, the history of ocular disease and underlying medical conditions. All subjects were required to undergo cognitive assessments, including the mini-mental state examination (MMSE), Montreal cognitive assessment scale (MOCA), and clinical dementia rating scale (CDR). Besides, intraocular pressure (IOP) and best-corrected visual acuity (BCVA) examinations were necessary.

Optical coherence tomography scanning

We performed two operations on both eyes of each subject using the Heidelberg Spectralis-OCT instrument (Heidelberg Engineering, Germany).

(1) Intensive horizontal scanning of the central macular area of the retina: 31 B-scans (each B-scan consists of 768 A-scans) were performed within the 6-mm diameter grid for the Early Treatment of Diabetic Retinopathy Study (ETDRS), and the macula thickness was measured in the ETDRS map [average of four quadrants of fovea (Ø 1 mm), inner ring (Ø 3 mm), and outer ring (Ø 6 mm)]. In the macular region, the inner and outer ring layers were segmented and analyzed with Heidelberg segmentation software, and the average macular thickness and the thickness of the following retinal layers were calculated: Macular RNFL (mRNFL), GCL, inner plexiform layer (IPL), INL, outer plexiform layer (OPL), outer nuclear layer (ONL), and retinal pigment epithelium (RPE).
(2) Circumferential scanning of the pRNFL: The pRNFL thickness was measured by the scanning technician in a circular scan over a 3.4 mm diameter area centered on the optic disc. For each pRNFL, 768 A-scans were performed with an ART value (average number of scans) of 100. pRNFL thickness was measured in each sector provided by Heidelberg software, namely global (G), superior quadrant (S), temporal quadrant (T), inferior quadrant (I), and nasal quadrant (N). All scans were performed according to OSCAR-IB consensus criteria (Tewarie et al., 2012) and were manually corrected by the scanning technician (ZXY) in case of unknown diagnosis to find obvious segmentation errors.

MR imaging acquisition

All MRI experiments were carried out on a 3T Siemens Prisma MRI scanner (Prisma, Siemens, Germany) with a 64-channel head/neck coil. Prior to imaging acquisition, participants were instructed to lie still, to let their mind wander, and to keep eyes closed once the scanning started. MRI-safe soft ear plugs were put into their ears to provide hearing protection. And the gap between their head and the coil was filled with foam paddings to minimize head movements.

The three-dimensional T1-weighted images (3D-T1WI) were acquired using a magnetization prepared rapid acquisition gradient echo (MPRAGE) sequence with the following parameters: Sagittal, 176 slices, slice thickness (ST) = 1 mm, repetition time (TR) = 2,300 ms, echo time (TE) = 2.98 ms, inversion time (TI) = 900 ms, data matrix = 248 × 256, field of view (FOV) = 248 × 256 mm^2, and flip angle (FA) = 9°.

DTI images were obtained using a single-shot echo-planar imaging (EPI) sequence, whose parameters were configured as 70 continuous axial-oblique (parallel to the anterior-posterior

commissural line) slices, 64 acquisitions with diffusion weighting (b = 1,000 s/mm2, 1 acquisition for each of 64 non-collinear diffusion sensitization gradients) together with three acquisitions without diffusion weighting (b = 0 s/mm2), ST = 2 mm, TR = 4,200 ms, TE = 68 ms, data matrix = 132 × 132, and FOV = 264 mm × 264 mm.

Resting-state fMRI data were collected using a gradient echo EPI sequence under an eye-closed condition. The online configuration of scanning parameters was specified as 75 continuous axial-oblique (parallel to the anterior-posterior commissural line) slices, ST = 2 mm, TR = 2,000 ms, TE = 30 ms, data matrix = 94 × 94, FOV = 220 mm × 220 mm, FA = 60°, and 240 volumes in total.

Region of interest segmentation

The segmentations of our regions of interest (ROIs) were carried out on 3D T1 images using automated programs in FreeSurfer (v7.0).[1] First, recon-all, the main FreeSurfer stream, was executed. It completed mainly the following processing stages: (1) Motion correction, (2) intensity normalization, (3) Talairach transformation, (4) non-brain tissue removal, (5) volumetric registration and labeling, (6) white matter segmentation, (7) spherical mapping and registration, and (8) cortical parcellation. Next, ROIs of hippocampus, LGN, and V1 were reconstructed by running the bash scripts of segmentHA_T1.sh (Iglesias et al., 2015), segmentThalamicNuclei.sh (Iglesias et al., 2018), and the recon-all -label-v1 (Hinds et al., 2008), respectively.

Probabilistic tractography

As suggested by Puzniak et al. (2021), to perform tractography of the visual system, the individual structures of optic chiasm, LGN, and V1 need to be provided at least. In our case, the locations of these structures were estimated automatedly as outlined above. To be specific, optic chiasm, LGN, and V1 were defined as the region with a label identifier of 85 from the aseg file, regions with label identifiers of 8,109 (L) and 8,209 (R) from the segmentation file of the thalamic nuclei, and the region with a label identifier of one from the threshold label file of V1, respectively. All these regions of interest were then transformed from fsaverage to native diffusion space through a two-step registration procedure. First, the segmentation files were registered to individual T1-weighted images through tkregister2. Next, the T1-weighted images were registered to individual FA images using a linear warping algorithm (**Supplementary Figure 1**).

All diffusion image preprocessing and fiber tracking were conducted using FMRIB Software Library (FSL v6.0).[2] The preprocessing steps were consisted of correction of motion and eddy current distortion, brain extraction, and local fitting of diffusion tensors. Probabilistic tractography was performed by employing the FDT toolbox. To calculate the probability of fiber connections from optic chiasm to LGN (the optic tract) and from LGN to V1 (the optic radiations), the algorithm was run using default parameters: curvature threshold = 0.2 mm, maximum number of steps per sample = 2,000, length of each step = 0.5 mm, and number of sample tracts = 5,000. To limit cross-hemispheric fiber bundles, tractography was performed separately for the left and right hemisphere by applying the contralateral target as an exclusion mask. The mean diffusion values (FA, MD, DA, and RD) of the optic tract and optic radiation fiber tracts were then extracted.

Fractional amplitude of low frequency fluctuations analysis

Fractional amplitude of low frequency fluctuations was calculated using the Data Processing and Analysis for Brain Imaging (DPABI V6.0) (Yan et al., 2016), a MATLAB toolbox developed based on Statistical Parametric Mapping (SPM12).[3] The resting-state fMRI images were first preprocessed through the following steps: (1) Format conversion from DICOM to NIFTI, (2) removal of the first 10 time points, (3) slice timing, (4) realignment, (5) co-registration to the skull stripped T1-weighted image, (6) nuisance covariates (Friston 24 head motion regressors, as well as white matter, ventricular CSF and global signals) regression, and (6) spatial normalization to the MNI 152 template. The preprocessed voxel-wise time series were then transformed to frequency domain *via* fast Fourier transform (FFT). fALFF was then calculated as the ratio of power spectrum of a specified frequency band (0.01–0.08 Hz) to that of the entire detectable frequency range (Zou et al., 2008). For standardization purposes, Fisher's r-to-z transformation was then performed to individual fALFF maps.

The mask file of V1 in individual T1 space was transformed to the MNI space by applying the same transform parameters generated by the aforementioned preprocessing step of spatial normalization. The regional mean of z-score fALFF maps for V1 was then extracted.

Statistical analysis

The average values of bilateral hemispheric data were calculated, and the Shapiro–Wilk test was used to test the distribution of normality of the data. Group comparisons were performed using the independent sample t-test or the Mann–Whitney U-test as appropriate. Categorical data were analyzed using the χ 2 test.

Spearman correlation analysis was used to assess the correlation between retinal structure and multimodal MRI findings in AD and HC groups, respectively.

Multiple linear regression model was developed based on the results of correlation analysis to explore the effects of multimodal MRI findings on retinal thickness in AD patients, and the results were expressed as standardized coefficients β and their corresponding 95% confidence intervals (CI), adjusting for covariates such as gender, age, years of education and dementia degree.

1 http://surfer.nmr.mgh.harvard.edu

2 https://www.fmrib.ox.ac.uk/fsl

3 http://www.fil.ion.ucl.ac.uk/spm

Diagnostic accuracy was performed using receiver operating characteristic (ROC) curve analysis. The area under the curve (AUC) and representative optimal sensitivity and specificity were used to evaluate the performance of the models. The Delong's test was conducted to compare the difference of two different diagnostic models.

All statistical tests were performed using the standard statistical software SPSS (version 26.0) and MedCalc (version 20.115), using a two-tailed test, and p-values < 0.05 were considered statistically significant. GraphPad Prism (version 9.0) and Origin (version 2022) was used to plot the graphs.

Results

A total of 97 subjects were included, including 49 AD patients and 48 HCs. Age and gender were matched between AD patients and HCs. No significant differences were observed in IOP and BCVA between two groups. About 33% of AD patients (16 patients) complained with visual deficits, including impaired visual acuity, color perception and visual field, compared with 6% of HCs (3 controls). The AD group had a shorter mean duration of education. There were significant differences in cognitive scores, as expected (Table 1).

Group difference in retinal structure and multimodal MRI

Compared to HCs, AD patients presented significantly thinner mean retinal thickness, macular volume, GCL thickness, IPL thickness, and ONL thickness, reduced by 2.70%, 2.67%, 5.82%, 4.06%, and 5.61%, respectively (Figure 1 and Supplementary Table 1). Additionally, comparison of pRNFL thickness revealed 9.66% reduction of temporal quadrant pRNFL thickness in AD group ($p < 0.001$), indicating that pRNFL thickness was preferentially reduced in the temporal quadrant (Figure 1).

Compared to HCs, there was a significant reduction of the relative volume of hippocampus (16.88%, $p < 0.001$) and LGN (29.27%, $p < 0.001$) in AD patients. No statistical change was found in the volume of V1 between the two group. In terms of the diffusion metrics of the visual pathway, we found significant decreases in the FA value of optic tract (3.75%, $p = 0.011$) and optic radiation (4.06%, $p = 0.006$) in AD patients. Measures of MD, DA and RD values increased among optic tract and optic radiation, but only met statistical significance in the optic radiation (Figure 2 and Supplementary Table 2). Besides, there were no significant differences in the fALFF value of V1 between AD patients and HCs (Figure 2).

TABLE 1 The demographic and clinical characteristics of the subjects.

Variables	AD	HCs	*P*-value
Number	49	48	NA
Age, year	64.88 ± 7.24	63.42 ± 5.31	0.261
Sex, m/f	19/30	17/31	0.732
Years of education	9.00 ± 4.22	10.85 ± 3.38	0.018*
MMSE	16.92 ± 7.56	28.00 ± 1.49	< 0.001***
MOCA	10.88 ± 6.34	22.04 ± 3.23	< 0.001***
CDR	1.15 ± 0.55	0	< 0.001***
IOP (mmHg)	15.14 ± 1.77	15.29 ± 1.70	0.674
BCVA	1.19 ± 0.25	1.14 ± 0.26	0.391
Visual deficits (%)	33%	6%	NA

AD, Alzheimer's disease; HCs, health controls; MMSE, mini-mental state examination; MoCA, montreal cognitive assessment; CDR, clinical dementia rating; IOP, intraocular pressure; BCVA, best-corrected visual acuity. *$p < 0.05$ and ***$p < 0.001$.

Correlation between retinal structure and multimodal MRI

Results of Spearman's correlation test revealed that the FA value of optic tract was highly correlated with mean retinal thickness, macular volume, GCL thickness, IPL thickness, ONL thickness, but not temporal quadrant pRNFL thickness (Figures 3,4 and Supplementary Table 3). There was no significant correlation between the FA value of optic tract and the thickness of any retinal layers in HCs (Supplementary Table 4).

In AD group, the relative volume of LGN was correlated with GCL thickness and IPL thickness in AD patients (Figures 4, 5 and Supplementary Table 3). No significant correlation was observed between the retinal thickness of any layer and the volume of hippocampus or V1 in the two group (Supplementary Table 4).

Furthermore, we found a significant positive correlation between the fALFF value of V1 and mean retinal thickness, macular volume, temporal quadrant pRNFL thickness in AD group (Figures 4, 5 and Supplementary Table 3). In HCs, no correlation was found between the fALFF value of V1 and the retinal thickness of any layer (Supplementary Table 4).

Based on the correlation results, we carried out multiple linear regression model to explore the effects of multimodal MRI findings on retinal structure in AD patients. After adjusted for gender, age, years of education and dementia degree, the FA value of optic tract demonstrated significant correlation with mean retinal thickness, macular volume, GCL thickness, IPL thickness, ONL thickness in AD patients (Table 2). In addition, the fALFF value of V1 were correlated with temporal quadrant pRNFL thickness ($\beta = 0.345$, $p = 0.044$) (Table 2).

Performance of combined diagnostic models

In the analysis of differences in retinal structure and multimodal MRI, we found the four parameters (thickness of GCL and temporal quadrant pRNFL, and volume of hippocampus and LGN) were significantly reduced in AD patients ($p < 0.001$). Based on the results, we carried out further analyses to evaluate the performance of the combination of these four parameters to differentiate AD patients from HCs by plotting ROC curves and calculating AUC. After adjusted by Age, the combined model showed the best performance to discriminate between AD patients and HCs (AUC = 0.936, sensitivity = 89.1%, specificity = 87.0%) (Figure 6).

10.3389/fnagi.2023.1088829

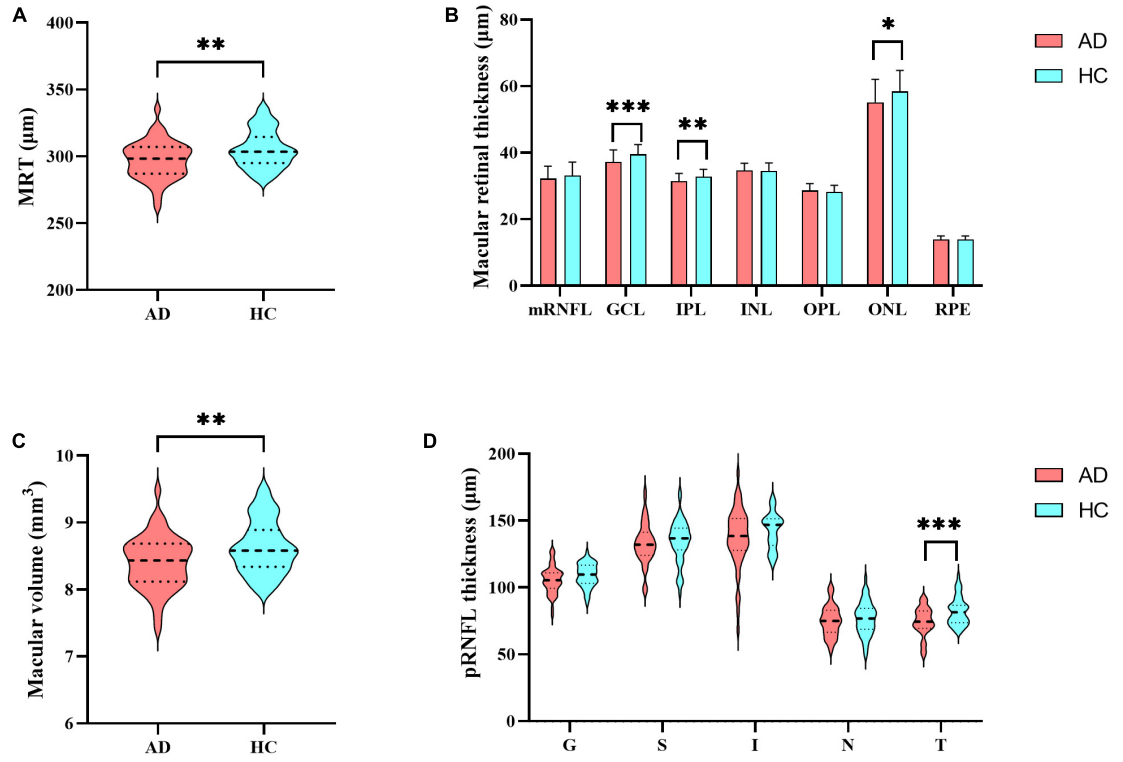

FIGURE 1
Differences in retinal thickness. **(A)** Mean retinal thickness; **(B)** the thickness of retinal layers in the macular region: mRNFL, GCL, IPL, INL, OPL, ONL and RPE; **(C)** macular volume; **(D)** peripapillary RNFL (pRNFL) thickness: global thickness (G), superior quadrant (S), inferior quadrant (I), nasal quadrant (N), temporal quadrant (T). MRT, mean retinal thickness; mRNFL, macular retinal nerve fiber layer; GCL, ganglion cell layer; IPL, inner plexiform layer; INL, inner nuclear layer; OPL, outer plexiform layer; ONL, outer nuclear layer; RPE, retinal pigment epithelium; pRNFL, peripapillary RNFL; G, global thickness; S, superior quadrant; I, inferior quadrant; N, nasal quadrant; T, temporal quadrant. Significant differences are indicated by square brackets. *Denotes $p < 0.05$, **denotes $p < 0.01$, and ***denotes $p < 0.001$.

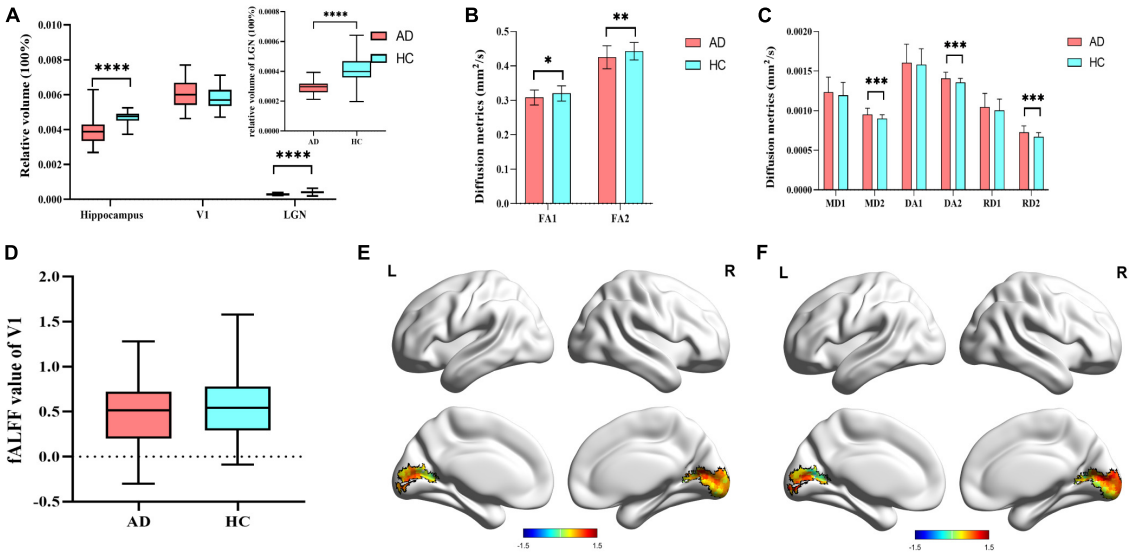

FIGURE 2
Differences in multimodal MRI. **(A)** Difference of 3D-T1WI results. **(B)** Difference of FA value in the visual pathway. FA1 represent FA value of optic tract, and FA2 represent FA value of optic radiation. **(C)** Difference of other diffusion metrics in the visual pathway. MD1, DA1, and RD1 represent MD, DA, and RD values of optic tract, respectively. MD2, DA2, and RD2 represent MD, DA, and RD values of optic radiation, respectively. **(D)** Difference of fALFF value of V1 in AD group and HCs group; **(E)** fALFF value of V1 in AD patients; **(F)** fALFF value of V1 in HCs. V1, primary visual cortex; LGN, lateral geniculate nucleus; FA, fractional anisotropy; MD, mean diffusivity; DA, axial diffusivity; RD, radial diffusivity; fALFF, fractional amplitude of low frequency fluctuations. Significant differences are indicated by square brackets. *Denotes $p < 0.05$, **denotes $p < 0.01$, ****means $p < 0.0001$.

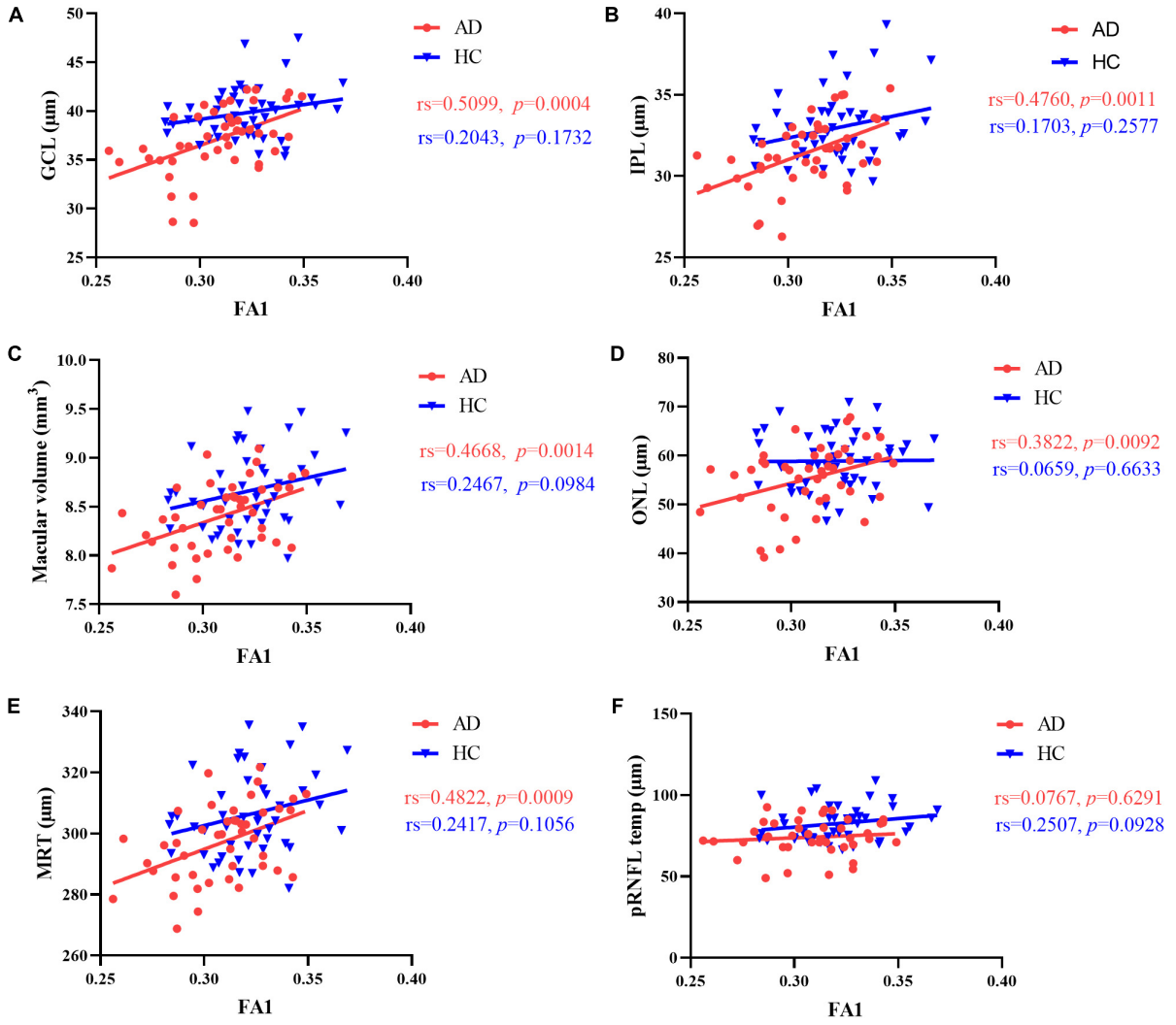

FIGURE 3
Correlation between FA value of optic tract and retinal thickness. In AD patients, there was a significant positive correlation between FA value of optic tract and **(A)** GCL thickness, **(B)** IPL thickness, **(C)** macular volume, **(D)** ONL thickness and **(E)** mean retinal thickness. **(F)** No correlation was found between FA value of optic tract and temporal quadrant pRNFL thickness. There was no correlation between FA value of optic tract and retinal thickness in HCs. MRT, mean retinal thickness; GCL, ganglion cell layer; IPL, inner plexiform layer; ONL, outer nuclear layer; pRNFL, peripapillary retinal nerve fiber layer; FA1, fractional anisotropy of the optic tract.

Discussion

Our study evaluated the changes of retinal thickness and multimodal MRI findings in AD patients. We also correlated OCT findings with multimodal MRI imaging in the study, and the results showed that retinal structure change was related to the loss of integrity of white matter fiber tracts in the visual pathway and the decreased LGN volume and functional metabolism of V1 in AD patients. In addition, a combined model with high auxiliary diagnostic efficacy of AD was generated, including thickness of GCL and temporal quadrant pRNFL, volume of hippocampus and LGN, and age, which can be applied to assist in the identification of probable AD patients. To the best of our knowledge, this is the first study on the correlation of retinal structure and brain multimodal MRI in AD patients.

Here we have shown, in agreement with previous studies, that the mean retinal thickness, macular volume, GCL, IPL, ONL, and temporal quadrant pRNFL thickness were significantly reduced in AD patients. Several previous studies have shown that pRNFL and GC-IPL layers are significantly thinner in early AD patients, and the latest studies indicated that macular GC-IPL layer may be more sensitive than pRNFL thickness (Cheung et al., 2021). Asanad et al. (2019) conducted the first fundus histology study on patients with AD using postmortem human tissues, and the results showed a gradient of retinal thickness reduction, temporal quadrant pRNFL, GCL, and IPL layers were thinned the most, followed by INL and ONL layers. In addition, AD mouse model experiment indicated that the degeneration of dendrites of retinal ganglion cells confined to the plexus layer in the retina preceded their cell loss (Williams et al., 2013). These findings, together with the findings of our study, suggest that changes in retinal structure may serve as an early diagnostic biomarker for AD.

Our results showed that the LGN volume of AD patients were significantly reduced. The changes of LGN in AD patients were

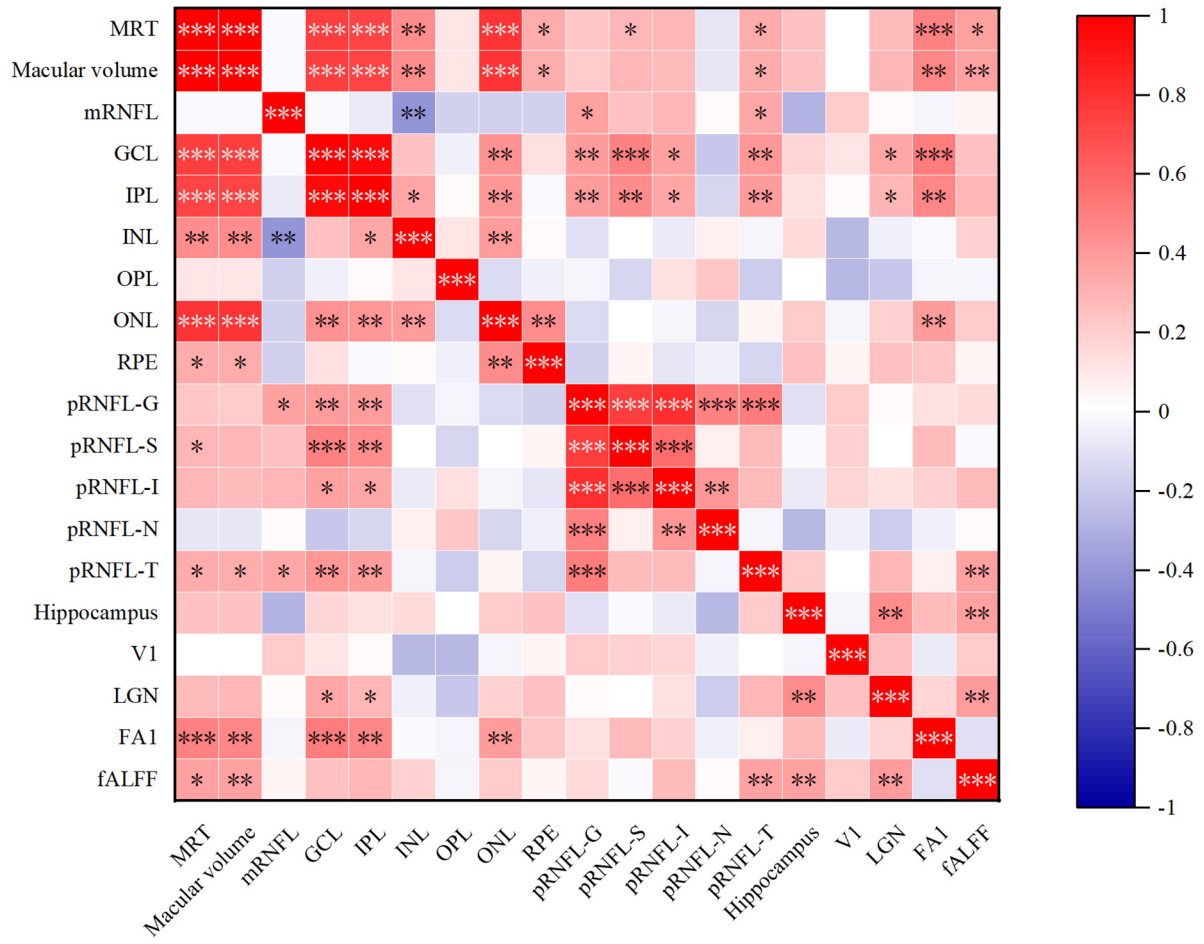

FIGURE 4
Heat map of correlation between retinal structure and multimodal MRI in AD group. MRT, mean retinal thickness; mRNFL, macular retinal nerve fiber layer; GCL, ganglion cell layer; IPL, inner plexiform layer; INL, inner nuclear layer; OPL, outer plexiform layer; ONL, outer nuclear layer; RPE, retinal pigment epithelium; pRNFL, peripapillary RNFL; G, global thickness; S, superior quadrant; I, inferior quadrant; N, nasal quadrant; T, temporal quadrant; V1, primary visual cortex; LGN, lateral geniculate nucleus; FA1, fractional anisotropy value of optic tract; fALFF, fractional amplitude of low frequency fluctuations. *$p < 0.05$, **$p < 0.01$, and ***$p < 0.001$.

rarely studied. Previous studies have found pathological changes such as significantly increased Aβ protein, decreased number of small cell neurons, and large-cell gliosis in LGN of AD patients, whereas the significance of LGN degeneration in AD patients has not been clarified (Erskine et al., 2016). Besides, we observed that volume and neuronal activity of V1 was not changed. Evidence from postmortem autopsy studies suggested that the visual cortex was not severely affected in patients with AD (Leuba and Saini, 1995). These studies confirmed that visual cortex was not affected in AD patients. Regarding to the diffusion metrics of the visual pathway, the first study by Nishioka et al. (2015) showed the changes of white matter fiber tracts in the visual pathway of AD patients. Reduction in FA and increases in MD DA and RD were observed in the optic nerve, less extensive similar changes were also found in the optic tract of AD patients. Likewise, our study showed the same changes in the optic tract. Besides, since the optic radiation is the axon of the geniculate striatum (Ogawa et al., 2014), and LGN volume of AD patients were significantly reduced. More significantly increases in MD, AD and RD and reduction in FA were found within optic radiation. These diffusional differences mirror white matter damage of visual pathway. The above results indicate that white matter damage extends to the visual system, which may contribute to the visual deficits in AD patients.

Studies have shown that thinning of GC-IPL in AD patients is associated with volume reduction of occipital and temporal lobes (Ong et al., 2015; Carazo-Barrios et al., 2021). In contrast with previous work, no correlation was observed between retinal structure and the volume of hippocampus or V1 in AD patients in our study, probably because most of the patients included in this study were mild-to-moderate AD patients, and the sample size was relatively small. Interestingly, significant correlation was presented between GC-IPL and the LGN volume, implying the important role of LGN in the retinal structural changes of AD patients. We found that fALFF value of V1 were positively correlated with temporal quadrant pRNFL thickness, indicating that temporal quadrant pRNFL thickness could reflect neuronal activity in V1. Since the foveal fibers occupy most of the temporal quadrant part of the optic nerve papilla (Jansonius et al., 2009), temporal quadrant pRNFL thickness is more

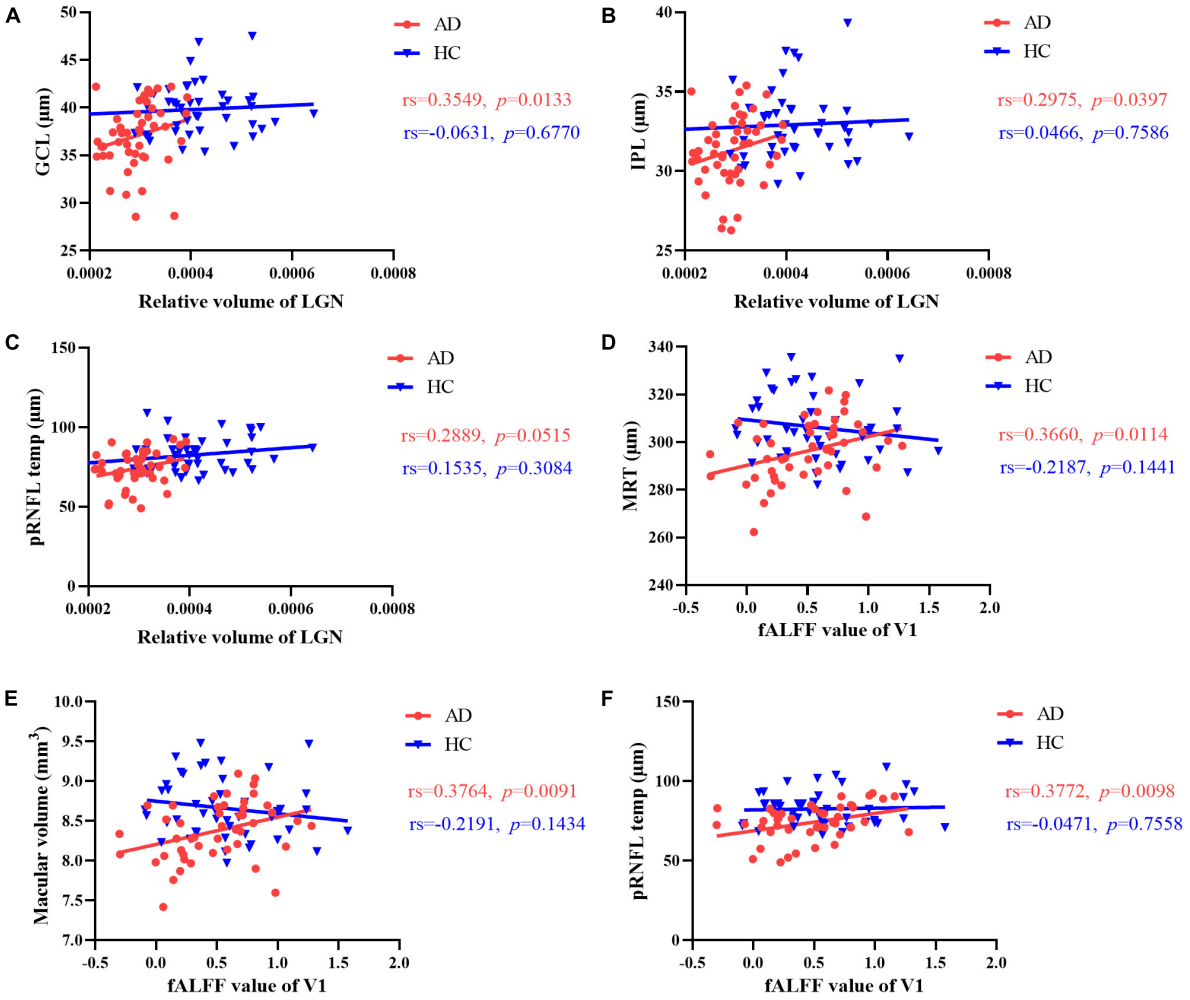

FIGURE 5
Correlation between brain structure, intrinsic activity changes and retinal thickness. The relative volume of LGN was correlated with **(A)** GCL thickness and **(B)** IPL thickness in AD patients. **(C)** No significant correlation was observed between temporal quadrant pRNFL thickness and the volume of LGN in the two group. In AD patients, there was a significant positive correlation between the fALFF value of V1 and **(D)** mean retinal thickness, **(E)** macular volume, **(F)** temporal quadrant pRNFL thickness. No correlation was found between fALFF value of V1 and the retinal thickness of any layer in HCs. GCL, ganglion cell layer; IPL, inner plexiform layer; MRT, mean retinal thickness; pRNFL, peripapillary retinal nerve fiber layer; LGN, lateral geniculate nucleus; fALFF, fractional amplitude of low frequency fluctuations; V1, primary visual cortex.

sensitive to reflect brain metabolism than other quadrant pRNFL thickness. These findings provide new functional features for the involvement of visual cortex in the development of retinal structural changes.

Remarkably, significant correlations were presented between the FA value of optic tract and mean retinal thickness, macular volume, GCL thickness and IPL thickness in AD patients. As the optic tract is a part of the RGC axon, the change of optic tract may be most related to the loss of RGC, and the RGC cell bodies are mainly in the macular GC-IPL layer (Song et al., 2018), thus explaining the correlation between the FA value of optic tract and the thickness of GC-IPL. However, no correlation was observed between the FA values of visual pathway and the thickness of pRNFL. The cell bodies and dendrites of RGCs are mainly located in the GC- IPL layer of the macula, while axons are clustered in the pRNFL layer. Since the macula contains more than 50% of the total RGCs and the cell bodies of RGCs are 10–20 times larger than the axon diameter, the macular GC-IPL is more sensitive to AD pathology than the pRNFL (Chan et al., 2019). In short, our study demonstrated that structural changes in the retina of AD patients was associated with damage to the white matter fiber tracts of the visual pathway.

In the present study, we found that FA value of optic tract correlated highly with macular volume, GCL and IPL thickness, besides LGN volume was correlated with GCL and IPL thickness in AD patients. Previous studies have confirmed that pathological features of AD can be found in the LGN and superior colliculus (Leuba and Saini, 1995). Thus, we speculated that there might be a trans-synaptic axonal retrograde lesions process in the visual pathway in AD patients. This hypothesis has been confirmed by several previous studies in which Van Buren et al. noted trans-synaptic retrograde lesions in the macaque visual system, and severe loss of ganglion cells in the retina corresponding to the lesion was observed after either surgical injury to the optic chiasma or ablation of the occipital lobe (Vanburen, 1963). Jindahra et al. (2009) demonstrated that both congenital and acquired visual

10.3389/fnagi.2023.1088829

TABLE 2 Multiple linear regression model of the effect of multimodal imaging on retinal structure in AD patients.

Variable	β	B	95% CI	*P*-value
GCL thickness (μm)				
FA1	0.474	71.708	(30.525, 112.890)	0.001**
Gender	−0.115	−0.771	(−2.785, 1.243)	0.443
Age	−0.117	−0.052	(−0.173, 0.068)	0.385
Years of education	−0.302	−0.250	(−0.496, -0.004)	0.047*
Dementia degree	−0.082	−0.473	(−2.034, 1.088)	0.543
Adjusted. R^2 = 0.255				
IPL thickness (μm)				
FA1	0.489	46.578	(20.875, 72.280)	0.001**
Gender	−0.232	−0.980	(−2.237, 0.277)	0.123
Age	−0.164	−0.046	(−0.121, 0.029)	0.225
Years of education	−0.299	−0.155	(−0.309, -0.002)	0.047*
Dementia degree	0.004	0.016	(−0.958, 0.991)	0.973
Adjusted. R^2 = 0.266				
Macular volume (mm^3)				
FA1	0.471	7.466	(3.266, 11.665)	0.001**
Gender	−0.278	−0.197	(−0.399, 0.004)	0.055
Age	−0.074	−0.003	(−0.017, 0.010)	0.604
Years of education	−0.254	−0.022	(−0.048, 0.003)	0.085
Dementia degree	−0.210	−0.130	(−0.291, 0.031)	0.110
fALFF	0.263	0.252	(−0.028, 0.533)	0.076
Adjusted. R^2 = 0.344				
pRNFL temp (μm)				
fALFF	0.345	10.197	(0.266, 20.128)	0.044*
Gender	0.159	3.510	(−3.485, 10.504)	0.317
Age	−0.028	−0.041	(−0.529, 0.447)	0.867
Years of education	−‘0.031	−0.082	(−0.959, 0.794)	0.850
Dementia degree	0.010	0.187	(−5.593, 5.966)	0.948
Adjusted. R^2 = 0.063				
ONL thickness (μm)				
FA1	0.317	98.613	(14.514, 182.712)	0.023*
Gender	−0.296	−4.088	(−8.200, 0.024)	0.051
Age	−0.230	−0.211	(−0.458, 0.035)	0.091
Years of education	−0.260	−0.441	(−0.944, 0.061)	0.083
Dementia degree	−0.337	−3.993	(−7.181, -0.805)	0.015*
Adjusted. R^2 = 0.265				
MRT (μm)				
FA1	0.471	264.966	(116.171, 413.761)	0.001**
Gender	−0.281	−7.073	(−14.213, 0.068)	0.052
Age	−0.070	−0.117	(−0.591, 0.357)	0.620
Years of education	−0.255	−0.792	(−1.697, 0.113)	0.084
Dementia degree	−0.209	−4.593	(−10.291, 1.105)	0.111
fALFF	0.262	8.929	(−1.010, 18.867)	0.077
Adjusted. R^2 = 0.344				

GCL, ganglion cell layer; IPL, inner plexiform layer; pRNFL, peripapillary retinal nerve fiber layer; ONL, outer nuclear layer; MRT, mean retinal thickness; FA1, fractional anisotropy (FA) value of the optic tract; fALFF, fractional amplitude of low frequency fluctuations. *$p < 0.05$ and **$p < 0.01$.

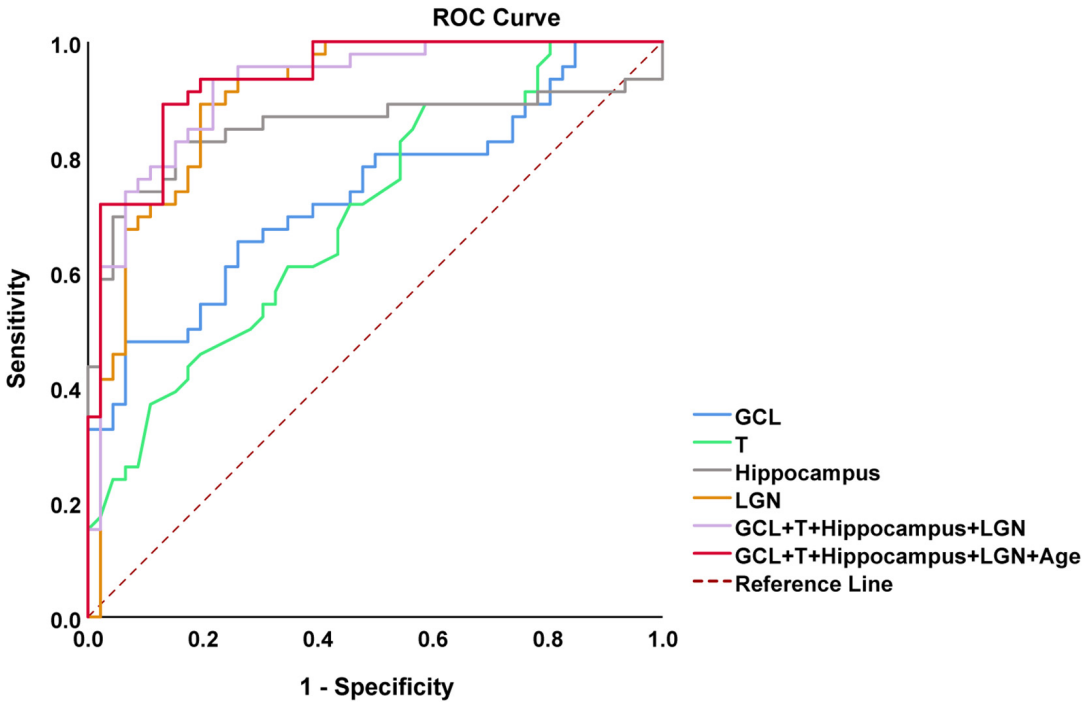

FIGURE 6
Receiving operating characteristic (ROC) curves analysis of combined OCT and multimodal MRI for diagnosis of AD. The model combining thickness of GCL and temporal quadrant pRNFL (T), volume of hippocampus and lateral geniculate nucleus (LGN), and age showed the best performance to identify AD patients [area under the curve (AUC) = 0.936, sensitivity = 89.1%, specificity = 87.0%]. AUC, area under the curve; ROC, receiver operating characteristic curve; OCT, optical coherence tomography; GCL, ganglion cell layer; pRNFL, peripapillary retinal nerve fiber layer.

pathway injuries in humans could cause thinning of the retinal nerve fiber layer through the study of patients with posterior knee lesions, which is likely due to the trans-synaptic axonal retrograde degenerative lesions following damage to the visual pathway. Furthermore, den Haan et al. (2018) found a correlation between RNFL thickness and posterior cortical atrophy in AD patients, which covered the cortex involved in visual processing. Consequently, the above studies provide evidence for trans-synaptic axonal retrograde lesions of the visual pathway in AD patients.

Some histopathological studies have identified Aβ protein deposition in the retina in AD animal models as well as in patients with early AD (Gupta et al., 2021). Although the mechanism of Aβ propagation pathology in AD remains unclear, a growing number of findings confirm that Aβ and Tau can be transmitted from one neuron to another along anatomically connected synapses (Lv et al., 2017). Several zoological studies have proved this theory. Nishioka et al. (2019) used transgenic tau mice to observe the diffusion change pattern caused by Aβ injection into LGN, and the change first appeared in the LGN and optic tract, and then in the optic nerve, implying that there is a process of trans-synaptic axonal retrograde lesions in the visual pathway of AD mice. Similarly, Sun et al. (2014) injected Aβ1-42 into the left ventricle of the mouse model, and DTI showed reduced FA and significantly increased RD in the optic nerve and optic tract 2 months later. These studies imply that there may be a process of trans-synaptic axonal retrograde lesions of Aβ pathologic protein in AD patients.

Although numerous studies have explored the possibility of retinal structure as an early diagnostic marker for AD, the diagnostic accuracy of retinal structure alone may not be sufficient due to the low specificity of retinal structural changes (Lemmens et al., 2020). In the current study, an AUC of 0.936 (CI 0.889–0.983) was achieved using a combination of OCT and multimodal MRI data, which improved the ability to assist detecting AD patients. Thus, OCT combined with multimodal MRI maybe serve as a potential auxiliary diagnostic tool for AD. Currently, most studies on the combination of OCT and MRI focus on the correlation between them. Some studies have found that retinal thickness is significantly related to brain volume (López-Cuenca et al., 2022; Mathew et al., 2023), but there is no study on the diagnosis of AD by combination of OCT and MRI yet.

The study also has certain limitations. Firstly, the case group was mostly mild-to-moderate AD patients due to the strong cooperation required for each examination, and the sample size was relatively small, so we failed to stratify AD patients according to the severity. Secondly, this study was a cross-sectional study, which is unable to observe the dynamic changes of each index longitudinally and to elucidate the causal relationship between retinal structure and multimodal MRI. Longitudinal study on retina and relevant brain MRI changes of early stages (such as subjective cognitive impairment, preclinical and prodromal AD and MCI) should be further explored. Thirdly, only a small part of patients involved in this study had undergone lumbar puncture or PET examination, that didn't reach the minimum sample size. We will explore comparing this combined model with CSF biomarkers and PET scans in future research. Last but not least, only AD patients and controls were included in our study, which indeed lacks diagnostic specificity. In the follow-up research, we will evaluate the retinal

structural characteristics of different types of dementia and explore disease-specific diagnostic indicators.

Conclusion

In summary, our study confirmed that the retinal structure and multimodal MRI findings of AD patients were significantly altered. The retinal structure change was related to the loss of integrity of white matter fiber tracts in the visual pathway and the decreased LGN volume and functional metabolism of V1 in AD patients. We speculate that the damage of white matter fiber tracts in the visual pathway may lead to the loss of retinal ganglion cells through trans-synaptic axonal retrograde lesions, which may be the cause of retinal structural changes in AD patients. Furthermore, our study supported that retinal imaging combined with multimodal MRI can contribute to a classification model for the identification of AD patients.

Data availability statement

The raw data supporting the conclusions of this article will be made available by the authors, without undue reservation.

Ethics statement

The studies involving human participants were reviewed and approved by the Ethics Committee of Xiangya Hospital of Central South University. The patients/participants provided their written informed consent to participate in this study.

Author contributions

XH, WZ, DW, and LS performed the study design, acquisition of data, analysis and interpretation of data, and drafting/revising the manuscript. BJ, QY, RC, YZ, XW, XX, and WL analyzed the data and revised the manuscript for intellectual content. XZ performed the OCT images scan. All authors contributed to the article and approved the submitted version.

Funding

This study was supported by the National Key R&D Program of China (no. 2020YFC2008500), the National Major Projects in Brain Science and Brain-like Research (no. 2021ZD0201803), the National Natural Science Foundation of China (nos. 81971029, 82071216, and 81901171), Hunan Innovative Province Construction Project (no. 2019SK2335), and Hu-Xiang Youth Project (no. 2021RC3028).

Acknowledgments

We thank all the patients and their families and all healthy volunteers for their involvement in this study. We are grateful to all our colleagues in the Department of Neurology, Xiangya Hospital, Central South University, China.

Conflict of interest

The authors declare that the research was conducted in the absence of any commercial or financial relationships that could be construed as a potential conflict of interest.

Publisher's note

All claims expressed in this article are solely those of the authors and do not necessarily represent those of their affiliated organizations, or those of the publisher, the editors and the reviewers. Any product that may be evaluated in this article, or claim that may be made by its manufacturer, is not guaranteed or endorsed by the publisher.

Supplementary material

The Supplementary Material for this article can be found online at: https://www.frontiersin.org/articles/10.3389/fnagi.2023.1088829/full#supplementary-material

References

Altıntaş, Ö, Gümüştaş, S., Cinik, R., Anık, Y., Özkan, B., and Karabaş, L. (2017). Correlation of the measurements of optical coherence tomography and diffuse tension imaging of optic pathways in amblyopia. *Int. Ophthalmol.* 37, 85–93. doi: 10.1007/s10792-016-0229-0

Alves, C., Jorge, L., Canário, N., Santiago, B., Santana, I., Castelhano, J., et al. (2019). Interplay between macular retinal changes and white matter integrity in early Alzheimer's disease. *J. Alzheimers Dis.* 70, 723–732. doi: 10.3233/jad-190152

Armstrong, R. A. (1996). Visual field defects in Alzheimer's disease patients may reflect differential pathology in the primary visual cortex. *Optom. Vis. Sci.* 73, 677–682. doi: 10.1097/00006324-199611000-00001

Arvanitakis, Z., Shah, R. C., and Bennett, D. A. (2019). Diagnosis and management of dementia: Review. *JAMA* 322, 1589–1599. doi: 10.1001/jama.2019.4782

Asanad, S., Ross-Cisneros, F. N., Nassisi, M., Barron, E., Karanjia, R., and Sadun, A. A. (2019). The retina in Alzheimer's disease: Histomorphometric analysis of an ophthalmologic biomarker. *Invest. Ophthalmol. Vis. Sci.* 60, 1491–1500. doi: 10.1167/iovs.18-25966

Bosch, B., Arenaza-Urquijo, E. M., Rami, L., Sala-Llonch, R., Junqué, C., Solé-Padullés, C., et al. (2012). Multiple DTI index analysis in normal aging, amnestic MCI and AD. Relationship with neuropsychological performance. *Neurobiol. Aging* 33, 61–74. doi: 10.1016/j.neurobiolaging.2010.02.004

Carazo-Barrios, L., Archidona-Arranz, A., Claros-Ruiz, A., García-Basterra, I., Garzón-Maldonado, F. J., Serrano-Castro, V., et al. (2021). Correlation between retinal nerve fibre layer thickness and white matter lesions in Alzheimer's disease. *Int. J. Geriatr. Psychiatry* 36, 935–942. doi: 10.1002/gps.5496

Chan, V. T. T., Sun, Z., Tang, S., Chen, L. J., Wong, A., Tham, C. C., et al. (2019). Spectral-domain OCT measurements in Alzheimer's disease: A systematic review and meta-analysis. *Ophthalmology* 126, 497–510. doi: 10.1016/j.ophtha.2018.08.009

Cheung, C. Y., Mok, V., Foster, P. J., Trucco, E., Chen, C., and Wong, T. Y. (2021). Retinal imaging in Alzheimer's disease. *J. Neurol. Neurosurg. Psychiatry* 92, 983–994. doi: 10.1136/jnnp-2020-325347

Chiasseu, M., Alarcon-Martinez, L., Belforte, N., Quintero, H., Dotigny, F., Destroismaisons, L., et al. (2017). Tau accumulation in the retina promotes early neuronal dysfunction and precedes brain pathology in a mouse model of Alzheimer's disease. *Mol. Neurodegener.* 12:58. doi: 10.1186/s13024-017-0199-3

Chiquita, S., Rodrigues-Neves, A. C., Baptista, F. I., Carecho, R., Moreira, P. I., Castelo-Branco, M., et al. (2019). The retina as a window or mirror of the brain changes detected in Alzheimer's disease: Critical aspects to unravel. *Mol. Neurobiol.* 56, 5416–5435. doi: 10.1007/s12035-018-1461-6

Coppola, G., Di Renzo, A., Ziccardi, L., Martelli, F., Fadda, A., Manni, G., et al. (2015). Optical coherence tomography in Alzheimer's disease: A meta-analysis. *PLoS One* 10:e0134750. doi: 10.1371/journal.pone.0134750

Criscuolo, C., Cerri, E., Fabiani, C., Capsoni, S., Cattaneo, A., and Domenici, L. (2018). The retina as a window to early dysfunctions of Alzheimer's disease following studies with a 5xFAD mouse model. *Neurobiol. Aging* 67, 181–188. doi: 10.1016/j.neurobiolaging.2018.03.017

den Haan, J., Janssen, S. F., van de Kreeke, J. A., Scheltens, P., Verbraak, F. D., and Bouwman, F. H. (2018). Retinal thickness correlates with parietal cortical atrophy in early-onset Alzheimer's disease and controls. *Alzheimers Dement.* 10, 49–55. doi: 10.1016/j.dadm.2017.10.005

Drew, L. (2018). An age-old story of dementia. *Nature* 559, S2–S3. doi: 10.1038/d41586-018-05718-5

Erskine, D., Taylor, J. P., Firbank, M. J., Patterson, L., Onofrj, M., O'Brien, J. T., et al. (2016). Changes to the lateral geniculate nucleus in Alzheimer's disease but not dementia with Lewy bodies. *Neuropathol. Appl. Neurobiol.* 42, 366–376. doi: 10.1111/nan.12249

Frisoni, G. B., Fox, N. C., Jack, C. R. Jr., Scheltens, P., and Thompson, P. M. (2010). The clinical use of structural MRI in Alzheimer disease. *Nat. Rev. Neurol.* 6, 67–77. doi: 10.1038/nrneurol.2009.215

Ge, Y. J., Xu, W., Ou, Y. N., Qu, Y., Ma, Y. H., Huang, Y. Y., et al. (2021). Retinal biomarkers in Alzheimer's disease and mild cognitive impairment: A systematic review and meta-analysis. *Ageing Res. Rev.* 69:101361. doi: 10.1016/j.arr.2021.101361

Golzan, S. M., Goozee, K., Georgevsky, D., Avolio, A., Chatterjee, P., Shen, K., et al. (2017). Retinal vascular and structural changes are associated with amyloid burden in the elderly: Ophthalmic biomarkers of preclinical Alzheimer's disease. *Alzheimers Res. Ther.* 9:13. doi: 10.1186/s13195-017-0239-9

Gupta, V. B., Chitranshi, N., den Haan, J., Mirzaei, M., You, Y., Lim, J. K., et al. (2021). Retinal changes in Alzheimer's disease- integrated prospects of imaging, functional and molecular advances. *Prog. Retin. Eye Res.* 82:100899. doi: 10.1016/j.preteyeres.2020.100899

Hinds, O. P., Rajendran, N., Polimeni, J. R., Augustinack, J. C., Wiggins, G., Wald, L. L., et al. (2008). Accurate prediction of V1 location from cortical folds in a surface coordinate system. *Neuroimage* 39, 1585–1599. doi: 10.1016/j.neuroimage.2007.10.033

Iglesias, J. E., Augustinack, J. C., Nguyen, K., Player, C. M., Player, A., Wright, M., et al. (2015). A computational atlas of the hippocampal formation using ex vivo, ultra-high resolution MRI: Application to adaptive segmentation of in vivo MRI. *Neuroimage* 115, 117–137. doi: 10.1016/j.neuroimage.2015.04.042

Iglesias, J. E., Insausti, R., Lerma-Usabiaga, G., Bocchetta, M., Van Leemput, K., Greve, D. N., et al. (2018). A probabilistic atlas of the human thalamic nuclei combining ex vivo MRI and histology. *Neuroimage* 183, 314–326. doi: 10.1016/j.neuroimage.2018.08.012

Jansonius, N. M., Nevalainen, J., Selig, B., Zangwill, L. M., Sample, P. A., Budde, W. M., et al. (2009). A mathematical description of nerve fiber bundle trajectories and their variability in the human retina. *Vis. Res.* 49, 2157–2163. doi: 10.1016/j.visres.2009.04.029

Jiao, B., Liu, H., Guo, L., Liao, X., Zhou, Y., Weng, L., et al. (2021). Performance of plasma amyloid β, total tau, and neurofilament light chain in the identification of probable Alzheimer's disease in South China. *Front. Aging Neurosci.* 13:749649. doi: 10.3389/fnagi.2021.749649

Jindahra, P., Petrie, A., and Plant, G. T. (2009). Retrograde trans-synaptic retinal ganglion cell loss identified by optical coherence tomography. *Brain* 132(Pt 3), 628–634. doi: 10.1093/brain/awp001

Jorge, L., Canário, N., Martins, R., Santiago, B., Santana, I., Quental, H., et al. (2020). The retinal inner plexiform synaptic layer mirrors grey matter thickness of primary visual cortex with increased amyloid β load in early Alzheimer's disease. *Neural Plast.* 2020:8826087. doi: 10.1155/2020/8826087

Koronyo, Y., Biggs, D., Barron, E., Boyer, D. S., Pearlman, J. A., Au, W. J., et al. (2017). Retinal amyloid pathology and proof-of-concept imaging trial in Alzheimer's disease. *JCI Insight* 2:e93621. doi: 10.1172/jci.insight.93621

Lemmens, S., Van Craenendonck, T., Van Eijgen, J., De Groef, L., Bruffaerts, R., de Jesus, D. A., et al. (2020). Combination of snapshot hyperspectral retinal imaging and optical coherence tomography to identify Alzheimer's disease patients. *Alzheimers Res. Ther.* 12:144. doi: 10.1186/s13195-020-00715-1

Leuba, G., and Kraftsik, R. (1994). Visual cortex in Alzheimer's disease: Occurrence of neuronal death and glial proliferation, and correlation with pathological hallmarks. *Neurobiol. Aging* 15, 29–43. doi: 10.1016/0197-4580(94)90142-2

Leuba, G., and Saini, K. (1995). Pathology of subcortical visual centres in relation to cortical degeneration in Alzheimer's disease. *Neuropathol. Appl. Neurobiol.* 21, 410–422. doi: 10.1111/j.1365-2990.1995.tb01078.x

Liao, C., Xu, J., Chen, Y., and Ip, N. Y. (2021). Retinal dysfunction in Alzheimer's disease and implications for biomarkers. *Biomolecules* 11:1215. doi: 10.3390/biom11081215

López-Cuenca, I., Marcos-Dolado, A., Yus-Fuertes, M., Salobrar-García, E., Elvira-Hurtado, L., Fernández-Albarral, J. A., et al. (2022). The relationship between retinal layers and brain areas in asymptomatic first-degree relatives of sporadic forms of Alzheimer's disease: An exploratory analysis. *Alzheimers Res. Ther.* 14:79. doi: 10.1186/s13195-022-01008-5

Lv, Z. Y., Tan, C. C., Yu, J. T., and Tan, L. (2017). Spreading of pathology in Alzheimer's disease. *Neurotox. Res.* 32, 707–722. doi: 10.1007/s12640-017-9765-2

Mathew, S., WuDunn, D., Mackay, D. D., Vosmeier, A., Tallman, E. F., Deardorff, R., et al. (2023). Association of brain volume and retinal thickness in the early stages of Alzheimer's disease. *J. Alzheimers Dis.* 91, 743–752. doi: 10.3233/JAD-210533

McKhann, G. M., Knopman, D. S., Chertkow, H., Hyman, B. T., Jack, C. R. Jr., Kawas, C. H., et al. (2011). The diagnosis of dementia due to Alzheimer's disease: Recommendations from the National Institute on Aging-Alzheimer's Association workgroups on diagnostic guidelines for Alzheimer's disease. *Alzheimers Dement.* 7, 263–269. doi: 10.1016/j.jalz.2011.03.005

Mendez, M. F., Mendez, M. A., Martin, R., Smyth, K. A., and Whitehouse, P. J. (1990). Complex visual disturbances in Alzheimer's disease. *Neurology* 40(3 Pt 1), 439–443. doi: 10.1212/wnl.40.3_part_1.439

Mendola, J. D., Cronin-Golomb, A., Corkin, S., and Growdon, J. H. (1995). Prevalence of visual deficits in Alzheimer's disease. *Optom. Vis. Sci.* 72, 155–167. doi: 10.1097/00006324-199503000-00003

Mu, Y., and Gage, F. H. (2011). Adult hippocampal neurogenesis and its role in Alzheimer's disease. *Mol. Neurodegener.* 6:85. doi: 10.1186/1750-1326-6-85

Nishioka, C., Liang, H. F., Barsamian, B., and Sun, S. W. (2019). Amyloid-beta induced retrograde axonal degeneration in a mouse tauopathy model. *Neuroimage* 189, 180–191. doi: 10.1016/j.neuroimage.2019.01.007

Nishioka, C., Poh, C., and Sun, S. W. (2015). Diffusion tensor imaging reveals visual pathway damage in patients with mild cognitive impairment and Alzheimer's disease. *J. Alzheimers Dis.* 45, 97–107. doi: 10.3233/jad-141239

Ogawa, S., Takemura, H., Horiguchi, H., Terao, M., Haji, T., Pestilli, F., et al. (2014). White matter consequences of retinal receptor and ganglion cell damage. *Investig. Ophthalmol. Vis. Sci.* 55, 6976–6986. doi: 10.1167/iovs.14-14737

Ong, Y. T., Hilal, S., Cheung, C. Y., Venketasubramanian, N., Niessen, W. J., Vrooman, H., et al. (2015). Retinal neurodegeneration on optical coherence tomography and cerebral atrophy. *Neurosci. Lett.* 584, 12–16. doi: 10.1016/j.neulet.2014.10.010

Puzniak, R. J., Prabhakaran, G. T., Buentjen, L., Schmitt, F. C., and Hoffmann, M. B. (2021). Tracking the visual system—from the optic chiasm to primary visual cortex. *Zeitschrift Epileptologie* 34, 57–66. doi: 10.1007/s10309-020-00384-y

Santangelo, R., Huang, S. C., Bernasconi, M. P., Falautano, M., Comi, G., Magnani, G., et al. (2020). Neuro-retina might reflect Alzheimer's disease stage. *J. Alzheimers Dis.* 77, 1455–1468. doi: 10.3233/jad-200043

Snyder, P. J., Alber, J., Alt, C., Bain, L. J., Bouma, B. E., Bouwman, F. H., et al. (2021). Retinal imaging in Alzheimer's and neurodegenerative diseases. *Alzheimers Dement.* 17, 103–111. doi: 10.1002/alz.12179

Song, X. Y., Puyang, Z., Chen, A. H., Zhao, J., Li, X. J., Chen, Y. Y., et al. (2018). Diffusion tensor imaging detects microstructural differences of visual pathway in patients with primary open-angle glaucoma and ocular hypertension. *Front. Hum. Neurosci.* 12:426. doi: 10.3389/fnhum.2018.00426

Sun, S. W., Liang, H. F., Mei, J., Xu, D., and Shi, W. X. (2014). In vivo diffusion tensor imaging of amyloid-β-induced white matter damage in mice. *J. Alzheimers Dis.* 38, 93–101. doi: 10.3233/jad-130236

Teipel, S., Drzezga, A., Grothe, M. J., Barthel, H., Chételat, G., Schuff, N., et al. (2015). Multimodal imaging in Alzheimer's disease: Validity and usefulness for early detection. *Lancet Neurol.* 14, 1037–1053. doi: 10.1016/s1474-4422(15)00093-9

Tewarie, P., Balk, L., Costello, F., Green, A., Martin, R., Schippling, S., et al. (2012). The OSCAR-IB consensus criteria for retinal OCT quality assessment. *PLoS One* 7:e34823. doi: 10.1371/journal.pone.0034823

Vanburen, J. M. (1963). Trans-synaptic retrograde degeneration in the visual system of primates. *J. Neurol. Neurosurg. Psychiatry* 26, 402–409. doi: 10.1136/jnnp.26.5.402

Wang, D., Hui, S. C., Shi, L., Huang, W. H., Wang, T., Mok, V. C., et al. (2013). Application of multimodal MR imaging on studying Alzheimer's disease: A survey. *Curr. Alzheimer Res.* 10, 877–892. doi: 10.2174/15672050113109990150

Wang, H., Feng, T., Zhao, Z., Bai, X., Han, G., Wang, J., et al. (2022). Classification of Alzheimer's disease based on deep learning of brain structural and metabolic data. *Front. Aging Neurosci.* 14:927217. doi: 10.3389/fnagi.2022.927217

Wang, X., Jiao, B., Liu, H., Wang, Y., Hao, X., Zhu, Y., et al. (2022). Machine learning based on optical coherence tomography images as a diagnostic tool for Alzheimer's disease. *CNS Neurosci. Therap.* 28, 2206–2217. doi: 10.1111/cns.13963

Weiler, M., Teixeira, C. V., Nogueira, M. H., de Campos, B. M., Damasceno, B. P., Cendes, F., et al. (2014). Differences and the relationship in default mode network intrinsic activity and functional connectivity in mild Alzheimer's disease and amnestic mild cognitive impairment. *Brain Connect.* 4, 567–574. doi: 10.1089/brain.2014.0234

Wierenga, C. E., and Bondi, M. W. (2007). Use of functional magnetic resonance imaging in the early identification of Alzheimer's disease. *Neuropsychol. Rev.* 17, 127–143. doi: 10.1007/s11065-007-9025-y

Williams, P. A., Thirgood, R. A., Oliphant, H., Frizzati, A., Littlewood, E., Votruba, M., et al. (2013). Retinal ganglion cell dendritic degeneration in a mouse model of Alzheimer's disease. *Neurobiol. Aging* 34, 1799–1806.

Xi, Q., Zhao, X. H., Wang, P. J., Guo, Q. H., Yan, C. G., and He, Y. (2012). Functional MRI study of mild Alzheimer's disease using amplitude of low frequency fluctuation analysis. *Chin. Med. J.* 125, 858–862.

Yan, C. G., Wang, X. D., Zuo, X. N., and Zang, Y. F. (2016). DPABI: Data processing & analysis for (resting-state) brain imaging. *Neuroinformatics* 14, 339–351. doi: 10.1007/s12021-016-9299-4

Zhang, B., Xu, Y., Zhu, B., and Kantarci, K. (2014). The role of diffusion tensor imaging in detecting microstructural changes in prodromal Alzheimer's disease. *CNS Neurosci. Ther.* 20, 3–9. doi: 10.1111/cns.12166

Zhang, J., Shi, L., and Shen, Y. (2022). The retina: A window in which to view the pathogenesis of Alzheimer's disease. *Ageing Res. Rev.* 77:101590. doi: 10.1016/j.arr.2022.101590

Zhou, Y., Song, Z., Han, X., Li, H., and Tang, X. (2021). Prediction of Alzheimer's disease progression based on magnetic resonance imaging. *ACS Chem. Neurosci.* 12, 4209–4223. doi: 10.1021/acschemneuro.1c00472

Zou, Q. H., Zhu, C. Z., Yang, Y., Zuo, X. N., Long, X. Y., Cao, Q. J., et al. (2008). An improved approach to detection of amplitude of low-frequency fluctuation (ALFF) for resting-state fMRI: Fractional ALFF. *J. Neurosci. Methods* 172, 137–141. doi: 10.1016/j.jneumeth.2008.04.012

frontiers | Frontiers in Aging Neuroscience

TYPE Original Research
PUBLISHED 10 March 2023
DOI 10.3389/fnagi.2023.1133705

OPEN ACCESS

EDITED BY
Woon-Man Kung,
Chinese Culture University,
Taiwan

REVIEWED BY
Sergio A Castillo-Torres,
Servicio de Movimientos Anormales,
Fleni,
Argentina
Daniele Urso,
King's College London,
United Kingdom

*CORRESPONDENCE
Zhenhua Liu
✉ liuzhenhua@csu.edu.cn
Lifang Lei
✉ Lei_lifang@qq.com

SPECIALTY SECTION
This article was submitted to Parkinson's Disease and Aging-related Movement Disorders, a section of the journal Frontiers in Aging Neuroscience

RECEIVED 29 December 2022
ACCEPTED 20 February 2023
PUBLISHED 10 March 2023

CITATION
Zhou X, Xiang Y, Song T, Zhao Y, Pan H, Xu Q, Chen Y, Sun Q, Wu X, Yan X, Guo J, Tang B, Lei L, Liu Z and for Parkinson's Disease & Movement Disorders Multicenter Database and Collaborative Network in China (PD-MDCNC) (2023) Characteristics of fatigue in Parkinson's disease: A longitudinal cohort study. *Front. Aging Neurosci.* 15:1133705. doi: 10.3389/fnagi.2023.1133705

Characteristics of fatigue in Parkinson's disease: A longitudinal cohort study

Xiaoxia Zhou[1], Yaqin Xiang[1], Tingwei Song[1], Yuwen Zhao[1], Hongxu Pan[1], Qian Xu[1], Yase Chen[1], Qiying Sun[2,3], Xinyin Wu[4], Xinxiang Yan[1,3], Jifeng Guo[1,3,5], Beisha Tang[1,3,5], Lifang Lei[6]*, Zhenhua Liu[1,3,5]* and for Parkinson's Disease & Movement Disorders Multicenter Database and Collaborative Network in China (PD-MDCNC)

[1]Department of Neurology, Xiangya Hospital, Central South University, Changsha, China, [2]Department of Geriatrics, Xiangya Hospital, Central South University, Changsha, China, [3]National Clinical Research Center for Geriatric Disorders, Xiangya Hospital, Central South University, Changsha, China, [4]Department of Epidemiology and Health Statistics, Xiangya School of Public Health, Central South University, Changsha, China, [5]Key Laboratory of Hunan Province in Neurodegenerative Disorders, Central South University, Changsha, China, [6]Department of Neurology, The Third Xiangya Hospital, Central South University, Changsha, China

Objective: To assess the prevalence, evolution, clinical characteristics, correlates and predictors of fatigue as well as to investigate the influence of comorbid fatigue on the longitudinal changes in motor and non-motor symptoms over a 2-year longitudinal follow-up period in a large cohort of patients with Parkinson's disease (PD).

Materials and methods: A total of 2,100 PD patients were enrolled from the Parkinson's Disease & Movement Disorders Multicenter Database and Collaborative Network in China (PD-MDCNC), and their motor and non-motor symptoms were assessed biennially using comprehensive scales, including the 16-item Parkinson Fatigue Scale (PFS-16). Each PD patient was categorized as PD with or without fatigue on the basis of a cut-off mean PFS-16 score of 3.3.

Results: The prevalence of fatigue in our cohort was 36.8%. Compared to PD patients without fatigue, PD patients with fatigue were more likely to be older, have a longer disease duration, and higher baseline levodopa equivalent daily dose (all $p<0.05$). Moreover, PD patients with fatigue showed more severe motor and non-motor phenotypes than those without fatigue. Overall, high total Unified Parkinson's Disease Rating Scale (UPDRS) score (odds ratio [OR]=1.016, 95% confidence interval [CI]: 1.009–1.024), Non-Motor Symptoms Scale score (OR=1.022, 95% CI: 1.015–1.029), postural instability and gait difficulty (PIGD) subtype (OR=1.586, 95% CI: 1.211–2.079), presence of excessive daytime sleepiness (EDS; OR=1.343, 95% CI: 1.083–1.666), and wearing-off (OR=1.282, 95% CI: 1.023–1.607) were significantly associated with fatigue in PD patients (all $p<0.05$). High total UPDRS score at baseline (OR=1.014, 95% CI: 1.002–1.027, $p=0.028$) increased the risk of developing fatigue during follow-up. Although significant, the odds ratios were low and confidence intervals were narrow. Analysis of disease progression showed significant group differences in motor and non-motor symptoms. In comparison with the never-fatigue group, the persistent-fatigue group showed significantly greater progression in motor, autonomic dysfunction, sleep, depression and cognitive symptoms (all $p<0.05$).

Conclusion: Increased disease severity, presence of the PIGD subtype, EDS, and wearing-off were associated with fatigue in PD patients. Significant subgroup-level differences were observed in the progression of motor and non-motor symptoms across different fatigue subgroups of PD patients.

KEYWORDS

Parkinson's disease, fatigue, longitudinal, PD-MDCNC, progression

1. Introduction

Parkinson's disease (PD) is the most common movement disorder and second-most common neurodegenerative disorder in the world after Alzheimer's disease, affecting >1% of the population aged ≥65 years and expected to double in prevalence by 2030 (Aarsland et al., 2021). PD is pathologically characterized by dopaminergic neuronal loss in the substantia nigra pars compacta and the presence of intracellular inclusions containing α-synuclein aggregates (Armstrong and Okun, 2020; Liu et al., 2022). Considering that the progression of PD can span decades, it has adverse and profound consequences for patients, caregivers, and the society (Bloem et al., 2021).

Apart from cardinal motor features, such as bradykinesia (slowness of movement), rigidity, and resting tremor, PD is also associated with a heterogeneous spectrum of non-motor symptoms that contribute greatly to the overall disease burden (Schapira et al., 2017; Aarsland et al., 2021). Notably, fatigue is a common but less visible symptom of PD and affects approximately half of all patients (Kluger, 2017), which is often considered by patients with PD to be one of the most disabling symptoms affecting their daily activities and quality of life (Stocchi et al., 2014). As demonstrated by the growing number of research articles, interest in the subject is increasing. Furthermore, expert opinions on raising awareness on fatigue have been published (Lazcano-Ocampo et al., 2020). Considering that fatigue has diverse clinical manifestation, large clinical heterogeneity with many confounding factors, and lacks of clear pathogenesis and treatment to date, the understanding of fatigue in PD is insufficient. Although previous studies on fatigue in PD have mostly focused on the clinical features and factors associated with PD, fatigue has also been shown to be associated with other common non-motor symptoms of PD, including cognitive impairment, depression, apathy, anxiety, autonomic dysfunction, daytime somnolence, and sleep disturbances, which adversely affects patients' quality of life (Stocchi et al., 2014; Fu et al., 2016; Kluger et al., 2017; Siciliano et al., 2018; Ongre et al., 2021; Ou et al., 2021; Zhou et al., 2021; Béreau et al., 2022). However, the results of these studies are not always consistent. For example, Ongre et al. reported that a higher level of fatigue was associated with better cognitive functioning, whereas Kluger et al. and Siciliano et al. found that fatigue is associated with cognitive decline. Moreover, most published investigations were limited in size (sample size <500), and knowledge regarding the longitudinal progression of fatigue (Ongre et al., 2021; Ou et al., 2021) in PD is currently limited. Furthermore, the potential influence of the presence of concomitant fatigue in PD on the rate of progression of other phenotypic features has not been characterized.

In the light of these discrepancies and gaps in the literature, we conducted a longitudinal cohort study of patients with PD with a 2-year follow-up period. The aims of this study were to assess the prevalence and evolution, clinical characteristics, correlates and predictors of fatigue, as well as to investigate the influence of comorbid fatigue on the longitudinal changes in motor and non-motor symptoms in a large cohort of patients with PD.

2. Materials and methods

2.1. Participants

The participants were enrolled from the Parkinson's Disease & Movement Disorders Multicenter Database and Collaborative Network in China (PD-MDCNC) between January 2017 and August 2022. At least two neurological specialists confirmed the clinical diagnosis of PD according to the Movement Disorder Society Clinical Diagnostic Criteria for Parkinson's Disease (Postuma et al., 2015), including diagnoses of either clinically established or probable PD. The exclusion criteria were as follows: (1) failure to complete the 16-item Parkinson's Fatigue Scale (PFS-16) questionnaire at baseline and follow-up, (2) missing data ≥10%, or (3) diagnosis of other causes of parkinsonism on baseline or follow-up assessments. The clinical data of all participants were stored in the PD-MDCNC.[1] Written informed consent was obtained from all participants. This study was approved by the Ethics Committee of Xiangya Hospital and conducted in accordance with the ethical guidelines of the Declaration of Helsinki.

2.2. Clinical assessments

The participants underwent comprehensive and standardized clinical assessments at baseline and at the 2-year follow-up. Before conducting the assessments, all researchers were trained to ensure equal understanding of the scales as well as the methods and phrasing used for clinical data collection. Baseline clinical information, including age, sex, age at onset, and disease duration, was collected. Treatments were recorded during the baseline and 2-year follow-up interviews. The levodopa equivalent daily dose (LEDD) was calculated using a commonly used method (Tomlinson et al., 2010). Clinical examinations of motor symptoms and a broad range of non-motor symptoms were performed on the basis of a series of PD assessment scales. Motor symptoms were assessed based on the Unified Parkinson's Disease Rating Scale (UPDRS) and Hoehn and Yahr

1 http://www.pd-mdcnc.com

stages, defining motor subtypes as tremor dominant (TD), postural instability and gait difficulty (PIGD), or indeterminate. The ratio of the mean UPDRS tremor score (8 items) to the mean UPDRS PIGD score (5 items) was used to define the TD (ratio ≥ 1.5), PIGD (ratio ≤ 1), and indeterminate subtypes (ratio > 1.0 and < 1.5; Jankovic et al., 1990; Stebbins et al., 2013). Motor complications, such as dyskinesia and wearing-off were diagnosed by clinicians, and the severities of dyskinesia and wearing-off were evaluated by UPDRS part IV-A and 9-item Wearing-off Questionnaire (WOQ-9), respectively. Freezing of gait (FOG) was evaluated using the New Freezing of Gait Questionnaire (NFOGQ).

In addition to motor symptoms, we evaluated a broad range of non-motor symptoms based on the Non-Motor Symptoms Scale (NMSS), Scales for outcomes in Parkinson's disease-Autonomic Dysfunction (SCOPA-AUT), Mini-Mental State Examination (MMSE), Rapid Eye Movement Sleep Behavior Disorder Questionnaire-Hong Kong (RBDQ-HK), Epworth Sleepiness Scale (ESS), Parkinson's Disease Sleep Scale (PDSS), Hyposmia Rating Scale (HRS), Functional Constipation Diagnostic Criteria Rome III, and Hamilton Depression Rating Scale (HAMD-17). Quality of life was assessed using the Parkinson's disease questionnaire (PDQ-39). Patients with illiteracy, primary education, and above junior education were identified as having cognitive impairment when the MMSE scores were below 17, 20 and 24 points, respectively. Hyposmia was defined as a total HRS score less than 22.5. Probable rapid eye movement sleep behavior disorder (pRBD) was defined as a total RBDQ-HK scale score no less than 18. Excessive daytime sleepiness (EDS) was defined as a total ESS score higher than 10. Depression was defined as a total HAMD-17 score higher than 7. Details regarding these clinical scales have been provided in our previous study (Zhao et al., 2020; Deng et al., 2022; Zhou X. et al., 2022; Zhou Z. et al., 2022).

2.3. Definition of fatigue

Fatigue was assessed using PFS-16, which has been developed for use in routine clinical practice and recommended for screening and rating the severity of fatigue. The PFS is a 16-item patient-rated scale that encompasses the physical aspects of fatigue and its impact on patients' daily functioning. Item scores ranged from 1 (strongly disagree) to 5 (strongly agree), with the PFS-16 mean score calculated as the mean of all individual item scores (range: 1.0–5.0). Based on a previous study (Brown et al., 2005; Friedman et al., 2010), we used a threshold PFS-16 mean score of 3.3 to define the presence of fatigue in our study. Considering that fatigue was not necessarily persistent, we classified fatigue into the following four types (Alves et al., 2004): "never fatigue" referred to cases showing no fatigue at baseline and the 2-year follow-up; "non-persistent fatigue" indicated fatigue that disappeared during the 2-year follow-up; "new-onset fatigue" indicated fatigue that first appeared at the 2-year follow-up; and "persistent fatigue" indicated fatigue that appeared at both the baseline and 2-year follow-up.

2.4. Statistical analyses

Continuous variables were summarized using descriptive statistics, and categorical variables were summarized using patient counts and percentages. For the analysis of cross-sectional data, comparisons between patients with and without fatigue were made using the chi-squared test and multivariable logistic regression for qualitative variables, and Student's t-test or nonparametric Mann–Whitney test and multivariable linear regression for quantitative variables. Most comparisons were adjusted for age and sex, and for additional variables thought to be potential confounders.

Spearman correlation analysis was used to analyze relationships between the presence of fatigue and other clinical variables. Binary logistic regression models were used to assess the factors associated with fatigue in PD and included as many variables as possible. A binary dependent variable of fatigue was assigned a value of 0 when the PFS-16 mean score was <3.3 and a value of 1 when the score was ≥3.3. The following covariates were included in the logistic model after analysis of multicollinearity (variance inflation factor < 10): age, sex, body mass index (BMI), disease duration, LEDD, total UPDRS score, NMSS score, PDSS score, PDQ-39 score, SCOPA-AUT score, motor subtype, severity of PD (Hoehn and Yahr stages 1–2.5 vs. stages 3–5), constipation (presence vs. absence), cognitive impairment (presence vs. absence), hyposmia (presence vs. absence), pRBD (presence vs. absence), EDS (presence vs. absence), depression (presence vs. absence), FOG (presence vs. absence), wearing-off (presence vs. absence), and dyskinesia (presence vs. absence).

The binary logistic regression model was also used to investigate the clinical predictors for fatigue in PD. The analysis was based on the patients who had no fatigue at baseline. The clinical outcome was the new occurrence of fatigue during follow-up. In the multivariate model, the covariates of the above binary logistic regression analysis after analysis of multicollinearity (variance inflation factor < 10) were included as covariates.

For the analysis of longitudinal data, the outcomes of clinical evaluations were compared using a paired-sample t-test, Wilcoxon matched-pair signed-rank test, or McNemar–Bowker test. We used generalized estimating equation (GEE) for comprehensive longitudinal comparison of the progression of the four fatigue subgroups. In each separate GEE for progression, the clinical characteristics at follow-up were defined as dependent variables. To reduce the "regression toward mean" bias, the analysis was adjusted for age at baseline, sex, disease duration, and baseline values of the clinical factors (Vickers and Altman, 2001). All analyses were performed using SPSS version 25.0 (IBM Corp., Armonk, NY, United States). Two-tailed p-values <0.05 were considered the threshold for statistically significant differences in all analyses.

3. Results

3.1. Overview, prevalence, and evolution of fatigue

Overall, 2,100 patients were eligible for inclusion in the study. The main demographic and clinical characteristics of the patients are summarized in Table 1. At baseline, the mean age, age at onset, and disease duration were 60.47 ± 10.21, 55.06 ± 10.81, and 5.42 ± 4.52 years, respectively. Approximately half of the patients were men (49.9%) and three-quarters of the patients (77.4%) were in Hoehn and Yahr stages 1–2.5. The baseline LEDD was 490.05 ± 278.44 mg (Table 1).

A total of 772 (36.8%) patients were identified as experiencing fatigue on the basis of the baseline PFS-16 score (PFS-16 mean

10.3389/fnagi.2023.1133705

TABLE 1 Demographic and clinical characteristics of patients with PD at baseline.

Characteristics	Overall (*n*=2,100)	PD with fatigue (*n*=772)	PD without fatigue (*n*=1,328)	*p* value[a]	*p* value[b]
Age at baseline	60.47 ± 10.21	61.49 ± 10.00	59.88 ± 10.28	**<0.001**	NA
Age at onset	55.06 ± 10.81	55.31 ± 10.48	54.91 ± 11.00	0.272	NA
Gender ratio (male)	1,047(49.9%)	387(50.1%)	660(49.7%)	0.849	NA
BMI	22.78 ± 5.22	22.59 ± 7.46	22.89 ± 3.27	**<0.001**	0.507
PD duration	5.42 ± 4.52	6.20 ± 4.80	4.97 ± 4.28	**<0.001**	NA
LEDD	490.05 ± 278.44	525.00 ± 280.70	469.73 ± 275.19	**<0.001**	**0.010**
Motor symptoms					
UPDRS total score	39.86 ± 20.40	48.45 ± 20.77	34.86 ± 18.43	**<0.001**	**<0.001**
UPDRS Part III score	25.15 ± 13.97	30.08 ± 14.38	22.29 ± 12.88	**<0.001**	**<0.001**
Bradykinesia score	9.29 ± 6.00	11.09 ± 6.34	8.25 ± 5.53	**<0.001**	**<0.001**
Rigidity score	5.19 ± 4.00	6.38 ± 4.26	4.49 ± 3.67	**<0.001**	**<0.001**
Tremor score	3.33 ± 3.30	3.61 ± 3.73	3.16 ± 3.02	**0.256**	0.140
Postural instability score	3.73 ± 2.76	4.64 ± 2.99	3.20 ± 2.46	**<0.001**	**<0.001**
Motor subtype				**<0.001**	
Tremor-dominant	460(21.9%)	115(14.9%)	345(26.0%)		
Intermediate type	291(13.9%)	95(12.3%)	196(14.8%)		**0.038**
PIGD-dominant	1,349(64.2%)	562(72.8%)	787(59.3%)		**<0.001**
Hoehn and Yahr stages				**<0.001**	**<0.001**
Stages of 1–2.5	1,625(77.4%)	516(66.8%)	1,109(83.5%)		
Stages of 3–5	475(22.6%)	256(33.2%)	219(16.5%)		
Freezing of gait[c]	588(28.0%)	286(37.0%)	302(22.7%)	**<0.001**	**<0.001**
Non-motor symptoms					
NMSS total score	33.96 ± 25.55	46.71 ± 28.67	26.55 ± 20.13	**<0.001**	**<0.001**
PDSS total score	119.28 ± 28.60	110.88 ± 25.33	124.16 ± 29.26	**<0.001**	**<0.001**
PDQ-39 total score	26.09 ± 31.46	36.03 ± 28.81	20.31 ± 31.50	**<0.001**	**<0.001**
SCOPA-AUT score	8.07 ± 5.42	9.61 ± 5.71	7.17 ± 5.04	**<0.001**	**<0.001**
Constipation[d]	760(36.2%)	355(46.0%)	405(30.5%)	**<0.001**	**<0.001**
CI[e]	149(7.1%)	78(10.1%)	71(5.3%)	**<0.001**	**0.002**
MMSE score	26.73 ± 3.37	26.23 ± 3.75	27.03 ± 3.09	**<0.001**	**<0.001**
Hyposmia[f]	899(42.8%)	386(50.0%)	513(38.6%)	**<0.001**	**<0.001**
HRS score	19.58 ± 6.22	18.62 ± 6.60	20.13 ± 5.92	**<0.001**	**<0.001**
pRBD[g]	882(42.0%)	397(51.4%)	485(36.5%)	**<0.001**	**<0.001**
RBDQ-HK score	16.32 ± 16.43	20.23 ± 17.43	14.06 ± 15.38	**<0.001**	**<0.001**
EDS[h]	677(32.2%)	333(43.1%)	344(25.9%)	**<0.001**	**<0.001**
ESS score	7.37 ± 6.16	9.01 ± 6.50	6.41 ± 5.75	**<0.001**	**<0.001**
Depression[i]	685(32.6%)	371(48.1%)	314(23.6%)	**<0.001**	**<0.001**
HAMD score	5.31 ± 5.19	7.35 ± 5.79	4.12 ± 4.38	**<0.001**	**<0.001**
Motor complications					
Wearing-off[j]	757(36.0%)	358(46.4%)	399(30.0%)	**<0.001**	**<0.001**
Dyskinesia[k]	288(13.7%)	138(17.9%)	150(11.3%)	**<0.001**	**0.002**

Data are mean ± SD or *n* (%), unless otherwise indicated. *p* value[a] are from the chi-squared test, Student's *t*-test or nonparametric Mann–Whitney test; *p* value[b] are from multivariable linear or logistic regression (controlled for sex, age, disease duration). Significant *p* values are indicated in bold. [c–k]Evaluated, respectively, by New Freezing of Gait Questionnaire (NFOGQ), Functional Constipation Diagnostic Criteria Rome III (ROME III), MMSE, HRS, RBDQ-HK, ESS, HAMD, 9-item Wearing-off Questionnaire (WOQ-9) and UPDRS part IV-A. PD, Parkinson's disease; BMI, body mass index; LEDD, levodopa equivalent daily dose; UPDRS, unified Parkinson's disease rating scale; PIGD, postural instability and gait difficulty; NMSS, non-motor symptom scale; PDSS, Parkinson's disease sleep scale; PDQ-39, The Parkinson's disease questionnaire (PDQ-39); SCOPA-AUT, scales for outcomes in Parkinson's disease-autonomic dysfunction; CI, cognitive impairment; MMSE, Mini-mental state examination; HRS, Hyposmia rating scale; pRBD, probable rapid eye movement sleep behavior disorder; RBDQ-HK, rapid eye movement sleep Behavior disorder questionnaire-Hong Kong; EDS, excessive daytime sleepiness; ESS, Epworth sleepiness scale; HAMD, Hamilton depression rating scale (HAMD-17).

score ≥ 3.3 points). The prevalence of fatigue by disease duration group was 26.4% (disease duration ≤ 3 years), 41.2% (3 < disease duration < 10 years) and 46.4% (disease duration ≥ 10 years). The frequency of fatigue was 31.7 and 53.9% in patients with Hoehn and Yahr stages 1–2.5 and 3–5, respectively (Supplementary Table 1). Fatigue did not always persist from one visit to the next in every patient during the follow-up period (Figure 1). The results showed never fatigue in 54.4% (1,142/2,100), non-persistent fatigue in 11.3% (237/2,100), new-onset fatigue in 8.8% (186/2,100), and persistent fatigue in 25.5% (535/2,100) of the patients.

To control for the heterogeneity of patient timelines, we stratified PD cases into three subgroups based on disease duration, as shown in Supplementary Table 2. Most scores of the motor and non-motor symptoms, including fatigue, worsened and the prevalence of symptoms increased as the disease progressed. Additionally, we found that motor complications were prone to occur in patients with PD with longer disease duration.

3.2. Comparison of clinical characteristics between PD patients with and without fatigue

Compared to PD patients without fatigue, those with fatigue were more likely to be older (61.49 ± 10.00 vs. 59.88 ± 10.28 years, $p < 0.001$), have a longer disease duration (6.20 ± 4.80 vs. 4.97 ± 4.28 years, $p < 0.001$), and higher baseline LEDD (525.00 ± 280.70 vs. 469.73 ± 275.19 mg, $p = 0.010$). Patients with fatigue had higher total UPDRS, UPDRS part III, bradykinesia, rigidity, tremor, postural instability, total NMSS, total PDQ-39, total SCOPA-AUT, total RBDQ-HK, ESS, and HAMD scores than those without fatigue (all $p < 0.001$, except for tremor score, which showed $p = 0.140$). Patients with fatigue had lower PDSS, total MMSE, and HRS scores than those without fatigue (all $p < 0.001$). Patients with fatigue also showed a higher prevalence of constipation, cognitive problems, hyposmia, pRBD, EDS, depression, wearing-off, and dyskinesia (all $p < 0.05$). In summary, PD patients with fatigue showed more severe motor and non-motor phenotypes (Table 1; Figure 2).

3.3. Factors associated with fatigue in PD

Spearman correlation analyses between presence of fatigue and clinical factors are shown in Supplementary Table 3. BMI and the PDSS score (lower score indicate more severe sleep disturbance) were significantly and negatively correlated with the presence of fatigue. Other clinical factors apart from sex were significantly and positively associated with fatigue.

Binary logistic regression analyses were performed to investigate factors associated with fatigue at baseline (Table 2). The variables included in the logistic regression model are mentioned in the Methods section. As shown in Table 2, the univariate logistic regression revealed that age, longer disease duration, LEDD, a greater disease severity (total UPDRS score, Hoehn and Yahr stage), PIGD subtype, total NMSS score, PDSS score, PDQ-39 score, SCOPA-AUT score, presence of FOG, constipation, cognitive impairment, hyposmia, pRBD, EDS, depression, wearing-off and dyskinesia were associated with fatigue ($p < 0.05$). Other clinical variables, including sex and BMI, were not significantly associated with fatigue. We further explored the independent associated factors of fatigue in PD patients using multivariate logistic regression. The total UPDRS score (OR = 1.016, 95% CI: 1.009–1.024, $p < 0.001$), NMSS score (OR = 1.022, 95% CI: 1.015–1.029, $p < 0.001$), PIGD subtype (OR = 1.586, 95% CI: 1.211–2.079, $p = 0.001$), presence of EDS (OR = 1.343, 95% CI: 1.083–1.666, $p = 0.007$), and wearing-off (OR = 1.282, 95% CI: 1.023–1.607, $p = 0.031$) remained significantly associated with fatigue in patients with PD (Table 2).

In order to explore the related factors of fatigue in PD patients at different disease periods, we further performed subgroup analyses according to the disease duration and Hoehn and Yahr stage grouping. The multivariate logistic regression model demonstrated that total UPDRS score (OR = 1.031, 95% CI: 1.013–1.050, $p < 0.001$), NMSS score (OR = 1.026, 95% CI: 1.012–1.040, $p < 0.001$), PIGD subtype (OR = 1.917, 95% CI: 1.185–3.100, $p = 0.008$) and presence of FOG (OR = 0.500, 95% CI: 0.272–0.922, $p = 0.026$) were significantly associated with fatigue in PD patients with disease duration less than or equal to 3 years. More details are shown in Supplementary Table 4.

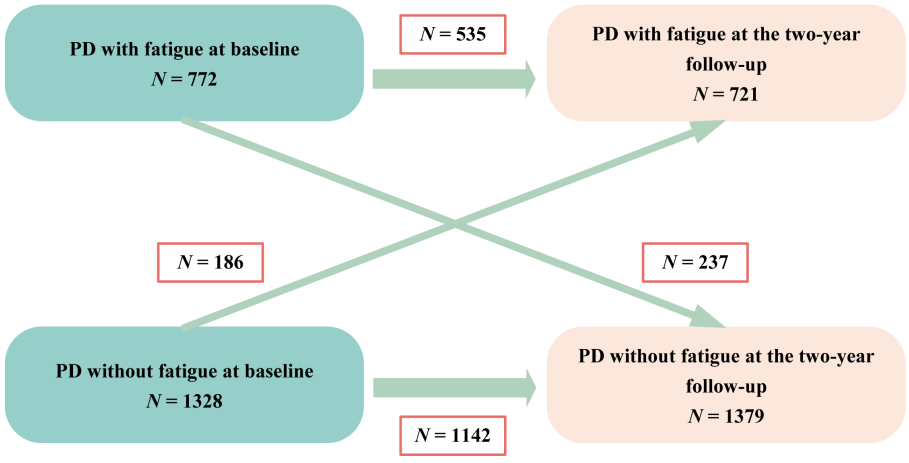

FIGURE 1
Diagram of fatigue change over time. PD, Parkinson's disease.

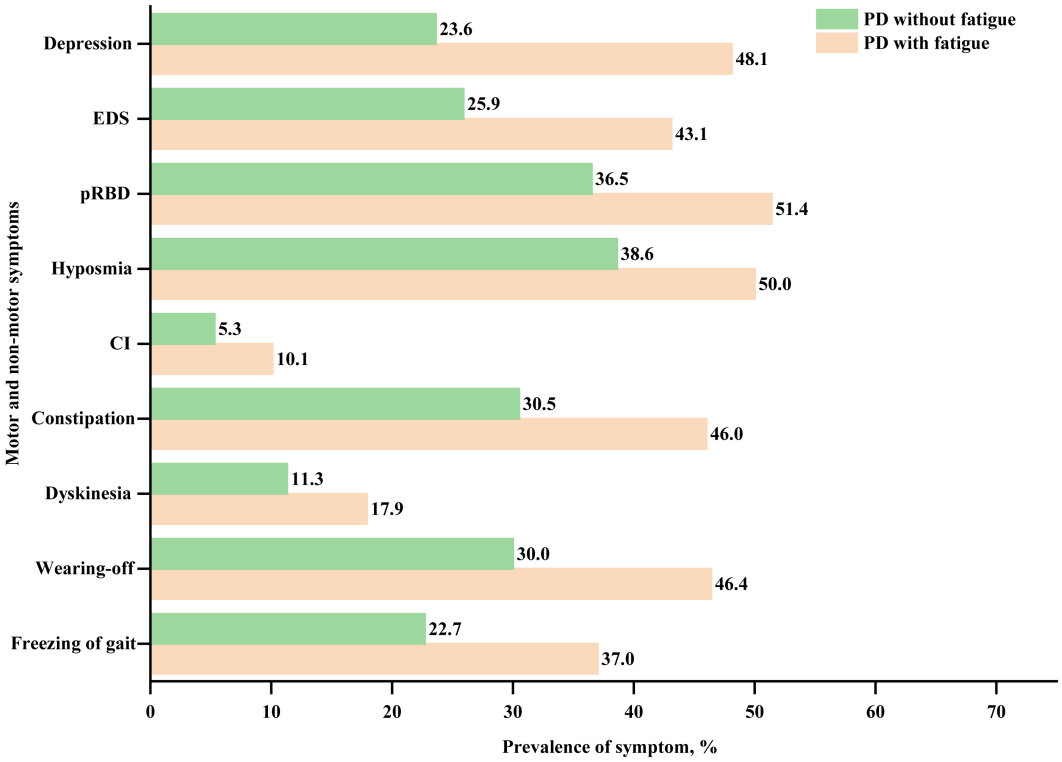

FIGURE 2
Frequency of motor and non-motor symptoms in PD with and without fatigue at baseline. PD, Parkinson's disease; CI, cognitive impairment; pRBD, probable rapid eye movement sleep behavior disorder; and EDS, excessive daytime sleepiness.

3.4. Predictors of fatigue in PD

The predictors for fatigue in PD are presented in Table 3. In the multivariate model, high total UPDRS score (OR = 1.014, 95% CI: 1.002–1.027, $p = 0.028$) increased the risk of developing fatigue during follow-up.

3.5. Disease progression in different fatigue subgroups

Most of the symptoms deteriorated significantly during the follow-up period. Overall, the total UPDRS, UPDRS part III, rigidity, postural instability, NMSS, PDSS, PDQ-39, SCOPA-AUT, MMSE, HRS, RBDQ-HK, and ESS scores worsened significantly from baseline to the 2-year follow-up ($p < 0.05$). The rates of Hoehn and Yahr stages 3–5, freezing of gait, wearing-off, dyskinesia, cognitive impairment, hyposmia, pRBD, and EDS increased significantly (all $p < 0.05$) except constipation and depression. With the persistence of fatigue, most other non-motor symptoms tend to increase in score or prevalence (Supplementary Tables 5 and 6).

Results from the GEE analysis showed significant group progression differences in motor and non-motor symptoms (Table 4 and Supplementary Table 6). In comparison with the never-fatigue group, the persistent-fatigue group showed significantly greater progression in the total UPDRS score (B = 9.477, 95% CI: 7.286–11.668), UPDRS part III score (B = 6.002, 95% CI: 4.507–7.498), and PDQ-39 score (B = 16.882, 95% CI: 13.063–20.701), highlighting the faster disease progression in the persistent-fatigue group (all $p < 0.001$). Similar progression was also observed in several non-motor features, namely, NMSS (B = 21.285, 95% CI: 18.276–24.293), PDSS (B = -10.827, 95% CI: −13.622 to −8.033), SCOPA-AUT (B = 4.147, 95% CI: 3.450–4.844), MMSE (B = -0.515, 95% CI: −0.856 to −0.174), HRS (B = -0.675, 95% CI: −1.286 to −0.065), RBDQ-HK (B = 3.630, 95% CI: 2.134–5.126), ESS (B = 3.203, 95% CI: 2.567–3.840), and HAMD (B = 3.137, 95% CI: 2.534–3.740) scores in the persistent-fatigue group compared to the never-fatigue group. In addition, in comparison with the never-fatigue group, the persistent-fatigue group had a worse prognosis, with more rapid progression in other domains, including freezing of gait (OR = 1.940, 95% CI: 1.541–2.442), wearing-off (OR = 2.255, 95% CI: 1.794–2.835), dyskinesia (OR = 1.971, 95% CI: 1.451–2.676), cognitive impairment (OR = 1.730, 95% CI: 1.227–2.440), pRBD (OR = 1.630, 95% CI: 1.277–2.081), EDS (OR = 2.800, 95% CI: 2.219–3.532), and depression (OR = 3.832, 95% CI: 3.013–4.874). All p-values were < 0.001, except that for cognitive impairment ($p = 0.002$).

In comparison with the never-fatigue group, the nonpersistent-fatigue group showed significantly greater progression in the freezing of gait (OR = 2.308, 95% CI: 1.707–3.119), pRBD (OR = 1.654, 95% CI: 1.190–2.300) and total SCOPA-AUT score (B = 0.972, 95% CI: 0.195–1.750). Other factors including total UPDRS, UPDRS part III, NMSS, PDSS, PDQ-39 scores, the rates of constipation, cognitive impairment, hyposmia, EDS, depression, wearing-off, and dyskinesia were not significantly different in the evolution of these symptoms between the never-fatigue and nonpersistent-fatigue group. Additional details are provided in Table 4 and Supplementary Table 6.

10.3389/fnagi.2023.1133705

TABLE 2 Factors Associated with Fatigue in PD.

	Univariate analysis			Multivariate analysis		
Variables (total cohort, *n*=2,100)	Odds ratio	95% CI	*p* value	Odds ratio	95% CI	*p* value
Sex (women vs. men)	0.983	0.823–1.174	0.849			
BMI	0.985	0.962–1.009	0.219			
Age	1.016	1.007–1.025	**0.001**			
Disease duration	1.062	1.041–1.083	**<0.001**			
LEDD	1.001	1.000–1.001	**<0.001**			
UPDRS total score	1.036	1.031–1.041	**<0.001**	1.016	1.009–1.024	**<0.001**
PIGD subtype (PIGD vs. TD)	2.142	1.690–2.716	**<0.001**	1.586	1.211–2.079	**0.001**
Hoehn and Yahr stages (3–5 vs. 1–2.5)	2.512	2.040–3.095	**<0.001**			
Freezing of gait (presence vs. absence)	1.999	1.646–2.428	**<0.001**			
NMSS total score	1.037	1.033–1.042	**<0.001**	1.022	1.015–1.029	**<0.001**
PDSS total score	0.979	0.975–0.982	**<0.001**			
PDQ-39 total score	1.027	1.023–1.032	**<0.001**			
SCOPA-AUT score	1.088	1.070–1.107	**<0.001**			
Constipation (presence vs. absence)	1.940	1.615–2.331	**<0.001**			
CI (presence vs. absence)	1.990	1.424–2.780	**<0.001**			
Hyposmia (presence vs. absence)	1.589	1.329–1.900	**<0.001**			
pRBD (presence vs. absence)	1.840	1.537–2.203	**<0.001**			
EDS (presence vs. absence)	2.170	1.798–2.619	**<0.001**	1.343	1.083–1.666	**0.007**
Depression (presence vs. absence)	2.988	2.472–3.612	**<0.001**			
Wearing-off (presence vs. absence)	2.013	1.675–2.420	**<0.001**	1.282	1.023–1.607	**0.031**
Dyskinesia (presence vs. absence)	1.709	1.331–2.196	**<0.001**			

p value are from logistic regression. Significant *p* values are indicated in bold. PD, Parkinson's disease; BMI, body mass index; LEDD, levodopa equivalent daily dose; UPDRS, unified Parkinson's disease rating scale; PIGD, postural instability and gait difficulty; TD, tremor-dominant; NMSS, non-motor symptom scale; PDSS, Parkinson's disease sleep scale; PDQ-39, The Parkinson's disease questionnaire (PDQ-39); SCOPA-AUT, scales for outcomes in Parkinson's disease-autonomic dysfunction; CI, cognitive impairment; pRBD, probable rapid eye movement sleep behavior disorder; EDS, excessive daytime sleepiness.

TABLE 3 Predictors of fatigue in PD.

Variables	Odds ratio	95% CI	*p* value
UPDRS total score	1.014	1.002–1.027	**0.028**

p value are from multivariable logistic regression. Significant *p* values are indicated in bold. PD, Parkinson's disease; UPDRS, Unified Parkinson's disease Rating Scale.

4. Discussion

This longitudinal cohort study systematically investigated the prevalence, evolution, and clinical correlates of fatigue among PD patients as well as assessed differences in disease progression across PD fatigue subgroups. Overall, approximately one-third of patients included in our study experienced fatigue. We found that PD patients with fatigue were more likely to be older, have a longer disease duration and higher baseline LEDD, and manifested more severe motor and non-motor phenotypes than PD patients without fatigue. We also found that increased disease severity, presence of the PIGD subtype, EDS, and wearing-off were associated with fatigue in patients with PD. To the best of our knowledge, this is the first study to assess longitudinal progression across different fatigue subgroups of PD patients. We observed significant subgroup-level differences in the progression of motor and non-motor symptoms. Our study provides evidence for the longitudinal progression of clinical symptoms in different fatigue subgroups of patients with PD and will facilitate the clinical management of fatigue.

We found that the overall frequency of fatigue in patients with PD was 36.8%, which is consistent with the study of Stocchi et al. (2014) and provides further evidence for fatigue as one of several common non-motor symptoms in patients with PD. The prevalence of fatigue in previous studies (Friedman et al., 2016; Siciliano et al., 2018) has been found to range from 33 to 70%, and the wide range of values may reflect differences in the study designs, especially the use of different fatigue rating scales and definitions of fatigue as well as the populations tested. We also found that the frequency of fatigue increased with the severity of PD, which is consistent with findings from previous studies (Stocchi et al., 2014; Fu et al., 2016; Ou et al., 2021). However, the results of the meta-analysis (Siciliano et al., 2018) showed that the prevalence of fatigue was not moderated by the disease severity.

Our study found that PD patients with fatigue were older, had longer disease duration, and had higher LEDD than those without fatigue. Additionally, PD patients with fatigue showed significantly greater disease severity scores and a higher prevalence of all motor and non-motor symptoms than those without fatigue. These findings indicate that fatigue exacerbates the symptoms and burden of PD patients and are in agreement with previous studies (Stocchi et al., 2014; Fu et al., 2016; Siciliano et al., 2018).

10.3389/fnagi.2023.1133705

TABLE 4 Progression of motor and non-motor outcomes in four different fatigue subgroups.

Outcome	Never fatigue (I=1,142)	Non-persistent fatigue (II=237)	New-onset fatigue (III=186)	Persistent fatigue (IV=535)	*P* value
Motor symptoms					
UPDRS total score	0*	−1.094 (−3.569 to 1.382)	10.616 (7.713 to 13.520)	9.477 (7.286 to 11.668)	P_{II} = 0.387, **P_{III} < 0.001, P_{IV} < 0.001**
UPDRS Part III score	0*	−1.089 (−2.849 to 0.670)	5.898 (3.870 to 7.926)	6.002 (4.507 to 7.498)	P_{II} = 0.225, **P_{III} < 0.001, P_{IV} < 0.001**
Bradykinesia score	0*	−0.029 (−0.778 to 0.721)	2.342 (1.448 to 3.236)	2.895 (2.251 to 3.538)	P_{II} = 0.940, **P_{III} < 0.001, P_{IV} < 0.001**
Rigidity score	0*	−0.256 (−0.784 to 0.272)	1.649 (1.020 to 2.279)	1.586 (1.139 to 2.034)	P_{II} = 0.342, **P_{III} < 0.001, P_{IV} < 0.001**
Tremor score	0*	−0.617 (−1.028 to −0.207)	0.093 (−0.437 to 0.622)	0.148 (−0.204 to 0.500)	**P_{II} = 0.003,** P_{III} = 0.732, P_{IV}=0.410
Postural instability score	0*	0.266 (−0.111 to 0.642)	0.963 (0.536 to 1.390)	0.860 (0.553 to 1.167)	P_{II} = 0.167, **P_{III} < 0.001, P_{IV} < 0.001**
Freezing of gait[a]	1*	2.308 (1.707 to 3.119)	1.885 (1.346 to 2.641)	1.940 (1.541 to 2.442)	**P_{II} < 0.001, P_{III} < 0.001, P_{IV} < 0.001**
Non-motor symptoms					
NMSS total score	0*	−0.018 (−3.091 to 3.055)	21.940 (17.548 to 26.332)	21.285 (18.276 to 24.293)	**P_{II}**=0.991, **P_{III} < 0.001, P_{IV} < 0.001**
PDSS total score	0*	−2.971 (−6.305 to 0.364)	−10.355 (−13.725 to −6.985)	−10.827 (−13.622 to −8.033)	P_{II}=0.081, **P_{III} < 0.001, P_{IV} < 0.001**
PDQ-39 total score	0*	2.592 (−1.148 to 6.332)	16.093 (12.593 to 19.593)	16.882 (13.063 to 20.701)	P_{II} = 0.174, **P_{III} < 0.001, P_{IV} < 0.001**
SCOPA-AUT score	0*	0.972 (0.195 to 1.750)	3.570 (2.600 to 4.541)	4.147 (3.450 to 4.844)	**P_{II} = 0.014, P_{III} < 0.001, P_{IV} < 0.001**
Constipation[b]	1*	0.996 (0.694 to 1.429)	2.233 (1.566 to 3.185)	2.124 (1.653 to 2.731)	P_{II} = 0.982, **P_{III} < 0.001, P_{IV} < 0.001**
CI[c]	1*	1.097 (0.635 to 1.894)	1.083 (0.609 to 1.927)	1.730 (1.227 to 2.440)	P_{II} = 0.740, P_{III} = 0.785, **P_{IV}=0.002**
MMSE score	0*	−0.010 (−0.364 to 0.343)	−0.107 (−0.546 to 0.332)	−0.515 (−0.856 to −0.174)	P_{II} =0.954, P_{III} = 0.632, **P_{IV}=0.003**
Hyposmia[d]	1*	1.330 (0.937 to 1.887)	1.553 (1.072 to 2.251)	1.221 (0.955 to 1.562)	P_{II} = 0.110, **P_{III} = 0.020,** P_{IV} = 0.112

(Continued)

TABLE 4 (Continued)

Outcome	Never fatigue (I=1,142)	Non-persistent fatigue (II=237)	New-onset fatigue (III=186)	Persistent fatigue (IV=535)	*P* value
HRS score	0*	−0.601 (−1.398 to 0.195)	−0.806 (−1.699 to 0.087)	−0.675 (−1.286 to −0.065)	P_{II} = 0.139, P_{III} = 0.077, **P_{IV} = 0.030**
pRBD[e]	1*	1.654 (1.190 to 2.300)	1.907 (1.320 to 2.755)	1.630 (1.277 to 2.081)	**P_{II}=0.003, P_{III}=0.001, P_{IV} < 0.001**
RBDQ-HK score	0*	1.374 (−0.483 to 3.231)	3.801 (1.559 to 6.043)	3.630 (2.134 to 5.126)	P_{II} = 0.147, **P_{III}=0.001, P_{IV} < 0.001**
EDS[f]	1*	0.895 (0.634 to 1.265)	2.876 (2.029 to 4.077)	2.800 (2.219 to 3.532)	P_{II} = 0.531, **P_{III} < 0.001, P_{IV} < 0.001**
ESS score	0*	−0.819 (−1.583 to −0.054)	3.514 (2.546 to 4.482)	3.203 (2.567 to 3.840)	P_{II} = 0.036, **P_{III} < 0.001, P_{IV} < 0.001**
Depression[g]	1*	1.109 (0.775 to 1.587)	3.508 (2.457 to 5.010)	3.832 (3.013 to 4.874)	P_{II} = 0.571, **P_{III} < 0.001, P_{IV} < 0.001**
HAMD score	0*	0.078 (−0.509 to 0.665)	3.184 (2.391 to 3.977)	3.137 (2.534 to 3.740)	P_{II} = 0.794, **P_{III} < 0.001, P_{IV} < 0.001**
Motor complications					
Wearing-off[h]	1*	1.288 (0.947 to 1.751)	2.114 (1.503 to 2.973)	2.255 (1.794 to 2.835)	P_{II} = 0.107, **P_{III} < 0.001, P_{IV} < 0.001**
Dyskinesia[i]	1*	1.335 (0.880 to 2.023)	1.724 (1.080 to 2.752)	1.971 (1.451 to 2.676)	P_{II} = 0.174, **P_{III}=0.022, P_{IV} < 0.001**

Data are B (95%CI) for continuous variables or OR (95%CI) for categorical variables, unless otherwise indicated. In each separate generalized estimating equation, the clinical characteristics at follow-up were defined as dependent variables and the analysis was adjusted for age at baseline, sex, disease duration, and baseline values of the clinical factors. *Reference group. Significant P values are indicated in bold. [a–i]Evaluated, respectively, by New Freezing of Gait Questionnaire (NFOGQ), Functional Constipation Diagnostic Criteria Rome III (ROME III), MMSE, HRS, RBDQ-HK, ESS, HAMD, 9-item Wearing-off Questionnaire (WOQ-9) and UPDRS part IV-A. PD, Parkinson's disease; UPDRS, Unified Parkinson's disease rating scale; NMSS, non-motor symptom scale; PDSS, Parkinson's disease sleep scale; PDQ-39, The Parkinson's disease questionnaire (PDQ-39); SCOPA-AUT, scales for outcomes in Parkinson's disease-autonomic dysfunction; CI, cognitive impairment; MMSE, Mini-mental state examination; HRS, Hyposmia rating scale; pRBD, probable rapid eye movement sleep behavior disorder; RBDQ-HK, rapid eye movement sleep behavior disorder questionnaire-Hong Kong; EDS, excessive daytime sleepiness; ESS, Epworth sleepiness scale; HAMD, Hamilton depression rating scale (HAMD-17).

Additionally, we investigated the factors associated with fatigue in order to improve the management of fatigue in patients with PD. In the multivariate logistic regression for the entire cohort, we found that the total UPDRS score, NMSS score and the presence of the PIGD subtype, EDS, and wearing-off were significantly associated with fatigue in patients with PD. Notably, fatigue has been reported to be reduced by dopaminergic drugs, such as levodopa (Lou et al., 2003), suggesting that dopaminergic deficits are involved in the development of fatigue in PD, which is further supported by our finding that more severe motor disabilities were associated with fatigue. However, the non-persistent nature of fatigue observed in many studies (Ongre et al., 2017; Ou et al., 2021; including our study) also suggests that dopaminergic mechanisms only partially contribute to the development of fatigue in PD. In fact, neither LEDD, Hoehn and Yahr stage nor disease duration were associated with fatigue in our study, providing indirect support for the hypothesis that fatigue in PD may result from the disruption of nondopaminergic pathways (Kluger, 2017; Siciliano et al., 2018). This implies that fatigue is independent of dopaminergic treatment in PD and instead an independent non-motor symptom of PD. Although "significant" in UPDRS and NMSS scores associated with fatigue, the odds ratios were close to 1.0 and confidence intervals were narrow, it is likely to be a very small association that may have limited clinical significance. Because UPDRS and NMSS scores are continuous variables, differences in scores between different patients can be large or small. Patients with severe symptoms can roughly be considered as more prone to fatigue than patients with very mild symptoms in clinical practice.

Our study also revealed a relationship between EDS and fatigue, which is consistent with the results of previous studies (Stocchi et al., 2014; Siciliano et al., 2018). Nevertheless, there are a few inconsistent findings in our study regarding factors associated with fatigue that should be noted. For example, some studies have shown that poor quality of life, sleep disorders, and depression (Ongre et al., 2021; Ou et al., 2021; Béreau et al., 2022) are related to fatigue, whereas we did

not find an association between fatigue and the patients' PDQ-39 score, PDSS score, the presence of pRBD, or depression as a whole. In order to determine whether the results of related factors are different due to different disease stages, we performed subgroup analyses of correlated factors grouped by disease duration and Hoehn and Yahr stages. We found that the total UPDRS score, NMSS score, PIGD subtype, and the absence of FOG were significantly associated with fatigue in PD patients with disease duration less than or equal to 3 years. The PDSS score was found to be associated with fatigue in patients with a disease course longer than 10 years; however, the OR value was close to 1 with little effect. No relationship was found between fatigue and PDQ-39, pRBD, or depression in each subgroup analysis, which may be ascribed to different inclusion criteria and confounding factors considered in previous studies (Ongre et al., 2021; Ou et al., 2021; Béreau et al., 2022). Our findings also differed from those of previous studies in that we found that the presence of the PIGD subtype and wearing-off were associated with fatigue. The link between fatigue and wearing-off further implicates that dopaminergic factors—either *via* direct dopaminergic neurotransmission or *via* indirect mechanisms—are key for the development of fatigue (Franke and Storch, 2017). Unfortunately, to date, there is no effective treatment for fatigue in patients with PD (Elbers et al., 2016), and rasagiline was only proposed as "possibly useful" (Seppi et al., 2019), deep brain stimulation may help improve fatigue in patients with PD (Lazcano-Ocampo et al., 2021). Therefore, PD patients with fatigue may benefit from the management of motor symptoms, wearing-off, and EDS because they are all associated with fatigue in these patients.

Our study also demonstrated that nearly all PD motor and non-motor symptoms significantly deteriorated over time, and that the occurrence of fatigue in PD was associated with worse baseline findings and faster progression rates, which are consistent with findings from previous studies. For example, data from the Oxford Parkinson's Disease Centre Discovery cohort demonstrated that almost all PD motor and non-motor symptoms measured in the study significantly increased over time (Liu et al., 2021). Other studies have also confirmed the longitudinal progression of both motor and non-motor symptoms, including autonomic dysfunction, EDS, and cognitive impairment (Amara et al., 2017; Simuni et al., 2018; Stanković et al., 2019; Myers et al., 2022). It should be noted that a subset of symptoms have shown stability, relief, and improvement in longitudinal studies (Cilia et al., 2020; Simuni et al., 2022). However, despite these inconsistencies, most studies have reported an overall deterioration of motor and non-motor symptoms, consistent with our data. In the subgroup analysis of our study, the persistent-fatigue group showed significantly greater progression in most symptoms, in comparison with the never-fatigue group. In comparison with the never-fatigue group, the nonpersistent-fatigue group showed more rapid progression in the freezing of gait, pRBD and total SCOPA-AUT score. However, other clinical features (including motor symptoms, wearing-off, dyskinesia, EDS, depression, quality of life and cognitive symptoms) were not significantly different in the evolution of these symptoms between these two groups. This reflected indirectly that the prognosis of patients with non-persistent fatigue was better than that of patients with persistent fatigue in the overall cohort, which further proves that fatigue can aggravate disease progression. Moreover, this suggests that the improvement of fatigue may alleviate motor and other non-motor symptoms to some extent. The results also provide indirect support for the hypothesis that progression during early PD in the persistent fatigue group may be faster than that in the non-persistent fatigue group.

The relationship between treatment and relief or aggravation of fatigue has not been thoroughly studied in the past. The factors influencing fatigue are quite numerous, and may include (in addition to the drugs regime) the amount of physical exercise and physical labor, emotional aspects, and diet, among others (Fu et al., 2016; Ongre et al., 2017; Lin et al., 2021; Ongre et al., 2021). A previous study analyzed factors associated with fatigue improvement, and found that patients with fatigue at baseline received higher doses of dopaminergic medication during follow-up than those without fatigue. Moreover, the study showed that the improvement of fatigue could not necessarily be attributed to changes in disease severity or other non-motor symptoms (such as depressive symptoms, sleep disorder, apathy, or cognitive impairment), and suggested an improved efficacy of dopamine agonists over levodopa in PD patients with fatigue (Ongre et al., 2017). However, the authors of this study did not take into account some additional confounding factors. Rigorous prospective cohort studies, with very strict design, precise group allocation, and with more confounding factors being considered, are needed in the future to further explore the relationship between the drug regime or other alleviating/aggravation factors, and the evolution of fatigue. Proposed pathophysiologic mechanisms of fatigue currently include increased circulating proinflammatory cytokines, dysfunction in nigrostriatal and extrastriatal dopaminergic pathways, involvement of nondopaminergic (particularly serotonergic) pathways, executive/prefrontal pathology, and involvement of the autonomic nervous system (Kluger, 2017; Lazcano-Ocampo et al., 2020). Further longitudinal studies are needed to corroborate our results and to investigate the specific neurobiological pathways related to fatigue in PD. To the best of our knowledge, no other studies have evaluated the longitudinal progression in PD patients with and without fatigue. The above findings suggest that screening for fatigue symptoms at baseline could improve the estimation of the subsequent disease trajectory, enabling better individualized treatment, information, and support to be offered to patients and their caregivers.

This study had some limitations. First, although the 2-year follow-up period was relatively short, we plan to address this by continuing to follow up our cohort of patients. Second, our study involved heterogeneity in clinical data collection and the data quality obtained from different investigators. Nevertheless, all researchers involved in the study received standardized and unified training to ensure consistency and quality of the data as much as possible. Third, PFS-16 was developed to assess a single construct reflecting the physical aspects of fatigue in patients with PD and to measure both the presence of fatigue and its severity. But this scale may not adequately reflect clinically significant non-physical aspects of fatigue and does not define fatigue. However, PFS-16 is a brief and easily completed scale developed specifically for PD, and meets the criteria for the designation of "recommended" as defined by the Movement Disorder Society for screening fatigue (Friedman et al., 2010). Fourth, the study was lacking in biomarkers for the characterization of

fatigue. Future studies combining clinical information and additional variables (i.e., genetics, neuroimaging markers, and other biomarkers) are warranted.

5. Conclusion

Increased disease severity, presence of the PIGD subtype, EDS, and wearing-off were associated with fatigue in patients with PD. Significant subgroup-level differences were observed in the progression of motor and non-motor symptoms across different fatigue subgroups of PD patients.

Data availability statement

The raw data supporting the conclusions of this article will be made available by the authors, without undue reservation.

Ethics statement

The studies involving human participants were reviewed and approved by Ethics Committee of Xiangya Hospital of Central South University. The patients/participants provided their written informed consent to participate in this study.

Author contributions

XZ: research project conception, organization, execution, statistical analysis design and execution of the study, patients' enrollment and follow up, and writing of the first manuscript draft. YX, TS, YZ, and HP: research project execution and patients' enrollment and follow up. QX, YC, QS, XY, JG, and BT: research project organization, execution, and manuscript review and critique. XW: statistical analysis design, execution, review and critique of the study and manuscript review and critique. LL and ZL: research project conception, organization, execution, and manuscript review and critique. All authors contributed to the article and approved the submitted version.

Funding

This study was supported by the Hunan Innovative Province Construction Project (Grant Nos. 2019SK2335 and 2021SK1010), Natural Science Foundation of Hunan Province (Grant No. 2022JJ40843), National Key Research and Development Program of China (Grant Nos. 2021YFC2501204 and 2016YFC306000), National Natural Science Foundation of China (Grant No. 82001359), and Scientific Research Project of Hunan Provincial Health Commission (Grant No. 202203074637).

Acknowledgments

We thank all subjects for their participation, all investigators for their efforts and support in this study. We would like to thank Editage (www.editage.cn) for English language editing.

Conflict of interest

The authors declare that the research was conducted in the absence of any commercial or financial relationships that could be construed as a potential conflict of interest.

Publisher's note

Supplementary material

The Supplementary material for this article can be found online at: https://www.frontiersin.org/articles/10.3389/fnagi.2023.1133705/full#supplementary-material

References

Aarsland, D., Batzu, L., Halliday, G. M., Geurtsen, G. J., Ballard, C., Ray Chaudhuri, K., et al. (2021). Parkinson disease-associated cognitive impairment. *Nat. Rev. Dis. Primers* 7:47. doi: 10.1038/s41572-021-00280-3

Alves, G., Wentzel-Larsen, T., and Larsen, J. P. (2004). Is fatigue an independent and persistent symptom in patients with Parkinson disease? *Neurology* 63, 1908–1911. doi: 10.1212/01.wnl.0000144277.06917.cc

Amara, A. W., Chahine, L. M., Caspell-Garcia, C., Long, J. D., Coffey, C., Högl, B., et al. (2017). Longitudinal assessment of excessive daytime sleepiness in early Parkinson's disease. *J. Neurol. Neurosurg. Psychiatry* 88, 653–662. doi: 10.1136/jnnp-2016-315023

Armstrong, M. J., and Okun, M. S. (2020). Diagnosis and treatment of Parkinson disease: a review. *JAMA* 323, 548–560. doi: 10.1001/jama.2019.22360

Béreau, M., Castrioto, A., Lhommée, E., Maillet, A., Gérazime, A., Bichon, A., et al. (2022). Fatigue in de novo Parkinson's disease: expanding the neuropsychiatric triad? *J. Parkinsons Dis.* 12, 1329–1337. doi: 10.3233/jpd-213116

Bloem, B. R., Okun, M. S., and Klein, C. (2021). Parkinson's disease. *Lancet* 397, 2284–2303. doi: 10.1016/s0140-6736(21)00218-x

Brown, R. G., Dittner, A., Findley, L., and Wessely, S. C. (2005). The Parkinson fatigue scale. *Parkinsonism Relat. Disord.* 11, 49–55. doi: 10.1016/j.parkreldis.2004.07.007

Cilia, R., Cereda, E., Akpalu, A., Sarfo, F. S., Cham, M., Laryea, R., et al. (2020). Natural history of motor symptoms in Parkinson's disease and the long-duration response to levodopa. *Brain* 143, 2490–2501. doi: 10.1093/brain/awaa181

Deng, P., Xu, K., Zhou, X., Xiang, Y., Xu, Q., Sun, Q., et al. (2022). Constructing prediction models for excessive daytime sleepiness by nomogram and machine learning: a large Chinese multicenter cohort study. *Front. Aging Neurosci.* 14:938071. doi: 10.3389/fnagi.2022.938071

Elbers, R. G., Berendse, H. W., and Kwakkel, G. (2016). Treatment of fatigue in Parkinson disease. *JAMA* 315, 2340–2341. doi: 10.1001/jama.2016.5260

Franke, C., and Storch, A. (2017). Nonmotor fluctuations in Parkinson's disease. *Int. Rev. Neurobiol.* 134, 947–971. doi: 10.1016/bs.irn.2017.05.021

Friedman, J. H., Alves, G., Hagell, P., Marinus, J., Marsh, L., Martinez-Martin, P., et al. (2010). Fatigue rating scales critique and recommendations by the movement disorders society task force on rating scales for Parkinson's disease. *Mov. Disord.* 25, 805–822. doi: 10.1002/mds.22989

Friedman, J. H., Beck, J. C., Chou, K. L., Clark, G., Fagundes, C. P., Goetz, C. G., et al. (2016). Fatigue in Parkinson's disease: report from a mutidisciplinary symposium. *NPJ Parkinsons Dis.* 2:15025. doi: 10.1038/npjparkd.2015.25

Fu, R., Luo, X. G., Ren, Y., He, Z. Y., and Lv, H. (2016). Clinical characteristics of fatigued Parkinson's patients and the response to dopaminergic treatment. *Transl. Neurodegener.* 5:9. doi: 10.1186/s40035-016-0056-2

Jankovic, J., McDermott, M., Carter, J., Gauthier, S., Goetz, C., Golbe, L., et al. (1990). Variable expression of Parkinson's disease: a base-line analysis of the DATATOP cohort. The Parkinson Study Group. *Neurology* 40, 1529–1534. doi: 10.1212/wnl.40.10.1529

Kluger, B. M. (2017). Fatigue in Parkinson's disease. *Int. Rev. Neurobiol.* 133, 743–768. doi: 10.1016/bs.irn.2017.05.007

Kluger, B. M., Pedersen, K. F., Tysnes, O. B., Ongre, S. O., Øygarden, B., and Herlofson, K. (2017). Is fatigue associated with cognitive dysfunction in early Parkinson's disease? *Parkinsonism Relat. Disord.* 37, 87–91. doi: 10.1016/j.parkreldis.2017.02.005

Lazcano-Ocampo, C., van Wamelen, D., Samuel, M., Silverdale, M., Rizos, A., Sauerbier, A., et al. (2021). Evaluation of the effect of bilateral subthalamic nucleus deep brain stimulation on fatigue in Parkinson's disease as measured by the non-motor symptoms scale. *Br. J. Neurosurg.* 1-4, 1–4. doi: 10.1080/02688697.2021.1961681

Lazcano-Ocampo, C., Wan, Y. M., van Wamelen, D. J., Batzu, L., Boura, I., Titova, N., et al. (2020). Identifying and responding to fatigue and apathy in Parkinson's disease: a review of current practice. *Expert. Rev. Neurother.* 20, 477–495. doi: 10.1080/14737175.2020.1752669

Lin, I., Edison, B., Mantri, S., Albert, S., Daeschler, M., Kopil, C., et al. (2021). Triggers and alleviating factors for fatigue in Parkinson's disease. *PLoS One* 16:e0245285. doi: 10.1371/journal.pone.0245285

Liu, Y., Lawton, M. A., Lo, C., Bowring, F., Klein, J. C., Querejeta-Coma, A., et al. (2021). Longitudinal changes in Parkinson's disease symptoms with and without rapid eye movement sleep behavior disorder: the Oxford discovery cohort study. *Mov. Disord.* 36, 2821–2832. doi: 10.1002/mds.28763

Liu, Z., Yang, N., Dong, J., Tian, W., Chang, L., Ma, J., et al. (2022). Deficiency in endocannabinoid synthase DAGLB contributes to early onset parkinsonism and murine nigral dopaminergic neuron dysfunction. *Nat. Commun.* 13:3490. doi: 10.1038/s41467-022-31168-9

Lou, J. S., Kearns, G., Benice, T., Oken, B., Sexton, G., and Nutt, J. (2003). Levodopa improves physical fatigue in Parkinson's disease: a double-blind, placebo-controlled, crossover study. *Mov. Disord.* 18, 1108–1114. doi: 10.1002/mds.10505

Myers, P. S., O'Donnell, J. L., Jackson, J. J., Lessov-Schlaggar, C. N., Miller, R. L., Foster, E. R., et al. (2022). Proteinopathy and longitudinal cognitive decline in Parkinson disease. *Neurology* 99, e66–e76. doi: 10.1212/wnl.0000000000200344

Ongre, S. O., Dalen, I., Tysnes, O. B., Alves, G., and Herlofson, K. (2021). Progression of fatigue in Parkinson's disease - a 9-year follow-up. *Eur. J. Neurol.* 28, 108–116. doi: 10.1111/ene.14520

Ongre, S. O., Larsen, J. P., Tysnes, O. B., and Herlofson, K. (2017). Fatigue in early Parkinson's disease: the Norwegian Park west study. *Eur. J. Neurol.* 24, 105–111. doi: 10.1111/ene.13161

Ou, R., Hou, Y., Liu, K., Lin, J., Jiang, Z., Wei, Q., et al. (2021). Progression of fatigue in early Parkinson's disease: a 3-year prospective cohort study. *Front. Aging Neurosci.* 13:701906. doi: 10.3389/fnagi.2021.701906

Postuma, R. B., Berg, D., Stern, M., Poewe, W., Olanow, C. W., Oertel, W., et al. (2015). MDS clinical diagnostic criteria for Parkinson's disease. *Mov. Disord.* 30, 1591–1601. doi: 10.1002/mds.26424

Schapira, A. H. V., Chaudhuri, K. R., and Jenner, P. (2017). Non-motor features of Parkinson disease. *Nat. Rev. Neurosci.* 18, 435–450. doi: 10.1038/nrn.2017.62

Seppi, K., Ray Chaudhuri, K., Coelho, M., Fox, S. H., Katzenschlager, R., Perez Lloret, S., et al. (2019). Update on treatments for nonmotor symptoms of Parkinson's disease-an evidence-based medicine review. *Mov. Disord.* 34, 180–198. doi: 10.1002/mds.27602

Siciliano, M., Trojano, L., Santangelo, G., De Micco, R., Tedeschi, G., and Tessitore, A. (2018). Fatigue in Parkinson's disease: a systematic review and meta-analysis. *Mov. Disord.* 33, 1712–1723. doi: 10.1002/mds.27461

Simuni, T., Caspell-Garcia, C., Coffey, C. S., Weintraub, D., Mollenhauer, B., Lasch, S., et al. (2018). Baseline prevalence and longitudinal evolution of non-motor symptoms in early Parkinson's disease: the PPMI cohort. *J. Neurol. Neurosurg. Psychiatry* 89, 78–88. doi: 10.1136/jnnp-2017-316213

Simuni, T., Merchant, K., Brumm, M. C., Cho, H., Caspell-Garcia, C., Coffey, C. S., et al. (2022). Longitudinal clinical and biomarker characteristics of non-manifesting LRRK2 G2019S carriers in the PPMI cohort. *NPJ Parkinsons Dis.* 8:140. doi: 10.1038/s41531-022-00404-w

Stanković, I., Petrović, I., Pekmezović, T., Marković, V., Stojković, T., Dragašević-Mišković, N., et al. (2019). Longitudinal assessment of autonomic dysfunction in early Parkinson's disease. *Parkinsonism Relat. Disord.* 66, 74–79. doi: 10.1016/j.parkreldis.2019.07.008

Stebbins, G. T., Goetz, C. G., Burn, D. J., Jankovic, J., Khoo, T. K., and Tilley, B. C. (2013). How to identify tremor dominant and postural instability/gait difficulty groups with the movement disorder society unified Parkinson's disease rating scale: comparison with the unified Parkinson's disease rating scale. *Mov. Disord.* 28, 668–670. doi: 10.1002/mds.25383

Stocchi, F., Abbruzzese, G., Ceravolo, R., Cortelli, P., D'Amelio, M., De Pandis, M. F., et al. (2014). Prevalence of fatigue in Parkinson disease and its clinical correlates. *Neurology* 83, 215–220. doi: 10.1212/wnl.0000000000000587

Tomlinson, C. L., Stowe, R., Patel, S., Rick, C., Gray, R., and Clarke, C. E. (2010). Systematic review of levodopa dose equivalency reporting in Parkinson's disease. *Mov. Disord.* 25, 2649–2653. doi: 10.1002/mds.23429

Vickers, A. J., and Altman, D. G. (2001). Statistics notes: Analysing controlled trials with baseline and follow up measurements. *BMJ* 323, 1123–1124. doi: 10.1136/bmj.323.7321.1123

Zhao, Y., Qin, L., Pan, H., Liu, Z., Jiang, L., He, Y., et al. (2020). The role of genetics in Parkinson's disease: a large cohort study in Chinese mainland population. *Brain* 143, 2220–2234. doi: 10.1093/brain/awaa167

Zhou, X., Liu, Z., Zhou, X., Xiang, Y., Zhou, Z., Zhao, Y., et al. (2022). The Chinese Parkinson's disease registry (CPDR): study design and baseline patient characteristics. *Mov. Disord.* 37, 1335–1345. doi: 10.1002/mds.29037

Zhou, Z., Zhou, X., Xiang, Y., Zhao, Y., Pan, H., Wu, J., et al. (2022). Subtyping of early-onset Parkinson's disease using cluster analysis: a large cohort study. *Front. Aging Neurosci.* 14:1040293. doi: 10.3389/fnagi.2022.1040293

Zhou, Z., Zhou, X., Zhou, X., Xiang, Y., Zhu, L., Qin, L., et al. (2021). Characteristics of autonomic dysfunction in Parkinson's disease: a large Chinese multicenter cohort study. *Front. Aging Neurosci.* 13:761044. doi: 10.3389/fnagi.2021.761044

frontiers | Frontiers in Aging Neuroscience

TYPE Mini Review
PUBLISHED 26 May 2023
DOI 10.3389/fnagi.2023.1117068

OPEN ACCESS

EDITED BY
Jiehui Jiang,
Shanghai University, China

REVIEWED BY
Richard Dodel,
University of Duisburg-Essen, Germany
Tobias Blum,
University of Duisburg-Essen, Germany,
in collaboration with reviewer RD

*CORRESPONDENCE
Wei Huang
✉ 13677080198@163.com

RECEIVED 06 December 2022
ACCEPTED 08 May 2023
PUBLISHED 26 May 2023

CITATION
Huang J, Yuan X, Chen L, Hu B, Jiang L, Shi T, Wang H and Huang W (2023) Subjective cognitive decline in patients with Parkinson's disease: an updated review.
Front. Aging Neurosci. 15:1117068.
doi: 10.3389/fnagi.2023.1117068

Subjective cognitive decline in patients with Parkinson's disease: an updated review

Juan Huang[1], Xingxing Yuan[2], Lin Chen[1], Binbin Hu[1], Lijuan Jiang[1], Ting Shi[1], Hui Wang[1] and Wei Huang[1]*

[1]Department of Neurology, Second Affiliated Hospital of Nanchang University, Nanchang, China, [2]Department of Anesthesiology, Changsha Hospital for Maternal and Child Health Care Affiliated to Hunan Normal University, Changsha, China

Cognitive impairment in patients with Parkinson's disease (PD) worsens the prognosis of PD and increases caregivers' burden and economic consequences. Recently, subjective cognitive decline (SCD), which refers to self-reported cognitive decline without detectable objective cognitive dysfunction, has been regarded as an at-risk state of mild cognitive impairment (MCI) and a prodromal stage for dementia in Alzheimer's disease (AD). However, studies on PD-SCD have thus far been scarce, and at present there is no consensus regarding the definition of SCD nor a gold standard as an evaluation tool. The present review aimed to look for an association between PD-SCD and objective cognitive function and found that PD with SCD occurred with brain metabolic changes, which were consistent with early aberrant pathological changes in PD. Moreover, PD patients with SCD were likely to progress to future cognitive impairment. It is necessary to establish a guideline for the definition and evaluation of SCD in PD. A larger sample size and more longitudinal investigations are needed to verify the predictive effectiveness of PD-SCD and to detect earlier subtle cognitive decline before MCI.

KEYWORDS

subjective cognitive decline (SCD), Parkinson's disease, cognitive impairment, objective cognitive function, mild cognitive impairment

Introduction

Cognitive dysfunction, one of the most common non-motor symptoms (NMSs) in Parkinson's disease (PD), is up to six times more common in PD than in the healthy aging population, worsens the prognosis of PD, and increases caregivers' burden and economic consequences (Aarsland et al., 2021). It was estimated that 40–50% of PD presents with mild cognitive impairment (MCI) at baseline, and 75–80% of MCI progresses to dementia in a longitudinal study (Hely et al., 2005; Stuart et al., 2016; Obeso et al., 2017). Recently, the process of cognitive decline in PD patients have received growing interest.

Subjective cognitive decline (SCD) refers to decreases in cognitive capacity without detectable impairment on neuropsychological tests, indicating intact cognitive functions, accompanied by pathological changes, and was believed to be an at-risk state of MCI and a prodromal stage for dementia in Alzheimer's disease (AD) (Reisberg et al., 2008; Jessen, 2010; Scheef et al., 2012; Jessen et al., 2014; Jack et al., 2018; Wirth et al., 2018). A study showed β-amyloid deposition and atrophy as well as brain activation in people with SCD, suggesting a compensatory mechanism, which might reflect early neuronal dysfunction together with memory performance preserved (Saykin et al., 2006; Rodda et al., 2009; Perrotin et al., 2012).

Thus, the state of SCD was recognized as an essential course of AD pathology and a risk factor for cognitive decline (Jessen et al., 2020). Similar to AD, SCD may be an intermediate state between cognitive normality and MCI in PD. Thus, a possible three-stage clinical performance related to cognition might be applicable to patients with PD, with SCD as the prodromal phase, followed by MCI, finally leading to dementia (Erro et al., 2012; Kjeldsen and Damholdt, 2019; Jones et al., 2021; Yoo et al., 2021; Ophey et al., 2022). Neuroimaging study focused on PD patients with SCD (PD-SCD) demonstrated reduced FDG metabolism in the middle frontal, middle temporal, and occipital areas and the angular gyrus of the cortex, which suggested there may be early pathological changes in PD-SCD (Ophey et al., 2022). Follow-up studies showed a significantly higher risk of developing PD-MCI and dementia for patients with PD-SCD compared to PD without SCD at baseline (Erro et al., 2014; Hong et al., 2014b; Galtier et al., 2019; Purri et al., 2020; Jones et al., 2021). However, there are inconsistent results, results just shown a correlation between SCD and depression, anxiety and other related mood features rather than cognitive dysfunction (Lehrner et al., 2014; Santangelo et al., 2014; Baschi et al., 2018; Barbosa et al., 2019). For example, in Barbosa's study, he regarded SCD as subjective cognitive complaints (SCC), and found SCD severity was related to depression (p = 0.026) rather than Montreal Cognitive Assessment (MoCA) scores (p = 0.141) in PD with normal cognition (PD-NC), which suggested clinician to alert affective disorder in PD-SCD (Barbosa et al., 2019). Study led by Baschi defined subjective memory complaints (SMC) as SCD, and results showed PD-SCD was significantly associated with anxiety (OR = 3.93) when compared to PD without SCD (Baschi et al., 2018).

Overall, cognitive impairment in PD is a huge financial burden to society as well as caregivers, and it is time to highlight the importance of identifying cognitive decline as early as possible (Aarsland et al., 2021). However, studies on PD-SCD have thus far been scarce, and there is no consensus regarding the definition of SCD nor is there a gold standard as an evaluation tool. Little is known about whether there is a clear association between SCD and cognitive dysfunction or later cognitive decline in PD.

The review aimed to outline how SCD has been used as a diagnostic criterion in studies on PD as well as to describe the possible correlation related to objective cognitive impairment, help recognize SCD as an at-risk state early indicator and allow clinicians to predict conversion to PD-D more accurately.

Methods

Our aim was to summarize the empirical literature on SCD in patients with PD. We used the following key words: "Parkinson's disease" (PD) and subjective complaints ("subjective cognitive decline" (SCD), "subjective cognitive impairment" (SCI), "subjective memory complaint(s)" (SMC), "subjective 'memory impairment" (SMI), or "subjective cognitive complaint(s)" (SCC) to search related literature in the PubMed, Web of Science, and Embase databases. All study designs and articles written in English from 1 January 1970 to 30 April 2023 were included; additionally, related reference lists were carried expand the literature results. **Table 1** show the detailed summary of included studies.

Results

Definition

Terminologies for SCD

The current available definition of SCD mainly focused on memory in the context of AD (Jessen et al., 2020). Unfortunately, at present there are no uniform definitions of SCD in PD, and researchers have also used the terms SMD (Siciliano et al., 2020), SMI (Song et al., 2014), SMC (Benito-León et al., 2011; Erro et al., 2012; Hong et al., 2012; Uemura et al., 2013; Lehrner et al., 2014; Baschi et al., 2018), SCI (Copeland et al., 2016; Mills et al., 2016; Hogue et al., 2018), or SCC (Dujardin et al., 2010; Santangelo et al., 2014; Koster et al., 2015; Castro et al., 2016; Mills et al., 2016; Dupouy et al., 2018; Hong et al., 2018; AlDakheel et al., 2019; Barbosa et al., 2019; Purri et al., 2020; Chua et al., 2021; Han et al., 2021; Jones et al., 2021; Pan et al., 2021; Xiao et al., 2021) as descriptions.

Assessment tools for SCD

Although patients with PD mainly exhibit severe deficits in executive function, attention and visuospatial function rather than memory (Kehagia et al., 2010), studies have been focused on memory-related questions. "Do you have any memory-related problems?," "Do you feel that your memory and thinking have gotten worse" or "Have you suffered from forgetfulness since the last interview? " were the questions adopted frequently to define SCD (Benito-León et al., 2011; Erro et al., 2012; Hong et al., 2012; Uemura et al., 2013; Hong et al., 2014a,b; Purri et al., 2020; Lee et al., 2020; Jones et al., 2021). Similarly, some studies applied the UPDRSI 1.1 [(1.1) cognitive impairment] to assess SCD (Mills et al., 2016; Hogue et al., 2018; Mills et al., 2020; Han et al., 2021; Xiao et al., 2021; Rosenblum et al., 2022a,b). Song and Castro defined the decreased self-awareness of attention/memory as SCD (Song et al., 2014; Castro et al., 2016). Siciliano adopted Multifactorial Memory Questionnaire (MMQ) to identify patients with SCD (Siciliano et al., 2020). In Rosenblum's study, he classified patients as suspected mild cognitive decline (sMCD) based on UPDRS-Cognitive Functional features score ≥ 1 [the mean score of seven MDS-UPDRS items chosen: (1.1) cognitive impairment, (2.1) speech, (2.4) eating, (2.5) dressing, (2.6) hygiene, (2.7) handwriting, and (2.8) doing hobbies], and regarded sMCD as SCD (Rosenblum et al., 2022a,b). Apart from the above studies measuring SCD by simple questions, other studies utilized questionnaires such as the subjective cognitive decline questionnaire (SCD-Q) (Ophey et al., 2022), Cognitive Complaints Interview (CCI) (Dujardin et al., 2010; Hong et al., 2018; Pan et al., 2021; Yoo et al., 2021), Parkinson's Disease Cognitive Function Rating Scale (PD-CFRS) (Siciliano et al., 2021), Parkinson's Disease Cognitive Questionnaire (PD-CQ) (Santangelo et al., 2014), Forgetfulness Assessment Inventory (FAI) (Lehrner et al., 2014), Non-Motor Symptoms Scale Domain-5 Score (NMSS-5) (Barbosa et al., 2019; Chua et al., 2021; Yang et al., 2022), Informant Questionnaire on Cognitive Decline in the Elderly (IQCODE) (Nakhla et al., 2021), and Self-Rating Scale of Memory Functions (SRMF) (Sitek et al., 2011). Galtier formulated a subjective cognitive decline semi-structured interview that included seven items (Galtier et al., 2019, 2021, 2022). A visual analog scale was applied by Dupouy et al. (2018)

TABLE 1 Detailed summary of the included studies.

References	Measure for SCD	Sample size	Terms for SCD	SCD domains	Design	Relevant results
Ophey et al., 2022	Subjective Cognitive Decline-Questionnaire (SCD-Q)	30 patients with PD	Subjective cognitive decline (SCD)	Memory, attention, language, executive functions, visuo-cognitive skills, social cognition	Cross-sectional	SCD being an early manifestation of future cognitive decline in PD, and early pathological changes in PD
Yang et al., 2022	Non-Motor Symptoms Scale Domain-5 (NMSs-5) Score ≥ 1	139 *de novo* patients with PD	Subjective cognitive decline (SCD)	Memory, attention	Cross-sectional study	Cognitive domains commonly impaired in PD-SCD were memory and attention; PD-SCD was significantly associated with worse HAMD and HAMA scores.
Rosenblum et al., 2022a	UPDRS-Cognitive Functional features ≥ 1	25 patients with suspected mild cognitive decline; 53 patients without suspected mild cognitive decline; 41 controls	Suspected mild cognitive decline (sMCD)	Memory, language, attention, executive function	Cross-sectional study	PD-sMCD shows higher depression and lower executive function and memory
Rosenblum et al., 2022b	UPDRS-Cognitive Functional features ≥ 1	25 patients with suspected of mild cognitive impairment (sMCI)	Suspected mild cognitive impairment (sMCI)	Memory, language, attention, executive function	Longitudinal study (1 year)	Self-reported cognitive decline may be a marker for identifying gradual cognitive ability decline in PD patients
Galtier et al., 2022	Subjective cognitive decline semi-structured interview	46 patients with PD and 20 controls	Subjective cognitive decline (SCD)	Attention, memory, language, visuospatial functions, executive functions	Longitudinal study (7.5 years)	PD-SCD showed a difficulty for action words
Pan et al., 2021	Cognitive Complaints Interview (CCI)	108 newly diagnosed patients with PD	Subjective cognitive complaints (SCCs)	Memory, language, and visuospatial function	Cross-sectional study	SCCs in early PD with different cognitive status appear to have different pathogenicity; attention/working memory of cognitively normal PD patients with SCCs declined.
Bejr-kasem et al., 2021	Informed by the subject, informant and/or judgment of the site investigator	131 *de novo* PD patients	Subjective cognitive decline	Not indicated	Longitudinal study (5 years)	Patients with minor hallucinations are associated with mid-term subjective cognitive decline.
Xiao et al., 2021	MDS-UPDRS-I 1.1 score > 0	134 patients with late-onset PD (LOPD) 198 patients with early-onset PD (EOPD)	Subjective cognitive complaints (SCCs)	Memory, attention, executive function and orientation	Cross-sectional study	SCCs are only associated with mood disorders in patients with LOPD and SCCs may reflect subthreshold cognitive impairment in the patients with EOPD
Han et al., 2021	MDS-UPDRS-I 1.1 score > 0	189 PD patients with normal cognition (PD-NC) 59 PD patients with SCC (PD-SCC) 135 PD patients with mild cognitive impairment (PD-MCI)	Subjective cognitive complaint (SCC)	Memory, attention, executive function and orientation	Longitudinal study (1–7 years)	PD-SCC patients exhibited faster deterioration of depression than PD-NC patients; PD-SCC showed memory dysfunction compared with PD-NC PD-SCC patients exhibited greater reductions in attention and executive function than the PD-NC group.
Yoo et al., 2021	Cognitive Complaints Interview (CCI)	153 drug-naïve and non-demented PD	Self-awareness of cognitive deficits	Memory, language, and visuospatial function	Cross-sectional	Structural connectivity of frontal lobes is closely associated with SCD in PD. Evaluating frontal structural connectivity from PD-SCD will be important in assessing the actual cognitive.
Siciliano et al., 2021	Parkinson's Disease Cognitive Functional Rating Scale (PD-CFRS)	90 non-demented patients with PD	Underestimators based on objective–subjective discrepancy	Self-reported impact of cognitive changes on daily functioning	Cross-sectional	underestimation of cognitive performance in PD was associated with the severity of fatigue and depressive symptoms.

(Continued)

TABLE 1 (Continued)

References	Measure for SCD	Sample size	Terms for SCD	SCD domains	Design	Relevant results
Nakhla et al., 2021	Informant Questionnaire of Cognitive Decline in the Elderly (IQCODE)	139 non-demented patients	informant-based cognitive decline	Learning, delayed recall, language, attention, and executive functioning	Cross-sectional	IQCODE was significantly associated with worse objective performance on global cognition, attention, learning, and executive function except for language or visuospatial function
Jones et al., 2021	A participant and/or informant endorsing "cognitive decline."	483 individuals newly diagnosed with PD	Subjective cognitive complaint (SCC)	Not indicated	Longitudinal study (5 years)	SCC at baseline was not associated with increased risk for future PD-MCI or PDD
Galtier et al., 2021	Subjective cognitive decline semi-structured interview	42 patients with PD and 19 controls	Subjective cognitive decline (SCD)	Attention, memory, language, visuospatial functions, executive functions	Longitudinal study (7.5 years)	PD-SCD patients showed difficulties in vs.-SP functions (executive functions).
Chua et al., 2021	Non-Motor Symptoms Scale Domain-5 (NMSs-5) Score $\geq$ 1.	121 PD patients	Subjective cognitive complaint (SCC)	Memory, attention	Cross-sectional	PD-SCD is highly prevalent and is associated with emotional factors (depression, anxiety, apathy)
Siciliano et al., 2020	Multifactorial Memory Questionnaire (MMQ)	100 patients with PD	Subjective memory decline (SMD)	Memory	Cross-sectional study	There may be a possible shared pathogenic underlying fatigue and SCD in PD patients
Purri et al., 2020	"Do you feel that your memory and thinking have gotten worse?"	153 PD patients with normal cognition	Subjective cognitive complaint (SCC)	Memory	Longitudinal study (4–5 years)	PD-SCD are more likely to progress to cognitive impairment in long term.
Mills et al., 2020	MDS-UPDRS-I 1.1 score > 0	336 patients with early-stage PD	Subjective cognitive complaint (SCC)	Memory, attention, executive function and orientation	Longitudinal study (>3 years)	PD-SCD were associated with development of PD-MCI over 3 years of follow-up
AlDakheel et al., 2019	MDS-UPDRS-I 1.1 score > 0 Neurobehavioral Inventory (NBI) score >0 or a yes response For General Complaint Question (GCQ)	139 non-demented PD patients	Subjective cognitive complaints (SCCs)	Memory, attention, executive function and orientation	Longitudinal study (1–2 years)	There was no correlation found between PD-SCCs and cognitive impairment; There was no predictive value of PD-SCCs over time
Galtier et al., 2019	Subjective cognitive decline semi-structured interview	43 PD patients and 20 controls	Subjective cognitive decline (SCD)	Attention, memory, language, visuospatial functions, executive functions	Longitudinal study (7.5 years)	PD-SCD is a risk factor for progression to dementia
Barbosa et al., 2019	Non-Motor Symptoms Scale Domain-5 (NMSs-5) Score $\geq$ 1.	128 PD patients	Subjective cognitive complaint (SCC)	Memory, attention	Cross-sectional	PD-SCD was found to be related to depression, anxiety and apathy
Hong et al., 2018	Cognitive Complaints Interview (CCI)	148 PD with cognitive normality (CN), 71 PD-MCI, and 31 PDD	Subjective cognitive complaint (SCC)	Memory, language, and visuospatial function	Cross-sectional	PD-SCD was related to depression score and was inversely correlated with cognitive performance
Hogue et al., 2018	MDS-UPDRS-I 1.1 score > 0)	351 drug-naive PD patients	Subjective cognitive impairment (SCI)	Memory, attention, executive function and orientation	Longitudinal study (3-year follow-up.)	There was no relationship between PD-SCD and depression, but PD-SCD had lower process speed and visuospatial functions. at baseline
Dupouy et al., 2018	Visual analog scale (VAS)	70 PD patients	Subjective cognitive complaint (SCC)	Memory, executive functions, spatial orientation, attention, and language	Cross-sectional	There was no relationship between SCD and the results of neuropsychological testing.
Baschi et al., 2018	Memory Assessment Clinics Questionnaire (MAC-Q) score $\geq$ 25	147 PD patients	Subjective memory complaints (SMC)	Memory	Cross-sectional	PD-SCD performs displayed significant lower performance in the MOCA test.
Mills et al., 2016	UPDRSI-1.1 score >0	759 PD patients and 481 controls	Subjective cognitive impairment (SCI)	Memory, attention, executive function and orientation	Cross-sectional	Visuospatial-executive performance and memory had the most significant impact on SCD

(Continued)

TABLE 1 (Continued)

References	Measure for SCD	Sample size	Terms for SCD	SCD domains	Design	Relevant results
Copeland et al., 2016	Existence of any self/informant-reported impairment in 5 cognitive domains	42 patients with PD-MCI	Subjective cognitive impairment (SCI)	Attention, memory, language, visuoperceptual skills, and executive functioning.	Cross-sectional	There was no relation between PD-SCD and cognitive domain
Castro et al., 2016	Existence of any self-reported impairment in memory and/or attention	31 PD without cognitive complaints 21 PD with cognitive complaints 25 controls	Subjective cognitive complaint (SCC)	Attention, memory	Cross-sectional	PD -SCD showed higher scores on HADS PD-without complaints showed poorer cognitive performance.
Koster et al., 2015	A 4-point Likert scale ranging	40 non-demented PD patients and 27 controls	Subjective cognitive complaint (SCC)	Attention, memory, executive functioning and process speed	Cross-sectional	PD-SCD had relationship with attention, executive function, processing speed but not memory
Song et al., 2014	Self-reported memory impairment	30 patients with PD-SCD 47 patients with PD without SCD	Subjective memory impairment (SMI)	Memory	Cross-sectional	PD-SCD group differed PD-without SCD group in MMSE. PD-SCD may be a predictive biomarker of predementia.
Santangelo et al., 2014	Parkinson's Disease Cognitive Questionnaire (PDCQ),	115 non-demented PD patients	Subjective cognitive complaints (SCC)	Attention, memory, language, visuoperceptual skills, and executive functioning	Cross-sectional	PD-SCD had association with depressive symptoms
Lehrner et al., 2014	Forgetfulness Assessment Inventory (FAI)	104 PD patients 248 controls	Subjective memory complaints (SMC)	Memory	Cross-sectional	Memory tests and depression were significantly correlated to SCD.
Hong et al., 2014b	"Do you feel that you have a declining memory?"	49 PD-SCD 23 controls	Subjective cognitive decline (SCD)	Memory	Cross-sectional	PD-SCD showed poorer performance in visual memory and executive functions and cortical thinning in the frontal, parahippocampal, and posterior cortical areas.
Hong et al., 2014a	"Do you feel that you have a declining memory?"	25 PD-SCD 21 PD without SCD	Subjective cognitive decline (SCD)	Memory	Longitudinal study (2.4-year low-up.)	PD-SCD showed more rapid decline in executive and visuospatial functions and was a risk factor for future cognitive decline
Erro et al., 2014	Item 12 of the non-motor symptoms questionnaire	76 newly diagnosed, untreated patients with PD	Subjective memory complaints (SMC)	Memory	Longitudinal study (2-year low-up.)	SCD were able to predict future development of MCI over 2 years
Uemura et al., 2013	Asking subjects about memory problems	105 PD-naMCI 89 PD-aMCI 99 Dementia 320 Control	Subjective memory complaints (SMC)	Memory	Cross-sectional	SCD was associated with significantly higher scores in depressive symptoms
Hong et al., 2012	"Do you have any memory-related problems?"	20 PD-SCD 15 PD without SCD	Subjective memory complaints (SMC)	Memory	Cross-sectional	PD-SCD had significantly decreased executive functions, process speed as well as decreased gray matter density in the anterior cingulate gyrus and right inferior parietal lobule
Sitek et al., 2011	Self-Rating Scale of Memory Functions (SRSMF)	45 PD patients 33 controls	Self-awareness of memory function	Memory	Cross-sectional	SCD was negatively affected by depressive symptoms.
Benito-León et al., 2011	"Do you suffer from forgetfulness since the last interview?"	46 PD patients 138 controls	Subjective memory complaints (SMC)	Memory	Cross-sectional	PD -SCD had prevalence of 58.7%.
Dujardin et al., 2010	Cognitive complaint interviews (CCI)	25 PD-SCD 25 PD without SCD	Subjective cognitive complaints (SCC)	Memory, language, and visuospatial function	Cross-sectional	PD-MCI and PDD are more frequent among PD-SCD

to assess five cognitive domains and helped establish a link between SCD and executive function, language and attention. Koster et al. developed a four-point Likert scale and obtained similar results to those of Koster et al. (2015). Copeland and colleagues took patients as well as their caregivers into account in five cognitive domains, the results showed little agreement between cognitive domains and patients/care partner with subjective reports (Copeland et al., 2016). Bejr-kasem defined patients with SCD according to information informed by the subject, informant and/or judgment of the site investigator, he showed patients with minor hallucinations were associated with mid-term subjective cognitive decline (Bejr-kasem et al., 2021). In order to clarify the relationship between PD-SCD and cognitive performance, AlDakheel adopted 4 methods to measure SCD, MDS-UPDRS-I 1.1 score $>$ 0, Neurobehavioral Inventory (NBI)-subject score $>$0, NBI-contact score $>$0, a yes response for General complaint question (GCQ), and he found there were little agreement between SCD and different methods, and no SCD method was associated with cognitive decline (AlDakheel et al., 2019).

Given that patients with PD manifest major impairments in executive function, attention and visuospatial function, not just memory (Kehagia et al., 2010), it is wise for evaluators to assess SCD with questionnaires/problems/interviews including five domains (memory, attention, executive functions, visuospatial functions, language). The definition of SCD should take the functions of these five domains into account, at the same time, the information provided by informant may be contribute to identify PD-SCD. Further research are required to help exploring the application and value of PD-SCD.

Prevalence

Since there are no guidelines for PD-SCD, researchers have classified PD-SCD differently, and some studies have classified PD-SCD as coexisting with objective impairment. For example, among PD patients in the Dujardin cross-sectional study, 32.22% matched a classification of PD-SCD, of these patients with SCD, 44.83% of PD-SCD met the dementia criteria, of these patients without SCD, just 25.41% met the dementia criteria, suggesting that PD-SCD has a higher probability of manifesting cognitive dysfunction than PD without SCD (Dujardin et al., 2010). Erro reported that approximately 25% of patients with PD underwent SCD, and PD-SCD at baseline may be a risk factor for PD-MCI (Erro et al., 2014). Lehrner studied PD-SCD with FAI and found that 31% of the PD patients reported SCD. Pan showed 30.3% and 12.1% of SCD in PD-MCI, PD-NC, respectively, he found SCD in PD-NC exhibited declined attention/working memory and thought there might be different pathogenicity in SCD with different cognitive status (Pan et al., 2021). Xiao classified patients into early-onset PD (EOPD) and late-onset PD (LOPD), there were 18.66% of EOPD and 24.74% of LOPD reported SCD (Xiao et al., 2021). Siciliano focused on PD with fatigue, and he found the prevalence of SCD was higher in fatigued PD patients when comparing with those with no fatigued (35 vs. 9%) (Siciliano et al., 2020). The PD-SCD evaluated by other studies demonstrated proportions of 32.6% (Baschi et al., 2018), 44.74% (Hogue et al., 2018), 85% (Barbosa et al., 2019), 29.7% (Lee et al., 2020), 23% (Jones et al., 2021), 32.3% (Siciliano et al., 2021), 28.6%, and 30.2% (Galtier et al., 2019, 2021).

Some researchers defined SCD as subjective cognitive impairment without objective cognitive decline. Purri described a 53% incidence of PD-SCD among PD patients with normal cognition and thought PD-SCD may be an indicator of subsequent cognitive impairment (Purri et al., 2020). Hong showed a proportion of 54.3% and found that PD-SCD can predict cognitive decline later (Hong et al., 2014a). Yang found the prevalence of PD-SCD was 28.1% (Yang et al., 2022). Galtier exhibited 30.5% were diagnosed with PD-SCD according to subjective cognitive decline semi-structured interview, and the longitudinal study result showed poor performance in verb naming test in PD-SCD, which suggested the role of linguistic impairment in PD-SCD (Galtier et al., 2022). Other studies demonstrated rates of 16.3% (Lehrner et al., 2014), 22.36% (Hogue et al., 2018), and 27.2% (Baschi et al., 2018).

Above all, there were some variations in the prevalence of PD-SCD among those studies, and the following reasons may be responsible for this. First, different demographic characteristics may contribute to the discrepancy; for example, an older cohort is prone to SCD since cognition declines with age. Second, the tool chosen to assess SCD may also be a factor, and a complete questionnaire may be more accurate than a single item. Third, the definition of SCD used in studies also influenced the results greatly, since PD may have normal memory but impaired planning ability, leading to some people being missed if the focus is only on memory. Finally, a state of anxiety, depression, and apathy in the PD group also accounted for the higher existence of SCD.

Neuroimaging

Although studies on neuroimaging in PD-SCD have been scarce, the existing results are encouraging. In a study of FDG-PET in PD with normal cognition (n = 18 as PD-SCD, n = 12 as PD control), results revealed reduced FDG metabolism in the middle frontal, middle temporal, occipital areas, and angular gyrus of the cortex. These regions may be neural correlates of PD-SCD, and could demonstrate an early pathological change in PD-SCD (Ophey et al., 2022), consistent with the finding of hypometabolism in the middle frontal gyrus and inferior parietal lobule in PD-MCI (Huang et al., 2008). Yoo classified PD patients had both CCI score $>$3 and intact cognition as underestimation of cognitive function, and the group here means to PD-SCD. MRI suggested a close association between the frontal lobes and PD-SCD and thought it important to measure frontal structural connectivity in the early stages of PD (Yoo et al., 2021). Song and colleagues found reduced perfusion in the frontal and inferior temporal cortical regions as well as the anterior cingulate gyrus and thalamus in PD-SCD patients compared to PD patients without SCD, which may provide a potential biomarker of predementia. Other studies by Hong found a decreased gray matter density and cortical thinning in the anterior cingulate gyrus, right inferior parietal lobule and parahippocampal cortices in PD-SCD (Hong et al., 2012, 2014b), suggesting an aberrant PD-related pathology.

The frontal lobe is responsible for executive functions, the temporal area is associated with semantic memory, the anterior cingulate gyrus seems to be relevant to verbal fluency, attention is dominated by the parietal lobe as well as the anterior cingulate

gyrus, and the occipital lobe plays a significant role in visuospatial ability (Mohanty et al., 2007; Hong et al., 2012, 2014b; Song et al., 2014; Ophey et al., 2022). The neuroimaging studies above revealed potential neural correlates that underlie PD-SCD, making PD-SCD a promising group to be emphasized in clinician. However, samples from neuroimaging studies to date are relatively small, and larger sample sizes and longitudinal studies are needed for further validation.

Association with emotion

Because SCD was mainly defined through several subjective questions, the mood features in patients with PD should be taken into account, as we mentioned before. Currently, the relationship between PD-SCD and emotional symptoms was debated, as some studies have described a marked correlation between anxiety, depression or apathy and PD-SCD, while other studies have not shown this. For example, Siciliano et al. (2021) defined underestimators as patients with subjective cognitive complaints but no objective cognitive impairment, they regarded PD-SCD as an underestimator actually and found a positive correlation between underestimator scores and fatigue, depression, and anxiety, suggesting a greater focus on mood features in patients with early PD in the clinical setting. In Yang et al.'s (2022) study, they defined PD-SCD according to NMSs-5 $\geq$ 1, subsequently, they found PD-SCD was associated with worse Hamilton Depression Scale (HAMD) and Hamilton Anxiety Scale (HAMA) scores. Rosenblum et al. (2022a) regarded PD patients with sMCD as PD-SCD, and he found PD-sMCD showed higher depression when compared to those with no suspected. Chua also obtained the association between PD-SCD and emotional factors (depression, anxiety, apathy) (Chua et al., 2021), and other studies also showed association between PD-SCD and emotional factors (Dujardin et al., 2010; Lehrner et al., 2014; Santangelo et al., 2014; Koster et al., 2015; Castro et al., 2016; Baschi et al., 2018; Barbosa et al., 2019; Purri et al., 2020; Han et al., 2021). At the same time, there still remains unclear between PD-SCD and emotions, since some studies showed no relation between these factors (Hong et al., 2012; Dupouy et al., 2018). According to Baschi, emotional disorders may be both a cause and a consequence of PD-SCD; for example, anxiety in individuals with PD-SCD may be caused by their awareness of cognitive function loss (Baschi et al., 2018). This data reinforced the point that when we encounter PD patients with emotional disorders, it is necessary to incorporate this information to further assess objective cognitive functions. Of course, the discrepancy of the results may be related to the methodology, as age, education, duration and severity of PD influenced moods and should be adjusted.

Assessment tools for objective cognitive performance

Studies have chosen complete neuropsychological tests for patients with PD, such as the MoCA/Mini Mental State Examination (MMSE) for global cognition, the semantic fluency/trail making test (TMT) for executive function, the word list verbal learning test for memory, the digit span test (DST)/symbol digits modalities test (SDMT) for attention, the naming test for language, and the Rey-Osterrieth complex figure test (ROCFT) for visuospatial ability. **Table 2** listed detailed information about neuropsychological tests.

Association with objective cognitive functions in cross-sectional study

Lehrner was interested in the relationship between cognitive complaints and cognitive impairment, he found significant correlations between PD-SCD and worse MMSE performance (Lehrner et al., 2014). Hong et al. (2014b) focused PD-SCD on memory impairment, he investigated the cognitive performance and cortical thickness (n = 49 PD-SCD, n = 23 controls), results showed PD-SCD have poorer performance in visual memory and executive functions, which was consistent with cortical thinning in frontal and posterior cortical areas, since frontal and posterior regions responsible for executive function and visual function, respectively. In Song et al.'s (2014) study, PD-SCD group (n = 30) differed PD-without SCD (n = 47) in global cognition measured by MMSE and suggested PD-SCD may be a predictive biomarker on predementia. Nakhla et al. (2021) took informant-based responses into account and measured them by IQCODE and ultimately found that higher scale scores were negatively correlated with objective performance, including attention, executive function, memory and global cognition. Hong et al. (2018) assessed PD-SCD by CCI and suggested that an increasing score was strongly correlated with poorer objective cognitive functions (global cognition and all five cognitive domains) after adjusting for a depressive score. Baschi found a lower MoCA score in PD-SCD patients than in PD patients without SCD (Baschi et al., 2018). Regression models analyzed by Mills et al. (2016) suggested lower scores on memory, executive and visuospatial functions in PD-SCD. Koster et al. (2015) showed that patients with PD have higher proportion of self-reported difficulties in attention and executive functions but not memory. Dujardin reported more objective cognitive dysfunction among PD patients with cognitive complaints than among PD patients without SCD (Dujardin et al., 2010). In a word, studies referred above showed a relationship between SCD and decreased cognitive manifestation, while the remaining reported mixed results (Castro et al., 2016; Copeland et al., 2016; Dupouy et al., 2018). Castro obtained a contradictory conclusion with the above results. In this study, PD with cognitive complaints performed at a higher level, suggesting better cognitive status (Castro et al., 2016). Additionally, Dupouy and Copeland found no association between neither the patient's nor the caregiver's complaints and the patient's objective cognitive manifestation (Copeland et al., 2016; Dupouy et al., 2018).

Attention and executive functions, which have neural correlates with the parietal and frontal lobes, were the most reported to have a strong correlation with the existence of PD-SCD, and these findings were consistent with the pathological changes in the early stage of PD. Some studies also found that PD-SCD was related to memory, and we think the results were affected by the assessed tools used as well as the targeted population. On the one hand, studies defined SCD as self-reported memory complaints, and the association investigated may be memory rather

TABLE 2 Detailed assessment tools about objective cognitive performance.

References	Global cognition	Attention/ working memory	Executive function	Language	Memory	Visuospatial function	Emotional evaluation
Ophey et al., 2022	Mini-Mental State Examination (MMSE); Parkinson Neuropsychometric Dementia Assessment (PANDA); Cognitive Failures Questionnaire (CFQ)	The Digit Span Test (DST)	Wisconsin Card Sorting Test (WCST); Alternating categories sport-fruit	Boston Naming Test (BNT)	Wechsler Memory Scale (WMS)	Block design subset	Beck Depression Inventory (BDI)
Yang et al., 2022	MMSE; Montreal Cognitive Assessment Scale (MoCA).	DST; Trail Making Test A (TMT-A); Stroop Color-Word Test (SCWT)	The Trail Making Test B (TMT-B); Clock Drawing Test (CDT); Animal Fluency Test (AFT)	BNT; the Wechsler Adult Intelligence Scale III (WAIS-III) Similarities Test	Auditory Verbal Learning Test (AVLT); Logical Memory Test (LMT)	Benton's Judgment of Line Orientation Test (JLOT); the Hooper Visual Organization Test (HVOT)	Hamilton Depression Scale (HAMD) Hamilton Anxiety Scale (HAMA)
Rosenblum et al., 2022a	MoCA Parkinson's Disease Cognitive Functional Rating Scale (PD-CFRS)		Daily Living Questionnaire (DLQ)	DLQ	DLQ		BDI
Rosenblum et al., 2022b	MoCA PD-CFRS	TMTA	DLQ TMTB	DLQ	DLQ		BDI
Galtier et al., 2022	MMSE			Action generation test (AGT); Anaphora test (APHT); Center-embedded subordinate clauses test (CESCT)			BDI
Pan et al., 2021	MMSE MoCA	DST TMT-A SCWT	TMT-B CDT VFT	BNT WAIS-III	AVLT LMT	JLOT HVOT	HAMD HAMA
Bejr-kasem et al., 2021	MoCA	Symbol Digit Modalities Test (SDMT)	Semantic fluency test	Letter Number Sequencing (LNS)	Hopkins Verbal Learning Test—Revised (HVLT-R)	JLOT	15-item Geriatric Depression Scale (GDS-15); State–Trait Anxiety Inventory (STAI)
Xiao et al., 2021	MoCA						HAMD HAMA
Han et al., 2021	MMSE	SDMT TMT-A	CWT; TMT-B	BNT AFT	AVLT; the Rey-Osterrieth Complex Figure Test (ROCFT)	CFT CDT	BDI
Yoo et al., 2021	MMSE						BDI
Siciliano et al., 2021	MoCA PD-CFRS						BDI; Parkinson Anxiety Scale (PAS); Apathy Evaluation Scale (AES)
Nakhla et al., 2021	An average of the six mentioned composites	Adaptive Digit; Ordering Test–Total; California Verbal Learning Test-II (CVLT-II); D-KEFS CWIT–Color Naming Condition	WCST–Perseverative Responses; D-KEFS CWIT–Inhibition/ Switching Condition;	D-KEFS Verbal Fluency–Category; Fluency Total Correct;	CVLT-II; LMT; WMS-III Visual Reproduction II	JLOT; WMS-III Visual Reproduction–Copy	GDS
Jones et al., 2021	MoCA	SDMT	AFT; LNS		HVLT	JOLT	

(Continued)

TABLE 2 (Continued)

References	Global cognition	Attention/ working memory	Executive function	Language	Memory	Visuospatial function	Emotional evaluation
Galtier et al., 2021	MMSE					JLOT; Facial Recognition Test (FRT); Block design subset	BDI
Chua et al., 2021	MMSE MoCA	WMS-IV Symbol Span; WAIS-IV Digit Span	Fruit fluency tests, frontal assessment battery	BNT; WMS-IV similarities	Alzheimer's Disease Assessment Scale-Cognitive (ADAS-Cog); ROCF	JLOT Rey-Osterrieth Complex Figure (ROCF) Copy	GDS Apathy Scale (AS); Hospital Anxiety and Depression Scale for Anxiety (HADS-A)
Siciliano et al., 2020	PD-Cognitive rating scale						BDI PAS AES
Purri et al., 2020	MoCA Mattis Dementia Rating Scale-2 (MDRS-2)	TMT-A SDMT	LNS phonemic verbal fluency; semantic verbal fluency (animals) TMT-B	BNT	HVLT-R	JLOT; CDT	GDS-15
Mills et al., 2020	MoCA						BDI
AlDakheel et al., 2019	MMSE	Delis Kaplan Executive Function System (DKEFS) Color Word; Interference Color Naming test WMS-III letter-number sequencing test,	Visual Verbal Test TMT-B	DKEFS Verbal Fluency; Category Fluency test; BNT	RCFT; CVLT-II	JLOT; Copy Trial of the RCFT	
Galtier et al., 2019	MMSE	DST	WCST (categories) letter fluency		CVLT; Spatial Recall Test (SRT)	JLOT; Block design	BDI
Barbosa et al., 2019	MoCA						Hospital Anxiety and Depression Scale (HADS); Apathy Scale.
Hong et al., 2018	Korean version of the Mini Mental State Examination (K-MMSE) Korean version of the Montreal Cognitive Assessment (K-MoCA)	TMT-A DST	Semantic fluency (animal); CDT	K-BNT; Word similarity	Delayed recall in Seoul Verbal Learning Test (SVLT)/RCFT	Copying task of RCFT; Clock copying (CLOX2)	BDI
Hogue et al., 2018		SDMT WAIS- III Letter Number Sequencing subtest	Letter number sequencing	Semantic fluency (animals)	HVLT	JLOT	GDS-15
Dupouy et al., 2018	MATTIS dementia rating scale.	TMT (B-A) SCWT, SDMT; Digit span; Benton visual retention test	WAIS-III-SDMT; semantic/ phonemic verbal fluencies	Semantic/phonemic verbal fluencies; the ExaDé confrontation naming test	free and cued selective reminding test (FCSRT); RCFT	RCFT; Visual Object and Space Perception Battery (VOSP)	Hamilton Anxiety and Depression Scale(HADS)
Baschi et al., 2018	MMSE MoCA	Visual search TMT-A	Frontal Assessment Battery Raven Colored Progressive Matrices	Aachener Aphasie Test naming; Token Test;	Rey Auditory Verbal Learning Test (R-AVLT); Story Recall Test	Constructional Apraxia; CDT	HADS
Mills et al., 2016	MoCA						

(Continued)

TABLE 2 (Continued)

References	Global cognition	Attention/ working memory	Executive function	Language	Memory	Visuospatial function	Emotional evaluation
Copeland et al., 2016		WMS–III DST; TMT-A	WCST; SCWT Interference Task score	BNT; semantic fluency (Animals)	Visuospatial Memory Test; HVLTR; LMT	JLOT; HVOT	
Castro et al., 2016	Parkinson's disease–cognition (SCOPA-COG)		TMT-B	Phonemic verbal fluency; BNT		CDT	Hospital anxiety and depression scale (HADS) BDI
Koster et al., 2015		SCWT; DST; SDMT	Letter Fluency; Letter-Number Sequencing	Animal fluency		CVLT-II	Minnesota Multiphasic Personality Inventory-2 Depression/ Psychasthenia
Song et al., 2014	MMSE						
Santangelo et al., 2014	MoCA						BDI
Lehrner et al., 2014	MMSE	TMT-(B-A)	TMT-A SCWT	Modified Boston Naming Test (mBNT); Semantic verbal fluency	Verbal Selective Reminding Test (VSRT)		BDI
Hong et al., 2014b	K-MMSE	DST; SCWT	Phonemic fluency Semantic fluency	k-BNT	SVLT; Visual memory	RCFT copy	BDI
Hong et al., 2014a	K-MMSE	DST; SCWT	Phonemic fluency Semantic fluency	k-BNT	SVLT; Visual memory	RCFT copy	BDI
Erro et al., 2014		Frontal assessment battery; TMT (B-A)	TMTB; SCWT; Phonological/ semantic fluency task		R-AVLT	JLOT; CDT	HADS
Uemura et al., 2013	MMSE						GDS-15
Hong et al., 2012	k-MMSE	DST	Go-no-go test Contrasting program	K-BNT	SVLT	RCFT	BDI
Sitek et al., 2011	MMSE	SCWT			AVLT		BDI
Benito-León et al., 2011	37-item version of MMSE		TMT	Animals/fruits Naming test	Story recall test		
Dujardin et al., 2010	MMSE	DST; SCWTt	Letter/number sequencing	Word-generation task	Buschke 16-item recall test Free recall		Montgomery and Asberg depression rating scale (MADRS)

than other domains. On the other hand, studies comparing PD-SCD and PD-MCI concurrently may increase the correlation with one another. Dupouy and Copeland found no association between SCD and objective cognitive performance, which may be due to the assessment used or the psychiatric symptoms among their cohort. Overall, the association between SCD and objective cognitive performance remains unclear now. SCD are subjective and may be influenced by countless factors and the conflicting results obtained can be associated with measurements of cognitive status, definition of SCD, sample size, study design and so on. Thus, it is difficult to show a clear relationship between the two, especially when the methods applied are not precise or extensive enough to evaluate SCD or objective cognitive functions.

Association with objective cognitive functions in longitudinal study

In Jones et al.'s (2021) study (n = 483 PD patients), a single item was used to assess PD-SCD, and the results revealed no relation

between PD-SCD at baseline and PD-MCI/PDD 5 years later. A longitudinal study (n = 139 non-demented PD patients) adopted 4 methods to elicit PD-SCD, it explored the link between PD-SCD and cognitive performance subsequently, results here showed there was no correlation between PD-SCD and cognitive decline and no predictive value of PD-SCD over time (1–2 years) (AlDakheel et al., 2019). Conversely, a follow-up study by Galtier suggested that PD-SCD patients (36.4%) are at higher risk of converting to dementia than PD without SCD (14.3%) 7.5 years later, and the PD-SCD group showed impairments in visuospatial and visuoperceptual functions, which was linked to thinning of posterior cortices (Galtier et al., 2021), at the same time, PD-SCD showed poor performance in verb naming test in the same longitudinal study (n = 46 PD, n = 20 controls), which suggested the possible linguistic dysfunction in PD-SCD (Galtier et al., 2022). Rosenblum followed up PD-sMCD (n = 25) and found self-reported cognitive decline may be a marker for predicting cognitive ability decline after 1 year (Rosenblum et al., 2022b). Han and colleagues regarded PD-SCD as an intermediate status of PD-NC and PD-MCI, they divided people into three groups: PD-NC (n = 189), PD-SCD (n = 59), PD-MCI (n = 135), the longitudinal study (1–7.5 years) found PD-SCD showed memory impairment and greater reductions in attention and executive function compared with PD-NC, which suggested PD-SCD may be high risk individuals progression to cognitive decline later (Han et al., 2021), and the results were similar to Hong's and Purri's study (Hong et al., 2014a; Purri et al., 2020). In Purri's study (n = 153 PD patients with normal cognition), they defined PS-SCD as subjective cognitive complaints with objective cognitive normality and found that the PD-SCD group performed worse on global cognition, executive function and processing speed than the PD without SCD group. Additionally, PD-SCD more easily converted cognitive impairment longitudinally, indicating that PD-SCD may be a warning of subtle cognitive decline (Purri et al., 2020). A larger longitudinal study (n = 336 patients with PD) led by Mills et al. (2020) showed that PD-SCD patients were more likely to develop PD-MCI over 3 years of follow-up and can be used to predict future cognitive impairment, which was similar to other studies (Hong et al., 2014a; Galtier et al., 2019). In Hong et al.'s (2014a) study, the findings were consistent with the conclusion that PD-SCD may be a risk factor for future cognitive dysfunction, since their results showed that PD-SCD could predict progression to decreased cognition 1–4 years later. Erro et al. (2014) also focused on the power of PD-SCD to predict further cognitive decline, he found patients with subjective memory decline at baseline (n = 76) were independent predictor, which can predict the progression to MCI with 2 years longitudinal study, Hogue et al.'s (2018) conclusion was similar to Erro, he created a regression model included SCD in baseline, and the model can predict future cognitive decline, which showed encouraging predictive value of PD-SCD.

In summary, the majority of the above studies considered PD-SCD to be risk factor for impaired objective cognition, and PD-SCD may be a potential way to identify early cognitive decline. However, some problems should be noted. Most studies evaluated PD-SCD with a single item partly concerned with memory, which could eventually influence the results, thus, assessing PD-SCD according to more comprehensive cognitive domains may contribute to the consistency of subjects selected. Secondly, emotional factors should be emphasized and adjusted when exploring the correlation between cognitive performance and PD-SCD, because emotional factors influenced cognitive function and may be linked with PD-SCD, which interfered the results. Thirdly, it may be potential way to associate longitudinal study with more neuroimaging researches in PD-SCD.

Conclusion

Subjective cognitive decline has been gaining increasing interest in recent years. Most of the results reported that patients with PD-SCD had a correlation with objective cognitive decline, and longitudinal studies also revealed a predictive risk for future cognitive dysfunction. Neuroimaging supported the above studies in terms of neural correlates as well as brain metabolism.

However, there are still some problems that need to be solved as soon as possible. First, it is necessary to establish a consensus on PD with SCD. According to the SCD consensus on patients with AD, we recommend that the definition of PD-SCD should be purely self/informant-reported cognitive decline, and this definition may contribute to proving a pre-MCI stage of subtle cognitive decline. Next, studies used different methods to evaluate SCD, and assessments of SCD ranged from a single item to several face-to-face questions and a complete questionnaire. Given the specific characteristics of cognitive impairment in PD, a questionnaire including all five domains should be adopted. Additionally, information derived from caregivers may be useful to detect PD-SCD. Finally, the sample size should be larger, and more longitudinal investigations are needed to verify the predictive effectiveness of PD-SCD.

Overall, a clear definition of PD-SCD would help identify earlier stages of cognitive impairment before PD-MCI, explore more risk factors associated with the existence of PD-SCD and allow for early attention and intervention in subtle cognitive decline stages, which may ultimately reduce the burden of cognitive impairment on society and caregivers.

Author contributions

JH had the idea for the manuscript. WH critically revised the work. All authors contributed to the study conception and design, performed the literature search, data analysis, and drafted the manuscript.

Funding

This work was supported by the Clinical Research Project of the Second Affiliated Hospital of Nanchang University, 2021efyC03.

Conflict of interest

The authors declare that the research was conducted in the absence of any commercial or financial relationships that could be construed as a potential conflict of interest.

Publisher's note

References

Aarsland, D., Batzu, L., Halliday, G. M., Geurtsen, G. J., Ballard, C., Ray Chaudhuri, K., et al. (2021). Parkinson disease-associated cognitive impairment. *Nat. Rev. Dis. Primers* 7:47. doi: 10.1038/s41572-021-00280-3

AlDakheel, A., Gasca-Salas, C., Armstrong, M. J., Duff-Canning, S., and Marras, C. (2019). Cognitive complaints in nondemented Parkinson's disease patients and their close contacts do not predict worse cognitive outcome. *Alzheimer Dis. Assoc. Disord.* 33, 147–153. doi: 10.1097/WAD.0000000000000301

Barbosa, R. P., Mendonça, M. D., Caetano, A. P., Lampreia, T. M., Miguel, R., and Bugalho, P. M. (2019). Cognitive complaints in Parkinson's disease patients: from subjective cognitive complaints to dementia and affective disorders. *J. Neural Transm.* 126, 1329–1335. doi: 10.1007/s00702-019-02042-8

Baschi, R., Nicoletti, A., Restivo, V., Recca, D., Zappia, M., and Monastero, R. (2018). Frequency and correlates of subjective memory complaints in Parkinson's disease with and without mild cognitive impairment: data from the Parkinson's disease cognitive impairment study. *J. Alzheimers Dis.* 63, 1015–1024. doi: 10.3233/JAD-171172

Bejr-kasem, H., Sampedro, F., Marín-Lahoz, J., Martínez-Horta, S., Pagonabarraga, J., and Kulisevsky, J. (2021). Minor hallucinations reflect early gray matter loss and predict subjective cognitive decline in Parkinson's disease. *Eur. J. Neurol.* 28, 438–447. doi: 10.1111/ene.14576

Benito-León, J., Louis, E. D., Posada, I. J., Sánchez-Ferro, Á, Trincado, R., Villarejo, A., et al. (2011). Population-based case–control study of cognitive function in early Parkinson's disease (NEDICES). *J. Neurol. Sci.* 310, 176–182. doi: 10.1016/j.jns.2011.06.054

Castro, P. C. F., Aquino, C. C., Felício, A. C., Doná, F., Medeiros, L. M. I., Silva, S. M. C. A., et al. (2016). Presence or absence of cognitive complaints in Parkinson's disease: mood disorder or anosognosia? *Arq. Neuropsiquiatr.* 74, 439–444. doi: 10.1590/0004-282x20160060

Chua, C. Y., Koh, M. R. E., Chia, N. S.-Y., Ng, S. Y.-E., Saffari, S. E., Wen, M.-C., et al. (2021). Subjective cognitive Complaints in early Parkinson's disease patients with normal cognition are associated with affective symptoms. *Parkinsonism Relat. Disord.* 82, 24–28. doi: 10.1016/j.parkreldis.2020.11.013

Copeland, J. N., Lieberman, A., Oravivattanakul, S., and Tröster, A. I. (2016). Accuracy of patient and care partner identification of cognitive impairments in Parkinson's disease-mild cognitive impairment: accuracy of patient and care partner identification. *Mov. Disord.* 31, 693–698. doi: 10.1002/mds.26619

Dujardin, K., Duhamel, A., Delliaux, M., Thomas-Antérion, C., Destée, A., and Defebvre, L. (2010). Cognitive complaints in Parkinson's disease: its relationship with objective cognitive decline. *J. Neurol.* 257, 79–84. doi: 10.1007/s00415-009-5268-2

Dupouy, J., Ory-Magne, F., Mekies, C., Rousseau, V., Puel, M., Rerat, K., et al. (2018). Cognitive complaint in early Parkinson's disease: a pilot study. *Acta Neurol. Scand.* 137, 59–66. doi: 10.1111/ane.12808

Erro, R., Santangelo, G., Barone, P., Picillo, M., Amboni, M., Longo, K., et al. (2014). Do subjective memory complaints herald the onset of mild cognitive impairment in Parkinson disease? *J. Geriatr. Psychiatry Neurol.* 27, 276–281. doi: 10.1177/0891988714532015

Erro, R., Santangelo, G., Picillo, M., Vitale, C., Amboni, M., Longo, K., et al. (2012). Link between non-motor symptoms and cognitive dysfunctions in de novo, drug-naive PD patients. *J. Neurol.* 259, 1808–1813. doi: 10.1007/s00415-011-6407-0

Galtier, I., Nieto, A., Lorenzo, J. N., and Barroso, J. (2019). Subjective cognitive decline and progression to dementia in Parkinson's disease: a long-term follow-up study. *J. Neurol.* 266, 745–754. doi: 10.1007/s00415-019-09197-0

Galtier, I., Nieto, A., Mata, M., Lorenzo, J. N., and Barroso, J. (2021). Analyses of visuospatial and visuoperceptual errors as predictors of dementia in Parkinson's disease patients with subjective cognitive decline and mild cognitive impairment. *J. Int. Neuropsychol. Soc.* 27, 722–732. doi: 10.1017/S1355617720001216

Galtier, I., Nieto, A., Mata, M., Lorenzo, J. N., and Barroso, J. (2022). Specific pattern of linguistic impairment in Parkinson's disease patients with subjective cognitive decline and mild cognitive impairment predicts dementia. *J. Int. Neuropsychol. Soc.* 13, 1–9. doi: 10.1017/S1355617722000571

Han, L., Wang, L., Xu, Z., Liang, X., Zhang, M., Fan, Y., et al. (2021). Disease progression in Parkinson's disease patients with subjective cognitive complaint. *Ann. Clin. Transl. Neurol.* 8, 2096–2104. doi: 10.1002/acn3.51461

Hely, M. A., Morris, J. G. L., Reid, W. G. J., and Trafficante, R. (2005). Sydney multicenter study of Parkinson's disease: non- L -dopa–responsive problems dominate at 15 years. *Mov. Disord.* 20, 190–199. doi: 10.1002/mds.20324

Hogue, O., Fernandez, H. H., and Floden, D. P. (2018). Predicting early cognitive decline in newly-diagnosed Parkinson's patients: a practical model. *Parkinsonism Relat. Disord.* 56, 70–75. doi: 10.1016/j.parkreldis.2018.06.031

Hong, J. Y., Lee, J. E., Sohn, Y. H., and Lee, P. H. (2012). Neurocognitive and atrophic patterns in Parkinson's disease based on subjective memory complaints. *J. Neurol.* 259, 1706–1712. doi: 10.1007/s00415-011-6404-3

Hong, J. Y., Lee, Y., Sunwoo, M. K., Sohn, Y. H., and Lee, P. H. (2018). Subjective cognitive complaints and objective cognitive impairment in Parkinson's disease. *J. Clin. Neurol. Seoul Korea* 14, 16–21. doi: 10.3988/jcn.2018.14.1.16

Hong, J. Y., Yun, H. J., Sunwoo, M. K., Ham, J. H., Lee, J.-M., Sohn, Y. H., et al. (2014b). Cognitive and cortical thinning patterns of subjective cognitive decline in patients with and without Parkinson's disease. *Parkinsonism Relat. Disord.* 20, 999–1003. doi: 10.1016/j.parkreldis.2014.06.011

Hong, J. Y., Sunwoo, M. K., Chung, S. J., Ham, J. H., Lee, J. E., Sohn, Y. H., et al. (2014a). Subjective cognitive decline predicts future deterioration in cognitively normal patients with Parkinson's disease. *Neurobiol. Aging* 35, 1739–1743. doi: 10.1016/j.neurobiolaging.2013.11.017

Huang, C., Mattis, P., Perrine, K., Brown, N., Dhawan, V., and Eidelberg, D. (2008). Metabolic abnormalities associated with mild cognitive impairment in Parkinson disease. *Neurology* 70, 1470–1477. doi: 10.1212/01.wnl.0000304050.05332.9c

Jack, C. R., Bennett, D. A., Blennow, K., Carrillo, M. C., Dunn, B., Haeberlein, S. B., et al. (2018). NIA-AA research framework: toward a biological definition of Alzheimer's disease. *Alzheimers Dement. J. Alzheimers Assoc.* 14, 535–562. doi: 10.1016/j.jalz.2018.02.018

Jessen, F. (2010). Prediction of dementia by subjective memory impairment effects of severity and temporal association with cognitive impairment dementia and subjective memory impairment. *Arch. Gen. Psychiatry* 67:414. doi: 10.1001/archgenpsychiatry.2010.30

Jessen, F., Amariglio, R. E., Buckley, R. F., van der Flier, W. M., Han, Y., Molinuevo, J. L., et al. (2020). The characterisation of subjective cognitive decline. *Lancet Neurol.* 19, 271–278. doi: 10.1016/S1474-4422(19)30368-0

Jessen, F., Wolfsgruber, S., Wiese, B., Bickel, H., Mösch, E., Kaduszkiewicz, H., et al. (2014). AD dementia risk in late MCI, in early MCI, and in subjective memory impairment. *Alzheimers Dement.* 10, 76–83. doi: 10.1016/j.jalz.2012.09.017

Jones, J. D., Uribe, C., Bunch, J., and Thomas, K. R. (2021). Beyond PD-MCI: objectively defined subtle cognitive decline predicts future cognitive and functional changes. *J. Neurol.* 268, 337–345. doi: 10.1007/s00415-020-10163-4

Kehagia, A. A., Barker, R. A., and Robbins, T. W. (2010). Neuropsychological and clinical heterogeneity of cognitive impairment and dementia in patients with Parkinson's disease. *Lancet Neurol.* 9, 1200–1213. doi: 10.1016/S1474-4422(10)70212-X

Kjeldsen, P. L., and Damholdt, M. F. (2019). Subjective cognitive complaints in patients with Parkinson's disease. *Acta Neurol. Scand.* 140, 375–389. doi: 10.1111/ane.13158

Koster, D. P., Higginson, C. I., MacDougall, E. E., Wheelock, V. L., and Sigvardt, K. A. (2015). Subjective cognitive complaints in parkinson disease without dementia: a preliminary study. *Appl. Neuropsychol. Adult* 22, 287–292. doi: 10.1080/23279095.2014.925902

Lee, J. E., Ju, Y. J., Chun, K. H., and Lee, S. Y. (2020). The frequency of sleep medication use and the risk of subjective cognitive decline (SCD) or SCD with functional difficulties in elderly individuals without dementia. *J. Gerontol. Ser. A* 75, 1693–1698. doi: 10.1093/gerona/glz269

Lehrner, J., Moser, D., Klug, S., Gleiß, A., Auff, E., Pirker, W., et al. (2014). Subjective memory complaints, depressive symptoms and cognition in Parkinson's disease patients. *Eur. J. Neurol.* 21, 1276–e77. doi: 10.1111/ene.12470

Mills, K. A., Mari, Z., Pontone, G. M., Pantelyat, A., Zhang, A., Yoritomo, N., et al. (2016). Cognitive impairment in Parkinson's disease: association between patient-reported and clinically measured outcomes. *Parkinsonism Relat. Disord.* 33, 107–114. doi: 10.1016/j.parkreldis.2016.09.025

Mills, K. A., Schneider, R. B., Saint-Hilaire, M., Ross, G. W., Hauser, R. A., Lang, A. E., et al. (2020). Cognitive impairment in Parkinson's disease: associations between subjective and objective cognitive decline in a large longitudinal study. *Parkinsonism Relat. Disord.* 80, 127–132. doi: 10.1016/j.parkreldis.2020.09.028

Mohanty, A., Engels, A. S., Herrington, J. D., Heller, W., Ringo Ho, M.-H., Banich, M. T., et al. (2007). Differential engagement of anterior cingulate cortex subdivisions for cognitive and emotional function. *Psychophysiology* 44, 343–351. doi: 10.1111/j.1469-8986.2007.00515.x

Nakhla, M. Z., Holiday, K. A., Filoteo, J. V., Zlatar, Z. Z., Malcarne, V. L., Lessig, S., et al. (2021). Informant-reported cognitive decline is associated with objective cognitive performance in Parkinson's disease. *J. Int. Neuropsychol. Soc.* 27, 439–449. doi: 10.1017/S1355617720001137

Obeso, J. A., Stamelou, M., Goetz, C. G., Poewe, W., Lang, A. E., Weintraub, D., et al. (2017). Past, present, and future of Parkinson's disease: a special essay on the 200th anniversary of the shaking palsy. *Mov. Disord. Off. J. Mov. Disord. Soc.* 32, 1264–1310. doi: 10.1002/mds.27115

Ophey, A., Krohm, F., Kalbe, E., Greuel, A., Drzezga, A., Tittgemeyer, M., et al. (2022). Neural correlates and predictors of subjective cognitive decline in patients with Parkinson's disease. *Neurol. Sci.* 43, 3153–3163. doi: 10.1007/s10072-021-05734-w

Pan, C., Ren, J., Hua, P., Yan, L., Yu, M., Wang, Y., et al. (2021). Subjective cognitive complaints in newly-diagnosed Parkinson's disease with and without mild cognitive impairment. *Front. Neurosci.* 15:761817. doi: 10.3389/fnins.2021.761817

Perrotin, A., Mormino, E. C., Madison, C. M., Hayenga, A. O., and Jagust, W. J. (2012). Subjective cognition and amyloid deposition imaging: a Pittsburgh Compound B positron emission tomography study in normal elderly individuals. *Arch. Neurol.* 69, 223–229. doi: 10.1001/archneurol.2011.666

Purri, R., Brennan, L., Rick, J., Xie, S. X., Deck, B. L., Chahine, L. M., et al. (2020). Subjective cognitive complaint in Parkinson disease patients with normal cognition: canary in the coal mine? *Mov. Disord. Off. J. Mov. Disord. Soc.* 35, 1618–1625. doi: 10.1002/mds.28115

Reisberg, B., Prichep, L., Mosconi, L., John, E. R., Glodzik-Sobanska, L., Boksay, I., et al. (2008). The pre–mild cognitive impairment, subjective cognitive impairment stage of Alzheimer's disease. *Alzheimers Dement.* 4, S98–S108. doi: 10.1016/j.jalz.2007.11.017

Rodda, J. E., Dannhauser, T. M., Cutinha, D. J., Shergill, S. S., and Walker, Z. (2009). Subjective cognitive impairment: increased prefrontal cortex activation compared to controls during an encoding task. *Int. J. Geriatr. Psychiatry* 24, 865–874. doi: 10.1002/gps.2207

Rosenblum, S., Meyer, S., Richardson, A., and Hassin-Baer, S. (2022a). Capturing subjective mild cognitive decline in Parkinson's disease. *Brain Sci.* 12:741. doi: 10.3390/brainsci12060741

Rosenblum, S., Meyer, S., Richardson, A., and Hassin-Baer, S. (2022b). Early identification of subjective cognitive functional decline among patients with Parkinson's disease: a longitudinal pilot study. *Sci. Rep.* 12:22242. doi: 10.1038/s41598-022-26280-1

Santangelo, G., Vitale, C., Trojano, L., Angrisano, M. G., Picillo, M., Errico, D., et al. (2014). Subthreshold depression and subjective cognitive complaints in Parkinson's disease. *Eur. J. Neurol.* 21, 541–544. doi: 10.1111/ene.12219

Saykin, A. J., Wishart, H. A., Rabin, L. A., Santulli, R. B., Flashman, L. A., West, J. D., et al. (2006). Older adults with cognitive complaints show brain atrophy similar to that of amnestic MCI. *Neurology* 67, 834–842. doi: 10.1212/01.wnl.0000234032.77541.a2

Scheef, L., Spottke, A., Daerr, M., Joe, A., Striepens, N., Kolsch, H., et al. (2012). Glucose metabolism, gray matter structure, and memory decline in subjective memory impairment. *Neurology* 79, 1332–1339. doi: 10.1212/WNL.0b013e31826c1a8d

Siciliano, M., Trojano, L., De Micco, R., Russo, A., Tedeschi, G., and Tessitore, A. (2020). Subjective memory decline in Parkinson's disease patients with and without fatigue. *Parkinsonism Relat. Disord.* 70, 15–19. doi: 10.1016/j.parkreldis.2019.11.017

Siciliano, M., Trojano, L., De Micco, R., Sant'Elia, V., Giordano, A., Russo, A., et al. (2021). Correlates of the discrepancy between objective and subjective cognitive functioning in non-demented patients with Parkinson's disease. *J. Neurol.* 268, 3444–3455. doi: 10.1007/s00415-021-10519-4

Sitek, E. J., Sołtan, W., Wieczorek, D., Robowski, P., and Sławek, J. (2011). Self-awareness of memory function in Parkinson's disease in relation to mood and symptom severity. *Aging Ment. Health* 15, 150–156. doi: 10.1080/13607863.2010.508773

Song, I.-U., Kim, J.-S., Chung, S.-W., Lee, K.-S., Oh, J.-K., and Chung, Y.-A. (2014). Early detection of subjective memory impairment in Parkinson's disease using cerebral perfusion SPECT. *Biomed. Mater. Eng.* 24, 3405–3410. doi: 10.3233/BME-141164

Stuart, S., Lord, S., Hill, E., and Rochester, L. (2016). Gait in Parkinson's disease: a visuo-cognitive challenge. *Neurosci. Biobehav. Rev.* 62, 76–88. doi: 10.1016/j.neubiorev.2016.01.002

Uemura, Y., Wada-Isoe, K., Nakashita, S., and Nakashima, K. (2013). Depression and cognitive impairment in patients with mild parkinsonian signs. *Acta Neurol. Scand.* 128, 153–159. doi: 10.1111/ane.12089

Wirth, M., Bejanin, A., La Joie, R., Arenaza-Urquijo, E. M., Gonneaud, J., Landeau, B., et al. (2018). Regional patterns of gray matter volume, hypometabolism, and beta-amyloid in groups at risk of Alzheimer's disease. *Neurobiol. Aging* 63, 140–151. doi: 10.1016/j.neurobiolaging.2017.10.023

Xiao, Y., Ou, R., Yang, T., Liu, K., Wei, Q., Hou, Y., et al. (2021). Different associated factors of subjective cognitive complaints in patients with early- and late-onset Parkinson's disease. *Front. Neurol.* 12:749471. doi: 10.3389/fneur.2021.749471

Yang, N., Ju, Y., Ren, J., Wang, H., Li, P., Ning, H., et al. (2022). Prevalence and affective correlates of subjective cognitive decline in patients with de novo Parkinson's disease. *Acta Neurol. Scand.* 146, 276–282. doi: 10.1111/ane.13662

Yoo, H. S., Kwon, H., Chung, S. J., Sohn, Y. H., Lee, J.-M., and Lee, P. H. (2021). Neural correlates of self-awareness of cognitive deficits in non-demented patients with Parkinson's disease. *Eur. J. Neurol.* 28, 4022–4030. doi: 10.1111/ene.15095

frontiers | Frontiers in Aging Neuroscience

TYPE Original Research
PUBLISHED 26 May 2023
DOI 10.3389/fnagi.2023.1207114

OPEN ACCESS

EDITED BY
Woon-Man Kung,
Chinese Culture University, Taiwan

REVIEWED BY
Konstantin Senkevich,
McGill University, Canada
Abhinav Jain,
Mayo Clinic, United States

*CORRESPONDENCE
Zhenhua Liu
✉ liuzhenhua@csu.edu.cn
Qiao Yu
✉ qiaoyu@csu.edu.cn

†These authors have contributed equally to this work

RECEIVED 17 April 2023
ACCEPTED 08 May 2023
PUBLISHED 26 May 2023

CITATION
Wang Y, Zhao Y, Pan H, Zeng Q, Zhou X, Xiang Y, Zhou Z, Xu Q, Sun Q, Tan J, Yan X, Li J, Guo J, Tang B, Yu Q and Liu Z (2023) Genetic analysis of dystonia-related genes in Parkinson's disease.
Front. Aging Neurosci. 15:1207114.
doi: 10.3389/fnagi.2023.1207114

Genetic analysis of dystonia-related genes in Parkinson's disease

Yige Wang[1,2], Yuwen Zhao[1], Hongxu Pan[1], Qian Zeng[1], Xiaoxia Zhou[1], Yaqin Xiang[1], Zhou Zhou[3], Qian Xu[1], Qiying Sun[3], Jieqiong Tan[4], Xinxiang Yan[1], Jinchen Li[2,3,4], Jifeng Guo[1,2,4,5], Beisha Tang[1,2,4,5], Qiao Yu[3*†] and Zhenhua Liu[1,2,4,5*†]

[1]Department of Neurology, Xiangya Hospital, Central South University, Changsha, Hunan, China, [2]National Clinical Research Center for Geriatric Disorders, Xiangya Hospital, Central South University, Changsha, Hunan, China, [3]Department of Geriatrics, Xiangya Hospital, Central South University, Changsha, Hunan, China, [4]Centre for Medical Genetics and Hunan Key Laboratory of Medical Genetics, School of Life Sciences, Central South University, Changsha, Hunan, China, [5]Key Laboratory of Hunan Province in Neurodegenerative Disorders, Central South University, Changsha, Hunan, China

Objective: Parkinson's disease (PD) and dystonia are two closely related movement disorders with overlaps in clinical phenotype. Variants in several dystonia-related genes were demonstrated to be associated with PD; however, genetic evidence for the involvement of dystonia-related genes in PD has not been fully studied. Here, we comprehensively investigated the association between rare variants in dystonia-related genes and PD in a large Chinese cohort.

Methods: We comprehensively analyzed the rare variants of 47 known dystonia-related genes by mining the whole-exome sequencing (WES) and whole-genome sequencing (WGS) data from 3,959 PD patients and 2,931 healthy controls. We initially identified potentially pathogenic variants of dystonia-related genes in patients with PD based on different inheritance models. Sequence kernel association tests were conducted in the next step to detect the association between the burden of rare variants and the risk for PD.

Results: We found that five patients with PD carried potentially pathogenic biallelic variants in recessive dystonia-related genes including *COL6A3* and *TH*. Additionally, we identified 180 deleterious variants in dominant dystonia-related genes based on computational pathogenicity predictions and four of which were considered as potentially pathogenic variants (p.W591X and p.G820S in *ANO3*, p.R678H in *ADCY5*, and p.R458Q in *SLC2A1*). A gene-based burden analysis revealed the increased burden of variant subgroups of *TH*, *SQSTM1*, *THAP1*, and *ADCY5* in sporadic early-onset PD, whereas *COL6A3* was associated with sporadic late-onset PD. However, none of them reached statistical significance after the Bonferroni correction.

Conclusion: Our findings indicated that rare variants in several dystonia-related genes are suggestively associated with PD, and taken together, the role of *COL6A3* and *TH* genes in PD is highlighted.

KEYWORDS

Parkinson's disease, dystonia-related genes, rare variants, whole-exome sequencing, whole-genome sequencing

1. Introduction

Parkinson's disease (PD), a progressive movement disorder, is the second most common neurodegenerative disorder after Alzheimer's disease. PD is characterized by motor symptoms, including bradykinesia, resting tremor, rigidity, and postural instability, as well as a wide variety of non-motor features, such as olfactory dysfunction, sleep disorders, and dysautonomia (Bloem et al., 2021). As a complex multifactorial disease, PD is caused by a combination of advancing age, genetic, environmental, and lifestyle factors, most of which have not yet been clearly identified (Lim et al., 2019; Bandres-Ciga et al., 2020; Blauwendraat et al., 2020). As another kind of movement disorder, dystonia is characterized by sustained or intermittent muscle contractions causing abnormal, often repetitive, movements, postures, or both. Dystonia can occur in isolation, in combination with other movement disorders, or coexist with a variety of other neurological or systemic manifestations (Albanese et al., 2013). In some conditions, dystonia is more likely a descriptive term rather than a specific diagnosis. The etiology of many forms of dystonia is recognized to be due to a large number of different causes and is still not fully elucidated, but genetic factors are involved unquestionably (Lohmann and Klein, 2013; Balint et al., 2018).

Parkinson's disease and dystonia have overlaps in clinical phenotypes and are both clinically and genetically heterogeneous conditions. Studies estimated that 30% or more of the patients suffering from PD may experience dystonia as a symptom or as a complication of treatment (Tolosa and Compta, 2006; Wickremaratchi et al., 2011). Dystonia is a common early symptom of young-onset PD and sometimes can precede overt parkinsonism, but it can also appear in the middle of advanced stages of PD (Shetty et al., 2019). Conversely, patients suffering from dopa-responsive dystonia (DRD), a specific type of dystonia characterized by lower limb dystonia in childhood with an excellent response to low doses of levodopa, frequently present with parkinsonism. Some DRD patients can even present prominent parkinsonism, leading to clinical difficulty to differentiate between DRD and young-onset PD (Wijemanne and Jankovic, 2015). Especially, dystonia is a prominent symptom for PD patients caused by several genes including *PRKN*, *PINK1*, *DJ-1,* and *PLA2G6* (Kasten et al., 2018; Niemann and Jankovic, 2019). Analogously, parkinsonism is commonly seen in subtypes of dystonia caused by genes such as *GCH1*, *TH*, *TAF1*, *ATP1A3,* and *PRKRA* (Phukan et al., 2011; Diez-Fairen et al., 2021).

These observed phenomena indicate a potential correlation between PD and dystonia and suggest the coexistence might be due to overlaps in the genetic background. Therefore, a possible role for dystonia-related genes (abbreviated as the "DYT genes" in this article) in PD is needed to be explored. Our previous research, consistent with other studies from different cohorts, had proven the role of *GCH1*, the most common cause of DRD, in the pathogenesis of PD (Mencacci et al., 2014; Guella et al., 2015; Chen et al., 2016; Pan et al., 2020). However, genetic evidence for the involvement of other DYT genes in PD has not been fully studied. To clarify the correlation between DYT genes and PD, we designed to comprehensively analyze the rare variants of the DYT genes in a large Chinese cohort of patients with PD and healthy controls by mining the whole-exome sequencing (WES) and whole-genome sequencing (WGS) data.

2. Materials and methods

2.1. Subjects

The enrolled subjects were recruited from Xiangya Hospital, Central South University and other sites of Parkinson's Disease & Movement Disorders Multicenter Database and Collaborative Network in China (PD-MDCNC, http://www.pd-mdcnc.com/). All subjects had undergone basic demographic data collection and peripheral blood sampling to prepare genomic DNA. PD patients are diagnosed according to the Movement Disorder Society (MDS) clinical diagnostic criteria (Postuma et al., 2015), and clinical features have been collected using neuropsychological tests including motor and non-motor manifestations.

In our study, sporadic PD patients were classified as sporadic early-onset PD (sEOPD) or sporadic late-onset PD (sLOPD) depending on the age at onset (AAO) with a cutoff at 50 years old. Controls were confirmed without neurological disorders and obvious family history of neurological disorders. Pathogenic or likely pathogenic variants in the established causative genes of PD were thoroughly screened and excluded from this study according to the previous description (Zhao et al., 2020). Genomic DNA was prepared from peripheral blood leukocytes following standard methods. All subjects or their guardians completed written informed consent, and the study protocol had been approved by the Medical Ethics Committee of Xiangya Hospital, Central South University.

2.2. Genotyping and quality control

All subjects were sequenced by WES or WGS depending on our previous or ongoing projects and reanalyzed in the current study. Specifically, familial PD (FPD), sEOPD, and neurological disease-free control group 1 were sequenced by WES, whereas sLOPD and control group 2 were sequenced by WGS. Data generation and quality control procedures for the WES and WGS have been described in detail previously (Pan et al., 2020). Briefly, the sequencing data were first processed following a bioinformatics pipeline (BWA-GATK-ANNOVAR), and subsequently, a series of procedures in quality control was accomplished by the PLINK software (Chang et al., 2015). For individuals with consanguineous family history, homozygosity mapping was performed with PLINK for detecting runs of homozygosity (ROH). Details of genotyping and quality control are shown in Supplementary Methods.

2.3. Gene selection

Our analysis included 47 autosomal DYT genes, collected from the Online Mendelian Inheritance in Man (OMIM, https://omim.org/), the Movement Disorder Society Genetic mutation database (MDSGene, https://www.mdsgene.org/), and widely accepted literature (Supplementary Table 1) (Lill et al., 2016; Balint et al.,

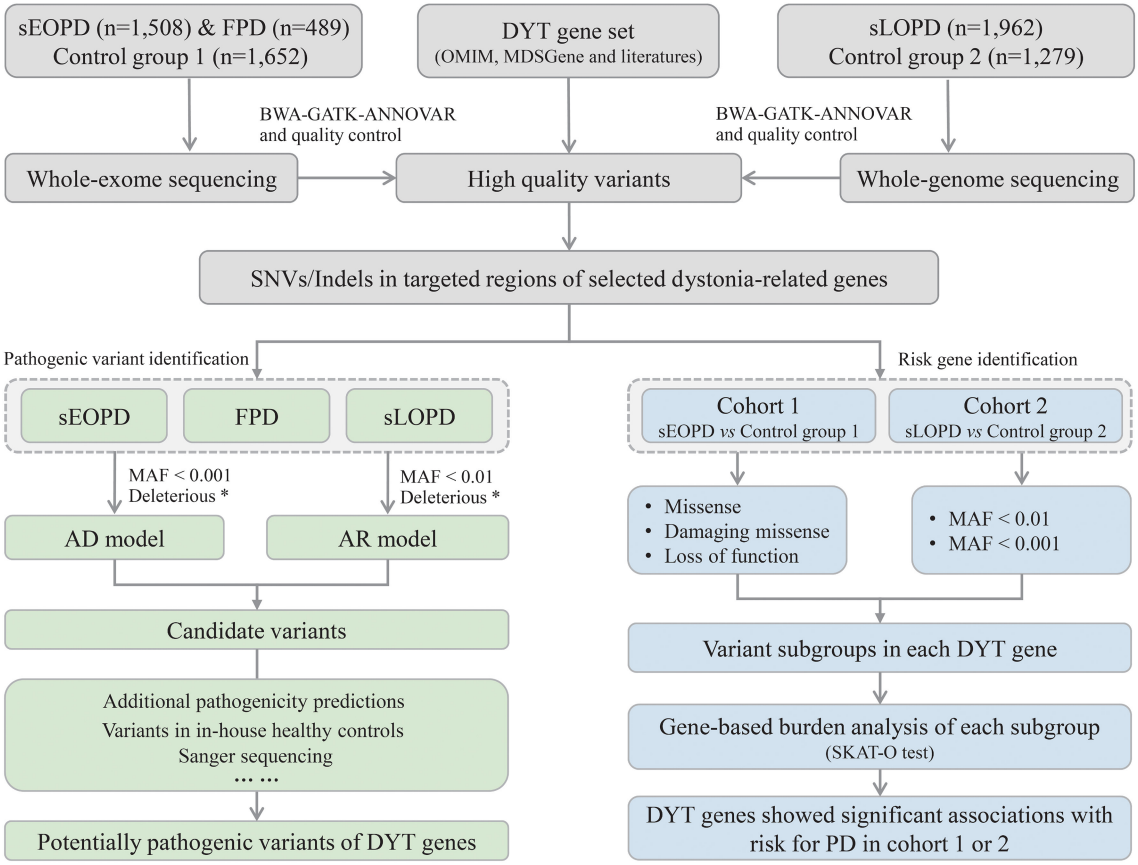

FIGURE 1
Workflow of the study design. sEOPD, sporadic early-onset Parkinson's disease; FPD, familial Parkinson's disease; sLOPD, sporadic late-onset Parkinson's disease; DYT, dystonia; SNVs, single nucleotide variants; Indels, small insertions/deletions; AD, autosomal dominant; AR, autosomal recessive; MAF, minor allele frequency. *Deleterious: the combination of damaging missense and loss-of-function variants.

2018; Wirth et al., 2020; Keller Sarmiento and Mencacci, 2021; Kuipers et al., 2021; Mencacci et al., 2021; Meng et al., 2021; Monfrini et al., 2021; van der Weijden et al., 2021). The protein–protein interactions of the DYT genes and established causative genes of PD assessed by the STRING v11 database (https://string-db.org/) were presented in Supplementary Figure 1 (Szklarczyk et al., 2019). Overall, we selected 19 genes with autosomal recessive (AR) inheritance including *HPCA*, *TH*, *PRKRA*, *COL6A3*, *MECR*, *PTS*, *QDPR*, *SLC6A3*, *SLC30A10*, *CP*, *DDC*, *SLC39A14*, *SLC18A2*, *SQSTM1*, *VPS41*, *COQ8A*, *VPS11*, *TSPOAP1*, and *MED27*, 25 genes with autosomal dominant (AD) inheritance including *TOR1A*, *TUBB4A*, *THAP1*, *PNKD*, *SLC2A1*, *PRRT2*, *SGCE*, *ATP1A3*, *CIZ1*, *CACNA1B*, *ANO3*, *GNAL*, *KCTD17*, *KMT2B*, *RHOBTB2*, *KCNA1*, *CACNA1A*, *YY1*, *GNAO1*, *GNB1*, *SCN8A*, *IRF2BPL*, *NR4A2*, *EIF2AK2*, and *DRD2*, as well as three genes with both inheritance patterns including *VPS16*, *SPR*, and *ADCY5*. It should be specially explained that variants of the *GCH1* gene had already been fully analyzed in the current cohorts previously, thus excluded from this study (Pan et al., 2020).

2.4. Criteria for rare variants in the DYT genes

The workflow of this study is shown in Figure 1. All high-quality single nucleotide variants and small insertions/deletions (SNVs and Indels) in protein-coding regions of the DYT genes were extracted from processed sequencing data, and then we analyzed from aspects of pathogenic variant identification and risk gene exploration with different subject groups. Minor allele frequency (MAF) of variants was defined by the East Asian population in Genome Aggregation Database (gnomAD) at thresholds of 0.01 and 0.001 (MAF $<$ 0.001 was considered a stricter threshold). ReVe score obtained from VarCards was used to predict pathogenicity for missense variants (Li et al., 2018). Damaging missense (missense variants with ReVe $\geq$ 0.7) and loss-of-function (stop gain/loss, frameshift, and splicing mutations falling within two base pairs of exon-intron junctions) variants, which have putative devastating effects on proteins, were defined as "deleterious."

2.5. Criteria for potentially pathogenic rare variants in the DYT genes

First, we filtered the rare deleterious variants with two different inheritance patterns under different criteria. For the AR inheritance pattern, filtered variants were deleterious homozygous or putative compound heterozygous states (the compound heterozygous state was not validated to be located on the different DNA strand) with MAF < 0.01 in gnomAD. For AD inheritance, filtered variants were deleterious heterozygous states with MAF < 0.001 in gnomAD. In particular, for genes that reported both recessive and dominant inheritance patterns in dystonia, we, respectively, filtered for different criteria in two conditions.

Subsequently, we scrutinized in-house WES and WGS data of healthy controls to exclude the variants carried by healthy individuals. We gave priority to the filtered variants predicted to be damaging by additional computational pathogenicity predictions including CADD, SIFT, LRT, MutationAssessor, PolyPhen2-HVAR, PolyPhen2-HDIV, and MutationTaster. In addition, we conservatively considered the pathogenicity of the loss-of-function variants, giving thought to variant-specific issues and disease mechanisms in variant interpretation. Variants that survived these criteria were further confirmed by Sanger sequencing and family segregation analysis when the samples were available, and then validated variants were considered potentially pathogenic. We re-evaluated the variants according to standards and guidelines from the American College of Medical Genetics and Genomics (ACMG), thus variants were further classified as pathogenic, likely pathogenic, or uncertain significance (Richards et al., 2015).

2.6. Burden analysis

Burden analysis was conducted to evaluate the aggregate association of rare variants with the disease, by optimized sequence kernel association test (SKAT-O) implanted in R (Wu et al., 2011). The variants were categorized into subgroups including missense, damaging missense, loss-of-function, as well as deleterious, with two MAF thresholds, including 0.01 and 0.001.

In the study, we performed SKAT-O for sEOPD and sLOPD compared with the corresponding control group. The SKAT-O test was conducted for each gene independently, considering each variant subgroup separately, with age, sex, and the first five principal components for population stratification as covariates. A p-value <0.001 (0.05/47) was considered statistically significant based on the Bonferroni correction and variant groups not surviving the Bonferroni correction, while uncorrected p-values <0.05 were considered "suggestive."

3. Results

3.1. Demographic characteristics

A total of 3,959 PD patients and 2,931 neurological disease-free controls were finally included in the analysis. Cohort 1 consisted of 1,508 sEOPD and 1,652 neurological disease-free controls (Control group 1) sequenced by WES, and cohort 2 consisted of 1,962 sLOPD and 1,279 neurological disease-free controls (Control group 2) sequenced by WGS. In addition, 153 probands of FPD with AR inheritance (ARPD) and 336 probands of FPD with AD inheritance (ADPD) were also sequenced by WES and included in the study. The detailed characteristics of each group are shown in Supplementary Table 2.

3.2. PD patients harboring potentially pathogenic variants of recessive DYT genes

For AR inheritance, we detected two deleterious homozygous variants and three pairs of deleterious putative compound heterozygous variants with MAF < 0.01, all of which were predicted to be damaging by multiple computational pathogenicity predictions and not present as biallelic forms in in-house healthy controls (Table 1). The results showed that the *COL6A3* gene was the most frequently mutated DYT gene in PD, and the variants of the *TH* gene were also found in one patient. All the potentially pathogenic variants of recessive DYT genes were confirmed by Sanger sequencing (Supplementary Figure 2), and the detailed phenotypes of carriers are shown in Supplementary Table 3.

The potentially pathogenic variants in *COL6A3* identified in the study are shown in Figure 2. Specifically, we identified a homozygous variant (p.A1638T) in exon 11 of *COL6A3* in the proband of a consanguineous family (AR-146) (Supplementary Figure 3A), located in a 5.36 Mb run of homozygosity (chr2: 237614085-242978914), detected based on homozygosity mapping using the WES data. The patient had an uneventful birth and normal development. At the age of 43, he developed mild rest tremors and clumsiness in his left hand. Subsequently, he had slowed movements in the right hand. A neurological examination performed at the age of 47 showed bilateral motor symptoms including rest tremor, bradykinesia, and rigidity, as well as non-motor symptoms including hyposmia, sleep disturbance, and urinary urgency. It should be noted that the patient presented no sign of dystonia. Brain magnetic resonance imaging (MRI) was reported to be normal, and the results of the electromyogram did not reveal abnormal findings (Supplementary Figure 3B). He responded well to the levodopa-benserazide therapy (500 mg per day) and showed no levodopa-induced dyskinesia. His parents have passed away, and a DNA sample of the unaffected sister was unavailable. In addition, three pairs of heterozygous variants of the *COL6A3* gene were detected in our patients (Table 1), which might form compound heterozygous states and play a role in PD. The patients harboring these variants manifested the typical symptoms of PD with no muscular dystrophy phenotypes or dystonia and were diagnosed as clinically established or probable PD, but one of them developed levodopa-induced dyskinesia.

For the *TH* gene, a novel homozygous variant (p.S19C) was identified in a sporadic patient with an AAO of 59 years. The initial symptoms of the patient were bradykinesia and muscle rigidity of the right lower limb, and over time, postural instability and gait difficulty were gradually manifested. The non-motor symptoms were also remarkable including rapid eye movement sleep behavior disorder (RBD), constipation, cognitive decline, and hyposmia.

TABLE 1 Patients with Parkinson's disease harboring potentially pathogenic variants of recessive dystonia-related genes.

Sample ID	Gene	Position (hg19)	Ref	Alt	Exonic function	Hom/Het	Nucleotide change	Amino acid alteration	MAF	CADD	ReVe	ACMG
AR-146	*COL6A3*	chr2:238275918	C	T	Missense	Hom	c.4912G>A	p.A1638T	0.0063/0.0099	29.6	0.851:D	US
EOPD-0488	*COL6A3*	chr2:238283448	G	A	Missense	Het	c.3286C>T	p.R1096C	0.0021/0.0012	23.3	0.728:D	US
		chr2:238266491	G	C	Missense	Het	c.6506C>G	p.P2169R	0.0003/0.0006	27.0	0.766:D	US
EOPD-1304	*COL6A3*	chr2:238283448	G	A	Missense	Het	c.3286C>T	p.R1096C	0.0021/0.0012	23.3	0.728:D	US
		chr2:238249328	G	A	Missense	Het	c.8231C>T	p.T2744M	0/0	27.9	0.889:D	US
EOPD-0766	*COL6A3*	chr2:238277596	G	A	Missense	Het	c.4510C>T	p.R1504W	0/0	24.4	0.856:D	US
		chr2:238270387	G	T	Missense	Het	c.6151C>A	p.P2051T	0/0	21.8	0.763:D	US
LOPD-0390	*TH*	chr11:2192961	G	C	Missense	Hom	c.56C>G	p.S19C	0.0001/NA	26.0	0.777:D	US

MAF, Minor allele frequency in the East Asian population of gnomAD exome database and genome database. NA means the variant was not found in the gnomAD exome or genome database. Hom, Homozygous; Het, Heterozygous; US, uncertain significance.

He was 67 years when he joined the recruitment, and a physical examination showed bilateral rigidity and bradykinesia without any sign of dystonia. Brain MRI was unremarkable. He responded well to dopaminergic therapies (the dose of levodopa-benserazide is 750 mg per day) and showed no levodopa-induced dyskinesia.

3.3. PD patients harboring potentially pathogenic variants of dominant DYT genes

For AD inheritance, we initially detected 180 heterozygous variants based on MAF < 0.001 and simultaneously predicted to have putative devastating effects on proteins (missense variants with ReVe ≥ 0.7 or loss-of-function variants) (Supplementary Table 4). After further filtering, four variants were considered potentially pathogenic variants (Table 2). All the variants were not present in gnomAD databases or in-house healthy controls and were loss-of-function variants or predicted to be damaging by multiple computational pathogenicity predictions. Five patients harboring the four potentially pathogenic variants of dominant DYT genes were confirmed by Sanger sequencing (Supplementary Figure 4), and the detailed phenotypes are shown in Supplementary Table 5.

Two novel variants of *ANO3* (p.W591X and p.G820S) were identified as heterozygous states in our cohort and were carried by three sEOPD patients. One patient harboring the loss-of-function variant p.W591X manifested as a tremor-dominant subtype and developed motor complications including drug-induced dyskinesia and wearing-off, as well as hyposmia and mild depression. The other two patients harboring the p.G820S showed typical motor symptoms whereas the non-motor symptoms were unremarkable. They all responded well to levodopa-benserazide therapy. Cranial MRIs were negative and other laboratory tests were unremarkable. Additionally, we detected a novel heterozygous variant of *ADCY5* (p.R678H) and a reported variant of *SLC2A1* (p.R458Q) in sLOPD patients. The carriers were also diagnosed as PD, with typical motor and non-motor symptoms.

Patients harboring the potentially pathogenic variants were diagnosed as clinically established or probable PD according to the MDS clinical diagnostic criteria (Postuma et al., 2015) and confirmed with no pathogenic or likely pathogenic SNVs/Indels and copy number variations (CNVs) in the established causative genes of PD by WES or WGS and multiplex ligation-dependent probe amplification.

3.4. Gene-based burden analysis

In cohort 1, a total of 2,534 variants with a MAF below 0.01 and 2,213 variants with a MAF below 0.001 in the protein-coding regions of 47 DYT genes in cases and controls passed the quality control and were included in the analysis. Similarly, a total of 2,073 variants with a MAF below 0.01 and 1,767 variants with a MAF below 0.001 were included in the analysis of cohort 2.

In cohort 1, we observed suggestive significant associations between loss-of-function variants of *TH* ($p = 0.0315$) and damaging missense variants of *SQSTM1* ($p = 0.0212$) and the

10.3389/fnagi.2023.1207114

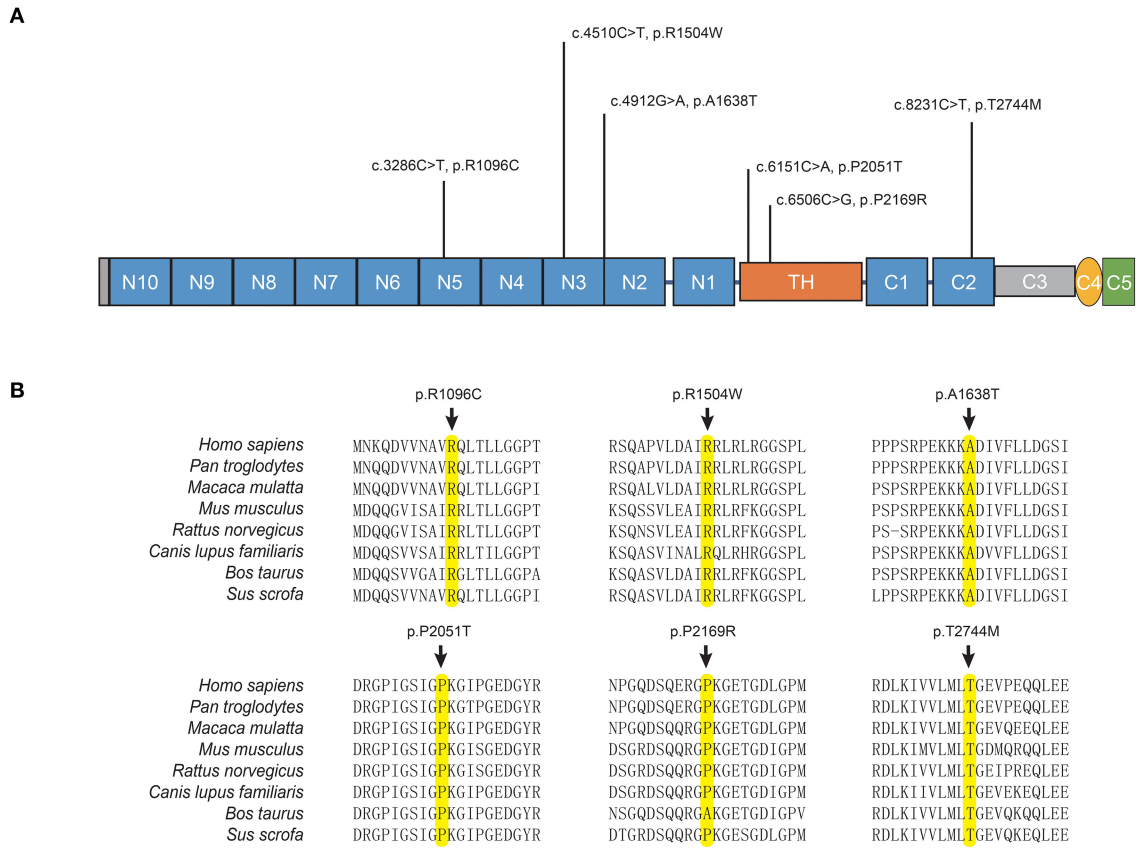

FIGURE 2
COL6A3 variants in Parkinson's disease. **(A)** Schematic representation of the domain organization of collagen VI α3 (NP_004360.2) and the localization of identified variants. Collagen VI α3 is composed of a collagen-like triple helical domain (TH) and N and C-terminal globular domains (N1–10 and C1–C5). **(B)** Alignment of multiple collagen VI α3 orthologs. The affected amino acid residues are highlighted in yellow.

increased risk for sEOPD. Without regard to pathogenicity, missense variants of *SQSTM1* ($p = 0.0022$), *THAP1* ($p = 0.0322$), and *ADCY5* ($p = 0.0486$) also reached a suggestive significance level. In cohort 2, we only detected suggestive associations between damaging missense variants of *COL6A3* ($p = 0.0346$) and the increased risk for sLOPD (Table 3). However, none of these variant subgroups of each DYT gene reached the statistical significance threshold after the Bonferroni correction ($p > 0.001$). The complete results of the burden analysis for each DYT gene are shown in Supplementary Table 6.

4. Discussion

Within two decades, the role of genetics in PD has been emphasized and better understood, but many gaps remain to be filled. We observed similarities in many aspects of PD and dystonia, which sparked our curiosity about the genetic overlaps in these two movement disorders. Consequently, we have comprehensively analyzed the rare variants in coding regions of DYT genes in a large Chinese cohort of PD patients and healthy controls by employing unbiased whole-exome and whole-genome approaches.

To our knowledge, this is the first and largest-ever study to explore the association between rare variants of DYT genes and PD. Firstly, we identified five patients with PD who carried potentially pathogenic biallelic variants in recessive dystonia-related genes, including *COL6A3* and *TH*. Secondly, we detected a total of 180 deleterious variants in dominant dystonia-related genes, four of which were considered potentially pathogenic variants, including p.W591X and p.G820S in *ANO3*, p.R678H in *ADCY5*, and p.R458Q in *SLC2A1*. Thirdly, the burden analysis revealed an increased burden of variant subgroups in *TH*, *SQSTM1*, *THAP1*, and *ADCY5* in sEOPD, as well as *COL6A3* in sLOPD, although statistical significance was not achieved after Bonferroni correction. Overall, our study provides evidence that several DYT genes contribute to the pathogenesis of PD, supported by a large sample size and robust methodologies.

The *COL6A3* gene encodes the alpha-3 chain of type VI collagen, which is an extracellular matrix (ECM) protein, playing a pivotal role in the central nervous system (CNS) and participating in various aspects of neurodevelopment and neurodegeneration by regulating autophagy and synaptic plasticity (Dityatev et al., 2010; Neill et al., 2021). Although the physiological role of Col6a3 in the CNS remains poorly understood, emerging data suggest its neuroprotective potential (Cheng et al., 2011; Cescon et al., 2016). Col6a3 was widely expressed throughout the adult mouse brain with the highest mRNA levels in the brainstem and midbrain (Zech et al., 2015). Biallelic loss-of-function mutations of *COL6A3*

TABLE 2 Patients with Parkinson's disease harboring potentially pathogenic variants of dominant dystonia-related genes.

Gene	Position (hg19)	Ref	Alt	Exonic function	Nucleotide change	Amino acid alteration	MAF	CADD	ReVe	ACMG	Sample ID	Hom/Het
ANO3	chr11:26621198	G	A	Stopgain	c.1773G>A	p.W591X	NA/NA	41	0.740:D	P	EOPD-0001	Het
ANO3	chr11:26669285	G	A	Missense	c.2458G>A	p.G820S	0/0	23.7	0.768:D	LP	EOPD-0190	Het
											EOPD-1469	Het
ADCY5	chr3:123044224	C	T	Missense	c.2033G>A	p.R678H	0/0	31	0.854:D	LP	LOPD-1445	Het
SLC2A1	chr1:43392818	C	T	Missense	c.1373G>A	p.R458Q	0/NA	26.3	0.812:D	LP	LOPD-0694	Het

MAF, Minor allele frequency in the East Asian population of gnomAD exome database and genome database. NA means the variant was not found in the gnomAD exome or genome database. Hom, Homozygous; Het, Heterozygous; P, Pathogenic; LP, Likely pathogenic.

TABLE 3 Suggestive associations between the burden of rare variants in dystonia-related genes and the increased risk for Parkinson's disease.

TH	Cohort 1	sEOPD	LoF	5	8	1	0.0315	5	8	1	0.0315
SQSTM1	Cohort 1	sEOPD	Dmis	12	11	3	0.0212	13	14	8	0.1939
SQSTM1	Cohort 1	sEOPD	Missense	29	28	12	0.0022	33	37	21	0.0054
THAP1	Cohort 1	sEOPD	Missense	5	5	0	0.0322	5	5	0	0.0322
ADCY5	Cohort 1	sEOPD	Missense	20	27	18	0.5357	23	45	27	0.0486
COL6A3	Cohort 2	sLOPD	Dmis	53	62	25	0.1212	63	143	64	0.0346

[a]Total number of accumulated allele counts of included variants detected in cases of the cohort.
[b]Total number of accumulated allele counts of included variants detected in controls of the cohort.
MAF, Minor allele frequency in the East Asian population of gnomAD exome database and genome database; sEOPD, Sporadic early-onset Parkinson's disease; sLOPD, Sporadic late-onset Parkinson's disease; LoF, Loss-of-function variants; Dmis, Damaging missense variants.

10.3389/fnagi.2023.1207114

can cause early-onset segmental isolated dystonia (DYT27) by affecting the EMC in the CNS (Zech et al., 2015). The genetic study of *COL6A3* in PD or other neurodegenerative diseases was insufficient. A previous study conducted in China reported a PD patient without dystonia symptoms carrying compound heterozygous variants in *COL6A3* gene. The study also observed an elevated aggregate variant burden of the *COL6A3* gene in 173 PD patients compared to 200 controls, thereby proposing a potential role of *COL6A3* in PD. However, it is important to note that this evidence is still preliminary (Jin et al., 2021). Here, we reported four patients with PD harboring potentially pathogenic biallelic variants in *COL6A3,* and all the patients showed typical manifestations of PD without dystonia or muscular dystrophy. None of the variants were located in previously reported hotspots for mutation in dystonia (exons 41 and 42), indicating variants in specific regions of *COL6A3* may have an association with PD (Domingo et al., 2016; Jin et al., 2021). We also observed an association between rare damaging variants of the *COL6A3* gene and an increased risk for sLOPD, which replicated the conclusion of the previous study with a larger sample size. As a result, the role of *COL6A3* in PD has been highlighted, although further evidence and mechanism explorations are needed.

TH is a well-established causative gene for DRD similar to *GCH1*, and mutations of *TH* and *GCH1,* resulting in deficiencies of the enzymes involved in the dopaminergic synthesis pathway, can present with dystonia and parkinsonism (Lee and Jeon, 2014; Wijemanne and Jankovic, 2015). The association between *GCH1* and PD has been proven previously, which was validated in the Chinese population (Pan et al., 2020). By contrast, the relationship between the *TH* gene and PD is not so clear, due to the limited number of research studies and inconsistencies across the studies (Bademci et al., 2012; Chen et al., 2020; Kawahata and Fukunaga, 2020). Previous studies were mainly focused on common variants of the *TH* gene and utilized a small sample size (Sutherland et al., 2008; Punia et al., 2010). With the rapid advances in genomic technology, subsequent studies performed genetic research between rare variants of *TH* and PD; however, the studies conducted are trivial due to their extremely rare presence with a small sample size (Hertz et al., 2006; Rengmark et al., 2016; Yan et al., 2018). In our cohort, we found a potentially pathogenic homozygous variant of *TH* in a patient with PD without symptoms of DRD, and we also provide suggestive evidence that loss-of-function variants in the *TH* gene might contribute to an increased risk for sEOPD, which help us fully understand the genetic risk for PD conferred by the *TH* gene.

ANO3 encodes anoctamin 3, which is highly expressed in the brain tissue, specifically in the striatum (Charlesworth et al., 2012). It is a transmembrane protein that belongs to a family of calcium-activated chloride channels and thus may play a role in signal transduction (Pedemonte and Galietta, 2014). Additionally, a previous study has reported an infantile-onset patient manifested dystonia, parkinsonism, and developmental regression, caused by a *de novo* missense variant in *ANO3* (Nelin et al., 2018). However, the exact role of anoctamin 3 remains uncertain, and the two variants found in our patients have not been fully researched in our study and have no other evidence to support the effects yet.

ADCY5 encodes isoform 5 of adenylyl cyclase, which is highly expressed in medium spiny neurons (MSNs) of the striatum. Adenylyl cyclase is responsible for the conversion of adenosine triphosphate (ATP) to cyclic adenosine-3′,5′-monophosphate (cAMP) and is involved in dopaminergic signaling. Dysfunction of the cAMP pathway can contribute to postsynaptic movement disorders such as dystonia, chorea, and parkinsonism (Abela and Kurian, 2018; Ferrini et al., 2021). A novel variant of *ADCY5* evaluated to be potentially pathogenic was identified in our cohort, and the burden of rare variants in *ADCY5* was increased in sEOPD, which suggested the involvement of *ADCY5* in the pathogenesis of PD, whereas research of the underlying mechanisms is further needed.

Additionally, we identified a variant in *SLC2A1* (p.R458Q) in one PD patient, which was evaluated to be potentially pathogenic. The variant has been recorded as a candidate causal variant of an individual with ataxic gait, global developmental delay, and disrupted sleep, which was included in the ClinVar database. Additionally, a missense variant occurring in the same codon (p.R458W) has been reported in individuals with features of *SLC2A1*-related disorder and has been demonstrated to result in a marked reduction in glucose transport, supporting the functional importance of this position in the protein (Arsov et al., 2012; Tzadok et al., 2014). Therefore, further studies are needed to confirm whether p.R458Q plays a role in PD onset or modification.

The burden analysis also showed the enrichment of extremely rare variants of the *SQSTM1* gene in sEOPD. The *SQSTM1* gene encodes p62, a prototype autophagy receptor, which is commonly found in protein aggregates associated with major neurodegenerative diseases (Deng et al., 2020). It was confirmed to play an essential role in the PINK1/Parkin-mediated mitophagy involved in the pathogenesis of PD (Geisler et al., 2010; Chu, 2019). Mutations in *SQSTM1* contribute to neurodegeneration in amyotrophic lateral sclerosis and frontotemporal dementia (Goode et al., 2016). We have completed an initial exploration and obtained a suggestive but encouraging result about the genetic association between *SQSTM1* and PD, which deserves further investigation. Additionally, *THAP1* was also nominated in the burden analysis, contributing to increased risk for sEOPD. *THAP1* encodes a transcription factor involved in the regulation of gene expression in the nervous system. The reported dysregulated genes by loss of Thap1 are functionally related to neurodevelopment, lysosomal lipid metabolism, myelin, cytoskeleton, synaptic transmission, and gliogenesis (Frederick et al., 2019; Domingo et al., 2021). Our results suggested the involvement of these genes in PD, but much remains to be understood about the underlying mechanisms.

As an exploratory study, limitations are inevitable. First, the DYT genes included in the study had been widely collected by researchers at the preliminary stage of the study, inevitably omitting some latest discovered genes and at the same time, a few controversial genes were incorporated, such as *CACNA1B* and *CIZ1*. The correlation between the two genes and DYT23 was pending confirmation, therefore, the pathogenicity of the variants located in the questioned genes was taken with caution. Besides, we initially detected a large number of variants under AD inheritance, whereas most of them were considered to be uncertain significance due to many aspects such as the reliability and the mechanisms of genes. The conservative interpretation of the variants led to the neglect of certain variants that merit further investigation. Second, we only focused on rare coding SNVs/Indels in this

study and did not consider more complex forms of variants, such as CNVs, as well as non-coding variants. The main reason for this decision was the undisclosed role of the DYT genes in PD, which we aimed to explore in the current study. We prioritized SNVs/Indels in coding regions as they were more likely to reveal possible genetic associations. While other types of variants are also important, their complex and potentially indirect mechanisms are currently challenging to elucidate. We will give more attention to the analysis and interpretation of non-coding and complex variants in future studies. Third, the pathogenicity of the discovered genes and variants still requires further validation through family segregation analysis and functional experiments, which have not been comprehensively investigated in our study. Family segregation analysis is a powerful tool for further classification of the identified candidate variants. In our study, we attempted to conduct family segregation analysis using Sanger sequencing in affected or unaffected parents and siblings of the proband whenever feasible. However, we encountered a limitation that most patients had no family history of PD or other neurodegenerative diseases, and unfortunately, DNA samples of their family members were not available. In addition, although it is the largest genetic study of the DYT genes in PD up to now, the sample size was insufficient for rare variants analysis, which may be the cause of little statistical significance detected.

In conclusion, our findings indicated that rare variants in several DYT genes are associated with PD, and the role of *COL6A3* and *TH* genes in PD is highlighted, although further evidence and mechanism explorations are still needed.

Data availability statement

The data analyzed in this study is subject to the following licenses/restrictions: The data that support the findings of this study are available from the corresponding author upon reasonable request. Requests to access these datasets should be directed to liuzhenhua@csu.edu.cn.

Ethics statement

The studies involving human participants were reviewed and approved by Medical Ethics Committee of Xiangya Hospital, Central South University. The patients/participants provided their written informed consent to participate in this study.

Author contributions

YW: conceptualization, data curation, formal analysis, methodology, and writing—original draft. YZ: data curation and writing—review and editing. HP and QZ: data curation and methodology. XZ, YX, and ZZ: data curation. QX, QS, JT, and XY: data curation and funding acquisition. JL, JG, and BT: funding acquisition and writing—review and editing. ZL and QY: project administration, supervision, funding acquisition, and writing—review and editing. All authors contributed to the article and approved the submitted version.

Funding

This study was supported by the Natural Science Foundation of Hunan Province (Grant No. 2022JJ40843), the National Natural Science Foundation of China (Grant No. 82001359), the Scientific Research Project of Hunan Provincial Health Commission (Grant No. 202203074637), the Hunan Innovative Province Construction Project (Grant Nos. 2019SK2335 and 2021SK1010), and the National Key Research and Development Program of China (Grant Nos. 2021YFC2501204 and 2016YFC306000).

Acknowledgments

The authors are grateful for the participation of all the subjects in this study. This study was supported in part by the Bioinformatics Center, Xiangya Hospital, Central South University.

Conflict of interest

The authors declare that the research was conducted in the absence of any commercial or financial relationships that could be construed as a potential conflict of interest.

Publisher's note

Supplementary material

The Supplementary Material for this article can be found online at: https://www.frontiersin.org/articles/10.3389/fnagi.2023.1207114/full#supplementary-material

References

Abela, L., and Kurian, M. A. (2018). Postsynaptic movement disorders: clinical phenotypes, genotypes, and disease mechanisms. *J. Inherit. Metab. Dis.* 41, 1077–1091. doi: 10.1007/s10545-018-0205-0

Albanese, A., Bhatia, K., Bressman, S. B., Delong, M. R., Fahn, S., Fung, V. S., et al. (2013). Phenomenology and classification of dystonia: a consensus update. *Mov. Disord.* 28, 863–73. doi: 10.1002/mds.25475

Arsov, T., Mullen, S. A., Rogers, S., Phillips, A. M., Lawrence, K. M., Damiano, J. A., et al. (2012). Glucose transporter 1 deficiency in the idiopathic generalized epilepsies. *Ann. Neurol.* 72, 807–15. doi: 10.1002/ana.23702

Bademci, G., Vance, J. M., and Wang, L. (2012). Tyrosine hydroxylase gene: another piece of the genetic puzzle of Parkinson's disease. *CNS Neurol. Disord. Drug Targets* 11, 469–81. doi: 10.2174/187152712800792866

Balint, B., Mencacci, N. E., Valente, E. M., Pisani, A., Rothwell, J., Jankovic, J., et al. (2018). Dystonia. *Nat. Rev. Dis. Primers* 4, 25. doi: 10.1038/s41572-018-0023-6

Bandres-Ciga, S., Diez-Fairen, M., Kim, J. J., and Singleton, A. B. (2020). Genetics of Parkinson's disease: an introspection of its journey towards precision medicine. *Neurobiol. Dis.* 137, 104782. doi: 10.1016/j.nbd.2020.104782

Blauwendraat, C., Nalls, M. A., and Singleton, A. B. (2020). The genetic architecture of Parkinson's disease. *Lancet Neurol.* 19, 170–178. doi: 10.1016/S1474-4422(19)30287-X

Bloem, B. R., Okun, M. S., and Klein, C. (2021). Parkinson's disease. *Lancet* 397, 2284–2303. doi: 10.1016/S0140-6736(21)00218-X

Cescon, M., Chen, P., Castagnaro, S., Gregorio, I., and Bonaldo, P. (2016). Lack of collagen VI promotes neurodegeneration by impairing autophagy and inducing apoptosis during aging. *Aging* 8, 1083–101. doi: 10.18632/aging.100924

Chang, C. C., Chow, C. C., Tellier, L. C., Vattikuti, S., Purcell, S. M., and Lee, J. J. (2015). Second-generation PLINK: rising to the challenge of larger and richer datasets. *Gigascience* 4, 7. doi: 10.1186/s13742-015-0047-8

Charlesworth, G., Plagnol, V., Holmstrom, K. M., Bras, J., Sheerin, U. M., Preza, E., et al. (2012). (2012). Mutations in ANO3 cause dominant craniocervical dystonia: ion channel implicated in pathogenesis. *Am. J. Hum. Genet.* 91, 1041-50. doi: 10.1016/j.ajhg.10024

Chen, C. M., Chen, Y. C., Chiang, M. C., Fung, H. C., Chang, K. H., Lee-Chen, G. J., et al. (2016). Association of GCH1 and MIR4697, but not SIPA1L2 and VPS13C polymorphisms, with Parkinson's disease in Taiwan. *Neurobiol. Aging* 39, 221e1–21e5. doi: 10.1016/j.neurobiolaging.12016

Chen, Y., Ou, R., Zhang, L., Gu, X., Yuan, X., Wei, Q. Q., et al. (2020). Contribution of five functional loci of dopamine metabolism-related genes to Parkinson's disease and multiple system atrophy in a Chinese population. *Front. Neurosci.* 14, 889. doi: 10.3389/fnins.2020.00889

Cheng, I. H., Lin, Y. C., Hwang, E., Huang, H. T., Chang, W. H., Liu, Y. L., et al. (2011). Collagen VI protects against neuronal apoptosis elicited by ultraviolet irradiation via an Akt/phosphatidylinositol 3-kinase signaling pathway. *Neuroscience* 183, 178–188. doi: 10.1016/j.neuroscience.03057

Chu, C. T. (2019). Mechanisms of selective autophagy and mitophagy: Implications for neurodegenerative diseases. *Neurobiol. Dis.* 122, 23-34. doi: 10.1016/j.nbd.07015

Deng, Z., Lim, J., Wang, Q., Purtell, K., Wu, S., Palomo, G. M., et al. (2020). ALS-FTLD-linked mutations of SQSTM1/p62 disrupt selective autophagy and NFE2L2/NRF2 anti-oxidative stress pathway. *Autophagy* 16, 917–931. doi: 10.1080/15548627.2019.1644076

Diez-Fairen, M., Alvarez Jerez, P., Berghausen, J., and Bandres-Ciga, S. (2021). The genetic landscape of Parkinsonism-related dystonias and atypical parkinsonism-related syndromes. *Int. J. Mol. Sci.* 22, 8100. doi: 10.3390./ijms22158100

Dityatev, A., Schachner, M., and Sonderegger, P. (2010). The dual role of the extracellular matrix in synaptic plasticity and homeostasis. *Nat. Rev. Neurosci.* 11, 735–46. doi: 10.1038/nrn2898

Domingo, A., Erro, R., and Lohmann, K. (2016). Novel dystonia genes: clues on disease mechanisms and the complexities of high-throughput sequencing. *Mov. Disord.* 31, 471–7. doi: 10.1002/mds.26600

Domingo, A., Yadav, R., Shah, S., Hendriks, W. T., Erdin, S., Gao, D., et al. (2021). Dystonia-specific mutations in THAP1 alter transcription of genes associated with neurodevelopment and myelin. *Am. J. Hum. Genet.* 108, 2145-2158. doi: 10.1016/j.ajhg.09017

Ferrini, A., Steel, D., Barwick, K., and Kurian, M. A. (2021). An update on the phenotype, genotype and neurobiology of ADCY5-related disease. *Mov. Disord.* 36, 1104–1114. doi: 10.1002/mds.28495

Frederick, N. M., Shah, P. V., Didonna, A., Langley, M. R., Kanthasamy, A. G., and Opal, P. (2019). Loss of the dystonia gene Thap1 leads to transcriptional deficits that converge on common pathogenic pathways in dystonic syndromes. *Hum. Mol. Genet.* 28, 1343–1356. doi: 10.1093/hmg/ddy433

Geisler, S., Holmstrom, K. M., Skujat, D., Fiesel, F. C., Rothfuss, O. C., Kahle, P. J., et al. (2010). PINK1/Parkin-mediated mitophagy is dependent on VDAC1 and p62/SQSTM1. *Nat. Cell Biol.* 12, 119–31. doi: 10.1038/ncb2012

Goode, A., Butler, K., Long, J., Cavey, J., Scott, D., Shaw, B., et al. (2016). Defective recognition of LC3B by mutant SQSTM1/p62 implicates impairment of autophagy as a pathogenic mechanism in ALS-FTLD. *Autophagy* 12, 1094–104. doi: 10.1080/15548627.2016.1170257

Guella, I., Sherman, H. E., Appel-Cresswell, S., Rajput, A., Rajput, A. H., and Farrer, M. J. (2015). Parkinsonism in GTP cyclohydrolase 1 mutation carriers. *Brain* 138, e349. doi: 10.1093/brain/awu341

Hertz, J. M., Ostergaard, K., Juncker, I., Pedersen, S., Romstad, A., Møller, L. B., et al. (2006). Low frequency of Parkin, Tyrosine Hydroxylase, and GTP Cyclohydrolase I gene mutations in a Danish population of early-onset Parkinson's Disease. *Eur. J. Neurol.* 13, 385–390. doi: 10.1111/j.1468-200601249.x

Jin, C. Y., Zheng, R., Lin, Z. H., Xue, N. J., Chen, Y., Gao, T., et al. (2021). Study of the collagen type VI alpha 3. (COL6A3). gene in Parkinson's disease. *BMC Neurol.* 21, 187. doi: 10.1186/s12883-021-02215-7

Kasten, M., Hartmann, C., Hampf, J., Schaake, S., Westenberger, A., Vollstedt, E. J., et al. (2018). Genotype-phenotype relations for the Parkinson's disease genes Parkin, PINK1, DJ1. MDSGene systematic review. *Mov. Disord.* 33, 730–741. doi: 10.1002/mds.27352

Kawahata, I., and Fukunaga, K. (2020). Degradation of tyrosine hydroxylase by the ubiquitin-proteasome system in the pathogenesis of Parkinson's disease and dopa-responsive dystonia. *Int. J. Mol. Sci.* 21, 3779. doi: 10.3390./ijms21113779

Keller Sarmiento, I. J., and Mencacci, N. E. (2021). Genetic dystonias: update on classification and new genetic discoveries. *Curr. Neurol. Neurosci. Rep.* 21, 8. doi: 10.1007/s11910-021-01095-1

Kuipers, D. J. S., Mandemakers, W., Lu, C. S., Olgiati, S., Breedveld, G. J., Fevga, C., et al. (2021). EIF2AK2 missense variants associated with early onset generalized dystonia. *Ann. Neurol.* 89, 485–497. doi: 10.1002/ana.25973

Lee, W. W., and Jeon, B. S. (2014). Clinical spectrum of dopa-responsive dystonia and related disorders. *Curr. Neurol. Neurosci. Rep.* 14, 461. doi: 10.1007/s11910-014-0461-9

Li, J., Zhao, T., Zhang, Y., Zhang, K., Shi, L., Chen, Y., et al. (2018). Performance evaluation of pathogenicity-computation methods for missense variants. *Nucl. Acids Res.* 46, 7793–7804. doi: 10.1093/nar/gky678

Lill, C. M., Mashychev, A., Hartmann, C., Lohmann, K., Marras, C., Lang, A. E., et al. (2016). Launching the movement disorders society genetic mutation database (MDSGene). *Mov Disord.* 31, 607–9. doi: 10.1002/mds.26651

Lim, S. Y., Tan, A. H., Ahmad-Annuar, A., Klein, C., Tan, L. C. S., Rosales, R. L., et al. (2019). Parkinson's disease in the Western Pacific Region. *Lancet Neurol.* 18, 865–879. doi: 10.1016/S1474-4422(19)30195-4

Lohmann, K., and Klein, C. (2013). Genetics of dystonia: what's known? What's new? What's next? *Mov. Disord.* 28, 899–905. doi: 10.1002/mds.25536

Mencacci, N. E., Brockmann, M. M., Dai, J., Pajusalu, S., Atasu, B., Campos, J., et al. (2021). Biallelic variants in TSPOAP1, encoding the active-zone protein RIMBP1, cause autosomal recessive dystonia. *J. Clin. Invest.* 131, 625. doi: 10.1172./jci140625

Mencacci, N. E., Isaias, I. U., Reich, M. M., Ganos, C., Plagnol, V., Polke, J. M., et al. (2014). Parkinson's disease in GTP cyclohydrolase 1 mutation carriers. *Brain*, 137, 2480–92. doi: 10.1093/brain/awu179

Meng, L., Isohanni, P., Shao, Y., Graham, B. H., Hickey, S. E., Brooks, S., et al. (2021). MED27 variants cause developmental delay, dystonia, and cerebellar hypoplasia. *Ann. Neurol.* 89, 828–833. doi: 10.1002/ana.26019

Monfrini, E., Cogiamanian, F., Salani, S., Straniero, L., Fagiolari, G., Garbellini, M., et al. (2021). A novel homozygous VPS11 variant may cause generalized dystonia. *Ann. Neurol.* 89, 834–839. doi: 10.1002/ana.26021

Neill, T., Kapoor, A., Xie, C., Buraschi, S., and Iozzo, R. V. (2021). A functional outside-in signaling network of proteoglycans and matrix molecules regulating autophagy. *Matrix Biol.* 100–101, 118–149. doi: 10.1016/j.matbio.04001

Nelin, S., Hussey, R., Faux, B. M., and Rohena, L. (2018). Youngest presenting patient with dystonia 24 and review of the literature. *Clin. Case Rep.* 6, 2070–2074. doi: 10.1002/ccr3.1671

Niemann, N., and Jankovic, J. (2019). Juvenile parkinsonism: Differential diagnosis, genetics, and treatment. *Parkinsonism Relat. Disord.* 67, 74–89. doi: 10.1016/j.parkreldis.06025

Pan, H. X., Zhao, Y. W., Mei, J. P., Fang, Z. H., Wang, Y., Zhou, X., et al. (2020). GCH1 variants contribute to the risk and earlier age-at-onset of Parkinson's disease: a two-cohort case-control study. *Transl. Neurodegener.* 9, 31. doi: 10.1186/s40035-020-00212-3

Pedemonte, N., and Galietta, L. J. (2014). Structure and function of TMEM16 proteins (anoctamins). *Physiol. Rev.* 94, 419–59. doi: 10.1152/physrev.00039.2011

Phukan, J., Albanese, A., Gasser, T., and Warner, T. (2011). Primary dystonia and dystonia-plus syndromes: clinical characteristics, diagnosis, and pathogenesis. *Lancet Neurol.* 10, 1074–85. doi: 10.1016/S1474-4422(11)70232-0

Postuma, R. B., Berg, D., Stern, M., Poewe, W., Olanow, C. W., Oertel, W., et al. (2015). MDS clinical diagnostic criteria for Parkinson's disease. *Mov. Disord.* 30, 1591–601. doi: 10.1002/mds.26424

Punia, S., Das, M., Behari, M., Mishra, B. K., Sahani, A. K., Govindappa, S. T., et al. (2010). Role of polymorphisms in dopamine synthesis and metabolism genes and association of DBH haplotypes with Parkinson's disease among North Indians. *Pharmacogenet. Genom.* 20, 435–41. doi: 10.1097/FPC.0b013e32833ad3bb

Rengmark, A., Pihlstrøm, L., Linder, J., Forsgren, L., and Toft, M. (2016). Low frequency of GCH1 and TH mutations in Parkinson's disease. *Parkinsonism Relat. Disord.* 29, 109–111. doi: 10.1016/j.parkreldis.05010

Richards, S., Aziz, N., Bale, S., Bick, D., Das, S., Gastier-Foster, J., et al. (2015). Standards and guidelines for the interpretation of sequence variants: a joint consensus recommendation of the American college of medical genetics and genomics and the association for molecular pathology. *Genet. Med.* 17, 405–24. doi: 10.1038/gim.2015.30

Shetty, A. S., Bhatia, K. P., and Lang, A. E. (2019). Dystonia and Parkinson's disease: what is the relationship? *Neurobiol. Dis.* 132, 104462. doi: 10.1016/j.nbd.05001

Sutherland, G., Mellick, G., Newman, J., Double, K. L., Stevens, J., Lee, L., et al. (2008). Haplotype analysis of the IGF2-INS-TH gene cluster in Parkinson's disease. *Am. J. Med. Genet. B Neuropsychiatr. Genet.* 147b, 495–459. doi: 10.1002./ajmg.b.30633

Szklarczyk, D., Gable, A. L., Lyon, D., Junge, A., Wyder, S., Huerta-Cepas, J., et al. (2019). STRING v11: protein-protein association networks with increased coverage, supporting functional discovery in genome-wide experimental datasets. *Nucleic Acids Res.* 47, D607–D613. doi: 10.1093/nar/gky1131

Tolosa, E., and Compta, Y. (2006). Dystonia in Parkinson's disease. *J. Neurol.* 253(Suppl 7), VII7–VII13. doi: 10.1007./s00415-006-7003-6

Tzadok, M., Nissenkorn, A., Porper, K., Matot, I., Marcu, S., Anikster, Y., et al. (2014). The many faces of Glut1 deficiency syndrome. *J. Child Neurol.* 29, 349–59. doi: 10.1177/0883073812471718

van der Weijden, M. C. M., Rodriguez-Contreras, D., Delnooz, C. C. S., Robinson, B. G., Condon, A. F., Kielhold, M. L., et al. (2021). A gain-of-function variant in dopamine D2 receptor and progressive chorea and dystonia phenotype. *Mov. Disord.* 36, 729–739. doi: 10.1002/mds.28385

Wickremaratchi, M. M., Knipe, M. D., Sastry, B. S., Morgan, E., Jones, A., Salmon, R., et al. (2011). The motor phenotype of Parkinson's disease in relation to age at onset. *Mov. Disord.* 26, 457–63. doi: 10.1002/mds.23469

Wijemanne, S., and Jankovic, J. (2015). Dopa-responsive dystonia–clinical and genetic heterogeneity. *Nat. Rev. Neurol.* 11, 414–24. doi: 10.1038/nrneurol.2015.86

Wirth, T., Mariani, L. L., Bergant, G., Baulac, M., Habert, M. O., Drouot, N., et al. (2020). Loss-of-function mutations in NR4A2 cause dopa-responsive dystonia parkinsonism. *Mov. Disord.* 35, 880–885. doi: 10.1002/mds.27982

Wu, M. C., Lee, S., Cai, T., Li, Y., Boehnke, M., and Lin, X. (2011). Rare-variant association testing for sequencing data with the sequence kernel association test. *Am. J. Hum. Genet.* 89, 82–93. doi: 10.1016/j.ajhg.05029

Yan, Y. P., Zhang, B., Shen, T., Si, X. L., Guo, Z. Y., Tian, J., et al. (2018). Study of GCH1 and TH genes in Chinese patients with Parkinson's disease. *Neurobiol. Aging* 68, 159e3–159e6. doi: 10.1016/j.neurobiolaging.02004

Zech, M., Lam, D. D., Francescatto, L., Schormair, B., Salminen, A. V., Jochim, A., et al. (2015). (2015). Recessive mutations in the alpha3 (VI) collagen gene COL6A3 cause early-onset isolated dystonia. *Am. J. Hum. Genet.* 96, 883–893. doi: 10.1016/j.ajhg.04010

Zhao, Y., Qin, L., Pan, H., Liu, Z., Jiang, L., He, Y., et al. (2020). The role of genetics in Parkinson's disease: a large cohort study in Chinese mainland population. *Brain* 143, 2220–2234. doi: 10.1093/brain/awaa167

frontiers | Frontiers in Pharmacology

TYPE Original Research
PUBLISHED 12 June 2023
DOI 10.3389/fphar.2023.1203349

OPEN ACCESS

EDITED BY
Woon-Man Kung,
Chinese Culture University, Taiwan

REVIEWED BY
Juexian Song,
Capital Medical University, China
Priyanka Baloni,
Purdue University, United States

*CORRESPONDENCE
Mosaburo Kainuma,
kainuma@med.u-toyama.ac.jp

RECEIVED 10 April 2023
ACCEPTED 30 May 2023
PUBLISHED 12 June 2023

CITATION
Kainuma M, Kawakatsu S, Kim J-D, Ouma S, Iritani O, Yamashita K-I, Ohara T, Hirano S, Suda S, Hamano T, Hieda S, Yasui M, Yoshiiwa A, Shiota S, Hironishi M, Wada-Isoe K, Sasabayashi D, Yamasaki S, Murata M, Funakoshi K, Hayashi K, Shirafuji N, Sasaki H, Kajimoto Y, Mori Y, Suzuki M, Ito H, Ono K and Tsuboi Y (2023), Metabolic changes in the plasma of mild Alzheimer's disease patients treated with Hachimijiogan.
Front. Pharmacol. 14:1203349.
doi: 10.3389/fphar.2023.1203349

Metabolic changes in the plasma of mild Alzheimer's disease patients treated with Hachimijiogan

Mosaburo Kainuma[1]*, Shinobu Kawakatsu[2], Jun-Dal Kim[3], Shinji Ouma[4], Osamu Iritani[5], Ken-Ichiro Yamashita[6], Tomoyuki Ohara[7], Shigeki Hirano[8], Shiro Suda[9], Tadanori Hamano[10], Sotaro Hieda[11], Masaaki Yasui[12], Aoi Yoshiiwa[13], Seiji Shiota[13], Masaya Hironishi[14], Kenji Wada-Isoe[15], Daiki Sasabayashi[16], Sho Yamasaki[17], Masayuki Murata[17], Kouta Funakoshi[18], Kouji Hayashi[19], Norimichi Shirafuji[10], Hirohito Sasaki[10], Yoshinori Kajimoto[14], Yukiko Mori[11], Michio Suzuki[16], Hidefumi Ito[12], Kenjiro Ono[20] and Yoshio Tsuboi[4]

[1]Department of Japanese Oriental Medicine Graduate School of Medicine and Pharmaceutical Sciences, University of Toyama, Toyama, Japan, [2]Aizu Medical Center, Department of Neuropsychiatry, Fukushima Medical University, Aizuwakamatsu, Japan, [3]Department of Research and Development, Division of Complex Biosystem Research (CBR), Institute of National Medicine (INM), University of Toyama, Toyama, Japan, [4]Department of Neurology, School of Medicine, Fukuoka University, Fukuoka, Japan, [5]Department of Geriatric Medicine, Kanazawa Medical University, Ishikawa, Japan, [6]Translational Neuroscience Center, Graduate School of Medicine, International University of Health and Welfare, Tochigi, Japan, [7]Department of Neuropsychiatry, Graduate School of Medical Sciences, Kyushu University, Fukuoka, Japan, [8]Department of Neurology, Graduate School of Medicine, Chiba University, Chiba, Japan, [9]Department of Psychiatry, Jichi Medical University, Tochigi, Japan, [10]Second Department of Internal Medicine, Division of Neurology, Faculty of Medical Sciences, University of Fukui, Fukui, Japan, [11]Department of Medicine, Division of Neurology, Showa University School of Medicine, Tokyo, Japan, [12]Department of Neurology, Wakayama Medical University, Wakayama, Japan, [13]Department of General Medicine, Oita University Faculty of Medicine, Oita, Japan, [14]Department of Internal Medicine, Wakayama Medical University Kihoku Hospital, Wakayama, Japan, [15]Department of Dementia Medicine, Kawasaki Medical School, Okayama, Japan, [16]Department of Neuropsychiatry, Graduate School of Medicine and Pharmaceutical Sciences, University of Toyama, Toyama, Japan, [17]Department of General Internal Medicine, Kyushu University Hospital, Fukuoka, Japan, [18]Department of Clinical Research Promotion, Kyushu University Hospital, Fukuoka, Japan, [19]Department of Rehabilitation, Fukui Health Science University, Fukui, Japan, [20]Department of Neurology, Kanazawa University Graduate School of Medical Sciences, Ishikawa, Japan

Background: Alzheimer's disease (AD), the most prevalent form of dementia, is a debilitating, progressive neurodegeneration. Amino acids play a wide variety of physiological and pathophysiological roles in the nervous system, and their levels and disorders related to their synthesis have been related to cognitive impairment, the core feature of AD. Our previous multicenter trial showed that hachimijiogan (HJG), a traditional Japanese herbal medicine (Kampo), has an adjuvant effect for Acetylcholine estelase inhibitors (AChEIs) and that it delays the deterioration of the cognitive dysfunction of female patients with mild AD. However, there are aspects

Abbreviations: AChEI; acetylcholinesterase inhibitor, AD; Alzheimer's disease, ADAS-Jcog; Alzheimer's Disease Assessment Scale-cognitive component-Japanese version, CREB; cAMP response element binding prote, HJG; Hachimijiogan, RED Cap; Research electronical data capture.

of the molecular mechanism(s) by which HJG improves cognitive dysfunction that remain unclear.

Objectives: To elucidate through metabolomic analysis the mechanism(s) of HJG for mild AD based on changes in plasma metabolites.

Methods: Sixty-seven patients with mild AD were randomly assigned to either an HJG group taking HJG extract 7.5 g/day in addition to AChEI or to a control group treated only with AChEI (HJG:33, Control:34). Blood samples were collected before, 3 months, and 6 months after the first drug administration. Comprehensive metabolomic analyses of plasma samples were done by optimized LC-MS/MS and GC-MS/MS methods. The web-based software MetaboAnalyst 5.0 was used for partial least square-discriminant analysis (PLS-DA) to visualize and compare the dynamics of changes in the concentrations of the identified metabolites.

Results: The VIP (Variable Importance in Projection) score of the PLS-DA analysis of female participants revealed a significantly higher increase in plasma metabolite levels after HJG administration for 6 months than was seen in the control group. In univariate analysis, the aspartic acid level of female participants showed a significantly higher increase from baseline after HJG administration for 6 months when compared with the control group.

Conclusion: Aspartic acid was a major contributor to the difference between the female HJG and control group participants of this study. Several metabolites were shown to be related to the mechanism of HJG effectiveness for mild AD.

KEYWORDS

metabolomic analysis, Alzheimer's disease, hachimijiogan, aspartic acid, kampo

Introduction

The cognitive and memory impairment of dementia patients has been shown to lead to negative changes in behavior and activities of daily life (Cipriani et al., 2020). Currently, more than 55 million people suffer from dementia worldwide, with an incidence of about 10 million each year. Alzheimer's disease (AD), the most prevalent form of dementia, is a debilitating, progressive form of neurodegeneration that accounts for 60%–70% of this disease that creates an enormous burden on public health systems around the world (World health Organization, 2023).

Numerous therapies have been developed in an attempt to alleviate or cure symptoms (Jeon et al., 2019). Notably, aducanumab was recently approved for mild AD (Billy et al., 2021); however, there is currently no available treatment that is an effective cure. The discovery and introduction of new therapeutic agents and strategies for AD are urgently needed.

"Kidney[™] deficiency" is one of the key pathologies of Kampo medicine, defined as a pattern characterized by an insufficient amount of essential qi of kidney. Hachimijiogan (HJG) is a traditional Japanese (herbal) medicine (Kampo) composed of eight herbs that is prescribed for the treatment of "Kidney[™] deficiency" (Terasawa, 1993; Kainuma et al., 2022). It is effective for various symptoms common to members of the older population, such as numbness, nocturia, lower back pain and coldness in the legs, and is used for cases of impotence, nephritis, diabetes, sciatica, bladder catarrh, lumbago, prostatic hypertrophy, and hypertension (Nakae et al., 2018). In Kampo, cognitive impairment is considered to be a sign of "Kidney[™] deficiency". We previously demonstrated the effectiveness of HJG for AD both *in vivo* and *in vitro*: improvement was seen in the spatial memory impairment of AD model rats and in cognitive function via cAMP response element binding protein (CREB) (Kubota et al., 2017; Moriyama et al., 2017). Although not conclusive, we reported in a clinical trial that HJG has an adjuvant effect for acetylcholinesterase inhibitors (AChEIs) and that it delays the deterioration of the cognitive dysfunction of mild AD patients (Kainuma et al., 2022). However, there are aspects of the molecular mechanism(s) by which HJG improves cognitive dysfunction that remain unclear.

Metabolomics is a system-biology technology that can be used to monitor the dynamic changes of endogenous small-molecule metabolites (Nicholson et al., 2002). Several blood metabolic biomarker studies of AD have reported that changes in phospholipids, polyamines, and amino acids have potential for use in diagnosis (Chouraki et al., 2017; Huo et al., 2020; Lin et al., 2019b; Olazarán et al., 2015; Orešič et al., 2011; Ozaki et al., 2022; Peña-Bautista et al., 2019; Shao et al., 2020; Trushina and Mielke, 2014; Wan et al., 2020; Wilkins and Trushina, 2018). Kampo medicines are multi-component, multi-targeted drugs that act on various targets in the body. To understand the complex actions of Kampo medicines, it is important to extensively study the biological reactions they induce and the relation of the components to these reactions. Because it has been shown to be a useful tool for elucidating complex pharmacological actions and evaluating the effects of Kampo medicines on the living body (Kitagawa et al., 2018; Yamashita et al., 2021; Kobayashi et al., 2022), comprehensive metabolomic analysis was used in this study to determine the mechanism(s) of the effectiveness of HJG for mild AD.

Methods

The data analyzed in this study was from our previous open-label, randomized, multicenter, control trials (Kainuma et al., 2020; Kainuma et al., 2022).

Ethics

The study was done in accordance with the principles of the Declarations of Helsinki and Tokyo and approved by the Kyushu University Hospital Clinical Research Review Board (CRB) (Fukuoka, Japan) (CRB approval number: KD 2019001). All participants gave written, informed consent.

Study design

This study started 2 August 2019 at three sites in Japan. Unfortunately, recruitment was delayed because of the COVID-19 pandemic, but we adjusted and were able to add 11 institutions by January of 2021. The study finished on 31 March 2022. In brief, our protocol was done with mild AD patients who met all the inclusion criteria:

1) Age: ≥50 to <85 years old, 2) Mild Alzheimer's disease (MMSE ≥21), 3) Taking the same dose of Donepezil, Galantamine, or Rivastigmine for more than 3 months, 4) Not taking Memantine, and 5) Written informed consent. Patients were excluded who were taking Kampo Medicine other than HJG for more than 3 months or who had a change in drug dosage that could affect the progression of cognitive function during the 3 months. The other major exclusion criteria are as follows: 1) Kidney dysfunction (eGFR<30 mL/min/1.73 m^2); 2) AST or ALT>100 IU/L; 3) Complication with gastric ulcer, bronchial asthma, or epilepsy; and 4) Judged by doctors not to be suited for study, such as having serious complications.

Participants were divided into an AChEI plus HJG group and an AChEI alone group to compare the effectiveness and safety of the addition of HJG. In addition to AChEI, the HJG group took 2.5 g of HJG extract 3 times/day (TSUMURA hachimijiogan Extract Granules for Ethical Use: TJ-7, HJG, Tokyo Japan), the usual adult daily dose. Randomization was done with the Randomization Module of Research Electronical Data Capture (RED Cap). A computer-generated list of random numbers was transferred to RED Cap for block randomization by age and sex, then the participants were randomly assigned at a 1:1 ratio. Participants, physicians and data evaluators were aware of the allocation group after randomization, but outcome evaluators were blinded.

The primary outcome was the change of the Cognitive Component of the Alzheimer's Disease Assessment Scale—Japanese Version (ADAS-Jcog) from baseline to 6 months, with assessments done at baseline and after 3 and 6 months. Blood tests were done at the same time points for the analyses of the metabolome, with samples collected at least 4 hours after breakfast. Plasma was separated by centrifugation at 2000 f for 25 min at 4°C, immediately stored at −80°C, and kept frozen until use.

Metabolomics analysis

We analyzed the plasma metabolome using gas chromatography-tandem mass spectrometry (GC-MS/MS; GCMS-TQ8040, Shimadzu, Kyoto, Japan) and liquid chromatography-tandem mass spectrometry (LC-MS/MS; Nexera X2 system connected with LCMS-8050, Shimadzu). We extracted, measured, and analyzed both hydrophilic and hydrophobic metabolites, including lipid mediators and phospholipids, in accordance with previously reported methods (Kitagawa et al., 2018; Yamashita et al., 2021).

Statistical analysis

The search for the HJG biomarkers was done through analysis of covariance of the change in metabolites from baseline, with the treatment group and baseline values as covariates. Continuous variables are expressed as the mean value and standard deviation.

A two-tailed test at the 5% level of significance was done for the statistical analyses. Two-tailed interval estimation was done with a 95% confidence interval (CI) and corresponding p values (with significance defined as $p < 0.05$). A t-test was used for comparison of the metabolomics of the HJG and control groups at each visit, with $p < 0.05$ representing a significant difference. JMP (Ver. 16, SAS Institute Japan Ltd.) was used for these analyses. In addition, to maximize class discrimination necessary for the identification discovery of potential metabolic biomarkers of between the HJG and Control groups, a supervised model of potential least squares discriminant analysis (PLS-DA) was applied. Variable importance in the projection (VIP) values were used in the PLS-DA model to estimate the discriminatory power of each variable for separation of the groups. The features, and variables with VIP values > 1 were considered important. The validation of all PLS-DA models was based on the leave-one-out cross validation method via parameters Q2 and R2. The significance of these models was demonstrated by permutation test with 2000 iterations using separation distance and p-value < 0.05.

Results

From among the 77 enrollees, the data of 67 (33 HJG and 34 control) were available for analysis: 2 of the 69 patients analyzed for the primary endpoint were not available for analysis due to hemolysis (Figure 1). No difference was found in the background factors between the HJG and control groups (Table 1).

Differential metabolite analysis

We conducted a comprehensive analysis of plasma metabolites to search for HJG biomarkers. The results for the plasma metabolites of male participants at 3 months in the HJG group showed significant change in hippuric acid, DHA, EPA, and phosphatidylcholine (PC) (36_1) and PC (36_2). At 6 months, hippuric acid, phenylacetic acid, suberic acid, tartaric acid, 2-

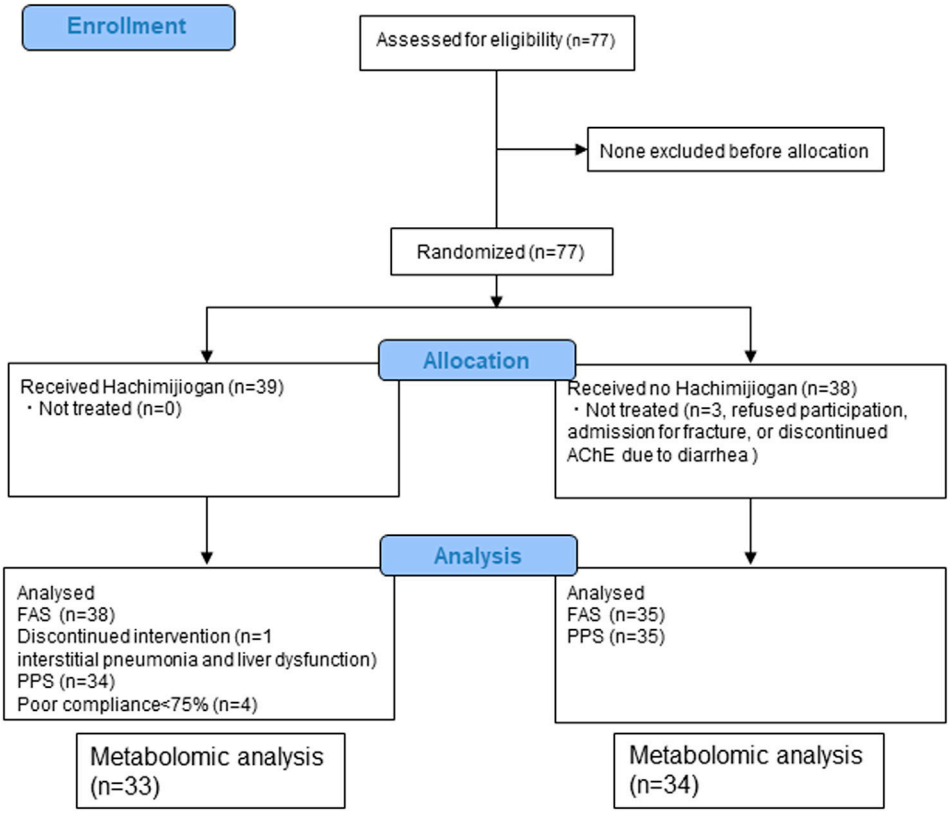

FIGURE 1
Enrollment, Randomization, and Trial completion.

Aminooctanoic acid, and 3-phosphoglyceric acid also showed more significant change in the HJG group than in the control group.

For the female participants of the HJG group at 3 months, suberic acid, tartaric acid and 1,5-anhydro-glucitol showed significant change. They also had significantly greater change of aspartic acid, 1-hexadecanol, 2-hydroxyisovaleric acid, 3-hydroxybutyric acid, and 3-hydroxyisobutyric acid at 6 months.

In the comparison of the metabolomics data for which more significant change from baseline was seen in the HJG group than in the control group at each testing point (day0, 3 M, and 6 M), the 3-phosphoglyceric acid of male participants at 6 months was significantly higher in the HJG group (Table 2). For the female participants, aspartic acid was significantly higher in the HJG group than in the control group (Table 3). In the analysis of aspartic acid, the difference in the change from baseline to 6 months of the HJG and control groups was 0.0099 (95% CI, 0.0015 to 0.0184 $p = 0.0223$) (Figure 2).

Visualization of metabolites

A PLS-DA model with unit variance scaling was used to visualize the differences in the metabolites of the HJG and Control groups and to determine which metabolites can be used to distinguish between the two groups, As shown in Figures 3, 4, plots of the PLS-DA score values of components 1 and 2 demonstrated visible clustering and clear separation between the HJG and control groups. Moreover, the VIP (Variable Importance in Projection) score of the PLS-DA analysis of male participants revealed significantly greater increases in 17,18-DHETE, EPA, DHA, and hippuric acid levels after HJG administration for 3 months than were seen in the control group. 3-phosphoglyce, O-phosphoethan, suberic acid, 17,18-DHETE, phenylacetic acid, hypotaurine, and aspartic acid had a significantly greater increase at 6 months.

In contrast, the VIP score of the PLS-DA analysis of female participants revealed a significantly greater increase in tartaric acid, tryptophan, suberic acid, pyridoxal, cysteine, and hippuric acid after HJG administration for 3 months, compared with the control group, and that proline, tartaric acid, alanine, cystathionine, and aspartic acid had a significantly greater increase at 6 months (Figures 5, 6).

Discussion

This is the first study to use metabolomic analysis to investigate the mechanism(s) of the action of HJG in a clinical study of dementia. The results of univariate and metabolomic analysis showed a significantly greater elevation of aspartic acid after

TABLE 1 Baseline characteristics.

	HJG group (n = 33)	Control group (n = 34)
Sex (male/female)	12/21	14/20
Age, years	75 ± 7.1	76 ± 7.3
Height (cm)	157 ± 9.4	157 ± 7.9
Body weight (kg)	55 ± 11	53 ± 10
Body mass index (Kg/m^2)	22 ± 3.7	21 ± 3.2
BUN (mg/dL)	17 ± 4.0	17 ± 5.3
Creatinine (mg/dL)	0.83 ± 0.20	0.79 ± 0.26
eGFR (mL/min/1.73 mm^2)	60 ± 14	67 ± 19
Albumin (g/dL)	4.1 ± 0.3	4.1 ± 0.3
HbA1c (%)	5.9 ± 0.6	6.1 ± 1.0
Systolic Hypertension (mmHg)	131 ± 17	133 ± 16
Diastolic Hypertension (mmHg)	76 ± 13	79 ± 11
Disease duration, years	3.7 ± 2.9	2.8 ± 2.2
Education (university/non university)	10/23	6/28
ADS-Jcog	14 ± 5.4	14 ± 5.7
IADL	5.3 ± 2.5	4.9 ± 2.2
NPI-Q score	4.9 ± 7.5	4.4 ± 8.5
Apathy scale	14 ± 7.4	14 ± 6.5
Hypertension, n (%)	14 (42%)	17 (50%)
Dyslipidemia, n (%)	11 (33%)	13 (38%)
Diabetes mellitus, n (%)	6 (18%)	6 (18%)
Old brain infarction, n (%)	1 (3%)	0 (0%)
AChE inhibitor		
Donepezil	17 (52%)	23 (68%)
Galantamine	10 (30%)	6 (18%)
Rivastigmine	6 (18%)	4 (12%)

6 months of HJG in female subjects when compared to controls. These results indicate that an increase in aspartic acid is an important mechanism in the action of HJG on cognitive function. Because this part of the analysis used the same female patients as were used for the primary endpoint, the significantly greater improvement in cognitive function at 6 months of these female patients treated with HJG (the difference in change from baseline at 6 months for female participants was 2.90 (90% CI, 0.09 to 5.71, $p = 0.090$) was shown not to be due to a synergistic effect with AchEI: it was the effect of HJG alone (Kainuma et al., 2022).

Aspartic acid is involved in the development of nerves and their activity in the central nervous system. It has been reported that the concentration of aspartic acid in blood and cerebrospinal fluid was decreased in an AD group compared to a normal group (D'Aniello et al., 2005; Olazarán et al., 2015). In their AD group, aspartic acid was also decreased in the brain, and a decrease in aspartic acid was reported to be correlated with the severity of AD (Kwo-On-Yuen et al., 1994). Of the many reports that use metabolome analysis of early stage AD (Chouraki et al., 2017; Lin et al., 2019a; Orešič, et al., 2011; Shao et al., 2020; Ozaki et al., 2022; Peña-Bautista et al., 2019), some have concluded that aspartic acid is useful for diagnosis (Huo et al., 2020; Olazarán et al., 2015; Trushina and Mielke, 2014; Wilkins and Trushina, 2018). These findings indicate that aspartic acid plays an important role in the maintenance of cognitive function. The results of our study indicate that HJG causes an increase of aspartic acid in the blood and a subsequent increase in aspartic acid in the brain, thereby suppressing the progress of cognitive function.

We previously reported in an *in vitro* study that HJG improves cognitive function through the phosphorylation of CREB (Kubota et al., 2017). Aspartic acid acts as a neurotransmitter and increases cAMP as a second messenger after stimulating receptors (D'Aniello

TABLE 2 Comparison of metabolites that had a significant difference in change from baseline (Male).

	Control			HJG		
	Day0	3M	6M	Day0	3M	6M
2-Aminooctanoic acid	0.003693 ± 0.001384	0.003932 ± 0.001711	0.003640 ± 0.001457	0.003912 ± 0.001962	0.004848 ± 0.002956	0.005183 ± 0.003472
3-Phosphoglyceric acid	0.000644 ± 0.000649	0.000552 ± 0.000312	0.000469 ± 0.001940	0.000870 ± 0.000529	0.000745 ± 0.000367	0.000815 ± 0.000418*
DHA	23.0969 ± 14.7251	16.6165 ± 10.3592	19.7715 ± 8.12547	23.0022 ± 14.5089	2 8.3068 ± 16.0475*	23.8425 ± 14.9368
EPA	3.87960 ± 2.96857	2.77862 ± 2.22006	3.14813 ± 1.49982	4.73024 ± 3.63317	6.02772 ± 3.99360*	5.36306 ± 3.849780
Hippuric acid	0.008413 ± 0.004493	0.006756 ± 0.005127	0.006799 ± 0.00464	0.008294 ± 0.009689	0.014966 ± 0.012421*	0.010992 ± 0.009915
PC (36_1)	29525625 ± 7838875.2	29992108 ± 10080484	29016862 ± 70877071.6	26260834 ± 11234604	32087620 ± 18430237	26650192 ± 8319154.6
PC (36_2)	183062364 ± 34245385	179692379 ± 38287164	169556757 ± 33394758	156467692 ± 45534033	183376700 ± 5684525	168844522 ± 50887932
Phenylacetic acid	0.001992 ± 0.001410	0.001965 ± 0.001427	0.001614 ± 0.001306	0.002155 ± 0.001514	0.002357 ± 0.001448	0.002563 ± 0.001682
Suberic acid	0.000955 ± 0.000267	0.000950 ± 0.000235	0.000872 ± 0.000190	0.000953 ± 0.000266	0.000964 ± 0.000187	0.000994 ± 0.000140
Tartaric acid	0.003790 ± 0.005934	0.002819 ± 0.002584	0.003532 ± 0.005427	0.002014 ± 0.000288	0.002772 ± 0.001098	0.002598 ± 0.000595

Mean ± SD. *$p < 0.05$.

TABLE 3 Comparison of metabolites that had a significant difference in change from baseline (Female).

	Control			HJG		
	Day0	3M	6M	Day0	3M	6M
Hexadecanol	0.003556 ± 0.001064	0.003724 ± 0.001236	0.003915 ± 0.001074*	0.003719 ± 0.000785	0.003770 ± 0.001004	0.003184 ± 0.000672
1,5-Anhydro-glucitol	0.002644 ± 0.001193	0.002899 ± 0.001379	0.002799 ± 0.001222	0.002580 ± 0.000993	0.002469 ± 0.000914	0.002679 ± 0.001137
2-Hydroxyisovaleric acid	0.023122 ± 0.008545*	0.022005 ± 0.007776	0.020061 ± 0.006961	0.017151 ± 0.005780	0.017675 ± 0.007805	0.019717 ± 0.008704
3-Hydroxybutyric acid	0.721135 ± 0.569033*	0.544997 ± 0.429438	0.501202 ± 0.359687″	0.326616 ± 0.341714	0.498769 ± 0.817871	0.191881 ± 0.156353
3-Hydroxyisobutyric acid	0.139914 ± 0.08404″	0.112181 ± 0.063638	0.105465 ± 0.056151″	0.079633 ± 0.053163	0.105273 ± 0.119125	0.061700 ± 0.028088
Aspartic acid	0.039730 ± 0.020842	0.041106 ± 0.016687	0.035451 ± 0.010251	0.038523 ± 0.014260	0.038809 ± 0.012114	0.045122 ± 0.016428*
Suberic acid	0.000945 ± 0.000313	0.000916 ± 0.000200	0.000981 ± 0.000207	0.000936 ± 0.000233	0.001029 ± 0.000188	0.000929 ± 0.000237
Tartaric acid	0.002395 ± 0.001089	0.001995 ± 0.000225	0.002935 ± 0.003280	0.002494 ± 0.001064	0.002797 ± 0.001203″	0.004170 ± 0.003245

Mean ± SD *$p < 0.05$, ″$p < 0.01$.

10.3389/fphar.2023.1203349

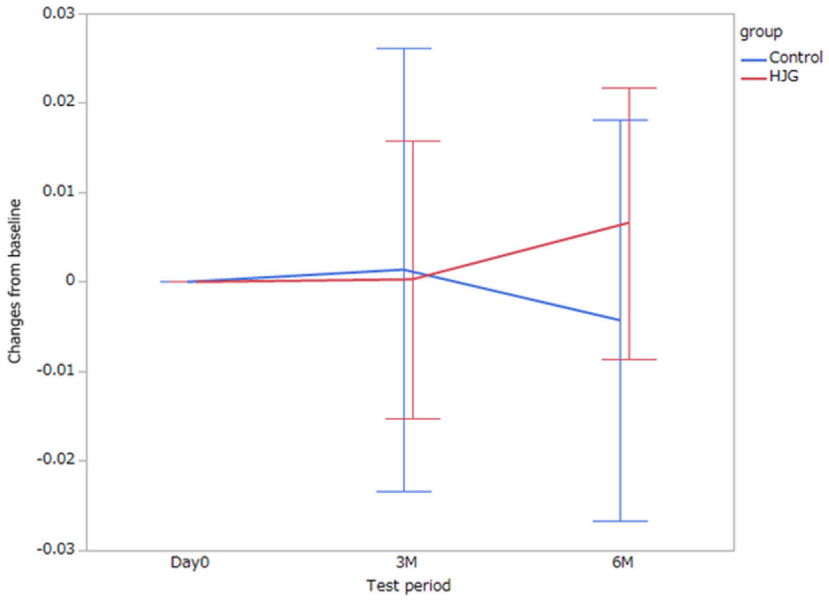

FIGURE 2
Difference between the HJG and control group female participants in the change of aspartic acid from baseline to 3 and 6 months.

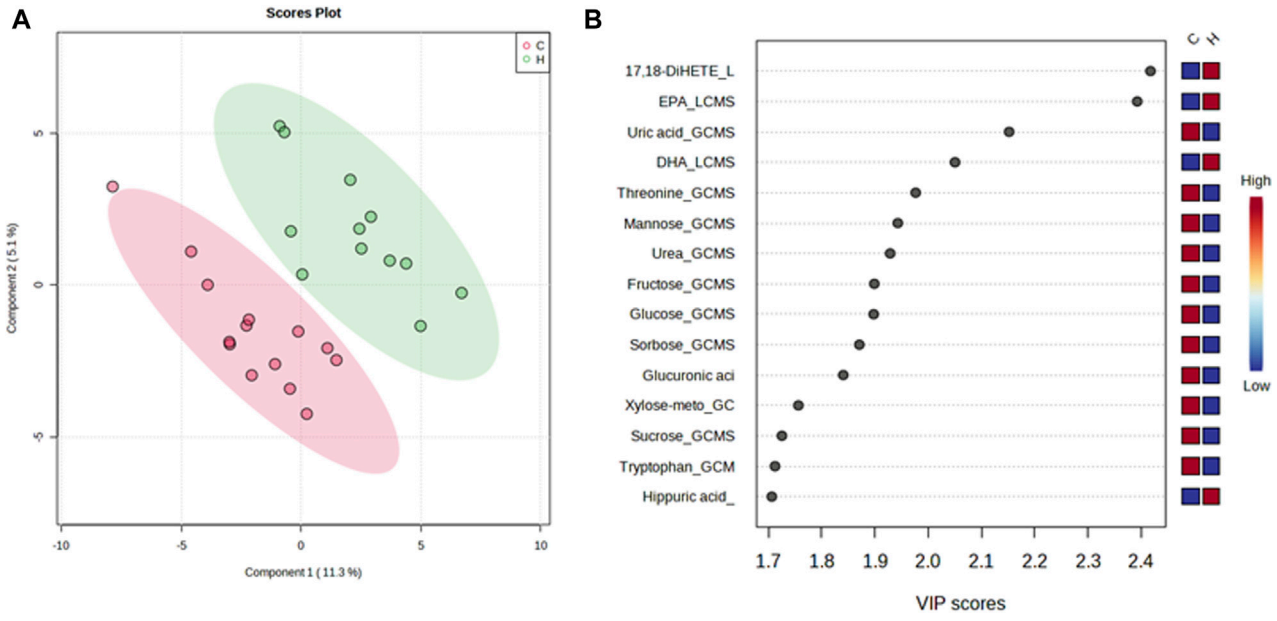

FIGURE 3
Partial least squares-discriminate analysis (PLS-DA) plot of the differential metabolites of the HJG and control group male participants and their importance in the projection (VIP) values at 3 months. **(A)** Score plot for PLS-DA of the HJG (H, green dots) (n = 12) and control groups (C, red dots) (n = 14). **(B)** The highest VIP values for the 1st component of PLS-DA. The blue to red color shift denotes low to high plasma metabolite concentrations.

et al., 2011.). Because cAMP is upstream of CREB phosphorylation, an aspartic acid-induced cAMP increase may induce CREB phosphorylation. The results of our study indicate that the increase in aspartic acid by HJG is involved in the phosphorylation of CREB. On the other hand, because aspartic acid in PC12 cells has been reported to increase during neuronal differentiation of PC12 cells (Sano et al., 2018), the increase in aspartic acid may be a product of HJG-induced neurite outgrowth.

Metabolomic analysis of donepezil has been done to examine lipid metabolism, but no significant findings were obtained, and there are no

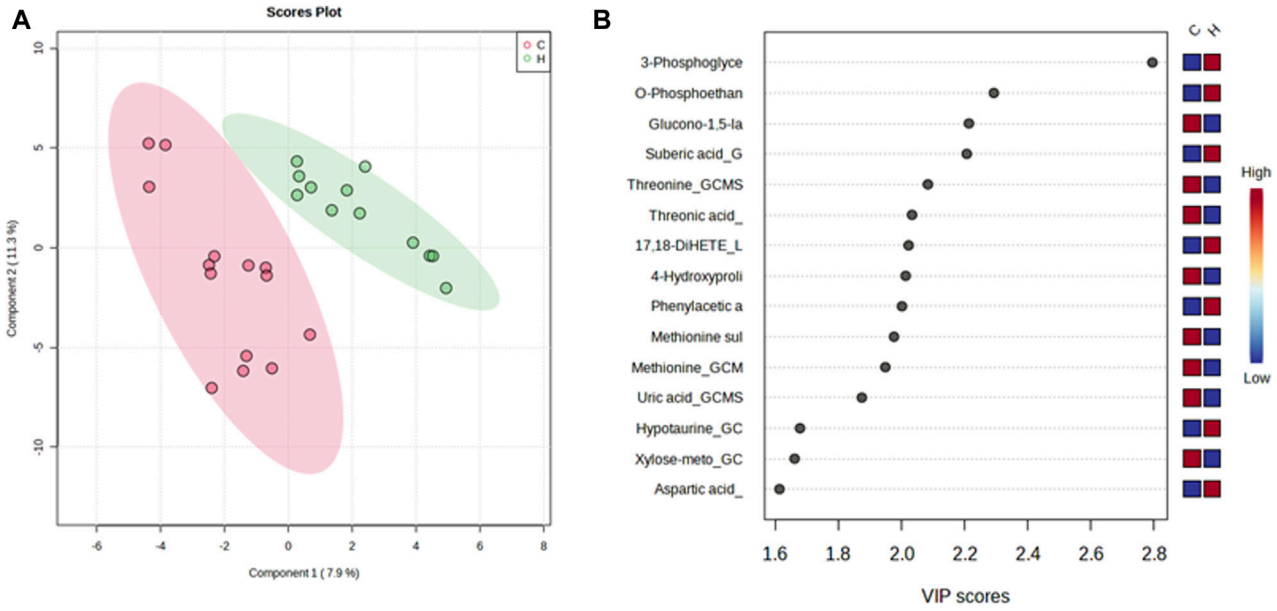

FIGURE 4
PLS-DA plot of differential metabolites and their corresponding VIP values for male participants at 6 months. **(A)** Score plot of the PLS-DA of the HJG (H, green dots) (*n* = 12) and control groups (C, red dots) (*n* = 14). **(B)** The highest VIP values for the 1st component of PLS-DA. The blue to red color shift denotes low to high plasma metabolite concentrations.

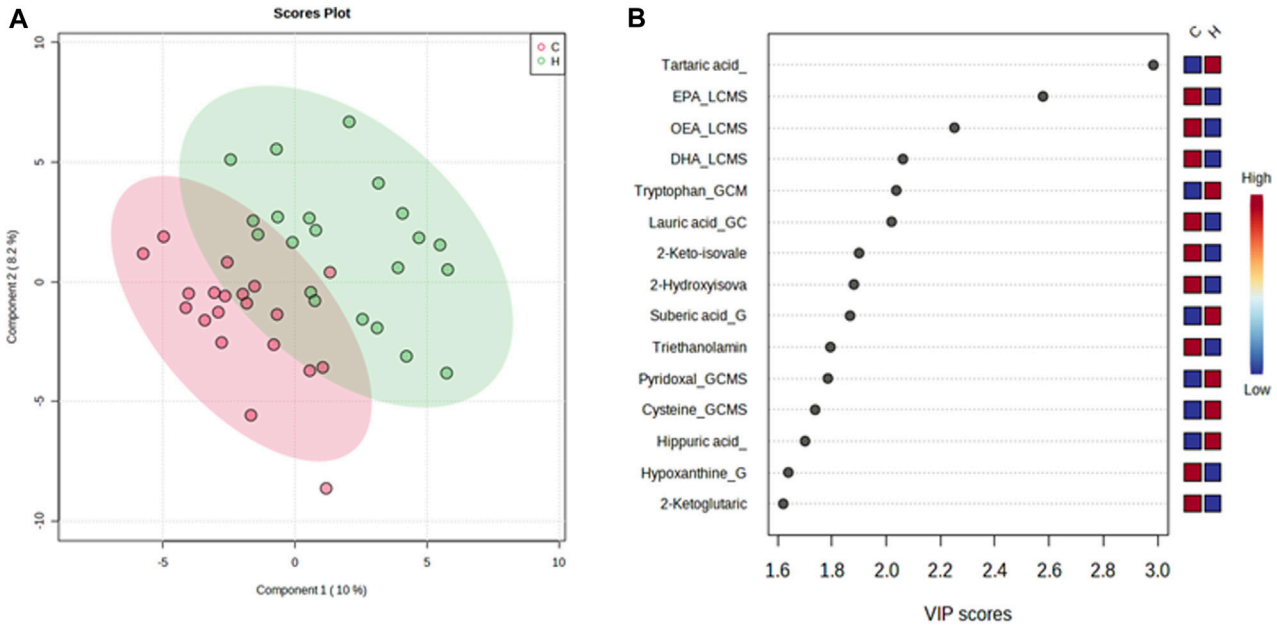

FIGURE 5
PLS-DA plot of differential metabolites and their corresponding VIP values for the female participants at 3 months. **(A)** Score plot of the PLS-DA of the HJG (H, green dots) (*n* = 21) and control groups (C, red dots) (*n* = 20). **(B)** The highest VIP values for the 1st component of PLS-DA. The blue to red color shift denotes low to high plasma metabolite concentrations.

reports of amino acid changes (Wan et al., 2020). There are also no reports on the use of metabolomics for responder analysis of dementia drugs other than donepezil. In this respect, responder analysis of HJG based on metabolome analysis, as used in this study is important, thus our results indicate that aspartic acid would be useful as a therapeutic drug for dementia.

The drugs used in Kampo medicine are combinations of two or more herbs, thus it is difficult to identify the causative agent in the

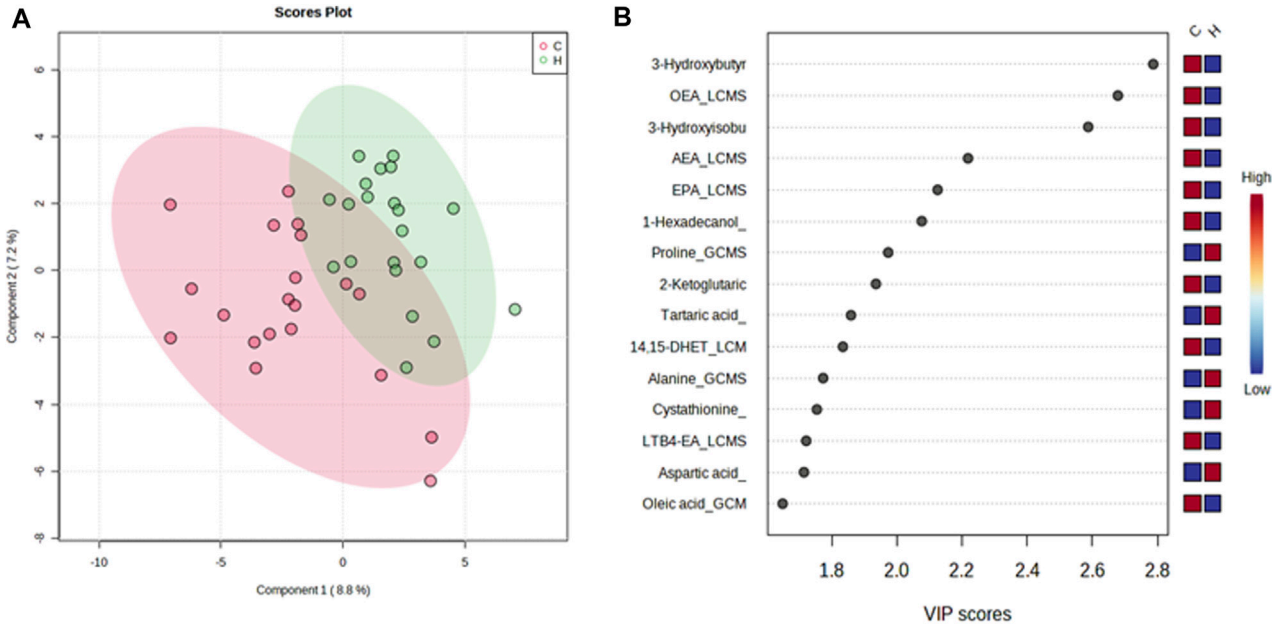

FIGURE 6
PLS-DA plot of differential metabolites and their corresponding VIP values for the female participants at 6 months. **(A)** Score plot of the PLS-DA of the HJG (H, green dots) (*n* = 21) and control groups (C, red dots) (*n* = 20). **(B)** The highest VIP values for the 1st component of PLS-DA. The blue to red color shift denotes low to high plasma metabolite concentrations.

same way as can be done for Western medicines. Although not detected in the univariate analysis in the present study, metabolomic analysis has shown that, in addition to aspartic acid, proline, tartaric acid, alanine, and cystathionine had significantly greater elevation after 6 months than was seen in our control group. Further, proline, alanine, and cystathionine has been correlated with cognitive decline associated with dementia (Xie et al., 2021; Lin et al., 2019b; Zhang et al., 2022). Therefore, it is possible that these substances may interact with each other to improve cognitive function.

The univariate metabolome analysis of the data of male participants showed significantly higher 3-phosphoglyceric acid in the HJG group. There are no reports of correlation between a change of 3-phosphoglyceric acid and cognitive impairment, but our data indicate that this may be related to the effect of HJG. On the other hand, although AD is more common in female patients and gender differences have been reported in the development of AD (Alzheimer's Association, 2023; Altmann et al., 2014; Tao et al., 2018), in the metabolome analysis of this study a significantly greater increase in aspartic acid was found in our male participants than in the controls after 6 months of HJG. This indicates that the results for men might be similar to those of women if we had had more male patients. Our experience has shown that patients who have signs of "Kidney[TM] deficiency" other than cognitive impairment who take HJG long term have less AD than patients who take it for shorter periods of time. Further studies are needed to confirm this observation.

There are several limitations to the present study. The sample size available for analysis was small, especially that of men. Also, the peripheral blood-brain relation of amino acid remains unknown. Finally, only Japanese populations were recruited for this study.

Conclusion

Aspartic acid was the main contributor to the difference between female patients treated with HJG in addition to AChEI and a control group treated with only AChEI. A combination of several metabolites was shown to be related to the mechanism of the effectiveness of HJG for mild AD.

Data availability statement

The raw data supporting the conclusion of this article will be made available by the authors, without undue reservation.

Ethics statement

The studies involving human participants were reviewed and approved by the Kyushu University Hospital Clinical Research Review Board (CRB) (Fukuoka, Japan) (CRB approval number: KD 2019001). The patients/participants provided their written informed consent to participate in this study.

Author contributions

Conceptualization: MK, SO, K-IY, TO, AY, MM, and YT. Investigation: SO, SK, OI, K-IY, TO, ShH, SSu, TH, SoH, MY, AY, SSh, MH, K-IW, DS, KH, NS, HS, YK, YM, MS, HI, KO, and YT,

project administration: MK, methodology: J-DK, KF, and MM, writing-original draft: MK, writing-review and editing: SK, J-DK, and YT. All authors contributed to the article and approved the submitted version.

Funding

This study was supported by a grant from the Japan Agency for Medical Research and Development (AMED) (grant number: JP19lk0310056).

Acknowledgments

Metabolomic analysis was outsourced to Tsumura & Co. (Tokyo, Japan). We also deeply thank Kiyoko Momota and Wakako Hiraoka for their efforts and support for our study.

Conflict of interest

The authors declare that the research was conducted in the absence of any commercial or financial relationships that could be construed as a potential conflict of interest.

Tsumura & Co. (Tokyo, Japan) provided TSUMURA hachimijiogan (TJ-7) Extract Granules for Ethical Use free of charge.

Publisher's note

References

Altmann, A., Tian, L., Henderson, V. W., and Greicius, M. D.Alzheimer's Disease Neuroimaging Initiative Investigators (2014). Sex modifies the APOE-related risk of developing Alzheimer disease. *Ann. Neurol.* 75, 563–573. doi:10.1002/ana.24135

Altzheimer's Association (2023). Altzheimer's disease a facts and Figures. Available at: https://www.alz.org/media/Documents/alzheimers-facts-and-figures (Accessed March 21, 2023).

Billy, D. B., Stein, P., and Cavazzoni, P. (2021). Approval of aducanumab for alzheimer disease—the FDA's perspective. *JAMA Intern Med.* 181, 1276–1278. doi:10.1001/jamainternmed.2021.4607

Chouraki, V., Preis, S. R., Yang, Q., Beiser, A., Li, S., Larson, M. G., et al. (2017). Association of amine biomarkers with incident dementia and Alzheimer's disease in the Framingham Study. *Alzheimers Dement.* 13, 1327–1336. doi:10.1016/j.jalz.2017.04.009

Cipriani, G., Danti, S., Picchi, L., Nuti, A., and Fiorino, M. D. (2020). Daily functioning and dementia. *Dement. Neuropsychol.* 14, 93–102. doi:10.1590/1980-57642020dn14-020001

D'Aniello, A., Fisher, G., Migliaccio, N., Cammisa, G., D'Aniello, E., and Patrizia Spinelli, P. (2005). Amino acids and transaminases activity in ventricular CSF and in brain of normal and Alzheimer patients. *Neurosci. Lett.* 388, 49–53. doi:10.1016/j.neulet.2005.06.030

D'Aniello, S., Somorjai, I., Jordi, G. F., Topo, E., and D'Aniello, A. (2011). D-Aspartic acid is a novel endogenous neurotransmitter. *FASEB J.* 25, 1014–1027. doi:10.1096/fj.10-168492

Honig, L. S., Vellas, B., Woodward, M., Boada, M., Bullock, R., Borrie, M., et al. (2018). Trial of solanezumab for mild dementia due to Alzheimer's disease. *N. Engl. J. Med.* 378, 321–330. doi:10.1056/NEJMoa1705971

Huo, Z., Yu, L., Yang, J., Zhu, Y., Bennett, D. A., and Zhao, J. (2020). Brain and blood metabolome for Alzheimer's dementia: Findings from a targeted metabolomics analysis. *Neurobiol. Aging* 86, 123–133. doi:10.1016/j.neurobiolaging.2019.10.014

Jeon, S. G., Song, E. J., Lee, D., Park, J., Nam, Y., Kim, J. I., et al. (2019). Traditional oriental medicines and Alzheimer's disease. *Aging Dis.* 10, 307–328. doi:10.14336/AD.2018.0328

Kainuma, M., Funakoshi, K., Ouma, S., Yamashita, K. I., Ohara, T., Yoshiiwa, A., et al. (2020). The efficacy and safety of hachimijiogan for mild alzheimer disease in an exploratory, open standard treatment controlled, randomized allocation, multicenter trial: A study protocol. *Med. Baltim.* 99 (38), e22370. doi:10.1097/MD.0000000000022370

Kainuma, M., Ouma, S., Kawakatsu, S., Iritani, O., Yamashita, K. I., Ohara, T., et al. (2022). An exploratory, open-label, randomized, multicenter trial of hachimijiogan for mild Alzheimer's disease. *Front. Pharmacol.* 13, 991982. Published online 2022 Oct 14. doi:10.3389/fphar.2022.991982

Kitagawa, H., Ohbuchi, K., Munekage, M., Fujisawa, K., Kawanishi, Y., Namikawa, T., et al. (2018). Data on metabolic profiling of healthy human subjects' plasma before and after administration of the Japanese Kampo medicine maoto. *Data Brief.* 3, 359–364. doi:10.1016/j.dib.2018.11.116

Kobayashi, A., Nagashima, K., Hu, A., Harada, Y., and Kobayashi, H. (2022). Effectiveness and safety of kamikihito, a traditional Japanese medicine, in managing anxiety among female patients with intractable chronic constipation. *Complement. Ther. Clin. Pract.* 46, 101526. doi:10.1016/j.ctcp.2021.101526

Kubota, K., Fukue, H., Sato, H., Hashimoto, K., Fujikane, A., Moriyama, H., et al. (2017). The traditional Japanese herbal medicine hachimijiogan elicits neurite outgrowth effects in PC12 cells and improves cognitive in AD model rats via phosphorylation of CREB. *Front. Pharmacol.* 8, 850. doi:10.3389/fphar.2017.00850

Kwo-On-Yuen, P. F., Newmark, R. D., Budinger, T. F., Kaye, J. A., M J Ball, M. J., and W Jagust, W. J. (1994). Brain N-acetyl-L-aspartic acid in Alzheimer's disease: A proton magnetic resonance spectroscopy study. *Brain Res.* 667, 167–174. doi:10.1016/0006-8993(94)91494-x

Lin, C. H., Yang, H. T., and Lane, H. Y. (2019a). D-glutamate, D-serine, and D-alanine differ in their roles in cognitive decline in patients with Alzheimer's disease or mild cognitive impairment. *Pharmacol. Biochem. Behav.* 185, 172760. doi:10.1016/j.pbb.2019.172760

Lin, C. N., Huang, C. C., Huang, K. L., Lin, K. J., Yen, T. C., and Kuo, H. C. (2019b). A metabolomic approach to identifying biomarkers in blood of Alzheimer's disease. *Ann. Clin. Transl. Neurol.* 27, 537–545. doi:10.1002/acn3.726

Mintun, M. A., Lo, A. C., Evans, C. D., Wessels, A. M., Ardayfio, P. A., Andersen, S. W., et al. (2021). Donanemab in early Alzheimer's disease. *N. Engl. J. Med.* 384, 1691–1704. doi:10.1056/NEJMoa2100708

Moriyama, H., Mishima, T., Kainuma, M., Watanabe, T., Nagao, M., Takasaki, K., et al. (2017). Effect of hachimijiogan on memory impairment induced by beta-amyloid combined with cerebral ischemia in rats. *Traditional Kampo Med.* 4, 51–54. doi:10.1002/tkm2.1069

Nakae, H., Hiroshima, Y., and Hebiguchi, M. (2018). Kampo medicines for frailty in locomotor disease. *Front. Nutr.* 26 (5), 31. doi:10.3389/fnut.2018.00031

Nicholson, J. K., Connelly, J., Lindon, J. C., and Holmes, E. (2002). Metabonomics: A platform for studying drug toxicity and gene function. *Nat. Rev. Drug. Discov.* 1, 153–161. doi:10.1038/nrd728

Olazarán, J., Gil-de-Gómez, L., Rodríguez-Martín, A., Valentí-Soler, M., Frades-Payo, B., Marín-Muñoz, J., et al. (2015). A blood-based, 7-metabolite signature for the early diagnosis of Alzheimer's disease. *J. Alzheimers Dis.* 45, 1157–1173. doi:10.3233/JAD-142925

Orešič, M., Hyötyläinen, T., Herukka, S-K., Sysi-Aho, M., Mattila, I., Seppänan-Laakso, T., et al. (2011). Metabolome in progression to Alzheimer's disease. *H.Transl Psychiatry* 1 (12), e57. doi:10.1038/tp.2011.55

Ozaki, T., Yoshino, Y., Tachibana, A., Shimizu, H., Mori, T., Nakayama, T., et al. (2022). Metabolomic alterations in the blood plasma of older adults with mild cognitive impairment and Alzheimer's disease (from the Nakayama Study). *Sci. Rep.* 12, 15205. doi:10.1038/s41598-022-19670-y

Peña-Bautista, C., Roca, M., Hervás, D., Cuevas, A., López-Cuevas, R., Vento, M., et al. (2019). Plasma metabolomics in early Alzheimer's disease patients diagnosed with amyloid biomarker. *J. Proteomics* 30, 144–152. doi:10.1016/j.jprot.2019.04.008

Sano, A., Shi, H., Suzuki, R., Shirataki, Y., and Sakagami, H. (2018). Change in amino acid pools during neuronal differentiation of PC12 cells. *Vivo* 32, 1403–1408. doi:10.21873/invivo.11392

Shao, Y., Ouyang, Y., Li, T., Liu, X., Xu, X., Li, S., et al. (2020). Alteration of metabolic profile and potential biomarkers in the plasma of Alzheimer's disease. *Aging Dis.* 11, 1459–1470. doi:10.14336/AD.2020.0217

Tao, Y., Peters, M. E., Drye, L. T., Devanand, D. P., Mintzer, J. F., Pollock, B. G., et al. (2018). Sex differences in the neuropsychiatric symptoms of patients with Alzheimer's disease. *Am. J. Alzheimers Dis. Other Demen* 33, 450–457. doi:10.1177/1533317518783278

Terasawa, K. (1993). *Kampo, Japanese oriental medicine*. Tokyo: KK Standard McIntyre.

Trushina, E., and Mielke, M. M. (2014). Recent advances in the application of metabolomics to Alzheimer's Disease. *Biochim. Biophys. Acta* 1842, 1232–1239. doi:10.1016/j.bbadis.2013.06.014

Wan, L., Lu, J., Huang, J., Huo, Y., Jiang, S., and Guo, C. (2020). Association between peripheral adiponectin and lipids levels and the therapeutic response to donepezil treatment in han Chinese patients with Alzheimer's disease. *Front. Aging Neurosci.* 12, 532386. doi:10.3389/fnagi.2020.532386

Wilkins, J. M., and Trushina, E. (2018). Application of metabolomics in Alzheimer's disease. *Front. Neurol.* 12 (8), 719. doi:10.3389/fneur.2017.00719

World health Organization (2018). World health organization. Available at: https://www.who.int/news-room/fact-sheets/detail/dementia (Accessed March 19, 2023).

Xie, K., Qin, Q., Long, Z., Yang, Y., Peng, C., Xi, C., et al. (2021). High-throughput metabolomics for discovering potential biomarkers and identifying metabolic mechanisms in aging and Alzheimer's disease. *Front. Cell Dev. Biol.* 9, 602887. doi:10.3389/fcell.2021.602887

Yamashita, H., Ohbuchi, K., Nagino, M., Ebata, T., Tsuchiya, K., Kushida, H., et al. (2021). Comprehensive metabolome analysis for the pharmacological action of inchinkoto, a hepatoprotective herbal medicine. *Metabolomics* 17, 106. doi:10.1007/s11306-021-01824-0

Zhang, J. Y., Ma, S., Liu, X., Du, Y., Zhu, X., Liu, Y., et al. (2022). Activating transcription factor 6 regulates cystathionine to increase autophagy and restore memory in Alzheimer' s disease model mice. *Biochem. Biophys. Res. Commun.* 615, 109–115. doi:10.1016/j.bbrc.2022.05.053

frontiers | Frontiers in Aging Neuroscience

TYPE Original Research
PUBLISHED 26 June 2023
DOI 10.3389/fnagi.2023.1169620

OPEN ACCESS

EDITED BY
Jiehui Jiang,
Shanghai University, China

REVIEWED BY
Firoz Akhter,
Stony Brook University, United States
Dhiraj,
National Eye Institute (NIH), United States

*CORRESPONDENCE
Shaoming Sang
✉ sangshaoming6202@126.com
Chunjiu Zhong
✉ zhongcj@163.com

†These authors have contributed equally to this work

RECEIVED 19 February 2023
ACCEPTED 08 June 2023
PUBLISHED 26 June 2023

CITATION
Jin B, Cheng X, Fei G, Sang S and Zhong C (2023) Identification of diagnostic biomarkers in Alzheimer's disease by integrated bioinformatic analysis and machine learning strategies.
Front. Aging Neurosci. 15:1169620.
doi: 10.3389/fnagi.2023.1169620

Identification of diagnostic biomarkers in Alzheimer's disease by integrated bioinformatic analysis and machine learning strategies

Boru Jin[1,2†], Xiaoqin Cheng[1,2†], Guoqiang Fei[1,2], Shaoming Sang[3*] and Chunjiu Zhong[1,2*]

[1]Department of Neurology, Zhongshan Hospital, Fudan University, Shanghai, China, [2]Collaborative Innovation Center for Brain Science, Fudan University, Shanghai, China, [3]Shanghai Raising Pharmaceutical Technology Co., Ltd. Shanghai, China

Background: Alzheimer's disease (AD) is the most prevalent form of dementia, and is becoming one of the most burdening and lethal diseases. More useful biomarkers for diagnosing AD and reflecting the disease progression are in need and of significance.

Methods: The integrated bioinformatic analysis combined with machine-learning strategies was applied for exploring crucial functional pathways and identifying diagnostic biomarkers of AD. Four datasets (GSE5281, GSE131617, GSE48350, and GSE84422) with samples of AD frontal cortex are integrated as experimental datasets, and another two datasets (GSE33000 and GSE44772) with samples of AD frontal cortex were used to perform validation analyses. Functional Correlation enrichment analyses were conducted based on Gene ontology (GO), Kyoto Encyclopedia of Genes and Genomes (KEGG), and the Reactome database to reveal AD-associated biological functions and key pathways. Four models were employed to screen the potential diagnostic biomarkers, including one bioinformatic analysis of Weighted gene co-expression network analysis (WGCNA)and three machine-learning algorithms: Least absolute shrinkage and selection operator (LASSO), support vector machine-recursive feature elimination (SVM-RFE) and random forest (RF) analysis. The correlation analysis was performed to explore the correlation between the identified biomarkers with CDR scores and Braak staging.

Results: The pathways of the immune response and oxidative stress were identified as playing a crucial role during AD. Thioredoxin interacting protein (TXNIP), early growth response 1 (EGR1), and insulin-like growth factor binding protein 5 (IGFBP5) were screened as diagnostic markers of AD. The diagnostic efficacy of TXNIP, EGR1, and IGFBP5 was validated with corresponding AUCs of 0.857, 0.888, and 0.856 in dataset GSE33000, 0.867, 0.909, and 0.841 in dataset GSE44770. And the AUCs of the combination of these three biomarkers as a diagnostic tool for AD were 0.954 and 0.938 in the two verification datasets.

Conclusion: The pathways of immune response and oxidative stress can play a crucial role in the pathogenesis of AD. TXNIP, EGR1, and IGFBP5 are useful biomarkers for diagnosing AD and their mRNA level may reflect the development of the disease by correlation with the CDR scores and Breaking staging.

KEYWORDS

Alzheimer's disease, biomarker, diagnosis, machine learning (ML), Bioinformatics

Introduction

Alzheimer's disease (AD) is the most prevalent form of dementia accounting for 60–80% of all cases (Alzheimer's Association, 2022), and is becoming one of the main causes of death and posing a huge burden on patients and their families (Katzman, 2008; Georges et al., 2020). It is reported that about 50% of people aged 80 suffer from this disorder (Nalbantoglu et al., 2005) and the number of that would accumulate up to 115 million by 2050, which means there are 7.7 million increased cases every year and one more suffers every 4 s (Sosa-Ortiz et al., 2012). AD is manifested by memory loss, executive dysfunctions, and other cognitive deficits affecting patients' ability to perform everyday activities (Querfurth and Laferla, 2010; Mckhann et al., 2011) and would eventually lead to the premature death of an individual occurring typically 3–9 years after diagnosis (Querfurth and Laferla, 2010). Due to the lack of effective treatments and the increasing average lifespan, AD has posed an enormous burden on worldwide economics and health (Alzheimer's Association, 2016; Robinson et al., 2017).

The major neuropathological features of AD are intracellular neurofibrillary tangles (NFTs) formed by hyperphosphorylated tau protein, extracellular senile plaques composed of aggregated β-amyloid (Aβ) fibers (Tabaton et al., 1991; Smith, 1998), and progressive brain atrophy causing by loss of synapses and neurons (Butterfield and Halliwell, 2019; Alzheimer's Association, 2021). Recently, attention has also been paid to other pathological markers including insulin resistance (de la Monte, 2017; Rad et al., 2018), oxidative stress (Perry et al., 2008; Jiang et al., 2016), neuroinflammation (Calsolaro and Edison, 2016), erythrocytic abnormality (Kosenko et al., 2020), mitochondrial dysfunction (Lustbader, 2004; Carvalho et al., 2019), and so forth. Several novel hypotheses were proposed such as the erythrocytic hypothesis (Kosenko et al., 2020), heart failure link to AD (Tublin et al., 2019), synaptic failure hypothesis (Tublin et al., 2019), and mitochondrial cascade hypothesis (Swerdlow et al., 2014). However, lacking a comprehensive understanding of the whole mechanism, none of these could precisely connect all the pathological events. There is an urgent need to detangle the mechanism of AD and identify useful biomarkers for diagnosis.

Bioinformatics analysis has evolved into an integrative field between computer science and biology, which allows the representation, storage, management, analysis, and investigation of numerous data types with diverse algorithms and computational tools (Mulder et al., 2017; Auslander et al., 2021). However, due to the quick development of next-generation sequencing and other emerging omics techniques, accumulated omics data at an astonishing speed and scope is urging for more effective approaches to conduct sophisticated analyses from various biomolecular levels, such as genomics, transcriptomics, proteomics, radiomics and metabolomics (Pevsner, 2015; Ayyildiz and Piazza, 2019). Fortunately, machine learning meets omics and exhibits extreme power in processing and modeling omics data with huge and diverse volumes (Li et al., 2022). Machine learning is a branch of artificial intelligence focusing on simulating human learning by exploring patterns in the data and applying self-improvement to continually enhance the performance of learning tasks (Auslander et al., 2021). Recently, the integrated bioinformatic analysis combined with machine-learning strategies was applied to the identification of potential pathways and diagnostic biomarkers of diseases, which has earned some praise (Journal of Nature Genetics, 2019; Auwul et al., 2021; Tran et al., 2021).

In our study, we integrated four frontal cortical datasets from the GEO database to discover novel pathways and identify diagnostic biomarkers of AD by bioinformatic analysis combined with machine learning strategies. The differential expressions and diagnostic efficacy of the identified biomarkers were verified in another two frontal cortical datasets of AD. The correlation analysis between the identified biomarkers and the CDR scores and Braaking staging. Finally, biomarkers associated with the key functional pathways in AD were identified and verified, which could also reflect the development of AD.

Materials and methods

A diagram of the workflow of the bioinformatics analyses combined with machine learning strategies is shown in **Figure 1**.

Data collection and data processing

We retrieved and downloaded six microarray expression profile datasets with the frontal cortex of AD patients from the National Center for Biotechnology Information (NCBI) Gene Expression Omnibus (GEO) database.[1] The search was conducted with the following keywords: ("Alzheimer's disease" and "Expression profiling by array"), and the species was restricted as "Homo sapiens." Four datasets (GSE5281, GSE131617, GSE48350, and GSE84422) from the platform of Affymetrix are used as

1 http://www.ncbi.nlm.nih.gov/geo

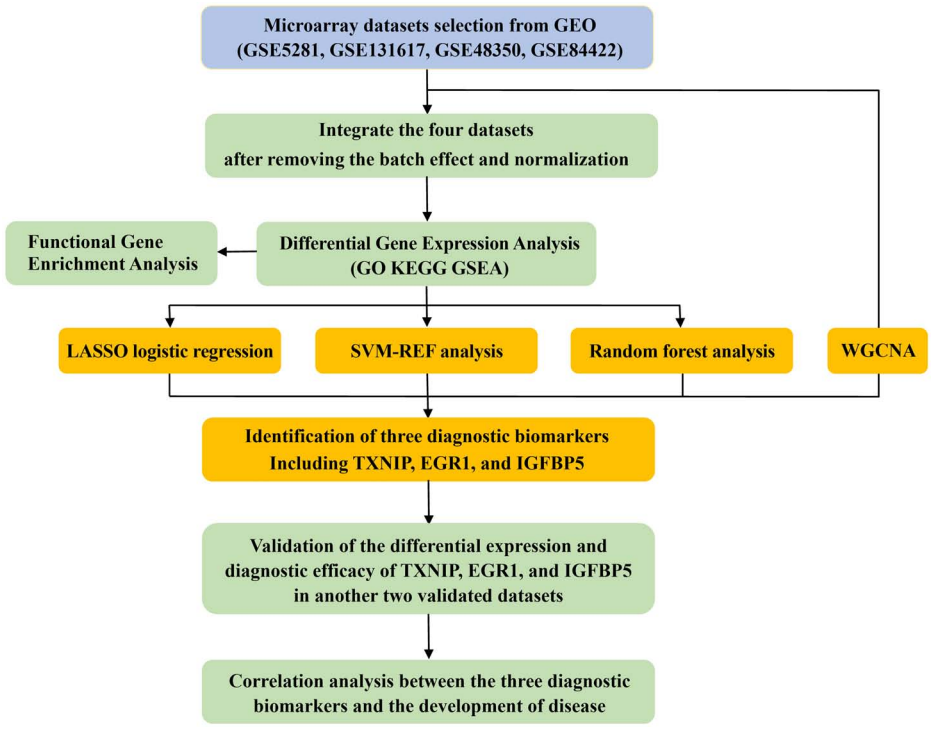

FIGURE 1
The workflow of the analysis process.

experimental datasets, and another two datasets (GSE33000 and GSE44772) from the platform of Rosetta/Merck were used as validation datasets.

Initially, referring to the annotation from the platforms, probes were annotated with gene symbols. Once there are multiple probes associated with the same gene, the average value of the expression would be calculated and applied. Then, the batch effect of the four experimental datasets was removed using the "Combat" function of the "SVA" package in R to fulfill normalization (Johnson et al., 2007). Finally, the validation of the differential expressions and diagnostic efficacy of identified biomarkers was performed on the validation datasets.

Differential gene expression analysis

After normalization, four datasets were merged into an integrated dataset including 87 frontal cortial samples of AD and 126 controls. The differential gene expression analysis was conducted on this integrated dataset with the "limma" package in R. The $|\log2FC|$ (fold change) >2 and adjusted $p < 0.05$ were regarded as thresholds for the screening. Heatmaps and volcano plots were performed with "pheatmap" and "EnhancedVolcano" packages in R.

Functional enrichment analysis

Focusing on all genes instead of only DEGs and demonstrating significantly enriched functional pathways more intuitively, gene set enrichment analysis (GSEA) was performed in R with clusterProfiler (Subramanian et al., 2005; Yu et al., 2012). Gene ontology (GO) enrichment analysis was conducted considering three hierarchical categories of biological process, molecular function, and cellular component with the "clusterProfiler" package in R (Yu et al., 2012). Pathway enrichment analysis was performed on Kyoto Encyclopedia of Genes and Genomes (KEGG) and Reactome database with "clusterProfiler" and "ReactomePA" packages in R (Yu et al., 2012; Yu and He, 2016; Minoru et al., 2017; Bijay et al., 2019).

Screening the diagnostic biomarkers

Four models were applied to screen the potential diagnostic biomarkers, including one bioinformatic analysis and three machine-learning algorithms. Weighted gene co-expression network analysis (WGCNA) is a bioinformatic method describing the correlation between genes and sample traits, which has been widely used for identifying candidate biomarkers or therapeutic targets (Langfelder et al., 2009). The least absolute shrinkage and selection operator (LASSO) is a shrinkage and variable selection method for regression models, which was applied to identify the diagnostic genes associated with discrimination with the "glmnet" package in R (Ranstam and Cook, 2018). Support vector machine-recursive feature elimination (SVM-RFE) was conducted in R using the "e1071" package with fivefold cross-validation (Sanz et al., 2018). Random forest (RF) analysis was performed in R with the "randomForest" package (Rigatti, 2017). Finally, the Venn diagram was plotted to visualize the overlapping potential

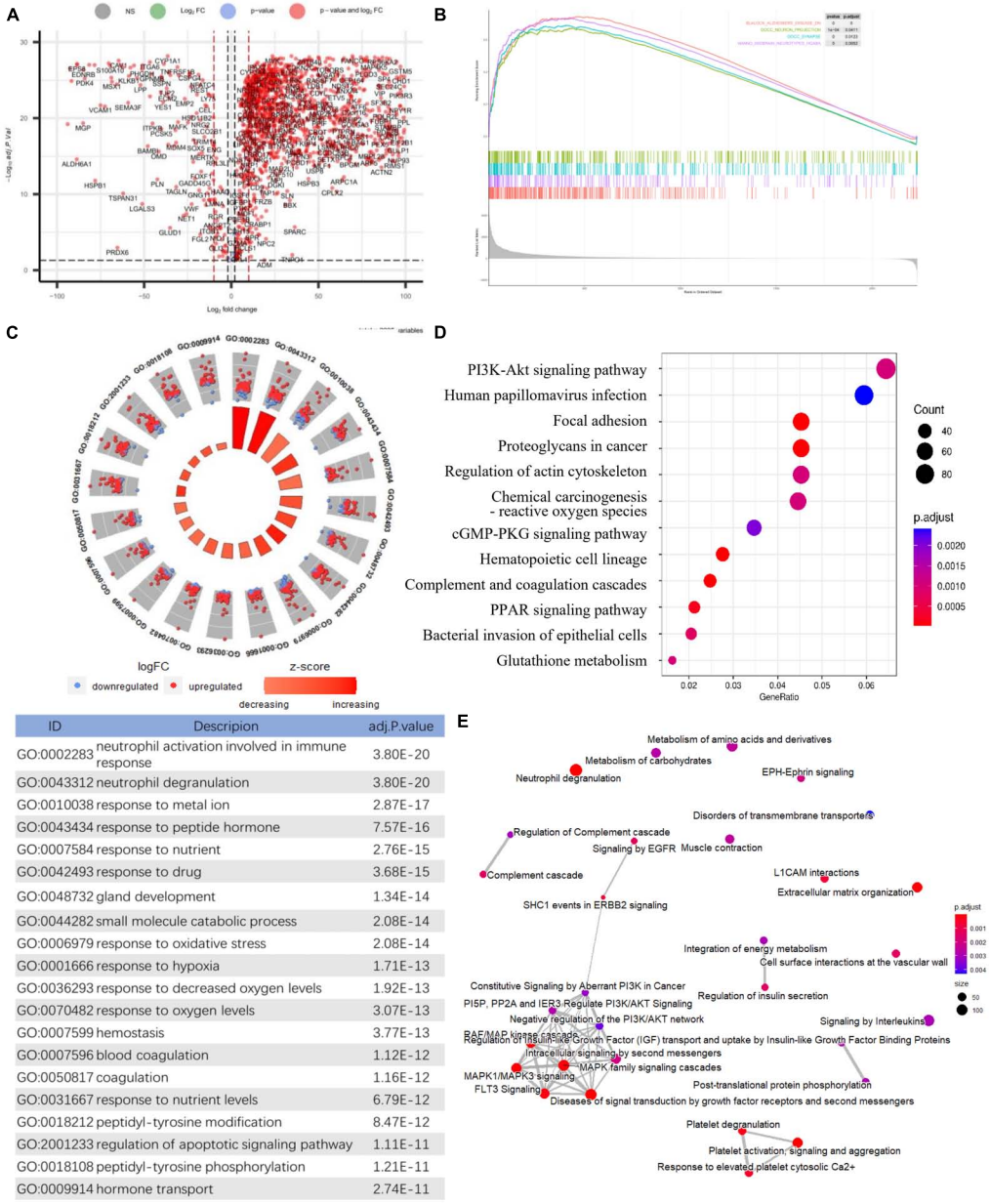

ID	Descripion	adj.P.value
GO:0002283	neutrophil activation involved in immune response	3.80E-20
GO:0043312	neutrophil degranulation	3.80E-20
GO:0010038	response to metal ion	2.87E-17
GO:0043434	response to peptide hormone	7.57E-16
GO:0007584	response to nutrient	2.76E-15
GO:0042493	response to drug	3.68E-15
GO:0048732	gland development	1.34E-14
GO:0044282	small molecule catabolic process	2.08E-14
GO:0006979	response to oxidative stress	2.08E-14
GO:0001666	response to hypoxia	1.71E-13
GO:0036293	response to decreased oxygen levels	1.92E-13
GO:0070482	response to oxygen levels	3.07E-13
GO:0007599	hemostasis	3.77E-13
GO:0007596	blood coagulation	1.12E-12
GO:0050817	coagulation	1.16E-12
GO:0031667	response to nutrient levels	6.79E-12
GO:0018212	peptidyl-tyrosine modification	8.47E-12
GO:2001233	regulation of apoptotic signaling pathway	1.11E-11
GO:0018108	peptidyl-tyrosine phosphorylation	1.21E-11
GO:0009914	hormone transport	2.74E-11

FIGURE 2
Identification of differentially expressed genes and Functional gene enrichment analyses. **(A)** Volcano plot; **(B)** GSEA profiles depicting the four significant GSEA sets in Alzheimer's disease; **(C)** GO analyses results of DEGs. **(D)** KEGG pathway analysis of DEGs. **(E)** Reactome pathway analysis of DEGs.

biomarkers among the four models as the candidate biomarkers (Bardou et al., 2014).

Validation of the candidate biomarkers

The differential expression of the candidate biomarkers was verified in the validation datasets of GSE33000 and GSE44772. The diagnostic efficacy of the candidate biomarkers was evaluated by receiver operating characteristic (ROCs) analysis with the area under the curves (AUCs) (Seshan et al., 2013). The correlation analysis was performed to explore the correlation between the candidate biomarkers with CDR scores and Braak staging.

Results

Identification of differentially expressed genes

After normalization, an integrated dataset with frontal cortical samples of AD was formed by four GEO datasets (GSE5281, GSE131617, GSE48350, and GSE84422), consisting of 87 AD patients and 126 control subjects. In the integrated dataset, the differential gene expression analysis identified 2235 DEGs, including 2029 downregulated genes and 206 upregulated genes in AD compared to the matched controls (Figure 2A and

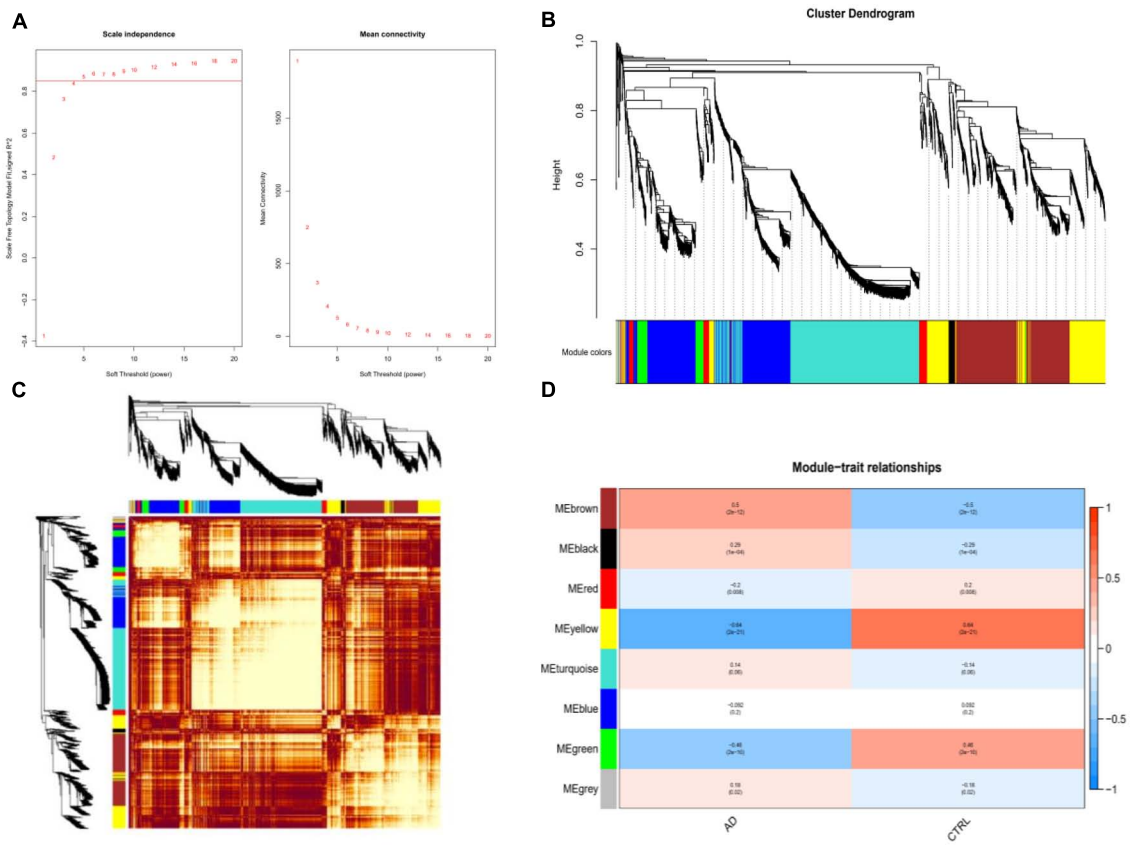

FIGURE 3
Weighted co-expression network analysis (WGCNA). **(A)** The scale-free fit index and the mean connectivity for various soft-thresholding powers of WGCNA. The left panel shows the scale-free fit index (*y*-axis) as a function of the soft-thresholding power (*x*-axis). The right panel displays the mean connectivity (degree, *y*-axis) as a function of the soft-thresholding power (*x*-axis). **(B)** Clustering dendrogram of differentially expressed genes related to Alzheimer's disease, with dissimilarity based on the topological overlap, together with assigned merged module colors and the original module colors. **(C)** Heatmap depicts the Topological Overlap Matrix (TOM) of genes selected for WGCNA. Light color represents lower overlap and red represents higher overlap. **(D)** Relationships of consensus modules with diseases. Each specified color represents a specific gene module.

Supplementary Table 1). The visualized DEG expressions in the integrated dataset were shown in the heatmap (Supplementary Figure 1).

Functional gene enrichment analyses

Gene set enrichment analysis in all detectable genes showed that genes in AD were mainly enriched in the following pathways: AD, neuron projection, synapses, multiple midbrain neurotypes, and so forth (Figure 2B). Also, GSEA_GO analysis revealed consistent results in pathway identification with GSEA analysis, in which dendrite and glutamatergic synapses were involved (Supplementary Table 1). GSEA_KEGG analysis showed that neurodegeneration and oxygen-related pathways were involved in AD, including the HIF-1 signaling and oxidative phosphorylation pathways (Supplementary Table 1). The results of the above GSEA analyses were further confirmed by GO, KEGG, and Reactome analysis on DEGs (Supplementary Table 1). The biological processes associated with immune response, oxidative stress, and apoptosis were significantly enriched by GO analysis (Figure 2C). PI3K-Akt signaling pathway was highlighted in both KEGG and Reactome analysis (Figures 2D, E).

Screening the diagnostic biomarkers

Weighted gene co-expression network analysis showed that eight remarkable co-expression gene modules identified were significantly correlated with AD (Figures 3A–D). LASSO logistic regression algorithm screened twelve potential diagnostic markers from DEGs (Figure 4A). SVM-RFE and RF analyses showed that there were 25 and 30 potential diagnostic markers associated with AD (Figures 4B, C). Among these potential biomarkers, there were three overlapping genes: thioredoxin interacting protein (TXNIP), early growth response 1 (EGR1), and insulin-like growth factor binding protein 5 (IGFBP5) (Figure 4D and Supplementary Table 1).

Validation of the candidate biomarkers

The expression changes of TXNIP, EGR1, and IGFBP5 were further validated in another two datasets GSE33000 and GSE44770. The results were consistent with the integrated dataset, in which TXNIP and IGFBP5 were significantly upregulated and EGR1 was downregulated (Figures 5A, B). The ROC analysis showed that the

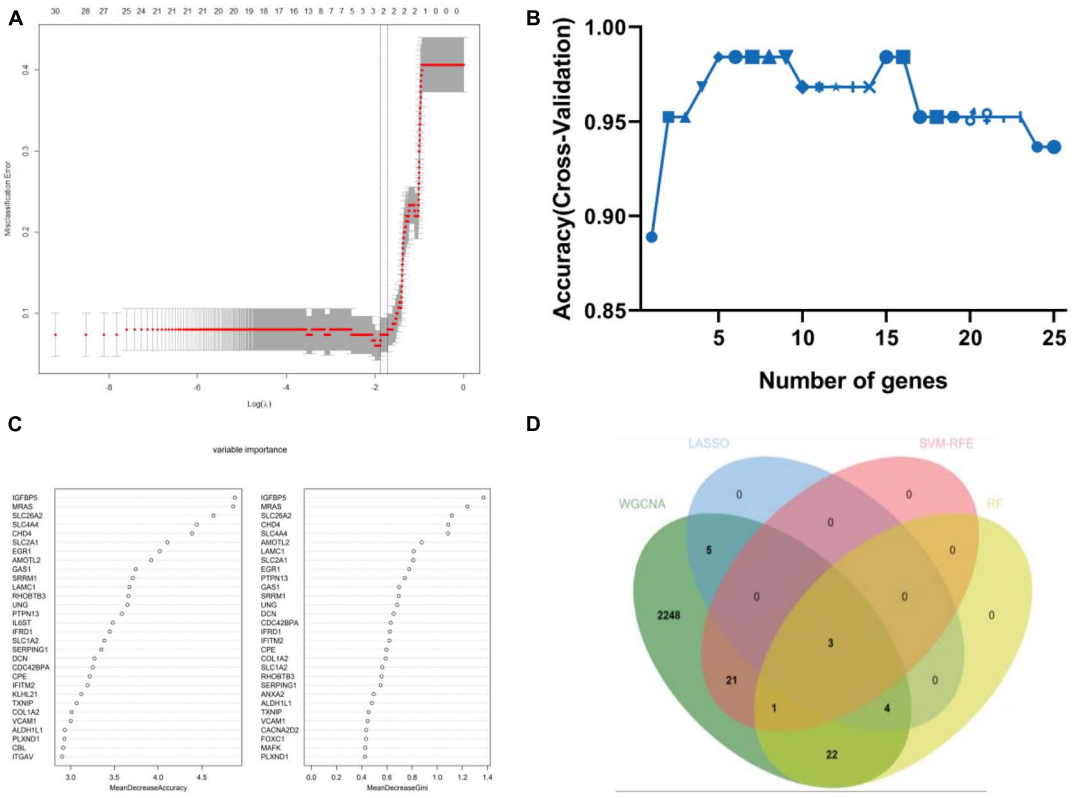

FIGURE 4
Machine-learning strategies for biomarker identification. **(A)** The cross-verification curve of least absolute shrinkage and selection operator (LASSO) logistic regression. **(B)** Support vector machine-recursive feature elimination (SVM-RFE) analysis. **(C)** Random forest (RF) analysis. **(D)** Venn diagram showed the intersection of diagnostic markers obtained by the four algorithms.

AUCs of TXNIP, EGR1, and IGFBP5 were 0.857, 0.888, and 0.856 in dataset GSE33000, 0.867, 0.909, and 0.841 in dataset GSE44770. The AUCs of the combination of these three biomarkers as a diagnostic tool for AD were 0.954 and 0.938 (Figure 5C). The correlation analysis indicated that TXNIP and IGFBP5 expressions were significantly correlated with CDR scores, and EGR1 and IGFBP5 expressions were significantly correlated with the Braak staging (Figure 6).

Discussion

The frontal cortex has always been viewed as the "motor" lobe associated with two cognitive functions of memory and motor (Fuster, 1993; Boyle, 2004; Hashimoto et al., 2017) and is very vulnerable to suffering from impairment in AD. And studies suggested that the frontal cortex is quite sensitive to subclinical changes which may help predict cognitive impairments and early disturbance of daily activities (Stoeckel et al., 2013; Marshall et al., 2019). Hence, we select the frontal cortical samples of AD to identify the diagnostic biomarkers. To enlarge the scale of the sample size and simultaneously avoid the batch effect, we integrated four AD frontal cortical datasets of transcriptome from the same platform to conduct the analyses, and another two frontal cortical datasets to perform further validation. Considering the extreme power of machine learning in processing and modeling omics data, the integrated bioinformatic analysis was combined with three machine-learning strategies to fulfill the identification of diagnostic biomarkers.

The differential gene expression analysis revealed 2235 DEGs in AD compared to the matched controls, including 2029 downregulated genes and 206 upregulated genes (Figure 2A). Multiple functional enrichment analyses found that several essential pathways were significantly enriched in AD patients, including AD, neurodegeneration, synapse, immune response, oxidative stress, apoptotic signaling pathway, and so forth. It is widely known that the loss of synapse correlates the best with cognitive impairment and even precedes neuronal loss in AD, and there are many factors contributing to synaptic dysfunction in AD, especially the above-identified: immune response and oxidative stress (DeKosky and Scheff, 1990; Britschgi and Wyss-Coray, 2007; Hong et al., 2016). Mounting studies show that oxidative stress can impair synapses and contribute to AD through most pathological hypotheses including the amyloid cascade hypothesis, tau hypothesis, inflammatory hypothesis, and so forth (Ansari and Scheff, 2010; Zhao and Zhao, 2013; Bai et al., 2022). Accumulating evidence has also stressed that immune responses involving glial cells and the complement system are prominently activated in the AD brain, which can prune excess synapses inappropriately and mediate synapse loss eventually (Akiyama et al., 2000; Wyss-Coray, 2006; Britschgi and Wyss-Coray, 2007; Hong et al., 2016; Rajendran and Paolicelli, 2018). Generally, our results confirmed

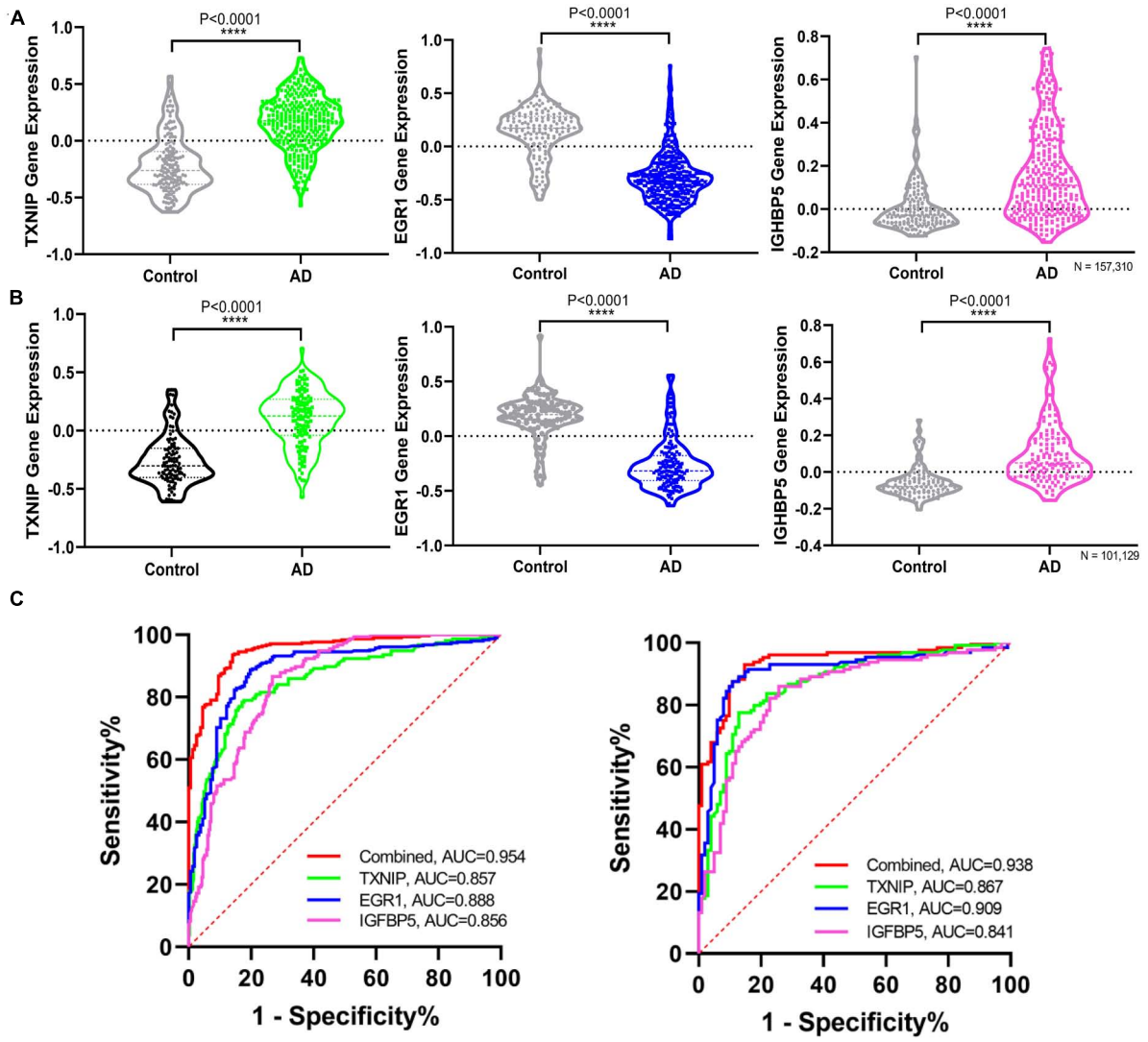

FIGURE 5
Validating the differential expression and diagnostic efficacy of the identified biomarkers. **(A)** Validation of the expression levels of the identified biomarkers in dataset GSE33000. **(B)** Validation of the expression levels of the identified biomarkers in dataset GSE44770. **(C)** Validation of the diagnostic efficacy of diagnostic biomarkers revealed by ROC analysis in the validation dataset GSE33000 and GSE44770 (TXNIP, EGR1, IGFBP5, and the combination of the three genes as a diagnostic tool).

the pathological pathways of synapse and apoptosis in AD and further stressed the crucial role of the immune response and oxidative stress in the pathogenesis of the disease.

Moreover, one bioinformatic analysis of WGCNA and three machine-learning strategies of LASSO, SVM-RFE, and RF analyses commonly identified that TXNIP, EGR1, and IGFBP5 could serve as biomarkers of AD, combining them as a tool gave rise to high AUCs of 0.954 and 0.938 in the two verification datasets (**Figure 5C**). The correlation analysis further revealed that the expressions of TXNIP and IGFBP5 were significantly correlated with the CDR scores, and the expressions of EGR1 and IGFBP5 were significantly correlated with the Braak staging (**Figure 6**).

Previous studies have shown that TXNIP as an endogenous inhibitor of antioxidant thioredoxin was found to increase in AD patients and AD mouse models, and could be a key coordinator of different pathological processes (Tsubaki et al., 2020). TXNIP connects oxidative stress and inflammation by interaction with the nucleotide-binding domain, leucine-rich-containing family, and pyrin domain-containing-3 (NLRP3) inflammasome complex (Wang et al., 2019; Eraky and Ramadan, 2022; Sbai et al., 2022). Recent studies also suggested that blocking the interaction of NLRP3 provides a significant effect, and thus TXNIP could serve as a therapeutic target (Zhang et al., 2021). Therefore, TXNIP closely associated with the identified pathways of immune response and oxidative stress can be a useful biomarker of AD. EGR1 has also been reported in previous gene-wide association analyses using brain expression data (Koldamova et al., 2014; Mukherjee et al., 2017; Lim et al., 2018), which was associated with Aβ toxicity and was invalided in a C. elegans model (Mukherjee et al., 2017). Functionally, EGR1 helps maintain the brain's cholinergic function during AD by regulating acetylcholinesterase (AChE) (Hu et al., 2019). EGR1 can bind to the BACE1 promoter and block the

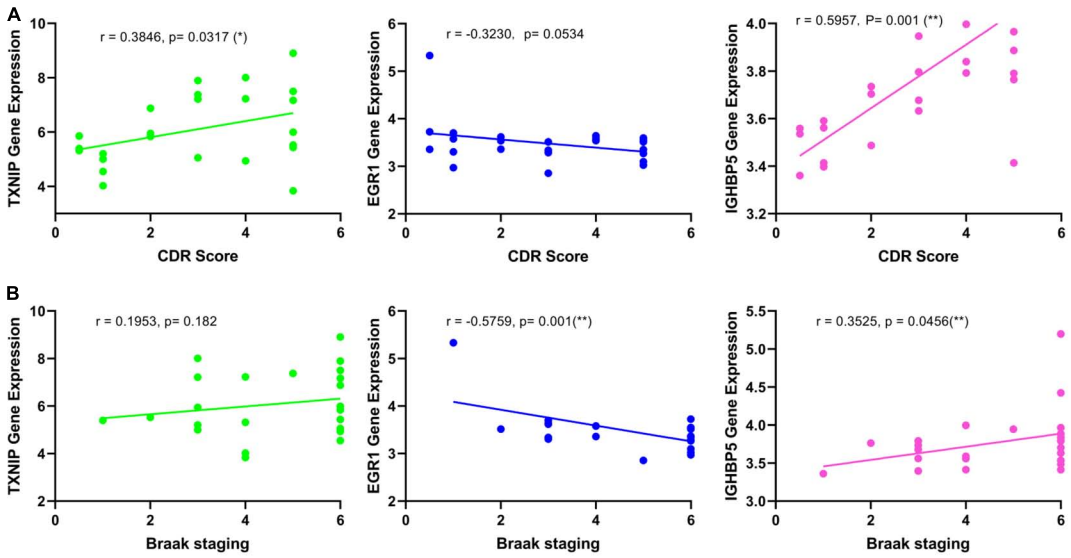

FIGURE 6
Correlation analysis of the identified biomarkers with the development of AD. **(A)** Correlation of the identified biomarkers with the CDR scores. **(B)** Correlation of the identified biomarkers with the Braak staging.

activation of the APP signaling to ultimately suppress the Aβ deposition and improve the cognitive function of AD (He et al., 2022). Studies also proposed EGR1 to be a key molecule affecting the activity of the nucleus basalis of Meynert by regulating synaptic activity and plasticity during AD (Zhu et al., 2016). Conclusively, EGR1 plays an important role in the development of AD and can serve as a useful biomarker. IGFBP5 is a pluripotent growth factor supporting neuronal survival and axon growth (Caroni and Grandes, 1990; Bach et al., 2005; Fernandez and Torres-Alemán, 2012; Rauskolb et al., 2017), which can coordinate the bioavailability and bioactivity of insulin-like growth factor 1 (IGF-1). IGFBP5 can modulate lipid metabolism and insulin sensitivity (Xiao et al., 2020), which are both associated with the cognitive impairment (Kao et al., 2020; Kellar and Craft, 2020). Studies have shown that IGFBP5 was associated with faster cognitive decline (Yu et al., 2018; Kim et al., 2019) and was found to increase in the brains (Rauskolb et al., 2022), cerebrospinal fluid (Salehi et al., 2008), and animal models of AD (Barucker et al., 2015).

Together, TXNIP, EGR1, and IGFBP5 served as potential biomarkers for AD diagnosis reflecting different pathogenetic pathways involved in the development of AD, which may be due to the complicated and multiple pathophysiological manifestations of AD. Besides the EGR1-associated Aβ deposition which has gained the most concern, our results suggested that the TXNIP-associated pathways of the immune response, oxidative stress, and especially their interaction should be paid more attention. More importantly, the identification of IGFBP5 highlights the role of insulin metabolism in the pathogenesis and development of AD. Evidence from epidemiological, clinical, and neuropathology has shown that patients with diabetes are at higher risk of developing AD due to impaired brain insulin signaling (Barbiellini Amidei et al., 2021; De Felice et al., 2022). Studies have repurposed anti-diabetes agents as novel therapeutics for AD, while how impaired insulin signaling and brain insulin resistance occurs remains unclear, urging further exploration.

There are some limitations of our study. Firstly, although we tried to select the same region of frontal cortex in AD brains from the same platform and have performed validation in another two verification datasets, the results still need more experimental confirmation for the data is from publicly available microarray datasets. Secondly, given the limited scale of sample size and type, the diagnostic efficacy of biomarkers should be further explored clinically, and even in samples of blood and cerebrospinal fluid. Thirdly, we fail to identify the early detecting biomarkers of AD due to the lack of datasets on patients with mild cognitive impairment (MCI), though early detection is the now most urgent need under the huge burden of increasing incidence and heavy cost. And we would like to perform the analysis of identifying the potential diagnostic biomarkers of MCI, once there were available datasets.

Conclusion

The integrated bioinformatic analysis combined with machine learning strategies can effectively help identify the functional pathways and diagnostic biomarkers in disease. Based on these methods, we stressed the crucial roles of immune response and oxidative stress in the pathogenesis of AD and identified three genes associated with the above two pathways as useful biomarkers, including TXNIP, EGR1, and IGFBP5. Furthermore, the expressions of TXNIP, EGR1, and IGFBP5 may reflect the development of AD by correlation with the CDR scores and Braak staging.

Data availability statement

The data presented in the study are deposited in the Gene Expression Omnibus (http://www.ncbi.nlm.nih.gov/geo) repository, accession numbers GSE5281, GSE131617, GSE48350, GSE84422, GSE33000, and GSE44772.

Author contributions

SS and CZ designed the study and accessed the funding. BJ and XC downloaded the data and performed the bioinformatics analysis. SS, GF, and BJ wrote the manuscript. All authors approved the submitted manuscript.

Funding

This study was supported by grants from the National Natural Science Foundation of China (81901081, 81870822, 91332201, and 82171408), Shanghai Municipal Science and Technology Major Project, and the Natural Science Foundation of Fujian Province (2020CXB049).

Conflict of interest

CZ, the corresponding author, holds shares of Shanghai Raising Pharmaceutical Co., Ltd., which is dedicated to developing drugs for the prevention and treatment of AD.

The remaining authors declare that the research was conducted in the absence of any commercial or financial relationships that could be construed as a potential conflict of interest.

Publisher's note

All claims expressed in this article are solely those of the authors and do not necessarily represent those of their affiliated organizations, or those of the publisher, the editors and the reviewers. Any product that may be evaluated in this article, or claim that may be made by its manufacturer, is not guaranteed or endorsed by the publisher.

Supplementary material

The Supplementary Material for this article can be found online at: https://www.frontiersin.org/articles/10.3389/fnagi.2023.1169620/full#supplementary-material

References

Akiyama, H., Barger, S., Barnum, S., Bradt, B., Bauer, J., Cole, G., et al. (2000). Inflammation and Alzheimer's disease. *Neurobiol. Aging.* 21, 383–421. doi: 10.1016/S0197-4580(00)00124-X

Alzheimer's Association (2016). 2016 Alzheimer's disease facts and figures. *Alzheimer's Dement.* 12, 459–509. doi: 10.1016/j.jalz.2016.03.001

Alzheimer's Association (2021). 2021 Alzheimer's disease facts and figures. *Alzheimers Dement.* 17, 327–406.

Alzheimer's Association (2022). 2022 Alzheimer's disease facts and figures. *Alzheimers Dement.* 18, 700–789. doi: 10.1002/alz.12638

Ansari, M., and Scheff, S. (2010). Oxidative stress in the progression of Alzheimer disease in the frontal cortex. *J. Neuropathol. Exp. Neurol.* 69, 155–167. doi: 10.1097/NEN.0b013e3181cb5af4

Auslander, N., Gussow, A., and Koonin, E. (2021). Incorporating machine learning into established bioinformatics frameworks. *Int. J. Mol. Sci.* 22:2903. doi: 10.3390/ijms22062903

Auwul, M., Rahman, M., Gov, E., Shahjaman, M., and Moni, M. (2021). Bioinformatics and machine learning approach identifies potential drug targets and pathways in COVID-19. *Brief. Bioinform.* 22:bbab120. doi: 10.1093/bib/bbab120

Ayyildiz, D., and Piazza, S. (2019). Introduction to bioinformatics. *Methods Mol. Biol.* 1986, 1–15. doi: 10.1007/978-1-4939-9442-7_1

Bach, L., Headey, S., and Norton, R. (2005). IGF-binding proteins–the pieces are falling into place. *Trends Endocrinol. Metab.* 16, 228–234. doi: 10.1016/j.tem.2005.05.005

Bai, R., Guo, J., Ye, X., Xie, Y., and Xie, T. (2022). Oxidative stress: the core pathogenesis and mechanism of Alzheimer's disease. *Ageing Res. Rev.* 77:101619. doi: 10.1016/j.arr.2022.101619

Barbiellini Amidei, C., Fayosse, A., Dumurgier, J., Machado-Fragua, M., Tabak, A., van Sloten, T., et al. (2021). Association between age at diabetes onset and subsequent risk of dementia. *JAMA* 325, 1640–1649. doi: 10.1001/jama.2021.4001

Bardou, P., Mariette, J., Escudié, F., Djemiel, C., and Klopp, C. (2014). jvenn: an interactive venn diagram viewer. *BMC Bioinformat.* 15:293. doi: 10.1186/1471-2105-15-293

Barucker, C., Sommer, A., Beckmann, G., Eravci, M., Harmeier, A., Schipke, C., et al. (2015). Alzheimer amyloid peptide aβ42 regulates gene expression of transcription and growth factors. *J. Alzheimers Dis.* 44, 613–624. doi: 10.3233/JAD-141902

Bijay, J., Lisa, M., Guilherme, V., Gong, C., Pascual, L., Antonio, F., et al. (2019). The reactome pathway knowledgebase. *Nucleic Acids Res.* 48, D498–D503.

Boyle, P. (2004). Assessing and predicting functional impairment in Alzheimer's disease: the emerging role of frontal system dysfunction. *Curr. Psychiatry Rep.* 6, 20–24. doi: 10.1007/s11920-004-0033-9

Britschgi, M., and Wyss-Coray, T. (2007). Systemic and acquired immune responses in Alzheimer's disease. *Int. Rev. Neurobiol.* 82, 205–233. doi: 10.1016/S0074-7742(07)82011-3

Butterfield, D., and Halliwell, B. (2019). Oxidative stress, dysfunctional glucose metabolism and Alzheimer disease. *Nat. Rev. Neurosci.* 20, 148–160. doi: 10.1038/s41583-019-0132-6

Calsolaro, V., and Edison, P. (2016). Neuroinflammation in Alzheimer's disease: current evidence and future directions. *Alzheimer's Dement.* 12, 719–732. doi: 10.1016/j.jalz.2016.02.010

Caroni, P., and Grandes, P. (1990). Nerve sprouting in innervated adult skeletal muscle induced by exposure to elevated levels of insulin-like growth factors. *J. Cell Biol.* 110, 1307–1317. doi: 10.1083/jcb.110.4.1307

Carvalho, C., Cardoso, S., Correia, S., and Moreira, P. (2019). Tortuous paths of insulin signaling and mitochondria in Alzheimer's disease. *Adv. Exp. Med. Biol.* 1128, 161–183. doi: 10.1007/978-981-13-3540-2_9

De Felice, F., Gonçalves, R., and Ferreira, S. (2022). Impaired insulin signalling and allostatic load in Alzheimer disease. *Nat. Rev. Neurosci.* 23, 215–230. doi: 10.1038/s41583-022-00558-9

de la Monte, S. (2017). Insulin resistance and neurodegeneration: progress towards the development of new therapeutics for Alzheimer's disease. *Drugs* 77, 47–65. doi: 10.1007/s40265-016-0674-0

DeKosky, S., and Scheff, S. (1990). Synapse loss in frontal cortex biopsies in Alzheimer's disease: correlation with cognitive severity. *Ann. Neurol.* 27, 457–464. doi: 10.1002/ana.410270502

Eraky, S., and Ramadan, N. (2022). Abo El-Magd NF. Ameliorative effects of bromelain on aluminum-induced Alzheimer's disease in rats through modulation of TXNIP pathway. *Int. J. Biol. Macromol.* 227, 1119–1131. doi: 10.1016/j.ijbiomac.2022.11.291

Fernandez, A., and Torres-Alemán, I. (2012). The many faces of insulin-like peptide signalling in the brain. *Nat. Rev. Neurosci.* 13, 225–239. doi: 10.1038/nrn3209

Fuster, J. (1993). Frontal lobes. *Curr. Opin. Neurobiol.* 3, 160–165. doi: 10.1016/0959-4388(93)90204-C

Georges, J., Miller, O., and Bintener, C. (2020). *Estimating the prevalence of dementia in Europe.* Luxembourg: Alzheimer Europe

Hashimoto, A., Matsuoka, K., Yasuno, F., Takahashi, M., Iida, J., Jikumaru, K., et al. (2017). Frontal lobe function in elderly patients with Alzheimer's disease and caregiver burden. *Psychogeriatrics* 17, 267–272. doi: 10.1111/psyg.12231

He, L., Liu, X., Li, H., Dong, R., Liang, R., and Wang, R. (2022). Polyrhachis vicina roger alleviates memory impairment in a rat model of Alzheimer's disease through the EGR1/BACE1/APP axis. *ACS Chem. Neurosci.* 13, 1857–1867. doi: 10.1021/acschemneuro.1c00193

Hong, S., Beja-Glasser, V., Nfonoyim, B., Frouin, A., Li, S., Ramakrishnan, S., et al. (2016). Complement and microglia mediate early synapse loss in Alzheimer mouse models. *Science* 352, 712–716. doi: 10.1126/science.aad8373

Hu, Y., Chen, X., Huang, S., Zhu, Q., Yu, S., Shen, Y., et al. (2019). Early growth response-1 regulates acetylcholinesterase and its relation with the course of Alzheimer's disease. *Brain Pathol.* 29, 502–512. doi: 10.1111/bpa.12688

Jiang, T., Sun, Q., and Chen, S. (2016). Oxidative stress: a major pathogenesis and potential therapeutic target of antioxidative agents in Parkinson's disease and Alzheimer's disease. *Prog. Neurobiol.* 147, 1–19. doi: 10.1016/j.pneurobio.2016.07.005

Johnson, W., Li, C., and Rabinovic, A. (2007). Adjusting batch effects in microarray expression data using empirical Bayes methods. *Biostatistics* 8, 118–127. doi: 10.1093/biostatistics/kxj037

Journal of Nature Genetics (2019). Deep learning for genomics. *Nat. Genet.* 51:1. doi: 10.1038/s41588-018-0328-0

Kao, Y., Ho, P., Tu, Y., Jou, I., and Tsai, K. (2020). Lipids and Alzheimer's disease. *Int. J. Mol. Sci.* 21:1505. doi: 10.3390/ijms21041505

Katzman, R. (2008). The prevalence and malignancy of Alzheimer disease: a major killer. *Alzheimers Dement.* 4, 378–380. doi: 10.1016/j.jalz.2008.10.003

Kellar, D., and Craft, S. (2020). Brain insulin resistance in Alzheimer's disease and related disorders: mechanisms and therapeutic approaches. *Lancet Neurol.* 19, 758–766. doi: 10.1016/S1474-4422(20)30231-3

Kim, N., Yu, L., Dawe, R., Petyuk, V., Gaiteri, C., De Jager, P., et al. (2019). Microstructural changes in the brain mediate the association of AK4, IGFBP5, HSPB2, and ITPK1 with cognitive decline. *Neurobiol. Aging.* 84, 17–25. doi: 10.1016/j.neurobiolaging.2019.07.013

Koldamova, R., Schug, J., Lefterova, M., Cronican, A., Fitz, N., Davenport, F., et al. (2014). Genome-wide approaches reveal EGR1-controlled regulatory networks associated with neurodegeneration. *Neurobiol. Dis.* 63, 107–114. doi: 10.1016/j.nbd.2013.11.005

Kosenko, E., Tikhonova, L., Alilova, G., Urios, A., and Montoliu, C. (2020). The erythrocytic hypothesis of brain energy crisis in sporadic alzheimer disease: possible consequences and supporting evidence. *J. Clin. Med.* 9:206. doi: 10.3390/jcm9010206

Langfelder, P., Horvath, S., Langfelder, P., and Horvath, S. (2009). WGCNA: an R package for weighted correlation network analysis. *BMC Bioinform.* 9:559. doi: 10.1186/1471-2105-9-559

Li, R., Li, L., Xu, Y., and Yang, J. (2022). Machine learning meets omics: applications and perspectives. *Brief. Bioinform.* 23:bbab460. doi: 10.1093/bib/bbab460

Lim, A., Gaiteri, C., Yu, L., Sohail, S., Swardfager, W., Tasaki, S., et al. (2018). Seasonal plasticity of cognition and related biological measures in adults with and without Alzheimer disease: analysis of multiple cohorts. *PLoS Med.* 15:e1002647. doi: 10.1371/journal.pmed.1002647

Lustbader, W. J. (2004). ABAD directly links a? To mitochondrial toxicity in Alzheimer\"s disease. *Science* 304, 448–452. doi: 10.1126/science.1091230

Marshall, G., Gatchel, J., Donovan, N., Muniz, M., Schultz, A., Becker, J., et al. (2019). Regional tau correlates of instrumental activities of daily living and apathy in mild cognitive impairment and Alzheimer's disease dementia. *J. Alzheimers Dis.* 67, 757–768. doi: 10.3233/JAD-170578

Mckhann, G., Knopman, D., Chertkow, H., Hyman, B., Jack, C., Kawas, C., et al. (2011). The diagnosis of dementia due to Alzheimer's disease: recommendations from the national institute on aging-Alzheimer's association workgroups on diagnostic guidelines for Alzheimer's disease. *Alzheimer's Dement.* 7, 263–269. doi: 10.1016/j.jalz.2011.03.005

Minoru, K., Miho, F., Mao, T., Yoko, S., and Kanae, M. (2017). KEGG: new perspectives on genomes, pathways, diseases and drugs. *Nucleic Acids Res.* 45, D353–D361. doi: 10.1093/nar/gkw1092

Mukherjee, S., Russell, J., Carr, D., Burgess, J., Allen, M., Serie, D., et al. (2017). Systems biology approach to late-onset Alzheimer's disease genome-wide association study identifies novel candidate genes validated using brain expression data and Caenorhabditis elegans experiments. *Alzheimers Dement.* 13, 1133–1142. doi: 10.1016/j.jalz.2017.01.016

Mulder, N., Adebiyi, E., Adebiyi, M., Adeyemi, S., Ahmed, A., Ahmed, R., et al. (2017). Development of bioinformatics infrastructure for genomics research. *Glob. Heart.* 12, 91–98. doi: 10.1016/j.gheart.2017.01.005

Nalbantoglu, J., Lacoste-Royal, G., and Gauvreau, D. (2005). Genetic factors in Alzheimer\"s disease. *J. Am. Geriatr. Soc.* 38, 564–568. doi: 10.1111/j.1532-5415.1990.tb02408.x

Perry, G., Moreira, P., Santos, M., Oliveira, C., Shenk, J., Nunomura, A., et al. (2008). Alzheimer disease and the role of free radicals in the pathogenesis of the disease. *Cns Neurol. Disord. Drug Targets* 7, 3–10. doi: 10.2174/187152708783885156

Pevsner, J. (2015). *Bioinformatics and functional genomics*. Hoboken, NJ: John Wiley & Sons.

Querfurth, H., and Laferla, F. (2010). Alzheimer's disease. *N. Engl. J. Med.* 362, 329–344. doi: 10.1056/NEJMra0909142

Rad, S., Arya, A., Karimian, H., Madhavan, P., Rizwan, F., Koshy, S., et al. (2018). Mechanism involved in insulin resistance via accumulation of beta-amyloid and neurofibrillary tangles: link between type 2 diabetes and Alzheimer's disease. *Drug Des. Deve. Ther.* 12, 3999–4021. doi: 10.2147/DDDT.S173970

Rajendran, L., and Paolicelli, R. (2018). Microglia-mediated synapse loss in Alzheimer's disease. *J. Neurosci.* 38, 2911–2919. doi: 10.1523/JNEUROSCI.1136-17.2017

Ranstam, J., and Cook, J. (2018). LASSO regression. *Br. J. Surg.* 105:1348. doi: 10.1002/bjs.10895

Rauskolb, S., Andreska, T., Fries, S., von Collenberg, C., Blum, R., Monoranu, C., et al. (2022). Insulin-like growth factor 5 associates with human Aß plaques and promotes cognitive impairment. *Acta Neuropathol. Commun.* 10:68. doi: 10.1186/s40478-022-01352-5

Rauskolb, S., Dombert, B., and Sendtner, M. (2017). Insulin-like growth factor 1 in diabetic neuropathy and amyotrophic lateral sclerosis. *Neurobiol. Dis.* 97(Pt B), 103–113. doi: 10.1016/j.nbd.2016.04.007

Rigatti, S. (2017). Random forest. *J. Insur. Med.* 47, 31–39. doi: 10.17849/insm-47-01-31-39.1

Robinson, M., Lee, B., and Hane, F. (2017). Recent progress in Alzheimer's disease research. Part 2: genetics and epidemiology. *J. Alzheimer's Dis.* 57, 317–330. doi: 10.3233/JAD-161149

Salehi, Z., Mashayekhi, F., and Naji, M. (2008). Insulin like growth factor-1 and insulin like growth factor binding proteins in the cerebrospinal fluid and serum from patients with Alzheimer's disease. *Biofactors* 33, 99–106. doi: 10.1002/biof.5520330202

Sanz, H., Valim, C., Vegas, E., Oller, J., and Reverter, F. (2018). SVM-RFE: selection and visualization of the most relevant features through non-linear kernels. *BMC Bioinform.* 19:432. doi: 10.1186/s12859-018-2451-4

Sbai, O., Djelloul, M., Auletta, A., Ieraci, A., Vascotto, C., and Perrone, L. (2022). AGE-TXNIP axis drives inflammation in Alzheimer's by targeting Aβ to mitochondria in microglia. *Cell Death Dis.* 13:302. doi: 10.1038/s41419-022-04758-0

Seshan, V., Gnen, M., and Begg, C. (2013). Comparing ROC curves derived from regression models. *Stat. Med.* 32, 1483–1493. doi: 10.1002/sim.5648

Smith, M. (1998). Alzheimer disease. *Int. Rev. Neurobiol.* 42, 1–54. doi: 10.1016/S0074-7742(08)60607-8

Sosa-Ortiz, A., Acosta-Castillo, I., and Prince, M. (2012). Epidemiology of dementias and Alzheimer's disease. *Arch. Med. Res.* 43, 600–608. doi: 10.1016/j.arcmed.2012.11.003

Stoeckel, L., Stewart, C., Griffith, H., Triebel, K., Okonkwo, O., den Hollander, J., et al. (2013). MRI volume of the medial frontal cortex predicts financial capacity in patients with mild Alzheimer's disease. *Brain Imaging Behav.* 7, 282–292. doi: 10.1007/s11682-013-9226-3

Subramanian, A., Tamayo, P., Mootha, V., Mukherjee, S., Ebert, B., Gillette, M., et al. (2005). Gene set enrichment analysis: a knowledge-based approach for interpreting genome-wide expression profiles. *Proc. Natl. Acad. Sci. U.S.A.* 102, 15545–15550. doi: 10.1073/pnas.0506580102

Swerdlow, R., Burns, J., and Khan, S. (2014). The Alzheimer's disease mitochondrial cascade hypothesis: progress and perspectives. *Biochim. Biophys. Acta Mol. Basis Dis.* 1842, 1219–1231. doi: 10.1016/j.bbadis.2013.09.010

Tabaton, M., Cammarata, S., Mancardi, G., Manetto, V., Autilio-Gambetti, L., Perry, G., et al. (1991). Ultrastructural localization of beta-amyloid, tau, and ubiquitin epitopes in extracellular neurofibrillary tangles. *Proc. Natl. Acad. Sci. U.S.A.* 88, 2098–2102. doi: 10.1073/pnas.88.6.2098

Tran, K., Kondrashova, O., Bradley, A., Williams, E., Pearson, J., and Waddell, N. (2021). Deep learning in cancer diagnosis, prognosis and treatment selection. *Genome Med.* 13:152. doi: 10.1186/s13073-021-00968-x

Tsubaki, H., Tooyama, I., and Walker, D. (2020). Thioredoxin-interacting protein (TXNIP) with focus on brain and neurodegenerative diseases. *Int. J. Mol. Sci.* 21:9357. doi: 10.3390/ijms21249357

Tublin, J., Adelstein, J., Del Monte, F., Combs, C., and Wold, L. (2019). Getting to the heart of Alzheimer disease. *Circ. Res.* 124, 142–149. doi: 10.1161/CIRCRESAHA.118.313563

Wang, C., Xu, Y., Wang, X., Guo, C., Wang, T., and Wang, Z. (2019). Dl-3-n-butylphthalide inhibits NLRP3 inflammasome and mitigates Alzheimer's-like pathology via Nrf2-TXNIP-TrX axis. *Antioxid Redox Signal.* 30, 1411–1431. doi: 10.1089/ars.2017.7440

Wyss-Coray, T. (2006). Inflammation in Alzheimer disease: driving force, bystander or beneficial response? *Nat. Med.* 12, 1005–1015.

Xiao, Z., Chu, Y., and Qin, W. (2020). IGFBP5 modulates lipid metabolism and insulin sensitivity through activating AMPK pathway in non-alcoholic fatty liver disease. *Life Sci.* 256:117997. doi: 10.1016/j.lfs.2020.117997

Yu, G., and He, Q. (2016). ReactomePA: an R/Bioconductor package for reactome pathway analysis and visualization. *Mol. Biosyst.* 12, 477–479. doi: 10.1039/C5MB00663E

Yu, G., Wang, L., Han, Y., and He, Q. (2012). clusterProfiler: an R package for comparing biological themes among gene clusters. *Omics* 16, 284–287. doi: 10.1089/omi.2011.0118

Yu, L., Petyuk, V., Gaiteri, C., Mostafavi, S., Young-Pearse, T., Shah, R., et al. (2018). Targeted brain proteomics uncover multiple pathways to Alzheimer's dementia. *Ann. Neurol.* 84, 78–88. doi: 10.1002/ana.25266

Zhang, M., Hu, G., Shao, N., Qin, Y., Chen, Q., Wang, Y., et al. (2021). Thioredoxin-interacting protein (TXNIP) as a target for Alzheimer's disease: flavonoids and phenols. *Inflammopharmacology* 29, 1317–1329. doi: 10.1007/s10787-021-00861-4

Zhao, Y., and Zhao, B. (2013). Oxidative stress and the pathogenesis of Alzheimer's disease. *Oxid. Med. Cell Longev.* 2013:316523.

Zhu, Q., Unmehopa, U., Bossers, K., Hu, Y., Verwer, R., Balesar, R., et al. (2016). MicroRNA-132 and early growth response-1 in nucleus basalis of Meynert during the course of Alzheimer's disease. *Brain* 139(Pt 3), 908–921. doi: 10.1093/brain/awv383

frontiers | Frontiers in Aging Neuroscience

TYPE Original Research
PUBLISHED 29 June 2023
DOI 10.3389/fnagi.2023.1189659

OPEN ACCESS

EDITED BY
Woon-Man Kung,
Chinese Culture University, Taiwan

REVIEWED BY
Gajanan Sathe,
Institute of Bioinformatics (IOB), India
Sreelakshmi K. Sreenivasamurthy,
Boston Children's Hospital and Harvard Medical School, United States

*CORRESPONDENCE
Xin Dong
✉ dongxin@shu.edu.cn
Qun Zhang
✉ zhangqun1120@sina.com

†These authors have contributed equally to this work and share first authorship

RECEIVED 19 March 2023
ACCEPTED 30 May 2023
PUBLISHED 29 June 2023

CITATION
Yang J, Wu S, Yang J, Zhang Q and Dong X (2023) Amyloid beta-correlated plasma metabolite dysregulation in Alzheimer's disease: an untargeted metabolism exploration using high-resolution mass spectrometry toward future clinical diagnosis.
Front. Aging Neurosci. 15:1189659.
doi: 10.3389/fnagi.2023.1189659

Amyloid beta-correlated plasma metabolite dysregulation in Alzheimer's disease: an untargeted metabolism exploration using high-resolution mass spectrometry toward future clinical diagnosis

Jingzhi Yang[1†], Shuo Wu[2†], Jun Yang[3], Qun Zhang[3*] and Xin Dong[4,5*]

[1]Institute of Translational Medicine, Shanghai University, Shanghai, China, [2]Neurology Department, Shanghai Baoshan Luodian Hospital, Shanghai, China, [3]Department of Internal Medicine, Shanghai Baoshan Elderly Nursing Hospital, Shanghai, China, [4]School of Medicine, Shanghai University, Shanghai, China, [5]Suzhou Innovation Center of Shanghai University, Suzhou, Jiangsu, China

Introduction: Alzheimer's disease (AD) is a leading cause of dementia, and it has rapidly become an increasingly burdensome and fatal disease in society. Despite medical research advances, accurate recognition of AD remains challenging. Epidemiological evidence suggests that metabolic abnormalities are tied to higher AD risk.

Methods: This study utilized case-control analyses with plasma samples and identified a panel of 27 metabolites using high-resolution mass spectrometry in both the Alzheimer's disease (AD) and cognitively normal (CN) groups. All identified variables were confirmed using MS/MS with detected fragmented ions and public metabolite databases. To understand the expression of amyloid beta proteins in plasma, ELISA assays were performed for both amyloid beta 42 (Aβ42) and amyloid beta 40 (Aβ40).

Results: The levels of plasma metabolites PAGln and L-arginine were found to significantly fluctuate in the peripheral blood of AD patients. In addition, ELISA results showed a significant increase in amyloid beta 42 (Aβ42) in AD patients compared to those who were cognitively normal (CN), while amyloid beta 40 (Aβ40) did not show any significant changes between the groups. Furthermore, positive correlations were observed between Aβ42/Aβ40 and PAGln or L-arginine, suggesting that both metabolites could play a role in the pathology of amyloid beta proteins. Binary regression analysis with these two metabolites resulted in an optimal model of the ROC (AUC = 0.95, $p < 0.001$) to effectively discriminate between AD and CN.

Discussion: This study highlights the potential of advanced high-resolution mass spectrometry (HRMS) technology for novel plasma metabolite discovery with high stability and sensitivity, thus paving the way for future clinical studies. The results of this study suggest that the combination of PAGln and L-arginine holds significant potential for improving the diagnosis of Alzheimer's disease (AD) in clinical settings. Overall, these findings have important implications for advancing our understanding of AD and developing effective approaches for its future clinical diagnosis.

KEYWORDS

Alzheimer's disease, neurodegenerative biomarkers, human plasma, high-resolution mass spectrometry, clinical diagnosis

1. Introduction

Alzheimer's disease (AD) is a form of neurological dementia that is progressive and irreversible; it has a significant negative impact on people's lives, society, and the economy (2021). Numbers of biochemical processes are affected in AD pathologies, which include the breakdown of amyloid precursor proteins, the phosphorylation of tau proteins, oxidative stress, poor energy, mitochondrial dysfunction, inflammation, membrane lipid dysregulation, or disruption of neurotransmitter pathways (de la Monte and Tong, 2014; Procaccini et al., 2016). It is increasingly clear that many neurodegenerative diseases have a pre-symptomatic phase, during which pathological changes accumulate prior to the onset of symptoms (Golde, 2022). Thereof, early diagnosis and therapy during the progression of AD are critical and a rapid pace of development should be adopted (Cummings et al., 2022). Nevertheless, the challenge of obtaining a prompt and accurate diagnosis has hindered the development of therapies for Alzheimer's disease (AD). As reported in a previous study, AD clinical trials are characterized by up to 80% screen failure rates (Aisen et al., 2016). Biomarkers enable the identification of the onset, profile, and severity of neurodegeneration-related brain alterations in particular patients who are in need of diagnosis, prognosis, and usage in clinical trials—as both inclusion and outcome measures—as the fieldwork to treat patients sooner and earlier (Bendlin and Zetterberg, 2022). The National Institute on Aging and Alzheimer's Association (NIA-AA) has proposed a research framework for using A/T/N biomarkers of β amyloid, tau, and neurodegeneration biomarkers to define Alzheimer's disease. These A/T/N biomarkers shall also serve as continuous measures to reflect different cognitive stages (Jack et al., 2018).

Currently, the availability of amyloid beta (A) PET and cerebrospinal fluid (CSF) biomarker tests for amyloid beta peptides, tau, and other neuroproteins (A/T/N classifiers) enables their use to diagnose brain amyloid pathology. However, there is still an unmet need for an accessible, radiation-free, minimally invasive, economical, quick, and analytically validated diagnostic approach to simplify clinical trial enrollment (Jack et al., 2016). Besides, the biochemical and physiological changes in the brain that characterize the illness beyond amyloid and tau deposition are still poorly understood, even though AD is currently characterized based on amyloid-plaque and tau neurofibrillary tangle deposition inside the neocortex (Jack et al., 2018).

Metabolome analysis has emerged as a novel strategy for the development of disease biomarkers in diagnosis, as well as for monitoring the progression of the disease with its underlying pathophysiology (Trivedi et al., 2017). The metabolome is a collection of small molecules that is produced by metabolic processes, arranged in biochemical pathways. It is impacted by various internal and external variables, including genetics (Holmes et al., 2008). It has been indicated that metabolomics appears to be of uttermost relevance in AD as several metabolic changes, such as higher insulin and insulin resistance levels, are associated with an increased risk of AD (Schrijvers et al., 2010). Thus, metabolites are now crucial diagnostic indicators of dementia before memory loss, defining its presence or absence.

As the plasma metabolome interacts and exchanges molecules with every organ and tissue, including the brain, it reflects various physiological and pathological changes. This makes it a promising avenue for identifying biomarkers for a range of disorders. Furthermore, interorgan communication is an important and conserved mechanism that maintains body homeostasis. Dysregulation of the systemic homeostatic system would result in metabolic and neurological disorders (Vogt and Bruning, 2013; Deleidi et al., 2015). Moreover, plasma is a bodily fluid that is simple to obtain and causes minimal discomfort to patients, which allows for the collection from large cohorts and repeated sampling (Lawton, 2008). Therefore, it is worth studying the systemic changes in blood metabolite levels associated with AD.

Analytical techniques have significantly improved, with high-resolution mass spectrometry (HRMS) instruments being readily available for determining the majority of chemical compounds (Niedzwiecki et al., 2020). Apart from determining the accurate properties of these metabolites, collective quantification is of great importance for metabolism study (Koek et al., 2011). The most popular mass spectrometers for UHPLC-HRMS are Orbitrap (OT) or TOF-based systems, as they enable the best MS data acquisition. However, according to instrument investigation, the resolution of a UHPLC-coupled OT instrument has been sacrificed in favor of achieving greater separation with higher acquisition rates (Kaufmann, 2018; de Souza et al., 2021). Furthermore, in line with our previous research on the discovery of AD urine metabolites, the OT systems for molecule detection displayed impressive stability performance (Zhang et al., 2022). Moreover, recent research that employs powerful bioinformatic techniques and high-throughput measurements of hundreds of metabolites has thoroughly documented the molecular alterations and disease-related pathways (Chandler et al., 2016; Sales et al., 2017; Uppal et al., 2017; Zhuang et al., 2021).

We performed a metabolomic analysis of the plasma of patients with AD and CN using high-resolution mass spectrometry (HRMS) from these viewpoints. Our current investigation supports the application of metabolomics analysis as a discrimination test between AD and CN, which may provide new insight for future clinical diagnosis.

2. Methods

2.1. Participant ascertainment and ethics approval

During the visits to the Shanghai Baoshan Senior Care Home, Baoshan District, No. 5425 Gonghe New Road, individuals between 60 and 80 years of age were recruited as participants, and a wide range of biospecimens and health indicators were collected. Standard cognitive screening, which includes medical history assessment, cognitive examination, and blood sampling, was conducted for all patients with Alzheimer's disease (AD). Regular biomedical indicators were obtained for cognitively normal (CN) individuals. The ethics committee of Shanghai Baoshan Luodian Hospital approved this study prior to the acquisition of clinical and genetic participants' data (Approval number: LDYY-KY-2020-04). The study was performed in accordance with the

ethical standards laid down in the 1964 Declaration of Helsinki and its later amendments.

2.2. ADAS-Cog assessment and participants' grouping

All study participants were fully informed of this research work, and written informed consent was obtained from all participants. The Alzheimer's Disease Assessment Scale—Cognitive (ADAS-Cog) Subscale test is a widely used cognitive test in research studies and clinical trials (Kueper et al., 2018; Zhang et al., 2022) and, therefore, was administered to evaluate the participants' recognition ability before the wet-lab experiments. Scores on the ADAS-Cog test range from 0 to 75, with a score above 18 indicating recognition impairment and leading to enrollment in the AD group. Conversely, a score below 18 indicates normal recognition ability and leads to enrollment in the CN group.

2.3. Plasma samples collection

Briefly, blood was collected in the morning, following an overnight fast of at least 8 h. EDTA blood tubes were used for plasma collection, which were then centrifuged at a speed of 3,000 g for 15 min at room temperature. The resulting supernatant was transferred and aliquoted into polypropylene tubes of 0.5 mL and stored at −80°C until further use. Quality control (QC) plasma was prepared by pooling an equal amount of individual plasma samples and was utilized to assess downstream sample preparation and MS measurements' stability.

2.4. Plasma protein biomarkers quantification

Plasma contents of total tau, APOE, amyloid beta-peptide 1-40, and amyloid beta-peptide 1-42 were measured using commercial ELISA kits according to the manufacturer's instructions (Total Tau, KHB0041, Invitrogen; APOE, ELH-ApoE4-1, RayBiotech; Amyloid beta 1-40, RE59781, IBL, and Amyloid beta 1-42, KHB3544, Thermo Fisher Scientific). Briefly, standard assays for detecting radioimmunoprecipitation assay-soluble samples were applied to the ELISA plates. After washing, a biotin-conjugated detection antibody was applied. Then, the positive reaction was enhanced with streptavidin–horseradish peroxidase and colored by 3,3′,5,5′-tetramethylbenzidine. The absorbance at 450 nm was applied, and the concentrations of four different proteins were calculated from the standard curves. All measurements were carried out in one round of experiments, and the results were read on a microplate photometer (Multiskan^{TM} FC, Thermo Fisher).

2.5. HRMS on untargeted metabolomics

The aliquoted frozen plasma sample was thawed and centrifuged at 14,000 g for 5 min. A measure of 300 microliters of methanol was added to 100 μL aliquot of plasma samples, vortexed for 5 min, and centrifuged at 14,000 g for another 5 min. The supernatant was transferred into a plastic tube, evaporated to dryness under a stream of nitrogen at 40°C, and reconstituted in 100 μL of acetonitrile, which contains 5 μg/mL 2-Chloro-L-phenylalanine (Sigma-Aldrich). A 5.0-μL aliquot of the reconstituted solution was injected into the UPLC MS system for online data acquisition. The same sample preparation steps were applied for QC samples. The plasma metabolites were separated on a Waters HPLC Column (XSelect HSS T3, 2.1 X 100 mm, 2.5 μm, MA, USA) that equilibrated at 37°C. The mobile phase consisted of 0.1% formic acid in water (A) as the aqueous phase and 0.1% formic acid in acetonitrile as the organic phase. The gradient elution (min, B) was set as 20 min: 0.0–2.0, 5%; 2.0–6.0, 50%; 6.0–15.0, 95%; 15.0–18.0, 95%; and 18.0–20.0, 5%. The eluent flow rate was set to 0.3 mL/min.

Sample extracts were analyzed using UPLC interfaced with the high-resolution MS system of Orbitrap (Dionex Ultimate 3000, Q-Exactive Plus, Thermo Scientific) in the positive electrospray ionization (ESI+) mode. The mass range was set to m/z 65–975. For the MS scan, the MS resolution was set to 35,000 with the automatic gain control (AGC) target set to 1×10^6 and the maximum ions injection time was set to 100 ms. For the MSMS scan, the MS resolution was set to 17,500 with the automatic gain control (AGC) target set to 1×10^5, and the maximum ion injection time was set to 50 ms. The stepped normalized collision energy (NCE) consisted of 20%, 25%, and 30% for ion fragmentation, and the isolation window was narrowed to 1.0 m/z for improving the MS feature identification. MS injection order followed the previous batch sequence setting (Zhang et al., 2022). In brief, QC samples were placed at the beginning, in between the samples, and at the end of the whole batch to examine the stability of the MS method.

2.6. Database search, data cleaning, and evaluation

The MS data underwent processing using Thermo Compound Discover 3.1 (Thermo Scientific, USA). An "Untargeted metabolomics workflow" was used to extract MS features and identify the nature of the compounds. In brief, MS raw files including QCs, ADs, and CNs were introduced into the data study. A specific sample type was selected for each of the individual raw data. The custom "Workflow Tree" was optimized according to the HRMS settings. Databases of mzCloud and mzVault were selected for compound identification. Then, the analysis was submitted to the job queue and resulted in a list with compound features, MS intensities, retention time (RT), MSMS spectrum, and so on. According to the database search results, MS features with more than 20% missing values were removed as these signals' quality was deemed uncertain for further validation and quantification. Also, those calculated MS intensities of lower than 10,000 were not included as their plasma levels were too low to be quantified with this method. To evaluate the stability of this untargeted approach, the intensities of selected metabolites and the internal standard (2-Chloro-L-phenylalanine) in all QC samples were analyzed.

TABLE 1 Demographic characteristics of the AD and CN groups.

Characteristics	AD group	CN group
n	29	29
Gender, female/male (%)	63.3	58.6
Age	69.0 ± 3.60	72.1 ± 7.1
Education year (y)	4 ± 2	6 ± 3
ADAS-Cog score (Score range)	72.65 ± 5.56 (53–75)	6.48 ± 6.45 (0–16.5)

Results are expressed as mean ± standard deviation.

TABLE 2 Plasma protein feature measurements by ELISA.

Protein features (unit)	AD group	CN group	*p*-value
Aβ40 (pg/mL)	333.908 ± 94.157	303.067± 114.857	0.142
Aβ42 (pg/mL)	9.422 ± 11.433	3.725 ± 2.722	0.001
TAU (pg/mL)	1,199.255 ± 959.953	2,217.143 ± 975.046	0.000
APOE (ng/mL)	32,617.841 ± 9,475.138	66,157.364 ± 108,855.517	0.002
Aβ42/Aβ40	0.027 ± 0.029	0.013 ± 0.010	0.001

Results are expressed as mean ± standard deviation; a $p < 0.05$ indicates statistical significance.

2.7. Metabolome-wide association study

Metabolome-wide association study (MWAS) was conducted with Simca-P 14.1 software (Umetrics, Umea, Sweden) (Wheelock and Wheelock, 2013). Data of normalized LC/MS peak areas were imported for multivariate analysis. Principal component analysis (PCA), partial least-squares discriminant analysis (PLS-DA), and orthogonal partial least-squares discriminant analysis (OPLS-DA) were performed separately for model development. The quality of the model was tested by cross-validation and permutation (Szymańska et al., 2012) and evaluated by the values of R^2X, R^2Y, and Q^2. By default, the model was run through seven rounds of cross-validation to establish the optimal number of principal components to minimize overfitting and the fact that both Q^2 and R^2 were near to 1, which shows that the model is excellent (Liang et al., 2011).

2.8. Metabolic pathway analysis

A metabolic pathway may be conceived of as a group of metabolites that arise from various regions of the metabolome and cooperate to control the processes of AD. Moreover, we looked at regulatory signatures related to the AD disease process using network extraction approaches. Thus, the Mummichog analysis was carried out using MetaboAnalyst (version 5.0). To identify m/z characteristics with a statistical significance of $p < 0.05$, Student's *t*-test analysis was performed. Features of m/z with calculated significance were then matched to the metabolic models of Kyoto Encyclopedia of Genes and Genomes (KEGG). Following validation of the m/z features that were mapped onto the metabolite networks, statistically significant values were reported. We took advantage of that technique to present further data on potential metabolic variations between AD and CN.

2.9. Metabolites MS/MS validation and semi-quantification

Metabolite annotation and identification were performed using both spectra of MS and MS/MS, which were further validated with the HMDB (https://hmdb.ca/) and PubChem (https://pubchem.ncbi.nlm.nih.gov/) databases. The MS and MS/MS fragments were all examined in each of the individual MS spectra. Discriminatory features that were associated with the significantly enriched pathways and a $p < 0.05$ were selected for semi-quantitation analysis. The semi-quantification was performed by calculating the relative responses (Rel. Res) of each metabolite, and the equation is listed as follows:

$$\begin{aligned} &Relative\ response(Rel.\ Res.) \\ &= Intenstiy\frac{validated\ metabolite}{Internal\ standard\ (2-Chloro-L-phenylalanine)} \end{aligned}$$

Further, the calculated relative responses were used to investigate the statistical differences between the AD and CN groups.

2.10. Statistical analysis

Continuous variables were compared using Student's *t*-test or the Mann–Whitney *U*-test. The area under the receiver operating characteristic curve [ROC (AUC)] was calculated to perform the discrimination power of the potential biomarkers for AD. Differential expression with metabolites and proteins between the AD and CN groups was demonstrated as boxplots. The correlation analysis was conducted between AD metabolites and protein biomarkers. Analyses were performed using GraphPad Prism (version 9.0.0, San Diego, USA). A $p < 0.05$ was considered statistically significant.

3. Results

3.1. Demographics characteristics of participants

Based on the results of the Alzheimer's Disease Assessment Scale—Cognitive (ADAS-Cog) Subscale, 29 participants scored between 53 and 75 and were classified as belonging to the Alzheimer's disease (AD) group, with an average score of 72.65 ± 5.56. Additionally, 29 participants scored between 0 and 16.5 and were included in the cognitively normal (CN) group, with an average score of 6.48 ± 6.45. Among the study participants, 63.3% of females were in the AD group, while 58.6% were in the CN group. Although the average education year was longer in the CN group (6y ± 3) than in the AD group (4y ± 2), there was no significant difference between the two groups. The average ages of the AD and CN groups were 69.0 years ± 3.60 and 72.1 years ± 7.1, respectively,

TABLE 3 Mass spectrometric characteristics of plasma metabolites and internal standard.

No.	Compound name	HMDB ID	KEGG ID	PubChem CID	Formula	MW	RT (min)	$[M+H]^+$	Identified MSMS fragment ions
1	Phenylacetylglutamine	HMDB06344	C04148	92258	C13 H16 N2 O4	264.11083	5.554	265.1183	223/115/101
2	L-Arginine	HMDB0000517	C00062	6322	C6 H14 N4 O2	174.11156	0.764	175.1191	175/116/130
3	Propionylcarnitine	HMDB0000824	C03017	107738	C10 H19 N O4	217.13121	0.977	218.1387	159/144
4	Creatine	HMDB0000064	C00300	586	C4 H9 N3 O2	131.06952	0.834	132.0769	132/114/100
5	Creatinine	HMDB0000562	C00791	588	C4 H7 N3 O	113.05909	0.821	114.0664	114/86/72
6	Indole-3-acetic acid	HMDB0000197	C00954	802	C10 H9 N O2	175.06323	7.021	176.0706	103/102/99
7	Pipecolic acid	HMDB0000070	C00408	849	C6 H11 N O2	129.07892	0.696	130.0863	130/110/84
8	Arachidonic acid	HMDB0001043	C00219	444899	C20 H32 O2	304.23991	15.685	305.2473	93/117/105
9	Choline	HMDB0000097	C00114	305	C5 H13 N O	103.10007	0.791	104.1073	60/58
10	Indole-3-lactic acid	HMDB0000671	C02043	92904	C11 H11 N O3	205.07378	6.52	206.0812	188/160/130
11	Proline	HMDB0000162	C00148	145742	C5 H9 N O2	115.06354	0.842	116.0706	70/116/68
12	Acetylcholine	HMDB0000895	C01996	187	C7 H15 N O2	145.11017	0.832	146.1150	87/60/43
13	Betaine	HMDB0000043	C00719	247	C5 H11 N O2	117.0791	5.575	118.0863	56/59/119
14	Bilirubin	HMDB0000054	C00486	5280352	C33 H36 N4 O6	584.26342	7.658	585.2705	285/539/253/286
15	Methyl indole-3-acetate	HMDB0029738	NA[a]	74706	C11 H11 N O2	189.07887	7.525	190.0861	130/172/101
16	Cortisol	HMDB0000063	C00735	5754	C21 H30 O5	362.20892	7.307	363.2160	327/309/121
17	L-Histidine	HMDB0000177	C00135	6274	C6 H9 N3 O2	155.06942	0.715	156.0767	125/84/79
18	Hypoxanthine	HMDB0000157	C00262	135398638	C5 H4 N4 O	136.03844	1.241	137.0457	137/119/95/81
19	Hexanoylcarnitine	HMDB0000756	NA[a]	6426853	C13 H25 N O4	259.17816	6.122	260.1856	85/201/99
20	Uric acid	HMDB0000289	C00366	1175	C5 H4 N4 O3	168.0283	1.239	169.0357	152/141
21	Ornithine	HMDB0000214	C00077	6262	C5 H12 N2 O2	132.08996	0.696	133.0983	125/79/84
22	Uracil	HMDB0000300	C00106	1174	C4 H4 N2 O2	112.02747	1.292	113.0348	96/70
23	Acetyl-L-carnitine	HMDB0000201	C02571	7045767	C9 H17 N O4	203.11572	0.891	204.1230	85/145
24	Decanoylcarnitine	HMDB0000651	C03299	10245190	C17 H33 N O4	315.24072	7.796	316.2482	85/257/155
25	Palmitoylcarnitine	HMDB0000222	C02990	461	C23 H45 N O4	399.33459	10.967	400.3419	85/341/239
26	5-Oxoproline	HMDB0000267	C01879	7405	C5 H7 N O3	129.04261	1.274	130.0500	84/85/131
27	Sphingosine 1-phosphate	HMDB0000277	C06124	5283560	C18 H38 N O5 P	379.24852	9.61	380.2557	346/223/101
28[b]	2-Chloro-L-phenylalanine	NA[a]	NA[a]	2761491	C9 H10 Cl N O2	199.04012	4.764	200.0472	154/183/118/165

[a]NA, not available.
[b]Internal standard.

10.3389/fnagi.2023.1189659

TABLE 4 Mass spectrometric signal intensities of 28 compounds in quality control (QC) samples across the analytical batch.

No.	Compound Name	HRMS signal intensity									Calculated value		
		QC 1	QC 2	QC 3	QC 4	QC 5	QC 6	QC 7	QC 8	QC 9	Average	SD	CV%
1	2-Chloro-L-phenylalanine	9529581	9088904	9485429	8742235	9469332	9395555	9548525	8850665	8704423	9,201,628	355,641	3.9%
2	Phenylacetylglutamine	382822	383624	392065	384992	387027	384947	373850	393136	341656	380,458	15,589	4.1%
3	Indole-3-acetic acid	124032	119284	121262	120338	114885	122387	107521	115021	118044	118,086	5,021	4.3%
4	Hexanoylcarnitine	58657	60892	58681	54927	57700	55457	54468	52743	56352	56,653	2,543	4.5%
5	Bilirubin	406307	399800	418485	422007	452406	407273	422593	383009	399875	412,417	19,611	4.8%
6	Ornithine	298137	292367	312863	298005	286066	294694	333486	295200	315194	302,890	14,805	4.9%
7	Methyl indole-3-acetate	226667	226120	228808	211032	224630	215322	215505	197252	199534	216,097	11,740	5.4%
8	Indole-3-lactic acid	39725	40016	38566	37977	34284	39277	35479	37280	35526	37,570	2,066	5.5%
9	Decanoylcarnitine	332006	330514	312064	327887	363043	342753	352238	303945	309703	330,461	19,901	6.0%
10	Uracil	34652	38553	34294	38542	33435	37115	33404	38183	37381	36,173	2,199	6.1%
11	L-Arginine	227217	200801	213641	226435	234702	207762	248974	233852	227311	224,522	14,871	6.6%
12	Palmitoylcarnitine	162114	139816	153831	152894	151122	149560	151737	158446	128209	149,748	10,146	6.8%
13	Cortisol	46274	42796	42073	37517	40200	45271	41367	41043	38296	41,649	2,891	6.9%
14	Uric acid	1467068	1499030	1419389	1601035	1732179	1657507	1486082	1505374	1406219	1,530,431	110,221	7.2%
15	Creatinine	866914	768723	865649	884379	862536	876028	894620	948036	1007037	885,991	64,959	7.3%
16	Sphingosine 1-phosphate	262005	266871	262232	240920	252065	242596	248322	230150	207334	245,833	18,644	7.6%
17	Acetyl-L-carnitine	2827805	2551314	2853465	2304034	2525169	2693666	2380845	2599126	2319824	2,561,694	204,268	8.0%
18	5-Oxoproline	293296	320502	273675	304564	321100	360339	338945	350682	314297	319,711	27,519	8.6%
19	Creatine	624589	755177	749724	796530	718671	748896	850668	752585	845281	760,236	6,8172	9.0%
20	Choline	1237398	1109407	1409400	1374631	1411754	1559393	1309037	1272301	1384232	1,340,839	127,715	9.5%
21	Hypoxanthine	108960	94697	93750	104105	122321	122007	110056	108137	117448	109,053	10,494	9.6%
22	Acetylcholine	111943	106859	124111	104598	88129	86441	95092	109266	124226	105,629	13,823	13.1%
23	L-Histidine	183886	196229	236228	288127	257609	260952	214771	274265	297919	245,554	40,360	16.4%
24	Proline	2299600	1450474	2030671	1514785	2035300	2526576	2160492	2444573	2252567	2,079,449	376,999	18.1%
25	Propionylcarnitine	113886	123703	94571	103424	105471	86245	65572	76310	75260	93,827	19,463	20.7%
26	Betaine	93875	137794	131380	114206	88957	114522	79435	128731	74935	107,093	23,476	21.9%
27	Pipecolic acid	274335	664566	749064	714482	704826	731427	705162	669263	700309	657,048	145,963	22.2%
28	Arachidonic acid	112458	120743	139285	116542	97998	101572	66210	93987	70134	102,103	23,556	23.1%

10.3389/fnagi.2023.1189659

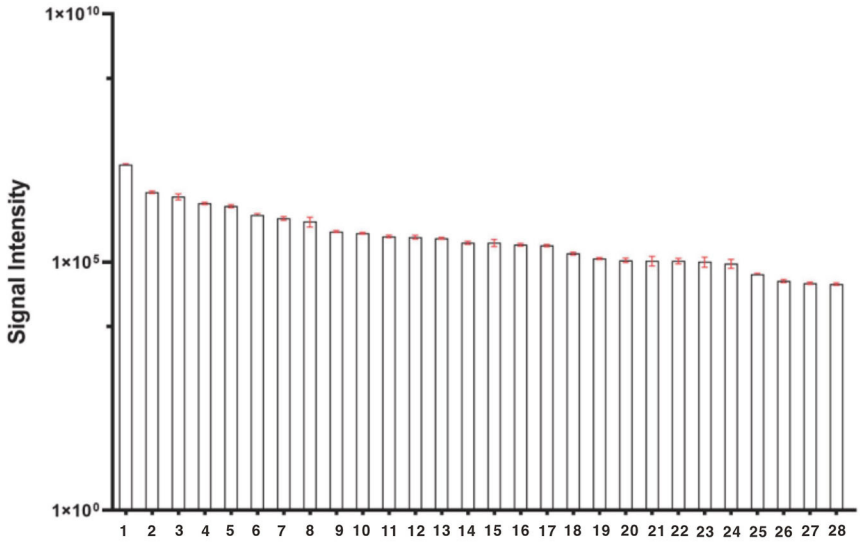

No.	Compound	CV%
1	2-Chloro-L-phenylalanine	3.9%
2	Acetyl-L-carnitine	8.0%
3	Proline	18.1%
4	Uric acid	7.2%
5	Choline	9.5%
6	Creatinine	7.3%
7	Creatine	9.0%
8	Pipecolic acid	22.2%
9	Bilirubin	4.8%
10	Phenylacetylglutamine	4.1%
11	Decanoylcarnitine	6.0%
12	5-Oxoproline	8.6%
13	Ornithine	4.9%
14	Sphingosine 1-phosphate	7.6%
15	L-Histidine	16.4%
16	L-Arginine	6.6%
17	Methyl indole-3-acetate	5.4%
18	Palmitoylcarnitine	6.8%
19	Indole-3-acetic acid	4.3%
20	Hypoxanthine	9.6%
21	Betaine	21.9%
22	Acetylcholine	13.1%
23	Arachidonic acid	23.1%
24	Propionylcarnitine	20.7%
25	Hexanoylcarnitine	4.5%
26	Cortisol	6.9%
27	Indole-3-lactic acid	5.5%
28	Uracil	6.1%

FIGURE 1
Bar column of average intensities and standard deviations of 28 compounds, including 27 metabolites and an internal standard of 2-Chloro-L-phenylalanine in all QC samples across the entire MS-analytical batches.

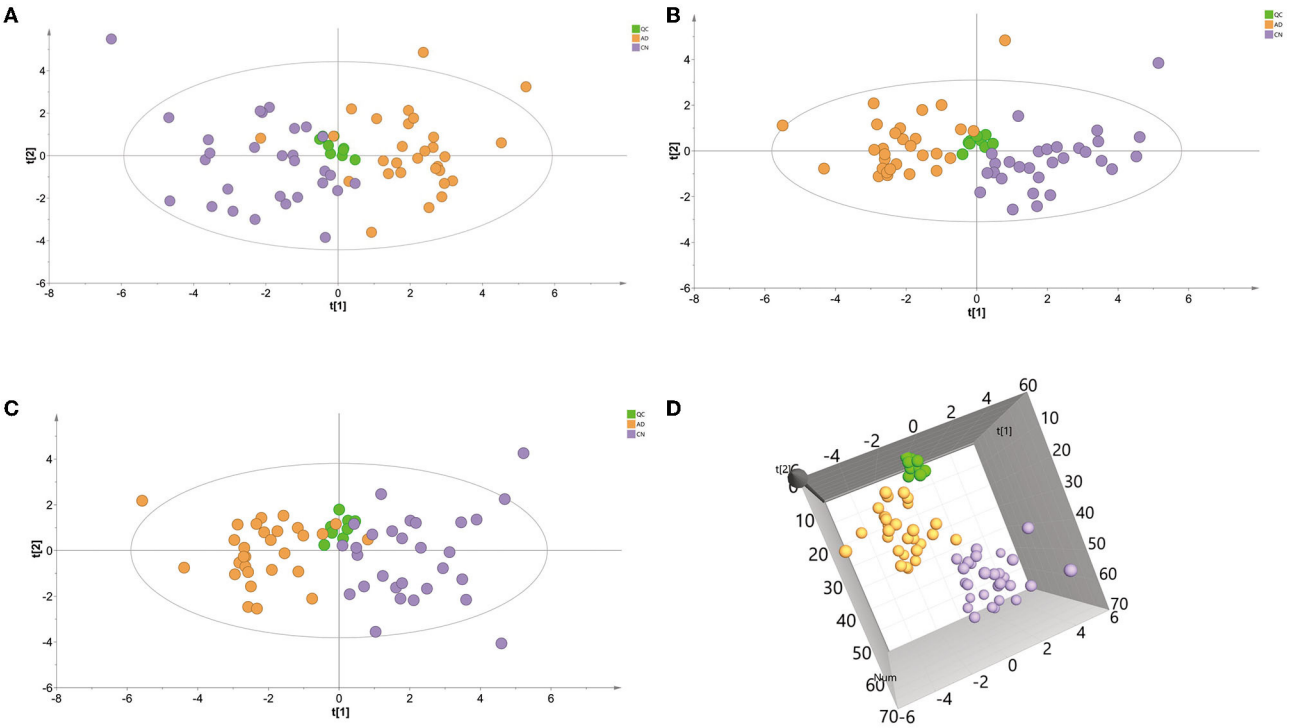

FIGURE 2
Multivariate data analysis of plasma samples in the ESI-positive mode. **(A)** Principal components analysis (PCA) score plot of the QC, AD, and CN groups. **(B)** Partial least-squares discriminant analysis (PLS-DA) score plot of the QC, AD, and CN groups. **(C)** Orthogonal partial least-squares discriminant analysis (OPLS-DA) score plot of the QC, AD, and CN groups. **(D)** A three-dimensional plot of the OPLS-DA model.

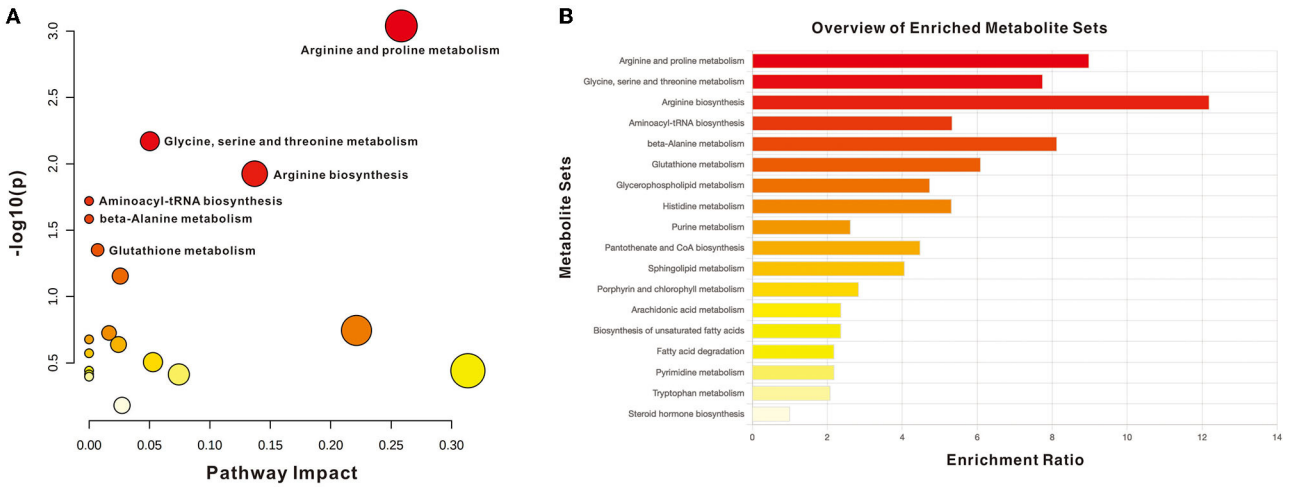

FIGURE 3
Summary of pathway analysis with MetaboAnalyst. **(A)** Pathway impact with significance ($p < 0.05$): arginine and proline metabolism, glycine, serine, and threonine metabolism, arginine biosynthesis, Aminoacyle-tRNA biosynthesis, and beta-alanine metabolism. **(B)** Metabolite sets enrichment overview.

with no significant difference in the age distribution between the two groups (Table 1).

3.2. AD protein biomarkers measurements

The biomarkers for AD protein, such as Amyloid beta 1-42 (Aβ42), Amyloid beta 1-40 (Aβ40), t-tau, and APOE, were measured in both the AD and CN groups, and the Aβ42/Aβ40 ratio was calculated. The plasma concentration of Aβ42 was noted to increase while the plasma concentrations of t-tau and APOE were observed to decrease significantly ($p < 0.0001$) in individuals with AD as compared to those without (CN). However, no significant difference was found in Aβ40 levels between the AD and CN groups. These observations are tabulated in Table 2 and are depicted as comparative boxplots in Supplementary Figure 1.

3.3. MWAS results

Using a high-resolution MS platform for the purpose of metabolome profiling, 612 distinct m/z characteristics with projected formulas or chemical names were acquired, where only those characteristics with an average batch determination rate of 80% or above were considered for further study (data are shown in Supplementary Table 1). Subsequently, a selection of the relative intensities was made, where those with CV% values <30% were chosen as criteria for further investigation, ultimately narrowing the list of chemicals down to 42. The databases of HMDB and PubChem were then utilized to validate the compound resources and MSMS fragmentation. This process resulted in the formation of a final endogenous compound list of 27 metabolites for the investigation of metabolite expression in both AD and CN groups (Table 3). The CV% of QC results was analyzed to ensure a convincing result in downstream analysis. As a result, the MS areas of nine QC samples were calculated for 27 metabolites and one internal standard, where the maximum value of the CV% is 23.1% for arachidonic acid and the minimum value of the CV% is 3.9% for 2-Chloro-L-phenylalanine. On average, the CV% value of the 28 compounds is 9.7%, indicating the MS measurement has good stability (refer to Table 4). Additionally, a plot of the average signal intensities and their standard deviations of 28 compounds are depicted in Figure 1.

3.4. Discrimination model evaluation

A principal component analysis (PCA) model was conducted with identified metabolites. The PCA ($R^2X = 0.331$ $Q^2 = 0.081$) scores plot showed an approximate separation between the AD and CN groups (Figure 2A), indicating a tendency of inter-group clustering. Additionally, the partial least-squares discriminant analysis (PLS-DA) model ($R^2X = 0.289$, $R^2Y = 0.477$, $Q^2 = 0.342$) and orthogonal partial least-squares discriminant analysis (OPLS-DA) model ($R^2X = 0.297$, $R^2Y = 0.456$, $Q^2 = 0.35$) were performed to compare the AD and CN groups. The corresponding score plots depicted in Figures 2B, C revealed a noticeable disjunction between the two groups. Moreover, a three-dimensional (3D) plot of the OPLS-DA model (Figure 2D) displayed a distinct separation between the AD and CN groups. These outcomes indicate plasma metabolic variations in AD patients.

3.5. Pathway analysis

The impact pathway was analyzed using MetaboAnalyst 5.0 (http://www.metaboanalyst.ca/). The results indicated that 27 endogenous metabolites were of close relevance to five biological pathways presenting statistical significance, which included the following: (1) arginine and proline metabolism, (2) glycine,

TABLE 5 KEGG-enriched molecular pathway with identified metabolites.

No.	Pathway name	Match status	Matched metabolites	*p*-value	Impact
1	Arginine and proline metabolism	4/38	L-Arginine, creatine, L-proline, and L-ornithine	0.0009	0.25841
2	Glycine, serine, and threonine metabolism	3/33	Choline, betaine, and creatine	0.0068	0.05034
3	Arginine biosynthesis	2/14	L-Arginine and L-ornithine	0.0119	0.13705
4	Aminoacyl-tRNA biosynthesis	3/48	L-Histidine, L-arginine, and L-proline	0.0191	0.00000
5	beta-Alanine metabolism	2/21	Uracil and L-histidine	0.0260	0.00000
6	Glutathione metabolism	2/28	5-Oxoproline and L-ornithine	0.0445	0.00709
7	Glycerophospholipid metabolism	2/36	Choline and acetylcholine	0.0700	0.02582
8	Histidine metabolism	1/16	L-histidine	0.1799	0.22131
9	Purine metabolism	2/65	Hypoxanthine and urate	0.1878	0.01651
10	Pantothenate and CoA biosynthesis	1/19	Uracil	0.2100	0.00000
11	Sphingolipid metabolism	1/21	Sphingosine 1-phosphate	0.2295	0.02434
12	Lysine degradation	1/25	L-pipecolic acid	0.2671	0.00000
13	Porphyrin and chlorophyll metabolism	1/30	Bilirubin	0.3117	0.05288
14	Biosynthesis of unsaturated fatty acids	1/36	Arachidonate	0.3618	0.00000
15	Arachidonic acid metabolism	1/36	Arachidonate	0.3618	0.3135
16	Fatty acid degradation	1/39	L-Palmitoylcarnitine	0.3856	0.00000
17	Pyrimidine metabolism	1/39	Uracil	0.3856	0.0743
18	Tryptophan metabolism	1/41	Indole-3-acetate	0.4009	0.00000
19	Steroid hormone biosynthesis	1/85	Cortisol	0.6597	0.02729

serine, and threonine metabolism, (3) arginine biosynthesis, (4) aminoacyle-tRNA biosynthesis, and (5) beta-alanine metabolism. The *p*-values obtained for these metabolites were as follows: 0.0009, 0.0068, 0.0119, 0.0191, and 0.0260, respectively. The KEGG pathway produced a bubble plot, which is shown in Figure 3A, while the metabolic features' enrichment result is displayed in Figure 3B. All pathways and their related metabolites are summarized in Table 5.

3.6. Potential plasma metabolic biomarkers of the AD and CN groups

Within the selected 27 endogenous metabolites, 14 compounds exhibited different regulation trends between the AD and CN groups. Specifically, phenylacetylglutamine and L-arginine were upregulated in the AD group compared with the CN group; acetyl-L-carnitine, sphingosine 1-phosphate, palmitoylcarnitine, 5-oxoproline, uracil, uric acid, hypoxanthine, L-histidine, decanoylcarnitine, ornithine, betaine, and cortisol exhibited downregulation in the AD group compared with the CN group. The expressions of metabolites that were upregulated and downregulated are presented as boxplots in Figure 4. However, the remaining 13 components showed no significant change between the AD and CN groups, and corresponding boxplots are included in Supplementary Figure 2.

3.7. Discrimination and correlation analysis with plasma biomarkers

The AUCs were utilized in this study to evaluate the diagnostic potential of various biomarkers. A value between 0 and 1 for the AUCs indicated the level of diagnostic accuracy ranging from no to great discrimination. The AUC values >0.8 were identified for phenylacetylglutamine (PAGln) and L-arginine, with AUC (PAGln) = 0.91 (95% confidence interval CI, 0.84, 0.99) and AUC (L-arginine) = 0.83 (95% confidence interval CI, 0.73, 0.93). To enhance the discrimination power of the model, a binary logistic regression was used with PAGln and L-arginine, which resulted in a model with an AUC of ROC of 0.95 (95% confidence interval CI, 0.90, 1.00). Figure 5A illustrates the ROC curves of the potential metabolic biomarkers. In addition, ROC analysis was performed to compare the discrimination ability between potential proteins and MS-discovered metabolites using Aβ42 and the ratio of Aβ42/Aβ40, respectively, with AUC (Aβ42) = 0.76 (95% confidence interval CI, 0.64, 0.89) and AUC (Aβ42/Aβ40) = 0.70 (95% confidence interval CI, 0.56, 0.83). Furthermore, the ROC curves of potential protein biomarkers are shown in Figure 5B. Pearson analysis indicated a positive correlation between Aβ42/Aβ40 and either PAGln or L-Arg. For Aβ42/Aβ40 and PAGln, $r = 0.5396$, $p < 0.0001$, while for Aβ42/Aβ40 and L-Arg, $r = 0.3240$, $p < 0.05$. Both correlation analyses indicated a statistically significant relationship between novel metabolites and the classical protein ratio (Figure 6).

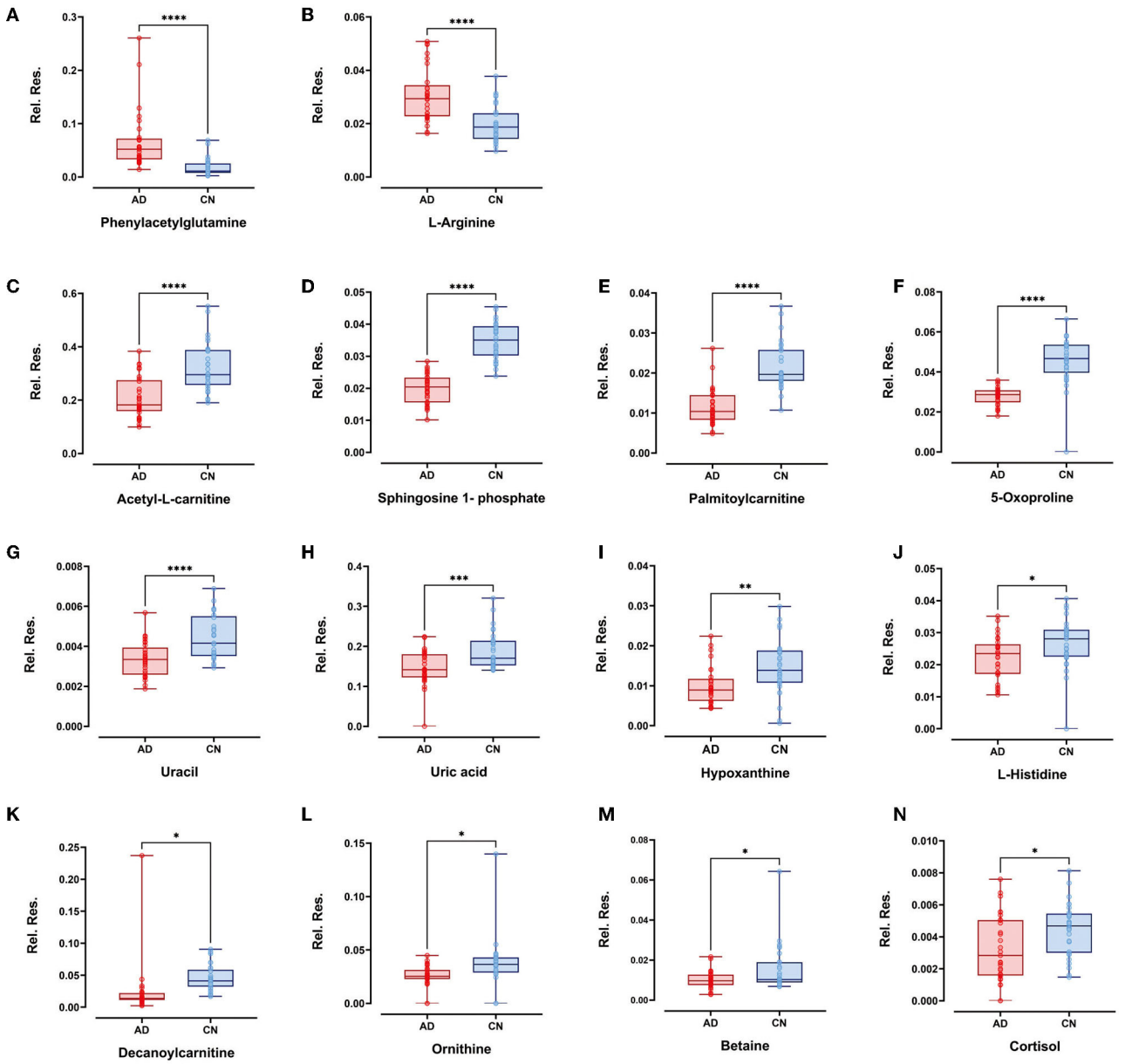

FIGURE 4
Boxplots showed upregulated plasma metabolites of **(A)** phenylacetylglutamine and **(B)** L-arginine ($p < 0.0001$). Boxplots showed downregulated plasma metabolites of **(C)** acetyl-L-carnitine, **(D)** sphingosine-1-phosphate, **(E)** palmitoylcarnitine, **(F)** 5-oxoproline, **(G)** uracil ($p < 0.0001$), **(H)** uric acid ($p < 0.001$); **(I)** hypoxanthine ($p < 0.01$); **(J)** L-histidine, **(K)** decanoylcarnitine, **(L)** ornithine, **(M)** betaine, and **(N)** cortisol ($p < 0.05$). Plots show data points from the minimum value to the maximum value for each group. Light pink dots represent AD patients, sky blue dots represent CN individuals, and dots were vertically aligned on the boxes for each group.

4. Discussion

There is an unmet demand for an examination that is simple, less intrusive, and affordable in the clinical diagnosis of AD. Untargeted metabolomics presents enormous potential in the exploration of new molecules implicated in the pathogenesis of AD. Using high-resolution mass spectrometry, we found that AD was closely linked to increased plasma levels of phenylacetylglutamine (PAGIn) and L-arginine (L-Arg). Furthermore, the AD group showed lower levels of metabolites of fatty acyls, sphingolipids, and steroids, in addition to other organic acids.

PAGIn, a gut microbiota-derived metabolite, which is derived from the essential amino acid phenylalanine, has been extensively studied as a toxin in chronic kidney disease and adverse cardiovascular events (Aronov et al., 2011; Poesen et al., 2016; Nemet et al., 2020; Yu et al., 2021). Emerging evidence have demonstrated that gut microbiota dysbiosis is functionally connected to brain immune dysfunctions (Sampson and Mazmanian, 2015). Also, the increased permeability of the gut and blood–brain barrier induced by microbiota dysbiosis may mediate or affect AD pathogenesis or other neurodegenerative disorders (Jiang et al., 2017). A metabolic profiling study on

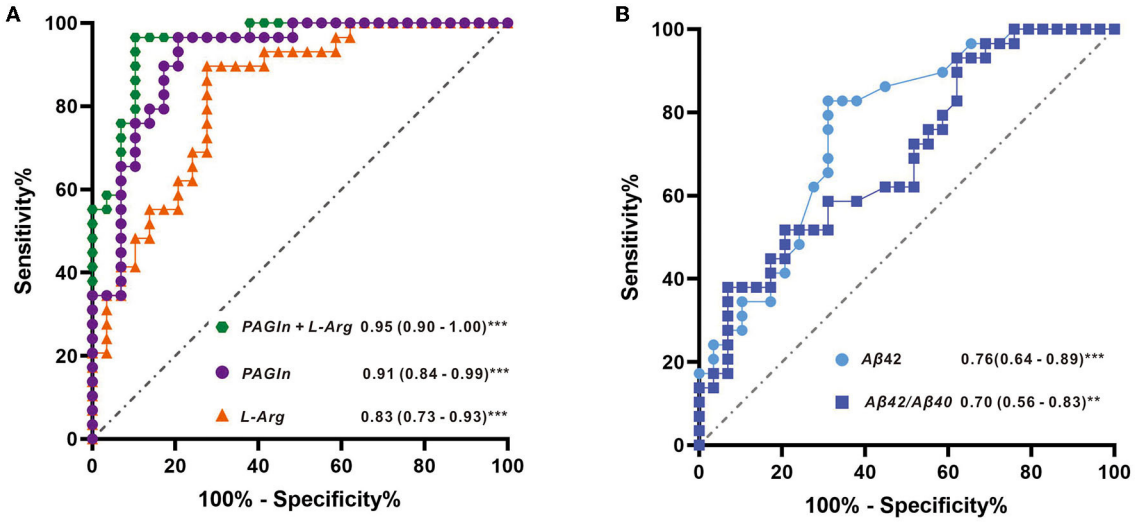

FIGURE 5
(A) ROC curves with metabolite features of L-arginine, PAGIn, and binary logistic regression of two metabolites (PAGIn + L-Arg) and **(B)** ROC curves with protein features of Aβ42 and the ratio of Aβ42/Aβ40.

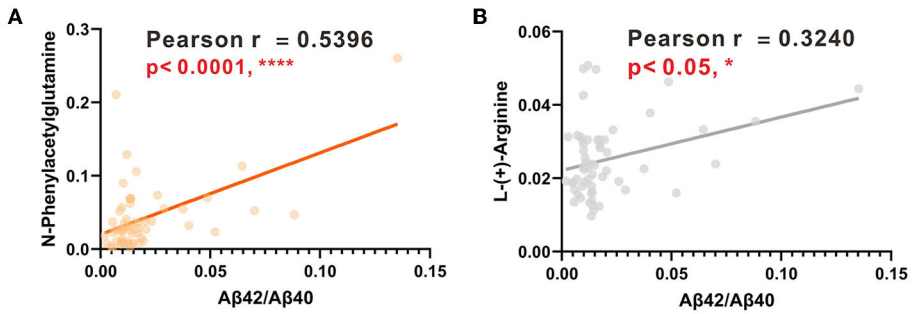

FIGURE 6
(A) Linear regression analysis between PAGIn and Aβ42/Aβ40. **(B)** Linear regression analysis between L-Arg and Aβ42/Aβ40.

Parkinson's disease (PD) using a mass spectrometry-based approach found that PAGIn was significantly elevated in the PD group as compared to the healthy controls, and its metabolic disturbances suggested that proteolytic metabolism was highly activated in PD (Shao et al., 2021). Nevertheless, limited findings have shown the dysregulation of plasma PAGIn in AD. This is our first observation documenting that plasma PAGIn is significantly elevated in AD patients, presenting an excellent discriminating power as a potential metabolite biomarker. Studies suggest that stochastic AD is associated with atherosclerosis, redox stress, inflammatory processes, and/or abnormal neurotransmitter and glucose metabolism in the brain (Yi et al., 2009). Thus, it is probable that PAGIn is involved in one or more pathophysiological processes, as previously stated. However, the underlying causes of PAGIn in Alzheimer's disease still require clarification.

L-Arg is a semi-essential amino acid that can be metabolized to form numerous bioactive molecules. Its involvement in AD is largely based on scattered information from a single pathway (Malinski, 2007). In a study examining arginine metabolism, researchers investigated three areas of the human brain: the superior frontal gyrus (SFG), the hippocampus (HPC), and the cerebellum (CE) in AD patients. They found that L-Arg was significantly elevated in the SFG area of AD patients, while L-ornithine (a product of arginase) showed a dramatic reduction in all three areas in AD (Liu et al., 2014). Interestingly, these findings were consistent with our results in the plasma metabolite investigation. The box plots illustrated that L-Arg was significantly elevated in the AD group, while its byproduct, L-ornithine, notably decreased in the AD group (Figures 4A, L). Furthermore, research has indicated that L-Arg has several direct and indirect effects on human vasculature, suggesting that it may play a crucial role in the pathogenesis of both atherosclerosis and AD. For instance, L-Arg has been found to be involved in diverse physiological and pathological processes, including neurotransmission (Chen and Chang, 2002), neurogenesis and neuroplasticity (Marcinkowska et al., 2022), cellular redox metabolism and redox stress (Perry et al., 2002; Tonnies and Trushina, 2017), inflammation (Wijnands et al., 2015), and regulation of cerebral blood flow (Matsuda et al., 2007).

In our previous study utilizing AD urine samples, an increase in potential diagnostic metabolites of uric acid, creatine, and choline was observed in the AD group as compared to the CN group. Conversely, in plasma samples, while uric acid displayed

a decreasing trend, both creatine and choline indicated no significant differences between the two groups (Zhang et al., 2022). The variability in the concentration of biomarkers in body fluids is due to the kidney's crucial role in reabsorbing certain substances from urine back into the bloodstream. Recent research also demonstrated a correlation between blood biomarker concentration with urinary biomarkers (Ho et al., 2015; Kukova et al., 2019). It appears that these metabolites undergo dynamic fluctuations during certain stages of Alzheimer's disease.

Besides, different biomarkers may denote the progression of Alzheimer's disease (Teunissen et al., 2022).

In addition, we investigated the AD biomarkers of Aβ40, Aβ42, APOE4, and TAU in blood to find their association with reported results (Rachakonda et al., 2004; Niedzwiecki et al., 2020; Thijssen et al., 2022). It has been suggested that the plasma ratio of Aβ42/Aβ40 is often used to discriminate amyloid PET positive and negative individuals across the clinical AD continuum (De Meyer et al., 2020; Verberk et al., 2020). In a case–control study, researchers used the ratio of Aβ42/Aβ40 in the discrimination test and acquired a good AUC(ROC), which is above 0.8 (Thijssen et al., 2022). Based on our ELISA results, we performed the discrimination test of ROC with Aβ42 and the Aβ42/Aβ40, which resulted in AUC (Aβ42) as 0.76 and AUC (Aβ42/Aβ40) as 0.70, and this was kept in line with reported cases.

Human APOE is a glycoprotein that is highly expressed in stressed neurons, astrocytes, microglia, vascular mural cells, and choroid plexus cells. It has been suggested that low plasma levels of APOE are linked to an elevated risk of developing future Alzheimer's disease and all forms of dementia in the general population (Rasmussen et al., 2015). Also, lower plasma concentrations of APOE were supported by the finding that APOE levels are negatively correlated with Aβ levels in multiple brain regions when analyzed in non-demented individuals (Shinohara et al., 2013). In this study, AD patients held lower APOE levels as compared to the CN participants, which presented a similar trend with reported cases.

Research suggested that Tau protein lost its ability to bind to microtubules, and therefore, its normal role of keeping the well-organized cytoskeleton is no longer effective (Kolarova et al., 2012). One prospective study indicated that high plasma Tau was found in patients with AD dementia compared with cognitively normal individuals and patients with MCI (Mattsson et al., 2016). However, another study revealed a significant decrease in plasma levels of total tau among individuals with MCI compared with cognitively normal controls, with a further highly significant reduction in AD patients compared with both MCI and normal controls (Sparks et al., 2012).

In our study, we observed a decrease in plasma t-tau levels in the AD group, which differs from the trends observed in other research groups (Mattsson et al., 2016; Shen, 2020). Another study that tested the alteration of plasma tau in AD found that plasma tau partly reflects AD pathology, but there is a considerable overlap with normal aging, especially in individuals without dementia (Mattsson et al., 2016). Recent studies suggested that elevated levels of tau in the blood are not specific to AD, which could also be found in other neuron degeneration conditions, such as Parkinson's disease, frontotemporal dementia, or amyotrophic lateral sclerosis (ALS) (Neumann et al., 2006; Boeve et al., 2022; Pan et al., 2022). Thus, future studies should test longitudinal plasma tau measurements in AD.

Nevertheless, the exciting and rapid developments in plasma-based assays hold promise for prescreening in research (reducing the need for, and associated costs with, lumbar punctures and PET scans), once properly validated, which would fulfill the diagnostic purposes in clinical practice. In this study, we employed the high-resolution mass spectrometer to screen the plasma metabolites, with the optimized and stabilized LCMS method, and we were able to determine hundreds of features that enable us to perform the discovery study. We found that both PAGIn and L-Arg showed pretty good discriminate power in separating AD patients from CN individuals, which exerted their underlying possibilities in clinical diagnosis. In addition, the combination group of PAGIn and L-Arg enhanced the diagnostic power from ROC (AUC) 0.91 to ROC (AUC) 0.95, thus improving the accuracy in AD discrimination with this test.

Epidemiological studies in different populations showed an independent relationship between the development of dementia and the incidence of cardiovascular diseases (CVD), implying the presence of shared biological processes (Cortes-Canteli and Iadecola, 2020; Stakos et al., 2020). Our results indicate that both plasma PAGIn and L-arginine are significant in separating Alzheimer's disease (AD) from cognitively normal individuals. However, limited investigations suggest that PAGIn and L-arginine are associated with AD but not CVD in plasma investigation. It is interesting to observe that, using mass spectrometry in one measurement, PAGIn and L-arginine were found to be significantly elevated in AD.

Besides, we introduced the discrimination analysis with Aβ42 and Aβ42/Aβ40. The best ROC of the protein biomarker is Aβ42 with an AUC of 0.76, which was in line with the literature. Moreover, protein–metabolite interactions are of importance in cellular procedure, since these compounds could serve as co-factors for proteins to mediate protein function. This has not been investigated in our previous studies on Alzheimer's disease. It is interesting to note the positive correlations between Aβ42/Aβ40 with PAGIn or L-Arg with statistical significance. This suggests that PAGIn and L-Arg hold great promise in the diagnosis of Alzheimer's disease. These findings should be further validated in future tests using clinical specimens.

However, our study has some limitations. First, it is restricted by the lack of access to pathology reports and APOE genotype information, which impacts the scope of clinical parameters that can be included in this article. In future research, MRI could be used to visualize decreased gray matter (GM) volume in AD patients or a positron emission tomography (PET) scan could be conducted to detect amyloid deposition in AD patients, as these methods are considered the "gold standard" for assessing AD states in clinical settings, and would support the diagnosis of metabolite biomarker studies. Second, the observational nature of the study design means that the causal links between two metabolites (PAGln and L-Arg) and AD cannot be established. Instead, a functional metabolomics technique must be used to uncover the underlying pathways. Third, our study was conducted at a single location and had a biased patient selection; the sample size was also small, which means that further validation at other research centers and larger sample sizes are required. Finally, absolute quantitation analysis of

differential metabolites was not performed due to a limited plasma sample, which should be done in future cohort studies to validate the findings.

5. Conclusion

In conclusion, our study showed that AD patients had an altered peripheral metabolism as compared to cognitively normal participants. We demonstrated the added advantage of examining metabolic expression signatures and constructing a comprehensive picture of metabolic change by examining categorization and regulatory signatures. Not only could studying additional signatures highlight potential predictive and regulatory indicators but could also uncover essential features that may have been overlooked when only investigating expression signatures. Particularly, PAGIn and L-Arg have been identified as potential essential features in metabolic alteration and showed an excellent discrimination ability in AD diagnosis. Our study also highlights a significant association between the AD protein ratio of Aβ42/Aβ40 and PAGIn or L-Arg. These findings indicate that protein biomarkers correlated with metabolites can strengthen AD diagnosis. Future studies will be required to corroborate these results and to clarify the specific roles of these metabolites in AD metabolic change.

Data availability statement

The data presented in the study are deposited in the MetaboLights public database. This data can be found here: https://www.ebi.ac.uk/metabolights/editor/study/MTBLS8045/.

Ethics statement

The studies involving human participants were reviewed and approved by the Ethics Committee of Shanghai Baoshan Luodian Hospital (Approval number: LDYY-KY-2020-04). The patients/participants provided their written informed consent to participate in this study.

Author contributions

XD and QZ contributed to the conception of this article. JiY performed the experiment and wrote the manuscript. SW performed the data collection and data analysis. JuY interpreted data for the work and joined in constructive discussions. All authors have read and agreed to the published version of the manuscript.

Funding

This work was supported by grants from the Science and Technology Innovation Special Fund (19-E-29) and the Science and Technology Committee of Shanghai Baoshan District.

Acknowledgments

We are grateful for the scientific discussion with colleagues from the Neurology Department and Clinical Research Center of Shanghai Baoshan Luodian Hospital. We would like to thank Xinru Liu for the collection of clinical documents and Junjie Chen for the plasma sample handling. We appreciate Shanghai Yunxiang Medical Technology Co., Ltd. (Shanghai, China) for providing a high-resolution mass spectrometer for metabolomics analysis.

Conflict of interest

The authors declare that the research was conducted in the absence of any commercial or financial relationships that could be construed as a potential conflict of interest.

Publisher's note

Supplementary material

The Supplementary Material for this article can be found online at: https://www.frontiersin.org/articles/10.3389/fnagi.2023.1189659/full#supplementary-material

References

(2021). 2021 Alzheimer's disease facts and figures. *Alzheimers. Dement.* 17, 327–406. doi: 10.1002/alz.12328

Aisen, P., Touchon, J., Andrieu, S., Boada, M., Doody, R., Nosheny, R. L., et al. (2016). Registries and cohorts to accelerate early phase Alzheimer's trials. A report from the E.U./U.S. clinical trials in Alzheimer's disease task force. *J. Prev. Alzheimers Dis.* 3, 68–74. doi: 10.14283/jpad.2016.97

Aronov, P. A., Luo, F. G., Plummer, N. S., Quan, Z., Holmes, S., Hostetter, T. H., et al. (2011). Colonic contribution to uremic solutes. *J. Am. Soc. Nephrol.* 22, 1769–1776. doi: 10.1681/ASN.2010121220

Bendlin, B. B., Zetterberg, H. (2022), The iterative process of fluid biomarker development and validation in Alzheimer's disease. *Alzheimers Dement (Amst)* 14, e12341. doi: 10.1002/dad2.12341

Boeve, B. F., Boxer, A. L., Kumfor, F., Pijnenburg, Y., and Rohrer, J. D. (2022). Advances and controversies in frontotemporal dementia: diagnosis, biomarkers, and therapeutic considerations. *Lancet Neurol.* 21, 258–272. doi: 10.1016/S1474-4422(21)00341-0

Chandler, J. D., Hu, X., Ko, E-J., Park, S., Lee, Y-T., Orr, M., et al. (2016). Metabolic pathways of lung inflammation revealed by high-resolution metabolomics (HRM) of H1N1 influenza virus infection in mice. *Am. J. Physiol. Regul. Integr. Comp. Physiol.* 311, R906–R916. doi: 10.1152/ajpregu.00298.2016

Chen, K. K., and Chang, L. (2002). Involvement of L-arginine/nitric oxide pathway at the paraventricular nucleus of hypothalamus in central neural regulation of penile erection in the rat. *Int. J. Impot. Res.* 14, 139–145. doi: 10.1038/sj.ijir.3900825

Cortes-Canteli, M., and Iadecola, C. (2020). Alzheimer's disease and vascular aging: JACC focus seminar. *J. Am. Coll. Cardiol.* 75, 942–951. doi: 10.1016/j.jacc.2019.10.062

Cummings, J., Lee, G., Nahead, P., Kambar, M., Zhong, K., Fonseca, J., et al. (2022). Alzheimer's disease drug development pipeline: 2022 *Alzheimers Dement (N Y)* 8, e12295. doi: 10.1002/trc2.12295

de la Monte, S. M., and Tong, M. (2014). Brain metabolic dysfunction at the core of Alzheimer's disease. *Biochem. Pharmacol.* 88, 548–559. doi: 10.1016/j.bcp.2013.12.012

De Meyer, S., Schaeverbeke, J. M., Verberk, I. M. W., Gille, B., De Schaepdryver, M., Luckett, E. S., et al. (2020). Comparison of ELISA- and SIMOA-based quantification of plasma Abeta ratios for early detection of cerebral amyloidosis. *Alzheimers. Res. Ther.* 12, 162. doi: 10.1186/s13195-020-00728-w

de Souza, L. P., Alseekh, S., Scossa, F., and Fernie, A. R. (2021). Ultra-high-performance liquid chromatography high-resolution mass spectrometry variants for metabolomics research. *Nat. Methods* 18, 733–746. doi: 10.1038/s41592-021-01116-4

Deleidi, M., Jaggle, M., and Rubino, G. (2015). Immune aging, dysmetabolism, and inflammation in neurological diseases. *Front. Neurosci.* 9, 172. doi: 10.3389/fnins.2015.00172

Golde, T. E. (2022). Alzheimer's disease - the journey of a healthy brain into organ failure. *Mol. Neurodegener.* 17, 18. doi: 10.1186/s13024-022-00523-1

Ho, J., Tangri, N., Komenda, P., Kaushal, A., Sood, M., Brar, R., et al. (2015). Urinary, plasma, and serum biomarkers' utility for predicting acute kidney injury associated with cardiac surgery in adults: a meta-analysis. *Am. J. Kidney Dis.* 66, 993–1005. doi: 10.1053/j.ajkd.2015.06.018

Holmes, E., Wilson, I. D., and Nicholson, J. K. (2008). Metabolic phenotyping in health and disease. *Cell.* 134, 714–717. doi: 10.1016/j.cell.2008.08.026

Jack, C. R. J., Bennett, D. A., Blennow, K., Carrillo, M. C., Dunn, B., Haeberlein, S. B., et al. (2018). NIA-AA research framework: toward a biological definition of Alzheimer's disease. *Alzheimers. Dement.* 14, 535–562. doi: 10.1016/j.jalz.2018.02.018

Jack, C. R. J., Bennett, D. A., Blennow, K., Carrillo, M. C., Feldman, H. H., Frisoni, G. B., et al. (2016). A/T/N: An unbiased descriptive classification scheme for Alzheimer disease biomarkers. *Neurology.* 87, 539–547. doi: 10.1212/WNL.0000000000002923

Jiang, C., Li, G., Huang, P., Liu, Z., and Zhao, B. (2017). The Gut Microbiota and Alzheimer's Disease. *J. Alzheimers. Dis.* 58, 1–15. doi: 10.3233/JAD-161141

Kaufmann, A. (2018). Analytical performance of the various acquisition modes in Orbitrap MS and MS/MS. *J. Mass Spectrom.* 53, 725–738. doi: 10.1002/jms.4195

Koek, M. M., Jellema, R. H., van der Greef, J., Tas, A. C., and Hankemeier, T. (2011). Quantitative metabolomics based on gas chromatography mass spectrometry: status and perspectives. *Metabolomics.* 7, 307–328. doi: 10.1007/s11306-010-0254-3

Kolarova, M., García-Sierra, F., Bartos, A., Ricny, J., and Ripova, D. (2012). Structure and pathology of tau protein in Alzheimer disease. *Int. J. Alzheimers. Dis.* 2012, 731526. doi: 10.1155/2012/731526

Kueper, J. K., Speechley, M., and Montero-Odasso, M. (2018). The Alzheimer's Disease Assessment Scale-Cognitive Subscale (ADAS-Cog): Modifications and Responsiveness in Pre-Dementia Populations. A Narrative Review. *J. Alzheimers. Dis.* 63, 423–444. doi: 10.3233/JAD-170991

Kukova, L. Z., Mansour, S. G., Coca, S. G., de Fontnouvelle, C. A., Thiessen-Philbrook, H. R., Shlipak, M. G., et al. (2019). Comparison of urine and plasma biomarker concentrations measured by aptamer-based versus immunoassay methods in cardiac surgery patients. *J. Appl. Lab Med* 4, 331–342. doi: 10.1373/jalm.2018.028621

Lawton, K. A, Berger, A, Mitchell, M, Milgram, K. E, Evans, A. M, Guo, L, et al. (2008). Analysis of the adult human plasma metabolome. *Pharmacogenomics.* 9, 383–397. doi: 10.2217/14622416.9.4.383

Liang, X., Chen, X., Liang, Q., Zhang, H., Hu, P., Wang, Y., et al. (2011). Metabonomic study of Chinese medicine Shuanglong formula as an effective treatment for myocardial infarction in rats. *J. Proteome Res.* 10, 790–799. doi: 10.1021/pr1009299

Liu, P., Fleete, M. S., Jing, Y., Collie, N. D., Curtis, M. A., Waldvogel, H. J., et al. (2014). Altered arginine metabolism in Alzheimer's disease brains. *Neurobiol. Aging* 35, 1992–2003. doi: 10.1016/j.neurobiolaging.2014.03.013

Malinski, T. (2007). Nitric oxide and nitroxidative stress in Alzheimer's disease. *J. Alzheimers. Dis.* 11, 207–218. doi: 10.3233/JAD-2007-11208

Marcinkowska, A. B., Biancardi, V. C., and Winklewski, P. J. (2022). Arginine-vasopressin, synaptic plasticity and brain networks. *Curr. Neuropharmacol.* 20, 2292–2302. doi: 10.2174/1570159X20666220222143532

Matsuda, H., Mizumura, S., Nagao, T., Ota, T., Iizuka, T., Nemoto, K., et al. (2007). An easy Z-score imaging system for discrimination between very early Alzheimer's disease and controls using brain perfusion SPECT in a multicentre study. *Nucl. Med. Commun.* 28, 199–205. doi: 10.1097/MNM.0b013e328013eb8b

Mattsson, N., Zatterberg, H., Janelize, S., Insel, P., Anderson, U., Stomrud, E., et al. (2016). Plasma tau in Alzheimer disease. *Neurology* 87, 1827–1835. doi: 10.1212/WNL.0000000000003246

Nemet, I., Saha, P. P., Gupta, N., Zhu, W., Romano, K. A., Skye, S. M., et al. (2020). A Cardiovascular Disease-Linked Gut Microbial Metabolite Acts via Adrenergic Receptors. Cell, 180, 862–877. e22. doi: 10.1016/j.cell.2020.02.016

Neumann, M., Sampathu, D. M., Kwong, L. K., Truax, A. C., Micsenyi, M. C., Chou, T. T., et al. (2006). Ubiquitinated TDP-43 in frontotemporal lobar degeneration and amyotrophic lateral sclerosis. *Science.* 314, 130–133. doi: 10.1126/science.1134108

Niedzwiecki, M. M., Walker, D. I., Howell, J. C., Watts, K. D., Jones, D. P., Miller, G. W., et al. (2020). High-resolution metabolomic profiling of Alzheimer's disease in plasma. *Ann Clin Transl Neurol* 7, 36–45. doi: 10.1002/acn3.50956

Pan, L., Li, C., Meng, L., Tian, L., He, M., Yuan, X., et al. (2022). Tau accelerates alpha-synuclein aggregation and spreading in Parkinson's disease. *Brain* 145, 3454–3471. doi: 10.1093/brain/awac171

Perry, G., Taddeo, M. A., Nunomura, A., Zhu, X., Zenteno-Savin, T., Drew, K. L., et al. (2002). Comparative biology and pathology of oxidative stress in Alzheimer and other neurodegenerative diseases: beyond damage and response. *Comp. Biochem. Physiol. C. Toxicol. Pharmacol.* 133, 507–513. doi: 10.1016/S1532-0456(02)00119-9

Poesen, R., Claes, K., Evenepoel, P., de Loor, H., Augustijns, P., Kuypers, D., et al. (2016). Microbiota-Derived Phenylacetylglutamine Associates with Overall Mortality and Cardiovascular Disease in Patients with CKD. *J. Am. Soc. Nephrol.* 27, 3479–3487. doi: 10.1681/ASN.2015121302

Procaccini, C., Santopaolo, M., Faicchia, D., Colamatteo, A., Formisano, L., de Candia, P., et al. (2016). Role of metabolism in neurodegenerative disorders. *Metab. Clin. Exp.* 65, 1376–1390. doi: 10.1016/j.metabol.2016.05.018

Rachakonda, V., Pan, T. H., and Le, W. D. (2004). Biomarkers of neurodegenerative disorders: how good are they? *Cell Res.* 14, 347–358. doi: 10.1038/sj.cr.7290235

Rasmussen, K. L., Tybjaerg-Hansen, A., Nordestgaard, B. G., and Frikke-Schmidt, R. (2015). Plasma levels of apolipoprotein E and risk of dementia in the general population. *Ann. Neurol.* 77, 301–311. doi: 10.1002/ana.24326

Sales, S., Knittelfelder, O., and Shevchenko, A. (2017). Lipidomics of Human Blood Plasma by High-Resolution Shotgun Mass Spectrometry. *Methods Mol. Biol.* 1619, 203–212. doi: 10.1007/978-1-4939-7057-5_16

Sampson, T. R., and Mazmanian, S. K. (2015). Control of brain development, function, and behavior by the microbiome. *Cell Host Microbe* 17, 565–576. doi: 10.1016/j.chom.2015.04.011

Schrijvers, E. M. C., Witteman, J. C. M., Sijbrands, E. J. G., Hofman, A., Koudstaal, P. J., Breteler, M. M. B. (2010). Insulin metabolism and the risk of Alzheimer disease: the Rotterdam Study. *Neurology* 75, 1982–1987. doi: 10.1212/WNL.0b013e3181ffe4f6

Shao, Y., Li, T., Liu, Z., Wang, X., Xu, X., Li, S., et al. (2021). Comprehensive metabolic profiling of Parkinson's disease by liquid chromatography-mass spectrometry. *Mol. Neurodegener.* 16, 4. doi: 10.1186/s13024-021-00425-8

Shen, X. N. (2020). Plasma amyloid, tau, and neurodegeneration biomarker profiles predict Alzheimer's disease pathology and clinical progression in older adults without dementia. *Alzheimers Dement (Amst).* 12, e12104. doi: 10.1002/dad2.12104

Shinohara, M., Petersen, R. C., Dickson, D. W., and Bu, G. (2013). Brain regional correlation of amyloid-beta with synapses and apolipoprotein E in non-demented individuals: potential mechanisms underlying regional vulnerability to amyloid-beta accumulation. *Acta Neuropathol.* 125, 535–547. doi: 10.1007/s00401-013-1086-9

Sparks, D. L., Kryscio, R. J., Sabbagh, M. N., Ziolkowski, C., Lin, Y., Sparks, L. M., et al. (2012). Tau is reduced in AD plasma and validation of employed ELISA methods. *Am. J. Neurodegener. Dis.* 1, 99–106.

Stakos, D. A., Stamatelopoulos, K, Bampatsias, D., Sachse, M., Zormpas, E., Vlachogiannis, N. I., et al. (2020). The Alzheimer's disease amyloid-beta hypothesis in cardiovascular aging and disease: JACC focus seminar. *J. Am. Coll. Cardiol.* 75, 952–967. doi: 10.1016/j.jacc.2019.12.033

Szymańska, E., Saccenti, E., Smilde, A. K., and Westerhuis, J. A. (2012). Double-check: validation of diagnostic statistics for PLS-DA models in metabolomics studies. *Metabolomics* 8, 3–16. doi: 10.1007/s11306-011-0330-3

Teunissen, C. E., Verberk, I. M. W., Thijssen, E. H., Vermunt, L., Hansson, O., Zetterberg, H., et al. (2022). Blood-based biomarkers for Alzheimer's disease: towards clinical implementation. *Lancet Neurol.* 21, 66–77. doi: 10.1016/S1474-4422(21)00361-6

Thijssen, E. H., Verberk, I. M. W., Kindermans, J., Abramian, A., Vanbrabant, J., Ball, A. J., et al. (2022). Differential diagnostic performance of a panel of plasma biomarkers for different types of dementia. *Alzheimers Dement (Amst)* 14, e12285. doi: 10.1002/dad2.12285

Tonnies, E., and Trushina, E. (2017). Oxidative stress, synaptic dysfunction, and alzheimer's disease. *J. Alzheimers. Dis.* 57, 1105–1121. doi: 10.3233/JAD-161088

Trivedi, D. K., Hollywood, K. A., and Goodacre, R. (2017). Metabolomics for the masses: the future of metabolomics in a personalized world. *New Horiz. Transl. Med.* 3, 294–305. doi: 10.1016/j.nhtm.2017.06.001

Uppal, K., Salinas, J. L., Monteiro, W. M., Val, F., Cordy, R. J., Liu, K., et al. (2017). Plasma metabolomics reveals membrane lipids, aspartate/asparagine and nucleotide metabolism pathway differences associated with chloroquine resistance in Plasmodium vivax malaria. *PLoS ONE.* 12, e0182819. doi: 10.1371/journal.pone.0182819

Verberk, I. M. W., Thijssen, E., Koelewijn, J., Mauroo, K., Vanbrabant, J., de Wilde, A., et al. (2020). Combination of plasma amyloid beta(1-42/1-40) and glial fibrillary acidic protein strongly associates with cerebral amyloid pathology. *Alzheimers. Res. Ther.* 12, 118. doi: 10.1186/s13195-020-00682-7

Vogt, M. C., and Bruning, J. C. (2013). CNS insulin signaling in the control of energy homeostasis and glucose metabolism - from embryo to old age. *Trends Endocrinol. Metab.* 24, 76–84. doi: 10.1016/j.tem.2012.11.004

Wheelock, A. M., and Wheelock, C. E. (2013). Trials and tribulations of 'omics data analysis: assessing quality of SIMCA-based multivariate models using examples from pulmonary medicine. *Mol. Biosyst.* 9, 2589–2596. doi: 10.1039/c3mb70194h

Wijnands, K. A. P., Castermans, T. M. R., Hommen, M. P. J., Meesters, D. M., and Poeze, M. (2015). Arginine and citrulline and the immune response in sepsis. *Nutrients* 7, 1426–1463. doi: 10.3390/nu7031426

Yi, J., Horkey, L. L., Friedlich, A. L., Shi, Y., Rogers, J., and Huang, S. (2009). L-arginine and Alzheimer's disease. *Int. J. Clin. Exp. Pathol.* 2, 211–238. Available online at: https://e-century.us/files/ijcep/2/3/IJCEP808005.pdf

Yu, F., Li, X., Feng, X., Wei, M., Luo, Y., Zhao, T., et al. (2021). Phenylacetylglutamine, a Novel Biomarker in Acute Ischemic Stroke. *Front Cardiovasc Med* 8, 798765. doi: 10.3389/fcvm.2021.798765

Zhang, Q., Wu, S., Liu, X., Yang, J., Dong, X., Zhou, Y., et al. (2022). An observation study of urinary biomarker exploratory in Alzheimer's disease using high-resolution mass spectrometry. *Biomed. Chromatogr.* 36, e5421. doi: 10.1002/bmc.5421

Zhuang, Z., Gao, M., Yang, R., Liu, Z., Cao, W., and Huang, T. (2021). Causal relationships between gut metabolites and Alzheimer's disease: a bidirectional Mendelian randomization study. *Neurobiol Aging, 100* 119. e15-119 e18. doi: 10.1016/j.neurobiolaging.2020.10.022

frontiers | Frontiers in Aging Neuroscience

TYPE Systematic Review
PUBLISHED 06 July 2023
DOI 10.3389/fnagi.2023.1199826

OPEN ACCESS

EDITED BY
Woon-Man Kung,
Chinese Culture University, Taiwan

REVIEWED BY
Anastasia Bougea,
National and Kapodistrian University of Athens, Greece
Artur Francisco Schumacher-Schuh,
Federal University of Rio Grande do Sul, Brazil
Violeta Pina,
University of Granada, Spain
Victor Manuel Campello, University of Barcelona, Spain, in collaboration with reviewer VP

*CORRESPONDENCE
Yuting Wang
✉ 15253669990@163.com

RECEIVED 04 April 2023
ACCEPTED 21 June 2023
PUBLISHED 06 July 2023

CITATION
Bian J, Wang X, Hao W, Zhang G and Wang Y (2023) The differential diagnosis value of radiomics-based machine learning in Parkinson's disease: a systematic review and meta-analysis.
Front. Aging Neurosci. 15:1199826.
doi: 10.3389/fnagi.2023.1199826

The differential diagnosis value of radiomics-based machine learning in Parkinson's disease: a systematic review and meta-analysis

Jiaxiang Bian[1], Xiaoyang Wang[1], Wei Hao[1], Guangjian Zhang[2] and Yuting Wang[2]*

[1]School of Clinical Medicine, Weifang Medical University, Weifang, China, [2]Department of Neurosurgery, Weifang People's Hospital, Weifang, China

Background: In recent years, radiomics has been increasingly utilized for the differential diagnosis of Parkinson's disease (PD). However, the application of radiomics in PD diagnosis still lacks sufficient evidence-based support. To address this gap, we carried out a systematic review and meta-analysis to evaluate the diagnostic value of radiomics-based machine learning (ML) for PD.

Methods: We systematically searched Embase, Cochrane, PubMed, and Web of Science databases as of November 14, 2022. The radiomics quality assessment scale (RQS) was used to evaluate the quality of the included studies. The outcome measures were the c-index, which reflects the overall accuracy of the model, as well as sensitivity and specificity. During this meta-analysis, we discussed the differential diagnostic value of radiomics-based ML for Parkinson's disease and various atypical parkinsonism syndromes (APS).

Results: Twenty-eight articles with a total of 6,057 participants were included. The mean RQS score for all included articles was 10.64, with a relative score of 29.56%. The pooled c-index, sensitivity, and specificity of radiomics for predicting PD were 0.862 (95% CI: 0.833–0.891), 0.91 (95% CI: 0.86–0.94), and 0.93 (95% CI: 0.87–0.96) in the training set, and 0.871 (95% CI: 0.853–0.890), 0.86 (95% CI: 0.81–0.89), and 0.87 (95% CI: 0.83–0.91) in the validation set, respectively. Additionally, the pooled c-index, sensitivity, and specificity of radiomics for differentiating PD from APS were 0.866 (95% CI: 0.843–0.889), 0.86 (95% CI: 0.84–0.88), and 0.80 (95% CI: 0.75–0.84) in the training set, and 0.879 (95% CI: 0.854–0.903), 0.87 (95% CI: 0.85–0.89), and 0.82 (95% CI: 0.77–0.86) in the validation set, respectively.

Conclusion: Radiomics-based ML can serve as a potential tool for PD diagnosis. Moreover, it has an excellent performance in distinguishing Parkinson's disease from APS. The support vector machine (SVM) model exhibits excellent robustness when the number of samples is relatively abundant. However, due to the diverse implementation process of radiomics, it is expected that more large-scale, multi-class image data can be included to develop radiomics

intelligent tools with broader applicability, promoting the application and development of radiomics in the diagnosis and prediction of Parkinson's disease and related fields.

Systematic review registration: https://www.crd.york.ac.uk/PROSPERO/display_record.php?RecordID=383197, identifier ID: CRD42022383197.

KEYWORDS

Parkinson's disease, radiomics, machine learning, diagnostic accuracy, meta-analysis, systematic review

1. Introduction

Parkinson's disease (PD) is the second utmost common neurodegenerative illness, and its prevalence is anticipated to more than double over the next 30 years (GBD 2016 Parkinson's Disease Collaborators, 2018; Tolosa et al., 2021). The increasing number of patients will impose a significant medical and economic burden on society. Currently, the diagnosis of PD depends on a set of standards proposed by the International Parkinson and Movement Disorder Society (MDS) in 2015 (Postuma et al., 2015). During this process, clinicians rely on limited support and exclusion criteria, as well as "Red flags" to evaluate patients, which is time-consuming and labor-intensive and is related to the experience of clinical experts. Moreover, in the early stages, it is challenging to accurately and timely identify PD due to overlapping symptoms with atypical Parkinson's syndrome (APS) (Respondek et al., 2019). Studies have shown that about 20–30% of patients with multiple system atrophy (MSA) or progressive supranuclear palsy (PSP) were initially misdiagnosed as idiopathic Parkinson's disease (IPD) in clinical practice (Saeed et al., 2020). In addition, in terms of the motor subtypes of PD, the postural instability and gait difficulty subtype (PIGD) has greater damage to the neurological function than the tremor-dominant subtype (TD) and has a relatively poor response to deep brain stimulation (DBS) and levodopa therapy (Sun et al., 2021). Given the above reasons, early and accurate identification of PD and differentiation of its subtypes have profound clinical significance for developing individualized treatment plans and predicting prognosis.

Radiomics has emerged as a result of the development of artificial intelligence and medical precision. It extracts high-dimensional data from clinical images (such as PET, MRI, and CT) that can be mined (Lambin et al., 2012, 2017). Through analyzing and constructing classification models, radiomics can be utilized alone or in conjunction with histological, demographic, genomic, or proteomic data to support evidence-based clinical decision-making (Rizzo et al., 2018). In recent years, radiomics has gradually demonstrated significant clinical utility in the diagnosis, differential diagnosis, severity assessment, and prediction of disease progression in Parkinson's disease (PD), Parkinson's syndrome, and other neurodegenerative disorders, through the utilization of various imaging techniques (Adeli et al., 2016; Klyuzhin et al., 2016; Rahmim et al., 2016).

However, radiomics encompasses diverse methods in its implementation and is highly correlated with the expertise of clinical experts. The diagnostic performance of radiomics needs to be comprehensively evaluated from an evidence-based perspective. Systematic reviews, as a component of evidence-based medicine, can provide relevant guidance to some extent in formulating clinical strategies. Therefore, we conducted this study to evaluate the accuracy of radiomics-based machine learning in diagnosing Parkinson's disease (PD) and to summarize some of the challenges currently faced by radiomics in order to provide a reference for future applications of radiomics.

2. Materials and methods

Our systematic review and meta-analysis were conducted based on the Preferred Reporting Items for Systematic Reviews and Meta-Analyses (PRISMA 2020) guidelines (Moher et al., 2009). The PRISMA guidelines are provided in **Supplementary Table 1**. This study was registered on PROSPERO (ID: CRD42022383197).

2.1. Inclusion and exclusion criteria

2.1.1. Inclusion criteria

(1) Patients clinically diagnosed with Parkinson's disease (PD) with complete imaging data.
(2) Fully constructed radiomics ML models for the diagnosis of PD.
(3) Studies without external validation were also included.
(4) Published studies employing the same or different machine learning (ML) algorithms on a single dataset.
(5) Studies reported in English were included.

2.1.2. Exclusion criteria

(1) Meta-analyses, reviews, guidelines, expert opinions, etc.
(2) Studies that only performed differential factor analysis and did not construct a complete ML model.
(3) Studies that lacked outcome indicators for ML model prediction accuracy (Roc, c-statistic, c-index, sensitivity,

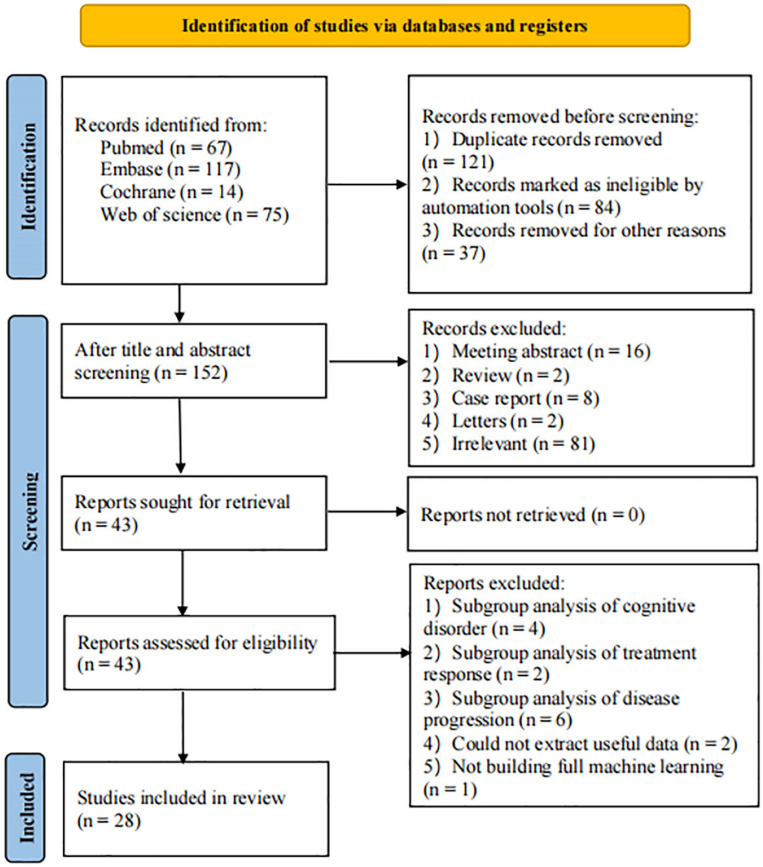

FIGURE 1
Literature screening flowchart.

specificity, accuracy, recall, precision, confusion matrix, diagnostic four-grid table, F1 score, calibration curve).

2.2. Literature search strategy

We performed a comprehensive search of the PubMed, Cochrane, Embase, and Web of Science databases for all available literature up to November 14th, 2022, utilizing a combination of subject headings and free-text terms. Our search was not restricted by language or geographic region. The detailed search strategy is shown in **Supplementary Table 2**.

2.3. Study selection and data extraction

We imported the retrieved literature into EndNote and removed duplicate articles. The remaining articles were screened based on their titles and abstracts. For the potentially relevant studies, we downloaded and read the full-text articles to determine their eligibility according to the inclusion and exclusion criteria. Before extracting the data, a standardized electronic spreadsheet was developed. The extracted information included the title, first author, publication year, country, study type, patient source, PD diagnostic criteria, radiomics source, whether complete imaging protocols were recorded, number of imaging reviewers involved, whether pre-experiments were conducted under different imaging parameters, whether repeated measurements were performed at different times, imaging segmentation software, texture extraction software, number of PD cases/images, total number of cases/images, number of PD cases/images in the training set, number of cases/images in the training set, method of generating the validation set, number of PD cases in the validation set, number of cases in the validation set, variable selection method, type of model used, modeling variables, whether radiomics scores were constructed, overfitting evaluation, whether the code and data were made publicly available, and model evaluation indications.

The literature screening and data extraction were independently conducted by two researchers (JB and XW), and cross-checking was performed afterward. In cases of disagreement, a third researcher (WH) was consulted to resolve the issue.

2.4. Quality assessment

The methodological quality of the included studies was assessed by the two researchers (JB and XW) using the Radiomics Quality Score (RQS), and an interactive check was conducted afterward (Lambin et al., 2012). If there was a dispute, a third researcher

TABLE 1 (A) Basic characteristic of the included studies; (B) Modeling information for included studies.

Schedule A							
No.	References	Country	Research type	Differential diagnosis	Patient source	Diagnostic criteria for Parkinson's disease	Radiomics source
1	Zhao et al., 2022	China	Case-control	PD vs. APS	Single center	The MDS PD Criteria	PET
2	Sun et al., 2022	China	Case-control	PD vs. HCs	Multi-center	The MDS PD Criteria	PET
3	Shiiba et al., 2022	Japan	Case-control	PD vs. HCs	Registration database	Not described	SPECT
4	Shi et al., 2022b	China	Case-control	PD vs. HCs	Registration database	Not described	MRI
5	Shi et al., 2022a	China	Case-control	PD vs. HCs	Registration database	Not described	MRI
6	Pang et al., 2022	China	Case-control	PD vs. MSA-p	Single center	Not described	MRI
7	Li et al., 2022	China	Case-control	PD vs. HCs	Single center	The MDS PD Criteria	MRI
8	Kim et al., 2022	Republic of Korea	Case-control	PD vs. MSA-p PD vs. MSA-c PD vs. PSP	Single center	The UK PD SBB criteria	MRI
9	Kang et al., 2022	China	Case-control	PD vs. HCs	Single center	The MDS PD Criteria	MRI
10	Guan et al., 2022	China	Case-control	PD vs. HCs	Single center	The UK PD SBB criteria	MRI
11	Ben Bashat et al., 2022	Israel	Case-control	PD vs. HCs	Single center	The MDS PD Criteria	MRI/SPECT
12	Zhang et al., 2021	China	Case-control	DPD vs. HCs NDPD vs. HCs DPD vs. NDPD	Single center	Not described	MRI
13	Tupe-Waghmare et al., 2021	India	Case-control	PD vs. HCs PD vs. APS	Single center	The UK PD SBB criteria	MRI
14	Sun et al., 2021	China	Case-control	PIGD vs. HCs TD vs. HCs PIGD vs. TD	Registration database	Not described	MRI
15	Shi et al., 2021	China	Case-control	PD vs. HCs	Registration database	The UK PD SBB criteria	MRI
16	Ren et al., 2021	China	Case-control	PD vs. HCs	Single center	The MDS PD Criteria	MRI
17	Li et al., 2021	China	Case-control	PD vs. HCs PD vs. DPD	Single center	The MDS PD Criteria	MRI
18	Hu et al., 2021	China	Case-control	PD vs. MSA	Single center	The MDS PD Criteria	MRI/PET
19	Dhinagar et al., 2021	United States	Case-control	PD vs. HCs	Registration database	Not described	MRI
20	Cao et al., 2021	China	Case-control	PD vs. HCs	Single center	Not described	MRI
21	Shu et al., 2020	China	Case-control	PD vs. HCs	Registration database	Not described	MRI
22	Pang et al., 2020	China	Case-control	PD vs. MSA-p	Single center	The UK PD SBB criteria	MRI
23	Liu et al., 2020	China	Case-control	PD vs. HCs	Single center	The UK PD SBB criteria	MRI
24	Cao et al., 2020	China	Case-control	PD vs. HCs	Single center	Not described	MRI
25	Xiao et al., 2019	China	Case-control	PD vs. HCs	Single center	Not described	MRI
26	Wu et al., 2019	China	Cohort study	PD vs. HCs	Multi-center	The UK PD SBB criteria	PET
27	Shinde et al., 2019	India	Case-control	PD vs. HCs PD vs. APS	Single center	The UK PD SBB criteria	MRI
28	Cheng et al., 2019	China	Case-control	PD vs. HCs	Single center	The UK PD SBB criteria	MRI

(Continued)

TABLE 1 (Continued)

Schedule B							
No.	References	Total sample size	Sample size in training set	Verification method	Sample size in validation set	Variable screening method	Type of model
1	Zhao et al., 2022	1017 (IPD 682, MSA 168, PSP 124, HCs 43)	737	External validation	280	Not described	CNN
2	Sun et al., 2022	406 (PD 125, HCs 281)	358	External validation	48	Not described	SVM, CNN
3	Shiiba et al., 2022	413 (PD 312, HCs 101)	224	Random sampling External validation	189	LASSO	SVM, KNN, LDA, DT
4	Shi et al., 2022b	143 (PD 86, HCs 57)	100	External validation	43	*T*-test, LASSO	SVM
5	Shi et al., 2022a	213 (PD123, HCs90)	213	fivefold cross validation 10-fold cross validation	–	*T*-tests, RFE	SVM
6	Pang et al., 2022	152 (PD 77, MSA-p 75)	107	Random sampling	45	LASSO, mRMR	SVM
7	Li et al., 2022	110 (PD 56, HCs 54)	60	External validation	50	LASSO	LR
8	Kim et al., 2022	128 (PD 56, MSA-p 34, MSA-c 21, PSP 17)	90 (PD 39 vs. MSA-P 24) (PD 39 vs. MSA-c 15) (PD 39 vs. PSP 12)	Random sampling	38 (PD 17 vs. MSA-P 10) (PD 17 vs. MSA-c 6) (PD 17 vs. PSP 5)	Autocorrelation and fisher score algorithm	KNN, SVM, GP, RF, DT, MLP, ADA, GNB, QDA
9	Kang et al., 2022	149 (PD 104, HCs 45)	104	Random sampling	45	LASSO	MLR, SVM
10	Guan et al., 2022	350 (PD 171, HCs 179)	244	External validation	106	RF	RF
11	Ben Bashat et al., 2022	127 (PD 46, HCs 81)	127	fivefold cross validation	–	PCA	SVM
12	Zhang et al., 2021	120 (PD 70, HCs 50)	84	Random sampling	36	LASSO	LASSO, RF, SVM
13	Tupe-Waghmare et al., 2021	201 (PD 65, APS 61 (MSA 31, PSP 30), HCs 75)	160	Random sampling	41 (PD 13 vs. HCs 15) (PD 13 vs. APS 13)	RFECV	RF
14	Sun et al., 2021	230 (PD 134, HCs 96)	185	Random sampling	45	LASSO	SVM, LR, MLP
15	Shi et al., 2021	100 (PD 59, HCs 41)	80	Random sampling	20	*T*-test, LASSO	LASSO
16	Ren et al., 2021	190 (PD 95, HCs 95)	126	Random sampling	64	LASSO, mRMR	RF, SVM, KNN, LR
17	Li et al., 2021	164 (PD 82, HCs 82)	164	fivefold cross validation	–	LASSO, Pearson correlation analyses, Multivariate analyses	LR
18	Hu et al., 2021	90 (PD 60, MSA 30)	63	Random sampling	27	LASSO, mRMR	LASSO, LR
19	Dhinagar et al., 2021	588 (PD 445, HCs 143)	424	Random sampling External validation	164	RFE	RF, CNN
20	Cao et al., 2021	116 (PD 67, HCs 49)	71	Random sampling	45	Mann-Whitney *U*-test	LR
21	Shu et al., 2020	336 (PD 168, HCs 168)	234	Random sampling	102	LASSO, mRMR, GBDT	SVM, Bayes, LR, RF, DT

(Continued)

TABLE 1 (Continued)

Schedule B							
No.	References	Total sample size	Sample size in training set	Verification method	Sample size in validation set	Variable screening method	Type of model
22	Pang et al., 2020	185 (PD 83, MSA-p 102)	129	Random sampling	56	*T*-tests, LASSO	SVM
23	Liu et al., 2020	138 (PD 69, HCs 69)	96	Random sampling	42	LASSO	LASSO
24	Cao et al., 2020	116 (PD 67, HCs 49)	93	Random sampling	23	Mann-Whitney *U*-test, LASSO	SVM, RF
25	Xiao et al., 2019	140 (PD 87, HCs 53)	140	sevenfold cross validation	–	ICC, RFE	LR, SVM, CNN
26	Wu et al., 2019	230 (PD 113, HCs 117)	146	Random sampling External validation	84	Autocorrelation and fisher score algorithm	SVM, RF
27	Shinde et al., 2019	100 (PD 45, APS 20 (MSA 15, PSP 5), HCs 35)	69 (PD 30 vs. HCs 25) (PD 30 vs. APS 14)	Random sampling	31 (PD 15 vs. HCs 10) (PD 15 vs. APS 6)	Average information gain	RF, CNN
28	Cheng et al., 2019	164 (PD 87, HCs 77)	164	threefold cross validation	–	ANOVA, RF, RFE	SVM

(A) The MDS PD criteria: the movement disorder society PD criteria; the UK PD SBB criteria: the UK PD society brain bank criteria.
(B) In article 8, 13, and 27, different research objects were used for training and verification, and the specific sample numbers were listed in the Table 2. In article 5, 11, 17, 25, and 28, the method of cross-validation is adopted, so there is no specific sample number of validation set 3. Article 5 used the same dataset of articles 4 and 15. Articles 20 and 24 were based on the same dataset. PCA, principle component analysis; RFE, recursive feature elimination; RFECV, recursive feature elimination with cross-validation; ICC, intraclass correlation coefficient; ANOVA, analysis of variance; MSA-c, multiple system atrophy-cerebellar type; MSA-p, multiple system atrophy-parkinsonian type.

(WH) was asked to assist in the decision-making process. RQS is a radiomics-specific quality assessment tool that scores the quality of the original study design based on 16 items (e.g., whether the image acquisition method and data were described in detail, whether measures were taken to prevent overfitting or multiple segmentation, whether the study was prospective, and whether the model was validated and how it was validated). Each criterion is assigned a numerical value that corresponds to the impact of the study on radiomics research, and the total score ranges from −8 to 36, which is then converted into a percentage score (0–100%). This score represents the rigor of model development and the evaluation of the study's impact on the field.

2.5. Outcome measures

The primary outcome measure of our systematic review is the c-index, which reflects the overall accuracy of the ML model. However, when there is a severe imbalance in the number of cases between the observation group and the control group, the c-index may not be sufficient to reflect the accuracy of the ML model for disease diagnosis. As a result, our primary outcome measures also included sensitivity and specificity.

2.6. Statistical analysis

Our analysis consists of three parts: (a) Diagnosis of Parkinson's disease [comparing PD patients and healthy controls (HC)], (b) Differential diagnosis of Parkinson's disease (comparing idiopathic PD patients and APS patients), and (c) Parkinson's disease subtypes (comparing TD and PIGD). This study reported the c-index with a 95% confidence interval (CI), which reflected the accuracy of ML models. In cases where the original literature lacks a 95% confidence interval or standard error of the c-index, they were estimated by the formula proposed by Debray et al. (2019). The meta-analysis of sensitivity and specificity requires the diagnostic fourfold table (true negatives, true positives, false negatives, and false positives), but few original studies directly reported a diagnostic fourfold table. Thus, we need to calculate the fourfold table by combining sensitivity and specificity with the number of cases. However, in cases where sensitivity and specificity are missing, Origin 2020 was used to extract them from the ROC curve.

A random effects model was used to perform the meta-analysis of the overall accuracy of the ML model, as reflected by the c-index, while a bivariate mixed effects model was used for the meta-analysis of the sensitivity and specificity (Reitsma et al., 2005). Statistical analysis was performed using Stata 15.0 (Stata Corporation, USA). A p-value < 0.05 was considered statistically significant.

3. Results

3.1. Study selection

Figure 1 illustrates the PRISMA flow diagram of the study selection. The search identified 67 studies from PubMed, 117 studies from Embase, 14 studies from Cochrane, and 75 studies

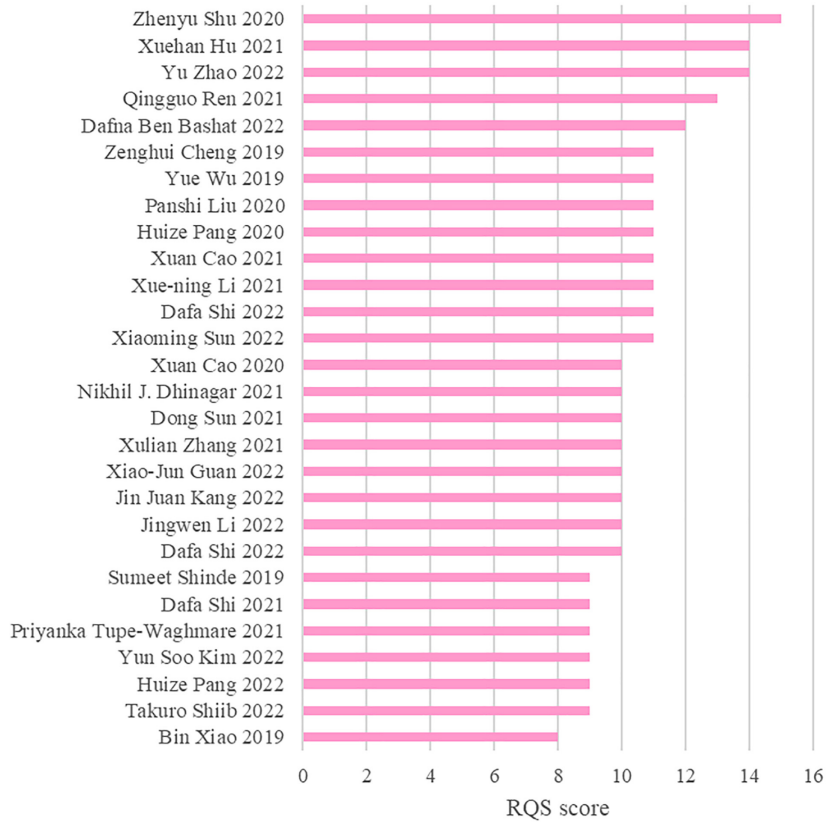

FIGURE 2
Bar chart (quality evaluation table).

from Web of Science. Following the exclusion of 121 duplicate studies, 43 studies were screened based on their titles or abstracts. Ultimately, a total of 28 articles (Cheng et al., 2019; Shinde et al., 2019; Wu et al., 2019; Xiao et al., 2019; Cao et al., 2020, 2021; Liu et al., 2020; Pang et al., 2020, 2022; Shu et al., 2020; Dhinagar et al., 2021; Hu et al., 2021; Li et al., 2021, 2022; Ren et al., 2021; Shi et al., 2021, 2022a, 2022b; Sun et al., 2021, 2022; Tupe-Waghmare et al., 2021; Zhang et al., 2021; Ben Bashat et al., 2022; Guan et al., 2022; Kang et al., 2022; Kim et al., 2022; Shiiba et al., 2022; Zhao et al., 2022) were deemed eligible and included in this meta-analysis.

3.2. Study characteristics

The characteristics of the studies included in this research are shown in **Table 1** and **Supplementary Table 4**. The original 28 studies were published between 2019 and 2022, with 27 of them from Asia (Cheng et al., 2019; Shinde et al., 2019; Wu et al., 2019; Xiao et al., 2019; Cao et al., 2020, 2021; Liu et al., 2020; Pang et al., 2020, 2022; Shu et al., 2020; Hu et al., 2021; Li et al., 2021, 2022; Ren et al., 2021; Shi et al., 2021, 2022a, 2022b; Sun et al., 2021, 2022; Tupe-Waghmare et al., 2021; Zhang et al., 2021; Ben Bashat et al., 2022; Guan et al., 2022; Kang et al., 2022; Kim et al., 2022; Shiiba et al., 2022; Zhao et al., 2022) and one from North America (Dhinagar et al., 2021). The study comprised a total of 6,057 participants, with 3,422 patients diagnosed with PD, 1,983 healthy controls, and 652 cases of APS (476 with MSA and 176 with PSP). Among these studies, 22 focused on the diagnosis of PD (Cheng et al., 2019; Shinde et al., 2019; Wu et al., 2019; Xiao et al., 2019; Cao et al., 2020, 2021; Liu et al., 2020; Shu et al., 2020; Dhinagar et al., 2021; Li et al., 2021, 2022; Ren et al., 2021; Shi et al., 2021, 2022a, 2022b; Sun et al., 2021, 2022; Zhang et al., 2021; Ben Bashat et al., 2022; Guan et al., 2022; Kang et al., 2022; Shiiba et al., 2022), while six studies focused on the differential diagnosis of PD and APS (Pang et al., 2020, 2022; Hu et al., 2021; Tupe-Waghmare et al., 2021; Kim et al., 2022; Zhao et al., 2022). In addition, two studies addressed the differential diagnosis of PD with or without depression (Li et al., 2021; Zhang et al., 2021), and one study fixated on the differential diagnosis of TD and PIGD (Sun et al., 2021). There were 14 ML models, including SVM (Support Vector Machine), CNN (Convolutional Neural Network), LR (Logistic Regression), LDA (Linear Discriminant Analysis), RF (Random Forest), LASSO (Least Absolute Shrinkage and Selection Operator), DT (Decision Tree), KNN (K-Nearest Neighbor), ANN (Artificial Neural Network), GNB (Gaussian Naive Bayes), GP (Gaussian Process), Bayes (Bayesian Network), ADA (Adaptive Boosting), and QDA (Quadratic Discriminant Analysis).

3.3. Quality analysis

Figure 2 illustrates the RQS scores and relative scores of all 28 studies included in this research, as evaluated by the two reviewers (JB and XW). The mean RQS score for the

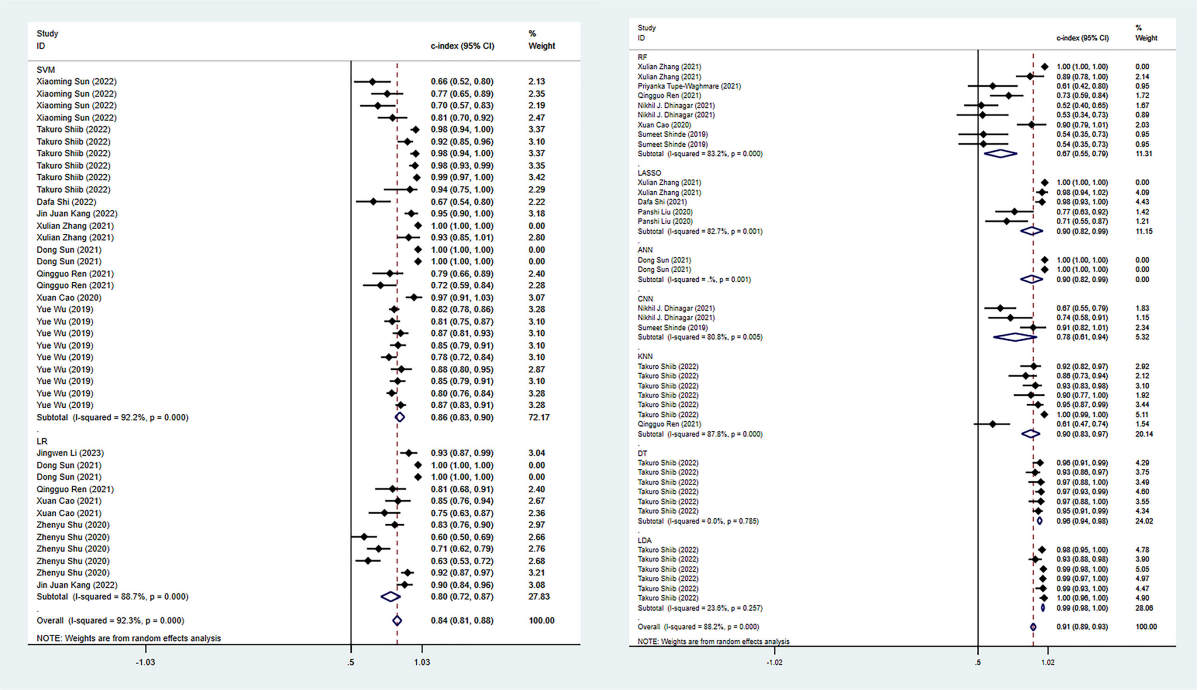

FIGURE 3
Meta-analysis results of c-index for PD diagnosis based on radiomics-based machine learning (Validation set). Due to the large amount of relevant data involved, the results of the verification set are presented in two parts, and the forest plot for the training set is provided in the **Supplementary material**.

TABLE 2 Meta-analysis results of sensitivity and specificity for PD diagnosis based on radiomics-based machine learning.

Model	Training set					Validation set				
	Number	Sen (95% CI)	I^2 (%)	Spe (95% CI)	I^2 (%)	Number	Sen (95% CI)	I^2 (%)	Spe (95% CI)	I^2 (%)
SVM	16	0.90 [0.83∼0.94]	88.7	0.94 [0.84∼0.98]	94.5	20	0.85 [0.79∼0.90]	59.0	0.90 [0.84∼0.94]	66.9
LR	11	0.88 [0.70∼0.96]	97.1	0.88 [0.72∼0.95]	96.5	12	0.81 [0.70∼0.89]	85.6	0.84 [0.71∼0.92]	85.7
RF	5	0.97 [0.70∼1.00]	98.2	0.97 [0.54∼1.00]	98.8	11	0.79 [0.69∼0.87]	71.6	0.81 [0.68∼0.90]	77.0
LASSO	3	0.81∼0.94	NA	0.75∼0.96	NA	5	0.91 [0.77∼0.97]	67.0	0.90 [0.58∼0.98]	82.5
ANN	2	1.00	NA	1.00	NA	2	1.00	NA	1.00	NA
CNN	2	0.80∼0.86	NA	0.83∼0.88	NA	3	0.56∼0.86	NA	0.67∼0.70	NA
KNN	1	0.74	NA	0.74	NA	1	0.55	NA	0.64	NA
DT	1	0.69	NA	0.92	NA	1	0.59	NA	0.92	NA
Bayes	1	0.76	NA	0.92	NA	1	0.77	NA	0.96	NA
LDA	NA	NA	NA	NA	NA	4	0.97 [0.86∼1.00]	93.7	0.92 [0.80∼0.97]	23.3
Overall	42	0.91 [0.86∼0.94]	95.4	0.93 [0.87∼0.96]	95.8	60	0.86 [0.81∼0.89]	81.4	0.87 [0.83∼0.91]	82.0

When the number of models is less than four, it is not possible to perform a meta-analysis using a bivariate mixed-effects model. Therefore, we only recorded the corresponding exact values and range. Number: the number of models included in various model types. SVM, support vector machine; LR, logistic regression; RF, random forest; LASSO, least absolute shrinkage and selection operator; ANN, artificial neural network; CNN, convolutional neural network; KNN, K-nearest neighbor; DT, decision tree; Bayes, Bayesian network; LDA, linear discriminant analysis.

studies was 10.64 (range 8–15), while the mean relative score was 29.56% (range 22.22–41.67%). All the studies reported well-documented image acquisition protocols and performed feature selection and data dimensionality reduction to reduce model overfitting. For model evaluation, most studies provided discriminant statistics (e.g., ROC curve, c-index, AUC) and their statistical significance (e.g., *p*-value, confidence interval), while calibration statistics were less frequently mentioned. Ten studies (Cao et al., 2020, 2021; Pang et al., 2020, 2022; Shu et al., 2020; Hu et al., 2021; Li et al., 2021; Zhang et al., 2021; Sun et al., 2022; Zhao et al., 2022) conducted multivariate analyzes of non-radiomics features, such as plasma FAM19A5, demographic and clinical characteristics, impaired sense of smell, and cognitive impairment, which provided more comprehensive integrated models. One study (Ben Bashat et al., 2022) also examined and discussed biological correlations; demonstrating phenotypic

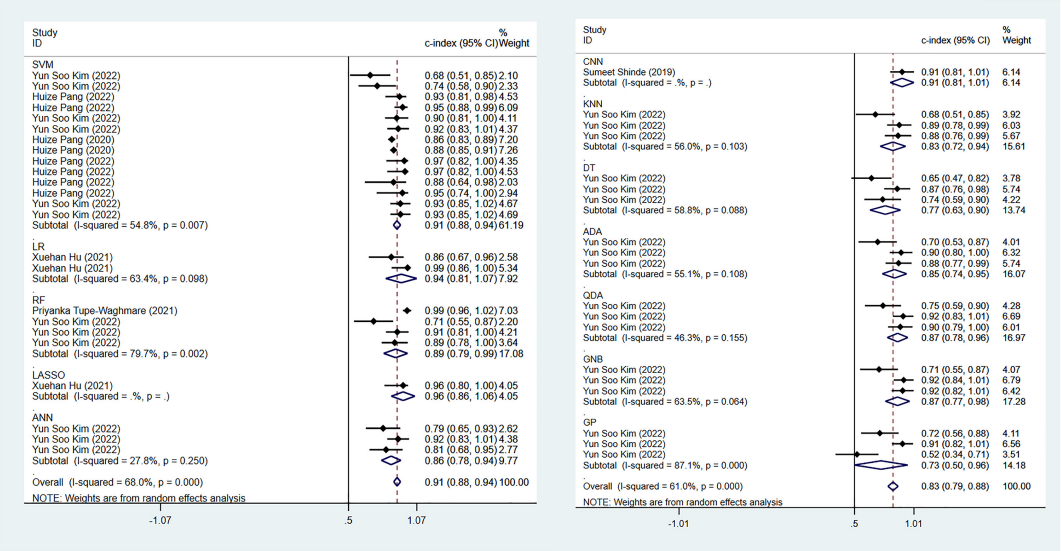

FIGURE 4
Meta-analysis results of c-index for differential diagnosis between PD and APS based on radiomics-based machine learning (Validation set).

differences that could be related to underlying gene-protein expression patterns broadens the perception of radiomics and biology. Nine studies (Liu et al., 2020; Shu et al., 2020; Cao et al., 2021; Ren et al., 2021; Shi et al., 2021; Guan et al., 2022; Li et al., 2022; Shiiba et al., 2022; Zhao et al., 2022) conducted cut-off value analysis to assess the risk of model diagnostic prediction accuracy. However, only five studies evaluated the potential clinical utility of the model by decision curve analysis (Wu et al., 2019; Shu et al., 2020; Hu et al., 2021; Ren et al., 2021; Zhao et al., 2022), and none performed a cost-effectiveness analysis. Since there is currently no clear gold standard for the clinical diagnosis of PD, it is challenging to evaluate the degree of consistency between the model and the current "gold standard" method.

Only one study has compared the diagnostic accuracy of ML models based on magnetic resonance imaging (MRI) with those based on dopamine transporter single-photon emission tomography (DAT-SPECT) imaging (Ben Bashat et al., 2022). Additionally, only two studies have prospectively validated the use of radiomic biomarkers (Sun et al., 2022; Zhao et al., 2022). No studies have investigated the stability of radiomics signatures across different scanners or time points. In terms of open science and data, most studies do not provide open-source code directly. The quality evaluation scores are shown in **Supplementary Table 3**.

3.4. Meta-analysis

3.4.1. Diagnosis of PD

In terms of the diagnosis of PD, 42 ML models in the training set reported a c-index, with a pooled c-index of 0.862 (95% CI: 0.833–0.891). In the validation set, 78 ML models reported a c-index, with a pooled c-index of 0.871 (95% CI: 0.853–0.890).

There were 42 fourfold tables for diagnosis that were available and could be directly or indirectly extracted in the training set, and the pooled sensitivity and specificity were 0.91 (95% CI: 0.86–0.94) and 0.93 (95% CI: 0.87–0.96), respectively. There were 60 models in the validation set, and the sensitivity and specificity for disease diagnosis were 0.86 (95% CI: 0.81–0.89) and 0.87 (95% CI: 0.83–0.91), respectively, as depicted in **Figure 3**, **Table 2** and **Supplementary Table 5**.

Among all the ML models constructed, support vector machine (SVM) and logistic regression (LR) showed ideal predictive performance in the training and validation sets with a larger sample size. Meanwhile, attention should also be paid to other models, such as CNN and LASSO, which demonstrated good diagnostic performance, despite a limited number of these models included in this study. Including more models in future studies can help verify their diagnostic potential.

3.4.2. Differential diagnosis PD and APS

Regarding the differential diagnosis between PD and APS, a total of 41 ML models reported a c-index, with a pooled c-index of 0.866 (95% CI: 0.843–0.889) in the training set, while in the validation set, 43 ML models reported a c-index, with a pooled c-index of 0.879 (95% CI: 0.854–0.903). The training set of 41 models had a pooled sensitivity and specificity of 0.86 (95% CI: 0.84–0.88) and 0.80 (95% CI: 0.75–0.84), respectively. Conversely, the validation set had a pooled sensitivity and specificity of 0.87 (95% CI: 0.85–0.89) and 0.82 (95% CI: 0.77–0.86), respectively. These results are detailed in **Figure 4**, **Table 3** and **Supplementary Table 6**. Notably, the SVM model showed good discrimination accuracy even with a relatively large number of models included in the analysis.

3.4.3. Differential diagnosis of PD and MSA

The pooled c-index, sensitivity, and specificity for differential diagnosis between PD and MSA were 0.857 (95% CI: 0.827–0.887), 0.86 (95% CI: 0.83–0.88), and 0.82 (95% CI: 0.77–0.87)

TABLE 3 Meta-analysis results of sensitivity and specificity for differential diagnosis between PD and APS based on radiomics-based machine learning.

Model	Training set					Validation set				
	Number	Sen (95% CI)	I^2 (%)	Spe (95% CI)	I^2 (%)	Number	Sen (95% CI)	I^2 (%)	Spe (95% CI)	I^2 (%)
SVM	10	0.88 [0.82∼0.92]	62.5	0.83 [0.75∼0.89]	69.7	10	0.86 [0.80∼0.90]	0.0	0.84 [0.77∼0.89]	0.0
LR	2	0.76∼0.93	NA	0.91∼1.00	NA	2	0.89∼0.94	NA	0.78∼1.00	NA
RF	3	0.81∼0.88	NA	0.63∼0.89	NA	4	0.84 [0.73∼0.92]	0.0	0.86 [0.61∼0.96]	54.7
LASSO	1	0.91	NA	0.95	NA	1	0.83	NA	1.00	NA
ANN	3	0.77∼0.81	NA	0.51∼0.84	NA	3	0.79∼0.88	NA	0.59∼0.91	NA
CNN	4	0.90 [0.83∼0.95]	0.0	0.88 [0.71∼0.95]	91.0	3	0.91∼1.00	NA	0.50∼0.90	NA
KNN	3	0.81∼0.90	NA	0.49∼0.87	NA	3	0.79∼0.90	NA	0.56∼0.83	NA
DT	3	0.81∼0.88	NA	0.56∼0.84	NA	3	0.80∼0.88	NA	0.51∼0.82	NA
ADA	3	0.80∼0.89	NA	0.49∼0.82	NA	3	0.79∼0.88	NA	0.54∼0.80	NA
QDA	3	0.81∼0.91	NA	0.60∼0.85	NA	3	0.81∼0.91	NA	0.63∼0.85	NA
GNB	3	0.82∼0.92	NA	0.54∼0.89	NA	3	0.80∼0.94	NA	0.57∼0.87	NA
GP	3	0.78∼0.88	NA	0.66∼0.90	NA	3	0.78∼0.90	NA	0.74∼0.91	NA
Overall	41	0.86 [0.84∼0.88]	21.8	0.80 [0.75∼0.84]	75.1	41	0.87 [0.85∼0.89]	0.0	0.82 [0.77∼0.86]	18.4

ADA, adaptive boosting; QDA, quadratic discriminant analysis; GNB, Gaussian naive Bayes; GP, Gaussian process.

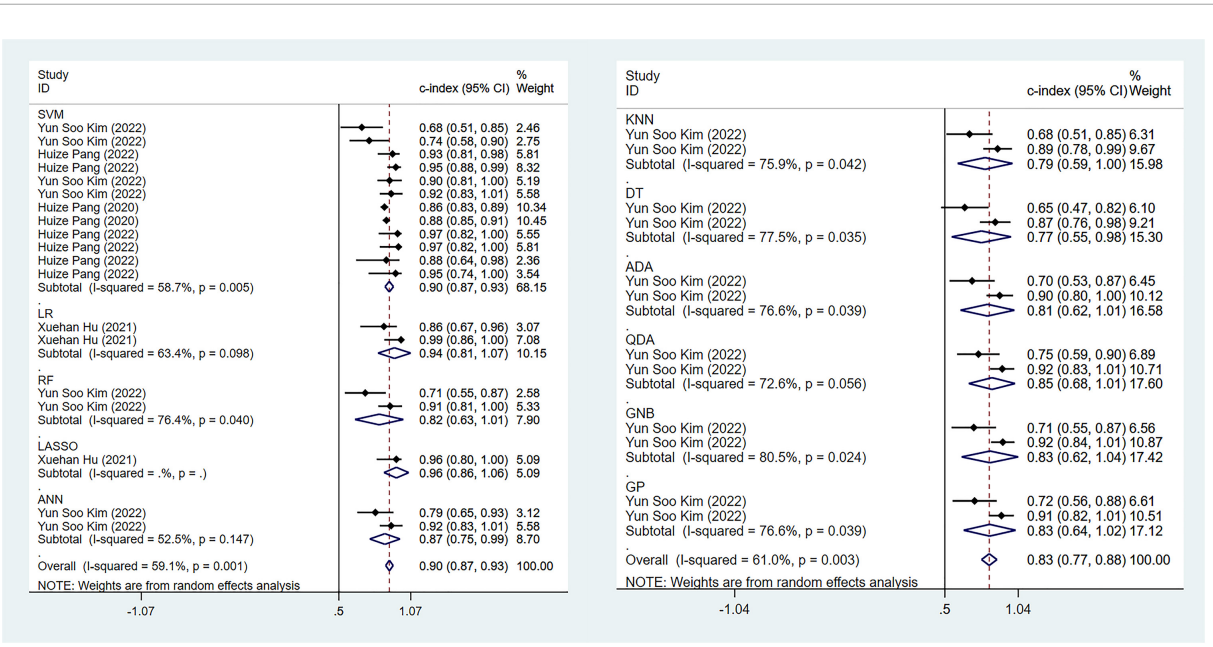

FIGURE 5
Meta-analysis results of c-index for differential diagnosis between PD and MSA based on radiomics-based machine learning (Validation set).

in the training set, which contained 27 models, respectively. In the validation set, which included 31 models, the pooled c-index, sensitivity, and specificity were 0.878 (95% CI: 0.852–0.905), 0.85 (95% CI: 0.82–0.88), and 0.82 (95% CI: 0.77–0.87), respectively. These results are presented in Figure 5, Table 4 and Supplementary Table 7.

3.4.4. Differential diagnosis between PD and PSP

The pooled c-index, sensitivity, and specificity for differential diagnosis between PD and PSP in the training set of 10 models were 0.871 (95% CI: 0.826–0.915), 0.87 (95% CI: 0.82–0.90), and 0.63 (95% CI: 0.53–0.71), respectively. In the validation set, the pooled c-index, sensitivity, and specificity were 0.863 (95% CI: 0.808–0.918), 0.88 (95% CI: 0.82–0.92), and 0.68 (95% CI: 0.54–0.79), respectively. These findings are presented in Figure 6, Table 5 and Supplementary Table 8.

3.4.5. Differential diagnosis between different motor subtypes of PD

Regarding the differential diagnosis between TD and PIGD motor subtypes, there were three models in the training set and validation set, respectively. The pooled c-index was 0.892 (95% CI:

TABLE 4 Meta-analysis results of sensitivity and specificity for differential diagnosis between PD and MSA based on radiomics-based machine learning.

Model	Training set					Validation set				
	Number	Sen (95% CI)	I^2 (%)	Spe (95% CI)	I^2 (%)	Number	Sen (95% CI)	I^2 (%)	Spe (95% CI)	I^2 (%)
SVM	8	0.89 [0.81∼0.93]	66.5	0.86 [0.81∼0.90]	0.0	8	0.86 [0.79∼0.90]	0.0	0.84 [0.76∼0.90]	0.0
LR	2	0.76∼0.93	NA	0.91∼1.00	NA	2	0.89∼0.94	NA	0.78∼1.00	NA
RF	2	0.81∼0.88	NA	0.63∼0.89	NA	2	0.79∼0.88	NA	0.68∼0.90	NA
LASSO	1	0.91	NA	0.95	NA	1	0.83	NA	1.00	NA
ANN	2	0.77∼0.81	NA	0.73∼0.84	NA	2	0.79∼0.88	NA	0.75∼0.91	NA
KNN	2	0.81∼0.89	NA	0.49∼0.87	NA	2	0.79∼0.89	NA	0.56∼0.83	NA
DT	2	0.81∼0.86	NA	0.56∼0.84	NA	2	0.80∼0.87	NA	0.51∼0.82	NA
ADA	2	0.80∼0.88	NA	0.49∼0.82	NA	2	0.79∼0.88	NA	0.54∼0.80	NA
QDA	2	0.81∼0.91	NA	0.60∼0.85	NA	2	0.81∼0.91	NA	0.63∼0.85	NA
GNB	2	0.82∼0.90	NA	0.54∼0.89	NA	2	0.80∼0.91	NA	0.63∼0.87	NA
GP	2	0.78∼0.88	NA	0.79∼0.90	NA	2	0.78∼0.90	NA	0.82∼0.91	NA
Overall	27	0.86 [0.83∼0.88]	32.1	0.82 [0.77∼0.87]	63.9	27	0.85 [0.82∼0.88]	0.0	0.82 [0.77∼0.87]	2.0

0.855–0.929) in the training set and 0.822 (95% CI: 0.724–0.920) in the validation set. The pooled sensitivity and specificity for TD subtype were between 0.85–0.88 and 0.77–0.82, respectively. For PIGD subtype, the pooled sensitivity and specificity were between 0.75–0.88 and 0.66–0.83, respectively. These results are presented in **Supplementary Tables 9**, **10**.

3.5. Overfitting evaluation

For the diagnosis and differential diagnosis of PD, no overfitting was observed for the ML models. Meanwhile, in the respective differential diagnoses, no overfitting was observed for the most commonly used ML model when there were relatively sufficient models. The detailed information is shown in **Supplementary Tables 5–9**.

4. Discussion

Our meta-analysis results indicated that radiomics demonstrated excellent diagnostic accuracy in PD diagnosis, with a pooled sensitivity and specificity of 0.91 and 0.93 in the training set, and 0.86 and 0.87 in the validation set, respectively. Furthermore, radiomics-based ML has good discrimination performance in differentiating PD from APS and classifying PD subtypes.

In recent years, researchers have made significant progress in exploring biomarkers for the diagnosis of Parkinson's disease (PD) (Parkinson Progression Marker Initiative, 2011; Tolosa et al., 2021). A meta-analysis of ML based on blood gene features for the prediction of idiopathic PD exhibited a sensitivity of 0.72 and specificity of 0.67 (Falchetti et al., 2020). Kalyakulina et al. (2022) conducted a meta-analysis of ML based on DNA methylation for the differentiation between PD cases and controls, with a classification accuracy of 0.76 using uncoordinated data and over 0.95 using coordinated data. di Biase et al. (2020) review reported an accuracy of over 0.83 for PD diagnosis using ML based on gait feature testing. Kwon et al. (2022) review demonstrated that the integration of clinically relevant biomarkers such as metabolomics, proteomics, and microRNA omics data from cerebrospinal fluid can serve as a powerful method for identifying PD and MSA. The aforementioned research results demonstrate that diagnostic models based on different variables have good performance in PD diagnosis. However, there have been no studies on the evaluation or integration of radiomics. Furthermore, the differentiation of PD and atypical parkinsonian syndromes (APS), as well as the classification of PD subtypes is rarely discussed. Previous studies have used conventional neuroimaging methods such as PET (Brajkovic et al., 2017), MRI, and molecular imaging (Atkinson-Clement et al., 2017; Loftus et al., 2023) for PD diagnosis based on visual assessment or statistical parameter mapping (SPM) analysis. Despite their high diagnostic accuracy, combining radiomics with artificial intelligence can save time and energy, reduce examination costs, and even improve diagnostic accuracy (Wu et al., 2019).

Previous studies have demonstrated that clinical factors, such as olfactory function (Alonso et al., 2021a,b), speech features, motor data, handwriting patterns, cardiac scintigraphy, cerebrospinal fluid (CSF), and serum markers, are closely associated with the diagnosis and severity assessment of Parkinson's disease (PD) and should not be disregarded when constructing diagnostic models (Mei et al., 2021; Rana et al., 2022). Halligan et al. (2021) have recommended that multivariable models should include clinical imaging biomarkers to evaluate their cumulative contribution to overall outcomes. A review by Zhang (2022) has shown that multimodal data, based on ML using imaging and clinical features, can enhance the accuracy of PD diagnosis and early detection. Additionally, Makarious et al. (2022) have demonstrated in their review that multimodal data-combined ML models is superior to single biomarker mode, and the model has been validated in the PD Biomarker Program (PDBP) dataset. The ten studies included in this meta-analysis (Cao et al., 2020, 2021; Pang et al., 2020, 2022; Shu et al., 2020; Hu et al., 2021; Li et al., 2021; Zhang et al., 2021; Sun et al., 2022; Zhao et al., 2022) also revealed that

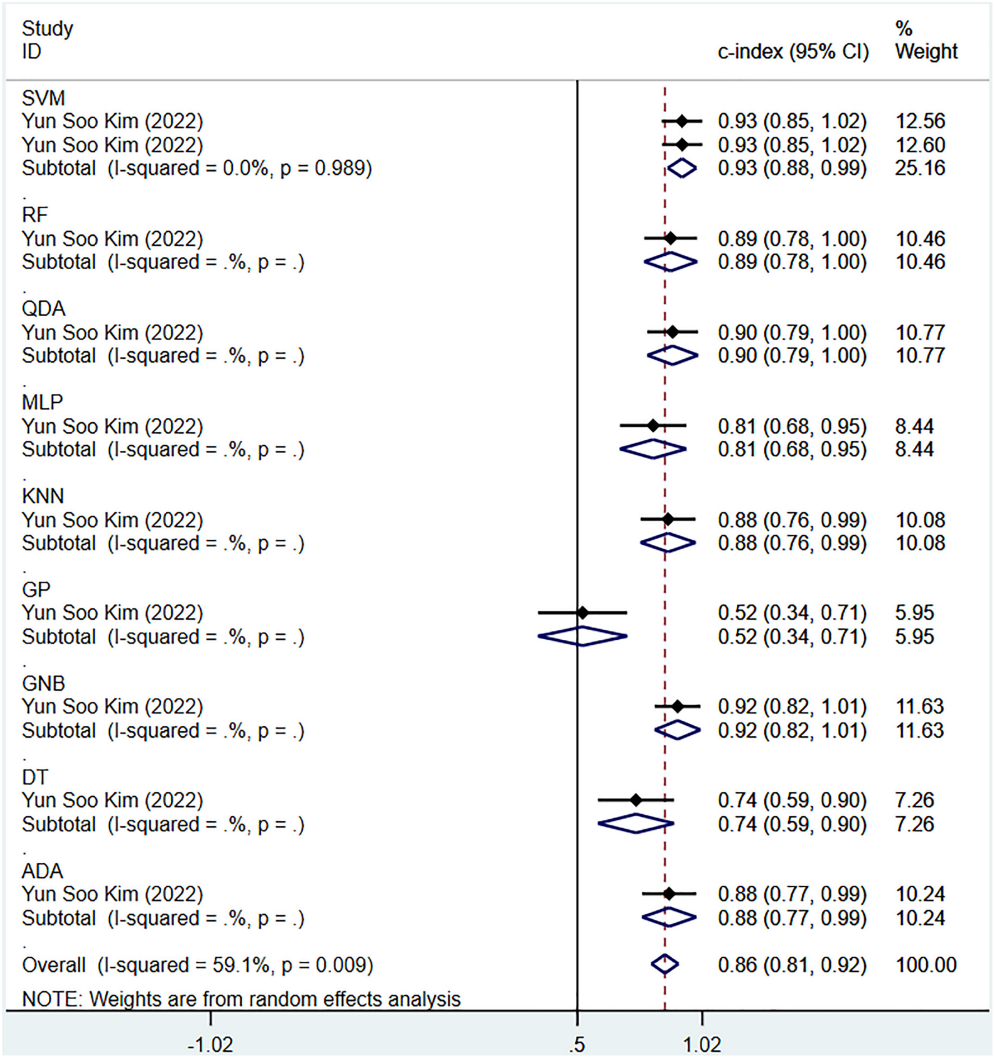

FIGURE 6
Meta-analysis results of c-index for differential diagnosis between PD and PSP based on radiomics-based machine learning (Validation set).

TABLE 5 Meta-analysis results of sensitivity and specificity for differential diagnosis between PD and PSP based on radiomics-based machine learning.

Model	Training set					Validation set				
	Number	Sen (95% CI)	I^2 (%)	Spe (95% CI)	I^2 (%)	Number	Sen (95% CI)	I^2 (%)	Spe (95% CI)	I^2 (%)
SVM	2	0.79∼0.91	NA	0.37∼0.75	NA	2	0.82∼0.91	NA	0.75∼0.79	NA
RF	1	0.87	NA	0.69	NA	1	0.88	NA	0.69	NA
ANN	1	0.80	NA	0.51	NA	1	0.80	NA	0.59	NA
KNN	1	0.90	NA	0.76	NA	1	0.90	NA	0.72	NA
DT	1	0.88	NA	0.67	NA	1	0.88	NA	0.60	NA
ADA	1	0.89	NA	0.65	NA	1	0.87	NA	0.62	NA
QDA	1	0.87	NA	0.71	NA	1	0.89	NA	0.68	NA
GNB	1	0.92	NA	0.59	NA	1	0.94	NA	0.57	NA
GP	1	0.79	NA	0.66	NA	1	0.81	NA	0.74	NA
Overall	10	0.87 [0.82∼0.90]	0.0	0.63 [0.53∼0.71]	0.0	10	0.88 [0.82∼0.92]	0.0	0.68 [0.54∼0.79]	0.0

comprehensive classification models, which combine clinical features and radiomics, have better predictive performance. Therefore, future radiomics analysis should incorporate other relevant variables to build more reliable models, and radiomic features can be added to existing diagnostic models to improve their diagnostic accuracy.

This study is the first systematic review and meta-analysis of radiomics-based ML in the diagnosis of PD and the differentiation of PD from APS. This study revealed that the main brain regions commonly used for diagnosis of PD were located in the substantia nigra-corpus striatum system, and some related areas such as the cerebral cortex. This was consistent with the pathological mechanism and features of PD. Some non-motor symptoms (olfactory disorder, depression, cognitive impairment, etc.) as non-radiomics variables for ML models had good value in diagnosing PD. Furthermore, we found that the major brain regions currently and commonly used to differentiate PD from APS were located in the basal ganglia system, especially the putamen area. UPDRS scores, as non-radiomics variables for ML model, were of good value in distinguishing PD from APD. The radiomics features commonly used to build ML models include first-order properties, shape features, and textural features [such as Gray Level Co-occurrence Matrix (GLCM), Gray Level Difference Matrix (GLDM), Gray-Level Run-Length Matrix (GLRLM)], etc.

We attempted to categorize models by type to determine the best model, but the number of some models, such as CNN, is limited due to their recent emergence, newer technology in deep learning (DL), and possible biases (Ching et al., 2018; Choi et al., 2020). DL has demonstrated greater potential for super-large datasets containing thousands or millions of cases (Camacho et al., 2018), whereas research datasets typically contain only hundreds of patients, making ML more suitable and cost-effective for building models for research purposes (Zhang et al., 2022). In our study, DL also demonstrated good diagnostic prediction performance, but we cannot draw definitive conclusions due to the limited number of the included studies. Further research is needed to endorse these findings. However, the SVM model still demonstrates excellent robustness even when the number of samples is relatively abundant. Additionally, we found that MRI was the main tool that used radiomics to predict PD diagnosis in clinical practice. In future work, incorporating data from various imaging modalities can further enhance the diagnostic capabilities for the disease. Our findings may advance the field of digital therapy and provide theoretical evidence for developing ML models for diagnosing PD in the future.

However, this study has certain limitations. Firstly, Currently, radiomics lacks a standardized operational guideline, which leads to variations in the process of region of interest (ROI) delineation and texture feature extraction among researchers. Even when multiple researchers are involved, it appears challenging to eliminate the impact of these variations. Additionally, the use of diverse dimensionality reduction methods or variable selection methods may contribute to high heterogeneity in radiomics studies targeting the same clinical question. Therefore, these factors may introduce a significant heterogeneity in systematic reviews related to radiomics. It is difficult to avoid such heterogeneity until standardized operational guidelines are widely adopted. Secondly, we observed that the included studies seemed to have relatively low scores, mainly due to the fact that the RQS scale is more inclined toward critical research on radiomics. Additionally, the RQS scale may be unsuitable for some models in clinical practice, making it difficult for some studies to obtain high RQS scores. Moreover, many related studies currently have a retrospective design, are single-center studies, and use internal validation or resampling methods (cross-validation), resulting in poor generalizability of the models and limiting the integration of ML models with clinical environments. Therefore, in the future, images from different hospitals and research centers are needed to externally validate the prediction model, making it adapt to a wider range of clinical scenarios. Furthermore, not all models are suitable for clinical practice, so the clinical effectiveness of diagnostic models must be strictly evaluated based on current diagnostic standards.

Imaging plays an indispensable role in the clinical diagnosis and treatment process. However, the interpretation of imaging data currently relies primarily on the expertise of clinical experts. In this regard, developing an intelligent radiomics reading tool based on standardized criteria would provide significant assistance to novice clinicians, especially in the diagnosis and treatment of complex diseases. This assistance in radiomics-based interpretation is crucial for clinical practice. Furthermore, promoting the development of radiomics can bring substantial value to the initial screening and diagnosis of many diseases, particularly in economically and medically underdeveloped regions.

However, radiomics currently faces several inevitable challenges and problems, with significant biases present in certain aspects of the radiomics implementation process. The development of radiomics did not adequately consider excessive parameter tuning, nor did it involve repeated measurements at different time points on the same patient (although this incurs certain costs, it is necessary for the development of such a tool). Moreover, the delineation of the ROI heavily relies on the expertise and knowledge of clinical experts. Therefore, in the development process, it is essential to incorporate ROI delineation from clinicians at different levels to generate imaging data, followed by the extraction of radiomics features using specific software. We have observed strong correlations among some of the extracted radiomics variables, making the selection of modeling variables a challenging task. Hence, it is crucial to compare different methods and identify the optimal variable selection approach to build ML models while avoiding overfitting. Additionally, in the process of constructing ML models, it may be advantageous to prioritize logistic regression (LR) as it offers good visualization and relatively straightforward predictive line plots. We hope that better standards for radiomics and ML will be established in the future, such as the standardization of image acquisition, segmentation, feature extraction, statistical analysis, and reporting formats, to achieve reproducibility and facilitate clinical application.

5. Conclusion

Our study suggested that radiomic-based ML exhibited high sensitivity and specificity in diagnosing Parkinson's disease (PD),

discriminating PD and atypical parkinsonian syndromes (APS), and distinguishing different subtypes of PD. This approach can serve as a potential method for screening, detecting, and diagnosing PD, making a significant contribution to clinical decision-making systems. However, due to the current lack of standardized operational guidelines, radiomics still faces numerous challenges in its current applications.

Data availability statement

The original contributions presented in this study are included in the article/**Supplementary material**, further inquiries can be directed to the corresponding author.

Author contributions

JB and XW: conceptualization. XW: resources. XW and WH: methodology. JB: formal analysis and investigation. JB and WH: writing—original draft preparation. GZ: writing—review and editing. YW: supervision. All authors read and approved the final manuscript.

Conflict of interest

The authors declare that the research was conducted in the absence of any commercial or financial relationships that could be construed as a potential conflict of interest.

Publisher's note

All claims expressed in this article are solely those of the authors and do not necessarily represent those of their affiliated organizations, or those of the publisher, the editors and the reviewers. Any product that may be evaluated in this article, or claim that may be made by its manufacturer, is not guaranteed or endorsed by the publisher.

Supplementary material

The Supplementary Material for this article can be found online at: https://www.frontiersin.org/articles/10.3389/fnagi.2023.1199826/full#supplementary-material

References

Adeli, E., Shi, F., An, L., Wee, C. Y., Wu, G., Wang, T., et al. (2016). Joint feature-sample selection and robust diagnosis of Parkinson's disease from MRI data. *Neuroimage* 141, 206–219. doi: 10.1016/j.neuroimage.2016.05.054

Alonso, C. C. G., Silva, F. G., Costa, L. O. P., and Freitas, S. (2021a). Smell tests can discriminate Parkinson's disease patients from healthy individuals: a meta-analysis. *Clin. Neurol. Neurosurg.* 211:107024. doi: 10.1016/j.clineuro.2021.107024

Alonso, C. C. G., Silva, F. G., Costa, L. O. P., and Freitas, S. (2021b). Smell tests to distinguish Parkinson's disease from other neurological disorders: a systematic review and meta-analysis. *Expert Rev. Neurother.* 21, 365–379. doi: 10.1080/14737175.2021.1886925

Atkinson-Clement, C., Pinto, S., Eusebio, A., and Coulon, O. (2017). Diffusion tensor imaging in Parkinson's disease: review and meta-analysis. *Neuroimage Clin.* 16, 98–110. doi: 10.1016/j.nicl.2017.07.011

Ben Bashat, D., Thaler, A., Lerman Shacham, H., Even-Sapir, E., Hutchison, M., Evans, K. C., et al. (2022). Neuromelanin and T(2)*-MRI for the assessment of genetically at-risk, prodromal, and symptomatic Parkinson's disease. *NPJ Parkinsons Dis.* 8:139. doi: 10.1038/s41531-022-00405-9

Brajkovic, L., Kostic, V., Sobic-Saranovic, D., Stefanova, E., Jecmenica-Lukic, M., Jesic, A., et al. (2017). The utility of FDG-PET in the differential diagnosis of Parkinsonism. *Neurol. Res.* 39, 675–684. doi: 10.1080/01616412.2017.1312211

Camacho, D. M., Collins, K. M., Powers, R. K., Costello, J. C., and Collins, J. J. (2018). Next-generation machine learning for biological networks. *Cell* 173, 1581–1592. doi: 10.1016/j.cell.2018.05.015

Cao, X., Lee, K., and Huang, Q. (2021). Bayesian variable selection in logistic regression with application to whole-brain functional connectivity analysis for Parkinson's disease. *Stat. Methods Med. Res.* 30, 826–842. doi: 10.1177/0962280220978990

Cao, X., Wang, X., Xue, C., Zhang, S., Huang, Q., and Liu, W. (2020). A radiomics approach to predicting Parkinson's disease by incorporating whole-brain functional activity and gray matter structure. *Front. Neurosci.* 14:751. doi: 10.3389/fnins.2020.00751

Cheng, Z., Zhang, J., He, N., Li, Y., Wen, Y., Xu, H., et al. (2019). Radiomic features of the Nigrosome-1 region of the substantia nigra: using quantitative susceptibility mapping to assist the diagnosis of idiopathic Parkinson's disease. *Front. Aging Neurosci.* 11:167. doi: 10.3389/fnagi.2019.00167

Ching, T., Himmelstein, D. S., Beaulieu-Jones, B. K., Kalinin, A. A., Do, B. T., Way, G. P., et al. (2018). Opportunities and obstacles for deep learning in biology and medicine. *J. R. Soc. Interface* 15:20170387. doi: 10.1098/rsif.2017.0387

Choi, R. Y., Coyner, A. S., Kalpathy-Cramer, J., Chiang, M. F., and Campbell, J. P. (2020). Introduction to machine learning. neural Networks, and deep learning. *Transl. Vis. Sci. Technol.* 9:14. doi: 10.1167/tvst.9.2.14

Debray, T. P., Damen, J. A., Riley, R. D., Snell, K., Reitsma, J. B., Hooft, L., et al. (2019). A framework for meta-analysis of prediction model studies with binary and time-to-event outcomes. *Stat. Methods Med. Res.* 28, 2768–2786. doi: 10.1177/0962280218785504

Dhinagar, N., Thomopoulos, S., Owens-Walton, C., Stripelis, D., Ambite, J. L., Ver Steeg, G., et al. (2021). 3D convolutional neural networks for classification of Alzheimer's and Parkinson's disease with T1-weighted brain MRI. *bioRxiv* [Preprint]. doi: 10.1101/2021.07.26.453903

di Biase, L., Di Santo, A., Caminiti, M. L., De Liso, A., Shah, S. A., Ricci, L., et al. (2020). Gait analysis in Parkinson's disease: an overview of the most accurate markers for diagnosis and symptoms monitoring. *Sensors* 20:3529. doi: 10.3390/s20123529

Falchetti, M., Prediger, R. D., and Zanotto-Filho, A. (2020). Classification algorithms applied to blood-based transcriptome meta-analysis to predict idiopathic Parkinson's disease. *Comput. Biol. Med.* 124:103925. doi: 10.1016/j.compbiomed.2020.103925

GBD 2016 Parkinson's Disease Collaborators (2018). Global, regional, and national burden of Parkinson's disease, 1990-2016: a systematic analysis for the global burden of disease study 2016. *Lancet Neurol.* 17, 939–953. doi: 10.1016/s1474-4422(18)30295-3

Guan, X. J., Guo, T., Zhou, C., Gao, T., Wu, J. J., Han, V., et al. (2022). A multiple-tissue-specific magnetic resonance imaging model for diagnosing Parkinson's disease: a brain radiomics study. *Neural. Regen. Res.* 17, 2743–2749. doi: 10.4103/1673-5374.339493

Halligan, S., Menu, Y., and Mallett, S. (2021). Why did European Radiology reject my radiomic biomarker paper? How to correctly evaluate imaging biomarkers in a clinical setting. *Eur. Radiol.* 31, 9361–9368. doi: 10.1007/s00330-021-07971-1

Hu, X., Sun, X., Hu, F., Liu, F., Ruan, W., Wu, T., et al. (2021). Multivariate radiomics models based on (18)F-FDG hybrid PET/MRI for distinguishing between Parkinson's disease and multiple system atrophy. *Eur. J. Nucl. Med. Mol. Imaging* 48, 3469–3481. doi: 10.1007/s00259-021-05325-z

Kalyakulina, A., Yusipov, I., Bacalini, M. G., Franceschi, C., Vedunova, M., and Ivanchenko, M. (2022). Disease classification for whole-blood DNA methylation: meta-analysis, missing values imputation, and XAI. *Gigascience* 11:giac097. doi: 10.1093/gigascience/giac097

Kang, J. J., Chen, Y., Xu, G. D., Bao, S. L., Wang, J., Ge, M., et al. (2022). Combining quantitative susceptibility mapping to radiomics in diagnosing Parkinson's disease and

assessing cognitive impairment. *Eur. Radiol.* 32, 6992–7003. doi: 10.1007/s00330-022-08790-8

Kim, Y. S., Lee, J. H., and Gahm, J. K. (2022). Automated differentiation of atypical parkinsonian syndromes using brain iron patterns in susceptibility weighted imaging. *Diagnostics* 12:637. doi: 10.3390/diagnostics12030637

Klyuzhin, I. S., Gonzalez, M., Shahinfard, E., Vafai, N., and Sossi, V. (2016). Exploring the use of shape and texture descriptors of positron emission tomography tracer distribution in imaging studies of neurodegenerative disease. *J. Cereb. Blood Flow Metab.* 36, 1122–1134. doi: 10.1177/0271678X15606718

Kwon, D. H., Hwang, J. S., Kim, S. G., Jang, Y. E., Shin, T. H., and Lee, G. (2022). Cerebrospinal fluid metabolome in Parkinson's disease and multiple system atrophy. *Int. J. Mol. Sci.* 23:1879. doi: 10.3390/ijms23031879

Lambin, P., Leijenaar, R. T. H., Deist, T. M., Peerlings, J., de Jong, E. E. C., van Timmeren, J., et al. (2017). Radiomics: the bridge between medical imaging and personalized medicine. *Nat. Rev. Clin. Oncol.* 14, 749–762. doi: 10.1038/nrclinonc.2017.141

Lambin, P., Rios-Velazquez, E., Leijenaar, R., Carvalho, S., van Stiphout, R. G., Granton, P., et al. (2012). Radiomics: extracting more information from medical images using advanced feature analysis. *Eur. J. Cancer* 48, 441–446. doi: 10.1016/j.ejca.2011.11.036

Li, J., Liu, X., Wang, X., Liu, H., Lin, Z., and Xiong, N. (2022). Diffusion tensor imaging radiomics for diagnosis of Parkinson's disease. *Brain Sci.* 12:851. doi: 10.3390/brainsci12070851

Li, X. N., Hao, D. P., Qu, M. J., Zhang, M., Ma, A. B., Pan, X. D., et al. (2021). Development and validation of a Plasma FAM19A5 and MRI-based radiomics model for prediction of Parkinson's disease and Parkinson's disease with depression. *Front. Neurosci.* 15:795539. doi: 10.3389/fnins.2021.795539

Liu, P., Wang, H., Zheng, S., Zhang, F., and Zhang, X. (2020). Parkinson's disease diagnosis using neostriatum radiomic features based on T2-weighted magnetic resonance imaging. *Front. Neurol.* 11:248. doi: 10.3389/fneur.2020.00248

Loftus, J. R., Puri, S., and Meyers, S. P. (2023). Multimodality imaging of neurodegenerative disorders with a focus on multiparametric magnetic resonance and molecular imaging. *Insights Imaging* 14:8. doi: 10.1186/s13244-022-01358-6

Makarious, M. B., Leonard, H. L., Vitale, D., Iwaki, H., Sargent, L., Dadu, A., et al. (2022). Multi-modality machine learning predicting Parkinson's disease. *NPJ Parkinsons Dis.* 8:35. doi: 10.1038/s41531-022-00288-w

Mei, J., Desrosiers, C., and Frasnelli, J. (2021). Machine learning for the diagnosis of Parkinson's disease: a review of literature. *Front. Aging Neurosci.* 13:633752. doi: 10.3389/fnagi.2021.633752

Moher, D., Liberati, A., Tetzlaff, J., and Altman, D. G. (2009). Preferred reporting items for systematic reviews and meta-analyses: the PRISMA statement. *BMJ* 339:b2535. doi: 10.1136/bmj.b2535

Pang, H., Yu, Z., Li, R., Yang, H., and Fan, G. (2020). MRI-based radiomics of basal nuclei in differentiating Idiopathic Parkinson's disease from parkinsonian variants of multiple system atrophy: a susceptibility-weighted imaging study. *Front. Aging Neurosci.* 12:587250. doi: 10.3389/fnagi.2020.587250

Pang, H., Yu, Z., Yu, H., Chang, M., Cao, J., Li, Y., et al. (2022). Multimodal striatal neuromarkers in distinguishing parkinsonian variant of multiple system atrophy from idiopathic Parkinson's disease. *CNS Neurosci. Ther.* 28, 2172–2182. doi: 10.1111/cns.13959

Parkinson Progression Marker Initiative (2011). The Parkinson progression marker initiative (PPMI). *Prog. Neurobiol.* 95, 629–635. doi: 10.1016/j.pneurobio.2011.09.005

Postuma, R. B., Berg, D., Stern, M., Poewe, W., Olanow, C. W., Oertel, W., et al. (2015). MDS clinical diagnostic criteria for Parkinson's disease. *Mov. Disord.* 30, 1591–1601. doi: 10.1002/mds.26424

Rahmim, A., Salimpour, Y., Jain, S., Blinder, S. A., Klyuzhin, I. S., Smith, G. S., et al. (2016). Application of texture analysis to DAT SPECT imaging: relationship to clinical assessments. *Neuroimage Clin.* 23, e1–e9. doi: 10.1016/j.nicl.2016.02.012

Rana, A., Dumka, A., Singh, R., Panda, M. K., Priyadarshi, N., and Twala, B. (2022). Imperative role of machine learning algorithm for detection of Parkinson's disease: review, challenges and recommendations. *Diagnostics* 12:2003. doi: 10.3390/diagnostics12082003

Reitsma, J. B., Glas, A. S., Rutjes, A. W., Scholten, R. J., Bossuyt, P. M., and Zwinderman, A. H. (2005). Bivariate analysis of sensitivity and specificity produces informative summary measures in diagnostic reviews. *J. Clin. Epidemiol.* 58, 982–990. doi: 10.1016/j.jclinepi.2005.02.022

Ren, Q., Wang, Y., Leng, S., Nan, X., Zhang, B., Shuai, X., et al. (2021). Substantia nigra radiomics feature extraction of Parkinson's disease based on magnitude images of susceptibility-weighted imaging. *Front. Neurosci.* 15:646617. doi: 10.3389/fnins.2021.646617

Respondek, G., Stamelou, M., and Höglinger, G. U. (2019). Classification of atypical parkinsonism per pathology versus phenotype. *Int. Rev. Neurobiol.* 149, 37–47. doi: 10.1016/bs.irn.2019.10.003

Rizzo, S., Botta, F., Raimondi, S., Origgi, D., Fanciullo, C., Morganti, A. G., et al. (2018). Radiomics: the facts and the challenges of image analysis. *Eur. Radiol. Exp.* 2:36. doi: 10.1186/s41747-018-0068-z

Saeed, U., Lang, A. E., and Masellis, M. (2020). Neuroimaging advances in Parkinson's disease and atypical Parkinsonian syndromes. *Front. Neurol.* 11:572976. doi: 10.3389/fneur.2020.572976

Shi, D., Zhang, H., Wang, G., Wang, S., Yao, X., Li, Y., et al. (2022b). Machine learning for detecting Parkinson's disease by resting-state functional magnetic resonance imaging: a multicenter radiomics analysis. *Front. Aging Neurosci.* 14:806828. doi: 10.3389/fnagi.2022.806828

Shi, D., Yao, X., Li, Y., Zhang, H., Wang, G., Wang, S., et al. (2022a). Classification of Parkinson's disease using a region-of-interest- and resting-state functional magnetic resonance imaging-based radiomics approach. *Brain Imaging Behav.* 16, 2150–2163. doi: 10.1007/s11682-022-00685-y

Shi, D., Zhang, H., Wang, S., Wang, G., and Ren, K. (2021). Application of functional magnetic resonance imaging in the diagnosis of Parkinson's disease: a histogram analysis. *Front. Aging Neurosci.* 13:624731. doi: 10.3389/fnagi.2021.624731

Shiiba, T., Takano, K., Takaki, A., and Suwazono, S. (2022). Dopamine transporter single-photon emission computed tomography-derived radiomics signature for detecting Parkinson's disease. *EJNMMI Res.* 12:39. doi: 10.1186/s13550-022-00910-1

Shinde, S., Prasad, S., Saboo, Y., Kaushick, R., Saini, J., Pal, P. K., et al. (2019). Predictive markers for Parkinson's disease using deep neural nets on neuromelanin sensitive MRI. *Neuroimage Clin.* 22:101748. doi: 10.1016/j.nicl.2019.101748

Shu, Z., Pang, P., Wu, X., Cui, S., Xu, Y., and Zhang, M. (2020). An integrative nomogram for identifying early-stage Parkinson's disease using non-motor symptoms and white matter-based radiomics biomarkers from whole-brain MRI. *Front. Aging Neurosci.* 12:548616. doi: 10.3389/fnagi.2020.548616

Sun, D., Wu, X., Xia, Y., Wu, F., Geng, Y., Zhong, W., et al. (2021). Differentiating Parkinson's disease motor subtypes: a radiomics analysis based on deep gray nuclear lesion and white matter. *Neurosci. Lett.* 760:136083. doi: 10.1016/j.neulet.2021.136083

Sun, X., Ge, J., Li, L., Zhang, Q., Lin, W., Chen, Y., et al. (2022). Use of deep learning-based radiomics to differentiate Parkinson's disease patients from normal controls: a study based on [(18)F]FDG PET imaging. *Eur. Radiol.* 32, 8008–8018. doi: 10.1007/s00330-022-08799-z

Tolosa, E., Garrido, A., Scholz, S. W., and Poewe, W. (2021). Challenges in the diagnosis of Parkinson's disease. *Lancet Neurol.* 20, 385–397. doi: 10.1016/s1474-4422(21)00030-2

Tupe-Waghmare, P., Rajan, A., Prasad, S., Saini, J., Pal, P. K., and Ingalhalikar, M. (2021). Radiomics on routine T1-weighted MRI can delineate Parkinson's disease from multiple system atrophy and progressive supranuclear palsy. *Eur. Radiol.* 31, 8218–8227. doi: 10.1007/s00330-021-07979-7

Wu, Y., Jiang, J. H., Chen, L., Lu, J. Y., Ge, J. J., Liu, F. T., et al. (2019). Use of radiomic features and support vector machine to distinguish Parkinson's disease cases from normal controls. *Ann. Transl. Med.* 7:773. doi: 10.21037/atm.2019.11.26

Xiao, B., He, N., Wang, Q., Cheng, Z., Jiao, Y., Haacke, E. M., et al. (2019). Quantitative susceptibility mapping based hybrid feature extraction for diagnosis of Parkinson's disease. *Neuroimage Clin.* 24:102070. doi: 10.1016/j.nicl.2019.102070

Zhang, J. (2022). Mining imaging and clinical data with machine learning approaches for the diagnosis and early detection of Parkinson's disease. *NPJ Parkinsons Dis.* 8:13. doi: 10.1038/s41531-021-00266-8

Zhang, J., Li, L., Zhe, X., Tang, M., Zhang, X., Lei, X., et al. (2022). The diagnostic performance of machine learning-based radiomics of DCE-MRI in predicting axillary lymph node metastasis in breast cancer: a meta-analysis. *Front. Oncol.* 12:799209. doi: 10.3389/fonc.2022.799209

Zhang, X., Cao, X., Xue, C., Zheng, J., Zhang, S., Huang, Q., et al. (2021). Aberrant functional connectivity and activity in Parkinson's disease and comorbidity with depression based on radiomic analysis. *Brain Behav.* 11:e02103. doi: 10.1002/brb3.2103

Zhao, Y., Wu, P., Wu, J., Brendel, M., Lu, J., Ge, J., et al. (2022). Decoding the dopamine transporter imaging for the differential diagnosis of parkinsonism using deep learning. *Eur. J. Nucl. Med. Mol. Imaging* 49, 2798–2811. doi: 10.1007/s00259-022-05804-x

frontiers | Frontiers in Aging Neuroscience

TYPE Original Research
PUBLISHED 06 July 2023
DOI 10.3389/fnagi.2023.1186470

OPEN ACCESS

EDITED BY
Woon-Man Kung,
Chinese Culture University, Taiwan

REVIEWED BY
Nihay Laham Karam,
University of Eastern Finland, Finland
Tara Patricia Hurst,
University of Oxford, United Kingdom

*CORRESPONDENCE
Tyson Dawson
✉ tysondawson@gmail.com

†These authors share first authorship

RECEIVED 14 March 2023
ACCEPTED 13 June 2023
PUBLISHED 06 July 2023

CITATION
Dawson T, Rentia U, Sanford J, Cruchaga C, Kauwe JSK and Crandall KA (2023) Locus specific endogenous retroviral expression associated with Alzheimer's disease. *Front. Aging Neurosci.* 15:1186470. doi: 10.3389/fnagi.2023.1186470

Locus specific endogenous retroviral expression associated with Alzheimer's disease

Tyson Dawson[1,2*†], Uzma Rentia[1†], Jessie Sanford[3], Carlos Cruchaga[3], John S. K. Kauwe[4] and Keith A. Crandall[1,2]

[1]Computational Biology Institute, The George Washington University, Washington, DC, United States, [2]Department of Biostatistics and Bioinformatics, Milken Institute School of Public Health, The George Washington University, Washington, DC, United States, [3]Department of Psychiatry, Washington University School of Medicine, St. Louis, MO, United States, [4]Department of Biology, Brigham Young University, Provo, UT, United States

Introduction: Human endogenous retroviruses (HERVs) are transcriptionally-active remnants of ancient retroviral infections that may play a role in Alzheimer's disease.

Methods: We combined two, publicly available RNA-Seq datasets with a third, novel dataset for a total cohort of 103 patients with Alzheimer's disease and 45 healthy controls. We use telescope to perform HERV quantification for these samples and simultaneously perform gene expression analysis.

Results: We identify differentially expressed genes and differentially expressed HERVs in Alzheimer's disease patients. Differentially expressed HERVs are scattered throughout the genome; many of them are members of the HERV-K superfamily. A number of HERVs are correlated with the expression of dysregulated genes in Alzheimer's and are physically proximal to genes which drive disease pathways.

Discussion: Dysregulated expression of ancient retroviral insertions in the human genome are present in Alzheimer's disease and show localization patterns that may explain how these elements drive pathogenic gene expression.

KEYWORDS

Alzheimer's disease, HERV, endogenous retrovirus, RNA-Seq, gene expression

1. Introduction

Alzheimer's disease is a chronic neurodegenerative disease and the leading cause of dementia (Alzheimer's Association, 2010); its precise pathogenesis is uncertain but involves neuroinflammation (Heneka et al., 2015), extracellular neuritic plaques comprised of misfolded amyloid-β peptides (Tiraboschi et al., 2004), and intracellular neurofibrillary tangles comprised of the microtubule-associated protein tau (Brion, 1998). Tau-mediated mechanisms have been associated with loss of genomic stability in affected neurons (Madabhushi et al., 2014) and with the activation of human endogenous retroviruses (HERVs) (Guo et al., 2018).

Human endogenous retroviruses (HERVs) are a constituent part of the human genome and comprise ∼8% of all human DNA sequences (Hoyt et al., 2022). HERV insertion and replication events have happened throughout evolutionary history (Bannert and Kurth, 2006; Feschotte and Gilbert, 2012). Though most HERVs remain largely neutralized from mutations and epigenetic control mechanisms (Groh and Schotta, 2017), they still retain transcriptional activity (Seifarth et al., 2005; Pehrsson et al., 2019) and serve cell-type-specific regulatory functions (Stauffer et al., 2004; Ohnuki et al., 2014; Buzdin et al., 2017). Indeed, among all the transposable elements, HERVs are the most enriched for apparent regulatory functions (Jacques et al., 2013; Sundaram et al., 2014). Systematic characterizations of the regulatory functions of HERVs are underway (Ito et al., 2017), but the regulatory relationships in particular diseases have yet to be robustly defined. HERV dysregulation has been observed in chronic inflammatory and neurodegenerative diseases including amyotrophic lateral sclerosis (Douville and Nath, 2014), multiple sclerosis (Perron et al., 1997; Mameli et al., 2012), and schizophrenia (Frank et al., 2005).

There are at least two ways in which tau-mediated HERV activation may play a role in the development of Alzheimer's disease: through the upregulation of HERVs or via the mobilization of HERVs. Tau may be involved in chromatin remodeling around HERV sequences, making regions in which HERVs are found increasingly transcriptionally accessible (Sun et al., 2018). HERV-derived nucleic acids, especially double-stranded DNA — which is a highly immunogenic pathogen-associated molecular pattern — may trigger the activation of innate immunity, as may HERV-derived proteins such as *env* which share structural similarity to extant viral proteins. In multiple sclerosis, HERVs have been shown to trigger an immune response *in vitro* (Perron et al., 2001), perhaps, as has been suggested, through the production of proinflammatory cytokines via the engagement of CD14/TLR4. In amyotrophic lateral sclerosis, proinflammatory stimuli seem to activate HERVs which, in turn, produce additional pro-inflammatory stimuli, hinting at a possible positive feedback mechanism in which epigenetically de-repressed HERVs amplify abnormal immune responses. Not only might the transcription of HERVs themselves be involved in pathogenesis, but the corresponding accessibility of HERV sequences may allow for more frequent and persistent presence of transcriptomic machinery at these loci and facilitate the transcription of nearby genes. The structure of prototypical HERVs – in which long terminal repeat regions flank viral proteins *gag*, *pro*, *pol* and *env* – allow these sequences to serve as active promoters for flanking sequences. The constituent loss of homeostatic balance that arises from this upregulation of HERV-proximal genes may contribute in some way to the Alzheimer's disease phenotype.

Recent studies have shed light on the possible role of the HERV-K and HERV-W *env* genes in neurodegenerative diseases, including Alzheimer's disease (Antony et al., 2004; Perron et al., 2005; Li et al., 2015; Ibba et al., 2018). Human toll-like receptor (TLR) 8 is responsive to a GUUGUGU motif found within the *env* gene of some HERV-K(HML-2) elements. Activation of hTLR8 upon binding to the *env* gene induces the canonical TLR pathway, ultimately leading to neuronal apoptosis, increased microglia, and the release of proinflammatory molecules including interferon. Such a process could contribute to phenotypic changes characteristic of Alzheimer's disease. Analysis of transcriptomic data from brain samples pointed to a correlation between upregulated HERV-K and TLR8 expression in the temporal cortex of Alzheimer's disease patients compared to age-matched controls (Dembny et al., 2020).

The role of HERVs in Alzheimer's disease has been explored at least since the early 2000's (Johnston et al., 2001) but, until now, studies have failed to quantify HERVs in both a high-throughput and locus-specific manner. Telescope is a tool that uses Bayesian reassignment to accurately classify HERV expression from RNA-Seq data (Bendall et al., 2019). Critically, telescope differs from other tools because it is able to estimate expression at locus-specific insertions rather than at the broad, subfamily level. Such accuracy allows us, for the first time, to comprehensively probe the expression of HERVs in Alzheimer's disease.

2. Materials and methods

2.1. RNA-Seq datasets

Here, we employ the use of three datasets. The first is from a heretofore unpublished cohort from Washington University, henceforth known as the WashU data. The study has been approved by the Institutional Review Board (Approval number: 201109148). Description of the data and raw data can be found at NIAGADS, dataset #00038.[1] For this cohort RNA was extracted from the Parietal cortex and RNA-Seq was generated using a Ribo-zero library with 30 million 150 × 2 reads (Del-Aguila et al., 2019; Dube et al., 2019; Li et al., 2020).

Participants in this study have provided written consent for providing their samples and clinical and demographic metadata. The other two datasets are publicly available via SRA: PRJEB28518 and PRJNA670209 (Nativio et al., 2020). PRJEB28518 used samples collected from post-mortem human brain samples collected at Seoul National University. PRJNA670209 used samples from frozen postmortem brain tissue from the Center for Neurodegenerative Disease Research brain bank (at UPenn) from both young and old patients sequenced on a NextSeq 500 machine.

2.2. RNA-Seq HERV identification and expression

Here, we use telescope (Bendall et al., 2019) to perform locus specific HERV quantification from RNA-Seq data. Telescope deals with the ambiguous mapping of repetitive HERV sequences by employing a Bayesian mixture model and expectation-maximization algorithm to reassign ambiguously mapped RNA-Seq fragments to the most likely locus of origin, thereby facilitating accurate, locus-specific HERV quantification. Our software pipeline uses fastQC (Andrews, 2010) to check for sequence quality, Trimmomatic (Bolger et al., 2014) to trim reads, then Bowtie2 (Langmead and Salzberg, 2012) to align reads to the Hg38 reference genome (GRCh38_no_alt_analysis_set_GCA_000001405.15) using the

1 https://www.niagads.org/datasets/ng00083

very-sensitive-local setting and allowing for a maximum of 100 alignments per read (–very-sensitive-local -k 100 –score-min L, 0, 1.6). The alignment files generated by Bowtie2 are fed into telescope which then uses the aforementioned Bayesian reassignment using up to 200 iterations of an expectation-maximization algorithm which has been modified to identify transposable elements (TEs) (–max_iter 200 –theta_prior 200000). With telescope, TEs are inferred when the hallmark genomic signatures of such elements are identified, including 5′ and 3′ long terminal repeats (LTRs) with an open reading frame between, thus inferring a functional TE. A total of 14,968 HERVs have thus been identified in the human genome and their annotation can be found at https://github.com/mlbendall/telescope_annotation_db/tree/master/builds/retro.hg38.v1. The output generated by telescope is a table of TEs (labeled by chromosomal location) and their expression as count values which are used in subsequent, downstream analyses.

2.3. RNA-Seq host gene expression

Host gene expression analysis was performed using fastQC for quality control, Trimmomatic for trimming of adapters and low-quality sequences, STAR (Dobin et al., 2013) for alignment, and FeatureCounts (Liao et al., 2014) for enumeration of transcripts.

2.4. Integrated gene and HERV expression

Arboreto (Moerman et al., 2019) was used to identify gene regulatory networks; specifically, it was used to identify those transcripts which show a high degree of correlation to each other. Variance-stabilization transformed counts of gene and HERV transcripts were used as input to Arboreto. The output was filtered to show those associations that existed between genes and HERVs (excluding HERV-HERV associations and gene-gene associations). Top associations, ranked by feature importance, were visualized in R using ggplot2.

2.5. Differential expression analysis

To account for sex-specific variance, genes that map to the Y chromosome were removed from the raw data. Batch effects associated with the provenance of the three datasets were removed using the ComBat-Seq function of the sva package in R v3.42.0 (Leek et al., 2012). Elements with low and consistent expression (which likely generate an uninformative signal and inflate adjusted *p*-values) were removed with the R package HTS Filter v1.34.0 which uses a Jaccard index filter to dynamically derive cutoff values to screen out uninformative transcriptomic data (Rau et al., 2013). Differential expression analysis comparing Alzheimer's data to normal samples was performed with DESeq2 v1.34.0 using a significance cutoff of $p = 0.05$ and condition (Alzheimer's or normal brain tissue) as factors in the DESeq model (Love et al., 2014). The R package ggplot2 v3.3.5 (Wickham, 2016) was used to visualize volcano plots, and the circlize v0.4.14 (Gu et al., 2014) package was used to visualize circos plots of differential HERV expression.

2.6. Proximal gene set enrichment and pathway analysis

Human endogenous retroviruses (HERVs) have been proposed as regulators that act on proximally-located genes (Buzdin et al., 2006; Rebollo et al., 2012; Sundaram et al., 2014; Yu et al., 2023). With this in mind, we sought to perform gene set enrichment analysis of those genes which were in the genomic neighborhood of the differentially expressed HERVs that were revealed in our analysis. Genes which flank or are intersected by HERVs have been documented for our telescope HERV annotation, available here: https://github.com/liniguez/telescope_metaannotations. Using an R script, differentially expressed HERVs were programmatically mapped to their closest upstream, downstream, and, in relevant cases, intersecting genes. The coefficient values associated with HERVs were assigned to their flaking/intersecting genes and these values were used as an input to omePath,[2] a generic tool for pathway enrichment analysis that allows users to calculate importance scores for omics features (i.e., expression of genes and HERVs) appropriate for their study design (e.g., adjusting for multivariable testing and confounding factors). Here, we use omePath with a gene ontology (GO) biological process reference database (The Gene Ontology Consortium, 2019) for mapping omics features to pathways. omePath identifies which pathways have significant associations with the underlying features by performing statistical tests using the feature scores in the pathways against all ranks to calculate a *p*-value and false discovery rate (FDR) for hypothesis testing.

3. Results

In this study, we use three datasets, two are publicly available and the third we publish as part of this paper (**Table 1**). We report that our samples had a median read count of ∼30 million and the median sample had 150,000 reads map to HERV sequences (**Supplementary Figure 1**). The HERV families with the most mapped reads were HERVL and ERVLE.

Due to the different provenance of our three datasets, we first sought to perform batch effect correction using ComBat-Seq on the count values of our HERV expression matrices. An initial PCA (principal component analysis) was performed before batch effect correction and, as expected, samples were clearly separated–not only by disease status but, more worryingly, by provenance

2 https://github.com/omicseye/omepath

TABLE 1 Brief description of datasets.

Dataset name	Number of AD patients	Number of healthy controls	Min # of reads	Median # of reads
WashU	81	17	3,096,385	29,422,202
PRJEB28518	10	10	21,645,208	44,218,524
PRJNA670209	12	18	26,043,105	38,416,313

The table outlines the number of patients in each cohort along with the minimum and median number of sequencing reads from each dataset.

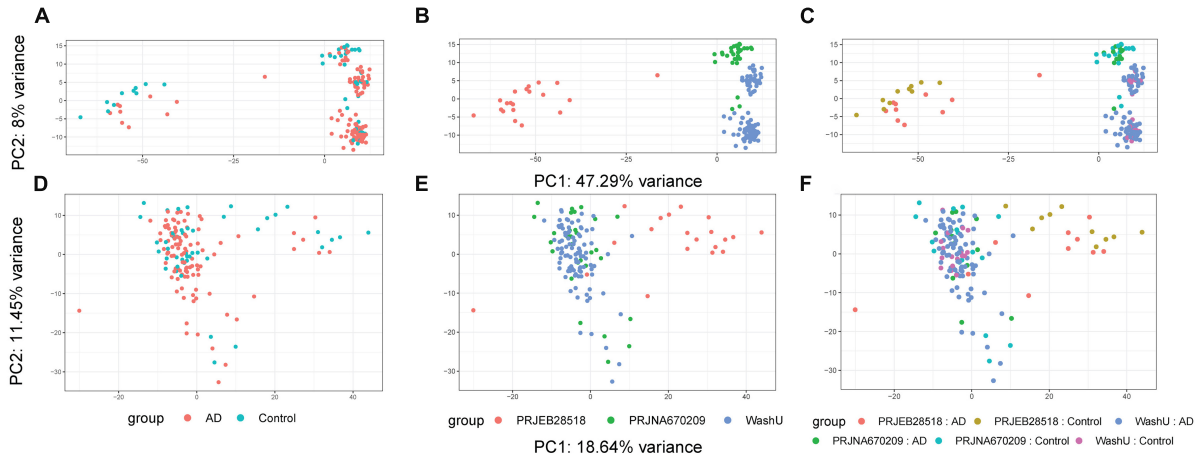

FIGURE 1
Results of batch effect correction on data structure shown via PCA. Before and after batch correction. Prior to batch correction using ComBat-Seq, much of the variance could be attributed to the provenance of the data sets. **(A)** PCA plot before batch effect correction colored by group. **(B)** PCA plot before batch effect correction colored by source. **(C)** PCA plot before batch effect correction colored by group and source. **(D)** PCA plot after batch effect correction colored by group. **(E)** PCA plot after batch effect correction colored by source. **(F)** PCA plot before batch effect correction colored by group and source.

FIGURE 2
Results of differential expression analysis of HERVs in combined Alzheimer's dataset. **(A)** Points in the volcano plot are individual HERV loci, their *X*-axis position represents their $\log_2$ fold change and their *Y*-axis position represents the $-\log_{10}$ of the *p*-value. Thus, HERVs higher on the plane and further to the edges represent more significantly aberrantly expressed HERVs where the bright green HERVs are those which have a FDR < 0.05 and are downregulated and the bright red HERVs are those which have a FDR < 0.05 and are upregulated. The top 4 most DE HERVs, ranked by *p*-value, are labeled. **(B)** Variance-stabilizing transformed counts of the most DE HERV, MER101_6q27d, are shown in box plots separated into two categories, AD patients and healthy controls.

(Figures 1A–C). After performing batch effect correction, samples were re-analyzed using the same PCA method and data provenance was no longer such a prominent factor (Figures 1D–F). With our count values thus corrected across our three datasets, we proceeded to the next analysis step.

Telescope quantified 13,666 distinct HERV loci expressed across the patients in our dataset. We performed differential expression using DESeq2 analysis on these HERVs between healthy and diseased patients. Doing so, we identified 698 HERVs that were differentially expressed (FDR adjusted *p*-value < 0.2) between

10.3389/fnagi.2023.1186470

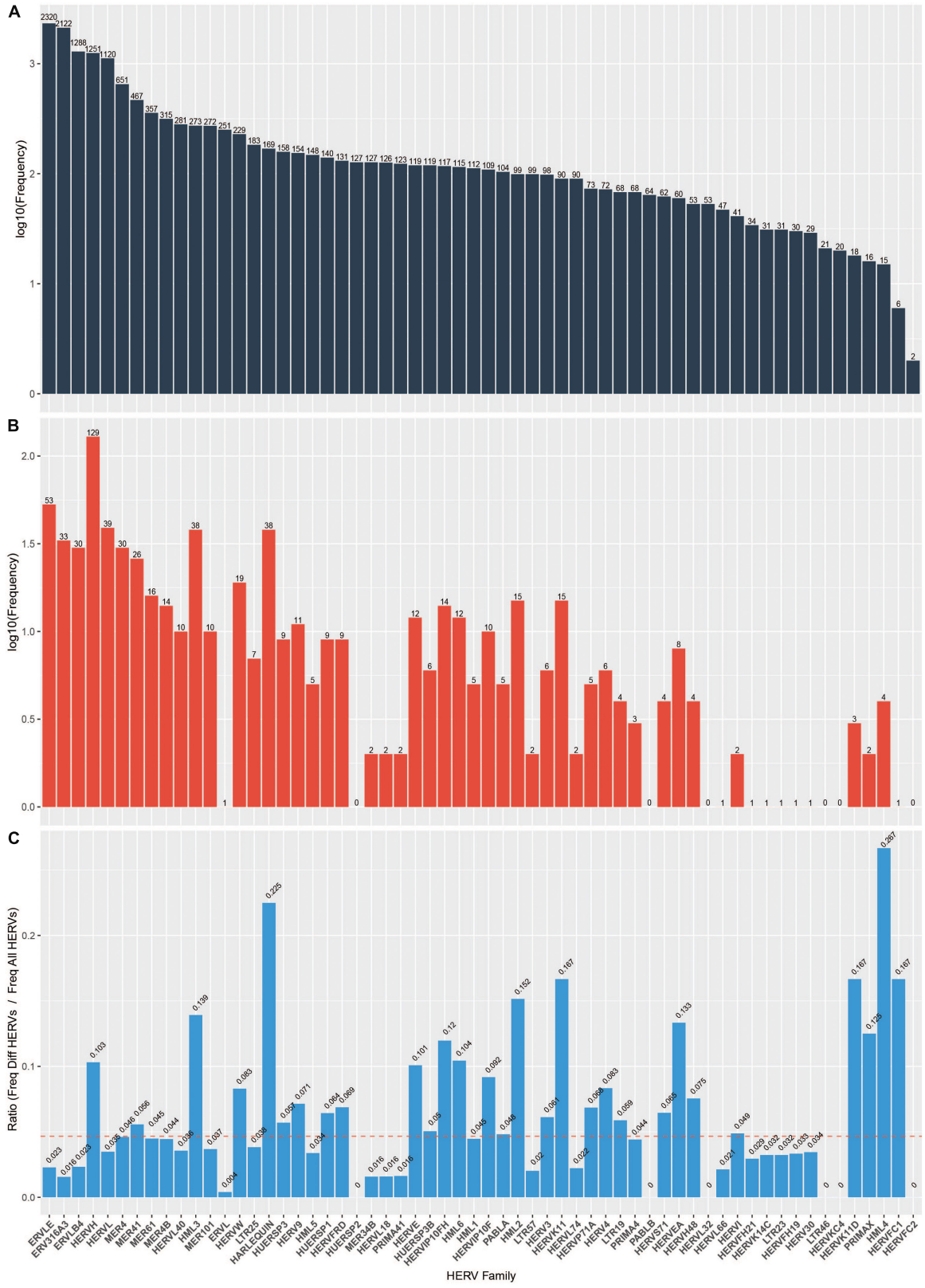

FIGURE 3
HERV frequency by family. **(A)** $\log_{10}$ frequency of HERV families in the database **(B)** $\log_{10}$ frequency of HERV families among the DE HERVs in our analysis **(C)** Ratio of frequency of DE HERVs in our analysis divided by frequency in the database. Dashed red line indicates the expected ratio (i.e., total number of HERVs in the database divided by total number of DE HERVs).

Alzheimer's and normal brain samples. Of the 698 elements, 187 were downregulated and 511 were upregulated (Figure 2).

As previously mentioned, HERVs can be divided into functional families. We sought to identify which families (if any) were disproportionately represented among the 698 significantly differentially expressed HERVs we identified. Indeed, members of HERV families including HML4, HARLEQUIN, HERVFC1, HERVK11D, HERVK11 are over-represented in the differentially expressed HERVs (Figure 3).

Because HERVs are dispersed throughout the human genome, we sought to identify whether particular genomic regions harbored a disproportionate number of differentially expressed HERVs. Significantly differentially expressed HERVs were scattered throughout the genome and showed no obvious pattern of chromosomal over-representation (Supplementary Figure 2).

Because HERVs are hypothesized to act as transcriptional regulators, especially for proximal genes, we chose to investigate whether HERVs play a role in activating genes that drive Alzheimer's disease. We queried the role of neighboring genes using a gene enrichment analysis. We identify pathways that are significantly enriched using this set of genes proximal to dysregulated HERVs (Figure 4).

To further explore patterns identified in previous research that show HERVK molecules as playing a particularly important role in modulating biological processes in Alzheimer's patients, we conducted a correlation analysis between the quantification of HERVK molecules and the expression of TLR-8 as well as the summed expression of genes that comprise an interferon signature (Catalina et al., 2019; Supplementary Table 2). We note that HERVK expression tends to positively correlate with expression of both TLR-8 and interferon signature genes (Figure 5) but that only a subset of HERVK loci are significantly correlated with either (Supplementary Figure 3). We also report that significant correlation patterns with TLR-8 and HERVK expression are absent at the family level. Specifically, the sum of neither HML1, HML2, HML3, HML4, HML5, HML6, HERVK11, HERVK11D,

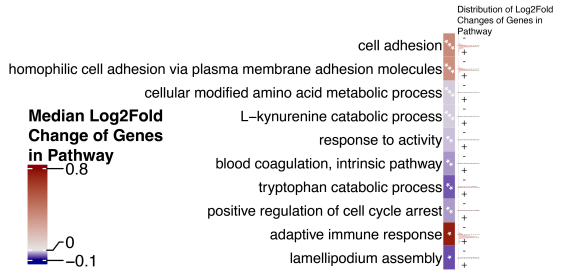

FIGURE 4
Gene set enrichment analysis of genes proximal to differentially expressed HERVs reveals dysregulated pathways that may be at play in AD. The top 10 most significant pathways, ranked by *p*-value are shown. Cells which contain one asterisk (*) represent pathways with *p*-values less than 0.05 but greater than 0.005. Cells which contain two asterisks (**) represent pathways with *p*-values less than 0.005 but greater than 0.001. Cells which contain three asterisks (***) represent pathways with *p*-values less than 0.001. Cells are annotated on the right with density plots showing the distribution of the $\log_2$ fold changes of genes in a given pathway. Cells are colored by the median $\log_2$ fold change of genes in the pathway to indicate the general directionality of the pathway in AD.

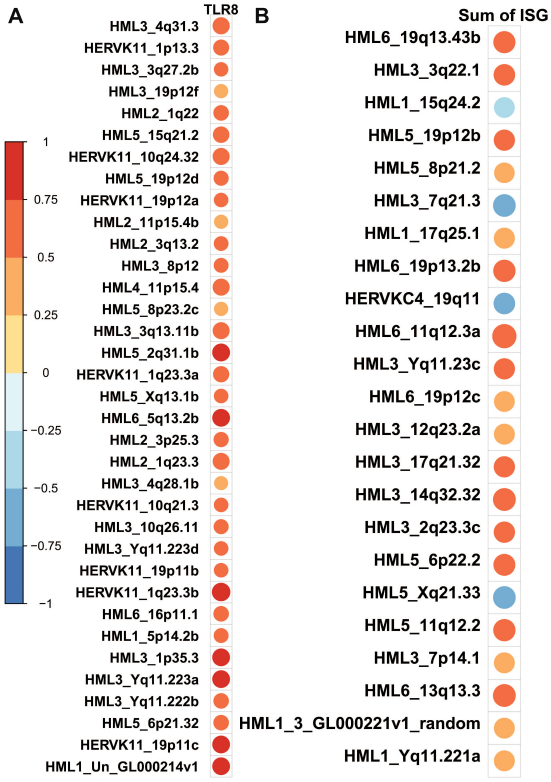

FIGURE 5
HERV-K loci which are significantly correlated with gene expression of interest tend to show positive correlations. Cells show circles whose size and color are indicative of the Pearson correlation coefficient associated with a correlation test between the transcript counts of the transcripts and HERV-K loci. Larger, redder circles indicate correlation coefficients that approach 1. Larger, bluer circles indicate correlation coefficients that approach −1. Only significant associations are shown in order to save space; a full depiction of the correlation between all HERV-K loci and TLR8 is given in the Supplementary material. **(A)** HERV-K loci which are significantly correlated with TLR8 expression all show a positive direction of such a correlation. **(B)** HERV-K loci which are significantly correlated with a sum of the expression of interferon-stimulated genes (ISG) mostly show a positive direction of such a correlation−19/23 correlation values are positive.

nor HERVKC4 elements, each families within the superfamily of HERVK, are significantly correlated with TLR-8 expression (Supplementary Figure 4).

We also sought to characterize the gene expression of the samples from our WashU RNA-Seq dataset. We report 1,514 upregulated genes in AD (FDR < 0.05) and 685 downregulated genes in AD (FDR < 0.05) (Figure 6). In order to compare the differentially expressed genes in our study — in which tissue was collected from the parietal lobe — with the results of other studies conducted in AD across brain regions, we obtained log fold change values from genes presented in a recent study (Figure 7A). Additionally, we used Arboreto to find HERVs that show the highest associations with DE genes and present scatter plots of the 5 strongest associations, ranked by feature importance (Figures 7B–F).

Finally, we conducted gene set enrichment analysis and identify chemotaxis and cell-cell adhesion as pathways that were the most statistically significantly enriched (Figure 8).

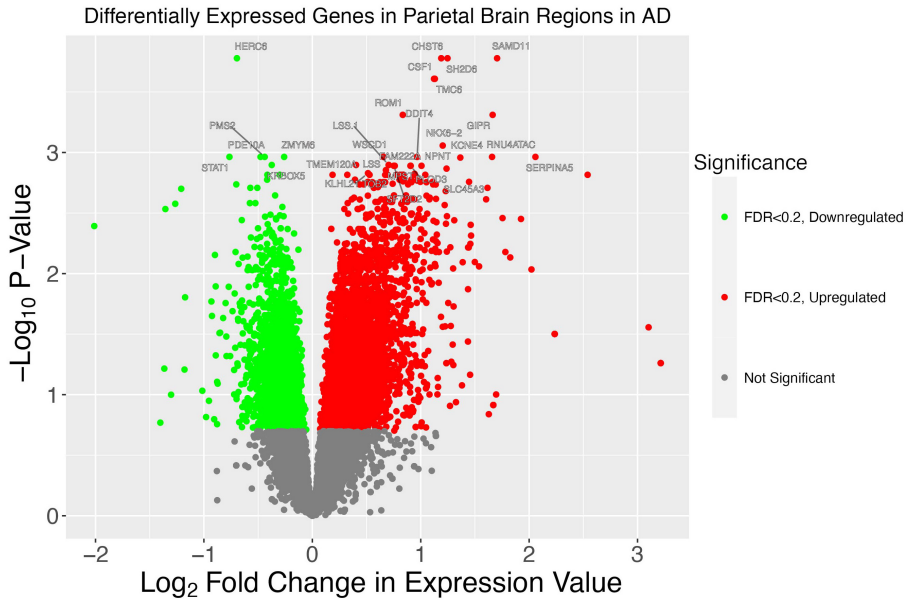

FIGURE 6
A volcano plot illustrates patterns of gene dysregulation in AD. On the *y*-axis the $-\log_{10}P$-value calculated using DESeq2 is shown. On the *x*-axis, the $\log_2$ fold change in expression value is shown. Each dot represents a gene. A handful of the genes with the most extreme *p*-values are shown. Red dots lie to the right of the $x = 0$ asymptote and represent genes with a greater expression in AD. Green dots lie to the left of the $x = 0$ asymptote and represent genes which have decreased expression in AD. All dots below the line of $-\log_{10}(0.2)$ are colored gray and represent genes which have a statistically insignificant change between conditions.

4. Discussion

In this analysis, we present locus-specific differential HERV expression patterns in Alzheimer's disease compared to normal brain samples. After filtering uninformative elements, 698 HERVs were found to be differentially expressed between Alzheimer's and normal brain samples. Of the 698 elements, 511 were upregulated and 187 were downregulated. Of the 62 families included in the analysis, several had more differentially expressed elements than would have been expected statistically. These families include HERV-K, HERV-W, HML3, HML2, HML4, and HML6, among others (**Figure 3**).

After identifying elements of interest, we conducted a differential gene expression analysis to assess dysregulation of elements proximal to individual HERV loci. We assessed the relationship between HERV-K and TLR8 expression, two elements that may work in tandem to cause neurodegeneration (Dembny et al., 2020). The association between TLR8 and each of the nine HERV-K families were found to be statistically insignificant (**Supplementary Figure 2**). However, when looking at individual loci, a number of elements had statistically significant Pearson correlation coefficients approaching one (**Figure 6**). Of note, all of the significant associations were positive. Similarly strong trends were observed by correlating HERV-K expression with the summed expression of a set of interferon signature genes. These results not only corroborate the findings of previous studies, they also highlight the benefit of looking beyond the family level of HERVs to specific transposable element insertions.

Next, gene set enrichment analysis of genes proximal to differentially expressed HERVs reveals dysregulated pathways that may be at play in AD. The pathways with the most statistically significant coefficient values were both linked to cell adhesion process, while the pathway with the largest absolute value of the coefficient was linked to the cell cycle. Disruptions to the cell cycle of neurons in the AD brain have been noted for several decades. As early as 1997, McShea et al. (1997) identified a number of dysregulated cell cycle mediators, such as cell-division cycle 2 (cdc2), cyclin B1 kinase, and cyclin-dependent kinase-4 (Cdk4) (Vincent et al., 1997). Soon after, evidence emerged that neurons in AD patients likely re-enter an ultimately lethal cell cycle (Yang et al., 2001), a cellular process that is now considered an early manifestation of neurodegenerative disease (Denechaud et al., 2023).

Our proximal gene analysis indicated that a member of the transmembrane (*TMEM*) protein family, *TMEM179* (ENSG00000258986), had the highest coefficient value at 2.623108848. The *TMEM* family is responsible for fulfilling a wide variety of important physiological functions such as mounting an immune response (Dodeller et al., 2008), collagen secretion (Zhang et al., 2020), dendritic lysosomal trafficking (Zhang et al., 2020), and smooth muscle contraction (Thomas-Gatewood et al., 2011), among other roles. The differential expression of the *TMEM* family has also been noted in several types of cancers (Schmit and Michiels, 2018). Of the expansive list of *TMEM* proteins, *TMEM179* is less frequently a subject of study. The sequence is located on human 14q32.33, which has previously been identified as a potential evolutionary breakpoint (Ruiz-Herrera et al., 2006; Longo et al., 2009). This protein has recently been identified as one of eight probable modulators of optic nerve necrosis in mice (Stiemke et al., 2020). It has also been demonstrated that *TMEM179* is expressed in oligodendrocyte precursor cells (OPCs), astrocytes, and neurons; and that it is found in the cortex, hippocampus, and

10.3389/fnagi.2023.1186470

FIGURE 7

A comparison of the fold change of genes across brain regions in AD. **(A)** Faceted plot is shown in which each panel represents a gene. Along the *x*-axis are brain regions and the fold change of the gene in patients with AD is expressed by the height of the bar. Each panel is colored into green and red regions to make it clear which direction the bars face, and, in turn, the corresponding fold change of the gene. The upper portion of each panel is colored red; bars which stretch into this region represent genes with a positive log fold change in AD. The lower portion of each panel is colored green; bars which stretch into this region represent genes with a negative log fold change in AD. Each tissue is also given its own color; some genes were not expressed in some tissues or not associated with a significant log fold change and, as a consequence, not every panel contains data for every tissue. Largely the patterns of log fold change remain consistent across tissues but there are exceptions in which genes show a different pattern of expression in the parietal lobe compared to other tissues. **(B–F)** Variance-stabilizing transformed counts of top 5 most-associated genes and HERVs as calculated by Arboreto.

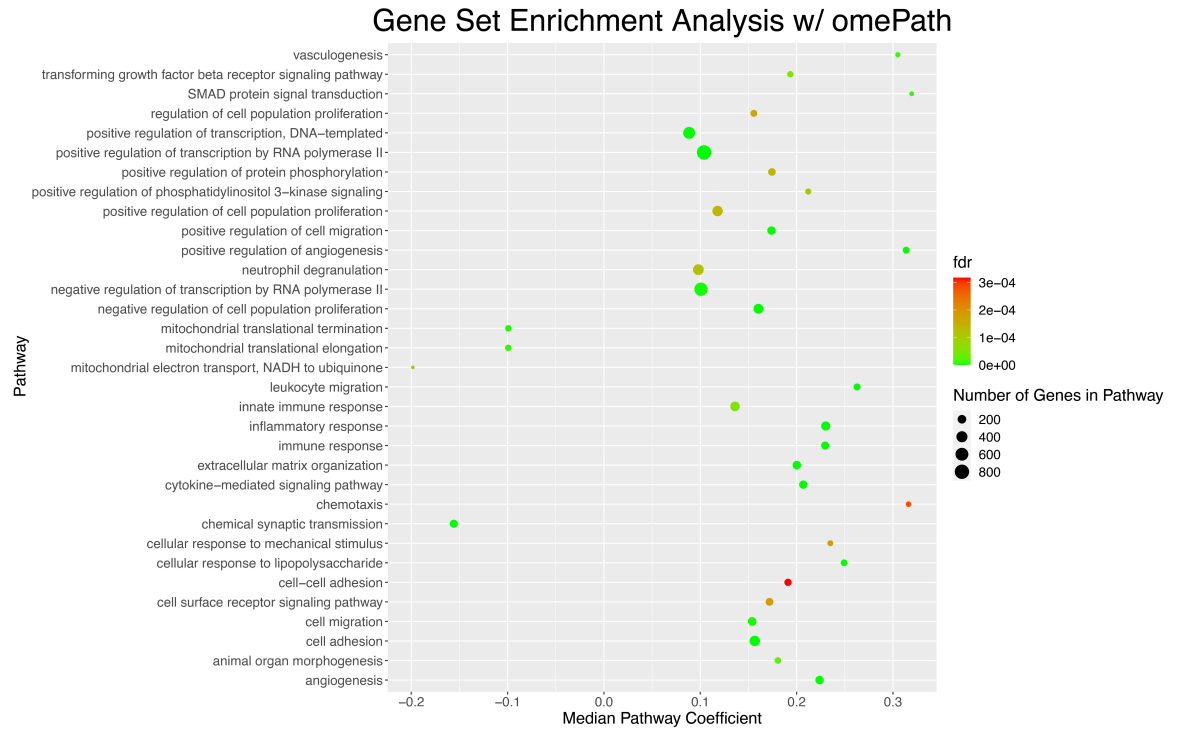

FIGURE 8
Gene set enrichment analysis of DE genes in AD highlights pathways that are significantly dysregulated in the parietal lobe. The top 33 pathways sorted by lowest *p*-value are shown. Each dot represents a pathway; the position of the dot on the *x*-axis represents the coefficient of the median gene in that pathway. The color of the gene, on a color scale from red to green, represents an increasingly more significant *p*-value associated with the dysregulation of the pathway. The size of the dot indicates the number of genes in the pathway; in this case pathways ranged from ~200 genes to ~800 genes.

hypothalamus of mice (He et al., 2021). However, the primary focus of the study was investigating the neurotoxic effects of arsenic and the protective effects of N-acetyl-cysteine (NAC) on OPCs. The investigators found that *TMEM179* was likely involved in modulating both neurotoxic and protective effects in OPCs, in addition to being involved in mitochondrial maintenance and apoptotic pathways (He et al., 2021). Notably, *TMEM179* was thought to inhibit apoptosis via suppression of protein kinase C β (PKCβ) (He et al., 2021), which is one of a handful of PKC isoforms often referred to as "memory kinases" for their role in transmembrane signal conduction (Sun and Alkon, 2014). Mice deficient in PKCβ also demonstrate deficits in cued conditioning and learning (Weeber et al., 2000). Most relevant though is the purported role of PKCβ in AD pathology. Studies have shown that when PKCβ fails to translocate to the plasma membrane, it can hyperphosphorylate tau (Gerschütz et al., 2013).

Accumulation of detritus could also be attributed to dysregulation of the *PSMB1* gene—which was found to have a $\log_2$ fold change value of 1.388246983. This gene encodes the β6 subunit of a proteasome beta-type family which in turn forms the core of the 20S proteasome. Proteasomes are key members of the ubiquitin–proteasome system (UPS) which is responsible for degradation of intracellular damaged, mutant, misfolded, or extraneous proteins (Glickman and Ciechanover, 2002). Critically, reduced UPS function has been noted throughout much of early Alzheimer's literature and could be linked to the accumulation of tau seen in the AD brain (López Salon et al., 2000; Keller et al., 2001). The 20S proteasome in particular is affected by this aberrant control of UPS function observed in AD. The phosphorylation and subsequent deactivation of nuclear factor erythroid 2-like factor 2 (Nrf2) in AD patients prevents the increased expression of the 20S proteasome (Ramsey et al., 2007; Pickering et al., 2012), which dwindles the already diminishing pool of competent proteasomes. While it is worth noting that researchers are still unclear whether defective proteasome function causes AD or if it arises as a consequence of the disease and simply exacerbates it (Lee et al., 2013), the increased expression of the *PSMB1* gene could still be an indication of the body attempting to compensate for reduced UPS activity.

Other overexpressed genes found in the analysis have less tangential relations to neurodegenerative changes. One such gene was *BASP1*, which had a $\log_2$ fold change value of 1.30198558. This gene plays a critical role in neurodevelopment, synaptic function, and nerve regeneration. More specifically, it is involved in enhanced neurite outgrowth (Korshunova et al., 2008), has implications for neurotransmission, synaptic plasticity, and information storage (Yamamoto et al., 1997; Han et al., 2013), and axonal regeneration after injury. Notably, recent studies have shown that levels of *BASP1* are decreased in AD patients (Musunuri et al., 2014), and the protein often demonstrates decreased phosphorylation in the temporal lobes compared to non-AD subjects (Tagawa et al., 2015).

A number of genes with both positive and negative correlation coefficients are classified as long non-coding RNAs (lncRNAs) and

pseudogenes. While these specific elements had little to no coverage in literature, lncRNAs in general have been implicated in a number of human diseases, including Alzheimer's. Although lncRNAs are not capable of forming functional proteins, they nonetheless play a crucial role in mediating the expression of neighboring protein-coding genes through chromatin modifications, transcriptional regulation, and post-transcriptional regulation (Mercer et al., 2009; Derrien et al., 2012; Marchese et al., 2017). Due to their regulatory roles, genomic rearrangements with lncRNA loci have been linked to cancers, neurological and cardiovascular disorders, and infectious or inflammatory disease (Esteller, 2011; Wapinski and Chang, 2011; DiStefano, 2018; Aznaourova et al., 2020). In the past decade, lncRNAs have been increasingly linked to AD pathology, with a number of elements having been identified as potential biomarkers in the blood (Kurt et al., 2020), plasma (Feng et al., 2018), extracellular vesicles (Straten et al., 2009; Wang et al., 2020), and cerebrospinal fluid (Straten et al., 2009; Wang et al., 2020). These identified elements (**Supplementary Table 1**) may also serve as biomarkers or play a role in AD pathology.

5. Conclusion

A total of 698 HERVs were identified as being significantly differentially expressed in Alzheimer's disease vs. healthy controls. These HERVs are physically proximal to genes in cell adhesion and immune response pathways. HERVs in the HERV-K superfamily are overrepresented among those differentially expressed and many loci are correlated with innate immune activation.

Further studies will be necessary to confirm the role of specific HERV loci in innate immunity and cell adhesion in neurodegenerative diseases like Alzheimer's Disease. Both *in vitro* and *in vivo* experimentation are warranted. Future studies may also probe the expression of other transposable elements or perform binding experiments to show to what degree certain HERV transcripts or proteins are immunogenic in AD.

Data availability statement

The data is available at https://www.niagads.org/datasets/ng00083. Circular RNAs in Alzheimer's disease brains – RNA-seq data. This dataset presents the results from processing ribosomal RNA (rRNA)-depleted RNA-seq data derived from human brain tissues donated by individuals with and without Alzheimer's disease (AD). At the individual-level, it includes data for circular and linear RNA counts as well as technical, clinical, and neuropathological phenotypes. At the summary statistic-level, it includes discovery, replication, and meta-analysis circular RNA (circRNA) differential expression and AD-trait correlation results www.niagads.org.

Ethics statement

The studies involving human participants were reviewed and approved by the Washington University Institutional Review Board. The patients/participants provided their written informed consent to participate in this study.

Author contributions

TD, UR, and JS: investigation. CC, JK, and KC: conceptualization, resources, review and editing, supervision, and funding acquisition. TD, UR, JS, CC, JK, and KC: methodology. TD and UR: writing. All authors contributed to the manuscript and approved the submitted version.

Funding

This work was supported by grants from the National Institutes of Health [R01AG044546 (CC), P01AG003991 (CC) RF1AG053303 (CC), RF1AG058501 (CC), U01AG058922 (CC), RF1AG071706 (CC), and R01AG078964 (CC)], the Chan Zuckerberg Initiative (CZI), the Michael J. Fox Foundation (CC), the Department of Defense (LI- W81XWH2010849), and the Alzheimer's Association Zenith Fellows Award (ZEN-22-848604, awarded to CC), and anonymous foundation. The recruitment and clinical characterization of research participants at Washington University were supported by the NIH P30AG06644, P01AG0399, and P01AG026276. This work was also supported by access to equipment made possible by the Hope Center for Neurological Disorders, the Neurogenomics and Informatics Center (NGI: https://neurogenomics.wustl.edu/) and the Departments of Neurology and Psychiatry at Washington University School of Medicine. The analytical component of this work was partially supported by funding from Brigham Young University.

Acknowledgments

We thank all the participants and their families, as well as the many involved institutions and their staff.

Conflict of interest

CC has received research support from: GlaxoSmithKline and Eisai. The funders of the study had no role in the collection, analysis, or interpretation of data; in the writing of the report; or in the decision to submit the manuscript for publication. CC is a member of the advisory board of Vivid Genomics and Circular Genomics and owns stocks. TD has received research support from AMPEL BioSolutions.

The remaining authors declare that the research was conducted in the absence of any commercial or financial relationships that could be construed as a potential conflict of interest.

Publisher's note

Supplementary material

The Supplementary Material for this article can be found online at: https://www.frontiersin.org/articles/10.3389/fnagi.2023.1186470/full#supplementary-material

SUPPLEMENTARY FIGURE 1
Read counts in Wash-U dataset of 98 patients. **(a)** The total number of reads from each sample is shown. Each bar represents a particular sample and its height represents the number of total reads. **(b)** A summary boxplot is shown to represent the distribution of reads across our samples. **(c)** The number of reads from each sample that mapped to HERVs is shown. The order of samples from panel a is preserved. **(d)** A heatmap shows the number of HERVs across families that mapped from each sample. Darker shades of red indicate a higher number of mapped HERVs from a sample to a HERV family.

SUPPLEMENTARY FIGURE 2
Genomic location of HERVs expressed in Alzheimer's disease. DE HERV loci are mapped to chromosomal locations and shown on a circos plot. The circos plot is a circular representation of the genome. The outermost ring is shaded according to cytogenetic bands with red bands corresponding to centromeres and black and gray bands corresponding to changes between bands and sub-bands that represent chromosomal structural features visible with a microscope. Chromosomes are labeled with text that surrounds this ring. The blue, dashed line in the center represents a $\log_2$ fold change of 0. Each dot represents a DE HERV in its corresponding chromosomal location, the color and distance from center are indicative of p-value and $\log_2$ fold change, respectively.

SUPPLEMENTARY FIGURE 3
Correlations between TLR-8 expression and expression of all HERV-K loci. Significant correlations have loci names written in red text.

SUPPLEMENTARY FIGURE 4
Correlation of sum of HERV-K expression across 9 HERV-K families and TLR8 expression.

References

Alzheimer's Association, (2021). Alzheimer's disease facts and figures. *Alzheimers Dement.* 17, 327–406.

Andrews, S. (2010). *FastQC: A quality control tool for high throughput sequence data*. Cambridge: Babraham Institute.

Antony, J. M., van Marle, G., Opii, W., Butterfield, D., Mallet, F., Yong, V., et al. (2004). Human endogenous retrovirus glycoprotein–mediated induction of redox reactants causes oligodendrocyte death and demyelination. *Nat. Neurosci.* 7, 1088–1095. doi: 10.1038/nn1319

Aznaourova, M., Schmerer, N., Schmeck, B., and Schulte, L. N. (2020). Disease-causing mutations and rearrangements in long non-coding RNA gene loci. *Front. Genet.* 11:527484. doi: 10.3389/fgene.2020.527484

Bannert, N., and Kurth, R. (2006). The evolutionary dynamics of human endogenous retroviral families. *Annu. Rev. Genomics Hum. Genet.* 7, 149–173.

Bendall, M. L., de Mulder, M., Iñiguez, L., Lecanda-Sánchez, A., Pérez-Losada, M., Ostrowski, M., et al. (2019). Telescope: Characterization of the retrotranscriptome by accurate estimation of transposable element expression. *PLoS Comput. Biol.* 15:e1006453. doi: 10.1371/journal.pcbi.1006453

Bolger, A. M., Lohse, M., and Usadel, B. (2014). Trimmomatic: A flexible trimmer for Illumina sequence data. *Bioinformatics* 30, 2114–2120.

Brion, J. P. (1998). Neurofibrillary tangles and Alzheimer's disease. *Eur. Neurol.* 40, 130–140.

Buzdin, A. A., Prassolov, V., and Garazha, A. V. (2017). Friends-enemies: Endogenous retroviruses are major transcriptional regulators of human DNA. *Front. Chem.* 5:35. doi: 10.3389/fchem.2017.00035

Buzdin, A., Kovalskaya-Alexandrova, E., Gogvadze, E., and Sverdlov, E. (2006). At least 50% of human-specific HERV-K (HML-2) long terminal repeats serve in vivo as active promoters for host nonrepetitive DNA transcription. *J. Virol.* 80, 10752–10762. doi: 10.1128/JVI.00871-06

Catalina, M. D., Bachali, P., Geraci, N. S., Grammer, A. C., and Lipsky, P. E. (2019). Gene expression analysis delineates the potential roles of multiple interferons in systemic lupus erythematosus. *Commun. Biol.* 2, 140. doi: 10.1038/s42003-019-0382-x

Del-Aguila, J. L., Benitez, B., Li, Z., Dube, U., Mihindukulasuriya, K., Budde, J., et al. (2019). TREM2 brain transcript-specific studies in AD and TREM2 mutation carriers. *Mol. Neurodegener.* 14:18. doi: 10.1186/s13024-019-0319-3

Dembny, P., Newman, A., Singh, M., Hinz, M., Szczepek, M., Krüger, C., et al. (2020). Human endogenous retrovirus HERV-K(HML-2) RNA causes neurodegeneration through Toll-like receptors. *JCI Insight* 5:e131093. doi: 10.1172/jci.insight.131093

Denechaud, M., Geurs, S., Comptdaer, T., Bégard, S., Garcia-Núñez, A., Pechereau, L., et al. (2023). Tau promotes oxidative stress-associated cycling neurons in S phase as a pro-survival mechanism: Possible implication for Alzheimer's disease. *Prog. Neurobiol.* 223:102386. doi: 10.1016/j.pneurobio.2022.102386

Derrien, T., Johnson, R., Bussotti, G., Tanzer, A., Djebali, S., Tilgner, H., et al. (2012). The GENCODE v7 catalog of human long noncoding RNAs: Analysis of their gene structure, evolution, and expression. *Genome Res.* 22, 1775–1789. doi: 10.1101/gr.132159.111

DiStefano, J. K. (2018). "The emerging role of long noncoding RNAs in human disease," in *Disease gene identification, methods in molecular biology*, ed. J. K. DiStefano (New York, NY: Springer), 91–110.

Dobin, A., Davis, C., Schlesinger, F., Drenkow, J., Zaleski, C., Jha, S., et al. (2013). STAR: Ultrafast universal RNA-seq aligner. *Bioinformatics* 29, 15–21. doi: 10.1093/bioinformatics/bts635

Dodeller, F., Gottar, M., Huesken, D., Iourgenko, V., and Cenni, B. (2008). The lysosomal transmembrane protein 9B regulates the activity of inflammatory signaling pathways. *J. Biol. Chem.* 283, 21487–21494. doi: 10.1074/jbc.M801908200

Douville, R. N., and Nath, A. (2014). Human endogenous retroviruses and the nervous system. *Handb. Clin. Neurol.* 123, 465–485.

Dube, U., Del-Aguila, J., Li, Z., Budde, J., Jiang, S., Hsu, S., et al. (2019). An atlas of cortical circular RNA expression in Alzheimer disease brains demonstrates clinical and pathological associations. *Nat. Neurosci.* 22, 1903–1912. doi: 10.1038/s41593-019-0501-5

Esteller, M. (2011). Non-coding RNAs in human disease. *Nat. Rev. Genet.* 12, 861–874.

Feng, L., Liao, Y., He, J., Xie, C., Chen, S., Fan, H., et al. (2018). Plasma long non-coding RNA BACE1 as a novel biomarker for diagnosis of Alzheimer disease. *BMC Neurol.* 18:4. doi: 10.1186/s12883-017-1008-x

Feschotte, C., and Gilbert, C. (2012). Endogenous viruses: Insights into viral evolution and impact on host biology. *Nat. Rev. Genet.* 13, 283–296.

Frank, O., Giehl, M., Zheng, C., Hehlmann, R., Leib-Mösch, C., Seifarth, W., et al. (2005). Human endogenous retrovirus expression profiles in samples from brains of patients with schizophrenia and bipolar disorders. *J. Virol.* 79, 10890–10901.

Gerschütz, A., Heinsen, H., Grünblatt, E., Wagner, A., Bartl, J., Meissner, C., et al. (2013). Neuron-specific mitochondrial DNA deletion levels in sporadic Alzheimer's disease. *Curr. Alzheimer Res.* 10, 1041–1046. doi: 10.2174/15672050113106660166

Glickman, M. H., and Ciechanover, A. (2002). The ubiquitin-proteasome proteolytic pathway: Destruction for the sake of construction. *Physiol. Rev.* 82, 373–428.

Groh, S., and Schotta, G. (2017). Silencing of endogenous retroviruses by heterochromatin. *Cell. Mol. Life Sci.* 74, 2055–2065.

Gu, Z., Gu, L., Eils, R., Schlesner, M., and Brors, B. (2014). Circlize implements and enhances circular visualization in R. *Bioinformatics* 30, 2811–2812. doi: 10.1093/bioinformatics/btu393

Guo, C., Jeong, H., Hsieh, Y., Klein, H., Bennett, D., De Jager, P., et al. (2018). Tau activates transposable elements in Alzheimer's disease. *Cell Rep.* 23, 2874–2880.

Han, M. H., Jiao, S., Jia, J., Chen, Y., Chen, C., Gucek, M., et al. (2013). The novel caspase-3 substrate Gap43 is involved in AMPA receptor endocytosis and long-term depression. *Mol. Cell. Proteomics* 12, 3719–3731. doi: 10.1074/mcp.M113.030676

He, Z., Zhang, Y., Zhang, H., Zhou, C., Ma, Q., Deng, P., et al. (2021). NAC antagonizes arsenic-induced neurotoxicity through TMEM179 by inhibiting oxidative stress in Oli-neu cells. *Ecotoxicol. Environ. Saf.* 223:112554. doi: 10.1016/j.ecoenv.2021.112554

Heneka, M. T., Carson, M., El Khoury, J., Landreth, G., Brosseron, F., Feinstein, D., et al. (2015). Neuroinflammation in Alzheimer's disease. *Lancet Neurol.* 14, 388–405.

Hoyt, S. J., Storer, J., Hartley, G., Grady, P., Gershman, A., de Lima, L., et al. (2022). From telomere to telomere: The transcriptional and epigenetic state of human repeat elements. *Science* 376:eabk3112.

Ibba, G., Piu, C., Uleri, E., Serra, C., and Dolei, A. (2018). Disruption by SaCas9 endonuclease of HERV-Kenv, a retroviral gene with oncogenic and neuropathogenic potential, inhibits molecules involved in cancer and amyotrophic lateral sclerosis. *Viruses* 10:412. doi: 10.3390/v10080412

Ito, J., Sugimoto, R., Nakaoka, H., Yamada, S., Kimura, T., Hayano, T., et al. (2017). Systematic identification and characterization of regulatory elements derived from human endogenous retroviruses. *PLoS Genet.* 13:e1006883. doi: 10.1371/journal.pgen.1006883

Jacques, P. E., Jeyakani, J., and Bourque, G. (2013). The majority of primate-specific regulatory sequences are derived from transposable elements. *PLoS Genet.* 9:e1003504. doi: 10.1371/journal.pgen.1003504

Johnston, J. B., Silva, C., Holden, J., Warren, K., Clark, A., and Power, C. (2001). Monocyte activation and differentiation augment human endogenous retrovirus expression: Implications for inflammatory brain diseases. *Ann. Neurol.* 50, 434–442. doi: 10.1002/ana.1131

Keller, J. N., Hanni, K. B., and Markesbery, W. R. (2001). Impaired proteasome function in Alzheimer's disease. *J. Neurochem.* 75, 436–439.

Korshunova, I., Caroni, P., Kolkova, K., Berezin, V., Bock, E., and Walmod, P. (2008). Characterization of BASP1-mediated neurite outgrowth. *J. Neurosci. Res.* 86, 2201–2213. doi: 10.1002/jnr.21678

Kurt, S., Tomatir, A. G., Tokgun, P. E., and Oncel, C. (2020). Altered expression of long non-coding RNAs in peripheral blood mononuclear cells of patients with Alzheimer's disease. *Mol. Neurobiol.* 57, 5352–5361.

Langmead, B., and Salzberg, S. L. (2012). Fast gapped-read alignment with Bowtie 2. *Nat. Methods* 9, 357–359. doi: 10.1038/nmeth.1923

Lee, M. J., Lee, J. H., and Rubinsztein, D. C. (2013). Tau degradation: The ubiquitin–proteasome system versus the autophagy-lysosome system. *Prog. Neurobiol.* 105, 49–59. doi: 10.1016/j.pneurobio.2013.03.001

Leek, J., Johnson, W. E., Parker, H. S., Jaffe, A. E., and Storey, J. D. (2012). The sva package for removing batch effects and other unwanted variation in high-throughput experiments. *Bioinformatics* 28, 882–883.

Li, W., Lee, M., Henderson, L., Tyagi, R., Bachani, M., Steiner, J., et al. (2015). Human endogenous retrovirus-K contributes to motor neuron disease. *Sci. Transl. Med.* 7:307ra153.

Li, Z., Farias, F., Dube, U., Del-Aguila, J., Mihindukulasuriya, K., Fernandez, M., et al. (2020). The TMEM106B FTLD-protective variant, rs1990621, is also associated with increased neuronal proportion. *Acta Neuropathol.* 139, 45–61. doi: 10.1007/s00401-019-02066-0

Liao, Y., Smyth, G. K., and Shi, W. (2014). featureCounts: An efficient general purpose program for assigning sequence reads to genomic features. *Bioinformatics* 30, 923–930. doi: 10.1093/bioinformatics/btt656

Longo, M. S., Carone, D., NISC Comparative Sequencing Program, Green, E., O'Neill, M., and O'Neill, R. J. (2009). Distinct retroelement classes define evolutionary breakpoints demarcating sites of evolutionary novelty. *BMC Genomics* 10:334. doi: 10.1186/1471-2164-10-334

López Salon, M., Morelli, L., Castaño, E. M., Soto, E. F., and Pasquini, J. M. (2000). Defective ubiquitination of cerebral proteins in Alzheimer's disease. *J. Neurosci. Res.* 62, 302–310.

Love, M., Huber, W., and Anders, S. (2014). Moderated estimation of fold change and dispersion for RNA-seq data with DESeq2. *Genome Biol.* 15:550. doi: 10.1186/s13059-014-0550-8

Madabhushi, R., Pan, L., and Tsai, L.-H. (2014). DNA damage and its links to neurodegeneration. *Neuron* 83, 266–282.

Mameli, G., Poddighe, L., Mei, A., Uleri, E., Sotgiu, S., Serra, C., et al. (2012). Expression and activation by epstein barr virus of human endogenous retroviruses-W in blood cells and astrocytes: Inference for multiple sclerosis. *PLoS One* 7:e44991. doi: 10.1371/journal.pone.0044991

Marchese, F. P. I, Raimondi, M., and Huarte. (2017). The multidimensional mechanisms of long noncoding RNA function. *Genome Biol.* 18:206.

McShea, A., Harris, P. L., Webster, K. R., Wahl, A. F., and Smith, M. A. (1997). Abnormal expression of the cell cycle regulators P16 and CDK4 in Alzheimer's disease. *Am. J. Pathol.* 150, 1933–1939.

Mercer, T. R., Dinger, M. E., and Mattick, J. S. (2009). Long non-coding RNAs: Insights into functions. *Nat. Rev. Genet.* 10, 155–159.

Moerman, T., Aibar, S. S., Bravo González-Blas, C., Simm, J., Moreau, Y., Aerts, J., et al. (2019). GRNBoost2 and Arboreto: Efficient and scalable inference of gene regulatory networks. *Bioinformatics* 35, 2159–2161. doi: 10.1093/bioinformatics/bty916

Musunuri, S., Wetterhall, M., Ingelsson, M., Lannfelt, L., Artemenko, K., Bergquist, J., et al. (2014). Quantification of the brain proteome in Alzheimer's disease using multiplexed mass spectrometry. *J. Proteome Res.* 13, 2056–2068.

Nativio, R., Lan, Y., Donahue, G., Sidoli, S., Berson, A., Srinivasan, A., et al. (2020). An integrated multi-omics approach identifies epigenetic alterations associated with Alzheimer's disease. *Nat. Genet.* 52, 1024–1035.

Ohnuki, M., Tanabe, K., Sutou, K., Teramoto, I., Sawamura, Y., Narita, M., et al. (2014). Dynamic regulation of human endogenous retroviruses mediates factor-induced reprogramming and differentiation potential. *Proc. Natl. Acad. Sci. U.S.A.* 111, 12426–12431. doi: 10.1073/pnas.1413299111

Pehrsson, E. C., Choudhary, M. N. K., Sundaram, V., and Wang, T. (2019). The epigenomic landscape of transposable elements across normal human development and anatomy. *Nat. Commun.* 10:5640. doi: 10.1038/s41467-019-13555-x

Perron, H., Garson, J., Bedin, F., Beseme, F., Paranhos-Baccala, G., Komurian-Pradel, F., et al. (1997). Molecular identification of a novel retrovirus repeatedly isolated from patients with multiple sclerosis. *Proc. Natl. Acad. Sci. U.S.A.* 94, 7583–7588. doi: 10.1073/pnas.94.14.7583

Perron, H., Jouvin-Marche, E., Michel, M., Ounanian-Paraz, A., Camelo, S., Dumon, A., et al. (2001). Multiple sclerosis retrovirus particles and recombinant envelope trigger an abnormal immune response in vitro, by inducing polyclonal Vβ16 T-lymphocyte activation. *Virology* 287, 321–332.

Perron, H., Lazarini, F., Ruprecht, K., Péchoux-Longin, C., Seilhean, D., Sazdovitch, V., et al. (2005). Human endogenous retrovirus (HERV)-W ENV and GAG proteins: Physiological expression in human brain and pathophysiological modulation in multiple sclerosis lesions. *J. Neurovirol.* 11, 23–33. doi: 10.1080/13550280590901741

Pickering, A., Linder, R. A., Zhang, H., Forman, H. J., and Davies, K. J. A. (2012). Nrf2-dependent induction of proteasome and Pa28αβ regulator are required for adaptation to oxidative stress. *J. Biol. Chem.* 287, 10021–10031.

Ramsey, C. P., Glass, C., Montgomery, M., Lindl, K., Ritson, G., Chia, L., et al. (2007). Expression of Nrf2 in neurodegenerative diseases. *J. Neuropathol. Exp. Neurol.* 66, 75–85.

Rau, A., Gallopin, M., Celeux, G., and Jaffrézic, F. (2013). Data-based filtering for replicated high-throughput transcriptome sequencing experiments. *Bioinformatics* 29, 2146–2152. doi: 10.1093/bioinformatics/btt350

Rebollo, R., Romanish, M. T., and Mager, D. L. (2012). Transposable elements: An abundant and natural source of regulatory sequences for host genes. *Annu. Rev. Genet.* 46, 21–42. doi: 10.1146/annurev-genet-110711-155621

Ruiz-Herrera, A., Castresana, J., and Robinson, T. J. (2006). Is mammalian chromosomal evolution driven by regions of genome fragility? *Genome Biol.* 7, R115.

Schmit, K., and Michiels, C. (2018). TMEM proteins in cancer: A review. *Front. Pharmacol.* 9:1345. doi: 10.3389/fphar.2018.01345

Seifarth, W., Frank, O., Zeilfelder, U., Spiess, B., Greenwood, A., Hehlmann, R., et al. (2005). Comprehensive analysis of human endogenous retrovirus transcriptional activity in human tissues with a retrovirus-specific microarray. *J. Virol.* 79, 341–352. doi: 10.1128/JVI.79.1.341-352.2005

Stauffer, Y., Theiler, G., Sperisen, P., Lebedev, Y., and Jongeneel, C. V. (2004). Digital expression profiles of human endogenous retroviral families in normal and cancerous tissues. *Cancer Immun.* 4:2.

Stiemke, A. B., Sah, E., Simpson, R., Lu, L., Williams, R., and Jablonski, M. (2020). Systems genetics of optic nerve axon necrosis during glaucoma. *Front. Genet.* 11:31. doi: 10.3389/fgene.2020.00031

Straten, G., Eschweiler, G. W., Maetzler, W., Laske, C., and Leyhe, T. (2009). Glial cell-line derived neurotrophic factor (GDNF) concentrations in cerebrospinal fluid and serum of patients with early Alzheimer's disease and normal controls. *J. Alzheimers Dis.* 18, 331–337. doi: 10.3233/JAD-2009-1146

Sun, M.-K., and Alkon, D. L. (2014). The memory kinases. *Prog. Mol. Biol. Transl. Sci.* 122, 31–59.

Sun, W., Samimi, H., Gamez, M., Zare, H., and Frost, B. (2018). Pathogenic tau-induced piRNA depletion promotes neuronal death through transposable element dysregulation in neurodegenerative tauopathies. *Nat. Neurosci.* 21, 1038–1048. doi: 10.1038/s41593-018-0194-1

Sundaram, V., Cheng, Y., Ma, Z., Li, D., Xing, X., Edge, P., et al. (2014). Widespread contribution of transposable elements to the innovation of gene regulatory networks. *Genome Res.* 24, 1963–1976. doi: 10.1101/gr.168872.113

Tagawa, K., Homma, H., Saito, A., Fujita, K., Chen, X., Imoto, S., et al. (2015). Comprehensive phosphoproteome analysis unravels the core signaling network that initiates the earliest synapse pathology in preclinical Alzheimer's disease brain. *Hum. Mol. Genet.* 24, 540–558. doi: 10.1093/hmg/ddu475

The Gene Ontology Consortium (2019). The gene ontology resource: 20 years and still going strong. *Nucleic Acids Res.* 47, D330–D338. doi: 10.1093/nar/gky1055

Thomas-Gatewood, C., Neeb, Z., Bulley, S., Adebiyi, A., Bannister, J., Leo, M., et al. (2011). TMEM16A channels generate Ca2+ -activated Cl - currents in cerebral artery smooth muscle cells. *Am. J. Physiol. Heart Circ. Physiol.* 301, H1819–H1827.

Tiraboschi, P., Hansen, L. A., Thal, L. J., and Corey-Bloom, J. (2004). The importance of neuritic plaques and tangles to the development and evolution of AD. *Neurology* 62, 1984–1989. doi: 10.1212/01.wnl.0000129697.01779.0a

Vincent, I., Jicha, G., Rosado, M., and Dickson, D. W. (1997). Aberrant expression of mitotic Cdc2/Cyclin B1 kinase in degenerating neurons of Alzheimer's disease brain. *J. Neurosci.* 17, 3588–3598. doi: 10.1523/JNEUROSCI.17-10-03588.1997

Wang, D., Wang, P., Bian, X., Xu, S., Zhou, Q., Zhang, Y., et al. (2020). Elevated plasma levels of exosomal BACE1-AS combined with the volume and thickness of

the right entorhinal cortex may serve as a biomarker for the detection of Alzheimer's disease. *Mol. Med. Rep.* 22, 227–238. doi: 10.3892/mmr.2020.11118

Wapinski, O., and Chang, H. Y. (2011). Long noncoding RNAs and human disease. *Trends Cell Biol.* 21, 354–361.

Weeber, E. J., Atkins, C., Selcher, J., Varga, A., Mirnikjoo, B., Paylor, R., et al. (2000). A role for the β isoform of protein kinase C in fear conditioning. *J. Neurosci.* 20, 5906–5914.

Wickham, H. (2016). *ggplot2*. New York: Springer International Publishing.

Yamamoto, Y., Sokawa, Y., and Maekawa, S. (1997). Biochemical evidence for the presence of NAP-22, a novel acidic calmodulin binding protein, in the synaptic vesicles of rat brain. *Neurosci. Lett.* 224, 127–130. doi: 10.1016/s0304-3940(97)13482-6

Yang, Y., Geldmacher, D. S., and Herrup, K. (2001). DNA replication precedes neuronal cell death in Alzheimer's disease. *J. Neurosci.* 21, 2661–2668. doi: 10.1523/JNEUROSCI.21-08-02661.2001

Yu, M., Hu, X., Pan, Z., Du, C., Jiang, J., Zheng, W., et al. (2023). Endogenous retrovirus-derived enhancers confer the transcriptional regulation of human trophoblast syncytialization. *Nucleic Acids Res.* 51, 4745–4759. doi: 10.1093/nar/gkad109

Zhang, Z., Bai, M., Barbosa, G., Chen, A., Wei, Y., Luo, S., et al. (2020). Broadly conserved roles of TMEM131 family proteins in intracellular collagen assembly and secretory cargo trafficking. *Sci. Adv.* 6:eaay7667. doi: 10.1126/sciadv.aay7667

frontiers | Frontiers in Aging Neuroscience

TYPE Original Research
PUBLISHED 12 July 2023
DOI 10.3389/fnagi.2023.1179752

OPEN ACCESS

EDITED BY
Chih-Yu Hsu,
Fujian University of Technology, China

REVIEWED BY
Andrzej Bogucki,
Medical University of Łódź, Poland
Agata Gajos,
Medical University of Łódź, Poland

*CORRESPONDENCE
Guohua Fan
✉ fangh22@126.com
Erlei Wang
✉ erlei_wang_jyj@163.com

RECEIVED 04 March 2023
ACCEPTED 22 June 2023
PUBLISHED 12 July 2023

CITATION
Bao Y, Ya Y, Liu J, Zhang C, Wang E and Fan G (2023) Regional homogeneity and functional connectivity of freezing of gait conversion in Parkinson's disease.
Front. Aging Neurosci. 15:1179752.
doi: 10.3389/fnagi.2023.1179752

Regional homogeneity and functional connectivity of freezing of gait conversion in Parkinson's disease

Yiqing Bao[1], Yang Ya[1], Jing Liu[2], Chenchen Zhang[1], Erlei Wang[1]* and Guohua Fan[1]*

[1]Department of Radiology, The Second Affiliated Hospital of Soochow University, Suzhou, China, [2]Department of Neurology, The Second Affiliated Hospital of Soochow University, Suzhou, China

Background: Freezing of gait (FOG) is common in the late stage of Parkinson's disease (PD), which can lead to disability and impacts the quality of life. Therefore, early recognition is crucial for therapeutic intervention. We aimed to explore the abnormal regional homogeneity (ReHo) and functional connectivity (FC) in FOG converters and evaluate their diagnostic values.

Methods: The data downloaded from the Parkinson's Disease Progression Markers Project (PPMI) cohort was subdivided into PD-FOG converters (n = 16) and non-converters (n = 17) based on whether FOG appeared during the 3-year follow-up; 16 healthy controls were well-matched. ReHo and FC analyses were used to explore the variations in spontaneous activity and interactions between significant regions among three groups of baseline data. Correlations between clinical variables and the altered ReHo values were assessed in FOG converter group. Last, logistic regression and receiver operating characteristic curve (ROC) were used to predict diagnostic value.

Results: Compared with the non-converters, FOG converters had reduced ReHo in the bilateral medial superior frontal gyrus (SFGmed), which was negatively correlated with the postural instability and gait difficulty (PIGD) score. ReHo within left amygdala/olfactory cortex/putamen (AMYG/OLF/PUT) was decreased, which was correlated with anxiety and autonomic dysfunction. Also, increased ReHo in the left supplementary motor area/paracentral lobule was positively correlated with the rapid eye movement sleep behavior disorder screening questionnaire. FOG converters exhibited diminished FC in the basal ganglia, limbic area, and cognitive control cortex, as compared with non-converters. The prediction model combined ReHo of basal ganglia and limbic area, with PIGD score was the best predictor of FOG conversion.

Conclusion: The current results suggested that abnormal ReHo and FC in the basal ganglia, limbic area, and cognitive control cortex may occur in the early stage of FOG. Basal ganglia and limbic area dysfunction combined with higher PIGD score are useful for the early recognition of FOG conversion.

KEYWORDS

Parkinson's disease, regional homogeneity, freezing of gait, receiver operating characteristic curve, functional connectivity

Introduction

Freezing of gait (FOG) is a distinct and serious gait impairment in the latter stage of Parkinson's disease (PD) (Giladi et al., 1997, 2001), characterized by a sudden transient and unexpected interruption in walking, usually during gait initiation or while turning. PD patients with FOG frequently fall, which can lead to disability and impacts the quality of life (Perez-Lloret et al., 2014). Therefore, it is very important to explore the pathophysiological mechanisms of FOG. Understanding the determinants of future FOG can provide important prognostic information for clinicians.

In the last decade, numerous neuroimaging studies have reported abnormal structural and functional changes associated with FOG in PD patients. Gray matter loss and hypoperfusion were observed in various cortical regions, especially frontal and parietal cortices (Matsui et al., 2005; Kostic et al., 2012; Tessitore et al., 2012). Meanwhile, using functional MRI, several studies have reported that FOG may be associated with abnormal activation in the cortical cognitive control, sensorimotor networks and basal ganglia, as well as abnormal functional connections (FC) between them (Shine et al., 2013a,b; Canu et al., 2015; Gilat et al., 2018). Nonetheless, most previous studies included patients who already had FOG symptoms, and only a few MRI studies followed PD patients developing FOG over time to identify predictive brain signs of FOG conversion. Dadar and colleagues found that the amyloid-β pathology may be related to future FOG in PD patients through increasing the burden of white matter hyperintensities (Dadar et al., 2021). During FOG conversion, the left thalamus swell and FOG converters had a marked reduction in thalamo-cortical coupling with limbic and cognitive regions over the 2 years (D'Cruz et al., 2021). In a recent longitudinal study, Sarasso et al. (2022) compared the graph theory indices and clinical data of FOG converters, non-converters, and FOG patients at baseline and over a 2-year follow-up period, showing that over time FOG converters have more dyskinesia, executive dysfunction, and emotional disorders, as well as decreased parietal clustering coefficient and sensorimotor local efficiency. In summary, these previous studies provide evidence of structural and functional abnormities during FOG conversion, which may be used as imaging biomarkers to predict FOG.

In this study, using rest-state fMRI data, we aimed to combine regional homogeneity (ReHo), an index evaluating local signal synchronization by measuring the similarity between the time series of a chosen voxel and its adjacent voxels (Zang et al., 2004), with voxel-based functional connectivity (FC) analysis and clinical data to explore FOG conversion in PD patients from the Parkinson's Disease Progression Markers Project (PPMI) cohort. Specifically, we used the second-year point-in-time data in PPMI cohort as baseline data and further subdivided it into FOG converters and non-converters based on whether FOG appeared during the following 3 years. Next, ReHo and FC analyses were performed in healthy controls and PD patients with and without FOG conversion to explore the changes of ReHo and FC in the early stage of FOG. Finally, logistic regression and characteristic curve (ROC) analysis were used to determine the best predictive model of FOG conversion with clinical data. Based on previous studies, we hypothesized that the alteration of ReHo and FC values in brain regions are specific to FOG converters in the early stage, and functional MRI combined with clinical features are most useful for the recognition of FOG conversion.

Materials and methods

Study design and participants

In this study, all data were used from the Parkinson's Progression Markers Project (PPMI), a large-scale, comprehensive, multicenter Biomarker Project, which was committed to multiple clinical examinations, neuroimaging, and longitudinal follow-ups (Parkinson Progression Marker Initiative, 2011). Patients received a comprehensive evaluation in ON medication state. Since most PD patients did not collect resting-state functional MRI data in the first year of baseline, so we used data from the second year of follow-up as a baseline and assessed FOG conversion during the 3-year follow-up using MDS-UPDRS items 2.13 and 3.11. In the present study, the FOG converter was considered to be present if the score was $\geq$ 1 for either MDS-UPDRS item 2.13 or 3.11 at any point during the follow-up, and a persistent score of 0 was defined as the FOG non-converter (Kim et al., 2019; Dadar et al., 2021).

Clinical assessments

Motor symptoms and disease severity were assessed using MDS-UPDRS III and HY stage. Based on MDS-UPDRS III, 11 items (2.10 and 3.15–18) were used for rest tremor score and 5 items (2.12–13 and 3.10–12) for postural instability and gait difficulty (PIGD) score (Stebbins et al., 2013; Dadar et al., 2021). Other clinical variables in this study included gender, duration, age, years of education, dominant hand, rapid eye movement (REM) sleep behavior disorder assessed by the

REM Sleep Behavior Disorder Screening Questionnaire (RBDSQ), excessive daytime sleepiness assessed by the Epworth Sleepiness Scale (ESS), overall cognitive function assessed by the Montreal Cognitive Assessment (MoCA), depression assessed by the Geriatric Depression Scale Score (GDS), anxiety evaluated by the State-Trait Anxiety Inventory (STAI), and autonomic dysfunction evaluated by the Autonomic Outcome Scale in Parkinson's disease (SCOPA-AUT). The PIGD, GDS, STAI, RBDSQ and SCOPA-AUT scores were sqrt-transformed (square root) to achieve a normal distribution.

MRI data acquisition and preprocessing

T1-weighted gradient echo three-dimensional (3D) magnetization-prepared rapid gradient-echo (MPRAGE) sequences [repetition time (TR) = 2,300 ms, flip angle (FA) = 9°, and 1 mm^3 isotropic voxels] were used to obtain high-resolution structural MRI images. Resting-state functional MRI scans were acquired with an echo-planar sequence (TR = 2,400 ms, FA = 80°, total of 210 volumes). The subjects were intended to close their eyes and rest and relax quietly. Functional images were preprocessed by data processing assistant for resting-state fMRI (DPARSF)[1] and Statistical Parametric Mapping (SPM12)[2] on the MATLAB r2018b platform as follows: (1) converting DICOM to NIFTI; (2) deleting the first 10 time points; (3) Slice timing correction; (4) Segmentation and realignment; (5) Regression of nuisance covariates (including white matter, cerebrospinal fluid, and Friston's 24 parameters of head motion); (6) Spatial normalization to Montreal Neurological Institute (MNI) space by resampling to 3 mm × 3 mm × 3 mm by DARTEL; (7) Filtering ($0.01 < f < 0.08$ Hz). Subjects with maximal translations exceeding 3 mm or rotations > 3° were excluded from the statistical analysis. Additionally, the mean frame-wise displacement (FD) (Jenkinson et al., 2002) was calculated and added as a covariate in the statistical analysis.

Statistical analysis

SPSS (Version 25.0. Armonk, NY, IBM Corp.) was used for clinical information analysis. Data normality was evaluated by the Shapiro–Wilk test. One-way analysis of variance, the Kruskal–Wallis test, two-sample *t*-test, or Wilcoxon Mann–Whitney test was utilized to compare the age, education experience, and clinical characteristics. Fisher's exact test was employed for comparisons of categorical variables and component ratios. $P < 0.05$ was considered statistically significant.

The regions showing significant ReHo differences between FOG converters and non-converters were defined as regions of interest (ROI), which were chosen as the seeds for FC analysis. ReHo and FC data were spatially smoothed using a 6 mm full-width at half-maximum Gaussian kernel. An analysis of covariance (ANCOVA) was used to explore the ReHo and FC differences among the three groups with mean FD as the covariate. ReHo and FC results were, respectively corrected by AlphaSim (voxel $P < 0.005$ and cluster $P < 0.01$) and Gaussian random field correction (GRF) method (voxel level $P < 0.001$ and cluster level $P < 0.05$) for multiple comparisons. Effective ReHo and FC values of clusters with significant differences among groups were extracted, followed by *post-hoc* Bonferroni test, and ReHo values were correlated with clinical variables via Pearson's correlation analysis.

Finally, the logistic regression model was used, including all MRI variables (i.e., ReHo and FC data) and clinical features with significant differences between groups at baseline. Univariate analysis was used to prove the influence of different factors on FOG conversion. We further excluded the possibility of collinearity and $P > 0.01$ factors in the univariable logistic analysis. Receiver operating characteristic (ROC) curve analysis was used to determine the best FOG prediction model.

Results

Demographic characteristics

A total of 17 FOG non-converters, 16 FOG converters, and 16 HCs were analyzed. The onset of PD patients included in our study was mostly laterality, with the right side being dominant in 63.6% of cases, and no difference was detected between the two groups with respect to age, gender, education year, dominant hand, and MoCA scores ($P > 0.05$). The rated values of H&Y, LEDD, ESS, GDS, RBDSQ, STAI, and tremor scores had no difference between converters and non-converters ($P > 0.05$), while MDS-UPDRS III, PIGD and SCOPA-AUT scores differed significantly across groups ($P < 0.05$) (**Table 1**).

ReHo values

The ReHo values of PD-FOG converter, non-converter, and HC groups differed significantly in the following locations: bilateral medial superior frontal gyrus (SFGmed), left amygdala/olfactory cortex/putamen (AMYG/OLF/PUT) and left supplementary motor area/paracentral lobule (SMA/PCL) (**Table 2**; **Figure 1**). Compared to PD-FOG non-converter group, the converter group showed decreased ReHo in the bilateral SFGmed, left OLF/PUT/AMYG ($P < 0.01$) (**Table 2**; **Figures 2A, B**), while increased ReHo in the left SMA/PCL ($P < 0.001$) (**Table 2**; **Figure 2C**). Compared to the HC group, the FOG converter group displayed decreased ReHo in the bilateral SFGmed ($P < 0.01$), left OLF/PUT/AMYG ($P < 0.001$) (**Table 2**; **Figures 2A, B**), while increased ReHo in the left SMA/PCL ($P < 0.05$) (**Table 2**; **Figure 2C**).

Correlation analysis

In PD-FOG converter group, the PIGD score was negatively correlated with the ReHo value in the bilateral SFGmed ($r = -0.547$,

1 http://www.restfmri.net/forum/dparsf
2 http://www.fil.ion.ucl.ac.uk/spm

TABLE 1 Demographic and clinical characteristics.

	FOG non-converters (n = 17)	FOG converters (n = 16)	HCs (n = 16)	P-value
Future FOG (Yes/No)	NO	YES	NA	<0.001
% Right-handed	88.2%	93.8%	87.5%	>0.05[a]
Age (years)	60.65 ± 9.33	63.34 ± 7.72	62.88 ± 9.03	0.640[b]
Gender (M/F)	11/6	11/5	13/3	0.624[a]
Education (year)	14.59 ± 3.02	15.75 ± 1.73	16.31 ± 1.85	0.161[b]
MoCA	28.00 (25.00, 30.00)	26.50 (24.25, 28.75)	28.00 (26.25, 28.75)	0.533[c]
Duration (months)	27.43 (26.23, 29.20)	27.40 (25.95, 29.88)	NA	0.885[d]
% Dominant side (right)	52.9%	75.0%	NA	0.141[a]
MDS-UPDRS III	15.76 ± 7.61	24.31 ± 11.03	NA	0.014[e]
PIGD	0.50 ± 0.55	1.24 ± 0.65	NA	0.001[e]
Tremor	4.82 ± 4.39	4.94 ± 4.28	NA	0.940[e]
H-Y stage	2.0 (1.0, 2.0)	2.0 (2.0, 2.0)	NA	0.090[d]
LEDD, mg	429.70 ± 222.07	505.70 ± 293.99	NA	0.407[e]
ESS	6.94 ± 3.91	8.13 ± 4.69	NA	0.436[e]
GDS	1.37 ± 0.87	1.54 ± 0.69	NA	0.543[e]
RBDSQ	1.89 ± 0.67	2.09 ± 0.82	NA	0.453[e]
STAI	8.04 ± 1.35	8.30 ± 0.97	NA	0.521[e]
SCOPA-AUT	2.98 ± 0.94	3.72 ± 0.97	NA	0.033[e]

HCs, healthy controls; MoCA, Montreal Cognitive Assessment; MDS-UPDRS, movement disorders society unified Parkinson's Disease rating scale; FOG, freezing of gait; H&Y, hoehn and yahr stage; LEDD, levodopa equivalent daily dose; GDS, geriatric depression scale score; ESS, epworth sleepiness scale score; RBDSQ, rem sleep behavior disorder questionnaire score; STAI, State-Trait anxiety inventory; SCOPA-AUT, scale for outcomes in Parkinson's Disease-Autonomic; Dominant side, side most affected at PD symptom onset; PIGD, postural instability and gait difficulty score; NA, not applicable. $P < 0.05$ was considered significant. [a]By Fisher's exact test. [b]By One-way analysis of variance. [c]By Kruskal-Wallis H test. [d]By Mann-Whitney U test. [e]By two-sample t-test.

TABLE 2 ReHo differences among the three groups.

AAL regions	Number of voxels	Peak MNI coordinates			F-value
		x	y	z	
Cluster 1					
SFGmed.L	30	3	54	27	12.104
SFGmed.R	21				
Cluster 2					
SMA.L	15	−18	−12	60	10.055
PCL.L	9				
Cluster 3					
OLF.L	15	−18	6	−15	14.025
PUT.L	12				
AMYG.L	10				

SFGmed.L, left medial superior frontal gyrus; SFGmed.R, right medial superior frontal gyrus; SMA.L, left supplementary motor area, PCL.L, left paracentral lobule. OLF.L, left olfactory cortex; PUT.L, left putamen; AMYG.L, left amygdala. AAL, automated anatomical labeling.

$P = 0.028$). Meanwhile, the ReHo value in the left OLF/PUT/AMYG was negatively correlated with SCOPA ($r = -0.535$, $P = 0.033$) and STAI scores ($r = -0.536$, $P = 0.032$). In contrast, a significantly positive correlation was found between the RBDSQ and the ReHo value in the left SMA/PCL ($r = 0.759$, $P = 0.001$) (Figure 2D).

FC analysis

When the ROI was set to the left OLF/PUT/AMYG, three groups showed significantly different FC between left superior temporal gyrus/middle temporal gyrus/temporal pole/rolandic operculum (STG/MTG/TP/Rol), right fusiform gyrus/lingual gyrus (FFG/LING) and left OLF/PUT/AMYG (Table 3; Figure 3A). When the ROI was set to the left SMA/PCL, three groups showed significantly different FC between left middle frontal gyrus (MFG) and left SMA/PCL (Table 3; Figure 3D). When the ROI was set to the SFGmed, no cluster survived after GRF correction.

Compared to FOG non-converter group, the converter group showed decreased FC between left STG/MTG/TP/Rol ($P < 0.01$) (Table 3; Figure 3B) and left OLF/PUT/AMYG, left MFG ($P < 0.05$) and left SMA/PCL (Table 3; Figure 3E).

Compared to HC group, the FOG converter group showed decreased FC between left STG/MTG/TP/Rol ($P < 0.001$) (Table 3; Figure 3B), right FFG/LING ($P < 0.001$) (Table 3; Figure 3C) and left OLF/PUT/AMYG, left MFG ($P < 0.001$) and left SMA/PCL (Table 3; Figure 3E).

Compared to HC group, the FOG non-converter group showed decreased FC between right FFG/LING ($P < 0.01$) (Table 3; Figure 3C) and left OLF/PUT/AMYG, left MFG ($P < 0.001$) and left SMA/PCL (Table 3; Figure 3E).

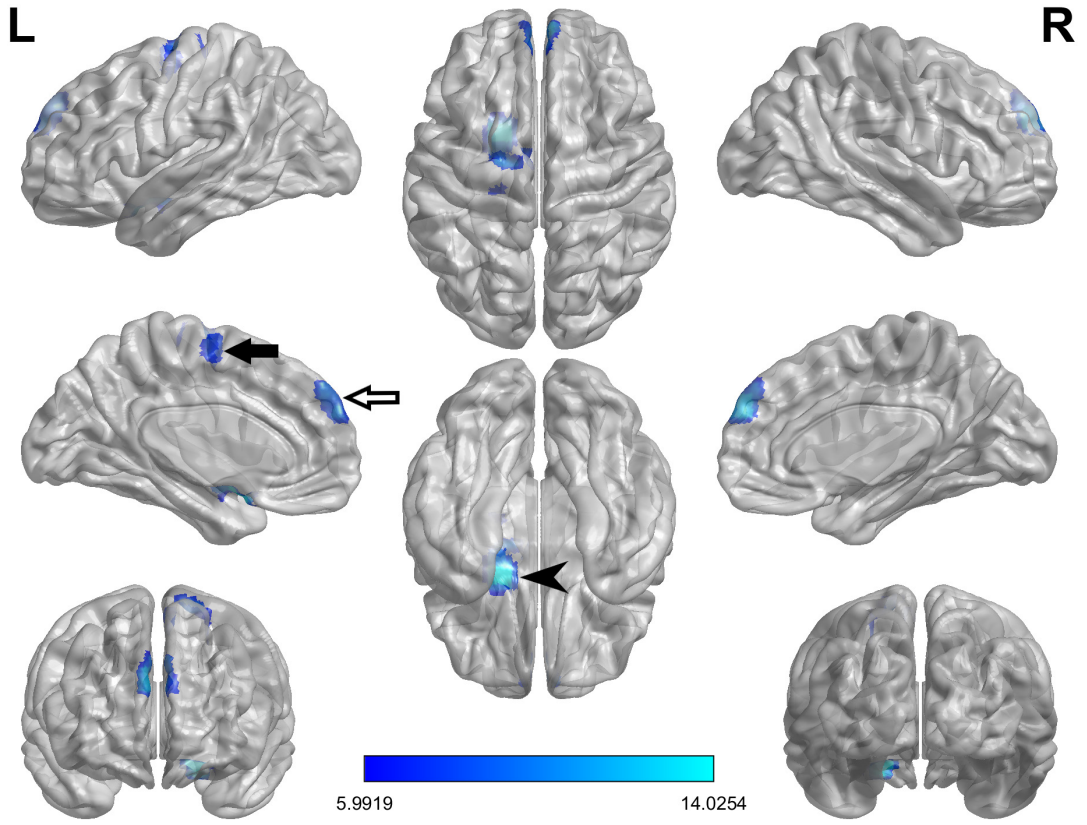

FIGURE 1
The ANCOVA test reveals significant differences in the ReHo index among FOG converter, FOG non-converter, and HC groups in the following regions: bilateral SFGmed (white arrow), left AMYG/PUT/OLF (black arrowhead) and left SMA/PCL (black arrow).

ReHo and FC data as predictors of FOG

The results of the logistic regression analyses are presented in Table 4. In the univariable logistic regression analyses, the decreased ReHo value in the SFGmed [odds ratio (OR): 0.76, 95% confidence interval (CI): 0.62–0.93, P = 0.007], left OLF/PUT/AMYG (OR: 0.46, 95% CI: 0.27–0.78, P = 0.004) and the increased ReHo value in the left SMA (OR: 1.61, 95% CI: 1.17–2.22, P = 0.003) were significantly associated with FOG conversion. Decreased FC between left OLF/PUT/AMYG and left STG/MTG/TP/Rol (OR: 0.11, 95% CI: 0.03–0.49, P = 0.004), left SMA/PCL and left MFG (OR: 0.18, 95% CI: 0.04–0.80, P = 0.024) were related to FOG conversion. In addition, MDS-UDPRS III (OR: 1.01, 95% CI: 1.00–1.02, P = 0.025), PIGD (OR: 1.23, 95% CI: 1.06–1.42, P = 0.007), and SCOPA-AUT score (OR: 1.09, 95% CI: 1.00–1.20, P = 0.047) were predictive of FOG conversion.

TABLE 3 FC differences among the three groups.

Brain regions (AAL)	Number of voxels	Peak MNI coordinates			*F*-value
		x	*y*	*z*	
left SMA/PCL					
MFG.L	47	−42	21	45	5.4072
left OLF/PUT/AMYG					
STG.L	68	−51	3	−6	3.9717
TPOsup.L	15				
MTG.L	14				
Rol.L	3				
FFG.R	89	27	−45	−12	3.8388
LING.R	25				

SMA, supplementary motor area; PCL, paracentral lobule; OLF, olfactory cortex; PUT, putamen; AMYG, amygdala; MFG.L, left middle frontal gyrus; STG.L, left superior temporal gyrus; TPOsup.L, left temporal pole (TP): superior temporal gyrus; MTG.L, left middle temporal gyrus; Rol.L, left rolandic operculum, FFG.R, right fusiform gyrus; LING.R, right lingual gyrus. AAL, automated anatomical labeling.

Predictive value of clinical and ReHo data

Stepwise selected by logistic regression, the final best prediction model for FOG conversion included PIGD score (OR: 1.31, 95% CI: 1.04–1.64, P = 0.021) and ReHo value in basal ganglia and limbic area (i.e., left OLF/PUT/AMYG) (OR: 0.39, 95% CI: 0.18–0.85, P = 0.017). The ROC curve analysis showed that the combined model of ReHo value and clinical variable distinguished between PD-FOG converters and non-converters [area under curve (AUC) = 0.94, 95% CI: 0.87–1], with a sensitivity of 87.5% and specificity of 94.1% (Figure 4).

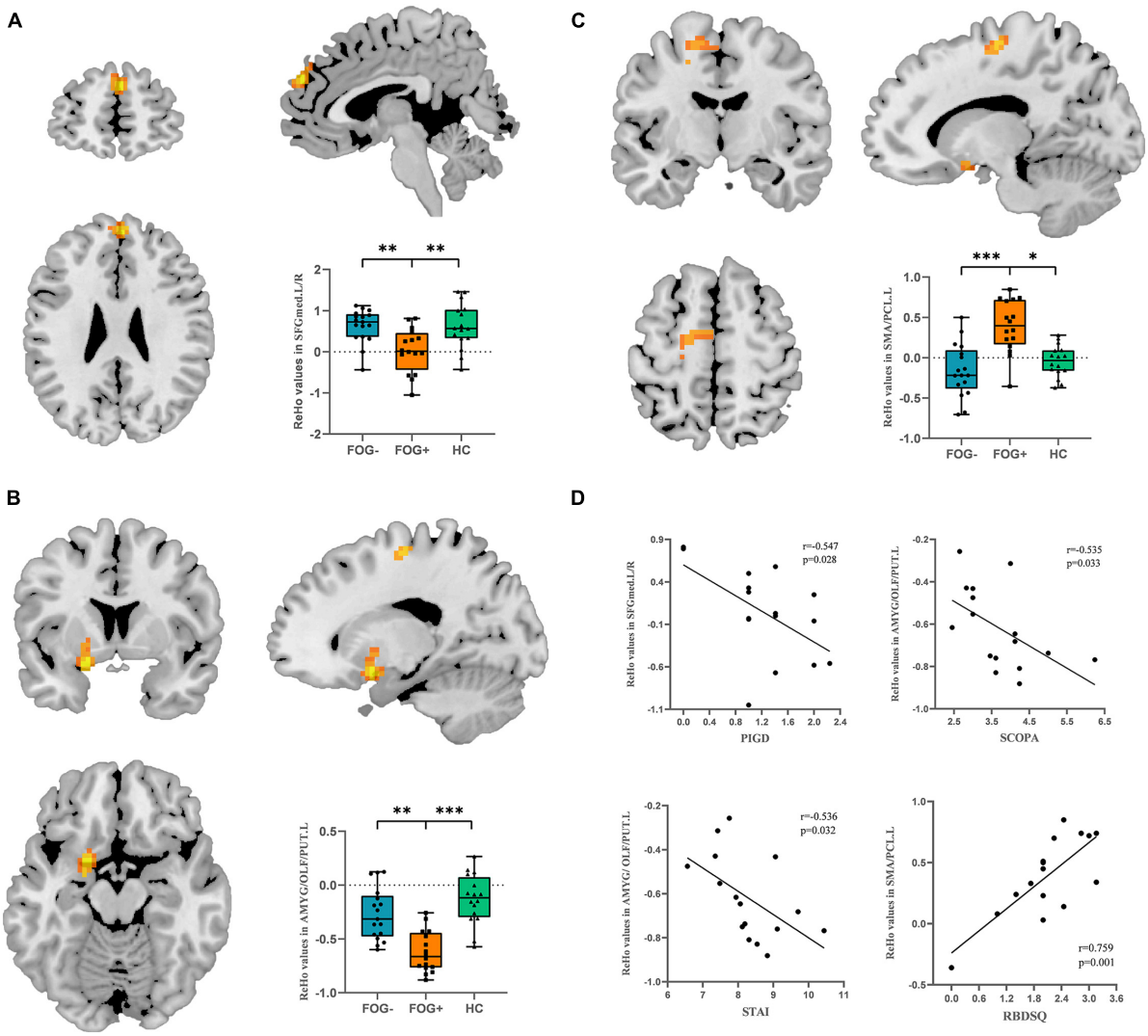

FIGURE 2
Post hoc analysis of ReHo differences. **(A)** Bilateral SFGmed demonstrated hypoactivity in FOG converters compared to FOG non-converter and HC groups. **(B)** Left OLF/PUT/AMYG demonstrated hypoactivity in FOG converters compared to FOG non-converter and HC groups. **(C)** Left SMA/PCL demonstrated significant hyperactivity in FOG converters compared to FOG non-converter and HC groups (Bonferroni corrected, $*P < 0.05$, $**P < 0.01$, $***P < 0.001$). **(D)** Correlation analysis between STAI, SCOPA scores and ReHo value in the left OLF/PUT/AMYG, RBDSQ and ReHo value in the left SMA/PCL ($P < 0.05$), PIGD score and ReHo value in the bilateral SFGmed. FOG+, FOG converters; FOG−, FOG non-converters.

Discussion

In this study, we analyzed the differences in MRI variables and clinical features of FOG converters and non-converters in PD patients, as well as their values in identifying FOG converters at the follow-up. The current results supported that cognitive control cortex, basal ganglia, and limbic area dysfunction may be related to PD-FOG conversion, and the decreased ReHo value in basal ganglia and limbic area, combined with PIGD score is the best initial predictive model.

Significantly decreased ReHo value within left putamen in the FOG converter group may suggest that such regional impairment contributes to the pathophysiology of FOG conversion in this study. In PD patients, several studies (Goldstein et al., 2017; Kish et al., 2017) have reported dopamine deficiency in the striatum and found that the most severely affected region was putamen. The putamen was suggested to be involved in self-initiated movement and its dysfunction was shown to relate to bradykinesia (Rodriguez-Oroz et al., 2009; Prodoehl et al., 2010; Dirnberger and Jahanshahi, 2013). A positron emission tomography (PET) study has also reported a relationship between FOG and dysfunction within the putamen; FOG was correlated with reduced F-Dopa uptake in the putamen of the right hemisphere (Pikstra et al., 2016). FOG converters also showed increased ReHo value in the left SMA/PCL and decreased FC between left SMA/PCL and MFG compared to non-converters. MFG, a critical brain region of the cognitive control network, is responsible for executive functions in the cognitive control network (MacDonald et al., 2000), while SMA plays a crucial role in the early preparation of voluntary movements (Cunnington et al., 2002). Hence, we assumed that neural activation can be expected in cortical motor regions as a compensation strategy for basal ganglia

dysfunction and abnormal functional connectivity in the prefrontal cortex (Sabatini et al., 2000; Eckert et al., 2006; Redgrave et al., 2010). These findings were in keeping with the decreased activation of putamen and increased activation of cortical motor regions in FOG during motor block (Wu and Hallett, 2005; Vercruysse et al., 2014), as insufficient compensatory brain activity which might result in difficulties in stride length regulation, ultimately leading to FOG. In contrast to our findings, Zhou et al. (2018) demonstrated that PD-FOG patients had reduced ReHo value in the left SMA. We consider it might be due to the inadequate compensatory ability of the motor cortex in the late stage of FOG; it may also be due to the formation of indirect basal ganglia pathways leading to subcortical overactivation, thus inhibiting cortical activity. Furthermore, we also discovered that RBDSQ was positively correlated with the ReHo value of left SMA in FOG converters. Similar to our results, during REM sleep, compared to the eyes closed awake condition, activity was higher in SMA in a magnetoencephalographic tomography (Ioannides et al., 2004). One reason for this could be the significant overlap between functional neuroanatomy that controls REM sleep, arousal and locomotion as well as multiple neural circuits affected in RBD and PD with FOG. However, the pathophysiology between REM and FOG also remains unclear; thus, more research is needed in this area.

The current findings indicated that the dysfunction in limbic brain region may be a risk factor for FOG conversion. Olfactory cortex is a significant part of the limbic system. Microstructural white matter reductions are present in the central olfactory system of early-stage PD patients (Ibarretxe-Bilbao et al., 2010), and additionally compared to PD patients without FOG, FOG patients had more severe olfactory deficits (Glover et al., 2021). In Alzheimer's disease, olfaction is a strong predictor of cognitive decline, with atrophy in the amygdala, hippocampus, and olfactory cortex (Vasavada et al., 2015; MacDonald et al., 2018; Lian et al., 2019). In this study, the olfactory cortex in FOG converters exhibited a reduced ReHo expression compared to non-converters, which may be related to the production of cognitive load and a decline in attention control. Decreased FC of left basal ganglia and limbic area with left temporal cortex including left STG, MTG, and TP was observed in this study as well. Included in the default-mode network (DMN), the temporal lobe is related to memory, visual-spatial ability, and the ability to read the social attention cues of others (Rektorova et al., 2014). Mild cognitive impairment (MCI) patients had atrophy and reduced ALFF value of the temporal cortex (Pereira et al., 2012; Gao et al., 2016). This result is attributed to a link between cognitive impairment and degeneration or inactivation in the temporal gyrus. FOG patients seem to have difficulty in execution and acquisition of automation compared to non-FOG patients (Hackney and Earhart, 2010; Spildooren et al., 2010; Vandenbossche et al., 2013). Loss of automation indicated significant pressure on cognitive resources (Vandenbossche et al., 2012). Perhaps, this might explain that FOG patients use the same attention resources to control their mood. Thus, due to executive dysfunction, FOG episodes occur when cognitive resources overload (Eysenck et al., 2007). Furthermore, served

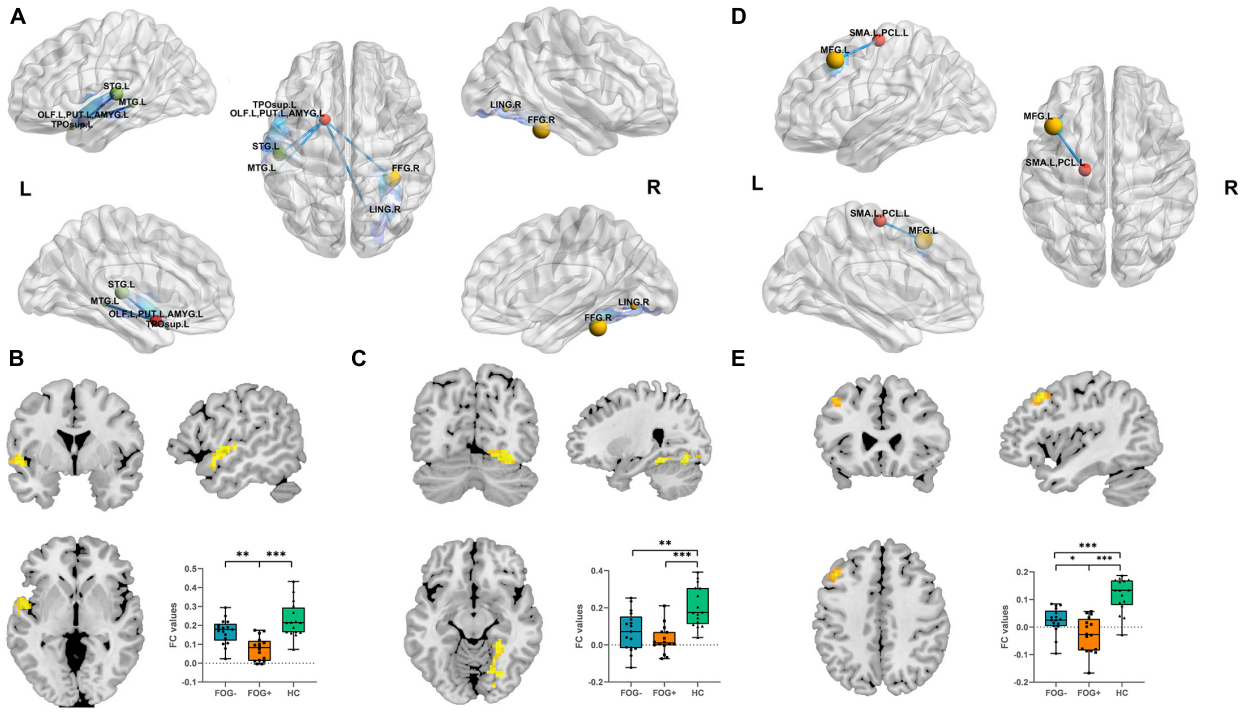

FIGURE 3
(A) Altered left OLF/PUT/AMYG FC value regions among three groups. **(B)** FC results among three groups with respect to left OLF/PUT/AMYG and left STG/MTG/TP/RoI. **(C)** FC results among the three groups within left OLF/PUT/AMYG and right FFG/LING. **(D)** Altered left SMA/PCL FC value regions among the three groups. **(E)** FC results among the three groups within left SMA/PCL and MFG (Bonferroni-corrected, $^{*}P < 0.05$, $^{**}P < 0.01$, $^{***}P < 0.001$). FOG+, FOG converters; FOG−, FOG non-converters.

TABLE 4 Logistic regression analysis of clinical and MR data.

Variables	Univariate analysis		Multivariate analysis	
	OR (95% CI)	*P*	OR (95% CI)	*P*
	OR (95% CI)	P	OR (95% CI)	P
ReHo[1]	0.76 (0.62–0.93)	0.007		
ReHo[2]	0.46 (0.27–0.78)	0.004	0.39 (0.18–0.85)	0.017
ReHo[3]	1.61 (1.17–2.22)	0.003		
FC[1]	0.11 (0.03–0.49)	0.004		
FC[2]	0.18 (0.04–0.80)	0.024		
MDS-UPDRS III	1.01 (1.00–1.02)	0.025		
PIGD	1.23 (1.06–1.42)	0.007	1.31 (1.04–1.64)	0.021
SCOPA	1.09 (1.00–1.20)	0.047		
Tremor	1.00 (0.99–1.02)	0.938		
GDS	1.03 (0.94–1.13)	0.531		
RBDSQ	1.04 (0.94–1.14)	0.441		
STAI	1.02 (0.96–1.08)	0.510		

ReHo[1], ReHo value in bilateral SFGmed; ReHo[2], ReHo value in left OLF/PUT/AMYG; ReHo[3], ReHo value in left SMA/PCL; FC[1], FC value between left OLF/PUT/AMYG and left STG/MTG/TP/Rol; FC[2], FC value between left SMA/PCL and MFG. $P < 0.05$ was considered significant.

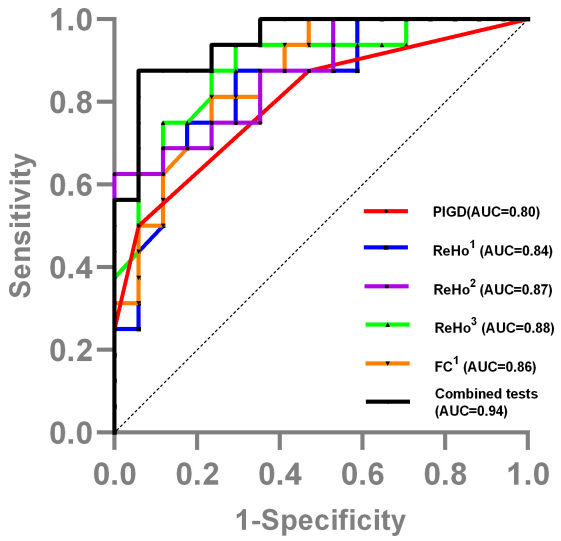

FIGURE 4
The ROC curve showed the value of clinical and MRI data in distinguishing PD-FOG converters and non-converters. ReHo[1], ReHo value in bilateral SFGmed; ReHo[2], ReHo value in left OLF/PUT/AMYG; ReHo[3], ReHo value in left SMA/PCL; FC[1], FC value between left OLF/PUT/AMYG and left STG/MTG/TP/Rol; Combined tests, the tests combined the PIGD score with the ReHo value in basal ganglia and limbic area.

as the subcortical hub of the limbic system, amygdala controlled both the emotional behavior and the autonomic nervous system (Ulrich-Lai and Herman, 2009). Previous studies have shown that there were higher heart rates and gastrointestinal autonomic dysfunction during FOG episodes (Maidan et al., 2010; Kwon et al., 2021). Meanwhile, emotional states have been shown to affect the motor control of gait (Naugle et al., 2011; Kyrdalen et al., 2019), and volume atrophy and hypoactivation in the amygdala have been found associated with major depressive disorder (Xia et al., 2004; Sheng et al., 2014; Li et al., 2022). Our study further supports the correlation between amygdala dysfunction and FOG conversion.

Notably, our findings suggested that FOG converters exhibited a negative correlation between the PIGD score and decreased ReHo value in the SFGmed. SFGmed belongs to the medial prefrontal lobe (mPFC) and has differential associations with executive function and attention allocation, value-based decision-making, and emotion regulation (DiGirolamo et al., 2001; Rushworth et al., 2002; Ragozzino, 2007). Hypoperfusion and reduced activation in bilateral mPFC has been reported in PD patients with difficulty initiating motor movement (Playford et al., 1992; Matsui et al., 2005). Gray matter atrophy in the mPFC has also been observed in PD patients with dyskinesia (Dagan et al., 2017; Zheng et al., 2022). Thus, dysfunction in mPFC could help reveal the neural pathophysiology related to the FOG. In our study, with no significant difference between the two study groups, FOG converters had higher LEDD and non-motor symptom scores; combined with higher PIGD scores, this result may indicate a low response to medication in FOG converters. PD patients with higher PIGD scores also had more severe motor and non-motor symptoms, rapid disease progression, and poorer experiences of daily living (Jankovic et al., 1990; Rajput et al., 2009); these phenomena might be due to the formation of Lewy bodies and significant amyloid plaque load in the mPFC (Selikhova et al., 2009).

This study has the significant advantage of combining MRI variables and clinical features, suggesting that basal ganglia and limbic area dysfunction combined with a higher PIGD score resulted in the highest predictive model accuracy (AUC = 0.94). Although with valuable findings, there are still some limitations in this study. First, the incidence of PD patients included in our study is mainly on the right side, which may be the reason why most abnormal brain regions and functional connections occurred on the left side. Second, there are a limited number of participants in our study. Therefore, more variables could not be added to the regression model, and thus, our findings should be interpreted with caution. In addition, we lacked a detailed gait assessment, such as gait speed, stride length, and other features to assess the motor status, which provided limited clinical data. However, our above study is prospective, and the results are similar to previous studies. Thus, our current grouping and sample size can explain the results, but the conclusions require a larger sample size and resampling by replication to eliminate the confounding factors and further explore their authenticity.

Conclusion

The current results supported that functional MRI could be considered a useful tool to identify FOG conversion in PD: the

basal ganglia and limbic area dysfunction could represent a marker of FOG conversion, together with the PIGD score. The important role of functional MRI to monitor disease conversion and to detect brain changes might precede the conversion of specific clinical features such as FOG. Thus, we hope that these abnormalities lay a foundation for improvement in early clinical early screening.

Data availability statement

The original contributions presented in this study are included in the article/supplementary material, further inquiries can be directed to the corresponding authors.

Ethics statement

Written informed consent was obtained from the individual(s) for the publication of any potentially identifiable images or data included in this article.

Author contributions

YB analyzed the data, plotted tables, and wrote the manuscript. YY and CZ re-analyzed the data and checked the figures. JL provided us with clinical scale analyses. EW and GF designed and organized the study. All authors contributed to the manuscript revision and read and approved the submitted version.

Funding

This work was partially supported by the Suzhou Municipal Science and Technology Project (Grant No. SKY2022011), the Elderly Health Research Project of Jiangsu Province (Grant No. LKZ2022009), and the Science and Technology Project for "Star of Medical Imaging" of Suzhou Medical Association (Grant No. 2022YX-M03).

Conflict of interest

The authors declare that the research was conducted in the absence of any commercial or financial relationships that could be construed as a potential conflict of interest.

Publisher's note

All claims expressed in this article are solely those of the authors and do not necessarily represent those of their affiliated organizations, or those of the publisher, the editors and the reviewers. Any product that may be evaluated in this article, or claim that may be made by its manufacturer, is not guaranteed or endorsed by the publisher.

References

Canu, E., Agosta, F., Sarasso, E., Volontè, M. A., Basaia, S., Stojkovic, T., et al. (2015). Brain structural and functional connectivity in Parkinson's disease with freezing of gait. *Hum. Brain Mapp.* 36, 5064–5078. doi: 10.1002/hbm.22994

Cunnington, R., Windischberger, C., Deecke, L., and Moser, E. (2002). The preparation and execution of self-initiated and externally-triggered movement: A study of event-related fMRI. *NeuroImage* 15, 373–385.

Dadar, M., Miyasaki, J., Duchesne, S., and Camicioli, R. (2021). White matter hyperintensities mediate the impact of amyloid ß on future freezing of gait in Parkinson's disease. *Parkinsonism Relat. Disord.* 85, 95–101. doi: 10.1016/j.parkreldis.2021.02.031

Dagan, M., Herman, T., Mirelman, A., Giladi, N., and Hausdorff, J. M. (2017). The role of the prefrontal cortex in freezing of gait in Parkinson's disease: Insights from a deep repetitive transcranial magnetic stimulation exploratory study. *Exp. Brain Res.* 235, 2463–2472. doi: 10.1007/s00221-017-4981-9

D'Cruz, N., Vervoort, G., Chalavi, S., Dijkstra, B. W., Gilat, M., and Nieuwboer, A. (2021). Thalamic morphology predicts the onset of freezing of gait in Parkinson's disease. *NPJ Parkinsons Dis.* 7:20. doi: 10.1038/s41531-021-00163-0

DiGirolamo, G. J., Kramer, A. F., Barad, V., Cepeda, N. J., Weissman, D. H., Milham, M. P., et al. (2001). General and task-specific frontal lobe recruitment in older adults during executive processes: A fMRI investigation of task-switching. *Neuroreport* 12, 2065–2071.

Dirnberger, G., and Jahanshahi, M. (2013). Executive dysfunction in Parkinson's disease: A review. *J. Neuropsychol.* 7, 193–224. doi: 10.1111/jnp.12028

Eckert, T., Peschel, T., Heinze, H. J., and Rotte, M. (2006). Increased pre-SMA activation in early PD patients during simple self-initiated hand movements. *J. Neurol.* 253, 199–207.

Eysenck, M. W., Derakshan, N., Santos, R., and Calvo, M. G. (2007). Anxiety and cognitive performance: Attentional control theory. *Emotion (Washington, D.C.)* 7, 336–353.

Gao, L., Wu, X., Zhang, J., Chan, P., and Wu, T. (2016). Brain activity in Parkinson's disease patients with mild cognitive impairment. *Sci. Bull.* 61, 1876–1883.

Giladi, N., Kao, R., and Fahn, S. (1997). Freezing phenomenon in patients with parkinsonian syndromes. *Mov. Disord.* 12, 302–305.

Giladi, N., Treves, T. A., Simon, E. S., Shabtai, H., Orlov, Y., Kandinov, B., et al. (2001). Freezing of gait in patients with advanced Parkinson's disease. *J. Neural Transm. (Vienna, Austria: 1996)* 108, 53–61.

Gilat, M., Ehgoetz Martens, K. A., Miranda-Domínguez, O., Arpan, I., Shine, J. M., Mancini, M., et al. (2018). Dysfunctional limbic circuitry underlying freezing of gait in Parkinson's disease. *Neuroscience* 374, 119–132. doi: 10.1016/j.neuroscience.2018.01.044

Glover, A., Pillai, L., Dhall, R., and Virmani, T. (2021). Olfactory deficits in the freezing of gait phenotype of Parkinson's disease. *Front. Neurol.* 12:656379. doi: 10.3389/fneur.2021.656379

Goldstein, D. S., Sullivan, P., Holmes, C., Mash, D. C., Kopin, I. J., and Sharabi, Y. (2017). Determinants of denervation-independent depletion of putamen dopamine in Parkinson's disease and multiple system atrophy. *Parkinsonism Relat. Disord.* 35, 88–91. doi: 10.1016/j.parkreldis.2016.12.011

Hackney, M. E., and Earhart, G. M. (2010). The effects of a secondary task on forward and backward walking in Parkinson's disease. *Neurorehabil. Neural Repair* 24, 97–106. doi: 10.1177/1545968309341061

Ibarretxe-Bilbao, N., Junque, C., Marti, M.-J., Valldeoriola, F., Vendrell, P., Bargallo, N., et al. (2010). Olfactory impairment in Parkinson's disease and white matter abnormalities in central olfactory areas: A voxel-based diffusion tensor imaging study. *Mov. Disord.* 25, 1888–1894. doi: 10.1002/mds.23208

Ioannides, A. A., Corsi-Cabrera, M., Fenwick, P. B. C., del Rio Portilla, Y., Laskaris, N. A., Khurshudyan, A., et al. (2004). MEG tomography of human cortex and brainstem activity in waking and REM sleep saccades. *Cereb. Cortex (New York, N.Y. 1991)* 14, 56–72.

Jankovic, J., McDermott, M., Carter, J., Gauthier, S., Goetz, C., Golbe, L., et al. (1990). Variable expression of Parkinson's disease: A base-line analysis of the DATATOP cohort. The Parkinson Study Group. *Neurology* 40, 1529–1534.

Jenkinson, M., Bannister, P., Brady, M., and Smith, S. (2002). Improved optimization for the robust and accurate linear registration and motion correction of brain images. *NeuroImage* 17, 825–841.

Kim, R., Lee, J., Kim, H.-J., Kim, A., Jang, M., Jeon, B., et al. (2019). CSF β-amyloid42 and risk of freezing of gait in early Parkinson disease. *Neurology* 92, e40–e47. doi: 10.1212/WNL.0000000000006692

Kish, S. J., Boileau, I., Callaghan, R. C., and Tong, J. (2017). Brain dopamine neurone 'damage': Methamphetamine users vs. Parkinson's disease - a critical assessment of the evidence. *Eur. J. Neurosci.* 45, 58–66. doi: 10.1111/ejn.13363

Kostic, V. S., Agosta, F., Pievani, M., Stefanova, E., Jecmenica-Lukic, M., Scarale, A., et al. (2012). Pattern of brain tissue loss associated with freezing of gait in Parkinson disease. *Neurology* 78, 409–416. doi: 10.1212/WNL.0b013e318245d23c

Kwon, K.-Y., Park, S., Lee, E. J., Lee, M., and Ju, H. (2021). Association of fall risk factors and non-motor symptoms in patients with early Parkinson's disease. *Sci. Rep.* 11:5171. doi: 10.1038/s41598-021-84720-w

Kyrdalen, I. L., Thingstad, P., Sandvik, L., and Ormstad, H. (2019). Associations between gait speed and well-known fall risk factors among community-dwelling older adults. *Physiother. Res. Int.* 24:e1743. doi: 10.1002/pri.1743

Li, X., Chen, X., Zhou, Y., Dai, L., Cui, L.-B., Yu, R., et al. (2022). Altered regional homogeneity and amplitude of low-frequency fluctuations induced by electroconvulsive therapy for adolescents with depression and suicidal ideation. *Brain Sci.* 12:1121. doi: 10.3390/brainsci12091121

Lian, T.-H., Zhu, W.-L., Li, S.-W., Liu, Y.-O., Guo, P., Zuo, L.-J., et al. (2019). Clinical, structural, and neuropathological features of olfactory dysfunction in patients with Alzheimer's disease. *J. Alzheimers Dis. JAD* 70, 413–423. doi: 10.3233/JAD-181217

MacDonald, A. W., Cohen, J. D., Stenger, V. A., and Carter, C. S. (2000). Dissociating the role of the dorsolateral prefrontal and anterior cingulate cortex in cognitive control. *Science (New York, N.Y.)* 288, 1835–1838.

MacDonald, S. W. S., Keller, C. J. C., Brewster, P. W. H., and Dixon, R. A. (2018). Contrasting olfaction, vision, and audition as predictors of cognitive change and impairment in non-demented older adults. *Neuropsychology* 32, 450–460. doi: 10.1037/neu0000439

Maidan, I., Plotnik, M., Mirelman, A., Weiss, A., Giladi, N., and Hausdorff, J. M. (2010). Heart rate changes during freezing of gait in patients with Parkinson's disease. *Mov. Disord.* 25, 2346–2354. doi: 10.1002/mds.23280

Matsui, H., Udaka, F., Miyoshi, T., Hara, N., Tamaura, A., Oda, M., et al. (2005). Three-dimensional stereotactic surface projection study of freezing of gait and brain perfusion image in Parkinson's disease. *Mov. Disord.* 20, 1272–1277.

Naugle, K. M., Hass, C. J., Joyner, J., Coombes, S. A., and Janelle, C. M. (2011). Emotional state affects the initiation of forward gait. *Emotion (Washington, D.C.)* 11, 267–277. doi: 10.1037/a0022577

Parkinson Progression Marker Initiative (2011). The Parkinson Progression Marker Initiative (PPMI). *Prog. Neurobiol.* 95, 629–635. doi: 10.1016/j.pneurobio.2011.09.005

Pereira, J. B., Ibarretxe-Bilbao, N., Marti, M.-J., Compta, Y., Junqué, C., Bargallo, N., et al. (2012). Assessment of cortical degeneration in patients with Parkinson's disease by voxel-based morphometry, cortical folding, and cortical thickness. *Hum. Brain Mapp.* 33, 2521–2534. doi: 10.1002/hbm.21378

Perez-Lloret, S., Negre-Pages, L., Damier, P., Delval, A., Derkinderen, P., Destée, A., et al. (2014). Prevalence, determinants, and effect on quality of life of freezing of gait in Parkinson disease. *JAMA Neurol.* 71, 884–890. doi: 10.1001/jamaneurol.2014.753

Pikstra, A. R. A., van der Hoorn, A., Leenders, K. L., and de Jong, B. M. (2016). Relation of 18-F-Dopa PET with hypokinesia-rigidity, tremor and freezing in Parkinson's disease. *NeuroImage Clin.* 11, 68–72. doi: 10.1016/j.nicl.2016.01.010

Playford, E. D., Jenkins, I. H., Passingham, R. E., Nutt, J., Frackowiak, R. S., and Brooks, D. J. (1992). Impaired mesial frontal and putamen activation in Parkinson's disease: A positron emission tomography study. *Ann. Neurol.* 32, 151–161.

Prodoehl, J., Spraker, M., Corcos, D., Comella, C., and Vaillancourt, D. (2010). Blood oxygenation level-dependent activation in basal ganglia nuclei relates to specific symptoms in de novo Parkinson's disease. *Mov. Disord.* 25, 2035–2043. doi: 10.1002/mds.23360

Ragozzino, M. E. (2007). The contribution of the medial prefrontal cortex, orbitofrontal cortex, and dorsomedial striatum to behavioral flexibility. *Ann. N. Y. Acad. Sci.* 1121, 355–375.

Rajput, A. H., Voll, A., Rajput, M. L., Robinson, C. A., and Rajput, A. (2009). Course in Parkinson disease subtypes: A 39-year clinicopathologic study. *Neurology* 73, 206–212. doi: 10.1212/WNL.0b013e3181ae7af1

Redgrave, P., Rodriguez, M., Smith, Y., Rodriguez-Oroz, M. C., Lehericy, S., Bergman, H., et al. (2010). Goal-directed and habitual control in the basal ganglia: Implications for Parkinson's disease. *Nat. Rev. Neurosci.* 11, 760–772. doi: 10.1038/nrn2915

Rektorova, I., Biundo, R., Marecek, R., Weis, L., Aarsland, D., and Antonini, A. (2014). Grey matter changes in cognitively impaired Parkinson's disease patients. *PLoS One* 9:e85595. doi: 10.1371/journal.pone.0085595

Rodriguez-Oroz, M. C., Jahanshahi, M., Krack, P., Litvan, I., Macias, R., Bezard, E., et al. (2009). Initial clinical manifestations of Parkinson's disease: Features and pathophysiological mechanisms. *Lancet Neurol.* 8, 1128–1139. doi: 10.1016/S1474-4422(09)70293-5

Rushworth, M. F. S., Hadland, K. A., Paus, T., and Sipila, P. K. (2002). Role of the human medial frontal cortex in task switching: A combined fMRI and TMS study. *J. Neurophysiol.* 87, 2577–2592.

Sabatini, U., Boulanouar, K., Fabre, N., Martin, F., Carel, C., Colonnese, C., et al. (2000). Cortical motor reorganization in akinetic patients with Parkinson's disease: A functional MRI study. *Brain* 123(Pt 2), 394–403.

Sarasso, E., Basaia, S., Cividini, C., Stojkovic, T., Stankovic, I., Piramide, N., et al. (2022). MRI biomarkers of freezing of gait development in Parkinson's disease. *NPJ Parkinsons Dis.* 8:158. doi: 10.1038/s41531-022-00426-4

Selikhova, M., Williams, D. R., Kempster, P. A., Holton, J. L., Revesz, T., and Lees, A. J. (2009). A clinico-pathological study of subtypes in Parkinson's disease. *Brain* 132, 2947–2957. doi: 10.1093/brain/awp234

Sheng, K., Fang, W., Su, M., Li, R., Zou, D., Han, Y., et al. (2014). Altered spontaneous brain activity in patients with Parkinson's disease accompanied by depressive symptoms, as revealed by regional homogeneity and functional connectivity in the prefrontal-limbic system. *PLoS One* 9:e84705. doi: 10.1371/journal.pone.0084705

Shine, J. M., Matar, E., Ward, P. B., Bolitho, S. J., Gilat, M., Pearson, M., et al. (2013a). Exploring the cortical and subcortical functional magnetic resonance imaging changes associated with freezing in Parkinson's disease. *Brain* 136, 1204–1215. doi: 10.1093/brain/awt049

Shine, J. M., Matar, E., Ward, P. B., Frank, M. J., Moustafa, A. A., Pearson, M., et al. (2013b). Freezing of gait in Parkinson's disease is associated with functional decoupling between the cognitive control network and the basal ganglia. *Brain* 136, 3671–3681. doi: 10.1093/brain/awt272

Spildooren, J., Vercruysse, S., Desloovere, K., Vandenberghe, W., Kerckhofs, E., and Nieuwboer, A. (2010). Freezing of gait in Parkinson's disease: The impact of dual-tasking and turning. *Mov. Disord.* 25, 2563–2570. doi: 10.1002/mds.23327

Stebbins, G. T., Goetz, C. G., Burn, D. J., Jankovic, J., Khoo, T. K., and Tilley, B. C. (2013). How to identify tremor dominant and postural instability/gait difficulty groups with the movement disorder society unified Parkinson's disease rating scale: Comparison with the unified Parkinson's disease rating scale. *Mov. Disord.* 28, 668–670. doi: 10.1002/mds.25383

Tessitore, A., Amboni, M., Cirillo, G., Corbo, D., Picillo, M., Russo, A., et al. (2012). Regional gray matter atrophy in patients with Parkinson disease and freezing of gait. *AJNR Am. J. Neuroradiol.* 33, 1804–1809. doi: 10.3174/ajnr.A3066

Ulrich-Lai, Y. M., and Herman, J. P. (2009). Neural regulation of endocrine and autonomic stress responses. *Nat. Rev. Neurosci.* 10, 397–409. doi: 10.1038/nrn2647

Vandenbossche, J., Deroost, N., Soetens, E., Coomans, D., Spildooren, J., Vercruysse, S., et al. (2012). Freezing of gait in Parkinson's disease: Disturbances in automaticity and control. *Front. Hum. Neurosci.* 6:356. doi: 10.3389/fnhum.2012.00356

Vandenbossche, J., Deroost, N., Soetens, E., Coomans, D., Spildooren, J., Vercruysse, S., et al. (2013). Impaired implicit sequence learning in Parkinson's disease patients with freezing of gait. *Neuropsychology* 27, 28–36. doi: 10.1037/a0031278

Vasavada, M. M., Wang, J., Eslinger, P. J., Gill, D. J., Sun, X., Karunanayaka, P., et al. (2015). Olfactory cortex degeneration in Alzheimer's disease and mild cognitive impairment. *J. Alzheimers Dis. JAD* 45, 947–958. doi: 10.3233/JAD-141947

Vercruysse, S., Spildooren, J., Heremans, E., Wenderoth, N., Swinnen, S. P., Vandenberghe, W., et al. (2014). The neural correlates of upper limb motor blocks in Parkinson's disease and their relation to freezing of gait. *Cereb. Cortex (New York, N.Y. 1991)* 24, 3154–3166. doi: 10.1093/cercor/bht170

Wu, T., and Hallett, M. (2005). A functional MRI study of automatic movements in patients with Parkinson's disease. *Brain* 128, 2250–2259.

Xia, J., Chen, J., Zhou, Y., Zhang, J., Yang, B., Xia, L., et al. (2004). Volumetric MRI analysis of the amygdala and hippocampus in subjects with major depression. *J. Huazhong Univ. Sci. Technol. Med. Sci.* 24, 500–502.

Zang, Y., Jiang, T., Lu, Y., He, Y., and Tian, L. (2004). Regional homogeneity approach to fMRI data analysis. *NeuroImage* 22, 394–400.

Zheng, J. H., Sun, W. H., Ma, J. J., Wang, Z. D., Chang, Q. Q., Dong, L. R., et al. (2022). Differences in neuroanatomy and functional connectivity between motor subtypes of Parkinson's disease. *Front. Neurosci.* 16:905709. doi: 10.3389/fnins.2022.905709

Zhou, C., Zhong, X., Yang, Y., Yang, W., Wang, L., Zhang, Y., et al. (2018). Alterations of regional homogeneity in freezing of gait in Parkinson's disease. *J. Neurol. Sci.* 387, 54–59. doi: 10.1016/j.jns.2018.01.021

frontiers | Frontiers in Aging Neuroscience

TYPE Original Research
PUBLISHED 14 July 2023
DOI 10.3389/fnagi.2023.1216509

OPEN ACCESS

EDITED BY
Woon-Man Kung,
Chinese Culture University, Taiwan

REVIEWED BY
Liu Qing,
Second People's Hospital of Guiyang, China
Laura Mitrea,
University of Agricultural Sciences and Veterinary Medicine of Cluj-Napoca, Romania
Mahmoud Salami,
Kashan University of Medical Sciences, Iran
Kai-Ming Jhang,
Changhua Christian Hospital, Taiwan

*CORRESPONDENCE
Can Sheng
canyeweiwu2013@163.com
Feng Chen
fenger0802@163.com
Ying Han
hanying@xwh.ccmu.edu.cn

RECEIVED 04 May 2023
ACCEPTED 12 June 2023
PUBLISHED 14 July 2023

CITATION
He B, Sheng C, Yu X, Zhang L, Chen F and Han Y (2023) Alterations of gut microbiota are associated with brain structural changes in the spectrum of Alzheimer's disease: the SILCODE study in Hainan cohort.
Front. Aging Neurosci. 15:1216509.
doi: 10.3389/fnagi.2023.1216509

Alterations of gut microbiota are associated with brain structural changes in the spectrum of Alzheimer's disease: the SILCODE study in Hainan cohort

Beiqi He[1], Can Sheng [2]*, Xianfeng Yu[3], Liang Zhang[1], Feng Chen [4]* and Ying Han [1,3,5,6]*

[1]School of Biomedical Engineering, Hainan University, Haikou, China, [2]Department of Neurology, The Affiliated Hospital of Jining Medical University, Jining, China, [3]Department of Neurology, Xuanwu Hospital of Capital Medical University, Beijing, China, [4]Department of Radiology, Hainan General Hospital (Hainan Affiliated Hospital of Hainan Medical University), Haikou, China, [5]Center of Alzheimer's Disease, Beijing Institute for Brain Disorders, Beijing, China, [6]National Clinical Research Center for Geriatric Disorders, Beijing, China

Background: The correlation between gut microbiota and Alzheimer's disease (AD) is increasingly being recognized by clinicians. However, knowledge about the gut–brain–cognition interaction remains largely unknown.

Methods: One hundred and twenty-seven participants, including 35 normal controls (NCs), 62 with subjective cognitive decline (SCD), and 30 with cognitive impairment (CI), were included in this study. The participants underwent neuropsychological assessments and fecal microbiota analysis through 16S ribosomal RNA (rRNA) Illumina Miseq sequencing technique. Structural MRI data were analyzed for cortical anatomical features, including thickness, sulcus depth, fractal dimension, and Toro's gyrification index using the SBM method. The association of altered gut microbiota among the three groups with structural MRI metrics and cognitive function was evaluated. Furthermore, co-expression network analysis was conducted to investigate the gut–brain–cognition interactions.

Results: The abundance of *Lachnospiraceae*, *Lachnospiracea_incertae_sedis*, *Fusicatenibacter*, and *Anaerobutyricum* decreased with cognitive ability. *Rikenellaceae*, *Odoribacteraceae*, and *Alistipes* were specifically enriched in the CI group. *Mediterraneibacter* abundance was correlated with changes in brain gray matter and cerebrospinal fluid volume ($p = 0.0214$, $p = 0.0162$) and significantly with changes in cortical structures in brain regions, such as the internal olfactory area and the parahippocampal gyrus. The three colonies enriched in the CI group were positively correlated with cognitive function and significantly associated with changes in cortical structure related to cognitive function, such as the precuneus and syrinx gyrus.

Conclusion: This study provided evidence that there was an inner relationship among the altered gut microbiota, brain atrophy, and cognitive decline. Targeting the gut microbiota may be a novel therapeutic strategy for early AD.

KEYWORDS

Alzheimer's disease, gut microbiota, 16S ribosomal RNA, brain structural, magnetic resonance imaging

1. Introduction

Alzheimer's disease (AD) is the most common form of dementia, imposing a heavy economic and social burden worldwide. Currently, the pathogenesis of AD remains unclear. Due to the lack of effective treatments in the stage of AD dementia, exploring new mechanisms of AD may be vital for providing successful therapeutic strategies (Chowdhary et al., 2021; Gauthier et al., 2021).

Recently, gut microbiota may be a critical factor in developing AD. Gut microbiota can interact with individual brain physiological activity through the microbiota–gut–brain axis, leading to the development of a variety of neurodegenerative diseases, such as AD and Parkinson's disease (Main and Minter, 2017; Cryan et al., 2019). Current studies have demonstrated that the structure of intestinal microbiota in patients with AD and mild cognitive impairment (MCI) is altered compared with cognitively normal adults (Cattaneo et al., 2017; Zhuang et al., 2018; Liu et al., 2019). In addition, our previous studies have also confirmed the similar alterations of specific gut microbiota, such as phylum *Firmicutes*, phylum *Bacteroidetes*, and their corresponding genus, in subjective cognitive decline (SCD) and amyloid-β (Aβ) positive cognitively normal individuals (Sheng et al., 2021, 2022), providing the preliminary evidence of altered gut microbiota in preclinical AD. Furthermore, these altered gut microbiotas are found to be associated with cognitive function and global brain Aβ burden (Chen et al., 2020; Li et al., 2020). Kim et al. confirmed that transplantation of fecal microbiota of wild-type mice into transgenic mice model of AD could improve Aβ plaque formation and cognitive impairment. Thus, alterations of gut microbiota are involved in the pathogenesis of the AD mice model (Kim et al., 2020). However, knowledge about the gut–brain interaction remains largely unknown.

A growing body of evidence suggests several pathways potentially connecting the intestinal microbiota and brain, including neuroimmune, gut microbiota-derived metabolites, neurotransmitters, and enteroendocrine signaling. The intestinal microbiota may influence brain amyloidosis and central nervous system (CNS) homeostasis through these substances or influence neural messages carried by the vagal and spinal afferent neurons, further leading to the development of AD (Kowalski and Mulak, 2019; Mahmoudian Dehkordi et al., 2019; Fung, 2020). However, studies describing the effect of gut microbiota on brain structural and functional changes in AD are few.

Recent advances in brain imaging have provided an opportunity for elucidating the gut–brain–cognition interactions. The evidence of brain volume atrophy and cortex lesions in AD is commonly shown using structural magnetic resonance imaging (sMRI) (Vemuri and Jack, 2010; Whitwell, 2018). De Santis et al. (2019) proposed a possible framework called radiomicrobiomics, which highlighted that the combination of gut microbiota with brain imaging techniques will greatly enhance our understanding of the microbiota–gut–brain axis in regulating cognition in AD (Cryan et al., 2019). Based on the amygdala-based functional connectivity and voxel-based morphometry (VBM) analysis, Zheng et al. (2020) revealed that the disrupted distribution of genus *Roseburia* regulated the amygdala-based functional connectivity in patients with end-stage renal disease. One recent study reported that gut bacteria *Odoribacter* was positively associated with hippocampal volume, which might be mediated by acetic acids (Liang et al., 2022). However, current studies focusing on the interactions between gut microbiota, brain, and cognition in AD, especially in the whole spectrum of AD are still limited.

This study aimed to (1) explore the characteristics of intestinal microbiota in the spectrum of AD in the Hainan cohort; (2) investigate the correlation between gut microbiota and brain atrophy; and (3) elucidate the interrelationship between gut microbiota, brain structure, and cognitive function using co-expression network analysis.

2. Materials and methods

2.1. Participants

One hundred and twenty-seven participants were recruited between November 2021 and July 2022 for the Sino Longitudinal Study on Cognitive Decline (SILCODE) (Li et al., 2019). Participants in the present study were recruited from Memory Clinic in both Hainan General Hospital and Hainan Cancer Hospital, including normal control (NC) ($n = 35$), individuals with SCD ($n = 62$), and patients with cognitive impairment (CI) (MCI, $n = 16$; mild AD dementia, $n = 14$). The criteria for individuals with NC were as follows: (1) objective neuropsychological assessments within the normal range, adjusted for age, gender, and years of education; and (2) without complaints of cognitive decline or concerns about cognitive decline. Individuals with SCD were diagnosed according to the criteria proposed by Jessen et al. (2014, 2020), which were as follows: (1) self-experienced, persistent cognitive decline, mainly in the memory domain but not in other cognitive domains, which was not related to the acute event; (2) the onset was within 5 years; (3) issues associated with SCD; (4) the objective neuropsychological examination was within the normal range, adjusted for age, gender, and years of education; (5) failure to meet the diagnostic criteria for MCI or AD dementia (Jessen et al., 2014, 2020). The definition of MCI was in accordance with the criteria proposed by Jak and Bondi in 2014. Participants were considered to have MCI if any one of the following three criteria were met: (1) impaired scores (defined as >1 SD below the age/education-corrected normative means) on both measures in at least one cognitive domain (memory, language, or speed/executive function); (2) impaired scores in each of the three cognitive domains (memory, language, or speed/executive function); (3) Functional Activity Questionnaire (FAQ) ≥ 9 (Bondi et al., 2014). The diagnosis of AD dementia was based on the frameworks of the Diagnostic and Statistical Manual of Mental Disorders (fifth edition) and the National Institute on Aging—Alzheimer's Association (NIA-AA) workgroups (McKhann et al., 2011; Association American Psychiatric, 2013). In our study, patients with MCI and mild AD were defined as individuals with CI.

The exclusion criteria were as follows: (1) those with left-handedness or double-handedness; (2) those suffered from cerebrovascular or psychiatric disorders or other neurological disorders that may lead to cognitive impairment or congenital

intellectual disability; (3) those with an experience of traumatic brain injury that may lead to cognitive impairment; (4) those with severe sensory impairment or infectious disease that cannot complete the examination; (5) those who cannot undergo MRI scan, such as having metal implants or claustrophobia; (6) those with a history of taking probiotics, prebiotics, synbiotics, antibiotics, or medications to regulate gut microbiota within the last 3 months; (7) those with a history of long-term use of corticosteroids, immunosuppressants, or immunostimulatory drugs; and (8) those suffered from severe gastrointestinal disorders, such as irritable bowel syndrome, inflammatory bowel disease, and severe digestive and absorption abnormalities.

All clinical information was collected according to standard procedures as experienced neurologists and memory clinic specialists prescribed. Research activities in this study were conducted following the ethical standards of the Declaration of Helsinki. The Medical Research Ethics Committee and Institutional Review Board of Xuanwu Hospital at Capital Medical University approved them. Written informed consent was obtained at the time when participants were recruited.

2.2. Neuropsychological assessments

Demographic information was collected on age, gender, and years of education. An experienced neurologist interviewed each participant and their informant about their essential physical condition, recorded the assessment of their self-perceived abilities, and sought confirmation from their informants.

All participants carried on the following neuropsychological tests: (1) memory domain: Auditory Verbal Learning Test—Huashan version (AVLT-H) (Zhao et al., 2012); (2) executive domain: Shape Trails Test (STT-A and B) (Zhao et al., 2013); (3) language domain: Animal Fluency Test (AFT) (Guo et al., 2007) and Boston Naming Test (BNT) (Guo, 2006); (4) global cognitive function: Montreal Cognitive Assessment—Basic (MoCA-B) (Chen et al., 2016), Mini-Mental State Examination (MMSE) (Li et al., 2016), Memory and Executive Screening Scale (MES) (Guo et al., 2012), and Everyday Cognition (Ecog) (Farias et al., 2008); (5) daily functional activities: FAQ (González et al., 2022); (6) emotional state: Hamilton Depression Rating Scale (HAMD), Hamilton Anxiety Rating Scale (HAMA), and Geriatric Depression Scale (GDS) (Aikman and Oehlert, 2001); (7) sleep state: Pittsburgh Sleep Quality Index (PSQI) (Buysse et al., 1989), REM sleep behavior disorder screening questionnaire (RBDSQ) (Nomura et al., 2015), and Epworth Sleepiness Scale (ESS) (Johns, 1991); (8) Clinical symptom: Clinical Dementia Rating (CDR) (Lim et al., 2005).

2.3. Fecal sample collection and DNA extraction

In this study, fecal sample collection and preservation operations were carried out by the standardized fecal procedure proposed by the International Human Microbiome Standard (IHMS) and the Human Microbiome Project (HMP) (https://www.hmpdacc.org).

According to the instructions, the QIAamp DNA Stool Mini Kit (Qiagen, Hilden, Germany) was used to extract DNA from the fecal samples in a Class II biosafety laboratory. After extraction, the DNA concentration was quantified using the UV microspectrophotometer Thermo Nano-Drop 2000 (Thermo Scientific, MA, USA). The total DNA was checked for quality by 1% agarose gel electrophoresis. Finally, after assessing the DNA integrity and fragment size, the qualified DNA extracts were suspended in H_2O and stored at −80°C prior to subsequent analysis.

2.4. 16s rRNA gene amplicon and sequencing

The 16S rRNA amplification region selected for this study is the V3-V4, using universal primers (341F and 806R) linked with indices and sequencing adaptors. The forward primer (5′-3′) was CCTAC GGGRSGCAGCAG (341F), and the reverse primer (5′-3′) was GGACTACVVGGGTATCTAATC (806R). The 5′ end of the universal primers was added to fit the Illumina NovaSeq PE250 sequencing of the splice and index sequences. The diluted genomic DNA was used as a template for PCR amplification using the KAPA HiFi Hotstart Ready Mix PCR kit high-fidelity enzyme. The 2% agarose gel electrophoresis was used to examine PCR products, and then the PCR product recovery was completed using the AxyPrep DNA Gel Extraction kit (AXYGEN). Amplified samples were subjected to library quality control using a Thermo Nano-Drop 2000 UV microspectrophotometer and 2% agarose gel electrophoresis. Qualified samples were subjected to library quantification using Qubit and homogenized according to the data available for each sample.

The completed amplified DNA samples were sequenced using the Illumina NovaSeq PE250 platform, resulting in paired-end sequencing (PE250) data. Paired-end reads from the double-end sequencing were spliced into a single sequence using PANDAseq software-long reads with a high variation region. The final clean reads were selected to be in the range of 250–500 nt.

2.5. Sequence analysis

In this study, the clean reads that completed the quality check were subjected to chimera removal operations and cluster analysis using the USEARCH tool. For clustering analysis, the clustering results were judged using a 97% similarity threshold to obtain operational taxonomic units (OTUs), each considered as a species representative (Edgar, 2010). For clean reads with identical sequences, the singletons were filtered out and matched to the OTU sequences one by one, and those that can be matched to the OTUs were output as mapped reads. All sequences were randomly sampled and leveled based on sufficient sequencing depth to avoid bias in analysis results due to differences in the quality of sequencing data among samples. The sequence with the highest abundance value in each OTU was selected as its representative sequence and compared to the sequences of known species in the 16S database for similarity, completing the species annotation of

OUT. The 16S database used in this study is the RDP database (http://rdp.cme.msu.edu/index.jsp) (Cole et al., 2014).

The alpha and beta diversity in this study was assessed using QIIME software. The alpha diversity indices were used to assess the alpha diversity, and five alpha diversity indices (Chao1, Observed species, Simpson, Shannon, and PD_whole_tree) were selected for analysis in our study. Beta diversity was assessed by calculating the phylogenetic distance of the UniFrac values, which were divided into Weighted UniFrac concerning sequence abundance and Unweighted UniFrac without reference to sequence abundance.

This study uses the Kruskal.test function in R studio's stats tool package to analyze the inter-group differences in microbiota structure. First, the linear discriminant analysis (LDA) typical method was used by LEfSe, a cloud tool of the National Microbial Science Data Center (https://nmdc.cn/analyze/detailsid=600676b70b38496ee0c90921), as the processing platform, to estimate the influence of each species' abundance on the differences among groups and analyze the microbiota information and enrichment that had a significant response to the sample grouping information. Then, the significant difference information of the distribution of bacteria between different groups was screened using the rank sum test method, and the microbiota with the significant difference in relative abundance value between groups was obtained. The threshold value was $p < 0.05$ and was corrected by a false discovery rate (FDR).

2.6. Structural MRI scan and data preprocessing

The MRI data acquisition equipment involved in this study was a 3-T MR imager (Magnetom Trio Tim; Siemens, Erlangen, Germany) at the Radiology Department of Hainan General Hospital, using a magnetization-prepared rapid acquisition gradient-echo sequence to acquire three-dimensional T1-weighted images at the sagittal plane. T1-weighted imaging (T1W1) acquisition parameters: matrix = 256 × 256, FOV = 256 × 256 mm^2, gap = 0, layer thickness = 1 mm, number of layers = 192, flip angle = 12°, TE = 2.9 ms, TR = 6.7 ms, TI = 450 ms, and voxel = $(1\,mm)^3$. The participants were asked to close their eyes and enter a quiet state without falling asleep and to keep their torsos as motionless as possible until the scan was completed.

The raw image data required a format conversion using Dcm2nii software to convert the DICOM format to the Nifti format required by the SPM 12 software. It was followed by preprocessing on MATLAB (R 2012b, MathWorks, Natick, MA, USA) using SPM 12 and the CAT 12 toolkit, including origin and bias field inhomogeneity correction. It segments the images into different gray matter, white matter, and cerebrospinal fluid volume (CSF) data files by CAT 12/s AMAP method. The images were normalized by the DARTEL algorithm function in the toolkit, aligned sample by sample image to a template of 555 healthy subjects in the IXI database (http://www.brain-development.org), and smoothed (Rajapakse et al., 1997). Total surface area (TSA), total intracranial volume (TIV), and actual and relative volumes of gray matter, white matter, and CSF (relative volumes were calculated by dividing each component volume by TIV) were calculated using the VBM method (Ashburner and Friston, 2000). The analysis of cortical morphology required re-aligning the samples with the DK40 template using algorithmic functions from the CAT 12 toolkit and the SBM method to complete the analysis of cortical anatomical features, including thickness, sulcus depth, fractal dimension, and Toro's gyrification index (Riccelli et al., 2017).

2.7. Statistical analysis

The statistical analysis was performed by IBM SPSS software (version 23, IBM, Armonk, NY, USA). For all intra-group statistical and inter-group comparison work on grouped data, the Shapiro–Wilk test (test of normality) and Levene's test (chi-square test) were performed before selecting the appropriate parametric or non-parametric test, respectively. A one-way ANOVA test was used for analyses of inter-group variance for continuous, normally distributed data, and the Kruskal–Wallis test for continuous, non-normally distributed data. The Pearson chi-square test was used to analyze inter-group variability for categorical variables.

When calculating correlations among the altered gut microbiota abundance, the structural index, and the neuropsychological assessments, biased correlation analysis was used through a linear mixed-effects model with age, years of education, and TIV as covariates, the aim of which was to exclude the influence of other confounding factors on the results. GraphPad Prism (version 9.0, GraphPad, San Diego, CA, USA) was used to describe the correlation.

Using Cytoscape to perform Spearman correlation analysis on the abundance of the screened gut microbiota, cortical index, volumetric index, and cognitive-related neuropsychological assessments and reflect significant interrelationships ($p < 0.05$), the results were tested by FDR to estimate the relationship between the pathways represented by the above feature values as a Network diagram for overall representation.

3. Results

3.1. Demographic and neuropsychological assessments

The results of demographic information and neuropsychological assessments of the NC, SCD, and CI participants are shown in Table 1. For all three groups of participants, there were no statistical differences in age, gender, or years of education ($p > 0.05$). There were also no statistical differences among the three groups in PSQI, RBDSQ, and ESS ($p > 0.05$). In the results of the three scales assessing mood (HAMD, HAMA, GDS), the differences among the three groups were statistically significant ($p = 0.026$, $p = 0.017$, and $p = 0.049$, respectively), and the SCD group had the highest scores in both HAMD and HAMA. There were extreme statistically significant differences ($p < 0.001$) in MMSE, MoCA-B, and FAQ scales, and the CI group had the most severe cognitive impairment on each of the scales.

TABLE 1 Demographic and neuropsychological assessments for all participants.

Characteristics	Total ($n = 127$)	Group			p-value
		NC ($n = 35$)	SCD ($n = 62$)	CI ($n = 30$)	
Sex (F/M)	83/44	24/11	41/21	18/12	0.757
Age (y)	69 (65, 72)	69 (65, 71.5)	67 (65, 71)	71.5 (66, 77)	0.102
Education (y)	14 (12, 16)	14 (12, 16)	15 (12, 16)	12 (10.25, 13.75)	0.139
HAMD	5.28 ± 4.46	3.57 ± 3.53	6.06 ± 4.80	5.63 ± 4.31	0.026
HAMA	6.41 ± 5.37	4.23 ± 4.46	7.29 ± 5.06	7.13 ± 6.34	0.017
GDS	3.20 ± 2.61	2.31 ± 1.92	3.40 ± 2.87	3.80 ± 2.57	0.049
PSQI	5.19 ± 3.58	5.00 ± 3.64	5.69 ± 3.93	4.37 ± 2.58	0.236
RBDSQ	1.74 ± 1.81	1.69 ± 1.81	1.92 ± 1.88	1.43 ± 1.70	0.477
ESS	6.02 ± 4.73	4.51 ± 3.74	6.29 ± 4.29	7.23 ± 6.14	0.056
MMSE	26.72 ± 4.38	28.77 ± 1.48	28.03 ± 2.14	21.60 ± 5.96	<0.001
AVLT-H N5	5.71 ± 3.46	8.31 ± 2.04	6.00 ± 3.00	2.07 ± 2.46	<0.001
AVLT-H N7	20.46 ± 3.92	22.83 ± 1.52	21.08 ± 2.72	16.43 ± 4.91	<0.001
STT-A	83.87 ± 41.70	70.57 ± 25.02	68.55 ± 30.66	131.07 ± 42.73	<0.001
STT-B	172.91 ± 65.26	137.40 ± 35.34	152.60 ± 39.77	256.33 ± 64.09	<0.001
AFT	19.24 ± 6.79	22.54 ± 5.08	20.44 ± 5.15	12.93 ± 7.52	<0.001
BNT	25.48 ± 4.84	26.77 ± 2.75	26.85 ± 2.79	21.13 ± 7.13	<0.001
MES	85.72 ± 15.92	92.49 ± 5.83	91.23 ± 6.99	66.47 ± 21.35	<0.001
FAQ	1.87 ± 4.96	0.06 ± 0.24	0.74 ± 1.48	0.74 ± 1.48	<0.001
Ecog	1.55 ± 0.63	1.18 ± 0.24	1.48 ± 0.44	2.12 ± 0.85	<0.001
MoCA-B	24.13 ± 5.66	26.86 ± 2.38	25.84 ± 2.41	17.43 ± 7.68	<0.001
CDR	0.22 ± 0.56	0 ± 0	0 ± 0	0.82 ± 0.15	<0.001

NC, normal control; SCD, subjective cognitive decline; CI, cognitive impairment; M, male; F, female; y, year; HAMD, Hamilton Depression Rating Scale; HAMA, Hamilton Anxiety Rating Scale; GDS, Geriatric Depression Scale; PSQI, Pittsburgh Sleep Quality Index; RBDSQ, REM Sleep Behavior Disorder Questionnaire; ESS, Epworth Sleeping Scale; MMSE, Mini-Mental State Examination; AVLT-H N5, Auditory Verbal Learning Test—long-delayed recall; AVLT-H N7, Auditory Verbal Learning Test—recognition; STT-A, Shape Trails Test Part A; STT-B, Shape Trails Test Part B; AFT, Animal Fluency Test; BNT, Boston Naming Test; MES, Memory and Executive Screening Scale; FAQ, Functional Activities Questionnaire; Ecog, Everyday Cognition; MoCA-B, Montreal Cognitive Assessment—Basic; CDR, Clinical Dementia Rating.

3.2. The overall gut microbial communities among the three groups

A total of 1,227 OTUs were analyzed from the fecal samples collected from all the participants, of which 198 OTUs were shared between the NC and SCD groups, 44 OTUs were shared between the SCD and CI groups, and 608 OTUs were shared between the three groups (Figure 1A). A total of 13 phyla, 26 orders, 44 families, 74 families, and 216 genera of microorganisms were detected in all OTUs. The accumulation curves for all the detected OTU crop species showed a sharp rise followed by a gentle rise, indicating that the sampling operation parameters were set correctly, and the sampling was adequate in the pre-treatment (Supplementary Figure 1).

In the Kruskal–Wallis test for the six alpha diversity indices among the three groups, chao 1, PD_whole_tree, Shannon, and Simpson showed no statistical difference in the between-group analysis ($p = 0.76$, $p = 0.49$, $p = 0.15$, $p = 0.15$; $p > 0.05$) (Figure 1B). In this study, the PCoA method was used to cluster the species composition of the samples for both weighted and unweighted UniFrac values, and the results showed no significant clustering between samples for species diversity among the groups (Figure 1C), and no significant clustering between samples using the NMDS method (Supplementary Figure 2).

In this study, all samples detected were analyzed for species annotation and abundance, and the distribution of the dominant phylum and the composition of the dominant genus were consistent with the results of previous studies on the ecological structure of human-derived intestinal microbiota, as observed in the overall sample microbiota ecological structure (Supplementary Figure 3). The study analyzed the three groups of samples at different biological taxonomic levels (Figure 1D; Supplementary Figure 4). The qualitative and non-quantitative histograms show that at the phylum level, the phylum *Firmicutes* was enriched in the NC group. In contrast, the abundance of the phylum *Firmicutes* was significantly lower, and the abundance of the phylum *Bacteroidetes* was significantly higher in the CI group compared with the NC group. At the genus level, the beneficial intestinal bacteria such as *Faecalibacterium* and *Lachnospiracea* were enriched in the NC group compared with the CI group. The

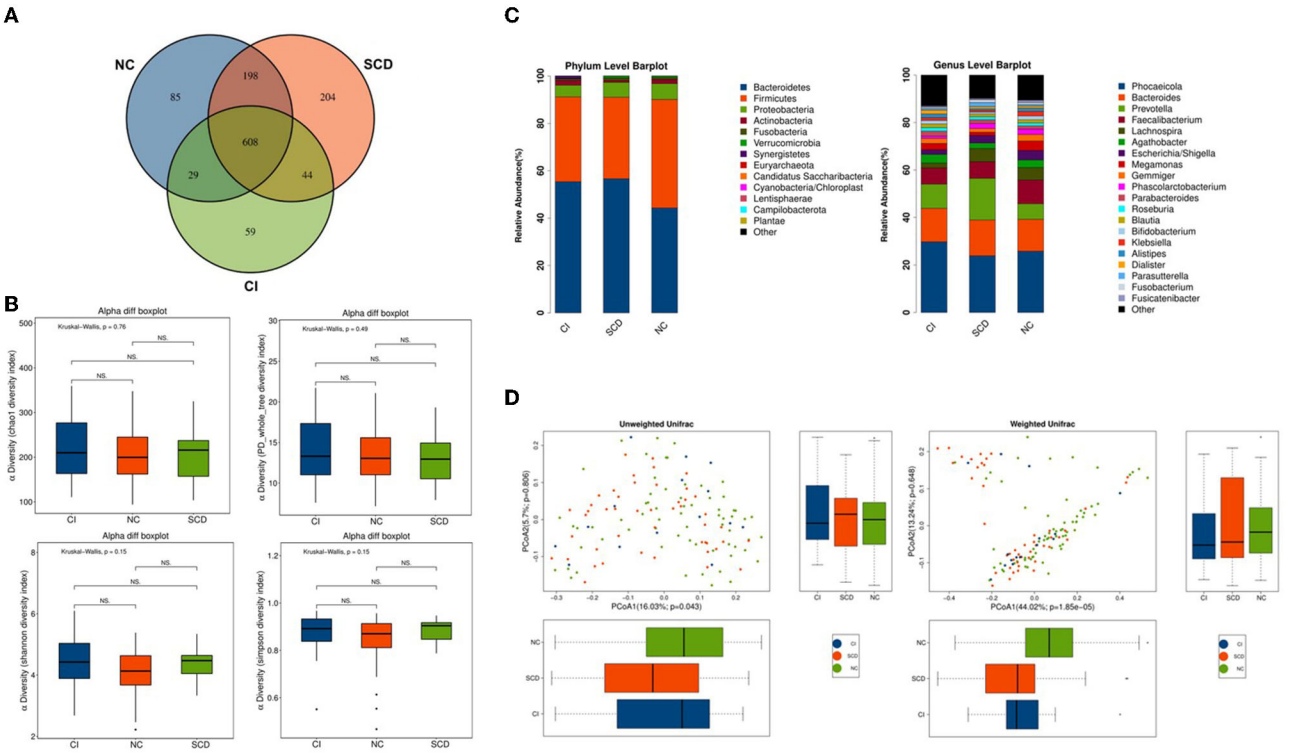

FIGURE 1
The overall structure of the gut microbiota based on the analysis of microbial diversity among NC, SCD, and CI. **(A)** Venn diagram illustrated the overlap of the OTUs identified in the gut microbiota among the three groups. **(B)** The alpha diversity of gut microbiota among the three groups. Each box plot represented the median, interquartile range, minimum, and maximum values. *P*-values were determined using the Kruskal–Wallis test. There were no significant differences in Chao1, PD_whole_tree, Shannon, and Simpson indices among the three groups. **(C)** The beta diversity among unweighted Unifrac and weighted Unifrac of the three groups using the principal coordinates analysis (PCoA). **(D)** Bar graphs indicate the bacterial community among the three groups at phylum and genus taxonomic levels.

abundance of these groups was reduced in comparison with the CI group.

3.3. Alterations of the gut microbiota among the three groups

In this study, to accurately know the information about the groups that were significantly different among the three groups, LEfSe analysis was used to assess the magnitude of the effect of the abundance of different species on the effect of group differences, to identify the groups or species that had a significant differential effect on the group information. As shown in Figure 2A, a total of thirty-two species were screened for the presence of statistical differences between groups at different biological taxonomic levels, of which seven were specifically enriched in the NC group, eight were specifically enriched in the SCD group, and seventeen were specifically enriched in the CI group. To further identify the groups that differed in abundance between groups, the rank sum test was used to analyze the significance of differences between groups, as shown in Figure 2B. Twenty groups (including all biological taxonomic classes) differed significantly among the groups, the phylum *Firmicutes*, class *Clostridia*, order *Clostridiales*, family *Lachnospiraceae*, genus *Fusicatenibacter*, genus *Lachnospiracea_incertae_sedis*, and *Anaerobutyricum* showed a progressively decreased prevalence from NC to SCD and CI; compared with both CI and SCD subjects, the NC population demonstrated a significant decrease in the abundance of phylum *Bacteroidetes*, class *Bacteroidia*, and order *Bacteroidales*.

Based on the results of the analysis of the differences between the three groups and the biological background of the screened groups, it was decided to retain nine distinct groups for the study. Among them, *Lachnospiraceae* (LDA = 4.64), *Lachnospiracea_incertae_sedis* (LDA = 3.40), *Fusicatenibacter* (LDA = 3.29), and *Anaerobutyricum* (LDA = 2.69) had decreasing abundance with cognitive ability and a decreasing trend between groups; the abundance of family *Rikenellaceae* (LDA = 3.65) and *Odoribacteraceae* (LDA = 3.06), and genus *Mediterraneibacter* (LDA = 3.18) and *Alistipes* (LDA = 3.65) in individuals with SCD were significantly reduced compared with others and enriched in the CI group.

3.4. Correlation between altered gut microbiota and brain structural features

In this study, sMRI image data from 100 participants acquired using a 3.0 T MRI machine were analyzed by the VBM method

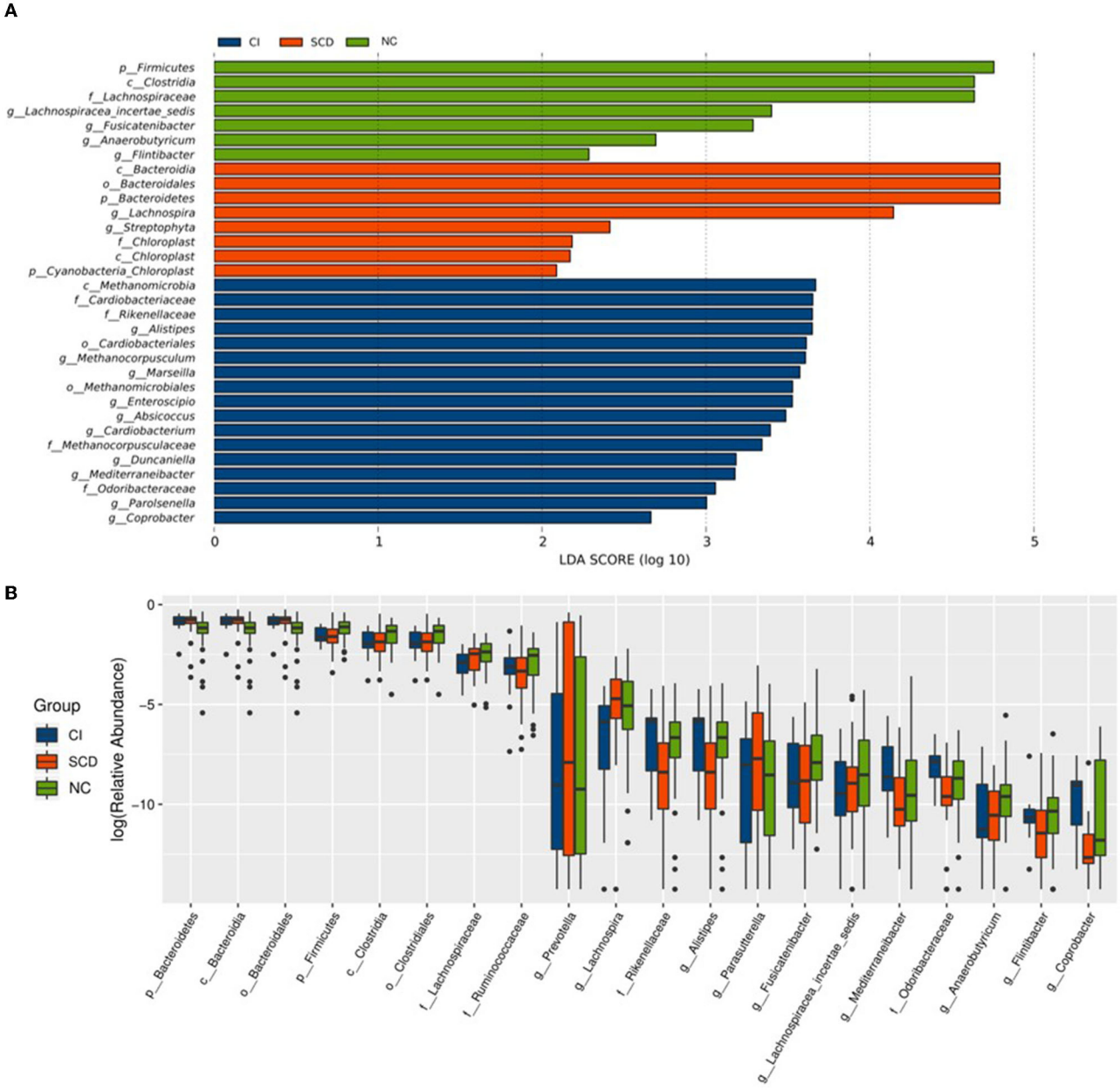

FIGURE 2
Alterations of the gut microbiota among the three groups. **(A)** The LEfSe analysis among NC, SCD, and CI. As shown in the histogram of LDA scores for differentially abundant taxa, the LDA scores indicated the enrichment of taxa in the NC group (green), the LDA scores indicated the enriched taxa in the SCD group (red), and the LDA scores indicated the enriched taxa in the CI group (blue). The LDA scores (log10) > 2 and $p < 0.05$ were listed. **(B)** The difference analysis of rank sum test among NC, SCD, and CI. The abscissa is the differential taxa, and the ordinate is the relative abundance log2, with different colors representing different groups.

to obtain eight volume metrics, including the actual volume of each group of TIV, TSA, gray matter, white matter, and CSF (GM_abs, WM_abs, CSF_abs) and the relative volume of comparison individual TIV (GM_rel, WM_ rel, CSF_rel). As shown in Table 2, CSF_abs indicated statistical inter-group difference ($p = 0.013$); TSA displayed a significantly inter-group difference ($p = 0.004$); WM_abs, GM_abs, CSF_rel, WM_rel, and GM_rel were shown extremely statistically inter-group difference ($p < 0.001$); there was no statistically significant difference among the groups in TIV ($p = 0.093$). There are consistent with previous relevant studies.

Participants' cortical morphology was analyzed using SBM, during which four participants' data that could not be aligned with the DK40 template were censored. Four cortical indices (thickness, sulcus depth, fractal dimension, and Toro's gyrification index) were calculated for the 72 brain regions delineated. Due to the plethora of results, Supplementary Table 1 presents the cortical index statistics for the 43 specific brain regions correlated with the

TABLE 2 Statistical table of sMRI volume indices calculated by VBM.

The indices of volumetry	Total ($n = 100$)	Groups			p-value
		NC ($n = 25$)	SCD ($n = 51$)	CI ($n = 24$)	
CSF_abs	341.9750 ± 70.0590	343.3282 ± 66.5699	325.3959 ± 62.5599	375.7958 ± 78.6731	0.013
WM_abs	497.3981 ± 60.2879	512.9503 ± 67.7562	508.8576 ± 52.2553	456.8464 ± 51.4591	<0.001
GM_abs	613.3541 ± 57.34508	627.9692 ± 61.2396	626.0984 ± 47.0597	571.0485 ± 54.4706	<0.001
CSF_rel	0.2349 ± 0.0398	0.2308 ± 0.0324	0.2219 ± 0.0328	0.2667 ± 0.0442	<0.001
WM_rel	0.3422 ± 0.0244	0.3452 ± 0.0227	0.3485 ± 0.0210	0.3259 ± 0.0263	<0.001
GM_rel	0.4228 ± 0.0240	0.4240 ± 0.0209	0.4295 ± 0.0212	0.4074 ± 0.0263	<0.001
TSA	1,838.7473 ± 156.9746	1,871.1383 ± 175.8909	1,865.9549 ± 131.4432	1,747.1906 ± 157.1386	0.004
TIV	1,452.7272 ± 134.3649	1,484.2477 ± 159.9418	1,460.3519 ± 121.3357	1,403.6906 ± 123.6676	0.093

NC, normal control; SCD, subjective cognitive decline; CI, cognitive impairment; CSF_abs, cerebrospinal fluid's absolute value; WM_abs, white matter's absolute value; GM_abs, gray matter's absolute value; CSF_rel, cerebrospinal fluid's relative tissue volume; WM_rel, white matter's relative tissue volume; GM_rel, gray matter's relative tissue volume; TSA, total surface area; TIV, total intracranial volume.

characteristic microbiotas in subsequent analysis. As shown in the table, these regions reveal statistical inter-group differences among the three groups: the entorhinal, the lateral prefrontal, the medial orbitofrontal, the temporal pole, the pars orbitalis, the superior parietal, and the supramarginal gyrus, particularly in the thickness of entorhinal, lateral orbitofrontal, temporal pole, the sulcus depth of pars orbitalis, the Toro's gyrification index of superior parietal, and supramarginal.

Correlations between sMRI brain volume metrics and characteristic microbiota abundance were performed using partial correlation analysis, adjusted for age, years of education, and TIV. As shown in Figures 3A–C, the *Mediterraneibacter*'s abundance was positively correlated with CSF_rel ($r = 0.2436$, $p = 0.0162$) and negatively correlated with GM_rel ($r = -0.2333$, $p = 0.0214$); the *Mediterraneibacter*'s abundance was negatively correlated with GM_abs ($r = -0.2176$, $p = 0.0297$); and the *Odoribacteraceae*'s abundance was negatively correlated with GM_abs ($r = -0.2176$, $p = 0.0297$).

The correlation between characteristic microbiota and brain cortex structure is shown in Figure 3D, with characteristic microbiota abundance correlating to varying degrees with several cortical indicators in multiple brain regions. As visualized in the heatmap, the *Rikenellaceae*'s abundance was negatively correlated with thickness of the lateral orbitofrontal cortex in both right and left brain ($r = -0.286$, $p = 0.005$; $r = -0.239$, $p = 0.021$); the *Odoribacteraceae*'s abundance was negatively correlated with sulcus depth of the left parahippocampal gyrus ($r = -0.475$, $p < 0.001$), with Toro's gyrification index of the left precuneus ($r = -0.256$, $p = 0.013$), with Toro's gyrification index of the superior parietal cortex in both right and left brain ($r = -0.207$, $p = 0.046$; $r = -0.246$, $p = 0.018$), and with Toro's gyrification index of the left supramarginal cortex ($r = -0.32$, $p = 0.002$); the *Lachnospiraceae*'s abundance was positively correlated with thickness of the entorhinal cortex in both right and left brain ($r = 0.277$, $p = 0.007$; $r = 0.282$, $p = 0.006$), with Toro's gyrification index of the left precuneus ($r = 0.217$, $p = 0.037$), and with Toro's gyrification index of the superior parietal cortex in both right and left brain ($r = 0.242$, $p = 0.02$; $r = 0.231$, $p = 0.026$); the *Lachnospiracea_ incertae_sedis*'s abundance was negatively correlated with fractal dimension of the left fusiform gyrus ($r = -0.296$, $p = 0.004$); the *Fusicatenibacter*'s abundance was negatively correlated with fractal dimension of the left lateral orbitofrontal cortex ($r = -0.286$, $p = 0.006$); the *Anaerobutyricum*'s abundance was negatively correlated with thickness of the temporal pole in both right and left brain ($r = -0.389$, $p < 0.001$; $r = -0.41$, $p < 0.001$); the *Alistipes*'s abundance was negatively correlated with thickness of the left lateral orbitofrontal cortex ($r = -0.286$, $p = 0.005$); and the Mediterraneibacter's abundance was negatively correlated with thickness of the left entorhinal cortex ($r = -0.292$, $p = 0.004$), with the thickness of temporal pole in both right and left brain ($r = -0.335$, $p = 0.001$; $r = -0.28$, $p = 0.007$), and positively correlated with Toro's gyrification index in the left parahippocampal gyrus ($r = 0.28$, $p = 0.006$).

3.5. Network analysis among altered gut microbiota, neuroimaging features, and cognition

Using a linear mixed-effects model, we analyzed the correlations between the nine abundance values of distinct groups and the results of the eleven neuropsychological scales after excluding the effects of age and education (Figure 4A). The abundance of *Mediterraneibacter* and *Alistipes* all correlated with the results of the different tables. The abundance of *Rikenellaceae* indicated a positive correlation with the FAQ results ($r = 0.228$, $p = 0.011$) and negative correlations with the results of MMSE, MES, AVLT-H N5, BNT, and MoCA-B ($r < 0$, $p < 0.05$). The abundance of *Odoribacteraceae* indicated positive correlations with STT-A and STT-B results ($r > 0$, $p < 0.05$) and negative correlations with BNT, MES, MoCA-B, and MMSE results ($r < 0$, $p < 0.05$). The abundance of *Lachnospiraceae* indicated a positive correlation with MES ($r = 0.189$, $p = 0.036$) and a negative correlation with the FAQ results ($r = -0.206$, $p = 0.022$). The abundance of *Alistipes* indicated a positive correlation with the FAQ results ($r = 0.228$, $p = 0.011$) and negative correlations with the MMSE, MES, AVLT-H N5, BNT, and MoCA-B results ($r < 0$, $p < 0.05$). The abundance of *Mediterraneibacter* performed a positive correlation with Ecog

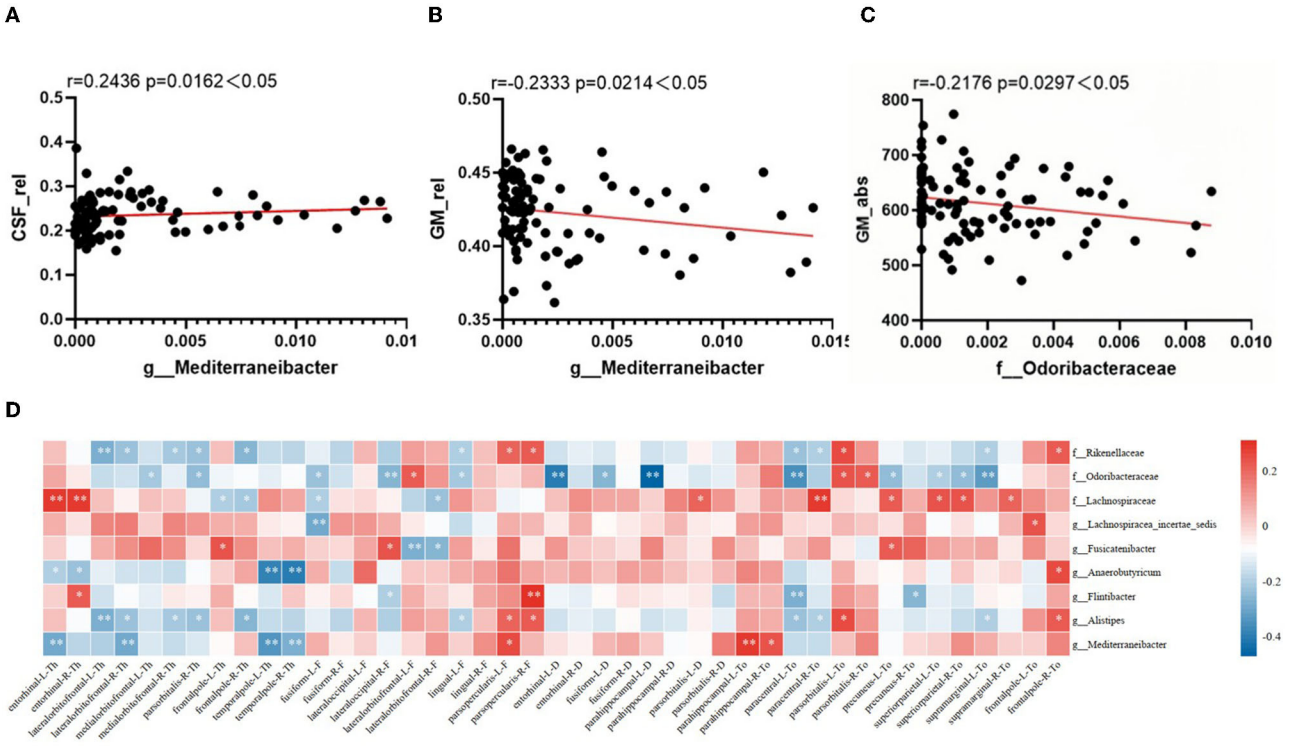

FIGURE 3
Correlation between altered characteristic taxa and brain structural features. **(A–C)** The result of correlation analysis between characteristic taxa abundance and sMRI volume index. **(A)** Scatter chart of correlation analysis between the abundance of *Mediterraneibacter* and cerebrospinal fluid's relative tissue volume. **(B)** Scatter chart of correlation analysis between the abundance of *Mediterraneibacter* and gray matter's relative tissue volume. **(C)** Scatter chart of correlation analysis between the abundance of *Odoribacteraceae* and gray matter's absolute value. **(D)** Heatmap of correlation between characteristic GM abundance and sMRI cortical index. The correlation coefficients (Corr) are displayed. Red or blue signifies a positive or negative correlation, respectively. $*p < 0.05$, $**p < 0.01$.

($r = 0.183$, $p = 0.041$) and negative correlations with MMSE, MES, AVLT-H N5, BNT, VFT, and MoCA-B results ($r < 0$, $p < 0.05$).

After implementing a linear mixed-effects model and regressing the effects of age and years of education, the results of the correlation analysis between 43 cortical indicators and the results of 11 neuropsychological scales were obtained. As shown in Figure 4B, cortical thickness in the entorhinal, the lateral orbitofrontal, the medial orbitofrontal, and the temporal pole, the cortical fractal dimension of the lateral occipital, the sulcus depth of the parahippocampal gyrus and pars orbitalis, and the cortical Toro's gyrification index of the paracentral, precuneus, superior parietal, and supramarginal gyrus showed positive correlations with MMSE, AVLT-H, VFT, BNT, MES, and MoCA-B results ($r > 0$, $p < 0.05$) and negative correlations with STT, FAQ, and Ecog results ($r < 0$, $p < 0.05$). The fractal dimension of the fusiform and lateral orbitofrontal showed positive correlations with STT, FAQ, and Ecog results ($r > 0$, $p < 0.05$) and negative correlations with MMSE, AVLT-H, VFT, BNT, MES, and MoCA-B results ($r < 0$, $p < 0.05$).

The results of the screened nine characteristic microbiota abundances, 43 cortical indicators, seven volumetric indicators, and neuropsychological assessment scales were subjected to an interaction network correlation analysis using Cytoscape to understand the interaction of colony characteristics and further explain the mechanism of formation of differences between characteristic colony groups. There was a tight correlation between the three feature values, forming a complete network of mechanisms (Figure 4C).

4. Discussion

In this study, we found nine specific gut microbiota that possibly related to the development of AD, of which four were negatively correlated with cognitive function, and one was positively correlated with cognitive function. In addition, three specificities were enriched in the cognitively impaired population. The joint analysis of the abundance of nine specific microbiota and individual brain structure sMRI image biomarkers found a significant correlation. *Mediterraneibacter* abundance was positively correlated to CSF and negatively correlated to gray matter volume. Moreover, we found a significant correlation between specific gut microbiota abundance and changes in cortical structure in brain regions related to cognitive function, such as entorhinal, fusiform, parahippocampal, precuneus, and superior parietal.

The gut microbiota compositions in the whole spectrum of AD were similar to that in previous studies, with the phylum *Firmicutes* enriched in the NC group and the phylum *Bacteroides* enriched in the CI group at the phylum level. In the study of Vogt et al. (2017) the abundance of phylum *Firmicutes* in AD was significantly lower than that of healthy controls, and the abundance

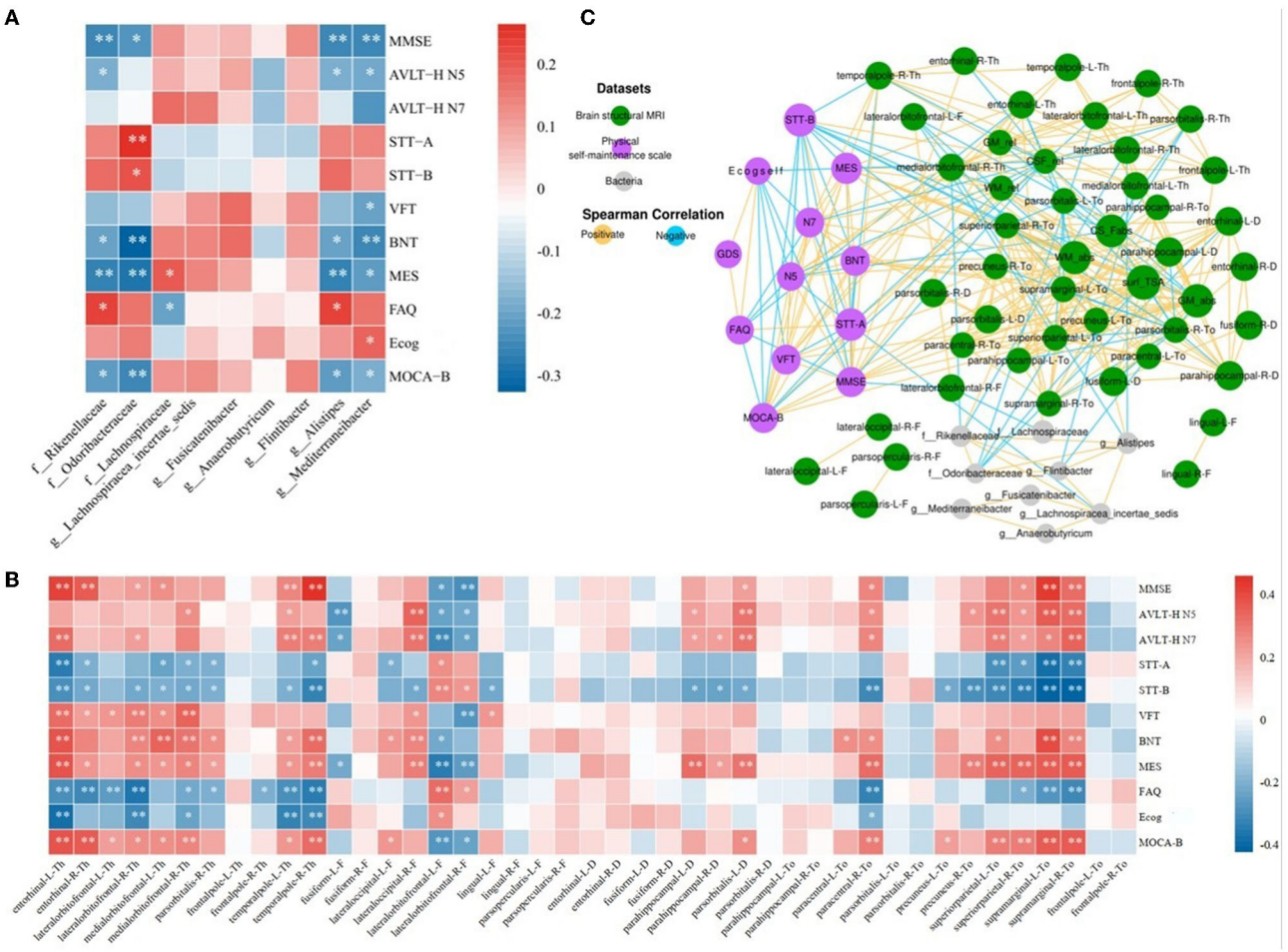

FIGURE 4
Network analysis among characteristic taxa, neuroimaging features, and cognition. **(A)** Heatmap of correlations between the night characteristic taxa and neuropsychological assessments. **(B)** Heatmap of correlation between the neuropsychological assessments and sMRI cortical index. **(C)** Significant associations among characteristic taxa, neuroimaging features, and neuropsychological assessments. The Spearman correlation was used to calculate pairwise correlations of all the measurements. The network shows significant correlations (FDR < 0.05) between each pair of measurement types. The size of nodes represents the number of connections with others. Orange edge, Spearman correlation coefficient > 0; blue edge, Spearman correlation coefficient < 0. $*p < 0.05$, $**p < 0.01$.

of phylum *Bacteroides* was significantly increased. Similarly, the decreased *Firmicutes* in the AD population was also confirmed in a cross-sectional study with the research cohort of the Chinese population (Liu et al., 2019). Decreased Firmicutes promote the production of toxic metabolites and pro-inflammatory cytokines, resulting in fewer beneficial substances for intestinal stability, damaging the intestinal epithelial barrier, and subsequently causing the blood–brain barrier dysfunction through peripheral circulation and neuroinflammation, which finally cause brain lesions (Bhat and Kapila, 2017; Cerovic et al., 2019; Liu et al., 2020). There were no significant differences in intra-group alpha diversity analysis and between-group beta diversity analysis and noticeable clustering effect among the three groups. It may be due to a decrease in the number of beneficial bacteria in the intestine and an increase in pathogenic bacteria as the disease progresses. In brief, compared with previous studies based on the Xuanwu cohort (Sheng et al., 2021, 2022), there were common and specific gut microbiota changes in the Hainan cohort. In addition to individual differences in the gut flora, we considered that the regional differences may also influence the distribution of individual gut microbiota.

From the perspective of whole brain volume, SCD shows gray matter and white matter atrophy similar to that in AD in brain regions, such as the hippocampus, medial temporal lobe, anterior cuneiform, and temporoparietal region (Sun et al., 2016, 2019; Hu et al., 2019). In addition, *Mediterraneibacter* was found to be correlated with regional brain structural indices. Some studies have reported that *Mediterraneibacter* and *Odoribacteraceae* participate in bile acid spectrum metabolism and indirectly regulate many individual functions, such as intestinal barrier, neuroinflammation, and immune response (Kim et al., 2019; Sato et al., 2021). Three studies have demonstrated that bile acid can affect metabolism and immune response by regulating Th17 and promoting the production and regulation of homeostasis by Treg cells in the colon tissue (Campbell et al., 2020; Song et al., 2020; Paik et al., 2022). In AD studies, serum concentrations of primary bile acids were significantly reduced in AD patients compared with cognitively

normal older adults, while levels of secondary bile acids and deoxycholic acids produced by gut microbiota were elevated. It suggests that potential gut microbiota dysregulation in AD patients may be caused by increased gut colonization by anaerobic bacteria capable of dehydroxylation of primary bile acids (Mahmoudian Dehkordi et al., 2019).

At present, it has been proved that short-chain fatty acids (SCFA) can inhibit Aβ deposition by interfering with the assembly of Aβ40 and Aβ42 polypeptides into soluble and neurotoxic Aβ aggregates *in vitro* (Ho et al., 2018). In a study of elderly cohorts, the level of individual gut microbiota-derived SCFA was negatively correlated with the pathological degree of Aβ deposition in the brain (Marizzoni et al., 2020). Studies on AD have shown that butyric acid at the gut–blood barrier (GBB) interface promotes the antimicrobial activity of intestinal macrophages, limits bacterial translocation, and enhances intestinal barrier function by providing energy to intestinal epithelial cells and increasing connection integrity (Mathewson et al., 2016). At the blood–brain barrier (BBB) interface, SCFA, mainly butyrate, increases the expression of tight junction proteins in the frontal cortex and hippocampus in mice and acts as a histone deacetylase inhibitor, transcriptional regulator, and anti-inflammatory molecule to maintain brain microvascular homeostasis (Braniste et al., 2014; Chriett et al., 2019). The characteristic microbiota *Lachnospiracea_incertae_sedis*, *Fusicatenibacter*, and *Anaerobutyricum* in the phylum *Firmicutes* analyzed in our study were all SCFA-producing bacteria. In this report, *Lachnospiraceae* was positively correlated with cortical thickness in the entorhinal zone, the Toro's gyrification index in the precuneus zone, and the Toro's gyrification index in the superior parietal, and these indicators were also positively correlated with the degree of cognitive impairment. The abundance of Lachnospiraceae and *Lachnospiracea_ incertae_sedis* was negatively correlated with the fractal dimension of the left fusiform cortex, and *Fusicatenibacter* was negatively correlated with the fractal dimension of the lateral prefrontal cortex. Moreover, the three cortical indicators of the two brain regions also showed an inverse correlation with the neuropsychological assessments. In the study of Thaker et al. (2017) the severity of Aβ deposition in the brain of AD patients and the severity of pathological changes in NFT are positively correlated with the thickness of the entorhinal cortex. The meta-analysis study of the pars orbitalis cortex by Belyk et al. (2017) found that as a semantic information-processing brain region, it is also involved in processing emotional perception signals and belongs to the convergence area of the functional and dynamic perception network. The precuneus is part of the posterior parietal cortex inside the cerebral hemisphere, and its cognitive function involves episodic memory, subspace, self-related information processing, metacognition, and consciousness processes. In a study for early AD therapy, researchers significantly improved episodic memory through stimulation of the precuneus (Koch et al., 2018).

Several microbiotas associated with gastrointestinal and psychiatric disorders have been reported to colonize the gut specifically in AD patients, and this condition affects cognitive function in individuals with AD (Mitrea et al., 2022; Rønnow Sand et al., 2022). *Rikenellaceae*, *Odoribacteraceae*, and *Alistipes* were specifically enriched in the intestines of individuals with CI in our study. The abundance was significantly correlated with the degree of cognitive impairment. In their correlation studies with individual cortical indicators, the primary brain areas affected were the frontal pole, fusiform, lingua, parahippocampal, precuneus, superior parietal, and supramarginal gyrus. However, there are few studies involving the impact of the abovementioned bacteria on brain structural alterations and cognitive impairment.

Currently, there are few studies demonstrating the interaction among gut microbiota, structural brain lesions, and individual cognitive function. In this study, we conducted a joint analysis of three types of characteristic indicators (characteristic GM abundance, sMRI imaging indices, and neuropsychological scale results), and the results showed that there were complex connections between various indicators, which further confirmed the existence of gut microbiota changes in early AD risk groups. In summary, it is suggested that these three microbiotas are related to the decline of individual cognitive function. Their increased abundance may affect the stable structure of specific brain regions, thereby impairing cognitive function. However, further experiments are needed to study the mediator substances and pathways of this effect.

There are several limitations to this study: (1) It is a single-center cross-sectional study of an elderly population in Hainan with a relatively small sample size; however, a larger sample size from multiple centers would be useful and necessary to provide more evidence. The results of this study will require a longitudinal study and randomized controlled trial of participants to determine whether the effect of the specific microbiota on disease progression is confounded by other factors. (2) The 16S rRNA high-throughput assay technique used in the current study achieves low resolution, is sensitive to the specific primers selected and the number of PCR cycles, and may be followed up with a macro-genome sequencing approach that extends taxonomic resolution to the species or strain level, as well as analyses potential functional information. (3) We have only confirmed that alterations in gut microbiota show effects on cognitive performance and brain structure, but the causal nature of the interaction between gut microbiota and cognitive function remains unclear. Subsequent inclusion of biomarkers such as gut microbiota metabolites and intra-blood cytokines will provide more comprehensive insights into the potential mechanisms that form a closed-loop study of gut–brain interactions in AD progression.

5. Conclusion

The present study characterized the gut microbiota and brain structure in the spectrum of AD. It confirmed the possible interactions of gut microbiota alterations on brain structure and cognitive function, providing a new perspective on the pathogenesis of AD and a potential target for AD treatments.

Data availability statement

The datasets presented in this study can be found in online repositories. The names of the repository/repositories and accession number(s) can be found below: https://www.ncbi.nlm.nih.gov/bioproject/PRJNA984461.

Ethics statement

The studies involving human participants were reviewed and approved by the Medical Ethics Committee of Xuanwu Hospital, Capital Medical University, Beijing, China. The patients/participants provided their written informed consent to participate in this study. Written informed consent was obtained from the individual(s) for the publication of any potentially identifiable images or data included in this article.

Author contributions

BH and CS contributed to the conception and design of the study. BH organized the database, performed the statistical analysis, and wrote the first draft of the manuscript. CS wrote sections of the manuscript and contributed to manuscript revision. XY and LZ contributed to the manuscript revision. YH and FC contributed to the manuscript revision, read, and approved the submitted version. All authors contributed to the article and approved the submitted version.

Funding

This study was supported by STI2030-Major Projects (2022ZD0211800), the National Natural Science Foundation of China (Grant No. 82020108013), the Sino-German Cooperation Grant (M-0759), the Science and Technology Development Plan Project of Shandong Medical and Health (Grant No. 202203070774), and the Doctoral Research Fund Project in the Affiliated Hospital of Jining Medical University (Grant No. 2022-BS-02).

Acknowledgments

The authors would like to thank all participants who donated their samples and colleagues who collected the samples.

Conflict of interest

The authors declare that the research was conducted in the absence of any commercial or financial relationships that could be construed as a potential conflict of interest.

Publisher's note

All claims expressed in this article are solely those of the authors and do not necessarily represent those of their affiliated organizations, or those of the publisher, the editors and the reviewers. Any product that may be evaluated in this article, or claim that may be made by its manufacturer, is not guaranteed or endorsed by the publisher.

Supplementary material

The Supplementary Material for this article can be found online at: https://www.frontiersin.org/articles/10.3389/fnagi.2023.1216509/full#supplementary-material

References

Aikman, G. G., and Oehlert, M. E. (2001). Geriatric depression scale. *J. Am. Geriatr. Soc.* 22, 63–70. doi: 10.1300/J018v22n03_07

Ashburner, J., and Friston, K. J. (2000). Voxel-based morphometry–the methods. *Neuroimage* 11 (6 Pt 1), 805–821. doi: 10.1006/nimg.2000.0582

Association American Psychiatric (2013). *Diagnostic and Statistical Manual of Mental Disorders Fifth Edition (DSM-5.)* Arlington, VA: American Psychiatric Pub.

Belyk, M., Brown, S., Lim, J., and Kotz, S. A. (2017). Convergence of semantics and emotional expression within the IFG pars orbitalis. *Neuroimage* 156, 240–248. doi: 10.1016/j.neuroimage.2017.04.020

Bhat, M. I., and Kapila, R. (2017). Dietary metabolites derived from gut microbiota: critical modulators of epigenetic changes in mammals. *Nutr. Rev.* 75, 374–389. doi: 10.1093/nutrit/nux001

Bondi, M. W., Edmonds, E. C., Jak, A. J., Clark, L. R., Delano-Wood, L., McDonald, C. R., et al. (2014). Neuropsychological criteria for mild cognitive impairment improves diagnostic precision, biomarker associations, and progression rates. *J. Alzheimers Dis.* 42, 275–289. doi: 10.3233/JAD-140276

Braniste, V., Al-Asmakh, M., Kowal, C., Anuar, F., Abbaspour, A., Tóth, M., et al. (2014). The gut microbiota influences blood-brain barrier permeability in mice. *Sci. Transl. Med.* 6, 263ra158. doi: 10.1126/scitranslmed.3009759

Buysse, D. J., Reynolds, C. F. 3rd, Monk, T. H., Berman, S. R., and Kupfer, D. J. (1989). The Pittsburgh Sleep Quality Index: a new instrument for psychiatric practice and research. *Psychiatry Res.* 28, 193–213. doi: 10.1016/0165-1781(89)90047-4

Campbell, C., McKenney, P. T., Konstantinovsky, D., Isaeva, O. I., Schizas, M., Verter, J., et al. (2020). Bacterial metabolism of bile acids promotes generation of peripheral regulatory T cells. *Nature* 581, 475–479. doi: 10.1038/s41586-020-2193-0

Cattaneo, A., Cattane, N., Galluzzi, S., Provasi, S., Lopizzo, N., Festari, C., et al. (2017). Association of brain amyloidosis with pro-inflammatory gut bacterial taxa and peripheral inflammation markers in cognitively impaired elderly. *Neurobiol. Aging* 49, 60–68. doi: 10.1016/j.neurobiolaging.2016.08.019

Cerovic, M., Forloni, G., and Balducci, C. (2019). Neuroinflammation and the gut microbiota: possible alternative therapeutic targets to counteract Alzheimer's disease? *Front. Aging Neurosci.* 11, 284. doi: 10.3389/fnagi.2019.00284

Chen, C., Ahn, E. H., Kang, S. S., Liu, X., Alam, A., and Ye, K. (2020). Gut dysbiosis contributes to amyloid pathology, associated with C/EBPβ/AEP signaling activation in Alzheimer's disease mouse model. *Sci. Adv.* 6, eaba0466. doi: 10.1126/sciadv.aba0466

Chen, K. L., Xu, Y., Chu, A. Q., Ding, D., Liang, X. N., Nasreddine, Z. S., et al. (2016). Validation of the Chinese version of montreal cognitive assessment basic for screening mild cognitive impairment. *J. Am. Geriatr. Soc.* 64, e285–e290. doi: 10.1111/jgs.14530

Chowdhary, N., Barbui, C., Anstey, K. J., Kivipelto, M., Barbera, M., Peters, R., et al. (2021). Reducing the risk of cognitive decline and dementia: WHO recommendations. *Front. Neurol.* 12, 765584. doi: 10.3389/fneur.2021.765584

Chriett, S., Dabek, A., Wojtala, M., Vidal, H., Balcerczyk, A., and Pirola, L. (2019). Prominent action of butyrate over β-hydroxybutyrate as histone deacetylase inhibitor, transcriptional modulator and anti-inflammatory molecule. *Sci. Rep.* 9, 742. doi: 10.1038/s41598-018-36941-9

Cole, J. R., Wang, Q., Fish, J. A., Chai, B., McGarrell, D. M., Sun, Y., et al. (2014). Ribosomal Database Project: data and tools for high throughput rRNA analysis. *Nucleic Acids Res.* 42 (Database issue), D633–D642. doi: 10.1093/nar/gkt1244

Cryan, J. F., O'Riordan, K. J., Cowan, C. S., M., Sandhu, K. V., Bastiaanssen, T. F., et al. (2019). The microbiota-gut-brain axis. *Physiol. Rev.* 99, 1877–2013. doi: 10.1152/physrev.00018.2018

De Santis, S., Moratal, D., and Canals, S. (2019). Radiomicrobiomics: advancing along the gut-brain axis through big data analysis. *Neuroscience* 403, 145–149. doi: 10.1016/j.neuroscience.2017.11.055

Edgar, R. C. (2010). Search and clustering orders of magnitude faster than BLAST. *Bioinformatics* 26, 2460–2461. doi: 10.1093/bioinformatics/btq461

Farias, S. T., Mungas, D., Reed, B. R., Cahn-Weiner, D., Jagust, W., Baynes, K., et al. (2008). The measurement of everyday cognition (ECog): scale development and psychometric properties. *J. Neuropsychol.* 22, 531–544. doi: 10.1037/0894-4105.22.4.531

Fung, T. C. (2020). The microbiota-immune axis as a central mediator of gut-brain communication. *Neurobiol. Dis.* 136, 104714. doi: 10.1016/j.nbd.2019.104714

Gauthier, S., RosaNeto, P., Morais, J. A., and Webster, C. (2021). *World Alzheimer Report 2021: Journey Through the Diagnosis of Dementia*. London: Alzheimer's Disease International.

González, D. A., Gonzales, M. M., Resch, Z. J., Sullivan, A. C., and Soble, J. R. (2022). Comprehensive evaluation of the functional activities questionnaire (FAQ) and its reliability and validity. *J Assess.* 29, 748–763. doi: 10.1177/1073191121991215

Guo, Q. H. (2006). Boston naming test in Chinese Elderly, patient with mild cognitive impairment and Alzheimer's dementia. *J. Chin. Mental Health J.* 20, 81–84.

Guo, Q. H., Jin, L. L., and Hong, Z. (2007). A specific phenomenon of animal fluency test in Chinese elderly. *J. Chinese Mental Health J.* 21, 622–625. doi: 10.1016/j.conbuildmat.2005.08.001

Guo, Q. H., Zhou, B., Zhao, Q. H., Wang, B., and Hong, Z. (2012). Memory and Executive Screening (MES): a brief cognitive test for detecting mild cognitive impairment. *J. BMC Neurol.* 12, 119. doi: 10.1186/1471-2377-12-119

Ho, L., Ono, K., Tsuji, M., Mazzola, P., Singh, R., and Pasinetti, G. M. (2018). Protective roles of intestinal microbiota derived short chain fatty acids in Alzheimer's disease-type beta-amyloid neuropathological mechanisms. *Exp. Rev. Neurother.* 18, 83–90. doi: 10.1080/14737175.2018.1400909

Hu, X., Teunissen, C. E., Spottke, A., Heneka, M. T., Düzel, E., Peters, O., et al. (2019). Smaller medial temporal lobe volumes in individuals with subjective cognitive decline and biomarker evidence of Alzheimer's disease-Data from three memory clinic studies. *Alzheimers Dement.* 15, 185–193. doi: 10.1016/j.jalz.2018.09.002

Jessen, F., Amariglio, R. E., Buckley, R. F., van der Flier, W. F., Han, Y., Molinuevo, J. L., et al. (2020). The characterisation of subjective cognitive decline. *Lancet Neurol.* 19, 271–278. doi: 10.1016/S1474-4422(19)30368-0

Jessen, F., Amariglio, R. E., van Boxtel, M., Breteler, M., Ceccaldi, M., Chételat, G., et al. (2014). A conceptual framework for research on subjective cognitive decline in preclinical Alzheimer's disease. *Alzheimers Dement.* 10, 844–852. doi: 10.1016/j.jalz.2014.01.001

Johns, M. W. (1991). A new method for measuring daytime sleepiness: the Epworth sleepiness scale. *Sleep*. 14, 540–545. doi: 10.1093/sleep/14.6.540

Kim, J. S., Lee, K. C., Suh, M. K., Han, K. I., Eom, M. K., Lee, J. H., et al. (2019). Mediterraneibacter butyricigenes sp. nov., a butyrate-producing bacterium isolated from human faeces. *J. Microbiol.* 57, 38–44. doi: 10.1007/s12275-019-8550-8

Kim, M. S., Kim, Y., Choi, H., Kim, W., Park, S., Lee, D., et al. (2020). Transfer of a healthy microbiota reduces amyloid and tau pathology in an Alzheimer's disease animal model. *Gut* 69, 283–294. doi: 10.1136/gutjnl-2018-317431

Koch, G., Bonn,ì, S., Pellicciari, M. C., Casula, E. P., Mancini, M., Esposito, R., et al. (2018). Transcranial magnetic stimulation of the precuneus enhances memory and neural activity in prodromal Alzheimer's disease. *Neuroimage* 169, 302–311. doi: 10.1016/j.neuroimage.2017.12.048

Kowalski, K., and Mulak, A. (2019). Brain-Gut-Microbiota Axis in Alzheimer's Disease. *J. Neurogastroenterol. Motil.* 25, 48–60. doi: 10.5056/jnm18087

Li, H., Jia, J., and Yang, Z. (2016). Mini-mental state examination in elderly Chinese: a population-based normative study. *J. Alzheimers Dis.* 53, 487–496. doi: 10.3233/JAD-160119

Li, X., Wang, X., Su, L., Hu, X., and Han, Y. (2019). Sino Longitudinal Study on Cognitive Decline (SILCODE): protocol for a Chinese longitudinal observational study to develop risk prediction models of conversion to mild cognitive impairment in individuals with subjective cognitive decline. *BMJ Open* 9, e028188. doi: 10.1136/bmjopen-2018-028188

Li, Z., Zhu, H., Guo, Y., Du, X., and Qin, C. (2020). Gut microbiota regulate cognitive deficits and amyloid deposition in a model of Alzheimer's disease. *J. Neurochem.* 155, 448–461. doi: 10.1111/jnc.15031

Liang, X., Fu, Y., Cao, W. T., Wang, Z., Zhang, K., Jiang, Z., et al. (2022). Gut microbiome, cognitive function and brain structure: a multi-omics integration analysis. *Transl. Neurodegener.* 11, 49. doi: 10.1186/s40035-022-00323-z

Lim, W. S., Chin, J. J., Lam, C. K., Lim, P. P., and Sahadevan, S. (2005). Clinical dementia rating: experience of a multi-racial Asian population. *Alzheimers Dis. Assoc. Disord.* 19, 135–142. doi: 10.1097/01.wad.0000174991.60709.36

Liu, P., Wu, L., Peng, G., Han, Y., Tang, R., Ge, J., et al. (2019). Altered microbiomes distinguish Alzheimer's disease from amnestic mild cognitive impairment and health in a Chinese cohort. *Brain Behav. Immun.* 80, 633–643. doi: 10.1016/j.bbi.2019.05.008

Liu, S., Gao, J., Zhu, M., Liu, K., and Zhang, H. L. (2020). Gut microbiota and dysbiosis in Alzheimer's disease: implications for pathogenesis and treatment. *Mol. Neurobiol.* 57, 5026–5043. doi: 10.1007/s12035-020-02073-3

Mahmoudian Dehkordi, S., Arnold, M., Nho, K., Ahmad, S., Jia, W., Xie, G., et al. (2019). Altered bile acid profile associates with cognitive impairment in Alzheimer's disease-An emerging role for gut microbiome. *Alzheimers Dement.* 15, 76–92. doi: 10.1016/j.jalz.2018.07.217

Main, B. S., and Minter, M. R. (2017). Microbial immuno-communication in neurodegenerative diseases. *Front. Neurosci.* 11, 151. doi: 10.3389/fnins.2017.00151

Marizzoni, M., Cattaneo, A., Mirabelli, P., Festari, C., Lopizzo, N., Nicolosi, V., et al. (2020). Short-chain fatty acids and lipopolysaccharide as mediators between gut dysbiosis and amyloid pathology in Alzheimer's disease. *J. Alzheimers Dis.* 78, 683–697. doi: 10.3233/JAD-200306

Mathewson, N. D., Jenq, R., Mathew, A. V., Koenigsknecht, M., Hanash, A., Toubai, T., et al. (2016). Gut microbiome-derived metabolites modulate intestinal epithelial cell damage and mitigate graft-versus-host disease. *Nat. Immunol.* 17, 505–513. doi: 10.1038/ni.3400

McKhann, G. M., Knopman, D. S., Chertkow, H., Hyman, B. T., Jack, C. R., Jr, Kawas, C. H., et al. (2011). The diagnosis of dementia due to Alzheimer's disease: recommendations from the National Institute on Aging-Alzheimer's Association workgroups on diagnostic guidelines for Alzheimer's disease. *Alzheimers Dement.* 7, 263–269. doi: 10.1016/j.jalz.2011.03.005

Mitrea, L., Nemeş, S. A., Szabo, K., Teleky, B. E., and Vodnar, D. C. (2022). Guts imbalance imbalances the brain: a review of gut microbiota association with neurological and psychiatric disorders. *Front. Med.* 9, 813204. doi: 10.3389/fmed.2022.813204

Nomura, T., Inoue, Y., Kagimura, T., Kusumi, M., and Nakashima, K. (2015). Validity of the Japanese version of the REM Sleep Behavior Disorder (RBD) Screening Questionnaire for detecting probable RBD in the general population. *J. Psychiatry Clin. Neurosci.* 69, 477–482. doi: 10.1111/pcn.12286

Paik, D., Yao, L., Zhang, Y., Bae, S., D'Agostino, G. D., Zhang, M., et al. (2022). Human gut bacteria produce T(H)17-modulating bile acid metabolites. *Nature* 603, 907–912. doi: 10.1038/s41586-022-04480-z

Rajapakse, J. C., Giedd, J. N., and Rapoport, J. L. (1997). Statistical approach to segmentation of single-channel cerebral MR images. *IEEE Trans. Med. Imaging* 16, 176–186. doi: 10.1109/42.563663

Riccelli, R., Toschi, N., Nigro, S., Terracciano, A., and Passamonti, L. (2017). Surface-based morphometry reveals the neuroanatomical basis of the five-factor model of personality. *Soc. Cogn. Affect. Neurosci.* 12, 671–684. doi: 10.1093/scan/nsw175

Rønnow Sand, J., Troelsen, F. S., Horváth-Puhó, E., Henderson, V. W., Sørensen, H. T., and Erichsen, R. (2022). Risk of dementia in patients with inflammatory bowel disease: a Danish population-based study. *Aliment. Pharmacol. Ther.* 56, 831–843. doi: 10.1111/apt.17119

Sato, Y., Atarashi, K., Plichta, D. R., Arai, Y., Sasajima, S., Kearney, S. M., et al. (2021). Novel bile acid biosynthetic pathways are enriched in the microbiome of centenarians. *Nature* 599, 458–464. doi: 10.1038/s41586-021-03832-5

Sheng, C., Lin, L., Lin, H., Wang, X., Han, Y., and Liu, S. L. (2021). Altered gut microbiota in adults with subjective cognitive decline: the SILCODE Study. *J. Alzheimers Dis.* 82, 513–526. doi: 10.3233/JAD-210259

Sheng, C., Yang, K., He, B., Du, W., Cai, Y., and Han, Y. (2022). Combination of gut microbiota and plasma amyloid-β as a potential index for identifying preclinical Alzheimer's disease: a cross-sectional analysis from the SILCODE study. *Alzheimers Res. Ther.* 14, 35. doi: 10.1186/s13195-022-00977-x

Song, X., Sun, X., Oh, S. F., Wu, M., Zhang, Y., Zheng, W., et al. (2020). Microbial bile acid metabolites modulate gut RORγ(+) regulatory T cell homeostasis. *Nature* 577, 410–415. doi: 10.1038/s41586-019-1865-0

Sun, Y., Dai, Z., Li, Y., Sheng, C., Li, H., Wang, X., et al. (2016). Subjective cognitive decline: mapping functional and structural brain changes—A combined resting-state functional and structural MR imaging study. *J. Radio.* 281, 185–92. doi: 10.1148/radiol.2016151771

Sun, Y., Wang, X., Wang, Y., Dong, H., Lu, J., Scheininger, T., et al. (2019). Anxiety correlates with cortical surface area in subjective cognitive decline: APOE ε4 carriers versus APOE ε4 non-carriers. *Alzheimers Res. Ther.* 11, 50. doi: 10.1186/s13195-019-0505-0

Thaker, A. A., Weinberg, B. D., Dillon, W. P., Hess, C. P., Cabral, H. J., Fleischman, D. A., et al. (2017). Entorhinal cortex: antemortem cortical thickness and postmortem neurofibrillary tangles and amyloid pathology. *Am. J. Neuroradiol.* 38, 961–965. doi: 10.3174/ajnr.A5133

Vemuri, P., and Jack, C. R. Jr. (2010). Role of structural MRI in Alzheimer's disease. *Alzheimers Res. Ther.* 2, 23. doi: 10.1186/alzrt47

Vogt, N. M., Kerby, R. L., Dill-McFarland, K. A., Harding, S. J., Merluzzi, A. P., Johnson, S. C., et al. (2017). Gut microbiome alterations in Alzheimer's disease. *Sci. Rep.* 7, 13537. doi: 10.1038/s41598-017-13601-y

Whitwell, J. L. (2018). Alzheimer's disease neuroimaging. *Curr. Opin. Neurol.* 31, 396–404. doi: 10.1097/WCO.0000000000000570

Zhao, Q., Guo, Q., Li, F., Zhou, Y., Wang, B., and Hong, Z. (2013). The Shape Trail Test: application of a new variant of the Trail making test. *PLoS ONE* 8, e57333. doi: 10.1371/journal.pone.0057333

Zhao, Q., Lv, Y., Zhou, Y., Hong, Z., and Guo, Q. (2012). Short-term delayed recall of auditory verbal learning test is equivalent to long-term delayed recall for identifying amnestic mild cognitive impairment. *PLoS ONE* 7, e51157. doi: 10.1371/journal.pone.0051157

Zheng, L. J., Lin, L., Zhong, J., Zhang, Z., Ye, Y. B., Zhang, X. Y., et al. (2020). Gut dysbiosis-influence on amygdala-based functional activity in patients with end stage renal disease: a preliminary study. *Brain Imaging Behav.* 14, 2731–2744. doi: 10.1007/s11682-019-00223-3

Zhuang, Z. Q., Shen, L. L., Li, W. W., Fu, X., Zeng, F., Gui, L., et al. (2018). Gut microbiota is altered in patients with Alzheimer's Disease. *J. Alzheimers Dis.* 63, 1337–1346. doi: 10.3233/JAD-180176

frontiers | Frontiers in Aging Neuroscience

TYPE Review
PUBLISHED 03 August 2023
DOI 10.3389/fnagi.2023.1206572

OPEN ACCESS

EDITED BY
Woon-Man Kung,
Chinese Culture University, Taiwan

REVIEWED BY
Tadanori Hamano,
University of Fukui, Japan
Sergey Bachurin,
Institute of Physiologically Active Compounds (RAS), Russia

*CORRESPONDENCE
Yong Peng
✉ 1779342446@qq.com

RECEIVED 16 April 2023
ACCEPTED 10 July 2023
PUBLISHED 03 August 2023

CITATION
Peng Y, Jin H, Xue Y-h, Chen Q, Yao S-y, Du M-q and Liu S (2023) Current and future therapeutic strategies for Alzheimer's disease: an overview of drug development bottlenecks.
Front. Aging Neurosci. 15:1206572.
doi: 10.3389/fnagi.2023.1206572

Current and future therapeutic strategies for Alzheimer's disease: an overview of drug development bottlenecks

Yong Peng[1,2]*, Hong Jin[1,2], Ya-hui Xue[1,2], Quan Chen[1,2], Shun-yu Yao[1,2], Miao-qiao Du[1,2] and Shu Liu[1,2]

[1]Neurology Department, The First Affiliated Hospital of Hunan Traditional Chinese Medical College, Zhuzhou, Hunan, China, [2]Neurology Department, The Third Affiliated Hospital of Hunan University of Chinese Medicine, Zhuzhou, Hunan, China

Alzheimer's disease (AD) is the most common chronic neurodegenerative disease worldwide. It causes cognitive dysfunction, such as aphasia and agnosia, and mental symptoms, such as behavioral abnormalities; all of which place a significant psychological and economic burden on the patients' families. No specific drugs are currently available for the treatment of AD, and the current drugs for AD only delay disease onset and progression. The pathophysiological basis of AD involves abnormal deposition of beta-amyloid protein (Aβ), abnormal tau protein phosphorylation, decreased activity of acetylcholine content, glutamate toxicity, autophagy, inflammatory reactions, mitochondria-targeting, and multi-targets. The US Food and Drug Administration (FDA) has approved five drugs for clinical use: tacrine, donepezil, carbalatine, galantamine, memantine, and lecanemab. We have focused on the newer drugs that have undergone clinical trials, most of which have not been successful as a result of excessive clinical side effects or poor efficacy. Although aducanumab received rapid approval from the FDA on 7 June 2021, its long-term safety and tolerability require further monitoring and confirmation. In this literature review, we aimed to explore the possible pathophysiological mechanisms underlying the occurrence and development of AD. We focused on anti-Aβ and anti-tau drugs, mitochondria-targeting and multi-targets, commercially available drugs, bottlenecks encountered in drug development, and the possible targets and therapeutic strategies for future drug development. We hope to present new concepts and methods for future drug therapies for AD.

KEYWORDS

Alzheimer's disease, β-amyloid protein, tau protein, mitochondria-targeting, multi-targets, clinical trials

1. Introduction

Alzheimer's disease (AD) is a chronic progressive disease with a hidden onset, unknown etiology, and long-term course. It is characterized mainly by cognitive dysfunction, such as aphasia and agnosia, and mental symptoms, such as hallucinations, delusions, and behavioral abnormalities, which significantly reduce the quality of life of older people

(Alzheimer's Association, 2022). The number of patients with AD worldwide is expected to exceed 150 million by 2050, according to the 2022 Alzheimer's Disease Facts and Figures report (Man et al., 2023). Despite extensive research, the etiology of AD is complex, and its pathogenesis remains unknown. The primary hypotheses are abnormal deposition of beta-amyloid protein (Aβ), abnormal phosphorylation of tau protein, and nervous system inflammation, among others. Unfortunately, no drugs that can block AD progression are currently available.

Five drugs, Tacrine, Donepezil, Carbalatine, Galanthamine, and Memantine, have been approved by the Food and Drug Administration (FDA) for clinical use. Recently, FDA also approved Lecanemab. The first four types of drugs are acetylcholinesterase inhibitors (AChEIs), which can inhibit the activity of acetylcholinesterase (AChE) to prevent the degradation of acetylcholine in the synaptic gap, increasing the cholinergic effects, maintaining neuronal activity, and improving memory and learning abilities. Memantine is an N-methyl-D-aspartate (NMDA) receptor antagonist that can reduce the neurotoxicity of excitatory amino acids in the synaptic cleavage and reduce neuronal apoptosis. However, these drugs only manage symptoms and delay the onset of AD but do not cure it. Lecanemab (BAN2401), an IgG1 monoclonal antibody, was well tolerated during the trial, although some participants experienced ARIA-E (Swanson et al., 2021). In a multicenter, double-blind, 18-month Phase III trial, Lecanemab reduced amyloid markers in patients with early AD; longer trials are required to determine the effectiveness and safety of this drug (van Dyck et al., 2023).

Several drugs are undergoing clinical trials for AD, but unfortunately, many have been terminated because of poor efficacy or large adverse reactions. Existing clinical trials have focused on two pathological features of AD: amyloid plaques (Aβ), tau protein, mitochondria-targeting, and multi-targets. Therefore, we classified AD's future treatment strategies into four main aspects: resistance against Aβ or anti tau protein treatment, mitochondria-targeting, and multi-targets agents.

Abbreviations: Aβ, beta-amyloid protein; Ach, acetylcholine; AChE, acetylcholinesterase; AChEI, acetylcholinesterase inhibitor; α-KGD, alpha-ketoglutarate dehydrogenase; AD, Alzheimer's disease; ADAS-Cog, Alzheimer's Disease Assessment Scale–Cognitive Subscale; ADCS-CGIC, Alzheimer's Disease Cooperative Study–Clinical Global Impression of Change scale; ADCS-ADL, Alzheimer's Disease Cooperative Study–Activities of Daily Living Inventory; AE, adverse effects; APP, amyloid precursor protein; ARIA, amyloid-related imaging abnormalities; ARIA-E, amyloid-related imaging abnormalities-edema; BACE-1, β-site amyloid precursor protein cleaving enzyme-1; BBB, blood–brain barrier; BChE, butyrylcholinesterase; C99, the membrane-bound carbon terminal 99 amino acid fragment; CaE, carboxylesterase; FDA, Food and Drug Administration; GSA-3β, glycogen synthase kinase 3β; iGluRs, ionotropic glutamate receptors; LMTM, leuco-methylthioninium bis (hydromethanesulfonate); mRC, mitochondrial respiratory chain; mGluRs, metabotropic glutamate receptors; ME, meningoencephalitis; MPT, mitochondrial permeability transition; MCI, mild cognitive impairment; NMDAR, anti-N-methyl-D-aspartate receptor; NbM, nucleus basalis of Meynert; NFTs, neurofibrillary tangles; NRF, nuclear respiratory factors; PGC-1, PPARγ coactivator-1; PoC, proof-of-concept; PPAR, peroxisome proliferator-activated receptor; PPIase, peptidyl-prolyl cis–trans isomerase; ROS, reactive oxygen species; TCA, tricarboxylic acid; ÒFAM, the mitochondrial transcription factor; TEAEs, treatment-related adverse reactions; TSPO, translocator protein; VGLUT, vesicular glutamate transporter.

2. Brief introduction of the physiological and pathological basis of AD

There were nine major mechanisms of the physiological and pathological basis of AD, such as Aβ deposition (Basisty et al., 2020), abnormal phosphorylation of tau protein (Jouanne et al., 2017; Hampel et al., 2019; Jo et al., 2020), decreasing acetylcholine activity (Cho et al., 2019; Babic Leko et al., 2021), glutamate toxicity (Ogbodo et al., 2022), autophagy (Reddy and Oliver, 2019; Luo et al., 2020), inflammatory response (Nho et al., 2019), neurovascular mechanism and mitochondrial hypothesis (Reddy and Reddy, 2017; Shevtsova et al., 2017, 2021; Wilkins and Morris, 2017; Liu et al., 2019), as well as "multi-target" agents (Makhaeva et al., 2019).

2.1. Aβ deposition

Beta-amyloid protein is an important biomarker used in the diagnosis of AD. Aβ plaques are formed by the hydrolysis of amyloid precursor protein (APP) through α, β, and γ secretory enzymes. Specifically, a portion of APP is cleaved by β-site APP-cleaving enzyme-1 (BACE-1) to produce a membrane-bound carbon terminal 99 amino acid fragment known as C99. C99 is then cleaved by γ-secretase to form Aβ1-40 and Aβ42. While Aβ monomers are typically soluble in small amounts and have no neurotoxicity, Aβ1–40 and Aβ42 are neurotoxic because of modulation by γ-secretase. They are more likely to accumulate into oligomers, which are eventually deposited in areas such as the olfactory cortex, hippocampus, and other areas of the cortex to form amyloid plaques. Ultimately, Aβ1–40 and Aβ42 lead to synaptic dysfunction, neuronal death, and cognitive decline (Basisty et al., 2020).

2.2. Abnormal phosphorylation of tau protein

Tau protein is a soluble microtubule-associated protein that combines with other tubules to form microtubules that coordinate various cellular functions. Abnormal phosphorylated tau protein forms neurofibrillary tangles (NFTs) that are deposited in the cytoplasm, rendering it unable to perform normal biological functions such as maintaining microtubule stability, reducing dissociation, and inducing microtubule bunching (Jouanne et al., 2017). It is also closely associated with cognitive decline. Protein kinases and phosphatases regulate tau protein phosphorylation. Studies have shown that Aβ can affect the activity of glycogen synthase kinase 3β (GSK-3β) and other protein kinases and the stability of the PP system, thus inducing tau protein deposition (Hampel et al., 2019). A study of 107 participants using Tau positron emission tomography (PET) scans found that mild cognitive decline in precursor AD was mainly related to abnormal tau protein accumulation in the medial and infratemporal cortex (Jo et al., 2020).

2.3. Acetylcholine activity was decreased

Acetylcholine is a neurotransmitter closely related to cognitive functions in the brain, such as learning and memory. The severity of AD is positively correlated with the degree of cholinergic deficiency. Cholinergic deficiency in patients with AD affects the blood–brain barrier (BBB), reducing neuronal excitability and weakening memory and learning functions. The nucleus basalis of Meynert (NbM) is the cerebral cortex's main source of cholinergic innervation. Extensive literature has shown that in the early stages of AD, patients have a significant loss of "large cell neurons" in the NbM and degeneration of nerve fibers (Ch4) in cholinergic NbM neurons. The degree of nerve fiber degeneration is associated with cognitive deficits (Cho et al., 2019). The number of Ch4 neurons is reduced by 80% in patients with AD compared with healthy controls (Babic Leko et al., 2021).

2.4. Glutamate toxicity

Glutamic acid is an excitatory amino acid in the nervous system that is involved in synaptic transmission, structural differentiation, learning, memory, and other neuronal functions. Ionotropic glutamate receptors (iGluRs) and metabotropic glutamate receptors (mGluRs) are distributed throughout the postsynaptic membranes of neurons. In patients with AD, the expression levels of vesicular glutamate transporters (VGLUT) 1 and 2 in the cerebral cortex are decreased, and the process of converting glutamic acid to glutamine is blocked, leading to excessive accumulation of glutamic acid between synapses. This accumulation acts on the anti-N-methyl-D-aspartate receptor (NMDAR), ultimately increasing Ca^{2+} concentration, neuroexcitatory toxicity, and neuronal apoptosis (Ogbodo et al., 2022).

2.5. Autophagy

Autophagy is a lysosome-mediated process that prevents abnormal protein aggregation and cell aging; it is essential for eliminating harmful substances in the body (Reddy and Oliver, 2019). Mitochondria play a crucial role in providing large amounts of adenosine triphosphate (ATP) for normal neuronal function. The removal of damaged mitochondria because of aging is vital for the maintenance of cellular homeostasis. Studies have shown that abnormal mitochondrial autophagy can lead to abnormal accumulation of the Aβ42 protein, even before the onset of the pathological symptoms of AD. Moreover, abnormal deposition of the Aβ42 protein has toxic effects on mitochondrial autophagy, inhibiting its normal function by suppressing key enzymes involved in mitochondrial metabolism (Luo et al., 2020).

2.6. Inflammatory response

Neuroinflammatory responses play a critical role in AD progression. Acute inflammation protects against brain injury and microglial cells act as phagocytes of the immune system. However, when the phagocytic capacity of microglia reaches maximum, their continuous activation results in the loss of their ability to clear Aβ plaques. Subsequently, the continuous deposition of Aβ plaques contributes to learning and memory dysfunction in patients with AD. Additionally, studies have shown that intestinal microbial disorders are closely associated with the occurrence of AD. Intestinal microbial disorders cause an increase in deoxycholic acid, which is deposited in the brain through the BBB, leading to apoptosis, reactive oxygen species (ROS) generation, inflammation, and neurodegeneration (Nho et al., 2019).

2.7. Mitochondrial hypothesis

The hypothesis of mitochondria-targeting drugs on AD included were as follows: (1) an improvement of the energy deficit related to neurodegeneration, including mitochondrial bioenergetics stimulants, mitochondrial biogenesis activators, and neuroprotectors and (2) increase in the resistance of mitochondria to the opening of mitochondrial permeability transition (MPT) pores (Shevtsova et al., 2021). There are some early signs in the early stage of AD and mild cognitive impairment (MCI), such as (1) the decrease in glucose consumption and disruption of mitochondrial bioenergetics (Chételat et al., 2003; Bachurin et al., 2018) and (2) disruption of glucose transport through BBB (Delbarba et al., 2016; Kuehn, 2020).

Alzheimer's disease might be called "type 3 diabetes" because insulin resistance increases the risk of dementia (Kandimalla et al., 2017; Neth and Craft, 2017). Insulin is associated with the brain's energy metabolism; insulin receptors are widely expressed in the brain's temporal lobe and hippocampus, which control memory and language (Watson and Craft, 2003). Also, the insulin-sensitive glucose transporter GLUT4 is important for memory and cognitive functions, which is expressed in the brain area, particularly in the hippocampus. Finally, additional glucose supply contributes to the activation of brain bioenergetics.

The activity and expression of the mitochondrial respiratory chain (mRC) decreased in early AD and its animal model (Yao et al., 2009). An Aβ-induced mitochondrial dysfunction of AD model was made by a transgenic *Caenorhabditis elegans* strain, which expressed human Aβ peptide specifically in neurons (GRU102). It showed that alterations in the tricarboxylic acid (TCA) cycle metabolism; reduced activity of a rate-limiting TCA cycle enzyme, i.e., alpha-ketoglutarate dehydrogenase (α-KGD); and low-level Aβ expression in GRU102 result in increasing protein carbonyl content, specifically in mitochondria. Moreover, metformin (an anti-diabetes drug) recovered Aβ-induced metabolic defects, reduced protein aggregation, and normalized the lifespan of GRU102 (Teo et al., 2019). Furthermore, metformin decreased the blood glucose level, α-KGD activity, and formation of Àβ aggregates. It can even extend the life span of *C. elegans*, enhancing the mRC activity and mitochondrial fission (Wang et al., 2019).

2.8. "Multi-target" agents

Multiple pathogenic factors (e.g., Aβ, metal ions, metal-bound Aβ, and ROS) are found in the brain of patients

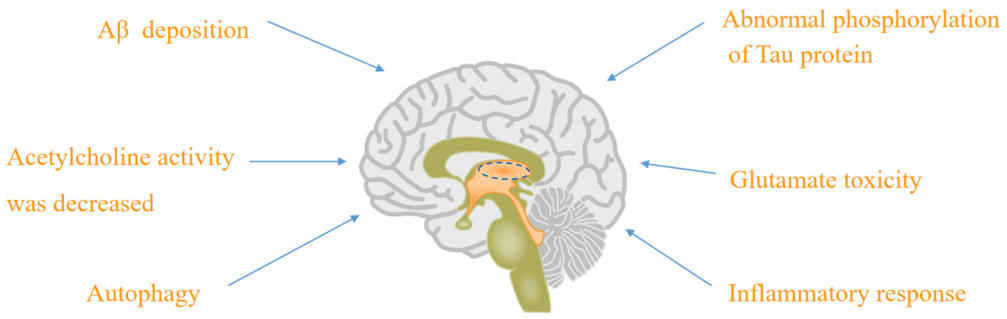

FIGURE 1
The physiological and pathological basis of AD: Aβ deposition, abnormal phosphorylation of tau protein, acetylcholine activity was decreased, glutamate toxicity, autophagy, and inflammatory response.

with AD. One of the modern approaches for creating multitarget agents for AD treatment is polypharmacophore design—building hybrid molecules that are conjugates of two or more different pharmacophores linked together with spacers (Bolognesi and Cavalli, 2016; Han et al., 2018).

Alzheimer's disease is a multifactorial neurodegenerative disease; therefore, logically multi-target drugs would be the best choice (Makhaeva et al., 2019). To date, there are five pharmacophores that demonstrate multi-target effects on AD, which are γ-carbolines, carbazoles, tetrahydrocarbazoles, phenothiazines, and aminoadamantanes. Biological activity of these compounds include inhibitory potency against AChE, butyrylcholinesterase (BChE), anti-carboxylesterase and anti-aggregation activities, and binding to the two sites of the NMDA subtype of the glutamate receptor to conduct potential cognition enhancement and neuroprotection against mitochondrial triggers of cell death (Makhaeva et al., 2019). There were selective BChE inhibitors (conjugates of γ-carbolines and phenothiazine I, γ-carbolines and carbazoles II, and aminoadamantanes and carbazoles III) as well as inhibitors of both cholinesterases (conjugates of γ-carbolines and methylene blue IV and bis-γ-carbolines with ditriazole-containing spacers V). These compounds exhibit combined potential for cognition enhancement, neuroprotection, and disease modification. Moreover, none of the conjugates exhibited high potency against carboxylesterase (CaE), thereby precluding potential drug–drug interactions through CaE inhibition (Makhaeva et al., 2019; **Figure 1**).

3. Therapeutic strategies for developing anti-AD drugs

The FDA has currently approved single-target drugs such as AChEI and NMDAR antagonists. There is a growing interest in developing multi-target drugs (Athar et al., 2021) that can address various aspects of AD pathology, including anti-Aβ deposition, tau protein phosphorylation, oxidative stress, and mitochondrial autophagy dysfunction. Many of these drugs are currently undergoing clinical trials.

3.1. Upcoming AD drugs targeting Aβ

The above FDA-approved therapies are only intended to ameliorate symptoms. Therefore, disease-modifying therapies are required to slow, modify, and control AD progression. The main mechanism of action of anti-Aβ drugs is to reduce the Aβ production, prevent its deposition, and accelerate its clearance.

3.1.1. β-Secretase inhibitor

β-Secretase inhibitors primarily reduce the production of amyloid beta. However, clinical trials of inhibitors targeting β-site APP-cleaving enzyme 1 (BACE1, also known as β-secretase 1) have largely been unsuccessful. Verubecestat, Lanabecestat, and Atabecestat are some of the molecules from the acyl guanidine class that have successfully reached the later stages of clinical trials. Nevertheless, they all failed to reach the market because of toxicity or a lack of clinical efficacy (Patel et al., 2022).

Verubecestat (MK-8931) was the first compound to enter Phase III trials because of its ability to cross the BBB and improve bioavailability. However, two Phase III clinical trials, EPOCH and APECS, were terminated prematurely after the drug failed to improve cognitive decline in participants and increased adverse events (AE) (Doggrell, 2019; Egan et al., 2019; Moussa-Pacha et al., 2020; Patel et al., 2022).

Lanabecestat (AZD3293) was studied in two Phase II/III and Phase III trials: AMARANTH and DAYBREAK-ALZ. These trials were designed to demonstrate its ability to slow the progression of mild AD. However, it was not found to slow cognitive decline in patients with mild AD at the mid-stage of the trial. Therefore, the trial was terminated prematurely (Wessels et al., 2020).

Atabecestat (JNJ-54861911), a potent BACE1 inhibitor, reduces the Aβ production in treating AD. Two Phase I trials, NCT01978548 and NCT02360657, showed an average 67 and 90% reduction in Aβ1-40 in the cerebrospinal fluid (CSF) of patients with early AD who received daily doses of 10 and 50 mg atabecestat for 4 weeks (Timmers et al., 2018). However, in a Phase II/III randomized, double-blind, placebo-controlled study, the trial was stopped early because of serious liver-related AE, and cognitive deterioration was found to be reversible after a 6-month follow-up of patients with AD (Sperling et al., 2021).

The BACE-1 inhibitor, Umibecestat (CNP520), has high selectivity and brain penetration, and animal toxicology studies have shown that it has a sufficiently safe range without AEs such as hair loss, cardiovascular damage, or liver toxicity (Neumann et al., 2018). However, trials of umibecestat at doses of 15 and 50 mg were stopped in two clinical prevention studies after the participants showed deterioration in the Neuropsychological State Cognition Test, even displaying significant brain shrinkage and weight loss (Vormfelde et al., 2020).

Elenbecestat (E2609) is another BACE-1 inhibitor that is an aminothiazine derivative. It has been shown to reduce the Aβ level in CSF (Roberts et al., 2021). In preclinical studies, without evidence of hypopigmentation, Elenbecestat reduced Aβ protein levels in rat and guinea pig brains, CSF, and plasma (Moriyama et al., 2017; Hsiao et al., 2019). In an elenbecestat healthy volunteer Phase I study (E2609-A001-002), it showed that Aβ decreased at 50 mg and increased at 100 and 400 mg (ClinicalTrials.gov.NCT01511783). This result was supported by an elenbecestat Phase II study (E2609-G000-201), which showed that CSF Aβ decreased at 50 mg in patients with MCI and early mild AD. Unfortunately, two elenbecestat global Phase III studies (E2609-G000-301 or MissionAD1) (ClinicalTrials.gov.NCT02956486) and (E2609-G000-302 or MissionAD2) were terminated because of an unfavorable risk-benefit ratio (Miranda et al., 2021).

3.1.2. γ-Secretase inhibitors

Semagacestat (LY450139) is a non-selective small-molecule γ-secretase inhibitor that targets the same mechanism as that of β-secretase inhibitors, aiming to reduce the deposition of Aβ amyloid protein. Two single-dose (140 mg), open-label, randomized crossover Phase III clinical trials showed that the clinical efficacy of semagacestat was independent of the preparation, food, and administration time. Additionally, the drug was well tolerated during the trial, and no safety concerns were reported (Willis et al., 2012). However, in a later Phase III trial (NCT00594568), the trial was terminated because of weight loss in patients treated with semagacestat and significantly higher rates of AEs, such as skin cancer and infection, than in the placebo group (Doody et al., 2013; Henley et al., 2014). Similarly, in a Phase II clinical trial of avagacestat in patients with mild-to-moderate AD, the trial was terminated because of the development of AEs such as brain microbleeds, diabetes, and skin cancer (Pinheiro and Faustino, 2019).

3.1.3. Drugs that enhance Aβ clearance (immunotherapy)

The two main types of immunotherapeutic drugs that can enhance the immune clearance of pathogens are active immunity (achieved through vaccination) and passive immunity (achieved through the administration of monoclonal antibodies).

3.1.4. Active immunity

The first anti-Aβ vaccine (AN1792) demonstrated the success of active immunotherapy in eliminating Aβ plaques, which could also be maintained for up to 14 years. However, in the Phase IIa clinical trial, approximately 6% of patients with AD treated with AN1792 developed meningoencephalitis (ME), leading to the termination of the trial. ME production may be related to the T-cell immune response (Nicoll et al., 2019).

A novel vaccine called ACC-001 was developed to avoid harmful T-cell responses and accelerate the clearance of Aβ plaques to address this issue (Pride et al., 2008). Phase II clinical trials of ACC-001 in patients with mild and moderate AD indicated that the vaccine had tolerable safety, regardless of whether the QS-21 adjuvant was used (Pasquier et al., 2016). Additionally, it was found that ACC-001 + QS-21 produced higher anti-Aβ antibody titers than the control group without QS-21 (Hull et al., 2017).

However, CAD106, an anti-Aβ vaccine containing peptide Aβ1-6, was terminated in another study of an AD prevention program because of abnormal changes in cognitive function, brain volume, and body weight in participants (Ohtake et al., 2017). In contrast, in Phase I clinical trials, ABvac40, the first active vaccine targeting the C-terminal of Aβ40, has shown good safety and tolerability (Lacosta et al., 2018).

3.1.5. Passive immunity

Bapineuzumab is a humanized monoclonal antibody that specifically targets Aβ and aims to reduce the abnormal deposition of Aβ plaques. In a Phase II study, treatment-emergent adverse events (TEAEs), including agitation and urinary tract infections, were reported in patients with severe AD. Bapineuzumab also causes amyloid-related imaging abnormalities (ARIA) with effusion or edema (ARIA-E) and ferriflavin deposition (Salloway et al., 2018). However, in two Phase III trials (NCT00575055 and NCT00574132), bapineuzumab did not significantly improve cognitive function in patients with AD (Salloway et al., 2014).

In contrast, gantenerumab is an IgG monoclonal antibody that accelerates the clearance of Aβ plaques through Fc receptor-mediated phagocytosis. A PET substudy clinical trial showed that a 1,200 mg dose of gantenerumab could stably clear Aβ plaques (Klein et al., 2019). No serious adverse events were reported after large-volume subcutaneous injection of gantenerumab (Portron et al., 2020). This drug can potentially reverse the pathology of amyloid plaques significantly and may alter the course of the disease by slowing or stopping its clinical progression (Bateman et al., 2022).

Crenezumab (RO5490245) is an IgG4 antibody with a high affinity for Aβ plaque oligomers and can be administrated at higher doses. No serious adverse events were reported in the GP29523 or GP40201 studies (Dolton et al., 2021). Two other Phase III multicenter trials were halted during mid-stage reviews because of the lack of clinical effectiveness of crenezumab (Ostrowitzki et al., 2022).

Ponezumab (PF-04360365), an IgG2 monoclonal antibody, was well tolerated in the trial but did not significantly affect Aβ deposition (Landen et al., 2017). In a double-blind, placebo-controlled Phase III trial of solanezumab at a dose of 400 mg every 4 weeks in patients with mild AD, no significant improvement in cognitive decline was observed, and cognitive decline preceded dysfunction in patients with mild AD throughout the trial. These findings could provide new insights into the prevention and treatment of AD at an early stage (Honig et al., 2018; Liu-Seifert et al., 2018).

Donanemab is currently in Phase III trials for the treatment of early AD. In the four Donanemab studies, 228 participants receiving Donanemab and 168 participants receiving placebo had low baseline levels of complete amyloid clearance. It was also found that in the Donanemab group, Tau accumulation was slower, and

TABLE 1 The anti-Aβ drugs are currently undergoing clinical trials or just approved including name of drugs, mechanism, company, and clinical trials.

Name of drug	Mechanism	Company	Clinical status
Verubecestat (MK-8931)	BACE 1 inhibitor	Merck Sharp (USA)	Phase III (terminated in 2019)
Lanabecestat (LY3314814)		Eli Lilly (USA)	Phase III (terminated in 2018)
Atabecestat (JNJ-54861911)		Janssen (USA)	Phase IIb/III (terminated in 2018)
Umibecestat (CNP520)		Novartis, Amgen, and Banner (USA)	Phase II/III (terminated in 2019)
Elenbecestat (E2609)		Biogen and Eisai (USA)	Phase III (terminated in 2019)
Semagacestat	γ-Secretase inhibitors	Eli Lilly (USA)	Phase III (terminated in 2011)
Avagacestat		Bristol-Myers Squibb (USA)	Phase II (terminated in 2013)
ACC-001	Active immunity	JANSSEN (USA)	Phase II (completed)
CAD106		Novartis (USA)	Phase II (terminated in 2010)
ABvac40		Araclon Biotech S.L.	Phase I (completed)
Bapineuzumab	Passive immunity	JANSSEN, Pfizer (USA)	Phase III (completed)
Gantenerumab		Hoffmann-La Roche	Phase III (completed)
Crenezumab		Hoffmann-La Roche	Phase III (terminated in 2019)
Ponezumab		Pfizer (USA)	Phase I (completed)
Solanezumab		Eli Lilly (USA)	Phase III (terminated in 2017)
Donanemab		Eli Lilly (USA)	Phase III (ongoing)
Aducanumab		Biogen	Approved (7th June 2021)

Donanemab was associated with ARIA-related AEs during the trial (Mintun et al., 2021; Rashad et al., 2022; Shcherbinin et al., 2022).

Aducanumab, a monoclonal antibody that targets soluble and insoluble Aβ aggregates (IgG1) and selectively binds to Aβ, received accelerated approval from the US FDA on 7 June 2021. It was the first new drug for the treatment of AD for 20 years, following the approval of the US FDA. It is currently under regulatory review in Japan and Europe to assess its safety and tolerability for long-term use (Dhillon, 2021). However, this drug can significantly increase the incidence of ARIA (Cummings et al., 2021; **Table 1** and **Figure 2**).

3.2. Anti-tau drugs

The role of the tau protein is not fully understood, but studies have shown that it plays an important role in the assembly and stabilization of cytoskeletal microtubules. Abnormal hyperphosphorylation of Tau (p-tau) reduces its affinity with bound microtubules, and Tau's abnormal phosphorylation leads to the aggregation and formation of NFT. The treatment of anti-tau drugs mainly includes three aspects: preventing tau hyperphosphorylation and aggregation, stabilizing microtubules, and accelerating tau clearance.

3.2.1. GSK-3β inhibitor

Tau phosphorylation is regulated by protein kinase and phosphatase. Among these, GSA-3β is associated with p-tau production and subsequent neuronal degeneration in AD (Wegmann et al., 2021). GSK-3β inhibitors can prevent tau hyperphosphorylation. Studies have shown that GSK-3β can reduce abnormal Tau phosphorylation and amyloid protein production *in vitro* and *in vivo*, a promising disease-modifying therapy for AD. Tideglusib, a thiadiazolone that irreversibly inhibits GSK-3β and reduces tau phosphorylation, did not show any clinical benefit in a double-blind, placebo-controlled Phase II trial demonstrating the clinical efficacy of GSK-3 inhibitors in AD and is subject to further study (Lovestone et al., 2015). Lithium was first used in psychiatry and was discovered by Australian psychiatrist John Cade in 1949 and has been widely used to treat manic episodes. In recent years, Lithium has been found to be an inhibitor of GSK3, involved in glucose metabolism, cell signaling and proliferation, and glial cell function regulation. Lithium can prevent amyloid formation and Tau hyperphosphorylation. There have been some case reports as well as case control studies showing that Lithium can reduce the symptoms of AD. However, clinically available Lithium has serious side effects (SAE) with long-term use. It requires constant monitoring of Lithium concentrations in the blood; safer and more effective Lithium is needed for clinical use (Haussmann et al., 2021; Hu et al., 2022; Muronaga et al., 2022; Luca and Luca, 2023).

3.2.2. Tau aggregation inhibitor

Tau accumulation is associated with neuron loss. Tau aggregation inhibitors such as methylthioninium chloride (methblue) and hydromethanesulfonate (LMTM) can reduce Tau accumulation.

Methylthioninium chloride (methylene blue) is also a drug with a long history of use, primarily in malaria, methemogenemia, and carbon monoxide poisoning, as well as histological dyes. Methylthioninium chloride failed to show clinical benefit for AD in a 24-week Phase II study (Tucker et al., 2018). LMTM is a compound with a higher bioavailability and lower toxicity than methylthioninium chloride. In one Phase III trial involving mild to moderate AD, LMTM failed to slow cognitive or functional decline, and another phase III trial involving healthy older people with mild to moderate AD is still being conducted (Seripa et al., 2016; Hashweh et al., 2020).

TRx-0014 (Rember) was completed in a Phase II study of patients with mild to moderate AD.

It showed improvements in the Alzheimer's Disease Assessment Scale–Cognitive Subscale (ADAS-Cog) over 24 weeks, as well as in the Alzheimer's Disease Cooperative Study–Clinical Global Impression of Change scale (ADCS-CGIC), the MMSE, and cerebral blood flow assessed by HMPAO-SPECT. Unfortunately, TRx-0014 showed no statistically significant effect on cognition in patients with mild AD (NCT00515333) (Wischik et al., 2015).

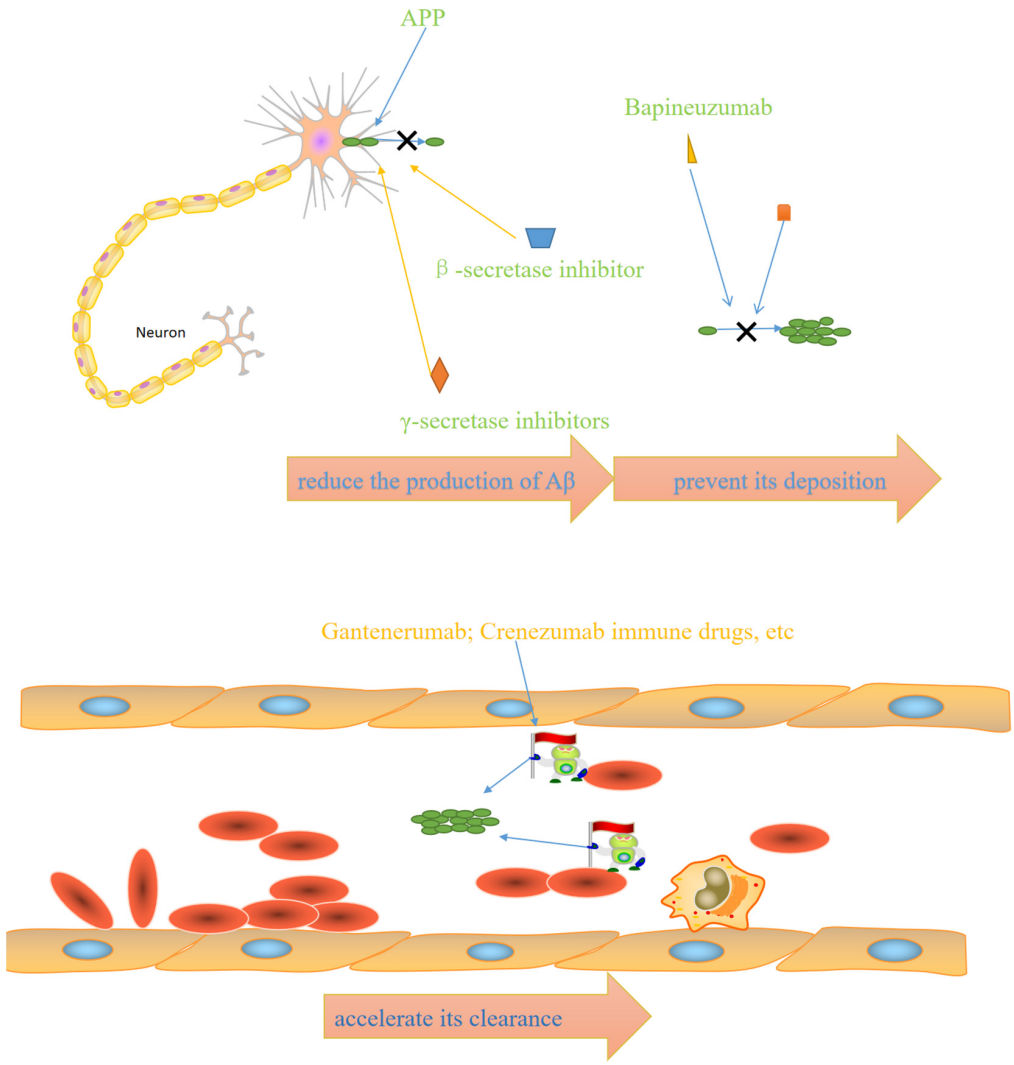

FIGURE 2
Mechanisms of anti-AD drugs: β-secretase inhibitors and γ-secretase inhibitors reduce the production of Aβ, bapineuzumab and other drugs prevent its deposition, immune drugs such as gantenerumab and crenezumab accelerate its clearance.

A Phase II trial of TRx0237 (LMT/hydromethylthionine) in mild-moderate AD (NCT01626391) was terminated early for administrative reasons (ClinicalTrials.gov.NCT01626391). Moreover, two Phase III studies [(NCT01689246)/the European Union Clinical Trials Registry (2012-002866-11), (NCT01689233) and the European Union Clinical Trials Registry (21012-002847-28)] confirmed that TRx0237 improved the cognition in patients with mild to moderate AD, such as changes in ADAS-Cog and Alzheimer's Disease Cooperative Study– Activities of Daily Living Inventory (ADCS-ADL) (Gauthier et al., 2016; Wilcock et al., 2018). A Phase II/III trial of TRx0237 Monotherapy in participants with AD (LUCIDITY/NCT03446001) was completed recently. The use of TRx0237 reflected as improvements in ADAS-Cog11 and ADCS-ADL23 (ClinicalTrials.gov.NCT03446001).

3.2.3. Stable microtubules

Davunetide (alternative names: NAP or NAPVSIPQ or A-L108 or CP201) is an eight amino-acid peptide derived from the neuroprotective fragment of activity-dependent neuroprotective protein (ADNP) (Gozes et al., 2009). Davunetide is a Src homology 3 (SH3) domain-ligand association site responsible for controlling signaling pathways regulating the cytoskeleton, direct microtubule end-binding protein interaction facilitating microtubule dynamics, and Tau microtubule interaction at the microtubule end-binding protein site EB1 and EB3 (Gozes and Shazman, 2023). Davunetide may contribute to the progression of several CNS disorders, such as Autism, Schizophrenia, AD (Idan-Feldman et al., 2011; Sragovich et al., 2017, 2019), and Progressive Supranuclear Palsy (Dale et al., 2020; VandeVrede et al., 2020). A placebo-controlled, ascending-dose 12 weeks Phase I study in participants with amnestic MCI (AL-108-21) was completed in 2013, showing that davunetide was generally safe and well tolerated. However, it failed to detect a statistically significant difference between the treatment groups on the composite cognitive memory score of efficacy data (Morimoto et al., 2013).

Epothilones are derived from *Sorangium cellulosum* and inhibit tubulin depolymerization, thus leading to the death of cancer cells (Ye et al., 2023). Moreover, Epothilone D can bind to tau protein,

thus effectively preventing nerve injury and improving cognitive performance in mouse models of AD (Brunden et al., 2010; Guo et al., 2020). Epothilone D (KOS-862) showed manageable toxicity, favorable PK profile, and the suggestion of clinical activity in Phase I clinical study of patients with advanced solid tumors and lymphoma (Konner et al., 2012) and in a Phase III trial in patients with advanced or metastatic breast cancer (Vahdat, 2008). Unfortunately, there were no publications regarding clinical trials of Epothilone D therapy in AD.

3.2.4. Active immunity

AADvac1 is a peptide that contains one of the epitopes of antibody DC8E8 (294KDNIKHVPGGGS305). AADvac1 is conjugated to keyhole limpet hemocyanin (KLH) along with aluminum hydroxide as an adjuvant. AADvac-1 therapy in patients with mild-to-moderate AD was completed in Phase I trials of (NCT01850238), without aberrant immune response or microhemorrhages (Novak et al., 2017, 2019); similar results were found in a follow-up study of 72 weeks (NCT02031198) (Novak et al., 2018). Moreover, cognitive decline (ADAS-cog11 value) in patients with mild-to-moderate AD was significantly reduced by AADvac1 (Novak et al., 2018). These results were confirmed in an AADvac-1 Phase II clinical trial (NCT02579252) (ClinicalTrials.gov.NCT02579252).

ACI-35 is a liposomal-anchored 16-amino acid tetra-palmitoylated phospho-tau peptide (393VYKSPVVSGDTSPRH L408) (Theunis et al., 2013). ACI-35 decreased soluble and insoluble Tau in tau-transgenic mouse models (Theunis et al., 2013).

3.2.5. Passive immunity

Gosuranemab is a humanized mouse monoclonal antibody (IPN002), which recognizes a phosphorylated epitope in the N-terminal region of Tau consisting of amino acid residues 15AGTYGLGDRK24 and targets extracellular Tau (Qureshi et al., 2018). Gosuranemab was found to be safe and well-tolerated in Phase 1 trials (NCT02460094) conducted on patients with PSP. Additionally, it demonstrated a reduction in unbound N-terminal Tau in CSF (Boxer et al., 2019). Unfortunately, AD biomarkers such as total Tau and ptau181 were not reduced by Gosuranemab (Tatebe et al., 2017; Yang et al., 2018). A Phase II clinical trial of Gosuranemab (TANGO trial, NCT03352557) is ongoing, with a completion date of 2024.

Tilavonemab (ABBV-8E12/C2N8E12/HJ8.5) is the humanized anti-Tau IgG4 antibody, which was found to be safe and tolerable as IV injections in Phase I trials (NCT02494024) (West et al., 2017). A Phase II trial of Tilavonemab for early AD (NCT02880956) found that Tilavonemab was tolerated generally well but found non-significant efficacy in treating patients with early AD (Florian et al., 2023).

Zagotenemab (LY3303560, MC-1 IgG1) is a humanized antibody that recognizes a conformational Tau epitope with a primary epitope located in the N-terminal region (Alam et al., 2017). Two Phase I trials of zagotenemab in healthy volunteers and patients with mild to moderate AD (NCT02754830 and NCT03019536) have been completed. However, no reports were released for unknown reasons (ClinicalTrials.gov.NCT02754830 and ClinicalTrials.gov.NCT03019536). Recently, a Phase II trial of zagotenemab (NCT03518073) was completed, showing that zagotenemab improves the clinical characteristics of patients with early AD. However, the trial showed an SAE occurrence of approximately 17% (ClinicalTrials.gov.NCT03518073).

Semorinemab (RO7105705) targets maximum binding across different extracellular Tau species, which was confirmed by preclinical studies in mouse models (Lee et al., 2016). Phase 1 Semorinemab (NCT02820896) studies have been completed; however, the corresponding report has not been made available. The study details can be found at https://beta.clinicaltrials.gov/study/NCT02820896. Recently, two ongoing Phase II trials have been completed: one involving participants with prodromal/probable AD (TAURIEL trial, NCT03289143) and another involving participants with moderate AD (NCT03828747). Both trials showed improvement in the

TABLE 2 The anti-tau drugs are currently undergoing clinical trials including name of drugs, mechanism, company, and clinical trials.

Name of drug	Mechanism	Company	Clinical status
Tideglusib	GSK-3β inhibitor	Noscira SA	Phase II (completed)
Lithium		National Institutes of Health Clinical Center (USA)	Phase II (completed)
Methylthioninium chloride (methylene blue)	Tau aggregation inhibitor	Allon Therapeutics/ Bristol-Myers/ Squibb (USA)	Phase II (completed) and Phase III (ongoing)
TRx-0014 (Rember)		University of Aberdeen (UK)	Phase II (completed)
TRx-0237 (LMT/hydromethylthionine)		TauRx	Phase II/III (completed)
Hydromethanesulfonate (LMTM)		The University of Texas Health Science Center at San Antonio (USA)	Phase II (ongoing)
Davunetide (NAP)	Stable microtubules	Allon Therapeutics Inc.	Phase I (completed)
AADvac1	Active immunity	Axon Neuroscience/ Weil am Rhein	Phase I/II (completed)
ACI-35		AC Immune	Phase I (completed)
Gosuranemab (BIIB092, BMS-986168, IPN007/IPN002) Tilavonemab (ABBV-8E12/ C2N8E12/HJ8.5)	Passive immunity	iPerian/Bristol-Meyers Squibb/Biogen (USA) C2N Diagnostics/ AbbVie	Phase II (ongoing) Phase II (ongoing)
Zagotenemab (LY3303560, MC-1 IgG1)		Eli Lilly (USA)	Phase II (ongoing)
Semorinemab		AC Immune/ Genentech/ Hoffmann-La Roch	

clinical characteristics of patients with AD (Teng et al., 2022; ClinicalTrials.gov.NCT03828747; **Table 2**).

3.3. Mitochondria-targeting drugs on AD

3.3.1. Insulin

Phase II/III clinical trials on insulin for AD (NCT01767909) have been completed. However, no cognitive or functional benefits were observed with a 12-months period of intranasal insulin treatment, although no clinically important AE was associated with the treatment (Craft et al., 2020).

3.3.2. Mitochondrial enhancers

"Mitochondrial enhancers" therapy in the early stages of AD included coenzyme Q (CoQ) and its synthetic analog, idebenone, which stimulate the mitochondrial electron transport chain activity, increase ATP production, and exhibit antioxidant- and free-radical-scavenging activity. Studies showed that the oxidized/total CoQ ratio was increased in the CSF of patients with AD (Isobe et al., 2009; Orsucci et al., 2011). Similar results were also observed in animal models, including older animals and diabetic rats (Yang et al., 2016). Clinical trials on these drugs (NCT00117403) have been completed, and they failed to show statistically significant efficacy (Gutzmann et al., 2002; Thal et al., 2003; Salloway et al., 2021).

Another mitochondrial enhancer, methylene blue, is a member of the phenothiazines family, which interacts with mitochondria and induces an alternative electron transfer to cytochrome oxidase, thus increasing its activity and possessing antioxidant properties (Tucker et al., 2018). Methylene blue is also a multi-target drug on several biotargets, such as mitochondria, membrane-associated transporters, and ion channels (Saitow and Nakaoka, 1997) and the activity of cholinergic, monoaminergic, or glutamatergic synaptic neurotransmission (Ramsay et al., 2007; Vutskits et al., 2008; Shevtsova et al., 2021). Unfortunately, a compound of methylene blue [Leuco-methylthioninium bis (hydromethanesulfonate; LMTM)] has failed to show a statistically significant positive effect in phase III clinical trials (NCT01689246) on AD (Gauthier et al., 2016). However, another phase III clinical trial showed that LMTM improved cognitive function, brain atrophy, and blood glucose in patients with AD (Wilcock et al., 2018). Thus, further evidence is needed to support its efficacy.

Mitochondrial dysfunction can be recovered through mitochondrial biogenesis, which includes peroxisome proliferator-activated receptor (PPAR) and transcription coactivators such as PPARγ coactivator-1 (PGC-1) family, nuclear transcription factors including nuclear respiratory factors 1 (NRF-1) and 2 (NRF-2), and the mitochondrial transcription factor (ÒFAM). The impairment of PGC-1α-mediated mitochondrial biogenesis appears in patients with AD (Qin et al., 2009) and AD model-3xTg mouse (Singulani et al., 2020).

Peroxisome proliferator-activated receptor (α, β/δ, γ) agonist, bezafibrate, decreases the tau protein level and microglia activation, enhances mitochondrial biogenesis, and improves behavioral characteristics in P301s transgenic mice (Dumont et al., 2012). Unfortunately, there were no clinical trial reports on Bezafibrate for AD treatment in ClinicalTrials.gov.

In mouse models, other PPAR-γ agonists such as thiazolidinediones, pioglitazone, and rosiglitazone showed improvement in memory. Rosiglitazone improved cognitive functions only in a small group of patients with MCI. However, some extensive clinical trials (REFLECT-2 and REFLECT-3) did not show a statistically significant efficacy (Harrington et al., 2011; Shevtsova et al., 2021). Recently, multiple trials on rosiglitazone therapy for AD, including a Phase IIb (NCT00334568) and Phase III [(AVA105640; NCT00428090), (AVA102677; NCT00550420); (study AVA10267, NCT00348309); (study AVA102670; NCT00348140)] trials were reported. These reports showed that six protein-predictive biomarkers (IL6, IL10, CRP, TNF, FABP-3, and PPY) could accurately classify 100% of rosiglitazone treatment responders. Unfortunately, this report did not mention any improvement in the cognitive function of patients with AD (O'Bryant et al., 2021).

3.3.3. Mitochondrial permeability transition inhibitors

Mitochondrial permeability transition inhibitors can prevent neurodegenerative processes and can be considered potential neuroprotectors. MPT inhibitors include modulators of mitochondrial calcium homeostasis and antioxidants. The MPT pore is considered a complex consisting of poly-R-3-hydroxybutyrate, polyphosphates, and calcium cations (PHB/polyp/Ca^{2+} complex) (Pavlov et al., 2005). An experiment showed that a decrease in the polyphosphate level increases the calcium retention capacity of mitochondria and reduces the probability of Ñà$^{2+}$-induced MPT pore opening (Abramov et al., 2007).

Cyclophilin D (peptidyl-prolyl cis–trans isomerase, PPIase) might be a master regulator of mitochondrial function, such as the mitochondrial redox status, presence of inorganic phosphate, and state of respiratory chain components, including complex I of the MRC, creatine kinase, and translocator protein (TSPO) peripheral benzodiazepine receptor (Azarashvili et al., 2015; Bernardi et al., 2015; Gutiérrez-Aguilar and Baines, 2015; Porter and Beutner, 2018). Cyclophilin family members have co-operations. For example, cyclophilin D is regulated by cyclosporin A through calcium. Cyclophilin D interacts with cardiolipin to release cytochrome C from mitochondria via tau protein-441, α-synuclein, and β-amyloid oligomers (Camilleri et al., 2013). There were some specific inhibitors, including cyclosporin À, alisporivir (Debio025) (Schiavone et al., 2017), N-methyl-4-isoleucine-cyclosporin (NIM811) (Springer et al., 2018), low-molecular-weight cyclophilin D ligands (4-aminobenzenesulfonamide derivative C-9) (Valasani et al., 2014, 2016), and cyclophilin D-independent MPT inhibitors (imidazole, thiadiazole, urea derivatives, N-phenylbenzamides, cinnamic anilides, and isoxazoles) (Valasani et al., 2016). Unfortunately, there are no clinical trials or animal model reports regarding these compounds (Shevtsova et al., 2021).

Dimebon prevents the opening of MPT pores and is considered a treatment for AD. Dimebon showed strong neuroprotective and cognition-enhancing effects in different animal models (Bachurin et al., 2001). Phase II clinical trials (NCT00377715) showed that Dimebon had a strong beneficial effect on memory and cognition in patients with AD (Doody et al., 2008). Unfortunately, this result was not supported by a phase III trial conducted

in multiple centers, possibly because of the involvement of a heterogeneous population with various neuropathologies unrelated to AD symptoms (MacKay et al., 2010).

Melatonin and its precursor, N-acetylserotonin (NAS), not only have the receptor-defined hormonal effect but also act as antioxidants and are accumulated in mitochondria. They stimulate the MRC, inhibit the MPT, and possess significant neuroprotective potential (Pandi-Perumal et al., 2013; Zhou et al., 2014; Tarocco et al., 2019; Shevtsova et al., 2021). Melatonin and NAS affect MPT induction conditions and have multimodal capabilities, such as regulators of endogenous and local MPT and synaptic and neuronal viability (Tarocco et al., 2019). One clinical trial in Japan showed that melatonin significantly prolonged sleep time (Asayama et al., 2003). Unfortunately, there was no significant improvement in sleep or agitation in two different clinical trials on melatonin treatment for AD in the USA (Singer et al., 2003; Gehrman et al., 2009). Interestingly, a significant improvement in cognitive performance, such as IADL and MMSE, was observed in a 24-weeks clinical trial on prolonged-release melatonin (PRM, also called Piromelatine) therapy for patients with AD, particularly in those with insomnia comorbidity (Wade et al., 2014). However, a recently completed phase II clinical trial (ReCognition, NCT02615002) on Piromelatine therapy for AD showed no statistically significant improvement in cognitive functions (Schneider et al., 2022).

Translocator protein density has been used as a biomarker for neuroinflammation in AD (Chen and Guilarte, 2008). Recently it showed that TSPO binding was greater in patients with AD than in age-matched controls or patients with MCI who had a positive amyloid scan (Kreisl et al., 2013). It showed that increased TSPO binding might play a pathophysiological role in the transition from MCI to AD (Lyoo et al., 2015). In a clinical trial (NCT00613119), TSPO binding (*V*T/*f*P)1) was greater in patients with AD than in healthy controls in expected temporoparietal regions and 2) was not significantly different among the three groups in the cerebellum (Lyoo et al., 2015; **Table 3**).

TABLE 3 Mitochondria-targeting drugs are currently undergoing clinical trials including name of drugs, mechanism, company, and clinical trials.

Name of drug	Mechanism	Company	Clinical status
Insulin (Humulin-RU-100)	Reduce blood glucose	Lilly (USA)	Phase II/III (completed)
Idebenone	mitochondrial enhancers	Wilhelm Griesinger Hospital (Germany)	Phase III (completed)
coenzyme Q	Antioxidants	National Institute on Aging (NIA), Alzheimer's Disease Cooperative Study (ADCS), Takeda America	Phase I/II (completed)
hydromethanesul fonate; (LMTM)		TauRx Therapeutics	Phase III (completed)
Rosiglitazone	PPAR-γ agonists	GlaxoSmithKline	Phase II (completed)
Melatonin	MPT inhibitors	Oregon Health and Science University	Phase II (completed)
prolonged-release melatonin (Circadin), Piromelatine		Neurim Pharmaceuticals Ltd. (Israel)	Phase II (completed)

TABLE 4 Multi-targets drugs are currently undergoing clinical trials including name of drugs, mechanism, company, and clinical trials.

Name of drug	Mechanism	Company	Clinical status
Dimebon (Latrepirdine)	Multi-targets	Medivation (USA), Pfizer, Novokuznetsk (Russia)	Phase III (completed)
Masitinib	Tyrosine kinase inhibitor	AB Science (France)	Unknown
Idalopirdine	5-HT6 receptor antagonist	H. Lundbeck A/S (Denmark)	Phase II/III (completed)
AVN-101		Avineuro Pharmaceuticals Inc. (USA)	Phase I (completed)

3.4. "Multi-target" agents on AD

3.4.1. γ-Carbolines

Dimebon is a compound of γ-carboline derivatives that conjugates with methylene blue (Bachurin et al., 2019; Makhaeva et al., 2019). Dimebon is a multitarget agent; its activities include protecting neurons from death, reducing the development of proteopathy, and increasing autophagy (Shevtsova et al., 2014; Skvortsova et al., 2018; Ustyugov et al., 2018). However, owing to a lack of statistically significant efficacy, the use of dimebon for AD was not confirmed through a phase II clinical trial (NCT00377715) (Doody et al., 2008).

3.4.2. Phenothiazine

Phenothiazine does not inhibit AChE and has a rather low anti-BChE activity, which was supported by molecular docking (Makhaeva et al., 2015). In a double transgenic mouse AD model, phenothiazine-based theranostic compounds inhibited Aβ aggregation and might act as imaging probes for amyloid plaques in AD on near-infrared fluorescent (NIRF) imaging (Dao et al., 2017). Unfortunately, there is no clinical trial report currently available on phenothiazine therapy for AD in the PubMed database.

3.4.3. Carbazoles

P7C3 is a neuroprotective aminopropyl carbazole identified on studies of postnatal hippocampal neurogenesis (Voorhees et al., 2018). P7C3 was named as it is the third compound (C3) of the seventh pool (P7) and has protective action on young hippocampal neurons in preventing neuron death; it has also been shown to inhibit cognitive decline in terminally aging rats (Pieper et al., 2010). Moreover, P7C3 molecules enhance the flux of nicotinamide adenine dinucleotide (NAD) in mammalian cells (Wang et al., 2014) and indirectly inhibit other critical cell death signaling events (Gu et al., 2017). P7C3 treatment shows neuroprotective effect in different animal models, such as amyotrophic lateral sclerosis (Tesla et al., 2012), Parkinson's disease (De Jesús-Cortés et al., 2012, 2015; Naidoo et al., 2014; Gu et al., 2017), traumatic brain injury (Dutca et al., 2014; Yin et al., 2014; Vázquez-Rosa et al., 2020), psychological stress–related hippocampal cell death (Walker et al., 2015), peripheral nerve crush injury (Kemp et al., 2015),

stroke (Kemp et al., 2015), and AD (TgF344-AD rat model) (Cohen et al., 2013; Voorhees et al., 2018). Unfortunately, there is no clinical trial report available on P7C3 therapy for AD in the PubMed database.

3.4.4. 5-HT

Idalopirdine is a novel selective 5-HT6 receptor antagonist that binds with ChEI, potentiates central acetyl choline levels and neuronal activity, and improves cognition in animal models (Herrik et al., 2016; Amat-Foraster et al., 2017).

A phase II, proof-of-concept (PoC) study of idalopirdine plus donepezil therapy for AD showed a significant improvement in cognitive performance of AD, such as in ADAS-cog and MMSE scores (Wilkinson et al., 2014). However, phase III development programs for idalopirdine therapy ("OLEX," idalopirdine only and "MEMOLEX," idalopirdine plus memantine) for AD showed no statistically significant efficacy.

AVN-101 is a very potent 5-HT7 receptor antagonist that blocks 5-HT6, 5-HT2A, and 5HT-2C receptors as well as histamine H1 and adrenergic 2A, 2B, and 2C receptors. AVN-101 shows good oral bioavailability, facilitates BBB permeability, and has a low toxicity and reasonable efficacy in animal models of CNS diseases (Ivachtchenko et al., 2016). Moreover, a phase I clinical study indicated that the AVN-101 is well tolerated (Ivachtchenko et al., 2016).

3.4.5. Tyrosine kinase inhibitor

Masitinib is an oral tyrosine kinase inhibitor that has demonstrated neuroprotective action in neurodegenerative diseases via inhibition of mast cell and microglia/macrophage activity, such as in cases of multiple sclerosis (AB07002) (Vermersch et al., 2022). Recently, a phase III clinical trial of masitinib therapy for AD (AB09004, NCT01872598) was completed, which demonstrated that masitinib causes significant improvement in ADAS-cog and ADCS-ADL scores (Dubois et al., 2023; **Table 4**).

4. Discussion

Alzheimer's disease is a neurodegenerative disease with increasing annual incidence. However, the pathogenesis of AD is complex, and its etiology has not been fully elucidated. Research and development of therapeutic drugs for AD are still in progress. Since AD has an insidious onset and slow disease progression, it can take up to 20 years from the onset of pathological changes to the appearance of clinically significant symptoms. Therefore, the early treatment of AD is crucial in controlling its progression. Anti-Aβ amyloid drugs are currently the focus of clinical trials; however, most clinical trials have been terminated because of AE and poor efficacy. For example, a clinical trial on aducanumab, donanemab, lecanemab, and other anti-Aβ drugs concluded that Aβ plaque clearance was closely related to the occurrence of ARIA-E (Wang et al., 2022). The high incidence of ARIAs suggests a need to clarify the early benefits of such interventions when conducting clinical trials (Loureiro et al., 2020). In clinical studies on donanemab, a trend toward slower Tau accumulation was observed. Thus, a future research direction would be to explore the relationship between reduced Aβ plaques and Tau levels, to achieve meaningful benefits for patients with AD. The accelerated FDA approval of aducanumab brought hope for AD drug development, and we look forward to more effective and economical treatments for patients with AD.

5. Conclusion

In conclusion, although there has not been a curative breakthrough in drug therapy for AD, progress is being made; new drugs with good efficacy, few adverse reactions, and economic feasibility will certainly be developed in the near future.

Author contributions

YP received funding support and developed the research hypothesis. YP, HJ, Y-hX, QC, S-yY, M-qD, and SL wrote the main manuscript. All authors jointly wrote the final manuscript as the end product.

Funding

This work was supported by the Scientific Research Project of Hunan Provincial Health Commission, China (No. C202303076574 to YP), Key Plans of Hunan Administration Traditional Chinese Medicine, China (No. A2023039 to YP), University-Hospital Joint-Fund of Hunan University of Chinese Medicine, China (No. 2022XYLH198 to YP), Fund for Creative Research Group of Affiliated First Hospital of Hunan Traditional Chinese Medical College, China (No. 2021B-003 to YP), and Technology Plan Project of Zhuzhou City, Hunan Province, China (No. 2021-009 to YP).

Conflict of interest

The authors declare that the research was conducted in the absence of any commercial or financial relationships that could be construed as a potential conflict of interest.

Publisher's note

References

Alzheimer's Association (2022). 2022 Alzheimer's disease facts and figures. *Alzheimers Dement.* 18, 700–789.

Abramov, A. Y., Fraley, C., Diao, C. T., Winkfein, R., Colicos, M. A., Duchen, M. R., et al. (2007). Targeted polyphosphatase expression alters mitochondrial metabolism and inhibits calcium-dependent cell death. *Proc. Natl. Acad. Sci. U.S.A.* 104, 18091–18096. doi: 10.1073/pnas.0708959104

Alam, R., Driver, D., Wu, S., Lozano, E., Key, S. L., Hole, J. T., et al. (2017). [O2–14–05]: preclinical characterization of an antibody [LY3303560] targeting aggregated tau. *Alzheimer Dement.* 13, 592–593.

Amat-Foraster, M., Leiser, S. C., Herrik, K. F., Richard, N., Agerskov, C., Bundgaard, C., et al. (2017). The 5-HT(6) receptor antagonist idalopirdine potentiates the effects of donepezil on gamma oscillations in the frontal cortex of anesthetized and awake rats without affecting sleep-wake architecture. *Neuropharmacology* 113, 45–59. doi: 10.1016/j.neuropharm.2016.09.017

Asayama, K., Yamadera, H., Ito, T., Suzuki, H., Kudo, Y., and Endo, S. (2003). Double blind study of melatonin effects on the sleep-wake rhythm, cognitive and non-cognitive functions in Alzheimer type dementia. *J. Nippon Med. Schl.* 70, 334–341.

Athar, T., Al Balushi, K., and Khan, S. A. (2021). Recent advances on drug development and emerging therapeutic agents for Alzheimer's disease. *Mol. Biol. Rep.* 48, 5629–5645.

Azarashvili, T., Krestinina, O., Baburina, Y., Odinokova, I., Grachev, D., Papadopoulos, V., et al. (2015). Combined effect of G3139 and TSPO ligands on Ca(2+)-induced permeability transition in rat brain mitochondria. *Arch. Biochem. Biophys.* 587, 70–77. doi: 10.1016/j.abb.2015.10.012

Babic Leko, M., Hof, P. R., and Simic, G. (2021). Alterations and interactions of subcortical modulatory systems in Alzheimer's disease. *Prog. Brain Res.* 261, 379–421. doi: 10.1016/bs.pbr.2020.07.016

Bachurin, S. O., Gavrilova, S. I., Samsonova, A., Barreto, G. E., and Aliev, G. (2018). Mild cognitive impairment due to Alzheimer disease: contemporary approaches to diagnostics and pharmacological intervention. *Pharmacol. Res.* 129, 216–226.

Bachurin, S. O., Makhaeva, G. F., Shevtsova, E. F., Boltneva, N. P., Kovaleva, N. V., Lushchekina, S. V., et al. (2019). Conjugates of methylene blue with γ-carboline derivatives as new multifunctional agents for the treatment of neurodegenerative diseases. *Sci. Rep.* 9:4873. doi: 10.1038/s41598-019-41272-4

Bachurin, S., Bukatina, E., Lermontova, N., Tkachenko, S., Afanasiev, A., Grigoriev, V., et al. (2001). Antihistamine agent Dimebon as a novel neuroprotector and a cognition enhancer. *Ann. N. Y. Acad. Sci.* 939, 425–435. doi: 10.1111/j.1749-6632.2001.tb03654.x

Basisty, N., Holtz, A., and Schilling, B. (2020). Accumulation of "Old Proteins" and the critical need for MS-based protein turnover measurements in aging and longevity. *Proteomics* 20:e1800403. doi: 10.1002/pmic.201800403

Bateman, R. J., Cummings, J., Schobel, S., Salloway, S., Vellas, B., Boada, M., et al. (2022). Gantenerumab: an anti-amyloid monoclonal antibody with potential disease-modifying effects in early Alzheimer's disease. *Alzheimers Res. Ther.* 14:178.

Bernardi, P., Rasola, A., Forte, M., and Lippe, G. (2015). The mitochondrial permeability transition pore: channel formation by F-ATP synthase, integration in signal transduction, and role in pathophysiology. *Physiol. Rev.* 95, 1111–1155. doi: 10.1152/physrev.00001.2015

Bolognesi, M. L., and Cavalli, A. (2016). Multitarget drug discovery and polypharmacology. *Chem. Med. Chem.* 11, 1190–1192.

Boxer, A. L., Qureshi, I., Ahlijanian, M., Grundman, M., Golbe, L. I., Litvan, I., et al. (2019). Safety of the tau-directed monoclonal antibody BIIB092 in progressive supranuclear palsy: a randomised, placebo-controlled, multiple ascending dose phase 1b trial. *Lancet Neurol.* 18, 549–558. doi: 10.1016/S1474-4422(19)30139-5

Brunden, K. R., Zhang, B., Carroll, J., Yao, Y., Potuzak, J. S., Hogan, A. M., et al. (2010). Epothilone D improves microtubule density, axonal integrity, and cognition in a transgenic mouse model of tauopathy. *J. Neurosci.* 30, 13861–13866. doi: 10.1523/JNEUROSCI.3059-10.2010

Camilleri, A., Zarb, C., Caruana, M., Ostermeier, U., Ghio, S., Högen, T., et al. (2013). Mitochondrial membrane permeabilisation by amyloid aggregates and protection by polyphenols. *Biochim. Biophys. Acta* 1828, 2532–2543. doi: 10.1016/j.bbamem.2013.06.026

Chen, M. K., and Guilarte, T. R. (2008). Translocator protein 18 kDa (TSPO): molecular sensor of brain injury and repair. *Pharmacol. Ther.* 118, 1–17. doi: 10.1016/j.pharmthera.2007.12.004

Chételat, G., Desgranges, B., de la Sayette, V., Viader, F., Eustache, F., and Baron, J. C. (2003). Mild cognitive impairment: can FDG-PET predict who is to rapidly convert to Alzheimer's disease? *Neurology* 60, 1374–1377.

Cho, H., Choi, J. Y., Lee, H. S., Lee, J. H., Ryu, Y. H., Lee, M. S., et al. (2019). Progressive tau accumulation in Alzheimer disease: 2-year follow-up study. *J. Nucl. Med.* 60, 1611–1621.

ClinicalTrials.gov.NCT01511783. *A Randomized, Double-Blind, Placebo-Controlled, Multiple Ascending Dose Study to Evaluate the Safety, Tolerability, Pharmacokinetics and Pharmacodynamics of E2609 in Healthy Subjects*. Available online at: https://www.clinicaltrials.gov/ct2/show/NCT01511783?term=E2609-A001-002&draw=2&rank=1

ClinicalTrials.gov.NCT01626391. *Safety Study of TRx0237 in Patients Already Taking Medications for Mild and Moderate Alzheimer's Disease*. Available online at: https://beta.clinicaltrials.gov/search?term=NCT01626391

ClinicalTrials.gov.NCT02579252. *24 Months Safety and Efficacy Study of AADvac1 in Patients With Mild Alzheimer's Disease (ADAMANT)*. Available online at: https://beta.clinicaltrials.gov/search?term=NCT02579252

ClinicalTrials.gov.NCT02754830. *A Study of LY3303560 in Healthy Participants and Participants With Alzheimer's Disease (AD)*. Available online at: https://beta.clinicaltrials.gov/search?term=NCT02754830

ClinicalTrials.gov.NCT02956486. *A Placebo-Controlled, Double-Blind, Parallel-Group, 24 Month Study With an Open-Label Extension Phase to Evaluate the Efficacy and Safety of Elenbecestat (E2609) in Subjects With Early Alzheimer's Disease*. Available online at: https://beta.clinicaltrials.gov/study/NCT02956486?distance=50&term=E2609-G000-301&rank=1; E2609-G000-302

ClinicalTrials.gov.NCT03019536. *A Study of LY3303560 in Participants With Mild Cognitive Impairment or Alzheimer's Disease*. Available online at: https://beta.clinicaltrials.gov/search?term=NCT03019536

ClinicalTrials.gov.NCT03446001. *Safety and Efficacy of TRx0237 in Subjects With Alzheimer's Disease Followed by Open-Label Treatment*. Available online at: https://beta.clinicaltrials.gov/search?term=NCT03446001

ClinicalTrials.gov.NCT03518073. *A Study of LY3303560 in Participants With Early Symptomatic Alzheimer's Disease*. Available online at: https://beta.clinicaltrials.gov/search?term=NCT03518073

ClinicalTrials.gov.NCT03828747. *A Study of Semorinemab in Patients With Moderate Alzheimer's Disease*. Available online at: https://beta.clinicaltrials.gov/search?term=NCT03828747

Cohen, R. M., Rezai-Zadeh, K., Weitz, T. M., Rentsendorj, A., Gate, D., Spivak, I., et al. (2013). A transgenic Alzheimer rat with plaques, tau pathology, behavioral impairment, oligomeric aβ, and frank neuronal loss. *J. Neurosci.* 33, 6245–6256.

Craft, S., Raman, R., Chow, T. W., Rafii, M. S., Sun, C. K., Rissman, R. A., et al. (2020). Safety, efficacy, and feasibility of intranasal insulin for the treatment of mild cognitive impairment and Alzheimer disease dementia: a randomized clinical trial. *JAMA Neurol.* 77, 1099–1109.

Cummings, J., Aisen, P., Apostolova, L. G., Atri, A., Salloway, S., and Weiner, M. (2021). Aducanumab: appropriate use recommendations. *J. Prev. Alzheimers Dis.* 8, 398–410.

Dale, M. L., Brumbach, B. H., Boxer, A. L., and Hiller, A. L. (2020). Associations between amantadine usage, gait, and cognition in PSP: a *post-hoc* analysis of the davunetide trial. *Front. Neurol.* 11:606925. doi: 10.3389/fneur.2020.606925

Dao, P., Ye, F., Liu, Y., Du, Z. Y., Zhang, K., Dong, C. Z., et al. (2017). Development of phenothiazine-based theranostic compounds that act both as inhibitors of β-amyloid aggregation and as imaging probes for amyloid plaques in Alzheimer's disease. *ACS Chem. Neurosci.* 8, 798–806.

De Jesús-Cortés, H., Miller, A. D., Britt, J. K., DeMarco, A. J., De Jesús-Cortés, M., Stuebing, E., et al. (2015). Protective efficacy of P7C3-S243 in the 6-hydroxydopamine model of Parkinson's disease. *NPJ Parkinsons Dis.* 1:15010. doi: 10.1038/npjparkd.2015.10

De Jesús-Cortés, H., Xu, P., Drawbridge, J., Estill, S. J., Huntington, P., Tran, S., et al. (2012). Neuroprotective efficacy of aminopropyl carbazoles in a mouse model of Parkinson disease. *Proc. Natl. Acad. Sci. U.S.A.* 109, 17010–17015. doi: 10.1073/pnas.1213956109

Delbarba, A., Abate, G., Prandelli, C., Marziano, M., Buizza, L., Arce Varas, N., et al. (2016). Mitochondrial alterations in peripheral mononuclear blood cells from Alzheimer's disease and mild cognitive impairment patients. *Oxid. Med. Cell. Longev.* 2016:5923938.

Dhillon, S. (2021). Aducanumab: first approval. *Drugs* 81, 1437–1443.

Doggrell, S. A. (2019). Lessons that can be learnt from the failure of verubecestat in Alzheimer's disease. *Expert Opin. pharmacother.* 20, 2095–2099. doi: 10.1080/14656566.2019.1654998

Dolton, M. J., Chesterman, A., Moein, A., Sink, K. M., Waitz, A., Blondeau, K., et al. (2021). Safety, tolerability, and pharmacokinetics of high-volume subcutaneous crenezumab, with and without recombinant human hyaluronidase in healthy volunteers. *Clin. Pharmacol. Ther.* 110, 1337–1348. doi: 10.1002/cpt.2385

Doody, R. S., Gavrilova, S. I., Sano, M., Thomas, R. G., Aisen, P. S., Bachurin, S. O., et al. (2008). Effect of dimebon on cognition, activities of daily living, behaviour, and global function in patients with mild-to-moderate Alzheimer's disease: a randomised, double-blind, placebo-controlled study. *Lancet* 372, 207–215. doi: 10.1016/S0140-6736(08)61074-0

Doody, R. S., Raman, R., Farlow, M., Iwatsubo, T., Vellas, B., Joffe, S., et al. (2013). A phase 3 trial of semagacestat for treatment of Alzheimer's disease. *N. Engl. J. Med.* 369, 341–350.

Dubois, B., López-Arrieta, J., Lipschitz, S., Doskas, T., Spiru, L., Moroz, S., et al. (2023). Masitinib for mild-to-moderate Alzheimer's disease: results from a randomized, placebo-controlled, phase 3, clinical trial. *Alzheimers Res. Ther.* 15:39.

Dumont, M., Stack, C., Elipenahli, C., Jainuddin, S., Gerges, M., Starkova, N., et al. (2012). Bezafibrate administration improves behavioral deficits and tau pathology in P301S mice. *Hum. Mol. Genet.* 21, 5091–5105. doi: 10.1093/hmg/dds355

Dutca, L. M., Stasheff, S. F., Hedberg-Buenz, A., Rudd, D. S., Batra, N., Blodi, F. R., et al. (2014). Early detection of subclinical visual damage after blast-mediated TBI enables prevention of chronic visual deficit by treatment with P7C3-S243. *Investig. Ophthalmol. Vis. Sci.* 55, 8330–8341. doi: 10.1167/iovs.14-15468

Egan, M. F., Mukai, Y., Voss, T., Kost, J., Stone, J., Furtek, C., et al. (2019). Further analyses of the safety of verubecestat in the phase 3 EPOCH trial of mild-to-moderate Alzheimer's disease. *Alzheimers Res. Ther.* 11:68. doi: 10.1186/s13195-019-0520-1

Florian, H., Wang, D., Arnold, S. E., Boada, M., Guo, Q., Jin, Z., et al. (2023). Tilavonemab in early Alzheimer's disease: results from a phase 2, randomized, double-blind study. *Brain* 146, 2275–2284. doi: 10.1093/brain/awad024

Gauthier, S., Feldman, H. H., Schneider, L. S., Wilcock, G. K., Frisoni, G. B., Hardlund, J. H., et al. (2016). Efficacy and safety of tau-aggregation inhibitor therapy in patients with mild or moderate Alzheimer's disease: a randomised, controlled, double-blind, parallel-arm, phase 3 trial. *Lancet* 388, 2873–2884.

Gehrman, P. R., Connor, D. J., Martin, J. L., Shochat, T., Corey-Bloom, J., and Ancoli-Israel, S. (2009). Melatonin fails to improve sleep or agitation in double-blind randomized placebo-controlled trial of institutionalized patients with Alzheimer disease. *Am. J. Geriatr. Psychiatry* 17, 166–169.

Gozes, I., and Shazman, S. (2023). A novel davunetide (NAPVSIPQQ to NAPVSIPQE) point mutation in activity-dependent neuroprotective protein (ADNP) causes a mild developmental syndrome. *Eur. J. Neurosci.* doi: 10.1111/ejn.15920 [Epub ahead of print].

Gozes, I., Stewart, A., Morimoto, B., Fox, A., Sutherland, K., and Schmeche, D. (2009). Addressing Alzheimer's disease tangles: from NAP to AL-108. *Curr. Alzheimer Res.* 6, 455–460.

Gu, C., Zhang, Y., Hu, Q., Wu, J., Ren, H., Liu, C. F., et al. (2017). P7C3 inhibits GSK3β activation to protect dopaminergic neurons against neurotoxin-induced cell death in vitro and in vivo. *Cell Death Dis.* 8:e2858.

Guo, B., Huang, Y., Gao, Q., and Zhou, Q. (2020). Stabilization of microtubules improves cognitive functions and axonal transport of mitochondria in Alzheimer's disease model mice. *Neurobiol. Aging* 96, 223–232. doi: 10.1016/j.neurobiolaging.2020.09.011

Gutiérrez-Aguilar, M., and Baines, C. P. (2015). Structural mechanisms of cyclophilin D-dependent control of the mitochondrial permeability transition pore. *Biochim. Biophys. Acta* 1850, 2041–2047. doi: 10.1016/j.bbagen.2014.11.009

Gutzmann, H., Kühl, K. P., Hadler, D., and Rapp, M. A. (2002). Safety and efficacy of idebenone versus tacrine in patients with Alzheimer's disease: results of a randomized, double-blind, parallel-group multicenter study. *Pharmacopsychiatry* 35, 12–18. doi: 10.1055/s-2002-19833

Hampel, H., Mesulam, M. M., Cuello, A. C., Khachaturian, A. S., Vergallo, A., Farlow, M. R., et al. (2019). Revisiting the cholinergic hypothesis in Alzheimer's disease: emerging evidence from translational and clinical research. *J. Prev. Alzheimers Dis.* 6, 2–15.

Han, J., Lee, H. J., Kim, K. Y., Lee, S. J. C., Suh, J. M., Cho, J., et al. (2018). Tuning structures and properties for developing novel chemical tools toward distinct pathogenic elements in Alzheimer's disease. *ACS Chem. Neurosci.* 9, 800–808. doi: 10.1021/acschemneuro.7b00454

Harrington, C., Sawchak, S., Chiang, C., Davies, J., Donovan, C., Saunders, A. M., et al. (2011). Rosiglitazone does not improve cognition or global function when used as adjunctive therapy to AChE inhibitors in mild-to-moderate Alzheimer's disease: two phase 3 studies. *Curr. Alzheimer Res.* 8, 592–606.

Hashweh, N. N., Bartochowski, Z., Khoury, R., and Grossberg, G. T. (2020). An evaluation of hydromethylthionine as a treatment option for Alzheimer's disease. *Expert Opin. Pharmacother.* 21, 619–627. doi: 10.1080/14656566.2020.1719066

Haussmann, R., Noppes, F., Brandt, M. D., Bauer, M., and Donix, M. (2021). Lithium: a therapeutic option in Alzheimer's disease and its prodromal stages? *Neurosci. Lett.* 760:136044. doi: 10.1016/j.neulet.2021.136044

Henley, D. B., Sundell, K. L., Sethuraman, G., Dowsett, S. A., and May, P. C. (2014). Safety profile of semagacestat, a gamma-secretase inhibitor: identity trial findings. *Curr. Med. Res. Opin.* 30, 2021–2032. doi: 10.1185/03007995.2014.939167

Herrik, K. F., Mørk, A., Richard, N., Bundgaard, C., Bastlund, J. F., and de Jong, I. E. M. (2016). The 5-HT6 receptor antagonist idalopirdine potentiates the effects of acetylcholinesterase inhibition on neuronal network oscillations and extracellular acetylcholine levels in the rat dorsal hippocampus. *Neuropharmacology* 107, 351–363. doi: 10.1016/j.neuropharm.2016.03.043

Honig, L. S., Vellas, B., Woodward, M., Boada, M., Bullock, R., Borrie, M., et al. (2018). Trial of Solanezumab for mild dementia due to Alzheimer's disease. *N. Engl. J. Med.* 378, 321–330.

Hsiao, C. C., Rombouts, F., and Gijsen, H. J. M. (2019). New evolutions in the BACE1 inhibitor field from 2014 to 2018. *Bioorganic Med. Chem. Lett.* 29, 761–777. doi: 10.1016/j.bmcl.2018.12.049

Hu, W., Zhao, M., Lian, J., Li, D., Wen, J., and Tan, J. (2022). Lithium cholesterol sulfate: a novel and potential drug for treating Alzheimer's disease and autism spectrum disorder. *CNS Neurol. Disord. Drug Targets*. doi: 10.2174/1871527321666220825114236 [Epub ahead of print].

Hull, M., Sadowsky, C., Arai, H., Le Prince Leterme, G., Holstein, A., Booth, K., et al. (2017). Long-term extensions of randomized vaccination trials of ACC-001 and QS-21 in mild to moderate Alzheimer's disease. *Curr. Alzheimer Res.* 14, 696–708. doi: 10.2174/1567205014666170117101537

Idan-Feldman, A., Schirer, Y., Polyzoidou, E., Touloumi, O., Lagoudaki, R., Grigoriadis, N. C., et al. (2011). Davunetide (NAP) as a preventative treatment for central nervous system complications in a diabetes rat model. *Neurobiol. Dis.* 44, 327–339. doi: 10.1016/j.nbd.2011.06.020

Isobe, C., Abe, T., and Terayama, Y. (2009). Increase in the oxidized/total coenzyme Q-10 ratio in the cerebrospinal fluid of Alzheimer's disease patients. *Dement. Geriatr. Cogn. Disord.* 28, 449–454. doi: 10.1159/000256209

Ivachtchenko, A. V., Lavrovsky, Y., and Okun, I. (2016). AVN-101: a multi-target drug candidate for the treatment of CNS disorders. *J. Alzheimers Dis.* 53, 583–620. doi: 10.3233/JAD-151146

Jo, T., Nho, K., Risacher, S. L., Saykin, A. J., and Alzheimer's Neuroimaging Initiative (2020). Deep learning detection of informative features in tau PET for Alzheimer's disease classification. *BMC Bioinform.* 21:496. doi: 10.1186/s12859-020-03848-0

Jouanne, M., Rault, S., and Voisin-Chiret, A. S. (2017). Tau protein aggregation in Alzheimer's disease: an attractive target for the development of novel therapeutic agents. *Eur. J. Med. Chem.* 139, 153–167.

Kandimalla, R., Thirumala, V., and Reddy, P. H. (2017). Is Alzheimer's disease a Type 3 Diabetes? A critical appraisal. *Biochim. Biophys. Acta Mol. Basis Dis.* 1863, 1078–1089.

Kemp, S. W. P., Szynkaruk, M., Stanoulis, K. N., Wood, M. D., Liu, E. H., Willand, M. P., et al. (2015). Pharmacologic rescue of motor and sensory function by the neuroprotective compound P7C3 following neonatal nerve injury. *Neuroscience* 284, 202–216. doi: 10.1016/j.neuroscience.2014.10.005

Klein, G., Delmar, P., Voyle, N., Rehal, S., Hofmann, C., Abi-Saab, D., et al. (2019). Gantenerumab reduces amyloid-beta plaques in patients with prodromal to moderate Alzheimer's disease: a PET substudy interim analysis. *Alzheimers Res. Ther.* 11:101. doi: 10.1186/s13195-019-0559-z

Konner, J., Grisham, R. N., Park, J., O'Connor, O. A., Cropp, G., Johnson, R., et al. (2012). Phase I clinical, pharmacokinetic, and pharmacodynamic study of KOS-862 (Epothilone D) in patients with advanced solid tumors and lymphoma. *Investig. New Drugs* 30, 2294–2302. doi: 10.1007/s10637-011-9765-7

Kreisl, W. C., Lyoo, C. H., McGwier, M., Snow, J., Jenko, K. J., Kimura, N., et al. (2013). In vivo radioligand binding to translocator protein correlates with severity of Alzheimer's disease. *Brain* 136, 2228–2238. doi: 10.1093/brain/awt145

Kuehn, B. M. (2020). In Alzheimer research, glucose metabolism moves to center stage. *JAMA* 323, 297–299.

Lacosta, A.-M., Pascual-Lucas, M., Pesini, P., Casabona, D., Pérez-Grijalba, V., Marcos-Campos, I., et al. (2018). Safety, tolerability and immunogenicity of an active anti-Aβ40 vaccine (ABvac40) in patients with Alzheimer's disease: a randomised, double-blind, placebo-controlled, phase I trial. *Alzheimers Res. Ther.* 10:12.

Landen, J. W., Andreasen, N., Cronenberger, C. L., Schwartz, P. F., Borjesson-Hanson, A., Ostlund, H., et al. (2017). Ponezumab in mild-to-moderate Alzheimer's disease: randomized phase II PET-PIB study. *Alzheimers Dement.* 3, 393–401. doi: 10.1016/j.trci.2017.05.003

Lee, S. H., Le Pichon, C. E., Adolfsson, O., Gafner, V., Pihlgren, M., Lin, H., et al. (2016). Antibody-mediated targeting of tau in vivo does not require effector function and microglial engagement. *Cell Rep.* 16, 1690–1700. doi: 10.1016/j.celrep.2016.06.099

Liu, P. P., Xie, Y., Meng, X. Y., and Kang, J. S. (2019). History and progress of hypotheses and clinical trials for Alzheimer's disease. *Signal Transduction Targeted Ther.* 4:29.

Liu-Seifert, H., Siemers, E., Sundell, K., Mynderse, M., Cummings, J., Mohs, R., et al. (2018). Analysis of the relationship of cognitive impairment and functional impairment in mild Alzheimer's disease in EXPEDITION 3. *J. Prev. Alzheimers Dis.* 5, 184–187.

Loureiro, J. C., Pais, M. V., Stella, F., Radanovic, M., Teixeira, A. L., Forlenza, O. V., et al. (2020). Passive antiamyloid immunotherapy for Alzheimer's disease. *Curr. Opin. Psychiatry* 33, 284–291.

Lovestone, S., Boada, M., Dubois, B., Hull, M., Rinne, J. O., Huppertz, H. J., et al. (2015). A phase II trial of tideglusib in Alzheimer's disease. *J. Alzheimers Dis.* 45, 75–88.

Luca, A., and Luca, M. (2023). Lithium in Alzheimer's disease: from prevention to treatment. *Psychogeriatrics* 23, 204–205.

Luo, F., Sandhu, A. F., Rungratanawanich, W., Williams, G. E., Akbar, M., Zhou, S., et al. (2020). Melatonin and autophagy in aging-related neurodegenerative diseases. *Int. J. Mol. Sci.* 21:7174. doi: 10.3390/ijms21197174

Lyoo, C. H., Ikawa, M., Liow, J. S., Zoghbi, S. S., Morse, C. L., Pike, V. W., et al. (2015). Cerebellum can serve as a pseudo-reference region in Alzheimer disease to detect neuroinflammation measured with PET radioligand binding to translocator protein. *J. Nucl. Med.* 56, 701–706. doi: 10.2967/jnumed.114.146027

MacKay, J., Harnett, S., and Machado, P. (2010). Pfizer and Medivation announce results from two phase 3 studies in Dimebon (Latrepirdine*) Alzheimer's disease clinical development program; 2010. Available online at: https://www.pfizer.com/news/press-release/press-release-detail/pfizer_and_medivation_announce_results_from_two_phase_3_studies_in_dimebon_latrepirdine_alzheimer_s_disease_clinical_development_program

Makhaeva, G. F., Lushchekina, S. V., Boltneva, N. P., Sokolov, V. B., Grigoriev, V. V., Serebryakova, O. G., et al. (2015). Conjugates of γ-Carbolines and Phenothiazine as new selective inhibitors of butyrylcholinesterase and blockers of NMDA receptors for Alzheimer Disease. *Sci. Rep.* 5:13164. doi: 10.1038/srep13164

Makhaeva, G. F., Shevtsova, E. F., Boltneva, N. P., Lushchekina, S. V., Kovaleva, N. V., Rudakova, E. V., et al. (2019). Overview of novel multifunctional agents based on conjugates of γ-carbolines, carbazoles, tetrahydrocarbazoles, phenothiazines, and aminoadamantanes for treatment of Alzheimer's disease. *Chem. Biol. Interact.* 308, 224–234. doi: 10.1016/j.cbi.2019.05.020

Man, V. H., He, X., Han, F., Cai, L., Wang, L., Niu, T., et al. (2023). Phosphorylation at Ser289 enhances the oligomerization of tau repeat R2. *J. Chem. Inform. Model.* 63, 1351–1361. doi: 10.1021/acs.jcim.2c01597

Mintun, M. A., Lo, A. C., Duggan Evans, C., Wessels, A. M., Ardayfio, P. A., Andersen, S. W., et al. (2021). Donanemab in early Alzheimer's disease. *N. Engl. J. Med.* 384, 1691–1704.

Miranda, A., Montiel, E., Ulrich, H., and Paz, C. (2021). Selective secretase targeting for Alzheimer's disease therapy. *J. Alzheimers Dis.* 81, 1–17.

Morimoto, B. H., Schmechel, D., Hirman, J., Blackwell, A., Keith, J., and Gold, M. (2013). A double-blind, placebo-controlled, ascending-dose, randomized study to evaluate the safety, tolerability and effects on cognition of AL-108 after 12 weeks of intranasal administration in subjects with mild cognitive impairment. *Dement. Geriatr. Cogn. Disord.* 35, 325–336. doi: 10.1159/000348347

Moriyama, T., Fukushima, T., Kokate, T., and Albala, B. (2017). [P3–037]: preclinical studies with elenbecestat, a novel BACE1 inhibitor, show no evidence of hypopigmentation. *Alzheimers Dement.* 13:944.

Moussa-Pacha, N. M., Abdin, S. M., Omar, H. A., Alniss, H., and Al-Tel, T. H. (2020). BACE1 inhibitors: current status and future directions in treating Alzheimer's disease. *Med. Res. Rev.* 40, 339–384.

Muronaga, M., Terao, T., Kohno, K., Hirakawa, H., Izumi, T., and Etoh, M. (2022). Lithium in drinking water and Alzheimer's dementia: epidemiological findings from national data base of Japan. *Bipolar Disord.* 24, 788–794. doi: 10.1111/bdi.13257

Naidoo, J., De Jesus-Cortes, H., Huntington, P., Estill, S., Morlock, L. K., Starwalt, R., et al. (2014). Discovery of a neuroprotective chemical, (S)-N-(3-(3,6-dibromo-9H-carbazol-9-yl)-2-fluoropropyl)-6-methoxypyridin-2-amine [(-)-P7C3-S243], with improved druglike properties. *J. Med. Chem.* 57, 3746–3754.

Neth, B. J., and Craft, S. (2017). Insulin resistance and Alzheimer's disease: bioenergetic linkages. *Front. Aging Neurosci.* 9:345. doi: 10.3389/fnagi.2017.00345

Neumann, U., Ufer, M., Jacobson, L. H., Rouzade-Dominguez, M. L., Huledal, G., Kolly, C., et al. (2018). The BACE-1 inhibitor CNP 520 for prevention trials in Alzheimer's disease. *EMBO Mol. Med.* 10:e9316. doi: 10.15252/emmm.201809316

Nho, K., Kueider-Paisley, A., MahmoudianDehkordi, S., Arnold, M., Risacher, S. L., Louie, G., et al. (2019). Altered bile acid profile in mild cognitive impairment and Alzheimer's disease: relationship to neuroimaging and CSF biomarkers. *Alzheimers dement.* 15, 232–244. doi: 10.1016/j.jalz.2018.08.012

Nicoll, J. A. R., Buckland, G. R., Harrison, C. H., Page, A., Harris, S., Love, S., et al. (2019). Persistent neuropathological effects 14 years following amyloid-beta immunization in Alzheimer's disease. *Brain* 142, 2113–2126.

Novak, P., Schmidt, R., Kontsekova, E., Kovacech, B., Smolek, T., Katina, S., et al. (2018). FUNDAMANT: an interventional 72-week phase 1 follow-up study of AADvac1, an active immunotherapy against tau protein pathology in Alzheimer's disease. *Alzheimers Res. Ther.* 10:108. doi: 10.1186/s13195-018-0436-1

Novak, P., Schmidt, R., Kontsekova, E., Zilka, N., Kovacech, B., Skrabana, R., et al. (2017). Safety and immunogenicity of the tau vaccine AADvac1 in patients with Alzheimer's disease: a randomised, double-blind, placebo-controlled, phase 1 trial. *Lancet Neurol.* 16, 123–134. doi: 10.1016/S1474-4422(16)30331-3

Novak, P., Zilka, N., Zilkova, M., Kovacech, B., Skrabana, R., Ondrus, M., et al. (2019). AADvac1, an active immunotherapy for Alzheimer's disease and non Alzheimer tauopathies: an overview of preclinical and clinical development. *J Prev Alzheimers Dis* 6, 63–69. doi: 10.14283/jpad.2018.45

O'Bryant, S. E., Zhang, F., Petersen, M., Johnson, L., Hall, J., and Rissman, R. A. (2021). A precision medicine approach to treating Alzheimer's disease using rosiglitazone therapy: a biomarker analysis of the REFLECT trials. *J. Alzheimers Dis.* 81, 557–568. doi: 10.3233/JAD-201610

Ogbodo, J. O., Agbo, C. P., Njoku, U. O., Ogugofor, M. O., Egba, S. I., Ihim, S. A., et al. (2022). Alzheimer's disease: pathogenesis and therapeutic interventions. *Curr. Aging Sci.* 15, 2–25.

Ohtake, Y., Kong, W., Hussain, R., Horiuchi, M., Tremblay, M. L., Ganea, D., et al. (2017). Protein tyrosine phosphatase σ regulates autoimmune encephalomyelitis development. *Brain Behav. Immun.* 65, 111–124. doi: 10.1016/j.bbi.2017.05.018

Orsucci, D., Mancuso, M., Ienco, E. C., LoGerfo, A., and Siciliano, G. (2011). Targeting mitochondrial dysfunction and neurodegeneration by means of coenzyme Q10 and its analogues. *Curr. Med. Chem.* 18, 4053–4064. doi: 10.2174/092986711796957257

Ostrowitzki, S., Bittner, T., Sink, K. M., Mackey, H., Rabe, C., Honig, L. S., et al. (2022). Evaluating the safety and efficacy of crenezumab vs placebo in adults with early alzheimer disease: two phase 3 randomized placebo-controlled trials. *JAMA Neurol.* 79, 1113–1121. doi: 10.1001/jamaneurol.2022.2909

Pandi-Perumal, S. R., BaHammam, A. S., Brown, G. M., Spence, D. W., Bharti, V. K., Kaur, C., et al. (2013). Melatonin antioxidative defense: therapeutical implications for aging and neurodegenerative processes. *Neurotoxicity Res.* 23, 267–300. doi: 10.1007/s12640-012-9337-4

Pasquier, F., Sadowsky, C., Holstein, A., Leterme Gle, P., Peng, Y., Jackson, N., et al. (2016). Two phase 2 multiple ascending-dose studies of vanutide cridificar (ACC-001) and QS-21 adjuvant in mild-to-moderate Alzheimer's disease. *J. Alzheimers Dis.* 51, 1131–1143.

Patel, S., Bansoad, A. V., Singh, R., and Khatik, G. L. (2022). BACE1: a key regulator in Alzheimer's disease progression and current development of its inhibitors. *Curr. Neuropharmacol.* 20, 1174–1193. doi: 10.2174/1570159X19666211201094031

Pavlov, E., Zakharian, E., Bladen, C., Diao, C. T., Grimbly, C., Reusch, R. N., et al. (2005). A large, voltage-dependent channel, isolated from mitochondria by water-free chloroform extraction. *Biophys. J.* 88, 2614–2625. doi: 10.1529/biophysj.104.057281

Pieper, A. A., Xie, S., Capota, E., Estill, S. J., Zhong, J., Long, J. M., et al. (2010). Discovery of a proneurogenic, neuroprotective chemical. *Cell* 142, 39–51.

Pinheiro, L., and Faustino, C. (2019). Therapeutic strategies targeting amyloid-beta in Alzheimer's disease. *Curr. Alzheimer Res.* 16, 418–452.

Porter, G. A. Jr., and Beutner, G. (2018). Cyclophilin D, somehow a master regulator of mitochondrial function. *Biomolecules* 8:176. doi: 10.3390/biom8040176

Portron, A., Jordan, P., Draper, K., Muenzer, C., Dickerson, D., van Iersel, T., et al. (2020). A phase I study to assess the effect of speed of injection on pain, tolerability, and pharmacokinetics after high-volume subcutaneous administration of gantenerumab in healthy volunteers. *Clin. Ther.* 42, 108–120.e1. doi: 10.1016/j.clinthera.2019.11.015

Pride, M., Seubert, P., Grundman, M., Hagen, M., Eldridge, J., and Black, R. S. (2008). Progress in the active immunotherapeutic approach to Alzheimer's disease: clinical investigations into AN1792-associated meningoencephalitis. *Neurodegener. Dis.* 5, 194–196. doi: 10.1159/000113700

Qin, W., Haroutunian, V., Katsel, P., Cardozo, C. P., Ho, L., Buxbaum, J. D., et al. (2009) PGC-1alpha expression decreases in the Alzheimer disease brain as a function of dementia. *Arch Neurol.* 66, 352–361.

Qureshi, I. A., Tirucherai, G., Ahlijanian, M. K., Kolaitis, G., Bechtold, C., and Grundman, M. (2018). A randomized, single ascending dose study of intravenous BIIB092 in healthy participants. *Alzheimers Dement.* 4, 746–755. doi: 10.1016/j.trci.2018.10.007

Ramsay, R. R., Dunford, C., and Gillman, P. K. (2007). Methylene blue and serotonin toxicity: inhibition of monoamine oxidase A (MAO A) confirms a theoretical prediction. *Br. J. Pharmacol.* 152, 946–951. doi: 10.1038/sj.bjp.0707430

Rashad, A., Rasool, A., Shaheryar, M., Sarfraz, A., Sarfraz, Z., Robles-Velasco, K., et al. (2022). Donanemab for Alzheimer's disease: a systematic review of clinical trials. *Healthcare* 11:32. doi: 10.3390/healthcare11010032

Reddy, A. P., and Reddy, P. H. (2017). Mitochondria-targeted molecules as potential drugs to treat patients with Alzheimer's disease. *Progr. Mol. Biol. Transl. Sci.* 146, 173–201. doi: 10.1016/bs.pmbts.2016.12.010

Reddy, P. H., and Oliver, D. M. (2019). Amyloid beta and phosphorylated tau-induced defective autophagy and mitophagy in Alzheimer's disease. *Cells* 8:488.

Roberts, C., Kaplow, J., Giroux, M., Krause, S., and Kanekiyo, M. (2021). Amyloid and APOE status of screened subjects in the Elenbecestat MissionAD phase 3 program. *J. Prev. Alzheimers Dis.* 8, 218–223. doi: 10.14283/jpad.2021.4

Saitow, F., and Nakaoka, Y. (1997). The photodynamic action of methylene blue on the ion channels of Paramecium causes cell damage. *Photochem. Photobiol.* 65, 902–907. doi: 10.1111/j.1751-1097.1997.tb01941.x

Salloway, S., Farlow, M., McDade, E., Clifford, D. B., Wang, G., Llibre-Guerra, J. J., et al. (2021). A trial of gantenerumab or solanezumab in dominantly inherited Alzheimer's disease. *Nat. Med.* 27, 1187–1196.

Salloway, S., Marshall, G. A., Lu, M., and Brashear, H. R. (2018). Long-term safety and efficacy of bapineuzumab in patients with mild-to-moderate Alzheimer's disease: a phase 2, open-label extension study. *Curr. Alzheimer Res.* 15, 1231–1243. doi: 10.2174/1567205015666180821114813

Salloway, S., Sperling, R., Fox, N. C., Blennow, K., Klunk, W., Raskind, M., et al. (2014). Two phase 3 trials of bapineuzumab in mild-to-moderate Alzheimer's disease. *N. Engl. J. Med.* 370, 322–333.

Schiavone, M., Zulian, A., Menazza, S., Petronilli, V., Argenton, F., Merlini, L., et al. (2017). Alisporivir rescues defective mitochondrial respiration in Duchenne

muscular dystrophy. *Pharmacol. Res.* 125, 122–131. doi: 10.1016/j.phrs.2017.09.001

Schneider, L. S., Laudon, M., Nir, T., Caceres, J., Ianniciello, G., Capulli, M., et al. (2022). A polymorphism cluster at the 2q12 locus may predict response to Piromelatine in patients with mild Alzheimer's disease. *J. Prev. Alzheimers Dis.* 9, 247–254. doi: 10.14283/jpad.2021.61

Seripa, D., Solfrizzi, V., Imbimbo, B. P., Daniele, A., Santamato, A., Lozupone, M., et al. (2016). Tau-directed approaches for the treatment of Alzheimer's disease: focus on leuco-methylthioninium. *Expert Rev. Neurother.* 16, 259–277. doi: 10.1586/14737175.2016.1140039

Shcherbinin, S., Evans, C. D., Lu, M., Andersen, S. W., Pontecorvo, M. J., Willis, B. A., et al. (2022). Association of amyloid reduction after Donanemab treatment with tau pathology and clinical outcomes: the TRAILBLAZER-ALZ randomized clinical trial. *JAMA Neurol.* 79, 1015–1024.

Shevtsova, E. F., Maltsev, A. V., Vinogradova, D. V., Shevtsov, P. N., and Bachurin, S. O. (2021). Mitochondria as a promising target for developing novel agents for treating Alzheimer's disease. *Med. Res. Rev.* 41, 803–827.

Shevtsova, E. F., Vinogradova, D. V., Kireeva, E. G., Reddy, V. P., Aliev, G., and Bachurin, S. O. (2014). Dimebon attenuates the Aβ-induced mitochondrial permeabilization. *Curr. Alzheimer Res.* 11, 422–429.

Shevtsova, E. F., Vinogradova, D. V., Neganova, M. E., Avila-Rodriguez, M., Ashraf, G. M., Barreto, G. E., et al. (2017). Mitochondrial permeability transition pore as a suitable target for neuroprotective agents against Alzheimer's disease. *CNS Neurol. Disord. Drug Targets* 16, 677–685. doi: 10.2174/1871527316666170424114444

Singer, C., Tractenberg, R. E., Kaye, J., Schafer, K., Gamst, A., Grundman, M., et al. (2003). A multicenter, placebo-controlled trial of melatonin for sleep disturbance in Alzheimer's disease. *Sleep* 26, 893–901.

Singulani, M. P., Pereira, C. P. M., Ferreira, A. F. F., Garcia, P. C., Ferrari, G. D., Alberici, L. C., et al. (2020). Impairment of PGC-1α-mediated mitochondrial biogenesis precedes mitochondrial dysfunction and Alzheimer's pathology in the 3xTg mouse model of Alzheimer's disease. *Exp. Gerontol.* 133:110882.

Skvortsova, V. I., Bachurin, S. O., Ustyugov, A. A., Kukharsky, M. S., Deikin, A. V., Buchman, V. L., et al. (2018). Gamma-carbolines derivatives as promising agents for the development of pathogenic therapy for proteinopathy. *Acta Naturae* 10, 59–62.

Sperling, R., Henley, D., Aisen, P. S., Raman, R., Donohue, M. C., Ernstrom, K., et al. (2021). Findings of efficacy, safety, and biomarker outcomes of atabecestat in preclinical alzheimer disease: a truncated randomized phase 2b/3 clinical trial. *JAMA Neurol.* 78, 293–301. doi: 10.1001/jamaneurol.2020.4857

Springer, J. E., Visavadiya, N. P., Sullivan, P. G., and Hall, E. D. (2018). Post-injury treatment with NIM811 promotes recovery of function in adult female rats after spinal cord contusion: a dose-response study. *J. Neurotrauma* 35, 492–499. doi: 10.1089/neu.2017.5167

Sragovich, S., Malishkevich, A., Piontkewitz, Y., Giladi, E., Touloumi, O., Lagoudaki, R., et al. (2019). The autism/neuroprotection-linked ADNP/NAP regulate the excitatory glutamatergic synapse. *Transl. Psychiatry* 9:2. doi: 10.1038/s41398-018-0357-6

Sragovich, S., Merenlender-Wagner, A., and Gozes, I. (2017). ADNP plays a key role in autophagy: from autism to schizophrenia and Alzheimer's Disease. *Bioessays* 39:1700054. doi: 10.1002/bies.201700054

Swanson, C. J., Zhang, Y., Dhadda, S., Wang, J., Kaplow, J., Lai, R. Y. K., et al. (2021). A randomized, double-blind, phase 2b proof-of-concept clinical trial in early Alzheimer's disease with lecanemab, an anti-Abeta protofibril antibody. *Alzheimers Res. Ther.* 13:80.

Tarocco, A., Caroccia, N., Morciano, G., Wieckowski, M. R., Ancora, G., Garani, G., et al. (2019). Melatonin as a master regulator of cell death and inflammation: molecular mechanisms and clinical implications for newborn care. *Cell Death Dis.* 10:317. doi: 10.1038/s41419-019-1556-7

Tatebe, H., Kasai, T., Ohmichi, T., Kishi, Y., Kakeya, T., Waragai, M., et al. (2017). Quantification of plasma phosphorylated tau to use as a biomarker for brain Alzheimer pathology: pilot case-control studies including patients with Alzheimer's disease and down syndrome. *Mol. Neurodegener.* 12:63. doi: 10.1186/s13024-017-0206-8

Teng, E., Manser, P. T., Pickthorn, K., Brunstein, F., Blendstrup, M., Sanabria Bohorquez, S., et al. (2022). Safety and efficacy of semorinemab in individuals with prodromal to mild alzheimer disease: a randomized clinical trial. *JAMA Neurol.* 79, 758–767. doi: 10.1001/jamaneurol.2022.1375

Teo, E., Ravi, S., Barardo, D., Kim, H. S., Fong, S., Cazenave-Gassiot, A., et al. (2019). Metabolic stress is a primary pathogenic event in transgenic Caenorhabditis elegans expressing pan-neuronal human amyloid beta. *eLife* 8:e50069. doi: 10.7554/eLife.50069

Tesla, R., Wolf, H. P., Xu, P., Drawbridge, J., Estill, S. J., Huntington, P., et al. (2012). Neuroprotective efficacy of aminopropyl carbazoles in a mouse model of amyotrophic lateral sclerosis. *Proc. Natl. Acad. Sci. U.S.A.* 109, 17016–17021. doi: 10.1073/pnas.1213960109

Thal, L. J., Grundman, M., Berg, J., Ernstrom, K., Margolin, R., Pfeiffer, E., et al. (2003). Idebenone treatment fails to slow cognitive decline in Alzheimer's disease. *Neurology* 61, 1498–1502. doi: 10.1212/01.wnl.0000096376.03678.c1

Theunis, C., Crespo-Biel, N., Gafner, V., Pihlgren, M., López-Deber, M. P., Reis, P., et al. (2013). Efficacy and safety of a liposome-based vaccine against protein Tau, assessed in tau.P301L mice that model tauopathy. *PLoS One* 8:e72301. doi: 10.1371/journal.pone.0072301

Timmers, M., Streffer, J. R., Russu, A., Tominaga, Y., Shimizu, H., Shiraishi, A., et al. (2018). Pharmacodynamics of atabecestat (JNJ-54861911), an oral BACE1 inhibitor in patients with early Alzheimer's disease: randomized, double-blind, placebo-controlled study. *Alzheimers Res. Ther.* 10:85. doi: 10.1186/s13195-018-0415-6

Tucker, D., Lu, Y., and Zhang, Q. (2018). From mitochondrial function to neuroprotection-an emerging role for methylene blue. *Mol. Neurobiol.* 55, 5137–5153. doi: 10.1007/s12035-017-0712-2

Ustyugov, A., Shevtsova, E., Ashraf, G. M., Tarasov, V. V., Bachurin, S. O., and Aliev, G. (2018). New therapeutic property of dimebon as a neuroprotective agent. *Curr. Med. Chem.* 25, 5315–5326.

Vahdat, L. T. (2008). Clinical studies with epothilones for the treatment of metastatic breast cancer. *Semin. Oncol.* 35, S22–S30.

Valasani, K. R., Sun, Q., Fang, D., Zhang, Z., Yu, Q., Guo, Y., et al. (2016). Identification of a small molecule cyclophilin D inhibitor for rescuing Aβ-mediated mitochondrial dysfunction. *ACS Med. Chem. Lett.* 7, 294–299.

Valasani, K. R., Vangavaragu, J. R., Day, V. W., and Yan, S. S. (2014). Structure based design, synthesis, pharmacophore modeling, virtual screening, and molecular docking studies for identification of novel cyclophilin D inhibitors. *J. Chem. Inform. Model.* 54, 902–912. doi: 10.1021/ci5000196

van Dyck, C. H., Swanson, C. J., Aisen, P., Bateman, R. J., Chen, C., Gee, M., et al. (2023). Lecanemab in early Alzheimer's disease. *N. Engl. J. Med.* 388, 9–21.

VandeVrede, L., Dale, M. L., Fields, S., Frank, M., Hare, E., Heuer, H. W., et al. (2020). Open-label phase 1 futility studies of salsalate and young plasma in progressive supranuclear palsy. *Mov. Disord. Clin. Pract.* 7, 440–447. doi: 10.1002/mdc3.12940

Vázquez-Rosa, E., Shin, M. K., Dhar, M., Chaubey, K., Cintrón-Pérez, C. J., Tang, X., et al. (2020). P7C3-A20 treatment one year after TBI in mice repairs the blood-brain barrier, arrests chronic neurodegeneration, and restores cognition. *Proc. Natl. Acad. Sci. U.S.A.* 117, 27667–27675. doi: 10.1073/pnas.2010430117

Vermersch, P., Brieva-Ruiz, L., Fox, R. J., Paul, F., Ramio-Torrenta, L., Schwab, M., et al. (2022). Efficacy and safety of Masitinib in progressive forms of multiple sclerosis: a randomized, phase 3, clinical trial. *Neurol. Neuroimmunol. Neuroinflamm.* 9:e1148. doi: 10.1212/NXI.0000000000001148

Voorhees, J. R., Remy, M. T., Cintrón-Pérez, C. J., El Rassi, E., Khan, M. Z., Dutca, L. M., et al. (2018). (-)-P7C3-S243 protects a rat model of Alzheimer's disease from neuropsychiatric deficits and neurodegeneration without altering amyloid deposition or reactive glia. *Biol. Psychiatry* 84, 488–498.

Vormfelde, S. V., Pezous, N., Lefevre, G., Kolly, C., Neumann, U., Jordaan, P., et al. (2020). A pooled analysis of three randomized phase I/IIa clinical trials confirms absence of a clinically relevant effect on the QTc interval by Umibecestat. *Clin. Transl. Sci.* 13, 1316–1326. doi: 10.1111/cts.12832

Vutskits, L., Briner, A., Klauser, P., Gascon, E., Dayer, A. G., Kiss, J. Z., et al. (2008). Adverse effects of methylene blue on the central nervous system. *Anesthesiology* 108, 684–692.

Wade, A. G., Farmer, M., Harari, G., Fund, N., Laudon, M., Nir, T., et al. (2014). Add-on prolonged-release melatonin for cognitive function and sleep in mild to moderate Alzheimer's disease: a 6-month, randomized, placebo-controlled, multicenter trial. *Clin. Interv. Aging* 9, 947–961. doi: 10.2147/CIA.S65625

Walker, A. K., Rivera, P. D., Wang, Q., Chuang, J. C., Tran, S., Osborne-Lawrence, S., et al. (2015). The P7C3 class of neuroprotective compounds exerts antidepressant efficacy in mice by increasing hippocampal neurogenesis. *Mol. Psychiatry* 20, 500–508. doi: 10.1038/mp.2014.34

Wang, D., Kowalewski, E. K., and Koch, G. (2022). Application of meta-analysis to evaluate relationships among ARIA-E Rate, amyloid reduction rate, and clinical cognitive response in amyloid therapeutic clinical trials for early Alzheimer's disease. *Ther. Innov. Regul. Sci.* 56, 501–516. doi: 10.1007/s43441-022-00390-4

Wang, T., Zhao, L., Liu, M., Xie, F., Ma, X., Zhao, P., et al. (2014). Oral intake of hydrogen-rich water ameliorated chlorpyrifos-induced neurotoxicity in rats. *Toxicol. Appl. Pharmacol.* 280, 169–176. doi: 10.1016/j.taap.2014.06.011

Wang, Y., An, H., Liu, T., Qin, C., Sesaki, H., Guo, S., et al. (2019). Metformin Improves Mitochondrial Respiratory Activity through Activation of AMPK. *Cell Rep.* 29, 1511–1523.e5.

Watson, G. S., and Craft, S. (2003). The role of insulin resistance in the pathogenesis of Alzheimer's disease: implications for treatment. *CNS Drugs* 17, 27–45.

Wegmann, S., Biernat, J., and Mandelkow, E. (2021). A current view on Tau protein phosphorylation in Alzheimer's disease. *Curr. Opin. Neurobiol.* 69, 131–138.

Wessels, A. M., Tariot, P. N., Zimmer, J. A., Selzler, K. J., Bragg, S. M., Andersen, S. W., et al. (2020). Efficacy and safety of Lanabecestat for treatment of early and mild Alzheimer Disease: the AMARANTH and DAYBREAK-ALZ randomized clinical trials. *JAMA Neurol.* 77, 199–209. doi: 10.1001/jamaneurol.2019.3988

West, T., Hu, Y., Verghese, P. B., Bateman, R. J., Braunstein, J. B., Fogelman, I., et al. (2017). Preclinical and clinical development of ABBV-8E12, a humanized anti-tau antibody, for treatment of Alzheimer's disease and other tauopathies. *J. Prev. Alzheimers Dis.* 4, 236–241. doi: 10.14283/jpad.2017.36

Wilcock, G. K., Gauthier, S., Frisoni, G. B., Jia, J., Hardlund, J. H., Moebius, H. J., et al. (2018). Potential of low dose leuco-methylthioninium Bis(Hydromethanesulphonate) (LMTM) monotherapy for treatment of mild Alzheimer's Disease: cohort analysis as modified primary outcome in a phase III clinical trial. *J. Alzheimers Dis.* 61, 435–457. doi: 10.3233/JAD-170560

Wilkins, H. M., and Morris, J. K. (2017). New therapeutics to modulate mitochondrial function in neurodegenerative disorders. *Curr. Pharm. Des.* 23, 731–752.

Wilkinson, D., Windfeld, K., and Colding-Jørgensen, E. (2014). Safety and efficacy of idalopirdine, a 5-HT6 receptor antagonist, in patients with moderate Alzheimer's disease (LADDER): a randomised, double-blind, placebo-controlled phase 2 trial. *Lancet Neurol.* 13, 1092–1099. doi: 10.1016/S1474-4422(14)70198-X

Willis, B. A., Zhang, W., Ayan-Oshodi, M., Lowe, S. L., Annes, W. F., Sirois, P. J., et al. (2012). Semagacestat pharmacokinetics are not significantly affected by formulation, food, or time of dosing in healthy participants. *J. Clin. Pharmacol.* 52, 904–913.

Wischik, C. M., Staff, R. T., Wischik, D. J., Bentham, P., Murray, A. D., Storey, J. M., et al. (2015). Tau aggregation inhibitor therapy: an exploratory phase 2 study in mild or moderate Alzheimer's disease. *J. Alzheimers Dis.* 44, 705–720.

Yang, C. C., Chiu, M. J., Chen, T. F., Chang, H. L., Liu, B. H., and Yang, S. Y. (2018). Assay of plasma phosphorylated tau protein (Threonine 181) and total tau protein in early-stage Alzheimer's disease. *J. Alzheimers Dis.* 61, 1323–1332. doi: 10.3233/JAD-170810

Yang, X., Zhang, Y., Xu, H., Luo, X., Yu, J., Liu, J., et al. (2016). Neuroprotection of coenzyme Q10 in neurodegenerative diseases. *Curr. Top. Med. Chem.* 16, 858–866.

Yao, J., Irwin, R. W., Zhao, L., Nilsen, J., Hamilton, R. T., and Brinton, R. D. (2009). Mitochondrial bioenergetic deficit precedes Alzheimer's pathology in female mouse model of Alzheimer's disease. *Proc. Natl. Acad. Sci. U.S.A.* 106, 14670–14675.

Ye, W., Liu, T., Zhang, W. M., Zhang, W., and Li, S. (2023). The improvement of epothilone D yield by the disruption of epoK gene in *Sorangium cellulosum* using TALEN system. *Mol. Biotechnol.* 65, 282–289. doi: 10.1007/s12033-022-00602-0

Yin, T. C., Britt, J. K., De Jesús-Cortés, H., Lu, Y., Genova, R. M., Khan, M. Z., et al. (2014). P7C3 neuroprotective chemicals block axonal degeneration and preserve function after traumatic brain injury. *Cell Rep.* 8, 1731–1740. doi: 10.1016/j.celrep.2014.08.030

Zhou, H., Wang, J., Jiang, J., Stavrovskaya, I. G., Li, M., Li, W., et al. (2014). N-acetyl-serotonin offers neuroprotection through inhibiting mitochondrial death pathways and autophagic activation in experimental models of ischemic injury. *J. Neurosci.* 34, 2967–2978. doi: 10.1523/JNEUROSCI.1948-13.2014

frontiers | Frontiers in Aging Neuroscience

TYPE Original Research
PUBLISHED 04 August 2023
DOI 10.3389/fnagi.2023.1236490

OPEN ACCESS

EDITED BY
Jiehui Jiang,
Shanghai University, China

REVIEWED BY
Hualin Chen,
Peking Union Medical College Hospital (CAMS), China
Chao Cheng,
Wuxi People's Hospital of Nanjing Medical University, China

*CORRESPONDENCE
Daojun Xie
✉ daojunxie@ahtcm.edu.cn

RECEIVED 07 June 2023
ACCEPTED 17 July 2023
PUBLISHED 04 August 2023

CITATION
Ma S, Wang D and Xie D (2023) Identification of disulfidptosis-related genes and subgroups in Alzheimer's disease.
Front. Aging Neurosci. 15:1236490.
doi: 10.3389/fnagi.2023.1236490

Identification of disulfidptosis-related genes and subgroups in Alzheimer's disease

Shijia Ma[1], Dan Wang[2] and Daojun Xie[2]*

[1]The First Affiliated Hospital of Anhui University of Chinese Medicine, Hefei, China, [2]Encephalopathy Center, The First Affiliated Hospital of Anhui University of Chinese Medicine, Hefei, China

Background: Alzheimer's disease (AD), a common neurological disorder, has no effective treatment due to its complex pathogenesis. Disulfidptosis, a newly discovered type of cell death, seems to be closely related to the occurrence of various diseases. In this study, through bioinformatics analysis, the expression and function of disulfidptosis-related genes (DRGs) in Alzheimer's disease were explored.

Methods: Differential analysis was performed on the gene expression matrix of AD, and the intersection of differentially expressed genes and disulfidptosis-related genes in AD was obtained. Hub genes were further screened using multiple machine learning methods, and a predictive model was constructed. Finally, 97 AD samples were divided into two subgroups based on hub genes.

Results: In this study, a total of 22 overlapping genes were identified, and 7 hub genes were further obtained through machine learning, including MYH9, IQGAP1, ACTN4, DSTN, ACTB, MYL6, and GYS1. Furthermore, the diagnostic capability was validated using external datasets and clinical samples. Based on these genes, a predictive model was constructed, with a large area under the curve (AUC = 0.8847), and the AUCs of the two external validation datasets were also higher than 0.7, indicating the high accuracy of the predictive model. Using unsupervised clustering based on hub genes, 97 AD samples were divided into Cluster1 (n = 24) and Cluster2 (n = 73), with most hub genes expressed at higher levels in Cluster2. Immune infiltration analysis revealed that Cluster2 had a higher level of immune infiltration and immune scores.

Conclusion: A close association between disulfidptosis and Alzheimer's disease was discovered in this study, and a predictive model was established to assess the risk of disulfidptosis subtype in AD patients. This study provides new perspectives for exploring biomarkers and potential therapeutic targets for Alzheimer's disease.

KEYWORDS

Alzheimer's disease, disulfidptosis, molecular clusters, machine learning, prediction model

Introduction

Alzheimer's disease (AD) is a prevalent neurodegenerative disorder characterized by progressive cognitive decline, accompanied by a decline in daily living abilities and psychiatric symptoms, and is the most common cause of dementia (McKhann et al., 2011). The incidence of AD is increasing year by year, with approximately 50 million AD patients

worldwide, and epidemiological data analysis predicts that the global incidence of AD will double by 2050 (Scheltens et al., 2021). AD was first discovered and reported by Aloïs Alzheimer in 1907, and over the past century, extensive research has been conducted, but the exact mechanism of AD remains largely unknown (Zhang G. et al., 2021), and there is still no effective treatment for preventing or slowing the progression of AD. Studies have shown that the preclinical latency period of AD can reach 20 years, indicating that we have a long time to intervene in the progression of the disease, making the discovery of AD biomarkers even more important.

Disulfidptosis is a newly discovered cell death mechanism that differs from traditional programmed cell death modes such as apoptosis, necrosis, autophagy, NETosis and pyroptosis (Jorgensen et al., 2016). Liu et al. (2023) found that cells with high expression of SLC7A11 undergo a previously uncharacterized form of cell death, called disulfidptosis, under glucose-deprived conditions due to the abnormal accumulation of disulfide molecules. Excessive accumulation of disulfide molecules induces disulfide stress in actin cytoskeleton proteins, resulting in an increase in disulfide bond levels within actin filaments. This leads to filament contraction and eventual disruption of the cellular skeleton structure, ultimately resulting in cell death. Inhibitors targeting specific cell death pathways have been used to treat various diseases, including neurodegenerative diseases (Deng et al., 2023). The discovery of the novel disulfidptosis mechanism of cell death induced by disulfide bonds in the cellular skeleton provides new potential targets for this form of treatment (Machesky, 2023).

Dendritic spines are excitatory synaptic protrusions located on dendritic shafts and are considered as pathological targets in Alzheimer's disease (Yu and Lu, 2012). Actin is the major cytoskeletal component of dendritic spines (Landis and Reese, 1983). Mounting evidence suggests that the actin cytoskeleton is crucial for synaptic function and plasticity (Selkoe, 2002). Dysregulation of actin cytoskeletal dynamics has been implicated in the pathological development of Alzheimer's disease (Pelucchi et al., 2020). Disulfide bond accumulation, which is the mechanism of disulfidptosis, can also lead to actin cytoskeleton damage. Thus suggesting a potential link between disulfidptosis and Alzheimer's disease, although the specific process of the link requires further analysis and investigation.

In this study, we aimed to explore potential mechanisms underlying AD by analyzing differentially expressed genes between normal and AD samples, utilizing the Gene Expression Omnibus (GEO) database. We performed a cross-referencing analysis between the differential genes and those associated with disulfidptosis, aiming to identify the differentially expressed disulfidptosis-related genes (DRGs). Subsequently, we applied various machine learning algorithms to identify key genes and developed a prediction model. The performance of the prediction model was validated using a nomogram and two external datasets. Finally, based on the expression profiles of seven disulfidptosis-related genes, we classified 97 AD patients into two disulfidptosis-related clusters and further evaluated the differences in immune cells between the two clusters, providing a new perspective for better understanding the potential molecular mechanisms underlying the pathogenesis of AD.

Materials and methods

Data acquisition and pre-processing

Three raw datasets (GSE132903, GSE48350, GSE5281, GSE33000, and GSE181279) were obtained from the GEO database using the "GEOquery" R program (Davis and Meltzer, 2007). These datasets contain gene expression data from both Alzheimer's disease patients and normal groups. The GSE132903 dataset contains 97 AD samples and 98 normal samples, the GSE48350 dataset contains 80 AD samples and 173 control samples, and the GSE5281 dataset contains 87 AD samples and 74 control samples, the GSE33000 dataset contains 310 AD samples and 157 control samples and the GSE181279 dataset contains 3 AD samples and 2 control samples.

Identification of differentially expressed genes associated with AD and disulfidptosis

Differential gene analysis was performed using the R package "limma" (Ritchie et al., 2015), $|\log2$ fold change (FC)$| > 0$ and $P < 0.05$ were selected as the threshold for differentially expressed genes (DEGs) between AD and normal samples in the dataset. Differential gene expression data were displayed using volcano plots and heatmaps. Gene ontology (GO) enrichment analysis and Kyoto Encyclopedia of Genes and Genomes (KEGG) pathway analysis were also performed using the "clusterProfiler" package (Yu et al., 2012) in R to further investigate the biological roles of DEGs.

Evaluating the immune cell infiltration

Single-sample gene set enrichment analysis (ssGSEA) was performed using the R package "GSVA." Twenty-eight immune gene sets were established, and the degree of immune cell infiltration was calculated for each sample based on the expression matrix of each sample (Hänzelmann et al., 2013). Four other algorithms, including quanTIseq, xCell, MCP-counter and Estimating the Proportion of Immune and Cancer cells (EPIC), were used to verify the stability of the ssGSEA results (Liu et al., 2022; Chen et al., 2023a). These analyses were performed by R package IOBR.

Construction of predictive model based on machine learning methods

According to the study by Liu et al. (2023) and Zhao et al. (2023a), a total of 26 DRGs were identified. By crossing DEGs with DRGs, differentially expressed DRGs were identified. Three machine learning techniques were then used to further screen the potential gene list for AD diagnosis (Yuan et al., 2023). The least absolute shrinkage and selection operator (LASSO) is a regression method that improves prediction accuracy and selects important

feature variables by using regularization techniques (Tibshirani, 1996). Support vector machine (SVM) can perform label prediction on feature vectors by establishing a threshold between the two classes (Noble, 2006). Random forest (RF) is a powerful method for predicting continuous variables and providing stable prediction results (Rigatti, 2017). The intersection genes resulting from LASSO regression, SVM and RF analyses were considered as central hub genes for AD diagnosis (Rajab et al., 2023). Next, a nomogram model for AD cluster occurrence was established using the rms R package (version 6.5.0). The pROC R package was used to perform receiver operating characteristic (ROC) analysis to evaluate the performance of the predictive model in discriminating AD from normal samples. The diagnostic value of the predictive model between AD and normal groups was validated using ROC analysis with two external brain tissue datasets, GSE5281 and GSE48350.

Validation by real-time PCR and differential expression of external datasets

Total RNA was extracted from the blood samples of AD and healthy controls (HCs) using TRIzol reagent Life Technologies (lot number: 248207), following the manufacturer's instructions. Subsequently, reverse transcription reactions were performed using RNA 1 μg and RevertAidTM M-MuLV reverse transcriptase (TaKaRa). Real-time PCR was conducted using 2 × SYBR Green qPCR Master Mix (High ROX) Servicebio (lot number: LT202201). The expression data were normalized using the 2-ΔΔCt method with β-actin as the internal reference. The primer sequences used for real-time fluorescence quantitative PCR analysis are provided in **Table 1**. We also performed differential analysis of the hub genes in GSE181279 and GSE33000. GSE181279 performed single-cell RNA-seq analysis. Quality control, data cleaning, and data analysis were performed using R packages such as "dplyr" and "Seurat." PCA analysis was conducted on the highly variable genes in the HC and AD groups, resulting in 4 clusters (HCs) and 6 clusters (AD), which were projected onto UMAP plots. The expression distribution of the hub genes in the control and AD groups was explored.

Subclusters analysis with seven disulfidptosis-related genes

Based on the expression profiles of 7 DRGs, we performed unsupervised hierarchical clustering analysis using ConsensusClusterPlus on 97 AD samples. Gene set variation analysis (GSVA) was conducted to elucidate the functional differences between the disulfidptosis subclusters identified through clustering analysis. The files "c2.cp.kegg.v7.4.symbols" and "h.all.v2023.1.Hs.symbols" were downloaded from the MSigDB online database for GSVA analysis. A heatmap was generated to visualize the distinct activity patterns of the two subclusters. DEGs were identified between the two disulfidptosis-related subclusters. Statistically significant values were considered when | log2 fold change (FC) | > 1 and adj. $p < 0.05$. GO and KEGG enrichment analyses were then conducted using the "clusterProfiler" package to describe their biological functions.

Results

Identification of DEGs and functional and pathway enrichment analysis

The dataset GSE132903 includes 97 AD samples and 98 normal samples. Using the R package "limma," a total of 11,637 DEGs were identified. **Figure 1** illustrates the specific analysis process, while **Figures 2A, B** display the volcano plot and heatmap of the DEGs, respectively. GO and KEGG enrichment pathway analysis was performed in R to explore the potential role of DEGs. The significant GO-BP (biological process) terms were mainly related to nervous system development, positive regulation of cellular metabolic process, establishment of localization. GO-CC (cellular component) analysis showed that the DEGs were significantly enriched in presynapse, cell junction, cell projection, nucleoplasm. GO-MF (molecular function) enriched pathways were mainly related to cytoskeletal protein binding, small molecule binding, enzyme binding, nucleoside phosphate binding (**Figure 2C**). The KEGG analysis revealed that these DEGs were enriched in pathways such as salmonella infection, Fc gamma R-mediated phagocytosis, axon guidance, ErbB signaling pathway, autophagy-animal, regulation of actin cytoskeleton and mitogen-activated protein kinase (MAPK) signaling pathway (**Figure 2D**). These results suggest that these DEGs have important implications for the research and can be further analyzed.

Evaluation of immune cell infiltration

The overall expression patterns of 22 DRGs in AD and normal samples are shown in **Figures 3A, B**. Except for NCKAP1, RAC1, ACTB, NDUFA11, GYS1, DSTN, and MYH10, which are expressed at lower levels in AD, most DRGs are expressed at higher levels in AD. A total of 22 key genes were identified by intersecting the 11,637 DEGs with the 26 DRGs (**Figure 3C**). To investigate whether there are differences in the immune system between AD and normal groups, an immune infiltration analysis was conducted using the ssGSEA algorithm, which revealed differences in the proportions of 28 infiltrating immune cell types between the AD and normal groups (**Figure 3D**). The results showed that AD patients had higher levels of activated CD8 T cell, CD56bright natural killer cell, CD56dim natural killer cell, central memory CD8 T cell, effector memory CD8 T cell, immature B cell, immature dendritic cell, mast cell, MDSC, natural killer cell, natural killer T cell and plasmacytoid dendritic cell, while gamma delta T cell and Type 1 T helper cell did not show significant differences (**Figure 3E**). To gain further insights into the tumor microenvironment (TME) contexture, we employed four additional methodologies, namely xCell, MCPcounter, EPIC, and quanTIseq (**Supplementary Figure 1**). Furthermore, the correlation analysis results also showed that Immune cells are closely associated with DRGs (**Figure 3F**). These results indicate that distinct immune cell types display unique infiltrations in AD

TABLE 1 Primer sequences for RT-qPCR.

Gene	Amplicon size (bp)	Forward primer (5′→3′)	Reverse primer (5′→3′)
Hu-β-actin	96	CCCTGGAGAAGAGCTACGAG	GGAAGGAAGGCTGGAAGAGT
Hu-MYH9	150	AAGCTGGTATGGGTGCCTTC	CTTGGGCGGGTTCATCTTCT
Hu-MYL6	196	GCATATCCTGTCGGGGTGAC	GCTGACGGCAAACATCATCC
Hu-DSTN	179	TTGCCAGGACAATCATTAACTGC	AATCCCAGTCCTCTCCTCAGA
Hu-ACTN4	180	GAACCGCTCGAAGTCCACAC	TGTGGCATTCATGTCCTCCC
Hu-GYS1	146	CGAATGGGGCGACAACTACT	TCTGTGCCAGGAACTTGCAG
Hu-IQGAP1	182	TCAGCCATTGTCAGCTCTGT	TCAAAGGCATCAGGAGCAACA

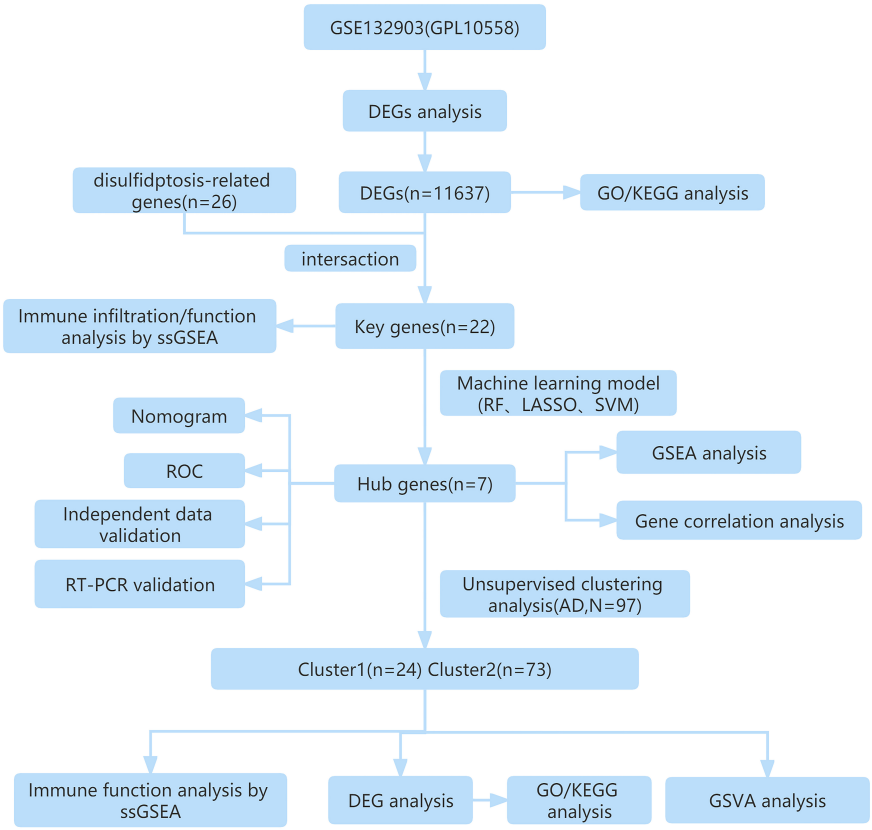

FIGURE 1
The study flow chart.

patients, and DRGs may serve as a crucial factor in regulating the immune infiltration status of AD patients.

Identification of the disulfidptosis-signature via machine learning

Based on 22 key genes, we used LASSO regression, random forest and SVM algorithms to screen for potential genes and construct a disulfidptosis-signature (Figures 4A–C). Ultimately, we identified eight disulfidptosis-related feature genes as hub genes, including MYL6, MYH9, IQGAP1, ACTN4, GYS1, DSTN, and ACTB (Figure 4D). We conducted gene set enrichment analysis (GSEA) analysis on the seven hub genes, which showed that these genes exhibit enrichment in immune and metabolic related pathways (Supplementary Figure 2). Most of the hub genes were highly correlated with each other and IQGAP1 had a strong synergistic relationship with MYH9 (coefficient = 0.68), while DSTN had a strong antagonistic relationship with ACTN4 (coefficient = 0.63) (Figure 5A). The diagnostic ability of each feature gene in predicting AD was evaluated through ROC curve analysis, and a nomogram model was developed as a predictive tool for AD diagnosis (Figure 5B). The AUC value of the ROC curve for GYS1, ACTB, MYL6, MYH9, IQGAP1, ACTN4 and DSTN were 0.627, 0.753, 0.672, 0.692, 0.637 and 0.753, respectively (Figure 5C). The calibration curve shows that the error between the actual risk and the predicted risk is small, which indicates that

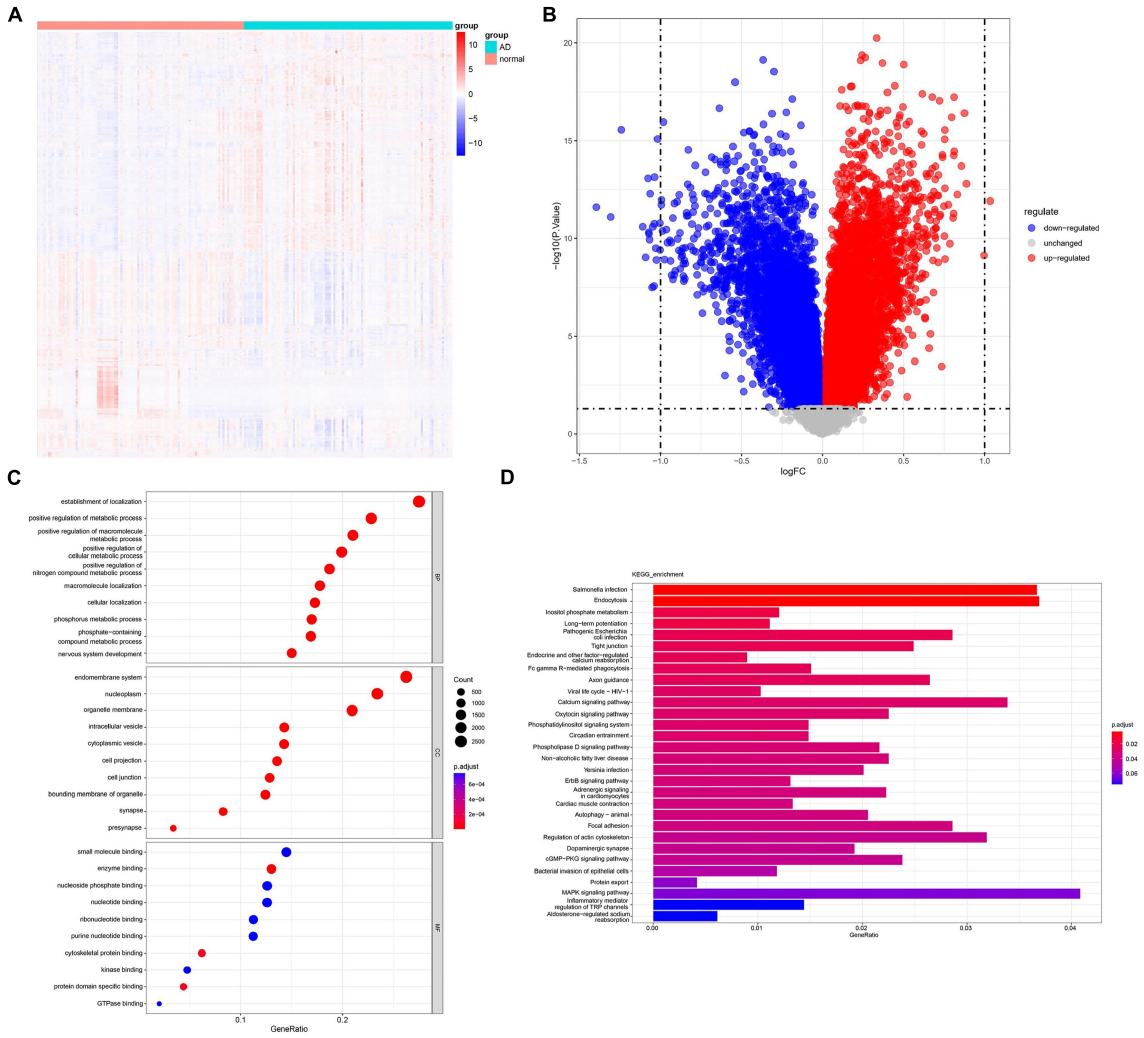

FIGURE 2
Analysis of differentially expressed genes and enriched pathways in AD. **(A)** An heatmap displays the expression levels of AD-related DEGs. **(B)** A volcano plot highlights the significant DEGs. **(C)** GO analysis shows enriched terms related to AD. **(D)** KEGG pathway analysis reveals enriched pathways in AD. DEGs, differentially expressed genes; GO, gene ontology; BP, biological process; CC, cellular component; MF, molecular function; KEGG, Kyoto Encyclopedia of Genes and Genomes.

the nomogram model has good prediction accuracy (Figure 5D). The AUC value of the ROC curve for nomogram was 0.8847 (Figure 5E). Further validation with external datasets GSE48350 and GSE5281 confirmed the diagnostic value of hub genes, with an AUC of 0.7306 for GSE48350 and 0.9217 for GSE5281 (Figures 5F, G). These results indicate that the nomogram model have good diagnostic value, and we can infer that these genes can accurately distinguish the AD group from the normal group.

Validation of hub genes expression through real-time PCR and differential analysis with external datasets

To validate the reliability of the hub genes, we collected blood samples from individuals with AD (n = 3) and healthy controls (HCs) (n = 3) for quantitative real-time reverse transcription-polymerase chain reaction (qRT-PCR). The results showed significantly elevated expression levels of MYH9, MYL6, ACTN4, IQGAP1, and GYS1 in AD patients compared to HCs, while the expression of DSTN was significantly decreased (Figure 6). Furthermore, the expression levels of the seven hub genes were validated in the GSE181279 and GSE33000 datasets. For GSE181279, we performed single-cell RNA sequencing (scRNA-seq) analysis, and quality control, data cleaning, and PCA analysis were conducted as shown in Supplementary Figure 3. The expression and distribution of hub genes are illustrated in Figure 7. The differential analysis results for GSE33000 can be found in Supplementary Table 1. Except for ACTB expression, the results from these two datasets were largely consistent, we considered the discrepancies of ACTB results to the heterogeneity of single-cell sequencing data, as well as differences in experimental methods, technology platforms, data processing, and analysis methods. These results suggest that these genes may have the potential to serve as biomarkers for AD diagnosis.

10.3389/fnagi.2023.1236490

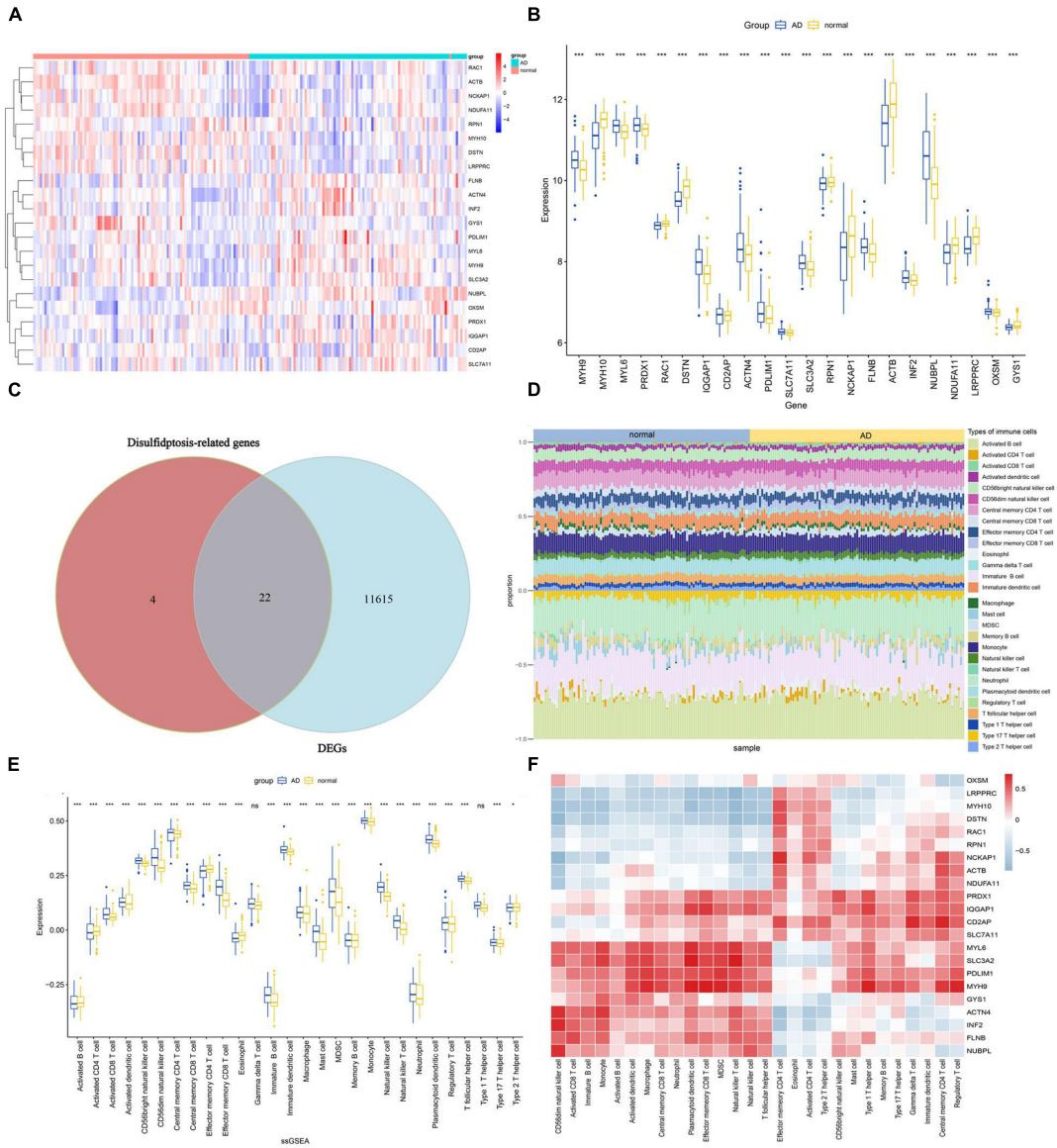

FIGURE 3
Expression of DRGs and immune cell infiltration in AD. **(A)** Heatmap showing the expression levels of DRGs. **(B)** Boxplot of DRGs expression levels. **(C)** Overlap of genes between DEGs and DRGs. **(D)** The proportions of 28 immune cells infiltrating in AD and normal were compared. **(E)** Boxplots illustrating the differences in immune infiltration between AD and normal. *$p < 0.05$, ***$p < 0.001$, ns, no significance. **(F)** Correlation analysis of 22 differentially expressed DRGs and infiltrated immune cells.

Consensus clustering analysis of disulfidptosis gene clusters

We performed consensus clustering analysis using the "Consensus Cluster Plus" package in R. Based on the expression profiles of the 7 hub genes, we grouped 97 AD samples. The stability of the clustering was found to be highest when $k = 2$, as demonstrated (**Figure 8A**), and the CDF curve showed fluctuations within the smallest consensus index range of 0.2 to 0.6 (**Figures 8B, C**). The same result was achieved from Nbclust testing (**Supplementary Figure 4**). We ultimately divided the 97 AD patients into two groups, namely Cluster1 ($n = 24$) and Cluster2 ($n = 73$). As shown in the PCA plot, the gene expression patterns between the clusters were distinct (**Figure 8D**). The expression levels of DRGs in the two subtypes were visualized by heatmap and boxplot (**Figures 8E, F**). With the exception of ACTN4 and GYS1, most DRGs had higher expression levels in Cluster2, including MYH9, MYL6, ACTB, DSTN, and IQGAP1.

GSVA of biological pathways between subclusters of disulfidptosis

Using GSVA analysis, we identified several enriched pathways that showed differential expression between the two subtypes, as visualized in a heat map. Based on KEGG pathways, Cluster1 showed higher expression levels in olfactory transduction, Notch signaling pathway and hedgehog signaling pathway, while Cluster2

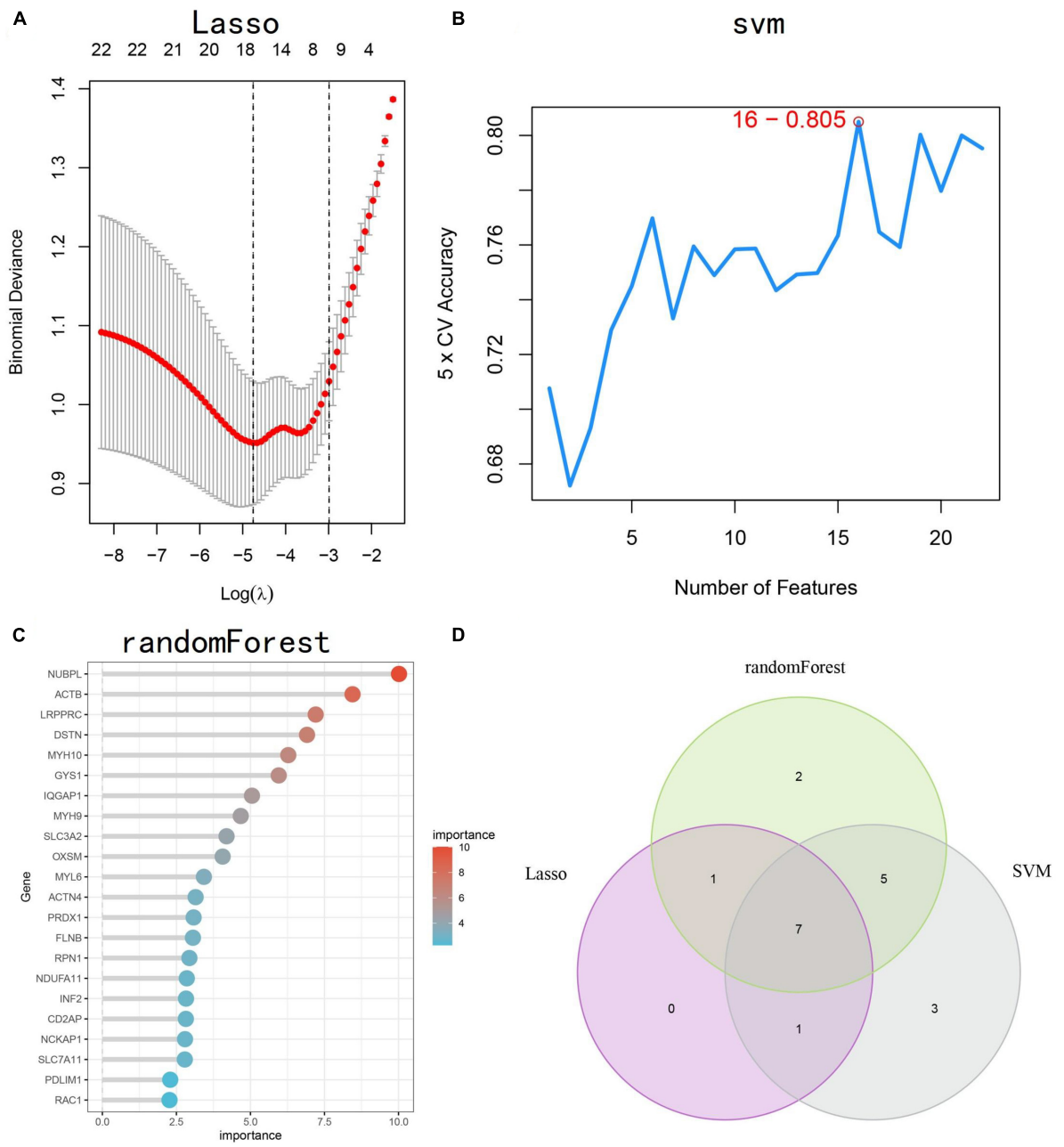

FIGURE 4
Identification of disulfidptosis-signature using machine learning. **(A–C)** Three different algorithms, LASSO regression, SVM, and RF, were used to construct disulfidptosis-signatures. **(D)** The Venn diagram shows the overlap of candidate genes identified by the three algorithms. LASSO, least absolute shrinkage and selection operator; SVM, support vector machine; RF, random forest.

showed higher activity in oxidative phosphorylation, valine leucine and isoleucine biosynthesis, cysteine and methionine metabolism, mismatch repair and Alzheimer's disease (Figure 9A). Cluster2 shows elevated expression in several metabolic pathways (including glucose metabolism, lipid metabolism, and amino acid metabolism), as well as disease pathways such as diabetes, Alzheimer's disease, and Parkinson's disease. Compared to Cluster1, Cluster2 showed higher Hallmark activity in PI3K AKT MTOR SIGNALING, MTORC1 SIGNALING, TGF BETA SIGNALING, APOPTOSIS, and IL2 STAT5 SIGNALING pathways (Figure 9B).

Functional distinctions between the two disulfidptosis subclusters

To gain further insight into the functional differences between the two subclusters, differential expression analysis was performed and a total of 298 DEGs were identified, including 90 upregulated and 208 downregulated genes. The distribution of these DEGs is shown in the volcano plot (Figure 10A). GO and KEGG enrichment analysis was then conducted on the 298 DEGs to gain a better understanding of potential

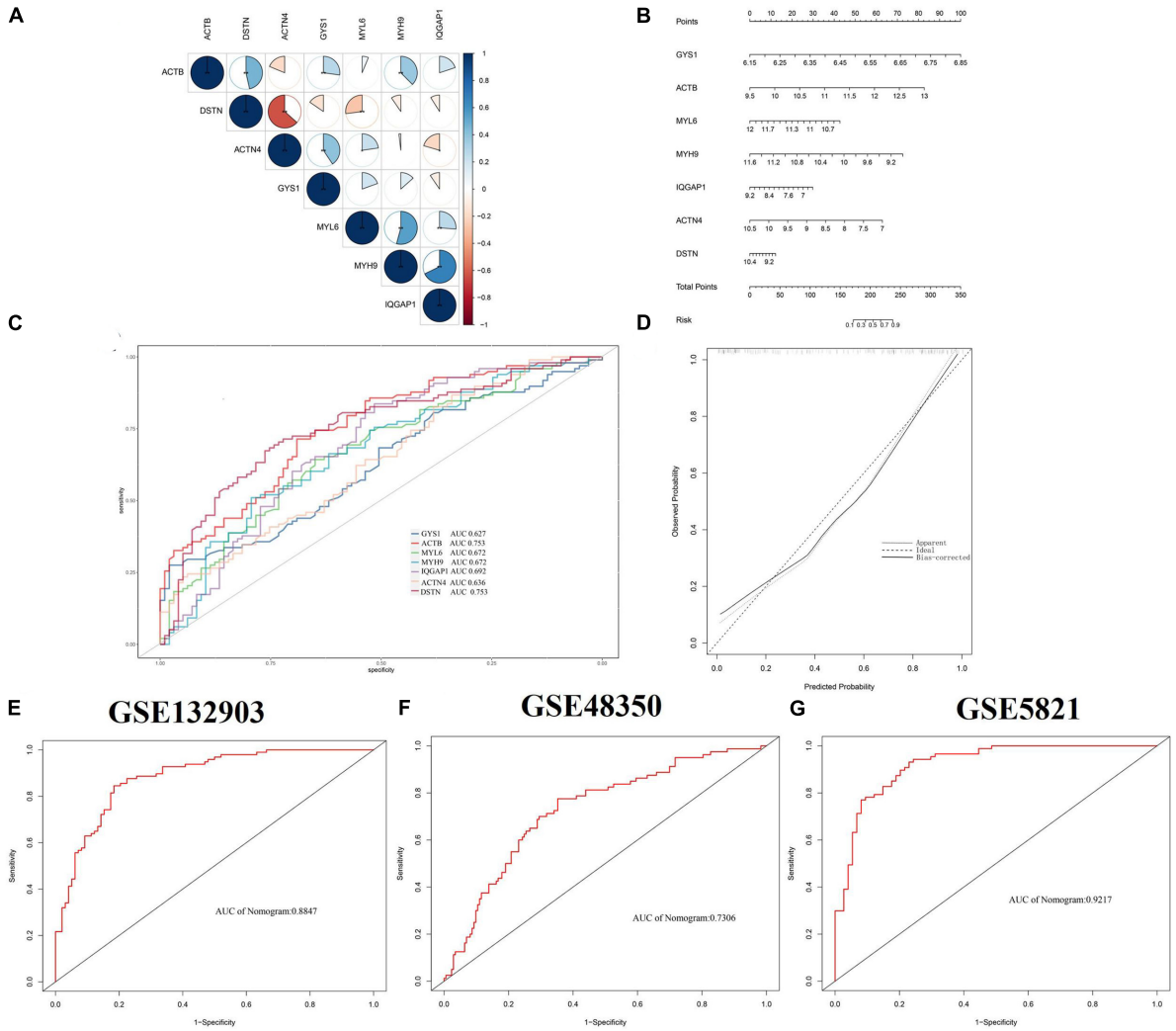

FIGURE 5
Validation of the diagnostic efficacy based on hub genes. **(A)** Correlation analysis of 7 hub genes. Positive correlations are represented by blue color while negative correlations are represented by red color. The pie chart depicts the correlation coefficients with varying sizes of each slice. $^{**}p < 0.05$. **(B)** Creating a nomogram to predict the risk of AD using hub genes. **(C)** ROC curve of hub genes in AD. **(D)** Calibration curve to evaluate prediction efficiency of nomogram model. **(E–G)** ROC curves from GSE132903, GSE48350, and GSE5821, respectively. ROC, receiver operating characteristic.

molecular processes and functions. GO analysis: (BP) shows gene enrichment in protein S-nitrosocysteine, regulation of transport, intracellular transport, nervous system development and intracellular localization; (CC) shows gene clustering in vesicle membrane, extracellular exosome, extracellular membrane-bounded organelle, extracellular vesicle and organelle membrane; (MF) shows cell enrichment in MHC class II protein complex binding, microtubule binding and protein-containing complex binding (Figure 10B). We performed KEGG enrichment analysis and found that these genes were mainly enriched in pathways such as Pathways of neurodegeneration—multiple diseases, Long-term potentiation, apelin signaling pathway and oxidative phosphorylation (Figures 10C, D). Subsequently, we conducted immune infiltration analysis on the two subgroups, and the results showed that the immune microenvironment between Cluster1 and Cluster2 had changed. Activated B cells, activated CD8 T cells, CD56dim natural killer cells, immature B cells, monocytes, natural killer cell and natural killer T cell were expressed at higher levels in Cluster1, while activated CD4 T cells, central memory CD4 T cells, effector memory CD4 T cells, eosinophil, immature dendritic cells, mast cell, memory B cells, neutrophil, regulatory T cells, type 1 T helper cells, type 17 T helper cells and type 2 T helper cells were expressed at higher levels in Cluster2 (Figure 10E). Moreover, the immune score of Cluster2 was relatively higher, indicating that Cluster2 may have a more significant level of immune infiltration (Figure 10F).

Discussion

As the most common neurodegenerative disease worldwide, Alzheimer's disease has been extensively studied, and some progress has been made (Zhao et al., 2023b). However, due to the lack of sufficient neurobiological markers and the heterogeneity of the pathogenesis of AD, the current therapeutic effects are still unsatisfactory (Byun et al., 2015; Cano et al., 2021). Therefore, it

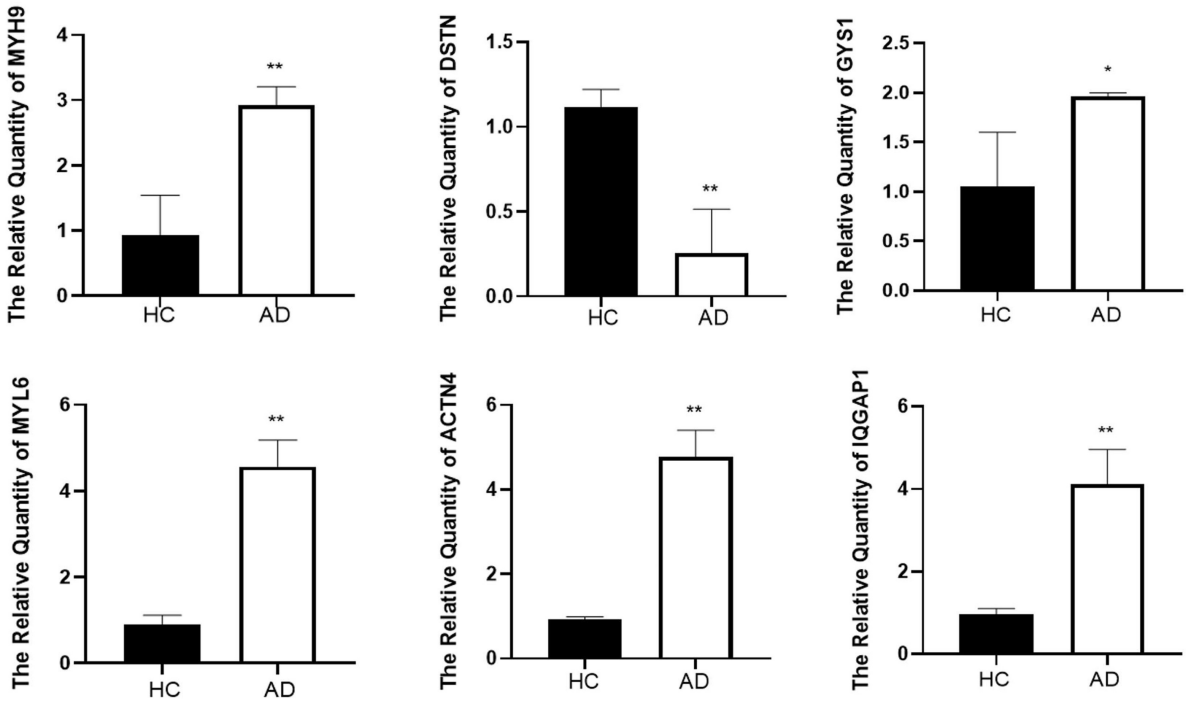

FIGURE 6
The result of quantitative real-time reverse transcription-polymerase chain reaction (qRT-PCR) illustrated the expression levels of hub genes in patients with AD (n = 3) and HC (n = 3). *p < 0.05, **p < 0.01.

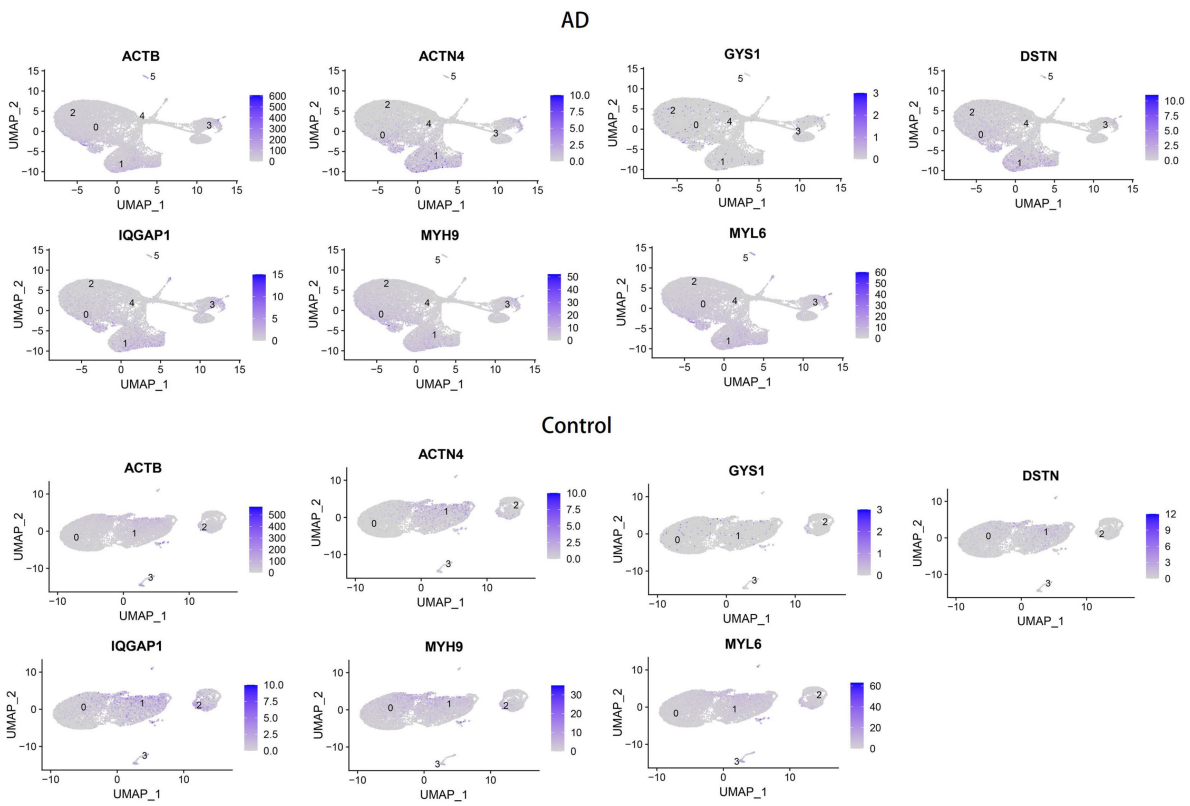

FIGURE 7
Verification of hub genes expression on single-cell RNA-seq analysis.

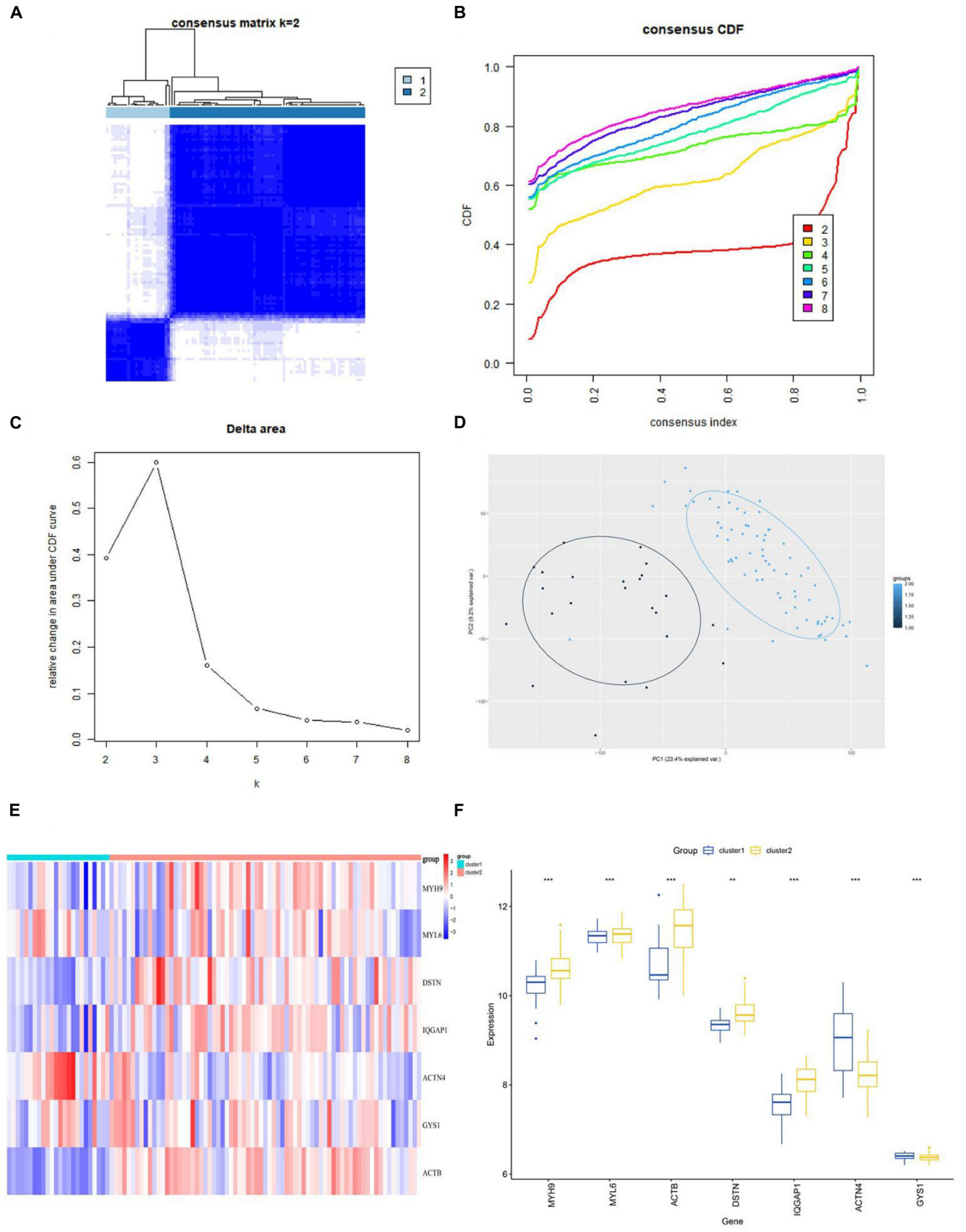

FIGURE 8
Identification of disulfidptosis subtypes in AD. **(A)** Consensus matrix displaying consensus values when $k = 2$. **(B,C)** CDF and CDF delta area curves were plotted to assess the quality of consensus clustering. **(D)** PCA diagram s depicting the distribution of different subclusters. **(E,F)** Differential expression of DRGs between subtypes is shown in the heatmap **(E)** and boxplot **(F)**. $^{**}p < 0.01$; $^{***}p < 0.001$; ns, no significance. CDF, cumulative distribution function; PCA, principal component analysis.

is crucial to identify more effective diagnostic markers to guide individualized treatment for AD. Disulfidptosis, a recently reported novel form of cell death, is mainly caused by the accumulation of disulfide bonds, leading to cytoskeleton collapse and subsequent cell death, which is closely related to disease progression (Chen et al., 2023b). However, the specific mechanism of disulfidptosis and its regulatory role in various diseases, as well as potential pathways, have not been further studied. Here, we attempted to

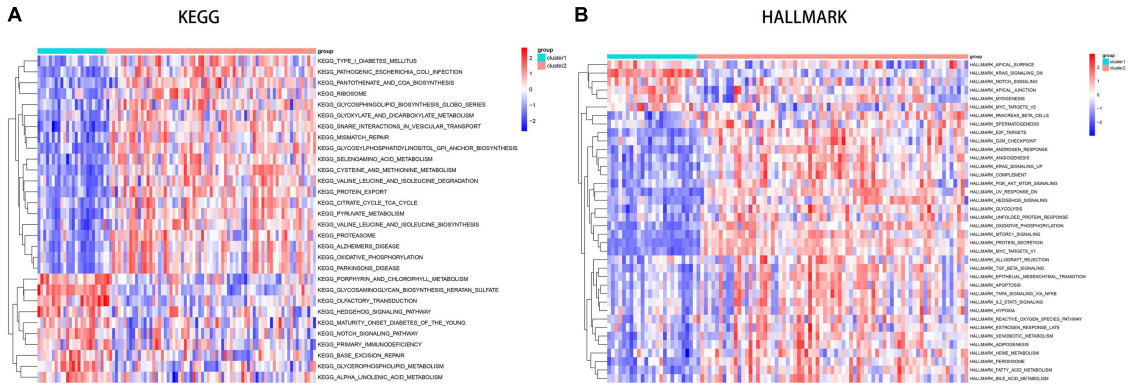

FIGURE 9
Analysis of key pathways between disulfidptosis subtypes using GSVA. **(A)** Pathway enrichment analysis based on the KEGG database. **(B)** Pathway enrichment analysis based on the Hallmark database.

elucidate the role of disulfidptosis-related genes in AD, linking disulfidptosis to the pathogenesis of AD, and identifying potential key genes through bioinformatics analysis to explore potential therapeutic targets.

In this study, we used the GEO database to investigate the gene expression levels of normal and AD patients and ultimately identified 11,637 DEGs. GO and KEGG enrichment analyses indicated that cells were enriched in positive regulation of metabolic process, cytoskeletal protein binding, MAPK signaling pathway, regulation of actin cytoskeleton and ErbB signaling pathway. Consistent with previous research conclusions that AD patients exhibit metabolic dysfunction in both the central and peripheral nervous system, as well as damage to the actin cytoskeleton in muscle cells leading to synaptic dysfunction and the MAPK and ErbB pathways have been identified as potential therapeutic targets for AD (Lee and Kim, 2017; Clarke et al., 2018; Pelucchi et al., 2020; Zhang H. et al., 2021).

Subsequently, we comprehensively evaluated the expression of DRGs in the brain tissues of both normal and AD individuals. Compared to the normal population, AD patients exhibited more abnormal expression of DRGs, indicating the important role of DRGs in the development of AD. Meanwhile, there were significant changes in the proportion of immune cells between normal and AD patients. Previous studies have shown that the immune system is closely related to AD (Mietelska-Porowska and Wojda, 2017), and our study showed that CD8 T cells, B cells, dendritic cells, mast cells, MDSCs, natural killer cells, and natural killer T cells were more highly infiltrated in AD patients, consistent with previous research (Salminen et al., 2018; Dai and Shen, 2021; Harcha et al., 2021).

In addition, we also found a correlation between these immune cells and DRGs. Furthermore, using three machine learning classifiers, we identified seven hub genes (MYL6, MYH9, IQGAP1, ACTN4, GYS1, DSTN, and ACTB) that are associated with AD. The diagnostic capability was validated using external datasets and clinical samples. Myosin II is an actin-binding protein composed of MHC (myosin heavy chain) IIs, RLCs (regulatory light chains) and ELCs (essential light chains) (Vierthaler et al., 2022). MYL6 is one of the ELCs, while MYH9 and MYH10 are part of the MHC family and encode non-muscle myosin II (NMM-II) which combines with the F-actin network to form the actomyosin cytoskeleton (Pecci et al., 2018; Acebedo et al., 2019); IQGAP1, a key regulatory factor for dendritic spine density, plays an important role in tissue cytoskeleton, microtubule network and cell adhesion by directly binding to actin and promoting actin filament crosslinking, and it also has a specific role in cognitive processes (Fukata et al., 1997; Briggs and Sacks, 2003; Gao et al., 2011; White et al., 2012); ACTN4, an important member of the actin-binding protein family, plays a crucial role in maintaining cell skeleton integrity, controlling cell movement, regulating mRNA metabolism and signal transduction (Khotin et al., 2010; Hsu and Kao, 2013; de Ribeiro et al., 2014); DSTN, a member of the actin depolymerizing factor (ADF)/cofilin family, plays a crucial role in regulating cell skeleton remodeling and actin filament turnover and has been linked to neurological damage (Zhang et al., 2020). DSTN protein has been proposed as a potential biomarker and regulatory protein for AD protection with Rb1 pretreatment (Hwang et al., 2016); Glycogen Synthase (GYS), belonging to the GT3 superfamily, is classified as a retaining glycosyltransferase (GT). Its function involves catalyzing the sequential addition of α-1, 4-linked glucose residues to the non-reducing end of a growing polysaccharide chain. GYS1, belonging to the GYS family, exhibits expression in multiple tissues, including muscle and brain (Inoue et al., 1988; McCorvie et al., 2022); beta-actin (ACTB) is a highly conserved cytoskeletal protein that plays a crucial role in cell growth and cell migration (Gu et al., 2021). ACTB is involved in various cellular processes, including cell motility, intracellular transport, and signal transduction. Its expression and function are essential for the proper functioning and dynamics of cells. The correlation analysis showed significant synergistic or antagonistic effects between these hub genes. Building a diagnostic model using these 7 hub genes may be useful in guiding the diagnosis of AD in clinical practice.

We used unsupervised clustering methods based on the expression of 7 features of double disulfidptosis-regulating factors to estimate molecular patterns in AD brain tissue and ultimately identified two distinct molecular subtypes. Immune infiltration analysis showed that Cluster2 had higher immune scores and relatively higher levels of immune infiltration. Moreover, most DRGs were expressed at higher levels in Cluster2. The KEGG analysis results highlight the close relationship between the

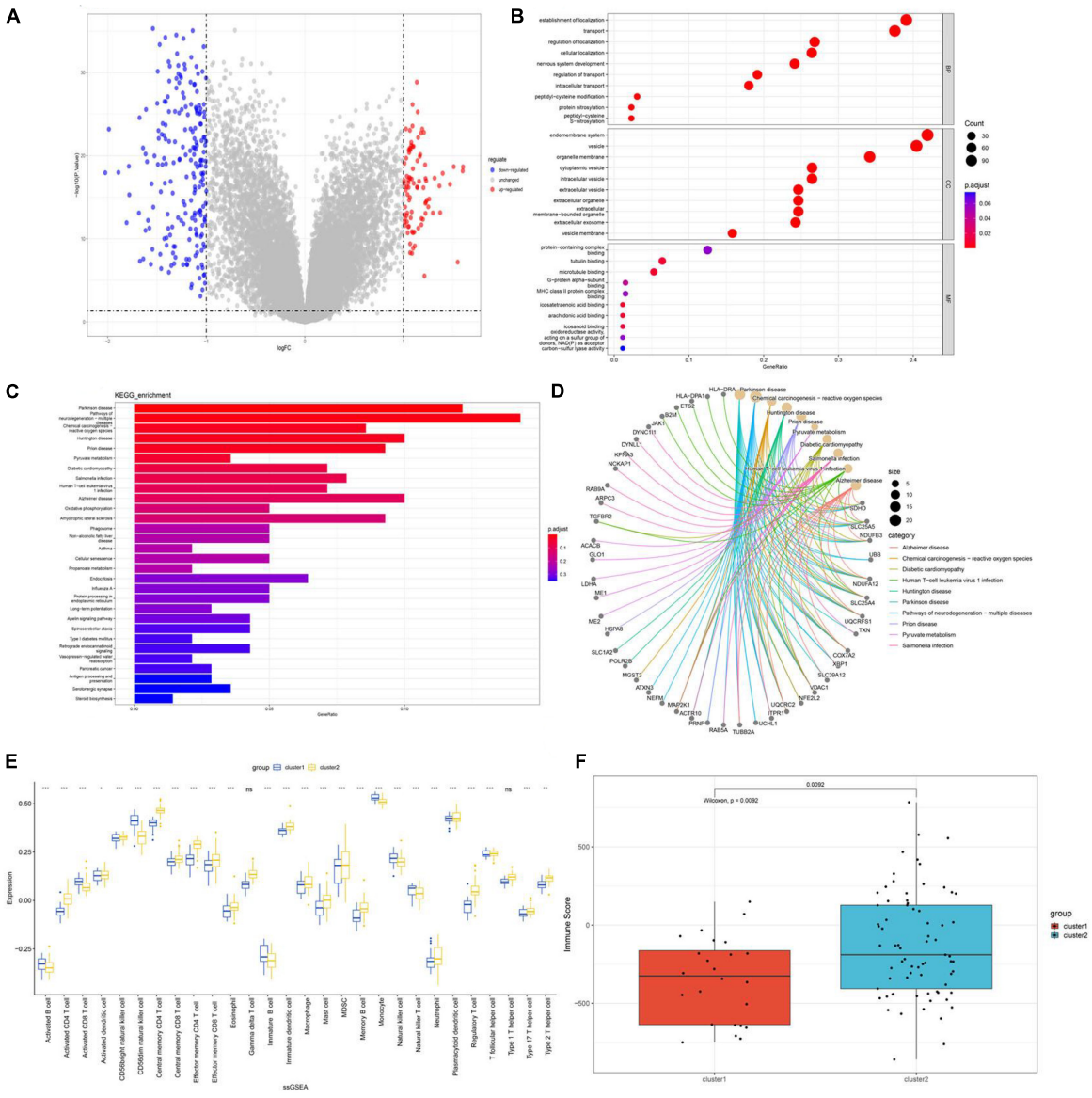

FIGURE 10
Functional enrichment analysis and infiltration of immune cells in disulfidptosis subtypes. **(A)** The volcano plot of DEGs. **(B)** GO analysis shows enriched terms **(C,D)** Enriched pathways based on KEGG analysis. **(E)** Correlation matrix of all 28 immune cell subtype compositions. **(F)** Boxplots depicting the immune score differences between the two disulfidptosis subtypes. *$p < 0.05$; **$p < 0.01$; ***$p < 0.001$.

DEGs of Cluster2 and Cluster1 and various processes, including metabolism, signal transduction, diseases, and neurodegeneration. The activation of the PI3K/Akt pathway has been shown to have beneficial effects on neurons and neural stem cells (Kitagishi et al., 2014; Razani et al., 2021), while dysfunction of the TGF-β/TβRII signaling axis in the AD brain may accelerate Aβ deposition and neurodegeneration (Das and Golde, 2006; Dammer et al., 2022). The GSVA analysis indicated an upregulation of Cluster2 in TGF BETA SIGNALING and PI3K AKT MTOR SIGNALING.

This study has some limitations that need to be emphasized. Firstly, as our current research is based on comprehensive bioinformatics analysis and RT-PCR validation. It lacks more experimental and clinical trial validation, our results need further confirmation. Additionally, it should be noted that the sample size of this study is relatively small, and larger studies are needed to verify the reliability of the results. Furthermore, this study only involved one group of AD patients and controls, without considering the potential effects of different factors such as age, sex, and race on the results. Moreover, more detailed clinical information is needed to verify the predictive performance of the model, and more external validation cohorts are needed to ensure the stability of the diagnostic model. Finally, more AD samples are needed to clarify the accuracy of the clustering related to disulfidptosis.

Conclusion

In summary, our study has revealed the correlation between the genes related to disulfidptosis and infiltrating immune cells,

and identified 7 feature genes associated with disulfidptosis, which accurately assess the AD subtypes and diagnose AD patients. Moreover, we have elucidated significant immune heterogeneity among different disulfidptosis subtypes of AD patients. Our study has, for the first time, revealed the involvement of disulfidptosis in the development of AD, providing new insights into the potential pathogenic processes and therapeutic strategies for AD.

Data availability statement

Publicly available datasets were analyzed in this study. This data can be found here: https://www.ncbi.nlm.nih.gov/geo/query/acc.cgi?acc=GSE33000, https://www.ncbi.nlm.nih.gov/geo/query/acc.cgi?acc=GSE181279. The accession numbers: GSE132903, GSE48350, GSE5821, GSE33000, and GSE181279.

Ethics statement

The studies involving human participants were reviewed and approved by the Medical Ethics Committee is affiliated to The First Affiliated Hospital of Anhui University of Chinese Medicine. The patients/participants provided their written informed consent to participate in this study.

Author contributions

SM designed the study, collected the original data, finished the analysis, and drafted the initial manuscript. DW helped revise the manuscript. DX provided the funding and supervised the study. All authors read and approved the final manuscript.

Funding

This research was supported by the National Natural Science Foundation of China (No. 8187140739).

Acknowledgments

We thank all researchers and participants of the GEO database for sharing these data.

Conflict of interest

The authors declare that the research was conducted in the absence of any commercial or financial relationships that could be construed as a potential conflict of interest.

Publisher's note

Supplementary material

The Supplementary Material for this article can be found online at: https://www.frontiersin.org/articles/10.3389/fnagi.2023.1236490/full#supplementary-material

References

Acebedo, A. R., Suzuki, K., Hino, S., Alcantara, M. C., Sato, Y., Haga, H., et al. (2019). Mesenchymal actomyosin contractility is required for androgen-driven urethral masculinization in mice. *Commun. Biol.* 2:95. doi: 10.1038/s42003-019-0336-3

Briggs, M. W., and Sacks, D. P. (2003). IQGAP proteins are integral components of cytoskeletal regulation. *EMBO Rep.* 4, 571–574. doi: 10.1038/sj.embor.embor867

Byun, M. S., Kim, S. E., Park, J., Yi, D., Choe, Y. M., Sohn, B. K., et al. (2015). Heterogeneity of regional brain atrophy patterns associated with distinct progression rates in Alzheimer's disease, Jo DG, editor. *PLoS One* 10:e0142756. doi: 10.1371/journal.pone.0142756

Cano, A., Turowski, P., Ettcheto, M., Duskey, J. T., Tosi, G., Sánchez-López, E., et al. (2021). Nanomedicine-based technologies and novel biomarkers for the diagnosis and treatment of Alzheimer's disease: From current to future challenges. *J. Nanobiotechnol.* 19:122. doi: 10.1186/s12951-021-00864-x

Chen, H., Yang, W., and Ji, Z. (2023a). Machine learning-based identification of tumor-infiltrating immune cell-associated model with appealing implications in improving prognosis and immunotherapy response in bladder cancer patients. *Front. Immunol.* 14:1171420. doi: 10.3389/fimmu.2023.1171420

Chen, H., Yang, W., Li, Y., Ma, L., and Ji, Z. (2023b). Leveraging a disulfidptosis-based signature to improve the survival and drug sensitivity of bladder cancer patients. *Front. Immunol.* 14:1198878. doi: 10.3389/fimmu.2023.1198878

Clarke, J. R., Ribeiro, F. C., Frozza, R. L., De Felice, F. G., and Lourenco, M. V. (2018). Metabolic Dysfunction in Alzheimer's disease: From basic neurobiology to clinical approaches. *JAD* 64, S405–S426. doi: 10.3233/JAD-179911

Dai, L., and Shen, Y. (2021). Insights into T-cell dysfunction in Alzheimer's disease. *Aging Cell* 20, e13511. doi: 10.1111/acel.13511

Dammer, E. B., Ping, L., Duong, D. M., Modeste, E. S., Seyfried, N. T., Lah, J. J., et al. (2022). Multi-platform proteomic analysis of Alzheimer's disease cerebrospinal fluid and plasma reveals network biomarkers associated with proteostasis and the matrisome. *Alz. Res. Therapy* 14:174. doi: 10.1186/s13195-022-01113-5

Das, P., and Golde, T. (2006). Dysfunction of TGF-β signaling in Alzheimer's disease. *J. Clin. Invest.* 116, 2855–2857. doi: 10.1172/JCI30284

Davis, S., and Meltzer, P. S. (2007). GEOquery: A bridge between the Gene Expression Omnibus (GEO) and BioConductor. *Bioinformatics* 23, 1846–1847. doi: 10.1093/bioinformatics/btm254

de Ribeiro, E. A., Pinotsis, N., Ghisleni, A., Salmazo, A., Konarev, P., and Kostan, J. (2014). The structure and regulation of human muscle α-actinin. *Cell* 159, 1447–1460. doi: 10.1016/j.cell.2014.10.056

Deng, L., He, S., Guo, N., Tian, W., Zhang, W., and Luo, L. (2023). Molecular mechanisms of ferroptosis and relevance to inflammation. *Inflamm. Res.* 72, 281–299. doi: 10.1007/s00011-022-01672-1

Fukata, M., Kuroda, S., Fujii, K., Nakamura, T., Shoji, I., Matsuura, Y., et al. (1997). Regulation of cross-linking of actin filament by IQGAP1, a target for Cdc42. *J. Biol. Chem.* 272, 29579–29583. doi: 10.1074/jbc.272.47.29579

Gao, C., Frausto, S. F., Guedea, A., Tronson, N., Jovasevic, V., Leaderbrand, K., et al. (2011). IQGAP1 regulates NR2A signaling, spine density, and cognitive processes. *J. Neurosci.* 31, 8533–8542. doi: 10.1523/JNEUROSCI.1300-11.2011

Gu, Y., Tang, S., Wang, Z., Cai, L., Lian, H., Shen, Y., et al. (2021). A pan-cancer analysis of the prognostic and immunological role of β-actin (ACTB) in human cancers. *Bioengineered* 12, 6166–6185. doi: 10.1080/21655979.2021.1973220

Hänzelmann, S., Castelo, R., and Guinney, J. (2013). GSVA: Gene set variation analysis for microarray and RNA-Seq data. *BMC Bioinform.* 14:7. doi: 10.1186/1471-2105-14-7

Harcha, P. A., Garcés, P., Arredondo, C., Fernández, G., Sáez, J. C., and van Zundert, B. (2021). Mast cell and astrocyte hemichannels and their role in Alzheimer's disease, ALS, and harmful stress conditions. *IJMS* 22:1924. doi: 10.3390/ijms22041924

Hsu, K. S., and Kao, H. Y. (2013). Alpha-actinin 4 and tumorigenesis of breast cancer. *Vit. Hormones* 93, 323–351. doi: 10.1016/B978-0-12-416673-8.00005-8

Hwang, J. S., Shim, J. S., Song, M. Y., Yim, S. V., Lee, S. E., and Park, K. S. (2016). Proteomic analysis reveals that the protective effects of ginsenoside Rb1 are associated with the actin cytoskeleton in β-amyloid-treated neuronal cells. *J. Ginseng Res.* 40, 278–284. doi: /10.1016/j.jgr.2015.09.004

Inoue, N., Matsukado, Y., Goto, S., and Miyamoto, E. (1988). Localization of glycogen synthase in brain. *J. Neurochem.* 50, 400–405. doi: 10.1111/j.1471-4159.1988.tb02926.x

Jorgensen, I., Zhang, Y., Krantz, B., and Miao, E. A. (2016). Pyroptosis triggers pore-induced intracellular traps (PITs) that capture bacteria and lead to their clearance by efferocytosis. *J. Exp. Med.* 213, 2113–2128. doi: 10.1084/jem.20151613

Khotin, M., Turoverova, L., Aksenova, V., Barlev, N., Borutinskaite, V., Vener, A., et al. (2010). Proteomic analysis of ACTN4-interacting proteins reveals it's a putative involvement in mRNA metabolism. *Biochem. Biophys. Res. Commun.* 397, 192–196. doi: 10.1016/j.bbrc.2010.05.079

Kitagishi, Y., Nakanishi, A., Ogura, Y., and Matsuda, S. (2014). Dietary regulation of PI3K/AKT/GSK-3β pathway in Alzheimer's disease. *Alzheimers Res. Ther.* 6:35. doi: 10.1186/alzrt265

Landis, D. M., and Reese, T. S. (1983). Cytoplasmic organization in cerebellar dendritic spines. *J. Cell Biol.* 97, 1169–1178. doi: 10.1083/jcb.97.4.1169

Lee, J. K., and Kim, N. J. (2017). Recent advances in the inhibition of p38 MAPK as a potential strategy for the treatment of Alzheimer's disease. *Molecules* 22:1287. doi: 10.3390/molecules22081287

Liu, X., Nie, L., Zhang, Y., Yan, Y., Wang, C., Colic, M., et al. (2023). Actin cytoskeleton vulnerability to disulfide stress mediates disulfidptosis. *Nat. Cell Biol.* 25, 404–414. doi: 10.1038/s41556-023-01091-2

Liu, Z., Liu, L., Weng, S., Guo, C., Dang, Q., Xu, H., et al. (2022). Machine learning-based integration develops an immune-derived lncRNA signature for improving outcomes in colorectal cancer. *Nat. Commun.* 13:816. doi: 10.1038/s41467-022-28421-6

Machesky, L. M. (2023). Deadly actin collapse by disulfidptosis. *Nat. Cell Biol.* 25, 375–376. doi: 10.1038/s41556-023-01100-4

McCorvie, T. J., Loria, P. M., Tu, M., Han, S., Shrestha, L., Froese, D. S., et al. (2022). Molecular basis for the regulation of human glycogen synthase by phosphorylation and glucose-6-phosphate. *Nat. Struct. Mol. Biol.* 29, 628–638. doi: 10.1038/s41594-022-00799-3

McKhann, G. M., Knopman, D. S., Chertkow, H., Hyman, B. T., Jack, C. R., Kawas, C. H., et al. (2011). The diagnosis of dementia due to Alzheimer's disease: Recommendations from the National Institute on Aging-Alzheimer's Association workgroups on diagnostic guidelines for Alzheimer's disease. *Alzheimers Dement.* 7, 263–269. doi: 10.1016/j.jalz.2011.03.005

Mietelska-Porowska, A., and Wojda, U. T. (2017). Lymphocytes and inflammatory mediators in the interplay between brain and blood in Alzheimer's disease: Potential pools of new biomarkers. *J. Immunol. Res.* 2017, 1–17. doi: 10.1155/2017/4626540

Noble, W. S. (2006). What is a support vector machine? *Nat. Biotechnol.* 24, 1565–1567. doi: 10.1038/nbt1206-1565

Pecci, A., Ma, X., Savoia, A., and Adelstein, R. S. (2018). MYH9: Structure, functions and role of non-muscle myosin IIA in human disease. *Gene* 664, 152–167. doi: 10.1016/j.gene.2018.04.048

Pelucchi, S., Stringhi, R., and Marcello, E. (2020). Dendritic spines in Alzheimer's disease: How the actin cytoskeleton contributes to synaptic failure. *IJMS* 21:908. doi: 10.3390/ijms21030908

Rajab, M. D., Jammeh, E., Taketa, T., Brayne, C., Matthews, F. E., Su, L., et al. (2023). Assessment of Alzheimer-related pathologies of dementia using machine learning feature selection. *Alz. Res. Therapy* 15:47. doi: 10.1186/s13195-023-01195-9

Razani, E., Pourbagheri-Sigaroodi, A., Safaroghli-Azar, A., Zoghi, A., Shanaki-Bavarsad, M., and Bashash, D. (2021). The PI3K/Akt signaling axis in Alzheimer's disease: A valuable target to stimulate or suppress? *Cell Stress Chaper.* 26, 871–887. doi: 10.1007/s12192-021-01231-3

Rigatti, S. J. (2017). Random forest. *J. Insur. Med.* 47, 31–39. doi: 10.17849/insm-47-01-31-39.1

Ritchie, M. E., Phipson, B., Wu, D., Hu, Y., Law, C., Shi, W., et al. (2015). limma powers differential expression analyses for RNA-sequencing and microarray studies. *Nucleic Acids Res.* 43:e47. doi: 10.1093/nar/gkv007

Salminen, A., Kaarniranta, K., and Kauppinen, A. (2018). The potential importance of myeloid-derived suppressor cells (MDSCs) in the pathogenesis of Alzheimer's disease. *Cell Mol. Life Sci.* 75, 3099–3120. doi: 10.1007/s00018-018-2844-6

Scheltens, P., De Strooper, B., Kivipelto, M., Holstege, H., Chételat, G., Teunissen, C. E., et al. (2021). Alzheimer's disease. *Lancet.* 397, 1577–1590. doi: 10.1016/S0140-6736(20)32205-4

Selkoe, D. (2002). Alzheimer's disease is a synaptic failure. *Science* 298, 789–791. doi: 10.1126/science.1074069

Tibshirani, R. (1996). Regression shrinkage and selection via the lasso. *J. R. Stat. Soc. Ser. B Methodol.* 58, 267–288. doi: 10.1111/j.2517-6161.1996.tb02080.x

Vierthaler, M., Sun, Q., Wang, Y., Steinfass, T., Poelchen, J., Hielscher, T., et al. (2022). ADCK2 knockdown affects the migration of melanoma cells via MYL6. *Cancers* 14:1071. doi: 10.3390/cancers14041071

White, C. D., Erdemir, H. S., and Sacks, D. B. (2012). IQGAP1 and its binding proteins control diverse biological functions. *Cell. Signall.* 24, 826–834. doi: 10.1016/j.cellsig.2011.12.005

Yu, G., Wang, L., Han, Y., and He, Q. Y. (2012). clusterProfiler: An R package for comparing biological themes among gene clusters. *OMICS* 16, 284–287. doi: 10.1089/omi.2011.0118

Yu, W., and Lu, B. (2012). Synapses and dendritic spines as pathogenic targets in Alzheimer's disease. *Neural Plastic.* 2012, 1–8. doi: 10.1155/2012/247150

Yuan, K., Zhao, S., Ye, B., Wang, Q., Liu, Y., Zhang, P., et al. (2023). A novel T-cell exhaustion-related feature can accurately predict the prognosis of OC patients. *Front. Pharmacol.* 14:1192777. doi: 10.3389/fphar.2023.1192777

Zhang, G., Zhang, Y., Shen, Y., Wang, Y., Zhao, M., and Sun, L. (2021). The potential role of ferroptosis in Alzheimer's disease. *JAD* 80, 907–925. doi: 10.3233/JAD-201369

Zhang, H., Zhang, L., Zhou, D., Li, H., and Xu, Y. (2021). ErbB4 mediates amyloid β—induced neurotoxicity through JNK/tau pathway activation: Implications for Alzheimer's disease. *J. Comp. Neurol.* 529, 3497–3512. doi: 10.1002/cne.25207

Zhang, H. J., Chang, W. J., Jia, C. Y., Qiao, L., Zhou, J., Chen, Q., et al. (2020). Destrin contributes to lung adenocarcinoma progression by activating Wnt/β-Catenin signaling pathway. *Mol. Cancer Res.* 18, 1789–1802. doi: 10.1158/1541-7786.MCR-20-0187

Zhao, S., Wang, L., Ding, W., Ye, B., Cheng, C., Shao, J., et al. (2023a). Crosstalk of disulfidptosis-related subtypes, establishment of a prognostic signature and immune infiltration characteristics in bladder cancer based on a machine learning survival framework. *Front. Endocrinol.* 14:1180404. doi: 10.3389/fendo.2023.1180404

Zhao, S., Ye, B., Chi, H., Cheng, C., and Liu, J. (2023b). Identification of peripheral blood immune infiltration signatures and construction of monocyte-associated signatures in ovarian cancer and Alzheimer's disease using single-cell sequencing. *Heliyon* 9:e17454. doi: 10.1016/j.heliyon.2023.e17454

frontiers | Frontiers in Neuroscience

TYPE Original Research
PUBLISHED 10 August 2023
DOI 10.3389/fnins.2023.1237284

OPEN ACCESS

EDITED BY
Woon-Man Kung,
Chinese Culture University, Taiwan

REVIEWED BY
Victor Montal,
Sant Pau Institute for Biomedical Research, Spain
Jacopo Sapienza,
San Raffaele Scientific Institute (IRCCS), Italy
Lisa C. Bratzke,
University of Wisconsin-Madison, United States

*CORRESPONDENCE
Jessica M. Collins
jessica.collins@utas.edu.au

RECEIVED 09 June 2023
ACCEPTED 20 July 2023
PUBLISHED 10 August 2023

CITATION
Collins JM, Bindoff AD, Roccati E, Alty JE, Vickers JC and King AE (2023) Does serum neurofilament light help predict accelerated cognitive ageing in unimpaired older adults? *Front. Neurosci.* 17:1237284. doi: 10.3389/fnins.2023.1237284

Does serum neurofilament light help predict accelerated cognitive ageing in unimpaired older adults?

Jessica M. Collins[1]*, Aidan D. Bindoff[1], Eddy Roccati[1], Jane E. Alty[1,2,3], James C. Vickers[1] and Anna E. King[1]

[1]Wicking Dementia Research and Education Centre, University of Tasmania, Hobart, TAS, Australia, [2]School of Medicine, University of Tasmania, Hobart, TAS, Australia, [3]Royal Hobart Hospital, Hobart, TAS, Australia

Introduction: Neurofilament light (NfL) is a blood biomarker of neurodegeneration. While serum NfL levels have been demonstrated to increase with normal ageing, the relationship between serum NfL levels and normal age-related changes in cognitive functions is less well understood.

Methods: The current study investigated whether cross-sectional serum NfL levels measured by single molecule array technology (Simoa®) mediated the effect of age on cognition, measured by a battery of neuropsychological tests administered biannually for 8 years, in a cohort of 174 unimpaired older adults (≥50 years) from the Tasmanian Healthy Brain Project. Mediation analysis was conducted using latent variables representing cognitive test performance on three cognitive domains - episodic memory, executive function, and language (vocabulary, comprehension, naming). Cognitive test scores for the three domains were estimated for each participant, coincident with blood collection in 2018 using linear Bayesian hierarchical models.

Results: Higher serum NfL levels were significantly positively associated with age ($p < 0.001$ for all domains). Cognitive test scores were significantly negatively associated with age across the domains of executive function ($p < 0.001$), episodic memory ($p < 0.001$) and language ($p < 0.05$). However, serum NfL levels did not significantly mediate the relationship between age and cognitive test scores across any of the domains.

Discussion: This study adds to the literature on the relationship between serum NfL levels and cognition in unimpaired older adults and suggests that serum NfL is not a pre-clinical biomarker of ensuing cognitive decline in unimpaired older adults.

KEYWORDS

biomarkers, neurofilament light, cognitive ageing, cognition, mediation analysis

1. Introduction

Cognitive decline with ageing is common; however, the onset, extent and rate of cognitive decline is highly variable between individuals (Rowe and Kahn, 1987; Nyberg et al., 2020). Age-related cognitive decline can range from minimal decline, which can be viewed as successful ageing through to levels of decline that meet criteria for mild cognitive impairment (MCI) and dementia (Rowe and Kahn, 1987; Nyberg et al., 2020). Cognitive impairment below the threshold of MCI and dementia is associated with a reduced quality of life (Roehr et al., 2017), and for some people may be a pre-clinical phase, on the spectrum of accelerated cognitive decline, continuous with dementia (Jessen et al., 2014). Being able to sensitively detect who has

accelerated cognitive ageing from normal cognitive ageing, will enable the early identification of people at risk of impairment, hence providing an opportunity for targeted dementia prevention.

Cognitive decline is due to age- and pathology-related neurodegenerative changes in the brain, which precede clinical cognitive changes by several years (Fleisher et al., 2015; Quiroz et al., 2018). Several blood-based biomarkers of these neurodegenerative changes in the brain have now been identified and are the subject of ongoing investigation (Alcolea et al., 2023). One such biomarker is the neuroaxonal protein neurofilament light (NfL), which is particularly abundant in a subset of neurons, typically projecting neurons, with wide calibre, myelinated axons (Kirkcaldie and Dwyer, 2017).

Increased serum and plasma levels of the NfL protein have been demonstrated in several neurodegenerative diseases including Alzheimer's disease (AD) (Lewczuk et al., 2018; Forgrave et al., 2019; Moscoso et al., 2021), frontotemporal dementia (Forgrave et al., 2019), motor neuron disease (Forgrave et al., 2019) and traumatic brain injury (Shahim et al., 2018). Thus, NfL does not appear to be a specific biomarker, for a particular neurological disorder, but is a general marker of neurodegenerative processes, particularly if they involve axonal pathology. Whilst NfL concentrations are slightly higher when measured in serum samples compared to plasma samples, the difference is minimal and NfL levels between the two sample types are highly correlated (Barro et al., 2020). Therefore, although the sample type may be important in the determination of reference ranges and diagnostic cut-off values, the associations between NfL levels, and measures of cognition and brain atrophy are expected to be concordant between serum and plasma samples.

NfL levels in serum and plasma have been demonstrated to significantly increase with aging in a multitude of studies (Disanto et al., 2017; Khalil et al., 2020; Quiroz et al., 2020; Kang et al., 2021). The biological source of the age-related increase in blood NfL levels is unclear but may reflect age-related neurodegeneration in the brain (Alirezaei et al., 2020; Khalil et al., 2020; Nyberg et al., 2020; Kang et al., 2021). Longitudinal analyses have revealed marked variability in age-related NfL increases in the blood (Khalil et al., 2020; Nyberg et al., 2020) and a study in neurologically inconspicuous community-dwelling adults has shown that serum NfL levels become more variable between individuals with increasing age (Khalil et al., 2020). In the same study, baseline serum NfL levels were shown to be a predictor of future brain volume loss and NfL levels increased in relation to brain volume loss (Khalil et al., 2020). Additionally, a study by Beydoun et al. (2023) demonstrated that plasma NfL has potential as a prognostic marker of white matter integrity in a study of middle-aged urban adults (mean age 47.9 years). Therefore, the variability in age-related increases in serum NfL levels in cognitively normal individuals, may be explained by pre-clinical neurodegenerative changes in the brain, beyond that of normal ageing, but not to the extent of clinical impairment. In support of this hypothesis, blood NfL levels are associated with risk of all-cause (de Wolf et al., 2020; Verberk et al., 2021) and AD dementia (de Wolf et al., 2020; Stocker et al., 2023). Furthermore, plasma NfL levels have been demonstrated to be a predictor of brain amyloid beta (Aβ) positivity as measured by Florbetapir-PET in participants with normal cognition suggesting it is a sensitive biomarker of the preclinical AD phase (Huang et al., 2022), however the relationship between Aβ burden and AD risk remains controversial.

Whilst studies have shown a relationship between serum and plasma NfL levels and cognition in people with mild cognitive impairment (MCI) (Lewczuk et al., 2018; Mattsson et al., 2019; Osborn et al., 2019) and AD (Lewczuk et al., 2018; Mattsson et al., 2019; Quiroz et al., 2020), the relationship between serum NfL levels and pre-clinical changes in cognitive status in unimpaired adults is less understood. Most of the literature on the relationship between NfL levels in the blood and cognition has been analysed in three main ways: first, the cross-sectional relationship between NfL and cognition at a single timepoint (Mielke et al., 2019; Osborn et al., 2019; Huang et al., 2022); second, the relationship between baseline NfL levels and future cognitive decline (Khalil et al., 2020; Verberk et al., 2021; Chatterjee et al., 2022); third, the longitudinal relationship between the rate of NfL change and cognitive decline trajectories (Mattsson et al., 2019; Mielke et al., 2019; Rauchmann et al., 2021). Furthermore, studies differ on the tools used to measure cognition, ranging from single instrument measures such as Mini Mental State Exam (MMSE) (Khalil et al., 2020; Chatterjee et al., 2022) to neuropsychological test batteries (Osborn et al., 2019; Rauchmann et al., 2021; Verberk et al., 2021).

When looking at the cross-sectional relationship between blood NfL and cognition, a study by Osbourn et al. found that higher plasma NfL was not associated with performance across multiple cognitive domains in unimpaired participants between the ages of 60 and 92 years (Osborn et al., 2019). In contrast to this, a more recent cross-sectional analysis in participants over 50 years of age, with normal cognition or objectively defined subtle cognitive impairment (Obj-SCD), showed that higher NfL levels were associated with lower global cognition, verbal episodic memory, visual episodic memory and executive function (Huang et al., 2022). However, when looking at subgroup analyses based on cognition (normal and Obj-SCD) and brain amyloid beta (Aβ+ and Aβ−) status there were differing results; NfL had a negative correlation with verbal episodic memory in the Aβ− normal cognition and Aβ− Obj-SCD groups, and a negative association with MMSE in the Aβ+ normal cognition group (Huang et al., 2022). A study of participants without dementia, but including people with both normal cognition and MCI, and a mean age of 76 years of age has also found no cross-sectional relationship between plasma NfL levels and global cognition or any cognitive measures using a 9-test neuropsychological battery (Mielke et al., 2019). This demonstrates that the association between blood NfL levels and cognition, in cognitively unimpaired older adults is complex and may vary based on both brain Aβ status and whether the cohort of cognitively normal participants includes those with subjective cognitive complaints or MCI.

Analysing the association between baseline blood NfL measures and cognition, a study by Khalil et al. (2020) demonstrated that baseline serum NfL levels correlated with future changes in MMSE scores over a mean follow-up time of 5.9 years, in a population of healthy adults aged between 38 and 85 years of age, but the annualised change in serum NfL was not related to the annualised change in MMSE scores. This is supported by a more recent study showing that baseline plasma NfL levels were significantly associated with prospective cognitive decline (measured by MMSE and the Preclinical Alzheimer's Cognitive Composite) in cognitively unimpaired participants with a mean age 74.2 (SD 7.2) years (Chatterjee et al., 2022). Conversely, Verberk and colleagues have shown that higher baseline serum NfL levels were not associated with the rate of decline across the cognitive domains of memory, attention, executive function, language and global cognition in cognitively normal participants with a mean baseline age of 61 years (Verberk et al., 2021). However, it is important to note that this study enrolled participants from a memory

clinic who despite not meeting criteria for MCI or dementia, did present at the memory clinic due to cognitive complaints (Verberk et al., 2021). Therefore, there is conflicting evidence for the relationship between higher baseline NfL levels in the blood as a predictor of future cognitive decline, and this may be a result of the cognitive measures used and/or the cohort studied.

When looking at the longitudinal relationship between plasma NfL levels and cognition, a study of participants without dementia but including those with both normal cognition and MCI, and a mean age of 76 years found that change in plasma NfL levels was associated with change in attention and global cognitive scores over a 30-month follow-up period (Mielke et al., 2019). Similarly, a study of participants with normal cognition through to dementia aged between 55 and 90 years of age demonstrated that plasma NfL rate of change was predictive of a memory composite score over a 4 year follow-up (Rauchmann et al., 2021). In contrast, in a cohort including cognitively unimpaired, MCI and AD dementia participants with a mean age of 72.9 (SD 7.1) years, faster increasing plasma NfL levels correlated with a faster decline in global cognition in participants with MCI and dementia, but not in cognitively unimpaired participants (Mattsson et al., 2019). When taken together the literature demonstrates that the relationship between blood NfL levels and cognitive functions is complex in cognitively normal older adults and requires further elucidation before NfL's clinical utility as a prognostic biomarker of cognitive decline can be determined.

The aim of the current study was to estimate the proportion of variance in cognitive functions mediated by pre-clinical neurodegeneration (measured by serum NfL), in order to gain a better understanding of the utility of serum NfL as a biomarker of pre-clinical cognitive decline. We have used longitudinal data from an extensive battery of cognitive tests in a cohort of cognitively unimpaired older adults in the Tasmanian Healthy Brain Project (THBP) to estimate cognitive functions in the same year (2018) as (cross-sectional) blood collection, on three cognitive domains (executive function, episodic memory, and language).

2. Methods

2.1. Participants

Participants were from the THBP, a longitudinal intervention study of older, community-dwelling Tasmanians which commenced in 2010 (Summers et al., 2013). Detailed information on the establishment of THBP and recruitment of its participants has been published previously (Summers et al., 2013). Briefly, adults aged between 50 and 79 years of age, without a history of prior conditions known to be associated with impaired neurological function, or neurological/psychiatric disorders were eligible. At recruitment, participants opted (non-random assignment) to undertake university-level education (completed at least 12.5% of 1 year full-time equivalent university study, later-life education intervention group) or no further education (comparison group). At baseline, participants also completed a medical health status questionnaire and data were collected on demographics using a specifically designed questionnaire including age (years), gender (options either "male" or "female"), education (in years) and occupational history (Summers et al., 2013). Education (in years) was calculated as the sum of the highest school leaving year and the number of years of further education (both determined using the baseline medical questionnaires) and the years of full-time-equivalent university study as part of the THBP (determined using academic transcripts).

All participants underwent annual cognitive assessments for the first 4 years of the study and then biennial thereafter. All THBP participants were invited to take part in the current study, with 174 (39 comparison group, 22%; 135 later-life education intervention 78%) of the remaining 410 participants at the time of collection in 2018 consenting to provide a blood sample. This project was approved by the University of Tasmania Health and Medical Research Committee (H0018265 and H0016317).

2.2. Cognitive assessments

Participants had comprehensive cognitive assessments between 2011 and 2022, as previously detailed (Summers et al., 2013). Briefly, a neuropsychological battery of tests was performed at each assessment, evaluating the cognitive domains of episodic memory [Paired Associates Learning Test - Cambridge Neuropsychological Test Automated Battery (CANTAB), Rey Auditory Verbal Learning Test, Rey Complex Figure Test, Wechsler Memory Scale (WMS)-III Logical Memory Test I & II], language [Wechsler Adult Intelligence Scale (WAIS)-III Vocabulary, WAIS-III Comprehension, Boston Naming Test] and executive function [Stroop Test C, Trail Making Test Part B, WAIS-III Digit Span Test, Controlled Oral Word Association Test].

Blood sample collection from consenting participants in 2018, did not necessarily coincide with a cognitive assessment, however all participants who provided blood had cognitive assessments before and after blood collection. We chose to single-impute cognitive tests scores for the year in which blood collection occurred (2018) by modelling individual trajectories on each test between 2015 and 2022 in order to make economical use of the available data using Bayesian hierarchical models (the decision process and methods are detailed in Supplementary material).

2.3. Blood collection and processing

The collection, processing and storage of blood was performed in 2018 according to the published guidelines for Alzheimer's disease research (O'Bryant et al., 2015). Non-fasting blood samples were collected under aseptic conditions by venepuncture using a 21-gauge (G) butterfly needle into BD Vacutainer™ SST™ II Advance tubes (Cat no. 367958). To prepare serum, blood was clotted at room temperature in a vertical position for 30 min and then centrifuged at 1,500 g for 10 min at 4°C. Each serum sample was aliquoted into 10 polypropylene, screw-top cryostorage tubes to prevent multiple freeze–thaw cycles and stored at −80°C. This process was completed in under 2 h from venepuncture.

2.4. Genotyping

APOE genotypes were available for the THBP cohort from a previous study (Ward et al., 2014). DNA was collected from THBP

participants with the Oragene DNA self-collection kit (Genotek, ON, Canada, 2012). A one-step amplified refractory mutation system PCR, followed by gel electrophoresis was used to determine *APOE* genotype. Using methods previously described (Donohoe et al., 1999), rs429358 and rs7412 were determined with PCR amplifications undertaken using ~50 ng of genomic DNA and PCR amplicons resolved on a 2% agarose gel. Samples were run in duplicate to ensure accuracy of genotyping, and genotyping repeated if results were unclear.

2.5. Serum NfL measurements

Serum NfL levels were measured using the NF-LIGHT™ (SR-X VERSION) single molecule array assay (SIMOA®) from Quanterix™ (cat number 103400). Serum samples were measured in duplicate using a 2-step assay on the SIMOA® SR-X™ platform (Quanterix™), according to manufacturer's protocols. Serum samples were diluted 4 times in sample diluent by adding 25 µL of serum to 75 µL of sample diluent. High- and low- quality control samples provided by Quanterix™ were run on each plate. If the intra-assay coefficient of variation between two duplicates was more than 20%, the sample was measured again. The average intra-assay coefficient of variation for included samples was 5.77%.

2.6. Statistics

Mediation analysis was conducted using latent variables representing cognitive test performance on three cognitive domains - episodic memory, executive function, and language. Cognitive test scores were estimated for each participant coincident with blood collection in 2018 using the hierarchical regression models, which considered age and length of time in the study in 2018. These scores were then standardized by converting to z-scores and reversing two items so that all items were positively correlated. We determined which cognitive tests to include on each cognitive domain using published literature (Smith et al., 2013; Faria et al., 2015) and earlier work using baseline results from the THBP (Ward et al., 2017), then proceeded using an iterative confirmatory factor analysis (CFA) approach to target a comparative fit index (CFI) > 0.95, and root mean squared error of approximation (RMSEA) < 0.05. If a model did not satisfy these criteria, we inspected the correlation matrix to identify items (cognitive tests) which were considered either redundant (highly correlated with another item) or poorly correlated with other items. The cognitive tests included for each cognitive domain, their loadings and 95% CIs are included in Table 1.

The $X \rightarrow M \rightarrow Y_d \leftarrow X$ paths were estimated using multiple linear regression, where X was participant age (mean-centered and standardized to unit SD), M was serum NfL concentration ($\log_e$-transformed due to right-skew), Y_d were the latent variable scores on cognitive domain *d* and years of education was included as a covariate (Figure 1). This model proposes that age causes both cognitive decline and neurodegeneration (measured using the proxy of NfL in serum), and that neurodegeneration is a mediator of age-related cognitive decline, evident in serum NfL concentrations.

We used the product of coefficients method to estimate the indirect a*b path ($X \rightarrow M \rightarrow Y_d$), direct path c' ($Y_d \leftarrow X$) and proportion mediated (a*b/(a*b + c'); see Figure 1). Standard errors were computed using bootstrapping (1×10^3 iterations). We considered a path coefficient to be significant at $\alpha = 0.05$. To avoid complexity we fitted a SEM for each cognitive domain rather than estimating all latent variables simultaneously. SEM was conducted using the 'lavaan' R package (Rosseel, 2012).

3. Results

Blood samples from $N = 174$ participants were analysed. Mean serum NfL concentration was 14.3 pg/mL (SD = 6.6). Some participants had insufficient cognitive assessment data to estimate cognitive domain scores, leaving $n = 143$ participants who undertook 528 cognitive assessments between 2015 and 2022. Mean age of participants was 65.5 years (SD = 6.8), 71.3% were female. Mean years of education was 17.1 years (SD = 3.2). The results of the CFA iterative approach for the cognitive domain latent variables, executive function, episodic memory, and language are included in Table 1 (further details on the CFA are included in Supplementary material).

3.1. Mediation

The standardised regression coefficient β = −0.728 [95% CI −0.848, −0.607] for the effect of age on executive function, adjusted for education and serum NfL was significant ($p < 0.001$; Figure 2A). The effect of age on serum NfL had the standardised regression coefficient β = 0.531 [95% CI 0.432, 0.630] which was also significant ($p < 0.001$), however the standardized regression coefficient β = 0.118 [95% CI −0.54, 0.289] for the effect of serum NfL on executive function was not ($p = 0.179$; Figure 2A). The indirect effect standardised regression coefficient β = 0.062 [95% CI −0.031, 0.156] was also not significant ($p = 0.190$), therefore serum NfL did not mediate the effect of age on executive function.

For episodic memory, the standardised regression coefficient β = −0.602 [95% CI −0.760, −0.444] for the effect of age, adjusted for education and serum NfL was significant ($p < 0.001$), as was the standardised regression coefficient β = 0.531 [95% CI 0.431, 0.631] for the effect of age on serum NfL ($p < 0.001$; Figure 2B). The standardised regression coefficient for the effect of serum NfL on episodic memory adjusted for age β = 0.121 [95% CI −0.044, 0.286] was not significant ($p = 0.151$; Figure 2B). The effect of age on episodic memory score was not mediated by serum NfL levels, with an indirect effect standardised regression coefficient of β = 0.064 [95% CI −0.025, 0.153] ($p = 0.159$).

The effect of age on language, adjusted for education and serum NfL was significant ($p < 0.05$) with the standardised regression coefficient β = −0.258 [95% CI −0.469, −0.048] (Figure 2C). The standardised regression coefficient β = 0.560 [95% CI 0.449, 0.672] for the effect of age of serum NfL levels was also significant ($p < 0.001$), however the standardised regression coefficient β = 0.075 [95% CI −0.162, 0.312] for the effect of serum NfL on language, adjusted for age was not significant ($p = 0.536$, Figure 2C). There was also no mediation of serum NfL levels on the effect of age on language as the indirect effect standardised regression coefficient of β = 0.042 [95% CI −0.090, 0.174] was not significant ($p = 0.534$).

The relationship between $\log_e$-transformed serum NfL and age and the distribution of $\log_e$-transformed serum NfL and the

TABLE 1 Cognitive domain latent variables, cognitive tests comprising them and factor loadings ± 95% CI.

Cognitive domain	Cognitive tests in model	LV loading	Lower CI of LV loading	Upper CI of LV loading	CFI	RMSEA	Model test statistic	value *p*	R^2
Executive Function	Trail making test part B	0.875	0.749	1.001	0.939	0.116	$\chi^2_7 = 20.6$	0.004	0.552
	Digit-span, WAIS-III	0.473	0.330	0.616					
	Stroop C	0.657	0.515	0.799					
Episodic Memory	Paired associates learning	0.707	0.604	0.811	0.995	0.033	$\chi^2_7 = 8.09$	0.325	0.367
	Rey complex figure test	0.877	0.782	0.973					
	Logical memory (I) subtest, WME	0.536	0.363	0.709					
Language	Boston naming test	0.481	0.291	0.671	0.928	0.109	$\chi^2_7 = 18.82$	0.009	0.329
	Vocabulary, WAIS-III	0.782	0.598	0.967					
	Comprehension, WAIS-III	0.643	0.464	0.882					

LV, latent variable; CI, confidence interval; CFI, comparative fit index; RMSEA, root mean squared error of approximation; WAIS-III, Wechsler Adult Intelligence Scale-Third; WME, Wechsler Memory Scale.

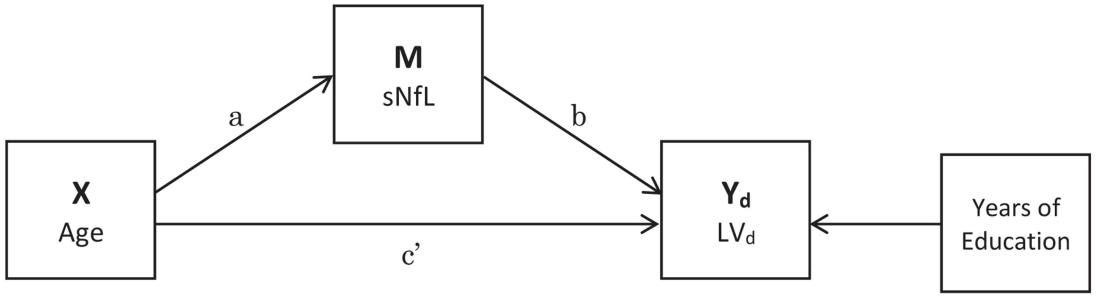

FIGURE 1
Mediation analysis pathways. The indirect pathway is a*b, the direct pathway is c' and the proportion mediated is a*b/(a*b + c'). Years of Education was included as a covariate. Latent variable (LV).

cognitive domain latent variables are shown in Figure 3. A sensitivity analysis was also performed using raw cognitive tests scores for participants who had cognitive testing coincident (in 2018) with blood collection, and the results support those of the Bayesian approach (full statistical methodology and results included in Supplementary material). Supplementary material also includes statistical methodology and results for the interactions between serum NfL and APOE genotype, age and APOE genotype and serum NfL and sex, on cognitive domain latent variables, none of which were statistically significant.

4. Discussion

The aim of the current study was to determine if serum NfL levels, used as a proxy measure of neurodegeneration, mediates the effects of age on cognitive functions, in unimpaired older adults. We hypothesised that in unimpaired older adults, age causes both cognitive decline and higher serum NfL levels, indicative of neurodegeneration, and that NfL levels (neurodegeneration) mediate age-related cognitive decline. This study did not detect a statistically significant mediation effect of serum NfL levels on the association between age and cognitive test scores across the domains of executive function, episodic memory or language, thereby negating this hypothesis.

The results of this study suggest that in cognitively unimpaired older adults, serum NfL levels do not provide us with any extra information on cognitive status beyond that which we can predict using chronological age. This is supported by several studies which have also demonstrated a lack of association between blood NfL levels and cognition, adjusted for age (Mielke et al., 2019; Osborn et al., 2019). It is possible that cognitive reserve compensates for the neuronal pathology/neurodegeneration indicated by blood NfL levels in unimpaired older adults and therefore no relationship between blood NfL levels and cognition is apparent. In support of this hypothesis, the current study demonstrated significant positive associations between years of education (a proxy of cognitive reserve) and cognitive tests score across all three cognitive domains.

In support of previous studies (Disanto et al., 2017; Khalil et al., 2020; Quiroz et al., 2020; Kang et al., 2021), blood NfL levels were

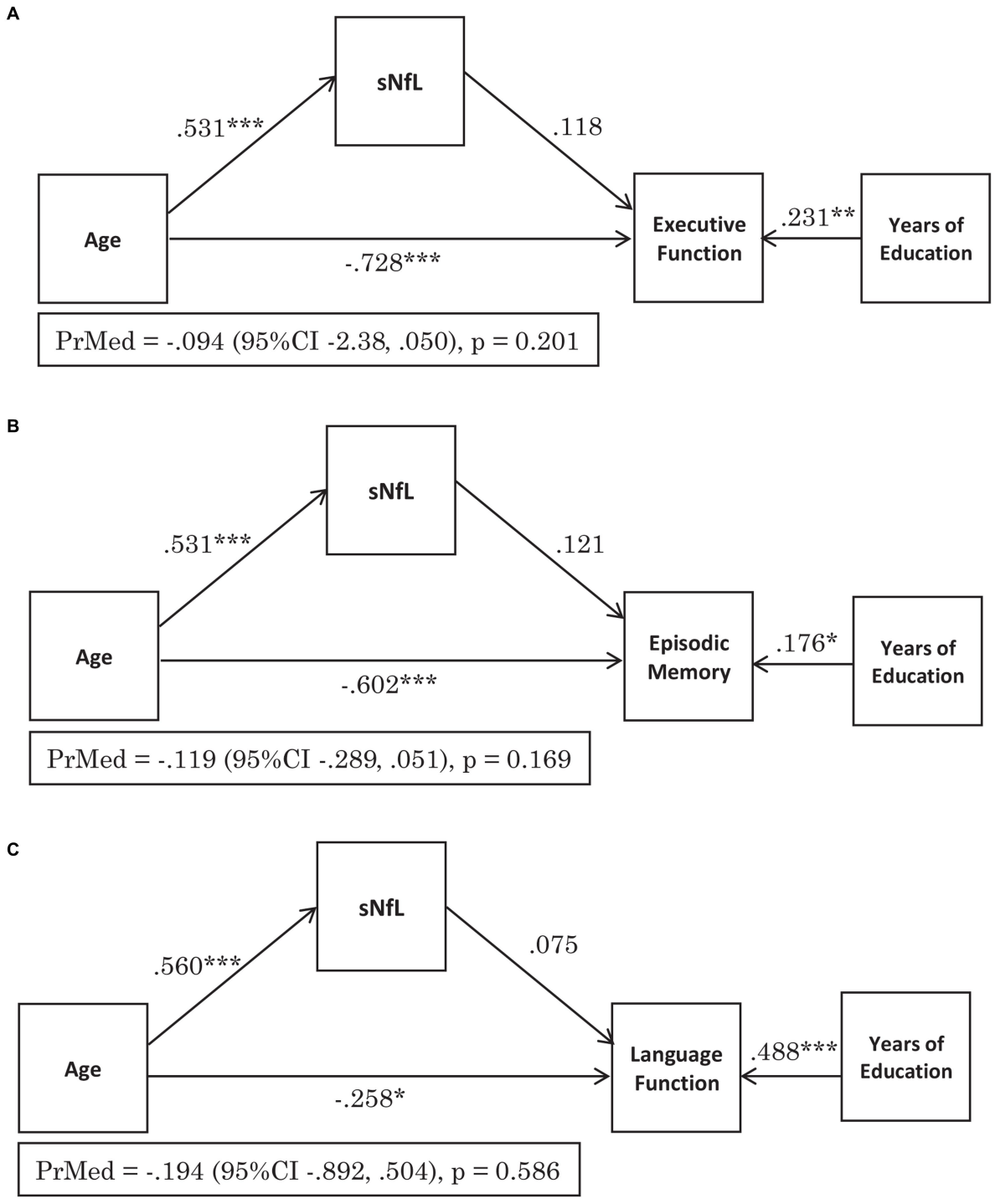

FIGURE 2
Serum NfL does not mediate the effect of age on cognitive function across the domains of: **(A)** Executive Function, **(B)** Episodic Memory and **(C)** Language. The figures demonstrate the standardised regression coefficients (β), *p*-values for the pathways and the proportion mediated (PrMed) β values, 95% confidence intervals (95% CI) and *p*-values. *$p < 0.05$, **$p < 0.01$, ***$p < 0.001$.

significantly correlated with age in this cohort of unimpaired older adults. The brain is known to undergo atrophy with ageing, with white matter loss greater than grey matter loss (Harada et al., 2013). In ageing, this atrophy is attributed to decreases in neuronal size, dendritic complexity and arborisation and the number of synaptic connections, rather than overt cell death (Harada et al., 2013). As NfL is expressed throughout the dendrites, cell body and axon of neurons (Yuan et al., 2017), it is possible that NfL is released and enters the blood when these cells undergo partial or complete degeneration however, the mechanisms underlying this remain unknown. This hypothesis is supported by studies demonstrating that the increase in NfL in the blood correlates with brain volume

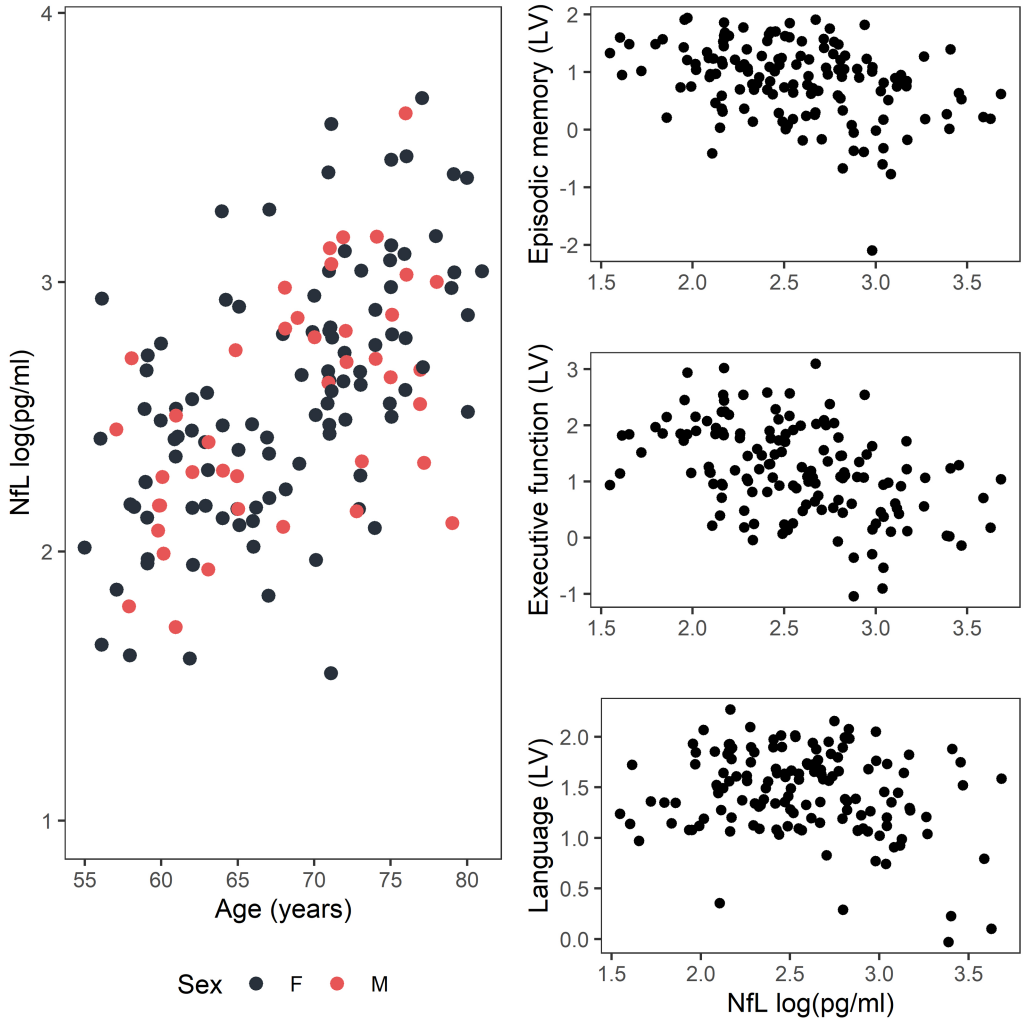

FIGURE 3
Distribution of data for the relationship between $\log_e$-transformed serum NfL and age for females (F, black) and males (M, red) and between $\log_e$-transformed serum NfL and the cognitive domain latent variables (LV) for episodic memory, executive function, and language.

loss on MRI (Mielke et al., 2019; Khalil et al., 2020) and reduced white matter integrity measured by DTI (Beydoun et al., 2023). Therefore, the increase in circulating NfL levels with age may be due to ageing-related neuronal damage and degeneration. However, the result of the current study and others (Mattsson et al., 2019; Osborn et al., 2019; Verberk et al., 2021) suggests that neurodegeneration indicated by blood NfL is not part of the causal relationship between aging and lower cognitive test scores in unimpaired older adults. Other factors may affect the levels of NfL in the blood, including glymphatic clearance (Plog et al., 2015), blood–brain barrier function (Uher et al., 2021) and kidney function (Akamine et al., 2020). Variability in NfL levels in the blood due to these confounding variables may be equal to or larger than the changes due to subtle, age-related or early neurodegenerative changes in the brains of unimpaired older adults. However, in MCI and dementia more extensive neurodegenerative changes in the brain may lead to NfL changes in the blood that far exceed the NfL changes caused by confounding factors such as kidney function. Therefore, the relationship between blood NfL levels and cognition may be more easily detected in MCI and dementia, hence resulting in the significant association reported for these conditions (Lewczuk et al., 2018; Mattsson et al., 2019; Osborn et al., 2019; de Wolf et al., 2020; Quiroz et al., 2020). It is also possible that the relationship between blood NfL levels and cognitive functions differs in disease compared to normal ageing and that the mechanisms of NfL release from cells to the blood are different.

In line with a substantial body of research demonstrating that cognitive test scores are significantly associated with age (Christensen, 2001; Deary et al., 2009), the current study demonstrated that higher age was associated with lower cognitive test scores across the cognitive domains of executive function, episodic memory and language. Age-related decline in cognitive test scores is likely due in part, but not solely, to neurodegeneration, with other molecular and biological factors, such as hormonal dysregulation and cognitive factors including changes in the speed/accuracy trade-off involved (Brebion, 2001; Deary et al., 2009; Bishop et al., 2010).

A novel aspect of the current study was a more thorough determination of cognitive function by using cognitive trajectories

for each participant between 2015 and 2022 and estimating their cognitive test scores coincident with the 2018 serum NfL analysis. This contrasts with previous cross-sectional studies that have looked at single timepoint cognitive test scores coincident with blood NfL measures (Osborn et al., 2019; Huang et al., 2022). This study used cognitive data both preceding and succeeding the NfL analysis to determine participants cognitive test scores more accurately at the time of NfL analysis, rather than relying on a single timepoint test score.

It is important to note that in our cohort of older adults, serum NfL levels were relatively low (range 4.7–39.8 pg./mL). This may reflect the demographics of the cohort, which in comparison to the general Australian population, have more years of education, a higher IQ and likely a higher socio-economic status (Thow et al., 2018). Thus, the low serum NfL concentrations may indicate healthier ageing of this cohort. However, the range of values seen in the current study are comparable to those published previously in a cohort of cognitively unimpaired older adults (Khalil et al., 2020).

A limitation of the current study is the cross-sectional measurement of serum NfL. Recent studies have shown that the rate of change of NfL in the blood, rather than the absolute concentration may be a better indicator of ensuing cognitive decline and dementia (Mielke et al., 2019; Hadjichrysanthou et al., 2020). Future studies focusing on the longitudinal relationship between blood NfL levels and cognitive change in unimpaired older adults are planned. Furthermore, mediation analyses assume that there is no measurement error or unmeasured confounding in the mediator. This is a limitation for NfL as we know that its levels are confounded by age (Khalil et al., 2020; Koini et al., 2021), body mass index (BMI; Koini et al., 2021) and kidney function (Akamine et al., 2020). We were able to adjust for age in our mediations analyses, but not for kidney function or BMI or any other unknown confounders. Furthermore, all lab-based assays will carry some amount of measurement error. Mediation analysis was chosen due to the strong colinear relationship between age, serum NfL and cognition however, this limitation must be kept in mind when interpreting the results of this study. It also should be noted that the current study did not gather information on the presence of subjective cognitive complaints, instead focusing on objective cognitive measures. It is possible that the relationship between serum NfL and cognition is different between cognitively unimpaired people with, and without, subjective cognitive changes.

In conclusion, the current study found no mediating effect of serum NfL levels on cognitive tests scores in unimpaired older adults. This study adds to the literature investigating the relationship between blood NfL levels and cognition during aging and suggests that serum NfL levels may not be useful in the pre-clinical detection of early cognitive changes.

Data availability statement

The original contributions presented in the study are included in the article/Supplementary material, further inquiries can be directed to the corresponding author.

Ethics statement

The studies involving human participants were reviewed and approved by University of Tasmania Health and Medical Research Committee. The patients/participants provided their written informed consent to participate in this study.

Author contributions

JC conducted serum NfL analysis. JC and AB conducted statistical analyses and prepared tables and figures. JC, AK, and JV conception and design of the study and funding acquisition. JC wrote the initial manuscript draft. All authors contributed to data interpretation, wrote sections of the manuscript, contributed to manuscript revisions, read and approved the submitted version of the manuscript.

Funding

This project is funded by National Health and Medical Research Council (NHRMC) Project grants (1003645 and 1108794) and Boosting Dementia Research Leadership Fellowship (APP1136913); the JO and JR Wicking Trust (Equity Trustees); and the Royal Hobart Hospital Research Foundation (20-003).

Acknowledgments

The technical assistance of Graeme McCormack is gratefully acknowledged.

Conflict of interest

The authors declare that the research was conducted in the absence of any commercial or financial relationships that could be construed as a potential conflict of interest.

Publisher's note

Supplementary material

The Supplementary material for this article can be found online at: https://www.frontiersin.org/articles/10.3389/fnins.2023.1237284/full#supplementary-material

References

Akamine, S., Marutani, N., Kanayama, D., Gotoh, S., Maruyama, R., Yanagida, K., et al. (2020). Renal function is associated with blood neurofilament light chain level in older adults. *Sci. Rep.* 10:20350. doi: 10.1038/s41598-020-76990-7

Alcolea, D., Beeri, M. S., Rojas, J. C., Gardner, R. C., and Lleo, A. (2023). Blood biomarkers in neurodegenerative diseases: implications for the clinical neurologist. *Neurology*. 4, 172–180. doi: 10.1212/WNL.0000000000207193

Alirezaei, Z., Pourhanifeh, M. H., Borran, S., Nejati, M., Mirzaei, H., and Hamblin, M. R. (2020). Neurofilament light chain as a biomarker, and correlation with magnetic resonance imaging in diagnosis of CNS-related disorders. *Mol. Neurobiol.* 57, 469–491. doi: 10.1007/s12035-019-01698-3

Barro, C., Chitnis, T., and Weiner, H. L. (2020). Blood neurofilament light: a critical review of its application to neurologic disease. *Ann. Clin. Transl. Neurol.* 7, 2508–2523. doi: 10.1002/acn3.51234

Beydoun, M. A., Noren Hooten, N., Weiss, J., Maldonado, A. I., Beydoun, H. A., Katzel, L. I., et al. (2023). Plasma neurofilament light as blood marker for poor brain white matter integrity among middle-aged urban adults. *Neurobiol. Aging* 121, 52–63. doi: 10.1016/j.neurobiolaging.2022.10.004

Bishop, N. A., Lu, T., and Yankner, B. A. (2010). Neural mechanisms of ageing and cognitive decline. *Nature* 464, 529–535. doi: 10.1038/nature08983

Brebion, G. (2001). Language processing, slowing, and speed/accuracy trade-off in the elderly. *Exp. Aging Res.* 27, 137–150. doi: 10.1080/03610730175007399

Chatterjee, P., Pedrini, S., Doecke, J. D., Thota, R., Villemagne, V. L., Dore, V., et al. (2022). Plasma A beta 42/40 ratio, p-tau181, GFAP, and NfL across the Alzheimer's disease continuum: a cross-sectional and longitudinal study in the AIBL cohort. *Alzheimers Dement.*:18. doi: 10.1002/alz.12724

Christensen, H. (2001). What cognitive changes can be expected with normal ageing? *Aust Nz J Psychiat.* 35, 768–775. doi: 10.1046/j.1440-1614.2001.00966.x

de Wolf, F., Ghanbari, M., Licher, S., McRae-McKee, K., Gras, L., Weverling, G. J., et al. (2020). Plasma tau, neurofilament light chain and amyloid-beta levels and risk of dementia; a population-based cohort study. *Brain* 143, 1220–1232. doi: 10.1093/brain/awaa054

Deary, I. J., Corley, J., Gow, A. J., Harris, S. E., Houlihan, L. M., Marioni, R. E., et al. (2009). Age-associated cognitive decline. *Br. Med. Bull.* 92, 135–152. doi: 10.1093/bmb/ldp033

Disanto, G., Barro, C., Benkert, P., Naegelin, Y., Schadelin, S., Giardiello, A., et al. (2017). Serum neurofilament light: a biomarker of neuronal damage in multiple sclerosis. *Ann. Neurol.* 81, 857–870. doi: 10.1002/ana.24954

Donohoe, G. G., Salomaki, A., Lehtimaki, T., Pulkki, K., and Kairisto, V. (1999). Rapid identification of apolipoprotein E genotypes by multiplex amplification refractory mutation system PCR and capillary gel electrophoresis. *Clin. Chem.* 45, 143–146. doi: 10.1093/clinchem/45.1.143

Faria, C. A., Alves, H. V. D., and Charchat-Fichman, H. (2015). The most frequently used tests for assessing executive functions in aging. *Dement Neuropsychol.* 9, 149–155. doi: 10.1590/1980-57642015DN92000009

Fleisher, A. S., Chen, K., Quiroz, Y. T., Jakimovich, L. J., Gutierrez Gomez, M., Langois, C. M., et al. (2015). Associations between biomarkers and age in the presenilin 1 E280A autosomal dominant Alzheimer disease kindred: a cross-sectional study. *JAMA Neurol.* 72, 316–324. doi: 10.1001/jamaneurol.2014.3314

Forgrave, L. M., Ma, M., Best, J. R., and DeMarco, M. L. (2019). The diagnostic performance of neurofilament light chain in CSF and blood for Alzheimer's disease, frontotemporal dementia, and amyotrophic lateral sclerosis: a systematic review and meta-analysis. *Alzheimers Dement (Amst).* 11, 730–743. doi: 10.1016/j.dadm.2019.08.009

Hadjichrysanthou, C., Evans, S., Bajaj, S., Siakallis, L. C., McRae-McKee, K., de Wolf, F., et al. (2020). The dynamics of biomarkers across the clinical spectrum of Alzheimer's disease. *Alzheimers Res. Ther.* 12:74. doi: 10.1186/s13195-020-00636-z

Harada, C. N., Natelson Love, M. C., and Triebel, K. L. (2013). Normal cognitive aging. *Clin. Geriatr. Med.* 29, 737–752. doi: 10.1016/j.cger.2013.07.002

Huang, Y. L., Li, Y. H., Xie, F., and Guo, Q. H. (2022). Associations of plasma phosphorylated tau181 and neurofilament light chain with brain amyloid burden and cognition in objectively defined subtle cognitive decline patients. *CNS Neurosci. Ther.* 28, 2195–2205. doi: 10.1111/cns.13962

Jessen, F., Amariglio, R. E., van Boxtel, M., Breteler, M., Ceccaldi, M., Chetelat, G., et al. (2014). A conceptual framework for research on subjective cognitive decline in preclinical Alzheimer's disease. *Alzheimers Dement.* 10, 844–852. doi: 10.1016/j.jalz.2014.01.001

Kang, M. S., Aliaga, A. A., Shin, M., Mathotaarachchi, S., Benedet, A. L., Pascoal, T. A., et al. (2021). Amyloid-beta modulates the association between neurofilament light chain and brain atrophy in Alzheimer's disease. *Mol. Psychiatry* 26, 5989–6001. doi: 10.1038/s41380-020-0818-1

Khalil, M., Pirpamer, L., Hofer, E., Voortman, M. M., Barro, C., Leppert, D., et al. (2020). Serum neurofilament light levels in normal aging and their association with morphologic brain changes. *Nat. Commun.* 11:9. doi: 10.1038/s41467-020-14612-6

Kirkcaldie, M. T. K., and Dwyer, S. T. (2017). The third wave: Intermediate filaments in the maturing nervous system. *Mol. Cell. Neurosci.* 84, 68–76. doi: 10.1016/j.mcn.2017.05.010

Koini, M., Pirpamer, L., Hofer, E., Buchmann, A., Pinter, D., Ropele, S., et al. (2021). Factors influencing serum neurofilament light chain levels in normal aging. *Aging-US.* 13, 25729–25738. doi: 10.18632/aging.203790

Lewczuk, P., Ermann, N., Andreasson, U., Schultheis, C., Podhorna, J., Spitzer, P., et al. (2018). Plasma neurofilament light as a potential biomarker of neurodegeneration in Alzheimer's disease. *Alzheimers Res. Ther.* 10:71. doi: 10.1186/s13195-018-0404-9

Mattsson, N., Cullen, N. C., Andreasson, U., Zetterberg, H., and Blennow, K. (2019). Association between longitudinal plasma neurofilament light and neurodegeneration in patients with Alzheimer disease. *JAMA Neurol.* 76, 791–799. doi: 10.1001/jamaneurol.2019.0765

Mielke, M. M., Syrjanen, J. A., Blennow, K., Zetterberg, H., Vemuri, P., Skoog, I., et al. (2019). Plasma and CSF neurofilament light: relation to longitudinal neuroimaging and cognitive measures. *Neurology* 93, e252–e260. doi: 10.1212/WNL.0000000000007767

Moscoso, A., Grothe, M. J., Ashton, N. J., Karikari, T. K., Lantero Rodriguez, J., Snellman, A., et al. (2021). Longitudinal associations of blood phosphorylated tau181 and neurofilament light chain with neurodegeneration in Alzheimer disease. *JAMA Neurol.* 78, 396–406. doi: 10.1001/jamaneurol.2020.4986

Nyberg, L., Boraxbekk, C. J., Sorman, D. E., Hansson, P., Herlitz, A., Kauppi, K., et al. (2020). Biological and environmental predictors of heterogeneity in neurocognitive ageing: Evidence from Betula and other longitudinal studies. *Ageing Res. Rev.* 64:101184. doi: 10.1016/j.arr.2020.101184

Nyberg, L., Lundquist, A., Nordin Adolfsson, A., Andersson, M., Zetterberg, H., Blennow, K., et al. (2020). Elevated plasma neurofilament light in aging reflects brain white-matter alterations but does not predict cognitive decline or Alzheimer's disease. *Alzheimers Dement (Amst).* 12:e12050. doi: 10.1002/dad2.12050

O'Bryant, S. E., Gupta, V., Henriksen, K., Edwards, M., Jeromin, A., Lista, S., et al. (2015). Guidelines for the standardization of preanalytic variables for blood-based biomarker studies in Alzheimer's disease research. *Alzheimers Dement.* 11, 549–560. doi: 10.1016/j.jalz.2014.08.099

Osborn, K. E., Khan, O. A., Kresge, H. A., Bown, C. W., Liu, D., Moore, E. E., et al. (2019). Cerebrospinal fluid and plasma neurofilament light relate to abnormal cognition. *Alzheimers Dement (Amst).* 11, 700–709. doi: 10.1016/j.dadm.2019.08.008

Plog, B. A., Dashnaw, M. L., Hitomi, E., Peng, W., Liao, Y., Lou, N., et al. (2015). Biomarkers of traumatic injury are transported from brain to blood via the glymphatic system. *J. Neurosci.* 35, 518–526. doi: 10.1523/JNEUROSCI.3742-14.2015

Quiroz, Y. T., Sperling, R. A., Norton, D. J., Baena, A., Arboleda-Velasquez, J. F., Cosio, D., et al. (2018). Association between amyloid and tau accumulation in young adults with autosomal dominant alzheimer disease. *JAMA Neurol.* 75, 548–556. doi: 10.1001/jamaneurol.2017.4907

Quiroz, Y. T., Zetterberg, H., Reiman, E. M., Chen, Y., Su, Y., Fox-Fuller, J. T., et al. (2020). Plasma neurofilament light chain in the presenilin 1 E280A autosomal dominant Alzheimer's disease kindred: a cross-sectional and longitudinal cohort study. *Lancet Neurol.* 19, 513–521. doi: 10.1016/S1474-4422(20)30137-X

Rauchmann, B. S., Schneider-Axmann, T., and Perneczky, R. (2021). Alzheimer's Disease Neuroimaging I. Associations of longitudinal plasma p-tau181 and NfL with tau-PET, abeta-PET and cognition. *J. Neurol. Neurosurg. Psychiatry* 92, 1289–1295. doi: 10.1136/jnnp-2020-325537

Roehr, S., Luck, T., Pabst, A., Bickel, H., Konig, H. H., Luhmann, D., et al. (2017). Subjective cognitive decline is longitudinally associated with lower health-related quality of life. *Int. Psychogeriatr.* 29, 1939–1950. doi: 10.1017/S1041610217001399

Rosseel, Y. (2012). lavaan: an R package for structural equation modeling. *J. Stat. Softw.* 48, 1–36. doi: 10.18637/jss.v048.i02

Rowe, J. W., and Kahn, R. L. (1987). Human aging: usual and successful. *Science* 237, 143–149. doi: 10.1126/science.3299702

Shahim, P., Tegner, Y., Marklund, N., Blennow, K., and Zetterberg, H. (2018). Neurofilament light and tau as blood biomarkers for sports-related concussion. *Neurology* 90, e1780–e1788. doi: 10.1212/WNL.0000000000005518

Smith, P. J., Need, A. C., Cirulli, E. T., Chiba-Falek, O., and Attix, D. K. (2013). A comparison of the Cambridge Automated Neuropsychological Test Battery (CANTAB) with "traditional" neuropsychological testing instruments. *J. Clin. Exp. Neuropsychol.* 35, 319–328. doi: 10.1080/13803395.2013.771618

Stocker, H., Beyer, L., Perna, L., Rujescu, D., Holleczek, B., Beyreuther, K., et al. (2023). Association of plasma biomarkers, p-tau181, glial fibrillary acidic protein, and neurofilament light, with intermediate and long-term clinical Alzheimer's disease risk: results from a prospective cohort followed over 17 years. *Alzheimers Dement.* 19, 25–35. doi: 10.1002/alz.12614

Summers, M. J., Saunders, N. L., Valenzuela, M. J., Summers, J. J., Ritchie, K., Robinson, A., et al. (2013). The Tasmanian Healthy Brain Project (THBP): a prospective longitudinal examination of the effect of university-level education in older adults in preventing age-related cognitive decline and reducing the risk of dementia. *Int. Psychogeriatr.* 25, 1145–1155. doi: 10.1017/S1041610213000380

Thow, M. E., Summers, M. J., Saunders, N. L., Summers, J. J., Ritchie, K., and Vickers, J. C. (2018). Further education improves cognitive reserve and triggers improvement in selective cognitive functions in older adults: The Tasmanian Healthy Brain Project. *Alzheimers Dement (Amst).* 10, 22–30. doi: 10.1016/j.dadm.2017.08.004

Uher, T., McComb, M., Galkin, S., Srpova, B., Oechtering, J., Barro, C., et al. (2021). Neurofilament levels are associated with blood-brain barrier integrity, lymphocyte extravasation, and risk factors following the first demyelinating event in multiple sclerosis. *Mult. Scler.* 27, 220–231. doi: 10.1177/1352458520912379

Verberk, I. M. W., Laarhuis, M. B., van den Bosch, K. A., Ebenau, J. L., van Leeuwenstijn, M., Prins, N. D., et al. (2021). Serum markers glial fibrillary acidic protein and neurofilament light for prognosis and monitoring in cognitively normal older people: a prospective memory clinic-based cohort study. *Lancet Healthy Longev.* 2, e87–e95. doi: 10.1016/S2666-7568(20)30061-1

Ward, D. D., Andel, R., Saunders, N. L., Thow, M. E., Klekociuk, S. Z., Bindoff, A. D., et al. (2017). The BDNF Val66Met polymorphism moderates the effect of cognitive reserve on 36-month cognitive change in healthy older adults. *Alzheimers Dement (NY).* 3, 323–331. doi: 10.1016/j.trci.2017.04.006

Ward, D. D., Summers, M. J., Saunders, N. L., Janssen, P., Stuart, K. E., and Vickers, J. C. (2014). APOE and BDNF Val66Met polymorphisms combine to influence episodic memory function in older adults. *Behav. Brain Res.* 271, 309–315. doi: 10.1016/j.bbr.2014.06.022

Yuan, A., Rao, M. V., and Veeranna, N. R. A. (2017). Neurofilaments and neurofilament proteins in health and disease. *Cold Spring Harb Perspect Biol* 9:a018309. doi: 10.1101/cshperspect.a018309

frontiers | Frontiers in Aging Neuroscience

TYPE Systematic Review
PUBLISHED 05 September 2023
DOI 10.3389/fnagi.2023.1234719

OPEN ACCESS

EDITED BY
Kuangyu Shi,
University of Bern, Switzerland

REVIEWED BY
Enquan Xu,
Duke University, United States
Dandan Wang,
Fudan University, China

*CORRESPONDENCE
Junyan Yao
junyanyao@shsmu.edu.cn

RECEIVED 09 June 2023
ACCEPTED 23 August 2023
PUBLISHED 05 September 2023

CITATION
Zhang Y, Zhang J, Wang Y and Yao J (2023) Global trends and prospects about synaptic plasticity in Alzheimer's disease: a bibliometric analysis.
Front. Aging Neurosci. 15:1234719.
doi: 10.3389/fnagi.2023.1234719

Global trends and prospects about synaptic plasticity in Alzheimer's disease: a bibliometric analysis

Yingying Zhang[1], Junyao Zhang[1], Yinuo Wang[1] and Junyan Yao[1,2]*

[1]Department of Anesthesiology, Shanghai General Hospital, Shanghai Jiao Tong University School of Medicine, Shanghai, China, [2]Department of Anesthesiology, Shanghai East Hospital, Tongji University School of Medicine, Shanghai, China

Background and purpose: In recent years, synaptic plasticity disorders have been identified as one of the key pathogenic factors and the early pathological characteristics of Alzheimer's disease (AD). In this study, we tried to use bibliometric analysis to gain a systematic understanding about synaptic plasticity in Alzheimer's disease.

Methods: We extracted relevant publications from the Web of Science Core Collection (WoSCC) on August 29th, 2022. Then, we used CiteSpace, VOSviewer and other online bibliometric platforms[1] to further analyze the obtained data.

Results: A total of 2,348 published articles and reviews about synaptic plasticity in AD from 2002 to 2022 were identified. During the past two decades, the overall trends of the numbers and citations of manuscripts were on the rise. The United States was the leading country with the largest number of publications which showed its crucial role in this field. The collaboration network analysis showed that the United States and China had the most frequent collaboration. In addition, Harvard University was the institution with the greatest number of publications and cited times. Among all authors, Selkoe DJ was the most influential author with the greatest cited times. The journal of Alzheimer's disease published the maximum number of documents in the field of synaptic plasticity in AD within 20 years. Furthermore, the results of keywords burst detection showed that the hot topics have shifted from the synaptic transmission, precursor protein and plaque formation to neuroinflammation, microglia and alpha synuclein.

Conclusion: This study analyzed 2,348 publications with 82,025 references covering the topic of synaptic plasticity in AD and presented the research trends. The results indicated that neuroinflammation, microglia and alpha synuclein were the current research hotspots, which implied the potential clinical applications to AD.

KEYWORDS

Alzheimer's disease, synaptic plasticity, bibliometric analysis, hotspots, VOSviewer, CiteSpace, co-citation

1 https://bibliometric.com/

Introduction

It has been forecasted that by 2050, the prevalence of dementia will double in Europe and triple worldwide (Scheltens et al., 2021). Alzheimer's disease (AD), a major cause of dementia, has becoming a global health concern. Nowadays, with the escalation of the aging process, the incidence of AD is also on increasing. The prevalence of AD not only damages the elderly's health, but also exerts a heavy burden on the family and society. Consequently, it is critical to find early diagnosis methods and effective therapeutic interventions for AD patients. Although the classical hypothesis of AD is the formation of amyloid plaques and neurofibrillary tangles (NFTs) mainly composed of amyloid-β (Aβ) peptides and hyper phosphorylated tau, the clinical therapeutic strategies based on this hypothesis still fail to achieve satisfactory results (Naseri et al., 2019). Thus, it is necessary to find new approaches to improve the treatment and diagnosis of AD.

The degeneration of synapses and dendritic spines are prior to the loss of neurons in many neurodegenerative diseases, especially in AD (Yu and Lu, 2012). As reported, the strength and efficiency of synaptic connections can be affected by the changes in the environment or the experience of the individuals (Krzeptowski et al., 2018; Mercerón-Martínez et al., 2021). This characteristic is defined as synaptic plasticity which is directly related to memory and learning process.

The mechanisms of synaptic plasticity refer to not only its morphological modifications, such as the regeneration of axons and the formation of new synapse but also its molecular changes that alter the cellular response to neurotrasmitters (Mercerón-Martínez et al., 2021). Over the years, long-term potentiation (LTP) and long-term depression (LTD), have generally been proposed to be the basis of cellular processes underlying learning and memory (Sweatt, 2016; Krzeptowski et al., 2018). LTP contributes to the formation of memory whereas LTD can inactive the memory (Nabavi et al., 2014). Therefore, LTP/LTD function together to modify the synaptic strength to encode the memories. Hence, when the efficacy of LTP decreases, the subjects' cognitive capacity subsequently shows a declining trend. Studies from AD mouse models have also denoted that soluble oligomers of Aβ can inhibit the hippocampal LTP *in vivo* and afterwards adversely affect the synaptic transmission (Selkoe, 2002). Previous studies have demonstrated that learning and synaptic dysfunctions appear before the formation of amyloid plaques and NFTs, suggesting that the disorders of synaptic efficacy underlie the initial development of AD (Selkoe, 2002).

Bibliometric analysis is an important statistical method that is used to quantitatively analyze large amounts of heterogeneous publications (Chen et al., 2014). In recent years, bibliometric analysis has been used to provide clear insights into many scientific fields. CiteSpace is a Java web-based visualizing processing tool widely used in bibliometric analysis, which can offer good support in analyzing data from multiple perspectives, including different countries/regions, institutions, journals, authors, co-citation references and keywords (Chen, 2004).

Over the past two decades, many publications have illustrated the correlation between synaptic plasticity and AD, however, the systematic summaries of these studies are still insufficient. Hence, it is necessary to collect data from relevant publications to assist investigators in understanding the vast amount of literature on this subject. Through evaluating the existing data, we can help researchers to identify detailed research focus, global research trends, hot sports and guide future academic decisions in the field of synaptic plasticity in AD.

In this study, we aimed to provide a comprehensive understanding of the developments in the field of synaptic plasticity in AD by analyzing the data obtained from the WoSCC. Furthermore, we identified the research trends and potential hot spots which may be helpful in future research planning and decision-making.

Methods

Data source and search strategies

A literature search was conducted using the WoSCC database (Clarivate Analytics, Philadelphia, PA, United States) with the following search strategy: Topic = (("synaptic plasticity" OR "synapse plasticity ") AND ("Alzheimer disease" OR "Alzheimer's disease")) AND language = English, limited time = from 2002 to 2022. We applied filters to limit the search to original articles and reviews, index = science citation index expanded (SCI-EXPANDED), timespan = 2002–2022. To reduce the bias incurred by frequent database updates, literature retrieval and data downloads were completed in 1 day on August 29th, 2022 by two authors (Yingying Zhang and Junyao Zhang) independently to obtain the primary data.

Data extraction and collection

The manuscripts conducted by the aforementioned search strategies were then screened and recorded for titles, countries/regions, institutions, journals, authors and cited references. The WoSCC data were converted to txt format and imported into Microsoft Excel 2021, VOSviewer (version 1.6.18), CiteSpace (version 5.8.R3), online analysis platform of bibliometry (see Footnote 1) for further bibliometric analysis.

Bibliometric analysis

All literature characteristics, including countries, institutions, journals, authors, co-citation references clusters and keywords with the strongest citation bursts were documented. The annual publication numbers and citation information of different countries/regions obtained from WoSCC were analyzed using Microsoft Excel 2021. CiteSpace v5.8.R3 was used to generate a visualization map in order to describe the co-cited authors/reference and to analyze keywords with strong citation bursts. The VOSviewer v1.6.18 was adopted to identify the intensity of cooperation between institutions and authors to illustrate the international influence of these institutions and authors in the field of synaptic plasticity in AD. In order to detect the research hotspots and predict research trends, we conducted the keywords co-occurrence network visualization map. Furthermore, the co-citation network visualization map of journals was also analyzed by VOSviewer.

Results

Bibliometric analysis of publication outputs and citation trend

A total of 2,348 publications were included in our study. The number of publications and citations were concluded using Microsoft Excel 2021 (Figure 1). There were few articles before 2008, the overall

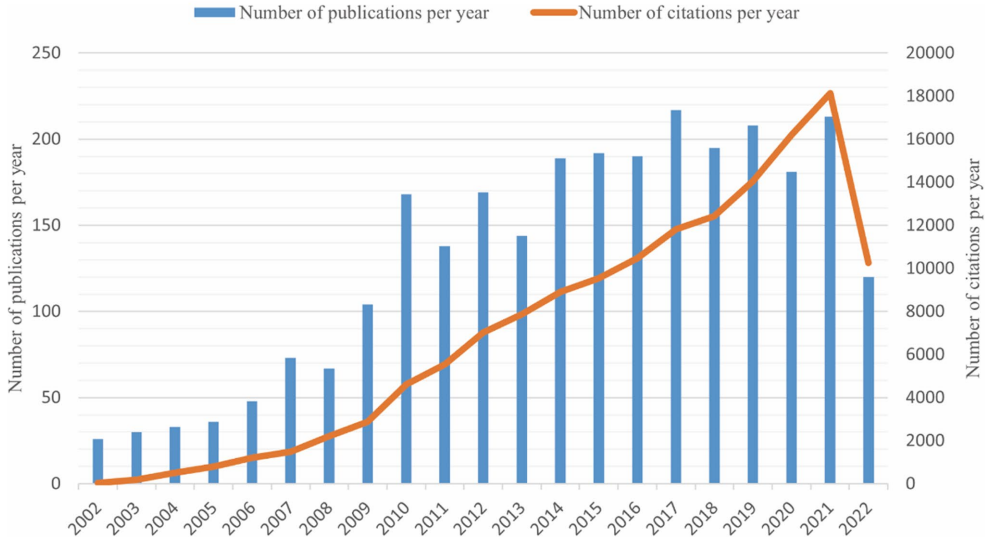

FIGURE 1
The trends of annual publications and citations on the topic of synaptic plasticity in Alzheimer's disease from 2002 to 2022.

trend was on the rise and reached its peak in 2017 with a total of 217 publications. This chart showed a surge increase in annual citation numbers between 2002 and 2021, presumably 62.87 times per item.

Bibliometric analysis of countries and regions

The distribution map of the top 20 productive countries was shown in Figure 2A. The United States had the largest number of publications (949) in this field, followed by China (399), Germany (193) and Italy (177). A national cooperation network analysis was conducted by an online analytical platform (Figure 2B). In this map, the United States was the center of the national cooperation which showed frequently cooperation with China, Italy, Ireland, UK, Germany and Canada. Nevertheless, other countries displayed less international cooperation than the United States.

Bibliometric analysis of institutions

In order to find out about the research institutions and interinstitutional cooperation efforts in the field of synaptic plasticity in AD, we conducted a visualization network map by VOSviewer (Figure 3A). The size of the circles represented the number of publications, therefore, the institution with more published articles tended to present larger circles. Links between the two institutions meat that they have collaboratively published articles. The length of the lines indicated the strength of the cooperation. The research network presented that Harvard University was the most productive institution and had the most frequent collaboration with other institutions. However, the cooperation among other institutions was relatively not close enough. As shown in Figure 3B, Harvard University, University Calif San Diego and National Institute of Aging had the most publications concentrated between 2012 and 2014, while publications from University Toronto, Columbia University and University College London were mainly published after 2016. Furthermore, Table 1 showed the top 10 prolific institutions. Seven institutions located in the United States, two located in China, and one located in Canada. Through analyzing these data, we can indicate that Harvard University contributed the most in the field of synaptic plasticity in AD followed by New York University and the University of San Diego.

Bibliometric analysis of journals

The WoSCC search showed that a total of 235 journals participated in the publication of synaptic plasticity in AD. Table 2 listed the top 10 productive journals, and the most prolific one was the journal of Alzheimer's disease which published 256 documents, followed by the Journal of Neuroscience (164) and Neurobiology of Aging (144). The co-citation network visualization map was shown in Figure 4A. The size of the node was correlated with the number of citations of each journal and this distribution trend could be understood more clearly in Figure 4B. The highest cited one was the journal of neuroscience with 17,166 citations, followed by Proceedings of the national academy of sciences of the United States of America-Physical sciences (9439) and Neuron (8549).

Bibliometric analysis of authors

The authors and their collaborations regarding synaptic plasticity in AD were shown in Figure 5A. In this visualization map, there were only four clusters, indicating that the collaboration of authors was not very close. The co-citation analysis of authors could reveal the core researchers and their contributions to a certain field. We conducted a visualization map of co-cited authors *via* CiteSpace (Figure 5B). Selkoe DJ from Harvard Medical School was the most cited author and has been cited 872 times in 2002. Shankar GM from Harvard Medical School has been cited 630 times in 2007 and thus ranks second, followed by Walsh DM (593), Hardy J (432) and Braak H (313). The other five major researchers and their institutions were also

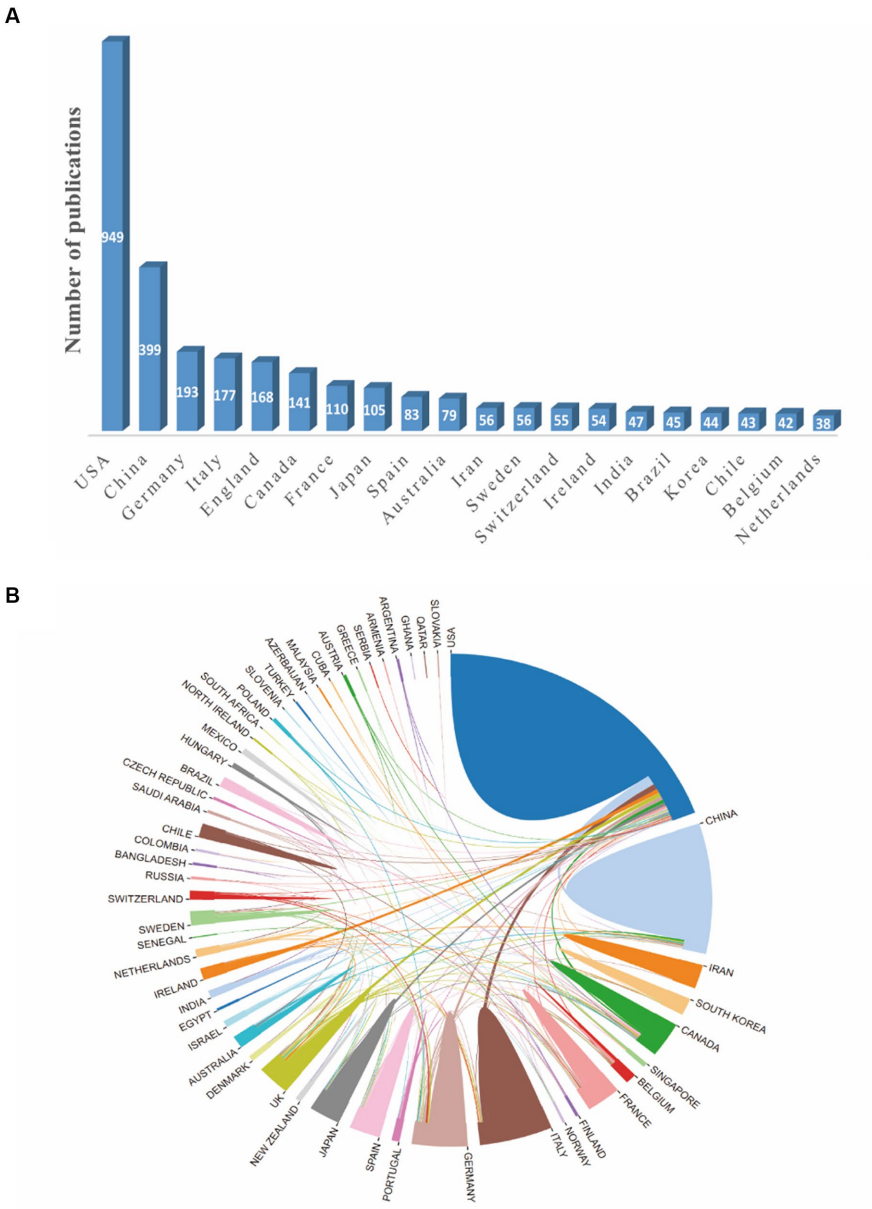

FIGURE 2
The network map of countries involved in the field of synaptic plasticity in Alzheimer's disease. **(A)** The distribution map of the top 20 productive countries. **(B)** The visualization map of collaboration among countries generated by an online analytical platform.

presented in Table 3 (Palop JJ from the University of California, Terry RD from the University of California-San Diego, Mattson MP from the Johns Hopkins University School of Medicine, Oddo S from the University of California, and Lambert MP from Perelman School of Medicine). It should be noted that the top three productive researchers called Selkoe DJ, Shankar GM and Walsh DM, were all members of Harvard Medical School. Consequently, it could be concluded that Harvard Medical School played a crucial role in this field.

Bibliometric analysis of references

In order to discover the present main topics and the evolution of synaptic plasticity in AD, the timeline view of co-citation documents clusters was conducted (Figure 6). It showed that in this scientific field, the focus of research seems to have shifted from conditional inactivation and calcium dyshomeostasis to early stage and brain insulin resistance. The top five highly cited references were presented in Table 4. Results showed that the highest cited reference was Amyloid-beta protein dimers isolated directly from Alzheimer's brains impair synaptic plasticity and memory which was published by Nature Medicine in 2008. It suggested that soluble Aβ oligomers can effectively inhibit LTP, enhance LTD, reduce dendritic spine density and also disrupt the memory of learned behavior in normal rats. This research denoted that soluble Aβ oligomers extracted from the cerebral cortex of AD brains can potently impair synapse structure and function (Shankar et al., 2008), which was consistent with the results of the article with the second highest citation. Researchers demonstrated that

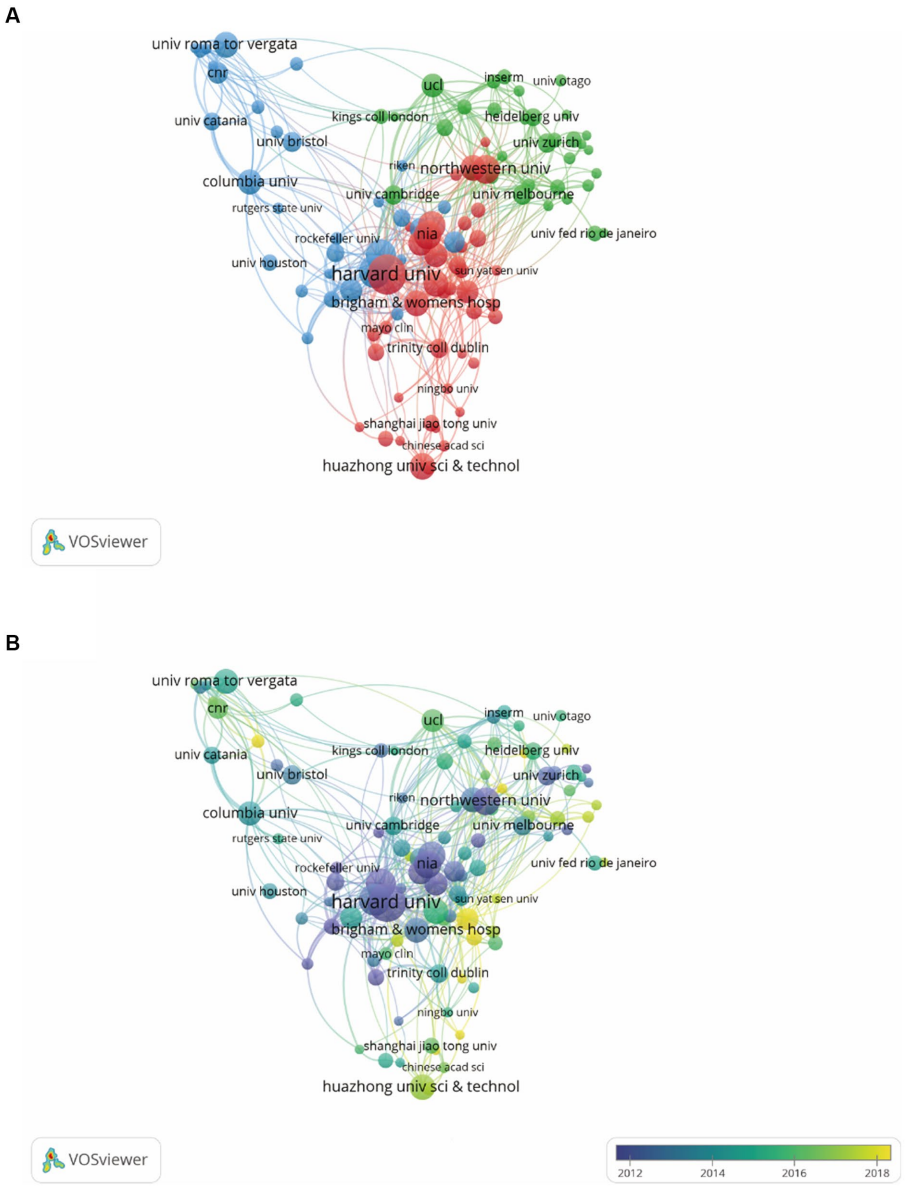

FIGURE 3
VOSviewer analysis of collaborations among different institutions. **(A)** The cooperation network map of institutions was based on VOSviewer. Size of the nodes represented the number of publications by each institution, and links between two nodes represented the frequency of the cooperation between two institutions. **(B)** The color of each circle referred to the average publication year for the institution.

without monomers and amyloid fibrils, Aβ oligomers can still disrupt synaptic plasticity *in vivo* (Walsh et al., 2002). The third highest-ranking article was published by Science in 2002, which suggested that synapses were the initial target in AD and its dysfunction appeared before Aβ plaque formation (Selkoe, 2002). This provided us with a new idea to intervene in the development of AD in the early stage. These high-citation references have made significant contributions in this field and deserve more attention in the future.

Bibliometric analysis of co-occurring keywords and burst detection with keywords

To identify the development in the field of synaptic plasticity in AD, we presented 50 keywords with a minimal occurrence of 87 times and classified into four clusters in Figure 7A. The size of each circle was positively correlated with the occurrence frequency of keywords. The green cluster contained some keywords such as synaptic plasticity, memory, neurotrophic factor and dentate gyrus. The red cluster contained some keywords such as Alzheimer's disease, long-term potentiation and amyloid precursor protein. In the yellow cluster, the main keywords were oxidative stress, dementia and neurodegeneration. The blue cluster keywords were dendritic spines, oligomers and phosphorylation. The keywords in the same cluster showed some correlation with each item. In Figure 7B, circles were colored differently according to the average occurrence time. It presented that "precursor protein," "peptide" and "central nervous system" have been researched earlier than 2014, whereas keywords such as "oxidative stress" and "mild cognitive impairment" were the current research focus in this field and may become hotspots in the future. Keywords burst detection was

TABLE 1 List of top 10 organizations.

Organization	Documents	Citations	Total link strength
Harvard Univ	64	10,301	414
NYU	49	4,618	229
Univ Calif San Diego	47	3,642	144
NIA	41	7,555	136
Northwestern Univ	41	6,498	265
Univ Calif Irvine	41	6,821	143
Shanxi Med Univ	39	1,162	46
Huazhong Univ Sci & Technol	38	1,064	40
Univ Toronto	37	1,749	89
Brigham & Women's Hosp	36	4,728	277

TABLE 2 List of top 10 journals.

Journals	Documents	Citations	Total link strength
Journal of Alzheimer's Disease	256	8,114	778
Journal of Neuroscience	164	19,782	995
Neurobiology of Aging	144	6,822	499
Journal of Neurochemistry	90	5,955	336
Molecular Neurobiology	85	2,644	251
Frontiers in Aging Neuroscience	79	1,624	202
Neurobiology of Disease	72	4,324	337
Neuroscience	67	2,230	174
Neuropharmacology	65	3,433	262
Behavioral Brain Research	54	2,841	206

conducted to identify the future emerging trends and current research hot topics. The top 25 keywords with the strongest citation burst were shown in Figure 7C. The red line indicated that the use of this keyword suddenly increased during this period of time and showed its beginning and ending years. In contrast, a blue line represented relative unpopularity. In the past two decades, precursor protein ranked first with the highest burst strength (14.68), followed by peptide (10.67), cortical neuron (10.59), secreted oligomer (9.59) and long-term potentiation (9.24). Some keywords burst with long durations, such as rat hippocampus, synaptic transmission and precursor protein, with a time span of 9, 8 and 8 years, respectively. In addition, the hot topics have switched from synaptic transmission, rat hippocampus, precursor protein and cortical neuron to plaque formation, secreted oligomer, impair synaptic plasticity and endoplasmic reticulum stress, and finally to depression, neuroinflammation, microglia, alpha synuclein and amyloid beta. This transition indicated that neuroinflammation, microglia and alpha synuclein have drawn the attention of peer investigators, indicating that they have become the new current research hotspots.

Discussion

In this study, we conducted bibliometric analysis *via* CiteSpace and VOSviewer to visually analyze a total of 2,348 publications from 2002 to 2022. We aimed to reveal the current research hotspot of synaptic plasticity in AD intuitively and provide guidance for future studies.

Research trends of synaptic plasticity in Alzheimer's disease

From the bibliometric analysis on the role of synaptic plasticity in AD publications over the past two decades, it was found that the number of published articles has gradually increased, indicating that synaptic plasticity was generally attracting attention in this field. 52 countries and 51 institutions were analyzed, respectively, by online bibliometric platform and VOSviewer. According to the results (Figure 2B), the United States, China, Italy and Germany contributed most in this field. By analyzing the institutional publication numbers and citations among all institutions, we figured out that Harvard University was the most productive one (Table 1). Based on these data, the United States is undoubtedly the world leader in this field. Meanwhile, our analysis showed that the United States and China had the most frequent cooperation because there are close academic exchanges between researchers in these two countries. By contrast, connections between other countries and organizations remain weak. This indicated that we should pay more attention to the cooperation between organizations in different countries in order to promote the development of this field. In China, AD has become one of the most urgent neurodegenerative diseases that needs to be solved. Researchers continuously try to find a new therapy method and have published substantial articles. However, the number of publications and citations is still insufficient, which indicates Chinese researchers need to further improve the quality and influence of their publications.

In order to evaluate the contribution of authors in this field, we ranked them based on their total number of citations. According to the data extracted from WoSCC, we found that Selkoe DJ ranked first with the most number of citations, followed by Shankar GM and Walsh DM. It should be noticed that these top three authors all come from Harvard Medical School, which was the most prolific institution we have referred above. Moreover, we also conducted the co-authorship visualization map to provide researchers the current partnerships and confirm potential collaborators.

Analyzing popular journals can provide researchers with a definite searching direction in this scientific research domain. We finally found that the Journal of Alzheimer's Disease has published the most documents, while the Journal of Neuroscience ranked first by citations (Table 2). In terms of publications and citations, we can conclude that the most influential one was the Journal of Neuroscience. Through the journals' rank, investigators can quickly find suitable journals for their own publications.

Through analyzing the timeline view of related references and the keywords citation bursts, we can understand the hotspots, research fronts and the evolution of this scientific research field. At the early stage, the effects of synaptic transmission, precursor protein, plaque formation and secreted oligomer have been studied over 5 years which indicated that these factors attracted researchers' attention and

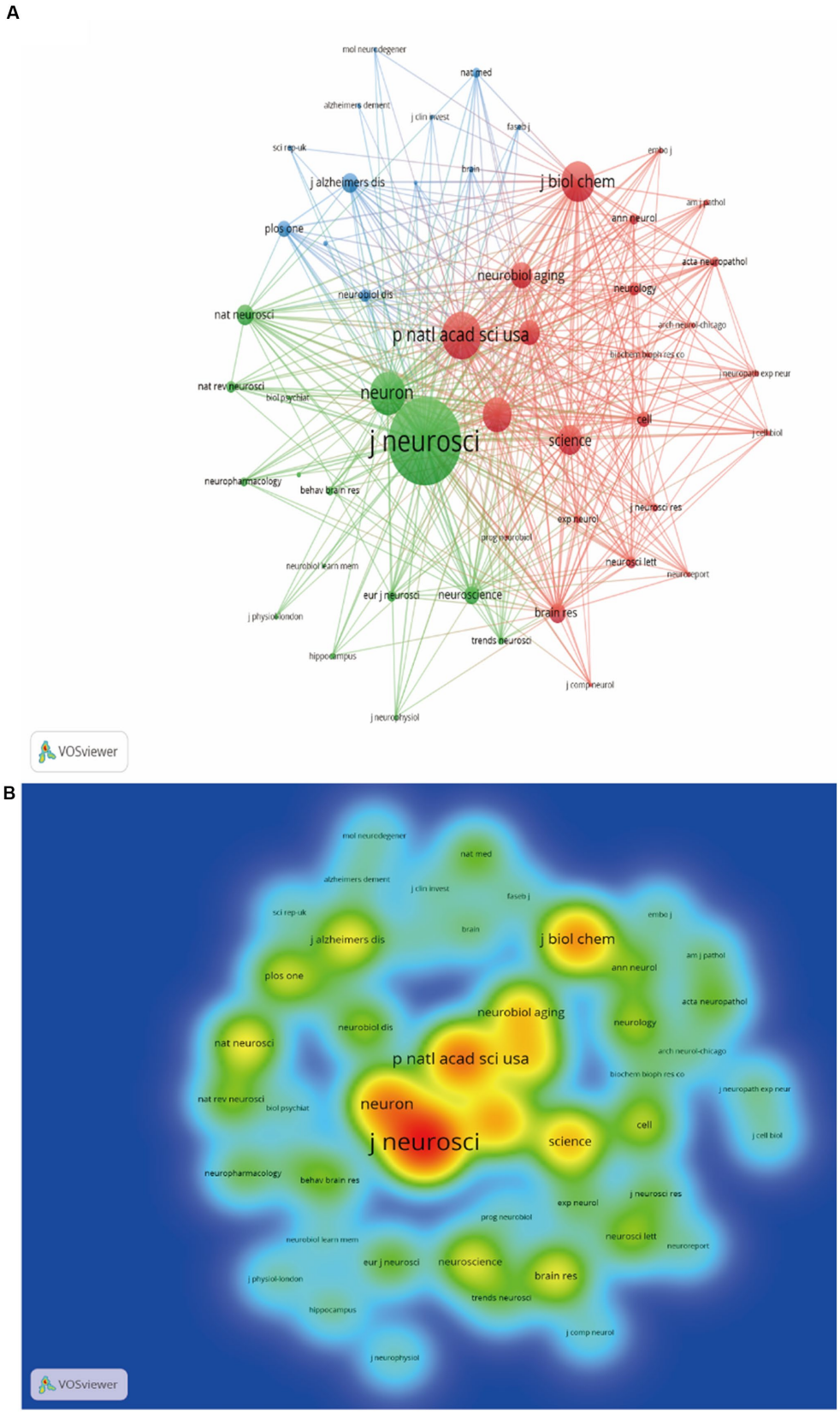

FIGURE 4
Analysis map of the most prolific journals. **(A)** The co-citation network visualization map of journals was based on VOSviewer. **(B)** The density visualization map of journals was based on VOSviewer.

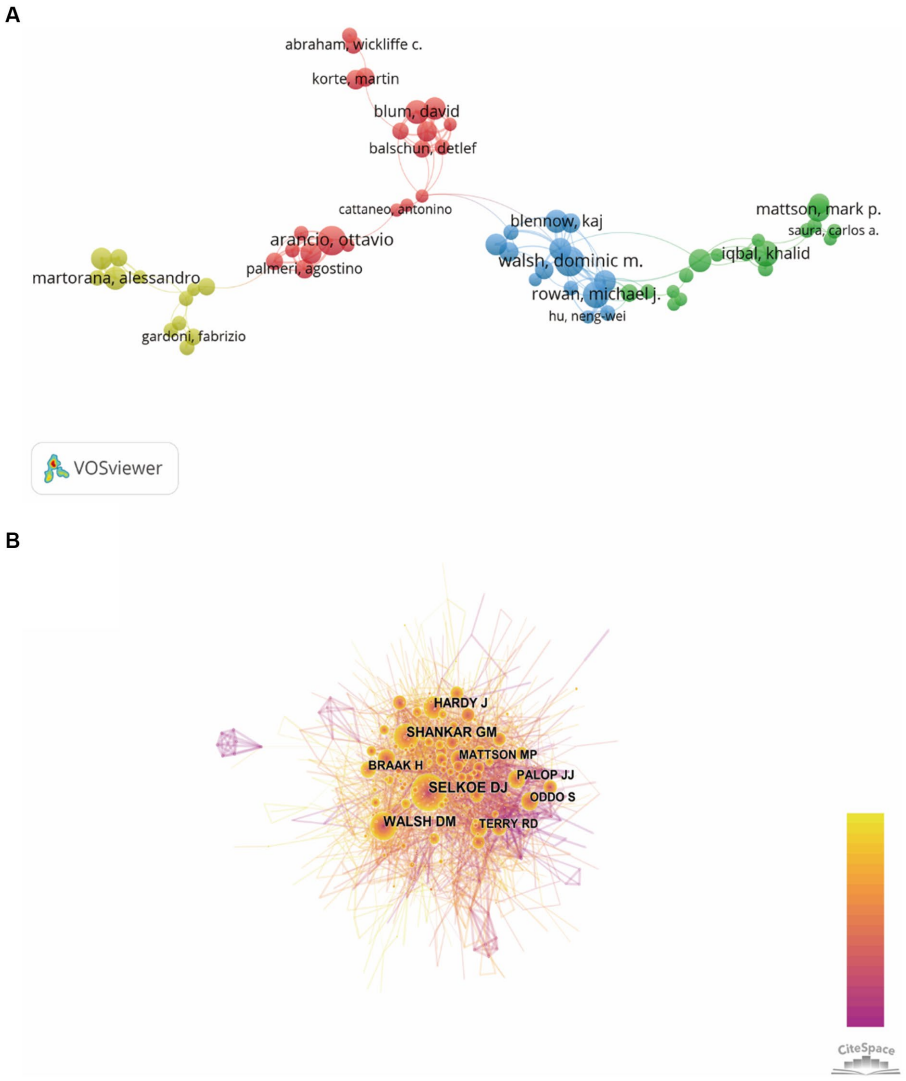

FIGURE 5
Visualization map of authors generated by VOSviewer and CiteSpace. **(A)** The co-authorship network visualization map of authors was based on VOSviewer. Circle size meat the number of authors' publications, and the length of lines meat the frequency of collaboration between those two authors. **(B)** The co-citation network visualization map of authors was based on CiteSpace. The node size represented the number of citations of each author, while the links referred to the frequency of the co-citation between two authors.

composed the research foundation in the field of synaptic plasticity in AD. Meanwhile, our research demonstrated that early stage, neuroinflammation, microglia and alpha synuclein have become the focal points of recent studies.

Research focus of synaptic plasticity in Alzheimer's disease

Publications with the highest citation number had been correlated with tremendous academic impact on a certain research field. Therefore, we analyzed the top 10 highly cited publications in recent 5 years, the results showed that the main influenced factors of synaptic plasticity in AD were therapeutic strategies, astrocyte and amyloid-β protein.

At present, despite comprehensive research into the pathophysiology of AD and a mass of drugs entering clinical development, no effective new drug has been approved since memantine in 2003 (Panza et al., 2019). Many reasons have been put forward to explain this failure, such as inappropriate patient selection, suboptimal dosing, drug exposure ('too little, too late') and inappropriate time of intervention (Polanco et al., 2018). Furthermore, the lack of a detailed understanding of the AD pathophysiology might lead to select of the wrong targets. Most of the drugs for AD target the accumulation of Aβ peptide. For example, AN-1792, CAD106, solanezumab and gantenerumab can stimulate Aβ clearance, while verubecestat, lanabecestat and elenbecestat can decrease Aβ production (Panza et al., 2019). Notably, anti-diabetes drugs, intervention of neuroinflammation and tau-targeting therapies have become promising new targets for treating AD. Craft et al. demonstrated that intranasal insulin detemir or regular insulin can effectively improve cognition and daily functioning of AD patients (Craft et al., 2017). In the early

years, researchers found that patients given some anti-inflammatory drugs could reduce the risk of developing AD (Abbott, 2018). Microglia gather around amyloid plaques and the areas of brain degeneration. Many studies have revealed that microglia have a central role in the link between inflammation and neurodegeneration (Zhou et al., 2020). Initially, the moderate activation of microglia can surround plaques and degrade Aβ by phagocytosis. Nevertheless, chronic overactivation of microglia tend to act a more proinflammatory role and less phagocytic ability (Marsh et al., 2016). It is necessary to fully understand the biology of microglia to consider how to design immune-based therapies for AD. Another promising target for intervention is tau. Although most of the anti-tau therapies have failed because of toxicity and/or lack of efficacy, the current new tau-targeting therapies have shown prospective effect in numerous preclinical studies (Mummery et al., 2023).

TABLE 3 List of top 10 authors.

Author	Citations	Institution
Selkoe DJ	872	*Harvard Medical School*
Shankar GM	630	*Harvard Medical School*
Walsh DM	563	*Harvard Medical School*
Hardy J	432	*University College London*
Braak H	313	*J.W. Goethe University*
Palop JJ	312	*The University of California*
Terry RD	298	*The University of California-San Diego*
Mattson MP	295	*The Johns Hopkins University School of Medicine*
Oddo S	295	*The University of California*
Lambert MP	275	*Perelman School of Medicine*

In recent years, the role of astrocytes in AD has also received increasing attention. It has been reported that astrocytes play an important role in regulating structural remodeling and functional plasticity of synapses (Santello et al., 2019). In addition, dynamic cellular imaging work revealed that astrocytes can intimately interact with neurons, while astrocyte-targeted mouse genetics illustrated that astrocytes participate in memory processes (Bindocci et al., 2017; Stobart et al., 2018). Despite the technical advances helping researchers further understand the role of astrocytes, they also highlight the incomplete comprehension of astrocyte biology. In pathological conditions, such as AD, astrocyte-neuron interactions can be substantially disrupted, with strong effect on brain circuits supporting memory formation and cognitive function (Santello et al., 2019). These findings suggest that therapeutic strategies targeting astrocyte pathways may have tremendous potential to fight against cognitive deficits in AD.

Walsh et al. revealed the influence of soluble Aβ oligomers on synaptic plasticity and memory (Walsh et al., 2002). They found that these soluble Aβ oligomers potently inhibited LTP, enhanced LTD, reduced dendritic spine density and also disrupted the memory of learned behavior in normal rodents (Walsh et al., 2002). In addition, Aβ can bind to distinct components of neuronal and non-neuronal plasma membranes to induce complex patterns of synaptic dysfunction and network disorganization (Mucke and Selkoe, 2012). In contrast, insoluble amyloid plaque cores from the AD cortex did not significantly alter synaptic plasticity and LTP, suggesting that plaque cores are largely inactive. However, this does not mean that insoluble amyloid plaque cores have no pathogenic role. Their accumulation may indicate that they act as reservoirs of small bioactive oligomers, and may release locally active Aβ species *in vivo* (Hardy and Selkoe, 2002; Yang et al., 2017). Hence, these studies concluded that soluble Aβ oligomers can impair synapse structure and function, and dimers

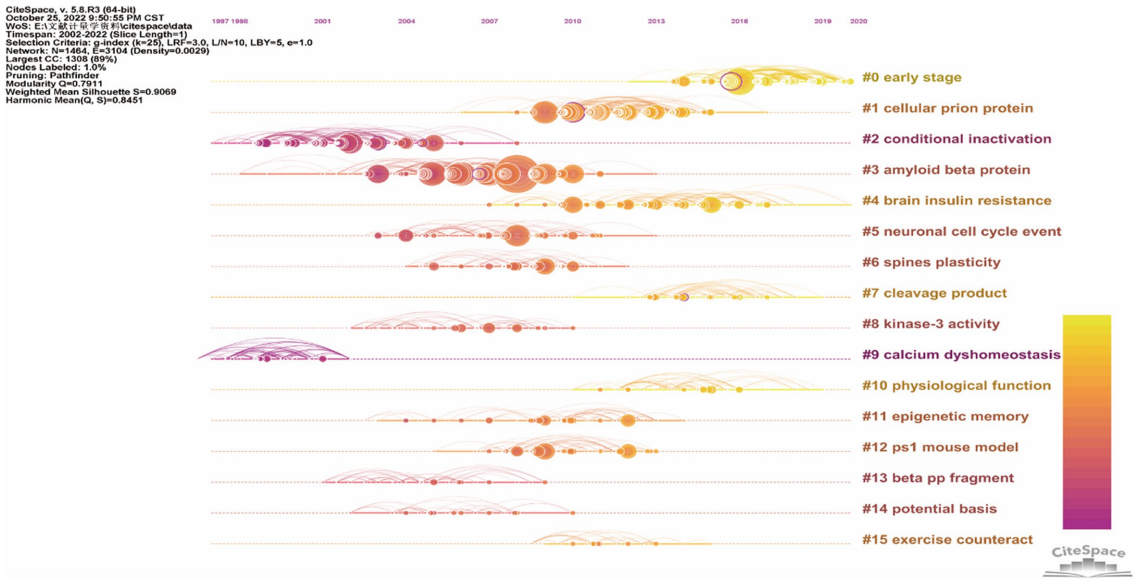

FIGURE 6
The timeline view of co-citation references clusters based on CiteSpace. The bold timeline indicated that the clustering topic was a hotspot during that period of time. Citation tree rings which had different sizes on the timeline represented some key documents with a high citation frequency.

are the smallest synaptotoxic species (Shankar et al., 2008). In addition, Aβ oligomers can interact with astrocytes and microglia. For instance, Aβ oligomers have been demonstrated to trigger astrogliosis and induce ROS generation in activated astrocytes (Wyssenbach et al., 2016; Pereira Diniz et al., 2017). As for microglia, it is possible that Aβ oligomers have a role in attracting microglia to plaques, while Aβ oligomers can also trigger a switch in microglial phenotype to pro-inflammatory phenotype, leading to produce excessive inflammatory factors (El-Shimy et al., 2015; Cline et al., 2018). These inflammatory factors, such as aberrant tumor necrosis factor (TNF), can cause synaptic dysfunction and memory loss (Ledo et al., 2016). Thus, the role of Aβ oligomers in the pathogenesis of AD is indispensable.

Research fronts of synaptic plasticity in Alzheimer's disease

Research fronts are the emerging hotspots or research topics. The timeline view of co-citation references clusters revealed that "early stage" has increasingly gained researchers' attention. Neuroinflammation, microglia and alpha synuclein have become the focal points of recent studies according to the analysis of keywords citation bursts. Although the hypothesis of amyloid-β deposition and neurofibrillary tangles can explain many aspects of AD pathogenesis, there still exist many pathological processes that cannot be sufficiently illustrated with this hypothesis. Hence, in the following discussion, we particularly focused on the emerging topic terms and the associated

TABLE 4 List of top 5 high cited reference.

Reference	Total citations	Author (year)
Amyloid-beta protein dimers isolated directly from Alzheimer's brains impair synaptic plasticity and memory	512	Shankar et al. (2008)
Naturally secreted oligomers of amyloid β protein potently inhibit hippocampal long-term potentiation in vivo	397	Walsh et al. (2002)
Alzheimer's Disease Is a Synaptic Failure	367	Selkoe (2002)
The amyloid hypothesis of Alzheimer's disease: progress and problems on the road to therapeutics	340	Hardy and Selkoe (2002)
Diffusible, nonfibrillar ligands derived from Abeta1-42 are potent central nervous system neurotoxins	265	Lambert (1998)

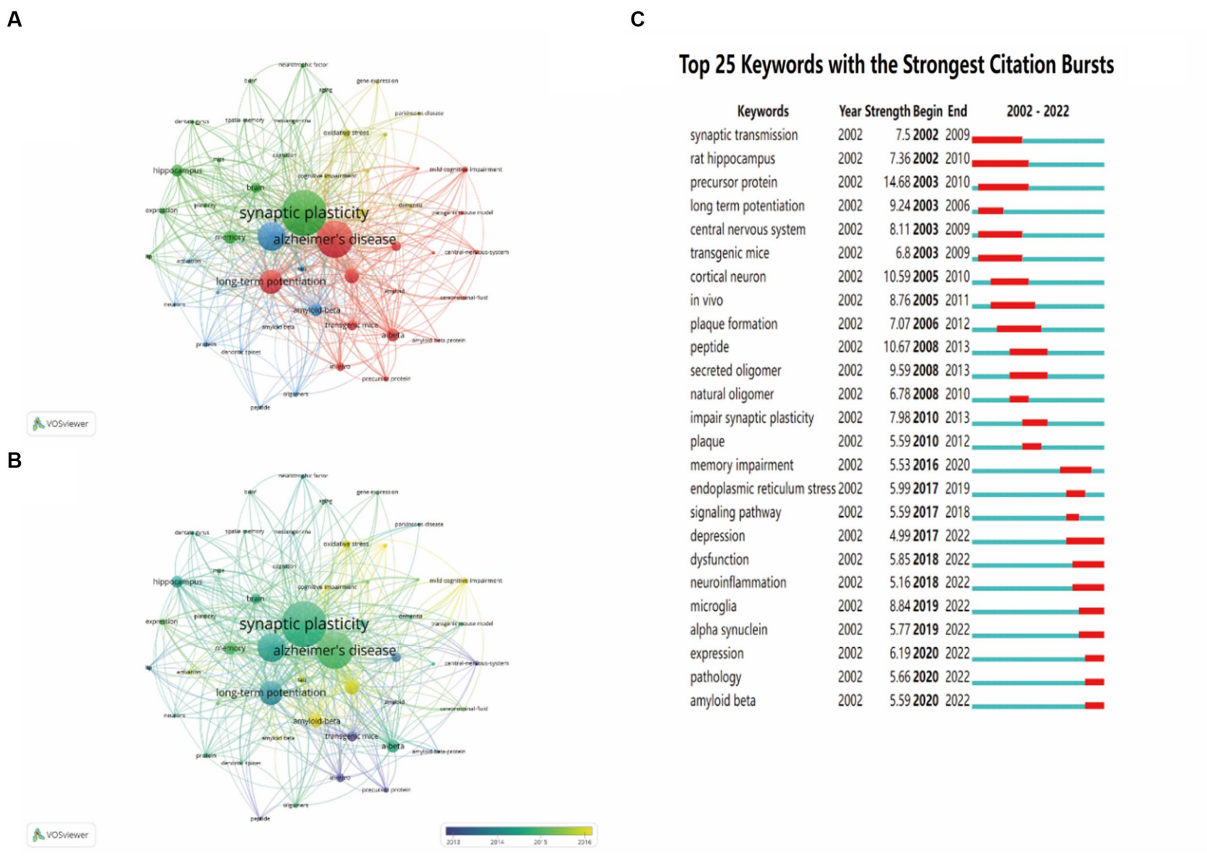

FIGURE 7
The analysis of keywords co-occurrence and keywords citation bursts. **(A)** The co-occurrence network visualization map of all keywords was based on VOSviewer. **(B)** The overlay visualization map of all keywords was based on VOSviewer. **(C)** The top 25 keywords with the strongest citation bursts were based on CiteSpace. Keywords marked in red indicated a sudden increase in usage frequency of this keyword during that period. Blue represented a relatively unpopular period of time.

publications, which can provide researchers new insights into the field of AD.

Neuroinflammation plays a significant role in the pathogenesis of AD with the discovery of increased levels of inflammatory markers. In addition, AD risk genes are identified associated with innate immune functions in patients. Neuroinflammation is intended to be a defense mechanism that can protect the body from removing or inhibiting diverse pathogens, but sustained inflammatory responses can induce neurotoxicity (Hickman et al., 2018).

In recent years, many researchers are prone to investigate the role of microglia in the development of AD. According to the results of keywords citation bursts, microglia has become one of the research hotspots. Microglia is the resident macrophage of the central nervous system (CNS) and the first responder to pathological insults, which play a critical role in regulating inflammatory processes of the CNS (Morales et al., 2014; Unger et al., 2020). It can act as the antigen-presenting cell to phagocytose the toxic product and release cytotoxic factors in order to protect the brain (Morales et al., 2014). Under normal conditions, microglia primarily exist in a resting state and have significant physiological functions in the regulation of synaptic transmission, neuronal activity and synaptic pruning (Akiyoshi et al., 2018). However, microglial excessive activation or dysfunction is positively correlated with cognitive impairment (Cornell et al., 2021). As for AD patients, extracellular amyloid-β and/or intraneuronal phosphorylated tau can both activate microglia (Merighi et al., 2022). Recent studies have proved that microglia participate in the modulation of synaptic plasticity, including LTP and LTD which are the cellular mechanism of learning and memory (Innes et al., 2019; Zhou et al., 2019). In the healthy brain, there is a balance between proinflammatory and anti-inflammatory factors released by microglia, while if disrupted, it can influence synaptic plasticity (Golia et al., 2019). Traditionally, microglia can be divided into the M1 (classically activated) and M2 (alternatively activated) based on their activation pattern. However, the switch between two definite phenotypes of microglia and astrocytes is complicated and may differ with the severity and stage of neurodegenerative disease (Kwon and Koh, 2020). At the beginning of Aβ pathology, microglia can exert a neuroprotective role by degrading and removing Aβ and tau, while with the evolution of AD, increasing in the size and number of amyloid plaques, the clearance ability of microglia decrease (Mawuenyega et al., 2010). Different species of Aβ aggregate can induce microglia activation and the production of pro-inflammatory cytokines (such as IL-1β, IL-6, IL-8 and TNF) in order to exhibit the neuroprotective effect, but these microglia cells later transfer to the neurotoxic (pro-inflammatory) phenotype resulting in neuronal dysfunction and death (Jimenez et al., 2008; Tang and Le, 2016). Pettigrew et al. reported that overexpression of TNF-α results in an increase in LTP, suggesting the synaptic networks may be hyperexcitable (Pettigrew et al., 2016). Nevertheless, compared to TNF-α, IL-β, another proinflammatory factor released by microglia, impairs LTP in the CA1 region (Hoshino et al., 2017). In conclusion, these results indicate that proinflammatory cytokines released by microglia have diverse effects on LTP and synaptic plasticity.

In addition to microglia, T cells, the crucial immune cells of the adaptive immune system, are also involved in AD pathology (Dai and Shen, 2021). During AD progression, activated CD8+ T and CD4+ T cells, the two major T-cell subsets, can gradually infiltrate into brain parenchyma due to increased permeability of the blood–brain barrier (BBB) (Cheng et al., 2014). Increased T cells promote crosstalk with microglia in the brain. Depletion of microglia eliminates T cell infiltration and depletion of T cells also largely blocks microglia activation (Chen et al., 2023). Recent studies demonstrated that the number of T cells were increased in brain regions with tauopathy rather than amyloid pathology alone (Merlini et al., 2018; Chen et al., 2023). Depleting T cells significantly reduce p-tau staining and tau-mediated neurodegeneration, demonstrating the critical role of T cells in mediating tau pathology (Chen et al., 2023). Further illuminating the correlation between T cells and tau protein might yield novel therapeutic targets for preventing neurodegeneration in AD.

Alpha-synuclein (α-syn) is considered the primary constituent protein of Lewy bodies, which is the defining hallmark of Lewy body dementia (LBD) including Parkinson's disease dementia (PDD) and dementia with Lewy bodies (DLB) (Hijaz and Volpicelli-Daley, 2020; Koga et al., 2021). α-Syn located at pre-synaptic terminals and was correlated with the distal reserve pool of synaptic vesicles. Knocking down or overexpression of α-syn resulted in deficiencies in synaptic transmissions, demonstrating that α-syn played a significant role in the regulation of neurotransmitter release and synaptic plasticity (Lashuel et al., 2013). α-Syn oligomers rather than monomers or fibrils can impair LTP through activated NMDA receptor (Diógenes et al., 2012). Consequently, the synaptic plasticity was compromised in AD patients. In recent years, researchers confirmed that α-syn oligomers could promote the formations of Aβ oligomers and stabilize their cross-β structures, whereas α-syn monomers suppressed Aβ aggregation, indicating that distinct structural forms of α-syn had different influences on Aβ aggregation (Atsmon-Raz and Miller, 2016; Chia et al., 2017; Shim et al., 2022). Hence, subsequent studies should be more focused on the different structural forms of α-syn to further illustrate the correlation between α-syn and Aβ. In addition, α-syn has also been reported as a protein that can directly interact with tau (Pan et al., 2022). The two proteins could promote mutual homogenous/heterogeneous aggregations. For example, α-syn could induce tau aggregation, in turn, tau could facilitate the fibrillization of α-syn (Hijaz and Volpicelli-Daley, 2020). Previous studies have demonstrated that the C-terminal of α-syn can directly interact with the microtubule binding domain of tau (Waxman and Giasson, 2011; Dasari et al., 2019). Interactions between these two proteins also accelerated tau phosphorylation, suggesting that increased α-syn in AD may promote tau pathology and further exacerbate cognitive decline (Bassil et al., 2020; Hu et al., 2020). Altogether, α-syn could be an emerging pathophysiological biomarker of AD and it may be crucial for assessing potential therapeutics for AD.

Limitations

The current study had several limitations. First, we only analyzed two document types (reviews and articles), other publications such as books or conference papers are not collected by bibliometric searches. Second, only English publications were enrolled in our research. Other significant articles using non-English languages, although few, were not considered. Third, we only indexed the documents in the WoSCC database due to the requirements of the CiteSpace software. Therefore, we may not analyze relevant articles only found in other databases such as PubMed and Scopus.

Conclusion

This study provided knowledge about synaptic plasticity in AD from a visualization and bibliometric perspective. We analyzed the publication trends hotspots and research fronts. In terms of publication trends, research on synaptic plasticity in AD steadily increased. Currently, the hotspots and research fronts have transferred from the synaptic transmission and precursor protein to neuroinflammation, microglia and alpha synuclein. Apart from the mechanism of Aβ peptides and hyper phosphorylated tau, researchers attempt to discover new mechanisms to explain some pathological processes that cannot be well illustrated with the traditional mechanism. This bibliometric study is beneficial for researchers to understand AD better by analyzing these development trends.

Data availability statement

The raw data supporting the conclusions of this article will be made available by the authors, without undue reservation.

Author contributions

JY conceived the project and designed the studies. YZ and JZ searched the literature together. YZ and YW analyzed the data. JY and YZ drafted the figures and wrote the manuscript. All authors contributed to the article and approved the submitted version.

Funding

This study was supported by grants (No. 82171183 and No. 81771269) from the National Natural Science Foundation of China. The funders had no role in the study design, data collection and analysis, decision to publish, or preparation of the manuscript.

Conflict of interest

The authors declare that the research was conducted in the absence of any commercial or financial relationships that could be construed as a potential conflict of interest.

Publisher's note

All claims expressed in this article are solely those of the authors and do not necessarily represent those of their affiliated organizations, or those of the publisher, the editors and the reviewers. Any product that may be evaluated in this article, or claim that may be made by its manufacturer, is not guaranteed or endorsed by the publisher.

References

Abbott, A. (2018). Is 'friendly fire' in the brain provoking Alzheimer's disease? *Nature* 556, 426–428. doi: 10.1038/d41586-018-04930-7

Akiyoshi, R., Wake, H., Kato, D., Horiuchi, H., Ono, R., Ikegami, A., et al. (2018). Microglia enhance synapse activity to promote local network synchronization. *eNeuro* 5:ENEURO.0088-18.2018. doi: 10.1523/ENEURO.0088-18.2018

Atsmon-Raz, Y., and Miller, Y. (2016). Non-amyloid-β component of human α-Synuclein oligomers induces formation of new Aβ oligomers: insight into the mechanisms that link Parkinson's and Alzheimer's diseases. *ACS Chem. Neurosci.* 7, 46–55. doi: 10.1021/acschemneuro.5b00204

Bassil, F., Brown, H. J., Pattabhiraman, S., Iwasyk, J. E., Maghames, C. M., Meymand, E. S., et al. (2020). Amyloid-Beta (Aβ) plaques promote seeding and spreading of alpha-Synuclein and tau in a mouse model of Lewy body disorders with Aβ pathology. *Neuron* 105, 260–275.e6. doi: 10.1016/j.neuron.2019.10.010

Bindocci, E., Savtchouk, I., Liaudet, N., Becker, D., Carriero, G., and Volterra, A. (2017). Three-dimensional Ca2+ imaging advances understanding of astrocyte biology. *Science* 356:eaai8185. doi: 10.1126/science.aai8185

Chen, C. (2004). Searching for intellectual turning points: progressive knowledge domain visualization. *Proc. Natl. Acad. Sci.* 101, 5303–5310. doi: 10.1073/pnas.0307513100

Chen, C., Dubin, R., and Kim, M. C. (2014). Emerging trends and new developments in regenerative medicine: a scientometric update (2000 – 2014). *Expert. Opin. Biol. Ther.* 14, 1295–1317. doi: 10.1517/14712598.2014.920813

Chen, X., Firulyova, M., Manis, M., Herz, J., Smirnov, I., Aladyeva, E., et al. (2023). Microglia-mediated T cell infiltration drives neurodegeneration in tauopathy. *Nature* 615, 668–677. doi: 10.1038/s41586-023-05788-0

Cheng, X., He, P., Yao, H., Dong, Q., Li, R., and Shen, Y. (2014). Occludin deficiency with BACE1 elevation in cerebral amyloid angiopathy. *Neurology* 82, 1707–1715. doi: 10.1212/WNL.0000000000000403

Chia, S., Flagmeier, P., Habchi, J., Lattanzi, V., Linse, S., Dobson, C. M., et al. (2017). Monomeric and fibrillar α-synuclein exert opposite effects on the catalytic cycle that promotes the proliferation of Aβ42 aggregates. *Proc. Natl. Acad. Sci. U. S. A.* 114, 8005–8010. doi: 10.1073/pnas.1700239114

Cline, E. N., Bicca, M. A., Viola, K. L., and Klein, W. L. (2018). The amyloid-β oligomer hypothesis: beginning of the third decade. *J. Alzheimers Dis.* 64, S567–S610. doi: 10.3233/JAD-179941

Cornell, J., Salinas, S., Huang, H.-Y., and Zhou, M. (2021). Microglia regulation of synaptic plasticity and learning and memory. *Neural Regen. Res.* 17, 705–716. doi: 10.4103/1673-5374.322423

Craft, S., Claxton, A., Baker, L. D., Hanson, A. J., Cholerton, B., Trittschuh, E. H., et al. (2017). Effects of regular and long-acting insulin on cognition and Alzheimer's disease biomarkers: a pilot clinical trial. *J. Alzheimers Dis.* 57, 1325–1334. doi: 10.3233/JAD-161256

Dai, L., and Shen, Y. (2021). Insights into T-cell dysfunction in Alzheimer's disease. *Aging Cell* 20:e13511. doi: 10.1111/acel.13511

Dasari, A. K. R., Kayed, R., Wi, S., and Lim, K. H. (2019). Tau interacts with the C-terminal region of α-synuclein, promoting formation of toxic aggregates with distinct molecular conformations. *Biochemistry* 58, 2814–2821. doi: 10.1021/acs.biochem.9b00215

Diógenes, M. J., Dias, R. B., Rombo, D. M., Vicente Miranda, H., Maiolino, F., Guerreiro, P., et al. (2012). Extracellular alpha-Synuclein oligomers modulate synaptic transmission and impair LTP via NMDA-receptor activation. *J. Neurosci.* 32, 11750–11762. doi: 10.1523/JNEUROSCI.0234-12.2012

El-Shimy, I. A., Heikal, O. A., and Hamdi, N. (2015). Minocycline attenuates Aβ oligomers-induced pro-inflammatory phenotype in primary microglia while enhancing Aβ fibrils phagocytosis. *Neurosci. Lett.* 609, 36–41. doi: 10.1016/j.neulet.2015.10.024

Golia, M. T., Poggini, S., Alboni, S., Garofalo, S., Ciano Albanese, N., Viglione, A., et al. (2019). Interplay between inflammation and neural plasticity: both immune activation and suppression impair LTP and BDNF expression. *Brain Behav. Immun.* 81, 484–494. doi: 10.1016/j.bbi.2019.07.003

Hardy, J., and Selkoe, D. J. (2002). The amyloid hypothesis of Alzheimer's disease: Progress and problems on the road to therapeutics. *Science* 297, 353–356. doi: 10.1126/science.1072994

Hickman, S., Izzy, S., Sen, P., Morsett, L., and Khoury, J. E. (2018). Microglia in neurodegeneration. *Nat. Neurosci.* 21, 1359–1369. doi: 10.1038/s41593-018-0242-x

Hijaz, B. A., and Volpicelli-Daley, L. A. (2020). Initiation and propagation of α-synuclein aggregation in the nervous system. *Mol. Neurodegener.* 15:19. doi: 10.1186/s13024-020-00368-6

Hoshino, K., Hasegawa, K., Kamiya, H., and Morimoto, Y. (2017). Synapse-specific effects of IL-1β on long-term potentiation in the mouse hippocampus. *Biomed. Res.* 38, 183–188. doi: 10.2220/biomedres.38.183

Hu, S., Hu, M., Liu, J., Zhang, B., Zhang, Z., Zhou, F. H., et al. (2020). Phosphorylation of tau and α-Synuclein induced neurodegeneration in MPTP mouse model of Parkinson's disease. *Neuropsychiatr. Dis. Treat.* 16, 651–663. doi: 10.2147/NDT.S235562

Innes, S., Pariante, C. M., and Borsini, A. (2019). Microglial-driven changes in synaptic plasticity: a possible role in major depressive disorder. *Psychoneuroendocrinology* 102, 236–247. doi: 10.1016/j.psyneuen.2018.12.233

Jimenez, S., Baglietto-Vargas, D., Caballero, C., Moreno-Gonzalez, I., Torres, M., Sanchez-Varo, R., et al. (2008). Inflammatory response in the hippocampus of PS1M146L/APP751SL mouse model of Alzheimer's disease: age-dependent switch in the microglial phenotype from alternative to classic. *J. Neurosci.* 28, 11650–11661. doi: 10.1523/JNEUROSCI.3024-08.2008

Koga, S., Sekiya, H., Kondru, N., Ross, O. A., and Dickson, D. W. (2021). Neuropathology and molecular diagnosis of Synucleinopathies. *Mol. Neurodegener.* 16:83. doi: 10.1186/s13024-021-00501-z

Krzeptowski, W., Hess, G., and Pyza, E. (2018). Circadian plasticity in the brain of insects and rodents. *Front. Neural Circuits* 12:32. doi: 10.3389/fncir.2018.00032

Kwon, H. S., and Koh, S.-H. (2020). Neuroinflammation in neurodegenerative disorders: the roles of microglia and astrocytes. *Transl. Neurodegener.* 9:42. doi: 10.1186/s40035-020-00221-2

Lashuel, H. A., Overk, C. R., Oueslati, A., and Masliah, E. (2013). The many faces of α-synuclein: from structure and toxicity to therapeutic target. *Nat. Rev. Neurosci.* 14, 38–48. doi: 10.1038/nrn3406

Ledo, J. H., Azevedo, E. P., Beckman, D., Ribeiro, F. C., Santos, L. E., Razolli, D. S., et al. (2016). Cross talk between brain innate immunity and serotonin Signaling underlies depressive-like behavior induced by Alzheimer's amyloid-β oligomers in mice. *J. Neurosci.* 36, 12106–12116. doi: 10.1523/JNEUROSCI.1269-16.2016

Marsh, S. E., Abud, E. M., Lakatos, A., Karimzadeh, A., Yeung, S. T., Davtyan, H., et al. (2016). The adaptive immune system restrains Alzheimer's disease pathogenesis by modulating microglial function. *Proc. Natl. Acad. Sci. U. S. A.* 113, E1316–E1325. doi: 10.1073/pnas.1525466113

Mawuenyega, K. G., Sigurdson, W., Ovod, V., Munsell, L., Kasten, T., Morris, J. C., et al. (2010). Decreased clearance of CNS amyloid-β in Alzheimer's disease. *Science* 330:1774. doi: 10.1126/science.1197623

Mercerón-Martínez, D., Ibaceta-González, C., Salazar, C., Almaguer-Melian, W., Bergado-Rosado, J. A., and Palacios, A. G. (2021). Alzheimer's disease, neural plasticity, and functional recovery. *J. Alzheimers Dis.* 82, S37–S50. doi: 10.3233/JAD-201178

Merighi, S., Nigro, M., Travagli, A., and Gessi, S. (2022). Microglia and Alzheimer's disease. *Int. J. Mol. Sci.* 23:12990. doi: 10.3390/ijms232112990

Merlini, M., Kirabali, T., Kulic, L., Nitsch, R. M., and Ferretti, M. T. (2018). Extravascular CD3+ T cells in brains of Alzheimer disease patients correlate with tau but not with amyloid pathology: An Immunohistochemical study. *Neurodegener Dis* 18, 49–56. doi: 10.1159/000486200

Morales, I., Guzmán-Martínez, L., Cerda-Troncoso, C., Farías, G. A., and Maccioni, R. B. (2014). Neuroinflammation in the pathogenesis of Alzheimer's disease. A rational framework for the search of novel therapeutic approaches. *Front. Cell. Neurosci.* 8:112. doi: 10.3389/fncel.2014.00112

Mucke, L., and Selkoe, D. J. (2012). Neurotoxicity of amyloid β-protein: synaptic and network dysfunction. *Cold Spring Harb. Perspect. Med.* 2:a006338. doi: 10.1101/cshperspect.a006338

Mummery, C. J., Börjesson-Hanson, A., Blackburn, D. J., Vijverberg, E. G. B., de Deyn, P. P., Ducharme, S., et al. (2023). Tau-targeting antisense oligonucleotide MAPTRx in mild Alzheimer's disease: a phase 1b, randomized, placebo-controlled trial. *Nat. Med.* 29, 1437–1447. doi: 10.1038/s41591-023-02326-3

Nabavi, S., Fox, R., Proulx, C. D., Lin, J. Y., Tsien, R. Y., and Malinow, R. (2014). Engineering a memory with LTD and LTP. *Nature* 511, 348–352. doi: 10.1038/nature13294

Naseri, N. N., Wang, H., Guo, J., Sharma, M., and Luo, W. (2019). The complexity of tau in Alzheimer's disease. *Neurosci. Lett.* 705, 183–194. doi: 10.1016/j.neulet.2019.04.022

Pan, L., Li, C., Meng, L., Tian, Y., He, M., Yuan, X., et al. (2022). Tau accelerates α-synuclein aggregation and spreading in Parkinson's disease. *Brain* 145, 3454–3471. doi: 10.1093/brain/awac171

Panza, F., Lozupone, M., Logroscino, G., and Imbimbo, B. P. (2019). A critical appraisal of amyloid-β-targeting therapies for Alzheimer disease. *Nat. Rev. Neurol.* 15, 73–88. doi: 10.1038/s41582-018-0116-6

Pereira Diniz, L., Tortelli, V., Matias, I., Morgado, J., Bérgamo Araujo, A. P., Melo, H. M., et al. (2017). Astrocyte transforming growth factor Beta 1 protects synapses against Aβ oligomers in Alzheimer's disease model. *J. Neurosci.* 37, 6797–6809. doi: 10.1523/JNEUROSCI.3351-16.2017

Pettigrew, L. C., Kryscio, R. J., and Norris, C. M. (2016). The TNFα-transgenic rat: hippocampal synaptic integrity, cognition, function, and post-ischemic cell loss. *PLoS One* 11:e0154721. doi: 10.1371/journal.pone.0154721

Polanco, J. C., Li, C., Bodea, L.-G., Martinez-Marmol, R., Meunier, F. A., and Götz, J. (2018). Amyloid-β and tau complexity — towards improved biomarkers and targeted therapies. *Nat. Rev. Neurol.* 14, 22–39. doi: 10.1038/nrneurol.2017.162

Santello, M., Toni, N., and Volterra, A. (2019). Astrocyte function from information processing to cognition and cognitive impairment. *Nat. Neurosci.* 22, 154–166. doi: 10.1038/s41593-018-0325-8

Scheltens, P., de Strooper, B., Kivipelto, M., Holstege, H., Chételat, G., Teunissen, C. E., et al. (2021). Alzheimer's disease. *Lancet* 397, 1577–1590. doi: 10.1016/S0140-6736(20)32205-4

Selkoe, D. J. (2002). Alzheimer's disease is a synaptic failure. *Science* 298, 789–791. doi: 10.1126/science.1074069

Shankar, G. M., Li, S., Mehta, T. H., Garcia-Munoz, A., Shepardson, N. E., Smith, I., et al. (2008). Amyloid β-protein dimers isolated directly from Alzheimer brains impair synaptic plasticity and memory. *Nat. Med.* 14, 837–842. doi: 10.1038/nm1782

Shim, K. H., Kang, M. J., Youn, Y. C., An, S. S. A., and Kim, S. (2022). Alpha-synuclein: a pathological factor with Aβ and tau and biomarker in Alzheimer's disease. *Alzheimers Res. Ther.* 14:201. doi: 10.1186/s13195-022-01150-0

Spillantini, M. G., Schmidt, M. L., Lee, V. M.-Y., Trojanowski, J. Q., Jakes, R., and Goedert, M. (1997). α-Synuclein in Lewy bodies. *Nature* 388, 839–840. doi: 10.1038/42166

Stobart, J. L., Ferrari, K. D., Barrett, M. J. P., Glück, C., Stobart, M. J., Zuend, M., et al. (2018). Cortical circuit activity evokes rapid astrocyte calcium signals on a similar timescale to neurons. *Neuron* 98, 726–735.e4. doi: 10.1016/j.neuron.2018.03.050

Sweatt, J. D. (2016). Neural plasticity and behavior – sixty years of conceptual advances. *J. Neurochem.* 139, 179–199. doi: 10.1111/jnc.13580

Tang, Y., and Le, W. (2016). Differential roles of M1 and M2 microglia in neurodegenerative diseases. *Mol. Neurobiol.* 53, 1181–1194. doi: 10.1007/s12035-014-9070-5

Unger, M. S., Li, E., Scharnagl, L., Poupardin, R., Altendorfer, B., Mrowetz, H., et al. (2020). CD8+ T-cells infiltrate Alzheimer's disease brains and regulate neuronal- and synapse-related gene expression in APP-PS1 transgenic mice. *Brain Behav. Immun.* 89, 67–86. doi: 10.1016/j.bbi.2020.05.070

Walsh, D. M., Klyubin, I., Fadeeva, J. V., Cullen, W. K., Anwyl, R., Wolfe, M. S., et al. (2002). Naturally secreted oligomers of amyloid β protein potently inhibit hippocampal long-term potentiation in vivo. *Nature* 416, 535–539. doi: 10.1038/416535a

Waxman, E. A., and Giasson, B. I. (2011). Induction of intracellular tau aggregation is promoted by α-Synuclein seeds and provides novel insights into the hyperphosphorylation of tau. *J. Neurosci.* 31, 7604–7618. doi: 10.1523/JNEUROSCI.0297-11.2011

Wyssenbach, A., Quintela, T., Llavero, F., Zugaza, J. L., Matute, C., and Alberdi, E. (2016). Amyloid β-induced astrogliosis is mediated by β1-integrin via NADPH oxidase 2 in Alzheimer's disease. *Aging Cell* 15, 1140–1152. doi: 10.1111/acel.12521

Yang, T., Li, S., Xu, H., Walsh, D. M., and Selkoe, D. J. (2017). Large soluble oligomers of amyloid β-protein from Alzheimer brain are far less neuroactive than the smaller oligomers to which they dissociate. *J. Neurosci.* 37, 152–163. doi: 10.1523/JNEUROSCI.1698-16.2016

Yu, W., and Lu, B. (2012). Synapses and dendritic spines as pathogenic targets in Alzheimer's disease. *Neural Plast.* 2012:247150, 1–8. doi: 10.1155/2012/247150

Zhou, L.-J., Peng, J., Xu, Y.-N., Zeng, W.-J., Zhang, J., Wei, X., et al. (2019). Microglia are indispensable for synaptic plasticity in the spinal dorsal horn and chronic pain. *Cell Rep.* 27, 3844–3859.e6. doi: 10.1016/j.celrep.2019.05.087

Zhou, Y., Song, W. M., Andhey, P. S., Swain, A., Levy, T., Miller, K. R., et al. (2020). Human and mouse single-nucleus transcriptomics reveal TREM2-dependent and -independent cellular responses in Alzheimer's disease. *Nat. Med.* 26, 131–142. doi: 10.1038/s41591-019-0695-9

frontiers | Frontiers in Aging Neuroscience

TYPE Original Research
PUBLISHED 09 November 2023
DOI 10.3389/fnagi.2023.1292417

OPEN ACCESS

EDITED BY
Woon-Man Kung,
Chinese Culture University, Taiwan

REVIEWED BY
Carlos Márquez,
University of Chile, Chile
Feng Han,
University of California, Berkeley, United States
Silvia Giovannini,
Catholic University of the Sacred Heart, Rome, Italy

*CORRESPONDENCE
Valeria Blasi
✉ vblasi@dongnocchi.it

RECEIVED 15 September 2023
ACCEPTED 26 October 2023
PUBLISHED 09 November 2023

CITATION
Isernia S, Blasi V, Baglio G, Cabinio M, Cecconi P, Rossetto F, Cazzoli M, Blasi F, Bruckmann C, Giunco F, Sorbi S, Clerici M and Baglio F (2023) The key role of depression and supramarginal gyrus in frailty: a cross-sectional study.
Front. Aging Neurosci. 15:1292417.
doi: 10.3389/fnagi.2023.1292417

The key role of depression and supramarginal gyrus in frailty: a cross-sectional study

Sara Isernia[1], Valeria Blasi[1]*, Gisella Baglio[1], Monia Cabinio[1], Pietro Cecconi[1], Federica Rossetto[1], Marta Cazzoli[1], Francesco Blasi[2], Chiara Bruckmann[2], Fabrizio Giunco[1], Sandro Sorbi[1], Mario Clerici[1,3] and Francesca Baglio[1]

[1]IRCCS Fondazione Don Carlo Gnocchi ONLUS, Milan, Italy, [2]Fondazione Istituto FIRC di Oncologia Molecolare, Milan, Italy, [3]Department of Pathophysiology and Transplantation, University of Milan, Milan, Italy

Background: The age-related decrease in reserve and resistance to stressors is recognized as frailty, one of the most significant challenges identified in recent years. Despite a well-acknowledged association of frailty with cognitive impairment, depression, and gray matter morphology, no clear data are available regarding the nature of this relationship. This cross-sectional study aims to disentangle the role of the behavioral, neuropsychological, and neural components as predictors or moderators of frailty.

Methods: Ninety-six older adults (mean age = 75.49 ± 6.62) were consecutively enrolled and underwent a clinical and MRI (3 T) evaluation to assess frailty, physical activity, global cognitive level, depression, wellbeing, autonomy in daily living, cortical thickness, and subcortical volumes.

Results: Results showed a full mediation of depression on the link between cortical thickness and frailty, while the cognitive level showed no significant mediating role. In particular, left supramarginal thickness had a predicting role on depression, that in turn impacted frailty occurrence. Finally, handgrip weakness was an early key indicator of frailty in this study's cohort.

Conclusion: These data substantiate the role of depression in mediating the link between neural integrity of the supramarginal gyrus and frailty. In the complexity of frailty, handgrip weakness seems to be an early key indicator. These results are relevant for the design of rehabilitation interventions aimed at reversing the frail condition.

KEYWORDS

frailty, aging, depression, cognitive impairment, brain, MRI, supramarginal gyrus

1. Introduction

The age-related decrease in reserve and resistance to stressors is recognized as frailty, one of the most significant global public health challenges in recent years due to the increase in the life expectancy in the general population (Dent et al., 2019). Frailty in older adults leads to significant vulnerability to adverse events and reduced ability to recover from health issues (Clegg et al., 2013).

Frailty has been conceptualized according to two principal models: the accumulative deficits multidimensional model, initially conceptualized by Mitnitski et al. (2001), and the frailty phenotype, proposed by Fried et al. (2001). The first is based on the Frailty Index (Rockwood and Mitnitski, 2007), calculated based on the degree of accumulation of health deficits, including

comorbidities, psychological factors, symptoms, and disabilities. The model of the frailty phenotype, instead, defines frailty as an independent syndrome based on five physical signs/symptoms: poor handgrip strength, slow gait speed, involuntary weight loss, exhaustion, and sedentary behavior (Fried et al., 2001). The frailty phenotype has been reported as a potential transition state between healthy and pathological aging, plausibly anticipating disability (Bandeen-Roche et al., 2006; Cheung et al., 2018). In the present study, we focused on this latter conceptualization of frailty as a medical syndrome (Bandeen-Roche et al., 2006; Xue, 2011; Dent et al., 2019) whose mechanisms involved are yet to be defined. This approach was considered more suitable for identifying risk factors in this transition state with consequent relevant implications for timely and effective therapeutic strategies.

Despite a well-acknowledged association of frailty with cognitive impairment (Kelaiditi et al., 2013; Ruan et al., 2015) and depression (Soysal et al., 2017), no clear data are available regarding the nature of this relationship. Specifically, several contributions investigated a potentially reversible condition, cognitive frailty, that is the simultaneous presence of both physical frailty and cognitive impairment (Kelaiditi et al., 2013; Ruan et al., 2015), leading to an enhanced risk of neurocognitive disorders (Avila-Funes et al., 2012; Panza et al., 2015a,b), functional disability, poor quality of life, and mortality (Sternberg et al., 2011; Feng et al., 2017; Sugimoto et al., 2018). Moreover, several studies (Avila-Funes et al., 2009; Bunce et al., 2019) advocated similar risk factors for physical frailty and cognitive impairment, such as lack of physical activity, reduced social stimulation, and higher hospitalization. Furthermore, several studies highlighted the link between depression and frailty (see Soysal et al., 2017 for a review and meta-analysis), but the direction of this relation is still under debate. Depression has been considered somehow a consequence of frailty or an overlapping syndrome due to the phenotypic similarity sharing the loss of energy, fatigue, poor sleep, and reduced interest (Mezuk et al., 2012; Buigues et al., 2015; Canevelli et al., 2015; Bunt et al., 2017). Additionally, other evidence considered depression and frailty as interrelated, with each condition representing a risk factor for the other (Chang et al., 2010; Soysal et al., 2017).

In this framework, the investigation of neural integrity can help in disentangling the causal relationship between frailty phenotype, cognitive level, and depression.

From a neurobiological perspective, frailty syndrome appears to be accompanied by changes in the microstructural integrity of cortical and subcortical gray matter (Avila-Funes et al., 2017; López-Sanz et al., 2018; Maltais et al., 2020; Tian et al., 2020). Moreover, in frail subjects, reduced brain volume (Del Brutto et al., 2017) has been shown in regions important for cognition and emotion processing, such as the hippocampus, amygdala, fusiform gyrus, medial prefrontal, and orbitofrontal cortex, inferior frontal gyrus, primary somatosensory cortex, insula, superior temporal sulcus, and cerebellum. Furthermore, the mean cortical thickness of areas involved in mobility and neurodegenerative diseases has also been linked to frailty (Lu et al., 2020). Finally, several studies showed a strong association between frailty and cerebrovascular disease explored in terms of white matter hyperintensities (WMH) (Avila-Funes et al., 2017; Siejka et al., 2020; Ducca et al., 2023).

To summarize, the frailty phenotype is strictly related to cognitive decay, depression, and loss of neural integrity. What remains to be clarified is the type of relationship between these factors. In this line, our study aimed to identify the best predictors of the frailty phenotype among cognitive impairment, depression, and loss of neural integrity and to examine their causal relationship. To achieve this aim, we characterized a cohort of 96 community-dwelling older adults.

2. Methods

A cross-sectional study was performed.

2.1. Participants

Participants were recruited considering the following inclusion criteria: (i) age > 65 y; (ii) Mini-Mental State Examination (MMSE) score > 18 [according to Pezzotti et al. (2008)] to exclude severe dementia; (iii) absence of MRI exam contraindications (i.e., pacemaker, or other not-MRI compatible metallic implants or prosthesis); (iv) signed the informed consent module approved by Don Gnocchi Foundation Ethics Committee; (v) absence of diagnosis of Parkinson's Disease, Alzheimer's disease or infectious disease; (vi) absence of an unstable condition of a cardiac, vascular, pulmonary, hepatic, renal, endocrine, hematological disease; (vii) no drug and/or alcohol abuse; (viii) absence of an unstable psychiatric condition.

They were consecutively enrolled between 2019 and 2022 at the Don Gnocchi Foundation Institute, both at the Palazzolo Institute and the IRCCS *S. Maria* Nascente Rehabilitation and Care clinic: they were community-dwelling older adults attending the rehabilitation and care service at the center, available to participate in the study after physician proposing the enrolment in the research or after reading information flyers at the clinic or after word of mouth. Participants could be either attending the clinic for any health-related problem such as memory complaints, cardiac or pulmonary disease, or orthopedic problems or could be volunteers operating at the clinic or informal caregivers accompanying a patient.

2.2. Procedure

The study's participants were involved in the research by taking part in a single session lasting about 1.5 h. The session included (1) a clinical and neuropsychological evaluation by a physician and a neuropsychologist and (2) a brain structural MRI examination.

2.2.1. Clinical and neuropsychological evaluation

For the clinical evaluation, each participant was screened in terms of the frailty phenotype (Fried et al., 2001) according to Fried's criteria (unintentional weight loss ≥4.5 kg in the prior year; grip strength measured with a manual dynamometer in the lowest 20% according to gender and Body Mass Index (BMI); poor endurance/exhaustion; walking time in the slowest 20% adjusting for gender and height using the 10 M walking test (Bohannon, 1997); kcal/week expenditure in the lowest 20% assessed by Minnesota Leisure Time Activity Questionnaire (Richardson et al., 1994). People meeting three or more criteria were classified as frail, those with one or two as pre-frail, and people without any as robust. Also, the level of a sedentary lifestyle was evaluated by the Physical Activity Scale for the Elderly [PASE, (Washburn et al., 1993)].

The neuropsychological evaluation comprised the Montreal Cognitive Assessment [MoCA, (Conti et al., 2015; Santangelo et al., 2015)] to measure the global cognitive level as well as subdomains

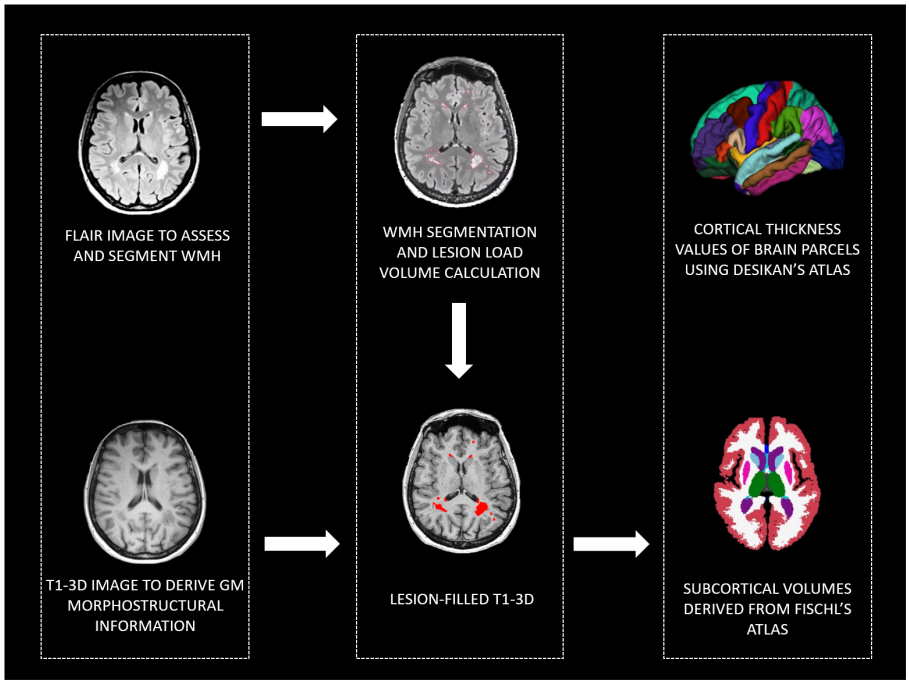

FIGURE 1
MRI pipeline to derive: WMH, cortical thickness values of brain parcels, and subcortical volumes. WMH, white matter hyperintensities; GM, gray matter, FLAIR, Fluid Attenuated Inversion Recovery; T1-3D, 3D T1 weighted.

according to the Uniform Data Set Guidelines (Dodge et al., 2020); the Center for Epidemiologic Studies Depression Scale [CES-D, (Radloff, 1977)] to assess depression symptoms; the Activity of Daily Living Inventory [ADCS-ADL, (Galasko et al., 1997; Reed et al., 2016)] to evaluate the level of autonomy in daily living; the 12-item Short Form Survey [SF12, (Jenkinson et al., 2001)] to measure physical and mental health-related wellbeing; the EuroQoL-5Dimensions-5Levels (Balestroni and Bertolotti, 2012) to measure the quality of life.

2.2.2. Brain structural MRI examination

To investigate brain morphology, all participants were given a single MRI examination (3 T Siemens PRISMA scanner) including T1-3D (MPRAGE, 0.8 mm^3, TR/TE: 2,300/3.1, FOV: 256 × 240 mm) to study brain morphometry; FLAIR (0.4 × 0.4 × 1 mm^3, TR/TE, 5,000/394 ms, FOV, 256 × 230 mm) to assess WMH; T2-weighted to exclude gross brain abnormalities. To extract morphometrical data, after manual segmentation of WMH on FLAIR acquisition, T1-3D images have been lesion filled and analyzed using the recon-all pipeline of Freesurfer software (v. 6.0).[1] Manual quality controls were performed according to Klapwijk et al. (2019). Manual corrections have been done when necessary. Brain parcellation was performed according to Fischl et al. (2002) and Desikan et al. (2006) atlases to extract brain thickness and subcortical volumes. Moreover, to control for possible cerebrovascular disease involvement, the total volume of the WMH was calculated (see Figure 1 for a graphical representation of the MRI processing steps). Extracted data have been included in second-level statistics, and subcortical volumes and WMH total volume have been normalized using total intracranial volume before entering statistical models.

1 https://surfer.nmr.mgh.harvard.edu/

2.3. Statistical analyses

JASP (v. 0.16.1.0; JASP Team 2020) software was utilized for the statistical analyses.

To check the normality distribution of variables, the Kolmogorov–Smirnov normality test, visual inspection of the histogram plot, skewness, and kurtosis were considered, and parametric or non-parametric statistical tests were used as adequate.

Descriptive statistics: to describe the demographics, the clinical and neural profile of participants, the means, medians, interquartile range (IDR), standard deviation, and frequencies were computed. Also, for each subject, the frailty level was considered by computing the frailty score by counting the number of physical criteria of Fried's frailty phenotype reported (0–5).

Direct group comparisons: to compare demographics, clinical, and neural profiles among Frail, Pre-Frail, and Robust groups, ANCOVA was performed (covariate: age for clinical variables; age and gender for neural variables). The *post hoc* test was computed to identify significant pairwise contrasts between groups. To compare nominal variables among groups, Chi-squared was utilized.

Correlation analyses: the association between frailty, clinical and neural profile (including only regions significantly different between groups at the ANCOVA analyses) was investigated by running partial correlations (covariate: age for clinical variables; age and gender for neural variables). According to Bonferroni's correction, a value of p threshold of 0.002 for clinical variables and 0.007 for neural variables was set to reduce the rate of false positives.

Regression analyses: clinical and neural indexes correlated with frailty scores were inserted as potential predictors in binary logistic regression. Regardless of the statistical significance, gender, age, and

MoCA were inserted into the model. The backward stepwise (Wald) option was used as the selection method. The binary dependent variable was group (pre-frail and frail vs. robust subjects).

Mediation analyses: to test the possible mediator role of clinical variables on the link between neural indexes and frailty, a mediation analysis was performed using the Structural Equation Modeling (SEM) module of JASP software (Biesanz et al., 2010). In detail, we explored: (1) the relationship between neural indexes (predictor, X) and frailty (outcome, Y) (direct effect of X on Y), (2) the relationship between clinical variables (moderator, M) and frailty (Y), (3) the relationship between neural indexes (X) and frailty (Y) following the incorporation of clinical variables (M) (indirect effect). The role of neural indices as moderators was also explored. The standard error estimation was computed (Robust Method option in JASP). All the analyses were adjusted for two covariates: age and sex.

Sample size calculation: the *a-priori* calculation of the study sample size was performed with G*Power software. To identify significant predictors of frailty in a multiple regression model, considering seven predictors in the model, a total sample size of about 90 subjects assured a good power (1-beta error probability = 0.90) with an alpha threshold = 0.05 and an effect size $f^2 = 0.15$.

3. Results

3.1. Participants

Overall, a 116 subjects were enrolled in the study as potentially eligible for research participation. Twenty participants were excluded from the analyses (11 did not complete the MRI examination, and 9 presented low-quality MRI data, such as movement artifacts due to a head motion). In total, 96 participants (58 females, mean age ± standard deviation = 75.49 ± 6.62, mean education ± standard deviation = 11.29 ± 3.85) were considered in the analyses. Among these, 17 were classified as frail, 45 were pre-frail, and 34 were robust.

3.2. Descriptive statistics: clinical and neuropsychological evaluation

The three groups showed significant differences in years of age (Frail > Pre-frail > Robust), depression level (CES-D, Frail > Pre-frail > Robust), physical health (SF-12, Frail < Pre-frail < Robust), and quality of life (EQ5D5L, Frail < Pre-frail < Robust). Also, the Robust group reported a higher score compared to Pre-frail and Frail group in the global cognitive level (MoCA, MMSE), especially attention (Robust > Frail, Pre-frail), physical activity in daily living (PASE, Robust > Frail, Pre-frail), and mental health (SF-12, Robust > Frail, Pre-frail) (Table 1).

A significant difference in Fried's frailty indicators distribution between the Frail and Pre-frail groups was highlighted, except for weakness. The weakness was the earliest indicator of risk of frailty, while exhaustion represented the symptom that most distinguished Frail from Pre-frail subjects (Table 2). Grouping together Frail and Pre-frails subjects, we found a significant difference between males and females in the frailty score ($t = -2.29$, $p = 0.026$, $d = 0.61$) and in the walking slowness ($t = -2.48$, $p = 0.016$, d = 0.67), which reached a lower level in female than male participants.

3.3. Investigation of neural indexes: MRI examination

The between-group comparison of neural indexes using ANCOVA (Frail, Pre-frail, and Robust groups) highlighted a higher cortical thickness in Robust than in Frail and Pre-frail groups in left parietal–temporal areas, such as postcentral ($F = 3.97$, $p = 0.022$, $\eta^2 = 0.07$, $\omega^2 = 0.05$), precuneus ($F = 3.12$, $p = 0.049$, $\eta^2 = 0.06$, $\omega^2 = 0.04$), superior temporal ($F = 3.50$, $p = 0.034$, $\eta^2 = 0.06$, $\omega^2 = 0.04$), supramarginal ($F = 4.88$, $p = 0.010$, $\eta^2 = 0.09$, $\omega^2 = 0.07$), and transverse temporal ($F = 4.04$, $p = 0.021$, $\eta^2 = 0.07$, $\omega^2 = 0.06$) gyri. Also, significant differences (Robust compared to Frail and Pre-frail groups) were found in the right lingual ($F = 3.24$, $p = 0.044$, $\eta^2 = 0.06$, $\omega^2 = 0.04$) and rostral middle frontal ($F = 4.43$, $p = 0.015$, $\eta^2 = 0.09$, $\omega^2 = 0.07$) gyri. No significant differences among groups were found in subcortical regions' volumes and WMH total volume.

3.4. Correlation analyses: behavioral and neural indexes associated with frailty score

Concerning demographic variables, age was associated with frailty score ($r = 0.476$, $p_{corr} = < 0.001$). Among behavioral measures, frailty score correlated with CES-D ($r = 0.634$, $p_{corr} = < 0.001$), $SF\text{-}12_{mental\ health}$ ($r = -0.394$, $p_{corr} = < 0.001$), EQ5D5L ($r = -0.396$, $p_{corr} = < 0.001$), and $ADCS_{domestic\ activity}$ ($r = -0.325$, $p_{corr} = 0.001$). Considering cortical thickness, frailty was associated with left supramarginal ($r = -0.288$, $p_{corr} = 0.005$), and right rostral middle frontal ($r = -0.292$, $p_{corr} = 0.004$) gyri.

No significant correlations were found between the frailty score and subcortical regions' volumes and between the frailty score and WMH total volume.

3.5. Predictors of frailty phenotype and mediation models

Possible predictors of frailty were selected based on correlations' results and inserted in a binary logistic regression model with a backward method.

The dependent variable was the presence of frailty (Frail and Pre-frail subjects groups versus Robust subjects group). Independent variables considered were: age, gender, MoCA, CES-D, $SF\text{-}12_{mental\ health}$, $ADCS_{domestic\ activity}$, left supramarginal, and right rostral middle frontal gyrus.

Four models were generated. The best model (Table 3) revealed the predictive role of CES-D, MoCA, and left supramarginal gyrus on the frailty condition (Accuracy = 0.865, AUC = 0.899, Sensitivity = 0.765, Specificity =0.919, Precision = 0.839). Also, the model highlighted a trend of the predictive effect of age and $ADCS_{domestic\ activity}$ on frailty.

The mediation model revealed a full mediation of depression on the link between the neural index and frailty. Specifically, Table 4 shows the significant mediation role of CES-D on the link between frailty and both the left supramarginal and the right rostral middle frontal gyri (Figure 2).

The same analyses have been run considering the mediating role of MoCA, and no statistically significant direct and/or indirect effects have been revealed.

Supplementary material report two additional mediation models testing the effect of the left supramaginal gyrus and of the right rostral middle frontal gyrus on the link between CES-D and frailty. Results yielded no statistically significant effects (see Supplementary Tables S1, S2).

TABLE 1 Subjects' characteristics and frailty groups' comparison.

	Frail subjects	Pre-frail subjects	Robust subjects	Test value	*p*-value	η^2	ω^2	*post-hoc*
N(%)	17 (18)	45 (47)	34 (35)					
Frailty score (Me, IQR)	3.00, 0.00	1.00, 1.00	0.00, 0.00					
Sex (Ma:Fe)	3:14	18:27	17:17	4.97^	0.083			
Age (Me, IQR)	78.00,11.00	75.00,10.00	71.50,6.75	9.58$	<0.001	0.17	0.15	F > P > R
Education (Me, IQR)	9.00, 5.00	13.00, 5.00	13.00, 3.00	1.08$	0.342			
CES-D (Me, IQR)	24.00, 16.00	13.00,18.00	7.00, 7.00	19.45$	<0.001	0.29	0.27	F > P > R
MMSE (Me, IQR)	25.70, 3.90	26.00, 3.00	27.00, 3.55	4.70$	0.011	0.09	0.07	R > F,P
MoCA (Me, IQR)	21.36, 5.96	21.83, 3.64	22.94, 3.01	4.71$	0.011	0.09	0.07	R > F,P
Memory (0–15)#	7.00, 5.00	9.00, 4.00	10.00, 5.00	2.79$	0.067			
Executive functions (0–13)#	10.00, 4.00	10.00, 4.00	11.50, 1.00	2.95$	0.057			
Attention (0–18)#	15.00, 6.00	16.00, 3.00	17.00, 2.00	4.03$	0.021	0.06	0.20	R > F
Language (0–6)#	5.00, 1.00	5.00, 2.00	5.00, 1.00	0.54$	0.583			
Visuospatial (0–7)#	6.00, 2.00	6.00, 2.00	6.00, 1.00	1.54$	0.219			
Orientation (0–6)#	6.00, 1.00	6.00, 0.00	6.00, 0.00	0.16$	0.851			
PASE (Me, IQR)	64.00, 37.00	71.00, 50.00	108.50, 63.25	5.01$	0.009	0.10	0.08	R > F,P
ADCS (Me, IQR)	77.00, 7.00	77.00, 5.00	78.00, 1.00	1.21$	0.304			
Basic (0–19)	19.00, 0.00	19.00, 0.00	19.00, 0.00	0.31$	0.734			
Communication (0–28)	28.00, 4.00	28.00, 0.00	28.00, 0.00	1.65$	0.197			
Domestic (0–20)	19.00, 3.00	20.00, 2.00	20.00, 0.00	2.57$	0.082			
Outside (0–13)	13.00, 2.00	13.00, 0.00	13.00, 0.00	0.37$	0.692			
SF12 (Me, IQR)								
Physical	37.14, 11.01	44.05, 13.70	46.05, 11.55	5.24$	0.007	0.10	0.08	R > P > R
Mental	48.41, 12.14	48.24, 14.97	54.77, 8.56	6.67$	0.002	0.12	0.10	R > F,P
EQ5D5L (Me, IQR)								
VAS	50.00, 20.00	70.00, 20.00	72.50,1 8.75	5.02$	0.009	0.10	0.08	R > P > R
Index	0.77, 0.20	0.86, 0.12	0.91, 0.07	7.39$	0.001	0.14	0.12	R > P > R

ADCS, Activities of Daily Living Inventory; Fe, female subjects; CES-D, Center for Epidemiologic Studies Depression Scale; EQ5D5L, EuroQoL-5Dimensions-5Levels; IQR interquartile range; Me, median; Ma, male; MMSE, Mini-Mental State Examination; MoCA, Montreal Cognitive Assessment.#derived from the MoCA test according to Dodge et al. (2020); PASE, Physical Activity Scale for the Elderly; SF12, 12-item Short Form Survey.

^Chi-squared test has been run.

$ANCOVA test has been run.

4. Discussion

The present study aimed to disentangle the complex relationship between frailty, clinical profile, and neural pattern, investigating each component's predicting and mediating role. The findings relied on a representative cohort of the general population of older people. As expected, frail people were a limited percentage of our study's total cohort of subjects; frailty subjects were older (Canevelli et al., 2015), with a prevalence of females (Hanlon et al., 2018; Williams et al., 2018). Frail and pre-frail subjects presented more depressive symptoms, lower physical activity, reduced quality of life and well-being, and lower global cognitive level than not-frail people.

The main result of the present study was the finding of a full mediation of depression on the link between frailty and brain cortical thickness in the supramarginal and rostral middle frontal gyri. Interestingly, in this link, no mediating role was found for the cognitive level. This datum suggests a twofold role of depression: a central role in the prediction of the risk of developing a frailty phenotype but also an explanatory role in the link between the neural integrity (cortical thickness) and the risk of developing a frailty phenotype. While the role of depression in the risk of developing Frailty is well acknowledged in some cohort and meta-analysis studies (Mezuk et al., 2012; Brown et al., 2014; Soysal et al., 2017; Chu et al., 2019), the second aspect linking depression to brain integrity and fragility is unprecedented.

Previous findings have demonstrated the strict relationship between frailty and depression, the latter being highly prevalent in both community dwelling and nursing home older adults (Giovannini et al., 2020). A recent meta-analysis involving 84,351 older adults (Chu et al., 2019) showed how older adults with depression were more prone to frailty than those without depression; this was especially true in men. Moreover, this risk was rated as high as an 80% probability of older adults with depression being frail (Pegorari and Tavares, 2014). Finally, Brown et al. (2014) found that the concurrence of specific characteristics of frailty, such as fatigue and slow gait speed, with depression in older adults was associated with an increased risk of

TABLE 2 Fried's frailty indicators frequency in the frail and pre-frail groups.

Fried's frailty indicator	Frail subjects % of cases on total	Pre-Frail subjects % of cases on total	χ^2	*p*
Handgrip weakness	82.35% (12/17)	64.44% (29/45)	1.86	0.172
Exhaustion	76.47% (13/17)	24.44% (11/45)	14.07	<0.001
Reduced Activity Level	58.82% (10/17)	22.22% (10/45)	7.56	0.006
Involuntary weight loss	47.06% (8/17)	11.11% (5/45)	9.62	0.002
Walking slowness	47.06% (8/17)	13.33% (6/45)	8.03	0.005

TABLE 3 Binary logistic regression model to test predictors of the frailty syndrome.

Predictors	β	Odds ratio	Wald	*p*	95% CI	
					Lower bound	Upper bound
CES-D	0.13	1.138	10.51	0.001	0.05	0.21
Left supramarginal gyrus	−5.49	0.004	3.97	0.046	−10.90	−0.09
MoCA	−0.23	0.792	4.00	0.046	−0.46	−0.00
$ADCS_{domestic\ activity}$	−0.74	0.477	3.67	0.055	−1.50	0.02
Age	0.09	1.094	2.98	0.084	−0.01	0.19
Intercept	25.40	0.00	4.42	0.036	1.72	49.08

CES-D, Center for Epidemiologic Studies Depression Scale; MoCA, Montreal Cognitive Assessment; ADCS, Activities of Daily Living Inventory; CI, Confidence Interval.

death; this association was stronger for older depressed women than men (Isernia et al., 2023). In fact, previous studies showed that depressive symptomatology is an early risk factor for frailty in women, where the increment of depression is evident already in pre-frail phenotype (Isernia et al., 2023). Altogether, the herein presented data together with the literature suggest the importance of treating depression in the cure and prevention of frailty. The role of depression in the frailty phenotype can be interpreted in many ways. One possibility is that the loss of interest and engagement in daily life activities (Vaughan et al., 2015; Gale et al., 2018) facilitates the risk of low physical activity, with consequent loss of physical capacities and increased risk for falls, and weight loss, all of which may increase the risk for frailty (Lohman et al., 2022). In this line, a recent meta-analysis showed how depression and frailty in older adults are each associated with an increased prevalence and incidence of the other and represent a risk factor for the development of the other (Soysal et al., 2017), thus pointing to a reciprocal interaction between the two conditions. According to this view, our results favor considering the reciprocal interaction between psychological and physical aspects of health for clinical care, supporting the notion that "mental health becomes health" (Schnittker, 2005).

As stated above, the novelty of this study relies on the finding of the mediating role of depression in the link between brain integrity and fragility involving two brain areas: the left supramarginal and the right rostral middle frontal gyri. It should be noted that only the left supramarginal gyrus was a significant predictor of frailty, suggesting a causal role in fragility.

Previous studies separately investigated the role of the left supramarginal gyrus in frailty syndrome and depression. Evidence from neuroimaging techniques (Suárez-Méndez et al., 2020) showed reduced functional connectivity of this area with frontal motor control regions in frailty subjects, suggesting a role in motor impairments in this population. Moreover, the left supramarginal gyrus, a multimodal/multisensory area, has been associated with an integrative role in the perception of the position and movement of own body in space (Proske and Gandevia, 2012). Finally, this area has been involved in emotion processing and regulation in patients with psychiatric disorders (Madeira et al., 2020), and an aberrant pattern of activation of this gyrus at rest has been highlighted in bipolar and major depression patients (Gong et al., 2020).

The herein presented results are in agreement with the above-reported evidence from literature suggesting how the relation of the left supramarginal gyrus thickness with frailty is mediated by depression through mechanisms involving reduced proprioception, movement guidance, and emotion regulation.

Regarding the specific left-lateralized contribution of the supramarginal gyrus, we registered an asymmetrical gray matter reduction in thickness of frail and pre-frail subjects, prevalent in the left hemisphere, that is peculiar to aging and people at risk of neurodegenerative conditions, showing the so-called "left hemisphere susceptibility" (Shi et al., 2009; Donix et al., 2013; Cabinio et al., 2018; Yang et al., 2019). The greater dependence on left hemisphere processing in older adults is also supported by the HAROLD model ("hemispheric asymmetry reduction in older adults"), which describes changes in functional recruitment of brain hemispheres in aging due to a global reorganization of neurocognitive networks as well as regional neural changes.

Concerning the role of depression on the link between frailty and the right rostral middle frontal gyrus, it is noteworthy that the latter is part of the dorsolateral prefrontal cortex, which is known to be implicated in executive functions and in late life depression (Aizenstein et al., 2009). Specifically, an altered functioning in the executive control circuit has been observed in patients with major depression, mainly related to the right rostral middle frontal gyrus hypo-activity, which may be amenable to treatment.

TABLE 4 Mediation models testing the role of the left supramarginal and right rostral middle frontal gyri's thickness on the link between depression and frailty.

		Estimate	SE	*z*-value	*p*	95% CI	
						Lower bound	Lower bound
Mediation role of left supramarginal gyrus							
Direct effect	L supramarginal ➔ frailty score	−0.16	0.09	−1.80	0.072	−0.33	0.01
Indirect effect	L supramarginal ➔ CES-D ➔ frailty score	−0.10	0.05	−2.18	0.029	−0.20	−0.01
Total effect	L supramarginal ➔ frailty score	−0.26	0.09	−2.82	0.005	−0.45	−0.08
Mediation role of right rostral middle frontal gyrus							
Direct effect	R rostral middle frontal ➔ frailty score	−1.34	0.79	−1.69	0.091	−2.89	0.21
Indirect effect	R rostral middle frontal ➔ CES-D ➔ frailty score	−0.98	0.45	−2.19	0.029	−1.85	−0.10
Total effect	R rostral middle frontal ➔ frailty score	−2.32	0.86	−2.69	0.007	−4.01	−0.63

CES-D, Center for Epidemiologic Studies Depression Scale; CI, Confidence Interval; L, left; R = right; SE, standard error.

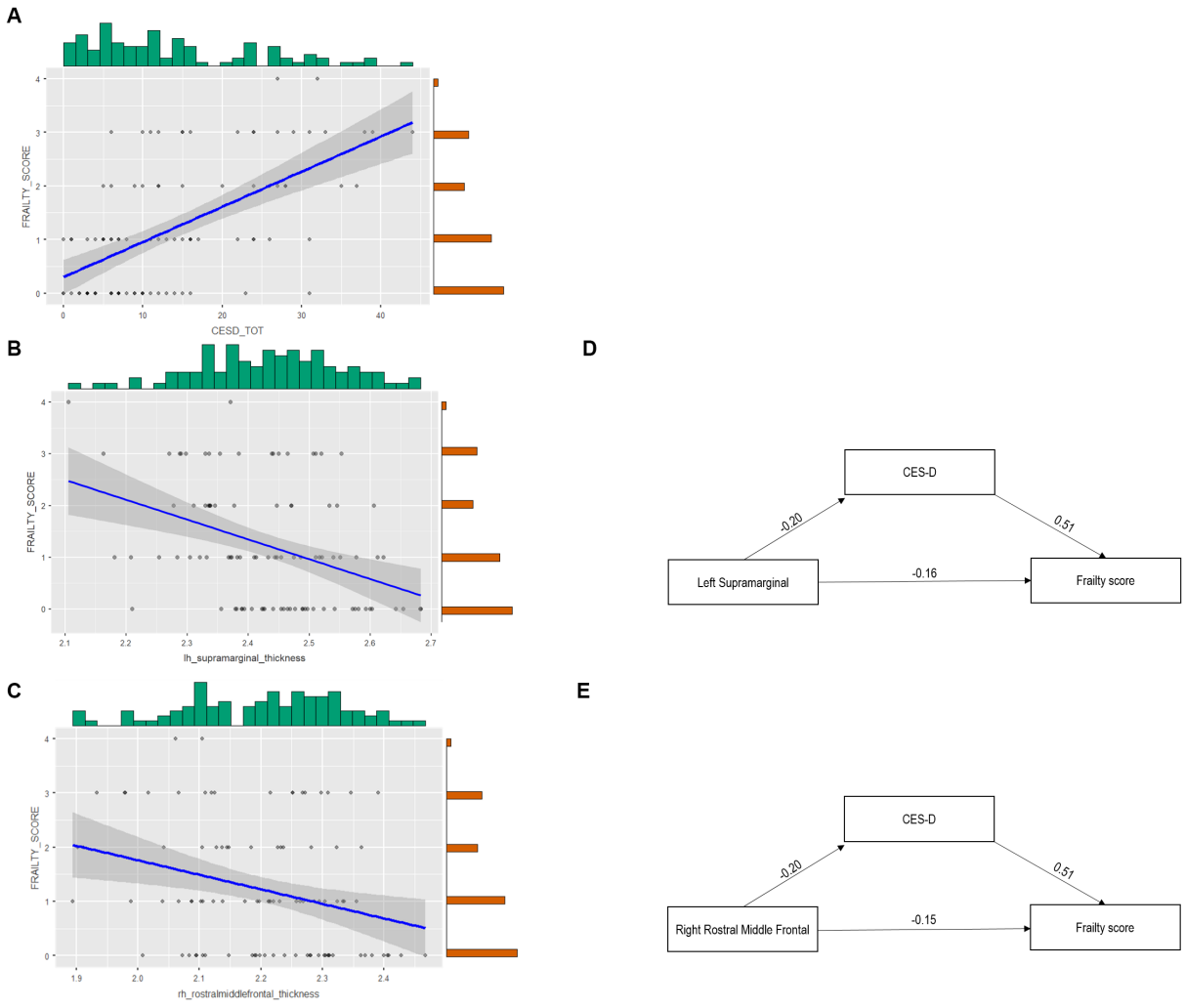

FIGURE 2
The complex link between cortical thickness, depression, and frailty. Panel **(A)** reports the Scatter plot depicting the link between frailty Score and CES-D. Panel **(B)** depicts the scatter plot of left supramarginal gyrus thickness and the frailty score. Panel **(C)** depicts the scatter plot of right rostral middle frontal gyrus thickness and the frailty score (light gray dots indicate that only one subject reported a certain relationship between variables, while dark gray dots suggest that more than one subject reported the relationship). Panel **(D)** reports the Mediation of CES-D on the link between left supramarginal thickness and the frailty score. Panel **(E)** shows the Mediation of CES-D on the link between right rostral middle frontal gyrus thickness and the frailty score.

Another finding in this study relates to the prevalence of frailty indicators in frail and pre-frail subjects, showing how handgrip weakness was the predominant symptom in both frail and pre-frail groups. At the same time, exhaustion was the indicator that most distinguished frail from pre-frail people. This is in line with previous research that reported handgrip weakness [i.e., Women's Health and Ageing Study II (Xue et al., 2008)] and exhaustion [i.e., inCHIANTI study (Stenholm et al., 2019)] as the earliest component of frailty. Thus, handgrip weakness may detect people at risk of frailty syndrome, while exhaustion may represent the leading indicator of actual frailty occurrence.

Some study limitations must be considered: our sample size is small, and the results need to be confirmed with a broader sample to assure generalizability. Also, further research adopting a longitudinal design may verify the findings related to the mediation model. Moreover, we restricted our model to investigate the link between neural patterns, depression, cognitive impairment, and frailty. However, additional significant variables, such as the muscle's integrity, nutritional lifestyle, and biomolecular data, should be considered.

Despite these caveats, the clinical implications of this study are significant. Clinicians should focus on depression and handgrip weakness, and interventions to prevent and reverse the frailty syndrome may act against muscle strength loss (Giovannini et al., 2021) isolation and disengagement in daily living. Especially differently to the current treatments targeted for frailty people, mainly operating on physical enhancement, social inclusion, and engagement should be considered. Accordingly, non-pharmacological treatments stimulating physical, emotional, and social processes, such as dance-based rehabilitation therapy (Meekums et al., 2015; Millman et al., 2021) or group activities (Savazzi et al., 2020), may show potential benefits for the frailty population.

5. Conclusion

In conclusion, this research supports the notion of frailty as a complex clinical entity in which depression mediates the association between brain integrity (supramarginal gyrus thickness) and Frailty. Moreover, our data showed how handgrip weakness is a crucial indicator of frailty. However, future contributions may confirm these results by adopting a longitudinal design and testing the effectiveness of rehabilitative interventions for people with frailty acting on depressive symptoms.

Data availability statement

The raw data supporting the conclusions of this article will be made available by the authors, without undue reservation.

Ethics statement

The study involving humans was approved by Don Gnocchi Foundation Ethics Committee. The studies were conducted in accordance with the local legislation and institutional requirements. The participants provided their written informed consent to participate in this study.

Author contributions

SI: Formal analysis, Investigation, Writing – original draft. VB: Conceptualization, Methodology, Supervision, Writing – original draft, Writing – review & editing. GB: Conceptualization, Validation, Writing – review & editing. MCab: Data curation, Writing – review & editing. PC: Investigation, Writing – review & editing. FR: Data curation, Writing – original draft. MCaz: Investigation, Writing – review & editing. FBl: Conceptualization, Funding acquisition, Writing – review & editing. CB: Investigation, Writing – review & editing. FG: Data curation, Writing – review & editing. SS: Supervision, Writing – review & editing. MCle: Supervision, Writing – review & editing. FBa: Funding acquisition, Supervision, Writing – original draft, Writing – review & editing.

Funding

The author(s) declare financial support was received for the research, authorship, and/or publication of this article. SI was supported with a scholarship from Fondazione Cariplo within the project "Transcription factor PREP1 in the frailty phenotype." This research was conducted with the financial support of the Italian Ministry of Health (Ricerca Corrente Rete IRCCS delle Neuroscienze e della Neuroriabilitazione- 2022).

Acknowledgments

We would like to thank all patients who participated in the study.

Conflict of interest

The authors declare that the research was conducted in the absence of any commercial or financial relationships that could be construed as a potential conflict of interest.

Publisher's note

Supplementary material

The Supplementary material for this article can be found online at: https://www.frontiersin.org/articles/10.3389/fnagi.2023.1292417/full#supplementary-material

References

Aizenstein, H. J., Butters, M. A., Wu, M., Mazurkewicz, L. M., Stenger, V. A., Gianaros, P. J., et al. (2009). Altered functioning of the executive control circuit in late-life depression: episodic and persistent phenomena. *Am. J. Geriatr. Psych. Off. J. Am. Assoc. Geriatr. Psych.* 17, 30–42. doi: 10.1097/JGP.0b013e31817b60af

Avila-Funes, J. A., Amieva, H., Barberger-Gateau, P., Le Goff, M., Raoux, N., Ritchie, K., et al. (2009). Cognitive impairment improves the predictive validity of the phenotype of frailty for adverse health outcomes: the three-city study. *J. Am. Geriatr. Soc.* 57, 453–461. doi: 10.1111/j.1532-5415.2008.02136.x

Avila-Funes, J. A., Carcaillon, L., Helmer, C., Carrière, I., Ritchie, K., Rouaud, O., et al. (2012). Is frailty a prodromal stage of vascular dementia? Results from the Three-City study. *J. Am. Geriatr. Soc.* 60, 1708–1712. doi: 10.1111/j.1532-5415.2012.04142.x

Avila-Funes, J. A., Pelletier, A., Meillon, C., Catheline, G., Periot, O., Trevin, O. F. I., et al. (2017). Vascular cerebral damage in frail older adults: the AMImage study. *J. Gerontol. A Biol. Sci. Med. Sci.* 72, 971–977. doi: 10.1093/gerona/glw347

Balestroni, G., and Bertolotti, G. (2012). EuroQol-5D (EQ-5D): an instrument for measuring quality of life. *Monaldi Arch. Chest Dis.* 78, 155–159. doi: 10.4081/monaldi.2012.121

Bandeen-Roche, K., Xue, Q. L., Ferrucci, L., Walston, J., Guralnik, J. M., Chaves, P., et al. (2006). Phenotype of frailty: characterization in the women's health and aging studies. *J. Gerontol. A Biol. Sci. Med. Sci.* 61, 262–266. doi: 10.1093/gerona/61.3.262

Biesanz, J. C., Falk, C. F., and Savalei, V. (2010). Assessing mediational models: testing and interval estimation for indirect effects. *Multivar. Behav. Res.* 45, 661–701. doi: 10.1080/00273171.2010.498292

Bohannon, R. W. (1997). Comfortable and maximum walking speed of adults aged 20-79 years: reference values and determinants. *Age Ageing* 26, 15–19. doi: 10.1093/ageing/26.1.15

Brown, P. J., Roose, S. P., Fieo, R., Liu, X., Rantanen, T., Sneed, J. R., et al. (2014). Frailty and depression in older adults: a high-risk clinical population. *Am. J. Geriatr. Psychiatry* 22, 1083–1095. doi: 10.1016/j.jagp.2013.04.010

Buigues, C., Padilla-Sánchez, C., Garrido, J. F., Navarro-Martínez, R., Ruiz-Ros, V., and Cauli, O. (2015). The relationship between depression and frailty syndrome: a systematic review. *Aging Ment. Health* 19, 762–772. doi: 10.1080/13607863.2014.967174

Bunce, D., Batterham, P. J., and Mackinnon, A. J. (2019). Long-term associations between physical frailty and performance in specific cognitive domains. *J. Gerontol. B Psychol. Sci. Soc. Sci.* 74, 919–926. doi: 10.1093/geronb/gbx177

Bunt, S., Steverink, N., Olthof, J., van der Schans, C. P., and Hobbelen, J. S. M. (2017). Social frailty in older adults: a scoping review. *Eur. J. Ageing* 14, 323–334. doi: 10.1007/s10433-017-0414-7

Cabinio, M., Saresella, M., Piancone, F., LaRosa, F., Marventano, I., Guerini, F. R., et al. (2018). Association between hippocampal shape, Neuroinflammation, and cognitive decline in Alzheimer's disease. *J. Alzheimers Dis.* 66, 1131–1144. doi: 10.3233/jad-180250

Canevelli, M., Cesari, M., and van Kan, G. A. (2015). Frailty and cognitive decline: how do they relate? *Curr. Opin. Clin. Nutr. Metab. Care* 18, 43–50. doi: 10.1097/mco.0000000000000133

Chang, S. S., Weiss, C. O., Xue, Q. L., and Fried, L. P. (2010). Patterns of comorbid inflammatory diseases in frail older women: the Women's health and aging studies I and II. *J. Gerontol. A Biol. Sci. Med. Sci.* 65, 407–413. doi: 10.1093/gerona/glp181

Cheung, J. T. K., Yu, R., Wu, Z., Wong, S. Y. S., and Woo, J. (2018). Geriatric syndromes, multimorbidity, and disability overlap and increase healthcare use among older Chinese. *BMC Geriatr.* 18:147. doi: 10.1186/s12877-018-0840-1

Chu, W., Chang, S. F., Ho, H. Y., and Lin, H. C. (2019). The relationship between depression and frailty in community-dwelling older people: a systematic review and Meta-analysis of 84,351 older adults. *J. Nurs. Scholarsh.* 51, 547–559. doi: 10.1111/jnu.12501

Clegg, A., Young, J., Iliffe, S., Rikkert, M. O., and Rockwood, K. (2013). Frailty in elderly people. *Lancet* 381, 752–762. doi: 10.1016/s0140-6736(12)62167-9

Conti, S., Bonazzi, S., Laiacona, M., Masina, M., and Coralli, M. V. (2015). Montreal cognitive Assessmen (MoCA)-Italian version: regression based norms and equivalent scores. *Neurol. Sci.* 36, 209–214. doi: 10.1007/s10072-014-1921-3

Del Brutto, O. H., Mera, R. M., Cagino, K., Fanning, K. D., Milla-Martinez, M. F., Nieves, J. L., et al. (2017). Neuroimaging signatures of frailty: a population-based study in community-dwelling older adults (the Atahualpa project). *Geriatr Gerontol Int* 17, 270–276. doi: 10.1111/ggi.12708

Dent, E., Martin, F. C., Bergman, H., Woo, J., Romero-Ortuno, R., and Walston, J. D. (2019). Management of frailty: opportunities, challenges, and future directions. *Lancet* 394, 1376–1386. doi: 10.1016/s0140-6736(19)31785-4

Desikan, R. S., Ségonne, F., Fischl, B., Quinn, B. T., Dickerson, B. C., Blacker, D., et al. (2006). An automated labeling system for subdividing the human cerebral cortex on MRI scans into gyral based regions of interest. *NeuroImage* 31, 968–980. doi: 10.1016/j.neuroimage.2006.01.021

Dodge, H. H., Goldstein, F. C., Wakim, N. I., Gefen, T., Teylan, M., Chan, K. C. G., et al. (2020). Differentiating among stages of cognitive impairment in aging: Version 3 of the Uniform Data Set (UDS) neuropsychological test battery and MoCA index scores. *Alzheimer's Dement.* 6:e12103. doi: 10.1002/trc2.12103

Donix, M., Burggren, A. C., Scharf, M., Marschner, K., Suthana, N. A., Siddarth, P., et al. (2013). APOE associated hemispheric asymmetry of entorhinal cortical thickness in aging and Alzheimer's disease. *Psychiatry Res.* 214, 212–220. doi: 10.1016/j.pscychresns.2013.09.006

Ducca, E. L., Gomez, G. T., Palta, P., Sullivan, K. J., Jack, C. R., Knopman, D. S., et al. (2023). Physical frailty and brain white matter abnormalities: the atherosclerosis risk in communities study. *J. Gerontol. A Biol. Sci. Med. Sci.* 78, 357–364. doi: 10.1093/gerona/glac111

Feng, L., Zin Nyunt, M. S., Gao, Q., Yap, K. B., and Ng, T. P. (2017). Cognitive frailty and adverse health outcomes: findings from the Singapore longitudinal ageing studies (SLAS). *J. Am. Med. Dir. Assoc.* 18, 252–258. doi: 10.1016/j.jamda.2016.09.015

Fischl, B., Salat, D. H., Busa, E., Albert, M., Dieterich, M., Haselgrove, C., et al. (2002). Whole brain segmentation: automated labeling of neuroanatomical structures in the human brain. *Neuron* 33, 341–355. doi: 10.1016/s0896-6273(02)00569-x

Fried, L. P., Tangen, C. M., Walston, J., Newman, A. B., Hirsch, C., Gottdiener, J., et al. (2001). Frailty in older adults: evidence for a phenotype. *J. Gerontol. A Biol. Sci. Med. Sci.* 56, M146–M156. doi: 10.1093/gerona/56.3.m146

Galasko, D., Bennett, D., Sano, M., Ernesto, C., Thomas, R., Grundman, M., et al. (1997). An inventory to assess activities of daily living for clinical trials in Alzheimer's disease. *Alzheimer Dis. Assoc. Disord.* 11, 33–39. doi: 10.1097/00002093-199700112-00005

Gale, C. R., Westbury, L., and Cooper, C. (2018). Social isolation and loneliness as risk factors for the progression of frailty: the English longitudinal study of ageing. *Age Ageing* 47, 392–397. doi: 10.1093/ageing/afx188

Giovannini, S., Coraci, D., Brau, F., Galluzzo, V., Loreti, C., Caliandro, P., et al. (2021). Neuropathic pain in the elderly. *Diagnostics* 11:613. doi: 10.3390/diagnostics11040613

Giovannini, S., Onder, G., van der Roest, H. G., Topinkova, E., Gindin, J., Cipriani, M. C., et al. (2020). Use of antidepressant medications among older adults in European long-term care facilities: a cross-sectional analysis from the SHELTER study. *BMC Geriatr.* 20:310. doi: 10.1186/s12877-020-01730-5

Gong, J., Wang, J., Qiu, S., Chen, P., Luo, Z., Huang, L., et al. (2020). Common and distinct patterns of intrinsic brain activity alterations in major depression and bipolar disorder: voxel-based meta-analysis. *Transl. Psychiatry* 10:353. doi: 10.1038/s41398-020-01036-5

Hanlon, P., Nicholl, B. I., Jani, B. D., Lee, D., McQueenie, R., and Mair, F. S. (2018). Frailty and pre-frailty in middle-aged and older adults and its association with multimorbidity and mortality: a prospective analysis of 493 737 UK biobank participants. *Lancet Public Health* 3, e323–e332. doi: 10.1016/s2468-2667(18)30091-4

Isernia, S., Cazzoli, M., Baglio, G., Cabinio, M., Rossetto, F., Giunco, F., et al. (2023). Differential roles of neural integrity, physical activity and depression in frailty: sex-related differences. *Brain Sci.* 13:950. doi: 10.3390/brainsci13060950

Jenkinson, C., Chandola, T., Coulter, A., and Bruster, S. (2001). An assessment of the construct validity of the SF-12 summary scores across ethnic groups. *J. Public Health Med.* 23, 187–194. doi: 10.1093/pubmed/23.3.187

Kelaiditi, E., Cesari, M., Canevelli, M., van Kan, G. A., Ousset, P. J., Gillette-Guyonnet, S., et al. (2013). Cognitive frailty: rational and definition from an (I.A.N.A./I.A.G.G.) international consensus group. *J. Nutr. Health Aging* 17, 726–734. doi: 10.1007/s12603-013-0367-2

Klapwijk, E. T., van de Kamp, F., van der Meulen, M., Peters, S., and Wierenga, L. M. (2019). Qoala-T: a supervised-learning tool for quality control of FreeSurfer segmented MRI data. *NeuroImage* 189, 116–129. doi: 10.1016/j.neuroimage.2019.01.014

Lohman, M. C., Mezuk, B., Fairchild, A. J., Resciniti, N. V., and Merchant, A. T. (2022). The role of frailty in the association between depression and fall risk among older adults. *Aging Ment. Health* 26, 1805–1812. doi: 10.1080/13607863.2021.1950616

López-Sanz, D., Suárez-Méndez, I., Bernabé, R., Pasquín, N., Rodríguez-Mañas, L., Maestú, F., et al. (2018). Scoping review of neuroimaging studies investigating frailty and frailty components. *Front. Med.* 5:284. doi: 10.3389/fmed.2018.00284

Lu, W. H., de Souto, B. P., Rolland, Y., Rodríguez-Mañas, L., Bouyahia, A., Fischer, C., et al. (2020). Cross-sectional and prospective associations between cerebral cortical thickness and frailty in older adults. *Exp. Gerontol.* 139:111018. doi: 10.1016/j.exger.2020.111018

Madeira, N., Duarte, J. V., Martins, R., Costa, G. N., Macedo, A., and Castelo-Branco, M. (2020). Morphometry and gyrification in bipolar disorder and schizophrenia: a comparative MRI study. *Neuroimage Clin.* 26:102220. doi: 10.1016/j.nicl.2020.102220

Maltais, M., de Souto, B. P., Perus, L., Mangin, J. F., Grigis, A., Chupin, M., et al. (2020). Prospective associations between diffusion tensor imaging parameters and frailty in older adults. *J. Am. Geriatr. Soc.* 68, 1050–1055. doi: 10.1111/jgs.16343

Meekums, B., Karkou, V., and Nelson, E. A. (2015). Dance movement therapy for depression. *Cochrane Database Syst. Rev.* 2016:CD009895. doi: 10.1002/14651858.CD009895.pub2

Mezuk, B., Edwards, L., Lohman, M., Choi, M., and Lapane, K. (2012). Depression and frailty in later life: a synthetic review. *Int. J. Geriatr. Psychiatry* 27, 879–892. doi: 10.1002/gps.2807

Millman, L. S. M., Terhune, D. B., Hunter, E. C. M., and Orgs, G. (2021). Towards a neurocognitive approach to dance movement therapy for mental health: a systematic review. *Clin. Psychol. Psychother.* 28, 24–38. doi: 10.1002/cpp.2490

Mitnitski, A. B., Mogilner, A. J., and Rockwood, K. (2001). Accumulation of deficits as a proxy measure of aging. *ScientificWorldJournal* 1, 323–336. doi: 10.1100/tsw.2001.58

Panza, F., Seripa, D., Solfrizzi, V., Tortelli, R., Greco, A., Pilotto, A., et al. (2015a). Targeting cognitive frailty: clinical and neurobiological roadmap for a single complex phenotype. *J. Alzheimers Dis.* 47, 793–813. doi: 10.3233/jad-150358

Panza, F., Solfrizzi, V., Barulli, M. R., Santamato, A., Seripa, D., Pilotto, A., et al. (2015b). Cognitive frailty: a systematic review of epidemiological and neurobiological evidence of an age-related clinical condition. *Rejuvenation Res.* 18, 389–412. doi: 10.1089/rej.2014.1637

Pegorari, M. S., and Tavares, D. M. (2014). Factors associated with the frailty syndrome in elderly individuals living in the urban area. *Rev. Lat. Am. Enfermagem* 22, 874–882. doi: 10.1590/0104-1169.0213.2493

Pezzotti, P., Scalmana, S., Mastromattei, A., and Di Lallo, D. (2008). The accuracy of the MMSE in detecting cognitive impairment when administered by general practitioners: a prospective observational study. *BMC Fam. Pract.* 9:29. doi: 10.1186/1471-2296-9-29

Proske, U., and Gandevia, S. C. (2012). The proprioceptive senses: their roles in signaling body shape, body position and movement, and muscle force. *Physiol. Rev.* 92, 1651–1697. doi: 10.1152/physrev.00048.2011

Radloff, L. S. (1977). The CES-D scale: a self-report depression scale for research in the general population. *Appl. Psychol. Meas.* 1, 385–401. doi: 10.1177/014662167700100306

Reed, C., Mark, B., Vellas, B., Andrews, J. S., Argimon, J. M., Bruno, G., et al. (2016). Identifying factors of activities of daily living important for cost and caregiver outcomes in Alzheimer's disease. *Int. Psychogeriatr.* 28, 247–259. doi: 10.1017/S1041610215001349

Richardson, M. T., Leon, A. S., Jacobs, D. R., Ainsworth, B. E., and Serfass, R. (1994). Comprehensive evaluation of the Minnesota leisure time physical activity questionnaire. *J. Clin. Epidemiol.* 47, 271–281. doi: 10.1016/0895-4356(94)90008-6

Rockwood, K., and Mitnitski, A. (2007). Frailty in relation to the accumulation of deficits. *J. Gerontol. A Biol. Sci. Med. Sci.* 62, 722–727. doi: 10.1093/gerona/62.7.722

Ruan, Q., Yu, Z., Chen, M., Bao, Z., Li, J., and He, W. (2015). Cognitive frailty, a novel target for the prevention of elderly dependency. *Ageing Res. Rev.* 20, 1–10. doi: 10.1016/j.arr.2014.12.004

Santangelo, G., Siciliano, M., Pedone, R., Vitale, C., Falco, F., Bisogno, R., et al. (2015). Normative data for the Montreal cognitive assessment in an Italian population sample. *Neurol. Sci.* 36, 585–591. doi: 10.1007/s10072-014-1995-y

Savazzi, F., Isernia, S., Farina, E., Fioravanti, R., D'Amico, A., Saibene, F. L., et al. (2020). "art, colors, and emotions" treatment (ACE-t): a pilot study on the efficacy of an art-based intervention for people with Alzheimer's disease. *Front. Psychol.* 11:1467. doi: 10.3389/fpsyg.2020.01467

Schnittker, J. (2005). When mental health becomes health: age and the shifting meaning of self-evaluations of general health. *Milbank Q.* 83, 397–423. doi: 10.1111/j.1468-0009.2005.00407.x

Shi, F., Liu, B., Zhou, Y., Yu, C., and Jiang, T. (2009). Hippocampal volume and asymmetry in mild cognitive impairment and Alzheimer's disease: Meta-analyses of MRI studies. *Hippocampus* 19, 1055–1064. doi: 10.1002/hipo.20573

Siejka, T. P., Srikanth, V. K., Hubbard, R. E., Moran, C., Beare, R., Wood, A., et al. (2020). White matter Hyperintensities and the progression of frailty-the Tasmanian study of cognition and gait. *J. Gerontol. A Biol. Sci. Med. Sci.* 75, 1545–1550. doi: 10.1093/gerona/glaa024

Soysal, P., Veronese, N., Thompson, T., Kahl, K. G., Fernandes, B. S., Prina, A. M., et al. (2017). Relationship between depression and frailty in older adults: a systematic review and meta-analysis. *Ageing Res. Rev.* 36, 78–87. doi: 10.1016/j.arr.2017.03.005

Stenholm, S., Ferrucci, L., Vahtera, J., Hoogendijk, E. O., Huisman, M., Pentti, J., et al. (2019). Natural course of frailty components in people who develop frailty syndrome: evidence from two cohort studies. *J. Gerontol. A Biol. Sci. Med. Sci.* 74, 667–674. doi: 10.1093/gerona/gly132

Sternberg, S. A., Wershof Schwartz, A., Karunananthan, S., Bergman, H., and Mark, C. A. (2011). The identification of frailty: a systematic literature review. *J. Am. Geriatr. Soc.* 59, 2129–2138. doi: 10.1111/j.1532-5415.2011.03597.x

Suárez-Méndez, I., Doval, S., Walter, S., Pasquín, N., Bernabé, R., Gallo, E. C., et al. (2020). Functional connectivity disruption in frail older adults without global cognitive deficits. *Front. Med.* 7:322. doi: 10.3389/fmed.2020.00322

Sugimoto, T., Sakurai, T., Ono, R., Kimura, A., Saji, N., Niida, S., et al. (2018). Epidemiological and clinical significance of cognitive frailty: a mini review. *Ageing Res. Rev.* 44, 1–7. doi: 10.1016/j.arr.2018.03.002

Tian, Q., Williams, O. A., Landman, B. A., Resnick, S. M., and Ferrucci, L. (2020). Microstructural neuroimaging of frailty in cognitively Normal older adults. *Front. Med.* 7:546344. doi: 10.3389/fmed.2020.546344

Vaughan, L., Corbin, A. L., and Goveas, J. S. (2015). Depression and frailty in later life: a systematic review. *Clin. Interv. Aging* 10, 1947–1958. doi: 10.2147/cia.s69632

Washburn, R. A., Smith, K. W., Jette, A. M., and Janney, C. A. (1993). The physical activity scale for the elderly (PASE): development and evaluation. *J. Clin. Epidemiol.* 46, 153–162. doi: 10.1016/0895-4356(93)90053-4

Williams, B., Jalilianhasanpour, R., Matin, N., Fricchione, G. L., Sepulcre, J., Keshavan, M. S., et al. (2018). Individual differences in corticolimbic structural profiles linked to insecure attachment and coping styles in motor functional neurological disorders. *J. Psychiatr. Res.* 102, 230–237. doi: 10.1016/j.jpsychires.2018.04.006

Xue, Q. L. (2011). The frailty syndrome: definition and natural history. *Clin. Geriatr. Med.* 27, 1–15. doi: 10.1016/j.cger.2010.08.009

Xue, Q. L., Bandeen-Roche, K., Varadhan, R., Zhou, J., and Fried, L. P. (2008). Initial manifestations of frailty criteria and the development of frailty phenotype in the Women's health and aging study II. *J. Gerontol. A Biol. Sci. Med. Sci.* 63, 984–990. doi: 10.1093/gerona/63.9.984

Yang, H., Xu, H., Li, Q., Jin, Y., Jiang, W., Wang, J., et al. (2019). Study of brain morphology change in Alzheimer's disease and amnestic mild cognitive impairment compared with normal controls. *Gen. Psych.* 32:e100005. doi: 10.1136/gpsych-2018-100005

frontiers | Frontiers in Pharmacology

TYPE Original Research
PUBLISHED 15 November 2023
DOI 10.3389/fphar.2023.1235406

OPEN ACCESS

EDITED BY
Jiehui Jiang,
Shanghai University, China

REVIEWED BY
Ioannis Zaganas,
University of Crete, Greece
Can Sheng,
Affiliated Hospital of Jining Medical University, China

*CORRESPONDENCE
Chengying Zheng,
zhengchengying@126.com

RECEIVED 06 June 2023
ACCEPTED 06 November 2023
PUBLISHED 15 November 2023

CITATION
Mei X, Zou C, Si Z, Xu T, Hu J, Wu X and Zheng C (2023), Antidepressant effect of bright light therapy on patients with Alzheimer's disease and their caregivers. *Front. Pharmacol.* 14:1235406. doi: 10.3389/fphar.2023.1235406

Antidepressant effect of bright light therapy on patients with Alzheimer's disease and their caregivers

Xi Mei[1], Chenjun Zou[2], Zizhen Si[3], Ting Xu[2], Jun Hu[2], Xiangping Wu[1] and Chengying Zheng[2]*

[1]Key Lab, Ningbo Kangning Hospital, Ningbo, Zhejiang, China, [2]Department of Geriatric, Ningbo Kangning Hospital, Ningbo, Zhejiang, China, [3]Medical College, Ningbo University, Ningbo, Zhejiang, China

Background: As a non-pharmacologic treatment, bright light therapy (BLT) is often used to improve affective disorders and memory function. In this study, we aimed to determine the effect of BLT on depression and electrophysiological features of the brain in patients with Alzheimer's disease (AD) and their caregivers using a light-emitting diode device of 14000 lux.

Methods: A 4-week case-control trial was conducted. Neuropsychiatric and electroencephalogram (EEG) examination were evaluated at baseline and after 4 weeks. EEG power in delta (1–4 Hz), theta (4–8 Hz), alpha (8–12 Hz), and beta (12–30 Hz) bands was calculated for our main analysis. Demographic and clinical variables were analyzed using Student's t test and the chi-square test. Pearson's correlation was used to determine the correlation between electrophysiological features, blood biochemical indicators, and cognitive assessment scale scores.

Results: In this study, 22 in-patients with AD and 23 caregivers were recruited. After BLT, the Hamilton depression scale score decreased in the fourth week. Compared with the age-matched controls of their caregivers, a higher spectral power at the lower delta and theta frequencies was observed in the AD group. After BLT, the EEG power of the delta and theta frequencies in the AD group decreased. No change was observed in blood amyloid concentrations before and after BLT.

Conclusion: In conclusion, a 4-week course of BLT significantly suppressed depression in patients with AD and their caregivers. Moreover, changes in EEG power were also significant in both groups.

KEYWORDS

bright light therapy, Alzheimer's disease, depression, EEG, biomarkers

Introduction

Alzheimer's disease (AD) is a progressive degenerative disease affecting cognitive functions and mental health. Its clinical manifestations include memory impairment and additional cognitive domain impairments in executive functions, attention, language, social cognition and judgment, psychomotor speed, and visuoperceptual or visuospatial abilities (Masters et al., 2015; Scheltens et al., 2016; Scheltens et al., 2021). Cognitive impairment is considered a transitional stage between normal aging and AD. China has a high prevalence of dementia and cognitive impairment (Jia et al., 2020).

AD may be accompanied by mental and behavioral symptoms, such as depressed mood and apathy in the initial stages, and also by psychotic symptoms, irritability, aggression, confusion, gait and mobility abnormalities, and seizures in the later stages (Altomari et al., 2022). In the long-term care process, caregivers of patients with AD may also suffer from mental health problems (Corrêa et al., 2019; Carbone et al., 2021). In previous studies, depression occurred in 50% of patients with AD, thereby increasing the caregivers' burden (Chi et al., 2014). Symptoms of depression can precede a clinical diagnosis of AD for years or occur around the onset of AD (Diniz et al., 2013). Caring for a loved one with AD can increase the risk of depression in caregivers, and symptoms of depression typically persist over time (Liu et al., 2017; Chai et al., 2018).

Aside from medication, a number of non-pharmacological treatments can be used to improve a patient's health condition. According to previous studies, exposure to bright light may improve sleep and ease depression and agitation in people with AD (Peter-Derex et al., 2015; van Maanen et al., 2016; Roccaro et al., 2020). Persons living with AD or vascular dementia who were exposed to bright light therapy (BLT) demonstrated significantly improved scores on the Mini-Mental State Examination (MMSE) scale, compared to exposure to dim light therapy (Lu et al., 2023). BLT has also been used for decades to treat nonseasonal depression and other mood disorders (Al-Karawi and Jubair, 2016; Wang et al., 2020).

Regardless of clinical manifestations, AD biomarkers, including amyloidosis, tauopathy, and neurodegeneration, are important for diagnosis and to evaluate the effectiveness of therapy in this disease (Jack et al., 2018). Electroencephalogram (EEG) biomarkers can be used to reflect the effects of AD neuropathology on functional brain networks (Pfurtscheller and Lopes da Silva, 1999). Because of its high temporal resolution, we can investigate EEG rhythms at different frequency bands during a resting-state condition in patients with cognitive decline (Caravaglios et al., 2023). Although changes in electrophysiological features are not specific for patients with AD, compared to older adults without cognitive impairment, patients with AD or dementia with mild cognitive impairment were characterized by changes in EEG rhythms during resting-state condition (Babiloni et al., 2020).

This study aimed to determine the effect of BLT on depression and electrophysiological features of the brain in patients with AD and their caregivers using a light-emitting diode device with an intensity of 14000 lux.

Methods

Participants

We recruited inpatients and their caregivers form Geriatric Center of Ningbo Kangning Hospital between September 2022 and March 2023. Potential participants were recommended to our experienced research psychiatrists for further study. Ultimately, 22 patients with AD and 23 caregivers were recruited in this study. The patients with AD were diagnosed using the Diagnostic and Statistical Manual of Mental Disorders, fifth edition criteria (First, 2013). All patients met the following inclusion and exclusion criteria: 1) diagnosed with AD by two research psychiatrists; 2) provision of informed consent; 3) disease course >3 months; 4) cholinesterase inhibitor (donepezil) and non-competitive N-methyl-d-aspartate receptor antagonist (memantine) use; 5) no history of other mental illnesses, including schizophrenia and delirium; and 6) no physical diseases.

Neuropsychiatric evaluation

The neuropsychological evaluation of cognition was confirmed by MMSE scores <17, 20, and 24 in people with no, primary school, and junior high school education, respectively (Li et al., 2016). The AD assessment scale—cognitive subscale (ADAScog) was used to evaluate patients' memory, language, and other cognitive impairments (Rosen et al., 1984). The Hamilton depression scale (HAMD) was adopted to evaluate depression in patients and their caregivers (Zimmerman et al., 2013).

Experimental protocol

The light therapy equipment used for treatment was designed by the Geriatric Center of Ningbo Kangning Hospital as described in our previous study (Zou et al., 2022). Light therapy with peak strength of 14000 lux was conducted from 9:00 a.m. to 9:30 a.m. each day for 4 weeks. The patients and their caregivers sat in front of the light therapy device with their eyes open to allow the light to reach the retinas for BLT. The distance between the participants and light source was 50 cm.

EEG examination and analysis

The participants were seated in a comfortable chair. A 128-channel EEG (EGI System 300; Electrical Geodesic Inc., Eugene, OR, United States) configured in the standard 10–20 montage was recorded with reference to linked mastoids. The sampling rate was 500 Hz using an amplifier with low and high cutoff frequencies of 0.1 and 100 Hz, respectively.

EEG recordings were compiled during a resting state using a structured testing and acquisition software platform (5 min with the eyes opened and 5 min with the eyes closed). During the open-eye task, participants were instructed to stare directly at a black fixation cross located in the center of a gray background. During the closed-eye task, they were instructed to close their eyes while maintaining wakefulness. NetStation software (Electrical Geodesic Inc., OR, United States) was used for recording. The impedance for all electrodes was kept below 50 kΩ. Offline data analysis was conducted with the open-source EEGLAB toolbox.

Blood enzyme-linked immunosorbent assay

Blood samples were collected before breakfast using a winged blood collection set. Approximately 5 mL of whole blood was collected in a procoagulant tube. To allow the measurement of plasma peptides, blood was immediately centrifuged at 1,400 rpm using a BY-600A type medical centrifuge (Beijing Baiyang Medical

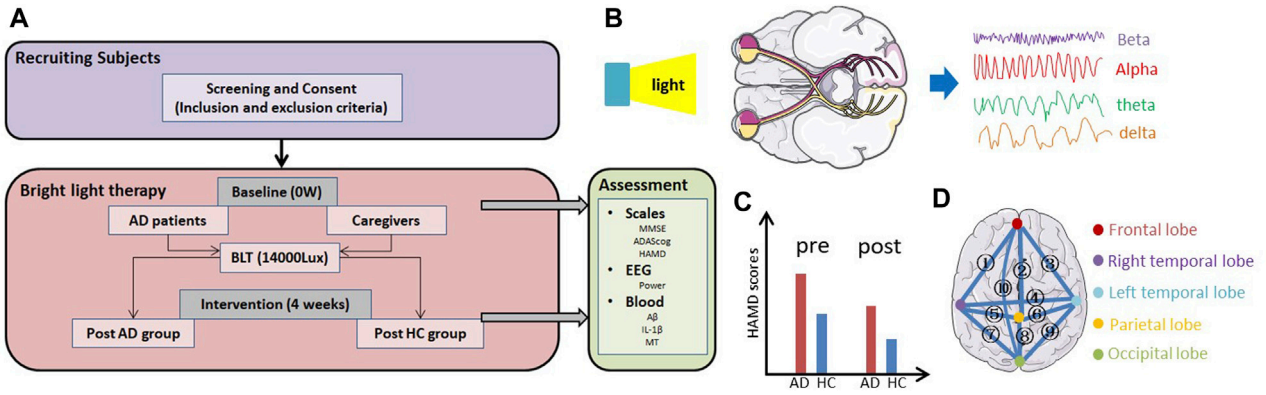

FIGURE 1
Overview of the study. **(A)** Protocol for bright light therapy in patients with AD and their caregivers (HC). **(B)** Light therapy modulated the EEG signal through the retina to the cortex. **(C)** HAMD scores, which reflect the level of depression in participants, may be change before and after therapy. **(D)** ① to ⑩ represent the relationship between the frontal and right temporal lobes, frontal and parietal lobes, frontal and left temporal lobes, right temporal and left temporal lobes, right temporal and parietal lobes, left temporal and parietal lobes, right temporal and occipital lobes, parietal and occipital lobes, left temporal and occipital lobes, frontal and occipital lobes.

Devices Co., Beijing, China) for 10 min. All blood samples were processed within 30 min of collection and immediately frozen at −80°C. Blood samples were thawed immediately before analysis.

Serum amyloid-β (Aβ), $Aβ_{40}$, $Aβ_{42}$, interleukin (IL)-1β, and melatonin (MT) levels were estimated using enzyme-linked immunosorbent assay kits (Shanghai Yuanye Bio-Technology Co., Shanghai, China). All procedures were performed according to the manufacturer's instructions. Absorbance was measured at 450 nm using a Sunrise-basic enzyme labeling instrument (Tecan Group Ltd., Mannedorf, Switzerland) with a reference wavelength of 690 nm. These measurements were transformed into concentrations by comparing the optical densities of the samples with the standard curve values.

Statistical analysis

Data are presented as the mean ± standard deviation (SD). Demographic and clinical variables were compared and analyzed between the different groups using Student's t test for continuous variables and the chi-square test for categorical variables. Pearson's correlation was used to determine the correlation among electrophysiological features, blood indicators, and cognitive assessment scale scores. Statistical significance was set at $p < 0.05$. Statistical Package for the Social Sciences (SPSS version 19.0, IBM Corp., Armonk, NY, United States) was used for all analyses.

Results

Clinical assessment

The protocol for BLT in patients with AD and their caregivers is shown in Figure 1. First, we recruited participants based on the inclusion and exclusion criteria. At baseline, all the participants were asked to complete assessments including neurophysiological scales (MMSE, ADAScog, and HAMD), EEG examination, and blood tests (i.e., Aβ, IL-1β, and MT levels). Subsequently, they were exposed to bright light at an illumination intensity of 14000 lux twice daily. After 4 weeks of therapy, the same assessments were repeated.

The characteristics of the patients included in this study are summarized in Table 1. In total, 22 patients with AD were included, with a mean age of 68.05 years, 10 men and 12 women. The caregiver group consisted of 23 individuals (8 men and 15 women) with a mean age of 65.04 years. Eleven patients with AD were taking memantine and nine were taking donepezil.

Effect of BLT on patients with AD and their caregivers

Blood test results and EEG parameters of patients with AD and their caregivers were evaluated. The results are presented in Table 2. After BLT, blood Aβ and IL-1β levels decreased significantly in both the AD and HC groups, whereas MT levels increased significantly in both groups. The HAMD score also decreased. Blood $Aβ_{40}$ and $Aβ_{42}$ levels were only significantly decreased in the HC group.

Changes in EEG power after BLT

Resting state EEG was performed in patients with AD and their caregivers with normal cognitive levels, as shown in Figures 2A–D. Compared to people with normal cognition, patients with AD had higher resting state EEG power at baseline. In the open-eye state (Figure 2A), the power of the HC group decreased, whereas that of the AD group increased, although no significant change in the EEG power after BLT was observed in both groups compared with that at baseline,. BLT suppressed the resting state power in the occipital lobe of patients with AD and in the frontal and right temporal lobes of caregivers in the HC group; however, these results were not significant. Regarding the differences in EEG power between the AD and HC groups in the closed-eye state (Figure 2B), the differences

TABLE 1 Patients' baseline characteristics.

Participant variables		AD (N=22)	HC (N=23)	t/χ^2	*p* value
Age (years)		68.05 (4.24)	65.04 (8.72)	−1.479	0.149
Sex (M/F)		10/12	8/15	1.800	0.180
Education (years)		6.09 (1.34)	5.91 (1.44)	−0.428	0.671
BMI		22.49(3.33)	23.91(2.02)	1.718	0.095
MMSE (scores)		15.91 (7.51)	29.09 (1.13)	8.145	**0.000**
ADAScog (scores)		39.39 (19.45)	6.74 (2.84)	−7.793	**0.000**
HAMD (scores)		3.26(2.82)	7.27(4.61)	−3.502	**0.001**
Blood Aβ (ng/mL)		426.30(69.59)	306.38(83.63)	−5.216	**0.000**
Blood $A\beta_{40}$ (pg/mL)		352.54 (86.61)	285.06 (80.86)	−2.703	**0.01**
Blood $A\beta_{42}$ (pg/mL)		663.62 (107.39)	525.18 (117.47)	−4.121	**0.000**
Blood IL-1β (pg/mL)		87.37 (13.49)	63.73 (13.33)	−5.912	**0.000**
Blood MT (pg/mL)		7.54(2.11)	10.03 (2.63)	3.482	**0.001**
EEG power (encephalic region)					
	Frontal	0.29(0.10)	0.22 (0.04)	−3.285	**0.003**
	Left temporal	0.26 (0.07)	0.24 (0.05)	−1.161	0.252
	Right temporal	0.28(0.10)	0.21(0.04)	−2.902	**0.007**
	Parietal	0.25(0.07)	0.19(0.04)	−2.918	**0.006**
	Occipital	0.27(0.07)	0.22(0.05)	−2.569	**0.014**
EEG power (wave band)					
	Delta	2.76(0.89)	2.22(0.46)	−2.523	**0.017**
	Theta	1.64(0.75)	1.15(0.46)	−2.641	**0.012**
	Alpha	0.80(0.27)	0.58(0.12)	−3.677	**0.001**
	Beta	0.48(0.23)	0.42(0.12)	−1.022	0.312
Medications					
	Memantine	11	0	NA	NA
	Donepezil	9	0	NA	NA
	Antidepressant	12	0	NA	NA

Data are presented as mean(standard deviation, SD). AD, Alzheimer's disease; HC, health control;MMSE, Mini-Mental State Examination; EEG, electroencephalography; PSD, power spectral density; NA, not applicable; HAMD, hamilton depression scale; ADAScog, Alzheimer's Disease Assessment Scale—Cognitive Subscale; MT, melatonin; IL, interleukin; BMI, body mass index. Resting state EEG, power was determined during the closed eye state. Delta band, 0–4 Hz; Theta band, 4–8 Hz; Alpha band, 8–13 Hz; Beta band, 13–30 Hz.Where bold values represents $p < 0.05$.

after BLT decreased in frontal, parietal and occipital lobes compared with that before BLT.

Regarding the EEG power band, differences were observed at baseline between patients with AD and their caregivers in the theta, alpha, and beta bands in the open-eye state and in the delta, theta, and alpha bands in the closed-eye state. Although no significant changes were observed in the power bands of both the AD and CG groups after BLT, differences were observed between the beta band in the open-eye state and that of the theta band in the closed-eye state, whereas the differences between the delta bands in the closed-eye state changed from significant to not significant.

Regarding the EEG topographic map (Figures 2E, F) the difference between pre- and post-therapy in the HC and AD groups was not significant in the open-eye state. In the closed-eye state, the differences between the delta, theta, and beta bands of the occipital lobe in the HC group were significant (P1 < 0.001); the differences between the theta and beta bands of the left temporal parietal lobe in the AD group were also significant (P2 < 0.001).

In Figure 3, the effects of BLT on the correlations between different regions of the cortex were investigated using the EEG power network in patients with AD and cognitive normal controls. The Pearson coefficient (r) was used to represent the connection strength between regions of the cortex as shown in Table 3. Compared with the pre therapy condition, significant improvements were observed in the numbers and strengths of connections after BLT.

TABLE 2 Participants'characteristics pre- and post-bright light therapy.

Variables	AD (N = 22)		t/χ^2	*p* value	HC (N = 23)		t/χ^2	*p* value
	Pre	Post			Pre	Post		
Blood Aβ (ng/mL)	426.30(69.59)	380.27(60.64)	4.436	**0.000**	306.38(83.63)	235.79(59.63)	5.713	**0.000**
Blood $A\beta_{40}$ (pg/mL)	352.54(86.61)	330.93(74.83)	1.417	0.171	285.06 (80.86)	199.63 (51.56)	4.185	**0.000**
Blood $A\beta_{42}$ (pg/mL)	663.62(107.39)	693.82(107.56)	−1.634	0.117	525.18 (117.47)	406.26(81.20)	6.241	**0.000**
Blood IL-1β (pg/mL)	87.37(13.49)	77.54(12.41)	3.976	**0.001**	63.73(13.33)	50.65(9.54)	3.671	**0.001**
Blood MT (pg/mL)	7.54(2.11)	9.42(2.20)	−3.701	**0.001**	10.03(2.63)	14.02 (1.78)	−6.480	**0.000**
EEG power (encephalic region)								
Frontal	0.29 (0.10)	0.31 (0.11)	−0.513	0.611	0.22 (0.04)	0.24 (0.06)	−1.455	0.153
Left temporal	0.26 (0.07)	0.27 (0.08)	−0.483	0.632	0.24 (0.05)	0.26 (0.07)	−1.211	0.232
Right temporal	0.28 (0.08)	0.28 (0.10)	−0.164	0.870	0.21 (0.04)	0.22 (0.05)	−0.692	0.493
Parietal	0.25 (0.07)	0.26 (0.08)	−0.644	0.523	0.20 (0.04)	0.22 (0.04)	−1.693	0.098
Occipital	0.27 (0.07)	0.28 (0.08)	−0.343	0.734	0.22 (0.05)	0.25 (0.06)	−1.467	0.149
EEG power (wave band)								
Delta	2.76 (0.89)	2.75 (0.90)	0.038	0.970	2.22 (0.46)	2.35 (0.54)	−0.819	0.417
Theta	1.64 (0.75)	1.73 (0.76)	−0.394	0.695	1.15 (0.46)	1.18 (0.49)	−0.205	0.838
Alpha	0.80 (0.27)	0.83 (0.25)	−0.409	0.684	0.58 (0.12)	0.62 (0.15)	−1.162	0.251
Beta	0.48 (0.23)	0.51 (0.19)	−0.556	0.581	0.42 (0.12)	0.49 (0.16)	−1.795	0.080
HAMD(scores)	7.23(4.61)	6.00(4.47)	2.494	**0.021**	3.26 (2.82)	1.87 (2.51)	4.449	**0.000**

Data are presented as mean (standard deviation, SD). AD, Alzheimer's disease; HC, health control; Aβ, β amyloid; MT, melatonin; EEG, electroencephalograph; HAMD, Hamilton depression scale. Resting state EEG, power was determined during the closed eye state. Delta band, 0–4 Hz; Theta band, 4–8 Hz; Alpha band, 8–13 Hz; Beta band, 13–30 Hz.Where bold values represents $p < 0.05$.

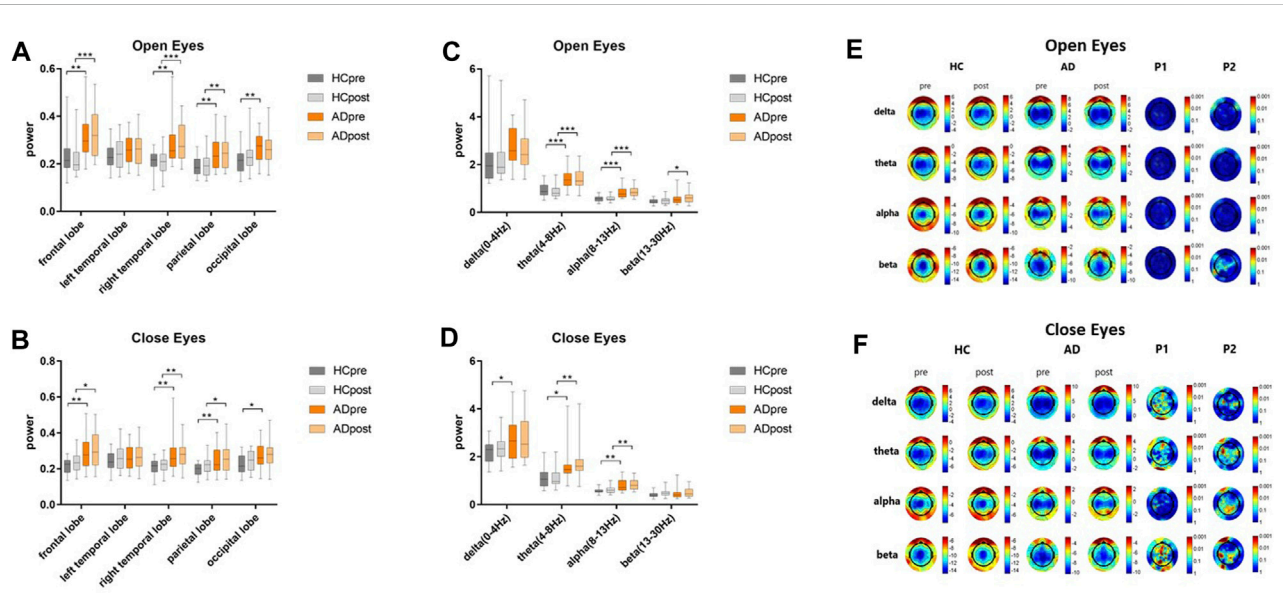

FIGURE 2
Resting state EEG power of patients with AD and their caregivers with normal cognition (CN group) in the open-eye **(A)** and closed-eye **(B)** states at the frontal, left temporal, right temporal, parietal, and occipital lobes, and in the open-eye **(C)** and closed-eye **(D)** states in the delta (0–4 Hz), theta (4–8 Hz), alpha (8–13 Hz), and beta (13–30 Hz) bands. The gray and orange bars represent the HC and AD groups, respectively before (dark color) and after (light color) bright light therapy. Resting state EEG topographic maps of patients with AD and their care givers with normal cognition (HC group) in the open-eye **(E)** and closed-eyes **(F)** states. P1 and P2 represent different *p* values before and after therapy in the HC and AD groups, respectively.

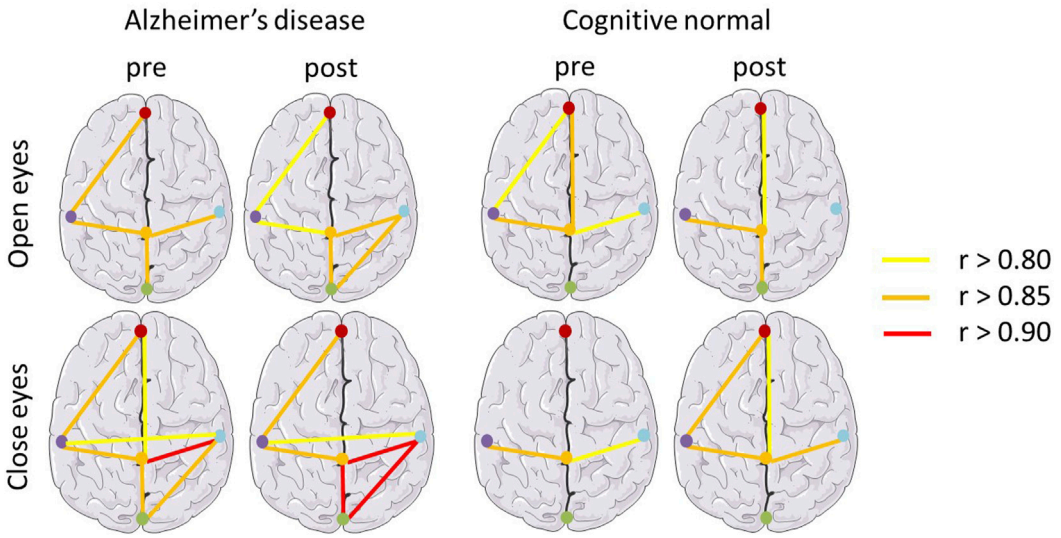

FIGURE 3
EEG power network of the brain in patients with Alzheimer's disease and cognitively normal controls. Pearson coefficient (r) was used to represent the connection strength between regions of the cortex. r values greater than 0.80, 0.85, 0.90 are represented by yellow, orange and red bars respectively.

TABLE 3 Correlation between regions of the cortex.

	AD_OE		AD_CE		HC_OE		HC_CE	
	pre	post	pre	post	pre	post	pre	post
①	0.869***	0.820***	0.876***	0.861***	0.813***	0.786***	0.733***	0.854***
②	0.726***	0.589**	0.805***	0.769***	0.885***	0.842***	0.754***	0.833***
③	0.597**	0.510*	0.798***	0.641**	0.714***	0.624**	0.634**	0.702***
④	0.710***	0.698***	0.831***	0.802***	0.755***	0.593**	0.743***	0.675***
⑤	0.854***	0.801***	0.855***	0.871***	0.865***	0.850***	0.852***	0.864***
⑥	0.865***	0.888***	0.941***	0.935***	0.847***	0.717***	0.845***	0.864***
⑦	0.641**	0.505*	0.686***	0.723***	0.772***	0.776***	0.762***	0.791***
⑧	0.855***	0.858***	0.889***	0.918***	0.769***	0.820***	0.723***	0.785***
⑨	0.784***	0.861***	0.891***	0.904***	0.776***	0.689***	0.700***	0.694***
⑩	0.496*	0.306	0.577**	0.570**	0.723***	0.725***	0.570**	0.759***

① to ⑩ represented relationship between frontal lobe and right temporal lobe, frontal lobe and parietal lobe, frontal lobe and left temporal lobe, right temporal lobe and left temporal lobe, right temporal lobe and parietal lobe, left temporal lobe and parietal lobe, right temporal lobe and occipital lobe, parietal lobe and occipital lobe, left temporal lobe and occipital lobe, frontal lobe and occipital lobe. *** $p < 0.001$, ** $p < 0.01$, * $p < 0.05$.

Pearson correlation between cognitive, blood, and EEG parameters

As shown in Figure 4, MMSE and ADAScog scores were both significantly correlated with the blood parameters of Aβ (r = −0.587, $p < 0.001$; r = 0.555, $p < 0.001$), $Aβ_{40}$ (r = −0.410, $p = 0.005$; r = 0.319, $p = 0.033$), $Aβ_{42}$ (r = −0.519, $p < 0.001$; r = 0.437, $p = 0.003$), IL-1β (r = −0.682, $p < 0.001$; r = 0.649, $p < 0.001$), and MT (r = 0.503, $p < 0.001$; r = −0.471, $p = 0.001$) respectively. The EEG parameter of the delta power band in the closed- ($p = 0.054$) and open-eye ($p = 0.187$) states showed no significant correlation with MMSE scores. The theta and delta power bands in the closed- ($p = 0.096$) and open-eye ($p = 0.127$) states showed no significant correlation with ADAScog scores. The EEG power of the left temporal lobe showed no significant correlation with both MMSE ($p = 0.072$) and ADAScog ($p = 0.069$) scores.

Discussion

BLT is a medical treatment that utilizes natural or artificial light to improve a health condition. Our study showed that BLT may affect the EEG power and blood indicators, and may suppress

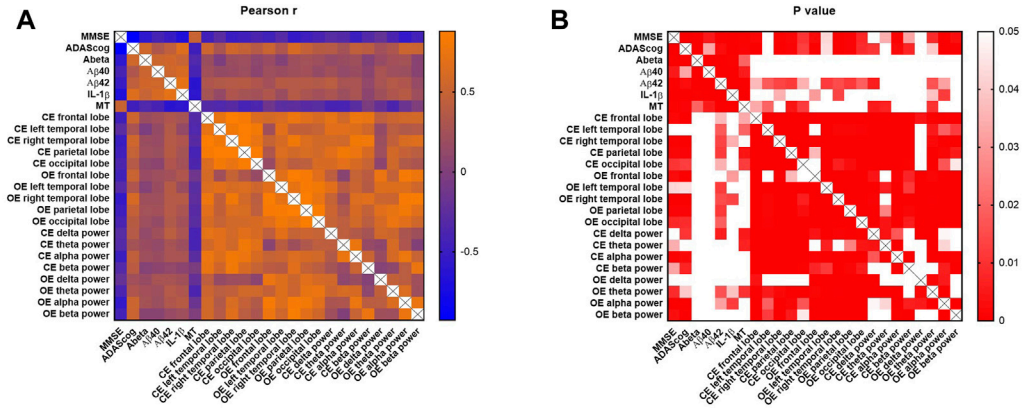

FIGURE 4
Pearson correlation analysis of cognitive, blood, and EEG parameters. MMSE and ADAScog scores represent the cognitive levels of participants. The blood parameters included Aβ, $Aβ_{40}$, $Aβ_{42}$, IL-1β and MT. EEG parameters included the power of five lobes (frontal, left temporal, right temporal, parietal, and occipital lobes) and four bands (delta [0–4 Hz], theta [4–8 Hz], alpha [8–13 Hz] and beta [13–30 Hz]). The scale bar represents the Pearson coefficient, r **(A)** and *p* values **(B)**. CE, closed-eye state; OE, open-eye state.

depression, potentially owing to its effects on the circadian system *via* brain regions that respond preferentially to light. Patients with AD have high EEG power and strong electrical activity and more wastage in the resting state (Hsiao et al., 2013). Although the EEG power may be high and electrical activity of nerve cells may be strong in patients with AD, the synaptic function is incomplete and the signal conduction between neurons is abnormal; therefore, the brain cannot perform the functions of execution, memory, and learning (Babiloni et al., 2023).

To the best of our knowledge, EEG has been used as a non-invasive tool to study AD for many years. In recent years, modern methods of EEG analysis have been used to investigate physiological brain aging and AD (Cassani et al., 2018). Many recent studies focused on EEG signals for AD diagnosis, identifying and comparing key steps of EEG-based AD detection (Poil et al., 2013; Jesus et al., 2021). Resting state EEG was used as an effective tool to detect and assess cognitive impairment in patients with early AD (Meghdadi et al., 2021; Özbek et al., 2021). Compared to age-matched controls, an increase in spectral power was observed at the lower delta and theta frequencies in the AD group (Meghdadi et al., 2021), which was also observed in our study. The power of the delta and theta bands in the AD group decreased after BLT. These indicators may be potentially used as therapy efficacy assessment indicators.

In this study, the control group included cognitively normal individuals, rather than patients with AD who were not exposed to BLT. To some extent, this method avoided the placebo effect in participants with or without BLT. Moreover, the baseline values of the AD group were considered the self-control condition (positive control). The caregiver group was considered the normal condition (negative control). In previous studies, low intensity light was used as a sham stimulation (Hirakawa et al., 2020), which may be an ideal sham procedure if the lighting device is adjustable.

According to a previous study, non-invasive phototherapy is emerging as a strategy for suppressing Aβ self-assembly against AD (Ma et al., 2023). However, developing efficient photosensitizers for Aβ oxygenation that are active in deep brain tissues through the scalp and skull while reducing side effects remains a daunting challenge. Although light treatment improved cognitive function in AD mice and cleared amyloid levels in the brain (Yao et al., 2020; Kim et al., 2022), no changes in blood amyloid concentrations before and after BLT were observed. Another study found that BLT resulted in less daytime sleeping and increased night-time sleeping in people with dementia (Tan et al., 2022). Aβ levels can be cleared during sleep although accumulate during sleep deprivation (Shokri-Kojori et al., 2018; Wang and Holtzman, 2020).

Phototherapy is an effective method of treatment for patients with seasonal affective disorders (Knapen et al., 2014; Meyerhoff et al., 2018). Research confirms that phototherapy markedly improved mood and sleep quality in older adults (Zhang et al., 2023). Light signals are projected through retinal ganglion cells to depressed brain areas to participate in non-visual imaging functions, thereby activating nerve cell activity, secreting neurotransmitters to induce physiological changes in neural pathways, and regulating circadian rhythms, mood, and sleep in the biological organism to improve depressive symptoms (Fernandez et al., 2018). Moreover, the circadian system is composed of the central autonomous clock, suprachiasmatic nucleus, and body systems that follow the signals of the suprachiasmatic nucleus which mediate the effects of light on cognition and mood (Fernandez et al., 2018). It continuously changes the homeostatic set points of the body over the day-night cycle. The circadian rhythm is a natural, internal process that regulates the sleep-wake cycle that repeats approximately every 24 h.

Several treatments for mood disorders are available, including medication (anticonvulsants, antipsychotics, lithium, antidepressants, and benzodiazepines) and psychotherapy (Otte et al., 2016). Anticonvulsants, antipsychotics, and lithium are used to stabilize mood whereas antidepressants are used to treat depressive and anxiety disorders. As a non-pharmacological treatment, BLT can avoid the side effects and drug interactions associated with drug therapy, and also have the advantages of good compliance and ease of operation, making it suitable for use in patients with AD and their caregivers to treat depression.

This study has the following limitations and strengths. First, the sample size was relatively small. Regarding the long therapy duration and advanced age of participants, clinical samples were prone to shedding, and the dropout rate was high. The strength of

this study is that we explored the non-pharmacological treatment BLT in patients with AD accompanied by depression, and revealed significant effects and useful clinical information regarding EEG power. Future studies will include a prolonged study duration and larger sample size to further investigate the association between changes in depression and EEG power.

Conclusion

BLT can suppress depression in patients with AD and their caregivers. Meanwhile, BLT significantly affected the EEG power and blood indicators. Non-pharmacological antidepressant therapy may be an effective and safe method for improving the emotional states of patients with AD and their caregivers.

Data availability statement

The original contributions presented in the study are included in the article/Supplementary material, further inquiries can be directed to the corresponding author.

Ethics statement

The studies involving humans were approved by the Ningbo Kangning Hospital ethics committee. The studies were conducted in accordance with the local legislation and institutional requirements. Written informed consent for participation in this study was provided by the participants'; legal guardians/next of kin.

Author contributions

XM, CZo, and ZS contributed to the original draft of the manuscript. TX and JH conducted the experiments. XW and CZh proofread the manuscript. All authors contributed to the article and approved the submitted version.

Funding

The study was funded by Ningbo City Key R&D plan "Jie Bang Gua Shuai" (2023Z170), Ningbo City Public welfare Science and technology Plan project (2022S025), Zhejiang Medical and Health Science and Technology Project (2022KY1174), Ningbo Medical and Health Leading Academic Discipline Project (2022-F28), and the Major Fund Project of Ningbo Science and Technology Bureau (2019B10034). The sponsor had no role in the design or conduct of this research.

Acknowledgments

We acknowledge the Ningbo Kangning Hospital and all hospital staff that were involved in patient treatment.

Conflict of interest

The authors declare that the research was conducted in the absence of any commercial or financial relationships that could be construed as a potential conflict of interest.

Publisher's note

References

Al-Karawi, D., and Jubair, L. (2016). Bright light therapy for nonseasonal depression: meta-analysis of clinical trials. *J. Affect. Disord.* 198, 64–71. doi:10.1016/j.jad.2016.03.016

Altomari, N., Bruno, F., Laganà, V., Smirne, N., Colao, R., Curcio, S., et al. (2022). A comparison of behavioral and psychological symptoms of dementia (bpsd) and bpsd sub-syndromes in early-onset and late-onset alzheimer's disease. *J. Alzheimer's Dis. JAD* 85, 691–699. doi:10.3233/JAD-215061

Babiloni, C., Blinowska, K., Bonanni, L., Cichocki, A., De Haan, W., Del Percio, C., et al. (2020). What electrophysiology tells us about alzheimer's disease: a window into the synchronization and connectivity of brain neurons. *Neurobiol. aging* 85, 58–73. doi:10.1016/j.neurobiolaging.2019.09.008

Babiloni, C., Lopez, S., Noce, G., Ferri, R., Panerai, S., Catania, V., et al. (2023). Relationship between default mode network and resting-state electroencephalographic alpha rhythms in cognitively unimpaired seniors and patients with dementia due to alzheimer's disease. *Cereb. Cortex* 33, 10514–10527. doi:10.1093/cercor/bhad300

Caravaglios, G., Muscoso, E. G., Blandino, V., Di Maria, G., Gangitano, M., Graziano, F., et al. (2023). Eeg resting-state functional networks in amnestic mild cognitive impairment. *Clin. EEG Neurosci.* 54, 36–50. doi:10.1177/15500594221110036

Carbone, E. A., de Filippis, R., Roberti, R., Rania, M., Destefano, L., Russo, E., et al. (2021). The mental health of caregivers and their patients with dementia during the covid-19 pandemic: a systematic review. *Front. Psychol.* 12, 782833. doi:10.3389/fpsyg.2021.782833

Cassani, R., Estarellas, M., San-Martin, R., Fraga, F. J., and Falk, T. H. (2018). Systematic review on resting-state eeg for alzheimer's disease diagnosis and progression assessment. *Dis. Markers* 2018, 5174815. doi:10.1155/2018/5174815

Chai, Y. C., Mahadevan, R., Ng, C. G., Chan, L. F., and Md Dai, F. (2018). Caregiver depression: the contributing role of depression in patients, stigma, social support and religiosity. *Int. J. Soc. psychiatry* 64, 578–588. doi:10.1177/0020764018792585

Chi, S., Yu, J. T., Tan, M. S., and Tan, L. (2014). Depression in alzheimer's disease: epidemiology, mechanisms, and management. *J. Alzheimer's Dis. JAD* 42, 739–755. doi:10.3233/JAD-140324

Corrêa, M. S., de Lima, D. B., Giacobbo, B. L., Vedovelli, K., Argimon, I. I. L., and Bromberg, E. (2019). Mental health in familial caregivers of alzheimer's disease patients: are the effects of chronic stress on cognition inevitable? *Stress Amsterdam, Neth.* 22, 83–92. doi:10.1080/10253890.2018.1510485

Diniz, B. S., Butters, M. A., Albert, S. M., Dew, M. A., and Reynolds, C. F., 3rd (2013). Late-life depression and risk of vascular dementia and alzheimer's disease: systematic review and meta-analysis of community-based cohort studies. *Br. J. psychiatry J. Ment. Sci.* 202, 329–335. doi:10.1192/bjp.bp.112.118307

Fernandez, D. C., Fogerson, P. M., Lazzerini Ospri, L., Thomsen, M. B., Layne, R. M., Severin, D., et al. (2018). Light affects mood and learning through distinct retina-brain pathways. *Cell* 175, 71–84. doi:10.1016/j.cell.2018.08.004

First, M. B. (2013). Diagnostic and statistical manual of mental disorders, 5th edition, and clinical utility. *J. Nerv. Ment. Dis.* 201, 727–729. doi:10.1097/NMD.0b013e3182a2168a

Hirakawa, H., Terao, T., Muronaga, M., and Ishii, N. (2020). Adjunctive bright light therapy for treating bipolar depression: a systematic review and meta-analysis of randomized controlled trials. *Brain Behav.* 10, e01876. doi:10.1002/brb3.1876

Hsiao, F. J., Wang, Y. J., Yan, S. H., Chen, W. T., and Lin, Y. Y. (2013). Altered oscillation and synchronization of default-mode network activity in mild alzheimer's disease compared to mild cognitive impairment: an electrophysiological study. *PloS one* 8, e68792. doi:10.1371/journal.pone.0068792

Jack, C. R., Jr., Bennett, D. A., Blennow, K., Carrillo, M. C., Dunn, B., Haeberlein, S. B., et al. (2018). Nia-aa research framework: toward a biological definition of alzheimer's disease. *Alzheimer's dementia* 14, 535–562. doi:10.1016/j.jalz.2018.02.018

Jesus, B., Jr., Cassani, R., McGeown, W. J., Cecchi, M., Fadem, K. C., and Falk, T. H. (2021). Multimodal prediction of alzheimer's disease severity level based on resting-state eeg and structural mri. *Front. Hum. Neurosci.* 15, 700627. doi:10.3389/fnhum.2021.700627

Jia, L., Du, Y., Chu, L., Zhang, Z., Li, F., Lyu, D., et al. (2020). Prevalence, risk factors, and management of dementia and mild cognitive impairment in adults aged 60 years or older in China: a cross-sectional study. *Lancet Public health* 5, e661–e671. doi:10.1016/S2468-2667(20)30185-7

Kim, S. H., Park, S. S., Kim, C. J., and Kim, T. W. (2022). Exercise with 40-hz light flicker improves hippocampal insulin signaling in alzheimer disease mice. *J. Exerc. Rehabil.* 18, 20–27. doi:10.12965/jer.2244042.021

Knapen, S. E., van de Werken, M., Gordijn, M. C., and Meesters, Y. (2014). The duration of light treatment and therapy outcome in seasonal affective disorder. *J. Affect. Disord.* 166, 343–346. doi:10.1016/j.jad.2014.05.034

Li, H., Jia, J., and Yang, Z. (2016). Mini-mental state examination in elderly Chinese: a population-based normative study. *J. Alzheimer's Dis. JAD* 53, 487–496. doi:10.3233/JAD-160119

Liu, S., Li, C., Shi, Z., Wang, X., Zhou, Y., Liu, S., et al. (2017). Caregiver burden and prevalence of depression, anxiety and sleep disturbances in alzheimer's disease caregivers in China. *J. Clin. Nurs.* 26, 1291–1300. doi:10.1111/jocn.13601

Lu, X., Liu, C., and Shao, F. (2023). Phototherapy improves cognitive function in dementia: a systematic review and meta-analysis. *Brain Behav.* 2023, e2952. doi:10.1002/brb3.2952

Ma, M., Wang, J., Jiang, H., Chen, Q., Xiao, Y., Yang, H., et al. (2023). Transcranial deep-tissue phototherapy for alzheimer's disease using low-dose x-ray-activated long-afterglow scintillators. *Acta biomater.* 155, 635–643. doi:10.1016/j.actbio.2022.10.049

Masters, C. L., Bateman, R., Blennow, K., Rowe, C. C., Sperling, R. A., and Cummings, J. L. (2015). Alzheimer's disease. *Nat. Rev. Dis. Prim.* 1, 15056. doi:10.1038/nrdp.2015.56

Meghdadi, A. H., Stevanović Karić, M., McConnell, M., Rupp, G., Richard, C., Hamilton, J., et al. (2021). Resting state eeg biomarkers of cognitive decline associated with alzheimer's disease and mild cognitive impairment. *PloS one* 16, e0244180. doi:10.1371/journal.pone.0244180

Meyerhoff, J., Young, M. A., and Rohan, K. J. (2018). Patterns of depressive symptom remission during the treatment of seasonal affective disorder with cognitive-behavioral therapy or light therapy. *Depress. anxiety* 35, 457–467. doi:10.1002/da.22739

Otte, C., Gold, S. M., Penninx, B. W., Pariante, C. M., Etkin, A., Fava, M., et al. (2016). Major depressive disorder. *Nat. Rev. Dis. Prim.* 2, 16065. doi:10.1038/nrdp.2016.65

Özbek, Y., Fide, E., and Yener, G. G. (2021). Resting-state eeg alpha/theta power ratio discriminates early-onset alzheimer's disease from healthy controls. *Clin. neurophysiology official J. Int. Fed. Clin. Neurophysiology* 132, 2019–2031. doi:10.1016/j.clinph.2021.05.012

Peter-Derex, L., Yammine, P., Bastuji, H., and Croisile, B. (2015). Sleep and alzheimer's disease. *Sleep. Med. Rev.* 19, 29–38. doi:10.1016/j.smrv.2014.03.007

Pfurtscheller, G., and Lopes da Silva, F. H. (1999). Event-related eeg/meg synchronization and desynchronization: basic principles. *Clin. Neurophysiol.* 110, 1842–1857. doi:10.1016/s1388-2457(99)00141-8

Poil, S. S., de Haan, W., van der Flier, W. M., Mansvelder, H. D., Scheltens, P., and Linkenkaer-Hansen, K. (2013). Integrative eeg biomarkers predict progression to alzheimer's disease at the mci stage. *Front. aging Neurosci.* 5, 58. doi:10.3389/fnagi.2013.00058

Roccaro, I., Smirni, D., and lux, F. (2020). Fiat lux: the light became therapy. An overview on the bright light therapy in alzheimer's disease sleep disorders. *J. Alzheimer's Dis. JAD* 77, 113–125. doi:10.3233/JAD-200478

Rosen, W. G., Mohs, R. C., and Davis, K. L. (1984). A new rating scale for alzheimer's disease. *Am. J. psychiatry* 141, 1356–1364. doi:10.1176/ajp.141.11.1356

Scheltens, P., Blennow, K., Breteler, M. M., de Strooper, B., Frisoni, G. B., Salloway, S., et al. (2016). Alzheimer's disease. *Lancet London, Engl.* 388, 505–517. doi:10.1016/S0140-6736(15)01124-1

Scheltens, P., De Strooper, B., Kivipelto, M., Holstege, H., Chételat, G., Teunissen, C. E., et al. (2021). Alzheimer's disease. *Lancet (London, Engl.* 397, 1577–1590. doi:10.1016/S0140-6736(20)32205-4

Shokri-Kojori, E., Wang, G. J., Wiers, C. E., Demiral, S. B., Guo, M., Kim, S. W., et al. (2018). B-amyloid accumulation in the human brain after one night of sleep deprivation. *Proc. Natl. Acad. Sci. U. S. A.* 115, 4483–4488. doi:10.1073/pnas.1721694115

Tan, J. S. I., Cheng, L. J., Chan, E. Y., Lau, Y., and Lau, S. T. (2022). Light therapy for sleep disturbances in older adults with dementia: a systematic review, meta-analysis and meta-regression. *Sleep. Med.* 90, 153–166. doi:10.1016/j.sleep.2022.01.013

van Maanen, A., Meijer, A. M., van der Heijden, K. B., and Oort, F. J. (2016). The effects of light therapy on sleep problems: a systematic review and meta-analysis. *Sleep. Med. Rev.* 29, 52–62. doi:10.1016/j.smrv.2015.08.009

Wang, C., and Holtzman, D. M. (2020). Bidirectional relationship between sleep and alzheimer's disease: role of amyloid, tau, and other factors. *Neuropsychopharmacology* 45, 104–120. doi:10.1038/s41386-019-0478-5

Wang, S., Zhang, Z., Yao, L., Ding, N., Jiang, L., and Wu, Y. (2020). Bright light therapy in the treatment of patients with bipolar disorder: a systematic review and meta-analysis. *PLoS One* 15, e0232798. doi:10.1371/journal.pone.0232798

Yao, Y., Ying, Y., Deng, Q., Zhang, W., Zhu, H., Lin, Z., et al. (2020). Non-invasive 40-hz light flicker ameliorates alzheimer's-associated rhythm disorder via regulating central circadian clock in mice. *Front. physiology* 11, 294. doi:10.3389/fphys.2020.00294

Zhang, M., Wang, Q., Pu, L., Tang, H., Chen, M., Wang, X., et al. (2023). Light therapy to improve sleep quality in older adults living in residential long-term care: a systematic review. *J. Am. Med. Dir. Assoc.* 24, 65–74.e1. doi:10.1016/j.jamda.2022.10.008

Zimmerman, M., Martinez, J. H., Young, D., Chelminski, I., and Dalrymple, K. (2013). Severity classification on the Hamilton depression rating scale. *J. Affect. Disord.* 150, 384–388. doi:10.1016/j.jad.2013.04.028

Zou, C., Mei, X., Li, X., Hu, J., Xu, T., and Zheng, C. (2022). Effect of light therapy on delirium in older patients with alzheimer's disease-related dementia. *J. psychiatric Res.* 149, 124–127. doi:10.1016/j.jpsychires.2022.03.003

Frontiers in
Aging Neuroscience

Explores the mechanisms of central nervous system aging and age-related neural disease

The third most-cited journal in the field of geriatrics and gerontology, with a focus on understanding the mechanistic processes associated with central nervous system aging.

Discover the latest Research Topics

See more →

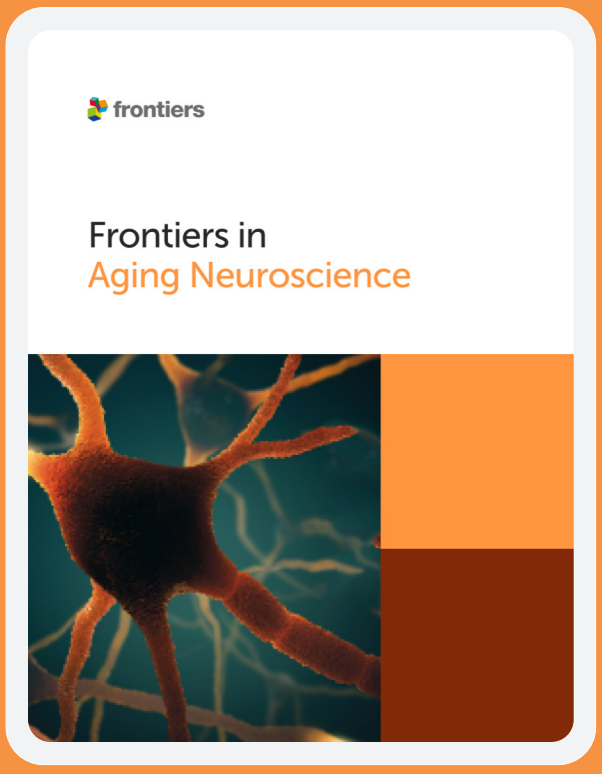

Frontiers

Avenue du Tribunal-Fédéral 34
1005 Lausanne, Switzerland
frontiersin.org

Contact us

+41 (0)21 510 17 00
frontiersin.org/about/contact